

Igor L. Shabalin

Ultra-High Temperature Materials II

Refractory Carbides I
(Ta, Hf, Nb and Zr Carbides)

 Springer

Ultra-High Temperature Materials II

Igor L. Shabalin

Ultra-High Temperature Materials II

Refractory Carbides I
(Ta, Hf, Nb and Zr Carbides)

A Comprehensive Guide and Reference Book

 Springer

Igor L. Shabalin
Materials and Physics Research Centre
The University of Salford
Manchester
UK

and

Department of High Temperature Materials
National Technical University of Ukraine
“Igor Sikorsky Kyiv Polytechnic Institute”
Kyiv
Ukraine

ISBN 978-94-024-1300-7 ISBN 978-94-024-1302-1 (eBook)
<https://doi.org/10.1007/978-94-024-1302-1>

Library of Congress Control Number: 2018935853

© Springer Nature B.V. 2019

This work is subject to copyright. All rights are reserved by the Publisher, whether the whole or part of the material is concerned, specifically the rights of translation, reprinting, reuse of illustrations, recitation, broadcasting, reproduction on microfilms or in any other physical way, and transmission or information storage and retrieval, electronic adaptation, computer software, or by similar or dissimilar methodology now known or hereafter developed.

The use of general descriptive names, registered names, trademarks, service marks, etc. in this publication does not imply, even in the absence of a specific statement, that such names are exempt from the relevant protective laws and regulations and therefore free for general use.

The publisher, the authors and the editors are safe to assume that the advice and information in this book are believed to be true and accurate at the date of publication. Neither the publisher nor the authors or the editors give a warranty, express or implied, with respect to the material contained herein or for any errors or omissions that may have been made. The publisher remains neutral with regard to jurisdictional claims in published maps and institutional affiliations.

Printed on acid-free paper

This Springer imprint is published by the registered company Springer Nature Singapore Pte Ltd..
The registered company address is: 152 Beach Road, #21-01/04 Gateway East, Singapore 189721, Singapore

This book is dedicated to two Russian men:

*—Colonel Logan S. Shabalin (1926–2016),
one of the Russian soldiers of WWII, my
beloved father*

and

*—Dr. Leonid I. Shabalin (born in 1979), my
beloved son*

Preface

This book is the second volume in my *Ultra-High Temperature Materials* series, which is devoted to the materials having melting (sublimation or decomposition) points around or above 2500 °C. In the preface to the first volume, I have already detailed all the motives that led me to the creation and establishment of this series of books, so here I consider it is sufficient only to refer to it. The second volume is not only the continuation of the first volume, but taking into account the system of references and addenda adopted in the series, it accumulates all the information presented in both volumes. Thus, any reader/user of this book is unlikely to be satisfied with the process of learning or searching for the information necessary for him without the usage of the previous volume.

Many thanks to the colleagues for their feedback on the chapters of the first volume, but I again ask everybody, who has any remarks, observations, or possibly corrections and personal opinions, concerning this book and its contents, to send them directly to my e-mail. It will be very useful for me to take into account all your responses before preparation and publishing of the succeeding volumes of the series.

This book would not have been possible to create without the permanent encouragement and warm support I have got for the last years from my best friends, my colleagues and co-authors such as Prof. D. Keith Ross, one of the best specialists in the UK in the area of materials characterization, former director of Institute for Materials Research (University of Salford, Manchester), the authors of many books on materials science of refractory compounds, Prof. Rostislav A. Andrievskii (Institute for Problems of Chemical Physics, Russian Academy of Sciences, Chernogolovka, Moscow Region) and Prof. George G. Gnesin (Institute for Problems of Materials Science, National Academy of Sciences of Ukraine, Kyiv). Probably, therefore, it is still difficult for me to imagine that these brilliant scientists, my close friends, recently passed away, are no longer with us.

For the invaluable and kind assistance in the preparation of this volume, I would like gratefully to acknowledge Prof. Alexander I. Savvatimskiy (Joint Institute for High Temperatures, Moscow, Russia), Prof. Irina V. Medvedeva (Institute of Metal Physics, Yekaterinburg, Russia), Prof. Anders E. W. Jarfors (Jönköping University,

Sweden), Dr. Yelena Vertyagina (University of Oxford, UK), Prof. Yury G. Gogotsi (Drexel University, Philadelphia, USA), Prof. Nikolai V. Obabkov, Prof. Vadim V. Kartashov, Prof. Peter E. Panfilov (Ural Federal University, Yekaterinburg, Russia), Prof. Artem R. Oganov (Stony Brook University, New York, USA), Dr. Suneel K. Kodambaka (University of California, Los Angeles, USA), Dr. Sergei A. Zykov (Institute of Metal Physics, Yekaterinburg, Russia), Prof. Mikhaylo S. Kovalchenko (Institute for Problems of Materials Science, Kyiv, Ukraine), Prof. Gopal S. Upadhyaya (formerly Indian Institute of Technology, Kanpur), Prof. Sergey S. Ordanyan and Dr. Dmitry P. Danilovich (St. Petersburg State Institute of Technology—Technical University, Russia), Prof. Koichi Niihara (Nagaoka University of Technology, Japan), Prof. Igor G. Korshunov (Ural State Mining University, Yekaterinburg, Russia), Prof. Anna Biedunkiewicz (West Pomeranian University of Technology, Szczecin, Poland), Prof. Anatoly G. Lanin (Luch Research & Production Association, Podolsk, Moscow Region, Russia), Dr. Vladimir M. Vishnyakov and Prof. John S. Colligon (University of Huddersfield, UK), Prof. W. Alan Oates, Dr. Wayne Y. Wang, Dr. Olga V. Umnova and Dr. Daniel J. Bull (University of Salford, Manchester, UK), Dr. Alexey S. Kurlov (Institute of Solid State Chemistry, Yekaterinburg, Russia), Dr. Florian Réjasse (University of Limoges, France), Prof. José M. F. Ferreira, University of Aveiro, Portugal), Dr. Patrick N. B. Anongba (Université Félix Houphouë-Boigny, Abidjan, Côte d'Ivoire), Dr. Stefano Guicciardi (Consiglio Nazionale delle Ricerche, Rome, Italy), Dr. Miron V. Luchka and Dr. Oleksandr V. Derevyanko (Institute for Problems of Materials Science, Kyiv, Ukraine), Prof. Shiro Shimado (Hokkaido University, Sapporo, Japan), Prof. Tatiana A. Prikhna (Institute of Superhard Materials, National Academy of Science of Ukraine, Kyiv, Ukraine), Prof. Valentyn A. Tatarenko (Institute for Metal Physics, Kyiv, Ukraine), Dr. Igor Yu. Konyashin (Element Six GmbH, Burghaun, Germany), John Cloughley (E4 Structures, Manchester, UK), Prof. Peter B. Barna (Research Institute for Technical Physics and Materials Science, Budapest, Hungary), Prof. László A. Gömze and Dr. Ludmila N. Gömze (University of Miskolc, Hungary), Dr. Mahdi G. Kakroudi (University of Tabriz, Iran), Prof. Namsrai Tsogbadrakh (National University of Mongolia, Ulaanbaatar, Mongolia).

I sincerely apologize if I have missed to mention the assistance of anybody else from the variety of scientists and researchers all around the world I have contacted with concerning the issues connected with the topics of this book.

Lastly, I wish to thank my relatives for their steadfast support during the last 4 years, which were necessary for the complete preparation of the book.

Manchester, UK
November 2017

Professor Igor L. Shabalin

Contents

1	Introduction	1
	References	7
2	Tantalum Carbides	9
2.1	Structures	9
2.2	Thermal Properties	15
2.3	Electro-magnetic and Optical Properties	29
2.4	Physico-mechanical Properties	43
2.5	Nuclear Physical Properties	61
2.6	Chemical Properties and Materials Design	63
	References	101
3	Hafnium Monocarbide	145
3.1	Structures	145
3.2	Thermal Properties	149
3.3	Electro-magnetic and Optical Properties	163
3.4	Physico-mechanical Properties	173
3.5	Nuclear Physical Properties	185
3.6	Chemical Properties and Materials Design	188
	References	218
4	Niobium Carbides	249
4.1	Structures	249
4.2	Thermal Properties	255
4.3	Electro-magnetic and Optical Properties	272
4.4	Physico-mechanical Properties	285
4.5	Nuclear Physical Properties	313
4.6	Chemical Properties and Materials Design	316
	References	368

5 Zirconium Monocarbide	423
5.1 Structures	423
5.2 Thermal Properties	432
5.3 Electro-magnetic and Optical Properties	457
5.4 Physico-mechanical Properties	476
5.5 Nuclear Physical Properties	517
5.6 Chemical Properties and Materials Design	527
References	597
Addendum	677
Index (Physical Properties)	723
Index (Chemical Systems)	739

About the Author



Igor L. Shabalin in his professional career has got over 45 years of experience in Ultra-High Temperature Materials Design, Science and Engineering. He was born in Russia, graduated in Technology of Less-Common Metals and received his M.Sc. and Ph.D. degrees from the Ural Polytechnic University (UPI), Yekaterinburg (former—Sverdlovsk), Russia. He has held academic positions at the UPI and was the founder of the Special Research Laboratory for Aerospace Industry (ONIL-123). As head of the laboratory and member of several scientific and technological councils, he established collaboration between universities and industry by running a variety of R&D projects and was involved in the management of some world leading programmes in rocketry and spacecraft development in the USSR Ministry of Aerospace Industry (MOM). In 2003, he immigrated to the United Kingdom and joined the University of Salford, Manchester, as a researcher in Materials in 2005. As he has developed his personal original approach to a special subclass of engineering materials—hetero-modulus composites and hybrids in ceramics, his research activity focuses mainly on high and ultra-high temperature ceramic composites with graphene-like (carbon and boron nitride) constituents. He has discovered in Russia in the 1980–90s and formulated later in the UK—mesoscopic temperature–pressure-dependent phenomenon in solid-state gas-exchange chemical reactions (surface processes) termed as “ridge effect”. From 1971 up to date, he has published about 300 scientific and technical papers and

holds more than 40 patents. In 2014, he was awarded the title of Honorary Professor of the Department of High Temperature Materials (National Technical University of Ukraine), which was founded by Grigorii V. Samsonov, one of the world famous scientists of the twentieth century in the field of physics and chemistry of refractory compounds.

Abstract

The work represents a thorough treatment of ultra-high temperature materials with melting points around or over 2500 °C. The second volume included physical (structural, thermal, electromagnetic, optical, mechanical and nuclear) and chemical (binary, ternary and multicomponent systems, solid-state diffusion, wettability, interaction with chemicals, gases and aqueous solutions) properties of refractory carbide materials: tantalum carbides (monocarbide TaC_{1-x} and semicarbide $\alpha/\beta\text{-Ta}_{2\pm x}\text{C}$), hafnium monocarbide HfC_{1-x} , niobium carbides (monocarbide NbC_{1-x} and semicarbide $\alpha/\beta/\gamma\text{-Nb}_{2\pm x}\text{C}$) and zirconium monocarbide ZrC_{1-x} . It will be of interest to researchers, engineers, postgraduate, graduate and undergraduate students alike. The reader/user is provided with the full qualitative and quantitative assessment for the materials, which could be applied in various engineering devices and environmental conditions in the wide range from cryogenic to ultra-high temperatures, on the basis of the latest updates in the field of physics, chemistry, nanotechnology, materials science and engineering.

Chapter 1

Introduction



Referring to the Volume I of this book [1], it is necessary to remind the fact that not only elemental carbon, but also its chemical compounds with various *p*-, *d*- and *f*-elements, termed as carbides, are of great interest for the materials designers and engineers, who are working in the area of ultra-high temperature materials, and so responsible for their technical applications in practice. If you look at the periodic table (*see* Table 1.1), where the melting (or decomposition) points of the binary compounds of chemical elements with carbon (carbides) are marked specially, you will find at least twenty carbide compounds of twelve elements (B, Si, Ti, V, Zr, Nb, Mo, Hf, Ta, W, Th, U), which are solid at the temperatures of around 2500 °C. Some refractory carbides have a bit higher melting points than the accepted decomposition point of carbon, while the most of refractory carbides have much higher melting points than the corresponding metals or non-metals, which form these compounds with carbon.

Namely, the refractory carbides possess the highest melting points among all the solids ever known [1–9]. This amazing property allow some carbides to save their physico-mechanical, thermophysical and physico-chemical stability, including hardness, strength and wear and erosion resistance, at the certain level up to ultra-high temperature ranges. The carbides are also very stable under the conditions of intensive nuclear radiation, when the radiation affects the solids jointly with higher temperatures. The extraordinary and very special behaviour of carbide compounds, formed by *d*- and *f*-elements (transition metals) and also called as metal-like (or interstitial) carbides, is caused by the specific chemical bonds between carbon and metal, which include and combine metallic, ionic and covalent interatomic bonding/interaction simultaneously [10–12]. The heterodesmic character of chemical bonding in transition metal carbides is almost always accompanied by non-stoichiometry and existence of wide homogeneity ranges of these carbide phases (variability of composition), e.g. titanium monocarbide TiC_{1-x} exists in the area of compositions from $\text{TiC}_{\sim 0.4}$ to $\text{TiC}_{\sim 1.0}$ in the same cubic crystal structure with only certain change of its lattice parameter (*see* section C–Ti in Table I-2.13; hereafter “I-0.00” is used to mark the sections, figures and tables of

Table 1.1 (continued)

³⁷ Rb (?)	³⁸ Sr SrC ₂ (1800)	³⁹ Y Y ₂ C ₂ (950) YC _{1-x} (~2380) Y ₄ C ₅ (1530) Y ₃ C _{4-x} (~1600) Y ₂ C _{3-x} (~1500) YC _{2-x} (~2380)	⁴⁰ Zr ZrC _{1-x} (3450)	⁴¹ Nb Nb _{2-x} C ₃ (30880) Nb ₄ C _{3-x} (1750) Nb ₆ C _{5-x} (~1100) NbC _{1-x} (3600)	⁴² Mo Mo _{2-x} C ₂ (2530) Mo ₃ C _{2-x} (2550) MoC _{1-x} (2600) MoC (1220)	⁴³ Tc TcC _{1-x} (?)	⁴⁴ Ru	⁴⁵ Rh	⁴⁶ Pd	⁴⁷ Ag	⁴⁸ Cd	⁴⁹ In	⁵⁰ Sn	⁵¹ Sb	⁵² Te	⁵³ I	⁵⁴ Xe
⁵⁵ Cs (?)	⁵⁶ Ba BaC ₂ (2000)	⁵⁷ La* La ₂ C _{3-x} (1415) LaC _{2-x} (2400)	⁷² Hf HfC _{1-x} (3950)	⁷³ Ta Ta _{2-x} C ₃ (3335) Ta ₄ C _{3-x} (2525) Ta ₆ C _{5-x} (1160) TaC _{1-x} (3990)	⁷⁴ W W _{2-x} C ₂ (2790) WC _{1-x} (2775) WC _{1-x} (2785)	⁷⁵ Re	⁷⁶ Os	⁷⁷ Ir	⁷⁸ Pt	⁷⁹ Au	⁸⁰ Hg	⁸¹ Tl	⁸² Pb	⁸³ Bi	⁸⁴ Po	⁸⁵ At (?)	⁸⁶ Rn
⁸⁷ Fr (?)	⁸⁸ Ra (?)	⁸⁹ Ac** (?)	¹⁰⁴ Rf (?)	¹⁰⁵ Db (?)	¹⁰⁶ Sg (?)	¹⁰⁷ Bh (?)	¹⁰⁸ Hs (?)	¹⁰⁹ Mt (?)	¹¹⁰ Ds (?)	¹¹¹ Rg (?)	¹¹² Cn (?)	¹¹³ Nh (?)	¹¹⁴ Fl (?)	¹¹⁵ Mc (?)	¹¹⁶ Lv (?)	¹¹⁷ Ts (?)	¹¹⁸ Og (?)

⁵⁸ Ce Ce ₂ C ₃ (~1600) CeC ₂ (2300)	⁵⁹ Pr Pr ₂ C _{3-5x} (1550) PrC ₂ (2320)	⁶⁰ Nd Nd ₂ C _{3-4x} (1620) NdC ₂ (2260)	⁶¹ Pm (?)	⁶² Sm Sm ₂ C (?) Sm ₂ C _{3-4x} (1325-?) SmC ₂ (~2300)	⁶³ Eu Eu ₂ C (?) EuC ₃ (?) EuC ₂ (1700-?)	⁶⁴ Gd Gd ₂ C (?) Gd ₂ C (?) Gd ₂ C _{3-4x} (?) GdC ₂ (2370)	⁶⁵ Tb Tb ₂ C (?) Tb ₂ C _{3-4x} (?) TbC ₃ (~2150)	⁶⁶ Dy Dy ₂ C (?) Dy ₂ C (?) Dy ₂ C _{3-4x} (?) DyC ₂ (2250-?)	⁶⁷ Ho Ho ₂ C (?) Ho ₂ C (?) Ho ₂ C _{3-4x} (?) HoC ₂ (2270-?)	⁶⁸ Er Er ₂ C (?) Er ₂ C _{3-4x} (?) ErC ₂ (2250-?)	⁶⁹ Tm Tm ₂ C (?) Tm ₂ C _{3-4x} (?) TmC ₂ (2180-?) TmC ₃ (?)	⁷⁰ Yb Yb ₂ C (?) YbC ₂ (?) Yb ₂ C _{3-4x} (?) Yb ₂ C _{4-5x} (?) Yb ₂ C _{4-5x} (?) YbC ₂ (?)	⁷¹ Lu Lu ₂ C (?) Lu ₂ C _{3-4x} (?) LuC ₂ (?)	¹⁰⁵ Lr (?)
⁹⁰ Th ThC _{1-4x} (2630) ThC _{2-3x} (2660)	⁹¹ Pa PaC (?) PaC ₂ (?)	⁹² U UC _{1-4x} (2530) U ₂ C ₃ (1820) UC _{2-3x} (2510)	⁹³ Np NpC _{1-3x} (?) Np ₂ C ₃ (?) NpC ₂ (?)	⁹⁴ Pu Pu ₂ C ₂ (575) PuC _{1-3x} (1655) Pu ₂ C _{3-4x} (2040) PuC ₂ (2230)	⁹⁵ Am Am ₂ C ₃ (?) AmC ₂ (?)	⁹⁶ Cm (?)	⁹⁷ Bk (?)	⁹⁸ Cf (?)	⁹⁹ Es (?)	¹⁰⁰ Fm (?)	¹⁰¹ Md (?)	¹⁰² No (?)	¹⁰³ Lr (?)	

*

**

Table 1.1 (continued)

Volume I of this book). Non-metallic or covalent carbides have also great resistance to the outer impact of high-temperature environment, but differ in kind of their chemical bonding from the metal-like carbides significantly, although non-stoichiometry might be inherent to their structures as well [13–15]. These both types of carbon compounds: interstitial (metal-like) and covalent carbides, according to the classification of inorganic compounds of carbon given earlier (*see* section I-2.6), can be used as materials or constituents of composite materials for high and ultra-high temperature technical applications.

The classification of refractory carbides into metallic and non-metallic is very important, since it is directly related to the physics of the transport properties of carbides. Naturally, the electrical and thermal conductivities of the former have a metallic character, while non-metallic refractory carbides are characterized mainly by semiconductor properties. A correct understanding of both the nature of refractory carbides and the manufacturing processes of materials on their basis allows material designers to obtain for carbide compositions the various necessary for practice temperature dependences of conductivities [16].

The refractory carbides vary sufficiently in their possible structures and compositions and physical and chemical properties. Some of them are exceedingly inert to chemical attacks, though their chemical stability has commonly a selective character. At higher temperatures all the carbides are susceptible to gas corrosion in oxidizing atmospheres, although some carbides have better resistance to oxidation than do the refractory metals, and most of them are more resistant to oxidation than graphite or other carbonaceous materials. A thorough consideration should be given to the atmosphere, in which refractory carbides are employed, as some of them can be attacked by reducing gas atmosphere at higher temperatures as well [17]. In order to realize successfully the high and ultra-high temperature properties of carbides, special attention must be paid first of all to the issues of their chemical compatibility in contact with various solid, liquid and gaseous substances in wide range of temperatures and pressures of the medium.

In addition to the extremely high melting points, carbides possess a wide range of other valuable properties, among which, in the first place, it is necessary to note their super-high hardness [18]. For massive machinery production all around the world, this property of carbides is much more important than anything else. So, for the reader/users, who are interested in ambient temperature applications of hard carbides, this book on ultra-high temperature materials will be interesting too. The fundamental significance of refractory carbides lies in the fact that in their lattices the breakdown of sp^3 -configurations has a considerable extent deferred to much higher temperatures than those at which it occurs in diamond, “champion of hardness”, in whose lattice there are no such stabilizers of electron configurations, as for example titanium or silicon in corresponding carbides. Thus, refractory carbides represent a unique compromise as their hardness, although less than that of diamond, is retained at the temperatures, which are unreachable in general for such material as diamond [19].

In this volume for each individual carbide compound or for a metal carbide family (various carbides of the same metal) being considered, as it was before for

the chemical elements (carbon and metals) in Volume I, a special section devoted to its structural features (partial variants of metal-carbon phase diagram, system and type of crystal structures, composition—lattice parameter relationships, possible phase transformations and slip systems, effects of contamination on structures, synthesized or theoretically predicted nanostructures, density of structures) fore-stalls the thorough and comprehensive description of data available in the literature on thermal, electro-magnetic and optical, physico-mechanical and nuclear physical properties of this carbide (or carbide family) with various compositions (carbon-metal ratios) within its homogeneity range and over very wide temperature range from 0 up to 2700–5000 K. The chemical properties of carbides (or carbides families) are considered in special sections by the analysis of interaction of carbides with metals, non-metals, various refractory compounds (carbides, nitrides, oxides, borides, silicides, intermetallides), gases and some common chemicals (acids, alkalis and salts in aqueous solutions and melts), diffusion processes in carbides and their wettabilities by various melts in the wide range of temperatures. As it was before in Volume I, the most reliable data (in author's opinion) on main physical properties of the ultra-high temperature carbide materials included in this volume are summarized in Addendum. Indeed, all the data in Addendum are based on the information given before in the corresponding chapters; however, every reader/user of the book has to be reminded that these data relate only to the quasi-stoichiometric compositions (or carbon-richest compositions for non-stoichiometric vanadium monocarbide) of the corresponding carbide materials.

The full amount of data on the structures and properties of refractory carbides, which is available in literature at the moment of the publication of this reference book was turn up to be too enormous, so it has been decided to divide all the information on ultra-high temperature carbide materials into three volumes. Honestly, it was one of the kind wishes of my readers/users, who took advantage of the feedback, to make the real content of the book more “deep” than “wide”. Thus, in this volume anyone can find all the necessary information on the transition metal carbides of 4–5 groups of the periodic table having the highest melting points (in the order of decreasing melting points): tantalum carbides (monocarbide TaC_{1-x} and semicarbide $\alpha/\beta\text{-Ta}_{2\pm x}\text{C}$), hafnium monocarbide HfC_{1-x} , niobium carbides (monocarbide NbC_{1-x} and semicarbide $\alpha/\beta/\gamma\text{-Nb}_{2\pm x}\text{C}$) and zirconium monocarbide ZrC_{1-x} . As far as possible, due to the reduction in the number of systems under the consideration, the author has tried to include in this volume all the latest research data on nanostructures of these refractory carbides, as well as the results of computer simulation for the properties of these carbides based on the quantum chemical and other theoretical approaches and calculations. In Table 1.1, all the refractory carbide systems relegated according to the classification adopted in this book to the ultra-high temperature materials are shaded gray; those carbide systems, which are considered in the second volume, are marked out in bold additionally. The next volumes of the reference book series will include data on metallic carbide systems, such as titanium, vanadium, tungsten, molybdenum, thorium and uranium carbides, as well as non-metallic refractory carbide systems, such as silicon and boron carbides.

There are no special sections devoted to the manufacturing methods of refractory carbides in the book chapters; however, anybody can find a lot of useful information on this issue in the sections, where the chemical properties of carbides and general principles of carbide containing materials design are described. The special author's remarks for readers/users of the book are following:

when it is not indicated specially, the value of percentage reported in the text of the book is given in mass percents;
some experimental and/or theoretically calculated data presented in the text, which are a bit doubtful in author's opinion, as they have not been confirmed in the literature sufficiently, are denoted by the special question marks.

Finally, it is necessary to recommend all the readers/users to become acquainted with the introduction of the previous volume [1], as those novel approaches to the description of materials that were substantiated there are also used by the author in this volume of book series.

References

1. Shabalin IL (2014) Ultra-high temperature materials I. Carbon (graphene/graphite) and refractory metals. Springer, Heidelberg
2. Kieffer R, Schwarzkopf P (1953) Hartstoffe und Hartmetalle (Refractory hard metals). Springer, Vienna (in German)
3. Storms EK (1967) The refractory carbides. Academic Press, New York
4. Toth LE (1971) Transition metal carbides and nitrides. Academic Press, New York
5. Kosolapova TYa (1971) Carbides: properties, production and applications. Plenum Press, New York
6. Samsonov GV, Upadhyaya GS, Neshpor VS (1974) Fizicheskoe materialovedenie karbidov (Physical materials science of carbides). Naukova Dumka, Kyiv (in Russian)
7. Upadhyaya GS (1996) Nature and properties of refractory carbides. Nova Science, Commack, New York
8. Pierson HO (1996) Handbook of refractory carbides and nitrides. Noyes Publications, Westwood, New Jersey
9. Lengauer W (2000) Transition metal carbides, nitrides and carbonitrides. In: Riedel R (ed) Handbook of ceramic hard materials. Wiley-VCH, Weinheim, pp. 202–252
10. Andrievskii RA, Lanin AG, Rymashevskii GA (1974) Prochnost tugoplavkikh soedinenii (Strength of refractory compounds). Metallurgiya, Moscow (in Russian)
11. Gubanov VA, Ivanovsky AL, Zhukov VP (1994) Electronic structure of refractory carbides and nitrides. Cambridge University Press, Cambridge
12. Gusev AI, Rempel AA, Magerl AJ (2001) Disorder and order in strongly nonstoichiometric compounds. Springer, Berlin
13. Kosolapova TYa, Andreeva TV, Barnitskaya TB, Gnesin GG, Makarenko GN, Osipova II, Prilutskii ÉV (1985) Nemetallicheskie tugoplavkie soedineniya (Non-metallic refractory compounds). Metallurgiya, Moscow (in Russian)
14. Gnesin GG (1977) Karbidokremnieve materialy (Silicon carbide materials). Metallurgiya, Moscow (in Russian)
15. Kislyi PS, Kuzenkova MA, Bodnaruk NI, Grabchuk BL (1988) Karbid bora (Boron carbide). Naukova Dumka, Kyiv (in Russian)

16. Gorinskii SG, Shabalin IL, Beketov AR, Podkovyrkin MI, Kokorin AF, Pakholkov VV (1980) Electrical resistivity of sintered TiC-SiC materials. *Powder Metall Met Ceram* 19(11):780–783
17. Sheipline VM, Runck RJ (1956) Carbides. In: Campbell IE (ed) *High temperature technology*. Wiley, Chapman and Hall, New York, London, pp. 114–130
18. Kislyi PS (1986) Tugoplavkie sverkhverdye materialy (Refractory super-hard materials). In: Novikov NV (ed) *Sinteticheskie sverkhverdye materialy (Synthetic super-hard materials)*, Vol. 1. Naukova Dumka, Kyiv, pp. 203–226 (in Russian)
19. Samsonov GV (1974) Some problems in the theory of the properties of carbides. In: Samsonov GV (ed) *Refractory carbides*. Consultants Bureau, New York, pp. 1–11

Chapter 2

Tantalum Carbides



2.1 Structures

Tantalum forms with carbon several chemical compounds (*see* also section C–Ta in Table I-2.13): tantalum monocarbide TaC_{1-x} with the extremely broad homogeneity range, low-temperature (ordered) $\alpha\text{-Ta}_{2+x}\text{C}$ and high-temperature (disordered) $\beta\text{-Ta}_{2\pm x}\text{C}$ modifications of tantalum semicarbide (the latter cannot be retained by quenching), close-packed (nanolamellar) $\varepsilon\text{-Ta}_3\text{C}_{2\pm x}$ and $\zeta\text{-Ta}_4\text{C}_{3-x}$ phases, also proposed $\text{Ta}_5\text{C}_{4\pm x}$, $\text{Ta}_6\text{C}_{5\pm x}$, $\text{Ta}_7\text{C}_{6\pm x}$ and $\text{Ta}_8\text{C}_{7\pm x}$ ordered phases and “surface” phase Ta_5C_2 [1–3, 17, 21, 76, 440, 679, 707, 730, 731]. Additionally, the absorption of a small amount of carbon was said to result in the ordered subcarbide Ta_{64}C [26, 528], which is more likely an example of a phase subject to controversies [27]. A high-temperature partial variant of tantalum – carbon phase diagram is given in Fig. 2.1, and the structural features of the tantalum carbides are presented in Table 2.1. The C/Ta atomic radii ratio calculated on the basis of Pauling’s atomic size of Ta (0.1457 nm, CN = 12) is 0.529 [115], 0.57 [90]; the ratio of Ta radii (in nm) in Me/MeC is 0.142/0.157 (10.5% expansion of Ta atoms in carbide) [155]. The structural transformation of TaC_{1-x} from NaCl type ($Fm\bar{3}m$) to CsCl type ($Pm\bar{3}m$) structure under ultra-high pressures (~100–700 GPa) has been predicted theoretically [410–412, 431, 706, 716].

In contrast to the other transition metal refractory carbides, within the homogeneity range TaC_{1-x} demonstrates practically a linear relationship (some kinds of exception are the data obtained by Santoro [122], Senczyk [399] and Gusev [754]) between lattice parameter and composition (*see* Fig. 2.2); in modified forms the following equations, earlier proposed by Bowman (for $0.01 \leq x \leq 0.29$) [78]:

$$a = 0.4457 - 0.0156x, \quad (2.1)$$

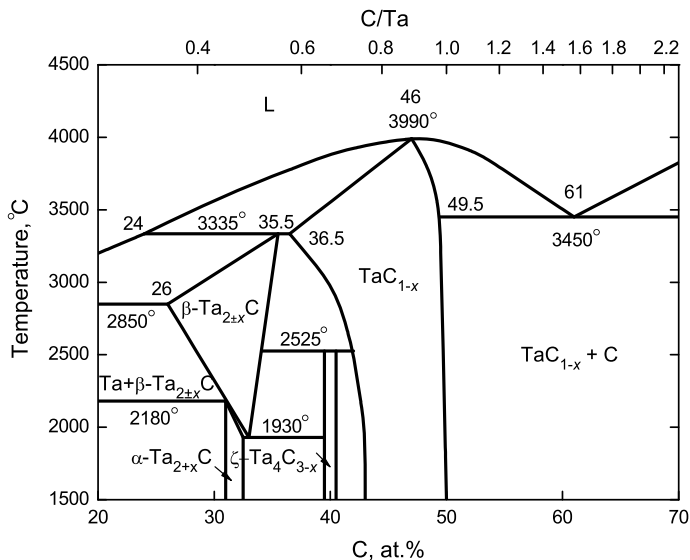


Fig. 2.1 High-temperature partial variant of tantalum – carbon equilibrium phase diagram [2, 4, 5, 80, 188, 463–468, 653, 757, 811]

later by Storms (for $0 < x \leq 0.28$) [17]:

$$a = 0.4458 - 0.0167x, \quad (2.2)$$

and then by Alexandre et al. [398] for materials (with $0 < x \leq 0.15$) reactively processed by hot isostatic pressing (HIP):

$$a = 0.4454 - 0.0102x, \quad (2.3)$$

can be recommended to describe it, where a is lattice parameter, nm and x is the value of index in TaC_{1-x} formula. However, in the contradiction to the linear relationships for the same correlation the complex (polynomial) functions were suggested by Senczyk ($0 \leq x \leq 0.30$) [399]:

$$a = 0.4457 - 0.0127x - 0.0130x^2 \quad (2.4)$$

and Gusev ($x \leq 0.329$) [754]:

$$a = 0.4456 - 0.0159x + 0.0077x^2. \quad (2.5)$$

Within the homogeneity range of semicarbide phase the lattice parameter a also declines with carbon content decreasing [16]. For parameters of formation and migration of lattice point defects (vacancies and interstitial atoms) in tantalum monocarbide *see* Sect. 2.5 (Table 2.19). At low temperatures for non-stoichiometric

Table 2.1 Structural properties (crystal structure, density) of tantalum carbide phases

Formula	Crystal structure						Density ^c , g cm ⁻³	References					
	System	Type	Space group	Lattice parameters ^a , nm					Z ^b				
				<i>a</i>	<i>c</i>	<i>cla</i>							
TaC _{1-x}	Cubic	NaCl	<i>Fm(-3)m</i>	0.4410 ^d	-	-	4	-	[17, 37, 78]				
				0.4424 ^e	-	-	4	-	[201]				
				0.4427	-	-	4	14.60	[9]				
				0.4438	-	-	4	14.57	[12]				
				0.4439 ^f	-	-	4	-	[758]				
				0.4445	-	-	4	-	[6]				
				0.4448	-	-	4	-	[10]				
				0.4450	-	-	4	-	[43]				
				0.4451	-	-	4	-	[14]				
				0.4452	-	-	4	14.53	[49]				
				0.4453 ^g	-	-	4	14.52	[8, 34, 46]				
				0.4454	-	-	4	14.48	[1, 13, 35, 123, 159]				
				0.4455	-	-	4	14.48	[11, 16, 17, 41, 50, 60]				
				0.4456 ^h	-	-	4	14.48	[15, 17, 48]				
				0.4460	-	-	4	14.45	[7]				
β -Ta _{2±x} C ⁱ	Hexagonal	NiAs	<i>P6₃/mmc</i>	0.3102	0.4940	1.593	1	-	[41]				
				0.3105	0.4935	1.589	1	15.03	[21]				
				0.3105	0.4945	1.593	1	-	[24, 25]				
				0.3108	0.4950	1.593	1	15.00	[23]				
				0.3119	0.4934	1.582	1	-	[32]				
α -Ta _{2+x} C ^{j,k}	Trigonal	CdI ₂ ^l	<i>P(-3)m1</i>	0.3094	0.4918	1.590	1	-	[449]				
				0.3097	0.4930	1.592	1	15.16	[6]				
				0.3100 ^m	0.4931 ^m	1.590 ^m	1	-	[21, 22]				
				0.3102 ⁿ	0.4940 ⁿ	1.593 ⁿ	1	-	[21, 22, 77]				
				0.3103	0.4936	1.591	1	-	[36]				
				0.3103	0.4937	1.591	1	15.08	[19]				
				0.3103 ⁿ	0.4938 ⁿ	1.591 ⁿ	1	15.08	[20, 21]				
				0.3104	0.4927	1.587	1	-	[34]				
				0.3104 ^o	0.4939 ^o	1.591 ^o	1	-	[33, 97]				
				0.3104	0.4940	1.591	1	15.04	[1, 35]				
				0.3104	0.4941	1.591	1	-	[43, 543]				
				0.3106	0.4945	1.592	1	-	[16, 17, 41]				
				0.3106	0.4964	1.593	1	-	[18]				
				0.3111	0.4948	1.590	1	-	[449]				
				ϵ -Ta ₃ C _{2±x} ^p	Trigonal	TiS	<i>R(-3)m</i>	0.3110	2.240	7.203	3	-	[3]
ζ -Ta ₄ C _{3-x} ^q	Trigonal	Sc ₂ Te ₃ ^r	<i>R(-3)m</i>					0.3116	3.000	9.628	3	15.01	[3, 28]
								0.3120	3.001	9.620	3	-	[34]
								0.3122 ^{q,r}	3.006 ^{q,r}	9.629 ^{q,r}	3	14.84	[29]
								0.3123 ^t	3.005 ^t	9.623 ^t	3	-	[32]
Ta ₆ C _{5±x} ^{s,u}	Mono- clinic or trigonal	-	<i>C2/m</i> , <i>C2/c</i> , <i>P3₁</i> , <i>P3₁12</i>	-	-	-	-	-	[2, 30, 31, 730]				

(continued)

Table 2.1 (continued)

- ^aWhen it is not indicated specially, value reported is for near-stoichiometric composition
- ^bNumber of formula units per lattice cell
- ^cCalculated from XRD or neutron diffraction patterns
- ^dCarbon content – 41.2 at.% (in equilibrium with semicarbide phase)
- ^eCalculated on the basis of density-functional theory (DFT)
- ^fNanocrystalline powders, specific surface area – 25 m² g⁻¹, mean particle size – 15-25 nm, carbon content – 49.0 at.%, oxygen content – 0.3-0.4 mas.%
- ^gMinimum interatomic distances: Ta-Ta and C-C – 0.314875 nm, Ta-C – 0.222650 nm [46]
- ^hCarbon content – 49.7 at.% (in equilibrium with graphite)
- ⁱIn contradiction to these data, β -Ta_{2±x}C was identified as orthorhombic (ζ -Fe₂N, *Pbcn*) with $a = 0.4940$ nm, $b = 0.6208$ nm, $c = 0.5370$ nm, $Z = 4$ [1], or orthorhombic (?) with $a = 0.4933$ nm, $b = 0.9866$ nm, $c = 0.8534$ nm [37]
- ^jIn contradiction to these data, α -Ta_{2±x}C was identified as orthorhombic (?) with $a = 0.2873$ nm, $b = 1.0250$ nm, $c = 0.4572$ nm [60]
- ^kAlso structured (vacancy ordered) in *Pnma*, *Pbcn*, *P3m1*, *I4₁/amd*, *R(-3)m*, *Fd(-3)m* and *P4/mmm* [730]
- ^lCadmium iodide antitype structure
- ^mCarbon content – 31.5 at.%
- ⁿCarbon content – 33 at.% C
- ^oCarbon content – 32-33 at.% C
- ^pIn contradiction to these data, Ta₄C_{3.04} (TaC_{0.76}) was identified as cubic (*Pm(-3)m*) with $a = 0.4424$ nm, $Z = 1$ and calculated density – 14.58 g cm⁻³ [47]
- ^qAlso GeSb₂Te₄ structure type proposed [29]
- ^rCarbon content – 40 at.% C
- ^sIncommensurate superstructure close to M₆C₅ type [30, 31]
- ^tAlso vacancy ordered Ta₅C_{4±x} (*P(-1)*, *C2/m*, *I4/m*), Ta₇C_{6±x} (*R(-3)*) and Ta₈C_{7±x} phases (*P4₃32*, *Fm(-3)m*) are supposed [730]

monocarbide TaC_{1-x} the slip system (110) <110> was determined, while for quasi-stoichiometric monocarbide the slip system (111) <110> is preferential at all temperatures [154–157, 159, 182, 381, 439, 517, 525, 533]; at temperatures above ~1200 °C slip can occur on other planes, e.g. in the systems (001) <010>, (011) <010> and (011) <110> [157, 381, 533]. At ambient temperatures Kiani et al. [564, 720] employing *in situ* electron microscopy method observed for TaC_{-0.85} single crystalline nanopillars the (1 $\bar{1}$ 0) <110> and (1 $\bar{1}$ 1) <110> slip systems; the DFT-calculated by them energy values, which characterize several different possible slip systems in quasi-stoichiometric TaC_{1-x}, are given in Table 2.2. The minimal Burgers vector of near-stoichiometric TaC_{1-x} ($\frac{1}{2}$ <110>) $b = 0.313$ nm [41]. Theoretically for α -Ta_{2±x}C phase with its trigonal symmetry easier slip would occur in (0001) <11 $\bar{2}$ 0> (on the basal plane); however (10 $\bar{1}$ 1) <11 $\bar{2}$ 3> (on a pyramidal plane) dislocation slip was confirmed experimentally [77, 189, 517]. The variations of the lattice parameter of TaC_{1-x} with temperature for the phases having different deviations from the stoichiometry are shown in Fig. 2.3.

In general, the contaminations, such as dissolved in TaC_{1-x} oxygen or/and nitrogen, which are always present in the materials, decrease the magnitude of lattice parameter by forming oxycarbide TaC_{1-x}O_y, carbonitride TaC_{1-x}N_z and oxycarbonitride TaC_{1-x}N_zO_y phases with various deviations from the stoichiometry

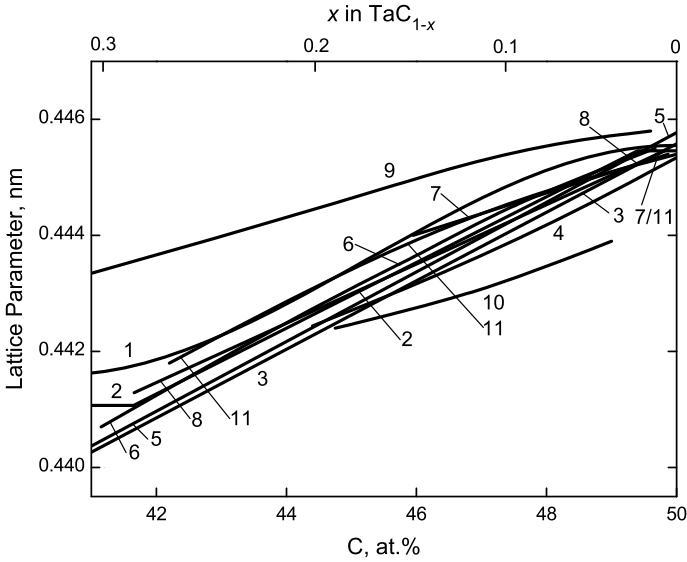


Fig. 2.2 Lattice parameter of TaC_{1-x} as a function of phase composition: 1 – [122], 2 – [17], 3 – for disordered structures [30, 754–756], 4 – [34], 5 – polynomial approximation [35, 123], 6 – [399], 7 – [398], 8 – synthesized by different methods [332, 753], 9 – [207], 10 – nanocrystalline powders (specific surface area – $\sim 25 \text{ m}^2 \text{ g}^{-1}$, mean particle size – 10-30 nm, content O – 0.3-0.4%) [758, 759], 11 – synthesized from the pure elements [604, 651, 766] (2-3, 5, 8 – on the basis of several sources)

Table 2.2 The DFT-calculated values of unstable stacking fault energies and total energies required to shear for the crystals of quasi-stoichiometric tantalum monocarbide TaC_{1-x} along different slip systems [564]

Slip system	Maximum $E_{\text{GSF}}(l)^a$, eV nm^{-2}	Shear total energy, eV nm^{-3}
(0 0 1) <110>	13.9	92
(1 $\bar{1}$ 0) <110>	10.3	492
(1 $\bar{1}$ 1) <110>	3.5	476
(0 0 1) <100>	16.8	–
(1 $\bar{1}$ 0) <100>	30.9	–
(1 $\bar{1}$ 0) <111>	33.6	–

^aThe generalized stacking fault energy E_{GSF} is a function of normalized displacement (l/b), where b is the Burgers vector for the slip direction; so $E_{\text{GSF}}(l)$ is defined as the energy per unit area required to shift one half of the supercell with respect to the other half by a distance l

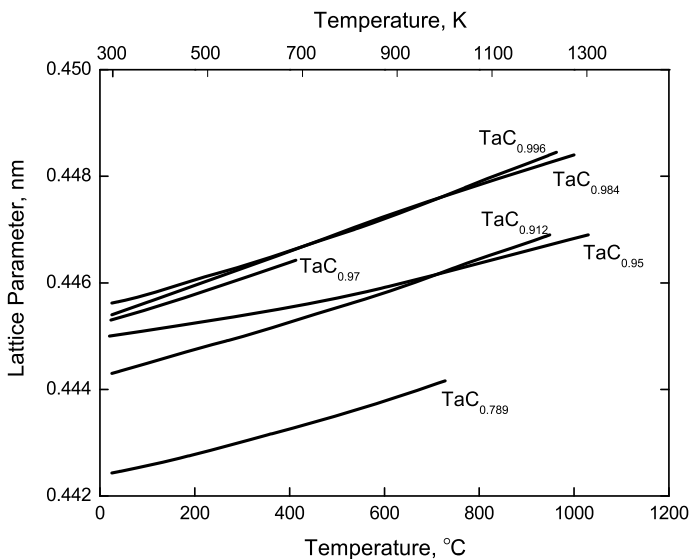


Fig. 2.3 Lattice parameter of TaC_{1-x} as a function of temperature for the phases having different deviations from the stoichiometry ($x = 0.004$ [48], $x = 0.016$ [79], $x = 0.03$ [46], $x = 0.05$ [43, 86], $x = 0.088$ and $x = 0.211$ [48])

(see also sections C–N–Ta and C–O–Ta in Table I-2.14); the effect of namely oxygen in this case is inconsiderable as its solubility in TaC_{1-x} is much lower in comparison with nitrogen [36, 63, 226, 530, 570].

Recently, due to the massive progress in nanotechnology, various nanostructures based on TaC_{1-x} , including nanorods (14–40 nm diameter, 800 nm length), nanowires, nanofibers (~40–90 nm in diameter, up to several micrometers in length), whiskers, thin films (300 nm thickness) and various (spherical, cubic-faceted) nanoparticles (40–250 nm), have been prepared [73, 74, 117, 450, 693, 702, 717–719, 758–760, 767–770, 816], as well as 2D-molecular $\text{Ta}_{n+1}\text{C}_n$ MXenes (Ta_2C , Ta_3C_2 , Ta_4C_3 , or $\text{Ta}_4\text{C}_3\text{T}_x$, where T are functional groups OH, O, F) – were synthesized and investigated in details theoretically [75, 563, 698, 699, 710, 715, 727, 749–751].

First Bowman [78] – for the X-ray density of synthesized from the elements TaC_{1-x} ($0.01 \leq x \leq 0.29$), and later Samsonov and Petrykina [705] – for the bulk density of hot-pressed TaC_{1-x} materials ($0 < x \leq 0.20$), proposed the equation:

$$d = 14.47 + 0.64x, \quad (2.6)$$

where d is the density, g cm^{-3} and x is the value of index in TaC_{1-x} formula. According to Storms [17], the X-ray density for monocarbide TaC_{1-x} phase with $x = 0.01$ is 14.48 g cm^{-3} and it increases as carbon is removed. The recommended values for the bulk (or pycnometric) density of pure poreless materials at room temperature are 14.8–15.0 and 14.4–14.6 g cm^{-3} – for the near-stoichiometric single-phase compositions of tantalum semicarbide $\text{Ta}_{2\pm x}\text{C}$ and monocarbide TaC_{1-x} , respectively [16, 37, 43, 59–61, 388, 442, 544, 701, 721].

2.2 Thermal Properties

Tantalum monocarbide TaC_{1-x} has the highest melting point of all the solid substances available; the incongruent melting point of $\beta\text{-Ta}_{2\pm x}\text{C}$ is about 500° lower. Within the homogeneity range of TaC_{1-x} the melting point of the phase varies (see Fig. 2.1); the maximum temperatures pertain to the nonstoichiometric compositions around $\sim\text{TaC}_{0.88-0.89}$ [17, 70, 71], and there are no sufficient proofs for complex carbides to be outperforming the maximum melting point of pure tantalum monocarbide phase [71]. The general thermodynamic properties of near-stoichiometric tantalum carbide phases are summarized in Tables 2.3 and 2.4. For the molar heat capacity of near-stoichiometric TaC_{1-x} $c_p = f(T, \text{K})$, $\text{J mol}^{-1} \text{K}^{-1}$, the following relationships were recommended in the literature:

in the range of temperatures from 300 to 4000 K [726]

$$c_p = 43.30 + (8.16 \times 10^{-3})T - (7.95 \times 10^5)T^{-2}, \quad (2.7)$$

in the range of temperatures from 300 to 2000 K [44, 52]

$$c_p = 30.46 + (6.904 \times 10^{-3})T, \quad (2.8)$$

in the range of temperatures from 1600 to 2300 K [52, 58]

$$c_p = 46.36 + (6.643 \times 10^{-3})T, \quad (2.9)$$

in the range of temperatures from 1300 to 2850 K [52, 55]

$$c_p = 47.72 + (5.532 \times 10^{-3})T, \quad (2.10)$$

in the range of temperatures from 1000 to 3000 K [52, 56]

$$c_p = 44.60 + (6.430 \times 10^{-3})T - (7.606 \times 10^5)T^{-2}, \quad (2.11)$$

in the range of temperatures from 370 to 3525 K [52, 57]

$$c_p = 46.02 + (3.714 \times 10^{-3})T - (2.826 \times 10^5)T^{-2} \\ + (6.620 \times 10^{13})T^{-2} \times \exp(-39000/T). \quad (2.12)$$

The variations of molar heat capacity with temperature for near-stoichiometric tantalum carbides $\text{Ta}_{2\pm x}\text{C}$ and TaC_{1-x} are demonstrated in Fig. 2.4 on the basis of several sources. For the molar heat capacity of monocarbide TaC_{1-x} phases with various deviations from the stoichiometry the following relationships were recommended:

Table 2.3 General thermodynamic properties of near-stoichiometric tantalum monocarbide TaC_{1-x}

Characteristics	Symbol	Unit	Value	References
Standard heat of formation (at 298.15 K) ^a	$-\Delta H^\circ_{298}$	kJ mol ⁻¹	142.4	[17]
			142.6 ± 6.0 ^b	[2, 818–820]
			142.7 ^c	[60, 578]
			143.4	[361, 362]
			144.1	[38]
			144.8	[1, 16, 39]
			144.9 ± 3.8	[37]
			146.4	[80, 205]
			150.0	[61]
			159.5	[35, 555]
			161.2	[43, 545]
Standard molar entropy ^d (at 298.15 K and 100 kPa)	S°_{298}	J mol ⁻¹ K ⁻¹	41.9	[61]
			42.26	[362]
			42.29 ± 0.84	[16, 17, 37, 43]
			42.34	[1]
			42.38	[38, 52, 53]
Molar enthalpy difference	$H_{298}-H_0$	kJ mol ⁻¹	6.460	[52, 53]
			6.460	[52, 53]
Standard molar heat capacity ^e (at 298.15 K and 100 kPa)	$c^\circ_{p,298}$	J mol ⁻¹ K ⁻¹	32.50	[44]
			32.52	[361]
			33.75 ^f	[360]
			33.89 ^g	[360]
			34.81 ^h	[360]
			35.42 ⁱ	[360]
			35.71 ^j	[360]
			35.82 ^k	[360]
			36.40	[60]
			36.50	[61]
			36.69	[17, 41]
			36.78	[1, 16, 54, 362]
			36.80	[38, 43, 52, 53]
Specific heat capacity (at 298.15 K)	c	J kg ⁻¹ K ⁻¹	188.0	[43]
			190.6	[16]
Molar enthalpy (heat) of melting (at the melting point)	ΔH_m	kJ mol ⁻¹	105	[16, 579]
Specific enthalpy (heat) of melting (at the melting point)		kJ kg ⁻¹	544	[16]

(continued)

Table 2.3 (continued)

Characteristics	Symbol	Unit	Value	References
Melting point	T_m	K (°C)	4050 (3780)	[545–549]
			4070 (3800)	[44]
			4150 ± 150	[43, 59, 61,
			(3880 ± 150)	66, 362, 388]
			4220 (3950)	[60]
			4235 (3965)	[576]
			4240 (3970)	[80]
			4250 (3980) ^l	[42, 554]
			4255 ± 50	[1, 22, 37, 41,
			(3985 ± 50)	115, 550–553]
			4260 ± 40	[4, 577]
			(3990 ± 40) ^m	
			4270 ± 200	[16, 17, 45, 70,
(4000 ± 200) ⁿ	71, 700]			
Boiling point	T_b	K (°C)	4420 (4150)	[442]
			5000–5100	[388]
			(4730–4830)	
			5050 (4780)	[59]
			5770 (5500)	[43, 44, 362]

^aEnthalpy (heat) of complete dissociation (atomization) from solid state at 298.15 K ($-\Delta_{at}H^\circ_{298}$, kJ mol⁻¹): 1642 ± 9 [1, 820], 1651 [572, 824], 1658 [573], 1987 [574]

^bExtrapolated to the stoichiometric composition of monocarbide

^cIn kJ per g-atom Ta

^dMolar entropy S°_T (at 1200 K), J mol⁻¹ K⁻¹, for TaC_{1-x} phases with different deviations from the stoichiometry: 109.42 ($x = 0$), 107.40 ($x = 0.05$), 105.36 ($x = 0.10$), 103.29 ($x = 0.15$), 101.20 ($x = 0.20$), 99.08 ($x = 0.25$) and 96.94 ($x = 0.30$) [52]

^eMolar heat capacity $c_{p,T}$ (at 1200 K), J mol⁻¹ K⁻¹, for TaC_{1-x} phases with different deviations from the stoichiometry: 52.63 ($x = 0$), 51.03 ($x = 0.05$), 49.41 ($x = 0.10$), 47.77 ($x = 0.15$), 46.11 ($x = 0.20$), 44.43 ($x = 0.25$) and 42.73 ($x = 0.30$) [52]

^fDisordered structure with carbon content – 44.8 at.%

^gOrdered structure with carbon content – 44.8 at.%

^hDisordered structure with carbon content – 45.7 at.%

ⁱOrdered structure with carbon content – 45.7 at.%

^jDisordered structure with carbon content – 46.8 at.%

^kOrdered structure with carbon content – 46.8 at.%

^lCarbon content – 46.2–47.4 at.%

^mCarbon content – 47 at.% [577]

ⁿCarbon content – ~44.4–47.4 at.% [17, 70, 71]

Table 2.4 General thermodynamic properties near-stoichiometric tantalum semicarbide $Ta_{2\pm x}C$

Characteristics	Symbol	Unit	Value	References
Standard heat of formation (at 298.15 K) ^a	$-\Delta H_{298}^{\circ}$	kJ mol^{-1}	193.6	[39]
			195.0 ± 8.4^b	[64]
			197.5	[16]
			197.6 ± 14.2	[37]
			200.4	[83]
			201.0	[17]
			202.6	[80]
			204.2	[84]
			208.4	[1, 60, 578]
			209.0^c	[64]
			209.1	[62]
			210.0 ± 8.4^d	[64]
			213.4	[38, 545]
Standard molar entropy (at 298.15 K and 100 kPa)	S_{298}°	$\text{J mol}^{-1} \text{K}^{-1}$	81.59	[1, 16]
			83.30	[43]
			83.32	[37]
			83.68	[38]
Standard molar heat capacity (at 298.15 K and 100 kPa)	$c_{p,298}^{\circ}$	$\text{J mol}^{-1} \text{K}^{-1}$	60.95	[1, 38]
			60.96	[16]
Specific heat capacity (at 298.15 K)	c	$\text{J kg}^{-1} \text{K}^{-1}$	162.0	[43]
			163.1	[16]
Molar enthalpy (heat) of vaporization (at 298.15 K) ^e	ΔH_v	kJ mol^{-1}	2483 ± 4	[575]
Melting point	T_m	$\text{K } (^{\circ}\text{C})$	3600 ± 30	[1, 17, 37,
			(3330 ± 30)	41, 59, 60,
				576]
			3610 ± 30	[4]
			(3335 ± 30)	
			$3670 (3400)$	[44, 362]
	$3770 (3500)$	[16, 38]		
Boiling point	T_b	$\text{K } (^{\circ}\text{C})$	$5740 (5465)$	[576]

^aEnthalpy of complete dissociation (atomization) from solid state at 298.15 K ($-\Delta_{at}H_{298}^{\circ}$): $2475 \pm 24 \text{ kJ mol}^{-1}$ [1]

^bFor $TaC_{0.455 \pm 0.002}$ composition

^cInterpolated to $TaC_{0.5}$ composition

^dFor $TaC_{0.507 \pm 0.002}$ composition

^eDue to an insignificant change in the phase composition of $Ta_{2.0}C$ during congruent vaporization, the calculation was carried out in accordance to the third law of thermodynamics with the assumption of phase composition constancy

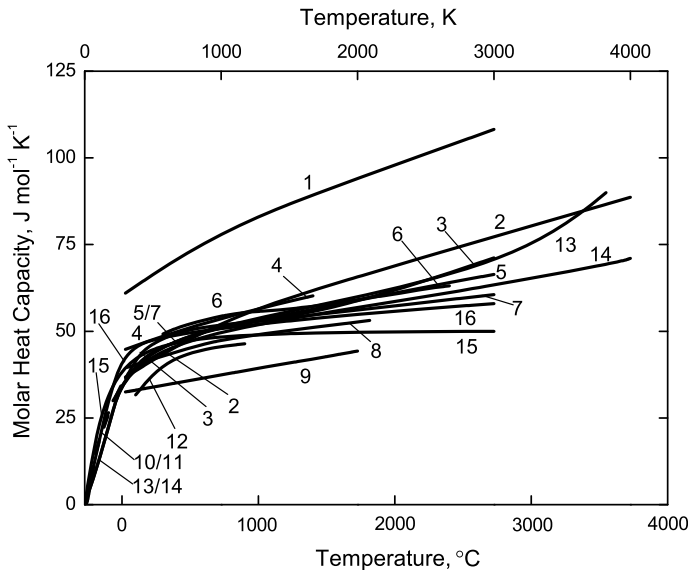


Fig. 2.4 Variation of molar heat capacity (1–14 – at constant pressure, c_p , and 15–16 – at constant volume, c_v) with temperature for near-stoichiometric tantalum carbides $Ta_{2-x}C$ (1 – [16]) and TaC_{1-x} (2 – [16, 81], 3 – [17, 209], 4 – [729], 5 – [80], 6 – [51], 7 – [82], 8 – $TaC_{0.99}$ [391, 392], 9 – [44], 10 – [43], 11 – [360], 12 – [771]; theoretically calculated: 13 – Slater’s approximation and 14 – Dugdale-MacDonald’s approximation on the basis of Debye-Grüneisen model [209], 15 – using projector augmented-wave (PAW) method within the generalized gradient approximation (GGA) of the Perdew-Burke-Ernzerhof scheme for ionic solids (PBEsol) [617], 16 – using density functional theory (DFT) within the GGA with the Perdew-Wang parameterization (PW91) [413]; 1-3, 5-7, 9-10 – on the basis of several sources)

for $TaC_{0.70}$ (in the range of temperatures from 1200 to 2300 K) [40, 52]

$$c_p = 37.46 + (5.698 \times 10^{-3})T, \quad (2.13)$$

for $TaC_{0.78}$ (in the range of temperatures from 1200 to 2300 K) [40, 52]

$$c_p = 38.07 + (6.770 \times 10^{-3})T, \quad (2.14)$$

for $TaC_{0.85}$ (in the range of temperatures from 1200 to 2300 K) [40, 52]

$$c_p = 38.41 + (8.158 \times 10^{-3})T, \quad (2.15)$$

for $TaC_{0.99}$ (in the range of temperatures from 300 to 3000 K) [17]

$$c_p = 57.74 - (9.20 \times 10^{-3})T + (46.39 \times 10^{-7})T^2 - (16.64 \times 10^5)T^{-2}, \quad (2.16)$$

for $\text{TaC}_{0.99}$ (in the range of temperatures from 1200 to 2300 K) [40, 52]

$$c_p = 39.26 + (10.134 \times 10^{-3})T \quad (2.17)$$

and for TaC_{1-x} in general (in the range of temperatures from 1200 to 2300 K) [52]

$$c_p = 41.40 + (9.356 \times 10^{-3})T - 31.74x - 4.15x^2, \quad (2.18)$$

or

$$c_p = 30.54 - (6.280 \times 10^{-3})T + [3.234 + (6.176 \times 10^{-3})T] \times e^{1-x}, \quad (2.19)$$

where x is the value of index in TaC_{1-x} formula. It should be emphasized specially that all the thermal properties of tantalum carbides are very sensitive to the deviation from the stoichiometry in the phases: for the standard heat of formation ΔH_{298}° , kJ mol⁻¹, molar enthalpy difference $H_T^\circ - H_{298}^\circ$, J mol⁻¹, and molar entropy S_T° , J mol⁻¹ K⁻¹, the following concentration and temperature-concentration dependencies within the homogeneity range of TaC_{1-x} were obtained by the calculations based on experimental data [2, 35, 39, 40, 52, 62, 818–820]:

$$\Delta H_{298}^\circ = 93.43x - 141.04, \quad (2.20)$$

$$\Delta H_{298}^\circ = 88.55x - 148.38, \quad (2.21)$$

$$\Delta H_{298}^\circ = 95.40 - 434.2(1-x) + 196.1(1-x)^2, \quad (2.22)$$

$$\Delta H_{298}^\circ = 56.39 - 343.4(1-x) + 144.4(1-x)^2 \pm 6.0, \quad (2.23)$$

$$H_T^\circ - H_{298}^\circ = 41.40T + (4.678 \times 10^{-3})T^2 + 25034x - 31.74xT - 4.150x^2T - 14488, \quad (2.24)$$

$$S_T^\circ = 95.34 \lg T + (9.356 \times 10^{-3})T - 73.10x \lg T - 9.56x^2 \lg T + 185.07x + 24.19x^2 - 195.38, \quad (2.25)$$

where T is temperature, K, and x is the value of index in TaC_{1-x} formula [Eqs. (2.24–2.25) were recommended for the range of temperatures from 1200 to 2300 K]. The thermodynamic functions for stoichiometric tantalum monocarbide are tabulated by Turchanin et al. [52, 53] in the range of temperatures from 0 to 3000 K, by Schick [81] and Chase [579] in the range of 0–6000 K, by Barin [38] in the range of 298.15–3500 K, thermodynamic functions of $\text{TaC}_{0.99}$ in the range of 298.15–3000 K are tabulated by Storms [17] and Toth [115]; for stoichiometric tantalum semicarbide the thermodynamic functions are tabulated by Barin [38] in the range of 298.15–3773 K and by Schick [81] in the range of 0–3773 K.

During the vaporization processes from the surface of tantalum carbides in a vacuum at high and ultra-high temperatures, the composition of the carbide phase

(C/Ta ratio) can change significantly. The resulting composition gradient cannot be accurately evaluated, but it was found to become worse as the temperature was increased [17]. The following equations were recommended for tantalum (P_{Ta} , Pa) and carbon (P_{C} , Pa) partial pressures over near-stoichiometric monocarbide phase for the range of about 2500–3000 K (2200–2700 °C) [16, 17]:

$$\lg P_{\text{Ta}} = -(4.777 \times 10^4)/T + 12.174, \quad (2.26)$$

$$\lg P_{\text{C}} = -(3.234 \times 10^4)/T + 10.041, \quad (2.27)$$

the estimation of tantalum partial pressures (P_{Ta} , Pa) and C/Ta atomic ratios in the gaseous phase in the Ta–C system carried out by Kulikov [576] led to such relationships as

for the conditions of $\text{Ta}_{2\pm x}\text{C}$ – TaC_{1-x} phases equilibrium:

at 1000–3270 K (730–3000 °C)

$$\lg P_{\text{Ta}} = -(4.377 \times 10^4)/T + 12.701, \quad (2.28)$$

$$\lg(\text{C}/\text{Ta}) = (2.087 \times 10^3)/T - 0.126, \quad (2.29)$$

at 3270–4270 K (3000–4000 °C)

$$\lg P_{\text{Ta}} = -(4.392 \times 10^4)/T + 12.748, \quad (2.30)$$

$$\lg(\text{C}/\text{Ta}) = (5.322 \times 10^3)/T - 1.115, \quad (2.31)$$

for the conditions of TaC_{1-x} –C phases equilibrium:

at 1000–3270 K (930–3000 °C)

$$\lg P_{\text{Ta}} = -(4.798 \times 10^4)/T + 12.087, \quad (2.32)$$

$$\lg(\text{C}/\text{Ta}) = (8.410 \times 10^3)/T + 3.191; \quad (2.33)$$

at 3270–4270 K (3000–4000 °C)

$$\lg P_{\text{Ta}} = -(4.684 \times 10^4)/T + 11.739, \quad (2.34)$$

$$\lg(\text{C}/\text{Ta}) = (6.157 \times 10^3)/T + 3.884, \quad (2.35)$$

at 4270–5700 K (4000–5400 °C)

$$\lg P_{\text{Ta}} = -(3.934 \times 10^4)/T + 9.925, \quad (2.36)$$

$$\lg(\text{C}/\text{Ta}) = (1.893 \times 10^4)/T + 1.105, \quad (2.37)$$

where T is temperature, K (*see* Table 2.5). The partial pressures of tantalum and carbon over the carbide phase as functions of composition at the fixed temperature 3000 K (2730 °C) are shown in Fig. 2.5 in comparison with the equilibrium pressure of carbon over graphite surface. At lower temperatures and short-term heating mainly carbon vaporized from the carbide surface in vacuum [16]. The solid monocarbide TaC_{1-x} loses carbon rapidly, being enriched with tantalum. Fesenko and Bolgar [125, 657] proposed for the evaporation rate of $\text{TaC}_{0.71}$ G , $\text{g cm}^{-2} \text{s}^{-1}$, as a function of temperature T , K, at 2970–3370 K (2700–3100 °C) the following equation:

$$\lg G = 9.10 - (4.49 \times 10^4)/T, \quad (2.38)$$

giving for 2700 and 3100 °C the values of 1.25×10^{-6} and $1.22 \times 10^{-4} \text{ g cm}^{-2} \text{s}^{-1}$, while for $\text{TaC}_{0.93}$ Deadmore [327] measured at 2225 and 2625 °C the values of 5×10^{-8} and $\sim 10^{-6} \text{ g cm}^{-2} \text{s}^{-1}$, respectively; and for $\text{TaC}_{0.96}$ (content O – 0.24%) Gusev [761] measured in vacuum ($1.3 \times 10^{-3} \text{ Pa}$) at 1900, 2200 and 2400 °C – 3.0×10^{-9} , 1.4×10^{-8} and $4.0 \times 10^{-8} \text{ g cm}^{-2} \text{s}^{-1}$, respectively (corresponding calculated partial pressures of Ta – 2.2×10^{-5} , 1.1×10^{-4} , $3.4 \times 10^{-4} \text{ Pa}$ and C – 2.1×10^{-5} , 1.0×10^{-4} , $2.5 \times 10^{-4} \text{ Pa}$, respectively), and established for the general evaporation rate G , $\text{g cm}^{-2} \text{s}^{-1}$, at 2100–2700 K (1830–2430 °C) the following relationship

$$\lg G = -(2.62 \pm 0.02) - (1.28 \times 10^4)/T. \quad (2.39)$$

Subsequently the monocarbide phase converts to two-phase ($\text{TaC}_{1-x} + \beta\text{-Ta}_{2\pm x}\text{C}$) area and then to the semicarbide phase area, where the congruently vaporizing composition shifts from $\text{TaC}_{0.53}$ at 2820 K (2550 °C) to $\text{TaC}_{0.47}$ at 3350 K (3080 °C) [35]. The small samples of monocarbide achieve the congruently vaporizing composition in 10 h at 2820 K (2550 °C) [65] and 100 h at 2400 K (2130 °C) [35]; in the range of temperatures from 2600 K (2330 °C) to 3400 K (3130 °C) this composition is described by the equation as follows [35, 65]:

$$\lg x = -6.8 \times 10^{-3} - (9.05 \times 10^2)/T, \quad (2.40)$$

where x is the value of index in TaC_{1-x} formula and T is temperature, K, and for the rate of congruent evaporation V , $\text{g cm}^{-2} \text{s}^{-1}$, in the Ta–C system at 3000–3400 K (2730–3130 °C) the equation is given as

$$\lg V = 8.725 - (4.2854 \times 10^4)/T, \quad (2.41)$$

while the similar equation was presented as well for the evaporation rate of near-stoichiometric $\beta\text{-Ta}_{2\pm x}\text{C}$ G , $\text{g cm}^{-2} \text{s}^{-1}$, as a function of temperature T , K, for the range of 3015–3355 K (2740–3080 °C) [1, 325]:

$$\lg G = 8.73 - (4.2854 \times 10^4)/T. \quad (2.42)$$

Table 2.5 Parameters of the gaseous phase in the Ta–C system in the conditions of $Ta_{2+x}C$ – TaC_{1-x} and TaC_{1-x} –C phases equilibria calculated on the basis of thermodynamic data [576]

Parameters	Temperature, K (°C)											
	1000 (730)	2000 (1730)	2500 (2230)	3000 (2730)	3270 (3000)	3770 (3500)	4000 (3730)	4270 (4000)	5000 (4730)	5700 (5430)		
					$Ta_{2+x}C$ – TaC_{1-x} phases equilibrium							
$\lg P_{Ta}$, Pa	-31.068	-9.240	-4.851	-1.914	-0.684	1.101	1.804	2.379	3.798	4.826		
$\lg P_{C_3}$, Pa	-29.102	-8.096	-3.941	-1.189	-0.060	1.606	2.203	2.855	4.029	4.950		
C/Ta^b	91.44	12.95	7.14	4.34	3.25	2.24	1.55	2.08	0.80	0.36		
Contents, vol. %:												
C	98.92	92.81	87.53	80.57	75.32	67.76	58.40	63.75	40.92	24.18		
C_2	–	0.02	0.15	0.53	0.83	0.78	1.48	2.44	2.10	1.14		
C_3	–	–	0.01	0.05	0.09	0.20	0.18	0.35	0.09	0.02		
Ta	1.08	7.17	12.31	18.85	23.76	31.26	39.94	33.46	56.83	74.66		
					TaC_{1-x} –C phases equilibrium							
$\lg P_{Ta}$, Pa	-35.888	-11.848	-7.067	-3.898	-2.584	-0.692	-0.018	0.718	2.062	3.023		
$\lg(C/Ta)$	11.601	6.914	6.303	5.924	5.763	5.738	5.537	5.325	4.798	4.426		

^aTotal gas pressure^bAtomic ratio in gaseous phase

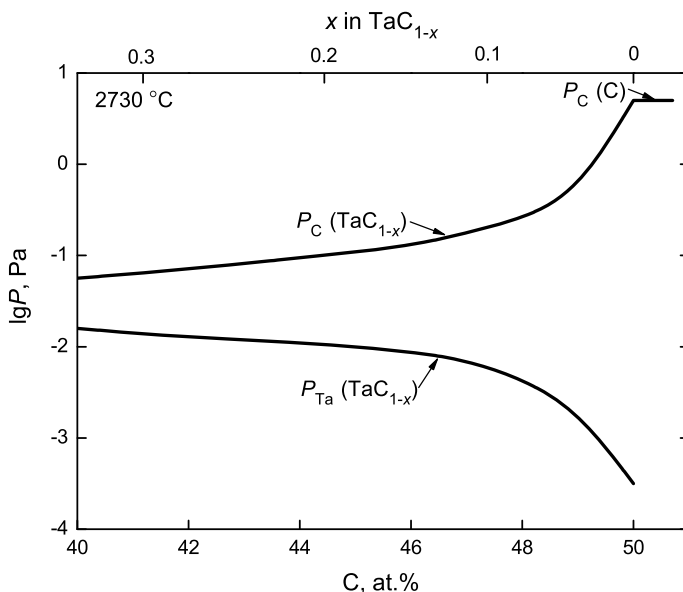


Fig. 2.5 Partial pressures of tantalum $P_{\text{Ta}}(\text{TaC}_{1-x})$ and carbon $P_{\text{C}}(\text{TaC}_{1-x})$ over tantalum monocarbide TaC_{1-x} phase, and vapour pressure of carbon over pure graphite $P_{\text{C}}(\text{C})$ as functions of monocarbide composition at 3000 K (2730 °C) calculated by Kaufman [16, 35, 115, 123, 363]

The values of general thermodynamic properties, vapour pressures and mass/linear vaporization rates for tantalum carbides are given in Addendum in comparison with other ultra-high temperature materials in the wide ranges of temperatures.

At room temperature thermal conductivity of near-stoichiometric tantalum monocarbide TaC_{1-x} , affected by porosity noticeably, is about $15\text{--}35 \text{ W m}^{-1} \text{ K}^{-1}$ (thermal diffusivity – $0.08 \text{ cm}^2 \text{ s}^{-1}$), and for near-stoichiometric tantalum semi-carbide $\alpha\text{-Ta}_{2+x}\text{C}$ the corresponding value is about $35 \text{ W m}^{-1} \text{ K}^{-1}$ [35, 37, 41, 43, 66, 67, 115, 139, 544–546, 701, 721, 729, 771]. Within the homogeneity range, as a consequence of conduction electrons scattering on the carbon sublattice vacancies and thermal lattice vibrations, the thermal conductivity of TaC_{1-x} declines with increasing carbon deficit (value of x) in the phase [16, 35, 41] that is shown in Fig. 2.6. The variation of thermal conductivity with temperature for near-stoichiometric TaC_{1-x} on the basis of several sources is shown in Fig. 2.7.

The mean coefficients of linear thermal expansion of near-stoichiometric phases $\alpha\text{-Ta}_{2+x}\text{C}$ and TaC_{1-x} at room temperature are $(3.7\text{--}7.8) \times 10^{-6} \text{ K}^{-1}$ [35, 37, 97, 123] and $(5.6\text{--}8.3) \times 10^{-6} \text{ K}^{-1}$ [46, 60, 72, 79, 93, 215, 582], respectively. The experimental data collected from the measurements of thermal expansion of

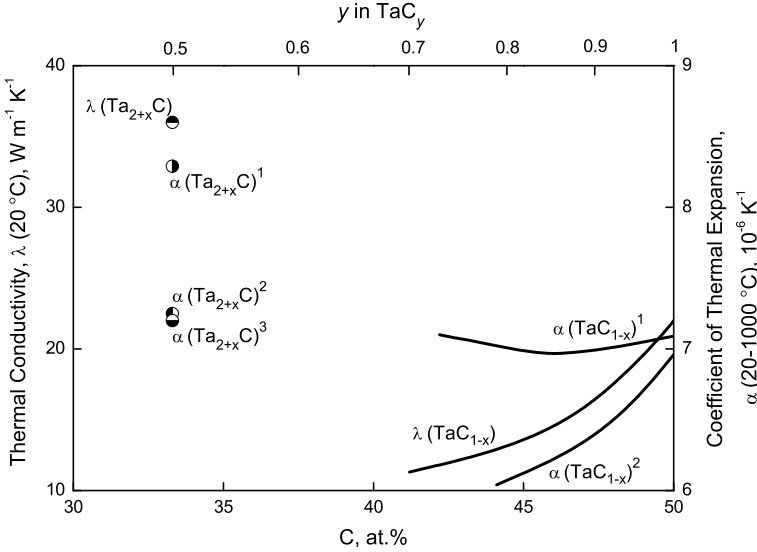


Fig. 2.6 Coefficients of thermal conductivity (λ) at 20 °C [35, 37, 41, 43] and linear thermal expansion (α) in the temperature range of 20–1000 °C (when it is not indicated specially) of tantalum monocarbide TaC_{1-x} (within the homogeneity range: 1 – hot-pressed and annealed, 6–10% porosity, content non-combined C $\leq 0.12\%$ [37, 326, 582, 651, 666]; 2 – [48]) and semicarbide $\alpha\text{-Ta}_{2+x}\text{C}$ (1 – in the range of 20–1200 °C [43]; 2 – hot-pressed and annealed, 6–10% porosity [582, 651]; 3 – in the range of 300–1200 °C [45, 828]) as functions of carbides composition

near-stoichiometric tantalum monocarbide TaC_{1-x} are listed in Table 2.6. The approximation function for the temperature dependence of relative thermal linear expansion $\Delta l/l_0 = f(T, \text{K})$, %, of near-stoichiometric TaC_{1-x} was recommended by Touloukian et al. [582] and based on the data for pure samples from several sources (accuracy within $\pm 5\%$ at $T < 2000$ K and within $\pm 7\%$ at $T > 2000$ K):

$$\Delta l/l_0 = -0.162 + (5.324 \times 10^{-4})T + (6.990 \times 10^{-8})T^2 + (2.780 \times 10^{-12})T^3, \quad (2.43)$$

where T is temperature, K, for 293–3200 K (20–2930 °C). On the basis of high-temperature X-ray measurements Houska [93] proposed for the average coefficient of linear thermal expansion α_m , K^{-1} , of near-stoichiometric sintered (in vacuum) $\text{TaC}_{-1.0}$ (content O – 0.02%) in the range of 25–2040 °C the following equation:

$$\alpha_m = 6.00 \times 10^{-6} + (0.56 \times 10^{-9})(t - 25), \quad (2.44)$$

where t is temperature, °C. The influence of carbon content on the thermal expansion of monocarbide phase within the homogeneity range can be seen in Figs. 2.3 and 2.6. The average values of coefficient of linear thermal expansion of near-stoichiometric tantalum semicarbide $\alpha\text{-Ta}_{2+x}\text{C}$ were evaluated as $7.2 \times 10^{-6} \text{ K}^{-1}$

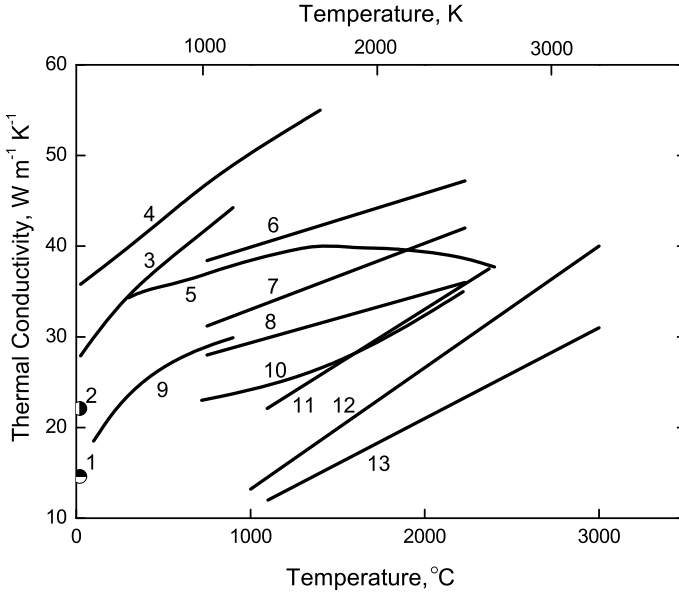


Fig. 2.7 Variation of thermal conductivity with temperature for tantalum monocarbide TaC_{1-x} materials on the basis of several sources: 1 – [66], 2 – [37, 67, 115, 545, 546], 3 – spark-plasma sintered, porosity – 1% [721], 4 – spark-plasma sintered, porosity <2% [729], 5 – as-hot-pressed [51, 68], 6 – $\text{TaC}_{0.98}$ [585], 7 – $\text{TaC}_{0.80}$ [585], 8 – $\text{TaC}_{0.74}$ [585], 9 – spark-plasma sintered, porosity – ~7% [771], 10 – hot-pressed [337], 11 – hot-pressed and heat-soaked at 2480 °C [68], 12 – [69], 13 – hot-pressed [35, 123] (when it is not indicated specially, data are given for near-stoichiometric compositions)

in the range of temperatures from 300 to 1200 °C [45] and $8.3 \times 10^{-6} \text{ K}^{-1}$ in the range of 20–1200 °C [43]. On the basis of X-ray measurements Lönnberg [97] proposed for the average coefficients of thermal expansion α_m , K^{-1} , along the main crystallographic directions a and c of near-stoichiometric $\alpha\text{-Ta}_{2+x}\text{C}$ in the temperature range of 25–1030 °C the following equations:

$$\alpha_{a,m} = 3.393 \times 10^{-6} + (2.834 \times 10^{-9})(t + 273), \quad (2.45)$$

$$\alpha_{c,m} = 1.769 \times 10^{-6} + (3.036 \times 10^{-9})(t + 273), \quad (2.46)$$

where $\alpha_{i,m}$ is the average coefficient of linear thermal expansion along the i -th direction, K^{-1} , and t is temperature, °C. In contrast to some other semicarbides of transition metals tantalum semicarbide $\alpha\text{-Ta}_{2+x}\text{C}$ displays smaller thermal expansion coefficients perpendicular to the basal plane than parallel to it. The carbon atoms in the structure of $\alpha\text{-Ta}_{2+x}\text{C}$ are more closely packed within the basal plane than perpendicular to it. It is most probable that this closer packing of the carbon atoms is responsible for the relatively high thermal expansion within the basal plane. Some recent works [204, 209, 413, 414, 561] are devoted to the calculations

Table 2.6 Average coefficients of linear thermal expansion α_m of near-stoichiometric tantalum monocarbide TaC_{1-x} in various temperature ranges

Temperature range, °C	$\alpha_m, 10^{-6} \text{ K}^{-1}$	References
20–200	5.89 ^a	[582]
20–300	5.97 ^a	[582]
20–400	6.03 ^a	[582]
20–500	6.10 ^a	[582]
	6.29 ± 0.29^b	[79]
	6.29	[86, 545]
	6.32	[88]
	6.65	[61]
20–600	6.18 ^a	[582]
	6.38	[43]
	6.41 ^c	[87]
	6.45	[51]
20–700	6.25 ^a	[582]
	6.45	[43]
	6.52 ^c	[87]
	6.55	[43, 51]
20–730	6.31	[677, 678]
20–800	6.33 ^a	[582]
	6.52	[43]
	6.56 ^c	[87]
	6.60	[51]
	8.2	[89]
20–850	6.84	[61]
20–900	6.41 ^a	[582]
20–1000	5.75 ^d	[85]
	6.46 ± 0.14^b	[79]
	6.49 ^a	[582]
	6.50	[67]
	6.61 ^e	[96, 546]
	6.64 ^c	[87]
	6.65	[51]
	6.67	[88]
	6.96 ^f	[48]
	7.1	[1, 37, 552]
	7.54	[41]
400–1000	4.09	[86]
20–1130	6.60	[677, 678]
20–1200	6.15 ^d	[85]
	6.64 ^a	[582]
	6.67 ^c	[87]
	6.70	[51]
	6.84	[43]
	6.90	[61]
	7.13 ^g	[93, 392]
8.29	[72, 90]	

(continued)

Table 2.6 (continued)

Temperature range, °C	α_m , 10^{-6} K^{-1}	References
20–1400	6.3 ^g	[115, 392, 393, 550]
	6.4 ^g	[68]
	6.40 ^d	[85]
	6.80 ^a	[582]
	6.89 ^c	[87]
	6.90	[51]
20–1500	7.02	[43]
	6.52 ^d	[85]
	6.67 ^e	[96]
	6.88 ^a	[582]
	7.05	[43, 51]
	7.11 ^c	[43, 87]
	7.12	[88]
20–1600	8.2	[94]
	6.58 ^d	[85]
	6.96 ^a	[582]
	7.15	[43]
	7.25	[51]
20–1730	7.29 ^c	[87]
	6.96	[16]
	7.08	[677, 678]
20–1800	6.66 ^d	[85]
	7.12 ^a	[582]
	7.34	[43]
	7.56	[51]
	7.59 ^c	[87]
20–2000	6.88 ^d	[85, 392]
	7.08 \pm 0.33 ^h	[729]
	7.29 ^a	[582]
	7.31 ^e	[96, 701]
	7.64	[88]
	7.90	[51]
	7.94 ^c	[87]
	5.0 ⁱ	[68, 92]
20–2050	7.41	[677, 678]
20–2130	7.46 ^a	[582]
20–2200	9.09	[61]
	6.78 ^d	[85]
	8.08	[43]
20–2300	8.20 ^c	[87]
	8.30	[43, 51]
	7.62 ^e	[96]
20–2400	7.63 ^a	[582]
	5.5 ⁱ	[68, 92]
20–2450		

(continued)

Table 2.6 (continued)

Temperature range, °C	$\alpha_m, 10^{-6} \text{ K}^{-1}$	References
20–2500	6.81 ^d	[85]
	7.50	[43, 51]
	7.71 ^a	[582]
	8.40	[88]
	8.46 ^c	[43, 87]
20–2600	7.80 ^{a, e}	[96, 582, 701]
	8.61 ^c	[51, 87]
20–2650	8.02	[86]
	8.2 ± 0.8	[43, 67, 91, 581]
20–2800	7.97 ^a	[582]
20–2900	8.06 ^a	[582]
	8.81 ^c	[87]
	8.85	[51]
20–3000	8.4 ^f	[95]

^aCalculated on the basis of approximation function

^bTaC_{0.98}, measured by high-temperature X-ray diffraction

^cHot-pressed TaC_{0.99} (27% porosity)

^dHot-pressed TaC_{0.98} (13% porosity), measured by an optical-micrometer method in Ar atmosphere

^eTaC_{0.99} hot-pressed at 3100–3150 °C and measured by dilatometric method

^fTaC_{0.997} measured by high-temperature X-ray diffraction

^gMeasured by high-temperature X-ray diffraction

^hSpark-plasma sintered (porosity <2%, mean grain size – 5.8 ± 0.2 μm), measured by dilatometric method in Ar atmosphere

ⁱHot-pressed TaC_{0.99} (25% porosity)

^jHot-pressed TaC_{0.97} measured by a dilatometric method

of coefficients of thermal expansion of tantalum carbides by means of theoretical modelling.

In comparison with other ultra-high temperature materials the values of thermal conductivity and thermal expansion of tantalum carbides in the wide range of temperatures are summarized in Addendum.

2.3 Electro-magnetic and Optical Properties

At room temperature the value of specific electrical resistance (resistivity) of near-stoichiometric tantalum monocarbide TaC_{1-x} lies within the area of 0.2–0.5 μΩ m, and for near-stoichiometric semicarbide α-Ta_{2+x}C it is about 0.4–0.5 μΩ m [1, 16, 35, 43, 60, 61, 90, 207, 372, 382, 388, 534, 544, 676, 830]. The variation of specific electrical resistance with temperature for near-stoichiometric TaC_{1-x} is shown on the basis of several sources in Fig. 2.8. In the wide temperature range from 300–500 up to 3000–3300 °C the resistance of monocarbide phase enlarges with increasing temperature, practically in accordance with linear relationship; that

is an evidence of mainly metallic type of conduction in TaC_{1-x} [35]. From the room temperature up to 800 °C, according to Nino et al. [721], the electrical resistivity of $\text{TaC}_{-1,0}$ materials (porosity – 1%) ρ , $\mu\Omega \text{ m}$, is obeyed the rule:

$$\rho = 0.35 + (5.70 \times 10^{-4})t, \quad (2.47)$$

for the interval of 1130–3230 °C Eckstein and Forman [102] recommended for near-stoichiometric tantalum monocarbide TaC_{1-x} the equation as follows:

$$\rho = 1.02 + (1.78 \times 10^{-4})(t + 273), \quad (2.48)$$

where t is temperature, °C. The single crystal $\text{TaC}_{0,99}$ resistivity measured by Allison et al. [100] at ultra-low and low temperatures is perfectly described in the interval from $T = 0$ to $T = 350 \text{ K}$ by the Wilson expression (in $\mu\Omega \text{ m}$):

$$\rho(T) = 0.125 + (5.353 \times 10^{-8})T^3 \int_0^{136/T} x^3 / \sinh^2 x dx, \quad (2.49)$$

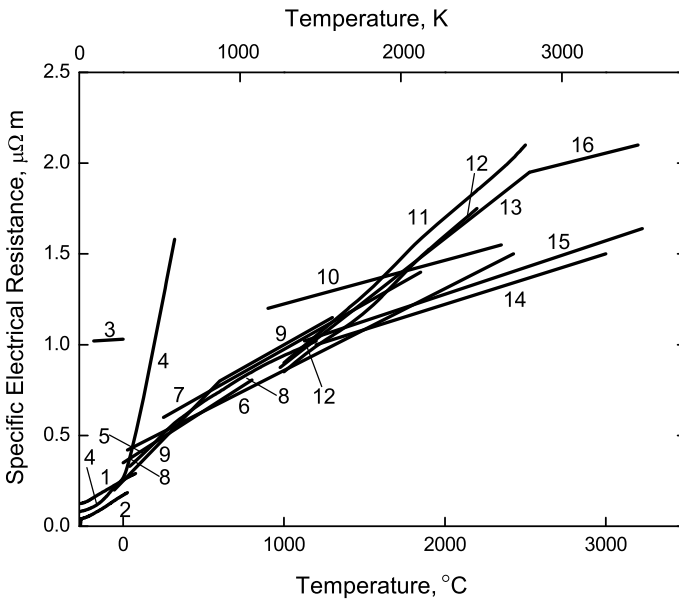


Fig. 2.8 Variation of specific electrical resistance with temperature for tantalum monocarbide TaC_{1-x} materials on the basis of several sources: 1 – single crystal $\text{TaC}_{0,99}$ [100]; 2 – hot-pressed $\text{TaC}_{0,997}$, porosity – ~11% [99]; 3 – sintered $\text{TaC}_{-1,0}$, porosity – 13% [104]; 4 – [51]; 5 – [103]; 6 – [105]; 7 – [98]; 8 – spark-plasma sintered, porosity – 1% [721]; 9 – sintered (in vacuum) $\text{TaC}_{0,98}$ [584, 585]; 10 – [345]; 11-12 – [61]; 13 – [101]; 14 – [69]; 15 – metal carburized in hydrocarbon atmosphere [102]; 16 – [106] (when it is not indicated specially, data are given for near-stoichiometric compositions)

Table 2.7 Average thermal coefficients of resistivity α_R of near-stoichiometric tantalum monocarbide TaC_{1-x} in various temperature ranges

Temperature range, °C	$\alpha_R, 10^{-3} \text{ K}^{-1}$	References
(-225)–(+20)	4.0 ^a	[100]
(-195)–0	0.53 ^b	[365]
(-190)–(+20)	0.25	[366]
20–25	1.5–2.5 ^c	[390]
	2.5 ^d	[206]
0–800	1.63 ^e	[721]
20–1000	0.79 ^f	[371, 583]
100–1100	1.38	[368, 369, 648]
20–1170	0.22	[367, 369, 648]
400–2000	1.07 ^g	[369, 648]
	0.99	[370]
20–2110	0.22	[367, 369, 648]

^aSingle crystal $\text{TaC}_{0.99}$, $d\rho/dT = 4.95 \times 10^{-4} \mu\Omega \text{ m K}^{-1}$

^bMaterials deposited from gas phase

^cCoating reactively sputter-deposited from Ar plasmas containing CH_4 , thickness – 1–25 μm

^dHot-pressed materials, carbon content – 49.5 at. %

^eSpark-plasma sintered materials (porosity – 1%)

^fThermal coefficient $\alpha = 1/\rho_\theta \times (d\rho/dT)_\theta$, corresponding to Debye temperature $\theta = 630 \text{ K}$ ($(d\rho/dT)_\theta = 3.3 \times 10^{-4} \mu\Omega \text{ m K}^{-1}$), corrected to the poreless state

^gHot-pressed materials

which can be simplified for $T \leq 25\text{--}40 \text{ K}$ up to $\rho(T) = 0.125 + AT^3$, where A is a constant. The data on the thermal coefficients of resistivity of near-stoichiometric TaC_{1-x} in the various temperature ranges are presented in Table 2.7. The variations of resistivity with temperature for the phases having different deviations from the stoichiometry are presented in Fig. 2.9. The specific electrical resistances in solid and liquid states and ratio of the resistivities at the melting point of TaC_{1-x} are $\rho_{\text{sol}} \approx 2.2\text{--}2.3 \mu\Omega \text{ m}$, $\rho_{\text{liq}} \approx 2.4 \mu\Omega \text{ m}$ and $\rho_{\text{liq}}/\rho_{\text{sol}} \approx 1.04\text{--}1.09$, respectively [112, 113].

Within the homogeneity range the resistivity of TaC_{1-x} enlarges considerably with increasing carbon deficit in non-metal sublattice, that is shown in Fig. 2.10, where the data from several sources are collected [1, 23, 37, 103, 107–111]; the variation of $d\rho/dT$ with composition at ambient temperatures is shown in Fig. 2.11. The superconducting transition temperature T_c of near-stoichiometric TaC_{1-x} is 9.1–11.0 K [35, 60, 73, 114–116, 356–358, 451, 661, 665, 688, 832]; it varies with composition considerably, e.g. falling from 9.7 K for $\text{TaC}_{0.99 \pm 0.01}$ up to 2.0 K for $\text{TaC}_{0.85 \pm 0.01}$ [114]. The highest temperature is reached for the most stoichiometric composition and any deviation therefrom results in a lowering and eventual disappearance ($<1.05 \text{ K}$ at $x \geq 0.25\text{--}0.30$) of T_c [114–116]. The transition temperature T_c of semicarbide $\alpha\text{-Ta}_{2+x}\text{C}$ phase having $x = 0.13$ is $<1.60\text{--}1.75 \text{ K}$ [115, 116], for the phase with $x = 0.08$ it is $<1.98 \text{ K}$ [831, 832], and for the stoichiometric phase $T_c = 3.26 \text{ K}$ [586].

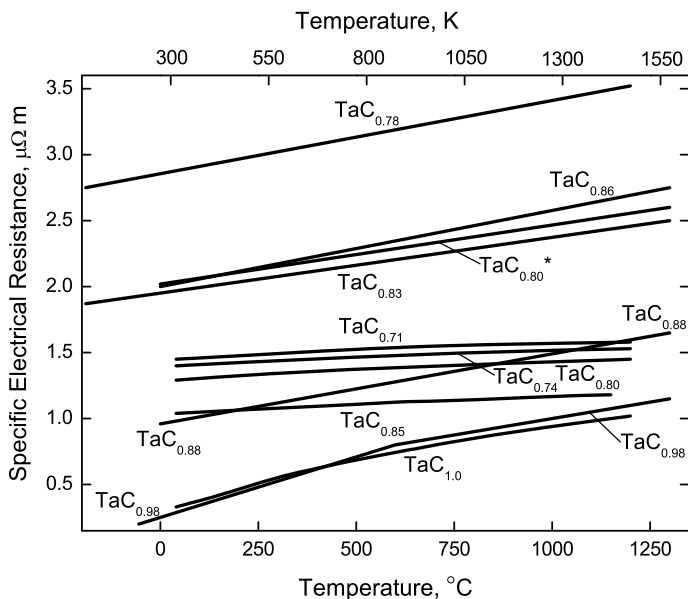


Fig. 2.9 Variations of specific electrical resistance with temperature for the TaC_{1-x} phases having different deviations from the stoichiometry ($x = 0.0, 0.15, 0.20, 0.26, 0.29$ [103]; sintered materials, $x = 0.02, 0.12, 0.14, 0.17, 0.20^*, 0.22$ [584, 585])

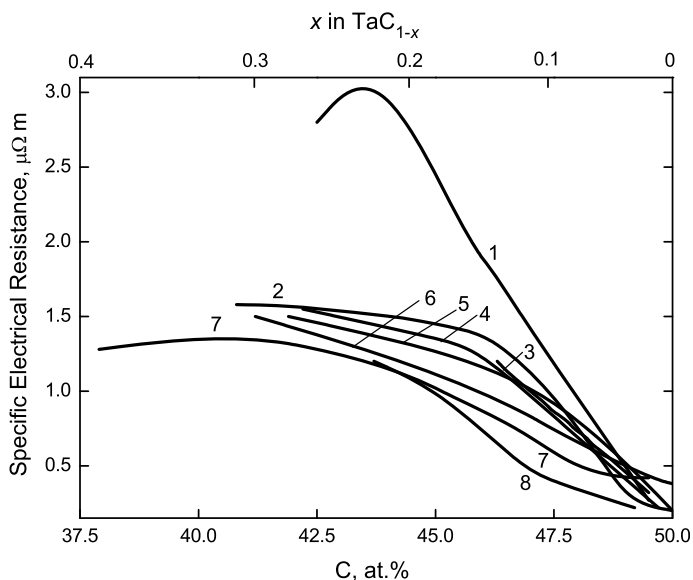


Fig. 2.10 Variations of specific electrical resistance at room temperature within the homogeneity range of tantalum monocarbide TaC_{1-x} materials on the basis of several sources: 1 – materials sintered in vacuum [584, 585], 2 – materials carburized by solid-state diffusion saturation [107], 3 – [321], 4 – [1, 23, 37, 111], 5 – materials carburized in propane [322, 522], 6 – [103, 108], 7 – [109, 660], 8 – [110]

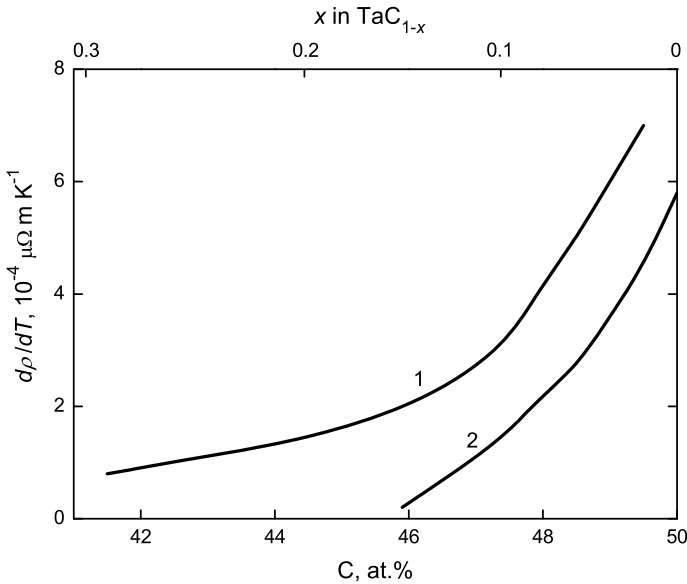


Fig. 2.11 Variation of dp/dT (slope of resistivity vs. temperature) at ambient temperatures with carbon content within the homogeneity range of tantalum monocarbide TaC_{1-x} based on: 1 – [103] and 2 – [107]

At room temperature the Hall and Seebeck coefficients of near-stoichiometric tantalum monocarbide TaC_{1-x} are $R = -(0.6-2.1) \times 10^{-10} \text{ m}^3 \text{ A}^{-1} \text{ s}^{-1}$ and $S = -(4.0-11.5) \mu\text{V K}^{-1}$, respectively [35, 37, 60, 111, 117, 328, 585, 587]; the reported values of these constants for nonstoichiometric TaC_{1-x} phases show considerable disagreement [35, 37, 108, 111, 123], experimental data obtained by Santoro and Dolloff [322, 522] for the Hall coefficient, Neshpor and Ordanyan [108] for the Seebeck coefficient and Borukhovich et al. [111, 585] for the Hall and Seebeck coefficients within the homogeneity range of tantalum monocarbide TaC_{1-x} for ambient and cryogenic temperatures are presented in Fig. 2.12.

Near-stoichiometric tantalum monocarbide TaC_{1-x} is a paramagnetic substance with molar magnetic susceptibility χ_m (SI) $\approx (120-250) \times 10^{-6} \text{ cm}^3 \text{ mol}^{-1}$ at room temperature very slightly varying with temperature in the range from -200 to $900 \text{ }^\circ\text{C}$ [35, 107, 118-120, 328, 329, 662]. The weak temperature influence and small absolute value of susceptibility indicate that the magnetic properties of TaC_{1-x} are determined primarily by conducting electrons [123]. With increasing carbon deficit within the homogeneity range the value of magnetic susceptibility of TaC_{1-x} declines to its diamagnetic (negative) minimum at $-(130-320) \times 10^{-6} \text{ cm}^3 \text{ mol}^{-1}$, corresponding to $\sim\text{TaC}_{0.80}$ composition (see Fig. 2.13), and then it enlarges again proceeding closer to the paramagnetic region [35, 118, 119, 122, 373, 589]. The temperature coefficient of magnetic susceptibility $d\chi/dT$ changes its sign with composition; it is positive for compositions near $\text{TaC}_{0.78}$ and negative

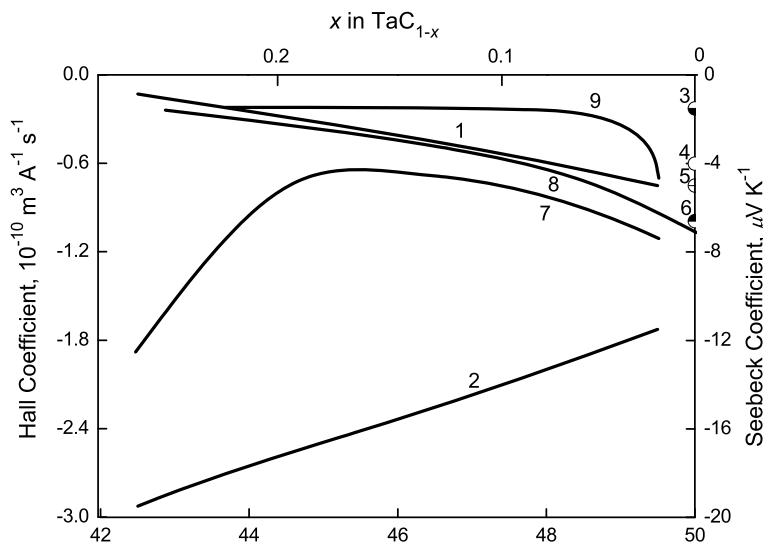


Fig. 2.12 Variations of Seebeck coefficient at room temperature (1 – [108]; 2 – [111, 585]; 3 – [588]; 4 – thin films deposited by r. f. sputtering technique, thickness – 0.3 μm [117]; 5 – hot-pressed materials [105]; 6 – [328]) and Hall coefficient at room (7 – sintered in vacuum [111, 585]; 8 – materials carburized in propane [322, 522]) and cryogenic, 77 K (9 – carburized in propane [322, 522]) temperatures within the homogeneity range of tantalum monocarbide TaC_{1-x}

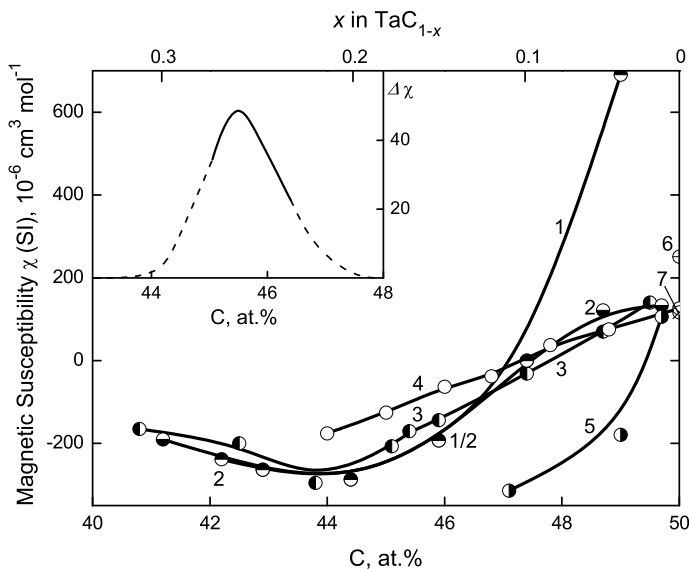


Fig. 2.13 Variation of molar magnetic susceptibility at room temperature within the homogeneity range of tantalum monocarbide TaC_{1-x} on the basis of several sources: 1 – [110]; 2 – contents: non-combined C $\leq 0.005\%$, N $\leq 0.005\%$, O $\leq 0.02\%$ [122]; 3 – disordered (for ordered state *see* data in the *Inset*) [119, 121, 654]; 4 – from 48.8 to 50 at.% C the values extrapolated [118, 589]; 5 – [107]; 6 – [329]; 7 – [328] (*Inset* – difference of the susceptibility magnitudes in disordered and ordered states $\Delta\chi = |\chi_{\text{disord}} - \chi_{\text{ord}}|$ determined for $\text{TaC}_{0.82}$ – $\text{TaC}_{0.85}$ phases, units are the same with the major plot [121, 654])

for near-stoichiometric compositions around $\text{TaC}_{0.97}$ [35, 119]. The χ - T curves of the monocarbide TaC_{1-x} with $x \leq 0.1$ and $x \geq 0.2$ exhibit no peculiarities since these compositions lie outside the $\text{TaC}_{0.81}$ to $\text{TaC}_{0.89}$ range, in which due to the ordering of carbon atoms and vacancies in TaC_{1-x} the reversible susceptibility jump corresponding to the region of temperature hysteresis is observed [121]. According to Santoro [122] tantalum semicarbide $\alpha\text{-Ta}_{2+x}\text{C}$ is also a paramagnetic substance with the value of its mass magnetic susceptibility something higher than that of near-stoichiometric monocarbide TaC_{1-x} , but $\zeta\text{-Ta}_4\text{C}_{3-x}$ is more likely diamagnetic.

According to Harris et al. [126] tantalum monocarbide TaC_{1-x} films (thickness 0.2–0.3 μm) in the condition of as-grown on metallic tantalum single-crystal with (100) orientation exhibit reflectance (reflective index) – 0.3–0.4 at a wavelength of about 0.1 μm . The variation of reflectance with angle of incidence for TaC_{1-x} film in high-vacuum ultraviolet range is given in Fig. 2.14, and the room-temperature reflectance spectrum of pure sintered near-stoichiometric TaC_{1-x} (porosity – 10%, grain size – 10–20 μm) from the ultraviolet wavelength region to the mid-infrared band is shown in Fig. 2.15. Optical properties of a nearly stoichiometric single crystal of tantalum monocarbide (specular reflectance at 0.03–6.0 eV and ellipsometry at 1.2–4.6 eV) were reported by Modine et al. [124], spin-resolved photoemission spectra of $\text{TaC}_{0.96}$ – by Garbe and Kirschner [671] and X-ray photoelectron spectra of TaC_{1-x} phases within the homogeneity range ($0 < x \leq 0.48$) – by Gruzalski and Zehner [670]. Optical spectra in the infrared (IR) and visible ranges as well as X-ray emission and absorption spectra were considered by Alyamovskii et al. [330], Ramqvist et al. [158], Kammori et al. [833] and

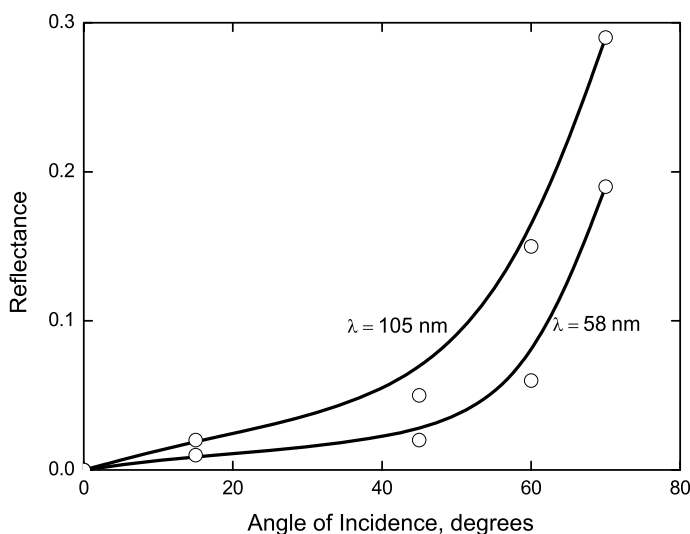


Fig. 2.14 Variation of reflectance with angle of incidence for as-grown (on metallic tantalum single-crystal with (100) orientation) TaC_{1-x} film (thickness – 0.2–0.3 μm) in high-vacuum ultraviolet range [126]

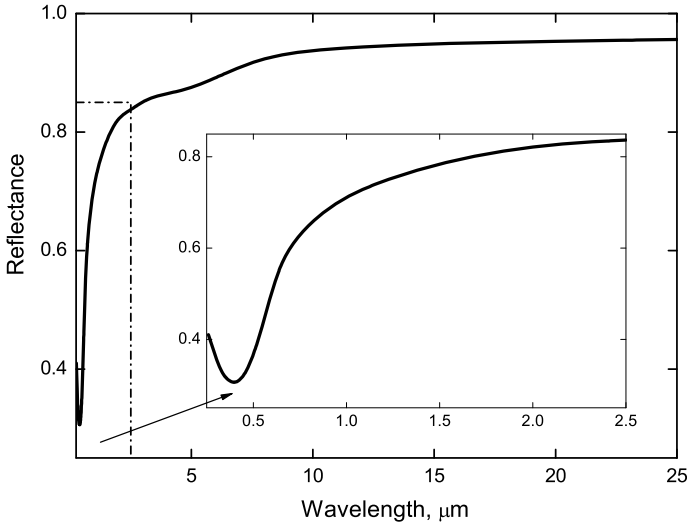


Fig. 2.15 Room-temperature reflectance spectrum of pure sintered TaC_{1-x} (porosity – 10%, grain size – 10-20 μm) from the ultraviolet wavelength region to the mid-infrared band [127, 128]

Upadhyaya [123]. The absorption wave numbers of basic maxima of IR band for tantalum carbides are 1080 cm^{-1} (for $\text{TaC}_{0.96}$), 1100 cm^{-1} (for $\text{TaC}_{0.73}$) and 1080 cm^{-1} (for $\text{Ta}_{1.96}\text{C}$) [330]. At the common conditions the colour of carbon-rich tantalum monocarbide TaC_{1-x} materials is brown in the dispersed state (powdered) or golden-brown (golden-yellow) in the compact state, the colour of tantalum semicarbide $\alpha\text{-Ta}_{2+x}\text{C}$ materials is gray [17, 37, 43, 60]. The colour intensity of TaC_{1-x} compact materials decreases sharply with an increase in deviation from the stoichiometry, so TaC_{1-x} phases with the value of index $x > 0.15$ are steel or silver in colour, i.e. very similar to that of transition metal carbides of group 4 [123].

The normal monochromatic emittance (spectral emissivity) $\varepsilon_{\lambda,T}$ of tantalum monocarbide TaC_{1-x} falls noticeably with wavelength λ growth and only slightly varies with temperature [16, 61, 123, 539]; the linear relationships for $\lambda = 0.4\text{--}1.1\ \mu\text{m}$

$$\varepsilon_{\lambda,T} = (0.693 \pm 0.015) - [(7.0 \pm 0.5) \times 10^{-5}](t + 273) - (0.147 \pm 0.01)\lambda, \quad (2.50)$$

where t is temperature, $^{\circ}\text{C}$, λ is wavelength, μm , was proposed by Danilyants et al. [151] in the temperature range $1430\text{--}3130\ ^{\circ}\text{C}$ for materials manufactured by remelting of pressed briquets with composition $\text{TaC}_{0.98}$, and for $\lambda = 0.65\ \mu\text{m}$

$$\varepsilon_{\lambda} = 0.4662 - (5.084 \times 10^{-5})(t + 273), \quad (2.51)$$

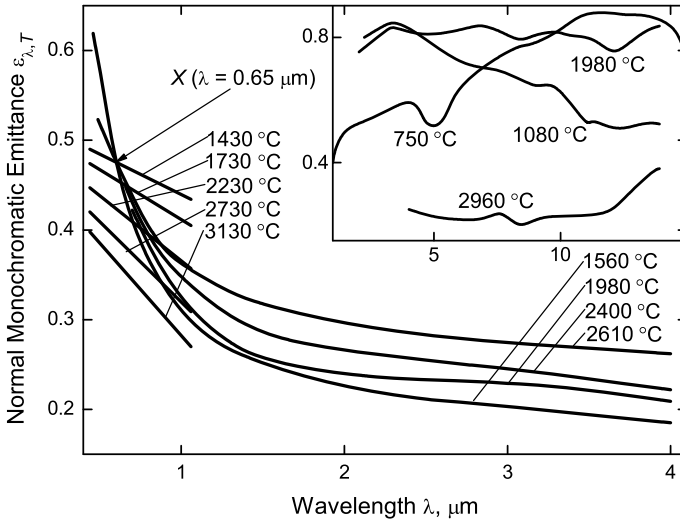


Fig. 2.16 Variations of normal monochromatic emittance $\epsilon_{\lambda,T}$ with wavelength λ for tantalum monocarbide TaC_{1-x} materials on the basis of several sources: remelted $\text{TaC}_{0.98}$, measured in high-purity Ar at 1430, 1730, 2230, 2730 and 3130 °C [151]; hot-pressed $\text{TaC}_{-1.0}$, measured in vacuum at 1560, 1980, 2400 and 2610 °C (X-point, or an isosbestic point, where $|1/\epsilon_{\lambda,T} \times d\epsilon_{\lambda,T}/dT|_{\lambda=X} = 0$, is marked specially) [138, 590, 595] (Inset – $\text{TaC}_{-1.0}$, measured in Ar + H_2 atmosphere at 1080, 1980 and 2960 °C [596, 597]; plasma-sprayed coating $\text{TaC}_{-1.0}$, measured at 750 °C [598, 599])

where t is temperature, °C, was obtained by Mackie et al. [129, 539] in the temperature range of 1100–1700 °C for arc-melted (via floating zone) polycrystalline monocarbide $\text{TaC}_{0.79 \pm 0.05}$. The variation of emittance $\epsilon_{\lambda,T}$ with wavelength and temperature for tantalum monocarbide is shown in Fig. 2.16. The data on monochromatic emittance ϵ_{λ} ($\lambda = 0.630\text{--}0.665 \mu\text{m}$) and integral (total) emittance ϵ_T for TaC_{1-x} materials produced by different manufacturing methods and measured at various temperatures are listed in Tables 2.8 and 2.9. According to Bober et al. [152], tantalum monocarbide shows in the solid and liquid states only a small variation of emissivity at $\lambda = 0.63 \mu\text{m}$ with temperature.

The thermionic emission characteristics (electron work function and Richardson constants) of various tantalum carbide phases are given in Fig. 2.17 and Table 2.10. The calculated values of emission current density for near-stoichiometric monocarbide TaC_{1-x} are about 0.2, 10^2 and $9 \times 10^3 \text{ A m}^{-2}$ at 730, 1230 and 1730 °C, respectively [16, 143]. Similar to some other transition metal carbides, single crystal TaC_{1-x} materials show following relationships between the effective thermionic work functions of different crystallographic planes: $\phi_{(210, 310)} < \phi_{(100)} \approx \phi_{(110)} \gg \phi_{(111)}$ [153]. A typical brightness characteristic ($U = 75 \text{ kV}$) of tantalum monocarbide

Table 2.8 Normal monochromatic emittance ε_λ ($\lambda = 0.630\text{--}0.665 \mu\text{m}$) of tantalum monocarbide TaC_{1-x} materials in various temperature ranges

Monochromatic emittance, ε_λ	Temperature range, °C	References
0.36–0.47 ^a	1430–3130	[151]
0.37–0.40 ^b	1150–1730	[129, 539]
0.40–0.46 ^c	2100–3200	[102]
0.43 ^d	1500–2100	[374]
0.43–0.53 ^e	1600–2700	[130]
0.45–0.47 ^f	1920–2110	[131]
0.45 ^g	1530–2530	[35, 138]
0.49–0.87 ^h	1550–3600	[594]
0.50–0.52 ⁱ	930–2830	[152]
0.50–0.85 (?) ^j	1500–3600	[135]
0.55 ^k	2430–2730	[16, 35]
0.54–0.83 ^l	1000–3000	[591, 833]
0.62–0.66 ^m	1000–2200	[1, 132]
0.62–0.85 ⁿ	800–1700	[37, 61, 72, 134]
0.67	1730	[16, 67]
0.80 ⁱ	1500	[133]

^aRemelted materials; ε_λ falls with the temperature growth linearly

^bArc-melted (via floating zone) polycrystalline $\text{TaC}_{0.79\pm 0.05}$, measured in vacuum $10^{-5}\text{--}10^{-6}$ Pa;

ε_λ falls with the temperature growth linearly (slope is $\sim 5.1 \times 10^{-5} \text{ K}^{-1}$)

^cMaterials manufactured by metal carburization; ε_λ grows with temperature increasing

^dFor $\lambda = 0.81 \mu\text{m}$, polished surface (with rough surface $\varepsilon_\lambda = 0.61$), after exposure to hot H_2 at 1120 °C for 1 h ε_λ increases to a value similar to that of material with a rough surface [375]

^eHot-pressed $\text{TaC}_{0.93}$ (5–15% porosity); ε_λ grows with temperature increasing

^f ε_λ grows with temperature increasing

^gSintered materials

^hSpecially polished materials; ε_λ falls with the temperature growth

ⁱHot-pressed materials; ε_λ grows very slightly with the temperature growth (linearly)

^jSharp decrease of emittance ε_λ was observed at $\sim 2000 \text{ °C}$; however, careful studies of this effect in carbide materials [123, 136, 137] showed that it results from the formation and subsequent thermal desorption of surface impurity films formed by interactions with oxygen and nitrogen

^kMaterials manufactured by metal carburization

^lSintered materials, measured in vacuum and Ar multiply; ε_λ falls with the temperature growth linearly

^mSintered materials; ε_λ falls with temperature increasing

ⁿPowdered materials on tantalum substrate; ε_λ grows with temperature increasing (almost linearly)

cathode (thermionic emitter for electron microscopy) is shown in Fig. 2.18. Field emission properties of TaC_{1-x} materials were reported in several works [153, 376, 377, 607, 608, 837].

Table 2.9 Integral (total) emittance ε_T of near-stoichiometric tantalum monocarbide TaC_{1-x} in various temperature ranges

Integral emittance, ε_T	Temperature range, °C	References
0.20–0.30 ^a	1300–2200	[138, 590]
0.25–0.92 ^b	500–2750	[592, 593]
0.36–0.44 ^c	1600–2700	[139]
0.39 ^d	2100–3200	[35, 102]
0.42–0.44 ^c	1000–2700	[1, 140]
0.42–0.54 ^f	1100–2900	[591, 834]
0.54–0.59 ^g	2000–3000	[35]

^aNormal emittance ε_T for hot-pressed materials, measured in Ar; ε_T increases with the temperature growth linearly

^bNormal emittance ε_T for hot-pressed materials, measured in Ar; dome-shaped curve $\varepsilon_T - T$ with the maximum at ~ 1100 °C ($\varepsilon_T = 0.37$ at 500 °C)

^c ε_T increases with the temperature growth

^dManufactured by metal carburization

^eNormal emittance ε_T for hot-pressed $\text{TaC}_{0.98\pm 0.03}$ (20–25% porosity); ε_T increases slightly with the temperature growth

^fHemispherical emittance ε_T for sintered materials; ε_T increases with the temperature growth

^gNormal emittance ε_T for hot-pressed materials; ε_T increases slightly with the temperature growth

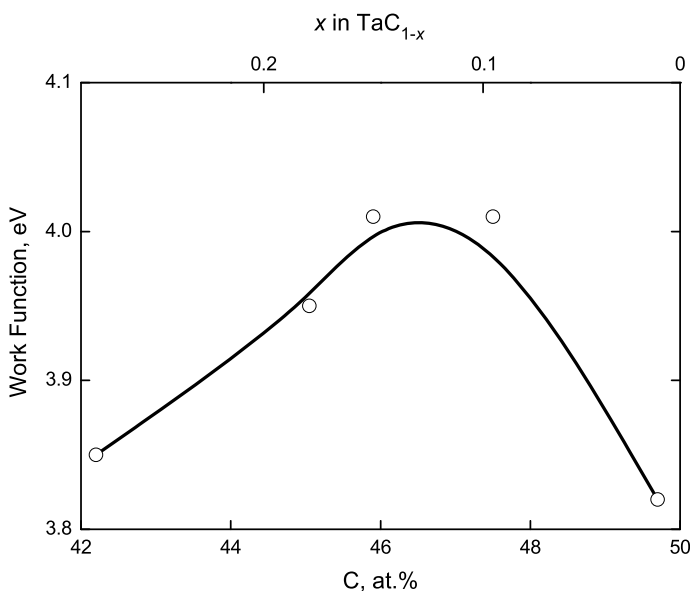
**Fig. 2.17** Variation of effective work function of tantalum monocarbide phase TaC_{1-x} at 1530 °C with carbon content (“total current” method) [35, 123, 141, 658, 666]

Table 2.10 Thermionic emission characteristics (electron work function and Richardson constant) of tantalum carbide phases

Composition	Work function ^a , $\varphi = \varphi_0 + (d\varphi/dT)_{av}T$, eV	Richardson constant, A, $10^4 \text{ A m}^{-2} \text{ K}^{-2}$	Temperature range, °C	Remarks ^b	References
Ta ₂ C	4.11	–	–	LMTO-calculated value	[673, 743, 744]
	$4.31 + (1.0 \times 10^{-4})T$	–	700–1300	TiM, metal-carburized	[1]
	4.73 ^c	–	–	UPS, single crystal (100)	[672–674, 743, 744]
TaC _{0.73}	3.85 ^d	–	1500	TiM, hot-pressed	[35, 123, 604]
	$4.17 - (1.8 \times 10^{-4})T$	–	1250–1800	TiM, hot-pressed	[1, 35, 142, 604]
TaC _{0.77}	3.40 ^d	–	1500	FEM, single crystal (100)	[153]
TaC _{0.82}	3.95 ^d	–	1500	TiM, hot-pressed	[35, 123, 604]
	$4.31 - (2.0 \times 10^{-4})T$	–	1200–1800	TiM, hot-pressed	[1, 142]
	4.01 ^d	–	1500	TiM, hot-pressed	[35, 123, 604]
TaC _{0.85}	4.30 ± 0.05	–	25	CPDM (W), hot-pressed	[1, 146]
	$4.46 - (2.5 \times 10^{-4})T$	–	1200–1800	TiM, hot-pressed	[1, 35, 142, 604]
	3.80 ± 0.05 ^d	–	–	TiM, metal-carburized	[1, 142]
TaC _{~0.90}	3.80 ± 0.1	165	–	TiM, metal-carburized	[1, 142]
	4.01 ^d	–	1500	TiM, hot-pressed	[35, 123, 604]
TaC _{0.91}	$4.37 - (2.0 \times 10^{-4})T$	–	1200–1800	TiM, hot-pressed	[1, 35, 142, 604]
	4.22 ± 0.06	–	–	CPDM, PeM, carburized	[1, 147]
TaC _{0.98}	3.82 ^d	–	1500	TiM, hot-pressed	[35, 123, 604]
TaC _{0.99}	$4.18 - (2.0 \times 10^{-4})T$	–	1200–1800	TiM, hot-pressed	[1, 35, 142, 604]
	3.05	2.1	–	TiM, powder	[1, 143]
TaC _{~1.0}	3.14	0.30	–	TiM, outgased powder	[1, 143]
	3.17 ± 0.06	0.22 ± 0.10	1300–2000	TiM, metal-carburized	[1, 102]
	From $(3.21 \pm 0.05)^d$ to $(3.87 \pm 0.1)^d$	–	From 1000 to 1300	TiM, metal-carburized (variation of φ_{eff} with temperature)	[1, 148]
TaC _{~1.0}	3.33 ^e	–	–	Single crystal (001), theoretically evaluated	[417]
	3.40	–	–	TiM, pyrolytic coating	[1, 378]
	3.61 ^f	–	–	Single crystal (001), theoretically evaluated	[417]

(continued)

Table 2.10 (continued)

Composition	Work function ^a , $\varphi = \varphi_0 + (d\varphi/dT)_{av}T$, eV	Richardson constant, A, $10^4 \text{ A m}^{-2} \text{ K}^{-2}$	Temperature range, °C	Remarks ^b	References
	3.64 ^d	–	1900	TiM, powder on W substrate	[1, 143]
	3.65 ^d	–	1700	TiM, powder	[145]
	3.77 ^d	–	1100	TiM, powder	[1, 145]
	3.77 ^d	–	2100	TiM, hot-pressed	[142]
	3.80 ± 0.05	–	1200–1700	TiM, metal-carburized	[679]
	3.80 ^d	–	2100	TiM, powder on W substrate	[1, 142]
	3.84 ^g	–	–	LMTO-calculated value for (001) surface	[673, 674, 743, 744]
	3.85	–	–	Calculated value (unrelaxed surface)	[743, 744]
	3.86	–	–	Theoretically evaluated (unrelaxed surface)	[673]
	3.93 ^d	–	25	TiM, powder	[145]
	3.95 ^d	7.64	2350	TiM, metal-carburized wire	[150]
	3.98 – (1.5 × 10 ⁻⁴)T	–	1100–1900	TiM, powder	[1, 35, 123, 145]
	4.15 ^d	–	1500	TiM, hot-pressed	[1, 144]
	4.16	–	–	Calculated value (relaxed surface)	[743, 744]
	4.2	–	–	Bulk materials for the CMOS device applications	[836]
	4.20 ± 0.04	–	1300	TiM, hot-pressed	[1, 149]
	4.24	–	–	Theoretically evaluated (relaxed surface)	[673]
	4.30 ^h	–	25	FEM, single crystal (001), clean surface	[542, 607–609, 743, 744]
	4.33 ^d	142.7	2350	TiM, electrolytic etching	[150]
	4.36 ⁱ	–	–	Single crystal (100), theoretically evaluated	[684]
	4.38 ± 0.05	–	25	CPDM, hot-pressed	[1, 149]
	4.38 ^c	–	–	UPS, single crystal (100)	[672–674, 743, 744]
	4.4 ^d	–	2100	TiM, sintered	[1, 142]
	4.5 ± 0.1	–	–	TiM, metal-carburized	[1, 142]
	4.54 ^d	4.01	2350	TiM, powder on Pt substrate	[150]
	4.70 ^j	–	25	FEM, single crystal (111), clean surface	[542, 607–609]

(continued)

Table 2.10 (continued)

Compo- sition	Work function ^a , $\varphi = \varphi_0 + (d\varphi/dT)_{av}T$, eV	Richardson constant, A, $10^4 \text{ A m}^{-2} \text{ K}^{-2}$	Temperature range, °C	Remarks ^b	References
	4.7	–	–	Nanocrystalline thin films sputtered on thermally oxi- dized Si wafers	[835]
	–	–	–	AeE, cold cathode, ~1 μm fibre, 800 A m^{-2} in vacuum $5.3 \times 10^{-7} \text{ Pa}$ for >1200 h	[1, 376, 377]

^a T is temperature, K

^bMethods applied for the experimental determination of the work function (TiM – thermionic method, UPS – ultraviolet photoemission spectroscopy technique, CPDM – contact potential difference method (second electrode is given in brackets), PeM – photoelectronic method, FEM – field emission microscopy, AeE – autoelectronic emission method) and manufacturing methods for the fabrication of a particular material (or its constitution) are marked

^cAbsolute work functions

^dThe values of effective electron work function

^eCalculated using the Perdew's generalized gradient approximation (GGA) for the fixed surface model

^fCalculated using the Perdew's GGA for the relaxed surface model

^gFull-potential linear-“muffin-tin”-orbital calculation technique (40-atom cell, no vacancies)

^hFor graphene-covered surface $\varphi = 3.9 \text{ eV}$

ⁱCalculated using the linear-muffin-tin-orbital with atomic sphere approximation (LMTO-ASA) technique

^jFor graphene-covered surface $\varphi = 3.5 \text{ eV}$

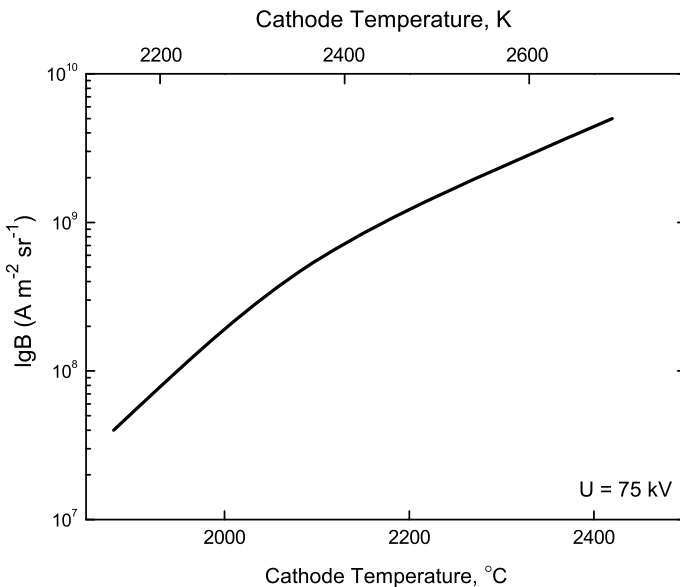


Fig. 2.18 Typical brightness (B) characteristic ($U = 75 \text{ kV}$) of tantalum monocarbide cathode (thermionic emitter with electron work functions $\varphi = 4.36 \text{ eV}$, $\varphi_{\text{eff}} = 4.33 \text{ eV}$, Richardson constant $A = 142.7 \times 10^4 \text{ A m}^{-2} \text{ K}^{-2}$, $T = 2635 \text{ K}$) produced by the carburization reaction of metal wire/foil with benzene vapour [150]

The recommended values of electrical resistivity, magnetic susceptibility, integral and spectral emittances and thermionic emission characteristics (electron work function and Richardson constant) for tantalum carbides are given in the wide range of temperatures in comparison with other ultra-high temperature materials in Addendum.

2.4 Physico-mechanical Properties

Most of the physico-mechanical properties of tantalum carbides are sensitive to the deviations from the stoichiometry, but also to the crystallographic directions in the materials; it has been just marked in Sect. 2.1 concerning the slip systems in TaC_{1-x} . At room temperature the hardness HV , GPa of near-stoichiometric tantalum monocarbide TaC_{1-x} is evaluated as 11.0 (mean grain size – 4–9 μm , porosity 3–8%, 5–15 N load) [724], 12.4 (for thin films on Ti) [686], 13.7 [403], 13.9 ± 0.7 (mean grain size – $5.8 \pm 0.2 \mu\text{m}$, porosity < 2%, 9.8 N load) [729], 14.0 [42, 332, 333], 14.0–14.3 (mean grain size – 15–25 μm , porosity < 2%, 98 N load) [721], 14.3 (for $\text{TaC}_{0.99}$, 1 N load) [601], 14.6 (for $\text{TaC}_{0.96}$, 200 N load) [1, 23], 14.7–19.6 [605], $(15.1\text{--}17.7) \pm (0.7\text{--}1.0)$ [35, 123, 171, 334], 15.2 [345], 15.5 [16], 15.7 (extrapolated to $\text{TaC}_{1.0}$) [109, 542], 15.7 ± 0.5 (0.3–49 N load) [16, 61, 90, 892], 16.7 [60], 16.9 ± 1.4 (for $\text{TaC}_{0.99}$, 0.5 N load) [37, 604], 17.0 ± 1.0 (contents: O – 0.05%, N – 0.05%, 0.5 N load) [164, 606], 17.7–19.6 (0.5–1.0 N load) [67, 197, 600, 602, 603], 17.8 (0.2–0.5 N load) [67, 600], 18.5 ± 0.8 (for $\text{TaC}_{0.98}$) [167] and 19.6 ± 1.0 (for $\text{TaC}_{0.95}(\text{N},\text{O})_{0.02}$, porosity – 3 to 5%, 0.5 N load) [168]; hardness HK , GPa is 18.0 [165] and 19.1 [387]. The hardness of $\text{TaC}_{\sim 1.0}$ in Mohs scale is 9–10 [442, 841], and in Rockwell scale HRA it is 82 kgf mm^{-2} (0.80 GPa) [37, 171], $\sim 88 \text{ kgf mm}^{-2}$ (~ 0.86 GPa) [392] and 89 kgf mm^{-2} (0.87 GPa) [388]. The variations of hardnesses HV/HK and microhardness $H\mu$ with carbon content within the homogeneity range of TaC_{1-x} and the orientation of indenter for the (100) surface of single crystal $\text{TaC}_{0.83}$ and $\text{TaC}_{0.96}$ are demonstrated in Fig. 2.19. According to Rowcliffe and Warren [381], a phase change occurs at hardness impressions made in TaC_{1-x} compositions in the interval from $\sim \text{TaC}_{0.75}$ to $\text{TaC}_{0.83}$, the maximal hardness in the Ta–C system, $\sim 37\text{--}51$ GPa (HK scale, 1 N load) is corresponding to composition $\text{TaC}_{0.83 \pm 0.01}$. The variation of hardness HV of near-stoichiometric tantalum monocarbide TaC_{1-x} with temperature based on several resources is presented in Fig. 2.20. In general, the exponential temperature dependency of hardness for TaC_{1-x} materials in the temperature range from 0 to 540 °C can be given by the following approximate relationship [16, 612–614]:

$$HV = 17.7 \exp[-(6.75 \times 10^{-4})t], \quad (2.52)$$

where HV is Vickers hardness, GPa and t is temperature, °C. Nino et al. [721] revealed that spark-plasma sintered $\text{TaC}_{\sim 1.0}$ materials over the range of grain sizes from 3 to 26 μm did not conform Hall-Petch type relationship. The hardness HV of

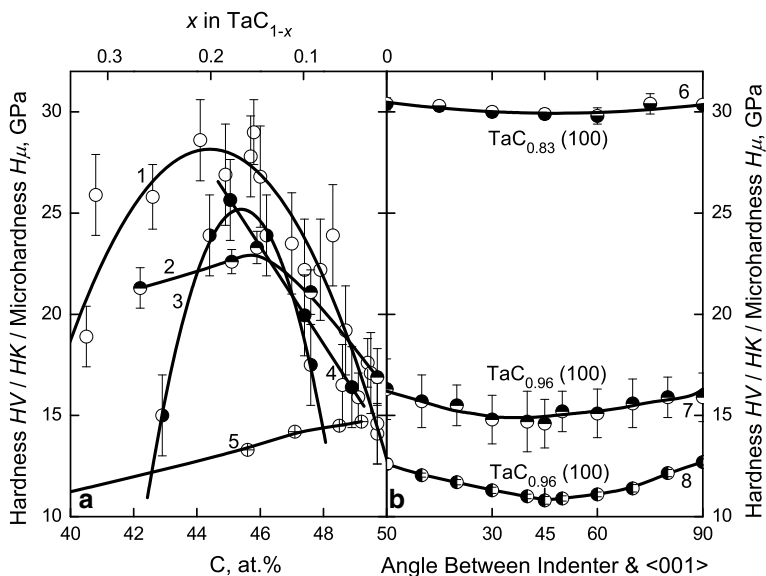


Fig. 2.19 Variations of the hardnesses HV (1, 5–6, 8) and HK (3–4, 7) and microhardness $H\mu$ (2) at room temperature of tantalum monocarbide TaC_{1-x} : (a) with deviation from the stoichiometry within the homogeneity range (1 – produced by gas carburization and hot-pressing methods, 200 N load [23, 332, 333]; 2 – hot-pressed and annealed in vacuum, 6–10% porosity, 0.5 N load [326, 666]; 3 – materials carburized in propane, 1 N load [110, 380, 527]; 4 – carburized by solid-state diffusion saturation, mean grain size – 10 μm , 1 N load [187, 380, 527]; 5 – [109]) and (b) with indenter orientation (angle between indenter axis and <001> direction) on the (100) surface of single crystal materials grown by floating-zone processes (6 – $TaC_{0.83}$, 2 N load [169, 170]; 7 – $TaC_{0.96}$, 1 N load [154, 155]; 8 – $TaC_{0.96}$, 2 N load [154, 155])

produced by gas carburization stoichiometric tantalum semicarbide $Ta_{-2.0}C$ at room temperature is ~ 13.3 GPa [23]; for sintered α - $Ta_{2+x}C$ Kotelnikov et al. [16] and Andrievskii and Spivak [41] recommended the value of 16.8 ± 1.6 GPa (0.3 N load), though Stern [605] and Ellinger [43] reported for hardnesses HV and HK much lower value of ~ 9.8 GPa. The data on hardness HK of tantalum monocarbide single crystals and microhardness $H\mu$ of various tantalum semicarbide and monocarbide compositions are listed in Tables 2.11 and 2.12. The mechanical properties of nanostructured TaC_{1-x} (99.5% purity), including its hardness HV , are presented in Table 2.13.

On the basis of several sources the variations of ultimate tensile σ_t and flexural (bending) σ_f strengths of tantalum monocarbide TaC_{1-x} with carbon content, temperature and mean grain size are shown in Figs. 2.21 and 2.22. The relationship $\sigma_f/\sigma_t \approx 2$ can be recommended for general estimations of the strength characteristics of TaC_{1-x} materials [42, 110, 615]. At room temperature the ultimate compressive strength for sintered (mean grain size – 5 to 20 μm , porosity – 5%) $TaC_{0.99}$ is evaluated as 1.75 GPa (at strain rate $3.7 \times 10^{-3} s^{-1}$) [1] and for sintered $TaC_{-1.0}$ – 0.84 GPa (corrected for porosity) [663]; the values of transverse rupture strength of

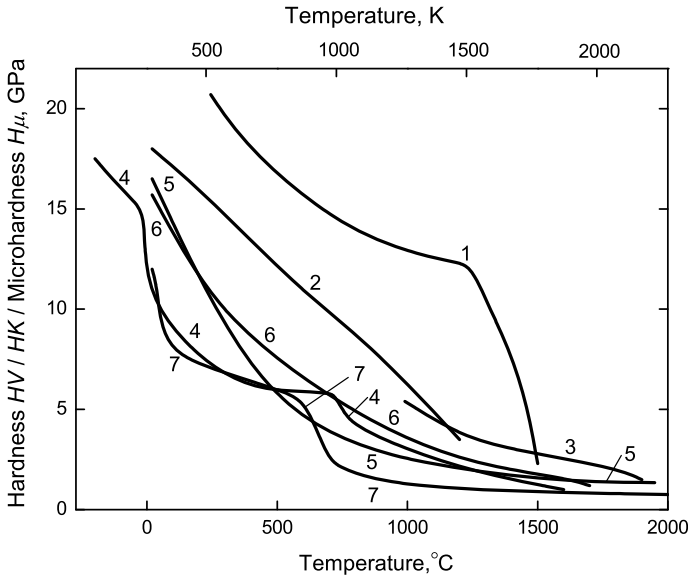


Fig. 2.20 Variation of hardnesses HV (2, 4–5, 7), HK (3) and microhardness $H\mu$ (1, 6) with temperature for TaC_{1-x} materials with various deviations from the stoichiometry based on several resources: 1 – single crystal (prepared by floating-zone process) $TaC_{0.83}$ (100), along the $\langle 001 \rangle$ direction, 2 N load [169, 170, 517]; 2 – sintered with temporary metallic binder (in high vacuum) $TaC_{-1.0}$, 3 N load [842]; 3 – arc-cast, 9.8 N load [517, 520]; 4 – sintered in vacuum $TaC_{0.95}$, 1 N load [42]; 5 – hot-pressed [1]; 6 – hot-pressed $TaC_{-1.0}$, porosity – 8%, 0.6–0.8 N load [425]; 7 – sintered [216] (when it is not indicated specially, data given are for quasi-stoichiometric composition)

spark-plasma sintered $TaC_{-1.0}$ (mean grain size – 4–9 μm , porosity 3–8%), measured by applying pressure through a ball-shaped indenter onto the disc-shaped samples, vary from 336 to 372 MPa [724]. The near-stoichiometric monocarbide TaC_{1-x} materials exhibit average fracture toughness K_{IC} of 5.6 ± 1.8 [704, 762], 3.8 ± 0.4 [721], 3.1 [771] and 2.7 ± 0.3 MPa $m^{1/2}$ [729] – for spark-plasma sintered materials, 5.3 ± 0.7 [34], 4.1 [892] and 3.7 ± 0.2 MPa $m^{1/2}$ [728] – for hot-pressed materials and 3.2 MPa $m^{1/2}$ – for hot isostatically pressed materials [398]. The fracture toughness was found to decrease with decreasing carbon content within the homogeneity range, as for $TaC_{0.8-0.9}$ compositions it was 3.8 ± 0.1 (for hot-pressed materials) [34] and 3.4 ± 0.9 MPa $m^{1/2}$ (for vacuum plasma sprayed materials) [181]; however, the opposite trend was revealed for materials prepared by hot-isostatic pressing, as for the same compositions K_{IC} increased up to 4.7 MPa $m^{1/2}$ [398]. For 99.5% purity nanostructured TaC_{1-x} with mean grain size in the range of 30–180 nm K_{IC} increases with decreasing the values of porosity and mean grain size (see Table 2.13). The exceptionally high values of fracture toughness were reported for two-phase carbide compositions: hot-pressed $TaC_{-0.6}$ materials containing ~80% $\zeta-Ta_4C_{3-x}$, $K_{IC} = 12.7 \pm 0.7$ MPa $m^{1/2}$ [34] and $TaC_{-0.7}$ materials,

Table 2.11 Microhardness $H\mu$, of tantalum monocarbide TaC_{1-x} ($0 < x \leq 0.17$) single crystals at room temperature (1 N load)

Surface	Indenter diagonal direction	Microhardness $H\mu$, GPa	References
		$x \approx 0$	
(001)	<001>	14.2 ± 0.5	[1, 159]
	<100>	16.2	[838, 839]
	<110>	14.7	[838, 839]
	< $\bar{1}10$ >	12.8 ± 0.5	[1, 159]
	–	24.0 ± 0.5	[1, 160]
	–	22.1 ± 0.5^a	[1, 160]
(110)	–	20.2 ± 0.5	[1, 160]
	–	19.1 ± 0.5^a	[1, 160]
(111)	< $\bar{1}\bar{1}0$ >	13.1 ± 0.5	[1, 159]
	< $\bar{1}\bar{1}\bar{2}$ >	14.9 ± 0.5	[1, 159]
	–	19.1 ± 0.5	[1, 160]
	–	18.4 ± 0.5^a	[1, 160]
		$x = 0.01 - 0.04$	
(100)	<010>	14.9 ± 0.5	[381]
		$x = 0.04$	
(001)	<100>	16.3 ± 0.9^b	[154, 155]
		12.6 ± 0.3^c	[154, 155]
	<010>	16.1 ± 0.5^b	[154, 155]
		10.8 ± 0.2^c	[154, 155]
	<110>	14.4 ± 0.5^b	[154, 155]
		12.7 ± 0.2^c	[154, 155]
(100)	<010>	15.2 ± 1.0^b	[381]
		$x = 0.17$	
(100)	<001>	30.4 ± 0.3^c	[169, 170]
	<010>	$\sim 38^b$	[381]
	<010>	30.4 ± 0.3^c	[169, 170]
	<011>	29.9 ± 0.3^c	[169, 170]

^aAnnealed at 2000 °C^bKnoop measurement (HK)^c2 N load

also containing lamellar ζ -phase, $K_{IC} = (11.9\text{--}13.8) \pm (0.8\text{--}0.9)$ MPa $\text{m}^{1/2}$ [523]. The stoichiometric semicarbide Ta_2C formed by hot-isostatic pressing was found to have K_{IC} of 9.7 ± 0.8 MPa $\text{m}^{1/2}$ [406]; for the spark plasma sintered semicarbide materials $K_{IC} = (4.8\text{--}6.4) \pm (0.6\text{--}0.7)$ MPa $\text{m}^{1/2}$ [405]. The mechanical properties, including hardness HV/HK , flexural strength σ_f and fracture toughness K_{IC} , of tantalum semicarbide Ta_{2+x}C materials prepared by different methods are given in Table 2.14. The ductile-to-brittle transition temperature of near-stoichiometric TaC_{1-x} is approximately half its melting point [178]; the reported values for the transition temperature of phases with various deviations from the stoichiometry are listed in Table 2.15. Tantalum semicarbide $\alpha\text{-Ta}_{2+x}\text{C}$ is brittle at room temperature but much more ductile than TaC_{1-x} in the range of temperatures around 1900 °C [189, 517, 524]. For detailed data on the slip systems in tantalum carbide phases

Table 2.12 Microhardness $H\mu$ of the various compositions of tantalum carbide phases at room temperature

Composition	Microhardness $H\mu$, GPa	Remarks	References
Ta ₂ C	~18	0.5 N load, physically vapour deposited (Ta in the presence of C ₂ H ₂) coatings	[400]
	15.5 ± 0.7 ^a	Hot isostatically pressed	[406]
	16.8 ± 1.6	0.3 N load, sintered	[37, 215]
	12.0	Sintered	[1, 161]
	9.4	–	[109, 517]
TaC _{0.73}	21.7 ± 1.0	0.5 N load, sintered in vacuum, contents: O – 0.12%, N – 0.06%	[1, 37]
TaC _{0.80}	~30	–	[42, 332]
	20.0 ± 0.5	9.8 N load, hot-pressed, mean grain size – 5.8 ± 2.4 μm, porosity – 3.3%	[34]
TaC _{0.8–0.9}	25.0 ± 7.2 ^b	0.5 N load, vacuum plasma sprayed, mean grain size – 60-90 nm	[181]
TaC _{0.82}	23.1 ± 0.6	0.5 N load, sintered in vacuum, contents: O – 0.12%, N – 0.02%	[1, 37]
TaC _{0.83}	29.4	0.25 N load, materials carburized in propane (maximal hardness revealed within the homogeneity range)	[110]
	23.5	1 N load, materials carburized in propane (maximal hardness revealed within the homogeneity range)	[110]
TaC _{0.84}	13.3	–	[109, 517]
TaC _{0.85}	23.8 ± 0.8	0.5 N load, sintered in vacuum, contents: O – 0.09%, N – 0.04%	[37]
TaC _{0.89}	14.2	–	[109, 517]
TaC _{0.90}	18.0 ± 0.4	9.8 N load, hot-pressed, mean grain size – 6.4 ± 3.7 μm, porosity – 3.5%	[34]
TaC _{0.91}	22.4 ^a	0.5 N load, physically vapour deposited (Ta in the presence of C ₂ H ₂) coatings	[400]
	21.5 ± 1.1	0.5 N load, sintered in vacuum, contents: O – 0.14%, N – 0.06%	[1, 37]
TaC _{0.93}	24.3 ^a	0.5 N load, physically vapour deposited (Ta in the presence of C ₂ H ₂) coatings	[400]
	15.1 ± 0.7	0.2-1.5 N load, hot-pressed and annealed at 1800 °C for 3 h, porosity – 20%, content: non-combined C – 0.3%	[171, 379]
TaC _{0.94}	15.7 ± 0.5	–	[90]
TaC _{0.95}	19.6 ± 1.0	0.5 N load, hot-pressed, porosity – 3-5%, contents: O + N – 0.02%	[168]
	10.5	1.0 N load, sintered in vacuum	[1, 42]

(continued)

Table 2.12 (continued)

Composition	Microhardness $H\mu$, GPa	Remarks	References
TaC _{0.96}	16.8	1.0 N load, sintered in vacuum, annealed, mean grain size – 15 μm , porosity – 4.5%, contents: non-combined C – 0.05%, O – 0.46%, N – 0.02%	[1, 41]
TaC _{0.97}	17.6 ^a	0.5 N load, physically vapour deposited (Ta in the presence of C ₂ H ₂) coatings	[400]
TaC _{0.98}	14.7	–	[109, 517]
	19.25	Deposited from gas phase	[163]
	18.5 \pm 0.8	–	[1, 167]
	18.0 ^a	Hot-pressed, mean grain size – 0.2 μm	[162]
	15.2 \pm 0.7	Pyrolytic materials	[610]
TaC _{0.99}	13.0 ^a	Hot-pressed, mean grain size – 4.0 μm	[162]
	17.2 \pm 1.4	1.0 N load, sintered in vacuum, contents: non-combined C – 0.12%, O – 0.11%, N – 0.03%	[1, 37]
	14.3 ^c	1.0 N load, sintered in vacuum, annealed, mean grain size – 12 μm , porosity – 4%, contents: non-combined C – 0.08%, O – 0.05%, N – 0.005%	[1, 41]
TaC _{~1.0}	25.0	–	[115, 544, 550, 551]
	24.5	DFT-computed theoretical value	[435]
	24.2 ^a	The highest value for materials sintered in vacuum (with fugitive binder), porosity – 7.5%	[387]
	21.3	DFT-computed theoretical value	[618]
	21.4	DFT-computed theoretical value	[844]
	19.9	Calculated on the basis of Simunek-Vackar's model	[383–385]
	19.5	–	[67]
	19.1 ^{a,d}	0.5 N load	[61, 387]
	18.9 \pm 3.4	20-30 N load, spark-plasma sintered, porosity – 5.4 \pm 0.7%, mean grain size – 4.5 \pm 0.9 μm	[704, 762]
	18.8 ^a	0.05 N load, hot-pressed, porosity – 5%	[335]
	18.0 ^a	Hot-pressed from ultra-dispersed powder	[1, 165]
	18.0	Hard coatings	[556, 557]
	18.0	3 N load, sintered with temporary metallic binder in high vacuum	[842]
	17.9	Sintered	[545, 548]
	17.6–19.6	0.2-0.5 N load	[67, 68]
	17.6–17.8	0.2 N load	[166, 174]
	17.6	0.5 N load	[600]
	17.0 \pm 1.0	0.5 N load, contents: O – 0.05%, N – 0.05%	[1, 164]
	17.0	Calculated on the basis of modified Hall-Petch relationship theory for nanocrystals	[324]
16.7 ^e	Deduced from the dislocation data measured by X-ray diffraction profile analysis	[558]	
16.7 ^f	0.2–10 N load, hot-pressed, porosity < 5%	[60, 535]	

(continued)

Table 2.12 (continued)

Composition	Microhardness $H\mu$, GPa	Remarks	References
	16.1 ^e	0.04–0.12 N load (extrapolated to 0.01 N load), coating ion-sputtered on a glass substrate, thickness – ~0.2 μm	[324, 558]
	16.0	1.2 N load	[61]
	15.7 ^h	On the basis of several published sources (extrapolated to defectless theoretical stoichiometry)	[109, 324, 558]
	~15.7 ⁱ	0.3 N load	[16, 61]
	15.5	0.5 N load	[67]
	15.5 \pm 0.6	2 N load, spark-plasma sintered, porosity – ~7%	[771]
	15.2	–	[840]
	(15.1–17.6) \pm (1.0–1.7)	–	[35, 123, 171, 334]
	~15.0	1 N load, single-crystal materials	[381, 663]
	14.7	Calculated on the basis of Xue's model	[383, 386]
	14.6 ^j	0.5–3.9 N load, hot filament chemical vapour deposited films on metal Ta substrate, thickness – 8 μm	[401]
	14.1 \pm 0.2	5 N load, hot-pressed, porosity – 6%, mean grain size – 3 μm	[402]
	(14–19) \pm (1–3)	Pulsed laser ablation deposited thin films on Ti substrate, thickness – 0.24–0.25 μm , approximate grain size – 10–100 nm	[611]
	~14.0	–	[42, 332]
	13.7–21.2 ^k	0–0.3 N load, chemical vapour deposited coatings, thickness 60–80 μm	[409]
	13.7 ^l	–	[403]
	13.5 \pm 0.2	9.8 N load, hot-pressed, mean grain size – 7.7 \pm 4.5 μm , porosity – 3%	[34]

^aKnoop measurement (*HK*)^bAverage for three directions^c3.8 GPa – at 1000 $^{\circ}\text{C}$ ^dProbably contaminated by W^eFor ion-sputtered coating the measured dislocation density $\rho = 1.65 \times 10^{12} \text{ cm}^{-2}$ ^fDetermined in accordance with the formula: $H\mu = 18.18P/d^2$, where P is the load on the indenter, N and d is the diagonal of the indentation, μm ; the values of other micromechanical characteristics: microbrittleness $\gamma_{\mu} = (D^2 - d^2)/d^2 = 0.55$, where D is the average size of the damageability zone, μm and brittle microstrength $\sigma_{\mu} = P/D^2 = 5.7 \text{ GPa}$ [535]^gMeasured using a Vickers diamond microindentation hardness tester^hRecommended for bulk samplesⁱ8.0 GPa – at 730 $^{\circ}\text{C}$, 4.5 – at 1230 $^{\circ}\text{C}$ [16, 166]^jMeasured using a Wilson microhardness tester^kNanoindentation with a typical probe depth of 1 μm ^lDiamond pyramid hardness measurement (*DPH*)

Table 2.13 Mechanical properties of nanostructured tantalum monocarbide TaC_{1-x} (99.5% purity)^a at room temperature [172, 203]

Relative density, %	Mean grain size, nm	Hardness HV^b , GPa	Fracture toughness K_{IC}^c , $\text{MPa m}^{1/2}$
88	184	13	3.9 ± 0.3
95	72	14	4.1 ± 0.4
96	33	21–22	5.1–6.8

^aManufactured by high-frequency induction heated sintering method

^b196 N load

^cEstimated according to $K_{IC} = 0.016P/C^{3/2}(E/HV)^{1/2}$, where P is the indentation load, C is the trace length of the crack measured from the centre of indentation and E is Young's modulus

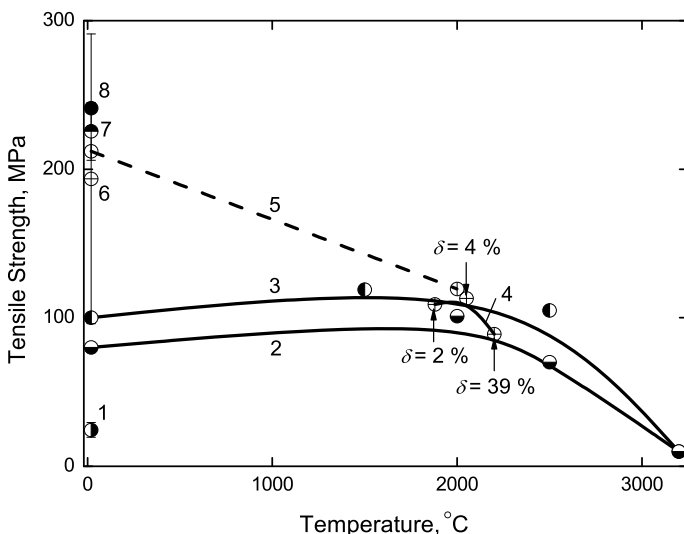


Fig. 2.21 Variations of tensile strength of near-stoichiometric tantalum monocarbide TaC_{1-x} with temperature on the basis of several sources: 1 – [35, 61]; 2 – sintered, 30% porosity [1, 173]; 3 – sintered, 20% porosity [1, 173]; 4 – carburized by solid-state diffusion saturation, mean grain size – $10 \mu\text{m}$ [123, 187, 389]; 5 – [61, 174]; 6 – hot-pressed $\text{TaC}_{0.93}$, 2–6% porosity [392, 396]; 7 – [61, 102]; 8 – hot-pressed $\text{TaC}_{0.95}$, mean grain size – $13 \mu\text{m}$, porosity – 7% [396, 540, 560] (elongation at rupture δ is indicated for curve 4)

structures *see* Sect. 2.1. The values of prolonged strength (creep resistance) are of great importance for the evaluation of operational time of components in the engineering practice. The examples of intermediate-temperature creep characteristics of hot isostatically pressed $\text{TaC}_{0.99}$ (porosity – 3%, mean grain size – $57 \mu\text{m}$) [182] are demonstrated in Fig. 2.23, high- and ultra-high temperature creep characteristics of various compositions TaC_{1-x} – in Fig. 2.24; steady-state creep activation energies Q and exponent constants n of TaC_{1-x} phases are listed in Table 2.16. The high-temperature creep mechanisms in tantalum semicarbide differ considerably from those in the monocarbide phase. Semicarbide $\alpha\text{-Ta}_{2+x}\text{C}$ phase

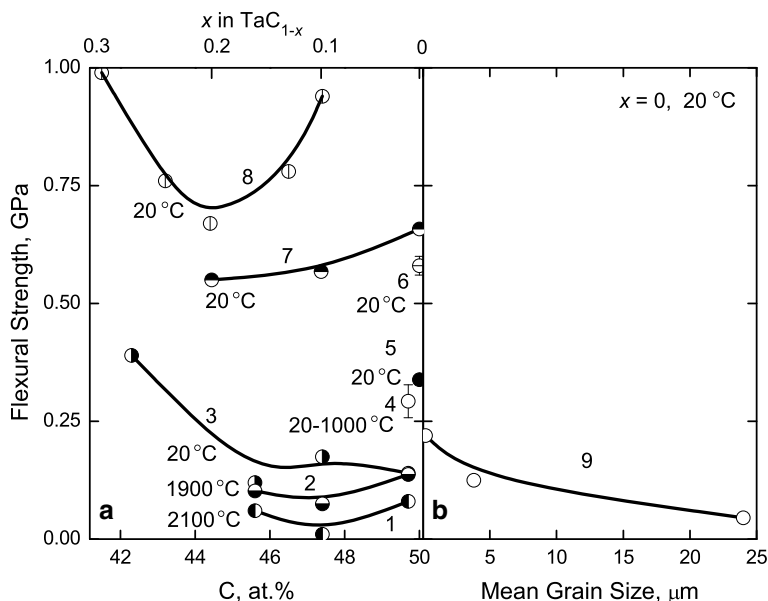


Fig. 2.22 Variations of flexural (bending) strength of TaC_{1-x} materials on the basis of several sources: (a) with deviation from the stoichiometry and temperature (1-3 – sintered [175, 737]; 4 – hot-pressed, 7–20% porosity, non-combined C – 0.03-0.07%, 3-point bending scheme [394, 395]; 5 – sintered at 2300 °C, mean grain size $\sim 2 \mu\text{m}$, 2.5% porosity [176]; 6 – hot-pressed, mean grain size $- 4.0 \pm 0.8 \mu\text{m}$, 6% porosity, 4-point bending scheme [728]; 7 – hot-pressed, mean grain size $- 7 \pm 3 \mu\text{m}$, 3% porosity [34]; 8 – materials carburized in propane, 3-point bending scheme [110, 380, 527]) and (b) with mean grain size (9 – sintered in H_2 at 2700 °C [177])

exhibits significantly more plasticity compared to TaC_{1-x} . The graphic stress-strain diagrams (curves) for different tantalum carbide materials at 1930 and 2160 °C are given in Fig. 2.25. Approximately, the following main dominating creep mechanisms can be established in some overlapping parametric ranges for tantalum monocarbide TaC_{1-x} materials with certain changes within the homogeneity range [183]:

vacancy-diffusional (or Nabarro-Herring) mechanism controlled by the bulk diffusion of metal in carbide (at temperatures from 2400 to 3000 °C and applied stresses from 8 to 70 MPa, with $Q \approx 600\text{--}640 \text{ kJ mol}^{-1}$ and $n = 1$);

dislocation-diffusional mechanism controlled by the bulk diffusion of metal in carbide (at 2500–3000 °C and 20–70 MPa, with $Q \approx 600\text{--}670 \text{ kJ mol}^{-1}$ and $n \approx 3.0\text{--}4.5$);

viscous dislocation sliding mechanism controlled by the bulk diffusion of carbon in carbide (at 1600–2200 °C and 50–200 MPa, with $Q \approx 400\text{--}500 \text{ kJ mol}^{-1}$ and $n \approx 3.5\text{--}5.0$).

At room temperature the values of Young's E , Coulomb's (shear) G and bulk (compression) K moduli, volume compressibility κ and Poisson's ratio ν of sub- and

Table 2.14 Mechanical properties of tantalum semicarbide $Ta_{2+x}C$ materials prepared by different manufacturing methods at room temperature [398, 405, 406]

Relative density, %	Mean grain size, μm	Hardness HV/HK , GPa	Flexural strength σ_f , MPa	Fracture toughness K_{IC} , $\text{MPa m}^{1/2}$	Young's modulus E , GPa
95.8 ^{a,b}	1.3	11.7 \pm 0.8 ^c	461 \pm 55 ^d	4.8 \pm 0.7 ^e	489 \pm 11 ^f
95.9 ^{a,g}	3.7	11.6 \pm 0.8 ^c	548 \pm 52 ^d	6.0 \pm 0.6 ^e	484 \pm 12 ^f
97.5 ^{a,g}	18	11.8 \pm 0.9 ^c	507 \pm 45 ^d	6.4 \pm 0.7 ^e	493 \pm 11 ^f
>98 ^h	–	15.5 \pm 0.7 ⁱ	550 \pm 50	(9.3–9.7) \pm 0.8 ^j	–

^aManufactured by spark plasma sintering method^bOpen porosity – 0.3% (density – 14.42 g cm^{-3})^cVickers hardness HV , 49 N load^d3-point bending scheme (fracture direction – normal to the pressing direction)^eEstimated according to the equation $K_{IC} = AP/C^{3/2}(E/HV)^{1/2}$, where A is a material-independent constant, P is the indentation load, C is the trace length of the crack measured from the centre of indentation and E is Young's modulus^fCalculated by the stress-strain curves recorded from tensile surfaces of the bending samples^gNo open porosity (density – 14.43–14.66 g cm^{-3})^hManufactured by HIP-reaction sintering in a metal Ti containerⁱKnoop microhardness^jMeasured by conventional single edge notched beam (SENB) method**Table 2.15** Ductile-to-brittle transition temperatures of tantalum monocarbide phases $TaC_{1-x}^{a,b}$

Composition	Temperature, K ($^{\circ}\text{C}$)	Characteristics	References
$TaC_{-1.0}$	2000 (1730) ^c	Hot-pressed, annealed (porosity – ~10%)	[42, 178]
	2020 (1750)	Carburized by solid-state diffusion saturation	[187, 389]
	2125 \pm 100 (1850 \pm 100)	On the basis of several sources	[517, 519]
	2300 (2030)	Carburized by solid-state diffusion saturation	[42]
$TaC_{0.98}$	2100–2200 (1830–1930)	Hot-pressed, annealed (porosity – 5–10%)	[175, 179]
	1170 (800)	Carburized, polycrystalline (bending scheme)	[437–439]
$TaC_{0.95}$	1550 (1280) ^d	Hot-pressed (mean grain size – 13 μm , porosity – 7%)	[540]
$TaC_{0.90}$	2025–2125 (1750–1850)	Hot-pressed, annealed (porosity – 5–10%)	[175, 179]
$TaC_{0.78}$	~1600 (1330)	–	[179, 180]
	1870 (1600)	–	[518]

^aFor near-stoichiometric TaC_{1-x} the following average values were estimated: Peierls stress $\tau_p = 4.0$ GPa, shear modulus – Peierls stress ratio $\tau_p/G = 0.021$ and slip activation energy barrier $q = 1.7$ eV [562]^bTransition temperature decreases almost linearly with the value of x growing [107, 175, 380]^cIn 4-point bending scheme only ~0.1% strain could be achieved prior to failure at 2000 $^{\circ}\text{C}$ ^dAt strain rates $\leq 8 \times 10^{-4} \text{ s}^{-1}$, permanent strains >5% achieved at 1280 $^{\circ}\text{C}$ and up to 40% at ≥ 1640 $^{\circ}\text{C}$

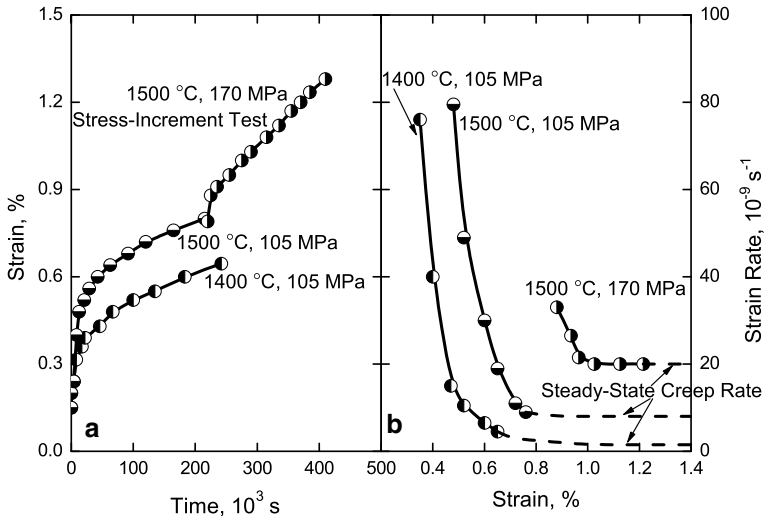


Fig. 2.23 Intermediate-temperature creep characteristics of hot isostatically pressed tantalum monocarbide $\text{TaC}_{0.99}$ (porosity – 3%, mean grain size – $57 \mu\text{m}$) at 1400–1500 °C and 105–170 MPa: (a) strain as a function of time and (b) strain rate as a function of strain (extrapolation to assumed values of steady-state creep rates is shown) [182]

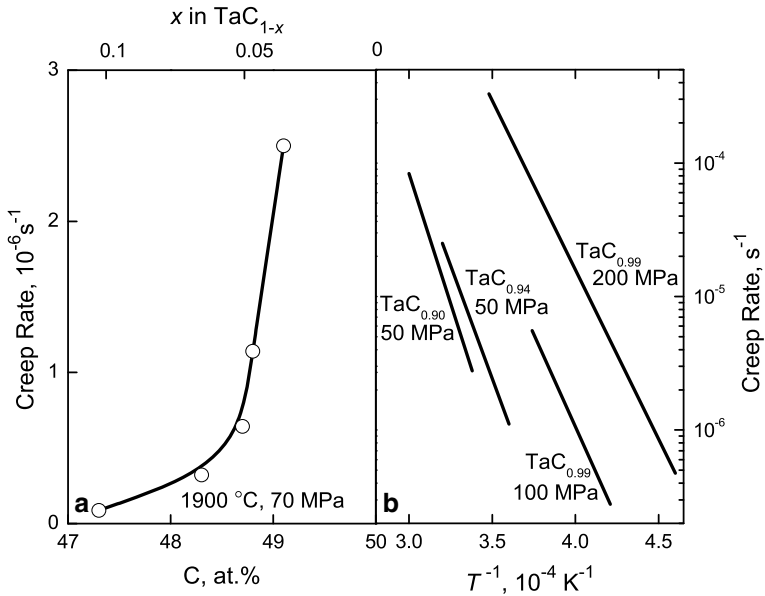


Fig. 2.24 High- and ultra-high temperature steady-state creep rate variations of tantalum monocarbide TaC_{1-x} materials: (a) – with deviation from the stoichiometry (materials carburized by solid-state diffusion saturation, mean grain size – $10 \mu\text{m}$ [187]) and (b) – with temperature ($\text{TaC}_{0.90}$ sintered and annealed in high-purity He atmosphere, porosity – 7%, mean grain size – $30 \mu\text{m}$ [186]; $\text{TaC}_{0.94}$ sintered in vacuum, porosity – $\leq 3\%$, mean grain size – $27 \mu\text{m}$, contents O + N – 0.13% [10]; $\text{TaC}_{0.99}$ sintered, porosity – 3%, mean grain size – $5 \mu\text{m}$, contents: non-combined C – 0.20%, O – 0.18%, N – 0.01%, W – 0.10% [422])

Table 2.16 Formal creep characteristics (activation energy Q , stress exponent constant n) of tantalum monocarbide phases TaC_{1-x} at various temperature and applied stress ranges

Composition	Load type ^a	Temperature range, °C	Applied stress range, MPa	Activation energy ^b , Q , kJ mol ⁻¹	Exponent constant ^b , n	References
TaC _{0.99-1.0} ^c	C	2350–2700	8–70	~610–630	1	[183]
TaC _{0.99} ^d	C	1400–1500	105–170	420	2	[182]
TaC _{0.99} ^e	C	2000–2400	60–100	485	3.5	[422–424]
	C	2000–2400	100–200	485	5	[422–424]
	C	2400–2600	100–200	615–630	4.2	[422–424]
TaC _{0.98}	F	1200–2200	–	560–600	–	[437, 438]
TaC _{0.97} ^f	F	2500–3000	0–15	610	1	[184]
TaC _{0.97} ^g	C	2700–3000	20–30	665	3	[534]
TaC _{0.95} ^h	F	2500–2850	7–12	610 ± 30	1	[168]
TaC _{0.95} ⁱ	C	1280–1640	–	~375	~13	[539, 540]
	C	1460–1810	–	400	4.5	[540, 683]
TaC _{0.94} ^j	C	2500–3050	50	800	–	[10]
TaC _{0.90} ^k	C	2550–3100	50	770	–	[185, 186]
TaC _{0.85-0.98} ^l	T	1950–2100	45–70	710	2–4	[187, 426]
TaC _{0.83} ^m	H	1200–1500	–	465	4.3	[169, 170]

^aDenoted: T – tension, F – flexure (bending), C – compression, H – hot hardness (measurement)

^bFor Q and n see the Eq. (I-3.17) and consideration in [683]

^cSintered materials, for TaC_{0.99} (porosity – 2-5%, mean grain size – 4-16 μm) $Q = 632$ kJ mol⁻², for TaC_{-1.0} (mean grain size – 10 μm) $Q = 607$ kJ mol⁻² and for TaC_{-1.0} (mean grain size – 16 μm) $Q = 615$ kJ mol⁻²

^dHot isostatically pressed (HIP), porosity – 3%, mean grain size – 57 μm

^eSintered, porosity – 3%, mean grain size – 5 μm, contents: non-combined C – 0.20%, O – 0.18%, N – 0.01%, W – 0.10%

^fHot-pressed, porosity – 3-5%

^gCharacteristics were determined for κ -creep (during hot-pressing densification of submicrometer powders) using Kovalchenko's equation for inhomogeneous deformation of viscous porous body:

$$\Delta X_n(\rho) = \int_{\rho_0}^{\rho} \frac{\rho^{\frac{5n+1}{2}}}{(1-\rho)^{\frac{n+1}{2}}} d\rho = B(P + P_L)^n \tau, \text{ where } \Delta X_n(\rho) \text{ is the difference between the primitives of}$$

the functions $X_n(\rho)$ taking for the current ρ and initial ρ_0 values of relative density, P is the applied pressure, P_L is the Laplace pressure, B and n are corresponding to those in Eq. (I-3.17)

^hHot-pressed, porosity – 3-5%, mean grain size – 33 μm, contents: (O + N)/Ta ratio is 0.02

ⁱHot-pressed in vacuum and annealed, porosity – 7%, mean grain size – 13 μm, characteristics were determined for the mechanical equation of state at the yield stress $d\gamma/dt = A(\tau_{0.2}/G)^n \exp(-Q/RT)$, where $d\gamma/dt$ is the plastic shear strain rate, which equals the true plastic strain rate divided by the Schmid factor; $\tau_{0.2}$ is the critical resolved shear stress, corresponding to 0.2% proof stress; G is Coulomb's (shear) modulus; R is the gas constant and T is absolute temperature, K

^jSintered in vacuum, porosity – ≤ 3%, mean grain size – 27 μm, contents: O + N – 0.13%

^kSintered, porosity – 7%, mean grain size – 30 μm

^lCarburized by solid-state diffusion saturation, mean grain size – 10 μm

^mSingle crystal prepared by floating-zone process, plane direction – (100) <001>

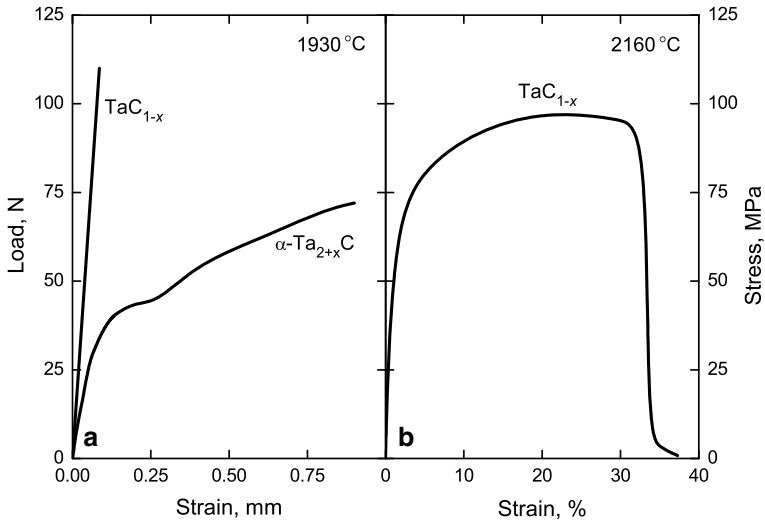


Fig. 2.25 The examples of stress-strain diagrams (curves) of tantalum carbides materials at high temperatures: (a) mid-point deflection at 4-point flexural (bending) scheme, 1930 °C, semicarbide $\alpha-Ta_{2+x}C$ and monocarbide TaC_{1-x} , prepared under similar conditions by hot isostatic pressing (HIP) [189] and (b) tensile scheme (elongation to failure – 33%), 2160 °C, monocarbide TaC_{1-x} , prepared by carburization (solid-state diffusion saturation), mean grain size – 10 μm [389, 517]

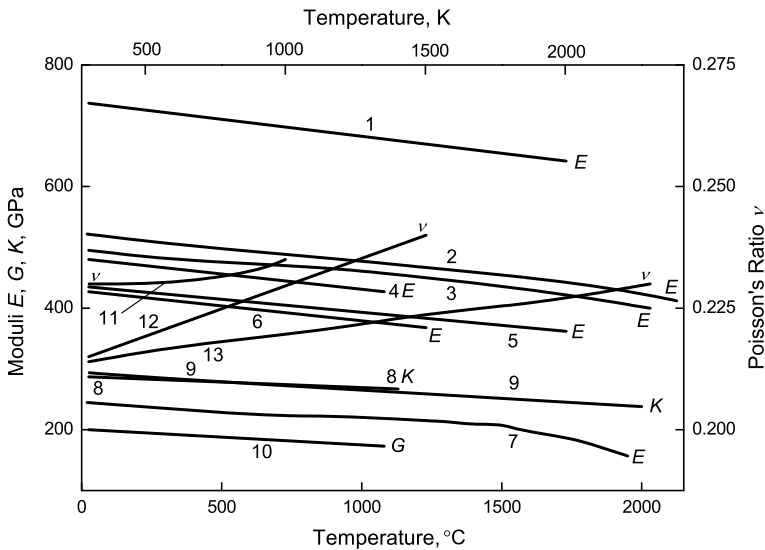


Fig. 2.26 Variations of elastic properties (1-7 – Young’s modulus E , 8-9 – bulk (compression) modulus K , 10 – Coulomb’s (shear) modulus G and 11-13 – Poisson’s ratio ν) of near-stoichiometric tantalum carbide phases with temperature: 1 – monocarbide TaC_{1-x} and 5 – semicarbide $\alpha-Ta_{2+x}C$ (recommended by Kotelnikov et al. [16]); 2 – $TaC_{0.99}$ (measured by Bukatov et al. [50]); 3 and 13 – $TaC_{0.95}$ with 3% porosity and contents $N = 0.27\%$ (given by Andrievskii and Spivak [41]); 4, 6, 8, 10, 12 – $TaC_{0.99}$ with 1% (4, 8, 10), 7% (12) and 12% (6) porosity (measured and calculated by Jun and Shaffer [190]); 7 – $TaC_{-1.0}$ (calculated on the basis of hardness-elasticity relationship by Travushkin et al. [216]); 9 – $TaC_{-1.0}$ (theoretically calculated by Cao et al. [413]); 11 – $TaC_{-1.0}$ (theoretically calculated by Varshney et al. [414, 415])

near-stoichiometric tantalum monocarbide TaC_{1-x} materials lie within the areas: $E = 240\text{--}580$ GPa [1, 35, 37, 41, 42, 50, 60, 61, 68, 90, 115, 123, 427, 544], $G = 200\text{--}250$ GPa [41, 42, 60, 192, 397, 407, 427], $K = 220\text{--}400$ GPa [41, 42, 192, 397, 407, 408], $\kappa = 2.84\text{--}3.33$ TPa^{-1} [41, 42, 195, 336] and $\nu = 0.20\text{--}0.25$ [41, 42, 192, 338, 427], while for near-stoichiometric tantalum semicarbide $\text{Ta}_{2\pm x}\text{C}$ materials $E = 440\text{--}530$ GPa [16, 404, 405] (see also Table 2.14), and calculated on the basis of density-functional theory (DFT) for $\alpha\text{-Ta}_{2+x}\text{C}$: $G = 148$ GPa, $K = 267$ GPa [435], $K = 246$ GPa [428] and for $\beta\text{-Ta}_{2\pm x}\text{C}$: $K = 229$ GPa [428]; the experimentally measured velocities of ultrasonic waves propagated in tantalum monocarbide TaC_{1-x} phases are

for single crystal $\text{TaC}_{0.90}$ [191]:

longitudinal velocity (along $\langle 100 \rangle$) V_S , m s^{-1}	5880 ± 70 ,
transversal velocity (along $\langle 110 \rangle$ and $\langle 100 \rangle$) V_T , m s^{-1}	2320 ± 100 ,
longitudinal velocity (along $\langle 110 \rangle$) V_S , m s^{-1}	5020 ± 70 ,
transversal velocity (along $\langle 110 \rangle$) V_T , m s^{-1}	3760 ;

for hot-pressed $\text{TaC}_{0.98\pm 0.12}$ (porosity – $11.7 \pm 1.4\%$) [206]:

longitudinal velocity V_S , m s^{-1}	6232 ± 10 ,
transversal velocity V_T , m s^{-1}	3744 ± 13 ;

for $\text{TaC}_{\sim 1.0}$ [429] (summarized on the basis of several sources):

average velocity V_m , m s^{-1}	4720 ;
--	----------

and theoretically estimated sound velocities for stoichiometric tantalum monocarbide $\text{TaC}_{\sim 1.0}$ are

by *ab initio* calculations (for zero pressure):

longitudinal velocity V_S , m s^{-1}	6518 (0 K) [414], 5172 (~ 300 K) [414], 5200 [419], 6190 [618], 6607 [716];
transversal velocity V_T , m s^{-1}	3850 (0 K) [414], 3057 (~ 300 K) [414], 3170 [419], 3517 [618], 3954 [716];
average velocity V_m , m s^{-1}	3490 [419], 3910 [618], 4369 [716];

by LMTO (linearized method of “muffin-tin” orbitals) calculations [429]:

average velocity V_m , m s^{-1}	4480 ;
--	----------

by TBFP (three body force potential) modeling calculations [419]:

longitudinal velocity V_S , m s^{-1}	6240 ;
transversal velocity V_T , m s^{-1}	3740 ;
average velocity V_m , m s^{-1}	4130 .

The variations of the elastic properties of near-stoichiometric tantalum carbide phases with temperature are shown in Fig. 2.26, for TaC_{1-x} the average rate of decay of the elastic modulus with temperature $1/E_{298\text{K}} \times dE/dT = -1.5 \times 10^{-4} \text{ K}^{-1}$ [562]; the elastic properties (stiffness coefficients c_{ij} and moduli E , K and Poisson’s ratio ν) of various tantalum monocarbide TaC_{1-x} phases are listed in Table 2.17. The DFT-calculated stiffness coefficients c_{ij} for $\alpha\text{-Ta}_{2+x}\text{C}$ are $c_{11} = 479$, $c_{33} = 500$,

Table 2.17 Elastic properties (stiffness coefficients c_{11} , c_{12} and c_{44} , Young's modulus E , bulk (compression) modulus K , Poisson's ratio ν)^a of tantalum monocarbide TaC_{1-x} phases

Compo- sition	Stiffness coefficients c_{ij}			Young's modulus E , GPa	Bulk modulus K , GPa	Poisson's ratio ν	References
	c_{11} , GPa	c_{12} , GPa	c_{44} , GPa				
TaC _{0.75} ^b	579	172	116	380 ^c	308 ^c	–	[434]
TaC _{0.875} ^b	684	147	157	488 ^d	337 ^d	–	[434]
TaC _{0.90}	505 ^e	73 ^e	79 ^e	477 ^f	229 ^f	0.15 ^f	[115, 191]
	500 ^g	90 ^g	80 ^g	–	–	–	[208]
TaC _{0.95} ^h	–	–	–	303	–	–	[115, 212]
	320	84	65	–	–	–	[41]
TaC _{0.96} ⁱ	–	–	–	270	–	–	[396, 540]
TaC _{0.96} ^j	–	–	–	527 ± 10	–	–	[1]
TaC _{0.97}	610	210	230	529 ^f	370 ^f	0.26 ^f	[155]
	709 ^b	147 ^b	169 ^b	515 ^{b,j}	337 ^{b,j}	–	[434]
TaC _{0.98} ^k	–	–	–	567 ± 68 ^{l,m}	332 ± 29 ^{l,m}	0.215 ± 0.02 ^l	[206]
	–	–	–	–	345 ± 9 ⁿ	–	[198]
TaC _{0.99}	–	–	–	550 ± 10 ^{l,o}	–	–	[1, 554]
	–	–	–	552 ⁱ	317 ⁱ	0.21 ⁱ	[50, 432]
TaC _{~1.0}	631 ^{p,q}	168 ^{p,q}	–	560 ^{p,q,r}	329 ^{p,q,r}	0.21 ^{p,q}	[190]
	634 ^s	200 ^s	–	538 ^{l,t}	345 ^{l,t}	0.24 ^l	[192, 427]
TaC _{~1.0}	–	–	–	–	343	–	[536]
	347 ^s	110 ^s	–	294	188 ^f	0.24	[207]
TaC _{~1.0}	595 ^u	–	153 ^u	–	–	–	[193, 562]
	621 ^v	155 ^v	167 ^v	550 ^v	318 ^v	0.21 ^v	[193]
TaC _{~1.0}	–	–	–	–	365 ^w	–	[115, 193]
	880 ^w	156 ^w	410 ^w	–	398 ^w	–	[199]
TaC _{~1.0}	733 ^v	112 ^v	315 ^v	–	319 ^v	–	[199]
	–	–	–	–	342 ^x	–	[210]
TaC _{~1.0}	–	–	–	–	433 ± 7 ^y	–	[200]
	907 ^w	108 ^w	211 ^w	–	371 ^w	–	[200]
TaC _{~1.0}	723 ^v	106 ^v	177 ^v	–	310 ^v	–	[200]
	611 ^w	243 ^w	159 ^w	439 ^{w,z}	365 ^{w,z}	0.30 ^w	[201]
TaC _{~1.0}	466 ^{a1}	224 ^{a1}	121 ^{a1}	320 ^{a1}	305 ^{a1,a2}	0.33 ^{a1}	[201]
	463 ^{a3}	223 ^{a3}	121 ^{a3}	320 ^{a2,a3}	303 ^{a2,a3}	0.32 ^{a3}	[201]
TaC _{~1.0}	454 ^v	227 ^v	120 ^v	312 ^{v,a4}	302 ^{v,a4}	0.33 ^v	[201]
	550 ^{a5}	150 ^{a5}	190 ^{a5}	479	283	–	[208, 562]
TaC _{~1.0}	–	–	–	514 ^{a6,a7}	317 ^{a6,a7}	0.23 ^{a6}	[209]
	740 ^x	165 ^x	176 ^x	–	357 ^{x,a8}	–	[211]
TaC _{~1.0}	–	–	–	480	–	–	[212]
	641 ^w	146 ^w	156 ^w	470 ^{w,a9}	311 ^{w,a9}	0.24 ^w	[204]
TaC _{~1.0}	–	–	–	288 ^{b1}	–	–	[196]
	–	–	–	534 ^{b1}	–	–	[197]
TaC _{~1.0}	–	–	–	562 ^{b1}	–	–	[194]
	–	–	–	–	309 ^{b2}	–	[195]
TaC _{~1.0}	–	–	–	265–275 ^{b3}	–	–	[202]
	–	–	–	–	324 ^{b4}	–	[339, 430]
TaC _{~1.0}	–	–	–	–	330 ^{b5}	–	[359]
	–	–	–	285 ^{b1}	–	–	[61, 214, 215, 436, 843]
TaC _{~1.0}	–	–	–	314 ^{b1}	–	0.17 ^{b1}	[388]

(continued)

Table 2.17 (continued)

Composition	Stiffness coefficients c_{ij}			Young's modulus E , GPa	Bulk modulus K , GPa	Poisson's ratio ν	References
	c_{11} , GPa	c_{12} , GPa	c_{44} , GPa				
	562 ^{b6}	159 ^{b6}	146 ^{b6}	492 ^{b6,b7}	294 ^{b6,b7}	0.22 ^{b6}	[416]
	571 ^{b8,b9}	169 ^{b8,b9}	195 ^{b8,b9}	487 ^{b8,b9,c1}	303 ^{b8,b9,c1}	0.23 ^{b8,b9}	[414, 415]
	422 ^{b8,c2}	120 ^{b8,c2}	140 ^{b8,c2}	356 ^{b8,c2,c3}	221 ^{b8,c2,c3}	0.23 ^{b8,c2}	[414, 415]
	–	–	–	–	316 ^{c4}	–	[417]
	–	–	–	–	356 ^{c5}	–	[417]
	–	–	–	–	320 ^{b8}	–	[418]
	704 ^{b8}	110 ^{b8}	170 ^{b8}	519 ^{b8,c6}	308 ^{b8,c6}	0.22 ^{b8}	[420]
	547 ^{c7}	119 ^{c7}	159 ^{c7}	504 ^{c7,c8}	262 ^{c7,c8}	0.18 ^{c7}	[419]
	370 ^{b8}	110 ^{b8}	153 ^{b8}	320 ^{b8,c9}	197 ^{b8,c9}	0.23 ^{b8}	[419]
	558 ^b	146 ^b	180 ^b	470 ^{b,d1}	305 ^{b,d1}	0.24 ^b	[421]
	694 ^{d2}	127 ^{d2}	127 ^{d2}	655 ^{d2,d3}	318 ^{d2,d3}	0.15 ^{d2}	[410]
	–	–	–	–	321 ^{d4}	–	[429, 430]
	–	–	–	–	286 ^{d5}	–	[429]
	–	–	–	–	391 ^b	–	[431]
	–	–	–	–	401 ^{d6}	–	[431]
	–	–	–	–	321 ^{d7}	–	[433]
	737 ^b	141 ^b	175 ^b	–	340 ^{b,d8}	–	[434, 435]
	–	–	–	562 ^{d9}	–	–	[541]
	–	–	–	560	–	–	[552]
	–	–	–	290	–	–	[545]
	486 ^{e1}	115 ^{e1}	130 ^{e1}	375 ^{e1,e2}	238 ^{e1,e2}	0.23 ^{e1}	[561, 562]
	778 ^{e3}	128 ^{e3}	181 ^{e3}	563 ^{e3,e4}	344 ^{e3,e4}	0.227 ^{e3}	[617]
	–	–	–	530	–	–	[569]
	–	–	–	–	323	–	[616]
	562 ^b	159 ^b	146 ^b	492 ^{b,b7}	294 ^{b,b7}	0.221 ^b	[618]
	–	–	–	525 ^{e5}	–	–	[668]
	–	–	–	466 ^{d3}	283 ^{d3}	–	[694]
	–	–	–	548 ± 26 ^{e6}	–	–	[704]
	747 ^{e7}	113 ^{e7}	175 ^{e7}	544 ^{e7,e8}	325 ^{e7,e8}	0.22 ^{e7}	[716]
	–	–	–	–	311 ^{e9}	–	[716]
	–	–	–	558 ^{f1}	–	–	[721]
	–	–	–	463 ± 43 ^{f2}	–	–	[722, 723]
	–	–	–	458 ± 7 ^{f3}	–	–	[729]
	–	–	–	436 ± 24 ^{f4}	–	–	[771]
	–	–	–	–	310 ^{b,f5}	–	[412]
	632 ^b	144 ^b	156 ^b	466 ^{b,f6}	307 ^{b,f6}	0.25 ^b	[844]
	–	–	–	720 (?)	–	–	[338, 397]

^aFor isotropic (or quasi-isotropic) materials [42]: $E = 2G(1 + \nu)$, $E = 3K(1 - 2\nu)$, $K = c_{12} + 2c_{44}/3$, $G = c_{44}$; the condition for the isotropy is given in Eq. (I-2.18)

^bCalculated on the basis of density-functional theory (DFT) with generalized gradient approximation (GGA) using the Perdew-Burke-Ernzerhof (PBE) functional

^cCalculated value of $G = 147$ GPa

^dCalculated value of $G = 195$ GPa

^eSingle crystal grown by Verneuil process

^fCalculated from the reported elastic properties

^gEstimation from phonon dispersion curves

^hHot-pressed in vacuum and annealed, porosity – 7%, mean grain size – 13 μm

(continued)

Table 2.17 (continued)ⁱSintered in vacuum, porosity – 4.5%, mean grain size – 15 μm ^jCalculated value of $G = 207 \text{ GPa}$ ^kHot-pressed, content O – 0.01 at. %^lCorrected to the poreless state (theoretical density)^mMeasured experimentally $G = 234 \pm 27 \text{ GPa}$ ⁿPowdered samples^oSintered in vacuum, porosity – 4.0%, mean grain size – 12 μm ^pHot-pressed samples, porosity – 6-12%; values measured experimentally (with minimal porosity):
 $E = 505 \text{ GPa}$, $G = 239 \text{ GPa}$, $K = 294 \text{ GPa}$, $\kappa = 3.33 \text{ TPa}^{-1}$ ^qObtained from elastic properties extrapolated to the poreless state^rMeasured experimentally $G = 202 \text{ GPa}$ ^sCalculated from the reported Young's modulus and Poisson's ratio^tMeasured experimentally $G = 216 \text{ GPa}$ and $\kappa = 2.84 \text{ TPa}^{-1}$ ^uSingle crystal^vCalculated on the basis DFT with GGA^wCalculated on the basis of DFT with local density approximation (LDA)^xEstimated theoretically by non-conserving pseudopotential and LDA^yNano-powdered samples^zCalculated value of $G = 169 \text{ GPa}$ ^{a1}Calculated on the basis of DFT with LDA together with Perdew-Burke-Ernzerhof (PBE) functional^{a2}Calculated value of $G = 121 \text{ GPa}$ ^{a3}Calculated on the basis of DFT with LDA together with the revised Perdew-Burke-Ernzerhof (RPBE) functional^{a4}Calculated value of $G = 118 \text{ GPa}$ ^{a5}Estimation from phonon dispersion curves (c_{11} is extrapolated from neutron data [213])^{a6}Calculated using the Debye-Grüneisen model combined with *ab initio* calculations^{a7}Calculated value of $G = 209 \text{ GPa}$ ^{a8}Calculated value of $G = 176 \text{ GPa}$ ^{a9}Calculated value of $G = 188 \text{ GPa}$ ^{b1}Measured experimentally and corrected for porosity^{b2} $\kappa = 3.24 \text{ TPa}^{-1}$ ^{b3}Spark-plasma sintered samples, measured from the segmented micrographs by computing stress analysis and object oriented finite element technique^{b4}Calculated on the basis of density-functional perturbation theory (DFPT)^{b5}From high pressure experiments^{b6}Calculated on the basis of DFT^{b7}Calculated value of $G = 166 \text{ GPa}$ ^{b8}From *ab initio* calculations^{b9}At 0 K^{c1}Calculated value of $G = 201 \text{ GPa}$ ^{c2}At ~300 K^{c3}Calculated value of $G = 144 \text{ GPa}$ ^{c4}Calculated on the basis of DFT with GGA using Perdew's functional^{c5}Calculated on the basis of DFT with GGA using RPBE functional^{c6}Calculated value of $G = 213 \text{ GPa}$ ^{c7}Calculated on the basis of three body force potential (TBFP) model^{c8}Calculated value of $G = 181 \text{ GPa}$ and $\kappa = 3.82 \text{ TPa}^{-1}$ ^{c9}Calculated value of $G = 144 \text{ GPa}$ and $\kappa = 5.08 \text{ TPa}^{-1}$ ^{d1}Calculated value of $G = 163 \text{ GPa}$ ^{d2}Calculated on the basis of interionic potential theory with modified ionic charge^{d3} $G = 190 \text{ GPa}$ ^{d4}Summarized value on the basis of critical reviews of all the available experimental data^{d5}Calculated on the basis of linearized method of "muffin-tin" orbitals (LMTO)^{d6}Calculated on the basis of DFT with LDA together with Ceperley-Alder (CA) type parametrization

(continued)

Table 2.17 (continued)

^{d7}Calculated on the basis of DFT with GGA using the plane-wave pseudopotential code Dacapo and Perdew's functional

^{d8}Calculated value of $G = 217$ GPa

^{d9}Calculated on the basis of experimental data for some TaC_{1-x} phase containing composites (corrected to zero porosity)

^{e1}Calculated on the basis of a modified interaction potential model with covalency (MIPMC_v)

^{e2}Calculated value of $G = 152$ GPa

^{e3}Calculated on the basis of DFT by projector augmented wave (PAW) method with GGA using PBE functional

^{e4}Calculated value of $G = 229$ GPa

^{e5}Experimentally measured by the method of continuous impression of an indenter

^{e6}Spark-plasma sintered, porosity – $5.4 \pm 0.7\%$, mean grain size – $4.5 \pm 0.9 \mu\text{m}$; evaluated through nanoindentation

^{e7}Calculated on the basis of DFT using PBE functional with GGA by FP-LAPW method

^{e8} $G = 223$ GPa

^{e9}Calculated on the basis of DFT using PBE functional with GGA by plane wave pseudo-potential (PP-PW) method

^{f1}Spark-plasma sintered, porosity < 2%, mean grain size – 15-25 μm ; measured experimentally by pulse-echo method and extrapolated to zero porosity

^{f2}Spark-plasma sintered, no porosity, mean grain size – $5 \pm 2 \mu\text{m}$; measured experimentally by nanoindentation on the polishing cross-section

^{f3}Spark-plasma sintered, porosity < 2%, mean grain size – $5.8 \pm 0.2 \mu\text{m}$; measured experimentally by Berkovich nanoindentation

^{f4}Spark-plasma sintered, porosity – $\sim 7\%$, mean grain size – $31 \pm 2 \text{nm}$; measured experimentally by indentation technique

^{f5}Calculated value of $G = 225$ GPa

^{f6}Calculated value of $G = 187$ GPa

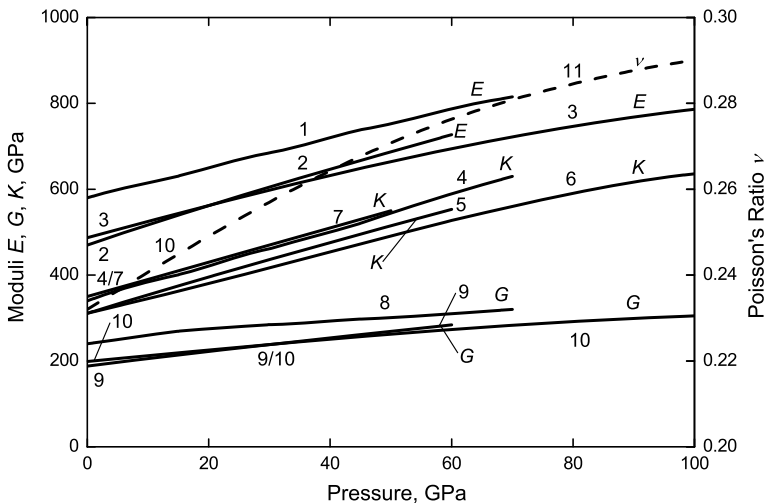


Fig. 2.27 Variations of elastic properties (1-3 – Young's modulus E , 4-7 – bulk (compression) modulus K , 8-10 – Coulomb's (shear) modulus G and 11 – Poisson's ratio ν) of near-stoichiometric tantalum monocarbide TaC_{1-x} with higher pressure: 1, 4, 8 – experimentally measured by Chen et al. [200]; 2, 5, 9 – calculated by Peng et al. [204]; 3, 6, 10-11 – calculated by Varshney et al. [414, 415] and 7 – calculated by Gautam and Kumar [617]

Table 2.18 Thermal shock/stress resistance (thermal strength) testing data on single phase tantalum monocarbide TaC_{1-x} materials

Materials and its characterization	Specimen shape and dimensions, mm	Method of thermal loading (testing)	Experimental results	References
TaC _{~1.0} , gas-phase deposited, contents: O + N ≤ 0.3%	Hollow cylinders: wall thickness – 0.8–1.2, height – 20	Direct resistance heating with 400 K s ⁻¹ , cooling by inert gas blow, cycle time – 3 min	Disintegration during the first heating-cooling cycle from 2400 to 50 °C	[41, 163]

$c_{44} = 133$, $c_{12} = 164$, $c_{13} = 149$, $c_{14} = -45$ (in GPa) [435]. The variations of the elastic moduli E , G and K and Poisson's ratio ν with higher pressure (up to 100 GPa) for near-stoichiometric tantalum monocarbide TaC_{1-x} experimentally measured and DFT-calculated are shown in Fig. 2.27. The testing data on thermal shock/stress resistance (thermal strength) of single phase tantalum monocarbide TaC_{1-x} materials are given in Table 2.18.

The magnitudes of physico-mechanical (strength, elasticity) properties of near-stoichiometric tantalum carbides in the wide range of temperatures are summarized in Addendum in comparison with other ultra-high temperature materials.

2.5 Nuclear Physical Properties

The comprehensive lists of isotopes for tantalum Ta and carbon C elements are presented in Tables I-6.2 and I-2.12, respectively. The nuclear physical properties of the elements, including isotopic mass range, total number of isotopes, thermal neutron macroscopic cross sections, moderating ability and capture resonance integral, are given in Table I-A.8.

The thermal neutron macroscopic cross sections for the binary compounds with the molecular formula A_xB_y are calculated according to the following equation:

$$\Sigma_i = [x\sigma_i(\text{A}) + y\sigma_i(\text{B})] \times (N_0\gamma/M), \quad (2.53)$$

where $\sigma_i(\text{A})$ and $\sigma_i(\text{B})$ are the microscopic cross sections of the elements A and B, respectively, N_0 is the Avogadro constant, γ is the density and M is the molecular mass of the compound. The calculated cross sections of near-stoichiometric tantalum carbide phases are listed in Table 2.19.

Table 2.19 Thermal neutron macroscopic cross sections^a of near-stoichiometric tantalum carbides [16, 217]

Phase	Macroscopic thermal neutron cross section of capture (absorption) Σ_a , cm ⁻¹	Macroscopic thermal neutron cross section of scattering Σ_s , cm ⁻¹
α -Ta _{2+x} C	1.00	~0.41
TaC _{1-x}	0.93	~0.48

^aFor 2200 m s⁻¹ neutrons

Table 2.20 Parameters of formation and migration of lattice point defects (vacancies and interstitial atoms) in near-stoichiometric tantalum monocarbide^a

Defect	Metal sublattice				Non-metal sublattice			
	E_f , eV	E_m , eV	S_f/k_B	S_m/k_B	E_f , eV	E_m , eV	S_f/k_B	S_m/k_B
Vacancy ^b [218, 739]	4.25	3.54	4.59	3.83	1.42	5.68	1.53	6.12
Vacancy ^c [538, 739]	3.79	3.31	4.11	3.60	1.10	3.31	1.19	3.60
Vacancy ^d [434]	3.5	–	–	–	0.26	4.0 ^e	–	–
Vacancy ^f [735]	1.63	–	–	–	–	–	–	–
Interstitial atom ^b [218]	20.59	0.71	22.37	0.77	6.39	0.71	6.94	0.77

^aDenoted: E_f – defect formation energy, E_m – defect migration energy, S_f – defect formation entropy, S_m – defect migration entropy, k_B – Boltzmann constant

^bCalculated on the basis of bonding model (relaxation displacement of atoms surrounding a defect is not taking into account)

^cCalculated on the basis of elastic continuum model

^d*Ab initio* simulation computed from the largest super-cell on the basis of the PAW pseudopotential using the PBE formulation

^eCalculated value of activation energy for carbon self-diffusion in tantalum monocarbide $E_A = 415 \text{ kJ mol}^{-1}$ (see also Table 2.25)

^fCalculated on the basis of data on the yield strength determined by hardness and elasticity experimental measurements

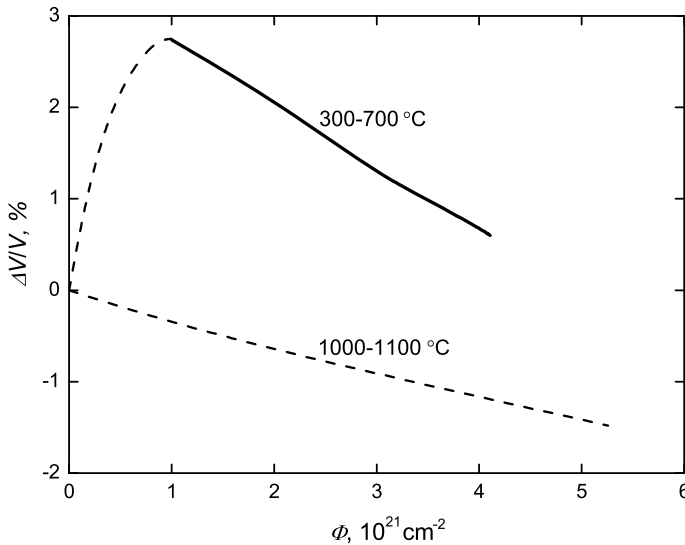


Fig. 2.28 The change in macroscopic volume (swelling/shrinkage) with fast neutron (>1 MeV) fluence Φ produced by ceramic technologies (hot-pressed, slip-cast, explosion-pressed) near-stoichiometric tantalum monocarbide TaC_{1-x} materials irradiated at different temperatures [218, 219, 619, 845, 846]

For the estimation of probable damage of tantalum monocarbide materials exposed to various types of radiation the parameters of formation and migration of lattice point defects (vacancies and interstitial atoms) are given in Table 2.20. Examples of such damage (swelling/shrinkage) produced by fast neutrons (>1 MeV) in the ranges of moderate and elevated temperatures are shown in Fig. 2.28. The fast neutron fluence more than $2 \times 10^{21} \text{ cm}^{-2}$ results in intensive failure of near-stoichiometric tantalum monocarbide hot-pressed (or sintered) materials [219]. As a result of damage the radiation-induced resistivity in $\text{TaC}_{0.99}$ increases noticeably but less than the same parameter in other refractory carbides; the contribution of the different defects to the damage rates were tentatively separated [220, 740]. The damage rate and recovery processes in $\text{TaC}_{0.99}$ irradiated with electrons of different energies were evaluated by Gosset et al. [221] and Allison et al. [331]; the threshold energy for carbon displacement was determined to be 23.2 ± 1.1 eV. The damage produced in TaC_{1-x} coating by bombardment with 90 keV protons to a dose $1.24 \times 10^{21} \text{ cm}^{-2}$ comprises erosion of the materials and its sputter etching; blisters could not be detected [401]. Preferential sputtering of carbon from the surface of TaC_{1-x} (depletion of carbon constituent) due to light ion (He^+ , H_2^+) bombardment ($E = 0.3\text{--}4$ keV, $\Phi = \sim 10^{18} \text{ cm}^{-2}$) was observed by Varga and Taglauer [847]. It was found that no significant deformations occur with deuterium ions D^+ implantation up to $\sim 10^{18} \text{ cm}^{-2}$ at 800 °C on tantalum monocarbide; however, steady-state irradiation in the range of temperatures 750–1250 °C with energetic (20–40 keV) He ions fluences between 6×10^{17} and $1 \times 10^{20} \text{ cm}^{-2}$ leads to extensive pore formation [222–224]. Deuterium retention in toughened, fine-grain and recrystallized W doped with 3.2 mol.% TaC_{1-x} , irradiated by 38 eV D^+ ions to fluences in the range of $6.0 \times 10^{20} - 1.8 \times 10^{21} \text{ cm}^{-2}$, was studied at 525 °C by Zibrov et al. [748]; the deuterium inventory in the materials was very low and comparable with that in pure polycrystalline W. Employing a positron annihilation method for the studies of atomic defects in the irradiated transition metal monocarbides at low temperatures, Rempel et al. [740, 848] proved that the recombination of interstitial tantalum atoms and vacancies in $\text{TaC}_{0.99}$ occurred at temperatures below 85 K.

Nuclear physical properties of tantalum carbides in comparison with other ultra-high temperature materials are also given in Addendum.

2.6 Chemical Properties and Materials Design

The comprehensive data on the chemical properties, compatibility (in the connection with both environmental resistance and composite materials design) and interaction behaviour of tantalum carbide phases at elevated, high and ultra-high temperatures with elements (metals, non-metals) are summarized in Table 2.21, with refractory compounds – in Table 2.22 and with gaseous media – in Table 2.23. The data on the oxidation resistance of tantalum carbide materials listed there are also accompanied by the graphic information in Figs. 2.29 and 2.30; the isothermal

Table 2.21 Chemical interaction and/or compatibility of tantalum carbide phases with elements (metals, non-metals) at elevated, high and ultra-high temperatures, including solid matters and molten media (reaction systems are given mainly in alphabetical order)^a

System	Atmosphere	Temperature range, °C	Interaction character, products and/or compatibility	References
TaC _{1-x} -Ag	-	1700	Addition of 5 mol.% Ag intensifies the densification of powdered carbide by spark plasma sintering (pressure 30 MPa, exposure 5 min)	[302]
TaC _{1-x} -Al	-	<1000	No interaction, lattice parameter of TaC _{1-x} is invariable; the particles of TaC _{1-x} show high stability and uniform distribution in melts	[1, 16, 225, 273-275, 302, 513, 514, 689-692, 742, 794, 876-878]
	He	1000-1400	Formation of Al ₄ C ₃ ; at higher temp. it decomposes	
	-	>1250	The formation of solid solutions; lattice parameter of TaC _{1-x} is decreasing considerably	
	-	-	Formation of Ta ₂ AlC, Ta ₃ AlC ₂ , Ta ₅ Al ₃ C _{1-x} , Ta ₃ Al ₂ C and α/β -Ta ₄ AlC ₃ (M _{n+1} AX _n -phases)	
	-	1400-2800	Addition of 1% Al does not affect the densification of powdered carbide by hot-pressing	
	-	1700	Testing in Al vapours results in the formation of refractory phase impregnated with Al in pores	
	-	1700	Addition of 5 mol.% Al intensifies the densification of powdered carbide by SPS (pressure 30 MPa, exposure 5 min) <i>See also</i> section TaC _{1-x} -Al ₄ C ₃ in Table 2.22 <i>See also</i> Table 2.24 <i>See also</i> section C-Al-Ta in Table I-2.14	
TaC _{1-x} -Al-Co	Ar	1350	Formation of η -Ta ₃ (Co,Al) ₃ C _{1±x} phases	[879]
TaC _{1-x} -Al-Cr	Ar	1350	Formation of η -Ta ₃ (Cr,Al) ₃ C _{1±x} phases	[879]
TaC _{1-x} -Al-Cu	Ar	1350	Formation of η -Ta ₃ (Cu,Al) ₃ C _{1±x} phases	[879]
TaC _{1-x} -Al-Fe	-	1000	Particles of TaC _{1-x} are rather stable in Fe - 15-26 at.% Al alloys during long-term exposures, although the formation of ε -(Fe,Al) _{2±x} Ta is observed; the solubility of Fe in carbide varies from 0.9 to 5.0 at.% and that of Al is very low	[822, 823, 879]
	Ar	1350	Formation of η -Ta ₃ (Fe,Al) ₃ C _{1±x} phases	
TaC _{1-x} -Al-Mn	Ar	1350	Formation of η -Ta ₃ (Mn,Al) ₃ C _{1±x} phases	[879]
TaC _{1-x} -Al-Ni	Ar	1350	Formation of η -Ta ₃ (Ni,Al) ₃ C _{1±x} phases	[879]
TaC _{1-x} -Al-Sn	-	-	Formation of Ta ₃ (Al,Sn) ₂ C ₂ (M _{n+1} AX _n -phase); Ta ₃ (Al _{0.6} Sn _{0.4})C ₂ was synthesized	[708, 709]
TaC _{1-x} -Al-V	Ar	1350	Formation of η -Ta ₃ (V,Al) ₃ C _{1±x} phases	[879]
TaC _{1-x} -Al-Zn	Ar	1350	Formation of η -Ta ₃ (Zn,Al) ₃ C _{1±x} phases	[879]
TaC _{1-x} -TiC _{1-x} -Al	-	-	Formation of (Ta,Ti) ₂ AlC (M _{n+1} AX _n -phase solid solution); (Ta _{0.6} Ti _{0.4}) ₂ AlC was synthesized <i>See also</i> section C-Al-Ta-Ti in Table I-2.14	[273-275, 469, 708]

(continued)

Table 2.21 (continued)

System	Atmosphere	Temperature range, °C	Interaction character, products and/or compatibility	References
TaC _{1-x} -VC _{1-x} -Al	-	-	Formation of (Ta,V) ₂ AlC (M _{n+1} AX _n -phase solid solution); (Ta _{0.35} V _{0.65}) ₂ AlC was synthesized <i>See also</i> section C-Al-Ta-V in Table I-2.14	[273–275, 469, 708]
α-Ta _{2+x} C-Al			<i>See</i> section C-Al-Ta in Table I-2.14	
TaC _{1-x} -Au	-	1700	Addition of 5 mol.% Au intensifies the densification of powdered carbide by SPS (pressure 30 MPa, exposure 5 min) considerably	[302]
TaC _{1-x} -β-B	-	>2400	Formation of TaB _{2±x} <i>See also</i> section C-B-Ta in Table I-2.14	[1]
α-Ta _{2+x} C-β-B			<i>See</i> section C-B-Ta in Table I-2.14	
TaC _{1-x} -Be	-	1400–2800	Addition of 1% Be does not affect the densification of powdered carbide by hot-pressing	[16, 343, 772]
	Vacuum	1500	Formation of terminal monocarbide (cubic) solid solution of substitutional-interstitial type	
	-	-	Formation of Be _x TaC _{0.76} (?) <i>See also</i> section C-Be-Ta in Table I-2.14	
TaC _{1-x} -Bi			<i>See</i> Table 2.24	
TaC _{1-x} -C	Ar/He	1900–2400	Addition of 0.1–0.8% C intensifies the densification of powdered carbide by hot-pressing	[1, 4, 5, 16, 61,
	Vacuum	<3300	TaC _{1-x} is compatible in contact with C (graphite) parts	188, 301, 463–468,
	-	~3400–3450	Eutectic TaC _{1-x} -C (graphite) <i>See also</i> section C-Ta in Table I-2.13	675, 697, 714]
TaC _{1-x} -C-Fe			<i>See</i> Table 2.24	
TaC _{1-x} -C-Fe-Mn			<i>See</i> Table 2.24	
TaC _{1-x} -β-Mo _{2±x} C-	-	1470–1500	Formation of complex monocarbonitride (Ta,Ti,W,Mo)(C,N) _{1-x} and complex intermetallic (Ti,W,Mo,Ce)(Co,Ni) _y with core-rim microstructures	[803]
TiC _{1-x} -δ-TiN _{1±x} -δ-WC _{1±x} -Ce-Co-Ni				

(continued)

Table 2.21 (continued)

System	Atmo- sphere	Temperature range, °C	Interaction character, products and/or compatibility	References
TaC _{1-x} - α/ϵ -Co	-	1100	TaC _{1-x} is in equilibrium with λ_2 -Co _{2±x} Ta and α -Co; η -Ta ₄ Co ₂ C _{1-x} is formed	[16, 226, 265, 270,
	-	~1250	The max. solid solubility of TaC _{1-x} in α -Co is ~1.0–2.5 mol.%	271, 293, 457, 460,
	-	1330–1400	Metallic Co on TaC _{1-x} plate instantaneously penetrates into the carbide and forms a eutectic (the process is identical in the case of both sintered and fused carbide materials)	784, 815, 871, 881]
	-	1340–1370	Eutectic TaC _{1-x} - α -Co; the solubility of TaC _{1-x} in α -Co is ~0.5–1.0 mol.%	
	-	1400	The max. solubility of TaC _{1-x} in molten Co is ~2.0 mol.%	
	-	1450	The solubility of Ta in Co-based binder phase in equilibrium with C is 4.0–4.5%	
	-	1500	The max. solubility of TaC _{1-x} in molten Co is ~4.0 mol.%	
	-	2750	Addition of 0.5–2.5 mas.% Co intensifies the densification of powdered carbide by hot-pressing <i>See also Table 2.24</i> <i>See also section C-Co-Ta in Table I-2.14</i>	
TaC _{1-x} -Cr ₃ C _{2-x} - β -Mo _{2±x} C- TiC _{1-x} - δ -TiN _{1±x} - δ -WC _{1±x} -Co- Ni	Vacuum	1400–1410	Formation of (Ta,Ti,W,Mo,Cr)(C,N) _{1-x} -Ti(C,N) _{1-x} -(Co,Ni,Mo) quasi-three-phase system with core-rim microstructures	[804]
TaC _{1-x} -Cr ₃ C _{2-x} - NbC _{1-x} - TiC _{1-x} -Co	-	-	Formation of (Ta,Ti,Nb,Cr)C _{1-x} -Co hard alloys (cermets)	[849]
TaC _{1-x} -HfC _{1-x} - Co	-	~1420–1445	Eutectic (Ta,Hf)C _{1-x} ($x = 0.06$ – 0.08)- α -Co <i>See also section C-Co-Hf-Ta in Table I-2.14</i>	[270]
TaC _{1-x} -HfC _{1-x} - β -Mo _{2±x} C- TiC _{1-x} - δ -TiN _{1±x} - δ -WC _{1±x} -Co	Vacuum	1400–1500	Formation of (Ta,Hf,Ti,W,Mo)(C,N) _{1-x} -Co two-phase cermet system with core-rim structures	[781]
TaC _{1-x} - β -Mo _{2±x} C- TiC _{1-x} - δ -TiN _{1±x} - VC _{1-x} - δ -WC _{1±x} -Co- Ni	Ar	1400	Formation of (Ta,Ti,W,Mo,V)(C,N) _{1-x} -Ti(C,N) _{1-x} -(Co,Ni,Mo) quasi-three-phase system with core-rim microstructures	[860]
TaC _{1-x} - β -Mo _{2±x} C- TiC _{1-x} - δ -TiN _{1±x} - δ -WC _{1±x} -Co- Ni	-	1400–1600	Formation of (Ta,Ti,W,Mo)(C,N) _{1-x} -(Co,Ni,Mo) cermet system with core-rim microstructures	[780, 790–792, 798, 857, 859–861]

(continued)

Table 2.21 (continued)

System	Atmosphere	Temperature range, °C	Interaction character, products and/or compatibility	References
TaC _{1-x} - β-Mo _{2±x} C- TiC _{1-x} - δ-WC _{1±x} -Co- Ni	-	1460	Formation of (Ta,Ti,W,Mo)C _{1-x} -(Co,Ni) two-phase cermet system with core-rim structure (the core structure of mixed carbide grains with either a high W or Ti content and rim structure with different metallic elements and distributions)	[785]
TaC _{1-x} -NbC _{1-x} - Co	-	~1410-1445	Eutectic (Ta,Nb)C _{1-x} (x = 0.18)-α-Co <i>See also</i> section C-Co-Nb-Ta in Table I-2.14	[270, 775]
TaC _{1-x} -NbC _{1-x} - TiC _{1-x} - δ-TiN _{1±x} -Co	Pure He	1550	Formation of complex monocarbonitride (Ta,Nb,Ti)(C,N) _{1-x} and complex intermetallics (Ti,Ta,Nb)Co _{1±x} , α-(Ti,Ta,Nb)Co _{2±x} and β-(Ti,Ta,Nb)Co _{2±x}	[783]
TaC _{1-x} -NbC _{1-x} - TiC _{1-x} - δ-TiN _{1±x} -Co- Ni	Pure He	1550	Formation of complex monocarbonitride (Ta,Nb,Ti)(C,N) _{1-x} and complex intermetallic (Ti,Ta,Nb)(Ni,Co) _{3±x} (orthorhombic modification)	[783, 864]
TaC _{1-x} -NbC _{1-x} - TiC _{1-x} - δ-TiN _{1±x} -VC _{1-x} - δ-WC _{1±x} -Co- Mo-Ni	-	-	Formation of complex monocarbonitride (cubic) (Ta,Nb,Ti,V,W)(C,N) _{1-x} phase	[793]
TaC _{1-x} -NbC _{1-x} - TiC _{1-x} - δ-TiN _{1±x} - δ-WC _{1±x} -Co	-	-	General consideration of the (Nb,Ta,Ti,W)(C,N) _{1-x} -δ-(W,Nb)C _{1±x} -α-Co system	[746, 863, 864]
TaC _{1-x} -NbC _{1-x} - TiC _{1-x} - δ-WC _{1±x} -Co	-	-	General consideration of the (Nb,Ta,Ti,W)C _{1-x} -δ-(W,Nb)C _{1±x} -α-Co system is presented	[272, 746, 784, 869, 872]
TaC _{1-x} -NbC _{1-x} - δ-WC _{1±x} -Co	-	-	General consideration of the (Nb,Ta,W)C _{1-x} -δ-(W,Nb)C _{1±x} -α-Co system is presented	[872]
TaC _{1-x} -TiC _{1-x} - Co	-	~1390-1450	Eutectic (Ta,Ti)C _{1-x} (x = 0.18-0.20)-α-Co	[270, 850]
TaC _{1-x} -TiC _{1-x} - δ-TiN _{1±x} -Co	Pure Ar/N ₂ , vacuum	1500	Formation of (Ta,Ti)C _{1-x} -Co two-phase cermet system <i>See also</i> section C-Co-Ta-Ti in Table I-2.14	[782, 797, 873]
TaC _{1-x} -TiC _{1-x} - δ-TiN _{1±x} - δ-WC _{1±x} -Co- Ni	Ar	1550	The liquid-phase sintering of powdered TiC _{0.5} N _{0.5} - 1.5 mol.% TaC _{1-x} - 1.5 mol.% δ-WC _{1±x} - 11 mol.% Co - 11 mol.% Ni composition leads to the formation of Ti(C,N) _{1-x} core/(Ti,W,Ta)(C,N) _{1-x} rim - microstructured hard alloy (cermet) system	[865]

(continued)

Table 2.21 (continued)

System	Atmo- sphere	Temperature range, °C	Interaction character, products and/or compatibility	References
TaC _{1-x} -TiC _{1-x} - δ-WC _{1±x} -Co	-	1250-1450	The max. solubility of (Ta,Ti,W)C _{1-x} in Co increases with temperature growth from ~3 to ~5 mol.%	[790, 850, 851, 867, 868, 870, 885]
	Vacuum	1450	Formation of (Ta,Ti,W)C _{1-x} - 30% Co two-phase and (Ta,Ti,W)C _{1-x} -δ-WC _{1±x} - 30% Co three-phase hard alloy (cermet) systems with Ti and W contents in the metal binder: 0.2% and 8% (two-phase system) and 0.1% and 10% (three-phase system), respectively; decrease in C content in the hard phase (with constant 10% molar fraction of TaC _{1-x} in it) from (Ta,Ti,W)C _{1.0} to (Ta,Ti,W)C _{0.85} leads to the increase of Ti and W contents in the metal binder - up to 1.2% and 22%, respectively	
TaC _{1-x} -TiC _{1-x} - δ-TiN _{1±x} - δ-WC _{1±x} -Co- Ni	-	1500	Formation of (Ta,Ti,W)C _{1-x} -Co two-phase hard metal (cermet) system with core-rim microstructures (with high Ti and Ta contents)	[790, 855, 856]
	Vacuum	1500	Formation of (Ta,Ti,W)(C,N) _{1-x} -(Co,Ni) two-phase cermet system with core-rim microstructures	
TaC _{1-x} -VC _{1-x} - Co	-	~1410-1445	Eutectic (Ta,V)C _{1-x} (x = 0.18)-(V,Ta)C _{1-x} (x = 0.17)-α-Co <i>See also</i> section C-Co-Ta-V in Table I-2.14	[271]
TaC _{1-x} - δ-WC _{1±x} -Co	-	-	General consideration of the (Ta,W)C _{1-x} - δ-(W,Ta)C _{1±x} -α-Co system are presented	[272, 680, 765, 790, 866]
	-	1400	The solid solubility of Ta in η ₂ -(Co,W) ₆ C is corresponding to Co _{3.04} W _{2.74} Ta _{0.22} C composition <i>See also</i> section C-Co-Ta-W in Table I-2.14	
TaC _{1-x} -ZrC _{1-x} - Co	-	1250	Eutectic (Ta,Zr)C _{1-x} (x = 0.18)-(Zr,Ta)C _{1-x} (x = 0.19)-α-Co <i>See also</i> section C-Co-Ta-Zr in Table I-2.14	[271]
α-Ta _{2+x} C-Co	-	~1675-1695	Eutectic TaC _{1-x} -Cr; the solubility of Cr in TaC _{1-x} is ~3.4 mol.% and that of TaC _{1-x} in Cr is ~2 mol.%	[226-229, 456, 681]
TaC _{1-x} -Cr	-	~1695	Eutectic (Ta,Cr)C _{1-x} (x = 0.21)-(Cr _y Ta _z) (y = 0.991, z = 0.009) <i>See also</i> section C-Cr-Ta in Table I-2.14	
α-Ta _{2+x} C-Cr	-	-	The solubility of Cr in α-Ta _{2+x} C is <2 at.% <i>See also</i> section C-Cr-Ta in Table I-2.14	[123, 226]

(continued)

Table 2.21 (continued)

System	Atmosphere	Temperature range, °C	Interaction character, products and/or compatibility	References	
TaC _{1-x} -Cs	Cs vapour, ~13 Pa	~2000	No effect upon structural characteristics of TaC _{1-x} and its thermionic emission parameters (some tens of hours exposure)	[147, 149, 458]	
α/β -Ta _{2+x} C-Cs	Cs vapour	–	No irreversible phenomena observed	[445, 458]	
TaC _{1-x} -Cu	Vacuum	~1200	No noticeable interaction between carbide particles (mean size – 1-2 μ m) and Cu melt	[16, 302, 763]	
		–	1700	Addition of 5 mol.% Cu intensifies the densification of powdered carbide by SPS (pressure 30 MPa, exposure 5 min) considerably <i>See also</i> Table 2.24	
TaC _{1-x} -Cu-Zr	–	1300	The infiltration of TaC _{1-x} preforms (porosity – 55%) by Cu – 22-67 at.% Zr alloy leads to the formation of compositions containing ZrC _{1-x} ($x \approx 0.4$) and α -Ta _{2+x} C phases along with the initial TaC _{1-x} and Cu constituents	[880]	
TaC _{1-x} - $\alpha/\gamma/\delta$ -Fe	–	1000	The interaction initiates along the grain boundaries of bulk γ -Fe	[16, 226, 265, 292, 457, 460, 628, 815, 874]	
		–	1100	TaC _{1-x} ($x > 0.15$) is in equilibrium with ϵ -Fe _{2+x} Ta and TaC _{1-x} ($0.01 \leq x \leq 0.15$) with γ -Fe	
		–	1200	Formation of new solid phases (20 μ m layer) in the contact zone between the bulk components	
		–	1250	The max. solubility of TaC _{1-x} in γ -Fe is ~0.15–0.30 mol.%	
		–	1360–1440	Metallic Fe on TaC _{1-x} plate instantaneously penetrates into the carbide and forms a eutectic (the process is identical in the case of both sintered and fused carbide materials)	
		–	~1440	Eutectic TaC _{1-x} - δ -Fe	
		–	2750	Addition of 0.5–2.5% Fe intensifies the densification of powdered carbide by hot-pressing	
		–	–	DFT calculated semicoherent interfacial energy at relaxed interface – 0.38 J m ⁻² <i>See also</i> Table 2.24	
TaC _{1-x} -TiC _{1-x} - δ -TiN _{1±x} -Fe	Pure N ₂ , vacuum	1500	Formation of (Ta,Ti)(C,N) _{1-x} -Fe two-phase cermet system <i>See</i> section C-Fe-Ta in Table I-2.14	[797]	
α -Ta _{2+x} C-Fe	–	–	<i>See</i> section C-Fe-Ta in Table I-2.14		
TaC _{1-x} -Ga	–	–	Formation of Ta ₂ GaC (M _{n+1} AX _n -phase) <i>See also</i> Table 2.24 <i>See also</i> section C-Ga-Ta in Table I-2.14	[273–275, 461]	

(continued)

Table 2.21 (continued)

System	Atmo- sphere	Temperature range, °C	Interaction character, products and/or compatibility	References
TaC _{1-x} -Ge			<i>See</i> Table 2.24	
TaC _{1-x} -Hf			<i>See</i> section C-Hf-Ta in Table I-2.14	
α -Ta _{2+x} C-Hf			<i>See</i> section C-Hf-Ta in Table I-2.14	
TaC _{1-x} -In			<i>See</i> Table 2.24	
TaC _{1-x} -Ir	-	~2030–2130	Eutectic (estimated) TaC _{1-x} ($x \approx 0.18$)-Ir <i>See also</i> section C-Ir-Ta in Table I-2.14	[226, 344]
α -Ta _{2+x} C-Ir			<i>See</i> section C-Ir-Ta in Table I-2.14	
TaC _{1-x} -K	-	~2000	No chemical reaction observed, no effect upon structural characteristics of TaC _{1-x} and its thermionic emission parameters (some tens of hours exposure)	[149, 458]
TaC _{1-x} - $\alpha/\beta/\gamma/\delta$ -Mn	-	-	The effect of Mn as an additive for hot-pres- suring process was studied <i>See also</i> Table 2.24	[16, 815]
TaC _{1-x} -Mo	-	1400	Under pressure 5 MPa the diffusion welded joint between TaC _{1-x} and Mo is produced (5–15 min exposure)	[1, 16, 21, 61, 215, 283, 285,
	Vacuum	≥ 1600	The initiation of reaction (5 h exposure) be- tween powdered TaC _{1-x} and compact dense metallic Mo	286, 462, 801, 802]
	Vacuum	2100–2200	Weak contact interaction (5 h exposure) be- tween the bulk components and formation of mixed carbide phases <i>See also</i> section C-Mo-Ta in Table I-2.14	
α -Ta _{2+x} C-Mo			<i>See</i> section C-Mo-Ta in Table I-2.14	
TaC _{1-x} -Cr ₃ C _{2-x}	Vacuum,	1450	The liquid-phase sintering of powdered	[862]
-TiC _{1-x} - δ -WC _{1±x} -Mo- Ni	0.01–0.1 Pa		(Ta _{0.14} Ti _{0.65} W _{0.21})C _{1-x} -Cr ₃ C _{2-x} -Mo-Ni compositions leads to the formation of core- rim structured (Ta,Ti,W,Mo)C _{1-x} phases em- bedded in the metallic Ni-based binder	
TaC _{1-x} -TiC _{1-x} - δ -TiNi _{1±x} - δ -WC _{1±x} -ZrC _{1-x} - -Mo-Ni	-	-	The formation of two- or three-phase cermet systems	[885]
TaC _{1-x} -TiC _{1-x} - Mo-Ni	Vacuum, 0.7–1.3 Pa	1200–1400	Hard alloys (Ti _{0.74–0.98} Ta _{0.02–0.26})C _{0.93–0.97} - 12% (Ni,Mo) were prepared	[883, 884]
TaC _{1-x} -TiC _{1-x} - δ -WC _{1±x} -Mo- Ni	-	1400–1500	Formation of (Ta,Ti,W,Mo)C _{1-x} -(Ni,Mo) hard alloy (cermet) system	[850, 885]

(continued)

Table 2.21 (continued)

System	Atmosphere	Temperature range, °C	Interaction character, products and/or compatibility	References
TaC _{1-x} -Mo-Re	Vacuum	2450	No interaction in the contact zone (1 h exposure) between Mo – 40 mas.% Re alloy and compact dense carbide materials	[287]
	Vacuum or He	2500	Interaction in the contact zone (15 min. exposure) between the compact dense materials	
	Vacuum or He	>2625	Being absorbed into the pores molten alloy dissolves (~25 vol.%) in TaC _{1-x} (25% porosity) materials completely <i>See also</i> sections C-Mo-Ta and C-Re-Ta in Table I-2.14	
TaC _{1-x} -Nb	Vacuum	1200	The initiation of reaction in powdered mixtures with the formation of solid solutions; under pressure 5 MPa the diffusion welded joint between TaC _{1-x} and Nb parts is produced (5–15 min exposure)	[1, 16, 37, 61, 215, 283–285]
	Vacuum	≥1600	The initiation of reaction between powdered TaC _{1-x} and compact dense Nb (exposure 5 h)	
	Vacuum	1600–1800	Formation of mixed carbide phases (α -Ta _{2+x} C – β -Nb _{2+x} C and TaC _{1-x} -NbC _{1-x} solid solutions)	
	Vacuum	>2000–2200	Intensive interaction between carbide and metallic phases <i>See also</i> section C-Nb-Ta in Table I-2.14 <i>See</i> section C-Nb-Ta in Table I-2.14	
α -Ta _{2+x} C-Nb				
TaC _{1-x} -Ni	Vacuum	1000	Formation of new solid phases initiates in the contact zone	[16, 226, 239, 265, 292, 457, 784, 815, 858, 881]
	–	1100	TaC _{1-x} is in equilibrium with Ni-Ta intermetallics and metal Ni; η -Ta ₄ Ni ₂ C _{1-x} is formed	
	–	1200	12 μ m layer of new solid phases forms in the contact zone for 1 h exposure	
	–	1250	The max. solubility of TaC _{1-x} in metallic Ni is ~1.5–3.0 mol.%	
	–	1300–1350	Metallic Ni on TaC _{1-x} plate instantaneously penetrates into the carbide and forms a eutectic (the process is identical in the case of both sintered and fused carbide materials)	
	–	~1340–1370	Eutectic TaC _{1-x} -Ni; the max. solubility of TaC _{1-x} in solid metallic Ni is ~2–4 mol.%	
	–	~1400	The max. solubility of TaC _{1-x} in molten Ni is 2.0 mol.%	
	–	2750	Addition of 0.5–2.5% Ni intensifies the densification of powdered carbide by hot-pressing <i>See also</i> Table 2.24 <i>See also</i> section C-Ni-Ta in Table I-2.14	
TaC _{1-x} -Ni-Cr	–	–	TaC _{1-x} (porosity – 6.0%) is impregnated perfectly by the Ni – 9.5 mas.% Cr alloy <i>See also</i> sections C-Ni-Ta and C-Cr-Ta in Table I-2.14	[1]

(continued)

Table 2.21 (continued)

System	Atmo- sphere	Temperature range, °C	Interaction character, products and/or compatibility	References
TaC _{1-x} -HfC _{1-x} -β-Mo _{2±x} C- TiC _{1-x} -δ-TiN _{1±x} -δ-WC _{1±x} -Ni	Vacuum	1400-1500	Formation of (Ta,Hf,Ti,W,Mo)(C,N) _{1-x} - (Ni,Mo) two-phase hard alloy (cermet) system with core-rim microstructures	[781]
TaC _{1-x} -HfC _{1-x} -TiC _{1-x} - δ-TiN _{1±x} -Ni	Vacuum	1500	The interaction of (Ta,Hf,Ti)C _{0.70} N _{0.30} mono- carbonitride phase with Ni is considered	[786]
TaC _{1-x} - β-Mo _{2±x} C- TiC _{1-x} -Ni	-	1350-1410	Powdered TiC _{1-x} - 3.5 mol.% β-Mo _{2±x} C - 3.5 mol.% TaC _{1-x} - 23.5 mol.% Ni compositions were sintered to form hard alloys (cermets)	[853]
TaC _{1-x} - β-Mo _{2±x} C- TiC _{1-x} -δ-TiN _{1±x} -Ni	-	1350-1480	Powdered Ti(C,N) - 2-22.5 vol.% TaC _{1-x} - 7 vol.% β-Mo _{2±x} C - 8 vol.% Ni compositions were heat-treated to form cermets	[852, 854]
TaC _{1-x} - β-Mo _{2±x} C- TiC _{1-x} -δ-TiN _{1±x} -δ-WC _{1±x} -Ni	-	1600	Formation of (Ta,Ti,W,Mo)(C,N) _{1-x} - Ni two- phase cermet system with core-rim structures	[780]
TaC _{1-x} -NbC _{1-x} -Ni	-	~1330-1350	Eutectic (Ta,Nb)C _{1-x} (x = 0.1-0.2) - Ni; the max. solubility of (Nb,Ta)C _{1-x} in Ni is ~3.0- 3.5 mol.% <i>See also</i> section C-Nb-Ni-Ta in Table I-2.14	[277, 775]
TaC _{1-x} -NbC _{1-x} -TiC _{1-x} - δ-TiN _{1±x} -Ni	Pure He	1550	Formation of complex monocarbonitride (Ta,Nb,Ti)(C,N) _{1-x} and complex intermetal- lide (Ti,Ta,Nb)Ni _{3±x} (hexagonal and ortho- rhombic modifications)	[783]
TaC _{1-x} -TiC _{1-x} - Ni	-	1000	Phase diagram of the system possesses one monovariant eutectic, but the alloys crystallize in a metastable state, as the carbide phase does not decompose into 2 solid solutions even af- ter long-term annealing (10 h exposure)	[738]
TaC _{1-x} -TiC _{1-x} - δ-TiN _{1±x} -Ni	Vacuum	~1400-1500	The interaction of (Ta,Ti)C _{0.50-0.70} N _{0.30-0.50} carbonitride phases with Ni is considered	[747, 773, 776-778, 786, 797]
TaC _{1-x} -TiC _{1-x} - δ-TiN _{1±x} - δ-WC _{1±x} -Ni	Vacuum	1500	The interaction of (Ta,Ti,W)C _{0.70} N _{0.30} mono- carbonitride phase with metallic Ni is consid- ered	[786, 865]
	Ar	1550	The liquid-phase sintering of powdered TiC _{0.5} N _{0.5} - 1.5 mol.% TaC _{1-x} - 1.5 mol.% δ-WC _{1±x} - 22 mol.% Ni composition leads to the formation of Ti(C,N) _{1-x} core/ (Ti,W,Ta)(C,N) _{1-x} rim - microstructured hard alloy (cermet) system	
TaC _{1-x} -ZrC _{1-x} - Ni	-	1000	Max. total solid solubility of carbides in Ni is ≤ ~2-3 mol.%	[807, 808]
	-	~1240-1270	Eutectic (Ta,Zr)C _{1-x} (x = 0.02)-(Zr,Ta)C _{1-x} (x = 0.17)-Ni	

(continued)

Table 2.21 (continued)

System	Atmo- sphere	Temperature range, °C	Interaction character, products and/or compatibility	References
α -Ta _{2+x} C-Ni TaC _{1-x} -Os	-	1500	See section C-Ni-Ta in Table I-2.14 The solid solubility of Os in TaC _{1-x} is low See also section C-Os-Ta in Table I-2.14	[226]
α -Ta _{2+x} C-Os TaC _{1-x} -Pb TaC _{1-x} -Pd	-	1200-1500	See section C-Os-Ta in Table I-2.14 See Table 2.24 The formation of (Pd,Ta) solid solutions and failure of TaC _{1-x} are occurred (8 h exposure); TaC _{1-x} is in equilibrium with (Pd _{0.84} Ta _{0.16}) bi- nary alloy See also section C-Pd-Ta in Table I-2.14	[1, 16, 226, 444]
α -Ta _{2+x} C-Pd TaC _{1-x} -Pt	-	1200-1500	See section C-Pd-Ta in Table I-2.14 The formation of (Pt,Ta) solid solutions and failure of TaC _{1-x} are occurred (8 h exposure); TaC _{1-x} is in equilibrium with Pt _{3±x} Ta See also section C-Pt-Ta in Table I-2.14	[1, 16, 226, 444]
α -Ta _{2+x} C-Pt TaC _{1-x} -Pu α -Ta _{2+x} C-Pu TaC _{1-x} -Re	-	~2420-2450	See section C-Pt-Ta in Table I-2.14 See section C-Pu-Ta in Table I-2.14 See section C-Pu-Ta in Table I-2.14 Eutectic TaC _{1-x} -Re; the max. solid solubility of Re in TaC _{1-x} is ~3-4 mol.% and that of TaC _{1-x} in Re is low too	[226, 243, 244, 287- 290, 745]
	Vacuum	2500	No interaction in the contact zone (1 h expo- sure) between the compact dense materials	
	-	-	Stable and compatible with each other as cer- met components	
	He	2655 ± 25	Melting 80 mol.% TaC _{0.94} + 20 mol.% Re composition results in the formation of TaC _{0.90} + Re-based solid solution	
	He	2700 ± 25	Melting 20 mol.% TaC _{0.70} + 80 mol.% Re composition results in the formation of TaC _{0.92} + χ -TaRe _{-3.5}	
	He	2730 ± 25	Melting 80 mol.% TaC _{0.70} + 20 mol.% Re composition results in the formation of TaC _{0.74} + χ -TaRe _{-1.9} See also section C-Re-Ta in Table I-2.14	
α -Ta _{2+x} C-Re	He	2775 ± 25	Melting 80 mol.% Ta _{2.06} C + 20 mol.% Re composition results in the formation of ~(Ta _{0.55} Re _{0.45}) solid solution + TaC _{0.70} + χ -TaRe _{3±x} (small amount) See also section C-Re-Ta in Table I-2.14	[283, 290]
TaC _{1-x} -Rh	-	≥ 1500	The interaction results in the formation of Rh _{3±x} Ta and C (graphite) See also section C-Rh-Ta in Table I-2.14	[226]
α -Ta _{2+x} C-Rh			See section C-Rh-Ta in Table I-2.14	

(continued)

Table 2.21 (continued)

System	Atmo- sphere	Temperature range, °C	Interaction character, products and/or compatibility	References
TaC _{1-x} -Ru	-	~1600	The interaction of non-stoichiometric carbides results in the formation of TaRu ₃ C _{1-x} ($x \approx 0.6$) <i>See also</i> section C-Ru-Ta in Table I-2.14	[226]
α -Ta _{2+x} C-Ru			<i>See</i> section C-Ru-Ta in Table I-2.14	
TaC _{1-x} -S	-	-	Formation of Ta ₂ S ₂ C (2 polytypes; C in carbosulfides is related to graphene sheets on (111) surfaces of TaC _{1-x}) <i>See also</i> section C-S-Ta in Table I-2.14	[278]
TaC _{1-x} -Sb			<i>See</i> Table 2.24	
TaC _{1-x} -Si	-	-	Formation of SiC and Ta silicides (or ternary phases, including M _{n+1} AX _n -phases, ?)	[16, 240, 241, 279, 566]
	-	1500-1700	During spark-plasma sintering the interaction leads to the formation of SiC and TaSi ₂ <i>See also</i> Table 2.24 <i>See also</i> section C-Si-Ta in Table I-2.14	
α -Ta _{2+x} C-Si			<i>See</i> section C-Si-Ta in Table I-2.14	
TaC _{1-x} -Sn			<i>See</i> Table 2.24	
TaC _{1-x} -Ta	Vacuum	>1200	Formation of α -Ta _{2+x} C in powdered mixtures	[1, 16, 61,
	-	1900	Under pressure 5 MPa the diffusion welded joint between TaC _{1-x} and Ta is produced (5-15 min exposure)	215, 283, 284, 811]
	Vacuum	>1900	Formation of α -Ta _{2+x} C and Ta-C solid solutions in the powdered mixtures of components	
	Vacuum	<2200	No interaction between powdered TaC _{1-x} and compact dense Ta (exposure 5 h) <i>See also</i> section C-Ta in Table I-2.13	
TaC _{1-x} - δ -TaN _{1-x} -Ta	N ₂	1250-1450	Formation of TaC _{1-x} N _y monocarbonitride (cubic) phase, α -Ta _{2+x} C _y N _z and γ -Ta _{2±x} N _y C _z semicarbonitride (hexagonal) phases and Ta(C,N) _{1-x} metallic solid solution	[16, 623]
β -Ta _{2±x} C-Ta		2800-2860	Eutectic β -Ta _{2±x} C-Ta	[2, 16, 17, 37]
			<i>See also</i> section C-Ta in Table I-2.13	
TaC _{1-x} -Tc			<i>See</i> section C-Ta-Tc in Table I-2.14	
TaC _{1-x} -Th			<i>See</i> section C-Ta-Th in Table I-2.14	
α -Ta _{2+x} C-Th			<i>See</i> section C-Ta-Th in Table I-2.14	
TaC _{1-x} - α/β -Ti	Vacuum, <7 × 10 ⁻⁴ Pa	1750-1800	Molten Ti reacts extensively with TaC _{1-x} crucibles resulting in the formation of an alloy, which soaks into carbide materials; a new phase is apparently formed as a distinct layer based on TiC _{1-x} between carbide and metal Ti	[16, 526]
	-	1830	Formation of mixed phases based on TiC _{1-x} and α -Ta _{2+x} C on the interface <i>See also</i> section C-Ta-Ti in Table I-2.14	

(continued)

Table 2.21 (continued)

System	Atmo- sphere	Temperature range, °C	Interaction character, products and/or compatibility	References
α -Ta _{2+x} C- α/β -Ti		1820	Solid solubility of Ti in α -Ta _{2+x} C is negligible <i>See also</i> section C-Ta-Ti in Table I-2.14	[16, 624]
TaC _{1-x} -Ti			<i>See</i> Table 2.24	
TaC _{1-x} - $\alpha/\beta/\gamma$ -U	-	1300-1310	The penetration depth of molten U into TaC _{1-x} [16] is 0.38 mm (40 min exposure) and 1.02 mm (4 h exposure); UC _{1±x} forms <i>See also</i> section C-Ta-U in Table I-2.14	
α -Ta _{2+x} C- $\alpha/\beta/\gamma$ -U		1700	The max. solid solubility of U in α -Ta _{2+x} C is <7 at.% <i>See also</i> section C-Ta-U in Table I-2.14	[16]
TaC _{1-x} -V			<i>See</i> section C-Ta-V in Table I-2.14	
α -Ta _{2+x} C-V			<i>See</i> section C-Ta-V in Table I-2.14	
TaC _{1-x} -W	-	1700	The addition of 10% TaC _{1-x} disperse inclusions to W leads to increasing the lattice parameter of metallic phase	[1, 37, 61, 215, 283, 286, 287]
	-	>1900-2200	The initiation of reaction and formation of mixed carbide phases	
	-	2000	Under pressure 5 MPa the diffusion welded joint between TaC _{1-x} and W is produced (5-15 min exposure)	
	Vacuum	≥ 2000	The initiation of reaction between powdered TaC _{1-x} and compact dense W (exposure 5 h)	
	-	2000-2500	Weak interaction between powdered TaC _{1-x} and compact dense metallic W	
	Vacuum	2600	No interaction in the contact zone (3 h exposure) between the compact dense materials	
	He	2600	No interaction in the contact zone (1 h exposure) between the compact dense materials	
	-	>2600	Intensive interaction <i>See also</i> section C-Ta-W in Table I-2.14	
β -Ta _{2±x} C-W		1700	The max. solid solubility of W in α -Ta _{2+x} C is ≤ 7 at.%	[16, 188, 226, 251-253]
		2860	Eutectic β -(Ta,W) _{2±x} C-(Ta,W) <i>See also</i> section C-Ta-W in Table I-2.14	
TaC _{1-x} - α/β -Zr	-	~1800	Eutectic (Ta,Zr)C _{1-x} -(Ta, β -Zr) <i>See also</i> section C-Ta-Zr in Table I-2.14	[188, 226, 255, 256]
α -Ta _{2+x} C-Zr			<i>See</i> section C-Ta-Zr in Table I-2.14	

^aThe parameters of wettability of TaC_{1-x} phases by liquid metals at various temperatures are listed in Table 2.24

Table 2.22 Chemical interaction and/or compatibility of tantalum carbide phases with refractory compounds at elevated, high and ultra-high temperatures (reaction systems are given mainly in alphabetical order)

System	Atmosphere	Temperature range, °C	Interaction character, products and/or compatibility	References
TaC _{1-x} -Al ₄ C ₃	-	Up to ~2000	No mutual solid solubilities Formation of Ta ₂ AlC, Ta ₃ AlC ₂ , Ta ₅ Al ₃ C _{1-x} , Ta ₃ Al ₂ C (?) and α/β -Ta ₄ AlC ₃ (M _{n+1} AX _n -phases) <i>See also</i> section TaC _{1-x} -Al in Table 2.21 <i>See also</i> section C-Al-Ta in Table I-2.14	[273–275, 513, 514, 689–692, 742]
TaC _{1-x} -AlN	Vacuum	1900–2300	High corrosion resistance against AlN sublimation process environment	[567]
TaC _{1-x} -Al ₂ O ₃	CO ₂ , 3.0 × 10 ⁻¹⁵ Pa	1000	Calculated equilibrium pressure of the interaction between the components	[471, 472, 565, 770]
	-	~1000–2000	Compatible with each other as composite components	
β -Ta _{2±x} C-Al ₂ O ₃	-	~1000–2000	Compatible with each other as composite components	[565]
TaC _{1-x} -B _{4±x} C	- Ar/He	>1500 1900–2400	Formation of TaB _{2±x} and C Addition of 0.3–0.4% B _{4±x} C intensifies the densification of powdered carbide by hot-pressing <i>See also</i> section C-B-Ta in Table I-2.14 <i>See</i> section C-B-Ta in Table I-2.14	[37, 266, 301, 342]
α -Ta _{2±x} C-B _{4±x} C	-	>2400	Formation of TaB _{2±x}	[16, 340, 341]
	-	-	<i>See also</i> section C-B-N-Ta in Table I-2.14	
TaC _{1-x} -CeN _{1±x}	-	-	Terminal mutual solid solubilities between the components (?)	[16]
TaC _{1-x} -CeP _{1±x}	-	-	Terminal mutual solid solubilities between the components (?)	[16]
TaC _{1-x} -CeS _{1±x}	-	-	Terminal mutual solid solubilities between the components (?)	[16]
TaC _{1-x} -Cr ₇ C _{3±x}	-	1000–2000	The max. solubility of “imaginary” phase ‘CrC _{1-x} ’ in TaC _{1-x} is ~10 mol.% and that of TaC _{1-x} in Cr ₇ C _{3±x} is ~1 mol.%	[226–229, 456, 681]
	-	~1720	Eutectic TaC _{1-x} -Cr ₇ C _{3±x} <i>See also</i> section C-Cr-Ta in Table I-2.14	
TaC _{1-x} -Cr ₂ O ₃	CO ₂ , 1.8 × 10 ⁻⁶ Pa	1000	Calculated equilibrium pressure of the interaction between the components	[471, 472]
TaC _{1-x} -DyN _{1±x}	-	-	Monocarbonitride (cubic) continuous solid solution (complete solubility in the system?)	[16]
TaC _{1-x} -ErN _{1±x}	-	-	Monocarbonitride (cubic) continuous solid solution (complete solubility in the system?)	[16]
TaC _{1-x} -EuN _{1±x}	-	-	Terminal mutual solid solubilities between the components (?)	[16]

(continued)

Table 2.22 (continued)

System	Atmosphere	Temperature range, °C	Interaction character, products and/or compatibility	References
TaC _{1-x} -EuO	-	-	Terminal mutual solid solubilities between the components (?)	[16]
TaC _{1-x} -Fe ₂ O ₃	CO ₂ , 1.5 Pa	1000	Calculated equilibrium pressure of the interaction between the components	[471, 472]
TaC _{1-x} -Fe ₃ C	-	-	Not (or very slightly) soluble in each other in solid state <i>See also</i> section C-Fe-Ta in Table I-2.14	[226, 460]
TaC _{1-x} -GdN _{1±x}	-	-	Terminal mutual solid solubilities between the components (?)	[16]
TaC _{1-x} -HfC _{1-x}	-	From ~890-905 to 3950	Monocarbide continuous solid solution (data on the higher melting points of (Ta,Hf)C _{1-x} in comparison with individual TaC _{1-x} and HfC _{1-x} are not confirmed); the critical point of the miscibility gap is corresp. to ~Ta _{0.55-0.58} Hf _{0.42-0.45} C _{1-x} composition	[3, 16, 71, 188, 226, 230, 231, 460, 625-627, 629, 650, 669, 682, 687, 696, 732, 805, 811, 826, 890, 895-897]
TaC _{1-x} -HfC _{1-x} -NbC _{1-x}	-	1900-2000	<i>See also</i> section C-Hf-Ta in Table I-2.14 Monocarbide (cubic) continuous solid solution (complete solubility in the system)	[16, 446, 460]
TaC _{1-x} -HfC _{1-x} -ThC _{1±x}	-	2000-2100	Terminal solid solution based on TaC _{1-x} - HfC _{1-x} monocarbide (cubic) continuous solid solution; the solubilities of ThC _{1±x} in TaC _{1-x} and HfC _{1-x} are <5 mol.% (solubilities of TaC _{1-x} and HfC _{1-x} in ThC _{1±x} are very low)	[16]
TaC _{1-x} -HfC _{1-x} -TiC _{1-x}	-	1900-2000	Monocarbide (cubic) continuous solid solution (complete solubility in the system)	[446, 460, 806]
TaC _{1-x} -HfC _{1-x} -UC _{1±x}	-	1900-2050	Monocarbide (cubic) continuous solid solutions with the miscibility gap limited by ~-(Hf _{0.4} U _{0.6})C _{1-x} - ~(Hf _{0.75} U _{0.25})C _{1-x} - ~(Ta _{0.12-0.15} Hf _{0.55} U _{0.30})C _{1-x} compositions <i>See also</i> section C-Hf-Ta-U in Table I-2.14	[16, 226, 446, 460]
TaC _{1-x} -HfC _{1-x} -VC _{1-x}	-	1900-2050	Monocarbide continuous solid solutions with great miscibility gap limited by ~-(Hf _{0.98} V _{0.02})C _{1-x} - ~(Hf _{0.03} V _{0.97})C _{1-x} - ~(Ta _{0.45-0.50} Hf _{0.20-0.25} V _{0.25-0.30})C _{1-x} compositions	[16, 446, 460, 891]
TaC _{1-x} -HfC _{1-x} -δ-WC _{1±x}	-	1900-2000	Extended solid solution based on TaC _{1-x} - HfC _{1-x} monocarbide (cubic) continuous solid solution; the solubilities of δ-WC _{1±x} in TaC _{1-x} and HfC _{1-x} are ~25-30 mol.% and ~40 mol.%, respectively (the solubilities of TaC _{1-x} and HfC _{1-x} in δ-WC _{1±x} are very low)	[16, 446]

(continued)

Table 2.22 (continued)

System	Atmosphere	Temperature range, °C	Interaction character, products and/or compatibility	References
TaC _{1-x} -HfC _{1-x} -ZrC _{1-x}	-	1900–2000	Monocarbide continuous solid solution (complete solubility in the system)	[16, 446]
α -Ta _{2+x} C- HfC _{1-x}	-	~1000–2000	The max. solubility of Hf in α -Ta _{2+x} C varies from ~1.5 to ~12 at. % <i>See also</i> section C-Hf-Ta in Table I-2.14	[188, 226, 230–231]
β -Ta _{2±x} C- HfC _{1-x}	-	~2000–3200	The max. solubility of Hf in β -Ta _{2±x} C varies from ~1.5 to ~18.5 at. % <i>See also</i> section C-Hf-Ta in Table I-2.14	[188, 226, 230, 231]
TaC _{1-x} -HfN _{1±x}	-	-	Monocarbonitride (cubic) continuous solid solution	[16]
TaC _{1-x} -HoN _{1±x}	-	-	Monocarbonitride (cubic) continuous solid solution (complete solubility in the system?)	[16]
TaC _{1-x} -LaB _{6±x}	Vacuum	1550	Interaction leads to the formation of Ta borides (50 h exposure)	[16]
TaC _{1-x} -LaN _{1±x}	-	-	Terminal mutual solid solubilities between the components (?)	[16]
TaC _{1-x} -LaP _{1±x}	-	-	Terminal mutual solid solubilities between the components (?)	[16]
TaC _{1-x} -LaS _{1-x}	-	-	Terminal mutual solid solubilities between the components (?)	[16]
TaC _{1-x} -LuN _{1±x}	-	-	Monocarbonitride (cubic) continuous solid solution (complete solubility in the system?)	[16]
TaC _{1-x} -MgO	-	>2000	Very weak interaction leads to the changes in microhardness near the contact zone	[1, 16, 232, 257, 447]
	Vacuum	>2200–2300	Very weak interaction (with the formation of TaC _x O _y oxycarbide phases) <i>See also</i> section C-Mg-O-Ta in Table I-2.14	
TaC _{1-x} -Mn ₅ C ₂ , Mn ₇ C ₃	-	-	Not (or very slightly) soluble in each other in the solid state	[460]
TaC _{1-x} - α -MoC _{1-x}	-	2000–2600	Monocarbide (cubic) continuous solid solution <i>See also</i> section C-Mo-Ta in Table I-2.14	[21, 226, 235, 236]
TaC _{1-x} - β -Mo _{2±x} C	-	-	The mutual temporary solubilities of the phases strongly depend on temperature <i>See also</i> section C-Mo-Ta in Table I-2.14	[35, 123]
α -Ta _{2+x} C- β -Mo _{2±x} C	-	1500–2200	The solubility of β -Mo _{2±x} C in α -Ta _{2+x} C increases from 5 to 30 mol. % and that of α -Ta _{2+x} C in β -Mo _{2±x} C – from ~30 to ~60 mol. % with temperature growth <i>See also</i> section C-Mo-Ta in Table I-2.14	[188, 276]
α -Ta _{2+x} C- β -Mo _{2±x} C- β -Nb _{2+x} C	-	1650–2000	The solubility of β -Mo _{2±x} C in α -Ta _{2+x} C- β -Nb _{2+x} C semicarbide continuous solid solution is low: from 3–4 mol. % in β -Nb _{2+x} C to 10–18 mol. % in α -Ta _{2+x} C; the solubilities of α -Ta _{2+x} C and β -Nb _{2+x} C in β -Mo _{2±x} C are 37–47 mol. % and 26–32 mol. %, respectively <i>See also</i> section C-Mo-Nb-Ta in Table I-2.14	[188, 276]

(continued)

Table 2.22 (continued)

System	Atmosphere	Temperature range, °C	Interaction character, products and/or compatibility	References
α -Ta _{2+x} C– β -Mo _{2±x} C– β -V _{2±x} C	–	1650–2000	Semicarbide continuous solid solutions with the miscibility gap limited by ~(Ta _{0.83–0.90} Mo _{0.10–0.17}) _{2±x} C– ~(Ta _{0.37–0.46} Mo _{0.54–0.63}) _{2±x} C– ~(Ta _{0.30–0.37} Mo _{0.35–0.38} V _{0.25–0.35}) _{2±x} C compositions <i>See also</i> section C–Mo–Ta–V in Table I-2.14	[188, 276]
β -Ta _{2±x} C– β -Mo _{2±x} C	–	2300–2500	Semicarbide (hexagonal) continuous solid solution <i>See also</i> section C–Mo–Ta in Table I-2.14	[21, 226, 235]
TaC _{1–x} –MoSi ₂	Ar	1850–1950	Interaction in the powder mixtures leads to the formation of (Mo,Ta) ₅ Si _{3±x} , SiC and ternary phases <i>See also</i> section C–Mo–Si–Ta in Table I-2.14	[16, 35, 123, 233, 234, 733, 894]
TaC _{1–x} –NbC _{1–x}	–	Up to 3600	Monocarbide continuous solid solution (complete solubility in the system, the variation of lattice parameter <i>a</i> , nm with composition for (Ta _{1–y} Nb _y)C _{1–x} phases ($x \approx 0$, $0 \leq y \leq 1$) is linear: $a = 0.4457 + 0.0013y$) <i>See also</i> section C–Nb–Ta in Table I-2.14	[16, 188, 226, 231, 238, 399, 460, 626, 627, 685, 741, 811]
TaC _{1–x} –NbC _{1–x} – –ThC _{1±x}	–	2000	Terminal solid solution based on TaC _{1–x} – NbC _{1–x} monocarbide (cubic) continuous solid solution; the solubilities of ThC _{1±x} in TaC _{1–x} and NbC _{1–x} are low	[16, 446]
TaC _{1–x} –NbC _{1–x} – –TiC _{1–x}	–	1900–2000	Monocarbide (cubic) continuous solid solution (complete solubility in the system) <i>See also</i> section C–Nb–Ta–Ti in Table I-2.14	[16, 446, 460, 767]
TaC _{1–x} – δ -TaN _{1–x} – NbC _{1–x} –TiC _{1–x}	–	1900–2000	Monocarbonitride (cubic) continuous solid solution (Ta,Nb,Ti)(C,N) _{1–x}	[767]
TaC _{1–x} –NbC _{1–x} – –UC _{1±x}	–	1900–2000	Monocarbide (cubic) continuous solid solution (complete solubility in the system)	[16, 446, 460]
TaC _{1–x} –NbC _{1–x} – –VC _{1–x}	–	1900–2000	Monocarbide (cubic) continuous solid solution (complete solubility in the system)	[16, 446, 460]
TaC _{1–x} –NbC _{1–x} – – δ -WC _{1±x}	–	1450	The max. solubility of δ -WC _{1±x} in TaC _{1–x} – NbC _{1–x} continuous solid solution is ~9 mol.%	[16, 280, 446, 685]
	–	1900–2000	The max. solubility of δ -WC _{1±x} in TaC _{1–x} – NbC _{1–x} continuous solid solution is ~30 mol.% <i>See also</i> section C–Nb–Ta–W in Table I-2.14	
TaC _{1–x} –NbC _{1–x} – –ZrC _{1–x}	–	1900–2000	Monocarbide (cubic) continuous solid solution (complete solubility in the system)	[16, 446, 460]
α -Ta _{2+x} C– β -Nb _{2+x} C	–	–	Semicarbide continuous solid solution <i>See also</i> section C–Nb–Ta in Table I-2.14	[188, 226, 231, 238]

(continued)

Table 2.22 (continued)

System	Atmosphere	Temperature range, °C	Interaction character, products and/or compatibility	References
α -Ta _{2+x} C– β -Nb _{2+x} C– γ -W _{2+x} C	–	1650–2000	The solubility of γ -W _{2+x} C in α -Ta _{2+x} C– β -Nb _{2+x} C semicarbide continuous solid solution is low: from 3–4 mol.% in β -Nb _{2+x} C to 11–14 mol.% in α -Ta _{2+x} C; the solubilities of α -Ta _{2+x} C and β -Nb _{2+x} C in γ -W _{2+x} C are 14–22 mol.% and 24–29 mol.%, respectively <i>See also</i> section C–Nb–Ta–W in Table I-2.14	[188, 276]
TaC _{1-x} – δ -NbN _{1-x}	–	–	Monocarbonitride (cubic) continuous solid solution (complete solubility in the system)	[16, 655, 882]
TaC _{1-x} – α -Nb ₅ Si _{3+x}	–	–	Interaction between the phases leads to the formation of new solid phases, including ternary phases	[16, 35, 123]
TaC _{1-x} –NbO	–	–	Terminal mutual solid solubilities between the components (?)	[16]
TaC _{1-x} –NdN _{1±x}	–	–	Terminal mutual solid solubilities between the components (?)	[16]
TaC _{1-x} – Nd ₂ Fe ₁₄ B	Pure Ar	1000	No solubility of Ta in complex boride phase	[799]
TaC _{1-x} –NpC _{1-x}	–	–	Terminal mutual solid solubilities between the components (?)	[16]
TaC _{1-x} –NpN _{1±x}	–	–	Monocarbonitride (cubic) continuous solid solution (complete solubility in the system?)	[16]
TaC _{1-x} –PrN _{1±x}	–	–	Terminal mutual solid solubilities between the components (?)	[16]
TaC _{1-x} –PuC _{1-x}	–	1400–1500	Max. terminal solid solubility of TaC _{1-x} in PuC _{1-x} is 17 mol.% and that of PuC _{1-x} in TaC _{1-x} is 67 mol.%	[1, 11, 16, 620, 621]
	–	>1600	Monocarbide continuous solid solution (complete solubility in the system?) <i>See also</i> section C–Pu–Ta in Table I-2.14	
TaC _{1-x} –PuN _{1±x}	–	–	Terminal mutual solid solubilities between the components (?)	[16]
TaC _{1-x} –PuP _{1±x}	–	–	Terminal mutual solid solubilities between the components (?)	[16]
TaC _{1-x} –PuS _{1±x}	–	–	Terminal mutual solid solubilities between the components (?)	[16]
TaC _{1-x} –ScC _{1-x}	–	–	Monocarbide continuous solid solution (complete solubility in the system?)	[16, 459]
TaC _{1-x} –ScN _{1±x}	–	–	Monocarbonitride (cubic) continuous solid solution (complete solubility in the system?)	[16]
TaC _{1-x} – α/β -SiC	–	–	Compatible with each other within the temperature range of the thermal stability of the phases <i>See also</i> section C–Si–Ta in Table I-2.14	[1, 16, 245, 725, 893]

(continued)

Table 2.22 (continued)

System	Atmosphere	Temperature range, °C	Interaction character, products and/or compatibility	References
α -Ta _{2+x} C- α/β -SiC			See section C-Si-Ta in Table I-2.14	
TaC _{1-x} - α/β -Si ₃ N ₄	-	~1400–1600	Interaction leads to the formation of Ta silicide phases and SiC; monocarbide TaC _{1-x} phase inhibits $\alpha \rightarrow \beta$ Si ₃ N ₄ transformation	[795, 796, 821]
TaC _{1-x} -SmN _{1±x}	-	-	Terminal mutual solid solubilities between the components?	[16]
TaC _{1-x} -TaB _{2±x}	-	≤ 2100	The components are compatible and virtually insoluble in each other	[14, 16, 24, 266–269]
	-	~2690–2770	Eutectic TaC _{1-x} -TaB _{2±x} ; the max. solid solubility of TaB _{2±x} in TaC _{1-x} is ~7 mol.% See also section C-B-Ta in Table I-2.14	
α -Ta _{2+x} C- TaB _{2±x}			See section C-B-Ta in Table I-2.14	
TaC _{1-x} - δ -TaN _{1-x}	-	~1500–1900	Monocarbonitride (cubic) continuous solid solution	[15, 63, 226, 237, 449, 570, 645, 889]
			See also section C-N-Ta in Table I-2.14	
TaC _{1-x} - δ -TaN _{1-x} -TiC _{1-x} - δ -TiN _{1±x}	Pure N ₂	1800	Monocarbonitride (cubic) continuous solid solution	[644, 797, 886, 887]
TaC _{1-x} - δ -TaN _{1-x} -‘TaO’	-	-	Formation of TaC _{1-x} N _y O _z oxycarbonitride (cubic) phase ^a based on TaC _{1-x} - δ -TaN _{1-x} continuous solid solution	[36]
α -Ta _{2+x} C- γ -Ta _{2±x} N	-	1100–1900	Semicarbonitride continuous solid solution	[226, 449]
			See also section C-N-Ta in Table I-2.14	
α -Ta _{2+x} C- γ -Ta _{2±x} N- ‘Ta ₂ O’	-	-	Formation of Ta ₂ C _x N _y O _z oxycarbonitride (hexagonal) solid solution based on α -Ta _{2+x} C- γ -Ta _{2±x} N continuous solid solution	[36]
	Ar	1700	Formation of oxycarbonitride (hexagonal) phase Ta ₂ C _{0.30–0.44} N _{0.05} O _{0.06–0.23} (0.50 ≤ x + y + z ≤ 0.60)	
TaC _{1-x} - α -Ta ₅ Si ₃	-	-	Formation of new solid phases, including ternary phases, in the contact zone See also section C-Si-Ta in Table I-2.14	[16, 35, 123]
TaC _{1-x} -TaSi ₂	-	-	Formation of new solid phases, including ternary phases; the solubility of TaC _{1-x} in TaSi ₂ is negligible See also section C-Si-Ta in Table I-2.14	[16, 35, 123, 282]
α -Ta _{2+x} C-TaSi ₂			See section C-Si-Ta in Table I-2.14	

(continued)

Table 2.22 (continued)

System	Atmosphere	Temperature range, °C	Interaction character, products and/or compatibility	References
TaC _{1-x} -Ta ₂ O ₅	Vacuum	>1200	Interaction results in the formation of metallic Ta	[36, 215, 449, 530, 752, 817]
	He, Ar 0.1–0.13 MPa	1300–1700	Formation of TaC _{1-x} O _y (TaC _{1-x} -‘TaO’ oxycarbide (cubic) solid solution) with approximate homogeneity limits: TaC _{0.7} -TaC _{0.7} O _{<0.05} -TaC _{0.95} O _{<0.05} -TaC _{0.99} <i>See also</i> section C–O–Ta in Table I-2.14	
α -Ta _{2+x} C-Ta ₂ O ₅	He, Ar 0.1–0.13 MPa	1300–1700	Formation of Ta ₂ C _x O _y oxycarbide (hexagonal) solid solution based on α -Ta _{2+x} C with approximate homogeneity limits: Ta _{2.5} C-Ta ₂ (C _{0.6} O _{0.2})-Ta ₂ (C _{0.4} O _{0.3})-Ta ₂ (C _{0.5} O _{0.4})-Ta _{2.0} C	[36, 449, 752]
	He	1700	Formation of oxycarbide (hexagonal) phase Ta ₂ C _{0.25-0.44} O _{0.09-0.24} (0.43 ≤ x + y ≤ 0.58) <i>See also</i> section C–O–Ta in Table I-2.14	
TaC _{1-x} TbN _{1±x}	–	–	Monocarbonitride (cubic) continuous solid solution (complete solubility in the system?)	[16]
TaC _{1-x} -TcC _{1-x}	–	–	Monocarbide continuous solid solution (complete solubility in the system?) <i>See also</i> section C–Ta–Tc in Table I-2.14	[453, 731]
α -Ta _{2+x} C-TcC _{1-x}	–	–	Mutual solid solubilities are low (?) <i>See also</i> section C–Ta–Tc in Table I-2.14	[453, 731]
TaC _{1-x} -ThC _{1±x} (α -Th, γ -ThC _{2-x})	–	1500	Compatible with each other (mutual solid solubilities are very low) <i>See also</i> section C–Ta–Th in Table I-2.14	[16, 226, 448]
TaC _{1-x} -ThC _{1±x} -TiC _{1-x}	–	>2000	Practically, no mutual solubilities between TaC _{1-x} -TiC _{1-x} monocarbide continuous solid solution and ThC _{1±x}	[16]
TaC _{1-x} -ThC _{1±x} -UC _{1±x}	–	>2000	Monocarbide continuous solid solutions with great miscibility gap because of low mutual solubilities in the TaC _{1-x} -ThC _{1±x} system	[16]
TaC _{1-x} -ThC _{1±x} -VC _{1-x}	–	>2000	Practically, no mutual solubilities between TaC _{1-x} -VC _{1-x} monocarbide continuous solid solution and ThC _{1±x}	[16]
TaC _{1-x} -ThC _{1±x} -ZrC _{1-x}	–	>2000	Practically, no mutual solubilities between TaC _{1-x} -ZrC _{1-x} monocarbide (cubic) continuous solid solution and ThC _{1±x}	[16]
α -Ta _{2+x} C-ThC _{1±x} (α -Th, γ -ThC _{2-x})	–	1500	Compatible with each other (mutual solid solubilities are very low) <i>See also</i> section C–Ta–Th in Table I-2.14	[16, 226, 448]
TaC _{1-x} -ThN _{1±x}	–	–	Extended monocarbonitride (cubic) solid solutions (terminal solubility?)	[16]
TaC _{1-x} -ThP _{1±x}	–	–	Terminal mutual solid solubilities between the components (?)	[16]
TaC _{1-x} -ThS _{1±x}	–	–	Terminal mutual solid solubilities between the components (?)	[16]

(continued)

Table 2.22 (continued)

System	Atmosphere	Temperature range, °C	Interaction character, products and/or compatibility	References
TaC _{1-x} -TiC _{1-x}	-	~0-3070 (or 1600-3070, ?)	Monocarbide continuous solid solution (the variation of lattice parameter <i>a</i> , nm with composition for (Ta _{1-y} Ti _y)C _{1-x} (<i>x</i> ≈ 0, 0 ≤ <i>y</i> ≤ 1) phases is linear: <i>a</i> = 0.4457 - 0.0128 <i>y</i>)	[16, 188, 226, 237, 246-248, 399, 473, 667, 685, 768, 787-789, 811]
	-	1700-2000	No complete homogenization is achieved (1 h exposure) for two-phase carbides mixture prepared by carbothermal reduction of oxides <i>See also</i> section C-Ta-Ti in Table I-2.14	
α-Ta _{2±x} C-TiC _{1-x}	-	1500-1800	The max. solubility of Ti in α-Ta _{2±x} C varies from ~6 to ~28 at. %	[246-248]
	-	2000	The max. solubility of Ti in α-Ta _{2±x} C varies from ~2 to ~30 at. % <i>See also</i> section C-Ta-Ti in Table I-2.14	
β-Ta _{2±x} C-TiC _{1-x}	-	2400-2600	The max. solubility of Ti in β-Ta _{2±x} C varies up to ~30 at. %	[246-248]
	-	3000	The max. solubility of Ti in β-Ta _{2±x} C varies up to ~20 at. %	
	-	3200	The max. solubility of Ti in β-Ta _{2±x} C varies up to ~10 at. % <i>See also</i> section C-Ta-Ti in Table I-2.14	
TaC _{1-x} -TiC _{1-x} - δ-TiN _{1±x}	Vacuum or Ar	1400-1800	Monocarbonitride (cubic) solid solution (Ta,Ti)(C,N) _{1-x}	[644, 773, 779, 787, 788, 886-888]
TaC _{1-x} -TiC _{1-x} - UC _{1±x}	-	2000-2050	Monocarbide continuous solid solutions with great miscibility gap because of low mutual solubilities in the TiC _{1-x} -UC _{1±x} system <i>See also</i> section C-Ta-Ti-U in Table I-2.14	[226, 446]
TaC _{1-x} -TiC _{1-x} - VC _{1-x}	-	1900-2000	Monocarbide (cubic) continuous solid solution (complete solubility in the system)	[446, 460]
TaC _{1-x} -TiC _{1-x} - δ-WC _{1±x}	-	1400-1500	Extended solid solution based on TaC _{1-x} -TiC _{1-x} monocarbide (cubic) continuous solid solution; the solubilities of δ-WC _{1±x} in TaC _{1-x} and TiC _{1-x} are ~10-15 and ~35-50 mol. %, respectively (the solubilities of TaC _{1-x} and TiC _{1-x} in δ-WC _{1±x} are very low)	[16, 67, 188, 280, 281, 446, 460, 774, 851, 867, 868]
	-	1900-2500	Extended solid solution based on TaC _{1-x} -TiC _{1-x} monocarbide continuous solid solution; the solubilities of δ-WC _{1±x} in TaC _{1-x} and TiC _{1-x} are ~30 and ~65 mol. %, respectively (the solubilities of TaC _{1-x} and TiC _{1-x} in δ-WC _{1±x} are very low) <i>See also</i> section C-Ta-Ti-W in Table I-2.14	
TaC _{1-x} -TiC _{1-x} - ZrC _{1-x}	-	1900-2000	Monocarbide (cubic) continuous solid solution (complete solubility in the system)	[16, 446, 460]

(continued)

Table 2.22 (continued)

System	Atmosphere	Temperature range, °C	Interaction character, products and/or compatibility	References
TaC _{1-x} - δ-TiN _{1±x}	-	-	The mutual solubilities of the phases are limited	[16, 67]
TaC _{1-x} -TiO _{1±x}	-	-	Terminal mutual solid solubilities between the components (?)	[16]
TaC _{1-x} -UC _{1±x}	-	1200–1700	Monocarbide continuous solid solution (a spacing-composition curve in the system is almost linear, complete solubility in the system)	[16, 226, 283, 460, 656, 734]
			<i>See also</i> section C-Ta-U in Table I-2.14	
TaC _{1-x} -UC _{1±x} - VC _{1-x}	-	2000–2050	Monocarbide continuous solid solution with great miscibility gap because of low mutual solubilities in the UC _{1±x} -VC _{1-x} system	[16, 226, 446]
			<i>See also</i> section C-Ta-U-V in Table I-2.14	
TaC _{1-x} -UC _{1±x} - ZrC _{1-x}	-	1900–2050	Monocarbide (cubic) continuous solid solution (complete solubility in the system)	[16, 226, 446, 460, 898]
			<i>See also</i> section C-Ta-U-Zr in Table I-2.14	
α-Ta _{2+x} C-UC _{1±x}			<i>See</i> section C-Ta-U in Table I-2.14	
TaC _{1-x} -α-UC _{2-x}	-	1700	The components are compatible; no solubility of TaC _{1-x} in α-UC _{2-x}	[283, 291]
			<i>See also</i> section C-Ta-U in Table I-2.14	
TaC _{1-x} -UN _{1-x}	-	-	Monocarbonitride (cubic) continuous solid solution (complete solubility in the system?)	[16]
			<i>See also</i> section C-N-Ta-U in Table I-2.14	
TaC _{1-x} -UP _{1±x}	-	-	Terminal mutual solid solubilities between the components (?)	[16]
TaC _{1-x} -US _{1±x}	-	-	Terminal mutual solid solubilities between the components (?)	[16]
TaC _{1-x} -VC _{1-x}	-	~500	Practically, no mutual solid solubilities between the components	[3, 16, 226, 227, 231, 399, 460, 627, 682, 736, 811]
	-	From 1200–1300 (or 1700–2500, ?) up to 2700	Monocarbide (cubic) continuous solid solution (complete solubility in the system, the variation of lattice parameter <i>a</i> , nm with composition for (Ta _{1-y} V _y)C _{1-x} phases ($x \approx 0$, $0 \leq y \leq 1$) is non-linear: $a = 0.4457 - 0.0162y - 0.0123y^2$)	
			<i>See also</i> section C-Ta-V in Table I-2.14	
TaC _{1-x} -VC _{1-x} - δ-WC _{1±x}	-	1900–2000	Extended solid solution based on TaC _{1-x} -VC _{1-x} monocarbide continuous solid solution; the solubilities of δ-WC _{1±x} in TaC _{1-x} and VC _{1-x} are ~30 and ~60 mol.%, respectively (the solubilities of TaC _{1-x} and VC _{1-x} in δ-WC _{1±x} are very low)	[16, 446]
			<i>See also</i> section C-Ta-V-W in Table I-2.14	
TaC _{1-x} -VC _{1-x} - ZrC _{1-x}	-	1900–2000	Monocarbide continuous solid solutions with great miscibility gap limited by ~(V _{0.99} Zr _{0.01})C _{1-x} - ~(V _{0.03} Zr _{0.97})C _{1-x} - ~(Ta _{0.65} V _{0.20} Zr _{0.15})C _{1-x} compositions	[16, 446, 460]

(continued)

Table 2.22 (continued)

System	Atmosphere	Temperature range, °C	Interaction character, products and/or compatibility	References
TaC _{1-x} -δ-VN _{1-x}	-	-	Monocarbonitride (cubic) continuous solid solution (complete solubility in the system?)	[16, 67, 882]
α-Ta _{2+x} C-	-	-	Semicarbidic continuous solid solution	[35, 123, 188, 226]
β-V _{2±x} C	-	1650–2000	Semicarbidic continuous solid solutions with the great miscibility gap limited by ~(Ta _{0.86-0.90} W _{0.10-0.14}) _{2+x} C- ~(Ta _{0.21-0.22} W _{0.78-0.79}) _{2+x} C- ~(Ta _{0.18-0.22} W _{0.30-0.35} V _{0.44-0.46}) _{2±x} C compositions <i>See also</i> section C-Ta-V-W in Table I-2.14	[188, 276]
α-Ta _{2+x} C-	-			
β-V _{2±x} C-	-			
α-W _{2+x} C	-			
TaC _{1-x} -β-W ₂ B _{5-x}	-	2290	Eutectic TaC _{1-x} -β-W ₂ B _{5-x}	[580]
TaC _{1-x} -γ-WC _{1-x}	-	~2500–2850	Monocarbide (cubic) continuous solid solution (complete solubility in the system) <i>See also</i> section C-Ta-W in Table I-2.14	[16, 188, 226, 236, 249–253]
TaC _{1-x} -δ-WC _{1±x}	-	1500	The max. solubility of W in TaC _{1-x} corresponds to ~-(Ta _{0.9} W _{0.1})C _{1-x} composition	[226, 249, 252, 253, 664, 829]
	-	1800	The max. solubility of W in TaC _{1-x} corresponds to ~-(Ta _{0.8} W _{0.2})C _{1-x} composition	
	-	2000	The max. solubility of W in TaC _{1-x} corresponds to compos. ~-(Ta _{0.7} W _{0.3})C _{1-x}	
	-	2760	The max. solubility of Ta in δ-WC _{1±x} is ~4 at.%. <i>See also</i> section C-Ta-W in Table I-2.14	
TaC _{1-x} -δ-WC _{1±x} -ZrC _{1-x}	-	1900–2000	Extended solid solution based on TaC _{1-x} -ZrC _{1-x} monocarbide (cubic) continuous solid solution; the solubilities of δ-WC _{1±x} in TaC _{1-x} and ZrC _{1-x} are ~30 mol.% (the solubilities of TaC _{1-x} and ZrC _{1-x} in δ-WC _{1±x} are very low) <i>See</i> section C-Ta-W in Table I-2.14	[16, 446]
α-Ta _{2+x} C-	-			
δ-WC _{1±x}	-			
TaC _{1-x} -α-W _{2+x} C	-	~1250–2100	The mutual solubilities of the phases strongly depend on temperature <i>See also</i> section C-Ta-W in Table I-2.14	[16]
α-Ta _{2+x} C-	-	1500–1950	The solubility of α-W _{2+x} C in α-Ta _{2+x} C increases from 5 to 12 mol.% and that of α-Ta _{2+x} C in α-W _{2+x} C – from ~8 to ~20 mol.% with temperature growth <i>See also</i> section C-Ta-W in Table I-2.14	[188]
α-W _{2+x} C	-			
β-Ta _{2±x} C-	-	2300–2450	The solubility of β-W _{2+x} C in α-Ta _{2+x} C increases from ~20 to ~40 mol.% and that of α-Ta _{2+x} C in β-W _{2+x} C – from ~30 to ~50 mol.% with temperature growth <i>See also</i> section C-Ta-W in Table I-2.14	[188]
β-W _{2+x} C	-			

(continued)

Table 2.22 (continued)

System	Atmosphere	Temperature range, °C	Interaction character, products and/or compatibility	References
β -Ta _{2±x} C– γ -W _{2±x} C	–	~2460–2790	Semicarbidic (hexagonal) continuous solid solution <i>See also</i> section C–Ta–W in Table I-2.14	[16, 188, 226, 251–253]
TaC _{1–x} –YC _{1±x}	–	–	Terminal mutual solid solubilities between the components (?)	[16]
TaC _{1–x} –YN _{1±x}	–	–	Terminal mutual solid solubilities between the components (?)	[16]
TaC _{1–x} –YbN _{1±x}	–	–	Monocarbonitride (cubic) continuous solid solution (complete solubility in the system?)	[16]
TaC _{1–x} –ZrC _{1–x}	–	~940–3400 (or ~1250–3400?)	Monocarbide (cubic) continuous solid solution (complete solubility in the system, the variation of lattice parameter <i>a</i> , nm with composition for (Ta _{1–y} Zr _y)C _{1–x} phases ($x \approx 0$, $0 \leq y \leq 1$) is non-linear: $a = 0.4457 + 0.0144y + 0.0091y^2$); the critical point of the miscibility gap is corresponding to \sim Zr _{0.30–0.35} Ta _{0.65–0.70} C _{1–x} composition	[16, 71, 188, 226, 231, 254–256, 399, 474, 622, 625, 627, 629, 659, 682, 696, 809–814]
	–	<1900	No solid solution is formed (1 h exposure) for two carbides powdered mixture treated by hot pressing	
	Ar, >0.1 MPa	1900–2000	Additions of TaC _{1–x} have no contribution to ZrC _{1–x} hot-pressing densification process, as the formation of solid solutions requires higher temperatures and longer time <i>See also</i> section C–Ta–Zr in Table I-2.14	
α -Ta _{2±x} C– ZrC _{1–x}	–	1775–1820	The max. solid solubility of Zr in α -Ta _{2±x} C varies up to ~12 at. %	[16, 188, 226, 231, 255, 256]
	–	–	<i>See also</i> section C–Ta–Zr in Table I-2.14	
β -Ta _{2±x} C– ZrC _{1–x}	–	2500	The max. solid solubility of Zr in β -Ta _{2±x} C varies up to ~14 at. %	[16, 188, 226, 231, 255, 256]
	–	–	<i>See also</i> section C–Ta–Zr in Table I-2.14	
TaC _{1–x} –ZrN _{1±x}	–	–	Monocarbonitride (cubic) continuous solid solution (complete solubility in the system)	[16, 67]
TaC _{1–x} –ZrP _{1±x}	–	–	Terminal mutual solid solubilities between the components (?)	[16]
TaC _{1–x} – β/γ -ZrO _{2–x}	–	≥ 2200	Formation of new solid phases (column-like crystals) in the interface between the compact dense materials <i>See also</i> section C–O–Ta–Zr in Table I-2.14	[1, 232, 257, 447, 695]

^aPractically, due to the serious difficulties in manufacturing transition metal carbide materials non-contaminated in any degree by O and N, all the materials labeled in literature as TaC_{1–x} with the appropriate certification more likely would have to be considered as TaC_{1–x}N_yO_z with low or very low values of *y* and *z* indexes

Table 2.23 Chemical interaction of tantalum carbide phases with gaseous media at elevated, high and ultra-high temperatures (reaction systems are given in alphabetical order)

System	Atmosphere	Temperature range, °C	Interaction character, products and/or compatibility	References
TaC _{1-x} -CO	CO	–	Formation of oxycarbide phases TaC _{1-x} O _y (extended substitution solid solution based on TaC _{1-x} with approximate homogeneity limits: TaC _{0.7} -TaC _{0.7} O _{<0.05} -TaC _{0.95} O _{<0.05} -TaC _{0.99}) <i>See also</i> section C-O-Ta in Table I-2.14	[16, 752]
TaC _{1-x} -CO ₂	CO ₂	–	Formation of oxycarbide phases TaC _{1-x} O _y (extended substitution solid solution based on TaC _{1-x} with approximate homogeneity limits: TaC _{0.7} -TaC _{0.7} O _{<0.05} -TaC _{0.95} O _{<0.05} -TaC _{0.99}) and subsequent formation of oxide scales <i>See also</i> section C-O-Ta in Table I-2.14	[16, 752]
TaC _{1-x} -Cl ₂	Cl ₂	<250	Compact dense TaC _{1-x} is resistant to Cl ₂	[16, 37, 345]
TaC _{1-x} -H ₂	Cl ₂	700–800	Powdered TaC _{1-x} decomposes easily	[16, 43, 60, 61, 139, 215, 364, 470, 639–642]
	H ₂ , 0.1 MPa	730–1330	The mass loss of compact TaC _{1-x} (6% porosity) observed in the range of 0.02–0.13% (1 h exposure) is a consequence of the formation and subsequent decomposition of the oxide phases (mainly Ta ₂ O ₅) due to residual O ₂ ; in comparison with vacuum (<1.5 Pa) H ₂ suppresses the mass loss of TaC _{1-x} (no hydride formation is observed)	
	H ₂	2000–2500	Weak interaction with the minimally determined mass changes	
	H ₂ , CH ₄	2300–2770	Decarbonization of carbide phases at CH ₄ content <0.125–0.250%	
	H ₂ , CH ₄	~3000–3900 3180	Noticeable decarbonization of carbide phases Decarbonization of carbide phases at CH ₄ content <0.25–0.50%	
TaC _{1-x} -H ₂ O	H ₂ O ^a	~700	Formation of various complex oxycarbide (?) phases	[139, 449]
	H ₂ O	800	TaC _{1-x} powders are burning (exothermic reaction)	
TaC _{1-x} -NH ₃ (25% N ₂ + 75% H ₂)	N ₂ , H ₂ , CH ₄	2300–2500	Decarbonization of carbide phases, if CH ₄ content <0.125–0.250%	[215]
	N ₂ , H ₂ , CH ₄	2770	Decarbonization of carbide phases, if CH ₄ content <0.25–0.50%	
	N ₂ , H ₂ , CH ₄	3180	Decarbonization of carbide phases, if CH ₄ content <0.5%	

(continued)

Table 2.23 (continued)

System	Atmosphere	Temperature range, °C	Interaction character, products and/or compatibility	References
TaC _{1-x} -N ₂	N ₂ , 0.1–30 MPa	1100–1800	High level stability; no interaction	[16, 35, 60, 63,
	N ₂	1250–1900 (?)	Formation of various monocarbonitride Ta ₂ C _x N _z phases	123, 139, 215, 226,
	N ₂ , ≤ 0.1 MPa	≤ 2700	No noticeable interaction of TaC _{1-x} materials with N ₂ atmosphere	237, 455, 623, 645]
	N ₂	3300	No interaction (if H ₂ is absent)	
	N ₂	~3900	Decarbonization of carbide phases Data available in literature are controversial <i>See also</i> section C–N–Ta in Table I-2.14	
α-Ta _{2+x} C–N ₂	N ₂	1250–1900	Formation of various semicarbonitride Ta ₂ C _x N _z phases <i>See also</i> section C–N–Ta in Table I-2.14	[63, 226, 237, 623]
TaC _{1-x} -O ₂ ^{b,c}	O ₂ (~0.8 Pa), Ar	50–360	In this temperature range the oxidation of sintered TaC _{-1.0} in gas mixture stream (5 ppm O ₂) with heating rate ~1.4 K min ⁻¹ leads to the maximal reaction rate ~7 × 10 ⁻¹⁰ mol cm ⁻² s ⁻¹ ; after a prolonged exposition at maximal temperature (8 ppm O ₂) the ratio of O/C = ~1.5 × 10 ⁻³ was achieved in solids	[1, 16, 36, 61, 139, 215, 240–242, 294–300, 454, 511, 568, 571, 643–645, 652, 703, 752, 771, 817]
	Air	400–500	The oxidation of hot-pressed (1–2% porosity) TaC _{1-x} initiates by the formation of oxycarbide phases TaC _{1-x} O _y (extended substitutional solid solution based on TaC _{1-x} with approximate homogeneity limits: TaC _{0.70} –TaC _{0.70} O _{<0.05} –TaC _{0.95} O _{<0.05} –TaC _{0.99}) with the subsequent occurrence of pentoxide β-Ta ₂ O ₅ C _x (with dissolved carbon in it, ?) and separation of carbon (sometimes metallic Ta was determined in the scale, ?); the oxidation resistance of TaC _{1-x} is higher than that of pure metal Ta	
	Air	~500–700	CVD-prepared TaC _{1-x} coating starts to be oxidized at > 508 °C; the initial oxidation product is Ta ₂ O _{3±x} (hexagonal) solid solution (?)	
	Air	600–700	The oxidation of hot-pressed (1–2% porosity) TaC _{1-x} evolves by the formation of oxide scales containing β-Ta ₂ O ₅ C _x , suboxide phases TaO _z (sometimes metallic Ta was determined as well, ?) and dispersed carbon phase	
	Air	690–900	During the oxidation of CVD-prepared TaC _{1-x} coating with increasing oxidation temperature Ta ₂ O _{3±x} (hexagonal) solid solution transforms into β-Ta ₂ O ₅ (orthorhombic) (?)	

(continued)

Table 2.23 (continued)

System	Atmosphere	Temperature range, °C	Interaction character, products and/or compatibility	References
	Air	700–1000	The oxidation rate of hot-pressed TaC _{1-x} grows sharply and oxidation kinetics is described by linear law during long-term exposures; however, oxide scales have good adherence with substrate	
	O ₂	700–1000	The non-isothermal oxidation of HIPed TaC _{0.99} (<2% porosity) in dynamic flow of pure O ₂ (5.6 cm ³ s ⁻¹) at 0.1 MPa at heating rate 1.7 × 10 ⁻² °C s ⁻¹ leads to increase in oxidation grade (fractional mass change corresponding to the complete oxidation) from 0 to 1	
	O ₂	750–850	The isothermal and isobaric (0.02–0.1 MPa) oxidation of HIPed TaC _{0.99} (<2% porosity) in dynamic flow of pure O ₂ (5.6 cm ³ s ⁻¹); temp. influence is described by apparent activation energy $E = 385 \pm 10$ kJ mol ⁻¹	
	Air	800	The oxidation mass gain of TaC _{1-x} is 4.93 and 12.9 g m ⁻² for 1 h and 2 h exposure, respectively	
	Air	900	The oxidation mass gain of TaC _{1-x} is 100 and 394 g m ⁻² for 1 h and 2 h exposure, respectively	
	Air	~900–1500	The oxidation product on the surface of CVD-prepared TaC _{1-x} coating is β-Ta ₂ O ₅ (orthorhombic) with chapped or porous structure; isolation and/or protective films are not formed	
	Air	1000–1200	The intensive oxidation of hot-pressed TaC _{1-x} accompanied with cracking and splitting of oxide scales; porous samples are disintegrated completely	
	Air	1100–1400	Severe oxidation of materials	
	Air	≥ ~1500	Liquid Ta ₂ O ₅ and β-Ta ₂ O ₅ (orthorhombic) phases coexist on the oxidized surface of CVD-prepared TaC _{1-x} coating	
	O ₂ , 10 ⁻¹ –10 ⁻³ Pa	1730–2230	During the oxidation of hot-pressed TaC _{1-x} a metallic surface layer formed by CO release simultaneously reacts with O ₂ forming volatile metal oxides; steady-state layer thickness is reached, if the rates of layer growth and metal evaporation are equal in the ablation process	
	O ₂ /C ₂ H ₂ torch	≥ ~2300	Massive molten Ta ₂ O ₅ (ablation layer); in solidified form – α-Ta ₂ O ₅ + β-Ta ₂ O ₅ wets substrate perfectly (?); the oxidation reaction of TaC _{1-x} CVD-prepared coatings (or hot-pressed materials with porosity <7%) is controlled by the mechanism of oxygen dissolution and diffusion from the gas-liquid interface through the melt to the TaC _{1-x} surface. The liquid oxide layer TaO ₂ acts as a dynamic component that promotes erosion of the TaC _{1-x} surface (?) <i>See also</i> section C–O–Ta in Table I-2.14	

(continued)

Table 2.23 (continued)

System	Atmosphere	Temperature range, °C	Interaction character, products and/or compatibility	References
α -Ta _{2+x} C–O ₂	Air or O ₂	–	Oxidation initiates by the formation of oxy-carbide phases Ta ₂ C _x O _y (extended solid solution based on α -Ta _{2+x} C with approximate homogeneity limits: Ta _{2.5} C–Ta ₂ (C _{0.6} O _{0.2})–Ta ₂ (C _{0.4} O _{0.3})–Ta ₂ (C _{0.5} O _{0.4})–Ta _{2.0} C)	[36, 295]
	O ₂	700–1000	The non-isothermal oxidation of HIPed α -Ta _{2+x} C (<2% porosity) in dynamic flow of pure O ₂ (5.6 cm ³ s ⁻¹) at 0.1 MPa at heating rate 1.7 × 10 ⁻² °C s ⁻¹ leads to increase in oxidation grade (fractional mass change corresponding to the complete oxidation) from 0 to 0.41	
	O ₂ , 0.02–0.1 MPa	750–850	The isothermal-isobaric oxidation of HIPed α -Ta _{2+x} C (<2% porosity) in dynamic flow of pure O ₂ (5.6 cm ³ s ⁻¹); temperature influence is described by apparent activation energy $E = 129 \pm 7$ kJ mol ⁻¹ See also section C–O–Ta in Table I-2.14	

^aIn the presence of H₂ in great excess

^bFine tantalum carbide powders are pyrophoric [320]

^cFor near-stoichiometric TaC_{1-x} the value of the Pilling–Bedworth ratio $\alpha = M_O d_C / M_C d_O = 1.91$, where M_O is molecular mass of the oxide phase formed on the oxidation of 1 mol of carbide phase, M_C is molecular mass of carbide phase, d_C and d_O are the densities of carbide and oxide phases, respectively [529]

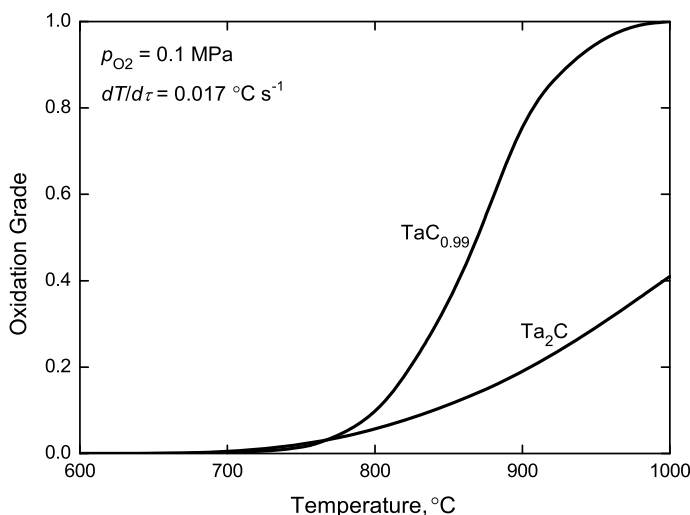


Fig. 2.29 Non-isothermal oxidation kinetics curves (heating rate – 1.7 × 10⁻² °C s⁻¹) for 4 × 4 × 4 mm samples of hot isostatically pressed tantalum carbide single-phase materials (porosity <2%) exposed to dynamic flow of pure oxygen (5.6 cm³ s⁻¹) under pressure 0.1 MPa; oxidation grade was defined by the fractional mass change, which was specified to the mass gain corresponding to the complete oxidation evaluated by considering that tantalum carbides are transformed to Ta₂O₅ according to the following reactions: 2TaC + 4½O₂ → Ta₂O₅ + 2CO₂ or Ta₂C + 3½O₂ → Ta₂O₅ + CO₂ [295]

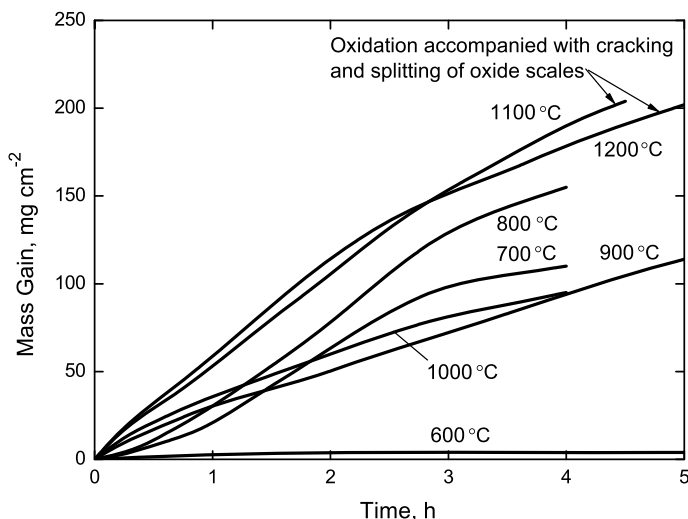


Fig. 2.30 Isothermal oxidation kinetics curves for 8 mm diameter disk-like samples of hot-pressed and subsequently annealed near-stoichiometric tantalum monocarbide materials (porosity 1–2%) in air [242, 296, 297]

Table 2.24 The parameters of wettability of tantalum monocarbide TaC_{1-x} phases with some liquid metals and alloys (melts)^a

Melt (purity)	Atmosphere	Temp., °C	Time, s	γ_{l-g} , mJ m ⁻²	W_a , mJ m ⁻²	W_m^b , kJ mol ⁻¹	θ , degree	References
$TaC_{0.78}$								
Cu	Vacuum	1100	1800	1360	1125	–	~100	[37, 258, 259, 347]
$TaC_{0.90}$								
Cu (0.2% Ag)	Vacuum	1100	900	1270	2325	–	34	[1, 260]
Cu	Vacuum	1100	1800	1360	1595	–	~80	[37, 258, 259, 347]
Cu (0.2% Ag)	Vacuum	1150	900	1255	2355	–	29	[1, 260]
$TaC_{0.94}$								
Cu (0.2% Ag)	Vacuum	1100	900	1270	1600	–	75	[1, 260]
Cu (0.2% Ag)	Vacuum	1150	900	1255	1845	–	62	[1, 260]
$TaC_{-1.0}$								
Al	Vacuum	900	900	914	165	8.0	145 ± 2	[261]
Al	Vacuum	900–1000	–	–	–	–	145–146	[259, 346]
Al (99.97%)	Vacuum	950–1000	1200	914	165	–	145	[1]
Al	He (high purity)	1000	900	914	350	–	128 ± 3	[1, 225]
Al (99.97%)	Vacuum	1150	60	914	215	–	140	[1]
Al (99.97%)	Vacuum	1150	180	914	235	–	138	[1]
Al (99.97%)	Vacuum	1150	300	914	325	–	130	[1]
Al (99.97%)	Vacuum	1150	600	914	375	–	126	[1]
Al (99.97%)	Vacuum	1150	1200	914	390	–	125	[1]

(continued)

Table 2.24 (continued)

Melt (purity)	Atmosphere	Temp., °C	Time, s	γ_{l-g} , mJ m ⁻²	W_{a^*} , mJ m ⁻²	$W_{m^*}^b$, kJ mol ⁻¹	θ , degree	References
Al (99.97%)	Vacuum	1200	60	914	455	–	120	[1]
Al (99.97%)	Vacuum	1200	120	914	1225	–	70	[1]
Al (99.97%)	Vacuum	1200	180	914	>1825	–	~0	[1]
Al	He (high purity)	1200	900	865	395	–	123 ± 3	[1, 225]
Al	He (high purity)	1400	900	865	940	–	85 ± 3	[1, 225]
Bi (99.999%)	Vacuum	320	900	390	114	5.4	135.0 ± 0.3	[1, 261, 346]
Co ^c	Vacuum	1420	300	1910	3770	–	13 ± 2	[260, 262, 346]
Co (99.98%)	Vacuum, Ar	1500	900	1805	>3670	–	~0	[1, 259, 261, 346]
Co ^d	Vacuum	1500	1200	1850	3700	–	10	[262, 263]
Cu	Vacuum	1100	–	–	–	–	~60	[37, 258, 347]
Cu	Vacuum	1100	–	–	–	–	75	[16, 362, 646]
Cu (0.2% Ag)	Vacuum	1100	900	1270	1525	–	78	[1, 260, 875]
Cu	Vacuum	1130	900	1351	318	15.1	140 ± 1	[1, 261, 346]
Cu (0.2% Ag)	Vacuum	1150	900	1255	1685	–	69	[1, 260]
Cu	Vacuum	1150	–	–	–	–	78	[346]
Cu (0.2% Ag)	Vacuum	1200	900	1240	1860	–	60	[1, 260]
Cu	Vacuum	1250	–	–	–	–	60	[346]
Cu	Vacuum	1250	–	–	–	–	36	[16, 362, 646]
Fe	Vacuum	1450–1490	60	1900	3650	–	23	[1, 259, 260, 346]
Fe (C-4.0, Mn-1.4, Si-2.5, S-0.1%) ^c	Pure Ar	1400–1450	900	–	–	–	~0	[1, 304, 346]
Fe (C-3.1, Mn-0.4, Si-1.6, S-0.02%) ^c	Pure Ar	1400–1450	900	–	–	–	~0	[1, 304, 346]
Fe (C-2.7, Mn-0.4, Si-1.2, S-0.2%) ^c	Pure Ar	1400–1450	900	–	–	–	~0	[1, 304, 346]
Fe (C-2.6, Mn-1.0, Si-1.0, Cr-0.3%) ^c	Pure Ar	1400–1450	900	–	–	–	~0	[1, 304, 346]
Fe (C-1.0, Cr-1.4, Mn-0.4, Si-0.3%) ^c	Pure Ar	~1500	900	–	–	–	~0	[304, 346]

(continued)

Table 2.24 (continued)

Melt (purity)	Atmosphere	Temp., °C	Time, s	γ_{l-g} , mJ m ⁻²	W_a , mJ m ⁻²	W_m^b , kJ mol ⁻¹	θ , degree	References
Fe (C-1.0, Cr-1.4, Mn-1.1, Si-0.6%) ^c	Pure Ar	~1500	900	–	–	–	~0	[304, 346]
Fe (C-0.8, Mn-0.2, Si-0.2, S-0.03%) ^c	Pure Ar	1500–1550	900	–	–	–	~0	[1, 304, 346]
Fe (C-0.2, Cr-14.5, Ni-2.7, Mn-0.5%) ^c	Pure Ar	1500–1550	900	–	–	–	~0	[1, 304, 346]
Fe (99.999%)	Vacuum, Ar	1550	900	1780	>3560	–	~0	[1, 261, 346]
Ga (99.99999%)	Vacuum	800	900	707	250	12.1	130 ± 2	[1, 261, 346]
Ge (99.9999%)	Vacuum	1000	900	600	230	11.0	128 ± 1	[1, 261, 346]
In (99.9995%)	Vacuum	250	900	559	56	2.7	154 ± 3	[1, 261, 346]
Mn (99.8%)	Vacuum, Ar	1300	900	1750	>3500	–	~0	[1, 261]
Ni	Vacuum	1380	300	1810	3550	–	16	[1, 260, 346]
Ni (99.99%)	Vacuum, Ar	1400	900	1700	>3400	–	~0	[1, 259, 261, 346]
Pb (99.98%)	Vacuum	400	900	480	171	8.2	130 ± 1	[1, 261, 346]
Sb (99.999%)	Vacuum	700	900	384	198	9.6	119 ± 3	[1, 261, 346]
Si (99.9999%)	Vacuum	1500	900	860	>1720	–	~0	[1, 261, 346]
Sn (99.999%)	Vacuum	300	900	554	130	6.2	140 ± 1	[1, 261, 346]
Tl (99.999%)	Vacuum	400	900	490	126	6.1	138 ± 1	[1, 261, 346]

^aThe parameters of wettability are given in accordance with Young-Dupré equation $W_a = \gamma_{l-g} \times (1 + \cos\theta)$ and Young's equation $\gamma_{s-l} = \gamma_{s-g} - \gamma_{l-g}\cos\theta$, where W_a is the work of adhesion, γ_{l-g} is the liquid-vapour interfacial energy (surface tension), γ_{s-l} is solid-liquid interfacial energy, γ_{s-g} is the solid-vapour interfacial energy and θ is the wetting contact angle [1]; compositions of melts are given in mass (weight) percentage

^b $W_m = W_a(M/d)^{2/3}N_A^{1/3}$, where W_m is the molar work of adhesion, M is the molecular mass and d is the density of chemical compound, N_A is the Avogadro constant [264]

^c $\gamma_{s-l} = 550 \pm 200$ mJ m⁻²

^d $\gamma_{s-l} = 0.905$ mJ m⁻²

^eSintered materials (porosity – 12-25%)

Table 2.25 Diffusion rates and related parameters in the systems containing tantalum, carbon and tantalum carbides phases at various temperatures.^a

Species pair	Temperature dependence of the diffusion coefficient (diffusivity) $D = D_0 \exp(-E_A/R)/T$, $\text{cm}^2 \text{ s}^{-1}$	Temperature range, K ($^{\circ}\text{C}$)	Remarks on materials characteristics and measurement method	References
C \rightarrow Ta	$6.7 \times 10^{-3} \exp(-19,400/T)$	460–2950 (190–2680)	Combined data from several sources	[35, 123, 307, 492]
	$3.8 \times 10^{-2} \exp(-24,300/T)$	2470–2950 (2200–2680)	Radiotracer ^{14}C with mechanical sectioning	[35, 123, 307]
	$2.57 \times 10^{-2} \exp(-21,500/T)$	1470–1870 (1200–1600)	^{14}C radiometric method, sectioning technique	[16, 501]
	$1.2 \times 10^{-2} \exp(-20,300/T)$	1720–2470 (1450–2200)	Radiotracer ^{14}C with mechanical sectioning	[502]
	$2.78 \times 10^{-3} \exp(-12,400/T)$	870–1670 (600–1400)	Radiotracer ^{14}C with mechanical sectioning	[503]
	$4 \times 10^{-3} \exp(-16,500 \pm 90)/T$	415–535 (140–260)	From the measurements of internal friction	[16, 308]
	$1.5 \times 10^{-2} \exp(-12,600-13,600)/T$	320–430 (50–160)	From various measurements of internal friction	[495–497]
	$(6.1 \pm 1.2) \times 10^{-3} \exp(-19,400 \pm 130)/T$	460–630 (190–360)	From the measurements of internal friction	[35, 123, 308, 499, 505]
	$[(0.54-1.40) \pm (0.1-0.3)] \times 10^{-2} \times \exp\{-[-19,300-19,900] \pm (100-130)/T\}$	460–630 (190–360)	Determined by the various methods of internal friction measurements	[308, 495, 498, 499]
	$8.54 \times 10^{-4} \exp(-26,400/T)$	1870–2170 (1600–1900)	–	[37]
	$(4.2_{-2.5}^{+6.1}) \exp(-46,000 \pm 2,000)/T$	1970–2470 (1700–2200)	Carbidization of metal Ta; calculated from the diffusion coefficients obtained from layer growth	[318]
	$84.6 \exp(-49,700/T)$	1570–1870 (1300–1600)	Calculation based on the growth of TaC_{1-x} phase layer	[504]

(continued)

Table 2.25 (continued)

Species pair	Temperature dependence of the diffusion coefficient (diffusivity) $D = D_0 \exp(-E_A/R)/T$, $\text{cm}^2 \text{s}^{-1}$	Temperature range, K ($^{\circ}\text{C}$)	Remarks on materials characteristics and measurement method	References
	$1.98 \times 10^4 \exp[(-9,700 \pm 3,300)/T]$, ?	1270–2070 (1000–1800)	Calculation based on the growth of α -Ta _{2+x} C phase layer	[493–495]
	$3.43 \times 10^{-6} \exp(-10,500/T)$	1270–2070 (1000–1800)	Calculation based on the thickness of α -Ta _{2+x} C layer	[16, 90]
	$9 \times 10^{-3} \exp(-21,100/T)$	—	Theoretical values evaluated by using the elastic constants of tantalum and diameter of carbon atom	[495, 500]
	$\sim \exp(-15,100/T)$	900–1000 (630–730)	Studied by high-temperature high-resolution Auger spectroscopy during the carbonization of Ta ribbons	[679]
C → TaC _{1-x}	$3.9 \exp[(-59,700 \pm 5,900)/T]$	2630–3230 (2360–2960)	Polycrystalline (hot-pressed) TaC _{1-x} ($x \approx 0.02$ – 0.08 , $\sim \text{Ta}_{0.93}\text{N}_{0.04}\text{O}_{0.01}\text{O}_{0.98}$, 15–20 μm grain size, 7–8% porosity, O + N $\leq 0.6\%$), ¹⁴ C radiotracer	[41, 123, 305, 314, 316, 508]
	1.66×10^{-10}	2500 (2230)	Calculated on the basis of developed statistic and thermodynamic theory of interstitial phases (for $x = 0.02$)	[559]
	2.58×10^{-9}	2800 (2530)		
	1.66×10^{-8}	3100 (2830)		
	$1.38 \exp(-45,100/T)$	2370–2920 (2100–2650)	Parameters of temperature variation of TaC _{1-x} layer growth rate constant upon contact saturation of solid metallic Ta by C	[35, 123, 531]
	$2.00 \exp(-45,600/T)$	2370–2920 (2100–2650)	Parameters of reaction-chemical diffusion, contact saturation of solid Ta by C; layer growth metallography method	[1, 37, 123, 309, 509]
	$1.04 \exp(-43,300/T)$	2070–2970 (1800–2700)	Parameters of reaction-chemical diffusion, contact saturation of solid Ta by C; layer growth metallography method	[1, 123, 310, 531]
	$0.18 \exp(-43,000 \pm 1,500/T)$	1970–2970 (1700–2700)	Parameters of reaction-chemical diffusion, contact saturation of solid Ta by C in the area of compos. TaC _{1-x} ($0.02 \leq x \leq 0.04$) (initial composition with $x = 0.34$); X-ray method	[1, 37, 123, 311, 316, 350, 509, 531]
	$0.135(-42,300/T)$	1970–2970 (1700–2700)	Parameters of reaction-chemical diffusion; diffusion couple (TaC _{0.84} -C) method	[349, 350]

(continued)

Table 2.25 (continued)

Species pair	Temperature dependence of the diffusion coefficient (diffusivity) $D = D_0 \exp(-E_A/R)/T$, $\text{cm}^2 \text{s}^{-1}$	Temperature range, K ($^{\circ}\text{C}$)	Remarks on materials characteristics and measurement method	References
	$4.88 \times 10^{-4} \exp(-28,400/T)$	2560–2810 (2290–2540)	Parameters of reaction-chemical diffusion, rate of carbidization of Ta obtained by deposition from gas phase on surface of graphite ($\text{TaC}_{0.89}$); X-ray method	[123, 312]
	$8.8 \exp(-49,700/T)$	2470–3020 (2200–2750)	Parameters of reaction-chemical diffusion, contact saturation of solid Ta by C; layer growth metallography method	[123, 313]
	$8.9 \times 10^{-2} \exp(-32,400/T)$	2100–2900 (1830–2630)	Chemical diffusion coefficients calculated on the basis of experiments on deposition of non-stoichiometric carbide TaC_{1-x} ($0.10 \leq x \leq 0.34$, porosity $\leq 10\%$) from $\text{CH}_4 + \text{H}_2$ gas phase ^b	[1, 37, 123, 315]
	$2.67 \exp(-50,900/T)$	2370–2970 (2100–2700)	Carbidization of 99.97% purified metal Ta in Ar atmosphere (equivalent single phase diffusion); gravimetric techniques	[316, 317]
	$4.9 \times 10^{-5} \exp(-17,100/T)$	2370–2970 (2100–2700)	Carbidization of 99.97% purified metal Ta in Ar–30 vol.% N_2 atmosphere (equivalent single phase diffusion); gravimetric techniques	[316, 317]
	4.75×10^{-8}	2870 (2600)	Carbidization of 99.97% purified metal Ta in Ar atmosphere (two phase diffusion); gravimetric techniques	[316, 317]
	$(2.3^{+1.5}_{-0.5}) \times 10^{-2} \exp(-42,000 \pm 1,000)/T$	1970–2470 (1700–2200)	Carbidization of metal Ta; calculated from the diffusion coefficients obtained by fitting a modified error function on the measured concentration profiles (for $\text{TaC}_{-1.0}$)	[318]
	$(1.1^{+2.8}_{-0.8}) \exp(-49,000 \pm 2,000)/T$	1970–2470 (1700–2200)	Carbidization of metal Ta; calculated from the diffusion coefficients obtained from layer growth	[318]
	$(0.14^{+0.25}_{-0.09}) \exp(-42,000 \pm 2,000)/T$	1970–2470 (1700–2200)	Carbidization of metal Ta; calculated from the diffusion coefficients obtained by fitting a modified error function on the measured concentration profiles (for $\text{TaC}_{0.77}$)	[318]
	$\sim \exp(-49,100 \pm 600)/T$	2000–2500 (1730–2230)	Parameters of reaction-chemical diffusion measured by diffusion couples method	[649]
	$4 \times 10^{-3} \exp(-38,100/T)$	—	The values of chemical diffusion coefficients summarized on the basis of several works	[372]

(continued)

Table 2.25 (continued)

Species pair	Temperature dependence of the diffusion coefficient (diffusivity) $D = D_0 \exp(-E_A/R)/T$, $\text{cm}^2 \text{ s}^{-1}$	Temperature range, K ($^{\circ}\text{C}$)	Remarks on materials characteristics and measurement method	References
$\text{C} \rightarrow \zeta\text{-Ta}_4\text{C}_{3-x}$	$(20_{-7}^{+1}) \exp(-58,500 \pm 1,000)/T$	1970–2420 (1700–2150)	Carbide of metal Ta; calculated from the diffusion coefficients obtained from layer growth	[318, 372]
$\text{C} \rightarrow \beta\text{-Ta}_{2\pm}\text{C}$	$10^3 \exp(-57,900/T)$	2370–2920 (2100–2650)	Parameters of reaction-chemical diffusion, contact saturation of solid Ta by C; metallography method	[1, 37, 123, 309, 316, 509]
	$7.0 \exp(-44,800/T)$	2070–2970 (1800–2700)	Parameters of reaction-chemical diffusion, contact saturation of solid Ta by C; metallography method	[1, 123, 310]
	$2.7 \exp(-42,800/T)$	2470–3020 (2200–2750)	Parameters of reaction-chemical diffusion, contact saturation of solid Ta by C; metallography method	[123, 313]
	2.97×10^{-7}	2870 (2600)	Carbide of 99.97% purified metal Ta in Ar atmosphere (two phase diffusion); gravimetric techniques	[316, 317]
	$(1.1_{-0.5}^{+2.3}) \times 10^5 \exp(-76,000 \pm 3,000)/T$	1970–2470 (1700–2200)	Carbide of metal Ta; calculated from the diffusion coefficients obtained by fitting a modified error function on the measured concentration profiles and from layer growth as well	[318, 372]
	$10^{-5} \exp(-75,400/T)$	–	The values of chemical diffusion coefficients summarized on the basis of several works	[372]
$\text{Ta} \rightarrow \text{TaC}_{1-x}$	$24.6 \exp(-61,200/T)$	–	Values calculated on the diffusion theory basis	[1, 37, 348]
	$\sim \exp(-62,400/T)$	–	General evaluation	[169, 170, 521]
	$\sim \exp(-76,300/T)$	–	Estimated on the basis of LeClaire's relation (connected with phase melting point)	[531]
$\text{W} \rightarrow \text{TaC}_{1-x}$	$(1.4_{-1.2}^{+6.5}) \exp(-60,400 \pm 4,000)/T$	2270–2820 (2000–2550)	Polycrystalline TaC_{1-x} ($x \approx 0.4\%$ porosity, $\text{O} + \text{N} \leq 0.2\%$), ^{185}W radiotracer	[41, 306, 507]
$\text{W} \rightarrow \text{TaC}_{1-x}$	–	–	The mixed carbide systems have the solid solutions, which possess a maximum value of the activation energy of W diffusion	[825]
$\text{W} \rightarrow$ (W,Ti) TaC_{1-x}	–	–		

(continued)

Table 2.25 (continued)

^aThe chemical diffusion coefficient concentration and temperature dependencies can be represented by an equation of the form $D' = D'_0 \exp(\beta x) \exp[-E'_A/(R)T]$, where β is the concentration factor and x is the value of index in TaC_{1-x} formula (for the ranges of $x = 0.01$ – 0.43 and $T = 1730$ – 2730 °C the recommended values are $D'_0 = 0.136 \text{ cm}^2 \text{ s}^{-1}$, $\beta = 6.0$ and $E'_A = 358 \text{ kJ mol}^{-1}$ [350]), and the discrepancy between chemical and self-diffusivities may be estimated on the basis of the thermodynamical relationship: $D' = D \times [1 + (d \ln \gamma_C / d \ln N_C)]$, where γ_C is the activity coefficient of carbon and N_C is the atomic fraction of carbon (evaluated at 2000 °C in TaC_{1-x} : at $x = 0.01$, $d \ln \gamma_C / d \ln N_C = 134$ and at $x = 0.20$, $d \ln \gamma_C / d \ln N_C = 9.4$ [506]); the approximate values of apparent activation energy for some diffusion controlled processes in TaC_{1-x} : α - Ta_{2+x}C and β - Ta_{2+x}C : (a) formation kinetics of α - Ta_{2+x}C during the $2\text{TaC}_{-1.0} + \text{Ta}$ interaction – $220 \pm 20 \text{ kJ mol}^{-1}$ (900–1200 °C) [711–713]; (b) formation kinetics of ζ - $\text{Ta}_4\text{C}_{3-x}$ ($x = 0.44$) during the $2\text{TaC}_{-1.0} + \text{Ta}$ interaction – $1010 \pm 150 \text{ kJ mol}^{-1}$ (1600–1800 °C) [711–713]; (c) recrystallization (grain growth) – 380 kJ mol^{-1} (sintered $\text{TaC}_{-1.0}$, 2400–2700 °C) [177]; (d) powder hot-pressing densification – 210 kJ mol^{-1} (β - $\text{Ta}_2\text{C}_{-1.0}$, viscous flow, 2700–3050 °C) [515, 516], 210 kJ mol^{-1} (β - $\text{Ta}_2\text{C}_{-1.0}$, mean particle size 15–25 μm , 2700 °C) [647], 295 kJ mol^{-1} ($\text{TaC}_{0.73}$, mean particle size 15–25 μm , 2700 °C) [647]; 325 kJ mol^{-1} ($\text{TaC}_{0.82}$, mean particle size 15–25 μm , 2700 °C) [647], 360 kJ mol^{-1} ($\text{TaC}_{0.91}$, mean particle size 15–25 μm , 2700 °C) [647], 405 kJ mol^{-1} ($\text{TaC}_{-1.0}$, viscous flow, 2700–3050 °C) [515, 516]; (e) indentation – 465 kJ mol^{-1} (single crystal $\text{TaC}_{0.83}$, 1200–1300 °C) [169]; (f) internal friction peaks characteristics (Marx-Wert formula) – 360 kJ mol^{-1} (sintered $\text{TaC}_{0.99}$, 1640 °C) [537]; data on creep – see Sect. 2.4 (Table 2.16), see also Sect. 2.5 (Table 2.20)

^bThe parameters probably contain significant contribution of surface and grain-boundary diffusion due to rather high porosity of the materials

Table 2.26 The interaction of near-stoichiometric tantalum monocarbide TaC_{1-x} materials with some chemical reagents in aqueous solutions [1, 37, 43, 90, 215, 319, 320, 345, 352, 353, 362, 512, 532]

Reagent, formula (density or concentration of aqueous solution) ^a	Treatment conditions		Character of interaction ^b
	Temperature, °C	Exposure time, h	
HCl (1:1)	20	24	No decomposition
	110–112	2	Decomposes up to ~2%
HCl (<i>d</i> = 1.19)	20	24	No decomposition
	120	2	Decomposes up to ~2%
H ₂ SO ₄ (1:4)	20	24	Decomposes up to ~1%
	115	2	Decomposes up to ~7%
H ₂ SO ₄ (<i>d</i> = 1.84)	20	24	No decomposition
	255	1.5	Decomposes up to ~75% (10% amorphous C) with the formation of stable oxysulfate; composition of released gases: CO ₂ 96.0, CO 2.2 and H ₂ 1.6 mol.% (CO ₂ and CO are products of the oxidation of amorphous C) ^c
	275	1.0	Decomposes up to ~80% (6.0% amorphous C) with the formation of stable oxysulfate; composition of released gases: CO ₂ 92.3, CO 6.0 and H ₂ 1.7 mol.% (CO ₂ and CO are products of the oxidation of amorphous C) ^c
HNO ₃ (1:1)	20	24	Decomposes completely (solution is transparent finally) ^c
	105	2	Decomposes up to ~1%
	110–114	1–2	Decomposes up to ~2%
HNO ₃ (<i>d</i> = 1.43)	20	24	No decomposition
	110–114	1–2	Decomposes up to ~1%
H ₃ PO ₄ (1:3)	≥100	2	Decomposes up to ~2%
H ₃ PO ₄ (<i>d</i> = 1.70)	20	24	Decomposes up to ~2%
	150–300	2	Decomposes very slightly
H ₂ C ₂ O ₄ ^d (saturated solution)	20	24	Decomposes up to ~3%
	100–105	2	Decomposes up to ~2%
NaOH (10%)	20	24	Decomposes up to ~1%
	108	2	No decomposition
NaOH (20%)	20	24	Decomposes up to ~1%
	108	2	Decomposes up to ~1%
H ₂ O ₂ (30%)	110	1	Decomposes up to ~15–17%
NH ₄ F (5%)	110	1	Decomposes up to ~10%
(NH ₄) ₂ S ₂ O ₈ (25–30%)	110	1	Decomposes up to ~10–12%
3HCl (1:1) + HNO ₃ (1:2)	110		No decomposition
3HCl (<i>d</i> = 1.19) + HNO ₃ (<i>d</i> = 1.43)	20	24	Decomposes up to ~1%
	110–115	2	Decomposes up to ~2%
HCl (<i>d</i> = 1.19) + H ₂ O ₂ (30%)	110	1	Decomposes up to ~1%

(continued)

Table 2.26 (continued)

Reagent, formula (density or concentration of aqueous solution) ^a	Treatment conditions		Character of interaction ^b
	Tempera- ture, °C	Exposure time, h	
HCl ($d = 1.19$) + (NH ₄) ₂ S ₂ O ₈ (25%)	–	–	Decomposes up to ~2%
HCl ($d = 1.19$) + Br ₂ (HBrO, HBr) (saturated solution)	–	–	Decomposes up to ~2%
H ₂ SO ₄ ($d = 1.84$) + HNO ₃ ($d = 1.43$)	20	24	Decomposes up to ~9%
	110	2	Decomposes up to ~4%
H ₂ SO ₄ (1:4) + H ₃ PO ₄ (1:3)	20	24	No decomposition
	≥150	2	Decomposes up to ~1%
H ₂ SO ₄ ($d = 1.84$) + H ₃ PO ₄ ($d = 1.70$)	20	24	Decomposes up to ~2%
	≥150	2	Decomposes ≥50% with the deposition of salts and hydrolysis
H ₂ SO ₄ (1:4) + H ₂ C ₂ O ₄ ^d (saturated solution)	20	24	Decomposes up to ~7%
	≥100	2	Decomposes up to ~2%
H ₂ SO ₄ ($d = 1.84$) + H ₂ C ₂ O ₄ ^d (saturated solution)	20	24	Decomposes up to ~3%
	≥100	2	Decomposes up to ~3%
H ₂ SO ₄ (1:4) + H ₂ O ₂ (30%)	110	1	Decomposes up to ~20–25%
H ₂ SO ₄ (1:4) + (NH ₄) ₂ S ₂ O ₈ (25%) (1–4)HNO ₃ ($d = 1.43$) + HF ($d = 1.15$) ^e	110	1	Decomposes up to ~2–5%
	20	–	Decomposes completely
HNO ₃ ($d = 1.43$) + NH ₄ F (5%)	110	0.5	Decomposes completely
	110–120	0.5	Decomposes completely; composition of released gases: CO ₂ 95–97, CO (traces) and H ₂ 2–3 mol.% (no precipi- tated C, solution is transparent)
H ₂ O ₂ (30%) + H ₂ C ₄ H ₄ O ₆ ^f (50%)	110	1	Decomposes up to ~40–50%
H ₂ O ₂ (30%) + H ₃ C ₆ H ₅ O ₇ ^g	110	1	Decomposes up to ~43%
H ₂ O ₂ (30%) + H ₄ C ₁₀ H ₁₂ N ₂ O ₈ ^h (saturated solution)	110	1	Decomposes up to ~96%
H ₂ O ₂ (30%) + NH ₄ F (NH ₄) ₂ S ₂ O ₈ + NH ₄ F	110	1	Decomposes up to ~96%
	–	–	Decomposes up to ~37%
4NaOH (20%) + Br ₂ (HBrO, HBr)	20	24	No decomposition
	100–110	2	Decomposes ≥50% with the deposition of salts
4NaOH (20%) + H ₂ O ₂ (30%)	20	24	Decomposes up to ~38%
	≥100	2	Decomposes ≥50% with the deposition of salts and hydrolysis
4NaOH (20%) + K ₃ [Fe(CN) ₆] (10%) ⁱ	20	24	Partly decomposes by hydrolysis
	≥100	2	Decomposes ≥50%

^aAll the ratios are given in volume fractions^bWhen it is not indicated specially, the character reported is related to the powders with mean particle size of 40–50 μm^cRepresented by the reaction equation: 2TaC_{1-x} + 4H₂SO₄ + 5SO₃ = Ta₂O(SO₄)₄ + 2(1 - x)C + 5SO₂ + 4H₂O^dOxalic acid^eα-Ta_{2+x}C decomposes completely in this solvent as well [37]^fTartaric acid

(continued)

Table 2.26 (continued)^gCitric acid^hEthylenediaminetetraacetic acid (EDTA)

ⁱRecommended chemical etching agents for TaC_{1-x}: (a) 10 g K₃[Fe(CN)₆] + 2–10 g KOH/NaOH + 100 ml H₂O (Murakami's reagent) [442]; (b) boiling aqueous solutions KOH (20%) + K₄[Fe(CN)₆] (20%) with exposure 3 min [347]; (c) boiling mixture of concentrated H₂SO₄ + (NH₄)₂S₂O₈ [441]; (d) H₂NSO₃H (20% sulfamic acid) with exposure 1 min (for thin films on different substrates) [442, 443]; (e) HF + 40% NH₄F (BHF solution) with exposure 4 s (for thin films on different substrates) [442, 443]; (f) 1 part HF (40%) + 3 parts concentrated HNO₃ with exposure 2 min [510]; (g) 40 ml HCl + 10 ml HNO₃ + 1 ml HF at 60–70 °C with exposure 4 min [381]; (h) 10 ml HNO₃ + 1 ml HF + 0.5 ml lactic acid CH₃CH(OH)CO₂H at 60–70 °C with exposure 0.5–1.0 min (for determination of the density of dislocations) [159]

oxidation kinetics of near-stoichiometric TaC_{1-x} materials given in the latter one can be termed in the context of ridge-effect model proposed by Shabalin [303, 452] with ridge temperature at air common conditions (for a certain partial oxygen pressure) nearby 800 °C, since the kinetics curves at temperatures ≥1000 °C are not reproducible and representative because of randomly cracking and splitting oxide scales. Data on the catalytic activities of tantalum carbides are given in several works [1, 351, 354, 355, 475–490, 630–639, 764, 800, 827, 899]; the examples of electrochemical behaviour of tantalum carbides are described in [355, 491, 639, 827]. The parameters of wettability of tantalum monocarbide phases with some liquid metals (melts) are listed in Table 2.24, the diffusion rates for the systems containing tantalum carbide phases are presented in species pairs within the various ranges of temperatures in the Table 2.25. The characters of chemical interaction of tantalum monocarbide phases with some common chemicals (acids, alkalis and salts in aqueous solutions) are summarized in Table 2.26.

In comparison with other ultra-high temperature materials the summarized data on the chemical behaviour of tantalum carbides are given in Addendum.

References

1. Kosolapova TYa (ed) (1990) Handbook of high-temperature compounds: properties, production and applications. Hemisphere, New York
2. Gusev AI, Rempel AA, Magerl AJ (2001) Disorder and order in strongly nonstoichiometric compounds. Springer, Berlin
3. Demyashev GM (2010) Review: transition metal-based nanolamellar phases. Prog Mater Sci 55:629–674
4. Lyakishev NP (ed) (1996) Diagrammy sostoyaniya dvoynikh metallicheskich sistem (Phase diagrams of binary metallic systems), Vol. 1. Mashinostroenie, Moscow (in Russian)
5. Massalski TB, Subramanian PR, Okamoto H, Kacprzak L (eds) (1990) Binary alloy phase diagrams, 2nd edn. ASM International, Metals Park, Ohio

6. Sridharan S, Nowotny H (1983) Studies in the ternary system Ti-Ta-Al and in the quaternary system Ti-Ta-Al-C. *Z Metallkd* 74(7):468–472
7. Matsumoto O, Yaguchi Y, Shiota Y, Kanzaki Y (1983) Formation of cubic solid solutions in the Mo-Nb-C and Mo-Ta-C systems by the carbonization of oxides in the plasma arc. *High Temp Sci* 16(4):243–250
8. Dubrovskaya LB, Nazarova SZ, Prekul AF (1982) Superconducting and normal properties of solid solutions $Nb_{1-x}Ta_xC_y$. *Phys Stat Sol A* 69(1):167–172
9. Valvoda V (1981) X-ray diffraction study of Debye temperature and charge distribution in tantalum monocarbide. *Phys Stat Sol A* 64(1):133–142
10. Kats SM, Ordanyan SS, Zaitsev GP (1981) High-temperature creep of solid solutions in the HfC-TaC system. *Inorg Mater* 17(11):1519–1522
11. Benedict U, Richter K, Walker CT (1978) Solubility study in the systems PuC-ZrC and PuC-TaC. *J Less-Common Met* 60(1):123–133
12. Kats SM, Ordanyan SS (1977) High-temperature creep of ZrC-TaC solid solutions. *Inorg Mater* 13(10):1426–1428
13. Dubrovskaya LB, Zaytsev GP, Ordanyan SS (1977) Magnetic susceptibility of solid solutions of hafnium and tantalum monocarbides. *Phys Met Metallogr* 44(6):173–177
14. Ordanyan SS, Unrod VI, Polishchuk VS, Storonkina NM (1976) Reactions in the system TaC-TaB₂. *Powder Metall Met Ceram* 15(9):692–695
15. Gatterer J, Dufek G, Etmayer P, Kieffer R (1975) Das kubische Tantalmonitrid (B1-Typ) und seine Mischbarkeit mit den isotypen Übergangsmetallnitriden und -carbiden (The cubic tantalum mononitride (B1-Type) and its miscibility with the isotypic mononitrides and monocarbides of the 4a and 5a group metals). *Monatsh Chem* 106(5):1137–1147 (in German)
16. Kotelnikov RB, Bashlykov SN, Galiakbarov ZG, Kashtanov AI (1968) Osobo tugoplavkie elementy i soedineniya (Extra-refractory elements and compounds). *Metallurgiya, Moscow* (in Russian)
17. Storms EK (1967) *The refractory carbides*. Academic Press, New York, London
18. Lissner F, Schleid T (2001) Refinement of the crystal structure of ditantalum monocarbide Ta₂C. *Z Krist New Cryst St* 216(3):329–330
19. Korolev YM, Gavrish AA, Glazunov MP, Spitsyn VI, Fedoseev GK (1975) Effect of Ta₂C texturation on quantitative X-ray diffraction analysis. *Russ J Inorg Chem* 20(11):1591–1593
20. Bowman AL, Wallace TC, Yarnell JL, Wenzel RG, Storms EK (1965) The crystal structures of V₂C and Ta₂C. *Acta Crystallogr* 19(1):6–9
21. Rudy E, Brukl CE, Windisch S (1968) Constitution of ternary Ta-Mo-C alloys. *J Am Ceram Soc* 51(5):239–250
22. Rudy E, Harmon DP (1966) Ta-C system. Partial investigation in the systems Nb-C and V-C. In: Ternary phase equilibria in transition metal-boron-carbon-silicon systems. Report AFML-TR-65-2, Contract USAF 33(615)-1249, Part 1, Vol. 5. Air Force Materials Laboratory, Wright-Patterson Air Force Base, Ohio, pp. 1–78
23. Ramqvist L (1968) Variation of hardness, resistivity and lattice parameter with carbon content of group 5b metal carbides. *Jernkontoret Ann* 152(9):465–475
24. Rudy E, Benesovsky F, Toth L (1963) Untersuchung der Dreistoffsysteme der Va-Metalle und VIa-Metalle mit Bor und Kohlenstoff (Investigation of the ternary systems of the Va metals and VIa metals with boron and carbon). *Z Metallkd* 54(6):345–353 (in German)
25. Rudy E, Benesovsky F (1962) Untersuchungen im System Tantal-Wolfram-Kohlenstoff (Investigations in the system tantalum-tungsten-carbon) *Monatsh Chem* 93(5):1176–1195 (in German)
26. Villagrana RE, Thomas G (1965) Interstitial ordering of carbon in tantalum. *Phys Stat Sol B* 9(2):499–518
27. Dahmen U, Thomas G (1979) Significance of oxygen on interstitial ordering in tantalum (The Ta₆₄C artifact). *Scripta Metall* 13:527–530
28. Yvon K, Parthe E (1970) On the crystal chemistry of the close packed transition metal carbides. I. The crystal structure of the ζ-V, Nb and Ta carbides. *Acta Crystallogr B* 26(2):149–153

29. Gusev AI, Kurlov AS, Lipatnikov VN (2007) Atomic and vacancy ordering in carbide ζ -Ta₄C_{3-x} ($0.28 \leq x \leq 0.40$) and phase equilibria in the Ta-C system. *J Solid State Chem* 180:3234–3246
30. Gusev AI, Rempel AA, Lipatnikov VN (1996) Incommensurate ordered phase in non-stoichiometric tantalum carbide. *J Phys Condens Matter* 8:8277–8293
31. Lipatnikov VN, Rempel AA (2005) Formation of the incommensurate ordered phase in TaC_y carbide. *JETP Lett* 81(7):326–330
32. Lipatnikov VN, Gusev AI (2006) Atomic-vacancy ordering in the carbide phase ζ -Ta₄C_{3-x}. *Phys Solid State* 48(9):1634–1645
33. Lönnberg B, Lundström T, Tellgren R (1986) A neutron powder diffraction study of Ta₂C and W₂C. *J Less-Common Met* 120:239–245
34. Hackett K, Verhoef S, Cutler RA, Shetty DK (2009) Phase constitution and mechanical properties of carbides in the Ta-C system. *J Am Ceram Soc* 92(10):2404–2407
35. Samsonov GV, Upadhyaya GS, Neshpor VS (1974) *Fizicheskoe materialovedenie karbidov* (Physical materials science of carbides). Naukova Dumka, Kyiv (in Russian)
36. Alyamovskii SI, Zainulin YuG, Shveikin GP (1981) *Oksikarbidy i oksinitridy metallov IVA i VA podgrupp* (Oxycarbides and oxynitrides of IVA and VA subgroups metals). Nauka, Moscow (in Russian)
37. Samsonov GV, Vinitskii IM (1980) *Handbook on refractory compounds*. IFI/Plenum, New York
38. Barin I (1995) *Thermochemical data of pure substances*, Vol. 1–2, 3rd edn. VCH, Weinheim, New York
39. Huber EJ Jr, Head EL, Holley CE Jr, Bowman AL (1963) Heats of formation of tantalum carbides. *J Phys Chem* 67(4):793–796
40. Bolgar AS, Guseva EA, Gorbatyuk VA, Fesenko VV (1968) Enthalpy and specific heat of tantalum carbide in its homogeneity region. *Powder Metall Met Ceram* 7(4):297–298
41. Andrievskii RA, Spivak II (1989) *Prochnost tugoplavkikh soedinenii i materialov na ikh osnove* (Strength of refractory compounds and materials based on them). *Metallurgiya, Chelyabinsk* (in Russian)
42. Andrievskii RA, Lanin AG, Rymashevskii GA (1974) *Prochnost tugoplavkikh soedinenii* (Strength of refractory compounds). *Metallurgiya, Moscow* (in Russian)
43. Krzhizhanovskii RE, Shtern ZYu (1977) *Teplofizicheskie svoistva nemetallicheskich materialov (karbidy)* (Thermophysical properties of non-metallic materials (carbides)). *Energiya, Leningrad* (in Russian)
44. Zefirov AP (ed), Vertyatin UD, Mashirev VP, Ryabtsev NG, Tarasov VI, Rogozkin BD, Korobov IV (1965) *Termodinamicheskie svoistva neorganicheskikh veschestv* (Thermodynamic properties of inorganic substances). *Atomizdat, Moscow* (in Russian)
45. Chirkin VS (1968) *Teplofizicheskie svoistva materialov yadernoi tekhniki* (Thermophysical properties of nuclear materials). *Atomizdat, Moscow* (in Russian)
46. Nakamura K, Yashima M (2008) Crystal structure of NaCl-type transition metal monocarbides MC (M = V, Ti, Nb, Ta, Hf, Zr), a neutron powder diffraction study. *Mater Sci Eng B* 148:69–72
47. Zubkov VG, Dubrovskaya LB, Geld PV, Tskhai VA, Dorofeev YuA (1969) *Neutrono-diffraktsionnoe issledovanie uporyadocheniya nestekhiometricheskikh kubicheskikh karbidov perekhodnykh metallov V gruppy* (Neutron diffraction study of the ordering of non-stoichiometric cubic carbides of group V transition metals). *Doklady AN SSSR* 184:874–876 (in Russian)
48. Fries RJ, Wahman LA (1967) Effect of stoichiometry on the thermal expansion of TaC_x. *J Am Ceram Soc* 50(9):475–477
49. Samsonov GV, Timofeeva II (1970) *Rentgenograficheskoe issledovanie dinamicheskikh harakteristik kristallicheskich reshetok nekotorykh faz vnedreniya* (X-ray diffraction study of dynamic characteristics of crystal lattices of some interstitial phases). *Dopov Akad Nauk Ukr RSR Ser A Fiz Mat Tekh Nauki* 32(9):831–833 (in Russian)
50. Bukatov VG, Knyazev VI, Korostin OS, Baranov VM (1975) Temperature dependence of the Young's modulus of metallic carbides. *Inorg Mater* 11(2):310–312

51. Portnoi KI, Chubarov VM (1967) Svoistva tugoplavkikh metallov i soedinenii (The properties of refractory metals and compounds). In: Tumanov AT, Portnoi KI (eds) Tugoplavkie materialy v mashinostroenii (Refractory materials in machinery construction). Mashinostroenie, Moscow, pp. 7–124 (in Russian)
52. Turchanin AG, Turchanin MA (1991) Termodinamika tugoplavkikh karbidov i karbonitridov (Thermodynamics of refractory carbides and carbonitrides). Metallurgiya, Moscow (in Russian)
53. Turchanin AG, Guseva EA, Fesenko VV (1971) Thermodynamic properties of refractory carbides in the temperature range 0-3000 K. I. Tantalum carbide. Powder Metall Met Ceram 10(10):823–825
54. Kelley KK (1940) The specific heats at low temperatures of tantalum oxide and tantalum carbide. J Am Chem Soc 62:818–819
55. Levinson LS (1963) High-temperature heat content of niobium carbide and of tantalum carbide. J Chem Phys 39(6):1550–1551
56. Sheindlin AE, Chekhovskoi VYa, Spilrain EE (1970) Research on thermophysical properties of solids at high temperatures at the Institute for High Temperatures of the USSR Academy of Sciences. High Temp High Press 2(1):1–6
57. Sheindlin AE, Belevich IS, Kozhevnikov IG (1972) Enthalpy and specific-heat of tantalum carbide in the range of 273–3600 K. High Temp 10(3):581–583
58. Petrova II, Chekhovskoi VYa (1978) True heat-capacity of zirconium, niobium and tantalum carbides by a pulse method. High Temp 16(6):1045–1050
59. Lide DR (ed) (2010) Handbook of chemistry and physics, 90th edn. CRC Press, Boca Raton, New York
60. Pierson HO (1996) Handbook of refractory carbides and nitrides. Noyes Publications, Westwood, New Jersey
61. Marmer EN, Gurvich OS, Maltseva LF (1967) Vysokotemperaturnye materialy (High-temperature materials). Metallurgiya, Moscow (in Russian)
62. Kornilov AN, Zaikin ID, Skuratov SM, Dubrovskaya LB, Shveikin GP (1967) Standard heats of formation of tantalum carbides from TaC phase. Russ J Phys Chem 41(2):172–174
63. Ritzhaupt-Kleissl H-J (1975) Hartstoffe im System Ta-TaC-TaN Einfluß von Zusammensetzung, Wärmebehandlung und Ausscheidungen auf die Härte bis 1300 °C (Hard materials in the system Ta-TaC-TaN, influence of composition, heat treatment and precipitates on the hardness to 1300 °C). KFK 2143. Institut für Material- und Festkörperforschung, Gesellschaft für Kernforschung MBH, Karlsruhe (in German)
64. Kornilov AN, Zaikin ID, Skuratov SM, Dubrovskaya LB, Shveikin GP (1964) Standartnyye teploty obrazovaniya karbidov tantalala iz fazy Ta₂C (Standard heats of formation of tantalum carbides from Ta₂C phase). Zh Fiz Khim 38(3):702–707 (in Russian)
65. Nikolskaya TA, Avarbe RG (1969) Temperature dependence and velocity of congruent evaporation of tantalum carbide phase. High Temp 7(6):1021–1023
66. Samsonov GV, Paderno VN (1963) Poluchenie i svoistva nekotorykh tugoplavkikh karbidnykh splavov (Preparation and properties of certain refractory carbide alloys). Zh Prikl Khim 36(12):2759–2762 (in Russian)
67. Kieffer R, Schwarzkopf P (1953) Hartstoffe und Hartmetalle (Refractory hard metals). Springer, Vienna (in German)
68. Hague JR, Lynch JF, Rudnick A, Holden FC, Duckworth WH (1964) Refractory ceramics for aerospace. Battelle Memorial Institute, The American Ceramic Society, Columbus, Ohio
69. Paderno YuB, Barantseva IG, Yupko VL (1965) Izmerenie teploprovodnosti i elektrostoprotivleniya ZrC, HfC, NbC i TaC pri vysokikh temperaturakh (Measurement of thermal conductivity and electrical resistance of ZrC, HfC, NbC and TaC at high temperatures). In: Grigoreva VV, Eremenko VN, Nazarchuk TN, Samsonov GV, Fedorchenko IM, Frantsevich IN (eds) Vysokotemperaturnye neorganicheskie soedineniya (High-temperature inorganic compounds). Naukova Dumka, Kyiv, pp. 199–204 (in Russian)
70. Storms EK (1964) A critical review of refractories. Report LA-TR-2942, Contract W-7405-eng-36. Los Alamos Scientific Laboratory, New Mexico, pp. 1–255
71. Andrievskii RA, Strelnikova NS, Poltoratskii NI, Kharkhardin ED, Smimov VS (1967) Melting point in systems ZrC-HfC, TaC-ZrC, TaC-HfC. Powder Metall Met Ceram 6(1):65–67

72. Samsonov GV, Paderno VN (1965) Preparation of solid solution alloys of hafnium carbide with carbides of titanium, zirconium, niobium and tantalum and determination of their physical properties. *Russ Metall* (1):119–126
73. Fukunaga A, Chu S, McHenry ME (1998) Synthesis, structure and superconducting properties of tantalum carbide nanorods and nanoparticles. *J Mater Res* 13(9):2465–2471
74. Shi L, Gu Y, Chen L, Yang Z, Ma J, Qian Y (2004) Formation of TaC nanorods with a low-temperature chemical route. *Chem Lett* 33(12):1546–1547
75. Lane NJ, Barsoum MW, Rondinelli JM (2013) Correlation effects and spin-orbit interactions in two-dimensional hexagonal 5d transition metal carbides $Ta_{n+1}C_n$ ($n = 1, 2, 3$). *Eur Phys Lett* 101(3):57004 (5 pp.)
76. Morris RA, Wang B, Thompson GB, Butts D (2013) Variations in tantalum carbide microstructures with changing carbon content. *Int J Appl Ceram Technol* 10(3):540–551
77. Wang B, De Leon N, Weinberger CR, Thompson GB (2013) A theoretical investigation of the slip systems of Ta_2C . *Acta Mater* 61:3914–3922
78. Bowman A (1961) The variation of lattice parameter with carbon content of tantalum carbide. *J Phys Chem* 65(9):1596–1598
79. Elliott RO, Kempter CP (1958) Thermal expansion of some transition metal carbides. *J Phys Chem* 62(5):630–631
80. Frisk K, Fernandez-Guillermet A (1996) Gibbs energy coupling of the phase diagram and thermochemistry in the tantalum-carbon system. *J Alloys Compd* 238:167–179
81. Schick HL (ed) (1966) Thermodynamics of certain refractory compounds, Vol. 1–2. Academic Press, New York, London
82. Hultgren R, Desai PD, Hawkins DT, Gleiser M, Kelley KK, Wagman DD (1973) Selected values of the thermodynamic properties of binary alloys. American Society for Metals, Metals Park, Ohio
83. Kulkarni AD, Worrell WL (1973) High-temperature thermodynamic stability of ditantalum carbide (Ta_2C). *Metall Trans* 4(4):931–933
84. Kubaschewski O (ed), Gerasimov YaI, Lavrentev VI, von Goldbeck O, Livey DT, Ferro R (1972) Tantalum: physico-chemical properties of its compounds and alloys. Atomic Energy Review, Special Issue N 3. International Atomic Energy Agency, Vienna, pp. 1–133
85. Miccioli BR, Shaffer PTB (1964) High-temperature thermal expansion behaviour of refractory materials. I. Selected monocarbides and binary carbides. *J Am Ceram Soc* 47(7):351–356
86. Nowotny H, Laube E (1961) Die thermische Ausdehnung des hochschmelzenden Phasen (The thermal expansion of high-melting point phases). *Planseeber Pulvermetall* 9:54–59 (in German)
87. Paderno YuB, Dudnik EM, Andreeva TV, Barantseva IG, Yupko VL (1965) Izmerenie koeffitsientov termicheskogo rasshireniya ZrC, HfC, NbC i TaC pri vysokikh temperaturakh (Measurement of the coefficients of thermal expansion of ZrC, HfC, NbC and TaC at high temperatures). In: Grigoreva VV, Eremenko VN, Nazarchuk TN, Samsonov GV, Fedorchenko IM, Frantsevich IN (eds) *Vysokotemperaturnye neorganicheskie soedineniya* (High-temperature inorganic compounds). *Naukova Dumka, Kyiv*, pp. 293–296 (in Russian)
88. Krikorian OH (1960) Thermal expansion of high-temperature materials. Report UCRL-TR-6132. Lawrence Radiation Laboratories, US Atomic Energy Commission, University of California, pp. 1–7
89. Sheplaine VM, Runck RJ (1956) Carbides. In: Campbell IE (ed) *High temperature technology*. Wiley, New York and Chapman and Hall, London, pp. 114–130
90. Samsonov GV (1964) Refractory transition metal compounds. Academic Press, New York
91. Koenig JH (1958) New developments in ceramics. *Mater Design Eng* 47(5):121–123
92. Neel DS, Pears CD, Oglesby S Jr (1962) The thermal properties of thirteen solid materials to 5000 °F or their destruction temperatures. Technical Report WADD-TR-60-924, Contract USAF 33(616)-6312. Southern Research Institute, University of Alabama, Birmingham, USA, pp. 1–216
93. Houska CR (1964) Thermal expansion of certain group IV and group V carbides at high temperatures. *J Am Ceram Soc* 47(6):310–311

94. Samsonov GV, Portnoi KI (1961) *Splavy na osnove tugoplavlikh soedinenii* (The alloys on the basis of refractory compounds). Oborongiz, Moscow (in Russian)
95. Kempter CP, Nadler MR (1965) Thermal expansion of tantalum monocarbide to 3020 °C. *J Chem Phys* 43(5):1739–1742
96. Jun CK, Shaffer PTB (1971) Thermal expansion of niobium carbide, hafnium carbide and tantalum carbide at high temperatures. *J Less-Common Met* 24(3):323–327
97. Lönnberg B (1986) Thermal expansion studies on the subcarbides of group V and VI transition metals. *J Less-Common Met* 120:135–146
98. Samsonov GV, Sinelnikova VS (1962) *Vysokotemperaturnye metallokeramicheskie materialy* (High-temperature sintered metal-powder materials). UkrSSR Academy of Sciences, Kyiv (in Russian)
99. Clinard FW Jr, Kempter CP (1968) Low-temperature electrical properties of some transition metals and transition-metal carbides. *J Less-Common Met* 15:59–73
100. Allison CY, Finch CB, Foegelle MD, Modine FA (1988) Low-temperature resistivity of transition-metal carbides. *Solid State Commun* 68(4):387–390
101. Golikova OA, Dzhaferov EO, Avgustinik AI, Klimashin GM (1970) Electrical properties of tantalum carbide at high temperatures. *Sov Phys Solid State* 11(8):1936–1940
102. Eckstein BH, Forman R (1962) Preparation and some properties of tantalum carbide. *J Appl Phys* 33(1):82–87
103. Neshpor VS, Airapetyants SV, Ordanyan SS, Avgustinik AI (1966) Effect of the chemical composition of the monocarbides of group IV and V transition metals in the homogeneity range on the temperature dependence of their resistivity and thermo-e.m.f. *Inorg Mater* 2(5):728–730
104. Sakurai J, Hayashi J, Mekata M, Tsuchida T, Takagi H (1961) Thermal conductivities of monocarbides in transition metals. *J Jpn Inst Met* 25(4):289–292 (in Japanese)
105. Lvov SN, Nemchenko VF, Samsonov GV (1960) *Nekotorye zakonomernosti elektricheskikh svoystv boridov, karbidov i nitridov perekhodnykh metallov IV-V grupp periodicheskoi sistemy* (Some regularities in the electric properties of borides, carbides and nitrides of transition metals within the IV-VI groups of the periodic system). *Doklady AN SSSR* 135(3):577–580 (in Russian)
106. Fesenko VV, Bolgar AS (1963) O kompleksnom izmerenii fiziko-khimicheskikh svoystv tugoplavlikh soedinenii pri vysokikh temperaturakh (On the complex measurement of physico-chemical properties of refractory compounds at high temperatures). In: Budnikov PP (ed) *Silikaty i oksidy v khimii vysokikh temperatur* (Silicates and oxides in the chemistry of high temperatures). Metallurgizdat, Moscow, pp. 135–148 (in Russian)
107. Steinitz R, Resnick R (1966) Electrical and magnetic properties of compositions in tantalum-carbon system. *J Appl Phys* 37(9):3463–3471
108. Neshpor VS, Ordanyan SS (1965) Certain electrical and thermal properties of tantalum monocarbide in the homogeneous region. *Inorg Mater* 1(4):442–444
109. Samsonov GV, Rukina VB (1957) Mikrotverdost i elektrosoprotivlenie karbida tantala v ego oblasti gomogenosti (Microhardness and electrical resistance of tantalum carbide in its homogeneous region). *Dopov Akad Nauk Ukr RSR* 3:247–249 (in Russian)
110. Santoro G (1963) Variation of some properties of tantalum carbide with carbon content. *Trans Metall Soc AIME* 227(6):1361–1368
111. Borukhovich AS, Geld PV, Tskhai VA, Dubrovskaya LB, Matveenkov II (1971) Conduction band of IVa and Va subgroup transition metal monocarbides. II. *Phys Stat Sol B* 45(1):179–187
112. Onufriev SV, Savvatimskii AI, Yanchuk VI (2011) Measurement of the thermal properties of zirconium and tantalum carbides at high temperatures (up to and above the melting point). *Meas Tech* 54(8):926–930
113. Knyazkov AM, Kurbakov SD, Savvatimskiy AI, Sheindlin MA, Yanchuk VI (2011) Melting of carbides by electrical pulse heating. *High Temp High Press* 40:349–358
114. Giorgi AL, Szklarz EG, Storms EK, Bowman AL, Matthias BT (1962) Effect of composition on the superconducting transition temperature of tantalum carbide and niobium carbide. *Phys Rev* 125(3):837–838

115. Toth LE (1971) Transition metal carbides and nitrides. Academic Press, New York, London
116. Toth LE, Ishikawa M, Chang YA (1968) Low temperature heat capacity of superconducting niobium and tantalum carbides. *Acta Mater* 16(9):1183–1187
117. Bhatt HD, Vedula R, Desu SB, Fralick GC (1999) Thin film TiC/TaC thermocouples. *Thin Solid Films* 342:214–220
118. Bittner H, Goretzki H (1962) Magnetische Untersuchungen der Carbide TiC, ZrC, HfC, VC, NbC und TaC (Magnetic studies of the TiC, ZrC, HfC, VC, NbC and TaC carbides). *Monatsh Chem* 93(5):1000–1004 (in German)
119. Dubrovskaya LB, Matveenko II (1965) Magnitnye svoistva kubicheskogo karbida tantalata (The magnetic properties of tantalum cubic carbide). *Fiz Met Metalloved* 19(2):199–204 (in Russian)
120. Borukhovich AS, Dubrovskaya LB, Matveenko II, Geld PV (1969) Magnetic susceptibility of niobium and tantalum monocarbides at low temperatures. *Phys Solid State* 11(3):681–686
121. Gusev AI, Rempel AA, Lipatnikov VN (1988) Magnetic susceptibility and atomic ordering in tantalum carbide. *Phys Stat Sol A* 106:459–466
122. Santoro GJ (1965) Magnetic susceptibilities of compositions in tantalum–tantalum carbide system. Technical Note NASA-TN-D-2638. NASA Lewis Research Center, Cleveland, Ohio, pp. 1–11
123. Upadhyaya GS (1996) Nature and properties of refractory carbides. Nova Science, Commack, New York
124. Modine FA, Major RW, Haywood TW, Gruzalski GR, Smith DY (1984) Optical properties of tantalum carbide from the infrared to the near ultraviolet. *Phys Rev B* 29(2):836–841
125. Fesenko VV, Bolgar AS (1969) Study of evaporation rates of carbides of titanium, zirconium, hafnium, niobium and tantalum at high temperatures. *High Temp* 7(2):226–233
126. Harris GL, Spencer MG, Jones A, Catchings RM (1992) SiC and TaC as optical materials. *Mater Sci Eng B* 11:89–91
127. Mercatelli L, Sani E, Sansoni P, Giannini A, Francini F, Sciti D (2011) Intrinsic spectral selectivity in ultra-high temperature ceramics for solar applications. *CLEO Europe EQEC* 5942843
128. Sani E, Mercatelli L, Sansoni P, Silvestroni L, Sciti D (2012) Spectrally selective ultra-high temperature ceramic absorbers for high-temperature solar plants. *J Renew Sustain Energy* 4(3):033104
129. Mackie WA, Carleson P, Fillion J, Hinrichs CH (1991) Normal spectral emittance of crystalline transition metal carbides. *J Appl Phys* 69(10):7236–7239
130. Deadmore D (1964) Normal spectral emittance (0.65 μ) of TaC-HfC solid solutions and tungsten above 1600 °C. *J Am Ceram Soc* 47(12):649–650
131. Coffman JA, Kibler GM, Riethof TR, Watts AA (1960) Carbonization of plastics and refractory materials research program. Report ARPA-24-59-6, Contract AF33(616)-6841. General Electric Co., pp. 1–46
132. Petrov VA (1969) Izluchatel'naya sposobnost' vysokotemperaturnykh materialov (The emissivity of high-temperature materials). Nauka, Moscow (in Russian)
133. Samsonov GV, Podchernyaeva IA, Fomenko VS (1969) Emission coefficient of high-melting compounds. *Powder Metall Met Ceram* 8(5):374–379
134. Samsonov GV, Fomenko VS, Paderno YuB (1962) Spectral emittance of the powders of some high-melting compounds. *Refract Indust Ceram* 3(1–2):35–37
135. Shaffer PTB (1963) Evidence for high-temperature forms of zirconium and tantalum monocarbides. *J Am Ceram Soc* 46(4):177–179
136. Grossman LN (1965) High-temperature thermophysical properties of zirconium carbide. *J Am Ceram Soc* 48(5):236–242
137. Kolesnichenko AN, Krasnoshchekov YaA, Nezhevenko LB, Pustogarov AV (1971) Izluchatel'naya sposobnost' karbida tsirkoniya pri vysokikh temperaturakh (The emittance of zirconium carbide at high temperatures). *Teplofiz Vysok Temp* 9(1):202–204 (in Russian)

138. Riethof T, Acchione BD, Branyan ER (1962) High-temperature spectral emissivity studies on some refractory metals and carbides. In: Herzfeld CM, Dahl AI (eds) *Temperature, its measurement and control in science and industry*, Vol. 3, Part 2. Reinholds, New York and Chapman & Hall, London, pp. 515–522
139. Shaffer PTB (1964) *Handbooks of high-temperature materials: No. 1 – Material index*. Plenum Press, Springer Science, New York
140. Sheindlin AE, Petrov VA, Vinnikova AN, Nikolaeva VA (1969) Integral normal emissivity of tantalum and hafnium carbides over temperature range 1300–3000 K. *High Temp* 7(2):236–238
141. Fomenko VS, Naumenko VYa, Okhremchuk LN, Podchernyaeva IA, Samsonov GV (1970) Glühemissionseigenschaften der Monokarbide von Übergangsmetallen der IV und V Gruppe im Homogenitätsbereich (The thermionic emission properties of transition metals monocarbides of groups IV and V in the homogeneity range). *Phys Stat Sol A* 2(3):K181–K184 (in German)
142. Fomenko VS (1981) *Emissionnye svoistva materialov* (The thermionic emission properties of materials). Naukova Dumka, Kyiv (in Russian)
143. Goldwater DL, Haddad RE (1951) Certain refractory compounds as thermionic emitters. *J Appl Phys* 22(1):70–73
144. Ingold JH (1963) Thermionic properties of some refractory metal carbides. *J Appl Phys* 34(7):2033–2039
145. Samsonov GV (ed), Fomenko VS (1966) *Handbook of thermionic properties*. Plenum Press, New York
146. Okhremchuk LN, Podchernyaeva IA, Podgrushko NF, Fomenko VS (1972) Voprosy raboty vykhoda perekhodnykh metallov (Problems of transition metals work function). *Radiotekhnika Elektronika* 17(1):205–206 (in Russian)
147. Baxter WJ (1971) Work function of tantalum carbide and the effects of adsorption and sputtering of cesium. *J Appl Phys* 42(7):2682–2688
148. Chaikovskii EF, Sotnikov VT, Vlasenko VA (1978) Vliyanie okisi ugleroda na rabotu vykhoda karbida tantala (Influence of carbon monoxide on work function of tantalum carbide). *Zh Tekh Fiz* 48(3):613–614 (in Russian)
149. Samsonov GV, Siman NI, Podchernyaeva IA, Fomenko VS (1976) Issledovanie energii adsorbtsii Cs i K na poverkhnosti tugoplavkikh karbidov (Study of Cs and K adsorption energies on surface of high-melting carbides). *Zh Tekh Fiz* 46(2):393–397 (in Russian)
150. Yada K, Masaoka H, Shoji Y, Tanji T (1989) Studies of refractory carbides, nitrides and borides as the thermionic emitters for electron microscopy. *J Electron Microscop Tech* 12:252–261
151. Danilyants GI, Kirillin AV, Novikov SV (1988) Emissivity of tantalum carbide at elevated temperatures. *High Temp* 26(1):65–69
152. Bober M, Karow HU, Mueller K (1980) Study of the spectral reflectivity and emissivity of liquid ceramics. *High Temp High Press* 12(2):161–168
153. Mackie WA, Hartman RL, Davis PR (1993) High current density field emission from transition metal carbides. *Appl Surf Sci* 67:29–35
154. Rowcliffe DJ, Hollox GE (1971) Plastic flow and fracture of tantalum carbide and hafnium carbide at low temperatures. *J Mater Sci* 6(10):1261–1269
155. Rowcliffe DJ, Hollox GE (1971) Hardness anisotropy, deformation mechanisms and brittle-to-ductile transition in carbide. *J Mater Sci* 6(10):1270–1276
156. Andrievskii RA, Rymashevskii GA, Sinelnikova VS (1972) Single crystals of refractory compounds – a review. I. *Powder Metall Met Ceram* 11(3):207–215
157. Andrievskii RA, Rymashevskii GA, Sinelnikova VS (1972) Single crystals of refractory compounds – a review. II. *Powder Metall Met Ceram* 11(10):796–809
158. Ramqvist L, Ekstig B, Källne E, Noreland E, Manne R (1971) X-ray emission spectra of VC_x, NbC_x, TaC_x and ZrC_x. *J Phys Chem Solids* 32(1):149–157
159. Popov VE, Vil'k YuN, TM Chekrygina, Gurin VN (1981) Morphology, microhardness and grinding ability of single-crystal powders. *Powder Metall Met Ceram* 20(8):578–581

160. Vahldiek FW, Mersol SA (1977) Slip and microhardness of IVa to VIa refractory materials. *J Less-Common Met* 55(2):265–278
161. Veretennikov BN, Solodov YuP, Pugachev YuI (1977) Changes in phase structure of tantalum carbides during prolonged heating in vacuum. *Inorg Mater* 13(6):828–831
162. Yohe WC, Ruoff AL (1978) Ultrafine-grain tantalum carbide by high pressure hot pressing. *Am Ceram Soc Bull* 57(12):1123–1130
163. Khusainov MA (1979) Termoprochnost tugoplavkikh materialov, poluchennykh gazofaznym osazhdeniem (Thermal strength of refractory materials manufactured by gas-phase deposition). Leningrad State University, Leningrad (in Russian)
164. Ordanyan SS, Zaitsev GP, Kats SM, Avgustinik AI (1976) Microhardness of alloys in system HfC-TaC. *Inorg Mater* 12(9):1293–1296
165. Yohe WC, Ruoff AL (1978) Ultrafine-grain tantalum carbide by high-pressure hot-pressing. *Am Ceram Soc Bull* 57(12):1123–1125
166. Atkins AG, Tabor D (1966) Hardness and deformation properties of solids at very high temperatures. *Proc R Soc London A* 292(1431):441–459
167. Shvab SA, Egorov FF (1983) Sintering kinetics, structure and some properties of heterophase materials of the titanium diboride – tantalum carbide system. *Powder Metall Met Ceram* 22(4):261–264
168. Spivak II, Klimenko VV (1973) Densification kinetics in the hot pressing and recrystallization of carbides. *Powder Metall Met Ceram* 12(11):883–887
169. Kumashiro Y, Nagai Y, Kato H (1982) The Vickers micro-hardness of NbC, ZrC and TaC single crystals up to 1500 °C. *J Mater Sci Lett* 1(2):49–52
170. Kumashiro Y, Nagai Y, Kato H, Sakuma E, Watanabe K, Misawa S (1981) The preparation and characteristics of ZrC and TaC single crystals using an r.f. floating-zone process. *J Mater Sci* 16(10):2930–2933
171. Ivanko AA (1968) Tverdost (The hardness). *Naukova Dumka, Kyiv* (in Russian)
172. Kim B-R, Woo K-D, Doh J-M, Yoon J-K, Shon I-J (2009) Mechanical properties and rapid consolidation of binderless nanostructured tantalum carbide. *Ceram Int* 35:3395–3400
173. Hivert A, Poulignier J (1968) Mechanical properties at high temperatures of some ultra-refractory carbides. *Rev Int Hautes Temp Refract* 5(1):55–61
174. Ramke WG, Latva JD (1963) Refractory ceramics and intermetallic compounds. *Aerosp Eng* 22(1):76–84
175. Johansen HA, Cleary JG (1966) The ductile-brittle transition in tantalum carbide. *J Electrochem Soc* 113(4):378–381
176. Liu J-X, Kan Y-M, Zhang G-J (2010) Pressureless sintering of tantalum carbide ceramics without additives. *J Am Ceram Soc* 93(2):370–373
177. Shvab SA, Egorov FF (1982) Structure and some properties of sintered tantalum carbide. *Powder Metall Met Ceram* 21(11):894–897
178. Kelly A, Rowcliffe DJ (1967) Deformation of polycrystalline transition metal carbides. *J Am Ceram Soc* 50(5):253–256
179. Hoffman M, Williams WS (1986) A simple model for the deformation behaviour of tantalum carbide. *J Am Ceram Soc* 69(8):612–614
180. Kurishita H, Suzuki E, Yoshinga H (1982) High-temperature deformation behaviour in tantalum carbide. *Eng Sci Rep* 4(1):43–48
181. Balani K, Gonzales G, Agarwal A, Hickman R, O'Dell JS, Seal S (2006) Synthesis, microstructural characterization and mechanical property evaluation of vacuum plasma sprayed tantalum carbide. *J Am Ceram Soc* 89(4):1419–1425
182. Kim C, Gottstein G, Grummon DS (1994) Plastic flow and dislocation structures in tantalum carbide: deformation at low and intermediate homologous temperatures. *Acta Metall Mater* 42(7):2291–2301
183. Zubarev PV (1985) Zharoprochnost faz vnedreniya (The heat-resistance of interstitial alloys). *Metallurgiya, Moscow* (in Russian)
184. Spivak II, Klimenko VV (1971) Study of diffusion effects on interstitial phases. *Phys Met Metallogr* 32(2):87–92

185. Kats SM, Ordanyan SS (1983) Extremal character of concentration dependence of creep rate of solid solutions of carbides in the $M^{IV}C$ - M^{VC} system. *Inorg Mater* 19(2):196–201
186. Kats SM, Ordanyan SS (1984) Creep in sintered polycrystalline niobium carbide and niobium carbide – based solid solutions. *Powder Metall Met Ceram* 23(5):414–418
187. Steinitz R (1966) Mechanical properties of refractory carbides at high temperatures. *Am Ceram Soc Bull* 45(4):467–470
188. Rudy E (1969) Compendium of phase diagram data. In: Ternary phase equilibria in transition metal-boron-carbon-silicon systems. Report AFML-TR-65-2, Contracts USAF 33(615)-1249 and USAF 33(615)-67-C-1513, Part 5. Air Force Materials Laboratory, Wright-Patterson Air Force Base, Ohio, pp. 1–689
189. De Leon N, Wang B, Weinberger CR, Matson LE, Thompson GB (2013) Elevated-temperature deformation mechanisms in Ta_2C : an experimental study. *Acta Mater* 61:3905–3913
190. Jun CK, Shaffer PTB (1971) Elastic moduli of niobium carbide and tantalum carbide at high temperature. *J Less-Common Met* 23(4):367–373
191. Bartlett RW, Smith CW (1967) Elastic constants of tantalum monocarbide $TaC_{0.96}$. *J Appl Phys* 38(13):5428–5429
192. Brown HL, Armstrong PE, Kempter CP (1966) Elastic properties of some polycrystalline transition-metal monocarbides. *J Chem Phys* 45(2):547–549
193. Lopez-de-la-Torre L, Winkler B, Schreuer J, Knorr K, Avalos-Borja M (2005) Elastic properties of tantalum carbide TaC. *Solid State Commun* 134:245–250
194. Tumanov VI, Yudkovskii SI, Chernyshev VV (1968) Relationship between physical and mechanical properties of carbides of groups IV–VI metals and their electron structure and thermodynamic parameters. *Russ Metall* (4):134–137
195. Champion AR, Drickamer HG (1965) The effect of high pressure on the compressibility of four cubic carbides. *J Phys Chem Solids* 26(12):1973–1975
196. Koster W, Rauscher W (1948) Beziehung zwischen dem Elastizitätsmodul von Zweistofflegierungen und ihrem Aufbau (The relationship between the modulus of elasticity of binary alloys and their structure). *Z Metallkd* 39(4):111–120 (in German)
197. Shaffer PTB, Watts RL (1961) Development of ultra refractory materials. Summary Report, Contract NOrd-17175. The Carborundum Company, Niagara Falls, New York, pp. 1–40
198. Liermann HP, Singh AK, Manoun B, Saxena SK, Zha CS (2005) Compression behaviour of $TaC_{0.98}$ under nonhydrostatic and quasi-hydrostatic pressures up to 76 GPa. *Int J Refract Met Hard Mater* 23:109–114
199. Sahnoun M, Daul C, Driz M, Parlebas JC, Demangeat C (2005) FP-LAPW investigation of electronic structure of TaN and TaC compounds. *Comput Mater Sci* 33(1–3):175–183
200. Chen H-H, Bi Y, Mao H-K, Xu J-A, Liu L, Jing Q-M, Li Z, Chen X-R, Wang Q-M (2013) High-pressure strength of nanocrystalline tantalum carbide TaC studied at a non-hydrostatic compression. *Int J Refract Met Hard Mater* 41:627–630
201. Li H, Zhang L, Zeng Q, Guan K, Li K, Ren H, Liu S, Cheng L (2011) Structural, elastic and electronic properties of transition metal carbides TMC (TM = Ti, Zr, Hf and Ta) from first-principles calculations. *Solid State Commun* 151:602–606
202. Bakshi SR, Bhargava A, Mohammadzadeh S, Agarwal A, Tsukanov I (2011) Computational estimation of elastic properties of spark plasma sintered TaC by meshfree and finite element methods. *Comput Mater Sci* 50:2615–2620
203. Shon I-J, Kim B-R, Ko I-Y, Nam K-S, Doh J-M (2010) Properties and rapid consolidation of binderless nanostructured tantalum carbide by pulsed current activated sintering. *J Ceram Process Res* 11(4):498–502
204. Peng F, Han L, Fu H, Cheng X (2009) First-principles calculations on elasticity and the thermodynamic properties of TaC under pressure. *Phys Stat Sol B* 246(7):1590–1596
205. Krikorian OH (1988) Thermal expansivity correlations for refractory materials with the NaCl-type structure. *High Temp High Press* 20:169–175
206. Dodd SP, Cankurtaran M, James B (2003) Ultrasonic determination of elastic and nonlinear acoustic properties of transition-metal carbide ceramics TiC and TaC. *J Mater Sci* 38(6):1107–1115

207. Krajewski A, D'Alessio L, De Maria G (1998) Physico-chemical and thermophysical properties of cubic binary carbides. *Cryst Res Technol* 33(3):341–374
208. Weber W (1973) Lattice dynamics of transition-metal carbides. *Phys Rev B* 8(11):5082–5092
209. Lu X-G, Selleby M, Sundman B (2007) Calculations of thermophysical properties of cubic carbides and nitrides using the Debye-Grüneisen model. *Acta Mater* 55:1215–1226
210. Kobayashi K (2001) First-principles study of the electronic properties of transition metal nitride surfaces. *Surf Sci* 493(1–3):665–670
211. Wu Z, Chen X-J, Struzhkin VV, Cohen RE (2005) Trends in elasticity and electronic structure of transition-metal nitrides and carbides from first principles. *Phys Rev B* 71(21):214103
212. Kral C, Lengauer W, Rafaja D, Ettmayer P (1998) Critical review on the elastic properties of transition metal carbides, nitrides and carbonitrides. *J Alloys Compd* 265:215–233
213. Smith HG, Gläser W (1970) Phonon spectra in TaC and HfC. *Phys Rev Lett* 25(23):1611–1613
214. Santhanam AT (1996) Application of transition metal carbides and nitrides in industrial tools. In: Oyama ST (ed) *The chemistry of transition metal nitrides*. Chapman & Hall, London, pp. 28–52
215. Kosolapova TYa (1971) *Carbides: properties, production and applications*. Plenum Press, New York
216. Travushkin GG, Knyazev VI, Belov VS, Rymashevskii GA (1973) Temperature threshold of brittle failure in interstitial phases. *Strength Mater* 5(5):639–641
217. Gordeev NV, Kardashev DA, Malyshev AV (1963) Yaderno-fizicheskie konstanty (Nuclear physics constants). Gosatomizdat, Moscow (in Russian)
218. Kovalchenko MS, Ogorodnikov VV, Rogovoi YuI, Krainii AG (1979) Radiatsionnoe povrezhdenie tugoplavkikh soedinenii (The radiation damage of refractory compounds). Atomizdat, Moscow (in Russian)
219. Keilholtz GW, Moore RE, Osborne MF (1968) Fast-neutron effects on the carbides of titanium, zirconium, tantalum, niobium and tungsten. *Nucl Appl* 4:330–336
220. Morillo J, De Novion CH, Dural J (1981) Neutron and electron radiation defects in titanium and tantalum monocarbides: an electrical resistivity study. *Radiat Eff Defects Solids* 55(1–2):67–77
221. Gosset D, Allison C, Morillo J (1984) Defaults d'irradiation électronique dans le carbure de tantale (Electron radiation defects in tantalum carbides). In: 26eme Colloque de metallurgie de Saclay: effets d'irradiation dans les matériaux (métaux, alliages, verres). Saclay, France, pp. 99–102 (in French)
222. Begrambekov LB, Nikopolskii MV, Telkovskii VG, Fedorov YuV (1987) Failure of metal carbides in ion irradiation. *Phys Chem Mater Treat* 21(4):322–325
223. Radel RF, Kulcinski GL (2005) Implantation of D and He in W-coated refractory carbides. *Fusion Sci Technol* 47(4):1250–1254
224. Zenobia SJ, Radel RF, Cipity BB, Kulcinski GL (2009) High temperature surface effects of He⁺ implantation in ICF fusion first wall materials. *J Nucl Mater* 389:213–220
225. Akhmatov VI, Kostikov VI, Melekhin VF, Stepanyuk VS, Shesterin YuA (1977) Smachivanie plazmennyykh pokrytii zhidkim alyuminiem (The wettability of plasma-sprayed coatings by aluminium). *Izv Vyssh Uchebn Zaved Chern Metall* (5):29–32 (in Russian)
226. Holleck H (1984) Binäre und ternäre Carbid- und Nitridsysteme der Übergangsmetalle (Binary and ternary carbide and nitride systems of the transition metals). Gebrüder Bornträger, Berlin (in German)
227. Eremenko VN, Velikanova TYa (1983) Use of the phase diagrams of ternary transition metal systems containing carbides in the development of heat-resisting hard alloys. *Powder Metall Met Ceram* 22(12):1010–1021
228. Velikanova TYa, Bondar AA, Dovbenko OI (2002) The Cr-Ta-C melting diagram in the (Cr)-(Ta)-(TaC) region. *Powder Metall Met Ceram* 41(7–8):400–406
229. Dovbenko OI, Bondar AA, Velikanova TYa, Bilous OO, Burka MP, Martseniuk PS, Shapoval TO, Tsyganenko NI (2003) Quasi-binary metal-carbide eutectic of Cr-Ta-C system. *Mater Lett* 57:2866–2871

230. Rudy E (1965) Ta-Hf-C system. In: Ternary phase equilibria in transition metal-boron-carbon-silicon systems. Report AFML-TR-65-2, Contract USAF 33(615)-1249, Part 2, Vol. 1. Air Force Materials Laboratory, Wright-Patterson Air Force Base, Ohio, pp. 1–84
231. Fedorov TF, Gladyshevskii EI (1965) Phase equilibria in ternary systems of transition metals of groups IV and V and carbon. *Powder Metall Met Ceram* 4(1):27–29
232. Krylov YuI, Balakir ÉA (1976) Karbidno-okisnye sistemy (Carbide-oxide systems). *Metallurgiya*, Moscow (in Russian)
233. Silvestroni L, Sciti D (2010) Sintering behaviour, microstructure and mechanical properties: a comparison among pressureless sintered ultra-refractory carbides. *Adv Mater Sci Eng* ID835018:1–11. <https://doi.org/10.1155/2010/835018>
234. Silvestroni L, Bellosi A, Melandri C, Sciti D, Liu JX, Zhang GJ (2011) Microstructure and properties of HfC and TaC-based ceramics obtained by ultrafine powder. *J Eur Ceram Soc* 31:619–627
235. Rudy E, Windisch S, Brukl CE (1967) Constitution of ternary Ta-Mo-C alloys. In: Ternary phase equilibria in transition metal-boron-carbide-silicon systems. Report AFML-TR-65-2, Contract USAF 33(615)-1249, Part 2, Vol. 17. Air Force Materials Laboratory, Wright-Patterson Air Force Base, Ohio, pp. 1–71
236. Eremenko VN, Velikanova TY, Shabanova SV, Artyukh LV (1973) Continuous series of solid solutions of carbides with NaCl structure in the ternary systems Mo(W)-Me^{IV,V}-C. *Powder Metall Met Ceram* 12(11):909–912
237. English JJ (1961) Binary and ternary phase diagrams of columbium, molybdenum, tantalum and tungsten. Report DMIC-152, Contract AF-33(616)-7747. Defence Metals Information Center, Battelle Memorial Institute, Columbus, pp. 1–226
238. Booker PH, Rudy E (1970) Phase equilibria studies in the Nb-Ta-C system. In: Phase equilibria investigations of binary, ternary and higher order systems. Report AFML-TR-69-117, Contract USAF 33(615)-67-C-1513, Part 3. Air Force Materials Laboratory, Wright-Patterson Air Force Base, Ohio, pp. 1–56
239. Jackson MR (1977) Composites of γ + TaC in the Ni-Ta-C ternary system. *Metall Trans A* 8(6):905–913
240. Laurila T, Zeng K, Molarius J, Riekkinen T, Suni I, Kivilahti JK (2002) Effect of oxygen on the reactions in Si/Ta/Cu and Si/TaC/Cu systems. *Microelect Eng* 64:279–287
241. Laurila T, Molarius J, Kivilahti JK (2004) Interfacial reactions in the Si/TaC/Cu systems. *Microelect Eng* 71:301–309
242. Voitovich RF (1981) Okislenie karbidov i nitridov (Oxidation of carbides and nitrides). *Naukova Dumka*, Kyiv (in Russian)
243. Gorshkova LV, Fedorov TF, Kuzma YuB (1967) Ternary systems niobium-rhenium-carbon and tantalum-rhenium-carbon. *Powder Metall Met Ceram* 6(4):287–290
244. Ordanyan SS (1975) Reactions of rhenium and other refractory metals with some metal-like compounds. *Powder Metall Met Ceram* 14(2):125–129
245. Schuster JC (1993–1994) Silicon carbide and transition metals: a critical evaluation of existing phase diagram data supplemented by new experimental results. *Int J Refract Met Hard Mater* 12(4):173–177
246. Rudy E (1970) The phase diagram of the systems Ti-Nb-C, Ti-Ta-C and Ti-Mo-C. In: Phase equilibria investigations of binary, ternary and higher order systems. Report AFML-TR-69-117, Contract USAF 33(615)-67-C-1513, Part 1. Air Force Materials Laboratory, Wright-Patterson Air Force Base, Ohio, pp. 1–132
247. Brukl CE, Harmon DP (1965) Ti-Ta-C system. In: Ternary phase equilibria in transition metal-boron-carbon-silicon systems. Report AFML-TR-65-2, Contract USAF 33(615)-1249, Part 2, Vol. 2. Air Force Materials Laboratory, Wright-Patterson Air Force Base, Ohio, pp. 1–67
248. Lukas HL (2010) Carbon – tantalum – titanium system. In: Effenberg G, Ilyenko S (eds) Ternary alloy systems, Subvol E, Part 2. Springer, Berlin, pp. 619–631
249. Rudy E (1965) Ta-W-C system. In: Ternary phase equilibria in transition metal-boron-carbon-silicon systems. Report AFML-TR-65-2, Contract USAF 33(615)-1249, Part 2, Vol. 8. Air Force Materials Laboratory, Wright-Patterson Air Force Base, Ohio, pp. 1–141

250. Hachisuka T (1968) Preparation of TaC-WC solid solutions and their properties. *J Jpn Soc Powder Metall* 15:110–117 (in Japanese)
251. Eremenko VN, Velikanova TYa (1973) Stroenie diagramm sostoyaniya troinykh sistem (Mo, W) – (Ti, Zr, Hf, V, Nb, Ta) – C (Structure of phase diagrams of the (Mo, W) – (Ti, Zr, Hf, V, Nb, Ta) – C ternary systems). In: Ageev VN (ed) *Obshchie zakonomernosti stroeniya diagramm sostoyaniya metallicheskih sistem* (The general regularities of the phase diagrams structures of metal systems). Nauka, Moscow, pp. 49–52 (in Russian)
252. Frisk K (1999) A thermodynamic analysis of the Ta-W-C and the Ta-W-C-N systems. *Z Metallkd* 90(9):704–711
253. Bochvar N, Rokhlin L, Lysova E (2010) Carbon – tantalum – tungsten system. In: Effenberg G, Ilyenko S (eds) *Ternary alloy systems, Subvol E, Part 3*. Springer, Berlin, pp. 1–17
254. Gusev AI (1985) Phase diagrams of the pseudo-binary TiC – NbC, TiC – TaC, ZrC – NbC, ZrC – TaC and HfC – TaC carbide systems. *Russ J Phys Chem* 59(3):336–340
255. Harmon DP, Brukl CE (1965) Zr-Ta-C system. In: *Ternary phase equilibria in transition metal-boron-carbon-silicon systems*. Report AFML-TR-65-2, Contract USAF 33(615)-1249, Part 2, Vol. 3. Air Force Materials Laboratory, Wright-Patterson Air Force Base, Ohio, pp. 1–72
256. Dobatkina T, Bochvar N (2010) Carbon – tantalum – zirconium system. In: Effenberg G, Ilyenko S (eds) *Ternary alloy systems, Subvol E, Part 3*. Springer, Berlin, pp. 18–30
257. Samsonov GV (ed) (1973) *The oxide handbook*. IFI/Plenum, New York
258. Goretzki H, Exner HE, Scheuermann W (1971) Electronic structure of refractory carbides and its relation to wetting. In: Hausner HH (ed) *Modern developments in powder metallurgy, Vol. 4 – Processes*. Plenum Press, New York, pp. 327–337
259. Vishnyakov LR, Grudina TV, Kadyrov VKh, Karpinos DM, Oleynik VI, Sapozhnikova AB, Tuchinskii LI (1985) *Kompozitsionnye materialy* (Composite materials). Naukova Dumka, Kyiv (in Russian)
260. Ramqvist L (1965) Wettability of metallic carbides by liquid Cu, Ni, Co and Fe. *Int J Powder Metall* 1(4):2–21
261. Samsonov GV, Panasyuk AD, Kozina GK (1968) Wetting of refractory carbides with liquid metals. *Powder Metall Met Ceram* 7(11):874–878
262. Warren R (1976) Determination of interfacial energy ratio in 2-phase systems by measurement of interphase contact. *Metallography* 9(3):183–191
263. Warren R (1980) Solid-liquid interfacial energies in binary and pseudo-binary systems. *J Mater Sci* 15(10):2489–2496
264. Samsonov GV, Panasyuk AD, Kozina GK, Dyakonova LV (1976) Kontaknoe vzaimod-eistvie karbida tsirkoniya s nikelovymi splavami (The contact interaction of zirconium carbide with nickel alloys). In: Samsonov GV, Kosolapova TYa, Gnesin GG, Fedorus VB, Domasevich LG (eds) *Karbidy i splavy na ikh osnove* (Carbides and alloys based on them). Naukova Dumka, Kyiv, pp. 56–59 (in Russian)
265. Chiotti PJ (1952) Experimental refractory bodies of high-melting nitrides, carbides and uranium dioxide. *J Am Ceram Soc* 35(5):123–130
266. Rogl P (2009) Boron – carbon – tantalum system. In: Effenberg G, Ilyenko S (eds) *Ternary alloy systems, Subvol E, Part 1*. Springer, Berlin, pp. 395–407
267. Lee Y-J, Kim SH, Lee T-H, Nersisyan HH, Lee K-H, Han M-H, Jeong S-U, Kang K-S, Bae K-K, Lee J-H (2014) Combustion synthesis and characterization of TaC, TaC/TaSi₂ and TaC/TaB nanoparticles. *Chem Eng Sci* 107:227–234
268. Soto G, Silva G, Contreras O (2006) A study on the flexibility of the hot-filament configuration and its implementation for diamond, boron carbide and ternary alloys deposition. *Surf Coat Technol* 201(6):2733–2740
269. Ordanyan SS (1980) Laws of interaction in the systems M^{IV}·V·C – M^{IV}·V·B₂. *Inorg Mater* 16(8):961–965
270. Shurin AK, Dmitrieva GP, Cherepova TS (1996) Phase equilibria in Co – Me'C – Me''C alloys. I. Systems with three-phase eutectic equilibria. *Powder Metall Met Ceram* 35(11–12):615–620

271. Shurin AK, Dmitrieva GP, Cherepova TS (1997) Phase equilibria in Co – Me'C – Me''C alloys. II. Systems with four-phase eutectic equilibrium. *Powder Metall Met Ceram* 36(3–4):193–196
272. Frisk K, Dumitrescu L, Ekroth M, Jansson B, Kruse O, Sundman B (2001) Development of a database for cemented carbides: thermodynamic modelling and experiments. *Phase Equilib* 22(6):645–655
273. Barsoum MW (2010) The $M_{n+1}AX_n$ phases and their properties. In: Riedel R, Chen I-W (eds) *Ceramics science and technology, Vol. 2 – Materials and properties*. Wiley-VCH, Weinheim, pp. 299–347
274. Sun ZM (2011) Progress in research and development on MAX phases: a family of layered ternary compounds. *Int Mater Rev* 56(3):143–166
275. Barsoum MW (2013) MAX phases: properties of machinable ternary carbides and nitrides. Wiley-VCH, Weinheim
276. Brukl CE (1972) Der Einfluß von Vanadin und Niob auf feste Subcarbidlösungen in den Systemen Tantal-Wolfram-Kohlenstoff und Tantal-Molybdän-Kohlenstoff (The influence of vanadium and niobium in solid subcarbide solutions in the systems tantalum-tungsten-carbon and tantalum-molybdenum-carbon). *Monatsh Chem* 103(3):820–830 (in German)
277. Shurin AK, Razumova NA, Dmitrieva GP, Khandros EL (1987) Diagramma sostoyaniya sistemy Ni – NbC_{0,8} – TaC_{0,9} (The constitution diagram of the Ni – NbC_{0,8} – TaC_{0,9} system). *Dopov Akad Nauk Ukr RSR Ser A Fiz Mat Tekh Nauki* 49(6):81–83 (in Russian)
278. Walter J, Boonchuduang W, Hara S (2000) XPS study on pristine and intercalated tantalum carbosulfide. *J Alloys Compd* 305:259–263
279. Islam MS, Islam AKMA (2011) Structural, elastic, electronic and optical properties of a new layered-ternary Ta₄SiC₃ compound. *Phys B* 406:275–279
280. Chatfield C (1986) The γ -WC solubility boundary in the quaternary TiC-NbC-TaC-WC system at 1723 K. *J Mater Sci* 21(2):577–582
281. Chatfield Ch (1983) Redetermination of the γ - α solubility line in the TiC-TaC-WC system at 1723 K. *Powder Metall Int* 15(1):18–19
282. Brewer L, Krikorian OH (1956) Reactions of refractory silicides with carbon and nitrogen. *J Electrochem Soc* 103(1):38–51, 103(12):701–703
283. Borisova AL (1985) Sovmestimost tugoplavkikh soedinenii s metallami i grafitom (The compatibility of refractory compounds with metals and graphite). *Naukova Dumka, Kyiv* (in Russian)
284. Borisova AL, Borisov YuS (1977) A thermodynamic evaluation of the effect of nonstoichiometry of compounds on the course of their solid-phase reactions. *Powder Metall Met Ceram* 16(6):440–447
285. Samsonov GV, Strashinskaya LV, Shiller ÉA (1962) Kontaktnoe vzaimodeistvie metallopodobnykh karbidov, nitridov i boridov s tugoplavkimi metallami pri vysokikh temperaturakh (The contact interaction of metal-like carbides, nitrides and borides with refractory metals at high temperatures). *Izv AN SSSR OTN Metall Toplivo* (5):167–180 (in Russian)
286. Strashinskaya LV, Stashevskaya IA (1974) An X-ray diffraction study of the reactions of molybdenum and tungsten with disperse inclusions. *Powder Metall Met Ceram* 13(5):420–422
287. Manning C, Stoops R (1968) High-temperature cermets: 1. Compatibility. *J Am Ceram Soc* 51(8):411–415
288. Ordanyan SS, Kosterova NV, Avgustinik AI (1971) Stroenie splavov v sisteme Ta-C-Re (The structure of alloys in the Ta-C-Re system). *Izv AN SSSR Neorg Mater* 7(1):64–66 (in Russian)
289. Ordanyan SS, Kosterova NV, Avgustinik AI (1969) Diagramma sostoyaniya sistemy TaC-Re (The substitution diagram of the TaC-Re system). *Izv AN SSSR Neorg Mater* 5(2):389–390 (in Russian)
290. Krikorian NH, Wallace TC, Krupka MC, Radosevich CL (1967) The reaction of some noble and transition metals with refractory carbides. *J Nucl Mater* 21(2):236–238

291. Benesovsky F, Rudy E (1961) Zur Kenntnis der System Uran – Zirconium (Hafnium, Niob, Tantal) – Kohlenstoff (To the knowledge of the uranium – zirconium (hafnium, niobium, tantalum) – carbon systems). *Planseeber Pulvermetall* 9(1/2):65–76 (in German)
292. Yurchenko OS (1971) Stability of iron and nickel during heating in contact with refractory compounds. *Powder Metall Met Ceram* 10(1):35–38
293. Shchetilina EA, Tumanov VI, Serebrova OI (1964) O rastvorimosti karbidov tugoplavkikh metallov v kobalte (On the solubility of carbides of refractory metals in cobalt). *Izv AN SSSR OTN Metall Toplivo* (6):142–147 (in Russian)
294. Szoekfalvi-Nagy A, Jehn H (1984) High-temperature oxidation of NbC and TaC at low oxygen pressures. *Z Metallkd* 75(5):389–394
295. Desmaison-Brut M, Alexandre N, Desmaison J (1997) Comparison of the oxidation behaviour of two dense hot isostatically pressed tantalum carbide (TaC and Ta₂C) materials. *J Eur Ceram Soc* 17(11):1325–1334
296. Voitovich RF, Pugach ÉA (1975) Vysokotemperaturnoe okislenie karbidov perekhodnykh metallov IV-VI grupp (High temperature oxidation of transition metals IV-VI groups carbides). In: Samsonov GV (ed) *Vysokotemperaturnye karbidy* (High-temperature carbides). Naukova Dumka, Kyiv, pp. 143–156 (in Russian)
297. Voitovich RF, Pugach ÉA (1976) Nekotorye osobennosti protsessy okisleniya karbidov metallov IV-VI grupp (The certain features of the oxidation process of metals IV-VI groups carbides). In: Samsonov GV, Kosolapova TYa, Gnesin GG, Fedorus VB, Domasevich LG (eds) *Karbidy i splavy na ikh osnove* (Carbides and alloys based on them). Naukova Dumka, Kyiv, pp. 233–234 (in Russian)
298. Li G-D, Xiong X, Huang B-Y, Zeng Y-L (2007) Oxidized characteristic and oxidized mechanism of TaC coating. *Chin J Nonferrous Met* 17(3):360–367 (in Chinese)
299. Lashtabeg A, Smart M, Riley D, Gillen A, Drennan J (2013) The effect of extreme temperature in an oxidising atmosphere on dense tantalum carbide (TaC). *J Mater Sci* 48(1):258–264
300. Paul A, Binner JGP, Vaidhyanathan B, Heaton ACJ, Brown PM (2013) Oxyacetylene torch testing and microstructural characterization of tantalum carbide. *J Microsc* 250(2):122–129
301. Zhang X, Hilmas GE, Fahrenholtz WG, Deason DM (2007) Hot-pressing of tantalum carbide with and without sintering additives. *J Am Ceram Soc* 90(2):393–401
302. Lui L, Zhong L, Zhang B, Lai Z, Ye F, Zhang Z, Zhou Y (2013) Densification of tantalum carbide ceramics with 5 mol.% Al, Cu, Ag and Au. *Scripta Mater* 69:574–577
303. Shabalin IL (2008) “Ridge effect” in oxidation kinetics of hetero-modulus ceramics based on titanium carbide. *Powd Metall Met Ceram* 47(1–2):137–150
304. Samsonov GV, Kozina GK, Panasyuk AD, Bondarchuk SN (1974) The reaction of refractory carbides with molten steels and cast irons. In: Samsonov GV (ed) *Refractory carbides*. Consultants Bureau, New York, pp. 433–440
305. Dergunova VS, Levinskii YuV, Shurshakov AN, Kravetskii GA (1974) Vzaimodeistvie ugleroda s tugoplavkimi metallami (The interaction of carbon with refractory metals). *Metallurgiya, Moscow* (in Russian)
306. Zagryazkin VN, Ushakov BF (1975) Diffuziya volframa v karbidakh tsirkoniya i tantara (Diffusion of tungsten in zirconium and tantalum carbides). *Izv AN SSSR Neorg Mater* 11(12):2238–2239 (in Russian)
307. Schmidt FA, Carlson ON (1972) Electrotransport of carbon in niobium and tantalum. *J Less-Common Met* 26(2):247–253
308. Powers RW, Doyle MV (1959) Diffusion of interstitial solutes in the group V transition metals. *J Appl Phys* 30(4):514–524
309. Brizes WF (1968) Diffusion of carbon in the carbides of tantalum. *J Nucl Mater* 26:227–231
310. Resnick R, Steinitz R, Seigle L (1965) Determination of diffusivity of carbon in tantalum and columbium carbides by layer-growth measurements. *Trans Met Soc AIME* 233(10):1915–1920
311. Resnick R, Seigle L (1966) Diffusion of carbon in tantalum monocarbide. *Trans Met Soc AIME* 236(12):1732–1739

312. Ambartsumyan RS, Babich BN (1970) Ob obrazovanii karbidov niobiya i tantala pri termicheskoi dissotsiatsii khloridov na grafitovoi podlozhke (On the formation of niobium and tantalum carbides at the thermal dissociation of chlorides on graphite substrate). *Izv AN SSSR Neorg Mater* 6(7):1224–1227 (in Russian)
313. Fromm E, Gebhardt E, Roy U (1966) Diffusion of carbon in carbide phase of tantalum. *Z Metallkd* 57(11):808–812
314. Andrievskii RA, Klimenko VV, Khromov YuF (1969) Samodiffuziya ugleroda v karbidakh perekhodnykh metallov IV i V grupp (The self-diffusion of carbon in transition metals IV and V groups carbides). *Fiz Met Metalloved* 28(2):298–203 (in Russian)
315. Vilk YuN, Nikolskii SS, Avarbe RG (1967) Temperature dependence of diffusion coefficient of carbon in nonstoichiometric zirconium, niobium and tantalum carbides. *High Temp* 5(4):545–548
316. Matzke Hj, Rondinella VV (1999) Diffusion in carbides, nitrides, hydrides and borides. In: Beke DL (ed) *Diffusion in non-metallic solids, Subvol B, Part 1*. Springer, Berlin, pp. 5/1–5/29
317. Johansen HA (1970) Kinetics of the carbiding reaction: tantalum carbide. *Planseeber Pulvermetall* 18:16–27
318. Rafaja D, Lengauer W, Wiesenberger H (1998) Non-metal diffusion coefficients for the Ta-C and Ta-N systems. *Acta Mater* 46(10):3477–3483
319. Kotlyar EE, Nazarchuk TN (1966) O nekotorykh khimicheskikh svoistvakh karbidov perekhodnykh metallov IV, V grupp periodicheskoi sistemy (On certain chemical properties of the transition metal carbides of IV, V groups of the periodic table). *Izv AN SSSR Neorg Mater* 2(10):1778–1780 (in Russian)
320. Samsonov GV (1962) *Analiz tugoplavkikh soedinenii* (The analysis of refractory compounds). Metallurgizdat, Moscow (in Russian)
321. Cooper JR, Hansler RL (1963) Variation of electrical resistivity of cubic tantalum carbide with composition. *J Chem Phys* 39(1):248–249
322. Santoro G, Dolloff RT (1968) Hall coefficient of tantalum carbide as a function of carbon content and temperature. *J Appl Phys* 39(5):2293–2296
323. Williams WS (1971) Transition-metal carbides. *Prog Solid State Chem* 6:57–118
324. Teng Z, Teng F, Wang Y (1995) Some applications of the Hall-Petch relationship for single-phase imperfect polycrystals. *Mater Charact* 34:237–240
325. Bolgar AS, Turchanin AG, Fesenko VV (1973) *Termodinamicheskie svoistva karbidov* (Thermodynamic properties of carbides). Naukova Dumka, Kyiv (in Russian)
326. Samsonov GV, Naumenko VY, Okhremchuk LN (1971) Herstellung und Eigenschaften von Karbiden der Übergangsmetalle in ihren Homogenitätsbereichen (Synthesis and properties of carbides of transition metals in their homogeneity range). *Phys Stat Sol A* 6(1):201–211 (in German)
327. Deadmore DL (1965) Vaporization of tantalum carbide – hafnium carbide solid solutions. *J Am Ceram Soc* 48(7):357–359
328. Samsonov GV, Paderno VN (1964) Über die Herstellung von Karbidmischkristallen und die Untersuchung ihrer physikalischen Eigenschaften (The production of mixed crystals of carbides and investigation of their physical properties). *Planseeber Pulvermetall* 12(1):19–30 (in German)
329. Costa P (1968) Electronic structure of transition carbides, nitrides and borides. In: Vahldiek FW, Mersol SA (eds) *Anisotropy in single-crystal refractory compounds, Vol. 1*. Plenum Press, New York, pp. 151–160
330. Alyamovskii SI, Shveikin GP, Geld PV (1966) Infrakrasnye spektry pogloshcheniya karbidov i nizshikh oksidov vanadiya, niobiya i tantala (The infrared absorption spectra of vanadium, niobium and tantalum carbides and lower oxides). *Zh Neorg Khim* 12(7):1738–1742 (in Russian)
331. Allison CY, Stoller RE, Kenik EA (1988) Electron microscopy of electron damage in tantalum carbide. *J Appl Phys* 63(5):1740–1743
332. Ramqvist L (1969) Preparation, properties and electronic structure of refractory carbides and related compounds. *Jernkontoret Ann* 153(4):159–179

333. Ramqvist L (1971) Electronic structure of cubic refractory carbides. *J Appl Phys* 42(5):2113–2127
334. Bazhenova LN, Ivanko AA (1969) Microhardness of carbides of certain transition metals. *Inorg Mater* 5(12):1763–1767
335. Sanders WA, Drell IL (1963) Compatibility of molten uranium dioxide with five refractory materials. Report NASA-TN-D-1442. National Aeronautics and Space Administration, Washington, DC, pp. 1–19
336. Frantsevich IN, Voronov FF, Bakuta SA (1982) Uprugie postoyannye i moduli uprugosti metallov i nemetallov (The elastic constants and elasticity moduli of metals and non-metals). *Naukova Dumka, Kyiv* (in Russian)
337. Touloukian YS, Powell RW, Ho CY, Klemens PG (1970) Thermophysical properties of matter. Vol. 2 – Thermal conductivity – nonmetallic solids. IFI/Plenum Data Corporation, New York
338. Frantsevich IN, Lyashchenko AB (1966) Young's moduli of the carbides of some transition metals. *Powder Metall Met Ceram* 5(7):573–574
339. Isaev EI, Simak SI, Abrikosov IA, Ahuja R, Vekilov YuKh, Katsnelson MI, Lichtenstein AI, Johansson B (2007) Phonon related properties of transition metals, their carbides and nitrides: a first principles study. *J Appl Phys* 101:123519-1–123519-18
340. Samsonov GV, Kulik OP, Polishchuk VS (1978) Poluchenie i metody analiza nitridov (The preparation and analysis methods of nitrides). *Naukova Dumka, Kyiv* (in Russian)
341. Golubev AS, Kurdyumov AV, Pilyankevich AN (1987) Nitrid bora: struktura, svoystva, poluchenie (Boron nitride: structure, properties, preparation). *Naukova Dumka, Kyiv* (in Russian)
342. Kislyi PS, Kuzenkova MA, Bodnaruk NI, Grabchuk BL (1988) Karbid bora (Boron carbide). *Naukova Dumka, Kyiv* (in Russian)
343. SpringerMaterials (2014) The Landolt-Börnstein database. The Be-C-Ta system. <http://www.springermaterials.com/docs/search?query=%22Be-C-Ta%22>. Accessed 8 Apr 2014
344. Strife JR, Smeggil JG, Worell WL (1990) Reaction of iridium with metal carbides in the temperature range of 1923 to 2400 K. *J Am Ceram Soc* 73(4):838–845
345. Samsonov GV, Umanskii YaS (1957) Tverdye soedineniya tugoplavkikh metallov (Hard compounds of refractory metals). *Metallurgizdat, Moscow* (in Russian)
346. Samsonov GV, Épik AP (1973) Tugoplavkie pokrytiya (Refractory coatings). *Metallurgiya, Moscow*
347. Samsonov GV, Kovalchenko MS (1962) Goryachee pressovanie (Hot pressing). *UkrSSR State Engineering Literature Publishing House, Kyiv* (in Russian)
348. Zagryazkin VN (1969) O mekhanizme diffuzii v monokarbidakh perekhodnykh metallov (On the mechanism of diffusion in transition metals monocarbides). *Fiz Met Metalloved* 28(2):292–297 (in Russian)
349. Wakelkamp W, Van Loo FJJ, Boelen B, Bastin GF, Metselaar R (1990) The diffusion of carbon in non-stoichiometric carbides. *Defect Diffus Forum* 66–69:1485–1490
350. Wallace TC, Sr, Butt DP (1996) Review of diffusion and vaporization of group 4 and 5 transition metal carbides. In: Oyama ST (ed) *The chemistry of transition metal carbides and nitrides*. Chapman & Hall, London, Glasgow, pp. 53–90
351. Ilchenko NI, Pyatnitsky YuI (1996) Carbides of transition metals as catalysts for oxidation reactions. In: Oyama ST (ed) *The chemistry of transition metal carbides and nitrides*. Chapman & Hall, London, Glasgow, pp. 311–327
352. Kopylova VP (1961) Khimicheskaya ustoychivost karbidov perekhodnykh elementov IV, V i VI grupp (The chemical stability of transition element carbides IV, V and VI groups). *Zh Prikl Khim* 34(9):1936–1939 (in Russian)
353. Umanskii YaS (1947) Karbidy tverdykh splavov (Carbides of hard alloys). *Metallurgizdat, Moscow* (in Russian)
354. Samsonov GV, Zhidkova TG, Klimak ZA (1975) O kataliticheskikh svoystvakh karbidov perekhodnykh metallov (On the catalytic properties of transition metal carbides). In: Samsonov GV (ed) *Vysokotemperaturnye karbidy (High-temperature carbides)*. *Naukova Dumka, Kyiv*, pp. 76–81 (in Russian)

355. Ham DJ, Lee JS (2009) Transition metal carbides and nitrides as electrode materials for low temperature fuel cells. *Energies* 2:873–899. <https://doi.org/10.3390/en20400873>
356. Thorwarth E, Dietrich M, Politis C (1976) Superconducting and normal state properties of tantalum carbonitrides under hydrostatic pressure. *Solid State Commun* 20(9):869–872
357. Klein BM, Papaconstantopoulos DA (1974) Electron-phonon interaction and superconductivity in transition metals and transition-metal carbides. *Phys Rev Lett* 32(21):1193–1195
358. Allen PB, Cohen ML (1972) Superconductivity and phonon softening. *Phys Rev Lett* 29(24):1593–1596
359. Drickamer HG, Lynch RW, Clendenen RL, Perez Albuern EA (1966) X-ray diffraction studies of the lattice parameters of solids under very high pressure. *Solid State Phys* 19:135–228
360. Gusev AI, Rempel AA, Lipatnikov VN (1996) Heat capacity of niobium and tantalum carbides NbC_y and TaC_y in disordered and ordered states below 300 K. *Phys Stat Sol B* 194:467–482
361. Kubaschewski O, Alcock CB (1979) *Metallurgical thermochemistry*, 5th edn. Pergamon Press, Oxford
362. Samsonov GV (1964) *Handbooks of high-temperature materials: No. 2 – Properties index*. Plenum Press, Springer Science, New York
363. Kaufman L (1964) Thermodynamic factors controlling the stability of solid phases at high temperatures. In: Waber JT, Chiotti P, Miner WN (eds) *Compounds of interest in nuclear reactor technology*. Metallurgical Society of American Institute of Mining Engineers, New York, pp. 193–225
364. Holland L (1957) *Vacuum deposition of thin films*. Wiley, New York
365. Meissner W, Franz H, Westerhoff H (1932) Messungen mit Hilfe von flüssigem Helium. XVI. Untersuchungen über die Supraleitfähigkeit von Carbiden, Nitriden, Boriden und Siliciden (Measurements using liquid helium. XVI. Studies on the superconductivity of carbides, nitrides, borides and silicides). *Z Phys* 75(7–8):521–530 (in German)
366. Agte C, Moers K (1931) Methoden zur Reindarstellung hochschmelzender Carbide, Nitride und Boride und Beschreibung einiger ihrer Eigenschaften (Methods for the purification of refractory carbides, nitrides and borides and description of some their properties). *Z Anorg Allg Chem* 198(1):233–275 (in German)
367. Becker K (1933) *Hochschmelzende Hartstoffe und ihre technische Anwendung (Refractory hard materials and their industrial application)*. Verlag Chemie, Berlin (in German)
368. Kolomoets NV, Neshpor VS, Samsonov GV, Semenkovich SA (1958) Thermoelectrical properties of some metal-like compounds. *Sov Phys Tech Phys* 3(11):2186–2193
369. Samsonov GV, Sinelnikova VS (1962) The resistivity of refractory compounds at high temperatures. *Powder Metall Met Ceram* 1(4):272–274
370. Samsonov GV (1956) The electrical conductivity of certain compounds of the transitional metals with boron, carbon and nitrogen and the electrical conductivity of alloys of these compounds. *Sov Phys Tech Phys* 1(4):695–701
371. Grebenkina VG, Denbnovetskaya EN (1974) Thermal coefficient of the electrical resistivity of carbides and their solid solutions. In: Samsonov GV (ed) *Refractory carbides*. Consultants Bureau, New York, pp. 269–274
372. Lengauer W (2000) Transition metal carbides, nitrides and carbonitrides. In: Riedel R (ed) *Handbook of ceramic hard materials*. Wiley-VCH, Weinheim, pp. 202–252
373. Gusev AI, Nazarova SZ (2005) Magnetic susceptibility of nonstoichiometric compounds of transition d-metals. *Phys Usp* 48(7):651–673
374. Ozaki Y, Zee RH (1995) Investigation of thermal and hydrogen effects on emissivity of refractory metals and carbides. *Mater Sci Eng A* 202(1–2):134–141
375. Cohron J, Ozaki Y, Chin B, Zee R (1994) Reactivity of refractory carbides with hot hydrogen. *AIP Conf Proc* 301:939
376. Stewart D, Rivlin VG, Wilson PD (1981) Field emission cold cathode devices based on eutectic systems. Final Technical Report RADC-TR-81-170, Contract/Grant AFOSR-77-3292, A1-A15. Rome Air Development Center, Air Force Systems Command, Griffiss Air Force Base, New York, pp. 1–89

377. Stewart D, Wilson PD, Latham RV, Allen NK (1981) Energy spectra of electrons field emitted from a broad area composite cathode of tantalum carbide. *J Mater Sci* 16(1):111–117
378. Hojo H, Nakayama K (1976) Coated emitters of transition metal carbides for vacuum measurement. *J Vac Soc Jpn* 19(9):312–317 (in Japanese)
379. Ivanko AA (1974) The microhardness of transition-metal carbides. In: Samsonov GV (ed) *Refractory carbides*. Consultants Bureau, New York, pp. 367–370
380. Hollox GE (1968/69) Microstructure and mechanical behaviour of carbides. *Mater Sci Eng* 3(3):121–137
381. Rowcliffe DJ, Warren WJ (1970) Structure and properties of tantalum carbide crystals. *J Mater Sci* 5(4):345–350
382. Williams WS (1999) Electrical properties of hard materials. *Int J Refract Met Hard Mater* 17(1):21–26
383. Tian Y, Xu B, Zhao Z (2012) Microscopic theory of hardness and design of novel superhard crystals. *Int J Refract Met Hard Mater* 33:93–106
384. Šimůnek A, Vackář J (2006) Hardness of covalent and ionic crystals: first-principle calculations. *Phys Rev Lett* 96(8):085501
385. Šimůnek A (2007) How to estimate hardness of crystals on a pocket calculator. *Phys Rev B* 75(17):172108
386. Li K, Wang X, Zhang F, Xue D (2008) Electronegativity identification of novel superhard materials. *Phys Rev Lett* 100(23):235504
387. Foster LS, Forbes LW Jr, Friar LB, Moody LS, Smith WH (1950) Sintering carbides by means of fugitive binders. *J Am Ceram Soc* 33(1):27–33
388. Hivert A (1966) Un matériau réfractaire résistant au choc thermique: le carbure de tantale imprégné (A refractory material resistant to thermal shock: impregnated tantalum carbide). In: *Proc. Int. conf. on materials for use in space*, Paris, France, 7–11 Feb 1966, No. 323, Centre National d'Études Spatiales (in French)
389. Steinitz R (1966) Mechanical properties of refractory carbides at high temperatures. In: Boltax A, Handwerk JH (eds) *Proc. Int. conf. on nuclear applications of non-fissionable ceramics*. American Nuclear Society, Illinois, pp. 75–100
390. Lee SL, Hefferman WJ, Walden JA (1995) Nondestructive evaluation of sputter-deposited tantalum carbide refractory coatings. Technical Report ARCCB-TR-95023. US Army Armament Research, Development and Engineering Centre, Watervliet, New York, pp. 1–19
391. Pankratz LB, Weller WW, King EG (1966) Thermodynamic data for molybdenum carbide and tantalum carbide. Report BM-RI-6861. Bureau of Mines, US Department of the Interior, Washington, DC, pp. 1–10
392. Lynch JF (1979) Engineering property data on selected ceramics, Vol. 2 Carbides. Report MCIC-HB-07. Metals and Ceramics Information Centre, Battelle Columbus Laboratories, Ohio, pp. 1–136
393. Mauer FA, Bolz LH (1955) Measurement of thermal expansion of cermet components by high-temperature X-ray diffraction. Report WADC-TR-55-473, Contracts AF33(616)-56-5 and AF33(616)-53-12. US Air Force, Wright Air Development Centre, Ohio, pp. 1–57
394. Lowrie R (1963) Research on physical and chemical principles affecting high temperature materials for rocket nozzles. Quarterly Progress Report, Contract DA 30-069-ORD-2787. Union Carbide Research Institute, Tarrytown, New York, pp. 1–50
395. Kebler RW, Aspinall SR, Schomaker V (1964) Research on physical and chemical principles affecting high temperature materials for rocket nozzles. Quarterly Progress Report, Contract DA 30-069-ORD-2787. Union Carbide Research Institute, Tarrytown, New York, pp. 1–56
396. Leipold MH, Nielsen TH (1967) The mechanical behaviour of tantalum carbide and magnesium oxide. Report TR-32-1201, Contract NAS7-100. Jet Propulsion Laboratory, California Institute of Technology, Pasadena, pp. 1–33
397. Frantsevich IN, Zhurakovskii EA, Lyashchenko AB (1967) Elastic constants and characteristics of the electron structure of certain classes of refractory compounds obtained by the metal-powder method. *Inorg Mater* 3(1):6–12

398. Alexandre N, Desmaison M, Valin F, Boncoeur M (1994) Synthesis of high toughness tantalum carbide Ta₂C by HIP-reaction sintering. In: Delaey L, Tas H (eds) Hot isostatic pressing '93. Proc. Int. conf. on hot isostatic pressing (HIP '93), Antwerp, Belgium, 21–23 Apr 1993. Elsevier, Amsterdam, pp. 443–450
399. Senczyk D (1984) The lattice parameters of MeC-type carbides, nitrides and carbonitrides of transition metals of IV and V groups of the periodic system. In: Proc. 11th conf. applied crystallography, Vol. 1. Kozubnik, Poland, pp. 234–240
400. Grossklauss W, Bunshah RF (1975) Synthesis and morphology of various carbides in the Ta-C system. *J Vac Sci Technol* 12(4):811–814
401. Dua AK, George VC (1994) TaC coatings prepared by hot filament chemical vapour deposition: characterization and properties. *Thin Solid Films* 247(1):34–38
402. Zhang X, Hilmas GE, Fahrenholtz WG (2009) Densification and mechanical properties of TaC-based ceramics. *Mater Sci Eng A* 501(1–2):37–43
403. Jones T (1956) The metallography of certain hot-pressed carbides possessing high melting points. In: Technical papers of the metallographic group meeting held at Bridgeport Brass Company, 7–8 Nov 1956, TID-7567, Part 15. US Atomic Energy Commission, Washington, DC, pp. 32–45
404. Teague MC, Hilmas GE, Fahrenholtz WG (2010) Mechanical properties of reactively processed W/Ta₂C-based cermets. *J Eur Ceram Soc* 30(11):2197–2201
405. Liu L, Liu H, Ye F, Zhang Z, Zhou Y (2012) Microstructure and mechanical properties of the spark plasma sintered Ta₂C ceramics. *Ceram Int* 38(6):4707–4713
406. Alexandre N, Desmaison M, Valin F, Boncoeur M (1997) Solid state reaction between tantalum (Ta) and tantalum carbide (TaC) powders during HIPing. *Key Eng Mater* (136/2):868–871
407. Bukatov VG, Korostin OS, Knyazev VI (1975) Internal friction of TaC_{0.99} from 20 to 2000 °C. *Inorg Mater* 11(2):313–315
408. Ajami FI, MacCrone RK (1974) Thermal expansion, Debye temperature and Gruneisen constant of carbides and nitrides. *J Less-Common Met* 38(2–3):101–110
409. Chen Z-K, Xiong X, Li G-D, Sun W, Long Y (2010) Texture structure and ablation behaviour of TaC coating on carbon/carbon composites. *Appl Surf Sci* 257(2):656–661
410. Singh A, Aynyas M, Sanyal SP (2009) High pressure behaviour and structural properties of transition metal carbides. *Phase Transit* 82(8):576–586
411. Bhardwaj P (2012) Structural study of transition metal carbides. *Acta Phys Polon A* 122(1):138–141
412. Zhao Z, Zhou X-F, Wang L-M, Xu B, He J, Liu Z, Wang H-T, Tian Y (2011) Universal phase transitions of B1-structured stoichiometric transition metal carbides. *Inorg Chem* 50:9266–9272
413. Cao Y, Zhu J, Liu Y, Long Z (2013) Thermodynamic properties of MC (M = V, Nb, Ta): first principles calculations. *Modern Phys Lett B* 27(19):1341035 (7 pp.)
414. Varshney D, Shriya S (2013) Elastic, mechanical and thermodynamic properties at high pressures and temperatures of transition metal monocarbides. *Int J Refract Met Hard Mater* 41:375–401
415. Varshney D, Shriya S, Singh N (2013) Mechanical stiffening of transition metal carbides: XC (X = Ti, Zr, Nb, Hf, Ta). In: Proc. 57th DAE solid state physics symp. 2012. AIP Conf Proc 1512:1016–1017
416. Liu YZ, Jiang YH, Zhou R, Feng J (2014) First principles study the stability and mechanical properties of MC (M = Ti, V, Zr, Nb, Hf and Ta) compounds. *J Alloys Compd* 582:500–504
417. Viñes F, Sousa C, Liu P, Rodriguez JA, Illas F (2005) A systematic functional theory study of the electronic structure of bulk and (001) surface of transition-metals carbides. *J Chem Phys* 122:174709 (11 pp.)
418. Tütüncü HM, Bağcı S, Duman S, Küçükerođan E, Srivastava GP (2012) First-principles study of electronic and dynamic properties of the TaC (001) surface. *Diamond Relat Mater* 25:19–23
419. Srivastava A, Diwan BD (2012) Elastic and thermodynamic properties of divalent transition metal carbides MC (M = Ti, Zr, Hf, V, Nb, Ta). *Can J Phys* 90:331–338

420. Yang J, Gao F (2012) First principles calculations of mechanical properties of cubic 5d transition metal monocarbides. *Phys B* 407:3527–3534
421. Li J, Wang X, Liu K, Li D, Chen L (2011) Crystal structures, mechanical and electronic properties of tantalum monocarbide and mononitride. *J Superhard Mater* 33(3):173–178
422. Zubarev PV, Kuraev AB (1992) Creep of monocarbides of transition metals of IV, V groups. III. Creep of hafnium, niobium and tantalum carbides. *Phys Met Metallogr* 73(6):649–653
423. Zubarev PV, Kuraev AB (1992) Creep of monocarbides of transition metals of IV, V groups. I. Creep of zirconium carbide. *Phys Met Metallogr* 73(6):643–646
424. Zubarev PV, Dementev LN, Shmelev AG (1980) Vliyanie rezhimov pressovaniya na vysokotemperaturnuyu polzuchest karbidov IV-VI grupp perekhodnykh metallov (The effect of pressing mode on high-temperature creep of groups IV-VI transition metals carbides). *Fiz Khim Obrab Mater* 3:91–95 (in Russian)
425. Skuratovskii VN, Tkachenko YuG, Borisenko VA (1969) A technique for the investigating the microhardness of refractory compounds within a wide temperature range. *Strength Mater* 1(4):393–396
426. Zubarev PV, Dementev LN (1971) Relation between the activation energies of high-temperature creep and diffusion in transition metal carbides. *Strength Mater* 3(9):1058–1061
427. Chang YA, Toth LE, Tyan YS (1971) On the elastic and thermodynamic properties of transition metal carbides. *Metall Trans* 2(1):315–320
428. Abderrahim FZ, Faraoun HI, Ouahrani T (2012) Structure, bonding and stability of semi-carbides M_2C and sub-carbides M_4C ($M = V, Cr, Nb, Mo, Ta, W$): a first principles investigation. *Phys B* 407:3833–3838
429. Gubanov VA, Ivanovsky AL, Zhukov VP (1994) Electronic structure of refractory carbides and nitrides. Cambridge University Press, Cambridge
430. Isaev EI, Ahuja R, Simak SI, Lichtenstein AI, Vekilov YuKh, Johansson B, Abrikosov IA (2005) Anomalously enhanced superconductivity and *ab initio* lattice dynamics in transition metal carbides and nitrides. *Phys Rev B* 72(6):064515
431. Srivastava A, Chauhan M, Singh RK (2011) High-pressure phase transitions in transition metal carbides XC ($X = Ti, Zr, Hf, V, Nb, Ta$): a first-principle study. *Phase Transit* 84(1):58–66
432. Friedrich A, Winkler B, Juarez-Arellano EA, Bayarjargal L (2011) Synthesis of binary transition metal nitrides, carbides and borides from the elements in the laser-heated diamond anvil cell and their structure-property relations. *Mater* 4:1648–1692. <https://doi.org/10.3390/ma4101648>
433. Vojvodic A, Ruberto C (2010) Trends in bulk electron-structural features of rocksalt early transition-metal carbides. *J Phys Condens Matter* 22:375501 (10 pp.)
434. Yu X-X, Thompson GB, Weinberger CR (2015) Influence of carbon vacancy formation on the elastic constants and hardening mechanisms in transition metal carbides. *J Eur Ceram Soc* 35:95–103
435. Yu X-X, Weinberger CR, Thompson GB (2014) *Ab initio* investigations of the phase stability in tantalum carbides. *Acta Mater* 80:341–349
436. McColm IJ (1990) Ceramic hardness. Plenum Press, New York
437. Martin J-L, Lacour-Gayet P, Costa P (1971) Variation de la contrainte avec la vitesse de deformation et la temperature pour le carbure de tantale entre 1200 et 2200 °C (The variation in strain with deformation rate and temperature for tantalum carbide between 1200 and 2200 °C). *C R Acad Sci Paris* 272:2127–2130 (in French)
438. Martin J-L, Lacour-Gayet P, Costa P (1972) Plastic deformation of tantalum carbide up to 2200 °C. In: Thomas G, Fulrath RM, Fisher RM (eds) Electron microscopy and structure of materials. Proc. 5th Int. materials symp. “The structure and properties of materials – techniques and applications of electron microscopy”, University of California, Berkeley, 13–17 Sept 1971. University of California Press, Berkeley, pp. 1131–1140
439. Rowcliffe DJ (1984) Plastic deformation of transition metal carbides. In: Tressler RE, Bradt RC (eds) Deformation of ceramic materials II. Plenum Press, New York, pp. 49–71
440. Rowcliffe DJ, Thomas G (1975) Structure of non-stoichiometric TaC. *Mater Sci Eng* 18(2):231–238

441. Markhasev BI, Pior NCh, Shumilova RG (1979) Travitel dlya vyyavleniya mikrostrukturnykh materialov na osnove karbidov niobiya, tantala i gafniya (An etching agent for revealing microstructure of materials on the base of niobium, tantalum and hafnium carbides). *Zavod Lab* 45(6):543–545 (in Russian)
442. Walker P, Tarn WH (1991) *CRC handbook of metal etchants*. CRC Press, Boca Raton
443. Hockman AJ, Feigelson RS (1983) Low temperature electro-synthesis of tantalum and niobium carbides. *J Electrochem Soc* 130(1):221–224
444. Raub E, Falkenburg G (1964) Reactionen zwischen Karbide und Platin oder Palladium während des Sinterns bei hohen Temperaturen (The reactions between carbides and platinum or palladium during sintering at high temperatures). *Z Metallkd* 55(4):190–192 (in German)
445. Gorbatiy NA, Ryabchenko EM (1965) Behaviour of adsorbed Cs films on single-crystal spikes of Ta and Ta₂C. *Phys Solid State* 7(4):921–926
446. Benesovsky F, Rudy E (1960) Pseudoternary carbide systems. *Metall* (9):875–876
447. Samsonov GV, Burykina AL, Strashinskaya LV, Pugach ÉA (1964) Reactions between magnesium oxide or zirconium dioxide and refractory compounds at high temperatures under vacuum. *Russ Metall* (4):70–77
448. Holleck H (1977) Zum Aufbau der Systeme Thorium – (Zirkon, Niob, Ruthenium, Rhodium) – Kohlenstoff (The structure of thorium – (zirconium, niobium, ruthenium, rhodium) – carbon systems). *J Nucl Mater* 66(3):273–282 (in German)
449. Schönberg N (1954) Ternary metallic phases in the Ta-C-N, Ta-C-O and Ta-N-O systems. *Acta Chem Scand* 8:620–623
450. Tao X, Li Y, Du J, Xia Y, Yang Y, Huang H, Gan Y, Zhang W, Li X (2011) A generic bamboo-based carbothermal method for preparing carbide (SiC, B₄C, TiC, TaC, NbC, Ti_xNb_{1-x}C and Ta_xNb_{1-x}C) nanowires. *J Mater Chem* 21(25):9095–9102
451. Vallance SR, Round DM, Ritter C, Cussen EJ, Kingman S, Gregory DH (2009) Ultrarapid microwave synthesis of superconducting refractory carbides. *Adv Mater* 21:4502–4504
452. Shabalin IL (2009) Oxidation behaviour of hetero-modulus ceramics based on titanium carbide. In: Lin H-T, Koumoto K, Kriven WM, Norton DP, Garsia E, Reimanis IE (eds) *Developments in strategic materials. Ceramic engineering and science proceedings, Vol. 29(10)*. Wiley, New York, pp. 261–278
453. Eremenko VN, Velikanova TYa, Bondar AA (1989) Phase equilibria at the solidus surface of the equilibrium diagram of ternary systems of technetium with carbon and d-transition metals of groups III-VII. *Powder Metall Met Ceram* 28(11):868–873
454. Voitovich RF, Pugach ÉA (1968) Okislenie tugoplavkikh soedinenii (Oxidation of refractory compounds). *Naukova Dumka, Kyiv* (in Russian)
455. Kieffer R, Nowotny H, Ettmayer P, Freudhofmeier M (1970) Über die Beständigkeit von Übergangsmetallcarbiden gegen Stickstoff bis zu 300 at (On the stability of transition metal carbides in nitrogen up to 300 atm). *Monatsh Chem* 101(1):65–82 (in German)
456. Rassaerts H, Benesovsky F, Nowotny H (1965) Untersuchungen in den systemen Nb- und Ta-Cr-C (Studies in the systems Nb- and Ta-Cr-C. *Planseeber Pulvermetall* 13(3):199–206 (in German)
457. Samsonov GV, Panasyuk AD, Kozina GK, Dyakonova LV (1972) Contact reaction of refractory compounds with liquid metals. 2. Reaction of carbides of subgroup Va and VIa metals with liquid transition metals. *Powder Metall Met Ceram* 11(8):629–631
458. Samsonov GV, Podchernyaeva IA, Siman NI, Fomenko VS (1976) Behaviour of refractory compounds in alkali metal media. *Powder Metall Met Ceram* 15(2):122–127
459. Velikanova TYa, Eremenko VN, Artyukh LV, Bondar AA, Gordiichuk OV (1989) Phase diagrams of Sc-M(IV-VII)-C systems. *Powder Metall Met Ceram* 28(9):711–718
460. Goldschmidt HJ (1967) *Interstitial alloys*. Butterworths, London
461. Jeitschko W, Nowotny H, Benesovsky F (1964) Die H-phasen Ti₂TiC, Ti₂PbC, Nb₂InC, Nb₂SnC und Ta₂GaC (The H-phases Ti₂TiC, Ti₂PbC, Nb₂InC, Nb₂SnC and Ta₂GaC). *Monatsh Chem* 95(2):431–435 (in German)
462. Samsonov GV, Yasinskaya GA, Shiller EA (1961) Interaction of certain oxides, carbides and high-melting metals at high temperatures. *Refract Indust Ceram* 2(7–8):274–277
463. Adelsberg LM, Cadoff LH, Tobin JM (1966) Group IVB and VB metal carbide-carbon eutectic temperatures. *J Am Ceram Soc* 49(10):573–574

464. Sara RV, Lowell CE (1964) Research study to determine phase equilibrium relations of selected metal carbides at high temperatures. Report WADD-TDR-60-143, Contract AF 33(657)-8025, Part 5. Research and Technology Division, Wright-Patterson Air Force Base, Ohio, pp. 1–55
465. Rudy E, Harmon DP (1965) Related binary systems. Ta-C system. Partial investigation in the systems Nb-C and V-C. In: Ternary phase equilibria in transition metal-boron-carbon-silicon systems. Report AFML-TR-65-2, Contract USAF 33(615)-1249, Part 1, Vol. 5. Air Force Materials Laboratory, Wright-Patterson Air Force Base, Ohio, pp. 1–78
466. Portnoi KI, Levinskii YuV, Fadeeva VI (1961) Vzaimodeistvie s uglerodom nekotorykh tugoplavkikh karbidov i ikh tverdykh rastvorov (Reaction with carbon of some refractory carbides and their solid solutions). *Izv AN SSSR OTN Metall Toplivo* (2):147–149 (in Russian)
467. Ellinger FH (1943) Tantalum-carbon system. *Trans Am Soc Met* 31:89–104
468. Nadler MR, Kemper CP (1960) Some solidus temperatures in several metal-carbon systems. *J Phys Chem* 64(10):1468–1471
469. Nowotny H, Rogl P, Schuster JC (1982) Structural chemistry of complex carbides and related compounds. *J Solid State Chem* 44:126–133
470. Cohron J, Zee R, Chin B (1994) Degradation of refractory metal carbides by hot hydrogen. *J Nucl Mater* 212–215:1488–1491
471. Loshak MG (1984) Prochnost i dolgovechnost tverdykh splavov (The strength and durability of hard alloys). *Naukova Dumka, Kyiv* (in Russian)
472. Vorobev YuP (2004) Karbidy v stalyakh (Carbides in steels). *Izv Chelyabinsk Nauch Tsentr* 2:34–60 (in Russian)
473. Kud IV, Likhoded LS, Eremenko LI, Makarenko GN, Fedorus VB, Prilutskii ÉV (2006) Features of (Ti, Me)C solid solution formation. *Powder Metall Met Ceram* 45(1–2):14–19
474. Wang X-G, Liu J-X, Kan Y-M, Zhang G-J (2012) Effect of solid solution formation on densification of hot-pressed ZrC ceramics with MC (M = V, Nb and Ta) additions. *J Eur Ceram Soc* 32:1795–1802
475. Lavrenko VA (1973) Rekombinatsiya atomov vodoroda na poverkhnostyakh tverdykh tel (The recombination of hydrogen atoms on the surfaces of solid bodies). *Naukova Dumka, Kyiv* (in Russian)
476. Buchner H, Gutjahr MA, Gross K, Beccu KD (1973) Über das Verhalten unterstöchiometrischer Übergangsmetallcarbide als Katalysatoren in Dehydrierungsprozessen (On the behaviour of under-stoichiometric transition metal carbides as catalysts in dehydrogenation processes). *Monatsh Chem* 104(1):160–165 (in German)
477. Ilchenko NI, Chebotareva NP, Shvidak NV (1976) Oxidation of ammonia on transition metal carbides. *React Kinet Catal Lett* 4(3):343–349
478. Chebotareva NP, Ilchenko NI, Golodets GI (1976) Kinetics and mechanism of oxidation of hydrogen on carbides of transition metals of groups IV–VI. *Theor Exp Chem* 12(2):154–162
479. Samsonov GV, Kharlamov AI (1975) Catalytic properties of refractory compound powders (survey). *Powder Metall Met Ceram* 14(9):699–707
480. Kharlamov AI, Rafal AN, Samsonov GV, Belov AS (1977) Catalytic activities of hafnium, tantalum and tungsten carbides in the high-temperature para/ortho conversion of hydrogen. *Theor Exp Chem* 13(1):92–94
481. Kharlamov AI, Kirillova NV, Yatsimirskii VK (1981) The catalytic properties of transition element carbides and nitrides in the oxidation of carbon monoxide. *Theor Exp Chem* 17(2):168–179
482. Kojima I, Miyazaki E, Inoue Y, Yasumori I (1979) Catalytic activities of TiC, WC and TaC for hydrogenation of ethylene. *J Catal* 59(3):472–474
483. Kojima I, Miyazaki E, Inoue Y, Yasumori I (1982) Catalysis by transition metal carbides. IV. Mechanism of ethylene hydrogenation and the nature of active sites on tantalum monocarbide. *J Catal* 73(1):128–135
484. Kojima I, Miyazaki E (1984) Catalysis by transition metal carbides. V. Kinetic measurements of hydrogenation of CO over TaC, TiC and Mo₂C catalysts. *J Catal* 89(1):168–171

485. Rafal AN (1983) Kinetika reaktsii s uchastiem vodoroda na beskisorodnykh tugoplavlykh soedinenii perekhodnykh metallov IV-VI grupp periodicheskoi sistemy (Kinetics of reactions involving hydrogen on oxygen-free refractory compounds of periodic system IV-VI groups transition metals). PhD thesis, Institute for Problems of Materials Science, Ukrainian SSR Academy of Sciences, Kyiv (in Russian)
486. Kharlamov AI, Kirillova NV (1983) Catalytic properties of powdered refractory compounds of transition elements. Carbides and nitrides – a review. *Powder Metall Met Ceram* 22(2):123–134
487. Ledoux MJ, Pham-Huu C (1992) High specific area carbides of silicon and transition metals for catalysis. *Catal Today* 15(2):263–284
488. Raevskaya LN, Pavlovsky FG, Kolotusha BI, Ilchenko NI (1991) Okislitel'naya kondensatsiya metana s uchastiem kisloroda i zakisi azota na karbidakh perekhodnykh metallov (Oxidative condensation of methane with participation of oxygen and nitrous oxide on carbides of transition metals). *Ukr Khim Zh* 57(10):1080–1084 (in Russian)
489. Oyama ST (1992) Preparation and catalytic properties of transition metal carbides and nitrides. *Catal Today* 15(2):179–200
490. Ledoux MJ, Pham-Huu C, Chianelli RR (1996) Catalysis with carbides. *Curr Opin Solid State Mater Sci* 1(1):96–100
491. Tomás-García AL, Jensen JO, Bjerrum NJ, Li Q (2014) Hydrogen evolution activity and electrochemical stability of selected transition metal carbides in concentrated phosphoric acid. *Electrochim Acta* 137:639–646
492. Gale WF, Totemeir TC (eds) (2004) *Smithells metals reference book*, 8th edn. Elsevier Butterworth Heinemann, ASM International Materials Information Society, Amsterdam
493. Samsonov GV, Latysheva VP (1956) Issledovanie diffuzii bora i ugleroda v nekotorye metally perekhodnykh grupp (A study of the diffusion of boron and carbon into certain transition groups metals). *Fiz Met Metalloved* 2(2):309–319 (in Russian)
494. Samsonov GV, Latysheva VP (1956) Diffuziya bora, ugleroda i azota v perekhodnye metally IV, V i VI grupp periodicheskoi sistemy (The diffusion of boron, carbon and nitrogen into transition metals of the IV, V and VI groups of the periodic system). *Doklady AN SSSR* 109(3):582–585 (in Russian)
495. Peterson NL (1960) Diffusion in refractory metals. Technical Report WADD-TR-60-793, Contract AF 33(616)-7382. US Air Force, Wright-Patterson Air Force Base, Ohio, pp. 1–164
496. Ke T-S (1948) Internal friction in the interstitial solid solutions of C and O in tantalum. *Phys Rev* 74(1):9–15
497. Wert CA (1950) Measurements on the diffusion of interstitial atoms in b.c.c. lattices. *J Appl Phys* 21(11):1196–1197
498. Powers RW, Doyle MV (1957) Carbon-tantalum internal friction peak. *J Appl Phys* 28(2):255–258
499. Cotton D, Jacquet P, Faure S, Vignal V (2014) Low-pressure carburizing process: modeling of carbon diffusion in carburized steels and tantalum. In: Lubben T, Zoch H-W, Schneider R (eds) *Proc. Eur. conf. on heat treatment and 21st IFHTSE congress*, Munich, Germany, 12–15 May 2014. Arbeitsgemeinschaft Wärmebehandlung Werkstofftechnik, Bremen, pp. 529–536
500. Ferro A (1957) Theory of diffusion constants in interstitial solid solutions of bcc metals. *J Appl Phys* 28(8):895–900
501. Nakonechnikov AI, Pavlinov LV, Bykov VN (1966) Diffusion of carbon in refractory metals with a bcc lattice. *Phys Met Metallogr* 22(2):73–77
502. Son P, Ihara S, Miyake M, Sano T (1969) Diffusion of carbon in vanadium. *J Jpn Inst Met* 33(1):1–3 (in Japanese)
503. Frantsevich IN, Kovenskii II (1961) Pro stan vugletsyu v titani, tantali ta volframi (On the state of carbon in titanium, tantalum and tungsten). *Dopov Akad Nauk Ukr RSR* 11:1471–1474 (in Ukrainian)

504. Zhunkovskii GL (1969) Issledovanie protsessov diffuzionnogo nasyshcheniya tugoplavkikh metallov uglerodom i borom v vakuume (A study of the processes of diffusion saturation of refractory metals with carbon and boron in vacuum). PhD thesis, Institute for Problems of Materials Science, Ukrainian SSR Academy of Sciences, Kyiv (in Russian)
505. Bokstein SZ, Bronfin MB, Kishkin ST (1967) Diffuzionnye kharakteristiki tugoplavkikh metallov ispolzuemykh pri vysokikh temperaturah (The diffusion characteristics of refractory metals applied at high temperatures). In: Tumanov AT, Portnoi KI (eds) Tugoplavkie materialy v mashinostroenii (Refractory materials in machinery construction). Mashinostroenie, Moscow, pp. 151–176 (in Russian)
506. Brizes WF, Salkovitz EI (1969) Comparison of the chemical and self-diffusivities in the transition metal monocarbides. *Scripta Metall* 3(9):659–662
507. Hj Matzke (1984) Point defects and transport properties in carbides. *Solid State Ionics* 12:25–45
508. Hj Matzke (1990) Mass transport in carbides and nitrides. In: Freer R (ed) *The physics and chemistry of carbides, nitrides and borides*. Kluwer Academic, Dordrecht, pp. 357–383
509. Murch GE, Bruff CM (1999) Chemical diffusion in bulk inhomogeneous nonmetallic compounds. In: Beke DL (ed) *Diffusion in non-metallic solids*. Subvol. B, Part 1. Springer, Berlin, pp. 10/1–10/62
510. Roeder E, Hornstra J (1968) Grain growth during hot-pressing of tantalum carbide. *J Am Ceram Soc* 51(4):224–225
511. Roebuck B, Almond EA, Kellie JLF (1986) Characterization of the particle size of cubic transition metal carbides by measurement of the rate of oxidation. In: *Horizons of powder metallurgy*. Proc. Int. powder metallurgy conf. and exhibition “The future of powder metallurgy”, 9828. Duesseldorf
512. Lukashenko TA, Tikhonov KI (1998) Korroziionnaya stoikost ryada karbidov i nitridov perekhodnykh metallov 4-6 grupp v kontsentrirrovannykh rastvorakh sernoi i fosfornoj kislot (Corrosion resistance of a number of carbides and nitrides of group 4-6 transition metals in concentrated solutions of sulfuric and phosphoric acids). *Zh Prikl Khim* 71(12):2017–2020 (in Russian)
513. Lin Z, Zhuo M, Zhou Y, Li M, Wang J (2006) Microstructures and theoretical bulk modulus of layered ternary tantalum aluminum carbides. *J Am Ceram Soc* 89(12):3765–3769
514. He X, Bai Y, Zhu C, Sun Y, Li M, Barsoum MW (2010) General trends in the structural, electronic and elastic properties of the M_3AlC_2 phases (M = transition metal): a first-principle study. *Comput Mater Sci* 49:691–698
515. Samsonov GV, Petrikina RYa (1970) Sintering of metals, carbides and oxides by hot pressing. *Phys Sintering* 2(3):1–20
516. Zhang X (2008) Densification and mechanical properties of tantalum carbide and tantalum diboride ceramics. PhD thesis, Missouri University of Science and Technology, Rolla
517. Thompson GB, Weinberger CR (2014) Tantalum carbides: their microstructures and deformation behavior. In: *Fahrenholtz WG, Wuchina EJ, Lee WE, Zhou Y (eds) Ultra-high temperature ceramics*. Wiley, Hoboken, New Jersey, pp. 291–315
518. Allison C, Hoffman M, Williams WS (1982) Electron energy loss spectroscopy of carbon in dissociated dislocations in tantalum carbide. *J Appl Phys* 53(10):6757–6761
519. Steinitz R (1968) Physical and mechanical properties of refractory compounds. In: *Hausner HH, Bowman MG (eds) Fundamentals of refractory compounds*. Plenum Press, New York, pp. 155–183
520. Koester RD, Moak DP (1967) Hot hardness of selected borides, oxides and carbides to 1900 °C. *J Am Ceram Soc* 50(6):290–296
521. Sarian S (1972) Carbon self-diffusion in disordered V_6C_5 . *J Phys Chem Solids* 33:1637–1643
522. Santoro GJ, Dolloff RT (1965) Hall coefficient of tantalum carbide as function of carbon content. Technical Note NASA-TN-D-3135. NASA Lewis Research Center, Cleveland, pp. 1–18
523. Limeng L, Feng Y, Zhou Y, Zhiguo Z (2010) Microstructure and mechanical properties of spark plasma sintered $TaC_{0.7}$ ceramics. *J Am Ceram Soc* 93(10):2945–2947

524. DiPietro S, Wuchina E, Opeka M, Buesking K, Spain J, Matson L (2007) Studies of phase stability and microstructure in the Ta-C system. *ECS Trans* 3(14):143–150
525. Lahiri D, Singh V, Rodrigues GR, Costa TMH, Gallas MR, Bakshi SR, Seal S, Agarwal A (2013) Ultrahigh-pressure consolidation and deformation of tantalum carbide at ambient and high temperatures. *Acta Mater* 61:4001–4009
526. Chapin EJ, Friske WH (1954) A metallurgical evaluation of refractory compounds for containing molten titanium. Part II – Carbon, graphite and carbides. Report NRL-4467. Naval Research Laboratory, Washington, DC, pp. 1–22
527. Hollox GE (1968) Microstructure and mechanical behaviour of carbides. Technical Report 68-10c, Contracts NASw-1290 and DA-31-124-ARO-D-467. Research Institute for Advanced Studies, Martin Marietta Corporation, Baltimore, pp. 1–59
528. Dahmen U (1979) Microstructures and phase transformations in interstitial alloys of tantalum. PhD thesis, Lawrence Berkeley Laboratory, University of California
529. Samsonov GV, Épik AP (1966) Coatings of high-temperature materials. Some properties of high-temperature compounds. In: Hausner HH (ed) *Coatings of high-temperature materials*. Springer, Plenum Press, New York, pp. 7–111
530. Kolchin OP, Berlin IK (1964) Vosstanovlenie tantala iz pyatiokisi karbotermicheskim metodom (The reduction of tantalum from pentoxide by carbothermic method). *Tsvet Met* (8):67–71 (in Russian)
531. Harrod DL, Fleischer LR (1968) On the role of diffusion in the plastic deformation of transition metal carbides. In: Vahldiek FW, Mersol SA (eds) *Anisotropy in single-crystal refractory compounds*, Vol. 1. Springer, Plenum Press, New York, pp. 341–356
532. Kotlyar EE, Nazarchuk TN (1972) Interaction of the carbides of group IV and V transition metals with various acids. In: Samsonov GV (ed) *Chemical properties and analysis of refractory compounds*. Consultants Bureau, New York, pp. 1–5
533. Chin GY (1975) Slip and twinning systems in ceramic crystals. In: Bradt RC, Tressler RE (eds) *Deformation of ceramic materials*. Plenum Press, New York, pp. 25–59
534. Kovalchenko MS, Ochkas LF (1976) Issledovanie uslovii polucheniya i nekotorykh svoystv materialov na osnove karbida tantala (Study of manufacturing conditions and some properties of materials based on tantalum carbide). In: Samsonov GV, Kosolapova TYa, Gnesin GG, Fedorus VB, Domasevich LG (eds) *Karbidy i splavy na ikh osnove (Carbides and alloys based on them)*. Naukova Dumka, Kyiv, pp. 50–54 (in Russian)
535. Samsonov GV, Tkachenko YuG, Berdikov VF, Bovkun GA (1976) Mikrotverdost, mikrokrupkost i khrupkaya mikroprochnost karbidov perekhodnykh metallov (Microhardness, microbrittleness and brittle microstrength of transition metal carbides). In: Samsonov GV, Kosolapova TYa, Gnesin GG, Fedorus VB, Domasevich LG (eds) *Karbidy i splavy na ikh osnove (Carbides and alloys based on them)*. Naukova Dumka, Kyiv, pp. 98–104 (in Russian)
536. Bukatov VG, Knyazev VI, Korostin OS, Baranov VM (1976) Izmenenie uprugikh kharakteristik v oblasti gomogennosti nekotorykh karbidov perekhodnykh metallov (Change of elastic characteristics in the range of homogeneity of some transition metal carbides). In: Samsonov GV, Kosolapova TYa, Gnesin GG, Fedorus VB, Domasevich LG (eds) *Karbidy i splavy na ikh osnove (Carbides and alloys based on them)*. Naukova Dumka, Kyiv, pp. 111–114 (in Russian)
537. Knyazev VI, Bukatov VG, Korostin OS (1976) Vnutrennee trenie nekotorykh monokarbidov perekhodnykh metallov v diapazone temperatur 20–2000 °C (The internal friction of some transition metal carbides in the temperature range of 20–2000 °C). In: Samsonov GV, Kosolapova TYa, Gnesin GG, Fedorus VB, Domasevich LG (eds) *Karbidy i splavy na ikh osnove (Carbides and alloys based on them)*. Naukova Dumka, Kyiv, pp. 114–121 (in Russian)
538. Ogorodnikov VV, Rogovoi YuI (1976) Tochechnye defekty v kubicheskikh monokarbidakh (Point defects in cubic monocarbides). In: Samsonov GV, Kosolapova TYa, Gnesin GG, Fedorus VB, Domasevich LG (eds) *Karbidy i splavy na ikh osnove (Carbides and alloys based on them)*. Naukova Dumka, Kyiv, pp. 129–137 (in Russian)
539. Kumashiro Y (2000) High-temperature characteristics. In: Kumashiro Y (ed) *Electric refractory materials*. Marcel Dekker, New York, pp. 191–222

540. Becher PF (1971) Mechanical behaviour of polycrystalline TaC. *J Mater Sci* 6(1):79–80
541. Mileiko ST (1997) Metal and ceramic based composites. Elsevier, Amsterdam
542. Ishizawa Y (2000) Transition metal carbide field emitters. In: Kumashiro Y (ed) *Electric refractory materials*. Marcel Dekker, New York, pp. 269–287
543. Pearson WB (1958) *Lattice spacings and structures of metals and alloys*. Pergamon Press, London
544. Berg G, Friedrich C, Broszeit E, Berger C (2000) Data collection of properties of hard materials. In: Riedel R (ed) *Handbook of ceramic hard materials*. Wiley-VCH, Weinheim, pp. 965–995
545. Kieffer R, Benesovsky F (1968) *Hartstoffe (Hard materials)*. Springer, Vienna (in German)
546. Frey H, Kienel G (1987) *Dünnschichttechnologie (Thin film technologie)*. VDI-Verlag, Düsseldorf (in German)
547. Hornbogen E (1987) *Werkstoffe: Aufbau und Eigenschaften von Keramik, Metallen, Polymer- und Verbundwerkstoffen (Materials: structure and properties of ceramics, metals, polymers and composites)*. Springer, Berlin (in German)
548. Schedler W (1988) *Hartmetall für Praktiker (Hard metal for the practitioner)*. VDI-Verlag, Düsseldorf (in German)
549. Dörre E (1986) *Nichtmetallische Hartstoffe (Non-metallic hard materials)*. In: Uetz H (ed) *Abrasion und Erosion (Abrasion and erosion)*. Hanser, München, pp. 433–437 (in German)
550. Freller H, Lorenz HP (1992) Kriterien für die anwendungsbezogene Auswahl von Hartstoffschichten (Criteria for selection of hard coatings for special applications). VDI-Verlag, Düsseldorf (in German)
551. Sundgren JE, Hentzell HTG (1986) A review of the present state of art in hard coatings grown from the vapour phase. *J Vac Sci Technol A* 4(5):2259–2279
552. Holleck H (1986) Material selection for hard coatings. *J Vac Sci Technol A* 4(6):2661–2669
553. Berger J (1992) *Beschichten mit Hartstoffen (Hard material coatings)*. VDI-Verlag, Düsseldorf (in German)
554. Bargel H-J, Schulze G (1988) *Werkstoffe (Materials)*. VDI-Verlag, Düsseldorf (in German)
555. Rühle M (1982) Zum technischen Stand der Dispersionshärtung. Teil 1. (State of the art dispersion hardening. Part 1.). *Metal* 36(12):1280–1287 (in German)
556. Haefler RA (1987) *Oberflächen- und Dünnschichttechnologie. Teil 1 – Beschichtung von Oberflächen (Surface and thin film technology. Part 1 – Coating surfaces)*. Springer, Berlin (in German)
557. Steffens H-D, Brandl W (1992) *Moderne Beschichtungsverfahren (Modern surface technology)*. Lehrstuhl für Werkstofftechnologie der Universität Dortmund (in German)
558. Zhang N, Wang Y (1992) Dislocations and hardness of hard coatings. *Thin Solid Films* 214(1):4–5
559. Lanin A (2013) *Nuclear rocket engine reactor*. Springer, Berlin
560. Leipold MH, Becher PF (1969) Pressure densification and grain growth in tantalum carbide. *Am Ceram Soc Bull* 48(4):404–407
561. Bhardwaj P, Singh S (2012) Structural phase stability and elastic properties of refractory carbides. *Int J Refract Met Hard Mater* 35:115–121
562. Wang J, Vandeperre LJ (2014) Deformation and hardness of UHTCs as a function of temperature. In: Fahrenholtz WG, Wuchina EJ, Lee WE, Zhou Y (eds) *Ultra-high temperature ceramics*. Wiley, Hoboken, New Jersey, pp. 236–266
563. Guo Z, Zhu L, Zhou J, Sun Z (2015) Microscopic origin of MXenes derived from layered MAX phases. *RSC Adv* 5(32):25403–25408
564. Kiani S, Ratsch C, Minor AM, Yang J-M, Kodambaka S (2015) *In situ* transmission electron microscopy observations of room-temperature plasticity in sub-micron-size TaC(100) and TaC(011) single crystals. *Scripta Mater* 100:13–16
565. Yeh C-L, Chen Y-S (2015) Studies of Ta, Al and carbon sources on combustion synthesis of alumina – tantalum carbide composites. *Mater Manuf Process* 30(3):298–302
566. Zhong L, Liu L, Worsch C, Gonzalez J, Springer A, Ye F (2015) Transient liquid phase sintering of tantalum carbide ceramics by using silicon as the sintering aid and its effect on microstructure and mechanical properties. *Mater Chem Phys* 149:505–511

567. Nakamura D, Suzumura A, Shigetoh K (2015) Sintered tantalum carbide coatings on graphite substrates: highly reliable protective coatings for bulk and epitaxial growth. *Appl Phys Lett* 106(8):082108
568. Gozzi D, Guzzardi G, Montozzi M, Cignini PL (1997) Kinetics of high temperature oxidation of refractory carbides. *Solid State Ionics* 101–103(2):1243–1250
569. Hampshire S (2014) Fundamental aspects of hard ceramics. In: Sarin VK, Llanes L, Mari D (eds) *Comprehensive hard materials*. Vol. 2 – Ceramics. Oxford, Elsevier, Amsterdam, pp. 3–28
570. Lyubimov VD, Shveikin GP, Alyamovskii SI (1983) Mekhanizm pryamogo vosstanovleniya oksidov tantalala i gafniya v srede azota (Direct reduction mechanism of tantalum and hafnium oxides in nitrogen medium). *Zh Neorg Khim* 28(4):1057–1060 (in Russian)
571. Berkowitz-Mattuck J, Larson JT, Quigley RF, Christiansen W (1963) Kinetics of oxidation of refractory metals and alloys at 1000–2000 °C. Report ASD-TDR-62-203, Contract AF33(616)-6154, Part 2. Arthur D. Little Inc., Cambridge, pp. 1–117
572. Ormont BF (1959) Energii atomizatsii i teploty obrazovaniya nekotorykh karbidov i nitridov i naibolee veroyatnye znacheniya dlya energii dissotsiatsii azota i energii sublimatsii ugleroda (Atomization energies and heats of formation of some carbides and nitrides and the most probable values for the dissociation energy of nitrogen and sublimation energy of carbon). *Zh Fiz Khim* 33(7):1455–1460 (in Russian)
573. Fujishiro S (1961) Thermodynamic properties of transition metal carbides and their periodicity. *J Jpn Soc Powder Metall* 8(2):73–76
574. Oshcherin BN (1965) Nekotorye voprosy termodinamiki karbidnykh faz vnedreniya v oblastiakh gomogennosti (The certain problems of thermodynamics of carbide interstitial phases within the homogeneity ranges). In: Grigoreva VV, Eremenko VN, Nazarchuk TN, Samsonov GV, Fedorchenko IM, Frantsevich IN (eds) *Vysokotemperaturnye neorganicheskie soedineniya (High-temperature inorganic compounds)*. Naukova Dumka, Kyiv, pp. 157–165 (in Russian)
575. Nikolskaya TA, Avarbe RG (1971) Nekotorye zakonomernosti ispareniya karbidov perekhodnykh metallov IV-V podgrupp v vakuume (Some regularity of transition metals of IV-V subgroups carbides evaporation in a vacuum). In: Kornilov II, Matveeva NM (eds) *Metallidy – stroenie, svoistva, primenenie (Metallides – structure, properties, application)*. Nauka, Moscow, pp. 127–134 (in Russian)
576. Kulikov IS (1988) Termodinamika karbidov i nitridov (Thermodynamics of carbides and nitrides). *Metallurgiya, Chelyabinsk* (in Russian)
577. Kaufman L, Bernstein H (1968) Thermodynamic properties of refractory transition metal compounds. In: Vahldiek FW, Mersol SA (eds) *Anisotropy in single-crystal refractory compounds*, Vol. 1. Springer, New York, pp. 269–297
578. Bowman AL, Krikorian NH (1976) Interstitial phases. In: Hannay NB (ed) *Treatise on solid state chemistry*. Vol. 3 – Crystalline and noncrystalline solids. Plenum Press, New York, pp. 253–292
579. Chase MW, Jr, ed (1998) NIST-JANAF thermochemical tables, 4th edn. *J Phys Chem Ref Data Monograph No. 9*. American Institute of Physics, New York
580. Ordanyan SS, Orekhov AN, Vikhman SV (2012) Interaction of W_2B_5 with $Me^{IV,V}C$ carbides. *Russ J Non-Ferrous Met* 55(1):91–94
581. Becker K, Ewest H (1930) Die physikalischen und wärmeausstrahlen Eigenschaften von Tantalcarbide (The physical and radiating properties of tantalum carbide). *Z Tech Physik* 11:216–220 (in German)
582. Touloukian YS, Kirby RK, Taylor RE, Lee TYR (1977) Thermophysical properties of matter. Vol. 13 – Thermal expansion – nonmetallic solids. IFI/Plenum Data Company, New York, Washington
583. Samsonov GV, Grebenkina VG (1968) Temperature coefficient of electroresistance of some high-melting compounds. *Powder Metall Met Ceram* 7(2):107–111

584. Dubrovskaya LB, Matveenko II, Geld PV (1965) Vliyanie temperatury i sostava na elektroprovodnost' β - i γ -faz sistemy tantal-uglerod (Effect of temperature and composition on the electrical conductivity of β - and γ -phases of the tantalum-carbon system). *Fiz Met Metalloved* 20(2):243–250 (in Russian)
585. Borukhovich AS (1978) Kinetic properties of IVa and Va subgroup transition metal monocarbides. *Phys Stat Sol A* 46(1):11–37
586. Lide DR (ed) (2010) CRC handbook of chemistry and physics, 90th edn. CRC Press, Boca Raton
587. Tsuchida T, Mekata M, Nakamura Y, Sakurai J, Takaki H (1961) Hall effect in carbides of transition metals. *J Phys Soc Jpn* 16(12):2453–2456
588. Costa P, Conte RR (1964) Physical properties of transition metal carbides and nitrides. In: Waber JT, Chiotti P, Miner WN (eds) *Compounds of interest in nuclear reactor technology*. Metallurgical Society of American Institute of Mining Engineers, New York, pp. 3–18
589. Goretzki H (1963) Untersuchung der magnetischen, elektrischen und thermoelektrischen Eigenschaften der Karbide und Nitride der 4a- und 5a-Gruppen Übergangsmetalle (A study of magnetic, electrical and thermoelectrical properties of carbides and nitrides of 4a and 5a groups transition metals). PhD thesis, Wien Universität (in German)
590. Riethof TR, DeSantis VJ (1963) Techniques for measuring normal spectral emissivity of conductive refractory compounds at high temperature. In: *Proc. symp. on measurement of thermal radiation properties of solids*, Dayton, Ohio, 5–7 Sept 1962. National Aeronautics and Space Administration, Washington, DC, pp. 565–584
591. Petrov VA, Chekhovskoi VYa, Sheindlin AE (1968) Emissivity and electrical resistivity of some refractory carbides. In: *Proc. 4th symp. on thermophysical properties*, University of Maryland, College Park, 1968. American Society of Mechanical Engineers, New York, pp. 270–277
592. Pears CD (1963) Some problems in emittance measurements of the higher temperatures and surface characterisation. In: *Proc. symp. on measurement of thermal radiation properties of solids*, Dayton, Ohio, 5–7 Sept 1962. National Aeronautics and Space Administration, Washington, DC, pp. 541–549
593. Neel DS, Pears CD, Oglesby S (1963) The thermal properties of twenty-six solid materials to 5000 °F or their destruction temperatures. Report ASD-TDR-62–765, Contract USAF 33(616)-7319. Southern Research Institute, University of Alabama, Birmingham, pp. 1–420
594. Shaffer PTB (1961) Development of ultra-refractory materials. Progress Report No. 25, Contract NORd-17175. The Carborundum Company, Niagara Falls, New York, pp. 1–4
595. Riethof TR (1961) High temperature spectral emissivity studies. General Electric Company, Missile and Space Vehicle Department, Philadelphia, Pennsylvania
596. Blau HH, Jr, Chaffee E, Jasperse JR, Martin WS (1960) High temperature thermal radiation properties of solid materials. Report AFCRC-TN-60-165, Contract USAF 19(604)-2639. Little (Arthur D.), Cambridge, Massachusetts, pp. 1–71
597. Touloukian YS, DeWitt DP (1972) *Thermophysical properties of matter, Vol. 8 – Thermal radiative properties – nonmetallic solids*. IFI/Plenum Data Corporation, New York, Washington
598. Adams JG (1962) The determination of spectral emissivities, reflectivities and absorptivities of materials and coatings. Technical Report NOR-61-189. Northrop Aircraft, Hawthorne, California, pp. 1–259
599. Touloukian YS, DeWitt DP, Hemicz RS (1972) *Thermophysical properties of matter, Vol. 9 – Thermal radiative properties – coatings*. IFI/Plenum Data Corporation, New York, Washington
600. Kieffer R, Kölbl F (1949) Tungsten carbide – free hard metals. *Powder Metall Bull* 4(1):4–17
601. Bukatov VG (1979) Issledovanie fiziko-mekhanicheskikh svoistv karbidov tugoplavkikh metallov i nekotorykh splavov na ikh osnove (Studies of physico-mechanical properties of refractory metal carbides and some alloys on their basis). PhD thesis, Moscow Institute of Steels and Alloys (in Russian)
602. Hausner HH, Friedemann HC (1962) *High temperature compounds – a data book*. General Astrometals Corporation, Yonkers, New York

603. Weber WP, Quirk JF, Lemmon AW Jr, Filbert RB Jr (1957) Properties of beryllium oxide and carbides of beryllium, molybdenum, niobium, tantalum and titanium. Report BMI-1165, Contract W-7405-eng-92. Battelle Memorial Institute, Columbus, Ohio, pp. 1–37
604. Naumenko VYa (1971) Tekhnologiya polucheniya i issledovanie nekotorykh svoystv karbidov perekhodnykh metallov IV-V grupp v oblastiakh ikh gomogenosti (Production technology and investigation of some properties of transition metal carbides IV-V groups in the regions of their homogeneity). PhD thesis, Institute for Problems of Materials Science, Ukrainian SSR Academy of Sciences, Kyiv (in Russian)
605. Stern KH (1996) Electrodeposition of refractory compounds from molten salts – borides, carbides and silicides. In: Stern KH (ed) Metallurgical and ceramic protective coatings. Chapman & Hall, London, Weinheim, New York, pp. 54–73
606. Weimer AW (ed) Carbide, nitride and boride materials synthesis and processing. Chapman & Hall, London, Weinheim, New York
607. Zaima S, Saito K, Adachi H, Shibata Y, Hojo H, Ono M (1980) Field emission from TaC. In: Yashiroo Y, Igata N (eds) Proc. 27th Int. field emission symp., University of Tokyo, Japan, pp. 348–352
608. Ono M, Hojo H, Shimizu H, Murakami H (1980) Tantalum carbide cathode for field emission guns. In: Yashiroo Y, Igata N (eds) Proc. 27th Int. field emission symp., University of Tokyo, Japan, pp. 353–358
609. Nagashima A, Nuka K, Satoh K, Itoh H, Ichinokawa T, Oshima C, Otani S (1993) Electronic structure of monolayer graphite on some transition metal carbide surfaces. Surf Sci 287–288(2):609–613
610. Khusainov MA (1989) Mechanical properties and special features of failure of carbides and nitrides of metals of groups IV-V deposited from the gas phase. Powder Metall Met Ceram 28(7):551–555
611. Ferro D, Rau JV, Albertini VR, Generosi A, Teghil R, Barinov SM (2008) Pulsed laser deposited hard TiC, ZrC, HfC and TaC films on titanium: hardness and an energy-dispersive X-ray diffraction study. Surf Coat Technol 202:1455–1461
612. Mukhopadhyay A, Raju GB, Basu B (2013) Ultra-high temperature ceramics: processing, properties and applications. In: Low IM, Sakka Y, Hu CF (eds) MAX phases and ultra-high temperature ceramics for extreme environments. IGI Global, Hershey, Pennsylvania, pp. 49–99
613. Wang HL, Hon MH (1999) Temperature dependence of ceramics hardness. Ceram Int 25(3):267–271
614. Kramer BM, Judd PK (1985) Computational design of wear coatings. J Vac Sci Technol A 3(6):2439–2444
615. Pisarenko GS, Rudenko VN, Tretyachenko GN, Troshchenko VT (1966) Prochnost materialov pri vysokikh temperaturakh (The strength of materials at high temperatures). Naukova Dumka, Kyiv (in Russian)
616. Ogorodnikov VV, Rogovoi YuI (1993) Rules of change in elastic, thermal and energy properties in a number of cubic transition metal monocarbides. Powder Metall Met Ceram 32(5):445–449
617. Gautam GS, Kumar KCH (2014) Elastic, thermochemical and thermophysical properties of rock salt-type transition metal carbides and nitrides: a first principles study. J Alloys Compd 587:380–386
618. Liu Y-Z, Jiang Y-H, Zhou R, Feng J (2014) First principles study the stability and mechanical properties of MC (C = Ti, V, Zr, Nb, Hf and Ta) compounds. J Alloys Compd 582:500–504
619. Patriarca P, Rucker DJ (1970) Fuels and materials development program. Technical Report ORNL-4480, Contract W-7405-ENG-26. Oak Ridge National Laboratory, Tennessee, pp. 1–255
620. Kotelnikov RB, Bashlykov SN, Kashtanov AI, Menshikova TS (1978) Vysokotemperaturnoe yadernoe toplivo (High-temperature nuclear fuel). Atomizdat, Moscow (in Russian)
621. Holleck H, Kleykamp H (1969) Thermodynamics of multi-component systems containing UC and PuC – a review. J Nucl Mater 32(1):1–19

622. Zhou P, Peng YB, Du Y, Wang SQ, Wen GH, Xie W, Chang KK (2013) A thermodynamic description of the C-Ta-Zr system. *Int J Refract Met Hard Mater* 41:408–415
623. Brauer G, Lesser R (1959) Karbonitride des Tantal (Tantalum carbonitrides). *Z Metallkd* 50(9):512–515 (in German)
624. McMullin JG, Norton JT (1953) The ternary system Ti-Ta-C. *Trans AIME* 197(9):1205–1208
625. Fischer JJ (1964) Hot-pressing mixed carbides of Ta, Hf and Zr. *Am Ceram Soc Bull* 43(3):183–185
626. Servant C, Danon CA (2004) CALPHAD modelling of the unmixing of transition metal carbide phases. *Calphad* 28(4):337–353
627. Markström A, Andersson D, Frisk K (2008) Combined *ab initio* and experimental assessment of $A_{1-x}B_xC$ mixed carbides. *Calphad* 32(4):615–623
628. Jung W-S, Chung S-H (2010) *Ab initio* calculation of interfacial energies between transition metal carbides and fcc iron. *Model Simul Mater Sci Eng* 18(7):075008
629. Ghaffari SA, Faghihi-Sani MA, Golestani-Fard F, Nojabayy M (2013) Diffusion and solid solution formation between the binary carbides of TaC, HfC and ZrC. *Int J Refract Met Hard Mater* 41:180–184
630. Orita M, Kojima I, Miyazaki E (1986) Catalysis by transition metal carbides. 7. Kinetic and XPS studies of the decomposition of methanol on TiC, TaC, Mo_2C , WC and W_2C . *Bull Chem Soc Jpn* 59(3):689–695
631. Miyazaki E, Kojima I, Orita M (1985) Synthesis of methyl formate from methanol over metal carbide catalysts. *J Chem Soc Chem Comm* 3:108–109
632. Kojima I, Miyazaki E, Yasumori I (1980) Synthesis of hydrocarbons from CO and H_2 over metal catalysts. *J Chem Soc Chem Comm* 12:573–574
633. Kojima I, Miyazaki E (1979) Hydrogenation activity and electronic structure of metal carbide catalysts. *Abstr Pap Am Chem Soc* 4:126–127
634. Michalsky R, Zhang Y-J, Medford AJ, Peterson AA (2014) Departures from the adsorption energy scaling relations for metal carbide catalysts. *J Phys Chem C* 118(24):13026–13034
635. Michalsky R, Zhang Y-J, Peterson AA (2014) Trends in the hydrogen evolution activity of metal carbide catalysts. *ACS Catal* 4(5):1274–1278
636. Regmi YN, Waetzig GR, Duffee KD, Schmuecker SM, Thode JM, Leonard BM (2015) Carbides of group IVA, VA and VIA transition metals as alternative HER and ORR catalysts and support materials. *J Mater Chem A* 3(18):10085–10091
637. Chen W-F, Muckerman JT, Fujita E (2013) Recent developments in transition metal carbides and nitrides as hydrogen evolution electrocatalysts. *Chem Comm* 49(79):8896–8909
638. Stottlemeyer AL, Kelly TG, Meng Q, Chen JG (2012) Reactions of oxygen-containing molecules on transition metal carbides: surface science insight into potential applications in catalysis and electrocatalysis. *Surf Sci Rep* 67:201–232
639. Rees EJ, Essaki K, Brady CDA, Burstein GT (2009) Hydrogen electrocatalysts from microwave-synthesized nanoparticulate carbides. *J Power Sources* 188(1):75–81
640. Aizawa T, Hayami W, Souda R, Otani S, Ishizawa Y (1997) Hydrogen adsorption on transition metal carbide (111) surfaces. *Surf Sci* 381:157–164
641. Tuffias RH, Duffy AJ, Arrieta VM, Abrams WM, Benander RE (1997) Materials and fabrication processes for operation in hot hydrogen. *AIP Conf Proc* 387:1613–1618
642. Mireles OR, Anghaie S, Cunningham B, Dooies B (2009) Material performance evaluation of TaC, WC and ZrC under prototypic nuclear thermal propulsion hot hydrogen environment. In: *Proc. 3rd topical meeting on nuclear and emerging technologies for space*, NETC 2009, Atlanta, Georgia, 14–19 June 2009. American Nuclear Society, Illinois, pp. 99–106
643. Johnsson M, Shimada S (2002) Oxidation of $Ta_xTi_{1-x}C$ whiskers under formation of carbon. *J Mater Sci Lett* 21(12):955–958
644. Shimada S, Seki Y, Johnsson M (2004) Thermoanalytical study on oxidation of $Ti_xTa_{1-x}C_yN_{1-y}$ whiskers with formation of carbon. *Solid State Ionics* 167(3–4):407–412

645. Shimada S, Johnsson M, Urbonaitė S (2004) Thermoanalytical study on oxidation of $TaC_{1-x}N_x$ powders by simultaneous TG-DTA-MS technique. *Thermochim Acta* 419(1–2):143–148
646. Lively DT, Murray P (1956) The wetting properties of solid oxides and carbides by liquid metals. In: Benesovsky F (ed) Proc. 2nd Plansee seminar on sintered high-temperature and corrosion resistance materials, Reutte, Tyrol, 19–23 June 1955. Metallwerk Plansee AG, Reutte, Tyrol, pp. 375–404
647. Samsonov GV, Kovalchenko MS, Petrykina RYa, Naumenko VYa (1970) Hot-pressing of the transition metals and their carbides in their homogeneity regions. *Powder Metall Met Ceram* 9(9):713–716
648. Samsonov GV, Sinelnikova VS (1964) Electrical resistance of refractory compounds at high temperatures. In: Samsonov GV (ed) Refractory transition metal compounds and high temperature cermets. Academic Press, New York, London, pp. 172–177
649. Lengauer W, Wiesenberger H, Jogue M, Rafaja D, Etmayer P (1996) Chemical diffusion in transition metal – carbon and transition metal – nitrogen systems. In: Oyama ST (ed) The chemistry of transition metal carbides and nitrides. Chapman & Hall, London, Glasgow, pp. 91–106
650. Emelyanov VS, Yevstyukhin AI, Godin YuG, Solovyev GI, Kokhtev SA (1967) Issledovanie karbidnoi oblasti sistemy Ta-Hf-C (Investigation of carbide region of Ta-Hf-C system). In: Emelyanov VS, Yevstyukhin AI (eds) Metallurgiya i metallovedenie chistykh metallov (Metallurgy and metallography of pure metals), Vol. 6. Atomizdat, Moscow, pp. 108–114 (in Russian)
651. Samsonov GV, Naumenko VYa (1970) Thermal expansion of transition metal carbides IV-V groups in their homogeneity regions. *High Temp* 8(5):1022–1024
652. Roebuck B, Almond EA, Kellie JLF (1986) Characterization of the particle size of cubic transition metal carbides by measurement of the rate of oxidation. In: Proc. Int. powder metall. conf. and exhibition (P/M'86), 9828. Duesseldorf, Germany
653. Wiesenberger H, Lengauer W, Etmayer P (1998) Reactive diffusion and phase equilibria in the V-C, Nb-C, Ta-C and Ta-N systems. *Acta Mater* 46(2):651–666
654. Nazarova SZ, Gusev AI (2001) Magnetic susceptibility as a method of investigation of short-range order in highly nonstoichiometric carbides. *J Struct Chem* 42(3):470–484
655. Bittner H, Goretzki H, Benesovsky F, Nowotny H (1963) Über einige Monocarbide-Mononitrid-Systeme und deren magnetische Eigenschaften (On some monocarbide-mononitride systems and their magnetic properties). *Monatsh Chem* 94(3):518–526 (in German)
656. Brownlee LD (1958) The pseudo-binary systems of uranium carbide with zirconium carbide, tantalum carbide and niobium carbide. *J Inst Met* 87(2):58–61
657. Fesenko VV, Bolgar AS (1963) Evaporation rate and vapour pressure of carbides, silicides, nitrides and borides. *Powder Metall Met Ceram* 2(1):11–17
658. Samsonov GV, Fomenko VS, Paderno VN, Rud BM (1964) Thermoemission characteristics of alloys of isomorphous carbides. *High Temp* 2(5):656–661
659. Avgustinik AI, Ordanyan SS (1966) Stroenie splavov sistemy Zr-C-Ta (The structure of alloys of the Zr-C-Ta system). *Zh Prikl Khim* 39(2):318–323 (in Russian)
660. Kuchma AY, Samsonov GV (1966) Obrazovanie stabilnykh elektronnykh konfiguratsii i nekotorye fizicheskie svoystva karbidov i nitridov perekhodnykh metallov v oblasti ikh gomogenosti (Formation of stable electron configurations and some physical properties of carbides and nitrides of transition metals in the range of their homogeneity). *Izv AN SSSR Neorg Mater* 2(11):1970–1974 (in Russian)
661. Willens RH, Buehler E, Matthias BT (1967) Superconductivity of the transition metal carbides. *Phys Rev* 159(2):327–330
662. Borukhovich AS, Dubrovskaya LB, Matveenko II, Geld PV (1970) Issledovanie magnitnoi vospriimchivosti kubiceskikh karbidov niobiya i tantala v oblasti nizkikh temperatur (A study of the magnetic susceptibility of cubic niobium and tantalum carbides in the low temperature range). In: Shveikin GP, Geld PV (eds) Issledovaniya soedinenii redkikh

- elementov. Trudy Instituta khimii (Studies of less-common element compounds. Proc. Institute of Chemistry), Vol. 20. USSR Academy of Sciences, Sverdlovsk, pp. 71–73 (in Russian)
663. Rice RW (1971) The compressive strength of ceramics. In: Kriegel WW, Palmour H, III (eds) *Ceramics in severe environments*. Proc. 6th university conference on ceramic science, North Carolina State University, Raleigh, 7–9 Dec 1970. Plenum Press, New York, pp. 195–229
664. Grebenkina VG, Sorokin VN, Yusov YuP, Perevezentsev AV (1973) Use of refractory carbides in resistors. *Powder Metall Met Ceram* 12(6):502–504
665. Savitskii EM, Baron VV, Efimov YuV, Bychkova MI, Myzenkova LF (1973) *Superconducting materials*. Plenum Press, New York
666. Samsonov GV, Fomenko VS, Podchernyaeva IA, Okhremchuk LN (1974) Thermionic emission properties of refractory compounds and materials based on them (a review). *Powder Metall Met Ceram* 13(10):836–842
667. Samsonov GV, Voronkin MA (1976) Properties of double carbides of titanium and group Va metals. *Powder Metall Met Ceram* 15(4):296–299
668. Kovalchenko MS, Bovkun GA, Tkachenko YuG, Ragozin IP (1983) Deformation properties of monocarbides of transition metals by the method of continuous impression of an indenter. *Powder Metall Met Ceram* 22(12):1034–1037
669. Valvoda V, Dobiášová L, Karen P (1985) X-ray diffraction analysis of diffusional alloying of HfC and TaC. *J Mater Sci* 20:3605–3609
670. Gruzalski GR, Zehner DM (1986) Defect states in substoichiometric tantalum carbide. *Phys Rev B* 34(6):3841–3848
671. Garbe J, Kirschner J (1989) Spin-resolved photoemission from the (100) face of tantalum carbide. *Phys Rev B* 39(9):6115–6120
672. Gruzalski GR, Lui S-C, Zehner DM (1990) Work-function changes accompanying changes in composition of (100) surfaces of HfC_x and TaC_x. *Surf Sci* 239(1–2):L517–L520
673. Price DL, Wills JM, Cooper BR (1993) Linear-muffin-tin-orbital calculation of TaC (001) surface relaxation. *Phys Rev B* 48(20):15301–15310
674. Price DL, Cooper BR, Wills JM (1993) Effect of carbon vacancies on carbide work functions. *Phys Rev B* 48(20):15311–15315
675. Nagashima A, Itoh H, Ichinokawa T, Oshima C, Otani S (1994) Change in the electronic states of graphite overlayers depending on thickness. *Phys Rev B* 50(7):4756–4763
676. Wang CC, Akbar SA, Chen W, Patton VD (1995) Electrical properties of high-temperature oxides, borides, carbides and nitrides. *J Mater Sci* 30:1627–1641
677. Singh M, Wiedemeier H (1997) Estimation of thermal expansion behaviour of some refractory carbides and nitrides. *J Mater Sci* 32(21):5749–5751
678. Eckerlin P, Kandler H (1971) *Structural data for elements and intermetallic phases*. Springer, Berlin
679. Gall NR, Rutkov EV, Tontegode AY (2001) Sequential Ta (100) carbonisation: from adsorption of single atoms to bulk carbide production. *Surf Sci* 472:187–194
680. Kruse O, Jansson B, Frisk K (2001) Experimental study of invariant equilibria in the Co-W-C and Co-W-C-Me (Me = Ti, Ta, Nb) systems. *J Phase Equilib* 22(5):552–555
681. Velikanova TYA, Bondar AA, Grytsiv AV, Dovbenko OI (2001) Metallochemistry of chromium with *d*-metals and carbon. *J Alloys Compd* 320:341–352
682. Gusev AI (2003) Analysis of surface segregation and solid-phase decomposition of substitutional solid solutions. *Dokl Phys Chem* 392(1–3):235–239
683. Siethoff H (2003) Correspondence of the plasticity of rocksalt structure ceramics and tetrahedrally coordinated semiconductors. *J Appl Phys* 94(5):3128–3134
684. Hugosson HW, Eriksson O, Jansson U, Ruban AV, Souvatzis P, Abrikosov IA (2004) Surface energies and work functions of the transition metal carbides. *Surf Sci* 557(1–3):243–254

685. Gusev AI (2006) Short-range order and diffuse scattering in nonstoichiometric compounds. *Phys Usp* 49(7):693–718
686. Latini A, Barinov SM, Ferro D, Rau JV, Scandurra R (2006) Electron beam deposited tantalum carbide film on titanium. *Powder Metall Prog* 6(1):20–25
687. Lavrentyev AA, Gabrelian BV, Vorzhev VB, Nikiforov IYa, Khyzhun OYu, Rehr JJ (2008) Electronic structure of cubic $\text{Hf}_x\text{Ta}_{1-x}\text{C}$ carbides from X-ray spectroscopy studies and cluster self-consistent calculations. *J Alloys Compd* 462:4–10
688. Noffsinger J, Giustino F, Louie SG, Cohen ML (2008) First principles study of superconductivity and Fermi-surface nesting in ultra-hard transition metal carbides. *Phys Rev B* 77(18):1805071–1805074
689. Wang J, Wang J, Zhou Y, Lin Z, Hu C (2008) *Ab initio* study of polymorphism in layered ternary carbides M_4AlC_3 ($\text{M} = \text{V}, \text{Nb}$ and Ta). *Scripta Mater* 58:1043–1046
690. Schuster JC, Nowotny H (1980) Investigations of the ternary systems (Zr, Hf, Nb, Ta)-Al-C and studies on complex carbides. *Z Metallkd* 71:341–346
691. Hu C, Zhang J, Bao Y, Wang J, Li M, Zhou Y (2008) *In situ* reaction synthesis and decomposition of Ta_2AlC . *Int J Mater Res (Z Metallkd)* 99(1):8–13
692. Hu C, He L, Zhang J, Bao Y, Wang J, Li M, Zhou Y (2008) Microstructure and properties of bulk Ta_2AlC ceramic synthesized by an *in situ* reaction/hot-pressing method. *J Eur Ceram Soc* 28(8):1679–1685
693. Li X, Westwood A, Brown A, Brydson R, Rand B (2009) A convenient general synthesis of carbide nanofibres via template reactions on carbon nanotubes in molten salt media. *Carbon* 47:201–208
694. Jiang X, Zhao J, Jiang X (2011) Correlation between hardness and elastic moduli of the covalent crystals. *Comput Mater Sci* 50(7):2287–2290
695. Klimov DA, Myktybekov B, Nizovtsev VE, Ukhov PA (2011) Perspektivy primeneniya nanostrukturnykh kompozitsionnykh materialov na osnove karbidov i oksidov tugoplavlykh metallov dlya aviakosmicheskikh obektov (Perspectives of the application of nanostructured composite materials based on carbides and oxides of refractory metals for aerospace facilities). *Trudy MAI*, Vol. 46, 9 pp. (in Russian) <http://www.mai.ru/upload/iblock/1a/1a1493319c8c15a70decf28b0a51172d.pdf> Accessed 10 Feb 2015
696. Simonenko EP, Ignatov NA, Simonenko NP, Ezhov YuS, Sevastyanov VG, Kuznetsov NT (2011) Synthesis of highly dispersed super-refractory tantalum-zirconium carbide Ta_4ZrC_5 and tantalum-hafnium carbide Ta_4HfC_5 via sol-gel technology. *Russ J Inorg Chem* 56(11):1681–1687
697. Batzill M (2012) The surface science of graphene: metal interfaces, CVD synthesis, nanoribbons, chemical modifications and defects. *Surf Sci Rep* 67:83–115
698. Kurtoglu M, Naguib M, Gogotsi Y, Barsoum MW (2012) First principles study of two-dimensional early transition metal carbides. *Mater Res Soc Commun* 2:133–137
699. Khazaei M, Arai M, Sasaki T, Chung C-Y, Venkataramanan NS, Estili M, Sakka Y, Kawazoe Y (2013) Novel electronic and magnetic properties of two-dimensional transition metal carbides and nitrides. *Adv Funct Mater* 23(17):2185–2192
700. Motzfeldt K (2013) High-temperature experiments in chemistry and materials science. Wiley, Chichester, West Sussex
701. Simonenko EP, Sevastyanov DV, Simonenko NP, Sevastyanov VG, Kuznetsov NT (2013) Promising ultra-high temperature ceramic materials for aerospace applications. *Russ J Inorg Chem* 58(14):1669–1693
702. Chen Y-J, Li J-B, Wei Q-M, Zhai H-Z (2001) Preparation and growth mechanism of TaC_x whiskers. *J Crystal Growth* 224:244–250
703. Nieto A, Kumar A, Lahiri D, Zhang C, Seal S, Agarwal A (2014) Oxidation behaviour of graphene nanoplatelet reinforced tantalum carbide composites in high-temperature plasma flow. *Carbon* 67:398–408
704. Nieto A, Lahiri D, Agarwal A (2014) Graphene nanoplatelets reinforced tantalum carbide consolidated by spark plasma sintering. *Mater Sci Eng A* 582:338–346
705. Samsonov GV, Petrykina RYa (1970) Sintering of metals, carbides and oxides by hot-pressing. *Phys Sinter* 2:1–20

706. Diwan BD (2014) Structural phase transition of refractory metal carbides at high pressure. *Can J Phys* 92:415–419
707. Gusev AI (2014) Nonstoichiometry and superstructures. *Phys Usp* 57(9):839–876
708. Naguib M, Bentzel GW, Shah J, Halim J, Caspi EN, Lu J, Hultman L, Barsoum MW (2014) New solid solution MAX phases: $(\text{Ti}_{0.5}\text{V}_{0.5})_3\text{AlC}_2$, $(\text{Nb}_{0.5}\text{V}_{0.5})_2\text{AlC}$, $(\text{Nb}_{0.5}\text{V}_{0.5})_4\text{AlC}_3$ and $(\text{Nb}_{0.8}\text{Zr}_{0.2})_2\text{AlC}$. *Mater Res Lett* 2(4):233–240
709. Etzkorn J, Ade M, Hillebrecht H (2007) Ta_3AlC_2 and Ta_4AlC_3 – single crystal investigations of two new ternary carbides of tantalum synthesized by the molten metal technique. *Inorg Chem* 46:1410–1418
710. Sun D, Hu Q, Chen J, Zhou A (2014) First principles calculations of the relative stability, structure and electronic properties of two-dimensional metal carbides and nitrides. In: Proc. 8th Int. conf. on high-performance ceramics (CICC 2013), Chongqing, China, 4–7 Nov 2013. *Key Eng Mater* 602–603:527–531
711. Sygnatowicz M, Cutler RA, Shetty DK (2014) Processing of dense $\zeta\text{-Ta}_4\text{C}_{3-x}$ by reaction sintering of Ta and TaC powder mixture. *J Am Ceram Soc* 97(12):3826–3834
712. Sygnatowicz M, Cutler RA, Shetty DK (2015) $\zeta\text{-Ta}_4\text{C}_{3-x}$: a high fracture toughness carbide with rising-crack-growth-resistance (R-curve) behaviour. *J Am Ceram Soc* 98(8):2601–2608
713. Meeks GJ, Dalton JS, Sparks TD, Shetty DK (2016) A functionally graded carbide in the Ta-C system. *J Am Ceram Soc* 99(2):392–394
714. Zou Z, Fu L, Song X, Zhang Y, Liu Z (2014) Carbide-forming groups IVB-VIB metals: a new territory in the periodic table for CVD growth of graphene. *Nano Lett* 14:3832–3839
715. Anasori B, Xie Y, Beidaghi M, Lu J, Hosler BC, Hultman L, Kent PRC, Gogotsi Y, Barsoum MW (2015) Two-dimensional ordered double transition metals carbides (MXenes). *ACS Nano* 9(10):9507–9516
716. Chauhan M, Gupta DC (2015) Electronic, mechanical, phase transition and thermo-physical properties of TMC (TM = V, Nb and Ta): high pressure *ab initio* study. *Phase Transit* 88(12):1193–1212
717. Kurlov AS, Belkov AM, Vyrodova TD, Gusev AI (2015) Effect of the nonstoichiometry of tantalum carbide TaC_y on the particle size of nanopowders prepared by milling. *Phys Solid State* 57(1):70–78
718. Gusev AI, Kurlov AS, Belkov AM, Belkova TD (2015) Effect of the milling energy on the anisotropy of deformation distortions in nanocrystalline powders of nonstoichiometric tantalum carbide TaC_y . *Phys Solid State* 57(6):1166–1176
719. Lu Y, Ye L, Han W, Sun Y, Qiu W, Zhao T (2015) Synthesis, characterization and microstructure of tantalum carbide – based ceramics by liquid polymeric precursor method. *Ceram Int* 41:12475–12479
720. Kiani S, Yang J-M, Kodambaka S (2015) Nanomechanics of refractory transition metal carbides: a path to discovering plasticity in hard ceramics. *J Am Ceram Soc* 98(8):2313–2323
721. Nino A, Hirabara T, Sugiyama S, Taimatsu H (2015) Preparation and characterization of tantalum carbide (TaC) ceramics. *Int J Refract Met Hard Mater* 52:203–208
722. Bakshi SR, Musaramthota V, Lahiri D, Singh V, Seal S, Agarwal A (2011) Spark-plasma sintered tantalum carbide: effect of pressure and nano-boron carbide addition on microstructure and mechanical properties. *Mater Sci Eng A* 528:1287–1295
723. Bakshi SR, Musaramthota V, Virzi DA, Keshri AK, Lahiri D, Singh V, Seal S, Agarwal A (2011) Spark-plasma sintered tantalum carbide – carbon nanotube composite: effect of pressure, carbon nanotube length and dispersion technique on microstructure and mechanical properties. *Mater Sci Eng A* 528:2538–2547
724. Khaleghi E, Lin Y-S, Meyers MA, Olevsky EA (2010) Spark plasma sintering of tantalum carbide. *Scripta Mater* 63:577–580
725. Liu L, Ye F, Zhang Z, Zhou Y (2011) Microstructure and mechanical properties of the spark-plasma sintered TaC/SiC composites. *Mater Sci Eng A* 529:479–484
726. Kubaschewski O, Alcock CB, Spencer PJ (1993) *Materials thermochemistry*, 6th edn. Pergamon Press, Oxford

727. Naguib M, Come J, Dyatkin B, Presser V, Taberna P-L, Simon P, Barsoum MW, Gogotsi Y (2012) MXene: a promising transition metal carbide anode for lithium-ion batteries. *Electrochem Commun* 16(1):61–64
728. Silvestroni L, Pienti L, Guicciardi S, Sciti D (2015) Strength and toughness: the challenging case of TaC-based composites. *Composites B* 72:10–20
729. Cedillos-Barraza O, Grasso S, Nasiri NA, Jayaseelan DD, Reece MJ, Lee WE (2016) Sintering behaviour, solid solution formation and characterization of TaC, HfC and TaC-HfC fabricated by spark-plasma sintering. *J Eur Ceram Soc* 36:1539–1548
730. Yu X-X, Weinberger CR, Thompson GB (2016) *Ab initio* investigations of the phase stability in group IVB and VB transition metal carbides. *Comput Mater Sci* 112:318–326
731. Wang Q, German KE, Oganov AR, Dong H, Feya OD, YaV Zubavichus, Murzin VYu (2016) Explaining stability of transition metal carbides – and why TaC does not exist. *RSC Adv* 6(20):16197–16202
732. Pan Y, Zhou P, Peng Y, Du Y, Luo F (2016) A thermodynamic description of the C-Hf-Ta system over the whole composition and temperature ranges. *Calphad* 53:1–9
733. Sani E, Mercatelli L, Meucci M, Balbo A, Silvestroni L, Sciti D (2016) Compositional dependence of optical properties of zirconium, hafnium and tantalum carbides for solar absorber applications. *Sol Energy* 131:199–207
734. Arabei BG, Levinskii YuV, Markov YuM, Portnoi KI (1978) Effect of alloying of uranium carbide on its interaction with carbon. *Atom Energy* 44(3):288–290
735. Balankin SA, Loshmanov LP, Skorov DM, Sokolov VS (1979) Raschet energii obrazovaniya vakansii v fazakh vnedreniya po dannym mekhanicheskikh svoystv (Calculation of vacancy formation energy in interstitial phases through mechanical properties data). In: Sobolev ND, Beskorovainyi NM, Morozov EM, Kulbakh AA, Markochev VM, Sapunov VT (eds) *Fizika i mekhanika deformatsii i razrusneniya* (Physics and mechanics of deformation and fracture), Vol. 7. Atomizdat, Moscow, pp. 8–12 (in Russian)
736. Fedorov ÉM, Andrievskii RA (1979) Thermodynamic stability of carbide solid solutions. *Inorg Mater* 15(3):357–360
737. Cannon WR, Langdon TG (1983) Review. Creep of ceramics. Part 1 – Mechanical characteristics. *J Mater Sci* 18:1–50
738. Dmitrieva GP, Razumova NA, Shurin AK, Khandros EL (1986) Phase equilibria in alloys of the Ni-TiC-MeC (Me: Zr, Hf, Nb, Ta) systems. *Russ Metall* (1):210–215
739. Ogorodnikov VV, Rogovoi YuI (1992) Simulating point defects in cubic monocarbides. *Inorg Mater* 28(5):763–767
740. Gusev AI, Rempel AA, Shveikin GP (1997) Nestekhiometriya i radiatsionnaya stoikost konstruksionnykh materialov (analiz dannykh) (Nonstoichiometry and structural materials resistance to radiation damage (data analysis)). *Doklady AN SSSR* 357(4):490–494 (in Russian)
741. Cherkashenko VM, Nazarova SZ, Gusev AI, Ivanovskii AL (2001) Electronic structure, chemical bonding and properties of binary carbides $M_xM'_yC_z$ in the crystalline and molecular states: XES, XPS and quantum-chemical studies. *J Struct Chem* 42(6):1002–1024
742. Wang J, Zhou Y (2009) Recent progress in theoretical prediction, preparation and characterization of layered ternary transition metal carbides. *Annu Rev Mater Res* 39:415–443
743. Yoshitake M (2012) Examination of work function of transition metal carbides and nitrides. *J Vac Soc Jpn* 55(7):349–353 (in Japanese)
744. Yoshitake M (2014) Generic trend of work functions in transition metal carbides and nitrides. *J Vac Sci Technol A* 32(6):061403
745. Ordanyan SS, Udalov YuP (2015) On the structure of the $SiC-Mo(W)Si_2-Me^d B_2$ systems and prospective development of refractory materials based on these systems. In: Ordanyan SS (ed) *Aktualnye problemy tekhnologii proizvodstva sovremennykh keramicheskikh materialov* (Current problems of the modern technology of ceramic materials). Polytechnic University Publishing House, Saint Petersburg, pp. 7–16 (in Russian)
746. Konyashin I, Lengauer W (2016) Sintering mechanisms of functionally graded cemented carbides. *Mater Sci Forum* 835:116–198

747. Zhilyaev VA, Patrakov EI (2016) Influence of alloying titanium carbonitride by transition metals of groups IV–VI on the interaction with nickel melt. *Russ J Non-Ferr Met* 57(2):141–147
748. Zibrov M, Mayer M, Gao L, Elgeti S, Kurishita H, Gasparyan Yu, Pisarev A (2015) Deuterium retention in TiC and TaC doped tungsten at high temperatures. *J Nucl Mater* 463:1045–1048
749. Khazaei M, Arai M, Sasaki T, Ranjbar A, Liang Y, Yunoki S (2015) OH-terminated two-dimensional transition metal carbides and nitrides as ultra-low work function materials. *Phys Rev B* 92(7):075411
750. Zha X-H, Luo K, Li Q, Huang Q, He J, Wen X, Du S (2015) Role of the surface effect on the structural, electronic and mechanical properties of the carbide MXenes. *EPL-Europhys Lett* 111:26007 (6 pp.)
751. Lei J-C, Zhang X, Zhou Z (2015) Recent advances in MXene: preparation, properties and applications. *Front Phys* 10(3):276–286
752. Dubrovskaya LB, Alyamovskii SI, Shveikin GP, Geld PV (1968) Oksikarbidnye fazy tantalata (Tantalum oxycarbide phases). *Zh Neorg Khim* 13(9):2331–2339 (in Russian)
753. Kikuchi M, Nagakura S, Oketani S (1971) Crystal structures of transition metal carbides. *J Iron Steel Inst Jpn* 57(6):1009–1053 (in Japanese)
754. Gusev AI (1989) Structural stability boundaries for nonstoichiometric compounds. *Phys Stat Sol A* 111(2):443–450
755. Gusev AI (1991) Disorder and long-range order in non-stoichiometric interstitial compounds. *Phys Stat Sol B* 163(1):17–54
756. Rempel AA (1996) Atomic and vacancy ordering in nonstoichiometric carbides. *Phys Usp* 39(1):31–56
757. Gusev AI, Rempel AA (1997) Phase diagrams of metal-carbon and metal-nitrogen systems and ordering in strongly nonstoichiometric carbides and nitrides. *Phys Stat Sol A* 163(2):273–304
758. Gusev AI, Kurlov AS, Belkova TD, Belkov AM (2015) Anisotropy of strain distortions in nanopowders of nonstoichiometric vanadium and tantalum carbides. *Int J Refract Met Hard Mater* 51:70–80
759. Kurlov AS, Gusev AI (2016) Effect of small particle sizes on the measured density of nanocrystalline powders of nonstoichiometric tantalum carbide TaC_y. *Phys Solid State* 58(8):1687–1693
760. Li PG, Lei M, Tang WH (2008) Route to transition metal carbide nanoparticles through cyanamide and metal oxide. *Mater Res Bull* 43:3621–3626
761. Gusev AI (1993) Vaporization of cubic carbides of vanadium, niobium and tantalum. *High Temp* 31(2):248–254
762. Zhang C, Boesl B, Silvestroni L, Sciti D, Agarwal A (2016) Deformation mechanism in graphene nanoplatelet reinforced tantalum carbide using high load *in situ* indentation. *Mater Sci Eng A* 674:270–275
763. Ichikawa K, Achikita M (1993) Electric conductivity and mechanical properties of carbide dispersion-strengthened copper prepared by compocasting. *Mater Trans JIM* 34(8):718–724
764. Choi J-G, Oh H-G, Back Y-S (1998) Tantalum carbide hydrodenitrogenation catalysts. *J Indust Eng Chem* 4(2):94–98
765. Morton CW, Wills DJ, Stjernberg K (2005) The temperature ranges for maximum effectiveness of grain growth inhibitors in WC-Co alloys. *Int J Refract Met Hard Mater* 23:287–293
766. Naumenko VYa (1970) Preparation of carbides of the IV–V groups transition metals in their homogeneity regions. *Powder Metall Met Ceram* 9(10):799–801
767. Carlsson M, Johnsson M, Nygren M (1999) Synthesis and characterization of Ti_{0.33}Ta_{0.33}Nb_{0.33}C and Ti_{0.33}Ta_{0.33}Nb_{0.33}C_xN_{1-x} whiskers. *J Am Ceram Soc* 82(8):1969–1976
768. Ahlén N, Johnsson M, Larsson A-K, Sundman B (2000) On the carbothermal vapour-liquid-solid (VLS) mechanism for TaC, TiC and Ta_xTi_{1-x}C whisker growth. *J Eur Ceram Soc* 20:2607–2618

769. Johnsson M (2004) Synthesis of boride, carbide and carbonitride whiskers. *Solid State Ionics* 172:365–368
770. Zhao G, Huang C, Liu H, Xu L, Chong X, Zou B, Zhu H (2012) A study on *in situ* growth of TaC whiskers in Al₂O₃ matrix powder for ceramic cutting tools. *Mater Res Bull* 47:2027–2031
771. Nisar A, Ariharan S, Venkateswaran T, Sreenivas N, Balani K (2016) Oxidation studies on TaC based ultra-high temperature ceramic composites under plasma arc jet exposure. *Corros Sci* 109:50–61
772. Zainulin YuG, Alyamovskii SI, Shveikin GP, Shchetnikov EN, Geld PV (1969) Vzaimodeistvie kubicheskikh karbidov titana, vanadiya, niobiya i tantala s berilliem (Interaction of cubic titanium, vanadium, niobium and tantalum carbides with beryllium). *Zh Prikl Khim* 42(3):693–695 (in Russian)
773. Naidoo M, Johnson O, Sigalas I, Herrmann M (2014) Influence of tantalum on the microstructure and properties of Ti(C,N)-Ni cermets. *Int J Refract Met Hard Mater* 42:97–102
774. Etmayer P (1986) Thermochemical estimation of the γ - α -solubility line in the TiC-TaC-WC system at 1723 K based on a ternary regular solid solution model. *Powder Metall Int* 18(6):404–406
775. Daoush WM, Park HS, Lee KH, Moustafa SF, Hong SH (2009) Effect of binder compositions on microstructure, hardness and magnetic properties of (Ta,Nb)C-Co and (Ta,Nb)C-Ni cemented carbides. *Int J Refract Met Hard Mater* 27(4):669–675
776. Kumar BVM, Basu B (2008) Fretting wear properties of TiCN-Ni cermets: influence of load and secondary carbide addition. *Metall Mater Trans A* 39:539–550
777. Kumar BVM, Balasubramaniam R, Basu B (2007) Electrochemical behaviour of TiCN-Ni-based cermets. *J Am Ceram Soc* 90(1):205–210
778. Kumar BVM, Basu B, Kang S, Ramkumar J (2006) Erosion wear behaviour of TiCN-Ni cermets containing secondary carbides (WC/NbC/TaC). *J Am Ceram Soc* 89(12):3827–3831
779. Liu N, Chen M, Xu Y, Zhou J, Shi M (2005) Effect of various carbides on the wettability in Ni/Ti(C,N) system. *J Wuhan Univ Technol* 20(3):35–39
780. Wang Y, Kou Z, Liu Y, Liu F, Duan W, Deng J, Ma Y, Ma D, Tan L, Li C, Zhang Y, He D (2016) Ti(C,N)-based cermets sintered under high pressure. *Int J Refract Met Hard Mater* 54:203–209
781. Zhou H, Huang C, Zou B, Liu H, Zhu H, Yao P, Wang J (2014) Effects of sintering processes on the mechanical properties and microstructure of Ti(C,N)-based cermet cutting tool materials. *Int J Refract Met Hard Mater* 47:71–79
782. Chicardi E, Córdoba JM, Sayagués MJ, Gotor FJ (2012) Inverse core-rim microstructure in (Ti,Ta)(C,N)-based cermets developed by a mechanically induced self-sustaining reaction. *Int J Refract Met Hard Mater* 31:39–46
783. Córdoba JM, Chicardi E, Gotor FJ (2012) Development of multicomponent-multiphase materials based on (Ti,Ta,Nb)C_xN_{1-x} carbonitride solid solutions. *Chem Eng J* 192:58–66
784. Etmayer P, Kolaska H, Lengauer W, Dreyer K (1995) Ti(C,N) cermets – metallurgy and properties. *Int J Refract Met Hard Mater* 13:343–351
785. Zhou S, Wang S, Wang L, Ding Z (2007) Effect of sintering atmosphere on microstructure and properties of TiC based cermets. *J Cent South Univ Technol* 14(2):206–209
786. Ahn S, Kang S (2001) Effect of various carbides on the dissolution behaviour of Ti(C_{0.7}N_{0.3}) in a Ti(C_{0.7}N_{0.3})-30Ni system. *Int J Refract Met Hard Mater* 19:539–545
787. Ahlén N, Johnsson M, Nygren M (1999) Oxidation behaviour of Ta_xTi_{1-x}C and Ta_xTi_{1-x}C_yN_{1-y} whiskers. *Thermochim Acta* 336:111–120
788. Ahlén N, Johnsson M, Nygren M (1998) Synthesis and characterization of Ta_xTi_{1-x}C and Ta_xTi_{1-x}C_yN_{1-y} whiskers. *J Eur Ceram Soc* 18:1513–1519
789. Ehm VT, Tashmetov MYu (1992) Struktur uporyadocheniya i fazovye prevrashcheniya v karbidakh Ti_{1-y}Ta_yC_{0.63} i Ti_{1-z}Nb_zC_{0.6} (Ordering structures and phase transformations in Ti_{1-y}Ta_yC_{0.63} and Ti_{1-z}Nb_zC_{0.6} carbides). *Fiz Met Metalloved* 3:112–116 (in Russian)
790. André H-O, Rolander U, Lindahl P (1993–1994) Phase composition in cemented carbides and cermets. *Int J Refract Met Hard Mater* 12:107–113

791. Zackrisson J, Andrén H-O (1999) Effect of carbon content on the microstructure and mechanical properties of (Ti,W,Ta,Mo)(C,N) – (Co,Ni) cermets. *Int J Refract Met Hard Mater* 17:265–273
792. Zackrisson J, Thuvander M, Lindahl P, Andrén H-O (1996) Atom probe analysis of carbonitride grains in (Ti,W,Ta,Mo)(C,N)(Co/Ni) cermets with different carbon content. *Appl Surf Sci* 94–95:351–355
793. Zhang S (1993) Titanium carbonitride – based cermets: processes and properties. *Mater Sci Eng A* 163:141–148
794. Kobashi M, Harata M, Choh T (1993) Dispersion behaviour of several carbides into molten aluminium and mechanical properties of TiC/Al composite. *J Jpn Inst Light Met* 43(10):522–527 (in Japanese)
795. Grigorev ON, Chugunova SI, Shatokhin AM, Yaroshenko VP (1981) Mechanical properties of silicon nitride composite materials. *Powder Metall Met Ceram* 20(7):502–505
796. Gogotsi YuG (1994) Review. Particulate silicon nitride – based composites. *J Mater Sci* 29:2541–2556
797. Semenov OV, Petrov NV, Maskhuliya LG, Ordanyan SS (1994) Wetting of titanium-tantalum carbonitride solid solution by iron subgroup metals. *Powder Metall Met Ceram* 33(11–12):588–592
798. Xiong J, Guo Z, Shen B, Cao D (2007) The effect of WC, Mo₂C, TaC content on the microstructure and properties of ultra-fine TiC_{0.7}N_{0.3}. *Mater Design* 28:1689–1694
799. Branagan DJ, Kramer MJ, McCallum RW (1996) Transition metal carbide formation in the Nd₂Fe₁₄B system and potential as alloying additions. *J Alloys Compd* 244:27–39
800. Kitchin JR, Nørskov JK, Barteau MA, Chen JG (2005) Trends in the chemical properties of early transition metal carbide surface: a density functional study. *Catal Today* 105:66–73
801. Takida T, Igarashi T, Doi Y, Nagae T, Hiraoka Y (1998) Low-temperature fracture behaviour of sintered molybdenum alloys dispersed with transition metal carbides prepared by spark plasma sintering. *J Jpn Soc Powder Metall* 45(11):1098–1104 (in Japanese)
802. Takida T, Igarashi T, Saito N, Nakamura M (1999) Stability of grain structures in sintered molybdenum alloys dispersed with carbide particles at high temperatures. *J Jpn Soc Powder Metall* 46(12):1261–1267 (in Japanese)
803. Zhu G, Liu Y, Ye J (2013) Influence of Ce-Co pre-alloyed powder addition on the microstructure and mechanical properties of Ti(C,N)-based cermets. *Int J Refract Met Hard Mater* 37:134–141
804. Wu P, Zheng Y, Zhao Y, Yu H (2010) Effect of TaC addition on the microstructure and mechanical properties of Ti(C,N)-based cermets. *Mater Design* 31:3537–3541
805. Nowotny H, Kieffer R, Benesovsky F (1960) Über die Systeme HfC-UC, HfC-TiC, HfC-ZrC, HfC-VC, HfC-NbC, HfC-TaC, HfC-Cr₂C₃, HfC-Mo₂C (MoC) und HfC-WC (On the systems HfC-UC, HfC-TiC, HfC-ZrC, HfC-VC, HfC-NbC, HfC-TaC, HfC-Cr₂C₃, HfC-Mo₂C (MoC) and HfC-WC). *Angew Chem* 72(1):37 (in German)
806. Lipke DW, Ushakov SV, Navrotsky A, Hoffman WP (2014) Ultra-high temperature oxidation of a hafnium carbide – based solid solution ceramic composite. *Corros Sci* 80:402–407
807. Shurin AK, Razumova NA, Dmitrieva GP, Khandros EL (1987) The phase diagram of Ni-ZrC-TaC system. *Powder Metall Met Ceram* 26(1):54–58
808. Shurin AK, Dmitrieva GP, Razumova NA (1988) Phase equilibria in ternary nickel-carbide alloys. *Russ Metall* (6):63–69
809. Gusev AI (1985) Prognoz i raschety fazovykh diagramm psevdobinarykh system na osnove tugoplavkikh soedinenii perekhodnykh metallov (Prediction and calculation of phase diagrams of pseudobinary systems based on high-melting transition metal compounds). In: Ageev NV (ed) *Raschety i eksperimentalnye metody postroeniya diagramm sostoyaniya* (Calculation and experimental methods of plotting phase diagrams). Nauka, Moscow, pp. 42–47 (in Russian)
810. Ogorodnikov VV, Ogorodnikova AA (1982) Calculation of the phase diagrams for pseudo-binary systems of cubic transition metal monocarbides. *Russ J Phys Chem* 56(11):1749–1751

811. Gusev AI (2000) Order-disorder transformations and phase equilibria in strongly nonstoichiometric compounds. *Phys Usp* 43(1):1–37
812. Carnahan RD, Janowski KR, Rossi RC (1969) Microstructure of zirconium based ternary carbide alloys. *Metallography* 2:65–77
813. Gladyshevskii EI, Fedorov TF, Gorshkova LV (1964) Sistema tsirkonii-tantal-uglerod (Zirconium-tantalum-carbon system). *Zh Neorg Khim* 9(5):1169–1173 (in Russian)
814. Simonenko EP, Simonenko NP, Ezhov YuS, Sevastyanov VG, Kuznetsov NT (2015) Study of the synthesis of nanocrystalline mixed tantalum-zirconium carbide. *Phys Atom Nucl* 78(12):1357–1365
815. Holleck H (1985) Ternäre Carbidssysteme mit Mangan, Eisen, Kobalt und Nickel und deren Bedeutung für verschleißfeste Werkstoffe (Ternary carbide systems with manganese, iron, cobalt and nickel and their significance for wear-resistant materials). *Metall* 39(7):634–645 (in German)
816. Johnsson M, Ahlén N, Nygren M (1997) Synthesis and characterization of transition metal carbide whiskers. *Key Eng Mater* 132–136:201–204
817. Worrell WL, Chipman J (1964) A thermodynamic analysis of the Ta-C-O, Cb-C-O and V-C-O systems. *Trans Metall Soc AIME* 230(7):1682–1686
818. Gusev AI, Rempel AA (2001) Nestekhiometriya, besporyadok i poryadok v tverdom tele (Nonstoichiometry, disorder and order in solids). Ural Division of the Russian Academy of Sciences, Yekaterinburg (in Russian)
819. Gusev AI (2007) Nestekhiometriya, besporyadok, blizhnii i dalnii poryadok v tverdom tele (Nonstoichiometry, disorder short-range and long-range order in solids). *Nauka Fizmatlit, Moscow* (in Russian)
820. Kurlov AS, Gusev AI (2014) High-energy milling of nonstoichiometric carbides: effect of nonstoichiometry on particle size of nanopowders. *J Alloys Compd* 582:108–118
821. Nino A, Sasago A, Sugiyama S, Taimatsu H (2016) Preparation of Si_3N_4 -TaC and Si_3N_4 -ZrC composite ceramics and their mechanical properties. *Int J Refract Met Hard Mater* 61:192–200
822. Schneider A, Falat L, Sauthoff G, Frommeyer G (2003) Constitution and microstructures of Fe-Al-M-C (M = Ti, V, Nb, Ta) alloys with carbides and Laves phase. *Intermetallics* 11:443–450
823. Falat L, Schneider A, Sauthoff G, Frommeyer G (2005) Mechanical properties of Fe-Al-M-C (M = Ti, V, Nb, Ta) alloys with strengthening carbides and Laves phase. *Intermetallics* 13:1256–1262
824. Smirnova VI, Ormont BF (1955) Zavisimost teplot i svobodnykh energii obrazovaniya karbidov tantala ot fazovogo i khimicheskogo sostava (Relation of heats and free energies of formation of tantalum carbides to phase and chemical composition). *Doklady AN SSSR* 100(1):127–130 (in Russian)
825. Baskin ML, Tretyakov VI, Chaporova IN (1962) Diffuziya volframa v monokarbidakh volframa, tantala, titana i v tverdykh rastvorakh TiC-WC i TiC-WC-TaC (Diffusion of tungsten in tungsten, tantalum and titanium monocarbides and solid solutions of TiC-WC and TiC-WC-TaC). *Fiz Met Metalloved* 14(3):422–427 (in Russian)
826. Barantseva IG, Paderno VN, Paderno YuB (1967) Some physical properties of alloys of the systems ZrC-NbC and TaC-HfC. *Powder Metall Met Ceram* 6(2):139–141
827. Lukashenko TA, Tikhonov KI, Sher ÉM (1999) Corrosion resistance and electrocatalytic activity of some refractory compounds of transition metals. *Refract Indust Ceram* 40(1–2):10–13
828. Chirkin VS (1959) Teplofizicheskie svoistva materialov. Spravochnik (Thermophysical properties of materials. Reference book). *Fizmatgiz, Moscow* (in Russian)
829. Samsonov GV, Grebenkina VG, Klimenko VS (1971) Coefficient of thermal expansion of refractory compounds. *Powder Metall Met Ceram* 10(8):643–647
830. Rudy E, Benesovsky F (1960) Über die elektrische Leitfähigkeit von hochschmelzenden harten Karbiden und Karbidmischkristallen (On the electrical conductivity of refractory hard carbides and carbide mixed crystals). *Planseeber Pulvermetall* 8:72–77 (in German)
831. Giorgi AL, Szklarz EG, Storms EK, Bowman AL (1963) Investigation of Ta_2C , Nb_2C and V_2C for superconductivity. *Phys Rev* 129(4):1524–1525

832. Samsonov GV (1965) Superconductivity of refractory compounds. In: Savitskii EM, Baron VV (eds) *Metal science and physics of superconductors*. Nauka, Moscow, pp. 65–71 (in Russian)
833. Kammori Ō, Sato K, Kurosawa F (1968) Infrared absorption spectra of metal carbides, nitrides and sulfides. *Jpn Analyst* 17(10):1270–1273 (in Japanese)
834. Petrov VA, Chekhovskoi VYa, Sheindlin AE, Nikolaeva VA (1969) Total hemispherical emissivity, spectral normal emissivity at a wavelength 0.65 μm and electrical resistivity of tantalum carbide at very high temperatures. *High Temp High Press* 1(1):657–661
835. Tuokedaerhan K, Tan R, Kakushima K, Ahmet P, Kataoka Y, Nishiyama A, Sugii N, Wakabayashi H, Tsutsui K, Natori K, Hattori T, Iwai H (2013) Stacked sputtering process for Ti, Ta and W carbide formation for gate metal application. *Appl Phys Lett* 103(11):111908 (3 pp.)
836. Hwang WS, Chan DSH, Cho BJ (2008) Metal carbides for band-edge work function metal gate CMOS devices. *IEEE Trans Electron Devices* 55(9):2469–2474
837. Shirokov EG (1970) Increasing total field emission current. *Sov Phys Tech Phys* 14(8):1134–1136
838. Brookes CA, O'Neill JB, Redfern BAW (1971) Anisotropy in hardness of single crystals. *Proc R Soc London A* 322(1548):73–88
839. Sirdeshmukh DB, Sirdeshmukh L, Subhadra KG (2006) *Micro- and macro-properties of solids*. Springer, Berlin, Heidelberg
840. Meerson GA, Umanskii YaS (1953) O tverdsti tugoplavkikh karbidov (On the hardness of refractory carbides). *Izv Sektora Fiz Khim Analiza AN SSSR* 22:104–110 (in Russian)
841. Plendl JN, Gielisse PJ (1962) Hardness of nonmetallic solids on an atomic basis. *Phys Rev* 125(3):828–832
842. Miyoshi A, Hara A (1965) High-temperature hardness of WC, TiC, TaC, NbC and their mixed carbides. *J Jpn Soc Powder Powder Metall* 12(2):78–84
843. Kashtalyan YuA (1970) Kharakteristiki uprugosti materialov pri vysokikh temperaturakh (Elasticity characteristics of materials at high temperature). *Naukova Dumka, Kyiv* (in Russian)
844. Ma S-Q, Liu Y, Ye J-W, Wang B (2014) Mechanical properties and electronic structure of N and Ta doped TiC: a first principles study. *Commun Theor Phys* 62:895–902
845. Patriarca P, Harms WO, Rucker DJ (1969) Fuels and materials development program. Quarterly Progress Report ORNL-4350, Contract W-7405-ENG-26, pp. 1–320. Oak Ridge National Laboratory, Tennessee
846. Patriarca P, Rucker DJ (1969) Fuels and materials development program. Quarterly Progress Report ORNL-4420, Contract W-7405-ENG-26. Oak Ridge National Laboratory, Tennessee, pp. 1–270
847. Varga P, Taglauer E (1981) Preferential sputtering of compounds due to light ion bombardment. *J Nucl Mater* 111–112:726–731
848. Rempel AA, Schaefer H-E, Forster M, Girka AI (1994) Atomic defects in transition metal carbides and SiC studied by positron annihilation. In: Barron AR, Fishman GS, Fury MA, Hepp AF (eds) *Covalent ceramics II: non-oxides*. Materials Research Society, Pittsburgh, pp. 299–304
849. Hinnüber J, Rüdiger O (1953) *Hartmetall-Legierungen hoher Korrosions- und Oxidationsbeständigkeit* (Hard metal alloys of high corrosion and oxidation resistance). *Arch Eisenhüttenwes* 24(5–6):267–274 (in German)
850. Kiparisov SS, Levinskii YuV, Petrov AP (1987) Karbid titana: poluchenie, svoistva, primeneniye (Titanium carbide: production, properties, application). *Metallurgiya, Moscow* (in Russian)
851. Panov VS, Chuvilin AM (2001) *Tekhnologiya i svoistva spechennykh tverdykh splavov i izdeli iz nikh* (Technology and properties of sintered hard alloys and products made from them). *MISIS, Moscow* (in Russian)
852. Ueki M, Saito Ts, Saito Ta, Kitamura K, Suzuki H (1988) Properties of TiC-TiN-Mo₂C-Ni alloy affected mainly by additional tantalum or tungsten carbide. *J Jpn Soc Powder Powder Metall* 35(1):27–32 (in Japanese)

853. Suzuki H, Terada O, Kitagawa N, Tsuchiya N (1990) The fine structure in nitrogen free TiC-Mo₂C-Ni cermet. J Jpn Soc Powder Powder Metall 37(6):873–877 (in Japanese)
854. Ueki M, Kitamura K, Suzuki H (1990) Properties of TiC-TiN-Mo₂C-Ni alloy affected by additional tantalum carbide. J Jpn Soc Powder Powder Metall 37(3):462–465 (in Japanese)
855. Andr n H-O, Rolander U, Lindahl P (1994) Atom-probe analysis of cemented carbides and cermets. Appl Surf Sci 76–77:278–284
856. Laoui T, Zou H, Van Der Biest O (1992) Analytical electron microscopy of the core/rim structure in titanium carbonitride cermets. Int J Refract Met Hard Mater 11(4):207–212
857. Yoshimura H, Sugizawa T, Nishigaki K, Doi H (1983) Reaction occurring during sintering and the characteristics of TiC-20TiN-15WC-10TaC-9Mo-5.5Ni-11Co cermet. Int J Refract Met Hard Mater 2(4):170–174
858. Kwon H-J, Kang S (2006) Instability of solid-liquid interface in transitional metal-carbide systems. J Mater Sci 41:4649–4653
859. Zhang H, Yan J, Zhang X, Tang S (2006) Properties of titanium carbonitride matrix cermets. Int J Refract Met Hard Mater 24(3):236–239
860. Wang J, Liu Y, Zhang P, Ye J, Tu M (2009) Effect of VC and nano-TiC addition on the microstructure and properties of micrometer grade Ti(C,N)-based cermets. Mater Design 30:2222–2226
861. Wang J, Liu Y, Feng Y, Ye J, Tu M (2009) Effect of NbC on the microstructure and sinterability of Ti(C_{0.7}N_{0.3})-based cermets. Int J Refract Met Hard Mater 27(3):549–551
862. Chen X, Xiong W, Qu J, Yang Q, Yao Z, Huang Y (2012) Microstructure and mechanical properties of (Ti,W,Ta)C-xMo-Ni cermets. Int J Refract Met Hard Mater 31:56–61
863. Wawrzik S, Zhou P, Buchegger C, Lengauer W (2015) Metallurgy and thermochemistry of cermet/hardmetal laminates. Int J Refract Met Hard Mater 50:282–289
864. Tsuda K (2016) History of development of cemented carbides and cermet. SEI Techn Rev 82:16–20
865. Verma V, Kumar BVM, Kang S (2016) Sliding wear behaviour of TaC-containing Ti(C,N)-WC-Ni/Co cermets. Int J Appl Ceram Technol 13(6):1033–1042
866. Suzuki H, Hayashi K, Lee WJ, Kubo Y (1979) Short-time bending creep-rupture strength of WC-(TaC,TiC)-Co cemented carbides. J Jpn Soc Powder Powder Metall 26(8):294–298 (in Japanese)
867. Cheburaeva PF, Chaporova IN (1986) The role of tantalum in the TiC-WC-TaC-Co hard metals. I. Effect of tantalum content on the composition and properties of the carbide and cobalt phases in the TiC-WC-TaC-Co hard metals. Powder Metall Met Ceram 25(4):327–331
868. Cheburaeva PF, Chaporova IN (1986) The role of tantalum in the TiC-WC-TaC-Co hard metals. II. Influence of tantalum content on the structure and properties of the TiC-WC-TaC-Co three-phase hard metals. Powder Metall Met Ceram 25(5):433–436
869. Perecherla A, Williams WS (1988) Room-temperature thermal conductivity of cemented transition metal carbides. J Am Ceram Soc 71(12):1130–1133
870. Faehrmann M, Klaus H, Poessnecker W (1991) Influence of carbon content on the properties of a WC-3TiC-6-TaC-9Co hardmetal. Powder Metall Int 23(4):211–215
871. Andersson G, Jansson B (2001) The solubility of cubic carbide formers in liquid cobalt. In: Kneringer G, R dhammer P, Wildner H (eds) Proc. 15th Int. Plansee seminar, Vol. 2. Plansee Holding AG, Reutte, Tyrol, Austria pp. 662–676
872. Barbatti C, Garcia J, Brito P, Pyzalla AR (2009) Influence of WC replacement by TiC and (Ta,Nb)C on the oxidation resistance of Co-based cemented carbides. Int J Refract Met Hard Mater 27:768–776
873. Chicardi E, C rdoba JM, Sayagu s MJ, Gotor FJ (2012) Absence of the core-rim microstructure in Ti_xTa_{1-x}C_yN_{1-y}-based cermets developed from a pre-sintered carbonitride master alloy. Int J Refract Met Hard Mater 33:38–43
874. Lekakh SN, Medvedeva NI (2015) *Ab initio* study of Fe adsorption on the (001) surface of transition metal carbides and nitrides. Comput Mater Sci 106:149–154
875. Eustathopoulos N, Nicholas MG, Drevet B (1999) Wettability at high temperatures. Elsevier Science, Oxford

876. Jeitschko W, Nowotny H, Benesovsky F (1963) Kohlenstoffhaltige ternäre Phasen ($\text{Nb}_3\text{Al}_2\text{C}$ und $\text{Ta}_3\text{Al}_2\text{C}$) (Carbonaceous ternary phases ($\text{Nb}_3\text{Al}_2\text{C}$ and $\text{Ta}_3\text{Al}_2\text{C}$)). *Monatsh Chem* 94(1):332–333 (in German)
877. Jeitschko W, Nowotny H, Benesovsky F (1963) Kohlenstoffhaltige ternäre Verbindungen (H-Phase) (Carbonaceous ternary compounds (H-phase)). *Monatsh Chem* 94(4):672–676 (in German)
878. Johnston J, Toth L, Kennedy K, Parker ER (1964) Superconductivity of $\text{Mo}_3\text{Al}_2\text{C}$. *Solid State Commun* 2(4):123
879. Reiffenstein E, Nowotny H, Benesovsky F (1965) Einige neue η -Carbide (Some new η -carbides). *Monatsh Chem* 96(5):1543–1546 (in German)
880. Wu D, Huangfu G, Wang D, Wei B, Wang Y, Zhou Y (2018) Microstructure and mechanical properties of ZrC-TaC_x composite fabricated by displacive compensation of porosity at 1300 °C. *Ceram Int* 44(1):246–253
881. Holleck H, Thümmel F (1967) Ternäre Komplex-carbide, -nitride und -oxide mit teilweise aufgefüllter Ti_2Ni -Struktur (Ternary complex carbides, nitrides and oxides with partial filled Ti_2Ni structure). *Monatsh Chem* 98(1):133–134 (in German)
882. Pessall N, Gold RE, Johansen HA (1968) A study of superconductivity in interstitial compounds. *J Phys Chem Solids* 29:19–38
883. Samsonov GV, Voronkin MA, Bronshtein DKh (1976) Tungsten-free hard alloys based on binary carbides. I. Preparation of alloys and characteristics of formation of their structure during sintering. *Powder Metall Met Ceram* 15(11):844–847
884. Samsonov GV, Voronkin MA, Linnikov AP, Loktionov VA (1976) Tungsten-free hard alloys based on binary carbides. II. Physico-mechanical properties of alloys. *Powder Metall Met Ceram* 15(12):927–931
885. Hachisuka T (1991) Fracture resistance of the $\text{TiC-Cr}_3\text{C}_2$ base multi-component ceramic composites as cutting tool. *J Jpn Soc Powder Powder Metall* 38(4):516–522 (in Japanese)
886. Semenov OV, Ordanyan SS, Maskhuliya LG (1987) Mekhanizm gomogenizatsii slozhnykh karbonitridnykh tverdykh rastvorov titana-tantala (The homogenization mechanism of titanium-tantalum complex carbonitride solid solutions). *Izv Vyssh Uchebn Zaved Khim Khim Technol* 30(10):17–20 (in Russian)
887. Semenov OV, Maskhuliya LG, Ordanyan SS (1988) Nekotorye fiziko-mekhanicheskie svoistva slozhnykh karbonitridnykh tverdykh rastvorov titana-tantala (Some physico-mechanical properties of titanium-tantalum complex carbonitride solid solutions). *Izv Vyssh Uchebn Zaved Khim Khim Technol* 31(11):21–23 (in Russian)
888. Naidoo M, Johnson O, Sigalas I, Herrmann M (2013) Preparation of Ti-Ta-(C,N) by mechanical alloying Ti(C,N) and TaC. *Int J Refract Met Hard Mater* 37:67–72
889. Du S, Zhang K, Meng Q, Ren P, Hu C, Wen M, Zheng W (2017) N dependent tribochemistry: achieving superhard wear-resistant low-friction TaC_xN_y films. *Surf Coat Technol* 328:378–389
890. Shahedifar V, Kakroudi MG (2018) Fracture behaviour improvement of TaC-based ceramic composites by fibrous structure. *Int J Refract Met Hard Mater* 71:15–20
891. Rezaei F, Kakroudi MG, Shahedifar V, Vafa NP (2017) Consolidation and mechanical properties of hot-pressed TaC-HfC-VC composites. *Ceram Int* 43(17):15537–15543
892. Rezaei F, Kakroudi MG, Shahedifar V, Vafa NP, Golrokhshari M (2017) Densification, microstructure and mechanical properties of hot-pressed tantalum carbide. *Ceram Int* 43(4):3489–3494
893. Pienti L, Silvestroni L, Landi E, Melandri C, Sciti D (2015) Microstructure, mechanical properties and oxidation behaviour of TaC- and HfC-based materials containing short SiC fiber. *Ceram Int* 41(1):1367–1377
894. Pienti L, Sciti D, Silvestroni L, Cecere A, Savino R (2015) Ablation tests on HfC- and TaC-based ceramics for aeropropulsive applications. *J Eur Ceram Soc* 35(5):1401–1411
895. Zhang C, Boesl B, Agarwal A (2017) Oxidation resistance of tantalum-hafnium carbide solid solutions under extreme conditions of a plasma jet. *Ceram Int* 43(17):14798–14806

896. Zhang C, Gupta A, Seal S, Boesl B, Agarwal A (2017) Solid solution synthesis of tantalum carbide – hafnium carbide by spark plasma sintering. *J Am Ceram Soc* 100(5):1853–1862
897. Foroughi P, Zhang C, Agarwal A, Cheng Z (2017) Controlling phase separation of $Ta_xHf_{1-x}C$ solid solution nanopowders during carbothermal reduction synthesis. *J Am Ceram Soc* 100(11):5056–5065
898. Chernetsov MV (2017) Integral materials studies of nuclear fuel at Institute of Reactor Materials. *Atom Energy* 121(4):255–258
899. Tardif A, Michel JM, Wach J (1971) Cinétique de décomposition du pentane sous 10^{-5} – 10^{-7} torr à la surface du tantale et des carbures Ta_2C et TaC, entre 1300 et 2300 K (Kinetics of pentane decomposition at 10^{-5} – 10^{-7} torr at the surface of tantalum and Ta_2C and TaC carbides, between 1300 and 2300 K). *Surf Sci* 26(1):255–268 (in French)

Chapter 3

Hafnium Monocarbide



3.1 Structures

Practically hafnium forms with carbon the only one chemical compound (see also section C–Hf in Table I-2.13) – hafnium monocarbide HfC_{1-x} with extremely broad homogeneity range, apart from low-temperature (<510–530 °C) ordered and metastable structures of $\text{Hf}_{2\pm x}\text{C}$ ($Fd(-3)m$, $R(-3)m$, $P3m1$, $Pnma$, $I4_1/amd$, $Pbcn$, $P4/mmm$), $\text{Hf}_3\text{C}_{2\pm x}$ ($C2/m$, $I4/mmm$, $P(-3)m1$, $Immm$), $\text{Hf}_4\text{C}_{3\pm x}$ ($C2/c$, $P(-3)m1$, $Pm(-3)m$), $\text{Hf}_5\text{C}_{4\pm x}$ ($P(-1)$, $C2/m$, $I4/m$), $\text{Hf}_6\text{C}_{5\pm x}$ ($C2/m$, $C2/c$, $P3_1I2$), $\text{Hf}_7\text{C}_{6\pm x}$ ($R(-3)$) and $\text{Hf}_8\text{C}_{7\pm x}$ ($P4_332$, $Fm(-3)m$) as well as molecular cluster Hf_8C_{12} , which are not confirmed sufficiently in literature [1–7, 332, 333, 483, 540, 541, 548]. The ordered structures should be in thermodynamic equilibrium with disordered hafnium monocarbide HfC_{1-x} phase; however, the latter one can exist as a metastable phase at a temperature below ~500 °C for an infinitely long time because the diffusion rate in this temperature range is extremely small [2]. A high-temperature partial variant of hafnium – carbon phase diagram is given in Fig. 3.1, and the microstructural features of hafnium monocarbide HfC_{1-x} are presented in Table 3.1. The C/Hf radii ratio calculated on the basis of Pauling’s atomic size of Hf (0.1585 nm, CN = 12) is 0.486 [9], 0.46 [32]; the ratio of Hf radii (in nm) in Me/MeC is 0.159/0.164 (2.5% expansion of Hf atoms in carbide) [42]. The phase transformation of HfC_{1-x} from NaCl type ($Fm(-3)m$) to CsCl type structure ($Pm(-3)m$) under very high pressures (~100–500 GPa) has been predicted theoretically [315, 322, 323, 326, 528].

The variation of the lattice parameter of hafnium monocarbide HfC_{1-x} phases with carbon content (or deviation from the stoichiometry) within the homogeneity range is shown in Fig. 3.2; in a modified form the following equations described this relationship in HfC_{1-x} were proposed by Senczyk (for $0 \leq x \leq 0.3$) [581]:

$$a = 0.4637 - 0.0017x - 0.01425x^2, \quad (3.1)$$

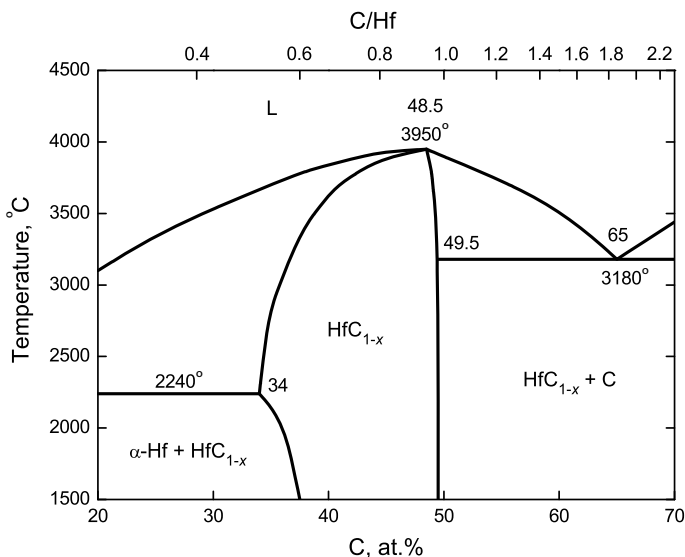


Fig. 3.1 High-temperature partial equilibrium phase diagram [2, 4, 6, 8–15, 17, 201, 343, 344, 426, 500, 559, 632]

and Gusev (for $x \leq 0.36$) [587]:

$$a = 0.4639 - 0.00125x - 0.00138x^2, \quad (3.2)$$

where a is lattice parameter, nm and x is the value of index in HfC_{1-x} formula. The wide data spread available in literature for the relationships between the lattice parameter and composition of HfC_{1-x} mainly could be explained by some difficulties in the contamination control of phase composition; the considerable solubilities of oxygen and nitrogen, which are always present in HfC_{1-x} , result in the formation of oxycarbide $\text{HfC}_{1-x}\text{O}_y$, carbonitride $\text{HfC}_{1-x}\text{N}_z$ and oxycarbonitride $\text{HfC}_{1-x}\text{N}_z\text{O}_y$ phases (see also sections C–Hf–N, C–Hf–N–O and C–Hf–O in Table I-2.14) with various deviations from the stoichiometry and noticeable decrease in the magnitude of lattice parameter [13, 28, 40, 223, 226, 402–408, 619]; the examples of oxygen effect on the completeness of metal and non-metal sublattices in HfC_{1-x} ($\text{HfC}_{1-x}\text{O}_y$) are given in Table 3.2.

The strong covalent character of chemical bonding in HfC_{1-x} determines the high value of C–Hf bond energy (enthalpy), which is about 5.60 ± 0.3 eV [165, 495, 496]. The calculated parameters of the electron structures of HfC_{1-x} monocarbides with minimal and maximal deviations from the stoichiometry are presented in Table 3.3.

Hafnium monocarbide has a uniquely stable crystal lattice at high temperatures compared with other transition metal carbides. HfC_{1-x} exhibits a marked anisotropy in its behaviour; in the $\langle 100 \rangle$ direction, it is relatively plastic compared with its

Table 3.1 Structural properties (crystal structure, density) of hafnium monocarbide phase

Formula	Crystal structure				Z ^b	Density ^c , g cm ⁻³	References
	System	Type	Space group	Lattice parameter ^a <i>a</i> , nm			
HfC _{1-x}	Cubic	NaCl	<i>Fm(-3)m</i>	0.4619 ^d	4	–	[12, 33]
				0.4620 ^e	4	–	[28]
				0.4623 ^f	4	–	[26]
				0.4629 ^g	4	–	[38]
				0.4630	4	12.74	[18]
				0.4630 ^h	4	12.47	[13]
				0.4631 ⁱ	4	–	[30]
				0.4633	4	12.71	[19]
				0.4635	4	12.70	[27, 32]
				0.4635 ^j	4	12.67	[34, 40]
				0.4637 ^g	4	–	[39]
				0.4637	4	12.68	[29]
				0.4637 ^k	4	12.53	[13]
				0.4638 ^l	4	12.60	[16]
				0.4639 ^m	4	12.66	[24, 37, 560]
				0.4640	4	12.66	[9, 20, 21, 35, 36]
				0.4640 ⁿ	4	12.65	[3, 4, 8]
				0.4641	4	12.65	[6, 17, 31]
				0.4642 ^o	4	12.67	[1, 13–15]
				0.4642 ^p	4	12.52	[557]
0.4643	4	12.63	[22]				
0.4648	4	12.59	[23]				
0.4674 ^q (?)	4	–	[25]				

^aWhen it is not indicated specially, value reported is for near-stoichiometric composition

^bNumber of formula units per lattice cell

^cCalculated from XRD or neutron diffraction patterns

^dCarbon content – 37.9 at.% (in equilibrium with α -Hf); the experimentally measured variation of lattice parameter with temp.: 20 °C – 0.4619 nm, 490 °C – 0.4632 nm, 680 °C – 0.4638 nm, 890 °C – 0.4643 nm

^eSamples also contain some O and N

^fSamples also contain some Zr

^gCalculated on the basis of density-functional theory (DFT) with local density approximation (LDA)

^hCarbon content – 40.0 at. %

ⁱMinimal interatomic distances: Hf–Hf and C–C – 0.327446 nm, Hf–C – 0.231539 nm

^jCarbon content – 48.7 at. %

^kCarbon content – 45.0 at. %

^lCarbon content – 47.4 at. %

^mReported thermal increment – $4.1 \times 10^{-6} \text{ K}^{-1}$

ⁿCarbon content – 49.7 at. % (in equilibrium with graphite)

^oCarbon content – 49.2 at. %

^pPrepared by SHS with charged C/Hf ratio – 1.0, carbon content – 47.4 at. %

^qIn the presence of excess carbon at temp. >1700 °C

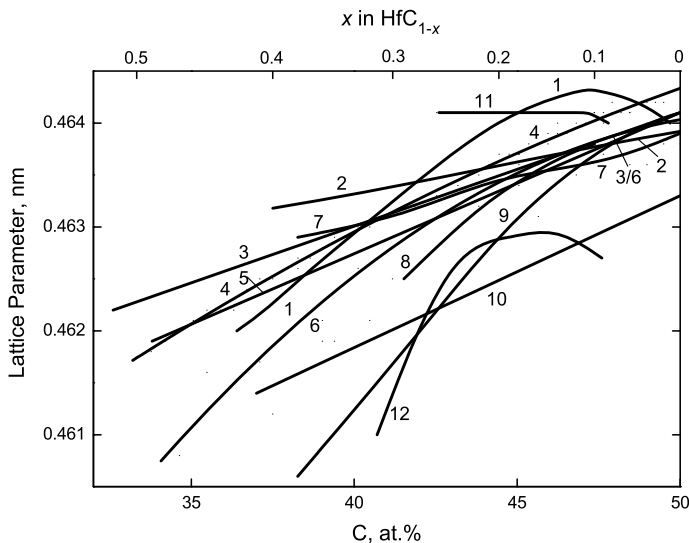


Fig. 3.2 Lattice parameter of HfC_{1-x} as a function of phase composition: 1 – synthesized by various methods [124, 558], 2 – [99], 3 – [17], 4 – polynomial approximation [14, 15], 5 – [22, 40], 6 – [8], 7 – synthesized from the elements [84, 423, 477, 561], 8 – [16], 9 – [6], 10 – [19], 11 – synthesized in loosely sintered hydride-carbon powdered mixtures in high vacuum (content O – $\sim 0.04\%$) and 12 – the same method realized in the compacted mixtures of the same powders (content O – $\sim 0.07\%$) [584, 585] (1, 4–6 – on the basis of several sources)

more brittle behaviour in the $\langle 110 \rangle$ direction, where cleavage occurs [147]. At room and low temperatures for monocarbide $\text{HfC}_{0.98}$ the preferred slip system $(110) \langle 1 \bar{1} 0 \rangle$ was determined by the experiments with single crystal materials [41, 42].

For parameters of formation and migration of lattice point defects (vacancies and interstitial atoms) in hafnium monocarbide *see* Sect. 3.5 (Table 3.17). Recently, due to the massive progress in nanotechnology, some nanostructures based on HfC_{1-x} ,

Table 3.2 The completeness of hafnium monocarbide HfC_{1-x} ($\text{HfC}_{1-x}\text{O}_y$) sublattices with various oxygen contents [40, 406]

Phase composition	Fraction of structural defects in sublattices	
	Metal	Non-metal
$\text{HfC}_{0.76}\text{O}_{0.07}$	0.030	0.195
$\text{HfC}_{0.76}\text{O}_{0.26}$	0.0525	0.0325
$\text{HfC}_{0.75}\text{O}_{0.24}$	0.055	0.0625
$\text{HfC}_{0.74}\text{O}_{0.25}$	0.0525	0.0625
$\text{HfC}_{0.69}\text{O}_{0.30}$	0.0625	0.075
$\text{HfC}_{0.66}\text{O}_{0.12}$	0.0625	0.2675
$\text{HfC}_{0.66}\text{O}_{0.21}$	0.0525	0.175
$\text{HfC}_{0.57}\text{O}_{0.13}$	0.0575	0.340

Table 3.3 The calculated parameters of the electron structures of hafnium monocarbide HfC_{1-x} phases with different deviations from the stoichiometry [490]

Parameter	Composition	
	$\text{HfC}_{-1.0}$	$\text{HfC}_{0.67}$
Electron configuration of Hf atom	$6s^{0.31} 6p^{0.93} 5d^{1.75}$	$6s^{0.46} 6p^{0.94} 5d^{1.89}$
Electron configuration of C atom	$2s^{1.17} 2p^{3.84}$	$2s^{1.25} 2p^{3.80}$
Charge of Hf atom	+1.0	+0.71
Charge of C atom	-1.0	-1.06
Populations of ($p + d$) states of the Hf atom	2.68	2.83
SWASC ^a d^{δ} , %	35.0	38.0
SWASC ^a sp^3 , %	37.4	36.9
Dissociation energy between Hf–Hf atoms, eV	0.230	0.695
Breakaway energy of Hf–Hf atoms, eV	7.62	10.25
Interaction energy Hf–C atoms, eV	0.82	0.48

^aStatistical weighting of the atoms with stable configuration

e.g. single-crystalline nanotubes (~60 nm in diameter and ~15 nm wall thickness) [398], nanowires (20–80 nm in diameter, several tens of micrometers in length) grown along $\langle 100 \rangle$ and $\langle 112 \rangle$ crystal directions [43, 44, 562, 563, 637], nanocrystal chains [399], nanofibers (~40–90 nm in diameter, up to several micrometers in length) [512], whiskers [375–377], thin films and coatings [148, 534, 593, 597, 598, 602, 606–610, 612, 614–616], nanopowders and nanoparticles [473, 508, 520, 635], have been synthesized and studied; 2D-molecular Hf_2C MXene [519, 533, 537, 555, 556] was examined using first principles calculations.

The recommended value for the bulk density of pure poreless near-stoichiometric HfC_{1-x} materials at room temperature is 12.60–12.65 g cm⁻³ [1, 4, 31, 35, 36, 45, 525].

3.2 Thermal Properties

Hafnium monocarbide HfC_{1-x} has one of the highest melting points of all the solid substances available. Within the homogeneity range of HfC_{1-x} the melting point of the phase varies (*see* Fig. 3.1); the maximum temperature is pertaining to the nonstoichiometric compositions around $\sim\text{HfC}_{0.89-0.94}$ [8, 21, 46, 47], and there are no sufficient proofs for the complex carbides to be outperforming the maximum melting point of hafnium monocarbide phase [46]. The general thermodynamic properties of near-stoichiometric hafnium monocarbide are summarized in Table 3.4. For the molar heat capacity $c_p = f(T, K)$, J mol⁻¹ K⁻¹, of hafnium monocarbide phases with various deviations from the stoichiometry, the following relationships were recommended in literature:

Table 3.4 General thermodynamic properties of near-stoichiometric monocarbide HfC_{1-x}

Characteristics	Symbol	Unit	Value	References
Standard heat of formation (at 298.15 K) ^a	$-\Delta H_{298}^{\circ}$	kJ mol^{-1}	208.4 ± 7.5	[1, 49]
			209.2	[51]
			209.5 ± 1.5^b	[8, 9, 56, 412]
			219.0	[383]
			223.0	[48]
			226.8 ± 2.1	[35, 50, 69, 490]
			228.1 ± 4.2	[36]
			230.1	[31, 55]
			234.1 ± 10.0^c	[2, 577–579]
			251.0	[54]
			309.0	[32, 45]
			338.0	[53]
			339.1	[52]
Standard molar entropy ^d (at 298.15 K and 100 kPa)	S_{298}°	$\text{J mol}^{-1} \text{K}^{-1}$	28.1 ± 8.2	[36]
			39.46 ^e	[8, 9]
			39.64	[58, 59]
			40.08	[1]
			41.22 ± 2.10	[31, 35, 54, 55]
			47.73 ^f	[45, 57]
Molar enthalpy difference	$H_{298} - H_0$	kJ mol^{-1}	6.355	[58]
			6.373	[8, 9]
Standard molar heat capacity ^g (at 298.15 K and 100 kPa)	$c_{p,298}^{\circ}$	$\text{J mol}^{-1} \text{K}^{-1}$	33.4	[61]
			34.42 ± 2.10	[29, 31, 54, 55]
			35.30	[45, 60]
			37.49 ^e	[4, 8, 9, 58, 59, 62]
			40.38	[1]
			54.7	[36]
Specific heat capacity (at 298.15 K)	c	$\text{J kg}^{-1} \text{K}^{-1}$	180.7	[31]
			196.8	[4]
Molar enthalpy (heat) of vaporization (at 298.15 K) ^{h,i}	ΔH_v	kJ mol^{-1}	1568 ± 2	[74]
Melting point	T_m	$\text{K (}^{\circ}\text{C)}$	4100 (3830) ^j	[14, 15, 22, 382, 383]
			4120 ± 40	[63]
			(3850 ± 40)	
			4160 ± 150	[45, 64–67]
			(3885 ± 150)	
			4165 ± 150	[32, 35, 36, 53, 68, 384–386]
(3890 ± 150)				

(continued)

Table 3.4 (continued)

Characteristics	Symbol	Unit	Value	References
			4170 (3900) ^k	[135, 420]
			4200 ± 40	[4, 9, 12, 13, 61,
			(3930 ± 40) ^l	82, 387, 410,
				411]
			4220 ± 25	[8, 12, 31, 388]
			(3950 ± 25)	
			4230 ± 20	[1]
			(3960 ± 20)	
Boiling point	T_b	K (°C)	4430 (4160)	[50]
			5190 (4920)	[410]
			5670 (5400) ^f	[32, 45]

^aEnthalpy (heat) of complete dissociation (atomization) from solid state at 298,15 K ($-\Delta_{at}H^\circ_{298}$, kJ mol⁻¹): 1546 ± 12 [1], 1640 [51], 1627 [409], 1674 [57], 1570 ± 10 [579]

^bCarbon content – 48.9 at. %

^cExtrapolated to the stoichiometric composition

^dMolar entropy S°_T (at 1200 K), J mol⁻¹ K⁻¹, for HfC_{1-x} phases with different deviations from the stoichiometry: 103.17 ($x = 0$), 102.49 ($x = 0.05$), 101.80 ($x = 0.10$), 101.11 ($x = 0.15$), 100.42 ($x = 0.20$), 99.73 ($x = 0.25$), 99.05 ($x = 0.30$), 98.36 ($x = 0.35$) and 97.67 ($x = 0.40$) [58]

^eCarbon content – 49.5 at. %

^fCalculated

^gMolar heat capacity $c_{p,T}$ (at 1200 K), J mol⁻¹ K⁻¹, for HfC_{1-x} phases with different deviations from the stoichiometry: 49.93 ($x = 0$), 49.34 ($x = 0.05$), 48.76 ($x = 0.10$), 48.17 ($x = 0.15$), 47.58 ($x = 0.20$), 47.00 ($x = 0.25$), 46.41 ($x = 0.30$), 45.83 ($x = 0.35$) and 45.24 ($x = 0.40$) [58]

^hDue to an insignificant change in the hafnium monocarbide phase composition during congruent vaporization, the calculation was carried out in accordance to the second and third laws of thermodynamics with the assumption of phase composition constancy

ⁱEnthalpy (heat) of sublimation of metallic Hf at 298,15 K, $\Delta_{sMc}H^\circ_{298} = 622.4$ kJ mol⁻¹ [580]

^jCarbon content – 47.5 at. %

^kCarbon content – 49.7 at. %

^lCarbon content – ~48.5 at. %

for HfC_{0.71} (in the range of temperatures from 1300 to 2500 K) [58, 69, 70]

$$c_p = 42.74 + (5.532 \times 10^{-3})T, \quad (3.3)$$

for HfC_{0.85} (in the range of temperatures from 1300 to 2500 K) [58, 69, 70]

$$c_p = 42.96 + (6.076 \times 10^{-3})T, \quad (3.4)$$

for HfC_{0.98} (in the range of temperatures from 298 to 3000 K) [4, 8]

$$c_p = 44.07 + (9.18 \times 10^{-3})T - (12.748 \times 10^{-7})T^2 - (8.181 \times 10^5)T^{-2}, \quad (3.5)$$

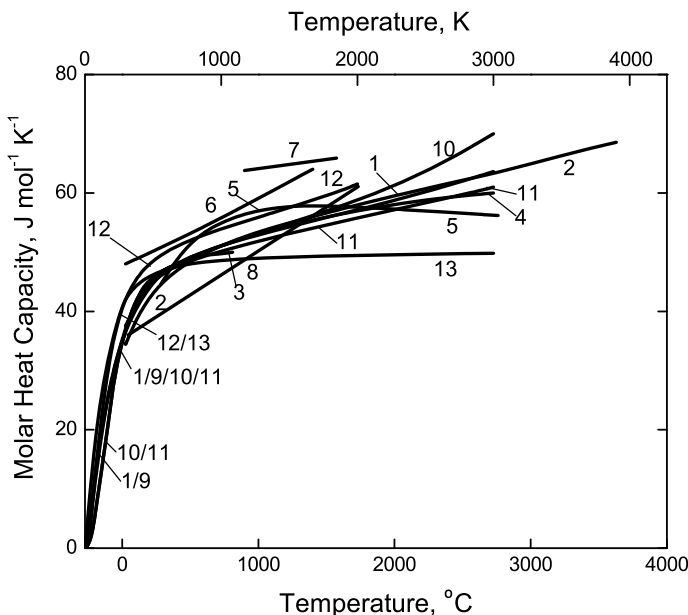


Fig. 3.3 Variation of molar heat capacity (1–11 – at constant pressure, c_p , and 12–13 – at constant volume, c_v) with temperature for near-stoichiometric hafnium carbide HfC_{1-x} (1 – [58, 59]; 2 – [54, 55]; 3 – [29]; 4 – [8]; 5 – [139]; 6 – [539]; 7 – $\text{HfC}_{0.96}$, contents: non-combined C – 0.03%, Zr – 3.45% [307]; 8 – [82, 309]; 9 – $\text{HfC}_{0.97}$, contents: non-combined C – 0.014%, O – 0.003%, N – 0.031%, Zr – 0.035%, Fe – 0.005% [491]; theoretically calculated: 10 – Slater’s approximation and 11 – Dugdale-MacDonald’s approximation on the basis of Debye-Grüneisen model [62]; 12 – *ab initio* calculated, based on the mean values between the corresponding generalized gradient approximation (GGA) and local density approximation (LDA) estimations [336]; 13 – using projector augmented-wave (PAW) method within the GGA of the Perdew-Burke-Ernzerhof scheme for ionic solids (PBEsol) [442]; 1–2, 4, 8 – on the basis of several sources; when it is not indicated specially, data given are for quasi-stoichiometric composition)

for $\text{HfC}_{0.99}$ (in the range of temperatures from 1300 to 2500 K) [58, 69–71]

$$c_p = 43.19 + (6.670 \times 10^{-3})T \quad (3.6)$$

and for HfC_{1-x} in general (in the range of temperatures from 1300 to 2500 K) [58]

$$c_p = 38.957 + (9.142 \times 10^{-3})T - 11.716x, \quad (3.7)$$

or

$$c_p = 41.018 + (8.174 \times 10^{-3})T + 7.738 \times 10^{-3}xT - 27.134x, \quad (3.8)$$

where x is the value of index in HfC_{1-x} formula. For the specific heat capacity of $\text{HfC}_{0.98}$ in the range of temperatures from 1290 to 2800 K the equation $c = f(T, K)$, $\text{J kg}^{-1} \text{K}^{-1}$ is given by Levinson [72] as

$$c = 243.4 + (27.73 \times 10^{-6})T. \quad (3.9)$$

The variations of molar heat capacity c_p with temperature for near-stoichiometric hafnium monocarbide are demonstrated on the basis of several sources in Fig. 3.3. The thermal properties of HfC_{1-x} are very sensitive to the deviation from the stoichiometry: for the standard heat of formation ΔH_{298}° , kJ mol⁻¹, molar enthalpy difference $H_T^\circ - H_{298}^\circ$, J mol⁻¹, and molar entropy S_T° , J mol⁻¹ K⁻¹, the following concentration and temperature-concentration dependencies within the homogeneity range of HfC_{1-x} were calculated from the experimental data [2, 49, 58, 73, 577–579]:

$$\Delta H_{298}^\circ = -208.4 - 69.36x + 662.85x^2, \quad (3.10)$$

$$\Delta H_{298}^\circ = 42.52 - 378.0(1-x) + 101.4(1-x)^2 \pm 10.0, \quad (3.11)$$

$$H_T^\circ - H_{298}^\circ = 38.957T + (4.571 \times 10^{-3})T^2 - 15724x - 11.716xT - 9600 \quad (3.12)$$

$$H_T^\circ - H_{298}^\circ = 41.018T + (4.087 \times 10^{-3})T^2 + (3.689 \times 10^{-3})xT^2 - 27.134xT - 11744 \quad (3.13)$$

$$S_T^\circ = 89.721\lg T + (9.142 \times 10^{-3})T + 69.321x - 26.98x\lg T - 184.06 \quad (3.14)$$

where T is temperature, K, and x is the value of index in HfC_{1-x} formula (Eqs. (3.12)–(3.14) were recommended for the range of temperatures from 1200 to 2500 K). The thermodynamic functions of stoichiometric hafnium carbide are tabulated by Turchanin et al. [58, 59] in the range of 0–3000 K, by Schick [55] in the range of 0–3900 K and by Barin [54] in the range of 298.15–3900 K, the thermodynamic functions of $\text{HfC}_{0.98}$ in the range of 298.15–3000 K – by Storms [8] and Toth [9], and $\text{HfC}_{0.97}$ in the range of 5–350 K – by Westrum and Feick [491].

During the vaporization processes from the surface of hafnium monocarbide at high and ultra-high temperatures in vacuum, the composition of the carbide phase (C/Hf ratio) can change noticeably. The following equation was recommended for hafnium partial pressure (P_{Hf} , Pa) over near-stoichiometric carbide phase in equilibrium with carbon ($\text{HfC}_{1-x} + \text{C}$) by Storms [8] for 2500–3200 K (2200–2900 °C):

$$\lg P_{\text{Hf}} = -(4.206 \times 10^4)/T + 13.306, \quad (3.15)$$

the estimation of hafnium partial pressures (P_{Hf} , Pa) in the gaseous phase in the Hf-C system carried out by Kulikov [410] led to such relationships as

for the conditions of congruent dissociation of quasi-stoichiometric HfC_{1-x} :
at 1000–2500 K (730–2230 °C)

$$\lg P_{\text{Hf}} = -(4.013 \times 10^4)/T + 12.620, \quad (3.16)$$

at 2500–4200 K (2230–3930 °C)

$$\lg P_{\text{Hf}} = -(4.076 \times 10^4)/T + 12.878, \quad (3.17)$$

at 4200–5000 K (3930–4730 °C)

$$\lg P_{\text{Hf}} = -(3.397 \times 10^4)/T + 11.262, \quad (3.18)$$

for the conditions of HfC_{1-x} -C phases equilibrium:

at 1000–2500 K (730–2230 °C)

$$\lg P_{\text{Hf}} = -(4.438 \times 10^4)/T + 12.675, \quad (3.19)$$

at 2500–4200 K (2230–3930 °C)

$$\lg P_{\text{Hf}} = -(4.372 \times 10^4)/T + 12.414, \quad (3.20)$$

at 4200–5000 K (3930–4730 °C)

$$\lg P_{\text{Hf}} = -(3.683 \times 10^4)/T + 10.773, \quad (3.21)$$

where T is temperature, K (*see* Table 3.5). The partial pressures of hafnium and carbon over the carbide phase as functions of composition at the fixed temperature of 3000 K (2730 °C) are shown in Fig. 3.4 in comparison with the equilibrium pressure of carbon over graphite surface. For the evaporation rate of $\text{HfC}_{0.95}$ G , $\text{g cm}^{-2} \text{ s}^{-1}$, as a function of temperature T , K, the following equation was proposed for the range of temperatures from 2600 K (2330 °C) to 3290 K (3020 °C) [1, 69]:

$$\lg G = 8.41 - (3.916 \times 10^4)/T. \quad (3.22)$$

For monocarbide phase $\text{HfC}_{0.99}$ at 2600 and 2900 °C the values of evaporation rate were estimated as 2.7×10^{-6} and $6.4 \times 10^{-5} \text{ g cm}^{-2} \text{ s}^{-1}$ [1, 69], while for carbide $\text{HfC}_{0.98}$ Deadmore [83] measured at 2225 and 2625 °C the values of 7×10^{-8} and $6 \times 10^{-6} \text{ g cm}^{-2} \text{ s}^{-1}$, respectively. For their high-vacuum experiments at 2800 K (2530 °C) Hojo and Nakayama [118] have evaluated the vapour pressure over a emitter coated by near-stoichiometric HfC_{1-x} and its evaporation rate as $8.29 \times 10^{-3} \text{ Pa}$ and $7.17 \times 10^{-7} \text{ g cm}^{-2} \text{ s}^{-1}$, respectively. Through a large part of the homogeneity range of HfC_{1-x} the vapour phase should receive metallic atoms mainly, although in a certain area of compositions congruent vaporization may occur [14, 15]. The change in the C/Me ratio of hafnium monocarbide phase established that at 2900 K (2630 °C) the congruently vaporizing composition corresponds to $\text{HfC}_{0.94}$ [20, 75], Nikolskaya and Avarbe [74] showed that this composition varies from $\text{HfC}_{0.99}$ at 2350 K (2080 °C) to $\text{HfC}_{0.91}$ at 3290 K (3020 °C), and in the temperature range of 2690–3290 K (2420–3020 °C) it could be described by the equation as follows:

Table 3.5 Parameters of the gaseous phase in the Hf-C system in the conditions of Hf-HfC_{1-x} phases equilibrium, congruent dissociation of quasi-stoichiometric HfC_{1-x} and HfC_{1-x}-C phases equilibrium calculated on the basis of thermodynamic data [410]

Parameters	Temperature, K (°C)									
	1000 (730)	1500 (1230)	2000 (1730)	2500 (2230)	3000 (2730)	3500 (3230)	3900 (3630)	4200 (3930)	5000 (4730)	5000 (4730)
	Hf-HfC _{1-x} phases equilibrium									
$\lg P_{\text{Hf}}, \text{Pa}$	-20.164	-9.413	-4.064	-0.896	1.111	2.493	3.296	3.930	-	-
$\lg P_{\Sigma}^{\text{a}}, \text{Pa}$	-20.164	-9.413	-4.064	-0.896	1.111	2.495	3.305	3.945	-	-
$\lg(C/\text{Hf})^{\text{b}}$	-15.656	-9.821	-6.813	-4.905	-3.470	-2.388	-1.661	-1.453	-	-
Contents, vol.%;										
C	-	-	-	-	0.02	0.27	1.44	2.10	-	-
C ₂	-	-	-	-	-	-	0.02	0.04	-	-
C ₃	-	-	-	-	-	-	-	0.003	-	-
Hf	100.0	100.0	100.0	100.0	99.97	99.59	97.87	96.62	-	-
HfC ^c	-	-	-	-	0.01	0.14	0.67	1.24	-	-
	Congruent dissociation of quasi-stoichiometric HfC _{1-x}									
$\lg P_{\text{Hf}}, \text{Pa}$	-27.493	-14.339	-7.520	-3.425	-0.702	1.242	2.439	3.174	4.468	4.468
$\lg P_{\Sigma}^{\text{a}}, \text{Pa}$	-27.192	-14.038	-7.219	-3.126	-0.407	1.530	2.721	3.454	4.758	4.758
Contents, vol.%;										
C	50.00	50.00	49.92	49.32	47.71	43.60	39.46	37.13	36.16	36.16
C ₂	-	-	0.04	0.31	1.12	2.46	3.64	4.44	5.07	5.07
C ₃	-	-	0.005	0.07	0.39	1.07	1.71	2.12	1.68	1.68
C ₄	-	-	-	-	-	-	-	0.005	0.01	0.01
C ₅	-	-	-	-	-	-	-	-	0.002	0.002
Hf	50.00	50.00	50.03	50.23	50.69	51.58	52.30	52.44	51.31	51.31
HfC ^c	-	-	0.004	0.07	0.39	1.29	2.59	3.85	5.77	5.77

(continued)

Table 3.5 (continued)

Parameters	Temperature, K (°C)									
	1000 (730)	1500 (1230)	2000 (1730)	2500 (2230)	3000 (2730)	3500 (3230)	3900 (3630)	4200 (3930)	5000 (4730)	
$\lg P_{\text{Hf}}, \text{ Pa}$	-31.700	-16.913	-9.521	-5.075	-2.134	-0.054	1.212	2.004	3.407	
$\lg P_{\text{C}}, \text{ Pa}$	-24.287	-11.719	-5.224	-1.156	1.595	3.564	4.771	5.455	6.394	
$\lg(\text{C}/\text{Hf})^b$	6.420	5.270	4.590	4.300	4.080	3.900	3.774	3.621	3.082	
Contents, vol. %:										
C	99.89	89.76	50.56	23.59	12.76	8.00	5.96	5.48	9.62	
C ₂	0.01	0.82	4.04	6.68	8.16	8.94	9.19	9.70	15.52	
C ₃	0.10	9.42	45.38	69.47	77.42	77.15	72.87	68.54	59.27	
C ₄	-	-	-	0.04	0.26	0.88	1.77	2.53	3.62	
C ₅	-	-	0.01	0.20	1.38	4.99	10.15	13.67	11.72	
Hf	-	-	0.005	0.012	0.019	0.024	0.028	0.036	0.103	
HfC ^c	-	-	-	0.001	0.004	0.012	0.023	0.038	0.133	

^aTotal gas pressure^bLogarithm of atomic ratio in gaseous phase^cGaseous molecule

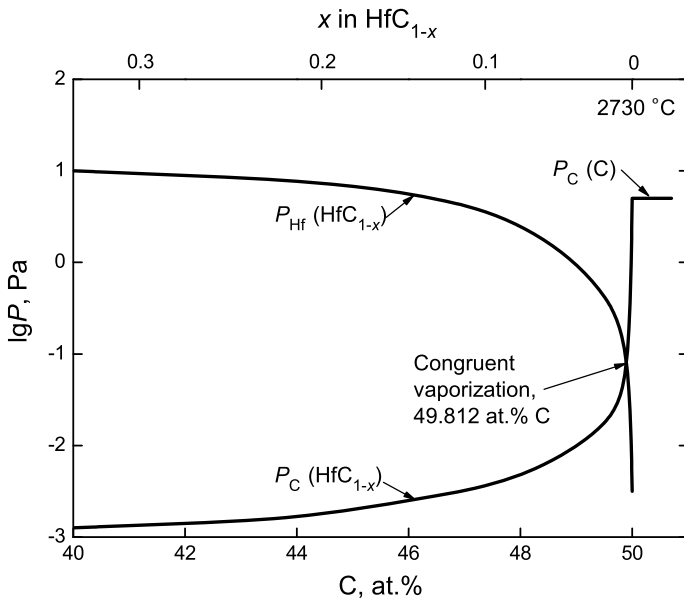


Fig. 3.4 Partial pressures of hafnium $P_{\text{Hf}}(\text{HfC}_{1-x})$ and carbon $P_{\text{C}}(\text{HfC}_{1-x})$ over hafnium carbide HfC_{1-x} phase, and vapour pressure of carbon over pure graphite $P_{\text{C}}(\text{C})$ as functions of carbide composition at 3000 K (2730 °C) calculated by Kaufman [9, 14, 15, 31, 296]; a congruently vaporizing composition is marked

$$\lg x = 3.149 - (1.372 \times 10^4)/T, \quad (3.23)$$

where x is the value of index in HfC_{1-x} formula and T is temperature, K, while for the rate of congruent vaporization of hafnium carbide materials from an open surface into a vacuum V , $\text{g cm}^{-2} \text{s}^{-1}$, for the range of 2580–3300 K (2310–3030 °C) the equation, which is similar to Eq. (3.22),

$$\lg V = 8.409 - (3.916 \times 10^4)/T, \quad (3.24)$$

was given, that is rather close to the results obtained by Fesenko and Bolgar [76] earlier.

The values of general thermodynamic properties, vapour pressures and vaporization rates for hafnium monocarbide are given in Addendum in comparison with other ultra-high temperature materials in the wide ranges of temperatures.

At room temperature thermal conductivity of near-stoichiometric hafnium monocarbide HfC_{1-x} is about $5\text{--}30 \text{ W m}^{-1} \text{ K}^{-1}$ (thermal diffusivity $\sim 0.04 \text{ cm}^2 \text{ s}^{-1}$) [1, 4, 32, 35, 36, 53, 61, 68, 77, 78, 82, 91, 154, 310, 378, 379, 525, 539]; it is affected by the porosity of carbide materials noticeably. Within the homogeneity range, as a consequence of conduction electrons scattering on the carbon sublattice vacancies and thermal lattice vibrations, the thermal conductivity of HfC_{1-x} declines

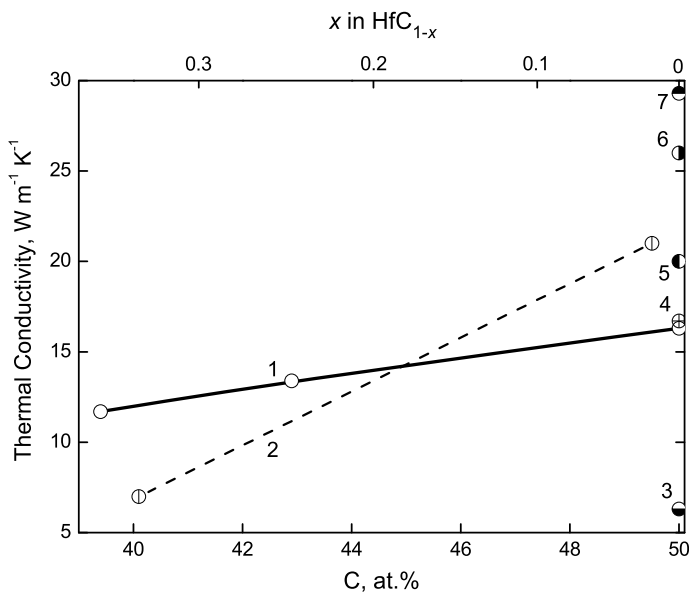


Fig. 3.5 Thermal conductivity of hafnium monocarbide HfC_{1-x} at room temperature (within the homogeneity range) as a function of carbide composition (1 – calculated on the basis of Goryachev’s method [1]; 2 – hot-pressed, porosity 5–10% [91]; 3 – [4, 35, 36]; 4 – [53]; 5 – [61]; 6 – [68, 77]; 7 – [32])

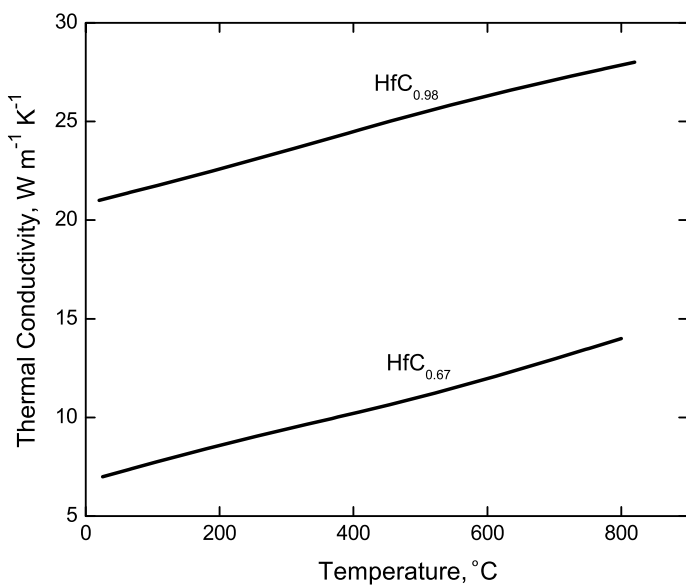


Fig. 3.6 Thermal conductivity of HfC_{1-x} as a function of temperature for the phases having different deviations from the stoichiometry [91]

with increasing carbon deficit (value of x) in the phase [14, 15] that is shown in Fig. 3.5; the difference in the temperature dependences of thermal conductivity for the HfC_{1-x} phases having different deviations from the stoichiometry is illustrated by Fig. 3.6. For the experimental data fit of thermal conductivity λ of $\text{HfC}_{0.96}\text{N}_{0.04}$ phase Lengauer et al. [29] obtained the following polynomial expression for the range of 300–1100 K (25–830 °C):

$$\lambda = 19.48 + (14.26 \times 10^{-3})T - (4.788 \times 10^{-6})T^2 - (4.614 \times 10^5)T^{-2}, \quad (3.25)$$

where T is temperature, K. The variation of thermal conductivity with temperature for near-stoichiometric HfC_{1-x} materials on the basis of several sources is shown in Fig. 3.7.

At room temperature the mean coefficient of linear thermal expansion of $\text{HfC}_{-1.0}$ is $(4.6\text{--}6.6) \times 10^{-6} \text{ K}^{-1}$ [34, 45, 61, 68, 81, 85, 139, 582]. The experimental data collected from the various measurements of thermal expansion of hafnium monocarbide are listed in Table 3.6. The approximation functions for the temperature

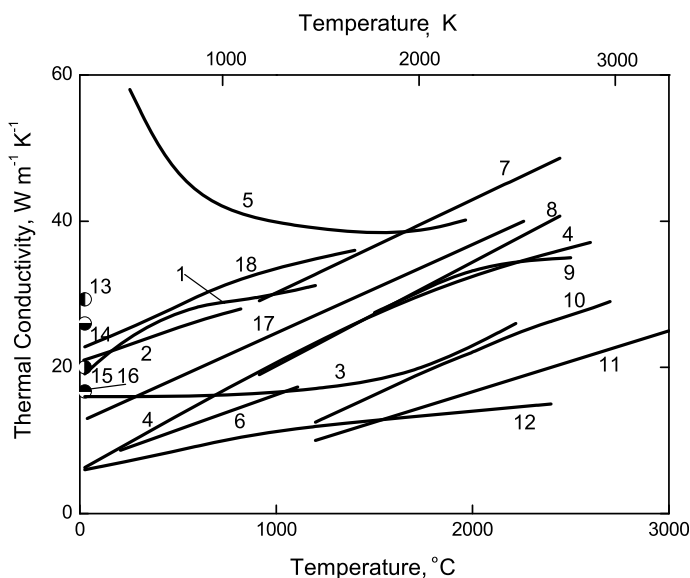


Fig. 3.7 Variation of thermal conductivity with temperature for near-stoichiometric hafnium monocarbide HfC_{1-x} on the basis of several sources: 1 – [378, 379]; 2 – hot-pressed $\text{HfC}_{0.98}$, porosity 5–10% [91]; 3 – [146]; 4 – chemically vapour deposited [4, 35, 36, 78]; 5 – hot-pressed and additionally heat-soaked at 2200 °C, porosity 6–12% [139]; 6 – hot-pressed, porosity 6–12% [139]; 7 – hot-pressed $\text{HfC}_{0.96}$, porosity 4–6%, contents: non-combined C – 0.03%, Zr – 3.45% [79, 307, 308]; 8 – hot-pressed $\text{HfC}_{0.96}$, porosity 4–6%, contents: non-combined C – 0.03%, Zr – 3.45% (repeated test) [79, 307, 308]; 9 – chemically vapour deposited [14, 15]; 10 – $\text{HfC}_{0.93}$, porosity 22–28% [81]; 11 – hot-pressed [14, 15]; 12 – hot-pressed, porosity 3% [310]; 13 – [32]; 14 – [68, 77]; 15 – [61]; 16 – [53]; 17 – [82]; 18 – spark-plasma sintered, porosity 15% [539]; when it is not indicated specially, data given are for quasi-stoichiometric composition

Table 3.6 Average coefficients of linear thermal expansion α_m of hafnium monocarbide HfC_{1-x} in various temperature ranges

Temperature range, °C	$\alpha_m, 10^{-6} \text{ K}^{-1}$	References
(-190)–(+25)	3.5 ± 0.4^a	[20]
	4.1 ± 0.7^b	[20]
	4.3 ± 0.4^c	[20]
(-190)–(+20)	3.15^d	[582]
	6.0	[45, 53]
20–200	6.22^d	[582]
100–200	6.3^e	[137]
20–230	6.39	[501, 502]
20–300	6.30^d	[582]
100–300	6.4^e	[137]
20–400	6.37^d	[582]
	6.50	[45, 53]
20–500	6.32	[138]
	6.45^d	[582]
100–500	6.5^e	[137]
20–540	4.6	[139]
20–610	6.59 ± 0.04^f	[85]
20–600	6.51^d	[582]
	6.66	[45, 53]
20–650	6.30	[53]
20–700	6.58^d	[582]
100–700	6.7^e	[137]
20–730	6.64	[501, 502]
20–800	6.5	[45, 53]
	6.63^d	[582]
20–815	6.3	[82]
20–900	5.1	[89]
	5.7–5.9	[77]
	6.68^d	[582]
100–900	6.6 ± 0.2^e	[137]
20–1000	6.19^g	[87]
	6.26	[138]
	-6.35^h	[91]
	6.6	[45, 53, 388]
	6.70 ± 0.08^i	[84, 490]
	6.73^d	[582]
20–1020	8.23	[4]
20–1020	5.0	[139]
20–1100	6.77^d	[582]
20–1200	6.06	[88]
	6.10	[92, 378, 381]
	6.67	[45, 53]

(continued)

Table 3.6 (continued)

Temperature range, °C	$\alpha_m, 10^{-6} \text{ K}^{-1}$	References
	6.73	[385]
	6.78 ⁱ	[389]
	6.82 ^d	[582]
20–1300	6.85 ^d	[582]
20–1330	6.89	[501, 502]
20–1400	6.80	[45, 53]
	6.89 ^d	[582]
	7.00	[90]
20–1500	6.59 ^g	[87]
	6.91 ^d	[582]
20–1600	6.87	[45, 53]
	6.94 ^d	[582]
20–1730	6.98	[501, 502]
	7.0	[31]
20–1800	6.66	[45, 53]
	6.97 ^d	[582]
	7.47	[90]
20–2000	6.8	[45, 53]
	7.00 ^d	[582]
	7.10 ^g	[87]
	7.66 ± 0.11 ^k	[539]
20–2025	7.14 ^l	[34]
500–2050	7.13 ^m	[582, 583]
20–2130	7.05	[501, 502]
20–2200	5.2	[67]
	6.9	[45, 53]
	7.06 ^d	[582]
815–2200	9.0	[82]
20–2400	6.9	[45, 53]
	7.14 ^d	[582]
	7.34 ^g	[87]
20–2500	7.18 ^d	[582]
20–2600	7.54 ^g	[87]
	7.24 ^d	[582]
20–2700	7.29 ^d	[582]
	7.3 ± 0.2 ⁿ	[86]
20–2800	7.34 ^d	[582]
20–2900	7.40 ^d	[582]
	8.01	[90]

(continued)

Table 3.6 (continued)^aPowdered HfC_{0.90}, measured by low-temperature X-ray diffraction method^bPowdered HfC_{0.97}, measured by low-temperature X-ray diffraction method^cPowdered HfC_{0.95}, measured by low-temperature X-ray diffraction method^dCalculated on the basis of approximation function^eFused HfC_{0.80} (contents: O – 0.05%, N – 0.003%, Zr – 2%), measured by dilatometric method^fHot-pressed HfC_{-1.0} (1–4% porosity), measured by dilatometric method^gHfC_{0.96} hot-pressed at 3100–3150 °C and measured by dilatometric method^hHot-pressed HfC_{0.67} and HfC_{0.98} (5–10% porosity), measured by dilatometric methodⁱFor HfC_{-1.0} (for HfC_{0.67} $\alpha_m = 6.79 \pm 0.08 \cdot 10^{-6} \text{ K}^{-1}$)^jMeasured by high-temperature X-ray diffraction^kSpark-plasma sintered HfC_{-1.0} (15% porosity, mean grain size – $5.8 \pm 0.2 \mu\text{m}$), measured by dilatometric method in Ar atmosphere^lSintered HfC_{0.95}, measured by high-temperature X-ray diffraction^mMaterials prepared by the diffusion saturation of metallic Hf by carbon, measured by telemicroscope method in He atmosphereⁿHfC_{-1.0} grains in a matrix of the arc-cast carbide-carbon eutectic materials, measured by high-temperature X-ray diffraction with the usage of (111) reflections

dependence of relative thermal linear expansion $\Delta l/l_0 = f(T, \text{K})$, %, of near-stoichiometric HfC_{1-x} was recommended by Touloukian et al. [582] on the basis of experimental data for pure samples [20, 86, 139, 310, 583] (accuracy within $\pm 5\%$ at $T < 1800 \text{ K}$ and within $\pm 10\%$ at $T > 1800 \text{ K}$):

for 293–2000 K (20–1730 °C):

$$\Delta l/l_0 = -0.170 + (5.521 \times 10^{-4})T + (1.041 \times 10^{-7})T^2 - (2.015 \times 10^{-11})T^3, \quad (3.26)$$

and for 2000–3200 K (1730–2930 °C):

$$\Delta l/l_0 = 7.367 \times 10^{-2} + (4.217 \times 10^{-4})T + (6.072 \times 10^{-8})T^2 + (3.374 \times 10^{-12})T^3, \quad (3.27)$$

where T is temperature, K. On the basis of high-temperature X-ray measurements Houska [34] proposed for the average coefficient of linear thermal expansion α_m, K^{-1} , of sintered (in vacuum) HfC_{0.95} (contents: non-combined C – 2.04%, N – 0.08%, O – 0.06%) in the temperature range of 25–2025 °C the following equation:

$$\alpha_m = 6.38 \times 10^{-6} + (0.38 \times 10^{-9})(t - 25), \quad (3.28)$$

where t is temperature, °C. The extrapolation of the relationship, obtained by Aigner et al. [92] for the range of 25–1200 °C, to hypothetical HfC_{1.0} phase gives the following expression for its coefficient of linear thermal expansion α, K^{-1} :

$$\alpha = \frac{2.2791 \times 10^{-6} + 0.494 \times 10^{-9}T}{0.46323 + 2.2791 \times 10^{-6}T + 0.247 \times 10^{-9}T^2}, \quad (3.29)$$

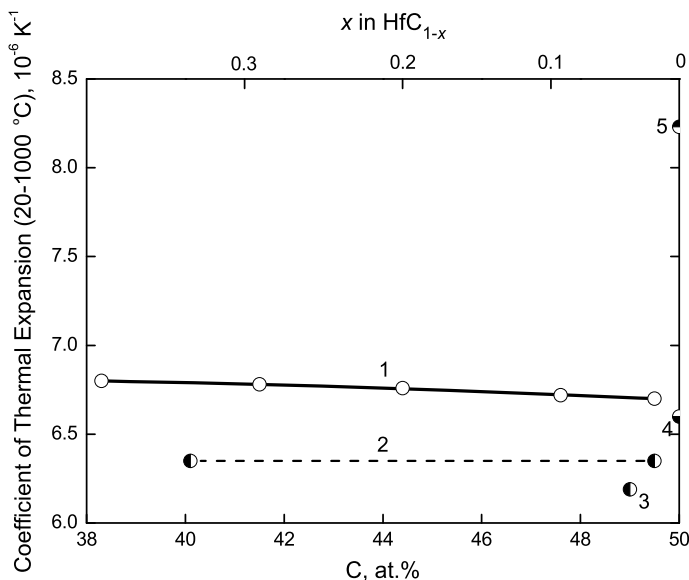


Fig. 3.8 Coefficient of linear thermal expansion in the temperature range of 20–1000 °C of hafnium monocarbide HfC_{1-x} (within the homogeneity range) materials as a function of carbide composition (1 – hot-pressed, 6–10% porosity, content non-combined C $\leq 0.16\%$, measured by dilatometric method [84, 480, 488]; 2 – hot-pressed, 5–10% porosity, measured by dilatometric method [91]; 3 – hot-pressed, measured by dilatometric method [87]; 4 – [45, 53]; 5 – [4])

where T is temperature, K. The influence of carbon content on the thermal expansion of HfC_{1-x} phase within the homogeneity range can be seen in Fig. 3.8; although according to Opeka et al. [91] there is no difference in thermal expansion behaviour measured by dilatometric method for hot-pressed $\text{HfC}_{0.67}$ and $\text{HfC}_{0.98}$ materials with 5–10% porosity. Some recent works [62, 318, 336, 391] are devoted to the calculations of coefficients of thermal expansion of hafnium monocarbide by means of theoretical modelling.

In comparison with other ultra-high temperature materials the values of thermal conductivity and thermal expansion of hafnium carbide in the wide range of temperatures are summarized in Addendum.

3.3 Electro-magnetic and Optical Properties

At room temperature the value of specific electrical resistance (resistivity) of near-stoichiometric hafnium monocarbide HfC_{1-x} lies within the area of 0.2–0.9 $\mu\Omega \text{ m}$ [1, 14, 15, 31, 45, 53, 68, 84, 300, 390, 490, 499, 586]. Anomalously high resistivity with a negative thermal coefficient was reported by Lei et al. [494] for a $\text{HfC}_{0.88}$ thin film (thickness – 1.2 μm) prepared by evaporation technique.

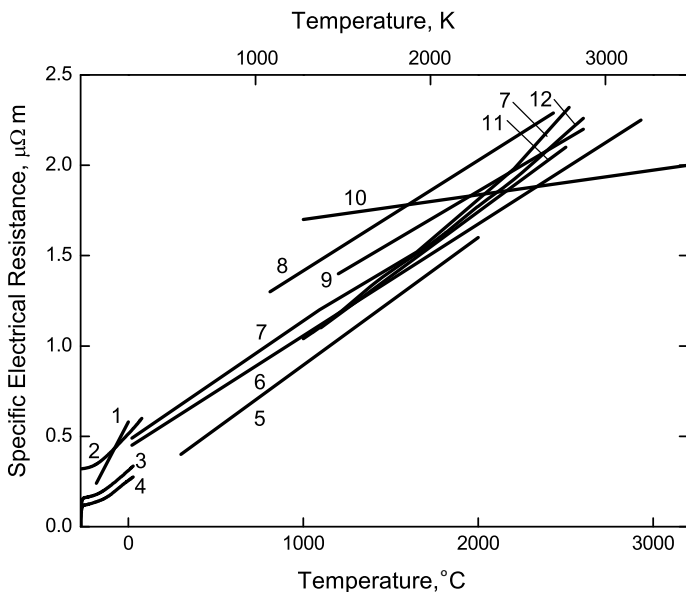


Fig. 3.9 Variation of specific electrical resistance (resistivity) with temperature for near-stoichiometric hafnium monocarbide HfC_{1-x} on the basis of several sources: 1 – sintered, 4% porosity [413]; 2 – single crystal $\text{HfC}_{0.99}$ [414]; 3 – hot isostatically pressed and subsequently sintered $\text{HfC}_{0.98}$, 26% porosity [93]; 4 – hot-pressed $\text{HfC}_{0.97}$, ~2.5% porosity [93]; 5 – [94]; 6 – counted for a pore-free state [31]; 7 – hot-pressed $\text{HfC}_{0.96}$, porosity 4%, contents: non-combined C – 0.03%, Zr – 3.45% and 8 – same (repeated test) [79, 307]; 9 – $\text{HfC}_{0.93}$, 22–28% porosity [81]; 10 – [95]; 11 – [45]; 12 – counted for a pore-free state [53]

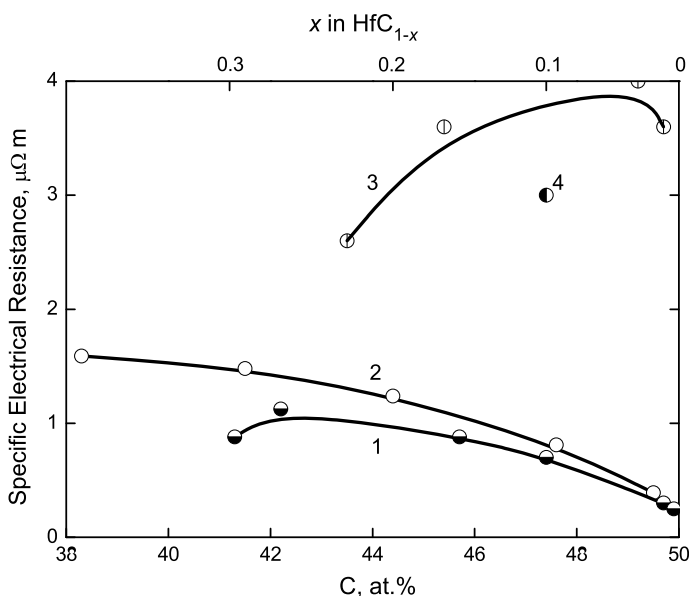
The variation of specific electrical resistance with temperature for near-stoichiometric HfC_{1-x} is shown on the basis of several sources in Fig. 3.9. In the wide temperature range from 0–200 °C up to 3000–3300 °C the resistance of monocarbide phase enlarges with increasing temperature, practically in accordance with linear relationship; that is an evidence of mainly metallic type of conduction in HfC_{1-x} [14, 15]. The single crystal $\text{HfC}_{0.99}$ resistivity measured by Modine et al. [414] at ultra-low, low and ambient temperatures is perfectly described in the interval from $T = 0$ to $T = 350$ K by the Wilson expression (in $\mu\Omega \text{ m}$):

$$\rho(T) = 0.322 + (1.467 \times 10^{-8})T^3 \int_0^{352/T} x^3 / \sinh^2 x dx. \quad (3.30)$$

The experimental data collected from the various measurements of thermal coefficient of resistivity for near-stoichiometric hafnium monocarbide are listed in Table 3.7. The data on the resistivity of HfC_{1-x} within the homogeneity range are contradictory; it was established that the resistivity enlarges with increasing carbon deficit in non-metal sublattice [84, 97], whereas in other work [96] the reverse

Table 3.7 Average values of thermal coefficients of resistivity α_R of near-stoichiometric hafnium monocarbide HfC_{1-x} in various temperature ranges

Temperature range, °C	$\alpha_R, 10^{-3} \text{ K}^{-1}$	References
(-195)–0	6.83 ^a	[367]
(-183)–0	7.74 ^b	[413]
(-123)–80	2.69 ^c	[414]
20–1000	0.94 ^d	[98]
	0.43 ^e	[494]
20–1150	0.41	[53]
300–2000	1.42	[1, 31, 94, 478, 479]
20–2890	0.27	[53]

^aMaterials deposited from gas phase^bSintered materials, 4% porosity^cSingle crystal $\text{HfC}_{0.99}$, $d\rho/dT = 9.1 \times 10^{-4} \mu\Omega \text{ m K}^{-1}$ ^dHot-pressed, counted for a pore-free state, $d\rho/dT = 5.0 \times 10^{-4} \mu\Omega \text{ m K}^{-1}$ ^eThin films prepared by activated reactive evaporation, carbon content – 46.8 at.%, thickness – 1.2 μm **Fig. 3.10** Variation of specific electrical resistance (resistivity) at room temperature within the homogeneity range of hafnium monocarbide HfC_{1-x} on the basis of several sources: 1 – [97]; 2 – sintered, 15–25% porosity [84]; 3 – [96]; 4 – [415]

picture was observed that is demonstrated in Fig. 3.10. In contrast to some other refractory transition metal carbides hafnium monocarbide HfC_{1-x} is not a superconductor along its full homogeneity range ($T_c < 1.23$ K) [14, 61, 293, 294, 487, 511]. At room temperature the Hall and Seebeck coefficients of near-stoichiometric hafnium monocarbide HfC_{1-x} are $R = -(11-18) \times 10^{-10} \text{ m}^3 \text{ A}^{-1} \text{ s}^{-1}$ and $S = -(3.5-12.5) \mu\text{V K}^{-1}$, respectively [14, 15, 68, 96, 101, 132, 415–418]; experimental data obtained by Golikova et al. [96] and Borukhovich et al. [415–417] for the Seebeck coefficients within the homogeneity range of HfC_{1-x} are presented in Fig. 3.11.

Near-stoichiometric hafnium monocarbide HfC_{1-x} is a diamagnetic substance with molar magnetic susceptibility χ_m (SI) $\approx -(200-500) \times 10^{-6} \text{ cm}^3 \text{ mol}^{-1}$ at room temperature slightly increasing with temperature in the range from 20 to 1000 °C [2, 5, 6, 9, 14–16, 100, 484, 509]. However, an increase in carbon deficit (value of x) in HfC_{1-x} results in changing in the magnetic properties of the phase from diamagnetic to paramagnetic, so the maximum of molar magnetic susceptibility χ_m (SI) $\approx (275-530) \times 10^{-6} \text{ cm}^3 \text{ mol}^{-1}$ is corresponding to the lowest carbon content in the phase and χ_m (SI) ≈ 0 – to the composition of $\text{HfC}_{0.77-0.80}$ (Fig. 3.12). Gusev and Zyryanova [5, 6] proposed for HfC_{1-x} within its homogeneity range the equation

$$\chi_m = A + BT^2, \quad (3.31)$$

which describes the relationship between magnetic susceptibility and temperature T , K in the interval from room temperature to disorder-order or order-disorder transformation temperatures (~ 800 K) and corresponds to the temperature dependence

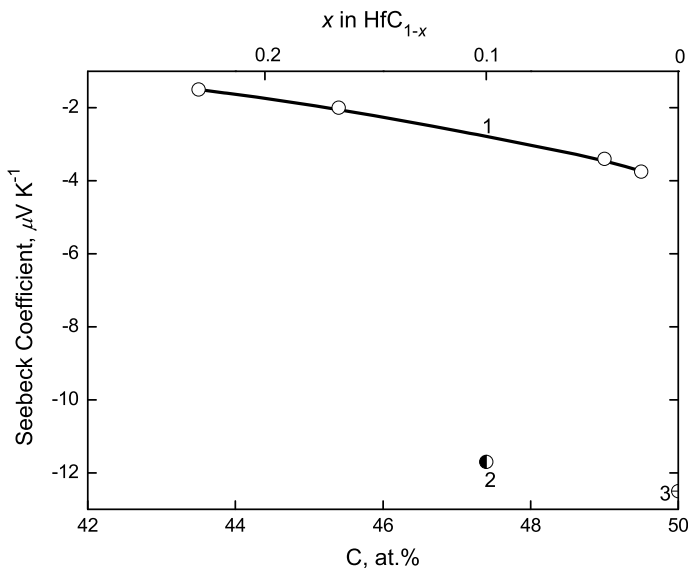


Fig. 3.11 Variation of Seebeck coefficient at room temperature within the homogeneity range of hafnium monocarbide HfC_{1-x} (1 – [96]; 2 – [415–417]; 3 – hot-pressed [101, 418])

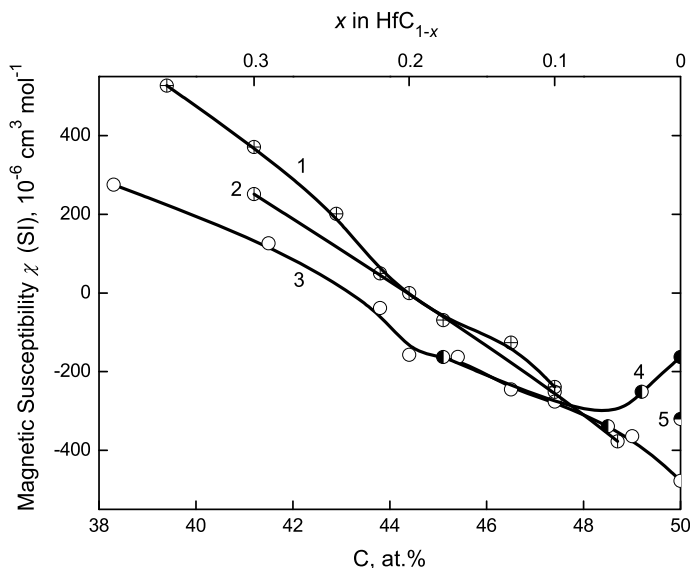


Fig. 3.12 Variation of molar magnetic susceptibility at room temperature within the homogeneity range of hafnium monocarbide HfC_{1-x} on the basis of several sources: 1 – [16], 2 – [1, 14, 15, 35], 3 – contents: non-combined C – 0.01–0.08%, O – 0.21–0.45%, N – 0.05–0.07% [5, 6, 484–486], 4 – [100], 5 – [77, 101]

of Pauli paramagnetism; where χ_m is the molar magnetic susceptibility (SI) of HfC_{1-x} , $\text{cm}^3 \text{mol}^{-1}$, A is the empirical constant increasing from $-353 \times 10^{-6} \text{cm}^3 \text{mol}^{-1}$ (for $x = 0.04$) to $248 \times 10^{-6} \text{cm}^3 \text{mol}^{-1}$ (for $x = 0.38$) and B is also the constant calculated from the experimental data (temperature coefficient) varying in the range of $(6620-10980) \times 10^{-14} \text{cm}^3 \text{mol}^{-1} \text{K}^{-2}$. The values of A and B in the function χ_m , which is sensitive to the ordering in the structure of HfC_{1-x} (see Sect. 3.1), change with disorder-order or order-disorder transformations [5, 6].

The room-temperature reflectance spectrum of pure spark plasma sintered HfC_{1-x} (porosity – 2%, grain size – $\sim 7 \mu\text{m}$) from the ultraviolet wavelength region to the mid-infrared band is shown in Fig. 3.13. The optical properties of quasi-stoichiometric HfC_{1-x} were reported by Delin et al. [588] on the basis of *ab initio* calculations, and IR absorption spectra – by Kammori et al. [589]. At common conditions the colour of hafnium monocarbide HfC_{1-x} in the dispersed state (powder) is grey or silver-gray [1, 35, 45, 61]. The normal monochromatic emittance (spectral emissivity) ε_λ of hafnium monocarbide slightly varies with temperature, the linear relationship for $\lambda = 0.65 \mu\text{m}$

$$\varepsilon_\lambda = 0.4322 + (1.065 \times 10^{-4})(t + 273), \quad (3.32)$$

where t is temperature, $^\circ\text{C}$, was obtained by Mackie et al. [105, 378] for arc-melted (via floating zone) polycrystalline $\text{HfC}_{0.86 \pm 0.03}$ in the temperature range 1150–1950 $^\circ\text{C}$, while Samsonov et al. [14] recommended linear equations, but with negative temperature coefficients:

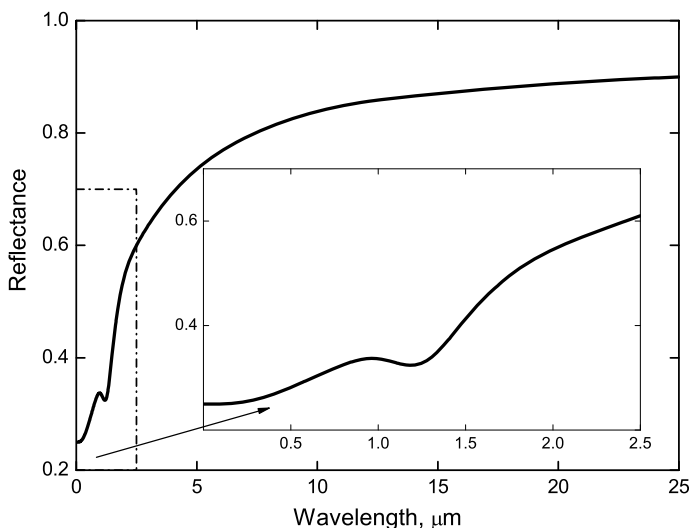


Fig. 3.13 Room-temperature reflectance spectrum of pure spark plasma sintered near-stoichiometric HfC_{1-x} (2% porosity, grain size $\sim 7 \mu\text{m}$) from the ultraviolet wavelength region to the mid-infrared band [102–104]

Table 3.8 Normal monochromatic emittance ε_λ ($\lambda = 0.650\text{--}0.665 \mu\text{m}$) of hafnium monocarbide HfC_{1-x} materials in various temperature ranges

Monochromatic emittance, ε_λ	Temperature range, $^\circ\text{C}$	References
0.51–0.73 ^a	1600–2700	[109]
0.55–0.70 ^b	700–2200	[105, 378]
0.66–0.67 ^c	2100–2200	[1, 106]
0.76 ^d	2000–3000	[14]
0.77 ^e	800–1600	[31, 32, 68, 107, 108, 421]
0.80 ^d	1000–1700	[14]
0.90 ^f	1400–1900	[419]

^aHot-pressed $\text{HfC}_{0.98}$ (5–15% porosity); ε_λ falls with the temperature growth linearly

^bArc-melted (via floating zone) polycrystalline $\text{HfC}_{0.86\pm 0.03}$, measured in vacuum $10^{-5}\text{--}10^{-6}$ Pa; ε_λ increases with the temperature growth linearly (slope is $\sim 1.1 \times 10^{-4} \text{K}^{-1}$)

^cPyrolytic coating; ε_λ falls with the temperature growth

^dHot-pressed materials

^ePowdered materials (coatings) on tantalum substrate

^fFor $\lambda = 0.81 \mu\text{m}$, the value is constant and rather independent on surface roughness and thermal treatment in vacuum and hot hydrogen

Table 3.9 Integral (total) emittance ε_T of near-stoichiometric hafnium monocarbide HfC_{1-x} in various temperature ranges

Integral emittance, ε_T	Temperature range, °C	References
0.34–0.60 ^a	850–1150	[524]
0.415–0.48 ^b	1000–2700	[1, 110]
0.42–0.485 ^c	2100–2600	[106, 420]
0.60–0.61 ^d	2000–3000	[14, 15]
0.60–0.85 ^e	1000–2700	[111]
0.65 ^f	3900	[420]

^aHemispherical emittance ε_T for hot-pressed $\text{HfC}_{-1.0}$ (<4% porosity, mean grain size $\sim 1 \mu\text{m}$, surface roughness $R_a = 0.3 \mu\text{m}$); ε_T increases with the temperature growth (addition of MoSi_2 increases ε_T – up to 0.53–0.72 in this temperature range)

^bNormal emittance ε_T for sintered $\text{HfC}_{-1.0}$ (9% porosity, contents: non-combined C – 1.16%, O – 0.1%); ε_T increases with the temperature growth linearly

^cNormal emittance ε_T for pyrolytic coating; ε_T increases with the temperature growth

^dNormal emittance ε_T for sintered materials

^eNormal emittance ε_T ; curve $\varepsilon_T - T$ with the maximum at $\sim 1300 \text{ }^\circ\text{C}$ and minimum at $\sim 2400 \text{ }^\circ\text{C}$

^fTheoretically calculated normal emittance ε_T for the stoichiometric composition

$$\varepsilon_\lambda = 0.73 - (3.75 \times 10^{-6})(t - 727), \quad (3.33)$$

$$\varepsilon_\lambda = 0.89 - (1.65 \times 10^{-4})(t - 727), \quad (3.34)$$

where t is temperature, $^\circ\text{C}$ and which are aimed for 730–1600 and 1300–2500 $^\circ\text{C}$ intervals, respectively. The data on monochromatic emittance ε_λ ($\lambda = 0.650\text{--}0.665 \mu\text{m}$) and integral (total) emittance ε_T for HfC_{1-x} materials produced by different manufacturing methods and measured at various temperatures are listed in

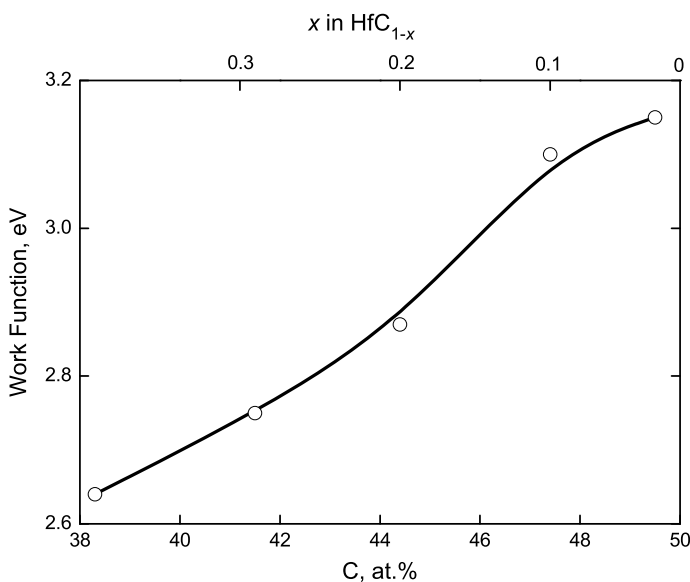
**Fig. 3.14** Variation of effective work function of hot-pressed hafnium monocarbide HfC_{1-x} materials at 1730 $^\circ\text{C}$ with carbon content [112, 113, 488]

Table 3.10 Thermionic emission characteristics (electron work function and Richardson constant) of hafnium monocarbide HfC_{1-x} phases

Composition	Work function ^a , $\phi = \phi_0 + (d\phi/dT)_{\text{av}}T$, eV	Richardson constant, A, $10^4 \text{ A m}^{-2} \text{ K}^{-2}$	Temperature range, °C	Remarks ^b	References
$\text{HfC}_{0.60}$	3.35	–	–	Theoretically evaluated	[498, 550, 551]
	3.87 ^c	–	–	PhES, single crystal (100)	[497, 498, 550, 551]
$\text{HfC}_{0.62}$	$2.52 + (6.0 \times 10^{-4})T$	–	1200–1700	TiM, hot-pressed	[1, 113, 590–592]
	3.60 ^d	–	1500	TiM, hot-pressed	[14, 15, 590–592]
$\text{HfC}_{0.67}$	3.66 ± 0.05	–	–	TiM, hot-pressed	[490]
$\text{HfC}_{0.71}$	$2.63 + (6.0 \times 10^{-4})T$	–	1200–1700	TiM, hot-pressed	[1, 113]
$\text{HfC}_{0.80}$	$2.75 + (6.0 \times 10^{-4})T$	–	1200–1750	TiM, hot-pressed	[1, 113]
$\text{HfC}_{0.88}$	3.32 ^d	–	1500	FEM, single crystal (100)	[297]
$\text{HfC}_{0.90}$	$3.00 + (5.0 \times 10^{-4})T$	–	1200–1750	TiM, hot-pressed	[1, 113]
$\text{HfC}_{0.95}$	4.15 ^d	–	1500	TiM, hot-pressed	[1, 114]
$\text{HfC}_{0.98}$	$3.05 + (5.0 \times 10^{-4})T$	–	1200–1700	TiM, hot-pressed	[1, 113, 590–592]
	3.95 ^d	–	1500	TiM, hot-pressed	[14, 15, 590–592]
$\text{HfC}_{-1.0}$	~2.04	10^{-5}	–	TiM, powder	[68, 122]
	2.94	–	–	FEM, thin films on W substrate	[595]
	$2.98 + (5.0 \times 10^{-4})T$	–	–	TiM, powder	[1, 115]
	2.99	–	–	FEM, thin films on Mo substrate	[595]
	3.00	0.3	–	TiM, powder on Ta foil	[1, 116]
	3.00	1.8	–	TiM, powder on Ta foil with MoSi_2 underlayer	[1, 116]
	3.25 ^d	–	1300	TiM, powder	[1, 117]
	3.40	–	–	TiM, pyrolytic coating	[1, 118]
	$3.42 + (1.75 \times 10^{-4})T$	–	1000–1900	TiM, powder	[1, 14, 15, 113]
	3.46 ^d	228	2300	TiM, powder on Pt substrate	[123, 594]
	3.57 ^d	107.9	2300	TiM, metal-carburized wire	[123, 594]
	3.6 ± 0.1	~15–30	–	TiM, sintered	[1, 113]
	3.63 ± 0.05	20	–	TiM, pressed	[1, 113]
	3.66 ^d	–	2100	TiM, hot-pressed	[1, 113]
	3.75 ^c	–	–	Single crystal (001), theoretically evaluated	[327]
	3.80 ± 0.04^d	–	1300	TiM, hot-pressed	[1, 119]
3.85 ^d	–	1900	TiM, powder on W substrate	[1, 120]	
3.86	–	–	Calculated value (unrelaxed surface)	[550]	

(continued)

Table 3.10 (continued)

Composition	Work function ^a , $\phi = \phi_0 + (d\phi/dT)_{av}T$, eV	Richardson constant, A, $10^4 \text{ A m}^{-2} \text{ K}^{-2}$	Temperature range, °C	Remarks ^b	References
	3.93 ^d	–	1650	TiM, sintered	[1, 113]
	3.94 ^d	39.8	2300	TiM, tip formed by electro-lytic etching	[123, 594]
	4.0	40	1000–1800	TiM, massive disk cathode	[1, 121]
	4.00 ± 0.05	–	–	TiM, hot-pressed	[490]
	4.02 ^f	–	–	Single crystal (001), theoretically evaluated	[327]
	4.10	–	2100	–	[50]
	4.15 ^d	–	1500	TiM, sintered	[1, 14, 15, 113, 114]
	4.28	–	–	Calculated value (relaxed surface)	[550]
	4.31 ^g	–	–	Single crystal (001), theoretically evaluated	[498, 550, 551]
	4.45 ^h	–	–	Single crystal (100), theoretically evaluated	[505, 550, 551]
	4.50 ⁱ	–	25	FEM, single crystal (001), clean surface	[380, 550, 551]
	4.5 ^j	–	–	PhES, nanocrystalline thin films	[593]
	4.52	–	–	FEM, thin films on W substrate, clean surface	[595]
	4.60	–	–	FEM, thin films on Mo substrate, clean surface	[595]
	4.63 ^c	–	–	PhES, single crystal (100)	[497, 498, 550, 551]
	4.90 ^k	–	25	FEM, single crystal (111), clean surface	[380]

^a T is temperature, K

^bMethods applied for the experimental determination of the work function (TiM – thermionic method, PhES – photoemission spectroscopy (with synchrotron radiation), FEM – field emission microscopy) and manufacturing methods for the fabrication of a particular material (or its constitution) are marked

^cAbsolute work functions

^dValues of effective electron work function

^eCalculated using the Perdew's generalized gradient approximation (GGA) for the fixed surface model

^fCalculated using the Perdew's GGA for the relaxed surface model

^gFull-potential linear-muffin-tin-orbital (FP-LMTO) calculation technique (40-atom cell, no vacancies)

^hLinear-muffin-tin-orbital with atomic sphere approximation (LMTO-ASA) calculation technique

ⁱFor graphene-covered surface $\phi = 4.3$ eV

^jIn the presence of considerable amounts of amorphous C (ratio C/Hf \approx 1.7)

^kFor graphene-covered surface $\phi = 3.7$ eV

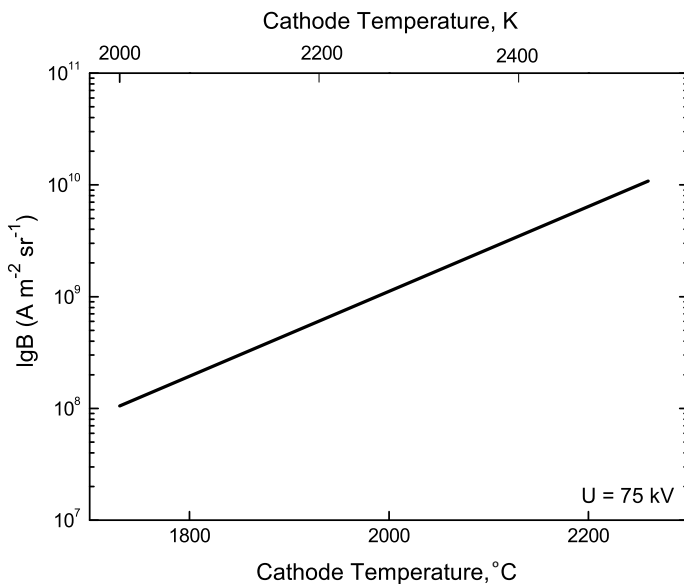


Fig. 3.15 Typical brightness (B) characteristic ($U = 75$ kV) of hafnium monocarbide cathode (thermionic emitter with electron work functions $\varphi = 3.69$ eV, $\varphi_{\text{eff}} = 3.94$ eV, Richardson constant $A = 39.8 \times 10^4$ A m $^{-2}$ K $^{-2}$, $T = 2575$ K) produced by carburization reaction of metal wire/foil with benzene vapour [123]

Tables 3.8 and 3.9. Thermodynamics of thermal radiation for stoichiometric hafnium monocarbide was considered by Fisenko and Lemberg [420].

The thermionic emission characteristics (electron work function and Richardson constants) of various hafnium monocarbide HfC_{1-x} phases are given in Fig. 3.14 and Table 3.10. The calculated values of emission current density for near-stoichiometric monocarbide HfC_{1-x} are about 3×10^{-4} , 0.3 and 50 A m $^{-2}$ at 730 °C, 1230 °C and 1730 °C, respectively [31]. Similar to some other transition metal carbides, single crystal HfC_{1-x} materials show following relationships between the effective thermionic work functions of different crystallographic planes: $\varphi_{(210,310)} < \varphi_{(100)} \approx \varphi_{(110)} \gg \varphi_{(111)}$ [297]. A typical brightness characteristic ($U = 75$ kV) of hafnium monocarbide cathode (thermionic emitter for electron microscopy) is shown in Fig. 3.15. Field emission properties of HfC_{1-x} single crystal tips and thin films (coatings) were reported in several works [297, 593, 595–616].

The recommended values of electrical resistivity, magnetic susceptibility, integral and spectral emittances and thermionic emission characteristics (electron work function and Richardson constant) for hafnium monocarbide materials are given in the wide range of temperatures in comparison with other ultra-high temperature materials in Addendum.

3.4 Physico-mechanical Properties

The physico-mechanical properties of hafnium monocarbide HfC_{1-x} are sensitive to the deviations from stoichiometry, but also to the crystallographic directions in the materials. At room temperature the hardness HV , GPa of near-stoichiometric hafnium monocarbide HfC_{1-x} is evaluated as 10.2 ± 0.7 (porosity – 15%, mean grain size – $1.8 \pm 0.2 \mu\text{m}$, 9.8 N load) [539], 16.4 (for $\text{HfC}_{0.95}$) [425], 21.0 (contents: non-combined C – 0.09%, O – 0.09%, N – 0.05%, porosity – 5%, mean grain size – $3 \mu\text{m}$, 1 N load) [427, 428], 22.6 [380], 24.8–31.4 [50, 154], 25.4 (0.5 N load) [77], 25.9 ± 1.6 [14, 15, 133], 26.0 ± 1.0 (contents: O + N – 0.1%, 0.5 N load) [131, 428], 26.1 [61], 27.0 ± 1.0 (for $\text{HfC}_{0.93}$, 1 N load) [4, 131], 27.8 ± 1.4 (for $\text{HfC}_{0.98}$, 0.5 N load) [35, 423], 28.1 ± 3.3 [129], 28.5 ± 3.0 (for monocarbide phase in contact with carbon, 0.5 N load) [31, 32, 424] and 29.0 (contents: O + N – 0.35%) [130]; hardness HK , GPa is 19.0–22.6 (0.5 N load) [422], 22.3 (extrapolated to $\text{HfC}_{1.0}$, 1 N load) [135] and 25.5 (for hafnium monocarbide HfC_{1-x} phase in contact with graphite, 1 N load) [17]. The hardness of near-stoichiometric hafnium monocarbide in Rockwell scale HRA is 84 kgf mm^{-2} (0.82 GPa) [4, 35, 129]. According to Avarbe et al. [426], the hardness HV , GPa of HfC_{1-x} (probably with noticeable oxygen contamination) is related with composition by the following equation (slightly modified):

$$HV = 19.6 + 0.51 \times (1 - x)/(2 - x), \quad (3.35)$$

where x is the value of index in HfC_{1-x} formula. According to Adams and Beall [135] the hardness HK of fused HfC_{1-x} materials in the interval between 50 and 30 at.% C changes with composition significantly and varies from 22.3 (value extrapolated to defectless theoretical stoichiometry) to 17.8 GPa (1 N load). The variations of hardnesses HV and HK with carbon content within the homogeneity range of HfC_{1-x} and indenter orientation for the (001) surface of $\text{HfC}_{0.98}$ single crystal are demonstrated in Fig. 3.16. The variation of the hardness HV of near-stoichiometric hafnium monocarbide HfC_{1-x} with temperature is presented in Fig. 3.17. In the range from 0 to 900 °C the hardness-temperature relationship for HfC_{1-x} materials can be described by the exponential equation [31, 432–434]:

$$HV = 29.4 \exp[-(14.7 \times 10^{-4})t], \quad (3.36)$$

or such approximate linear equation (for temperatures <500 °C) [560] as

$$HV = 34.4 - (2.03 \times 10^{-3})t, \quad (3.37)$$

where HV is Vickers hardness, GPa and t is temperature, °C. The data on hardness HK of hafnium monocarbide single crystals and microhardness $H\mu$ of various HfC_{1-x} compositions are listed in Tables 3.11 and 3.12.

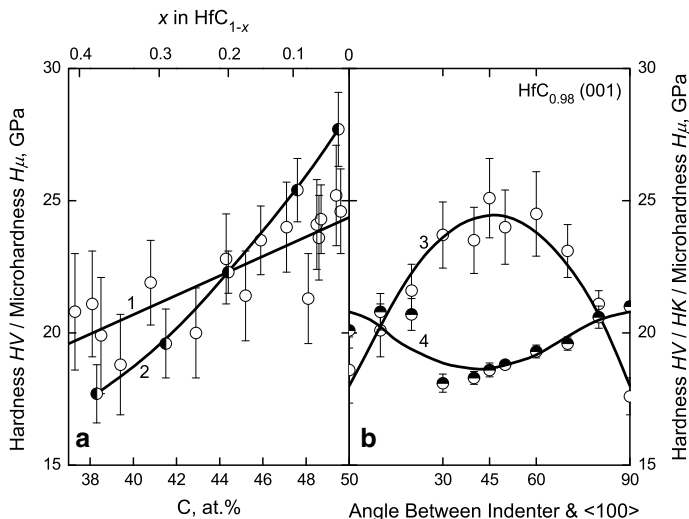


Fig. 3.16 Variations of the hardnesses HV (1, 4), HK (3) and microhardness H_{μ} (2) at room temperature for hafnium monocarbide HfC_{1-x} materials: (a) with deviation from the stoichiometry within the homogeneity range (1 – prepared by various methods, 200 N load [21, 124, 125]; 2 – hot-pressed, 0.5 N load [4, 35, 84, 488]) and (b) with indenter orientation (angle between indenter axis and $\langle 100 \rangle$ direction) on the (001) surface of single crystal materials grown by floating-zone processes (3 – $\text{HfC}_{0.98}$, 1 N load and 4 – $\text{HfC}_{0.98}$, 2 N load [41, 42, 493])

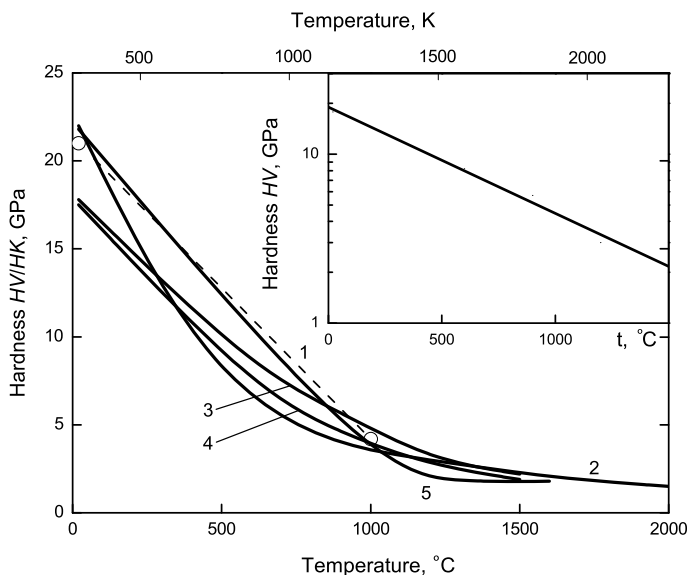


Fig. 3.17 Variations of the hardness HV/HK of hafnium monocarbide HfC_{1-x} with temperature: 1 – $\text{HfC}_{-1.0}$, sintered in vacuum and annealed (mean grain size – 3.0 μm , porosity – 5%, contents: non-combined C – 0.09%, O – 0.09%, N – 0.05%), 1 N (microhardness) load [1]; 2 – $\text{HfC}_{-1.0}$, hot-pressed and annealed in Ar atmosphere (porosity – 1%), 10 N load [126, 127]; 3 – $\text{HfC}_{0.87}$, fused (contents: O – 0.05%, N – 0.003%, Zr – 2%), 19.6 N load [137]; 4 – $\text{HfC}_{0.83}$, fused (contents: O – 0.05%, N – 0.003%, Zr – 2%), 19.6 N load [137]; 5 – $\text{HfC}_{-1.0}$, zone-melted with excess C (~5%), 11 N load [364] (Inset – fused $\text{HfC}_{0.87}$, in $\lg(HV) - t$, °C scale, 19.6 N load [137])

Table 3.11 Microhardness $H\mu$ (HK scale) of hafnium monocarbide HfC_{1-x} ($0 < x \leq 0.02$) single crystals at room temperature (1 N load)

Surface	Indentor diagonal direction	Microhardness $H\mu$, GPa	References
		$x \approx 0^a$	
(001)	<100>	18.1	[617, 618]
	<110>	24.5	[617, 618]
	–	26.0 ± 0.5	[128]
(110)	–	25.1 ± 0.5^b	[128, 335]
	–	22.9 ± 0.5	[128]
(111)	–	22.7 ± 0.5^b	[128, 335]
	–	24.1 ± 0.5	[128]
(001)	–	23.7 ± 0.5^b	[128, 335]
		$x = 0.02$	
(001)	<100>	19.0 ± 1.0	[41]

^aCrystals grown by controlled solidification from the melt^bAnnealed at 2100 °C**Table 3.12** Microhardness $H\mu$ of the various compositions of hafnium monocarbide HfC_{1-x} phase at room temperature

Composition	Microhardness $H\mu$, GPa	Remarks	References
$\text{HfC}_{0.62}$	17.7 ± 1.1	0.5 N load, sintered in vacuum, contents: O – 0.09%, N – 0.04%	[35, 84]
$\text{HfC}_{0.63}$	19.5^a	0.98 N load, fused, content non-combined C – ~0.05%	[135]
	15.8^a	19.6 N load, fused, non-combined C – ~0.05%	[135]
$\text{HfC}_{0.67}$	18.8 ± 1.2	0.5 N load, sintered in vacuum	[84, 490]
$\text{HfC}_{0.71}$	19.6 ± 1.3	0.5 N load, sintered in vacuum, contents: O – 0.09%, N – 0.03%	[35, 84]
$\text{HfC}_{0.80}$	22.3 ± 0.9	0.5 N load, sintered in vacuum, contents: O – 0.10%, N – 0.06%	[35, 84]
	21.0^a	0.98 N load, fused, non-combined C – 0.04%	[135]
$\text{HfC}_{0.82}$	18.2^a	19.6 N load, fused, non-combined C – 0.04%	[135]
	17.5 ± 0.9^b	19.6 N load, fused, contents: O – 0.05%, N – 0.003%, Zr – 2%	[137]
$\text{HfC}_{0.87}$	17.8 ± 0.6^b	19.6 N load, fused, contents: O – 0.05%, N – 0.003%, Zr – 2%	[137]
	25.4 ± 1.2	0.5 N load, sintered in vacuum, contents: O – 0.09%, N – 0.04%	[35, 84]
$\text{HfC}_{0.91}$	19 (22 ^a)	Electron beam deposited thin films on Ti substrate, thickness – $0.50 \pm 0.03 \mu\text{m}$, mean grain size <0.3 μm	[148]

(continued)

Table 3.12 (continued)

Compo- sition	Microhardness $H\mu$, GPa	Remarks	References
HfC _{0.95}	25.9 ± 1.6	0.2–1.5 N load, hot-pressed and annealed at 1800 °C for 3 h, porosity – 7%, non-combined C – 0.1%	[129, 298]
	16.4 ^c	–	[425]
HfC _{0.96}	28.8 ^d	Hot-pressed, mean grain size – 5–20 μm	[441]
	25.6	Hot-pressed, mean grain size – 5–20 μm	[441]
	24.5 ^a	0.5 N load, hot-pressed, porosity – 3–5%, mean grain size – 30 μm, contents: non-combined C – 0.03%, Zr – 3.45	[79, 80]
HfC _{0.97}	20.2 ^a	0.5 N load, hot-pressed, porosity – 1–2%, mean grain size – 13 μm, contents: non-combined C – 0.30%, O – 0.45%, N – 0.10%, Zr – 1.40	[79, 80]
	20.0 ^a	0.5 N load, sintered in vacuum, porosity – 4–7%, mean grain size – 42 μm, contents: non-combined C – 0.30%, O – 0.45%, N – 0.10%, Zr – 1.40	[79, 80]
HfC _{0.98}	27.7 ± 1.4	0.5 N load, sintered in vacuum, contents: non-combined C – 0.16%, O – 0.11%, N – 0.04%	[35, 84]
	27.4 ± 0.4	Pyrolytic materials	[430]
	25–28 ^a	1 N load, sintered, porosity – 1–7%	[17]
HfC _{~1.0}	29.0	Sintered in Ar, contents: O + N – 0.35%	[130, 299]
	28.5	–	[32, 108]
	28.4 ± 1.4	0.5 N load, sintered in vacuum	[84, 490]
	28.0	–	[14, 15]
	27.9	C ₂ H ₂ -reactive magnetron sputtered coatings	[321]
	27.7	1 N load, sintered	[64, 283]
	27.0	–	[9, 387]
	26.8	Calculated on the basis of Tian's model	[302]
	26.4 ± 1.6	–	[133]
	26.1	–	[61, 301]
	26.05 ^a	0.98 N load, hot-pressed, porosity – 2%	[136]
	26.0 ± 1.0	Sintered, contents: O + N – 0.1%	[131, 363]
	25.7	Calculated value	[429]
	25.0	–	[129]
	24.0	–	[134]
	23.0 ^d	0.5 N peak load, spark plasma sintered materials, porosity – 2%, mean grain size – 19 ± 1 μm	[103, 104, 435]
	22.8 ^a	0.98 N load, fused, non-combined C – 0.09%	[135]
	21.8 ^a	0.98 N load, zone-melted with excess C (~5%)	[364]
	21.0	Sintered in vacuum and annealed, porosity – 5%, mean grain size – 3.0 μm, contents: non-combined C – 0.09%, O – 0.09%, N – 0.05%	[1]
	20.1 ^e	0.2–10 N load, hot-pressed, porosity <5%	[371]
	19.4–23.0 ^a	0.5 N load	[67]

(continued)

Table 3.12 (continued)

Composition	Microhardness $H\mu$, GPa	Remarks	References
	19.4 ^a	19.6 N load, fused, content non-combined C – 0.09%	[135]
	18.8 ± 0.7	9.8 N load, spark plasma sintered materials, porosity – 2%, mean grain size – 19 ± 1 μm	[103, 104, 435]
	18 ± 2	Pulsed laser ablation deposited thin films on Ti substrate, thickness – 0.22 to 0.50 μm, approximate grain size – 10 to 100 nm	[431]
	17.3	Theoretical evaluation	[305]
	17.9	–	[304]
	15.9 ± 0.5	0.1 kN load, reactive spark plasma sintered materials, porosity – 8%, mean grain size <5 μm	[436]
	15.6	Calculated on the basis of Xue’s model	[302, 303]

^aKnoop measurement (*HK*)

^bMarshall micro-indentation diamond pyramid hardness testing in vacuum

^cDiamond pyramid hardness measurement (*DPH*)

^dEvaluated by a MTS XP diamond Berkovitch nanoindenter

^eDetermined in accordance with the formula: $H\mu = 18.18 P/d^2$, where P is the load on the indenter, N and d is the diagonal of the indentation, μm; the values of other micromechanical characteristics: microbrittleness $\gamma_\mu = (D^2 - d^2)/d^2 = 3.0$, where D is the average size of the damageability zone, μm and brittle microstrength $\sigma_\mu = PID^2 = 2.7$ GPa [371]

The variations of ultimate tensile and flexural (bending) strengths of near-stoichiometric hafnium monocarbide HfC_{1-x} with temperature determined in various experimental works are shown in Fig. 3.18 in comparison with the values of *ab initio* calculated strength characteristics. Spark-plasma sintered near-stoichiometric HfC_{1-x} (porosity 15%, mean grain size – 1.8 ± 0.2 μm) exhibits average fracture toughness K_{IC} of 2.9 ± 0.5 MPa m^{1/2} [539], and for cold-pressed and sintered near-stoichiometric HfC_{1-x} (porosity 3–4%, mean grain size – 2.8 ± 1.0 μm, content O – 0.02%) $K_{IC} = 1.73 \pm 0.09$ MPa m^{1/2} [149]. Brizes (cited by Hollox [438]) has reported that pure near-stoichiometric HfC_{1-x} materials are ductile at temperatures around 1600 °C. The values of prolonged strength (creep resistance) are of great importance for the evaluation of operational time of components in the engineering practice. The examples of ultra-high temperature creep characteristics of sintered and annealed in vacuum $\text{HfC}_{0.91}$ (porosity ≤ 10%, mean grain size – 22 μm, contents O + N – 0.24%) are demonstrated in Fig. 3.19; creep activation energies Q and exponent constants n of HfC_{1-x} phases are listed in Table 3.13. At room temperature the values of Young’s modulus E of near-stoichiometric hafnium monocarbide HfC_{1-x} materials lies within the area of 320–480 GPa [1, 3, 4, 9, 79, 82, 91, 150, 311, 314]; the reported values for

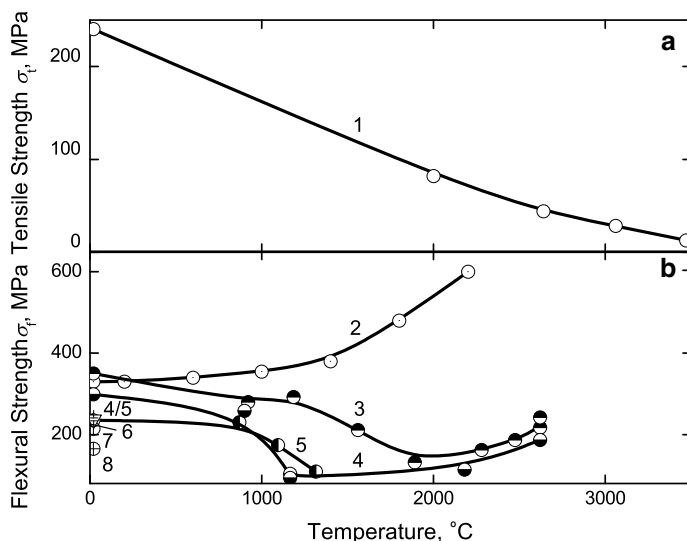


Fig. 3.18 Variations of (a) tensile σ_t (1 – sintered $\text{HfC}_{-1.0}$, data corrected to the poreless state [14, 53, 88, 140]) and (b) flexural (bending) σ_f (2 – sintered $\text{HfC}_{-1.0}$, data corrected to the poreless state [1, 141, 149]; 3 – hot-pressed $\text{HfC}_{-1.0}$, porosity – 5%, mean grain size – 8 μm , contents: non-combined C – 0.04%, O – 0.16%, N – 0.03%, Zr – 1.07, 3-point bending scheme [80, 306]; 4 – hot-pressed $\text{HfC}_{-1.0}$, porosity – 4%, mean grain size – 24 μm , contents: non-combined C – 0.04%, O – 0.16%, N – 0.03%, Zr – 1.07, 3-point bending scheme [80, 306]; 5 – [82, 312, 313]; 6 – hot-pressed $\text{HfC}_{0.96}$, porosity – 3–5%, mean grain size – 30 μm , contents: non-combined C – 0.03%, Zr – 3.45, 3-point bending scheme [79]; 7 – hot-pressed $\text{HfC}_{0.97}$, porosity – 1–2%, mean grain size – 13 μm , contents: non-combined C – 0.30%, O – 0.45%, N – 0.10%, Zr – 1.40, 4-point bending scheme [79]; 8 – sintered in vacuum $\text{HfC}_{0.97}$, porosity – 4 to 7%, mean grain size – 42 μm , contents: non-combined C – 0.30%, O – 0.45%, N – 0.10%, Zr – 1.40, 4-point bending scheme [79]) strengths with temperature for near-stoichiometric hafnium monocarbide HfC_{1-x} materials (the values of *ab initio* calculated ideal shear strength and ratio of the ideal strength to the elastic shear modulus for quasi-stoichiometric HfC_{1-x} are 30 GPa and ~ 0.13 , respectively [362])

Coulomb's (shear) modulus G of HfC_{1-x} are 193–195 GPa [9, 150], 193–199 GPa [3, 4] (determined experimentally) and 166 GPa [62], 175–189 GPa [163], 230 GPa [164], 236 GPa [362] (calculated theoretically), for bulk (compression) modulus K – 245–290 GPa [3, 4, 9, 150, 152], for volume compressibility κ – 4.06–4.78 TPa^{-1} [1, 3, 4, 150, 151] and Poisson's ratio ν – 0.17 to 0.22 [3, 4, 150, 154, 163]; the *ab initio* calculated sound velocities (at zero pressure) for near-stoichiometric hafnium monocarbide $\text{HfC}_{-1.0}$ are:

longitudinal velocity V_S , m s^{-1} 6964 (0 K) [318], 5474 (~ 300 K) [318], 6253 [315], 6530 [163], 6280–6450 [336], 6351 [444];

transversal velocity V_T , m s^{-1} 4273 (0 K) [318], 3339 (~ 300 K) [318], 3893 [315], 4090 [163], 3850–3950 [336], 3816 [444];

average velocity V_m , m s^{-1} 4250–4360 [336], 4880 [444].

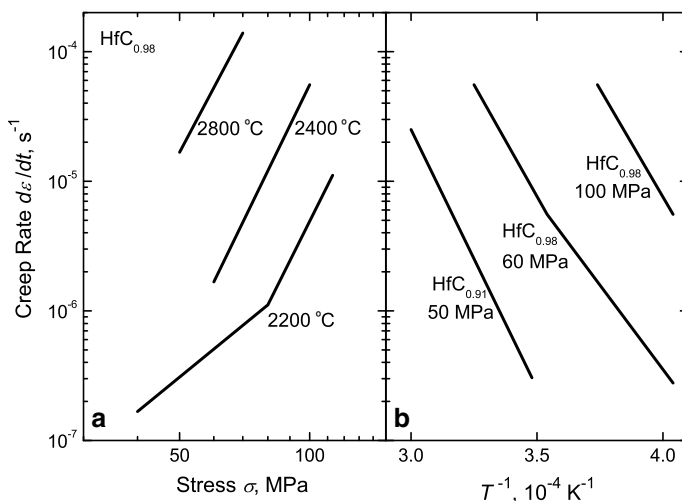


Fig. 3.19 High- and ultra-high temperature creep rate variations of near-stoichiometric hafnium monocarbide HfC_{1-x} materials with applied stress (a) and reciprocal temperature (b): $\text{HfC}_{0.91}$ (sintered and annealed in vacuum, porosity $\leq 10\%$, mean grain size – $22 \mu\text{m}$, contents O + N – 0.24%) [144] and $\text{HfC}_{0.98}$ (sintered, porosity – 5% , mean grain size – $22 \mu\text{m}$, contents: non-combined C – 0.05% , O – 0.10% , N – 0.01% , W – 0.02%) [328]

Table 3.13 Formal creep characteristics (activation energy Q , stress exponent constant n) of hafnium monocarbide phases HfC_{1-x} at various temperature and stress ranges^a

Composition	Load type ^b	Temperature range, °C	Stress range, MPa	Activation energy ^c , Q , kJ mol^{-1}	Exponent constant ^c , n	References
$\text{HfC}_{0.96-0.99}^d$	C	2400–2700	8–70	830 ± 60	1	[142]
$\text{HfC}_{0.98}^e$	C	2200–2400	60–100	435	2.6	[328–330]
	C	2200–2400	100–200	810	6.5	[328–330]
	C	2600–2800	60–100	810	5–6.5	[328–330]
$\text{HfC}_{0.94}^f$	F	2500–3050	10–16	815	1	[145]
$\text{HfC}_{0.93}^g$	F	2500–2950	10–17.5	815 ± 40	1	[143]
$\text{HfC}_{0.91}^h$	C	1950–2100	50	840	–	[144]

^aFor near-stoichiometric HfC_{1-x} the following average values were estimated: Peierls stress $\tau_P = 6.0 \text{ GPa}$, shear modulus – Peierls stress ratio $\tau_P/G = 0.032$ and slip activation energy barrier $q = 1.2 \text{ eV}$ [392]

^bDenoted: F – flexure (bending), C – compression

^cSee Eq. (I-3.17)

^dSintered, porosity – 3% , mean grain size – $11\text{--}15 \mu\text{m}$, contents: O/Hf and N/Hf ratios ≤ 0.03

^eSintered, porosity – 5% , mean grain size – $22 \mu\text{m}$, contents: non-combined C – 0.05% , O – 0.10% , N – 0.01% , W – 0.02%

^fHot-pressed, porosity – $3\text{--}5\%$

^gHot-pressed, porosity $\leq 5\%$, mean grain size – $80 \mu\text{m}$, contents: O $\leq 0.1\%$, N $\leq 0.09\%$

^hSintered and annealed, porosity $\leq 10\%$, mean grain size – $22 \mu\text{m}$, O + N – 0.24%

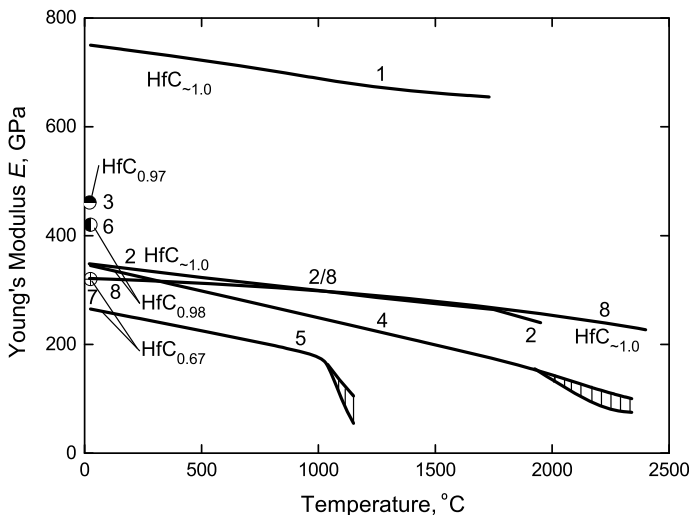


Fig. 3.20 Variations of Young's modulus E with temperature of hafnium carbide HfC_{1-x} phases: 1 – recommended by Kotelnikov et al. [31]; 2 – calculated on the basis of hardness-elasticity relationship by Travushkin et al. [126, 127]; 3 – hot-pressed and sintered materials, porosity – 4–7%, determined by the slope of stress-strain curves employing 4-point bending scheme by Sanders et al. [79]; 4–7 – hot-pressed materials, measured by Opeka et al. (4–5 – from flexural testing, upper lines correspond to the initial modulus (without plastic components) and lower lines correspond to the secondary modulus (with plastic components), 6 – from tensile testing of ring specimens and 7 – from ultrasonic measurements) [91]; 8 – hot-pressed materials, measured by Jun and Shaffer (resonant frequency technique) [82, 311]

The variations of Young's modulus E with temperature for the HfC_{1-x} phases with different deviations from the stoichiometry are shown in Fig. 3.20; the elastic properties (stiffness coefficients c_{ij} and moduli E , K and Poisson's ratio ν) of various HfC_{1-x} materials are listed in Table 3.14. The variations of the elastic characteristics with higher pressure (up to 100 GPa) for quasi-stoichiometric hafnium monocarbide $\text{HfC}_{-1.0}$ based on *ab initio* calculations are shown in Fig. 3.21. According to the calculations on the basis of DFT with LDA produced by Krasnenko and Brik [443] bulk (compression) modulus K of $\text{HfC}_{-1.0}$ arises at elevated hydrostatic pressures p (up to 50 GPa) linearly

$$K = 258.0 + 4.21p. \quad (3.38)$$

The testing data on thermal shock/stress resistance (thermal strength) of single phase hafnium monocarbide HfC_{1-x} materials are given in Table 3.15.

Table 3.14 Elastic properties (stiffness coefficients c_{11} , c_{12} and c_{44} , Young's modulus E , bulk (compression) modulus K , Poisson's ratio ν)^a of hafnium monocarbide phases HfC_{1-x}

Composition	Stiffness coefficients c_{ij}			Young's modulus E , GPa	Bulk modulus K , GPa	Poisson's ratio ν	References
	c_{11} , GPa	c_{12} , GPa	c_{44} , GPa				
$\text{HfC}_{0.67}$	–	–	–	265 ^{b,c}	–	–	[91]
	–	–	–	317 ^{b,d}	–	–	[91]
	–	–	–	320 ^{b,e}	–	–	[91]
$\text{HfC}_{0.75}^f$	464	101	131	366 ^g	223 ^g	–	[334]
$\text{HfC}_{0.88}^f$	508	107	162	425 ^h	223 ^h	–	[334]
$\text{HfC}_{0.96}^i$	–	–	–	430 ^j	203 ^j	–	[441]
$\text{HfC}_{0.97}$	535 ^f	110 ^f	170 ^f	445 ^{f,k}	252 ^{f,k}	–	[334]
	–	114 ^{l,m,n}	195 ^{l,m}	461 ^{l,m,o}	242 ^{l,m,o}	0.18 ^{l,m}	[3, 9, 82, 150, 314]
–	–	–	–	430 ^p	–	–	[151]
–	–	–	–	321 ^q	–	–	[79]
–	–	–	199	470	246	0.18	[4]
–	–	–	–	–	263	–	[157, 372]
$\text{HfC}_{0.98}$	–	–	–	345 ^{c,r}	–	–	[91]
	–	–	–	420 ^{d,r}	–	–	[91, 381]
	–	–	–	427 ^{e,r}	–	–	[91]
$\text{HfC}_{\sim 1.0}$	–	–	179 ^s	317–421 ^s	291 ^s	–	[9, 152]
	–	–	–	424 ^t	–	0.17	[154]
–	–	–	–	351 ^u	–	–	[67, 108]
–	–	–	–	480 \pm 10 ^v	–	–	[156]
–	–	–	–	352	–	–	[35, 155]
–	–	–	–	514 ⁿ	–	–	[1]
–	–	–	193	470	275	0.215	[4]
–	–	–	–	422	–	–	[14, 15]
–	500 ^w	114 ^w	180 ^w	433	243 ^w	–	[159, 392, 515]
–	574 ^x	107 ^x	180 ^x	–	260 ^x	–	[161]
–	–	–	–	–	238 ^x	–	[162, 331]
–	591 ^y	119 ^y	163 ^y	461 ^{y,z}	276 ^{y,z}	0.22 ^y	[39]
–	527 ^{a1}	107 ^{a1}	160 ^{a1}	431 ^{a1,a2}	247 ^{a1,a2}	0.21 ^{a1}	[39]
–	506 ^{a3}	105 ^{a3}	160 ^{a3}	422 ^{a3,a4}	238 ^{a3,a4}	0.205 ^{a3}	[39]
–	528 ^{a5}	111 ^{a5}	160 ^{a5}	431 ^{a2,a5}	250 ^{a2,a5}	0.21 ^{a5}	[39]
–	–	–	–	404 ^{a6,a7}	236 ^{a6,a7}	0.215 ^{a6}	[62]
–	577 ^{a8}	117 ^{a8}	171 ^{a8}	537 ^{a8,a9}	270 ^{a8,a9}	–	[164]
–	579 ^{a5}	103 ^{a5}	204 ^{a5}	–	260 ^{a5}	–	[287]
–	–	–	–	–	257 ^y	–	[288]
–	–	–	–	–	238 ^{b1}	–	[288]
–	–	–	–	–	218 ^f	–	[288]
–	554 ^{b2}	132 ^{b2}	228 ^{b2}	–	–	–	[295]
–	514 ^{b3}	98 ^{b3}	178 ^{b3}	449 ^{b3,b4}	237 ^{b3,b4}	0.18 ^{b3}	[315]
–	486 ^{a8}	106 ^{a8}	156 ^{a8}	–	233 ^{a8}	–	[316]
–	480 ^{a8}	103 ^{a8}	177 ^{a8}	–	–	–	[317]

(continued)

Table 3.14 (continued)

Composition	Stiffness coefficients c_{ij}			Young's modulus E , GPa	Bulk modulus K , GPa	Poisson's ratio ν	References
	c_{11} , GPa	c_{12} , GPa	c_{44} , GPa				
	570 ^{a8,b5}	140 ^{a8,b5}	214 ^{a8,b5}	513 ^{a8,b5,b6}	283 ^{a8,b5,b6}	0.20 ^{a8,b5}	[318, 319]
	428 ^{a8,b7}	100 ^{a8,b7}	149 ^{a8,b7}	373 ^{a8,b7,b8}	210 ^{a8,b7,b8}	0.20 ^{a8,b7}	[318, 319]
	533 ^{a8}	104 ^{a8}	162 ^{a8}	437 ^{a8,b9}	247 ^{a8,b9}	0.205 ^{a8}	[320]
	498 ^{c1}	113 ^{c1}	179 ^{c1}	455 ^{c1,c2}	241 ^{c1,c2}	0.19 ^{c1}	[163]
	548 ^{a8}	99 ^{a8}	192 ^{a8}	518 ^{a8,c3}	248 ^{a8,c3}	0.15 ^{a8}	[163]
	—	—	—	255 ^{c4}	—	—	[321]
	454 ^{c5}	87 ^{c5}	87 ^{c5}	426 ^{c5,c6}	218 ^{c5,c6}	0.16 ^{c5}	[322]
	465 ^{c1}	79 ^{c1}	91 ^{c1}	—	—	—	[323]
	556 ^y	105 ^y	152 ^y	—	248 ^y	—	[324]
	502 ^{a5}	97 ^{a5}	143 ^{a5}	—	—	—	[324]
	—	—	—	—	265 ^{c7}	—	[325]
	537 ^{c8}	112 ^{c8}	156 ^{c8}	498 ^{c8,c9}	254 ^{c8,c9}	0.17 ^{c8}	[305]
	—	—	—	—	243 ^{d1}	—	[327]
	—	—	—	—	242 ^{d2}	—	[327]
	—	—	—	—	310 ^f	—	[38]
	—	—	—	—	314 ^{d3}	—	[38]
	540 ^f	112 ^f	171 ^f	—	253 ^{f,d4}	—	[334]
	609 ^f	112 ^f	183 ^f	—	278 ^{f,d5}	—	[333]
	582 ^{d6}	103 ^{d6}	173 ^{d6}	—	263 ^{d6}	—	[336, 443]
	507 ^f	103 ^f	165 ^f	—	238 ^f	—	[336, 443]
	—	—	—	—	242–275 ^{d7}	—	[336]
	—	—	—	355	—	—	[386]
	—	—	—	464	—	—	[387]
	—	—	—	471	—	—	[388]
	474 ^{d8}	88 ^{d8}	98 ^{d8}	337 ^{d8,d9}	216 ^{d8,d9}	0.23 ^{d8}	[391, 392]
	—	—	—	450 ^{e1}	—	—	[104]
	—	—	—	386 ^{e2}	—	—	[439]
	—	—	—	—	246 ^{e3}	—	[440]
	551 ^{e4}	105 ^{e4}	175 ^{e4}	461 ^{e4,e5}	254 ^{e4,e5}	0.197 ^{e4}	[442]
	537 ^f	112 ^f	156 ^f	498 ^{f,c9}	254 ^{f,c9}	0.173 ^f	[444]
	—	—	—	350 ^{e6}	—	—	[153, 492]
	—	—	—	283 ± 10 ^{e7}	—	—	[539]
	—	—	—	—	242 ^{f,a2}	—	[326]
	—	—	—	740–750 (?)	—	—	[31, 158]

^aFor isotropic (or quasi-isotropic) materials [3]: $E = 2G(1 + \nu)$, $E = 3K(1 - 2\nu)$, $K = c_{12} + 2c_{44}/3$, $G = c_{44}$; the condition for the isotropy is given in Eq. (I-2.18)

^bHot-pressed, mean grain size >200 μm , porosity – 5–10%

^cFrom flexural stress versus deflection measurements

^dFrom ultrasonic measurements

^eFrom ring specimens tensile testing measurements

^fCalculated on the basis of density-functional theory (DFT) with generalized gradient approximation (GGA) using Perdew-Burke-Ernzerhof (PBE) functional

^gCalculated value of $G = 149$ GPa

^hCalculated value of $G = 176$ GPa

ⁱHot-pressed, corrected to the poreless state (true porosity – up to 12%), mean grain size – 5–20 μm ; ultrasonic wave velocity measurements

^jMeasured experimentally $G = 193$ GPa

(continued)

Table 3.14 (continued)^kCalculated value of $G = 184$ GPa^lHot-pressed, porosity – 3%, corrected to the poreless state^mFrom ultrasonic measurements, corrected to the poreless stateⁿCalculated value^oMeasured experimentally $G = 195$ GPa^pHot isostatically pressed and subsequently sintered, non-combined C – 0.05%^qHot-pressed, mean grain size – 13 μm , porosity – 4–7%, determined by the slope of stress-strain curves employing 4-point bending scheme^rHot-pressed, mean grain size – 40–60 μm , porosity – 5–10%^sSelf-bonded sintered^tPorosity – 5.0%^uHot-pressed, porosity – 6–8%^vSintered in vacuum and annealed, mean grain size – 3.0 μm , porosity – 5%, contents: non-combined C – 0.09%, O – 0.09%, N – 0.05%^wEstimation from phonon dispersion curves (c_{11} is extrapolated from neutron data [160])^xCalculated on the basis of density-functional perturbation theory (DFPT)^yCalculated on the basis of DFT with local density approximation (LDA)^zCalculated value of $G = 189$ GPa^{a1}Calculated on the basis of DFT with LDA together with PBE functional^{a2}Calculated value of $G = 178$ GPa^{a3}Calculated on the basis of DFT with LDA together with the revised Perdew-Burke-Ernzerhof (RPBE) functional^{a4}Calculated value of $G = 175$ GPa^{a5}Calculated on the basis of DFT using plane-wave pseudopotential (PWPP) method with GGA^{a6}Calculated using the Debye–Grüneisen model combined with *ab initio* calculations^{a7}Calculated value of $G = 166$ GPa^{a8}From *ab initio* calculations^{a9}Calculated value of $G = 230$ GPa^{b1}Calculated on the basis of DFT with Wu-Cohen GGA exchange-energy functional^{b2}At 80 K^{b3}Calculated on the basis of full-potential *ab initio* approach^{b4}Calculated value of $G = 190$ GPa^{b5}At 0 K^{b6}Calculated value of $G = 215$ GPa^{b7}At ~300 K^{b8}Calculated value of $G = 155$ GPa^{b9}Calculated value of $G = 181$ GPa^{c1}Calculated on the basis of three body force potential (TBFP) model^{c2}Calculated value of $G = 184$ GPa and $\kappa = 4.15$ TPa^{-1} ^{c3}Calculated value of $G = 205$ GPa and $\kappa = 4.03$ TPa^{-1} ^{c4}Coatings synthesized by C_2H_2 -reactive magnetron sputtering^{c5}Calculated on the basis of interionic potential theory with modified ionic charge^{c6}Calculated value of $G = 125$ GPa^{c7}First principles calculations using the plane-wave pseudopotential method^{c8}First principles calculations^{c9}Calculated value of $G = 177$ GPa^{d1}Calculated on the basis of DFT with GGA together with the Perdew's functional^{d2}Calculated on the basis of DFT with GGA using RPBE functional^{d3}Calculated on the basis of DFT with LDA using Ceperley-Alder (CA) type parametrization^{d4}Calculated value of $G = 187$ GPa^{d5}Calculated value of $G = 207$ GPa^{d6}On the basis of DFT with LDA using Ceperley-Alder-Perdew-Zunger (CA-PZ) functional^{d7}Calculated on the basis of Murnaghan equation of state

(continued)

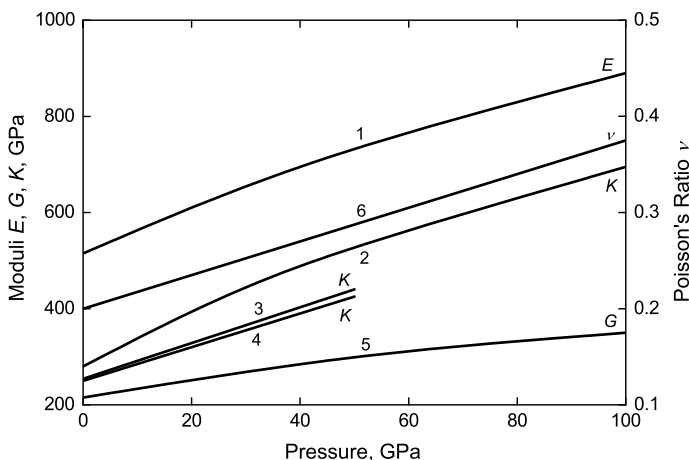
Table 3.14 (continued)^{d8}Calculated on the basis of a modified interaction potential model with covalency (MIPMC_v)^{d9}Calculated value of $G = 136$ GPa^{e1}Calculated by the data acquisition software of the nanoindentation measurements based on Oliver-Pharr model [437]^{e2}Hot-pressed, porosity – 6%; calculated from depth-sensing indentation (DSI) measurements^{e3}On the basis of interconsistency of the physical properties of transition metal monocarbides^{e4}Calculated on the basis of DFT by projector augmented wave (PAW) method with GGA using PBE functional^{e5}Calculated value of $G = 192$ GPa^{e6}Hot-pressed; experimentally measured by the method of continuous impression of an indenter^{e7}Spark-plasma sintered, mean grain size – 1.8 ± 0.2 μm , porosity – 15%; measured experimentally by Berkovich nanoindentation

Fig. 3.21 Variations of elastic properties (1 – Young’s modulus E , 2–4 – bulk (compression) modulus K , 5 – Coulomb’s (shear) modulus G and 6 – Poisson’s ratio ν) of quasi-stoichiometric hafnium monocarbide HfC_{1-x} with higher pressure (at 0 K) based on *ab initio* calculations: 1–2, 5–6 – by Varshney et al. [318, 319]; 3 – by Gautam and Kumar [442] and 4 – by Krasnenko and Brik [336, 443]

Table 3.15 Thermal shock/stress resistance (thermal strength) testing data on single phase hafnium monocarbide HfC_{1-x} materials

Materials and its characterization	Specimen shape and dimensions, mm	Method of thermal loading (testing)	Experimental results	References
HfC_{1-x} , gas-phase deposited, contents: $\text{O} + \text{N} \leq 0.3\%$	Hollow cylinders: wall thickness – 0.8–1.2, height – 20	Direct resistance heating with 400 K s^{-1} , cooling by inert gas blow, cycle time – 3 min	Disintegration after 2–3 heating-cooling cycles from 2870 to 50°C	[4, 141]

The magnitudes of physico-mechanical (strength, elasticity) properties of near-stoichiometric hafnium carbide HfC_{1-x} in the wide range of temperatures are summarized in Addendum in comparison with other ultra-high temperature materials.

3.5 Nuclear Physical Properties

The isotopes of element hafnium Hf (standard atomic mass – 178.49 u) from ¹⁵³Hf to ¹⁸⁸Hf, including metastable isomers (^{153m}Hf, ^{156m}Hf, ^{171m}Hf, ^{172m}Hf, ^{174m1–4}Hf, ^{177m1–3}Hf, ^{178m1–3}Hf, ^{179m1–2}Hf, ^{180m1–5}Hf, ^{181m1–3}Hf, ^{182m}Hf and ^{184m}Hf), and their general characteristics are summarized in Table 3.16; neutron nuclear physical properties of the isotopes of hafnium are given in Table 3.17. The comprehensive list of isotopes of element carbon C is presented in Table I-2.12 and its nuclear physical properties, including isotopic mass range, total number of isotopes, thermal neutron macroscopic cross sections, moderating ability and capture resonance integral, are given in Table I-A.8.

The thermal neutron macroscopic cross sections Σ_i (see Eq. 2.53) of near-stoichiometric hafnium monocarbide HfC_{1-x} (for 2200 m s⁻¹ neutrons) [31]:
 cross section of capture (absorption) Σ_a , cm⁻¹ 4.17
 cross section of scattering Σ_s , cm⁻¹ ~0.59

For the estimation of probable damage of hafnium monocarbide materials exposed to various types of radiation the parameters of formation and migration of lattice point defects (vacancies and interstitial atoms) are given in Table 3.18.

Table 3.16 General characteristics of the isotopes of hafnium [165–169]

Isotope	Mass, u	Abundance, %	Half-life period	Decay mode, excitation (radiation) energy, MeV
¹⁸⁰ Hf ^a	179.946550	35.08	–	–
¹⁷⁸ Hf ^a	177.943699	27.28	–	–
¹⁷⁷ Hf ^a	176.943221	18.60	–	–
¹⁷⁹ Hf ^a	178.945816	13.62	–	–
¹⁷⁶ Hf ^a	175.941409	5.26	–	–
¹⁷⁴ Hf ^b	173.940046	0.16	2.0 × 10 ¹⁵ year	α
¹⁸² Hf ^c	181.950554	–	8.9 × 10 ⁶ year	β ⁻
^{178m2} Hf	–	–	31 year	Isomer, γ, 2,446
¹⁷² Hf	171.939448	–	1.87 year	K-capture; γ, 0.28, 0.8
¹⁷⁵ Hf	174.941509	–	70 day	β ⁺
¹⁸¹ Hf	180.949101	–	42.39 day	β ⁻ , 0.408; γ, 0.004, 0.133, 0.136, 0.137, 0.346, 0.473, 0.482, 0.615
^{179m2} Hf	–	–	25.05 day	Isomer, γ, 1.106
¹⁷³ Hf	172.94051	–	23.6 h	β ⁺
¹⁷⁰ Hf	169.93961	–	16.01 h	K-capture
¹⁷¹ Hf	170.94049	–	12.1 h	β ⁺
^{180m1} Hf	–	–	5.47 h	Isomer, γ, 1.141
¹⁸⁴ Hf	183.95545	–	4.12 h	β ⁻
¹⁸³ Hf	182.95353	–	1.067 h	β ⁻
^{182m} Hf	–	–	1.025 min	β ⁻ (58%); Isomer (42%), 1.172
^{177m3} Hf	–	–	51.4 min	Isomer, γ, 2.740

(continued)

Table 3.16 (continued)

Isotope	Mass, u	Abundance, %	Half-life period	Decay mode, excitation (radiation) energy, MeV
¹⁶⁸ Hf	167.94057	–	25.95 min	β^+
¹⁶⁶ Hf	165.94218	–	6.77 min	β^+
¹⁸⁵ Hf	184.95882 (?)	–	3.5 min	β^-
¹⁶⁹ Hf	168.94126	–	3.24 min	β^+
¹⁸⁶ Hf	185.96089 (?)	–	2.6 min	β^-
¹⁶⁷ Hf	166.94260	–	2.05 min	β^+
¹⁶⁴ Hf	163.944367	–	111 s	β^+
¹⁶⁵ Hf	164.94457	–	76 s	β^+
^{184m} Hf	–	–	48 s	Isomer, β^- , 1.272
¹⁶³ Hf	162.94709	–	40.0 s	β^+ , α ($10^{-4}\%$)
¹⁶² Hf	161.94721	–	39.4 s	β^+ (99.99%), α (0.008%)
¹⁸⁷ Hf	186.96459 (?)	–	30 (?) s	?
^{171m} Hf	–	–	29.5 s	Isomer, γ , 0.022
¹⁸⁸ Hf	187.96685 (?)	–	20 (?) s	?
^{179m1} Hf	–	–	18.67 s	Isomer, γ , 0.375
¹⁶¹ Hf	160.950275	–	18.2 s	β^+ (99.7%), α (0.3%)
¹⁶⁰ Hf	159.950684	–	13.6 s	β^+ (99.3%), α (0.7%)
¹⁵⁹ Hf	158.953995	–	5.20 s	β^+ (59%), α (41%)
^{178m1} Hf	–	–	4.0 s	Isomer, γ , 1.147
¹⁵⁸ Hf	157.954799	–	2.84 s	β^+ (55%), α (45%)
¹⁵⁴ Hf	153.96486 (?)	–	2 s	β^+ , α (rare)
^{177m1} Hf	–	–	1.09 s	Isomer, γ , 1.315
¹⁵⁵ Hf	154.96339 (?)	–	890 ms	β^+ , α (rare)
^{153m} Hf	–	–	500 (?) ms	Isomer, γ , 0.750 (?)
¹⁵³ Hf	152.97069 (?)	–	400 (?) ms	?
¹⁵⁷ Hf	156.95840 (?)	–	115 ms	α (86%), β^+ (14%)
¹⁵⁶ Hf	155.95936	–	23 ms	α (97%), β^+ (3%)
^{181m3} Hf	–	–	1.5 ms	Isomer, γ , 1.738
^{156m} Hf	–	–	480 μ s	Isomer, γ , 1.959
^{181m2} Hf	–	–	~100 μ s	Isomer, γ , 1.040
^{180m6} Hf	–	–	90 μ s	Isomer, γ , 3.599
^{181m1} Hf	–	–	80 μ s	Isomer, γ , 0.595
^{178m3} Hf	–	–	68 μ s	Isomer, γ , 2.574
^{177m2} Hf	–	–	55.9 μ s	Isomer, γ , 1.342
^{180m3} Hf	–	–	15 μ s	Isomer, γ , 2.426
^{180m5} Hf	–	–	>10 μ s	Isomer, γ , 2.538
^{180m4} Hf	–	–	10 μ s	Isomer, γ , 2.486
^{174m4} Hf	–	–	3.7 μ s	Isomer, γ , 3.312
^{174m2} Hf	–	–	2.39 μ s	Isomer, γ , 1.798
^{174m3} Hf	–	–	2.39 μ s	Isomer, γ , 1.798
^{180m2} Hf	–	–	0.57 μ s	Isomer, γ , 1.374
^{172m} Hf	–	–	163 ns	Isomer, γ , 2.006
^{174m1} Hf	–	–	138 ns	Isomer, γ , 1.549

^aBelieved to undergo α decay (?)^bPrimordial radionuclide^cBelieved to occur naturally after the α decay of ¹⁸⁶W (?)

Table 3.17 Neutron nuclear physical properties of the isotopes of hafnium [170, 171, 445, 446, 620]

Isotope	Microscopic thermal neutron cross sections ^a , b		Macroscopic thermal neutron cross sections ^a , cm ⁻¹		Resonance integral for neutron capture I_γ , b
	Capture (absorption) σ_a	Scattering ^b σ_s	Capture (absorption) Σ_a	Scattering ^b Σ_s	
Hf ^c	104.1 ± 0.5	10.2 ± 0.4	4.67	0.45	1990 ± 50
¹⁸⁰ Hf	13.04 ± 0.07	22 ± 1	–	–	35 ± 1
¹⁷⁸ Hf	84 ± 4	4.4 ± 0.3	–	–	1950 ± 120
¹⁷⁷ Hf	370 ± 10	0.2 ± 0.2	–	–	7200 ± 200
¹⁷⁹ Hf	41 ± 3	7.1 ± 0.3	–	–	630 ± 30
¹⁷⁶ Hf	24 ± 3	5.5 ± 0.3	–	–	880 ± 40
¹⁷⁴ Hf	549 ± 7	15 ± 3	–	–	440 ± 40

^aFor 2200 m s⁻¹ neutrons^bTotal bound scattering cross sections^cOccurred naturally**Table 3.18** Parameters of formation and migration of lattice point defects (vacancies and interstitial atoms) in near-stoichiometric hafnium monocarbide^a

Defect	Metal sublattice				Non-metal sublattice			
	E_f , eV	E_m , eV	S_f/k_B	S_m/k_B	E_f , eV	E_m , eV	S_f/k_B	S_m/k_B
Vacancy ^b [172, 546]	3.98	3.32	4.38	3.65	1.33	5.32	1.46	5.84
Vacancy ^c [373, 546]	3.67	3.10	4.03	3.41	1.04	3.94	1.14	4.33
Vacancy ^d [334]	9.3	–	–	–	1.1	4.8 ^e	–	–
Vacancy ^f [545]	4.24	–	–	–	–	–	–	–
Di-vacancy ^g [621]	7.30	–	–	–	7.30	–	–	–
Interstitial atom ^b [172]	19.29	0.66	21.20	0.73	5.99	0.66	6.58	0.73

^aDenoted: E_f – defect formation energy, E_m – defect migration energy, S_f – defect formation entropy, S_m – defect migration entropy, k_B – Boltzmann constant^bCalculated on the basis of bonding model (relaxation displacement of atoms surrounding a defect is not taking into account)^cCalculated on the basis of elastic continuum model^d*Ab initio* simulation computed from the largest super-cell on the basis of the PAW pseudopotential using the PBE formulation^eCalculated value of activation energy $E_A = 570$ kJ mol⁻¹ (see also Table 3.23)^fCalculated on the basis of data on the yield strength determined by hardness and elasticity experimental measurements^gCalculated on the basis of PAW within GGA

Nuclear physical properties of hafnium monocarbide HfC_{1-x} in comparison with other ultra-high temperature materials are also given in Addendum.

3.6 Chemical Properties and Materials Design

The information on the chemical properties, compatibility and interaction of hafnium monocarbide HfC_{1-x} at elevated, high and ultra-high temperatures with elements (metals, non-metals) is summarized in Table 3.19, with refractory

Table 3.19 Chemical interaction and/or compatibility of hafnium carbide HfC_{1-x} with elements (metals, non-metals) at elevated, high and ultra-high temperatures, including solid matters and molten media (reaction systems are given mainly in alphabetical order)^a

System	Atmosphere	Temperature range, °C	Interaction character, products and/or compatibility	References
HfC_{1-x} -Al	-	<1000	No chemical interaction in the contact zone; lattice parameter of HfC_{1-x} is invariable	[1, 31, 173, 368,
	-	>1250	The formation of solid solutions (?); lattice parameter of HfC_{1-x} is decreasing slightly	447-449,
	-	1400-2800	Addition of 1% Al does not affect the densification of powdered carbide by hot-pressing	526, 549,
	-	1700	Testing in Al vapours results in the formation of refractory phase impregnated with Al in pores	564]
	-	-	Formation of HfAl_3C_3 , HfAl_4C_4 , $\text{Hf}_2\text{Al}_3\text{C}_4$, $\text{Hf}_2\text{Al}_4\text{C}_5$, $\text{Hf}_3\text{Al}_3\text{C}_5$, $\text{Hf}_3\text{Al}_4\text{C}_6$ and $\text{Hf}_5\text{Al}_3\text{C}$ <i>See also</i> section HfC_{1-x} - Al_4C_3 in Table 3.20 <i>See also</i> Table 3.22 <i>See also</i> section C-Al-Hf in Table I-2.14	
HfC_{1-x} -SiC-Al	-	-	Formation of $\text{Hf}(\text{Al}_{1-x}\text{Si}_x)_4\text{C}_4$, $\text{Hf}_2(\text{Al}_{1-x}\text{Si}_x)_4\text{C}_5$ and $\text{Hf}_3(\text{Al}_{1-x}\text{Si}_x)_4\text{C}_6$ <i>See also</i> section HfC_{1-x} - Al_4C_3 -Si in this table <i>See also</i> section HfC_{1-x} - Al_4C_3 -SiC in Table 3.20	[526]
HfC_{1-x} -SiC-TiC _{1-x} -Al	-	-	Formation of solid solutions $(\text{Ti}_{1-x}\text{Hf}_x)_3(\text{Si}_{1-x}\text{Al}_x)\text{C}_2$ based on Ti_3SiC_2 <i>See also</i> section HfC_{1-x} - Al_4C_3 -SiC-TiC _{1-x} in Table 3.20	[514]
HfC_{1-x} -β-B	-	1400-1500	The max. solubility of B in HfC_{1-x} is ~6 mol.% (?)	[31, 194,
	-	1500	Intensive interaction (small mass loss) with the formation of $\text{HfB}_{2\pm x}$ <i>See also</i> section C-B-Hf in Table I-2.14	527, 571]
HfC_{1-x} -Be	-	-	The effect of Be as an additive for hot-pressing process was studied <i>See</i> Table 3.22	[31]
HfC_{1-x} -Bi	-	-		
HfC_{1-x} -C	-	~3100-3280	Eutectic HfC_{1-x} -C (graphite)	[4, 12, 17, 22, 201, 343, 344, 518, 536]
HfC_{1-x} -C-Fe	-	-	<i>See also</i> section C-Hf in Table I-2.13 <i>See</i> Table 3.22	
HfC_{1-x} -C-Fe-Mn	-	-	<i>See</i> Table 3.22	

(continued)

Table 3.19 (continued)

System	Atmosphere	Temperature range, °C	Interaction character, products and/or compatibility	References
HfC _{1-x} -Cd	-	450	No chemical interaction	[368]
HfC _{1-x} - α/ϵ -Co	-	~1370-1420	Eutectic HfC _{1-x} - α -Co	[1, 13, 31,
	-	1500	The contact zone between bulk HfC _{1-x} and metallic Co includes eutectic alloy	35, 204,
	-	-	Addition of 1% Co intensifies the densification of powdered carbide by hot-pressing	455, 532]
			<i>See also</i> Table 3.22	
			<i>See also</i> section C-Co-Hf in Table I-2.14	
HfC _{1-x} -NbC _{1-x} -Co	-	~1360-1435	Eutectic (Hf,Nb)C _{1-x} ($x = 0.06-0.18$)- α -Co	[174]
			<i>See also</i> section C-Co-Hf-Nb in Table I-2.14	
HfC _{1-x} -TaC _{1-x} -Co			<i>See</i> section TaC _{1-x} -HfC _{1-x} -Co in Table 2.21	
			<i>See also</i> section C-Co-Hf-Ta in Table I-2.14	
HfC _{1-x} -TaC _{1-x} -TiC _{1-x} - δ -TiN _{1\pmx} - δ -WC _{1\pmx} - β -Mo _{2\pmx} C-Co			<i>See</i> section TaC _{1-x} -HfC _{1-x} -TiC _{1-x} - δ -TiN _{1\pmx} - δ -WC _{1\pmx} - β -Mo _{2\pmx} C-Co in Table 2.21	
HfC _{1-x} -TiC _{1-x} -Co	-	1370	Eutectic (Hf,Ti)C _{1-x} ($x = 0.06$)-(Ti,Hf)C _{1-x} ($x = 0.20$)- α -Co	[175]
			<i>See also</i> section C-Co-Hf-Ti in Table I-2.14	
HfC _{1-x} -VC _{1-x} -Co	-	1320	Eutectic (Hf,V)C _{1-x} ($x = 0.06$)-(V,Hf)C _{1-x} ($x = 0.17$)- α -Co	[175]
			<i>See also</i> section C-Co-Hf-V in Table I-2.14	
HfC _{1-x} -ZrC _{1-x} -Co	-	~1380-1435	Eutectic (Hf,Zr)C _{1-x} ($x = 0.06-0.19$)- α -Co	[174]
			<i>See also</i> section C-Co-Hf-Zr in Table I-2.14	
HfC _{1-x} -Cr	Ar	1790-1830	Eutectic HfC _{1-x} -Cr; the max. solubility of Cr in HfC _{1-x} is ~9 mol.% and that of HfC _{1-x} in Cr is ~1 mol.%	[1, 13,
	-	-	Stable and compatible with each other as cermet components	176, 204,
			<i>See also</i> section C-Cr-Hf in Table I-2.14	504, 552]
HfC _{1-x} -Cs	Cs vapour, ~13 Pa	~2000	No chemical reaction observed, no effect upon structural characteristics of HfC _{1-x} and its thermionic emission parameters (some tens of hours exposure)	[119, 339]
HfC _{1-x} -Cu			<i>See</i> Table 3.22	
HfC _{1-x} -Cu-Hf			<i>See</i> Table 3.22	
HfC _{1-x} -Cu-Hf-V			<i>See</i> Table 3.22	

(continued)

Table 3.19 (continued)

System	Atmosphere	Temperature range, °C	Interaction character, products and/or compatibility	References
HfC _{1-x} - $\alpha/\gamma/\delta$ -Fe	-	~1410–1490	Eutectic HfC _{1-x} - δ -Fe; the max. solubility of HfC _{1-x} in δ -Fe is ≤ 0.3 mol.%	[1, 13, 31, 35, 204,
	-	1550	The contact zone between bulk HfC _{1-x} and metallic Fe includes eutectic alloy	205, 464,
	-	-	DFT calculated semicoherent interfacial energy at relaxed interface -0.95 J m ⁻² <i>See also</i> Table 3.22 <i>See also</i> section C-Fe-Hf in Table I-2.14 <i>See</i> Table 3.22	532, 554]
HfC _{1-x} -Fe-Mn			<i>See</i> Table 3.22	
HfC _{1-x} -Ga			<i>See</i> Table 3.22	
HfC _{1-x} -Ge			<i>See</i> Table 3.22	
HfC _{1-x} - α/β -Hf	-	~2240–2360	Peritectic α -Hf (in equilibrium with HfC _{0.52})	[8–11, 31, 204]
			<i>See also</i> section C-Hf in Table I-2.13	
HfC _{1-x} -In	-	-	Formation of Hf ₂ InC ($M_{n+1}AX_n$ -phase)	[177, 178, 628]
			<i>See also</i> Table 3.22 <i>See also</i> section C-Hf-In in Table I-2.14	
HfC _{1-x} -TiC _{1-x} -In	-	-	Formation of (Hf,Ti) ₂ InC _{1+x} ($M_{n+1}AX_n$ -phase solid solution); (Hf _{0.5} Ti _{0.5})InC and (Hf _{0.53} Ti _{0.47})InC _{1.26} were synthesized	[177, 178, 529–531]
			<i>See also</i> section C-Hf-In-Ti in Table I-2.14	
HfC _{1-x} -Ir	-	1650–1930	Near-stoichiometric HfC _{1-x} reacts with Ir to form HfIr _{3+x} ($x \approx 0$) containing C deposits of varying morphology: large widely spaced at lower temperatures and smaller in size uniformly dispersed at higher temperatures	[13, 202]
			<i>See also</i> section C-Hf-In in Table I-2.14	
HfC _{1-x} -K	-	~2000	No chemical reaction observed, no effect upon structural characteristics of HfC _{1-x} and its thermionic emission parameters (some tens of hours exposure)	[119, 339]
HfC _{1-x} -Li	-	-	HfC _{1-x} is highly resistant to Li liquid environments	[393, 394]
HfC _{1-x} - $\alpha/\beta/\gamma/\delta$ -Mn	-	-	Intensive interaction; the formation of eutectic alloy and solid solutions	[1, 31, 341]
	-	-	Formation of metastable Mn ₃ Hf ₅ C (η -carbide type, ?)	
	-	-	The effect of Mn as an additive for hot-pressing process was studied <i>See also</i> Table 3.22 <i>See also</i> section C-Hf-Mn in Table I-2.14	

(continued)

Table 3.19 (continued)

System	Atmo- sphere	Temperature range, °C	Interaction character, products and/or compatibility	References
HfC _{1-x} -Mo	-	1250	The max. solubility of HfC _{1-x} in Mo is 0.25 mol.% (?)	[1, 13, 31, 53, 179-
	-	1500-2200	Formation of solid solutions (exposure 5 h)	182, 186,
	Vacuum	≥1800	The initiation of reaction between powdered HfC _{1-x} and compact dense Mo (exposure 5 h)	195, 204,
	-	2000-2200	Noticeable solid state interaction between bulk and dense materials	342, 552,
	-	2100	The max. solubility of HfC _{1-x} in Mo is 0.4 mol.%	569, 570]
	-	-	Stable and compatible with each other as cermet components	
	-	~2310-2370	Eutectic HfC _{1-x} -Mo; the max. solubility of Mo in HfC _{1-x} is ≥15 mol.% and that of HfC _{1-x} in Mo is 1.6 mol.% <i>See also</i> Table 3.22 <i>See also</i> section C-Hf-Mo in Table I-2.14	
HfC _{1-x} -Mo-Ni	Vacuum, 0.01-0.1 Pa	1450	The contact interaction of compact dense HfC _{1-x} (x = 0.05) with Ni-25% Mo melt leads to the preferential dissolution of C; after cooling the isolations based on β-Mo _{2±x} C (hexagonal) phase, surrounded by metal-semi-carbide eutectics, are formed in the metallic melt based on Ni (Hf content ≤2%) in parallel with Ni-HfNi ₅ eutectics	[624]
HfC _{1-x} -TiC _{1-x} -Mo-Ni	Vacuum, 0.01-0.1 Pa	1450	The interaction of Hf _{0.21} Ti _{0.79} C _{0.95} phase with Ni-25% Mo melt is characterized by preferential dissolution of C and subsequent precipitation of Hf _{0.01} Ti _{0.50} Mo _{0.50} C _{1-x} (from the melt saturated with Hf, Ti and C); after cooling the solidified Ni-HfNi ₅ eutectics was revealed	[624]
HfC _{1-x} -TiC _{1-x} -δ-TiN _{1±x} -Mo-Ni	Vacuum, 0.01-0.1 Pa	1450	The interaction of Hf _{0.20} Ti _{0.80} C _{0.75} N _{0.24} phase with molten Ni-20% Mo alloy leads to the accelerated incongruent dissolution of the components, preferentially - C and Hf, up to Hf _{0.07} Ti _{0.93} C _{0.20} N _{0.80} ; the metallic melts have a hypereutectic structure with primary precipitates of Hf _{0.02} Ti _{0.50} Mo _{0.48} (C,N) _{1-x} and Hf _{0.68} Ti _{0.14} Mo _{0.18} (C,N) _{1-x} in eutectics matrix	[623]
HfC _{1-x} -Nb	Vacuum	1000-1400	No interaction between powdered HfC _{1-x} and compact dense Nb	[1, 13, 31,
	Vacuum	1400-2200	The formation of solid solutions	53, 195,
	Vacuum	≥1400	The initiation of reaction between powdered HfC _{1-x} and compact dense Nb with the formation of solid solutions (Hf,Nb)C _{1-x} and non-combined C (exposure 5 h) <i>See also</i> section C-Hf-Nb in Table I-2.14	204]

(continued)

Table 3.19 (continued)

System	Atmo- sphere	Temperature range, °C	Interaction character, products and/or compatibility	References
HfC _{1-x} -Ni	Ar	1180–1215	Formation of a liquid phase in the powdered mixture (mean grain size ~ 50 μm) of the components	[1, 13, 31, 35, 183–185, 204, 450, 458–460, 532]
	–	~1310–1360	Eutectic HfC _{1-x} -Ni; the max. solubility of HfC _{1-x} in Ni is ≤0.7–1.0 mol.% and that of Ni in HfC _{1-x} is ~7.5 mol.%	
	–	1450	The contact zone between HfC _{1-x} and Ni includes eutectic alloy; carbide solid solutions are formed <i>See also</i> Table 3.22 <i>See also</i> section C-Hf-Ni in Table I-2.14	
HfC _{1-x} - β-Mo _{2±x} C-Ni	–	~1200–1240	Eutectic (Hf,Mo)C _{1-x} -β-(Mo,Hf) _{2±x} C-Ni <i>See also</i> section C-Hf-Mo-Ni in Table I-2.14 <i>See</i> section TaC _{1-x} -HfC _{1-x} -TiC _{1-x} - δ-TiN _{1±x} -Ni in Table 2.21	[218]
HfC _{1-x} -TaC _{1-x} - TiC _{1-x} - δ-TiN _{1±x} -Ni				
HfC _{1-x} -TaC _{1-x} - TiC _{1-x} - δ-TiN _{1±x} - δ-WC _{1±x} - β-Mo _{2±x} C-Ni			<i>See</i> section TaC _{1-x} -HfC _{1-x} -TiC _{1-x} - δ-TiN _{1±x} -δ-WC _{1±x} -β-Mo _{2±x} C-Ni in Table 2.21	
HfC _{1-x} -TiC _{1-x} - Ni	–	~1205–1235	Eutectic (Hf,Ti)C _{1-x} -(Ti,Hf)C _{1-x} -Ni (cast alloys show a tendency to crystallization in metastable state when the carbide phase does not decompose into two solid solutions)	[183, 451, 458–460, 624]
	Vacuum, 0.01–0.1 Pa	1450	Hf _{0,20} Ti _{0,80} C _{0,95} phase has higher dissolution rate in molten Ni; preferentially C and Hf are transferred into the melt, when attaining composition Hf _{0,05} Ti _{0,95} C _{<0,95} the dissolution becomes congruent <i>See also</i> section C-Hf-Ni-Ti in Table I-2.14	
HfC _{1-x} -TiC _{1-x} - Ni-Mo	Vacuum, 0.05 Pa	1450	The interaction of Hf _{0,20} Ti _{0,80} C _{0,96} phase with Ni–20% Mo melt is characterized by preferential dissolution of C and subsequent precipitation of Hf _{0,01} Ti _{–0,60} Mo _{–0,40} C _{1-x} (from the melt saturated with Hf, Ti and C)	[461, 624]
HfC _{1-x} -TiC _{1-x} - δ-TiN _{1±x} -Ni	Vacuum, 0.1–0.01 Pa	1450	The interaction of Hf _{0,20} Ti _{0,80} C _{0,75} N _{0,24} phase with molten Ni leads to the incongruent dissolution of the components, preferentially – C and Hf, and simultaneous decomposition of the initial phase with the formation of isolated Hf _{0,10} Ti _{0,90} (C,N) _{1-x} and Hf _{0,55} Ti _{0,45} (C,N) _{1-x} ; the metallic melts have a hypoeutectic structure with primary precipitates of Ni based phase and ternary eutectics (one of its constituents is Hf _{0,75} Ti _{0,25} (C,N) _{1-x})	[189, 227, 510, 553, 623]
	Vacuum	1450–1500	The interaction of (Hf,Ti)C _{0,60–0,70} N _{0,30–0,40} carbonitride phases with Ni is considered	

(continued)

Table 3.19 (continued)

System	Atmosphere	Temperature range, °C	Interaction character, products and/or compatibility	References
HfC _{1-x} -TiC _{1-x} - δ -TiN _{1±x} - δ -WC _{1±x} -Ni	Vacuum	1450–1500	The interaction of (Hf,Ti,W)C _{0.70} N _{0.30} carbonitride phase with Ni is considered	[510, 517]
HfC _{1-x} - δ -WC _{1±x} -Ni	–	~1000	Eutectic (Hf,W)C _{1-x} - δ -(W,Hf)C _{1±x} -Ni	[184]
			<i>See also</i> section C–Hf–Ni–W in Table I-2.14	
HfC _{1-x} -ZrC _{1-x} -Ni	Vacuum	1000	The max. solid solubility of (Zr,Hf)C _{1-x} in Ni is ≤ 1 mol.%	[185, 573]
	–	~1130–1330	Eutectic (Zr,Hf)C _{1-x} ($x = 0.02$ – 0.17)-Ni; the minimum on the line of eutectic solidification is 100–150 °C lower than the eutectic temperatures in ZrC _{1-x} -Ni and HfC _{1-x} -Ni systems	
			<i>See also</i> section C–Hf–Ni–Zr in Table I-2.14	
HfC _{1-x} -Os	–	–	The mutual solubilities of the components are low	[13]
			<i>See also</i> section C–Hf–Os in Table I-2.14	
HfC _{1-x} -Pb	–	450	No chemical interaction	[177, 178, 368]
	–	–	Formation of Hf ₂ PbC ($M_{n+1}AX_n$ -phase)	
			<i>See also</i> Table 3.22	
			<i>See also</i> section C–Hf–Pb in Table I-2.14	
HfC _{1-x} -Pd			<i>See</i> section C–Hf–Pd in Table I-2.14	
HfC _{1-x} -Pt			<i>See</i> section C–Hf–Pt in Table I-2.14	
HfC _{1-x} -Re	–	2000–2200	The max. solubility of Re in HfC _{1-x} is 2 mol.%	[1, 13, 186, 199, 200, 204, 346, 552]
	He	2500	No interaction in the contact zone between the compact dense materials (exposure 1 h)	
	–	2600	The max. solubility of Re in HfC _{1-x} is 4 mol.%	
	–	–	Stable and compatible with each other as cermet components	
	–	2690–2750	Eutectic HfC _{1-x} -Re; the max. solid solubility of Re in HfC _{1-x} is ~4–5 mol.% and that of HfC _{1-x} in Re is also low	
			<i>See also</i> section C–Hf–Re in Table I-2.14	
HfC _{1-x} -Rh	–	–	No solubility of Rh in HfC _{1-x}	[13]
			<i>See also</i> section C–Hf–Rh in Table I-2.14	
HfC _{1-x} -Ru	–	~2000	Eutectic HfC _{1-x} -Ru	[13]
			<i>See also</i> section C–Hf–Ru in Table I-2.14	
HfC _{1-x} -S	–	–	Formation of Hf ₂ SC ($M_{n+1}AX_n$ -phase)	[177, 178]
			<i>See also</i> section C–Hf–S in Table I-2.14	
HfC _{1-x} -Sb			<i>See</i> Table 3.22	
HfC _{1-x} -Si	–	≥ 1500	Intensive interaction; formation of SiC and Hf silicides (or ternary phases ?)	[1, 12, 31, 187, 188, 368]
			<i>See also</i> Table 3.22	
			<i>See also</i> section C–Hf–Si in Table I-2.14	

(continued)

Table 3.19 (continued)

System	Atmosphere	Temperature range, °C	Interaction character, products and/or compatibility	References
HfC _{1-x} -Al ₄ C ₃ -Si	-	-	Formation of Hf(Al _{1-x} Si _x) ₄ C ₄ , Hf ₂ (Al _{1-x} Si _x) ₄ C ₅ and Hf ₃ (Al _{1-x} Si _x) ₄ C ₆ <i>See also</i> section HfC _{1-x} -SiC-Al in this table <i>See also</i> section HfC _{1-x} -Al ₄ C ₃ -SiC in Table 3.20	[526]
HfC _{1-x} -Sn	-	350	No interaction	[177, 178,
	-	-	Formation of Hf ₂ SnC (M _{n+1} AX _n -phase) <i>See also</i> Table 3.22 <i>See also</i> section C-Hf-Sn in Table I-2.14	368, 627]
HfC _{1-x} -Ta	Vacuum	1000-1400	No interaction between powdered HfC _{1-x} and compact dense Ta	[1, 12, 13,
	Vacuum	1400-2200	Powdered HfC _{1-x} interacts with compact dense Ta slightly	31, 53,
	Vacuum	≥1400	The initiation of reaction between powdered HfC _{1-x} and compact dense Ta (exposure 5 h) <i>See also</i> section C-Hf-Ta in Table I-2.14	189, 195-197, 542]
HfC _{1-x} -Tc			<i>See</i> section C-Hf-Tc in Table I-2.14	
HfC _{1-x} -Th			<i>See</i> section C-Hf-Th in Table I-2.14	
HfC _{1-x} -Ti			<i>See</i> section C-Hf-Ti in Table I-2.14	
HfC _{1-x} -Tl	-	-	Formation of Hf ₂ TlC (M _{n+1} AX _n -phase) <i>See also</i> Table 3.22 <i>See also</i> section C-Hf-Tl in Table I-2.14	[177, 178]
HfC _{1-x} -U			<i>See</i> section C-Hf-U in Table I-2.14	
HfC _{1-x} -V	-	-	Stable and compatible with each other as cermet components <i>See also</i> section C-Hf-V in Table I-2.14	[552]
HfC _{1-x} -W	-	1000-1700	No interaction between powdered HfC _{1-x} and compact dense W	[1, 13, 31,
	-	1700-2200	The interaction between powdered HfC _{1-x} and compact dense W leads to the formation of new phases	53, 186,
	Vacuum	≥2000	The initiation of reaction between powdered HfC _{1-x} and compact dense W (exposure 5 h)	190, 191,
	-	-	Stable and compatible with each other as cermet components	195, 198,
	-	2790-2930	Eutectic HfC _{1-x} -W; the solubility of W in HfC _{1-x} is ~11 mol.% and that of HfC _{1-x} in W is ~1-3 mol.% <i>See also</i> section C-Hf-W in Table I-2.14	552]
HfC _{1-x} -Zn	-	550	No interaction	[368]
HfC _{1-x} -α/β-Zr	-	~2000	HfC _{1-x} is wetted readily by the molten Zr, which flows easily and reacts strongly on/with the carbide surface	[13, 192,
		2030	Eutectic (Hf,Zr)C _{1-x} -β-(Zr,Hf)-α-(Hf,Zr) <i>See also</i> section C-Hf-Zr in Table I-2.14	193, 203]

^aThe parameters of wettability of hafnium carbide HfC_{1-x} by liquid metals are listed in Table 3.22

Table 3.20 Chemical interaction and/or compatibility of hafnium carbide HfC_{1-x} with refractory compounds at elevated, high and ultra-high temperatures (reaction systems are given mainly in alphabetical order)

System	Atmosphere	Temperature range, °C	Interaction character, products and/or compatibility	References
$\text{HfC}_{1-x}\text{-Al}_4\text{C}_3$	–	–	Formation of $n\text{HfC} \cdot m\text{Al}_4\text{C}_3$ compounds: HfAl_4C_4 , $\text{Hf}_2\text{Al}_3\text{C}_4$, $\text{Hf}_2\text{Al}_4\text{C}_5$, $\text{Hf}_3\text{Al}_3\text{C}_5$, $\text{Hf}_3\text{Al}_4\text{C}_6$, HfAl_8C_7 and $\text{Hf}_3\text{Al}_8\text{C}_9$ <i>See also</i> section $\text{HfC}_{1-x}\text{-Al}$ in Table 3.19 <i>See also</i> section C-Al-Hf in Table I-2.14	[513, 526, 549, 564]
$\text{HfC}_{1-x}\text{-Al}_4\text{C}_3\text{-SiC}$	–	–	Formation of $\text{Hf}(\text{Al}_{1-x}\text{Si}_x)_4\text{C}_4$, $\text{Hf}_2(\text{Al}_{1-x}\text{Si}_x)_4\text{C}_5$ and $\text{Hf}_3(\text{Al}_{1-x}\text{Si}_x)_4\text{C}_6$ <i>See also</i> section $\text{HfC}_{1-x}\text{-SiC-Al}$ in Table 3.19 <i>See also</i> section $\text{HfC}_{1-x}\text{-Al}_4\text{C}_3\text{-Si}$ in Table 3.19	[526, 549]
$\text{HfC}_{1-x}\text{-Al}_4\text{C}_3\text{-SiC-TiC}_{1-x}$	–	–	Formation of solid solutions $(\text{Ti}_{1-x}\text{Hf}_x)_3(\text{Si}_{1-x}\text{Al}_x)_2\text{C}_2$ based on Ti_3SiC_2 <i>See also</i> section $\text{HfC}_{1-x}\text{-SiC-TiC}_{1-x}\text{-Al}$ in Table 3.19	[514]
$\text{HfC}_{1-x}\text{-Al}_4\text{C}_3\text{-YC}_{1\pm x}/\beta\text{-YC}_{2\pm x}$	–	–	Formation of $(\text{Hf,Y})\text{Al}_4\text{C}_4$, $(\text{Hf,Y})_2\text{Al}_4\text{C}_5$, $(\text{Hf,Y})_3\text{Al}_4\text{C}_6$, $(\text{Hf,Y})\text{Al}_8\text{C}_7$ and $(\text{Hf,Y})_3\text{Al}_8\text{C}_9$ is proposed	[513]
$\text{HfC}_{1-x}\text{-B}_{4\pm x}\text{C}$	–	>1800 (?)	Formation of $\text{HfB}_{2\pm x}$ <i>See also</i> section C-B-Hf in Table I-2.14	[206–209, 571]
$\text{HfC}_{1-x}\text{-}\alpha\text{-BN}$	–	–	Formation of $\text{HfB}_{2\pm x}$	[210, 211]
$\text{HfC}_{1-x}\text{-CeN}_{1\pm x}$	–	–	Terminal mutual solid solubilities between the components (?)	[31]
$\text{HfC}_{1-x}\text{-CeP}_{1\pm x}$	–	–	Terminal mutual solid solubilities between the components (?)	[31]
$\text{HfC}_{1-x}\text{-CeS}_{1\pm x}$	–	–	Terminal mutual solid solubilities between the components (?)	[31]
$\text{HfC}_{1-x}\text{-Cr}_3\text{C}_{2-x}$	–	–	The max. solubility of “imaginary” phase ‘ CrC_{1-x} ’ in HfC_{1-x} is ~9 mol.% and that of HfC_{1-x} in $\text{Cr}_3\text{C}_{2-x}$ is very low (?) <i>See also</i> section C-Cr-Hf in Table I-2.14	[13, 31, 176, 236, 341]
$\text{HfC}_{1-x}\text{-Cr}_3\text{C}_{2-x}\text{-}\beta\text{-Mo}_{2\pm x}\text{C-}\delta\text{-TiN}_{1\pm x}\text{-}\delta\text{-WC}_{1\pm x}$	Vacuum	1350–1600	Powdered $\text{TiC}_{1-x}\text{-15% } \delta\text{-TiN}_{1\pm x}\text{-25% } \delta\text{-WC}_{1\pm x}\text{-8% HfC}_{1-x}\text{-8% Cr}_3\text{C}_{2-x}\text{-4% } \beta\text{-Mo}_{2\pm x}\text{C}$ composition was heat-treated to prepare sintered materials	[630, 631]
$\text{HfC}_{1-x}\text{-DyN}_{1\pm x}$	–	–	Monocarbonitride (cubic) continuous solid solution (complete solubility in the system?)	[31]
$\text{HfC}_{1-x}\text{-ErN}_{1\pm x}$	–	–	Monocarbonitride (cubic) continuous solid solution (complete solubility in the system?)	[31]

(continued)

Table 3.20 (continued)

System	Atmosphere	Temperature range, °C	Interaction character, products and/or compatibility	References
HfC _{1-x} -EuN _{1±x}	-	-	Monocarbonitride (cubic) continuous solid solution (complete solubility in the system?)	[31]
HfC _{1-x} -EuO	-	-	Terminal mutual solid solubilities between the components (?)	[31]
HfC _{1-x} -Fe ₂ O ₃	-	800	The interaction initiates with the formation of α-Fe (traces)	[289]
		900	Formation of α-HfO _{2-x} and α-Fe (both in trace amounts)	
HfC _{1-x} -Fe ₃ C	-	-	Not (or very slightly) soluble in each other in solid state <i>See also</i> section C-Fe-Hf in Table I-2.14	[13, 341]
HfC _{1-x} -GdN _{1±x}	-	-	Monocarbonitride (cubic) continuous solid solution (complete solubility in the system?)	[31]
HfC _{1-x} -HfB _{1±x}	-	1500	Mutual solubilities of the components are ~5-7 mol.% <i>See also</i> section C-B-Hf in Table I-2.14	[31, 194, 207-209]
HfC _{1-x} -HfB _{2±x}	-	~3110-3140	Eutectic HfC _{1-x} -HfB _{2±x} ; the max. solid solubility of HfC _{1-x} in HfB _{2±x} is <2 mol.% and that of HfB _{2±x} in HfC _{1-x} is ~10 mol.% <i>See also</i> section C-B-Hf in Table I-2.14	[12, 13, 31, 130, 194, 207-209, 571]
HfC _{1-x} -HfN _{1±x}	-	1150	Monocarbonitride (cubic) continuous solid solution (HfC _x N _z , 0.6 ≤ x + z ≤ 1) within the homogeneity range: ~HfC _{0.60} -HfN _{0.72} -HfN _{1.0} -HfC _{0.98}	[1, 13, 31, 40, 223, 388, 407, 439, 441, 581, 629, 638]
		~2000	Monocarbonitride (cubic) continuous solid solution (HfC _x N _z , 0.6 ≤ x + z ≤ 1); (complete solubility in the system, the variation of lattice parameter <i>a</i> , nm with composition for Hf(C _{1-x} N _x) phases (0 ≤ x ≤ 1) is linear: <i>a</i> = 0.4640 - 0.0122 <i>x</i>) <i>See also</i> section C-Hf-N in Table I-2.14	
HfC _{1-x} -HfN _{1±x} -'HfO'	-	1600	Formation of HfC _{1-x} N _y O _z oxycarbonitride (cubic) phase ^a based on of HfC _{1-x} -HfN _{1±x} continuous solid solution with homogeneity limits: HfC _{0.75} O _{0.25} -HfN _{0.80} O _{0.20}	[28, 40, 388, 406, 408, 439]
		2000	Formation of HfC _{1-x} N _y O _z oxycarbonitride (cubic) phase based on of HfC _{1-x} -HfN _{1±x} continuous solid solution with homogeneity limits: HfC _{0.70} O _{0.30} -HfN _{0.75} O _{0.25} <i>See also</i> section C-Hf-N-O in Table I-2.14	

(continued)

Table 3.20 (continued)

System	Atmosphere	Temperature range, °C	Interaction character, products and/or compatibility	References
HfC _{1-x} - α/β -HfO _{2-x}	Vacuum	1000–2000	No noticeable interaction between the components (exposure 1 h)	[1, 17, 40, 213, 226, 388, 402–406, 439, 453, 471, 506, 507, 516, 523, 538, 619]
	1.0 Pa	1470–1730	Formation of HfC _{0.93–0.97} O _{0.04–0.07} oxycarbide (cubic) phase	
	CO, 9–133 kPa	1900	Formation of HfC _{1-x} O _y (HfC _{1-x} -‘HfO’ oxycarbide (cubic) solid solution) with the homogeneity range ~HfC _{0.75} O _{0.25} -HfC _{0.55} -HfC _{0.99}	
	Vacuum, CO	1900–2500	Formation of oxycarbide (cubic) phase HfC _{0.49–0.76} O _{0.07–0.33} (0.70 ≤ 1-x+y ≤ 1.03) <i>See also</i> section C-Hf-O in Table I-2.14	
HfC _{1-x} -HoN _{1±x}	–	–	Monocarbonitride (cubic) continuous solid solution (complete solubility in the system, ?)	[31]
HfC _{1-x} -LaN _{1±x}	–	–	Terminal mutual solid solubilities between the components (?)	[31]
HfC _{1-x} -LaP _{1±x}	–	–	Terminal mutual solid solubilities between the components (?)	[31]
HfC _{1-x} -LaS _{1-x}	–	–	Terminal mutual solid solubilities between the components (?)	[31]
HfC _{1-x} -LuN _{1±x}	–	–	Monocarbonitride (cubic) continuous solid solution (complete solubility in the system?)	[31]
HfC _{1-x} -MgO	Vacuum	<2000	No interaction	[1, 31, 35, 212, 213, 289]
	1.0 Pa	2200	The initiation of reaction between powdered HfC _{1-x} and compact dense MgO (exposure 1 h); microhardness of MgO declines	
HfC _{1-x} -Mn ₅ C ₂ , Mn ₇ C ₃	–	–	Not (or very slightly) soluble in each other in solid state <i>See also</i> section C-Hf-Mn in Table I-2.14	[341]
HfC _{1-x} - α -MoC _{1-x}	–	1400	Extended solid solution based on HfC _{1-x} with the homogeneity range from HfC _{0.56–0.99} to (Hf _{0.15} Mo _{0.85})C _{0.72–0.77}	[13, 31, 181, 214–216, 236, 341]
	–	~1400–1700	The max. solubility of HfC _{1-x} in α -MoC _{1-x} corresponds to compos. (Mo _{0.93–0.95} Hf _{0.05–0.07})C _{0.65–0.70} (the presence of Hf stabilizes α -MoC _{1-x})	
	–	~1700	Extended solid solution based on HfC _{1-x} with the homogeneity range from HfC _{0.54–0.99} to (Hf _{0.11} Mo _{0.89})C _{0.72–0.77}	
	–	>1700–2000	Monocarbide (cubic) continuous solid solution with the homogeneity range from HfC _{0.54–0.99} to MoC _{0.64–0.71} (the max. C content in the mixed monocarbide phase (Hf,Mo)C _{1-x} increases as Hf substitutes for Mo) <i>See also</i> section C-Hf-Mo in Table I-2.14	

(continued)

Table 3.20 (continued)

System	Atmosphere	Temperature range, °C	Interaction character, products and/or compatibility	References
HfC _{1-x} - α-MoC _{1-x} - TiC _{1-x}	-	1500–1650	Large miscibility gap connects the TiC _{1-x} - HfC _{1-x} and HfC _{1-x} -α-MoC _{1-x} boundary systems; addition of Mo to the TiC _{1-x} -HfC _{1-x} solid solution decreases the critical miscibility temp., while addition of Ti to HfC _{1-x} - α-MoC _{1-x} solid solution raises the critical temperature (no-maximum type ternary critical point) <i>See also</i> section C–Hf–Mo–Ti in Table I-2.14	[221]
HfC _{1-x} - α-MoC _{1-x} - VC _{1-x}	-	1500	Great miscibility gap between the VC _{1-x} - HfC _{1-x} and HfC _{1-x} -α-MoC _{1-x} boundary systems	[222]
	-	1500–2750	Addition of V to the HfC _{1-x} -α-MoC _{1-x} solid solution increases the critical miscibility temperature <i>See also</i> section C–Hf–Mo–V in Table I-2.14	
HfC _{1-x} - η-MoC _{1-x}	-	1700	The max. solubility of HfC _{1-x} in η-MoC _{1-x} is ~6 mol.% <i>See also</i> section C–Hf–Mo in Table I-2.14	[13, 181]
HfC _{1-x} - β-Mo _{2±x} C	-	1400–2000	The max. solubility of HfC _{1-x} in β-Mo _{2±x} C corresponds to compos. (Mo _{0.9} Hf _{0.1})C _{0.475–0.50} <i>See also</i> section C–Hf–Mo in Table I-2.14	[13, 31, 181, 236]
HfC _{1-x} -MoSi ₂	Ar	1900–1950	Interaction in powder mixtures leads to the formation of (Mo,Hf) ₅ Si _{3±x} and SiC <i>See also</i> section C–Hf–Mo–Si in Table I-2.14	[219, 220, 543, 634]
HfC _{1-x} -NbC _{1-x}	-	1200–2050	Monocarbide (cubic) continuous solid solution (complete solubility in the system) <i>See also</i> section C–Hf–Nb in Table I-2.14	[1, 13, 31, 224, 225, 341, 462, 503, 572, 632]
HfC _{1-x} - β-Nb _{2+x} C	-	1200–2050	The max. solubility of Hf in β-Nb _{2+x} C is ~5 at.% <i>See also</i> section C–Hf–Nb in Table I-2.14	[13, 31, 225]
HfC _{1-x} -NbC _{1-x} - TaC _{1-x}	-		<i>See</i> section TaC _{1-x} -HfC _{1-x} -NbC _{1-x} in Table 2.22	
HfC _{1-x} -NbC _{1-x} - ThC _{1±x}	-	>2000	Terminal solid solution based on HfC _{1-x} - NbC _{1-x} monocarbide (cubic) continuous solid solution; the solubilities of ThC _{1±x} in HfC _{1-x} and NbC _{1-x} are <5 mol.% (solubilities of HfC _{1-x} and NbC _{1-x} in ThC _{1±x} are very low)	[31]
HfC _{1-x} -NbC _{1-x} - TiC _{1-x}	-	1900–2000	Monocarbide (cubic) continuous solid solution (complete solubility in the system)	[31, 338]
HfC _{1-x} -NbC _{1-x} - UC _{1±x}	-	1900–2050	Monocarbide (cubic) continuous solid solutions with the small miscibility gap limited by ~ $(\text{Hf}_{0.4}\text{U}_{0.6})\text{C}_{1\pm x}$ ~ $(\text{Hf}_{0.75}\text{U}_{0.25})\text{C}_{1-x}$ ~ $(\text{Hf}_{0.5}\text{Nb}_{0.15-0.20}\text{U}_{0.3})\text{C}_{1-x}$ compositions <i>See also</i> section C–Hf–Nb–U in Table I-2.14	[13, 31, 338, 341]

(continued)

Table 3.20 (continued)

System	Atmo- sphere	Temperature range, °C	Interaction character, products and/or compatibility	References
HfC _{1-x} -NbC _{1-x} -VC _{1-x}	-	1900–2050	Monocarbide continuous solid solution with the miscibility gap limited by compos. ~(Hf _{0.98} V _{0.02})C _{1-x} - ~(Hf _{0.03} V _{0.97})C _{1-x} - ~(Hf _{0.2-0.3} Nb _{0.51-0.52} V _{0.2-0.3})C _{1-x} <i>See also</i> section C-Hf-Nb-V in Table I-2.14	[31, 224, 338]
HfC _{1-x} -NbC _{1-x} -δ-WC _{1±x}	-	1900–2000	The max. solid solubility of δ-WC _{1±x} in HfC _{1-x} -NbC _{1-x} monocarbide (cubic) continuous solid solution corresponds to ~(Hf _{0.6} W _{0.4})C _{1-x} and ~(Nb _{0.7} W _{0.3})C _{1-x} compositions; practically, no solubility of HfC _{1-x} and NbC _{1-x} in δ-WC _{1±x}	[31, 338]
HfC _{1-x} -NbC _{1-x} -ZrC _{1-x}	-	1900–2000	Monocarbide (cubic) continuous solid solution (complete solubility in the system)	[31, 338, 341]
HfC _{1-x} -NbC _{1-x} -δ-NbN _{1-x}	Pure N ₂	1200–2500	Monocarbonitride (cubic) continuous solid solution (complete solubility in the system)	[629]
HfC _{1-x} - δ-NbN _{1-x}	-	1600–2200	Monocarbonitride (cubic) continuous solid solution	[31, 629]
HfC _{1-x} -NbO	-	-	Terminal mutual solid solubilities between the components?	[31]
HfC _{1-x} -NdN _{1±x}	-	-	Monocarbonitride (cubic) continuous solid solution (complete solubility in the system?)	[31]
HfC _{1-x} - Nd ₂ Fe ₁₄ B	Pure Ar	1000	No solubility of Hf in complex boride phase, Hf carbide is stable in contact with it	[568]
HfC _{1-x} -NpC _{1-x}	-	-	Monocarbide (cubic) continuous solid solution (complete solubility in the system?)	[31]
HfC _{1-x} -NpN _{1±x}	-	-	Monocarbonitride (cubic) continuous solid solution (complete solubility in the system?)	[31]
HfC _{1-x} -PrN _{1±x}	-	-	Monocarbonitride (cubic) continuous solid solution (complete solubility in the system?)	[31]
HfC _{1-x} -PuC _{1-x}	-	-	Monocarbide (cubic) continuous solid solution (complete solubility in the system?)	[31]
HfC _{1-x} -PuN _{1±x}	-	-	Monocarbonitride (cubic) continuous solid solution (complete solubility in the system?)	[31]
HfC _{1-x} -PuP _{1±x}	-	-	Terminal mutual solid solubilities between the components (?)	[31]
HfC _{1-x} -PuS _{1±x}	-	-	Terminal mutual solid solubilities between the components (?)	[31]
HfC _{1-x} -ScC _{1-x}	-	-	Monocarbide continuous solid solution (complete solubility in the system)	[31, 340]
HfC _{1-x} -ScN _{1±x}	-	-	Monocarbonitride (cubic) continuous solid solution (complete solubility in the system?)	[31]
HfC _{1-x} -α/β-SiC	-	-	Compatible with each other within the temperature range of the thermal stability of the phases <i>See also</i> section C-Hf-Si in Table I-2.14	[1, 31, 228, 504, 633, 636]

(continued)

Table 3.20 (continued)

System	Atmo- sphere	Temperature range, °C	Interaction character, products and/or compatibility	References
HfC _{1-x} - α/β -Si ₃ N ₄	-	~1400–1600	Interaction leads to the formation of Hf silicide phases and SiC	[566,567]
HfC _{1-x} -SiO ₂	-	1000–1500	Interaction leads to the formation of SiC and HfO _{2-x}	[527]
HfC _{1-x} -SmN _{1±x}	-	-	Monocarbonitride (cubic) continuous solid solution (complete solubility in the system?)	[31]
HfC _{1-x} -TaC _{1-x}			<i>See</i> section TaC _{1-x} -HfC _{1-x} in Table 2.22 <i>See also</i> section C-Hf-Ta in Table I-2.14	
HfC _{1-x} -TaC _{1-x} - -ThC _{1±x}			<i>See</i> section TaC _{1-x} -HfC _{1-x} -ThC _{1±x} in Table 2.22	
HfC _{1-x} -TaC _{1-x} - -TiC _{1-x}			<i>See</i> section TaC _{1-x} -HfC _{1-x} -TiC _{1-x} in Table 2.22	
HfC _{1-x} -TaC _{1-x} - -UC _{1±x}			<i>See</i> section TaC _{1-x} -HfC _{1-x} -UC _{1±x} in Table 2.22 <i>See also</i> section C-Hf-Ta-U in Table I-2.14	
HfC _{1-x} -TaC _{1-x} - -VC _{1-x}			<i>See</i> section TaC _{1-x} -HfC _{1-x} -VC _{1-x} in Table 2.22	
HfC _{1-x} -TaC _{1-x} - - δ -WC _{1±x}			<i>See</i> section TaC _{1-x} -HfC _{1-x} - δ -WC _{1±x} in Table 2.22	
HfC _{1-x} -TaC _{1-x} - -ZrC _{1-x}			<i>See</i> section TaC _{1-x} -HfC _{1-x} -ZrC _{1-x} in Table 2.22	
HfC _{1-x} - α -Ta _{2±x} C			<i>See</i> section α -Ta _{2±x} C-HfC _{1-x} in Table 2.22 <i>See also</i> section C-Hf-Ta in Table I-2.14	
HfC _{1-x} - β -Ta _{2±x} C			<i>See</i> section β -Ta _{2±x} C-HfC _{1-x} in Table 2.22 <i>See also</i> section C-Hf-Ta in Table I-2.14	
HfC _{1-x} - δ -TaN _{1-x}	N ₂ , 3 MPa	1800	Monocarbonitride (cubic) continuous solid solution (complete solubility in the system)	[622]
HfC _{1-x} - ε -TaN _{1-x}	N ₂ , >0.1 MPa	1600–2000	Extended monocarbonitride (cubic) solid solutions; the max. solubility of ε -TaN _{1-x} (hexagonal) in HfC _{1-x} is ~75 mol.%	[18, 31]
HfC _{1-x} -TbN _{1±x}	-	-	Monocarbonitride (cubic) continuous solid solution (complete solubility in the system?)	[31]
HfC _{1-x} -TcC _{1-x}	-	-	Terminal mutual solid solubilities between the components (?) <i>See also</i> section C-Hf-Tc in Table I-2.14	[452,541]
HfC _{1-x} -ThC _{1±x}	-	-	Extended monocarbide solid solutions (terminal solubility?) <i>See also</i> section C-Hf-Th in Table I-2.14	[31, 341]
HfC _{1-x} -ThC _{1±x} - -TiC _{1-x}	-	>2000	Terminal solid solution based on HfC _{1-x} -TiC _{1-x} monocarbide (cubic) continuous solid solution; the solubilities of ThC _{1±x} in HfC _{1-x} and TiC _{1-x} are <5 and <3 mol.%, respectively (solubilities of HfC _{1-x} and TiC _{1-x} in ThC _{1±x} are very low)	[31]

(continued)

Table 3.20 (continued)

System	Atmosphere	Temperature range, °C	Interaction character, products and/or compatibility	References
HfC _{1-x} -ThC _{1±x} -UC _{1±x}	-	>2000	The max. solubility of HfC _{1-x} in ThC _{1±x} -UC _{1±x} monocarbide continuous solid solution corresponds to compositions ~($\text{Th}_{0.9}\text{Hf}_{0.1}$)C _{1±x} and ~($\text{U}_{0.6}\text{Hf}_{0.4}$)C _{1±x} , respectively, and that of ThC _{1±x} and UC _{1±x} in HfC _{1-x} correspond to compositions ~($\text{Hf}_{0.95}\text{Th}_{0.05}$)C _{1-x} and ~($\text{Hf}_{0.75}\text{U}_{0.25}$)C _{1-x} , respectively	[31]
HfC _{1-x} -ThC _{1±x} -VC _{1-x}	-	>2000	All the mutual solubilities between the carbides in the system are low	[31]
HfC _{1-x} -ThC _{1±x} -ZrC _{1-x}	-	2000-2100	Terminal solid solution based on HfC _{1-x} -ZrC _{1-x} monocarbide (cubic) continuous solid solution; the solubilities of ThC _{1±x} in HfC _{1-x} and ZrC _{1-x} are <5 and <10 mol.%, respectively (solubilities of HfC _{1-x} and ZrC _{1-x} in ThC _{1±x} are very low)	[31]
HfC _{1-x} -ThN _{1±x}	-	-	Extended monocarbonitride (cubic) solid solutions (terminal solubility?)	[31]
HfC _{1-x} -ThP _{1±x}	-	-	Terminal mutual solid solubilities between the components (?)	[31]
HfC _{1-x} -ThS _{1±x}	-	-	Terminal mutual solid solubilities between the components (?)	[31]
HfC _{1-x} -TiC _{1-x}	-	1500 ~1770-2050 >1900-2000	The miscibility gap in the solid state – from ~Hf _{0.1-0.2} Ti _{0.8-0.9} C _{1-x} to ~Hf _{0.50-0.75} Ti _{0.25-0.50} C _{1-x} The critical point in the miscibility gap at ~Hf _{0.35-0.45} Ti _{0.55-0.65} C _{1-x} Monocarbide continuous solid solution (complete solubility in the system); perfect homogenization after 7 h exposure <i>See also</i> section C-Hf-Ti in Table I-2.14	[13, 31, 192, 225, 229-231, 290, 457, 462, 463, 503, 575, 632]
HfC _{1-x} -TiC _{1-x} - UC _{1±x}	-	1900-2000	The max. solubility of UC _{1±x} in HfC _{1-x} -TiC _{1-x} monocarbide continuous solid solution corresponds to compos. ~($\text{Hf}_{0.75}\text{U}_{0.25}$)C _{1-x} (?) and ~($\text{Ti}_{0.95}\text{U}_{0.05}$)C _{1-x} and that of HfC _{1-x} and TiC _{1-x} in UC _{1±x} corresponds to compositions ~($\text{U}_{0.6}\text{Hf}_{0.4}$)C _{1±x} (?) and ~($\text{U}_{0.9}\text{Ti}_{0.1}$)C _{1±x} , respectively (or HfC _{1-x} -UC _{1±x} monocarbide continuous solid solution, ?) Data on the system available in the literature are contradictory	[31, 338]
HfC _{1-x} -TiC _{1-x} - VC _{1-x}	-	1900-2050	Monocarbide (cubic) continuous solid solution with the miscibility gap limited by compos. ~($\text{Hf}_{0.98}\text{V}_{0.02}$)C _{1-x} - ~($\text{Hf}_{0.03}\text{V}_{0.97}$)C _{1-x} - ~($\text{Hf}_{0.14-0.17}\text{Ti}_{0.73-0.75}\text{V}_{0.09-0.12}$)C _{1-x} <i>See also</i> section C-Hf-Ti-V in Table I-2.14	[224, 338, 341]

(continued)

Table 3.20 (continued)

System	Atmo- sphere	Temperature range, °C	Interaction character, products and/or compatibility	References
HfC _{1-x} -TiC _{1-x} - δ-WC _{1±x}	-	1540	(Hf,W)C _{1-x} -(Ti,W)C _{1-x} monocarbide con- tinuous solid solution with the miscibility gap limited by compos. Hf _{0.64} Ti _{0.36} C _{1-x} - Hf _{0.22} Ti _{0.78} C _{1-x} -Hf _{0.41} Ti _{0.27} W _{0.32} C _{1±x}	[31, 232, 338]
	-	1900-2000	(Hf,W)C _{1-x} -(Ti,W)C _{1-x} monocarbide (cubic) continuous solid solution (complete solubility); the max. solubility of δ-WC _{1±x} in the con- tinuous solid solution is corresponding to ~(Hf _{0.6} W _{0.4})C _{1-x} and ~(Ti _{0.3} W _{0.7})C _{1-x} composi- tions; practically, no solubility of HfC _{1-x} and TiC _{1-x} in δ-WC _{1±x} <i>See also</i> section C-Hf-Ti-W in Table I-2.14	
HfC _{1-x} -TiC _{1-x} - ZrC _{1-x}	-	1900-2000	Monocarbide (cubic) continuous solid solution (complete solubility in the system)	[31, 338, 341]
HfC _{1-x} -TiC _{1-x} - δ-NbN _{1-x}	Pure N ₂	1200-2500	Monocarbonitride (cubic) continuous solid solution (complete solubility in the system)	[629]
HfC _{1-x} - δ-TiN _{1±x}	-	1600-2200	Monocarbonitride (cubic) continuous solid solution	[31]
HfC _{1-x} -TiO _{1±x}	-	-	Terminal mutual solid solubilities between the components (?)	[31]
HfC _{1-x} -UC _{1±x}	-	~1730-2000	Extended monocarbide solid solutions (termi- nal solubility?)	[13, 31, 236, 341, 544]
	-	>~1730	Monocarbide (cubic) continuous solid solution (a spacing-composition curve in the system is almost linear, complete solubility in the sys- tem?) Data on the system available in the literature are contradictory <i>See also</i> section C-Hf-U in Table I-2.14	
HfC _{1-x} -UC _{1±x} - VC _{1-x}	-	≥1900-2000	The max. solubility of HfC _{1-x} in UC _{1±x} and VC _{1-x} corresponds to compos. ~(U _{0.6} Hf _{0.4})C _{1±x} and ~(V _{0.95} Hf _{0.05})C _{1-x} , respectively; and that of UC _{1±x} in HfC _{1-x} and VC _{1-x} corresponds to compos. ~(Hf _{0.75} U _{0.25})C _{1-x} and ~(V _{0.97} U _{0.03})C _{1-x} , respectively; and that of VC _{1-x} in HfC _{1-x} and UC _{1±x} corresponds to compos. ~(Hf _{0.95} V _{0.05})C _{1-x} and ~(U _{0.95} V _{0.05})C _{1±x} , respectively	[31, 338]
HfC _{1-x} -UC _{1±x} - ZrC _{1-x}	-	1900-2050	Monocarbide continuous solid solution with the small miscibility gap limited by ~(Hf _{0.4} U _{0.6})C _{1±x} - ~(Hf _{0.75} U _{0.25})C _{1-x} - ~(Hf _{0.45} Zr _{0.10} U _{0.45})C _{1±x} compositions <i>See also</i> section C-Hf-U-Zr in Table I-2.14	[13, 31, 338, 341]
HfC _{1-x} -β-UC _{2-x}	-	1800-2000	Practically, no solubility of HfC _{1-x} in α-UC _{2-x} <i>See also</i> section C-Hf-U in Table I-2.14	[13, 31]
HfC _{1-x} -UN _{1-x}	-	-	Monocarbonitride (cubic) continuous solid solution (complete solubility in the system?)	[31]

(continued)

Table 3.20 (continued)

System	Atmo- sphere	Temperature range, °C	Interaction character, products and/or compatibility	References
HfC _{1-x} -UP _{1±x}	-	-	Terminal mutual solid solubilities between the components (?)	[31]
HfC _{1-x} -US _{1±x}	-	-	Terminal mutual solid solubilities between the components (?)	[31]
HfC _{1-x} -UO _{2+x}	Vacuum, Ar	1930-2760	No interaction (exposure 10 min)	[1, 31, 213]
HfC _{1-x} -VC _{1-x}	-	1000	The mutual solid solubilities between HfC _{1-x} and VC _{1-x} are low	[3, 13, 31, 225,
	-	~2580-2650	Eutectic HfC _{1-x} -VC _{1-x} ; the max. mutual solubilities of HfC _{1-x} and VC _{1-x} in each other are ~15 mol.% Data on the system available in the literature are contradictory <i>See also</i> section C-Hf-V in Table I-2.14	233, 234, 236, 462, 552, 632]
HfC _{1-x} -VC _{1-x} - δ-WC _{1±x}	-	~1900-2000	The max. solubility of δ-WC _{1±x} in cubic carbides HfC _{1-x} and VC _{1-x} corresponds to compos. ~(Hf _{0,6} W _{0,4})C _{1±x} and ~(V _{0,4} W _{0,6})C _{1-x} , respectively; max. mutual solubilities of carbides HfC _{1-x} and VC _{1-x} corresponds to compos. ~(Hf _{0,9} V _{0,1})C _{1-x} and ~(V _{0,95} Hf _{0,05})C _{1-x} and with increasing V content in (Hf,V)C _{1-x} the max. solubility of W decreases there	[31, 234, 338]
	-	2580	(Hf,W)C _{1-x} -(V,W)C _{1-x} monocarbide continuous solid solution with the miscibility gap limited by compos. ~(Hf _{0,9} V _{0,1})C _{1-x} - ~(Hf _{0,1} V _{0,9})C _{1-x} - ~(Hf _{0,40-0,45} V _{0,40-0,45} W _{0,15})C _{1±x} ; the addition of δ-WC _{1±x} decreases the critical temp. of the miscibility gap	
HfC _{1-x} -VC _{1-x} - ZrC _{1-x}	-	1900-2050	Extended solid solution based on HfC _{1-x} -ZrC _{1-x} monocarbide (cubic) continuous solid solution; the massive miscibility gap limited by ~(Hf _{0,98} V _{0,02})C _{1-x} -~(Hf _{0,03} V _{0,97})C _{1-x} - ~(V _{0,97} Zr _{0,03})C _{1-x} -~(V _{0,08} Zr _{0,92})C _{1-x} compositions	[13, 31, 338, 552]
HfC _{1-x} -δ-VN _{1-x}	-	1600-2200	Monocarbonitride (cubic) continuous solid solution (?)	[18, 31]
	-	-	Terminal mutual solid solubilities between the components (?) Data on the system available in the literature are contradictory	
HfC _{1-x} - β-W ₂ B _{5-x}	-	2270	Eutectic HfC _{1-x} -β-W ₂ B _{5-x}	[521]
HfC _{1-x} -γ-WC _{1-x}	-	2550-2850	Monocarbide (cubic) continuous solid solution with the homogeneity range from HfC _{0,54-0,99} to WC _{0,60-0,66} (the max. C content in the mixed monocarbide phase (Hf,W)C _{1-x} increases as Hf substitutes for W; the presence of Hf stabilizes γ-WC _{1-x}) <i>See also</i> section C-Hf-W in Table I-2.14	[13, 31, 191, 235, 236, 341]

(continued)

Table 3.20 (continued)

System	Atmo- sphere	Temperature range, °C	Interaction character, products and/or compatibility	References
HfC _{1-x} - δ-WC _{1±x}	-	1800	The max. solubility of W in HfC _{1-x} corresponds to compos. ~($\text{Hf}_{0.7}\text{W}_{0.3}$)C _{1-x}	[13, 31, 191, 235, 236, 341]
	-	2400	The max. solubility of W in HfC _{1-x} corresponds to compos. ~($\text{Hf}_{0.4}\text{W}_{0.6}$)C _{1-x}	
	-	-	Practically, no solubility of HfC _{1-x} in δ-WC _{1±x} . <i>See also</i> section C-Hf-W in Table I-2.14	
HfC _{1-x} - δ-WC _{1±x} -ZrC _{1-x}	-	1900–2000	Extended solid solution based on HfC _{1-x} -ZrC _{1-x} monocarbide (cubic) continuous solid solution; the solubilities of δ-WC _{1±x} in HfC _{1-x} and ZrC _{1-x} are ~40 and ~30 mol.%, respectively (solubilities of ZrC _{1-x} and HfC _{1-x} in δ-WC _{1±x} are very low)	[31, 338]
HfC _{1-x} - γ-W _{2+x} C	-	2660	The max. solubility of Hf in γ-W _{2+x} C corresponds to compos. ($\text{W}_{0.94}\text{Hf}_{0.06}$) _{2.0} C _{0.99} <i>See also</i> section C-Hf-W in Table I-2.14	[13, 191, 341]
HfC _{1-x} -YC _{1±x}	-	-	Terminal mutual solid solubilities between the components (?)	[31]
HfC _{1-x} -YN _{1±x}	-	-	Monocarbonitride (cubic) continuous solid solution (complete solubility in the system?)	[31]
HfC _{1-x} -YbN _{1±x}	-	-	Monocarbonitride (cubic) continuous solid solution (complete solubility in the system?)	[31]
HfC _{1-x} -ZrC _{1-x}	-	from (-85)- (-100) up to 3400	Monocarbide (cubic) continuous solid solution, complete solubility in the system (data on the higher melting points of (Hf,Zr)C _{1-x} in comparison with individual HfC _{1-x} and ZrC _{1-x} are not confirmed); the critical point of the miscibility gap is corresponding to (-85)-(-100) °C and ~Hf _{0.50} Zr _{0.50} C _{1-x} composition (theoretically calculated)	[13, 31, 46, 192, 193, 225, 229, 290, 341, 454, 456, 457, 465, 565, 574–576, 632]
	-	2400–2800	Sintering process of the equimolar mixture of components was studied <i>See also</i> section C-Hf-Zr in Table I-2.14	
HfC _{1-x} -ZrN _{1±x}	-	-	Monocarbonitride (cubic) continuous solid solution (?)	[31]
HfC _{1-x} -ZrP _{1±x}	-	-	Terminal mutual solid solubilities between the components (?)	[31]
HfC _{1-x} - β/γ-ZrO _{2-x}	Vacuum	2000–2300	No interaction between dense compact HfC _{1-x} and powdered β/γ-ZrO _{2-x}	[1, 35, 213, 289]
	-	>2200	The initiation of reaction between powdered HfC _{1-x} and compact dense γ-ZrO _{2-x} (exposure 1 h)	

^aPractically, due to the serious difficulties in manufacturing transition metal carbide materials non-contaminated in any degree by O and N, all the materials labeled in literature as HfC_{1-x} with the appropriate certification more likely would have to be considered as HfC_{1-x}N_yO_z with low or very low values of y and z indexes

Table 3.21 Chemical interaction of hafnium monocarbide HfC_{1-x} with gaseous media at elevated, high and ultra-high temperatures (reaction systems are given in alphabetical order)

System	Atmosphere	Temperature range, °C	Interaction character, products and/or compatibility	References
HfC_{1-x} -CO	CO	1400	The equilibrium pressure of CO (p_{CO}) of the reaction $\text{HfC} + 2\text{CO} \leftrightarrow \alpha\text{-HfO}_2 + 3\text{C}$ is ~ 0.01 MPa	[28, 40, 242, 243, 388, 453, 523, 538]
	CO	1500–1640	p_{CO} (1500 °C) = ~ 0.02 MPa, p_{CO} (1600 °C) = ~ 0.05 MPa, p_{CO} (1640 °C) = ~ 0.1 MPa	
	CO	~ 1630	At pressures $< 1.33 \times 10^{-4}$ Pa the surface properties of single crystal HfC_{1-x} are stable	
	CO	~ 1600 – 1900	Formation of oxycarbide phases $\text{HfC}_{1-x}\text{O}_y$ (extended substitution solid solution based on HfC_{1-x} with approximate homogeneity limits: $\sim \text{HfC}_{0.75}\text{O}_{0.25}$ – $\text{HfC}_{0.55}$ – $\text{HfC}_{0.99}$) <i>See also</i> section C–Hf–O in Table I-2.14	
HfC_{1-x} -CO ₂	CO ₂	–	Formation of oxycarbide phases $\text{HfC}_{1-x}\text{O}_y$ (extended substitution solid solution based on HfC_{1-x} with approximate homogeneity limits: $\sim \text{HfC}_{0.75}\text{O}_{0.25}$ – $\text{HfC}_{0.55}$ – $\text{HfC}_{0.99}$) and subsequent formation of oxide scales	[28, 40, 237, 243, 388, 453, 523, 538]
	CO ₂ , $< 10^{-4}$ Pa	~ 1630	In the range of low pressures CO ₂ the surface properties of single crystal HfC_{1-x} are stable <i>See also</i> section C–Hf–O in Table I-2.14	
HfC_{1-x} -F ₂	F ₂ , 0.1 MPa	25	Arc-melted $\text{HfC}_{0.95}$ is resistant to F ₂	[245]
	F ₂ -He	~ 300	Detectable highly exothermic reaction starts (at fluorine partial pressure $p_{\text{F}_2} \geq 0.37$ kPa); the surface temperature of the samples increase rapidly	
	F ₂ -He	~ 300 – 400	Formation of solid HfF_4 , which is not adherent to the carbide surface; so, the $\text{HfC}_{0.95}$ surface is practically clean ($p_{\text{F}_2} = 0.37$ kPa)	
	F ₂ -He	~ 400 – 500	Formed solid HfF_4 is more adhered to the arc-melted $\text{HfC}_{0.95}$ surface, but it is abrupt crumbled ($p_{\text{F}_2} = 0.37$ kPa)	
	F ₂ (0.4–7.0 kPa), He (~ 100 kPa)	~ 550 – 900	Due to the volatilization of outer fluoride layers, arc-melted $\text{HfC}_{0.95}$ loses its mass (the reaction rate k is linear); k , $\text{mg cm}^{-2} \text{s}^{-1}$, varies from 0.03 (565 °C, $p_{\text{F}_2} = 0.37$ kPa; incomplete volatilization of HfF_4) to 0.8 (820 °C, $p_{\text{F}_2} = 7.0$ kPa); at temperatures > 600 – 650 °C apparent activation energy $E \approx 0$ and reaction rate is directly proportional to p_{F_2}	

(continued)

Table 3.21 (continued)

System	Atmo- sphere	Temperature range, °C	Interaction character, products and/or compatibility	References
HfC _{1-x} -H ₂	H ₂	–	Formation of carbohydride phases HfC _x H _y , (x = 0.50–0.58, y = 0.42–0.43, including Hf ₂ CH _x) via hydrogen dissolution in non-stoichiometric phases (dehydrogenation leads to the starting compositions again)	[31, 154, 244, 467–469, 520]
	H ₂	2230–2730	HfC _{1-x} is nonreactive with H ₂ ; it also has low permeability to H ₂	
	H ₂	<2480	HfC _{1-x} is resistant to H ₂	
	H ₂	>2760	HfC _{1-x} interacts with H ₂ <i>See also</i> section C–H–Hf in Table I-2.14	
HfC _{1-x} -H ₂ O	H ₂ O	400–500	No interaction	[154, 470, 489]
	H ₂ O, He	700–800	Hydrolysis of HfC _{1-x} materials in superheated steam leads to the evolution of H ₂ , CO, CO ₂ (delayed in release) and small amounts of CH ₄ , and precipitation of elemental C and C _n H _m wax (primary products), which are converted thereafter into CO ₂ and H ₂ ; a large amount of H ₂ evolves at the earlier stage while CO ₂ continues to evolve with some amount of H ₂ even after the ceasing of CO evolution	
HfC _{1-x} -N ₂	N ₂	20–1000	For wafers heated at 10 K min ⁻¹ rate the mass gain started in a range from 180 to 590 °C and achieved up to 1–6% in total	[1, 13, 29, 31, 35, 92, 153, 154, 223, 246, 365, 379, 381, 441, 527]
	N ₂ , ≤30 MPa	1100–1400	No interaction	
	N ₂	1150	Formation of monocarbonitride (cubic) continuous solid solution with the homogeneity range within ~HfC _{0.60} –HfN _{0.72} –HfN _{1.0} –HfC _{0.98} compositions	
	N ₂ flow	1500	No interaction, no mass change	
	N ₂ , 0.1–30 MPa	1500–1800	The formation of various monocarbonitride HfC _y N _z (0.6 ≤ x + z ≤ 1.0) phases Data available in literature are controversial <i>See also</i> section C–N–Hf in Table I-2.14	
HfC _{1-x} -O ₂ ^{a,b}	O ₂	20–25	At high O coverages single crystal HfC _{0.98} (100) surface reacts with the depletion of C atoms and formation of disordered oxide layers (finally – HfO _{2-x} -like layers)	[1, 35, 217, 237, 238, 248–262, 388, 394–396, 400, 439, 453, 471–476, 522, 523, 535, 538, 563, 619]
	O ₂ –Ar	400–420	Powdered (grain size ~1 μm, BET surface area ~1.0 m ² g ⁻¹) near-stoichiometric HfC _{1-x} starts to be oxidized (at partial pressures p _{O2} = 0.5–40 kPa) with formation of HfC _{1-x} O _y , α-HfO _{2-x} (monoclinic) and C (amorphous)	
	Air	410–435	The initiation of oxidation reaction for powdered HfC _{0.76} O _{0.07} , HfC _{0.78} O _{0.26} and HfC _{0.60}	

(continued)

Table 3.21 (continued)

System	Atmosphere	Temperature range, °C	Interaction character, products and/or compatibility	References
	Air	435–900	In this temperature range the oxidation of powdered HfC _{0.60} with heating rate 10 K min ⁻¹ leads to 13% total mass gain and maximal mass gain rate of 0.14 mg s ⁻¹ ; a certain amount of combined carbon was revealed in the final oxidation products due to the incomplete decomposition of ~HfO ₂ C intermediate phase ^c	
	O ₂ -Ar	480–600	Powdered (grain size ~1 μm, BET surface area ~0.33 m ² g ⁻¹) HfC _{0.98} oxidizes at p _{O2} = 4–16 kPa through the initial stage of oxycarbide phase HfC _{1-x} O _y formation and subsequent stages of O-diffusion-controlled in α-HfO _{2-x} (early) and phase-boundary-control-led (later) processes (both described by apparent activation energy E = 195 ± 15 kJ mol ⁻¹)	
	O ₂ -Ar	600–900	The oxidation of single crystal HfC _{0.96} with faces parallel to the (100) plane at p _{O2} = 2–8 kPa is accompanied with the formation of bilayered C containing α-HfO _{2-x} and described by linear kinetics with apparent activation energy (>700 °C) E = 160 kJ mol ⁻¹	
	Air	600–1200	The oxidation of compact (porosity 1–2%) near-stoichiometric HfC _{1-x} results in the formation of oxycarbide phase HfC _{1-x} O _y , C (amorphous) and oxide (α- and β-HfO _{2-x}) phases; occurrence of HfN _{1±x} and metal Hf (?) was detected too	
	O ₂ -Ar	700–1500	Single crystal HfC _{0.96} with faces parallel to the (200) plane at p _{O2} = 0.08–80.0 kPa oxidizes through the formation of oxycarbide HfC _{1-x} O _y , C and α-HfO _{2-x} with preferred (200), (020) or (002) orientation; the C containing oxide scale consists of compact/poreless (inner, ~23–25 at.% C) and porous (outer, ~6–11 at.% C) layers	
	O ₂ , 0.1 MPa	1000	Disintegration of dense zone-refined HfC _{0.97} (contents: O – 0.003%, N – 0.031%, Fe – 0.005%, Zr – 0.035%) samples into several pieces within 3 min	
	Air	1100–1400	Severe oxidation and disintegration of HfC _{1-x} materials	
	Air	1200	The oxidation mass gains of hot-pressed (1–2% porosity) HfC _{1-x} are 0.65 and 1.15 kg m ⁻² for 1 h and 2 h exposure, respectively	

(continued)

Table 3.21 (continued)

System	Atmo- sphere	Temperature range, °C	Interaction character, products and/or compatibility	References
	O ₂ , 2– 100 kPa	1200–1800	The oxidation rate constants decrease with temperature growth; CO is formed at the carbide-oxide interface and oxidized by incoming O ₂ to form CO ₂ in the outer layer of oxide scale where the morphology abruptly changed in comparison with the inner layer of scale	
	Air	1200–1800	The oxidation kinetics of hot-pressed (~10% porosity) near-stoichiometric HfC _{1-x} is controlled by gaseous diffusion via pores in the oxide (parabolic growth of the scale)	
	O ₂ -Ar	1400–2100	CVD-prepared HfC _{-0.5} film oxidizes by 93% Ar – 7% O ₂ gas flow (20 cm s ⁻¹) through the formation of 3 layers: residual carbide with dissolved O (HfC _{1-x} O _y), dense-appearing oxide containing carbon (HfO _{2-x} C _y) and porous outer oxide layer (α-HfO _{2-x})	
	Air	1500	The oxidation mass gains of the bulk samples of HfC _{0.67} , HfC _{0.82} and HfC _{0.98} are 1, 14 and 21 mg cm ⁻² , respectively (0.25 h exposure); morphological observations show the formation of a “maltese cross” protective oxide scale structure	
	O ₂ (0.6– 1.5 kPa), He (100 kPa, flow rate ~2 cm ³ s ⁻¹)	1500–2000	The oxidation of dense zone-refined HfC _{0.97} (contents: O – 0.003%, N – 0.031%, Fe – 0.005%) is linear in character and preferential along grain boundaries (the average oxidation mass gain is ~15–17 mg cm ⁻² for 1–1.5 h exposure at T = 1500–1600 °C)	
	Air	1800–2200	The oxidation kinetics of hot-pressed (~10% porosity) near-stoichiometric HfC _{1-x} is controlled by bulk (ambipolar) diffusion of O atoms (parabolic growth of the scale); the scale substantially densifies, yet remaining sufficiently porous to provide CO release	
	O ₂ /C ₂ H ₂ torch	~3000	The oxidation of CVD-prepared HfC _{1-x} coating by gas flow (pressure O ₂ /C ₂ H ₂ – 0.4/0.1 MPa, flow rate – 0.7–2 dm ³ s ⁻¹) leads to the formation of HfO _{2-x} C _y interlayer and HfO _{2-x} scale (β-HfO _{2-x} formed on the surface transforms to α-HfO _{2-x} upon cooling to room temperature); the oxide scale is composed of molten and porous (with micro-cracks and microholes as a result of CO/CO ₂ release) layers	
<i>See also section C–O–Hf in Table I-2.14</i>				

^aFine hafnium carbide powders are pyrophoric [247]

^bFor near-stoichiometric HfC_{1-x} the value of the Pilling-Bedworth ratio (based on the density of the low-temperature (monoclinic) α-HfO_{2-x} oxide phase) $\alpha = M_O d_C / M_C d_O = 1.44$, where M_O is molecular mass of the oxide phase formed on the oxidation of 1 mol of carbide phase, M_C is molecular mass of carbide phase, d_C and d_O are the densities of carbide and oxide phases, respectively [394]

^cBy analogy with the phase ZrO₂C reported by Guerlet and Lehr [401]

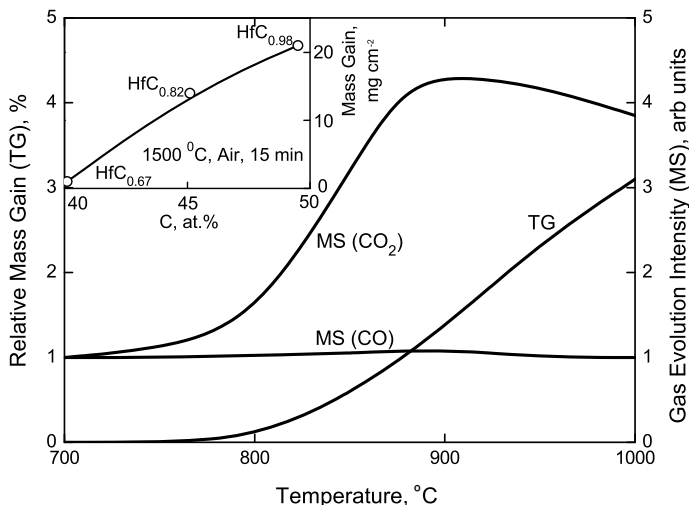


Fig. 3.22 Non-isothermal oxidation kinetics curves (heating rate – $0.17\text{ }^{\circ}\text{C s}^{-1}$) for ~60 mg samples of single crystal $\text{HfC}_{0.96}$ with faces parallel to the (100) plane exposed to a flowing atmosphere ($p = 20\text{ kPa}$) of the mixed gases of 20 vol.% O_2 and 80 vol.% Ar: TG – thermogravimetric (mass increase begins at $\sim 770\text{ }^{\circ}\text{C}$) and MS – mass-spectrometric (CO_2 gas evolution begins at $\sim 770\text{ }^{\circ}\text{C}$ with a maximum at $\sim 890\text{ }^{\circ}\text{C}$, CO gas was hardly detected); the complete oxidation and conversion of carbide to oxide in accordance with the reaction $\text{HfC}_{0.96} + 1.96\text{O}_2 \rightarrow \text{HfO}_2 + 0.96\text{CO}_2$ is corresponding to the relative mass gain of 10.5% [237] (Inset – the variation of oxidation mass gain with carbon content for HfC_{1-x} materials with different deviations from the stoichiometry [394–396])

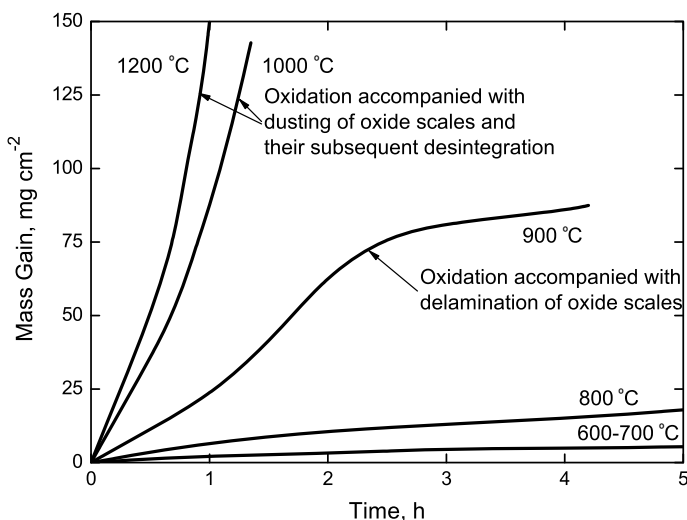


Fig. 3.23 Isothermal oxidation kinetics curves for 8 mm diameter disk-like samples of hot-pressed and subsequently annealed near-stoichiometric hafnium monocarbide HfC_{1-x} materials (porosity 1–2%) in air [238–241]

Table 3.22 The parameters of wettability of hafnium monocarbide HfC_{1-x} phases with some liquid metals and alloys (melts)^a

Melt (purity)	Atmosphere	Temp., °C	Time, s	γ_{l-g} , mJ m^{-2}	W_{a} , mJ m^{-2}	W_{m}^{b} , kJ mol^{-1}	θ , degree	References
$\text{HfC}_{0.99}$								
Co^{c}	–	1500	900	1805	3260	170	36 ± 2	[1, 263]
Fe^{d}	Vacuum	1550	900	1780	2870	150	52 ± 2	[1, 263]
Ni^{e}	–	1450	900	1700	3400	177	28 ± 2	[1, 263]
$\text{HfC}_{\sim 1.0}$								
Al (99.97%)	Vacuum	900	900	914	140	7.1	148 ± 3	[1, 35, 265, 272]
Al (99.97%)	Vacuum	1000	900	914	155	–	146 ± 3	[1, 35, 265, 272]
Bi (99.999%)	Vacuum	320	900	390	60	3.1	148 ± 2	[1, 35, 271, 272]
Co	Vacuum	1420	300	1910	3380	–	40	[1, 266, 271, 272]
Co^{c}	–	1500	1200	1805	3265	170	36	[1, 263, 267, 268]
Co (99.98%)	Ar	1500	1200	1805	3190	165	40	[1, 265, 345]
Co	Ar	1550	–	–	–	–	40	[35, 271, 272, 345]
Co	Vacuum	1550	–	–	–	–	36	[35, 271, 272]
Cu	Vacuum	1100	–	–	–	–	134	[35, 266, 271, 626]
Cu (99.99%)	Vacuum	1130	900	1351	316	16	140 ± 0.25	[1, 265, 272, 345]
Cu^{f}	Vacuum, 1.3 mPa	1150	3600	610	–	–	134	[625]
Cu (Hf – 2.75%) ^f	Vacuum, 1.3 mPa	1150	3600	–	–	–	146	[625]
Cu (Hf – 2.75, V – 0.8%) ^f	Vacuum, 1.3 mPa	1150	3600	–	–	–	105	[625]
Cu	Vacuum	1200	–	–	–	–	131	[35, 266, 271, 272]
Fe	Vacuum	1490	60	1900	3245	–	45	[1, 266, 269, 272]
Fe (C-4.0, Mn-1.4, Si-2.5, S-0.1%) ^g	Pure Ar	1400–1450	900	–	–	–	132	[1, 270, 272]
Fe (C-3.1, Mn-0.4, Si-1.6, S-0.02%) ^g	Pure Ar	1400–1450	900	–	–	–	122	[1, 270, 272]

(continued)

Table 3.22 (continued)

Melt (purity)	Atmosphere	Temp., °C	Time, s	γ_{1-g} , mJ m^{-2}	W_a , mJ m^{-2}	W_m^b , kJ mol^{-1}	θ , degree	References
Fe (C-2.7, Mn-0.4, Si-1.2, S-0.2%) ^g	Pure Ar	1400–1450	900	–	–	–	145	[1, 270, 272]
Fe (C-2.6, Mn-1.0, Si-1.0, Cr-0.3%) ^g	Pure Ar	1400–1450	900	–	–	–	140	[1, 270, 272]
Fe (C-1.0, Cr-1.4, Mn-0.4, Si-0.3%) ^g	Pure Ar	1500–1550	900	–	–	–	132	[1, 270, 272]
Fe (C-1.0, Cr-1.4, Mn-1.1, Si-0.6%) ^g	Pure Ar	1500–1550	900	–	–	–	145	[1, 270, 272]
Fe (C-0.8, Mn-0.2, Si-0.2, S-0.03%) ^g	Pure Ar	1500–1550	900	–	–	–	148	[1, 270, 272]
Fe (C-0.2, Cr-14.5, Ni-2.7, Mn-0.5%) ^g	Pure Ar	1500–1550	900	–	–	–	128	[1, 270, 272]
Fe ^d	Vacuum	1550	900	1780	2870	149	52	[1, 263, 271, 272]
Fe (99.999%)	Ar	1550	900	1780	270	14	148	[1, 265, 271, 272]
Ga (99.99999%)	Vacuum, Ar	800	900	707	115	6.1	147 ± 0.3	[1, 35, 271, 272]
Ge (99.9999%)	Vacuum	1000	900	600	140	7.3	140 ± 0.3	[1, 35, 271, 272]
In (99.9995%)	Vacuum	250	900	559	90	4.6	147 ± 0.6	[1, 35, 271, 272]
Mn (99.8%)	Vacuum	1300	900	1750	2115	110	78	[1, 265, 345]
Mn (99.8%)	Ar	1300	900	1750	1870	97	86	[1, 265, 345]
Mo	He	2610	–	–	–	–	14	[271]
Ni	Vacuum	1380	300	1810	3475	–	23	[1, 35, 266, 272]
Ni ^e	Vacuum, Ar	1450	900	1700	3200	170	28	[1, 263, 271, 272]
Ni (99.99%)	Ar	1450	900	1700	3060	177	37	[1, 265, 345]
Pb (99.98%)	Vacuum	400	900	480	64	3.3	150 ± 1	[1, 35, 271, 272]
Sb (99.999%)	Vacuum	700	900	384	137	7.1	130 ± 1	[1, 35, 271, 272]

(continued)

Table 3.22 (continued)

Melt (purity)	Atmo- sphere	Temp., °C	Time, s	γ_{l-g} , mJ m ⁻²	W_a , mJ m ⁻²	W_m^b , kJ mol ⁻¹	θ , degree	References
Si	Vacuum	1500	900	860	1650	84	23 ± 2	[1, 35, 272]
Sn (99.999%)	Vacuum	300	900	554	61	3.1	153 ± 2	[1, 35, 271, 272]
Tl (99.999%)	Vacuum	400	900	490	163	8.4	132 ± 3	[1, 35, 271, 272]

^aThe parameters of wettability are given in accordance with Young-Dupré equation $W_a = \gamma_{l-g} \times (1 + \cos\theta)$ and Young's equation $\gamma_{s-l} = \gamma_{s-g} - \gamma_{l-g}\cos\theta$, where W_a is the work of adhesion, γ_{l-g} is the liquid-vapour interfacial energy (surface tension), γ_{s-l} is solid-liquid interfacial energy, γ_{s-g} is the solid-vapour interfacial energy and θ is the wetting contact angle [1]; compositions of melts are given in mass (weight) percentage

^b $W_m = W_a(M/d)^{2/3}N_A^{1/3}$, where W_m is the molar work of adhesion, M is the molecular mass and d is the density of chemical compound, N_A is the Avogadro constant [264]

^c $\gamma_{s-l} = 1500$ mJ m⁻²

^d $\gamma_{s-l} = 1860$ mJ m⁻²

^e $\gamma_{s-l} = 1450$ mJ m⁻²

^fSintered materials (porosity – ≤2%, contents: non-combined C – 0.20%, O – 0.06%, N – 0.10%, Cr – 0.30%, Zr – 0.30%)

^gSintered materials (porosity – 3–6%)

compounds – in Table 3.20 and with gaseous media – in Table 3.21. The data on the oxidation resistance of HfC_{1-x} listed there are also accompanied by the graphic information in Figs. 3.22 and 3.23. Data on the catalytic activities of HfC_{1-x} are given in several works [1, 282, 286, 347–356, 466, 495, 542]; the examples of its electrochemical behaviour are described in [291, 292, 357, 374]. The parameters of wettability of HfC_{1-x} with some liquid metals (melts) are listed in Table 3.22, the diffusion rates for the systems containing HfC_{1-x} are presented in species pairs within the various ranges of temperatures in the Table 3.23. The characters of chemical interaction of hafnium monocarbide HfC_{1-x} with some common chemicals (acids, alkalies and salts in aqueous solutions) are summarized in Table 3.24.

Table 3.23 Diffusion rates and related parameters in the systems containing hafnium, carbon and hafnium monocarbide phases at various temperatures^{a, b}

Species pair	Temperature dependence of the diffusion coefficient (diffusivity) $D = D_0 \exp(-E_A/R)/T$, $\text{cm}^2 \text{ s}^{-1}$	Temperature range, K ($^{\circ}\text{C}$)	Remarks on materials characteristics and measurement method	References
$\text{C} \rightarrow \alpha\text{-Hf}$	$7.4 \exp(-37,600/T)$	1390–2030 (1120–1760)	Polycrystalline Hf (1.5 wt.% Zr), residual activity method using ^{14}C radioactive diffusant	[1, 14, 35, 273–275]
	$6.1 \times 10^{-5} \exp(-12,000/T)$, ?	1370–1570 (1100–1300)	Calculation based on the growth of HfC_{1-x} phase layer	[1]
$\text{C} \rightarrow \beta\text{-Hf}$	$4.2 \times 10^{-2} \exp(-20,100/T)$	2030–2400 (1760–2130)	Polycrystalline Hf (1.5 wt.% Zr), residual activity method using ^{14}C radioactive diffusant	[1, 14, 15, 35, 273]
	$0.8 \exp(-25,400/T)$	2070–2370 (1800–2100)	Polycrystalline Hf (3 wt.% Zr), diffusion couple method with determination of $c \sim x$ curves by calculation from an analytical solution	[274, 275]
$\text{C} \rightarrow \text{HfC}_{1-x}$	$6.3 \exp(-65,600 \pm 6600)/T$	2470–3070 (2200–2800)	Polycrystalline (hot-pressed) HfC_{1-x} ($x = 0.03$, $\text{Hf}(\text{C}_{0.95}\text{N}_{0.04}\text{O}_{0.01})_{0.97}$, 100–300 μm grain size, porosity <5%, $\text{O} + \text{N} \leq 0.05\%$), ^{14}C radiotracer	[4, 35, 277, 278, 358, 360, 361, 547]
	$4.7 \times 10^4 \exp(-64,500 \pm 3300)/T$	1860–2270 (1590–2000)	Polycrystalline (hot-pressed) HfC_{1-x} ($x \approx 0$, porosity – 5%, non-combined C – 0.9%), ^{14}C radiotracer	[4, 14, 15, 278, 280, 358]
	$2.62 \exp(-48,000/T)$	2570–3270 (2300–3000)	Parameters of temperature variation of HfC_{1-x} layer growth rate constant upon C saturation of liquid Hf in graphite crucible	[14, 15, 279]
	$8.6 \exp(-51,200/T)$	2570–3270 (2300–3000)	Parameters of reaction-chemical diffusion, C saturation of liquid Hf in graphite crucible; metallography method	[14, 15, 279, 281, 369]
$\text{Hf} \rightarrow \text{HfC}_{1-x}$	$1.48 \times 10^8 \exp(-92,000/T)$	–	Values calculated on the diffusion theory basis	[1, 35, 276]
	$\sim \exp(-75,200/T)$	–	Estimated on the basis of LeClair's relation (connected with phase melting point)	[369]

(continued)

Table 3.23 (continued)

^aThe chemical diffusion coefficient concentration and temperature dependencies can be represented by an equation of the form $D' = D'_0 \exp(\beta x) \exp(-E'_A/R/T)$, where β is the concentration factor and x is the value of index in HfC_{1-x} formula (for the ranges of $x = 0.01-0.50$ and $T = 2330-3030$ °C the recommended values are $D'_0 = 3.94 \text{ cm}^2 \text{ s}^{-1}$, $\beta = 9.2$ and $E'_A = 477 \text{ kJ mol}^{-1}$ [281]), and the discrepancy between chemical and self-diffusivities may be estimated on the basis of the thermodynamical relationship: $D' = D \times [1 + (d \ln \gamma_C / d \ln N_C)]$, where γ_C is the activity coefficient of carbon and N_C is the atomic fraction of carbon (evaluated at 2000 °C in HfC_{1-x} : at $x = 0.01$, $d \ln \gamma_C / d \ln N_C = 141$ and at $x = 0.20$, $d \ln \gamma_C / d \ln N_C = 15$ [359]); the approximate values of apparent activation energy for some diffusion controlled processes in HfC_{1-x} : (a) grain growth (particle coarsening) $- 210 \pm 5 \text{ kJ mol}^{-1}$ ($\text{HfC}_{-1.0}$, mean particle size 45–50 nm, in arc-melted W $- 3.6 \text{ mas. \% Re}$ alloy, 1900–2300 °C) [481]; (b) powder hot-pressing densification $- 160 \text{ kJ mol}^{-1}$ ($\text{HfC}_{0.71}$, mean particle size 10–20 μm , 2400–2600 °C) [477], 170 kJ mol^{-1} ($\text{HfC}_{0.80}$, mean particle size 10–20 μm , 2400–2600 °C) [477], 190 kJ mol^{-1} ($\text{HfC}_{0.91}$, mean particle size 10–20 μm , 2400–2600 °C) [477], 215 kJ mol^{-1} ($\text{HfC}_{-1.0}$, mean particle size 10–20 μm , 2400–2600 °C) [477]; data on creep – see Sect. 3.4 (Table 3.13), see also Sect. 3.5 (Table 3.18)

^bBy the studies of diffusion in $\text{HfC}_{1-x}\text{-TaC}_{1-x}$ powder blends annealing at 1900 °C (exposure time – from 5 to 200 h) it was found that Hf atoms have a higher intrinsic diffusivity compared with Ta atoms [397]

Table 3.24 The interaction of near-stoichiometric hafnium monocarbide HfC_{1-x} materials with some common chemical reagents in aqueous solutions [1, 32, 35, 36, 45, 64, 247, 283–285, 291, 292, 366, 370, 482]

Reagent, formula (density or concentration of aqueous solution) ^a	Treatment conditions		Character of interaction ^b
	Temperature, °C	Exposure time, h	
HCl (1:1)	20	24	Decomposes up to ~4%
	110–112	2	Decomposes up to ~57%
HCl ($d = 1.19$)	20	24	No decomposition
	100–120	2	No decomposition
H ₂ SO ₄ (1:4)	20	24	No decomposition
	110–116	2	Decomposes up to ~10–12%
H ₂ SO ₄ ($d = 1.84$)	20	24	No decomposition
	264–268	1	Decomposes completely (16.1% amorphous C); composition of released gases: CH ₄ 64.2, CO ₂ 31.8 and H ₂ 4.0 mol.% ^c
	290–300	1	Decomposes completely (6.3% amorphous C); composition of released gases: CH ₄ 16.2, CO ₂ 81.3 and H ₂ 2.4 mol.% (solution is transparent finally) ^c
HNO ₃ (1:1)	20	24	Decomposes up to ~25%
	100–105	2	Decomposes completely (no precipitated C, solution is transparent) ^d
HNO ₃ ($d = 1.43$)	20	24	Decomposes up to ~40%
	110–120	0.5	Decomposes completely with the formation of soluble nitrates (no precipitated C, solution is transparent); composition of released gases: CH ₄ (traces), CO ₂ 95–97 and H ₂ 2–3 mol.% (N oxides are not taking into account) ^d
H ₃ PO ₄ (1:3)	20	24	Decomposes up to ~2–3%
	≥100	2	Decomposes up to ~10%
H ₃ PO ₄ ($d = 1.70$)	20	24	Decomposes up to ~3%
	110	2	Decomposes up to ~10%
	230–240	1.5	Decomposes up to ~77%; composition of released gases: CH ₄ 62.1, CO ₂ 35.2 and H ₂ 3.0 mol.% ^c
	250	1	Decomposes completely with the formation of soluble phosphate HfO(H ₂ PO ₄) ₂ ; composition of released gases: CH ₄ 77.2, CO ₂ 19.3 and H ₂ 3.4 mol.% (dissolution proceeds very energetically and mainly finishes in 30–40 min) ^e

(continued)

Table 3.24 (continued)

Reagent, formula (density or concentration of aqueous solution) ^a	Treatment conditions		Character of interaction ^b
	Tempera- ture, °C	Exposure time, h	
	250–270	1.5	Decomposes completely with the formation of soluble phosphate $\text{HfO}(\text{H}_2\text{PO}_4)_2$; composition of released gases: CH_4 69.3, CO_2 28.9 and H_2 1.7 mol.% (resultant solution is transparent, on heavily diluting with H_2O the amorphous precipitates appear, which after heating transform into pyrophosphate $\text{Hf}_2\text{P}_2\text{O}_7$) ^c
HClO_4 ($d = 1.67$)	20	24	Decomposes up to ~3%
	≥ 100	2	Decomposes up to ~98%
$\text{H}_2\text{C}_2\text{O}_4^f$ (saturated solution)	20	24	Decomposes up to ~2–3%
	≥ 100	2	Decomposes up to ~10%
Organic acids	110	1	No decomposition
NaOH (10%)	20	24	No decomposition
	108	2	Decomposes up to ~2%
NaOH (20%)	20	24	No decomposition
	108–110	2	Decomposes up to ~1–2%
H_2O_2 (30%)	110	1	Practically, no decomposition
NaCl (3%)	–	–	The oxide film forms on the HfC_{1-x} anode under electrolysis at potentials between -0.2 and $+1.9$ V; the film consists of the upper layer formed in polymolecular chemisorption of O_2 and Cl_2 gases followed by the $\text{HfO}_{2-x} + \text{C}$ layer and inner oxycarbide HfC_xO_y layers
Na_2SO_4	–	–	Under electrolysis HfC_{1-x} has a wider passivity region than metal Hf and dissolves anodically faster
NaNO_3	–	–	Under electrolysis HfC_{1-x} has a wider passivity region than metal Hf and dissolves anodically faster
NH_4F (5%)	–	–	Decomposes up to ~23%
$(\text{NH}_4)_2\text{S}_2\text{O}_8$ (25%)	–	–	Decomposes completely
3HCl ($d = 1.19$) + HNO_3 ($d = 1.43$)	20	24	Decomposes up to ~86%
	106–110	2	Decomposes completely
3HCl (1:1) + HNO_3 (1:2)	110	1	Decomposes almost completely
HNO_3 ($d = 1.43$) + H_2SO_4 ($d = 1.84$)	20	24	Decomposes completely
	110	2	Decomposes completely
H_2SO_4 (1:4) + H_3PO_4 (1:3)	20	24	Decomposes almost completely
	≥ 150	2	Decomposes completely
H_2SO_4 ($d = 1.84$) + H_3PO_4 ($d = 1.70$)	20	24	Decomposes up to ~1–3%
	250	2	Decomposes almost completely with the deposition of salts
H_2SO_4 (1:4) + $\text{H}_2\text{C}_2\text{O}_4^f$ (saturated solution)	20	24	No decomposition
	≥ 100	2	Decomposes up to ~5%

(continued)

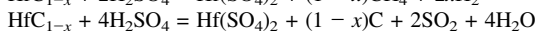
Table 3.24 (continued)

Reagent, formula (density or concentration of aqueous solution) ^a	Treatment conditions		Character of interaction ^b
	Tempera- ture, °C	Exposure time, h	
H ₂ SO ₄ (<i>d</i> = 1.84) + H ₂ C ₂ O ₄ ⁱ (saturated solution)	20	24	Decomposes up to ~2%
	≥100	2	Decomposes up to ~34–37%
HCl (<i>d</i> = 1.19) + H ₂ O ₂ (30%)	110	1	Decomposes almost completely
HCl (<i>d</i> = 1.19) + (NH ₄) ₂ S ₂ O ₈ (25%)	–	–	Decomposes completely
HCl (<i>d</i> = 1.19) + Br ₂ (HBrO, HBr) (saturated solution)	–	–	Decomposes almost completely
H ₂ SO ₄ (1:4) + H ₂ O ₂ (30%)	110	1	Decomposes completely
H ₂ SO ₄ (1:4) + (NH ₄) ₂ S ₂ O ₈ (25%) ^g	110	1	Decomposes completely
H ₂ SO ₄ (1:1) + (NH ₄) ₂ S ₂ O ₈ (25%)	110	1	Decomposes completely
4HNO ₃ (<i>d</i> = 1.43) + HF (<i>d</i> = 1.13)	20	24	Decomposes completely
	110	1	Decomposes completely
H ₂ O ₂ (30%) + H ₂ C ₂ O ₄ ⁱ (50%)	110	1	Decomposes completely
H ₂ O ₂ (30%) + H ₂ C ₄ H ₄ O ₆ ^h (50%)	20	24	No decomposition
	110	1	Decomposes up to ~3%
H ₂ O ₂ (30%) + H ₃ C ₆ H ₅ O ₇ ⁱ	110	1	Decomposes up to ~2%
H ₂ O ₂ (30%) + H ₄ C ₁₀ H ₁₂ N ₂ O ₈ ⁱ (saturated solution)	110	1	Decomposes up to ~3%
H ₂ O ₂ (30%) + NH ₄ F	110	1	Decomposes completely
(NH ₄) ₂ S ₂ O ₈ + H ₄ C ₁₀ H ₁₂ N ₂ O ₈ ⁱ	–	–	Decomposes up to ~28%
(NH ₄) ₂ S ₂ O ₈ + NH ₄ F	–	–	Decomposes completely
4NaOH (20%) + Br ₂ (HBrO, HBr)	20	24	Decomposes up to ~12–19%
	≥100	2	Decomposes up to ~36%
4NaOH (20%) + H ₂ O ₂ (30%)	20	24	Decomposes up to ~47–66%
	100–110	2	Dissolves completely with hydrolytic deposition of metal
4NaOH (20%) + K ₃ [Fe(CN) ₆] (10%)	20	24	Decomposes up to ~14–17%
	≥100	2	Decomposes up to ~63–76%

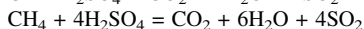
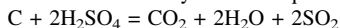
^aAll the ratios are given in volume fractions

^bWhen it is not indicated specially, the character reported is related to the powders with mean particle size of 40–50 μm

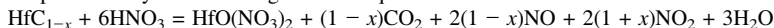
^cThe decomposition of HfC_{1-x} starts at 200–220 °C, at 230–250 °C the dissolution is very energetical and decomposition, accompanied by the release of amorphous finely-dispersed C, mainly finishes in 30–40 min; represented by the main reaction equations:



as well as secondary reaction equations:



^dRepresented by the following reaction equation:



^eRepresented by the following reaction equation:



^fOxalic acid

(continued)

Table 3.24 (continued)

^aRecommended chemical etching agents for HfC_{1-x}: **(a)** boiling mixture of concentrated H₂SO₄ + (NH₄)₂S₂O₈ [337]; **(b)** 10 g K₃[Fe(CN)₆] + 2–10 g KOH/NaOH + 100 ml H₂O (Murakami's reagent for metallographic analysis) [185]; **(c)** 5% Br₂ solution in CH₃OH (methanol) (for the separation of carbide phases from metal-carbide alloys) [185]

^bTartaric acid

ⁱCitric acid

^jEthylenediaminetetraacetic acid (EDTA)

In comparison with other ultra-high temperature materials the summarized data on the chemical behaviour of hafnium monocarbide are given in Addendum.

References

1. Kosolapova TYa (ed) (1990) Handbook of high-temperature compounds: properties, production and applications. Hemisphere, New York
2. Gusev AI, Rempel AA, Magerl AJ (2001) Disorder and order in strongly nonstoichiometric compounds. Springer, Berlin
3. Andrievskii RA, Lanin AG, Rymashevskii GA (1974) Prochnost tugoplavkikh soedinenii (Strength of refractory compounds). Metallurgiya, Moscow (in Russian)
4. Andrievskii RA, Spivak II (1989) Prochnost tugoplavkikh soedinenii i materialov na ikh osnove (Strength of refractory compounds and materials based on them). Metallurgiya, Chelyabinsk (in Russian)
5. Gusev AI, Zyryanova AN (1999) Atomic-vacancy ordering and magnetic susceptibility of nonstoichiometric hafnium carbide. JETP Let 69(4):324–329
6. Gusev AI, Zyryanova AN (2000) Ordering and magnetic susceptibility of non-stoichiometric hafnium carbide. Phys Stat Sol A 177:419–437
7. Guo BC, Wei S, Purnell J, Buzza S, Castleman AW (1992) Metallo-carbohedrenes [M₈C₁₂ (M = V, Zr, Hf and Ti)]: a class of stable molecular cluster ions. Science 256:515–516
8. Storms EK (1967) The refractory carbides. Academic Press, New York, London
9. Toth LE (1971) Transition metal carbides and nitrides. Academic Press, New York, London
10. Massalski TB, Subramanian PR, Okamoto H, Kacprzak L (eds) (1990) Binary alloy phase diagrams, 2nd edn. ASM International, Metals Park, Ohio
11. Lyakishev NP (ed) (1996) Diagrammy sostoyaniya dvoinykh metallicheskich sistem (Phase diagrams of binary metallic systems), Vol. 1. Mashinostroenie, Moscow (in Russian)
12. Rudy E (1969) Compendium of phase diagram data. In: Ternary phase equilibria in transition metal-boron-carbon-silicon systems. Report AFML-TR-65-2, Contracts USAF 33(615)-1249 and USAF 33(615)-67-C-1513, Part 5. Air Force Materials Laboratory, Wright-Patterson Air Force Base, Ohio, pp. 1–689
13. Holleck H (1984) Binäre und ternäre Carbid- und Nitridsysteme der Übergangsmetalle (Binary and ternary carbide and nitride systems of the transition metals). Gebrüder Bornträger, Berlin, Stuttgart (in German)
14. Samsonov GV, Upadhyaya GS, Neshpor VS (1974) Fizicheskoe materialovedenie karbidov (Physical materials science of carbides). Naukova Dumka, Kyiv (in Russian)
15. Upadhyaya GS (1996) Nature and properties of refractory carbides. Nova Science, Commack, New York
16. Bittner H, Goretzki H (1962) Magnetische Untersuchungen der Carbide TiC, ZrC, HfC, VC, NbC und TaC (Magnetic studies of the TiC, ZrC, HfC, VC, NbC and TaC carbides). Monatsh Chem 93(5):1000–1004 (in German)

17. Cotter PG, Kohn JA (1954) Industrial diamond substitutes: I. Physical and X-ray study of hafnium carbide. *J Am Ceram Soc* 37(9):415–420
18. Nowotny H, Benesovsky F, Rudy E (1960) Hochschmelzende Systeme mit Hafniumkarbid und -nitrid (Refractory systems with hafnium carbide and nitride). *Monatsh Chem* 91(2): 348–356 (in German)
19. Benesovsky F, Rudy E (1960) Beitrag zum Aufbau des Systeme Zr-C und Hf-C (Contributions to the construction of the systems Zr-C and Hf-C). *Planseeber Pulvermetall* 8:66–71 (in German)
20. Krikorian NH, Wallace TC, Anderson JL (1963) Low-temperature thermal expansion of the group 4a carbides. *J Electrochem Soc* 110(6):587–588
21. Ramqvist L (1968) Variation of lattice parameter and hardness with carbon content of group 4b metal carbides. *Jernkontoret Ann* 152(10):517–523
22. Sara RV (1965) The hafnium – carbon system. *Trans Metall Soc AIME* 233(9):1683–1691
23. Samsonov GV, Morosov VV (1971) Carbohydride der Uebergangsmetalle (Carbohydrides of the transition metals). *Monatsh Chem* 102:1667–1678 (in German)
24. Samsonov GV, Timofeeva II (1970) Rentgenograficheskoe issledovanie dinamicheskikh kharakteristik kristallicheskikh reshetok nekotorykh faz vnedreniya (X-ray diffraction study of dynamic characteristics of crystal lattices of some interstitial phases). *Dopov Akad Nauk Ukr RSR Ser A Fiz Mat Tekh Nauki* 32:831–833 (in Russian)
25. Achour M, Zaug J, Pialoux A (1975) Etude de la carboreduction progressive du dioxyde de hafnium. III. Determination du parametre cristallin de la phase HfC limite puis sous vide par diffraction des rayons X entre 1000 et 2000 °C (Study of the progressive reduction of hafnium dioxide by carbon. III. Determination of the lattice parameter of the boundary phase HfC in vacuum by X-ray diffraction between 1000 and 2000 °C). *Rev Int Hautes Temp Refract* 12(3):289–294 (in French)
26. Kieffer R, Nowotny HN, Ettmayer P, Dufek G (1972) Neue Untersuchungen ueber die Mischbarkeit von Uebergangsmetallnitriden und -karbiden (New investigations on the miscibility of transition metal nitrides and carbides). *Metall* 26:701–708 (in German)
27. Dubrovskaya LB, Zaytsev GP, Ordanyan SS (1977) Magnetic susceptibility of solid solutions of hafnium and tantalum monocarbides. *Phys Metal Metallogr* 44:173–177
28. Constant K, Kieffer R, Ettmayer P (1975) Uber das pseudoternare System ‘HfO’-HfN-HfC (On the pseudoternary system ‘HfO’-HfN-HfC). *Monatsh Chem* 106:973–981 (in German)
29. Lengauer W, Binder S, Aigner K, Ettmayer P, Guillou A, Debuigne J, Groboth G (1995) Solid state properties of group IVb carbonitrides. *J Alloys Compd* 217:137–147
30. Nakamura K, Yashima M (2008) Crystal structure of NaCl-type transition metal monocarbides MC (M = V, Ti, Nb, Ta, Hf, Zr), a neutron powder diffraction study. *Mater Sci Eng B* 148:69–72
31. Kotelnikov RB, Bashlykov SN, Galiakbarov ZG, Kashtanov AI (1968) Osobo tugoplavkie elementy i soedineniya (Extra-refractory elements and compounds). *Metallurgiya, Moscow* (in Russian)
32. Samsonov GV (1964) Refractory transition metal compounds. Academic Press, New York
33. Kolomoets NV, Neshpor VS, Samsonov GV, Semenkovich SA (1958) Thermoelectric properties of some metal-like compounds. *Sov Phys Tech Phys* 3(11):2186–2193
34. Houska CR (1964) Thermal expansion of certain group IV and group V carbides at high temperatures. *J Am Ceram Soc* 47(6):310–311
35. Samsonov GV, Vinitskii IM (1980) Handbook on refractory compounds. IFI/Plenum, New York
36. Kosolapova TYa (1971) Carbides: properties, production and applications. Plenum Press, New York
37. Nartowski AM, Parkin IP, MacKenzie M, Craven AJ, MacLeod I (1999) Solid state metathesis routes to transition metal carbides. *J Mater Chem* 9(6):1275–1281
38. Srivastava A, Chauhan M, Singh RK (2011) High-pressure phase transitions in transition metal carbides XC (X = Ti, Zr, Hf, V, Nb, Ta): a first-principle study. *Phase Transit* 84(1):58–66

39. Li H, Zhang L, Zeng Q, Guan K, Li K, Ren H, Liu S, Cheng L (2011) Structural, elastic and electronic properties of transition metal carbides TMC (TM = Ti, Zr, Hf and Ta) from first principles calculations. *Solid State Commun* 151:602–606
40. Alyamovskii SI, Zainulin YuG, Shveikin GP (1981) Oksikarbidy i oksinitridy metallov IVA i VA podgrupp (Oxycarbides and oxynitrides of IVA and VA subgroups metals). Nauka, Moscow (in Russian)
41. Rowcliffe DJ, Hollox GE (1971) Plastic flow and fracture of tantalum carbide and hafnium carbide at low temperatures. *J Mater Sci* 6(10):1261–1269
42. Rowcliffe DJ, Hollox GE (1971) Hardness anisotropy, deformation mechanisms and brittle-to-ductile transition in carbide. *J Mater Sci* 6(10):1270–1276
43. Yuan J, Zhang H, Tang J, Shinya N, Nakajima K, Qin L-C (2012) Synthesis and characterization of single crystalline hafnium carbide nanowires. *J Am Ceram Soc* 95(7):2352–2356
44. Tian S, Li H, Zhang Y, Zhang S, Wang Y, Ren J, Qiang X (2013) Single-crystalline hafnium carbide nanowire growth below the eutectic temperature by CDV. *J Cryst Growth* 384:44–49
45. Krzhizhanovskii RE, Shtern ZYu (1977) Teplofizicheskie svoistva nemetallicheskih materialov (karbidy) (Thermophysical properties of non-metallic materials (carbides)). Energiya, Leningrad (in Russian)
46. Andrievskii RA, Strelnikova NS, Poltoratskii NI, Kharkhardin ED, Smirnov VS (1967) Melting point in systems ZrC-HfC, TaC-ZrC, TaC-HfC. *Powder Metall Met Ceram* 6(1):65–67
47. Storms EK (1964) A critical review of refractories. Report LA-TR-2942, Contract W-7405-ENG-36. Los Alamos Scientific Laboratory, New Mexico, pp. 1–255
48. Zhelankin VI, Kutsev VS (1964) Zavisimost teploty obrazovaniya karbida gafniya ot sostava (Dependence of the heat of formation of hafnium carbide upon the composition). *Zh Fiz Khim* 38(3):562–564 (in Russian)
49. Kornilov AN, Chelovskaya NV, Zhelankin VI, Shveikin GP (1977) Enthalpies of formation of hafnium carbides. *J Chem Thermodyn* 9(7):629–642
50. Portnoi KI, Chubarov VM (1967) Svoistva tugoplavkikh metallov i soedinenii (The properties of refractory metals and compounds). In: Tumanov AT, Portnoi KI (eds) *Tugoplavkie materialy v mashinostroenii* (Refractory materials in machinery construction). Mashinostroenie, Moscow, pp. 7–124 (in Russian)
51. Ormont BF (1959) Energii atomizatsii i teploty obrazovaniya nekotorykh karbidov i nitridov i naibolee veroyatnye znacheniya dlya energii dissotsiatsii azota i energii sublimatsii ugleroda (Atomization energies and heats of formation of some carbides and nitrides and the most probable values for the dissociation energy of nitrogen and sublimation energy of carbon). *Zh Fiz Khim* 33(7):1455–1460 (in Russian)
52. Zefirov AP (ed), Veryatin UD, Mashirev VP, Ryabtsev NG, Tarasov VI, Rogozkin BD, Korobov IV (1965) *Termodinamicheskie svoistva neorganicheskikh veschestv* (Thermodynamic properties of inorganic substances). Atomizdat, Moscow (in Russian)
53. Marmar ÉN, Gurvich OS, Maltseva LF (1967) *Vysokotemperaturnye materialy* (High-temperature materials). Metallurgiya, Moscow (in Russian)
54. Barin I (1995) *Thermochemical data of pure substances*, Vol. 1–2, 3rd edn. VCH, Weinheim, New York
55. Schick HL (ed) (1966) *Thermodynamics of certain refractory compounds*, Vol. 1–2. Academic Press, New York, London
56. Mah AD (1964) Heats of formation of zirconium carbide and hafnium carbide. Report BM-RI-6518. US Bureau of Mines, US Department of the Interior, Washington, DC, pp. 1–8
57. Oshcherin BN (1965) Nekotorye voprosy termodinamiki karbidnykh faz vnedreniya v oblasti gomogenosti (The certain problems of thermodynamics of carbide interstitial phases within the homogeneity ranges). In: Grigoreva VV, Eremenko VN, Nazarchuk TN, Samsonov GV, Fedorchenko IM, Frantsevich IN (eds) *Vysokotemperaturnye neorganicheskie soedineniya* (High-temperature inorganic compounds). Naukova Dumka, Kyiv, pp. 157–165 (in Russian)

58. Turchanin AG, Turchanin MA (1991) Termodinamika tugoplavkikh karbidov i karbonitridov (Thermodynamics of refractory carbides and carbonitrides). Metallurgiya, Moscow (in Russian)
59. Turchanin AG, Polyakov AE (1982) Thermodynamic properties of hafnium carbide in the temperature range 0–3000 K. *Inorg Mater* 18(3):335–338
60. Samsonov GV, Portnoi KI (1961) Splavy na osnove tugoplavkikh soedinenii (Alloys on the basis of refractory compounds). Oborongiz, Moscow (in Russian)
61. Pierson HO (1996) Handbook of refractory carbides and nitrides. Noyes Publications, Westwood, New Jersey
62. Lu X-G, Selleby M, Sundman B (2007) Calculations of thermophysical properties of cubic carbides and nitrides using the Debye-Grüneisen model. *Acta Mater* 55:1215–1226
63. Fesenko VV, Bolgar AS (1963) O kompleksnom izmerenii fiziko-khimicheskikh svoistv tugoplavkikh soedinenii pri vysokikh temperaturakh (On the complex measurement of physico-chemical properties of refractory compounds at high temperatures). In: Budnikov PP (ed) Silikaty i oksily v khimii vysokikh temperatur (Silicates and oxides in the chemistry of high temperatures). Metallurgizdat, Moscow, pp. 135–148 (in Russian)
64. Samsonov GV, Umanskii YaS (1957) Tverdye soedineniya tugoplavkikh metallov (Hard compounds of refractory metals). Metallurgizdat, Moscow (in Russian)
65. Sanders WA, Grisaffe SJ (1960) The hot-pressing of hafnium carbide (melting point, 7030 °F). Technical Note NASA-TN-D-303. NASA Lewis Research Center, Cleveland, Ohio, pp. 1–15
66. Kieffer R, Schwarzkopf P (1953) Hartstoffe und Hartmetalle (Refractory hard metals). Springer, Vienna (in German)
67. Hague JR, Lynch JF, Rudnick A, Holden FC, Duckworth WH (1964) Refractory ceramics for aerospace. Battelle Memorial Institute, The American Ceramic Society, Columbus, Ohio
68. Samsonov GV, Paderno VN (1965) Preparation of solid solution alloys of hafnium carbide with carbides of titanium, zirconium, niobium and tantalum and determination of their physical properties. *Russ Metall* (1):119–126
69. Bolgar AS, Turchanin AG, Fesenko VV (1973) Termodinamicheskie svoistva karbidov (Thermodynamic properties of carbides). Naukova Dumka, Kyiv (in Russian)
70. Guseva EA, Bolgar AS, Turchanin AG, Fesenko VV, Morozov VV (1971) Experimental study of heat contents of hafnium carbides in region of homogeneity at high temperatures. *Rus J Phys Chem* 45(11):1671–1674
71. Bolgar AS, Guseva EA, Fesenko VV (1967) Thermodynamic properties of zirconium and hafnium carbides in the range 298–2500 K. *Powder Metall Met Ceram* 6(1):31–33
72. Levinson LS (1964) High-temperature heat content of tungsten carbide and hafnium carbide. *J Chem Phys* 40(5):1437–1438
73. Turchanin AG (1984) Equations for the enthalpy and specific heat of hafnium carbide as functions of temperature and concentration in the homogeneity region. *Inorg Mater* 20(5):739–741
74. Nikolskaya TA, Avarbe RG (1971) Nekotorye zakonomernosti ispareniya karbidov perekhodnykh metallov IV-V podgrupp v vakuume (Some regularity of transition metals of IV-V subgroups carbides evaporation in a vacuum). In: Kornilov II, Matveeva NM (eds) Metallidy – stroenie, svoistva, primeneniye (Metallides – structure, properties, application). Nauka, Moscow, pp. 127–134 (in Russian)
75. Hansler RL (1965) Preferential vaporization of carbon from hafnium carbide. *J Electrochem Soc* 112(8):881
76. Fesenko VV, Bolgar AS (1969) Study of evaporation rates of carbides of titanium, zirconium, hafnium, niobium and tantalum at high temperatures. *High Temp* 7(2):226–233
77. Samsonov GV, Paderno VN (1963) Poluchenie i svoistva nekotorykh tugoplavkikh karbidnykh splavov (Preparation and properties of certain carbide alloys). *Zh Prikl Khim* 36(12):2759–2762 (in Russian)
78. Fridlender BA, Neshpor VS, Sokolov VV (1973) Thermal conductivities of pyrolytic hafnium nitride and carbide. *High Temp* 11(2):376–379

79. Sanders WA, Creagh JR, Zalabak C, Gangler JJ (1963) Preliminary investigation of the fabrication and properties of hafnium carbide. In: Ault GM, Barclay WF, Munger HP (eds) Proc. of technical conf. on high-temperature materials II. Cleveland, Ohio, 26–27 Apr 1961. Interscience Publishers, New York, pp. 469–483
80. Sanders WA, Probst HB (1968) Mechanical properties of hafnium carbide to 2635 °C. *Am Ceram Soc Bull* 47(4):354–358
81. Paderno YuB, Barantseva IG, Yupko VL (1965) Izmerenie teploprovodnosti i elektrosovotivleniya ZrC, HfC, NbC i TaC pri vysokikh temperaturakh (Measurement of thermal conductivity and electrical resistance of ZrC, HfC, NbC and TaC at high temperatures). In: Grigoreva VV, Eremenko VN, Nazarchuk TN, Samsonov GV, Fedorchenko IM, Frantsevich IN (eds) *Vysokotemperaturnye neorganicheskie soedineniya* (High-temperature inorganic compounds). Naukova Dumka, Kyiv (in Russian), pp. 199–204
82. Lynch JF (1979) Engineering property data on selected ceramics, Vol. 2 – Carbides. Report MCIC-HB-07. Metals and Ceramics Information Centre, Battelle Columbus Laboratories, Ohio, pp. 1–136
83. Deadmore DL (1965) Vaporization of tantalum carbide – hafnium carbide solid solutions. *J Am Ceram Soc* 48(7):357–359
84. Samsonov GV, Naumenko VY, Okhremchuk LN (1971) Herstellung und Eigenschaften von Karbiden der Übergangsmetalle in ihren Homogenitätsbereichen (Synthesis and properties of carbides of transition metals in their homogeneity range). *Phys Status Solidi A* 6(1):201–211 (in German)
85. Grisaffe SJ (1960) Thermal expansion of hafnium carbide. *J Am Ceram Soc* 43(9):494
86. Richardson JH (1965) Thermal expansion of three group IVa carbides to 2700 °C. *J Am Ceram Soc* 48(10):497–499
87. Jun CK, Shaffer PTB (1971) Thermal expansion of niobium carbide, hafnium carbide and tantalum carbide at high temperatures. *J Less Common Met* 24(3):323–327
88. Ramke WG, Latva JD (1963) Refractory ceramics and intermetallic compounds. *Aerospace Eng* 22(1):76–84
89. Nowotny H, Laube E (1961) Die thermische Ausdehnung des hochschmelzenden Phasen (The thermal expansion of high-melting point phases) *Planseeber Pulvermetall* 9:54–59 (in German)
90. Paderno YuB, Dudnik EM, Andreeva TV, Barantseva IG, Yupko VL (1965) Izmerenie koeffitsientov termicheskogo rasshireniya ZrC, HfC, NbC i TaC pri vysokikh temperaturakh (Measurement of the coefficients of thermal expansion of ZrC, HfC, NbC and TaC at high temperatures). In: Grigoreva VV, Eremenko VN, Nazarchuk TN, Samsonov GV, Fedorchenko IM, Frantsevich IN (eds) *Vysokotemperaturnye neorganicheskie soedineniya* (High-temperature inorganic compounds). Naukova Dumka, Kyiv, pp. 293–296 (in Russian)
91. Opeka MM, Talmy IG, Wuchina EJ, Zaykoski JA, Causey SJ (1999) Mechanical, thermal and oxidation properties of refractory hafnium and zirconium compounds. *J Eur Ceram Soc* 19:2405–2414
92. Aigner K, Lengauer W, Rafaja D, Ettmayer P (1994) Lattice parameters and thermal expansion of $Ti(C_xN_{1-x})$, $Zr(C_xN_{1-x})$, $Hf(C_xN_{1-x})$ and TiN_{1-x} from 298 to 1473 K as investigated by high-temperature X-ray diffraction. *J Alloys Compd* 215:121–126
93. Clinard FW Jr, Kempter CP (1968) Low-temperature electrical properties of some transition metals and transition-metal carbides. *J Less Common Met* 15:59–73
94. Samsonov GV, Sinelnikova VS (1962) *Vysokotemperaturnye metallokeramicheskie materialy* (High-temperature sintered metal-powder materials). UkrSSR Academy of Sciences, Kyiv (in Russian)
95. Strasser A, Koch LJ (1963) Thermal conductivity of carbides. *Nucleonics* 21(11):6–10
96. Golikova OA, Avgustinik AI, Klimashin GM, Kozlovskii LV, Ordanyan SS, Snetkova VA (1966) Electrical properties of carbides of transition metals in group 4. *Sov Phys Solid State* 7(12):2995–3002

97. Kuchma AYa, Samsonov GV (1966) Obrazovanie stabilnykh elektronnykh konfiguratsii i nekotorye fizicheskie svoystva karbidov i nitridov perekhodnykh metallov v oblasti ikh gomogennosti (Formation of stable electron configurations and some physical properties of carbides and nitrides of transition metals in the range of their homogeneity). *Izv AN SSSR Neorg Mater* 2(11):1970–1974 (in Russian)
98. Grebenkina VG, Denbnovetskaya EN (1974) Thermal coefficient of the electrical resistivity of carbides and their solid solutions. In: Samsonov GV (ed) *Refractory carbides*. Consultants Bureau, New York, London, pp. 269–274
99. Timofeeva II, Klochkov LA (1974) Variation in the lattice parameters and static distortions in the homogeneity range of transition metal monocarbides. In: Samsonov GV (ed) *Refractory carbides*. Consultants Bureau, New York, London, pp. 239–245
100. Samsonov GV, Kuchma AYa (1968) Magnetic susceptibility of zirconium, hafnium and niobium monocarbides. *Inorg Mater* 4(8):1195–1197
101. Samsonov GV, Paderno VN (1964) Über die Herstellung von Karbidmischkristallen und die Untersuchung ihrer physikalischen Eigenschaften (The production of mixed crystals of carbides and investigation of their physical properties). *Planseeber Pulvermetall* 12(1):19–31 (in German)
102. Mercatelli L, Sani E, Sansoni P, Giannini A, Francini F, Sciti D (2011) Intrinsic spectral selectivity in ultra-high temperature ceramics for solar applications. *CLEO Europe EQEC* 5942843
103. Sani E, Mercatelli L, Jafrancesco D, Sans J-L, Sciti D (2012) Ultra-high temperature ceramics for solar receivers: spectral and high-temperature emittance characterization. *J Eur Opt Rap Public* 7(12052):1–5
104. Sciti D, Guicciardi S, Nygren M (2008) Densification and mechanical behaviour of HfC and HfB₂ fabricated by spark plasma sintering. *J Am Ceram Soc* 91(5):1433–1440
105. Mackie WA, Carleson P, Fillion J, Hinrichs CH (1991) Normal spectral emittance of crystalline transition metal carbides. *J Appl Phys* 69(10):7236–7239
106. Zapadaeva TE, Petrov VA, Sokolov VV (1980) Emissivity of stoichiometric hafnium carbide at high temperatures. *High Temp* 18(1):68–75
107. Samsonov GV, Fomenko VS, Paderno YuB (1962) Spectral emittance of the powders of some high-melting compounds. *Refract Indust Ceram* 3(1–2):35–37
108. Samsonov GV, Paderno VN (1961) Poluchenie i nekotorye svoystva karbida gafniya (Preparation and certain properties of hafnium carbide). *Zh Prikl Khim* 34(5):963–969 (in Russian)
109. Deadmore D (1964) Normal spectral emittance (0.65 μ) of TaC-HfC solid solutions and tungsten above 1600 °C. *J Am Ceram Soc* 47(12):649–650
110. Sheindlin AE, Petrov VA, Vinnikova AN, Nikolaeva VA (1969) Integral normal emissivity of tantalum and hafnium carbides over temperature range 1300–3000 K. *High Temp* 7(2):236–238
111. Pears CD (1963) Some problems in emittance measurements at the higher temperatures and surface characterization. In: Richmond JC (ed) *Measurement of thermal radiation properties of solids*. NASA Office of Scientific and Technical Information, Washington, DC, pp. 541–550
112. Fomenko VS, Naumenko VYa, Okhremchuk LN, Podchernyaeva IA, Samsonov GV (1970) Glühemissionseigenschaften der Monokarbide von Übergangsmetallen der IV und V Gruppe im Homogenitätsbereich (The thermionic emission properties of transition metals monocarbides of groups IV and V in the homogeneity range). *Phys Status Solidi A* 2(3):K181–K184 (in German)
113. Fomenko VS (1981) Emissionnye svoystva materialov (The thermionic emission properties of materials). *Naukova Dumka, Kyiv* (in Russian)
114. Ingold JH (1963) Thermionic properties of some refractory metal carbides. *J Appl Phys* 34(7):2033–2039
115. Denbnovetskaya EN, Lavrenko VA, Podchernyaeva IA, Protsenko TG, Siman NI, Fomenko VS (1971) Electron work function and surface recombination of hydrogen for alloys of the system HfC-WC. *Powder Metall Met Ceram* 10(4):289–291

116. Gorbatyi NA, Lvov GV, Perederii VA, Reshetnikov LV, Fekhetdinov FA (1966) Termoelektronnaya emissiya karbidov gafniya i tsirkoniya (Thermionic emission of hafnium and zirconium carbides). *Izv AN SSSR Ser Fiz* 30(12):1942–1949 (in Russian)
117. Samsonov GV, Fomenko VS, Paderno VN, Rud BM (1964) Thermoemission characteristics of alloys of isomorphous carbides. *High Temp* 2(5):656–658
118. Hojo H, Nakayama K (1976) Coated emitters of transition metal carbides for vacuum measurement. *J Vac Soc Jpn* 19(9):312–317 (in Japanese)
119. Samsonov GV, Siman NI, Podchernyaeva IA, Fomenko VS (1976) Issledovanie energii adsorbtsii Cs i K na poverkhnosti tugoplavkikh karbidov (Study of Cs and K adsorption energies on surface of high-melting carbides). *Zh Tekh Fiz* 46(2):393–397 (in Russian)
120. Matskevich TL, Krachino TV, Kazantsev AP (1963) Thermionic emission of HfB_2 , HfC , HfO_2 , VC and a solid solution of $(\text{UC})_1(\text{ZrC})_4$. *Sov Phys Tech Phys* 7(10):934–940
121. Ingold JH (1961) Thermionic properties of HfC . *J Appl Phys* 32(12):2651
122. Samsonov GV, Paderno YuB, Fomenko VS (1965) K voprosu o termoemissionnykh kharakteristikakh perekhodnykh metallov i ikh soedinenii (To the problem of thermionic emission characteristics of transition metals and their compounds). In: Grigoreva VV, Eremenko VN, Nazarchuk TN, Samsonov GV, Fedorchenko IM, Frantsevich IN (eds) *Vysokotemperaturnye neorganicheskie soedineniya* (High-temperature inorganic compounds). *Naukova Dumka, Kyiv*, pp. 108–115 (in Russian)
123. Yada K, Masaoka H, Shoji Y, Tanji T (1989) Studies of refractory carbides, nitrides and borides as the thermionic emitters for electron microscopy. *J Electron Microsc Tech* 12:252–261
124. Ramqvist L (1969) Preparation, properties and electronic structure of refractory carbides and related compounds. *Jernkontoret Ann* 153(4):159–179
125. Ramqvist L (1971) Electronic structure of cubic refractory carbides. *J Appl Phys* 42(5):2113–2127
126. Travushkin GG, Knyazev VI, Belov VS, Rymashevskii GA (1973) Temperature threshold of brittle failure in interstitial phases. *Strength Mater* 5(5):639–641
127. Kovalchenko MS, Dzhemelinskii VV, Borisenko VA (1969) Temperature dependence of the hardness of titanium, zirconium and hafnium carbides. *Strength Mater* 1(5):515–518
128. Vahldiek FW, Mersol SA (1977) Slip and microhardness of IVa to VIa refractory materials. *J Less Common Met* 55(2):265–278
129. Ivanko AA (1968) Tverdst (The hardness). *Naukova Dumka, Kyiv* (in Russian)
130. Ordanyan SS, Unrod VI, Lutsenko AE (1977) Reactions in system HfC-HfB_2 . *Inorg Mater* 13(3):451–453
131. Ordanyan SS, Zaitsev GP, Kats SM, Avgustinik AI (1976) Microhardness of alloys in system HfC-TaC . *Inorg Mater* 12(9):1293–1296
132. Tsuchida T, Mekata M, Nakamura Y, Sakurai J, Takaki H (1961) Hall effect in carbides of transition metals. *J Phys Soc Jpn* 16(12):2453–2456
133. Bazhenova LN, Ivanko AA (1969) Microhardness of carbides of certain transition metals. *Inorg Mater* 5(12):1763–1767
134. Westbrook JH, Stover ER (1967) Carbides for high-temperature applications. In: Campbell IE, Sherwood EM (eds) *High-temperature materials and technology*. Wiley, New York, pp. 312–348
135. Adams RP, Beall RA (1963) Preparation and evaluation of fused hafnium carbide. Report BM-RI-6304. Bureau of Mines, US Department of the Interior, Washington DC, pp. 1–17
136. Sanders WA, Drell IL (1963) Compatibility of molten uranium dioxide with five refractory materials. Report NASA-TN-D-1442. National Aeronautics and Space Administration, Washington DC, pp. 1–19
137. Adams RP, Copeland MI, Deardorff DK, Lincoln RL (1968) Cast hafnium carbide – carbon alloys: preparation, evaluation and properties. Report BM-RI-7137. Bureau of Mines, US Department of the Interior, Washington DC, pp. 1–50
138. Krikorian OH (1960) Thermal expansion of high temperature materials. Report UCLRL-6132. Office of Technical Services, US Department of Commerce, Washington DC, pp. 1–10

139. Neel DS, Pears CD, Oglesby S, Jr (1962) The thermal properties of thirteen solid materials to 5000 °F or their destruction temperatures. Technical Report WADD-TR-60-924, Contract USAF 33(616)-6312. Southern Research Institute, University of Alabama, Birmingham, USA, pp. 1–216
140. Kislyi PS (1979) Poluchenie izdelii iz tugoplavkikh soedinenii metodami poroshkovoi metallurgii (The manufacture of articles from refractory compounds by powder metallurgy methods). *Zh Vsesoyuz Khim Obshchestva Im D I Mendeleev* 24(3):270–276 (in Russian)
141. Khusainov MA (1979) Termoprochnost tugoplavkikh materialov, poluchennykh gazofaznym osazhdeniem (Thermal strength of refractory materials manufactured by gas-phase deposition). Leningrad State University, Leningrad (in Russian)
142. Zubarev PV (1985) Zharoprochnost faz vnedreniya (The heat-resistance of interstitial alloys). *Metallurgiya*, Moscow (in Russian)
143. Spivak II, Klimenko VV (1973) Sinterization kinetics in the hot pressing and recrystallization of carbides. *Powder Metall Met Ceram* 12(11):883–887
144. Kats SM, Ordanyan SS, Zaitsev GP (1981) High-temperature creep of solid solutions in the HfC-TaC system. *Inorg Mater* 17(11):1519–1522
145. Spivak II, Klimenko VV (1971) A study of diffusion effects on interstitial phases. *Phys Met Metallogr* 32(2):87–92
146. Touloukian YS (ed) (1967) Thermophysical properties of high temperature solid materials, Vol. 6. Macmillan, New York
147. Lewis D, Porter LJ (1970) Plastic deformation in hafnium carbide. *J Less-Common Met* 22:439–444
148. Ferro D, Barinov SM, Rau JV, Latini A, Scandurra R, Brunetti B (2006) Vickers and Knoop hardness of electron beam deposited ZrC and HfC thin films on titanium. *Surf Coat Technol* 200:4701–4707
149. Liu J-X, Huang X, Zhang G-J (2013) Pressureless sintering of hafnium carbide – silicon carbide ceramics. *J Am Ceram Soc* 96(6):1751–1756
150. Brown HL, Armstrong PE, Kempter CP (1966) Elastic properties of some polycrystalline transition-metal monocarbides. *J Chem Phys* 45(2):547–549
151. Frantsevich IN, Voronov FF, Bakuta SA (1982) Uprugie postoyannye i moduli uprugosti metallov i nemetallov (The elastic constants and elasticity moduli of metals and non-metals). *Naukova Dumka*, Kyiv (in Russian)
152. Lynch JF, Ruderer CG, Duckworth WH (1966) Engineering properties of selected ceramic materials. The American Ceramic Society, Columbus, Ohio
153. Kral C, Lengauer W, Rafaja D, Ettmayer P (1998) Critical review on the elastic properties of transition metal carbides, nitrides and carbonitrides. *J Alloys Compd* 265:215–233
154. Shaffer PTB (1964) Handbooks of high-temperature materials: No. 1 – Materials index. Plenum Press, Springer, New York
155. Santhanam AT (1996) Application of transition metal carbides and nitrides in industrial tools. In: Oyama ST (ed) *The chemistry of transition metal carbides and nitrides*. Chapman & Hall, London, Glasgow, pp. 28–52
156. Frantsevich IN, Gnesin GG, Kurdyumov AV, Karyuk GG, Bochko AV, Semenenko NP (1980) Sverkhтвердые материалы (Super-hard materials). *Naukova Dumka*, Kyiv (in Russian)
157. Bukatov VG, Knyazev VI, Korostin OS, Baranov VM (1975) Temperature dependence of the Young's modulus of metallic carbides. *Inorg Mater* 11(2):310–312
158. Frantsevich IN, Lyashchenko AB (1966) Young's moduli of the carbides of some transition metals. *Powder Metall Met Ceram* 5(7):573–574
159. Weber W (1973) Lattice dynamics of transition-metal carbides. *Phys Rev B* 8(11):5082–5092
160. Smith HG, Gläser W (1970) Phonon spectra in TaC and HfC. *Phys Rev Lett* 25(23):1611–1613
161. Wu Z, Chen X-J, Struzhkin VV, Cohen RE (2005) Trends in elasticity and electronic structure of transition-metal nitrides and carbides from first principles. *Phys Rev B* 71(21):214103
162. Isaev EI, Simak SI, Abrikosov IA, Ahuja R, Vekilov YuKh, Katsnelson MI, Lichtenstein AI, Johansson B (2007) Phonon related properties of transition metals, their carbides and nitrides: a first principles study. *J Appl Phys* 101:123519-1 – 123519-18

163. Srivastava A, Diwan BD (2012) Elastic and thermodynamic properties of divalent transition metal carbides MC (M = Ti, Zr, Hf, V, Nb, Ta). *Can J Phys* 90:331–338
164. He LF, Lin ZJ, Wang JY, Bao YW, Zhou YC (2008) Crystal structure and theoretical elastic property of two new ternary ceramics $\text{Hf}_3\text{Al}_4\text{C}_6$ and $\text{Hf}_2\text{Al}_4\text{C}_5$. *Scripta Mater* 58:679–682
165. Lide DR (ed) (2010) CRC handbook of chemistry and physics, 90th edn. CRC Press, Boca Raton, New York
166. Samsonov GV (ed) (1976) *Svoistva elementov (Properties of elements)*, 2nd ed., Vol. 1. Metallurgiya, Moscow (in Russian)
167. Audi G, Wapstra AH, Thibault C, Blachot J, Bersillon O (2003) The NUBASE evaluation of nuclear and decay properties. *Nucl Phys A* 729:3–128
168. De Laeter JR, Böhlke JK, De Bièvre P, Hidaka H, Peiser HS, Rosman KJR, Taylor PDP (2003) Atomic weights of the elements. Review 2000 (IUPAC Technical report). *Pure Appl Chem* 75(6):683–800
169. Wieser ME (2006) Atomic weights of the elements 2005. (IUPAC Technical report). *Pure Appl Chem* 78(11):2051–2066
170. Sears VF (1992) Neutron scattering lengths and cross sections. *Neutron News* 3(3):26–37
171. Noguere G, Courcelle A, Palau JM, Siegler P (2005) Low neutron energy cross sections of the hafnium isotopes. JEF/DOC-1077. JEFF Meeting 4–5 May 2005, OECD/NEA, Issy-les-Moulineaux, France. https://www.oecd-nea.org/dbdata/nds_jefreports/jefreport-23/supp/jefdoc/jefdoc-1077.pdf. Accessed 18 March 2014
172. Kovalchenko MS, Ogorodnikov VV, Rogovoi YuI, Krainii AG (1979) *Radiatsionnoe povrezhdenie tugoplavkikh soedinenii (The radiation damage of refractory compounds)*. Atomizdat, Moscow (in Russian)
173. Kubaschewski O (1990) The Al-C-Hf (aluminium-carbon-hafnium) system. *Ternary Alloys VCH* 3:494–496
174. Shurin AK, Dmitrieva GP, Cherepova TS (1996) Phase equilibria in Co – Me'C – Me''C alloys. 1. Systems with three-phase eutectic equilibria. *Powder Metall Met Ceram* 35(11–12):615–620
175. Shurin AK, Dmitrieva GP, Cherepova TS (1997) Phase equilibria in Co – Me'C – Me''C alloys. 2. Systems with four-phase eutectic equilibrium. *Powder Metall Met Ceram* 36(3–4):193–196
176. Velikanova TYa, Bondar AA, Grytsiv AV, Dovbenko OI (2001) Metallochemistry of chromium with *d*-metals and carbon. *J Alloys Compd* 320:341–352
177. Barsoum MW (2010) The $M_{n+1}AX_n$ phases and their properties. In: Riedel R, Chen I-W (eds) *Ceramics science and technology, Vol. 2 – Materials and properties*. Wiley – VCH, Weinheim, pp. 299–347
178. Barsoum MW (2013) *MAX phases: properties of mashinable carbides and nitrides*. Wiley – VCH, Weinheim
179. Savitskii EM, Burkhanov GS (1971) *Metallovedenie splavov tugoplavkikh i redkikh metallov (Metallography of refractory and less-common metal alloys)*, 2nd edn. Nauka, Moscow (in Russian)
180. Ordanyan SS, Kraskovskaya AA, Avgustinnik AI (1966) Fazovaya diagramma sistemy HfC-Mo (Phase diagram of the HfC-Mo). *Izv AN SSSR Neorg Mater* 2(2):299–302 (in Russian)
181. Rokhlin L, Kolchugina N, Dobatkina T, Semenova E (2010) Carbon – hafnium – molybdenum system. In: Effenberg G, Ilyenko S (eds) *Ternary alloy systems, Subvol. E, Part 2*. Springer, Berlin, Heidelberg, pp. 409–428
182. Eremenko VN, Shabanova SV, Velikanova TYa, Petrenko LA (1975) Structure of alloys and phase equilibria of the system Hf-Mo-C. I. Projection of the solidus surface of the partial system Mo-HfC-Hf. *Powder Metall Met Ceram* 14(7):555–561
183. Dmitrieva GP, Razumova NA, Shurin AK (1984) Phase equilibrium diagram of the Ni-TiC-HfC system. *Powder Metall Met Ceram* 23(2):159–162
184. Raevskaya MV, Tatarkina AL, Kulova LK (1981) Fazovye ravnovesiya v kvazi-troinykh sistemakh nikel – karbid volframa (WC) – karbid tsirkoniya (ZrC) i nikel – karbid volframa (WC) – karbid gafniya (HfC) (Phase equilibria in the nickel – tungsten carbide (WC) – zirconium carbide (ZrC) and nickel – tungsten carbide (WC) – hafnium carbide (HfC) quasiternary systems). In: Drits ME (ed) *Fazovye ravnovesiya v metallicheskih splavakh (Phase equilibria in metallic alloys)*. Nauka, Moscow, pp. 273–276 (in Russian)

185. Shurin AK, Dmitrieva GP, Razumova NA, Khandros EL (1987) Phase diagram of the Ni-ZrC-HfC. *Powder Metall Met Ceram* 26(9):754–757
186. Kosterova NV, Ordanyan SS, Neshpor VS, Ostrovskii EK (1980) Thermoionic properties of cermets of eutectic compositions in Me(IV) – (C,B) – (Mo,Re,W) systems. *Powder Metall Met Ceram* 19(1):61–66
187. Brukl CE (1966) The Zr-Si-C, Hf-Si-C, Zr-Si-B, and Hf-Si-B systems. In: Ternary phase equilibria in transition metal-boron-carbon-silicon systems. Report AFML-TR-65-2, Contract USAF 33(615)-1249, Part 2, Vol. 10. Air Force Materials Laboratory, Wright-Patterson Air Force Base, Ohio, pp. 1–95
188. Cacciamani G, Riani P (2010) Carbon – hafnium – silicon system. In: Effenberg G, Ilyenko S (eds) Ternary alloy systems. Subvol. E, Part 2. Springer, Berlin, Heidelberg, pp. 429–432
189. Kumar BVM, Basu B (2008) Fretting wear properties of TiCN-Ni cermets: influence of load and secondary carbide addition. *Metall Mater Trans A* 39:539–550
190. Eremenko VN, Velikanova TYa, Artyukh LV, Akselrod GM, Vishnevskii AS (1976) Issledovanie splavov troinykh sistem W-HfC-C i W-ZrC-C pri subsolidusnykh temperaturakh (A study of ternary systems W-HfC-C and W-ZrC-C alloys at subsolidus temperatures). *Dopov Akad Nauk Ukr RSR Ser A Fiz Mat Tekh Nauki* 38(1):83–89 (in Russian)
191. Eremenko VN, Velikanova TYa, Artyukh LV, Vishnevskii AS (1975) Phase diagram of ternary system hafnium-tungsten-carbon. Solidus surface projection. *Rev Int Hautes Temp Refract* 12(3):209–213
192. Brukl CE, Harmon DP (1966) The Ti-Zr-C, Ti-Hf-C and Zr-Hf-C systems. In: Ternary phase equilibria in transition metal-boron-carbon-silicon systems. Report AFML-TR-65-2, Contract USAF 33(615)-1249, Part 2, Vol. 4. Air Force Materials Laboratory, Wright-Patterson Air Force Base, Ohio, pp. 1–78
193. Bittermann H, Rogl P (2002) Critical assessment and thermodynamic calculation of ternary system C-Hf-Zr (carbon-hafnium-zirconium). *J Phase Equilib* 23(3):218–235
194. Nowotny H, Rudy E, Benesovsky F (1961) Untersuchungen in den Systemen – Hafnium-Bor-Kohlenstoff und Zirconium-Bor-Kohlenstoff (Investigations in the systems hafnium-boron-carbon and zirconium-boron-carbon). *Monatsh Chem* 92(2):393–406 (in German)
195. Samsonov GV, Strashinskaya LV, Shiller EA (1962) Kontaktnoe vzaimodeistvie metallopodobnykh karbidov, nitridov i boridov s tugoplavkimi metallami pri vysokikh temperaturakh (The contact interaction of metal-like carbides, nitrides and borides with refractory metals at high temperatures). *Izv AN SSSR OTN Metall Toplivo* 5:167–180 (in Russian)
196. Rudy E, Nowotny H (1963) Untersuchungen im System Hafnium-Tantal-Kohlenstoff (Investigations in the system hafnium-tantalum-carbon). *Monatsh Chem* 94(3):507–517 (in German)
197. Emelyanov VS, Yevstyukhin AI, Godin YuG, Solovyev GI, Kokhtev SA (1967) Issledovanie karbidnoi oblasti v sisteme Ta-Hf-C (Investigation of carbide region of Ta-Hf-C system). In: Emelyanov VS, Yevstyukhin AI (eds) *Metallurgiya i metallovedenie chistykh metallov (Metallurgy and metallography of pure metals)*, Vol. 6. Atomizdat, Moscow, pp. 108–114 (in Russian)
198. Zakharov AM, Naumkin OP, Kurganov GV (1974) Tungsten-rich corner of W-Zr-C and W-Hf-C ternary systems. *Russ Metall* (1):136–139
199. Fedorov TF, Gladyshevskii EI, Gorshkova LV (1966) O fazovykh ravnovesiyakh v troinoi sisteme Hf-Re-C (On phase equilibria in the ternary system Hf-Re-C). *Izv AN SSSR Metall* (6):134–136 (in Russian)
200. Manning C, Stoops R (1968) High-temperature cermets. I. Compatibility. *J Am Ceram Soc* 51(8):411–415
201. Adelsberg LM, Cadoff LH, Tobin JM (1966) Group IVB and VB metal carbide – carbon eutectic temperatures. *J Am Ceram Soc* 49(10):573–574
202. Strife JR, Smeggil JG, Worell WL (1990) Reaction of iridium with metal carbides in the temperature range of 1923 to 2400 K. *J Am Ceram Soc* 73(4):838–845

203. McDevitt SM, Billings GW, Indacochea JE (2002) High temperature interaction behavior at liquid metal – ceramic interfaces. *J Mater Eng Performance* 11(4):392–401
204. Borisova AL (1985) Sovmestimost tugoplavkikh soedinenii s metallami i grafitom (The compatibility of refractory compounds with metals and graphite). *Naukova Dumka, Kyiv* (in Russian)
205. Shurin AK, Dmitrieva GP (1974) Phase diagrams of iron alloys with zirconium and hafnium carbides. *Metal Sci Heat Treat* 16(7–8):665–667
206. Kislyi PS, Kuzenkova MA, Bodnaruk NI, Grabchuk BL (1988) Karbid bora (Boron carbide). *Naukova Dumka, Kyiv* (in Russian)
207. Rogl P (2009) Boron – carbon – hafnium system. In: Effenberg G, Ilyenko S (eds) Ternary alloy systems, Subvol. E, Part 1. Springer, Berlin, Heidelberg, pp. 282–305
208. Rudy E, Windisch S (1966) Phase diagrams of the systems Ti-B-C, Zr-B-C and Hf-B-C. In: Ternary phase equilibria in transition metal - boron - carbon - silicon systems. Report AFML-TR-65-2, Contract USAF 33(615)-1249, Part 2, Vol. 13. Air Force Materials Laboratory, Wright Patterson Air Force Base, Ohio, pp. 1–212
209. Bittermann H, Rogl P (1998) The system boron – carbon – hafnium. In: Effenberg G (ed) Phase diagrams of ternary metal-boron-carbon systems. ASM International, Materials Park, Ohio, pp. 102–141
210. Samsonov GV, Kulik OP, Polishchuk VS (1978) Poluchenie i metody analiza nitridov (The preparation and analysis methods of nitrides). *Naukova Dumka, Kyiv* (in Russian)
211. Golubev AS, Kurdyumov AV, Pilyankevich AN (1987) Nitrid bora: struktura, svoystva, poluchenie (Boron nitride: structure, properties, preparation). *Naukova Dumka, Kyiv* (in Russian)
212. Burykina AL, Strashinskaya LV (1965) A study of new materials operating in contact with certain solid and liquid metals and compounds. *Mater Sci* 1(5):385–389
213. Samsonov GV (ed) (1973) The oxide handbook. IFI/Plenum, New York, London
214. Eremenko VN, Shabanova SV, Velikanova TYa, Petrenko LA (1975) Structure of alloys and the phase equilibrium diagram of the system Hf-Mo-C. II. *Powder Metall Met Ceram* 14(8):643–648
215. Eremenko VN, Shabanova SV, Velikanova TYa (1977) Structure of alloys and the phase equilibrium diagram of the system Hf-Mo-C. V. Isothermal section of the system Hf-Mo-C at 1700 °C. *Powder Metall Met Ceram* 16(9):712–717
216. Eremenko VN, Shabanova SV, Velikanova TYa (1977) Structure of alloys and the phase equilibrium diagram of the system Hf-Mo-C. VI. Isothermal section of the Hf-Mo-C system at 1400 °C. *Powder Metall Met Ceram* 16(10):772–777
217. McClaine LA (ed) (1962) Thermodynamic and kinetic studies for a refractory materials program. Technical Report ASD-TDR-62-204, Contract AF33(616)-7472, Part 1. Air Force Materials Laboratory, Wright-Patterson Air Force Base, Ohio, pp. 1–92
218. Dmitrieva GP, Razumova NA, Shurin AK (1984) Phase equilibria in alloys of the Ni-HfC-Mo₂C system. *Powder Metall Met Ceram* 23(9):714–718
219. Silvestroni L, Sciti D (2010) Sintering behaviour, microstructure and mechanical properties: a comparison among pressureless sintered ultra-refractory carbides. *Adv Mater Sci Eng* ID835018:1–11. <https://doi.org/10.1155/2010/835018>
220. Silvestroni L, Bellosi A, Melandri C, Sciti D, Liu JX, Zhang GJ (2011) Microstructure and properties of HfC and TaC-based ceramics obtained by ultrafine powder. *J Eur Ceram Soc* 31:619–627
221. Rogl P, Naik SK, Rudy E (1977) A constitutional diagram of the system TiC-HfC-MoC. *Monatsh Chem* 108(6):1325–1337
222. Rogl P, Naik SK, Rudy E (1977) A constitutional diagram of the system VC_{0.88}-HfC_{0.98}- (MoC). *Monatsh Chem* 108(6):1339–1352
223. Binder S, Lengauer W, Ettmayer P, Bauer J, Debuigne J, Bohn M (1995) Phase equilibria in the systems Ti-C-N, Zr-C-N and Hf-C-N. *J Alloys Compd* 217(1):128–136
224. Rudy E, Nowotny H, Benesovsky F, Kieffer R, Neckel A (1960) Über Hafniumkarbid enthaltende Karbidssysteme (On hafnium carbide containing carbide systems). *Monatsh Chem* 91(1):176–187 (in German)

225. Fedorov TF, Gladyshevskii EI (1965) Phase equilibria in ternary systems of transition metals of groups IV and V and carbon. *Powder Metall Met Ceram* 4(1):27–29
226. Kosolapova TYa, Fedorus VB, Kuzma YuB (1966) Vzaimodeistvie karbidov perekhodnykh metallov s ikh okislami (Interaction between carbides of transition metals and their oxides). *Izv AN SSSR Neorg Mater* 2(8):1516–1520 (in Russian)
227. Kumar BVM, Balasubramaniam R, Basu B (2007) Electrochemical behaviour of TiCN-Ni-based cermets. *J Am Ceram Soc* 90(1):205–210
228. Schuster JC (1993–1994) Silicon carbide and transition metals: a critical evaluation of existing phase diagram data supplemented by new experimental results. *Int J Refract Met Hard Mater* 12(4):173–177
229. Gusev AI (1984) Calculation of phase diagrams of pseudobinary systems based on high-melting carbides of titanium, zirconium, hafnium and vanadium. *Inorg Mater* 20(7):976–981
230. Bandyopadhyay D, Sharma RC, Chakraborti N (2000) The C-Hf-Ti (carbon-hafnium-titanium) system. *J Phase Equilib* 21(6):535–538
231. Voroshilov YuV, Gorshkova LV, Popova AM, Fedorov TF (1967) Ternary systems Ti-Zr-C and Ti-Hf-C. *Powder Metall Met Ceram* 6(5):403–405
232. Rogl P, Naik SK, Rudy E (1977) A constitutional diagram of the system TiC-HfC-WC. *Monatsh Chem* 108(5):1189–1211
233. Andrievskii RA, Spivak II, Klimenko VV (1972) O proyavlenii sverkhplastichnosti u tugoplavkikh soedinenii (On manifestation of superplasticity in refractory compounds). *Doklady AN SSSR* 203(6):1279–1281 (in Russian)
234. Rogl P, Naik SK, Rudy E (1977) A constitutional diagram of the system VC_{0.88}-HfC_{0.98}-WC. *Monatsh Chem* 108(5):1213–1234
235. Eremenko VN, Velikanova TY, Shabanova SV, Artyukh LV (1973) Continuous series of solid solutions of carbides with NaCl structure in the ternary systems Mo(W)-Me^{IV,V}-C. *Powder Metall Met Ceram* 12(11):909–912
236. Nowotny H, Kieffer R, Benesovsky F (1960) Uber die Systeme HfC-UC, HfC-TiC, HfC-ZrC, HfC-VC, HfC-NbC, HfC-TaC, HfC-Cr₂C₃, HfC-Mo₂C (MoC) und HfC-WC (On the systems HfC-UC, HfC-TiC, HfC-ZrC, HfC-VC, HfC-NbC, HfC-TaC, HfC-Cr₂C₃, HfC-Mo₂C (MoC) and HfC-WC). *Angew Chem* 72(1):37 (in German)
237. Shimada S, Nakajima K, Inagaki M (1997) Oxidation of single crystals of hafnium carbide in a temperature range of 600 to 900 °C. *J Am Ceram Soc* 80(7):1749–1756
238. Voitovich RF, Pugach ÉA (1973) High-temperature oxidation of ZrC and HfC. *Powder Metall Met Ceram* 12(11):916–920
239. Voitovich RF, Pugach ÉA (1975) Vysokotemperaturnoe okislenie karbidov perekhodnykh metallov IV-VI grupp (High-temperature oxidation of transition metals IV-VI groups carbides). In: Samsonov GV (ed) *Vysokotemperaturnye karbidy* (High-temperature carbides). Naukova Dumka, Kyiv, pp. 143–156 (in Russian)
240. Voitovich RF, Pugach ÉA (1976) Nekotorye osobennosti protsessa okisleniya karbidov metallov IV-VI grupp (The certain features of the oxidation process of metals IV-VI groups carbides). In: Samsonov GV, Kosolapova TYa, Gnesin GG, Fedorus VB, Domasevich LG (eds) *Karbidy i splavy na ikh osnove* (Carbides and alloys based on them). Naukova Dumka, Kyiv, pp. 233–234 (in Russian)
241. Voitovich RF (1981) Okislenie karbidov i nitridov (Oxidation of carbides and nitrides). Naukova Dumka, Kyiv (in Russian)
242. Achour M, Pialoux A, Dode M (1975) Etude de la carboreduction progressive du dioxyde de hafnium. 2. Determination de la pression de l'equilibre monovariant: $\alpha\text{-HfO}_2 + 3\text{C} \leftrightarrow \text{HfC} + 2\text{CO}$, entre 1300 °C et 1650 °C. Isothermes de carboreduction de l' $\alpha\text{-HfO}_2$ en presence d'un excès de carbone (Study of progressive reduction of hafnium dioxide by carbon. II. Determination of the monovariant equilibrium pressure: $\alpha\text{-HfO}_2 + 3\text{C} \leftrightarrow \text{HfC} + 2\text{CO}$ between 1300 °C and 1650 °C. Isotherms of $\alpha\text{-HfO}_2$ reduction by carbon in the presence of carbon excess). *Rev Int Hautes Temp Refract* 12(3):281–287 (in French)
243. Lovell JM, Mackie WA, Magera GG (2012) Hafnium carbide thermal sources in O₂, CO and CO₂ environments. In: Proc. IEEE 9th Int. vacuum electron sources conf. IVESC-2012, Monterey, California, pp. 303–304
244. Tuffias RH, Duffy AJ, Arrieta VM, Abrams WM, Benander RE (1997) Materials and fabrication processes for operation in hot hydrogen. *AIP Conf Proc* 387:1613–1618

245. Kuriakose AK, Margrave JL (1964) Kinetics of reaction of elemental fluorine. II. The fluorination of hafnium carbide and hafnium boride. *J Phys Chem* 68(8):2343–2345
246. Kieffer R, Nowotny H, Etmayer P, Freudhofmeier M (1970) Über die Beständigkeit von Übergangsmetallcarbiden gegen Stickstoff bis zu 300 at (On the stability of transition metal carbides in nitrogen up to 300 atm). *Monatsh Chem* 101(1):65–82 (in German)
247. Samsonov GV (1962) Analiz tugoplavkikh soedinenii (The analysis of refractory compounds). Metallurgizdat, Moscow (in Russian)
248. Shirotori Y, Ozawa K, Edamoto K, Otani S (2006) Formation of oxide layer on HfC (100) surface studied by photoemission spectroscopy. *e-J Surf Sci Nanotech* 4:219–226
249. Shimada S (2002) A thermoanalytical study on the oxidation of ZrC and HfC powders with formation of carbon. *Solid State Ionics* 149(3–4):319–326
250. Shimada S, Inagaki M, Matsui K (1992) Oxidation kinetics of hafnium carbide in the temperature range of 480 to 600 °C. *J Am Ceram Soc* 75(10):2671–2678
251. Shimada S, Yunazar F, Otani S (2000) Oxidation of hafnium carbide and titanium carbide single crystals with the formation of carbon at high temperatures and low oxygen pressures. *J Am Ceram Soc* 83(4):721–728
252. Shimada S (2001) Formation and mechanism of carbon-containing oxide scales by oxidation of carbides (ZrC, HfC, TiC). *Mater Sci Forum* 369–372(1):377–384
253. Shimada S (2001) Oxidation and mechanism of single crystal carbides with formation of carbon. *J Ceram Soc Jpn* 109(3):S33–S42
254. Bargeron CB, Benson RC (1988) X-ray microanalysis of a hafnium carbide film oxidized at high temperature. *Surf Coat Technol* 36:111–115
255. Bargeron CB, Benson RC, Newman RW, Jette AN, Phillips TE (1993) Oxidation mechanisms of hafnium carbide and hafnium diboride in the temperature range 1400 to 2100 °C. *Johns Hopkins APL Techn Digest* 14(1):29–36
256. Bargeron CB, Benson RC, Jette AN, Phillips TE (1993) Oxidation of hafnium carbide in the temperature range 1400 to 2060 °C. *J Am Ceram Soc* 76(4):1040–1046
257. Holcomb GR (1988) The high temperature oxidation of hafnium carbide. PhD thesis, Ohio State University, Columbus, Ohio
258. Courtright EL, Prater JT, Holcomb GR, Pierre GRSt, Rapp RA (1991) Oxidation of hafnium carbide with additions of tantalum and praseodymium. *Oxid Met* 36(5–6):423–437
259. Holcomb GR, Pierre GRSt (1993) Application of a counter-current gaseous diffusion model to the oxidation of hafnium carbide at 1200 to 1530 °C. *Oxid Met* 40(1–2):109–118
260. Berkowitz-Mattuck JB (1967) High-temperature oxidation. IV. Zirconium and hafnium carbides. *J Electrochem Soc* 114(10):1030–1033
261. Wang Y-L, Xiong X, Li G-D, Zhang H-B, Chen Z-K, Sun W, Zhao X-J (2012) Microstructure and ablation behavior of hafnium carbide coating for carbon/carbon composites. *Surf Coat Technol* 206:2825–2832
262. Wang Y-L, Xiong X, Zhao X-J, Li G-D, Chen Z-K, Sun W (2012) Structural evolution and ablation mechanism of a hafnium carbide coating on C/C composite in an oxyacetylene torch environment. *Corros Sci* 61:156–161
263. Samsonov GV, Panasyuk AD, Kozina GK, Dyakonova LV (1972) Contact reaction of refractory compounds with liquid metals. I. Reaction of carbides of subgroup IVa metals with the iron group metals. *Powder Metall Met Ceram* 11(7):568–571
264. Samsonov GV, Panasyuk AD, Kozina GK, Dyakonova LV (1976) Kontaknoe vzaimod-eistvie karbida tsirkoniya s nikelievymi splavami (The contact interaction of zirconium carbide with nickel alloys). In: Samsonov GV, Kosolapova TYa, Gnesin GG, Fedorus VB, Domasevich LG (eds) *Karbidy i splavy na ikh osnove* (Carbides and alloys based on them). Naukova Dumka, Kyiv, pp. 56–59 (in Russian)
265. Samsonov GV, Panasyuk AD, Kozina GK (1968) Wetting of refractory carbides with liquid metals. *Powder Metall Met Ceram* 7(11):874–878
266. Ramqvist L (1965) Wettability of metallic carbides by liquid Cu, Ni, Co and Fe. *Int J Powder Metall* 1(4):2–21
267. Warren R (1980) Solid-liquid interfacial energies in binary and pseudo-binary systems. *J Mater Sci* 15(10):2489–2496

268. Warren R, Waldron MB (1972) Surface and interfacial energies in systems of certain refractory metal monocarbides with liquid cobalt. *Nature Phys Sci* 235(56):73–74
269. Panasyuk AD (1979) Physico-chemical principles of contact interaction in the system infusible compound – liquid metal. *Inorg Mater* 15(4):445–448
270. Samsonov GV, Kozina GK, Panasyuk AD, Bondarchuk SN (1974) The reaction of refractory carbides with molten steels and cast irons. In: Samsonov GV (ed) *Refractory carbides*. Consultants Bureau, New York, London, pp. 433–440
271. Vishnyakov LR, Grudina TV, Kadyrov VKh, Karpinos DM, Oleynik VI, Sapozhnikova AB, Tuchinskii LI (1985) *Kompozitsionnye materialy (Composite materials)*. Naukova Dumka, Kyiv (in Russian)
272. Samsonov GV, Épik AP (1973) *Tugoplavkie pokrytiya (Refractory coatings)*. Metallurgiya, Moscow (in Russian)
273. Meshcheryakov GYa, Andrievskii RA, Zagryazkin VN (1968) Diffusion of carbon in hafnium. *Phys Met Metallogr* 25(1):176–179
274. Gale WF, Totemeier TC (eds) (2004) *Smithells Metals Reference Book*, 8th edn. Elsevier, ASM International, Amsterdam, Boston
275. Carlson ON, Schmidt FA, Sever JC (1973) Electrotransport of carbon, nitrogen and oxygen in hafnium metal. *Metall Trans* 4(10):2407–2411
276. Zagryazkin VN (1969) O mekhanizme diffuzii v monokarbidakh perekhodnykh metallov (On the mechanism of diffusion in transition metals monocarbides). *Fiz Met Metalloved* 28(2):292–297 (in Russian)
277. Andrievskii RA, Klimenko VV, Khromov YuF (1969) Samodiffuziya ugleroda v karbidakh perekhodnykh metallov IV i V grupp (Self-diffusion of carbon in IV and V groups transition metals monocarbides). *Fiz Met Metalloved* 28(2):298–303 (in Russian)
278. Dergunova VS, Levinskii YuV, Shurshakov AN, Kravetskii GA (1974) *Vzaimodeistvie ugleroda s tugoplavkimi metallami (The interaction of carbon with refractory metals)*. Metallurgiya, Moscow (in Russian)
279. Adelsberg LM, Cadoff LH (1967) Reactions of liquid titanium and hafnium with carbon. *Trans Met Soc AIME* 239(6):933–935
280. Andrievskii RA, Ereemeev VS, Zagryazkin VN, Panov AS (1967) Diffuziya ugleroda v karbidakh perekhodnykh metallov IV-VI grupp periodicheskoi sistemy (Diffusion of carbon in carbides of periodic table IV-VI groups transition metals). *Izv AN SSSR Neorg Mater* 3(12):2158–2164 (in Russian)
281. Wallace TC Sr, Butt DP (1996) Review of diffusion and vaporization of group 4 and 5 transition metal carbides. In: Oyama ST (ed) *The chemistry of transition metal carbides and nitrides*. Chapman & Hall, London, Glasgow, pp. 53–90
282. Ilchenko NI, Pyatnitsky YuI (1996) Carbides of transition metals as catalysts for oxidation reactions. In: Oyama ST (ed) *The chemistry of transition metal carbides and nitrides*. Chapman & Hall, London, Glasgow, pp. 311–327
283. Umanskii YaS (1947) *Karbidy tverdykh splavov (Carbides of hard alloys)*. Metallurgizdat, Moscow (in Russian)
284. Kopylova VP (1961) *Khimicheskaya ustoichivost karbidov perekhodnykh elementov IV, V i VI grupp (The chemical stability of transition element carbides IV, V and VI groups)*. *Zh Prikl Khim* 34(9):1936–1939 (in Russian)
285. Kotlyar EE, Nazarchuk TN (1966) O nekotorykh khimicheskikh svoistvakh karbidov perekhodnykh metallov IV, V grupp periodicheskoi sistemy (On certain chemical properties of the transition metal carbides of IV, V groups of the periodic table). *Izv AN SSSR Neorg Mater* 2(10):1778–1780 (in Russian)
286. Samsonov GV, Zhidkova TG, Klimak ZA (1975) O kataliticheskikh svoistvakh karbidov perekhodnykh metallov (On the catalytic properties of transition metal carbides). In: Samsonov GV (ed) *Vysokotemperaturnye karbidy (High-temperature carbides)*. Naukova Dumka, Kyiv, pp. 76–81
287. Maouche D, Louail L, Ruterana P, Maamache M (2008) Formation and stability of di-transition-metal carbides $Ti_xZr_{1-x}C$, $Ti_xHf_{1-x}C$ and $Hf_xZr_{1-x}C$. *Comput Mater Sci* 44(2):347–350

288. Tran F, Laskowski R, Blaha P, Schwarz K (2007) Performance on molecules, surfaces and solids of the Wu-Cohen GGA exchange-correlation energy functional. *Phys Rev B* 75(11):115131 (14 pp.)
289. Krylov YuI, Balakir ÉA (1976) *Karbidno-okisnye sistemy (Carbide-oxide systems)*. Metallurgiya, Moscow (in Russian)
290. Adjaoud O, Steinle-Neumann G, Burton BP, Van de Walle, A (2009) First-principles phase diagram calculations for the HfC-TiC, ZrC-TiC and HfC-ZrC solid solutions. *Phys Rev B* 80(13):134112 (7 pp.)
291. Lavrenko VA, Talash VN, Desmason-Brut M, Rudenko YuB (2009) Protective oxide layers formed during electrochemical oxidation of hafnium carbide. *Powder Metall Met Ceram* 48(9–10):595–599
292. Abramov YuA, Kamkin AN, Davydov AD (1979) Anodic solution of hafnium and its carbide. *Protect Met* 15(2):185–186
293. Klein BM, Papaconstantopoulos DA (1974) Electron-phonon interaction and superconductivity in transition metals and transition-metal carbides. *Phys Rev Lett* 32(21):1193–1195
294. Allen PB, Cohen ML (1972) Superconductivity and phonon softening. *Phys Rev Lett* 29(24):1593–1596
295. Roedhammer P, Gmelin E, Weber W (1975) Influence of phonon anomalies on the specific heat of transition metal carbides. *Solid State Commun* 16(10–11):1205–1208
296. Kaufman L (1964) Thermodynamic factors controlling the stability of solid phases at high temperatures. In: Waber JT, Chiotti P, Miner WN (eds) *Compounds of interest in nuclear reactor technology*. Metallurgical Society of American Institute of Mining Engineers, New York, pp. 193–225
297. Mackie WA, Hartman RL, Davis PR (1993) High current density field emission from transition metal carbides. *Appl Surf Sci* 67:29–35
298. Ivanko AA (1974) The microhardness of transition-metal carbides. In: Samsonov GV (ed) *Refractory carbides*. Consultants Bureau, New York, London, pp. 367–370
299. Artamonov AYa, Bovkun GA (1974) Some aspects of the abrasive wear of transition-metal carbides. In: Samsonov GV (ed) *Refractory carbides*. Consultants Bureau, New York, London, pp. 371–376
300. Williams WS (1999) Electrical properties of hard materials. *Int J Refract Met Hard Mater* 17(1):21–26
301. Guo X, Li L, Liu Z, Yu D, He J, Liu R, Xu B, Tian Y, Wang H-T (2008) Hardness of covalent compounds: roles of metallic component and d-valence electrons. *J Appl Phys* 104(2):023503
302. Tian Y, Xu B, Zhao Z (2012) Microscopic theory of hardness and design of novel superhard crystals. *Int J Refract Met Hard Mater* 33:93–106
303. Li K, Wang X, Zhang F, Xue D (2008) Electronegativity identification of novel superhard materials. *Phys Rev Lett* 100(23):235504
304. Shackelford JF, Alexander W (eds) (2001) *CRC materials science and engineering handbook, 3rd edn*. CRC Press, Boca Raton, London
305. Liu YZ, Jiang YH, Zhou R, Feng J (2014) First principles study the stability and mechanical properties of MC (M = Ti, V, Zr, Nb, Hf and Ta) compounds. *J Alloys Compd* 582:500–504
306. Sanders WA, Probst HB (1969) High-temperature mechanical properties of polycrystalline hafnium carbide and hafnium carbide containing 13 vol.% hafnium diboride. Report NASA-TN-D-5008. NASA Lewis Research Centre, Cleveland, Ohio, pp. 1–20
307. Pike JN (1960) Research in physical and chemical principles affecting high temperature materials for rocket nozzles. Semiannual Progress Report. Union Carbide Research Institute, Tarrytown, New York, Parma Research Centre, Cleveland, Ohio, pp. 1–80
308. Pike JN, Doar JF (1961) High temperature thermal conductivity measurements. Part II. The rectangular bar method; experimental techniques. Report C-10. Union Carbide Corporation and National Carbon Company Parma Research Laboratories, Cleveland, Ohio, pp. 1–43
309. Kelley KK (1960) Contribution to the data on theoretical metallurgy. XIII. High temperature heat content, heat capacity and entropy data for the elements and inorganic compounds. Bulletin N 584. US Bureau of Mines, US Department of the Interior, Washington, DC, pp. 1–232

310. Pike JN (1965) Research in physical and chemical principles affecting high temperature materials for rocket nozzles. Final Report, Contract DA-30-069-ORD-2787, Vol. 2. Union Carbide Research Institute, Tarrytown, New York, pp. 1–288
311. Jun CK, Shaffer PTB (1970) Advanced ceramic systems for rocket nozzle applications. Summary Report, Contract N00017-70-C-4402. Carborundum Company, Niagara Falls, New York, pp. 1–134
312. Juenke EF (1964) A review of recent research on refractory metal carbides and borides. Report SR-GEMP-267, Contract AEC-AT(40-1)-2847. Nuclear Materials and Propulsion Operation, General Electric Company, Cincinnati, Ohio, pp. 1–24
313. Steele SR, Pappis J, Schilling H, Simpson J (1968) Chemical vapour deposited materials for electron tubes. Report RDTR-ECOM-0156-1, Contract DAA-B07-68-C-0156. Raytheon Company, Waltham, Massachusetts, pp. 1–88
314. Chang YA, Toth LE, Tyan YS (1971) On the elastic and thermodynamic properties of transition metal carbides. *Metall Trans* 2(1):315–320
315. Chauhan M, Gupta DC (2013) Electronic, mechanical, phase transition and thermo-physical properties of TiC, ZrC and HfC: high pressure computational study. *Diam Relat Mater* 40:96–106
316. Feng W, Cui S, Hu H, Zhang G, Lv Z (2011) Electronic structure and elastic constants of $\text{TiC}_x\text{Nb}_{1-x}$, $\text{Zr}_x\text{Nb}_{1-x}\text{C}$ and $\text{HfC}_x\text{Nb}_{1-x}$ alloys: a first-principles study. *Phys B* 406:3631–3635
317. Kamiş T, Bağcı S, Tütüncü HM, Duman S, Srivastava GP (2011) *Ab initio* calculation of phonons in bulk HfC and the HfC (001) (1×1) surface. *Philos Mag* 91(6):946–957
318. Varshney D, Shriya S (2013) Elastic, mechanical and thermodynamic properties at high pressures and temperatures of transition metal monocarbides. *Int J Refract Met Hard Mater* 41:375–401
319. Varshney D, Shriya S, Singh N (2013) Mechanical stiffening of transition metal carbides: XC (X = Ti, Zr, Nb, Hf, Ta). In: Proc. 57th DAE solid state physics symp. 2012. AIP Conf Proc 1512:1016–1017
320. Yang J, Gao F (2012) First principles calculations of mechanical properties of cubic 5d transition metal monocarbides. *Phys B* 407:3527–3534
321. Li G, Li G (2010) Microstructure and mechanical properties of hafnium carbide coatings synthesized by reactive magnetron sputtering. *J Coat Technol Res* 7(3):403–407
322. Singh A, Aynyas M, Sanyal SP (2009) High pressure behaviour and structural properties of transition metal carbides. *Phase Transit* 82(8):576–586
323. Bhardwaj P (2012) Structural study of transition metal carbides. *Acta Phys Polon A* 122(1):138–141
324. Zaoui A, Bouhafs B, Ruterana P (2005) First-principles calculations on the $\text{TiC}_x\text{Nb}_{1-x}$, $\text{Zr}_x\text{Nb}_{1-x}\text{C}$ and $\text{HfC}_x\text{Nb}_{1-x}$ alloys. *Mater Chem Phys* 91:108–115
325. Li H, Zhang L, Zeng Q, Ren H, Guan K, Liu Q, Cheng L (2011) First-principles study of the structural, vibrational, phonon and thermodynamic properties of transition metal carbides TMC (TM = Ti, Zr, Hf). *Solid State Commun* 151:61–66
326. Zhao Z, Zhou X-F, Wang L-M, Xu B, He J, Liu Z, Wang H-T, Tian Y (2011) Universal phase transitions of B1-structured stoichiometric transition metal carbides. *Inorg Chem* 50:9266–9272
327. Viñes F, Sousa C, Liu P, Rodriguez JA, Illas F (2005) A systematic density functional theory study of the electronic structure of bulk and (001) surface of transition-metals carbides. *J Chem Phys* 122:174709 (11 pp.)
328. Zubarev PV, Kuraev AB (1992) Creep of monocarbides of transition metals of IV, V groups. III. Creep of hafnium, niobium and tantalum carbides. *Phys Met Metallogr* 73(6):649–653
329. Zubarev PV, Kuraev AB (1992) Creep of monocarbides of transition metals of IV, V groups. I. Creep of zirconium carbide. *Phys Met Metallogr* 73(6):643–646
330. Zubarev PV, Dementev LN, Shmelev AG (1980) Vliyaniye rezhimov pressovaniya na vysokotemperaturnuyu polzuchest karbidov IV-VI grupp perekhodnykh metallov (The effect of pressing mode on high-temperature creep of groups IV-VI transition metals carbides). *Fiz Khim Obrab Mater* (3):91–95 (in Russian)

331. Isaev EI, Ahuja R, Simak SI, Lichtenstein AI, Vekilov YuKh, Johansson B, Abrikosov IA (2005) Anomalously enhanced superconductivity and *ab initio* lattice dynamics in transition metal carbides and nitrides. *Phys Rev B* 72(6):064515
332. Gusev AI, Rempel AA (1993) Superstructures of non-stoichiometric interstitial compounds and the distribution functions of interstitial atoms. *Phys Stat Sol A* 135(1):15–58
333. Zeng Q, Peng J, Oganov A, Zhu Q, Xie C, Zhang X, Dong D, Zhang L, Cheng L (2013) Prediction of stable hafnium carbides: stoichiometries, mechanical properties and electronic structure. *Phys Rev B* 88(21):214107
334. Yu X-X, Thompson GB, Weinberger CR (2015) Influence of carbon vacancy formation on the elastic constants and hardening mechanisms in transition metal carbides. *J Eur Ceram Soc* 35:95–103
335. McColm IJ (1990) *Ceramic hardness*. Plenum Press, New York, London
336. Krasnenko V, Brik MG (2012) First-principles calculations of hydrostatic pressure effects on the structural, elastic and thermodynamic properties of cubic monocarbides XC (X = Ti, V, Cr, Nb, Mo, Hf). *Solid State Sci* 14:1431–1444
337. Markhasev BI, Pior NCh, Shumilova RG (1979) Travitel dlya vyyavleniya mikrostrukturnykh materialov na osnove karbidov niobiya, tantalala i gafniya (An etching agent for revealing microstructure of materials on the base of niobium, tantalum and hafnium carbides). *Zavod Lab* 45(6):543–545 (in Russian)
338. Benesovsky F, Rudy E (1960) Pseudoternary carbide systems. *Metall* (9):875–876
339. Samsonov GV, Podchernyaeva IA, Siman NI, Fomenko VS (1976) Behaviour of refractory compounds in alkali metal media. *Powder Metall Met Ceram* 15(2):122–127
340. Velikanova TYa, Eremenko VN, Artyukh LV, Bondar AA, Gordichuk OV (1989) Phase diagrams of Sc-M(IV-VII)-C systems. *Powder Metall Met Ceram* 28(9):711–718
341. Goldschmidt HJ (1967) *Interstitial alloys*. Butterworths, London
342. Samsonov GV, Yasinskaya GA, Shiller EA (1961) Interaction of certain oxides, carbides and high-melting metals at high temperatures. *Refract Indust Ceram* 2(7–8):274–277
343. Rudy E (1965) Related binary systems. Hf-C system. In: Ternary phase equilibria in transition metal-boron-carbon-silicon systems. Report AFML-TR-65-2, Contract USAF 33(615)-1249, Part 1, Vol. 4, Air Force Materials Laboratory, Wright-Patterson Air Force Base, Ohio, pp. 1–48
344. Portnoi KI, Levinskii YuV, Fadeeva VI (1961) Vzaimodeistvie s uglerodom nekotorykh tugoplavkikh karbidov i ikh tverdykh rastvorov (Reaction with carbon of some refractory carbides and their solid solutions). *Izv AN SSSR OTN Metallurgiya Toplivo* (2):147–149 (in Russian)
345. Kozina GK (1970) Issledovanie kontaktnogo vzaimodeistviya tugoplavkikh karbidov i materialov na ikh osnove s zhidkimi metallami i splavami (A study of the contact interaction of refractory carbides and materials on their basis with liquid metals and alloys). PhD thesis, Institute for Problems of Materials Science, Ukrainian SSR Academy of Sciences, Kyiv (in Russian)
346. Ordanyan SS (1975) Reactions of rhenium and other refractory metals with some metal-like compounds. *Powder Metall Met Ceram* 14(2):125–129
347. Rafal AN (1983) Kinetika reaktsii s uchastiem vodoroda na beskislorodnykh tugoplavkikh soedinenii perekhodnykh metallov IV-VI grupp periodicheskoi sistemy (Kinetics of reactions involving hydrogen on oxygen-free refractory compounds of periodic system IV-VI groups transition metals). PhD thesis, Institute for Problems of Materials Science, Ukrainian SSR Academy of Sciences, Kyiv (in Russian)
348. Ilchenko NI, Chebotareva NP, Shvidak NV (1976) Oxidation of ammonia on transition metal carbides. *React Kinet Catal Lett* 4(3):343–349
349. Chebotareva NP, Ilchenko NI, Golodets GI (1976) Kinetics and mechanism of oxidation of hydrogen on carbides of transition metals of groups IV-VI. *Theor Exp Chem* 12(2):154–162
350. Samsonov GV, Kharlamov AI (1975) Catalytic properties of refractory compound powders (survey). *Powder Metall Met Ceram* 14(9):699–707
351. Kharlamov AI, Rafal AN, Samsonov GV, Belov AS (1977) Catalytic activities of hafnium, tantalum and tungsten carbides in the high-temperature para/ortho conversion of hydrogen. *Theor Exp Chem* 13(1):92–94

352. Kharlamov AI, Kirillova NV, Yatsimirskii VK (1981) The catalytic properties of transition element carbides and nitrides in the oxidation of carbon monoxide. *Theor Exp Chem* 17(2):168–179
353. Kharlamov AI, Kirillova NV (1983) Catalytic properties of powdered refractory compounds of transition elements. Carbides and nitrides – a review. *Powder Metall Met Ceram* 22(2):123–134
354. Raevskaia LN, Pavlovskiy FG, Kolotusha BI, Ilchenko NI (1991) Okislitel'naya kondensatsiya metana s uchastiem kisloroda i zakisi azota na karbidakh perekhodnykh metallov (Oxidative condensation of methane with participation of oxygen and nitrous oxide on carbides of transition metals). *Ukr Khim Zh* 57(10):1080–1084 (in Russian)
355. Oyama ST (1992) Preparation and catalytic properties of transition metal carbides and nitrides. *Catal Today* 15(2):179–200
356. Ledoux MJ, Pham-Huu C, Chianelli RR (1996) Catalysis with carbides. *Current Opinion Solid State Mater Sci* 1(1):96–100
357. Semenov-Kobzar AA, Obolonchik VA, Akinina ZS (1969) Stability of transition metal carbides under anodic polarization conditions. *Powder Metall Met Ceram* 8(5):399–402
358. Matzke Hj, Rondinella VV (1999) Diffusion in carbides, nitrides, hydrides and borides. In: Beke DL (ed) *Diffusion in non-metallic solids. Subvol. B, Part 1*. Springer, Berlin, Heidelberg, pp. 5/1–5/29
359. Brizes WF, Salkovitz EI (1969) Comparison of the chemical and self-diffusivities in the transition metal monocarbides. *Scripta Metall* 3(9):659–662
360. Matzke Hj (1984) Point defects and transport properties in carbides. *Solid State Ionics* 12:25–45
361. Matzke Hj (1990) Mass transport in carbides and nitrides. In: Freer R (ed) *The physics and chemistry of carbides, nitrides and borides*. Kluwer Academic, Dordrecht, pp. 357–383
362. Jhi S-H, Louie SG, Cohen ML, Morris JW, Jr (2001) Mechanical instability and ideal shear strength of transition metal carbides and nitrides. *Phys Rev Lett* 87(7):075503/1–075503/4
363. Holleck H (1986) Material selection for hard coatings. *J Vac Sci Technol A* 4(6):2661–2669
364. Koester RD, Moak DP (1967) Hot hardness of selected borides, oxides and carbides to 1900 °C. *J Am Ceram Soc* 50(6):290–296
365. Castillo DG, Jones PF (1993) Studies of hafnium carbide wafers using thermogravimetric analyzer. Technical Report. Phillips Laboratory, Edwards Air Force Base, California, pp. 1–11
366. Samsonov GV (1964) *Handbooks of high-temperature materials: No. 2 – Properties index*. Plenum Press, Springer Science, New York
367. Meissner W, Franz H, Westerhoff H (1932) Messungen mit Hilfe von flüssigem Helium. XVI. Untersuchungen über die Supraleitfähigkeit von Carbiden, Nitriden, Boriden und Siliciden (Measurements using liquid helium. XVI. Studies on the superconductivity of carbides, nitrides, borides and silicides). *Z Phys* 75(7–8):521–530 (in German)
368. Samsonov GV, Kislyi PS (1965) Vysokotemperaturnye nemetallicheskie termopary i nakonechniki (High-temperature non-metallic thermocouples and cap fittings). *Naukova Dumka, Kyiv* (in Russian)
369. Harrod DL, Fleischer LR (1968) On the role of diffusion in the plastic deformation of transition metal carbides. In: Vahldiek FW, SA Mersol (eds) *Anisotropy in single-crystal refractory compounds, Vol. 1*. Springer, Plenum Press, New York, pp. 341–356
370. Kotlyar EE, Nazarchuk TN (1972) Interaction of the carbides of group IV and V transition metals with various acids. In: Samsonov GV (ed) *Chemical properties and analysis of refractory compounds*. Consultants Bureau, New York, London, pp. 1–5
371. Samsonov GV, Tkachenko YuG, Berdikov VF, Bovkun GA (1976) Mikrotverdost, mikrohrupkost i hrupkaya mikroprochnost karbidov perekhodnykh metallov (Microhardness, microbrittleness and brittle microstrength of transition metal carbides). In: Samsonov GV, Kosolapova TYa, Gnesin GG, Fedorus VB, Domasevich LG (eds) *Karbidy i splavy na ikh osnove* (Carbides and alloys based on them). *Naukova Dumka, Kyiv*, pp. 98–104 (in Russian)

372. Bukatov VG, Knyazev VI, Korostin OS, Baranov VM (1976) *Izmenenie uprugikh kharakteristik v oblasti gomogennosti nekotorykh karbidov perekhodnykh metallov* (Change of elastic characteristics in the range of homogeneity of some transition metal carbides). In: Samsonov GV, Kosolapova TYa, Gnesin GG, Fedorus VB, Domasevich LG (eds) *Karbidy i splavy na ikh osnove* (Carbides and alloys based on them). Naukova Dumka, Kyiv, pp. 111–114 (in Russian)
373. Ogorodnikov VV, Rogovoi YuI (1976) *Tochechnye defekty v kubicheskikh monokarbidakh* (Point defects in cubic monocarbides). In: Samsonov GV, Kosolapova TYa, Gnesin GG, Fedorus VB, Domasevich LG (eds) *Karbidy i splavy na ikh osnove* (Carbides and alloys based on them). Naukova Dumka, Kyiv, pp. 129–137 (in Russian)
374. Brynza AP, Khmelovskaya SA, Fedorus VB, Silina ZR (1976) *Issledovanie khimicheskoi stoikosti i elektrokhimicheskogo povedeniya karbidov* (A study of the chemical resistance and electrochemical behaviour of carbides). In: Samsonov GV, Kosolapova TYa, Gnesin GG, Fedorus VB, Domasevich LG (eds) *Karbidy i splavy na ikh osnove* (Carbides and alloys based on them). Naukova Dumka, Kyiv, pp. 199–208 (in Russian)
375. Futamoto M, Yuito I, Kawabe U (1983) Hafnium carbide and nitride whisker growth by chemical vapour deposition. *J Cryst Growth* 61(1):69–74
376. Motojima S, Kawashima Y (1996) Chemical vapour growth of HfC whiskers and their morphology. *J Mater Sci* 31(14):3697–3700
377. Motojima S, Kawashima Y (1996) HfC offers high temperature reinforcement. *Adv Compos Bull* 8:2–3
378. Kumashiro Y (2000) High-temperature characteristics. In: Kumashiro Y (ed) *Electric refractory materials*. Marcel Dekker, New York, Basel, pp. 191–222
379. Lengauer W, Eder A (2005) Carbides: transition metal solid-state chemistry. In: King RB (ed) *Encyclopedia of inorganic chemistry*. Wiley, Chichester, pp. 674–690
380. Ishizawa Y (2000) Transition metal carbide field emitters. In: Kumashiro Y (ed) *Electric refractory materials*. Marcel Dekker, New York, Basel, pp. 269–287
381. Lengauer W (2000) Transition metal carbides, nitrides and carbonitrides. In: Riedel R (ed) *Handbook of ceramic hard materials*. Wiley – VCH, Weinheim, pp. 202–252
382. Rühle M (1982) *Zum technischen Stand der Dispersionshärtung. Teil 1. (State of the art dispersion hardening. Part 1.)*. *Metall* 36(12):1280–1287 (in German)
383. Kubaschewski O, Alcock CB (1979) *Metallurgical thermochemistry*, 5th edn. Pergamon Press, Oxford, New York
384. Haefer RA (1987) *Oberflächen- und Dünnschichttechnologie. Teil 1 – Beschichtung von Oberflächen. (Surface and thin film technology. Part 1 – Coating surfaces.)*. Springer, Berlin (in German)
385. Frey H, Kienel G (1987) *Dünnschichttechnologie (Thin film technologie)*. VDI-Verlag, Düsseldorf (in German)
386. Rother B, Vetter J (1992) *Plasma Beschichtungsverfahren und Hartstoffschichten (Plasma coating processes and hard material layers)*. Deutscher Verlag für Grundstoffindustrie, Leipzig (in German)
387. Sundgren JE, Hentzell HTG (1986) A review of the present state of art in hard coatings grown from the vapour phase. *J Vac Sci Technol A* 4(5):2259–2279
388. Brundiers GD (1975) *Herstellung, Aufbau und Eigenschaften von Hafniumverbindungen im System Hf-C-N-O (Preparation, structure and properties of hafnium compounds in the system Hf-C-N-O)*. PhD thesis (KfK-2161), Kernforschungszentrum Karlsruhe, Institut für Material -und Festkörperforschung, Karlsruhe Universität (in German)
389. Bleckmann H (1971) *Röntgenographische Bestimmung der thermischen Ausdehnung an verschiedenen metallischen und nichtmetallischen Hartstoffen (X-ray determination of thermal expansion in various metallic and non-metallic hard materials)*. PhD thesis, Rheinisch-Westfälische Technische Hochschule, Aachen (in German)
390. Berg G, Friedrich C, Broszeit E, Berger C (2000) Data collection of properties of hard materials. In: Riedel R (ed) *Handbook of ceramic hard materials*. Wiley – VCH, Weinheim, pp. 965–995
391. Bhardwaj P, Singh S (2012) Structural phase stability and elastic properties of refractory carbides. *Int J Refract Met Hard Mater* 35:115–121

392. Wang J, Vandeperre LJ (2014) Deformation and hardness of UHTCs as a function of temperature. In: Fahrenholtz WG, Wuchina EJ, Lee WE, Zhou Y (eds) Ultra-high temperature ceramics. Wiley, Hoboken, New Jersey, pp. 236–266
393. Gangler J (1971) NASA research on refractory compounds. *High Temp High Press* 3(5): 487–502
394. Wuchina EJ, Opeka M (2014) The group IV carbides and nitrides. In: Fahrenholtz WG, Wuchina EJ, Lee WE, Zhou Y (eds) Ultra-high temperature ceramics. Wiley, Hoboken, New Jersey, pp. 361–390
395. Wuchina EJ, Opeka M (1999) Oxidation of Hf-based ceramics. *Electrochem Soc Proc* (38):477–488
396. Wuchina EJ, Opeka M (2001) The oxidation behaviour of HfC, HfN and HfB₂. *Electrochem Soc Proc* (12):136–143
397. Valvoda V, Dobiášová L, Karen P (1985) X-ray diffraction analysis of diffusional alloying of HfC and TaC. *J Mater Sci* 20:3605–3609
398. Tian S, Li H, Zhang Y, Ren J, Qiang X, Wang J (2014) Catalyst-assisted growth of single-crystalline hafnium carbide nanotubes by chemical vapour deposition. *J Am Ceram Soc* 97(1):48–51
399. Tian S, Li H, Zhang Y, Ren J, Qiang X, Zhang S (2014) Hafnium carbide nanocrystal chains for field emitters. *Appl Surf Sci* 305:697–701
400. Zhilyaev VA, Zainulin YuG, Alyamovskii SI, Shveikin GP (1972) High-temperature oxidation of zirconium and hafnium oxycarbides and oxynitrides. *Powder Metall Met Ceram* 11(8):632–636
401. Guerlet JP, Lehr P (1967) Sur l'oxydation du zirconium par l'oxyde carbon (On oxidation of zirconium by carbon monoxide). *Compt Rend Acad Sci C* 264(23):1833–1835 (in French)
402. Zhelankin VI, Kutsev VS, Ormont BF (1959) Issledovanie ravnovesiya pri vysokotemperaturnom vosstanovlenii dnuokisi gafniya HfO₂ (Equilibrium study of the high temperature reduction of hafnium dioxide HfO₂). *Zh Fiz Khim* 33(9):1988–1991 (in Russian)
403. Zhelankin VI, Kutsev VS, Ormont BF (1961) Issledovanie ravnovesiya vosstanovleniya HfO₂ uglerodom pri vysokih temperaturakh (Equilibrium study of reduction of HfO₂ by carbon at high temperatures). *Zh Fiz Khim* 35(11):2608–2611 (in Russian)
404. Zhelankin VI, Kutsev VS, Ormont BF (1962) Usloviya obrazovaniya karbida gafniya pri vosstanovlenii oksida gafniya uglerodom (Conditions for the formation of hafnium carbide during the reduction of hafnium dioxide with carbon). *Zh Neorg Khim* 7(8):1762–1764 (in Russian)
405. Zverev GL (1968) Vzaimodeistvie okislov tsirkoniya i gafniya so svoimi karbidami (Interaction of zirconium and hafnium oxides with their carbides). *Izv AN SSSR Neorg Mater* 4(7):1197–1199 (in Russian)
406. Alyamovskii SI, Zainulin YuG, Shveikin GP, Geld PV (1971) Kubicheskie oksikarbid gafniya (Cubic hafnium oxycarbide). *Zh Neorg Khim* 16(6):1480–1484 (in Russian)
407. Portnoi KI, Levinskii YuV (1963) Vysokotemperaturnoe ravnovesie reaktsii HfN + C ↔ HfC + ½N₂ (High temperature equilibrium of the reaction HfN + C ↔ HfC + ½N₂). *Zh Fiz Khim* 37(11):2467–2470 (in Russian)
408. Lyubimov VD, Shveikin GP, Alyamovskii SI (1983) Mekhanizm pryamogo vosstanovleniya okislov tantalala i gafniya v srede azota (Direct reduction mechanism of tantalum and hafnium oxides in nitrogen medium). *Zh Neorg Khim* 28(4):1057–1060 (in Russian)
409. Fujishiro S (1961) Thermodynamic properties of transition metal carbides and their periodicity. *J Jpn Soc Powder Powder Metall* 8(2):73–76
410. Kulikov IS (1988) Termodinamika karbidov i nitridov (Thermodynamics of carbides and nitrides). *Metallurgiya, Chelyabinsk* (in Russian)
411. Kaufman L, Bernstein H (1968) Thermodynamic properties of refractory transition metal compounds. In: Vahldiek FW, Mersol SA (eds) Anisotropy in single-crystal refractory compounds, Vol. 1. Springer, New York, pp. 269–297
412. Bowman AL, Krikorian NH (1976) Interstitial phases. In: Hannay NB (ed) Treatise on solid state chemistry, Vol. 3. Crystalline and noncrystalline solids. Plenum Press, New York, London, pp. 253–292

413. Sakurai J, Hayashi J, Mekata M, Tsuchida T, Takagi H (1961) Thermal conductivities of monocarbides in transition metals. *J Jpn Inst Met* 25(4):289–292 (in Japanese)
414. Modine FA, Foegelle MD, Finch CY, Allison CY (1989) Electrical properties of transition metal carbides of group IV. *Phys Rev B* 40(14):9558–9564
415. Borukhovich AS (1978) Kinetic properties of IVa and Va subgroup transition metal monocarbides. *Phys Stat Sol A* 46(1):11–37
416. Geld PV, Tskhai VA, Borukhovich AS, Dubrovskaya LB, Matveenko II (1970) Conduction band of IVa and Va subgroup transition metal monocarbides. I. *Phys Stat Sol* 42:85–93
417. Borukhovich AS, Geld PV, Tskhai VA, Dubrovskaya LB, Matveenko II (1971) Conduction band of IVa and Va subgroup transition metal monocarbides. II. *Phys Stat Sol B* 45(1):179–187
418. Lvov SN, Nemchenko VF, Samsonov GV (1962) Effect of nonmetallic atoms on the electric properties of high-melting compounds of transition metals. *Powder Metall Met Ceram* 1(4):231–236
419. Ozaki Y, Zee RH (1995) Investigation of thermal and hydrogen effects on emissivity of refractory metals and carbides. *Mater Sci Eng A* 202(1–2):134–141
420. Fisenko AI, Lemberg V (2012) Radiative properties of stoichiometric hafnium, titanium and zirconium carbides: thermodynamics of thermal radiation. *Int J Thermophys* 33:513–527
421. Samsonov GV, Podchernyaeva IA, Fomenko VS (1969) Emission coefficient of high-melting compounds. *Powder Metall Met Ceram* 8(5):374–379
422. Hausner HH, Friedemann HC (1962) High temperature compounds – a data book. General Astrometals Corporation, Yonkers, New York
423. Naumenko VYa (1971) Tekhnologiya polucheniya i issledovanie nekotorykh svoystv karbidov perekhodnykh metallov IV-V grupp v oblastiakh ikh gomogenosti (Production technology and investigation of some properties of transition metal carbides IV-V groups in the regions of their homogeneity). PhD thesis, Institute for Problems of Materials Science, Ukrainian SSR Academy of Sciences, Kyiv (in Russian)
424. Curtis CE, Doney LM, Johnson JR (1954) Some properties of hafnium oxide, hafnium silicate, calcium hafnate and hafnium carbide. *J Am Ceram Soc* 37(10):458–465
425. Jones T (1956) The metallography of certain hot-pressed carbides possessing high melting points. In: Technical papers of the metallographic group meeting held at Bridgeport Brass Company, 7–8 Nov 1956, TID-7567, Part 1. US Atomic Energy Commission, Washington DC, pp. 32–45
426. Avarbe RG, Avgustinik AI, Vilks YuN, Konraskov YuD, Nikolskii SS, Omelchenko YuA, Ordanyan SS (1962) Diagramma sostoyaniya sistemy Hf-HfC (Phase diagram of the Hf-HfC system). *Russ J Appl Chem* 35(9):1899–1902
427. Bukatov VG (1979) Issledovanie fiziko-mekhanicheskikh svoystv karbidov tugoplavkikh metallov i nekotorykh splavov na ikh osnove (Studies of physico-mechanical properties of refractory metal carbides and some alloys on their basis). PhD thesis, Moscow Institute of Steels and Alloys (in Russian)
428. Weimer AW (ed) Carbide, nitride and boride materials synthesis and processing. Chapman & Hall, London, Weinheim, New York
429. Jhi S-H, Ihm J, Louie SG, Cohen ML (1999) Electronic mechanism of hardness enhancement in transition-metal carbonitrides. *Nature* 399(6732):132–134
430. Khusainov MA (1989) Mechanical properties and special features of failure of carbides and nitrides of metals of groups IV-V deposited from the gas phase. *Powder Metall Met Ceram* 28(7):551–555
431. Ferro D, Rau JV, Albertini VR, Generosi A, Teghil R, Barinov SM (2008) Pulsed laser deposited hard TiC, ZrC, HfC and TaC films on titanium: hardness and an energy-dispersive X-ray diffraction study. *Surf Coat Technol* 202:1455–1461
432. Mukhopadhyay A, Raju GB, Basu B (2013) Ultra-high temperature ceramics: processing, properties and applications. In: Low IM, Sakka Y, Hu CF (eds) MAX phases and ultra-high temperature ceramics for extreme environments. IGI Global, Hershey, Pennsylvania, pp. 49–99
433. Wang HL, Hon MH (1999) Temperature dependence of ceramics hardness. *Ceram Int* 25(3):267–271
434. Kramer BM, Judd PK (1985) Computational design of wear coatings. *J Vac Sci Technol A* 3(6):2439–2444

435. Sciti D, Nygren M (2008) Spark plasma sintering of ultra-refractory compounds. *J Mater Sci* 43:6414–6421
436. Sun S-K, Zhang G-J, Wu W-W, Liu J-X, Suzuki T, Sakka Y (2013) Reactive spark plasma sintering of ZrC and HfC ceramics with fine microstructures. *Scripta Mater* 69:139–142
437. Oliver WC, Pharr GM (1992) An improved technique for determining hardness and elastic modulus using load and displacement sensing indentation experiments. *J Mater Res* 7(6): 1564–1583
438. Hollox GE (1968/69) Microstructure and mechanical behaviour of carbides. *Mater Sci Eng* 3(3):121–137
439. Brozek V, Ctibor P, Cheong D-I, Yang S-H, Mastny L, Novak M (2011) Preparation and properties of ultra-high temperature ceramics based on ZrC and HfC. *Solid State Phenom* 170:37–40
440. Ogorodnikov VV, Rogovoi YuI (1993) Rules of change in elastic, thermal and energy properties in a number of cubic transition metal monocarbides. *Powder Metall Met Ceram* 32(5):445–449
441. Yang Q, Lengauer W, Koch T, Scheerer M, Smid I (2000) Hardness and elastic properties of $Ti(C_xN_{1-x})$, $Zr(C_xN_{1-x})$ and $Hf(C_xN_{1-x})$. *J Alloys Compd* 309:L5–L9
442. Gautam GS, Kumar KCH (2014) Elastic, thermochemical and thermophysical properties of rock salt – type transition metal carbides and nitrides: a first principles study. *J Alloys Compd* 587:380–386
443. Krasnenko V, Brik MG (2014) First principles calculations of the structural, elastic and electronic properties of MN_xC_{1-x} ($M = Ti, Zr, Hf; 0 \leq x \leq 1$) carbonitrides at ambient and elevated pressure. *Solid State Sci* 28:1–8
444. Liu Y-Z, Jiang Y-H, Zhou R, Feng J (2014) First principles study the stability and mechanical properties of MC ($C = Ti, V, Zr, Nb, Hf$ and Ta) compounds. *J Alloys Compd* 582:500–504
445. Mughabghab SF (1984) Neutron cross sections, Vol. 1 – Neutron resonance parameters and thermal cross sections, Part B – $Z = 61-100$. Academic Press, Orlando
446. Mughabghab SF (2003) Thermal neutron capture cross sections resonance integral and G-factors. IAEA Nuclear Data Section, Vienna
447. He L-F, Lin Z-J, Wang J-Y, Bao Y-W, Zhou Y-C (2008) Crystal structure and theoretical elastic property of two new ternary ceramics $Hf_3Al_4C_6$ and $Hf_2Al_4C_5$. *Scripta Mater* 58(8):679–682
448. He X, Bai Y, Zhu C, Sun Y, Li M, Barsoum MW (2010) General trends in the structural, electronic and elastic properties of the M_3AlC_2 phases ($M =$ transition metal): a first-principle study. *Comput Mater Sci* 49:691–698
449. Schuster JC, Nowotny H (1980) Investigations of the ternary systems (Zr,Hf,Nb,Ta)–Al–C and studies on complex carbides. *Z Metallkd* 71:341–346
450. Shurin AK, Dmitrieva GP (1974) Issledovanie fazovykh ravnesii i struktury splavov Ni-ZrC i Ni-HfC (Examination of phase equilibria and structure of the Ni-ZrC and Ni-HfC alloys). *Metallofizika (Akad Nauk Ukr SSR Inst Metallofiz)* (53):97–100 (in Russian)
451. Dmitrieva GP, Razumova NA, Shurin AK, Khandros EL (1986) Phase equilibria in the alloys of the Ni-TiC-MeC ($Me = Zr, Hf, Nb, Ta$) systems. *Russ Metall* (1):210–215
452. Eremenko VN, Velikanova TYa, Bondar AA (1989) Phase equilibria at the solidus surface of the equilibrium diagram of ternary systems of technetium with carbon and d-transition metals of groups III-VII. *Powder Metall Met Ceram* 28(11):868–873
453. Zainulin YuG, Shveikin GP, Alyamovskii SI, Geld PV (1971) Coefficients of thermal expansion of cubic (NaCl type) oxycarbides and oxynitrides of zirconium and hafnium. *High Temp* 9(3):496–499
454. Fischer JJ (1964) Hot-pressing mixed carbides of Ta, Hf and Zr. *Am Ceram Soc Bull* 43(3):183–185
455. Dmitrieva GP, Shurin AK (1973) Fazovye ravnesiya i struktura splavov Co-ZrC i Co-HfC (The phase equilibria and structure of Co-ZrC and Co-HfC alloys). *Dopov Akad Nauk Ukr RSR Ser A Fiz Mat Tekh Nauki* 35(9):845–848 (in Russian)

456. Umanskii YaS, Fadeeva VI (1965) Diffuznoe rasseyanie rentgenovskikh luchei tverdyim rastvorom HfC-ZrC (Diffuse X-ray scattering of the HfC-ZrC solid solution). *Fiz Met Metalloved* 20(5):719–722 (in Russian)
457. Gusev AI (2006) Short-range order and diffuse scattering in nonstoichiometric compounds. *Phys Usp* 49(7):693–718
458. Zhilyaev VA, Patrakov EI (2006) Mekhanizm zhidkofaznogo vzaimodeistviya dvoynykh karbidov (Ti,Me)C s nikelom (The mechanism of liquid-phase interaction of double carbides (Ti,Me)C with nickel). *Konstruk Kompoz Mater* (4):199–201 (in Russian)
459. Zhilyaev VA, Patrakov EI (2015) Regularities of the contact interaction of double carbides (Ti_{1-n}Me_n)C with nickel. *Russ J Non-Ferr Met* 56(3):329–332
460. Zhilyaev VA (2015) Regularities of reactions of group IV, V transition metal carbides with nickel. *Russ J Non-Ferr Met* 56(5):575–579
461. Zhilyaev VA, Patrakov EI (2006) Osobennosti vzaimodeistviya dvoynykh karbidov (Ti,Me)C s Ni-Mo raspalvom (The particularities of the interaction of double carbides (Ti,Me)C with Ni-Mo melt). *Konstruk Kompoz Mater* 4:196–199 (in Russian)
462. Markström A, Andersson D, Frisk K (2008) Combined *ab-initio* and experimental assessment of A_{1-x}B_xC mixed carbides. *Calphad* 32(4):615–623
463. Kieffer R, Nowotny H, Neckel A, Ettmayer P, Usner L (1968) Zur Entmischung von kubischen Mehrstoffcarbiden (On the miscibility of multicomponent cubic carbides). *Monatsh Chem* 99(3):1020–1027 (in German)
464. Jung W-S, Chung S-H (2010) *Ab initio* calculation of interfacial energies between transition metal carbides and fcc iron. *Model Simul Mater Sci Eng* 18(7):075008
465. Ghaffari SA, Faghihi-Sani MA, Golestani-Fard F, Nojabayy M (2013) Diffusion and solid solution formation between the binary carbides of TaC, HfC and ZrC. *Int J Refract Met Hard Mater* 41:180–184
466. Stottlemeyer AL, Kelly TG, Meng Q, Chen JG (2012) Reactions of oxygen-containing molecules on transition metal carbides: surface science insight into potential applications in catalysis and electrocatalysis. *Surf Sci Rep* 67:201–232
467. Goretzki H, Bittner H, Nowotny H (1964) Der Einfluß von Wasserstoff auf Titancarbid (The influence of hydrogen on titanium carbide). *Monatsh Chem* 95(6):1521–1526 (in German)
468. Samsonov GV, Antonova MM, Morozov VV (1970) Ternary systems Me-C-H and Me-N-H. *Powder Metall Met Ceram* 9(4):318–327
469. Aizawa T, Hayami W, Souda R, Otani S, Ishizawa Y (1997) Hydrogen adsorption on transition metal carbide (111) surfaces. *Surf Sci* 381:157–164
470. Uchida K, Imoto S, Kyō B (1977) Hydrolysis of titanium and zirconium carbonitrides. *Trans Jpn Inst Met* 18(10):727–734
471. Shimada S (2001) Interfacial reaction on oxidation of carbides with formation of carbon. *Solid State Ionics* 141–142:99–104
472. Shimada S, Hayashi S, Yunazar F (2002) High-temperature oxidation of (Ti_{0.5}Hf_{0.5})C ceramics fabricated by hot-pressing. *J Ceram Soc Jpn* 110:167–172
473. Patra N, Nasiri NA, Jayaseelan DD, Lee WE (2016) Low-temperature solution synthesis of nanosized hafnium carbide using pectin. *Ceram Int* 42(1):1959–1963
474. McClaine LA (ed) (1963) Thermodynamic and kinetic studies for a refractory materials program. Technical Report ASD-TDR-62-204, Contract AF33(616)-7472, Part 2. Air Force Materials Laboratory, Wright-Patterson Air Force Base, Ohio, pp. 1–142
475. McClaine LA (ed) (1964) Thermodynamic and kinetic studies for a refractory materials program. Technical Report ASD-TDR-62-204, Contract AF33(616)-7472, Part 3. Air Force Materials Laboratory, Wright-Patterson Air Force Base, Ohio, pp. 1–236
476. Berkowitz-Mattuck J, Larson JT, Quigley RF, Christiansen W (1963) Kinetics of oxidation of refractory metals and alloys at 1000–2000 °C. Report ASD-TDR-62-203, Contract AF33(616)-6154, Part 2. Arthur D. Little Inc., Cambridge, Massachusetts, pp. 1–117
477. Samsonov GV, Kovalchenko MS, Petrykina RYa, Naumenko VYa (1970) Hot-pressing of the transition metals and their carbides in their homogeneity regions. *Powder Metall Met Ceram* 9(9):713–716

478. Samsonov GV, Sinelnikova VS (1964) Electrical resistance of refractory compounds at high temperatures. In: Samsonov GV (ed) *Refractory transition metal compounds and high temperature cermet*s. Academic Press, New York, London, pp. 172–177
479. Samsonov GV, Sinelnikova VS (1962) The resistivity of refractory compounds at high temperatures. *Powder Metall Met Ceram* 1(4):272–274
480. Samsonov GV, Naumenko VYa (1970) Thermal expansion of transition metal carbides IV-V groups in their homogeneity regions. *High Temp* 8(5):1022–1024
481. Liu M, Cowley J (1993) Hafnium carbide growth behaviour and its relationship to the dispersion hardening in tungsten at high temperatures. *Mater Sci Eng A* 160:159–167
482. Lukashenko TA, Tikhonov KI (1998) Korroziionnaya stoikost ryada karbidov i nitridov perekhodnykh metallov 4–6 grupp v kontsentrirovannykh rastvorakh semoi i fosfornoj kislot (Corrosion resistance of a number of carbides and nitrides of group 4–6 transition metals in concentrated solutions of sulfuric and phosphoric acids). *Zh Prikl Khim* 71(12):2017–2020 (in Russian)
483. Rohmer M-M, Benard M, Poblet J-M (2000) Structure, reactivity and growth pathways of metalcarbohedrenes M_8C_{12} and transition metal/carbon clusters and nanocrystals: a challenge to computational chemistry. *Chem Rev* 100:495–542
484. Nazarova SZ, Gusev AI (2001) Magnetic susceptibility as a method of investigation of short-range order in highly nonstoichiometric carbides. *J Struct Chem* 42(3):470–484
485. Zyryanova AN, Gusev AI (1998) Magnetic susceptibility and ordering in nonstoichiometric hafnium carbide. *Russ J Phys Chem A* 72(12):2034–2041
486. Zyryanova AN, Nazarova SZ, Gusev AI (1998) Magnetic susceptibility anomaly as evidence for ordering of nonstoichiometric hafnium carbide HfC_y . *Dokl Phys Chem* 359(1–3):91–96
487. Savitskii EM, Baron VV, Efimov YuV, Bychkova MI, Myzenkova LF (1973) *Superconducting materials*. Plenum Press, New York, London
488. Samsonov GV, Fomenko VS, Podchernyaeva IA, Okhremchuk LN (1974) Thermionic emission properties of refractory compounds and materials based on them (a review). *Powder Metall Met Ceram* 13(10):836–842
489. Kyō B, Uchida K, Imoto S (1975) Hydrolysis of hafnium nitrides and carbides. *J Jpn Inst Met* 39(3):305–311 (in Japanese)
490. Samsonov GV, Goryachev YuM, Okhremchuk LN, Podchernyaeva IA, Fomenko VS (1977) Electron energy spectrum and physical properties of transition metal carbides in the region of homogeneity. *Russ Phys J* 20(1):30–36
491. Westrum EF Jr, Feick G (1977) Heat capacities of $HB_{2.035}$ and $HfC_{0.968}$ from 5 to 350 K. *J Chem Thermodyn* 9:293–299
492. Kovalchenko MS, Bovkun GA, Tkachenko YuG, Ragozin IP (1983) Deformation properties of monocarbides of transition metals by the method of continuous impression of an indenter. *Powder Metall Met Ceram* 22(12):1034–1037
493. Rowcliffe DJ (1984) Plastic deformation of transition metal carbides. In: Tressler RE, Bradt RC (eds) *Deformation of ceramic materials II*. Plenum Press, New York and London, pp. 49–71
494. Lei J-F, Okimura H, Brittain JO (1990) The electrical resistance of the group IV transition metal monocarbides and mononitrides in the temperature range 20–1000 °C. *Mater Sci Eng A* 123:129–140
495. Simões JAM, Beauchamp JL (1990) Transition metal – hydrogen and metal – carbon bond strengths: the keys to catalysis. *Chem Rev* 90(4):629–688
496. Luo Y-R (2007) *Comprehensive handbook of chemical bond energies*. CRC Press, Boca Raton, London, New York
497. Gruzalski GR, Lui S-C, Zehner DM (1990) Work-function changes accompanying changes in composition of (100) surfaces of HfC_x and TaC_x . *Surf Sci* 239(1–2):L517–L520
498. Price DL, Cooper BR, Wills JM (1993) Effect of carbon vacancies on carbide work functions. *Phys Rev B* 48(20):15311–15315
499. Wang CC, Akbar SA, Chen W, Patton VD (1995) Electrical properties of high-temperature oxides, borides, carbides and nitrides. *J Mater Sci* 30:1627–1641
500. Bittermann H, Rogl P (1997) Critical assessment and thermodynamic calculation of the binary system hafnium-carbon (Hf-C). *J Phase Equilib* 18(4):344–356

501. Singh M, Wiedemeier H (1997) Estimation of thermal expansion behaviour of some refractory carbides and nitrides. *J Mater Sci* 32(21):5749–5751
502. Eckerlin P, Kandler H (1971) Structural data for elements and intermetallic phases. Springer, Berlin
503. Gusev AI (2003) Analysis of surface segregation and solid-phase decomposition of substitutional solid solutions. *Dokl Phys Chem* 392(1–3):235–239
504. Pisarenko VA, Rakitskii AN, Samelyuk AV (2003) Diffusion interaction in fiber-reinforced composites of the chromium alloy – silicon carbide system. *Powder Metall Met Ceram* 42(5–6):297–301
505. Hugosson HW, Eriksson O, Jansson U, Ruban AV, Souvatzis P, Abrikosov IA (2004) Surface energies and work functions of the transition metal carbides. *Surf Sci* 557(1–3): 243–254
506. Arun R, Subramanian M, Mehrotra GM (1990) Oxidation behaviour of TiC, ZrC and HfC dispersed in oxide matrices. In: Tressler E, McNallan M (eds) *Ceramic transactions, Vol. 10 – Corrosion and corrosive degradation of ceramics*. Westerville, Ohio, The American Ceramic Society, pp. 211–223
507. McCauley RA (2004) *Corrosion of ceramic and composite materials*, 2nd edn. Marcel Dekker, New York, Basel
508. Sacks MD, Wang C-A, Yang Z, Jain A (2004) Carbothermal reduction synthesis of nanocrystalline zirconium carbide and hafnium carbide powders using solution-derived precursors. *J Mater Sci* 39:6057–6066
509. Gusev AI, Nazarova SZ (2005) Magnetic susceptibility of nonstoichiometric compounds of transition d-metals. *Phys Usp* 48(7):651–673
510. Ahn S, Kang S (2001) Effect of various carbides on the dissolution behaviour of $Ti(C_{0.7}N_{0.3})$ in a $Ti(C_{0.7}N_{0.3})$ –30Ni system. *Int J Refract Met Hard Mater* 19:539–545
511. Noffsinger J, Giustino F, Louie SG, Cohen ML (2008) First principles study of superconductivity and Fermi-surface nesting in ultra-hard transition metal carbides. *Phys Rev B* 77(18):1805071–1805074
512. Li X, Westwood A, Brown A, Brydson R, Rand B (2009) A convenient general synthesis of carbide nanofibres via templated reactions on carbon nanotubes in molten salt media. *Carbon* 47:201–208
513. Sugiura K, Iwata T, Nakano H, Fukuda K (2009) $[Zr_{0.72}Y_{0.28}]Al_4C_4$: a new member of the homologous series $(MC)_n(T_4C_3)_m$ ($M = Zr, Y$ and $Hf, T = Al, Si, Ge$). *J Solid State Chem* 182(7):1619–1623
514. Wan D-T, He L-F, Zheng L-L, Zhang J, Bao Y-W, Zhou Y-C (2010) A new method to improve the high-temperature mechanical properties of Ti_3SiC_2 by substituting Ti with Zr, Hf or Nb. *J Am Ceram Soc* 93(6):1749–1753
515. Jiang X, Zhao J, Jiang X (2011) Correlation between hardness and elastic moduli of the covalent crystals. *Comput Mater Sci* 50(7):2287–2290
516. Klimov DA, Myktybekov B, Nizovtsev VE, Ukhov PA (2011) Perspektivy primeneniya nanostrukturnykh kompozitsionnykh materialov na osnove karbidov i oksidov tugoplavlikh metallov dlya aviakosmicheskikh obektov (Perspectives of the application of nanostructured composite materials based on carbides and oxides of refractory metals for aerospace facilities). *Trudy MAI, Vol. 46, 9 pp.* (in Russian). <http://www.mai.ru/upload/iblock/1a/1a1493319c8c15a70decf28b0a51172d.pdf>. Accessed 10 Feb 2015
517. Kwon WT, Park JS, Kim S-W, Kang S (2004) Effect of WC and group IV carbides on the cutting performance of Ti(C,N) cermet tools. *Int J Machine Tools Manufact* 44:341–346
518. Batzill M (2012) The surface science of graphene: metal interfaces, CVD synthesis, nano-ribbons, chemical modifications and defects. *Surf Sci Rep* 67:83–115
519. Kurtoglu M, Naguib M, Gogotsi Y, Barsoum MW (2012) First principles study of two-dimensional early transition metal carbides. *MRS Commun* 2:133–137
520. Epshteyn A, Purdy AP, Pettigrew KA, Miller JB, Stroud RM (2009) Sonochemical synthesis of air-insensitive carbide-stabilized hafnium subhydride nanopowder. *Chem Mater* 21(15):3469–3472

521. Ordanyan SS, Orekhov AN, Vikhman SV (2012) Interaction of W_2B_5 with $Me^{IV,VC}$ carbides. *Russ J Non-Ferrous Met* 55(1):91–94
522. Charpentier L, Balat-Pichelin M, Sciti D, Silvestroni L (2013) High-temperature oxidation of Zr- and Hf-carbides: influence of matrix and sintering additive. *J Eur Ceram Soc* 33(15–16):2867–2878
523. Réjasse F, Rapaud O, Pradeilles N, Maître A, Trolliard G (2013) Experimental study of group IVB metals oxycarbides. In: David N, Jaubert J-N, Privat R (eds) *Proc. 39th joint European days on equilibrium between phases*, Nancy, France, 19–21 Mar 2013. MATEC Web Conf 3:01077. <http://dx.doi.org/10.1051/mateconf/20130301077>. Accessed 28 May 2016
524. Sani E, Mercatelly L, Sans J-L, Silvestroni L, Sciti D (2013) Porous and dense hafnium and zirconium ultra-high temperature ceramics for solar receivers. *Opt Mater* 36:163–168
525. Simonenko EP, Sevastyanov DV, Simonenko NP, Sevastyanov VG, Kuznetsov NT (2013) Promising ultra-high temperature ceramic materials for aerospace applications. *Russ J Inorg Chem* 58(14):1669–1693
526. Zhou Y-C, He L-F, Lin Z-J, Wang J-Y (2013) Synthesis and structure-property relationships of a new family of layered carbides in Zr-Al(Si)-C and Hf-Al(Si)-C systems. *J Eur Ceram Soc* 33:2831–2865
527. Blum YD, Kleebe H-J (2004) Chemical reactivities of hafnium and its derived boride, carbide and nitride compounds at relatively mild temperatures. *J Mater Sci* 39(19):6023–6042
528. Diwan BD (2014) Structural phase transition of refractory metal carbides at high pressure. *Can J Phys* 92:415–419
529. Gupta S, Hoffman EN, Barsoum MW (2006) Synthesis and oxidation of Ti_2InC , Zr_2InC , $(Ti_{0.5}Zr_{0.5})_2InC$ and $(Ti_{0.5}Hf_{0.5})_2InC$ in air. *J Alloys Compd* 426:168–175
530. Barsoum MW, Golczewski J, Seifert JJ, Aldinger F (2002) Fabrication and electrical and thermal properties of Ti_2InC , Hf_2InC and $(Ti, Hf)_2InC$. *J Alloys Compd* 340:173–179
531. Naguib M, Bentzel GW, Shah J, Halim J, Caspi EN, Lu J, Hultman L, Barsoum MW (2014) New solid solution MAX phases: $(Ti_{0.5}V_{0.5})_3AlC_2$, $(Nb_{0.5}V_{0.5})_2AlC$, $(Nb_{0.5}V_{0.5})_4AlC_3$ and $(Nb_{0.8}Zr_{0.2})_2AlC$. *Mater Res Lett* 2(4):233–240
532. Abdelkader HS, Faraoun HI (2014) Properties of interfaces between iron-group metals (Fe, Co, Ni) and HfC via first principles modeling. *J Mater Sci* 49:407–414
533. Sun D, Hu Q, Chen J, Zhou A (2014) First principles calculations of the relative stability, structure and electronic properties of two-dimensional metal carbides and nitrides. In: *Proc. 8th Int. conf. on high-performance ceramics (CICC 2013)*, Chongqing, China, 4–7 Nov 2013. *Key Eng Mater* 602–603:527–531
534. Wang S, Zhang K, An T, Hu C, Meng Q, Ma Y, Wen M, Zheng W (2015) Structure, mechanical and tribological properties of HfC_x films deposited by reactive magnetron sputtering. *Appl Surf Sci* 327:68–76
535. Lipke DW, Ushakov SV, Navrotsky A, Hoffman WP (2014) Ultra-high temperature oxidation of a hafnium carbide – based solid solution ceramic composite. *Corros Sci* 80:402–407
536. Zou Z, Fu L, Song X, Zhang Y, Liu Z (2014) Carbide-forming groups IVB-VIB metals: a new territory in the periodic table for CVD growth of graphene. *Nano Lett* 14:3832–3839
537. Guo Z, Zhu L, Zhou J, Sun Z (2015) Microscopic origin of MXenes derived from layered MAX phases. *RSC Adv* 5(32):25403–25408
538. Réjasse F, Trolliard G, Rapaud O, Maître A, David J (2015) TEM study of the reaction mechanisms involved in the carbothermal reduction of hafnia. *RSC Adv* 5:45341–45350
539. Cedillos-Barraza O, Grasso S, Nasiri NA, Jayaseelan DD, Reece MJ, Lee WE (2016) Sintering behaviour, solid solution formation and characterization of TaC, HfC and TaC-HfC fabricated by spark-plasma sintering. *J Eur Ceram Soc* 36:1539–1548
540. Yu X-X, Weinberger CR, Thompson GB (2016) *Ab initio* investigations of the phase stability in group IVB and VB transition metal carbides. *Comput Mater Sci* 112:318–326
541. Wang Q, German KE, Oganov AR, Dong H, Feya OD, Zubavichus YaV, Murzin VYu (2016) Explaining stability of transition metal carbides – and why TcC does not exist. *RSC Adv* 6(20):16197–16202

542. Gazaryan KG, Nersesyan GA, Mkrtchyan DzhS, Mnatsakanyan RA (1992) Transition metal carbides as catalysts for *n*-heptane conversion. *Petroleum Chem* 32(6):486–491
543. Sani E, Mercatelli L, Meucci M, Balbo A, Silvestroni L, Sciti D (2016) Compositional dependence of optical properties of zirconium, hafnium and tantalum carbides for solar absorber applications. *Sol Energy* 131:199–207
544. Arabei BG, Levinskii YuV, Markov YuM, Portnoi KI (1978) Effect of alloying of uranium carbide on its interaction with carbon. *Atom Energy* 44(3):288–290
545. Balankin SA, Loshmanov LP, Skorov DM, Sokolov VS (1979) Raschet energii obrazovaniya vakansii v fazakh vnedreniya po dannym mekhanicheskikh svoistv (Calculation of vacancy formation energy in interstitial phases through mechanical properties data). In: Sobolev ND, Beskorovainyi NM, Morozov EM, Kulbakh AA, Markochev VM, Sapunov VT (eds) *Fizika i mekhanika deformatsii i razrusneniya* (Physics and mechanics of deformation and fracture), Vol. 7. Atomizdat, Moscow (in Russian), pp. 8–12
546. Ogorodnikov VV, Rogovoi Yul (1992) Simulating point defects in cubic monocarbides. *Inorg Mater* 28(5):763–767
547. Gusev AI, Rempel AA, Shveikin GP (1997) Nestekhiometriya i radiatsionnaya stoikost konstruksionnykh materialov (analiz dannykh) (Nonstoichiometry and structural materials resistance to radiation damage (data analysis)). *Doklady AN SSSR* 357(4):490–494 (in Russian)
548. Cherkashenko VM, Nazarova SZ, Gusev AI, Ivanovskii AL (2001) Electronic structure, chemical bonding and properties of binary carbides $M_xM'_yC_z$ in the crystalline and molecular states: XES, XPS and quantum-chemical studies. *J Struct Chem* 42(6):1002–1024
549. Wang J, Zhou Y (2009) Recent progress in theoretical prediction, preparation and characterization of layered ternary transition metal carbides. *Annu Rev Mater Res* 39:415–443
550. Yoshitake M (2012) Examination of work function of transition metal carbides and nitrides. *J Vac Soc Jpn* 55(7):349–353 (in Japanese)
551. Yoshitake M (2014) Generic trend of work functions in transition metal carbides and nitrides. *J Vac Sci Technol A* 32(6):061403
552. Ordanyan SS, Udalov YuP (2015) On the structure of the $SiC-Mo(W)Si_2-Me^d B_2$ systems and prospective development of refractory materials based on these systems. In: Ordanyan SS (ed) *Aktualnye problemy tekhnologii proizvodstva sovremennykh keramicheskikh materialov* (Current problems of the modern technology of ceramic materials). Polytechnic University Publishing House, Saint Petersburg, pp. 7–16 (in Russian)
553. Zhilyaev VA, Patrakov EI (2016) Influence of alloying titanium carbonitride by transition metals of groups IV–VI on the interaction with nickel melt. *Russ J Non-Ferr Met* 57(2):141–147
554. Lekakh SN, Medvedeva NI (2015) *Ab initio* study of Fe adsorption on the (001) surface of transition metal carbides and nitrides. *Comput Mater Sci* 106:149–154
555. Khazaei M, Arai M, Sasaki T, Ranjbar A, Liang Y, Yunoki S (2015) OH-terminated two-dimensional transition metal carbides and nitrides as ultra-low work function materials. *Phys Rev B* 92(7):075411
556. Zha X-H, Luo K, Li Q, Huang Q, He J, Wen X, Du S (2015) Role of the surface effect on the structural, electronic and mechanical properties of the carbide MXenes. *EPL-Europhys Lett* 111:26007 (6 pp.)
557. Shabalin IL, Luchka MV, Shabalin LI (2007) Vacuum SHS in systems with group IV transition metals for production of ceramic compositions. *Phys Chem Solid State* 8(1):159–175
558. Kikuchi M, Nagakura S, Oketani S (1971) Crystal structures of transition metal carbides. *J Iron Steel Inst Jpn* 57(6):1009–1053 (in Japanese)
559. Gusev AI, Rempel AA (1997) Phase diagrams of metal-carbon and metal-nitrogen systems and ordering in strongly nonstoichiometric carbides and nitrides. *Phys Stat Sol A* 163(2):273–304
560. Krajewski A, D'Alessio L, De Maria G (1998) Physico-chemical and thermophysical properties of cubic binary carbides. *Cryst Res Technol* 33(3):341–374
561. Naumenko VYa (1970) Preparation of carbides of the IV–V groups transition metals in their homogeneity regions. *Powder Metall Met Ceram* 9(10):799–801

562. Ren J, Zhang Y, Li J, Tian S, Fei T, Li H (2016) Effects of deposition temperature and time on HfC nanowires synthesized by CVD on SiC-coated C/C composites. *Ceram Int* 42: 5623–5628
563. Ren J, Zhang Y, Hu H, Fei T, Li H (2016) Oxidation resistance and mechanical properties of HfC nanowire-toughened ultra-high temperature ceramic coating for SiC-coated C/C composites. *Appl Surf Sci* 360:970–978
564. He LF, Bao YW, Wang JY, Li MS, Zhou YC (2009) Microstructure and mechanical and thermal properties of ternary carbides in Hf-Al-C system. *Acta Mater* 57:2765–2774
565. Kellie JLF, Davies P, Retelsdorf HJ (1984) Production of zirconium hafnium and zirconium niobium carbides. *Int J Refract Met Hard Mater* 3(3):136–141
566. Grigorev ON, Chugunova SI, Shatokhin AM, Yaroshenko VP (1981) Mechanical properties of silicon nitride composite materials. *Powder Metall Met Ceram* 20(7):502–505
567. Gogotsi YuG (1994) Review. Particulate silicon nitride – based composites. *J Mater Sci* 29:2541–2556
568. Branagan DJ, Kramer MJ, McCallum RW (1996) Transition metal carbide formation in the $Nd_2Fe_{14}B$ system and potential as alloying additions. *J Alloys Compd* 244:27–39
569. Ryan NE, Soffa WA, Crawford RC (1968) Orientation and habit plane relationships for carbide and nitride precipitates in molybdenum. *Metallogr* 1:195–220
570. Takida T, Igarashi T, Saito N, Nakamura M (1999) Stability of grain structures in sintered molybdenum alloys dispersed with carbide particles at high temperatures. *J Jpn Soc Powder Powder Metall* 46(12):1261–1267 (in Japanese)
571. Rogl P, Bittermann H (1999) Ternary metal boron carbides. *Int J Refract Met Hard Mater* 17:27–32
572. Stecher P, Benesovsky F, Neckel A, Nowotny H (1964) Untersuchungen in den Systemen Titan (Zirkonium, Hafnium) – Niob – Kohlenstoff (Investigations in the systems titanium (zirconium, hafnium) – niobium – carbon). *Monatsh Chem* 95(6):1630–1645 (in German)
573. Shurin AK, Dmitrieva GP, Razumova NA (1988) Phase equilibria in ternary nickel-carbide alloys. *Russ Metall* (6):63–69
574. Gladyshevskii EI, Popova NM, Fedorov TF (1963) Mutual solubility of zirconium, niobium and hafnium carbides. *Russ J Inorg Chem* 8(8):1040–1041
575. Nowotny H, Kieffer R, Benesovsky F, Brukl C (1959) Über die Teilsysteme: TiC-HfC und ZrC-HfC (On subsystems: TiC-HfC and ZrC-HfC). *Monatsh Chem* 90(1):86–88 (in German)
576. Mozhukhin EI, Kondratev NN (1982) Issledovanie protsessov tverdogfaznogo spekaniya karbidov titana, tsirkoniya i gafniya (Study of the processes of solid-phase sintering of titanium, zirconium and hafnium carbides). *Izv Vyssh Uchebn Zaved Chem Metall* (3):12–15 (in Russian)
577. Gusev AI, Rempel AA (2001) Nestekhiometriya, besporyadok i poryadok v tverdom tele (Nonstoichiometry, disorder and order in solids). Ural Division of the Russian Academy of Sciences, Yekaterinburg (in Russian)
578. Gusev AI (2007) Nestekhiometriya, besporyadok, blizhnii i dalnii poryadok v tverdom tele (Nonstoichiometry, disorder, short-range and long-range order in solids). Nauka Fizmatlit, Moscow (in Russian)
579. Kurlov AS, Gusev AI (2014) High-energy milling of nonstoichiometric carbides: effect of nonstoichiometry on particle size of nanopowders. *J Alloys Compd* 582:108–118
580. Glushko VP, Gurvich LV (eds) (1982) Thermodynamic properties of individual substances, Vol. IV, Parts 1–2. Nauka, Moscow
581. Senczyk D (1984) The lattice parameters of MeC-type carbides, nitrides and carbonitrides of transition metals of IV and V groups of the periodic system. In: Proc. 11th conf. on applied crystallography, Vol. 1. Kozubnik, Poland, pp. 234–240
582. Touloukian YS, Kirby RK, Taylor RE, Lee TYR (1977) Thermophysical properties of matter, Vol. 13 – Thermal expansion – nonmetallic solids. IFI/Plenum Data Corporation, New York, Washington
583. Brizes WF (1968) Mechanical properties of the groups IVB and VB transition metal monocarbides. Report NASA-CR-95887, Contract N68-30720. Space Research Coordination Centre, University of Pittsburgh, Pennsylvania

584. Norton JT, Lewis RK (1963) Properties of non-stoichiometric metallic carbides. Technical Report NASA-CR-52083, Contract NASw-663. Advanced Metals Research Corporation, Somerville, Massachusetts, pp. 1–18
585. Norton JT, Lewis RK (1964) Properties of non-stoichiometric metallic carbides. Final Report NASA-CR-58046, Contract NASw-663. Advanced Metals Research Corporation, Somerville, Massachusetts, pp. 1–42
586. Rudy E, Benesovsky F (1960) Über die elektrische Leitfähigkeit von hochschmelzenden harten Karbiden und Karbidmischkristallen (On the electrical conductivity of refractory hard carbides and carbide mixed crystals). *Planseeber Pulvermetall* 8:72–77 (in German)
587. Gusev AI (1989) Structural stability boundaries for nonstoichiometric compounds. *Phys Stat Sol A* 111:443–450
588. Delin A, Eriksson O, Ahuja R, Johanson B, Brooks MSS, Gasche T, Auluck S, Wills JM (1996) Optical properties of the group IVB refractory metal compounds. *Phys Rev B* 54(3):1673–1681
589. Kammori Ô, Sato K, Kurosawa F (1968) Infrared absorption spectra of metal carbides, nitrides and sulfides. *Jpn Analyst* 17(10):1270–1273 (in Japanese)
590. Fomenko WS, Lawrenko WA, Ochremtschuk LN, Podtschernjaeva IA, Prozenko TG, Samsonow GW (1971) Korrelation von Abtrennungsarbeit von Übergangsmetall Karbide in Homogenitätsbereich mit Oberflächenrekombination von Wasserstoffatomen (Correlation of work function of transition metal carbides in homogeneity region with surface recombination of hydrogen atoms). *Rev Int Hautes Temp* 8(3–4):315–318 (in German)
591. Samsonov GV, Naumenko VYa, Okhremchuk LN, Podchernyaeva IA, Fomenko VC (1972) Termoemissionnye svoistva karbidov perekhodnykh metallov IV-V grupp v oblastiakh ikh gomogenosti (The thermionic emission properties of transition metal carbides IV-V groups in their homogeneity regions). In: Samsonov GV (ed) *Elektronnoe stroenie i fizicheskie svoistva tverdogo tela* (Electron structure and physical properties of solids), Vol. 2. Naukova Dumka, Kyiv, pp. 147–156 (in Russian)
592. Samsonov GV, Podchernyaeva IA, Fomenko VS, Lavrenko VA, Okhremchuk LN, Protsenko TG (1972) Correlation between the work functions of transition metal carbides in their homogeneity regions and surface recombination of hydrogen atoms. *Powder Metall Met Ceram* 11(5):389–392
593. Back T, Fairchild SB, Averett K, Maruyama B, Pierce N, Cahay M, Murray PT (2013) Pulsed-laser deposited transition metal carbides for field emission cathode coatings. *ACS Appl Mater Interfaces* 5:9241–9246
594. Zaima S, Adachi H, Shibata Y (1984) Promising cathode materials for high brightness electron beams. *J Vac Sci Technol B* 2(1):73–78
595. Charbonnier FM, Mackie WA, Xie T, Davis PR (1999) Enhanced field emission from carbide-coated field emitters and device applications. *Ultramicroscopy* 79:73–82
596. Yu ML, Hussey BW, Kratschmer E, Chang THP, Mackie WA (1995) Improved emission stability of carburized HfC <100> and ultrasharp tungsten field emitters. *J Vac Sci Technol B* 13(6):2436–2440
597. Jiang J, Zhang JH, Feng T, Jiang BY, Wang YJ, Zhang FM, Dai LJ, Wang X, Liu XH, Zou SC (2005) Improved emission stability of HfC-coated carbon nanotubes field emitters. *Solid State Commun* 135(6):390–393
598. Nicolaescu D, Sato T, Nagao M, Filip V, Kanemaru S, Itoh J (2004) Characterization of enhanced field emission from HfC-coated Si emitter arrays through parameter extraction. In: *Proc. 6th Int. vacuum microelectronics conf. (IVMC 2003)*, Osaka, Japan, 07–11 July 2003. *J Vac Sci Technol B* 22(3):1227–1233
599. Nicolaescu D, Nagao M, Sato T, Filip V, Kanemaru S, Itoh J (2005) Emission statistics for Si and HfC emitter arrays after residual gas exposure. In: *Proc. 17th Int. vacuum nanoelectronics conf. (IVNC-04)*, Cambridge, Massachusetts, 11–16 July 2004. *J Vac Sci Technol B* 23(2):707–717
600. Nicolaescu D, Nagao M, Filip V, Kanemaru S, Itoh J (2005) General analytical relationship for electric field of gated field emitters. *Jpn J Appl Phys Part 1* 44(6A):3854–3859
601. Nicolaescu D, Nagao M, Sato T, Filip V, Kanemaru S, Itoh J (2005) Emission statistics for HfC emitter arrays after residual gas exposure. *Jpn J Appl Phys Part 1* 44(8):5959–5963

602. Nicolaescu D, Nagao M, Sato T, Filip V, Kanemaru S, Itoh J (2006) Parameter dispersion characterization for arrays of HfC-coated emitters on poly-Si substrate. In: Proc. 18th Int. vacuum nanoelectronics conf., Oxford, UK, 10–14 July 2005. *J Vac Sci Technol B* 24(2):1045–1051
603. Yu ML, Kim HS, Hussey BW, Chang THP, Mackie WA (1996) Energy distributions of field emitted electrons from carbide tips and tungsten tips with diamond-like carbon coatings. *J Vac Sci Technol B* 14(6):3797–3801
604. Yu ML, Lang ND, Hussey BW, Chang THP, Mackie WA (1996) New evidence for localized electronic states on atomically sharp field emitters. *Phys Rev Lett* 77(8):1636–1639
605. Mackie WA, Morrissey JL, Hinrichs CH, Davis PR (1992) Field emission from hafnium carbide. In: Proc. 38th Nat. symp. of the American Vacuum Society, Seattle, Washington, 11–15 Nov 1991. *J Vac Sci Technol A* 10(4/3):2852–2856
606. Rakhshandehroo MR, Pang SW (1999) High current density Si field emission devices with plasma passivation and HfC coating. *IEEE Trans Electron Devices* 46(4):792–797
607. Sato T, Saida M, Horikawa K, Adachi K, Nagao M, Kanemaru S, Yamamoto S, Sasaki M (2005) Field emission distributions from HfC thin films studied with STM. In: Proc. 12th Int. display workshops in conjunction with Asia Display 2005 (IDW/AD'05), Takamatsu, Japan, 06–09 Dec 2005, Vols. 1–2. Institute of Image Information & Television Engineers, Tokyo, pp. 1705–1708
608. Sato T, Yamamoto S, Nagao M, Matsukawa T, Kanemaru S, Itoh J (2003) Fabrication and characterization of HfC coated Si field emitter arrays. In: Proc. 15th Int. vacuum microelectronics conf. (IVMC), Lyon, France, 07–11 July 2002. *J Vac Sci Technol B* 21(4):1589–1593
609. Yang YC, Liu L, Wei Y, Liu P, Jiang KL, Li QQ, Fan SS (2010) *In situ* fabrication of HfC-decorated carbon nanotube yarns and their field emission properties. *Carbon* 48(2):531–537
610. Yang YC, Qian L, Tang J, Liu L, Fan SS (2008) A low-vacuum ionization gauge with HfC-modified carbon nanotube field emitters. *Appl Phys Lett* 92(15):153105 (3 pp.)
611. Nagao M, Yasumuro C, Sacho Y, Tanoue H, Kanemaru S, Itoh J (2006) HfC field emitter array controlled by built-in poly-Si thin film transistor. In: Proc. 18th Int. vacuum nanoelectronics conf., Oxford, UK, 10–14 July 2005. *J Vac Sci Technol B* 24(2):936–939
612. Zhang JH, Yang CR, Wang YJ, Feng T, Yu WD, Jiang J, Wang X, Liu XH (2006) Improvement of the field emission of carbon nanotubes by hafnium coating and annealing. *Nanotechnol* 17(1):257–260
613. Sato T, Saida M, Nagao M, Yamamoto S, Sasaki M (2006) A new method for nanometer scale imaging of field emission current distribution. In: Proc. 7th IEEE Int. vacuum electronics conf. (IVEC)/6th IEEE Int. vacuum electron sources conf. (IVESC), Monterey, California, 25–27 Apr 2006. Institute of Electrical and Electronics Engineers, New York, pp. 475–476
614. Nagao M, Sacho Y, Matsukawa T, Kanemaru S, Itoh J (2005) Fabrication of HfC-coated Si field emitter arrays with built-up poly-Si thin film transistor. In: Proc. 17th Int. microprocesses and nanotechnology conf., Osaka, Japan, 26–29 Oct 2004. *Jpn J Appl Phys Part 1* 44(7B-SI):5740–5743
615. Sato T, Saida M, Horikawa K, Sasaki M, Nagao M, Kanemaru S, Matsukawa T, Itoh J, Yamamoto S (2005) Scanning tunneling microscopy observations of hafnium carbide thin films as a field emission material. In: Proc. 17th Int. vacuum nanoelectronics conf. (IVNC-04), Cambridge, Massachusetts, 11–16 July 2004. *J Vac Sci Technol B* 23(2):741–744
616. Nagao M, Sacho Y, Sato T, Matsukawa T, Kanemaru S, Itoh J (2004) Fabrication of polycrystalline silicon field emitter arrays with hafnium carbide coating for thin film transistor controlled field emission displays. In: Proc. 16th Int. microprocesses and nanotechnology conf., Tokyo, Japan, 29–31 Oct 2003. *Jpn J Appl Phys Part 1* 43(6B):3919–3922
617. Brookes CA, O'Neill JB, Redfern BAW (1971) Anisotropy in hardness of single crystals. *Proc R Soc Lond A* 322(1548):73–88
618. Sirdeshmukh DB, Sirdeshmukh L, Subhadra KG (2006) *Micro- and macro-properties of solids*. Springer, Berlin, Heidelberg

619. Réjasse F, Rapaud O, Trolliard G, Masson O, Maître A (2017) Experimental investigation and thermodynamic evaluation of the C-Hf-O ternary system. *J Am Ceram Soc* 100(8):3757–3770
620. Mughabghab SF (2006) Atlas of neutron resonances, 5th edn. Elsevier, Amsterdam, Boston
621. Razumovskiy VI, Popov MN, Ding H, Odqvist J (2015) Formation and interaction of point defects in group IVb transition metal carbides and nitrides. *Comput Mater Sci* 104:147–154
622. Gatterer J, Dufek G, Etmayer P, Kieffer R (1975) Das kubische Tantalmonitrid (B1-Typ) und seine Mischbarkeit mit den isotypen Übergangsmetallnitriden und -carbiden (The cubic tantalum mononitride (B1 type) and its miscibility with the isotypic transition metal nitrides and carbides). *Monatsh Chem* 106(5):1137–1147 (in German)
623. Zhilyaev VA, Patrakov EI, Pelts AD (1990) Kontaktnoe vzaimodeistvie legirovannykh karbonitridov titana s rasplavami na osnove nikelya (The contact interaction of alloyed titanium carbonitrides with nickel based melts). In: Nauch. soobshcheniya 7-oi Vsesoyuznoi konf. po strukture i svoistvam metallicheskih i shlakovykh rasplavov (Proc. 7th All-Union conf. on structure and properties of metallic and slag melts), Vol. 3, Part 3, pp. 232–235. Chelyabinsk Polytechnical Institute, Chelyabinsk (in Russian)
624. Zhilyaev VA, Patrakov EI (2016) Regularities of the contact interaction of double carbides ($(\text{Ti}_{1-n}\text{Me}_n^{\text{IV,V}})\text{C}$) with the Ni-Mo melt. *Russ J Non-Ferr Met* 57(6):610–617
625. Mortimer DA, Nicholas MG (1973) The wetting of carbon and carbides by copper alloys. *J Mater Sci* 8:640–648
626. Eustathopoulos N, Nicholas MG, Drevet B (1999) Wettability at high temperatures. Elsevier Science, Oxford
627. Jeitschko W, Nowotny H, Benesovsky F (1963) Kohlenstoffhaltige ternäre Verbindungen (H-Phase) (Carbonaceous ternary compounds (H-phase)). *Monatsh Chem* 94(4):672–676 (in German)
628. Jeitschko W, Nowotny H, Benesovsky F (1963) Die H-Phasen Ti_2InC , Zr_2InC , Hf_2InC und Ti_2GeC (The H-phases Ti_2InC , Zr_2InC , Hf_2InC and Ti_2GeC). *Monatsh Chem* 94(6):1201–1205 (in German)
629. Pessall N, Gold RE, Johansen HA (1968) A study of superconductivity in interstitial compounds. *J Phys Chem Solids* 29:19–38
630. Hachisuka T (1990) Toughening phenomena in $\text{TiC-TiN-Mo}_2\text{C-WC-HfC-Cr}_2\text{C}_3$ multi-component ceramic composite. *J Jpn Soc Powder Powder Metall* 37(7):1029–1036 (in Japanese)
631. Hachisuka T (1991) Fracture resistance of the $\text{TiC-Cr}_3\text{C}_2$ base multi-component ceramic composites as cutting tool. *J Jpn Soc Powder Powder Metall* 38(4):516–522 (in Japanese)
632. Gusev AI (2000) Order-disorder transformations and phase equilibria in strongly nonstoichiometric compounds. *Phys Usp* 43(1):1–37
633. Pienti L, Silvestroni L, Landi E, Melandri C, Sciti D (2015) Microstructure, mechanical properties and oxidation behaviour of TaC- and HfC-based materials containing short SiC fiber. *Ceram Int* 41(1):1367–1377
634. Pienti L, Sciti D, Silvestroni L, Cecere A, Savino R (2015) Ablation tests on HfC- and TaC-based ceramics for aeropropulsive applications. *J Eur Ceram Soc* 35(5):1401–1411
635. Bokhonov BB, Dudina DV (2017) Synthesis of ZrC and HfC nanoparticles encapsulated in graphitic shells from mechanically milled Zr-C and Hf-C powder mixtures. *Ceram Int* 43(16):14529–14532
636. Duan L, Zhao X, Wang Y (2017) Comparative ablation behaviours of C/SiC-HfC composites prepared by reactive melt infiltration and precursor infiltration and pyrolysis routes. *Ceram Int* 43(18):16114–16120
637. Tian S, Zhang Y, Ren J, Qiang X, Zhang S, Li H (2017) High-aspect-ratio HfC nanobelts accompanied by HfC nanowires: synthesis, characterization and field emission properties. *Appl Surf Sci* 402:344–351
638. Aisyah IS, Wyzomirska M, Calka A, Wexler D (2017) Nitrogenation of hafnium carbide powders in AC and DC plasma by electrical discharge assisted mechanical milling. *J Alloys Compd* 715:192–198

Chapter 4

Niobium Carbides



4.1 Structures

Niobium forms with carbon several chemical compounds (*see* also section C–Nb in Table I-2.13): niobium monocarbide NbC_{1-x} with the extremely broad homogeneity range, several modifications of niobium semicarbide, such as ordered low-temperature $\alpha\text{-Nb}_2\text{C}$ and middle-temperature $\beta\text{-Nb}_{2+x}\text{C}$ and disordered high-temperature $\gamma\text{-Nb}_{2\pm x}\text{C}$, as well as $\varepsilon\text{-Nb}_3\text{C}_{2+x}$, $\zeta\text{-Nb}_4\text{C}_{3-x}$, $\text{Nb}_5\text{C}_{4\pm x}$, $\text{Nb}_6\text{C}_{5\pm x}$, $\text{Nb}_7\text{C}_{6\pm x}$ and $\text{Nb}_8\text{C}_{7\pm x}$ ordered phases [1–7, 154, 415, 861–864, 930, 931, 958, 1095, 1096]. It should be mentioned that there are no forcible scientific arguments in favour of existence of the both ε - and ζ -phases as well as the data on molecular clusters Nb_8C_{12} are not confirmed sufficiently in the literature [4, 8, 12, 841, 891]. A high-temperature partial variant of niobium – carbon phase diagram is given in Fig. 4.1, and the structural features of the niobium carbides are presented in Table 4.1. The C/Nb radii ratio calculated on the basis of Pauling’s atomic size of Nb (0.1456 nm, CN = 12) is 0.530 [7], or 0.56 [63]; the ratio of Nb radii (in nm) in Me/MeC is 0.143/0.157 (10.0% expansion of Nb atoms in carbide) [690]. Under the higher pressures of $\sim 60\text{--}600$ GPa the structural transformation of NbC_{1-x} from NaCl type ($Fm(-3)m$) to CsCl type ($Pm(-3)m$) structure has been predicted theoretically [385–387, 391, 392, 738, 926]. The relationships between the lattice parameter and composition of NbC_{1-x} on the basis of several sources are given in Fig. 4.2; in the modified forms the following equations for $0 \leq x \leq 0.3$ in NbC_{1-x} earlier proposed by Kempter et al. [68] and later by Senczyk [1030]:

$$a = 0.4471 - 0.00268x - 0.03457x^2, \quad (4.1)$$

and recently by Gusev et al. (for disordered structures, $0 \leq x \leq 0.30$) [73, 359, 962, 1023]:

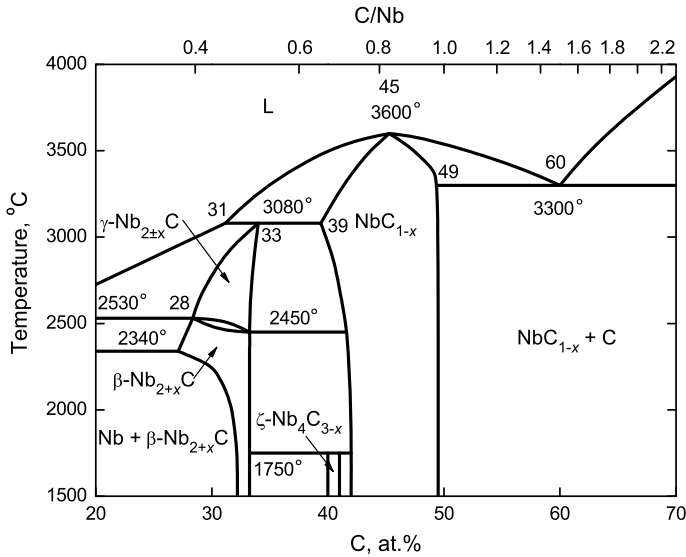


Fig. 4.1 High-temperature partial variant of niobium – carbon equilibrium phase diagram [3–7, 9, 58, 106, 144, 146, 415, 768, 818, 840, 859, 885, 886, 959, 964, 1029, 1034, 1094]

$$a = 0.4467 + 0.00493x - 0.07323x^2, \quad (4.2)$$

$$a = 0.4447 + 0.00378(0.1956 - x)^{1/3}, \quad (4.3)$$

can be recommended to describe it, where a is lattice parameter, nm and x is the value of index in NbC_{1-x} formula; within the homogeneity range of semicarbide $\text{Nb}_{2\pm x}\text{C}$ phase both the lattice parameters a and c also decline with decreasing carbon content [77, 82, 85]. The minimal Burgers vector of near-stoichiometric NbC_{1-x} ($1/2 \langle 110 \rangle$) $b = 0.316$ nm [2]; accordingly to the latter equation [359]:

$$b = 0.3144 + 0.00267(0.1956 - x)^{1/3}. \quad (4.4)$$

The parameters of formation and migration of NbC_{1-x} lattice point defects (vacancies and interstitial atoms) are given in Sect. 4.5 (Table 4.14). At low temperatures for non-stoichiometric monocarbide the slip system (111) $\langle 110 \rangle$ was determined, this system is also more preferential for NbC_{1-x} with various x at higher temperatures [10, 11, 87, 292, 297, 298, 690, 698, 1048]; it is necessary to add that for $\text{NbC}_{0.87}$ – by Turchin et al. [703] and for $\text{NbC}_{0.83}$ ($\text{Nb}_6\text{C}_{5\pm x}$ phase with non-cubic short- or long-range ordering) – by Morgan and Lewis [296], the coexistence of slip systems (110) $\langle 1\bar{1}0 \rangle$ and (111) $\langle 1\bar{1}0 \rangle$ were also determined [713]. The variations of the lattice parameter of NbC_{1-x} with temperature for the phases having different deviations from the stoichiometry are shown in Fig. 4.3.

Table 4.1 Structural properties (crystal structure, density) of niobium carbide phases

Formula	Crystal structure						Density ^c , g cm ⁻³	Reference	
	System	Type	Space group	Lattice parameters ^a , nm					Z ^b
				<i>a</i>	<i>b</i>	<i>c</i>			
NbC _{1-x}	Cubic	NaCl	<i>Fm</i> (-3) <i>m</i>	0.4430 ^d	-	-	4	-	[69, 77]
				0.4431 ^d	-	-	4	-	[58]
				0.4432 ^d	-	-	4	-	[6, 68]
				0.4432 ^e	-	-	4	7.79	[46]
				0.4433	-	-	4	-	[66, 67]
				0.4442	-	-	4	-	[27]
				0.4454 ^f	-	-	4	-	[18, 69]
				0.4457	-	-	4	-	[64]
				0.4460	-	-	4	-	[65]
				0.4461	-	-	4	-	[62, 159]
				0.4462	-	-	4	7.84	[29]
				0.4463	-	-	4	-	[24]
				0.4464 ^g	-	-	4	-	[69]
				0.4465 ^h	-	-	4	7.76	[21, 28]
				0.4467	-	-	4	7.82	[39]
				0.4467 ⁱ	-	-	4	7.78	[37, 38]
				0.4468 ^j	-	-	4	-	[36]
				0.4468	-	-	4	7.81	[30]
				0.4469	-	-	4	7.81	[10, 11, 22]
				0.4469 ^k	-	-	4	7.75	[41, 69]
0.4469 ^l	-	-	4	7.70	[59]				
0.4470 ^m	-	-	4	-	[58, 80]				
0.4470 ^m	-	-	4	7.78	[25, 31, 32]				
0.4471	-	-	4	7.80	[33, 34, 42]				
0.4471 ⁿ	-	-	4	7.77	[43]				
0.4471 ^o	-	-	4	7.72	[40]				
0.4471 ^p	-	-	4	7.79	[6, 68, 77, 388]				
				0.4473	-	-	4	7.80	[26]
γ-Nb _{2±x} C	Hexagonal	NiAs	<i>P6₃/mmc</i>	0.3100	-	0.5003 ^q	1	7.89	[50]
				0.3114	-	0.4985 ^r	1	7.85	[51]
				0.3116	-	0.4958 ^s	1	7.88	[56, 57]
				0.3117	-	0.4964 ^s	1	7.87	[53]
				0.3118	-	0.4955 ^s	1	-	[79]
				0.3118	-	0.4958 ^s	1	-	[59]
				0.3118	-	0.4961 ^s	1	-	[76]
				0.3119	-	0.4953 ^s	1	-	[64]
				0.3119	-	0.4959 ^s	1	-	[71, 718]
				0.3120	-	0.4957 ^{s,u}	1	-	[77]
				0.3122	-	0.4964 ^s	1	7.79	[84]

(continued)

Table 4.1 (continued)

Formula	Crystal structure			Lattice parameters ^a , nm			Density ^c , g cm ⁻³	Reference			
	System	Type	Space group	<i>a</i>	<i>b</i>	<i>c</i>					
				<i>Z</i> ^b							
				0.3123	–	0.4966 ^{s,u}	1	–	[82]		
				0.3124	–	0.4963 ^s	1	7.83	[54]		
				0.3125	–	0.4752 ^t	1	8.17	[52]		
				0.3125	–	0.4983 ^s	1	–	[17]		
				0.3126	–	0.4965 ^s	1	7.85	[10, 11, 69]		
				0.3126	–	0.4966 ^s	1	–	[61]		
				0.3126	–	0.4972 ^s	1	–	[2, 3, 6]		
				0.3127	–	0.4965 ^{s,u}	1	–	[58]		
				0.3127	–	0.4972 ^{s,v}	1	7.80	[6, 58, 81]		
				0.3128	–	0.4970 ^{s,v}	1	–	[77]		
				0.3128	–	0.4973 ^s	1	7.80	[55]		
				0.3128	–	0.4974 ^s	1	–	[62, 63]		
				0.3065–	–	0.4999–	1	–	[29]		
				0.3135	–	0.4909 ^w	–	–	–		
β -Nb _{2+x} C ^x	Trigonal	ϵ -Fe ₂ N	<i>P</i> (–3) <i>I</i> <i>m</i>	0.5401	–	0.4955 ^y	3	–	[2, 3, 61]		
				(or	0.5407	–	0.4968 ^y	3	–	[77]	
			<i>P</i> (–3) <i>m</i> <i>l</i>	0.5407	–	0.4974 ^y	3	–	[7, 70]		
				0.5408	–	0.4965 ^y	3	–	[1, 10, 11]		
				0.5417	–	0.4972 ^y	3	7.80	[47]		
α -Nb ₂ C ^x	Orthorhombic	ζ -Fe ₂ N	<i>Pbcn</i>	1.089	1.236	0.4968	–	–	[61, 77, 79]		
				1.076	1.254	0.4966	–	–	[78]		
			–	<i>Pnma</i>	1.0906	0.3096	0.4969	–	–	[2, 3, 6, 60]	
			–		<i>Pna2</i> ₁	1.092	0.3090	0.4974	–	–	[7, 35, 69]
			–	(or <i>Pmc2</i> ₁)	1.074–	0.3099–	0.4926–	–	–	[29]	
			–	–	1.086	0.3135	0.4907	–	–	–	
			Monoclinic	–	<i>Pm</i>	1.076	0.3135	0.4966	4	7.84	[48]
						1.090	0.3095	0.4967	4	–	[229]
						1.091	0.3095	0.4975	4	7.82	[47]
						1.092	0.3090	0.4970	4	–	[1]
1.094	0.3099	0.4982				4	7.45	[19]			
ϵ -Nb ₃ C _{2+x}	Hexagonal	–	–	1.1460	–	1.830 ^f	–	–	[12, 15]		
ζ -Nb ₄ C _{3-x}	Trigonal	Sn ₄ P ₃	<i>R</i> (–3) <i>m</i>	0.3140	–	3.010 ^z	3	7.90	[12, 13, 69]		
				0.4445	–	–	1	–	[154, 155]		
Nb ₆ C _{5±x}	Monoclinic	Nb ₆ C ₅	<i>C2/m</i>	0.5447 ^{a1}	0.9435 ^{a1}	0.5447 ^{a1}	2	7.77	[4, 20, 150]		
				0.5461 ^{a1}	0.9458 ^{a1}	0.5461 ^{a1}	2	7.72	[14, 16, 49]		
	Trigonal	–	<i>P3</i> ₁	0.5464 ^{a2}	–	1.5422 ^{a2}	3	7.70	[4, 23, 45, 77, 149]		
Nb ₈ C _{7±x} ^{a3}	Cubic	–	<i>P4</i> ₃ <i>32</i>	0.8974 ^{a4}	–	–	4	–	[154]		

^aWhen it is not indicated specially, value reported is for near-stoichiometric compositions^bNumber of formula units per lattice cell^cCalculated from XRD or neutron diffraction patterns^dCarbon content – 41.0–41.5 at.% (in equilibrium with semicarbide phase)^eCarbon content – 43.2 at.%^fCarbon content – 45.0 at.%^gCarbon content – 47.0 at.%

(continued)

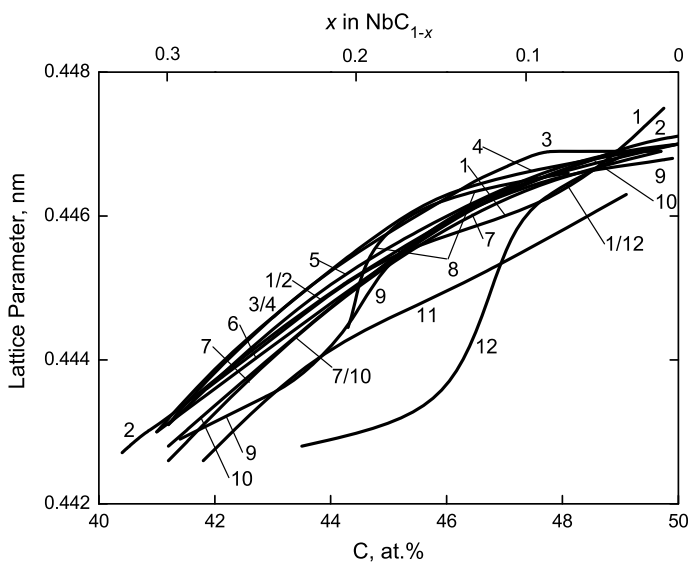
Table 4.1 (continued)^hCarbon content – 47.9 at.%ⁱCarbon content – 49.0 at.%^jCarbon content – 48.0 at.%^kCarbon content – 48.5–49.0 at.%^lCarbon content – 46.9 at.%^mCarbon content – 49.5–49.7 at.%ⁿCarbon content – 49.2 at.%^oCarbon content – 47.7 at.%^pCarbon content – 49.7–49.9 at.% (in equilibrium with graphite)^q $cla = 1.61$ ^r $cla = 1.60$ ^s $cla = 1.59$ ^t $cla = 1.52$ ^uCarbon content – 32.0–32.9 at.%^vCarbon content – 33.3 at.%^w $cla = 1.63$ –1.57^xAlso structured (vacancy ordered) in $P3m1$, $I4_1/amd$, $R(-3)m$, $Fd(-3)m$ and $P4/mmm$ [930]^y $cla = 0.92$ ^z $cla = 9.59$ ^{a1}Carbon content – ~ 45.5 at.%; $\alpha = \gamma = 90^\circ$, $\beta = 109.47^\circ$ ^{a2}Carbon content – 44.1–44.8 at.%^{a3}Also vacancy ordered $Nb_5C_{4\pm x}$ ($P(-1)$, $C2/m$, $I4/m$) and $Nb_7C_{6\pm x}$ ($R(-3)$) are supposed [930]^{a4}Calculated on the basis of density-functional theory (DFT) with generalized gradient approximation of Perdew-Burke-Ernzerhof (GGA-PBE)

Fig. 4.2 Lattice parameter of NbC_{1-x} as a function of phase composition: 1 – synthesized from the elements [191, 772, 833, 968], 2 – [6, 68, 72], 3 – [82, 85], 4 – [77], 5 – [36, 75], 6 – [69], 7 – polynomial approximation of experimental data [10, 11, 218, 848], 8 and 9 – for ordered and disordered structures, respectively [73, 74, 359, 961–963], 10 – synthesized by different methods [266, 960], 11 – [76], 12 – [83] (1, 3, 5–9 – on the basis of several sources, for single crystal NbC_{1-x} materials see Fig. 4.23)

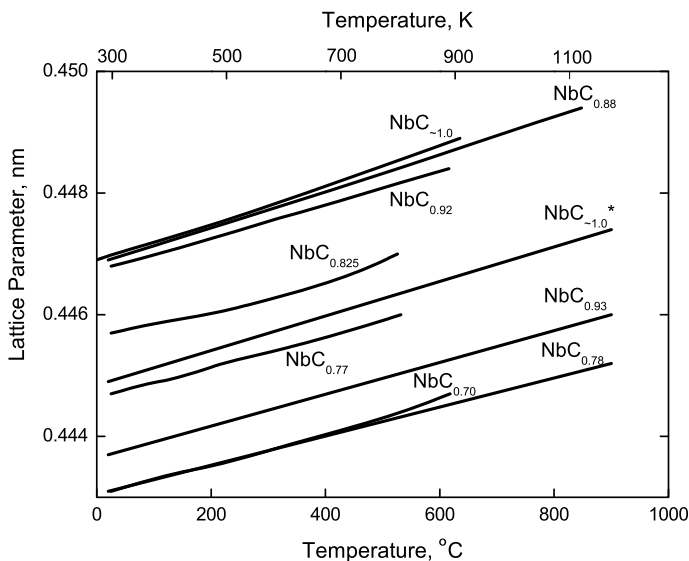


Fig. 4.3 Lattice parameter of NbC_{1-x} as a function of temperature for the phases having different deviations from the stoichiometry ($x \approx 0$ [75]; $x = 0^*$, $x = 0.07$ and $x = 0.22$ [699]; $x = 0.08$, $x = 0.175$, $x = 0.23$ and $x = 0.30$ [36]; $x = 0.12$ [82, 86])

In general, the contaminations, such as dissolved in NbC_{1-x} oxygen or/and nitrogen, which are always present in the material, decrease the magnitude of lattice parameter by forming oxycarbide $\text{NbC}_{1-x}\text{O}_y$, carbonitride $\text{NbC}_{1-x}\text{N}_z$ and oxycarbonitride $\text{NbC}_{1-x}\text{N}_z\text{O}_y$ phases with various deviations from the stoichiometry (see also sections C–N–Nb and C–Nb–O in Table I-2.14) [59, 69, 495, 742, 743].

The strong covalent character of chemical bonding in NbC_{1-x} determines the high value of C–Nb bond energy (enthalpy), which is about 5.89 ± 0.1 eV [870], or 5.85 ± 0.1 eV [871], or 5.43 ± 0.15 eV [130, 872], or 5.39 ± 0.15 eV [873].

Recently, due to the massive progress in nanotechnology, various nanostructures based on niobium carbides, including nanosheets (8–12 nm in sizes) [100], nanocrystalline coatings/films [97–99, 921], nanowires (various types, e.g. 1–3 nm diameter, within the inner space of CNTs) [101, 532], nanorods (2–30 nm diameter, up to 20 μm length) [88, 91, 714], nanotubes (20–60 nm diameter, up to 1–10 μm in length) [92], nanofibres (40–90 nm diameter, up to 1–10 μm in length) [96], whiskers (0.1–3.5 μm diameter, up to 10–100 length/diameter ratios) [89, 90, 884, 936, 969, 970], solid cage shape particles [90] and various (in types) nanoparticles (from 5 to 500 nm) [91, 93–95, 509, 877, 902, 917, 927, 965], have been synthesized, as well as 2D-molecular $\text{Nb}_{n+1}\text{C}_n$ (or $(\text{Nb},\text{M})_2\text{CT}_x$, $\text{Nb}_4\text{C}_3\text{T}_x$, where T are functional groups OH, O, F and others, and M are co-host carbide metals) MXenes [102, 103, 471, 740, 909, 918, 920, 923–925, 928, 957, 1019].

According to Storms et al. [6, 68], the X-ray density of niobium monocarbide NbC_{1-x} phase drops from 7.79 g cm^{-3} for $\text{NbC}_{0.99}$ (value extrapolated to $\text{NbC}_{1.0}$ phase – 7.796 g cm^{-3}) to a minimum of 7.72 g cm^{-3} for $\text{NbC}_{0.79}$ and then rises to

7.73 g cm⁻³ for the composition corresponding to the NbC_{1-x}-Nb_{2±x}C phase boundary, while the X-ray density of Nb_{2±x}C semicarbide phase in equilibrium state with NbC_{1-x} monocarbide is 7.80 g cm⁻³. The recommended values for the bulk (or pycnometric) density of pure poreless materials at room temperature are about 7.80–7.85 and 7.75–7.80 g cm⁻³ – for the near-stoichiometric single-phase compositions of niobium semicarbide Nb_{2±x}C and monocarbide NbC_{1-x}, respectively [130, 307, 308, 719, 818, 1034].

4.2 Thermal Properties

Niobium monocarbide NbC_{1-x} has one of the highest melting points of all the solid substances available; the incongruent melting point of γ -Nb_{2±x}C is about 500° lower. Within the homogeneity range of NbC_{1-x} the melting point of the phase varies (*see* Fig. 4.1); the maximum temperatures pertain to the non-stoichiometric compositions around \sim NbC_{0.79–0.84} [6, 9, 105, 106]. The general thermodynamic properties of near-stoichiometric niobium carbide phases are summarized in Tables 4.2 and 4.3. For the molar heat capacity of near-stoichiometric niobium monocarbide NbC_{1-x} $c_p = f(T, K)$, J mol⁻¹ K⁻¹, the following relationships were recommended in the literature:

in the range of temperatures from 50 to 1600 K [80]

$$c_p = 56.07 \exp(-115.40/T), \quad (4.5)$$

in the range of temperatures from 300 to 670 K [124, 127, 128]

$$c_p = 45.94 + (5.78 \times 10^{-3})T - (9.71 \times 10^5)T^{-2}, \quad (4.6)$$

in the range of temperatures from 300 to 1800 K [125, 127, 128]

$$c_p = 45.15 + (7.22 \times 10^{-3})T - (9.00 \times 10^5)T^{-2}, \quad (4.7)$$

in the range of temperatures from 500 to 2400 K [126–128]

$$c_p = 47.03 + (5.23 \times 10^{-3})T - (10.63 \times 10^5)T^{-2}, \quad (4.8)$$

in the range of temperatures from 600 to 2500 K [80]

$$c_p = 43.06 + (7.76 \times 10^{-3})T. \quad (4.9)$$

in the range of temperatures from 670 to 1800 K [124, 127, 128]

$$c_p = 47.20 + (4.94 \times 10^{-3})T - (10.46 \times 10^5)T^{-2}, \quad (4.10)$$

Table 4.2 General thermodynamic properties of near-stoichiometric niobium monocarbide NbC_{1-x}

Characteristics	Symbol	Unit	Value	Reference
Standard heat of formation (at 298.15 K) ^a	$-\Delta H^\circ_{298}$	kJ mol ⁻¹	125.6	[117]
			129.7 ± 2.5 ^b	[109]
			132.8 ± 3.4 ^c	[108, 140]
			133.1 ± 3.8 ^d	[141]
			134.3	[113]
			134.7	[82, 107]
			138.2	[142]
			139.7 ^e	[1, 721]
			140.6 ± 10.0 ^{f,g}	[4-7, 62-64, 108, 111, 118, 753, 1021-1023]
			142.1 ± 2.7 ^g	[109]
Standard molar entropy ^h (at 298.15 K and 100 kPa)	S°_{298}	J mol ⁻¹ K ⁻¹	145.6	[112]
			34.69 ^e	[1, 6]
			34.89	[141]
			34.97 ^e	[127-129]
			35.06	[122]
			35.28	[140]
			35.40 ± 0.20	[114, 124]
			36.40	[5, 132]
			37.07 ⁱ	[125]
			37.25 ± 2.9	[62, 63, 67, 82, 118]
Molar enthalpy difference	$H_{298} - H_0$	kJ mol ⁻¹	37.66	[125, 170]
			5.422 ^c	[127, 128]
Standard molar heat capacity ^j (at 298.15 K and 100 kPa)	$c^\circ_{p,298}$	J mol ⁻¹ K ⁻¹	33.24 ^k	[74, 143]
			33.35 ^l	[6, 122]
			33.70 ^m	[74, 143]
			33.78 ⁿ	[74, 143]
			34.38 ^o	[74, 143]
			34.70 ^p	[74, 143]
			34.73 ^q	[74, 143]
			36.23 ^e	[127-129]
			36.62	[126]
			36.78 ^e	[1, 2, 6, 122]
			36.82 ^r	[7, 67, 80, 84, 114, 124]
			37.18	[5, 125, 132]
			37.35	[62, 63, 82]
Specific heat capacity (at 298.15 K)	c	J kg ⁻¹ K ⁻¹	354.4	[5, 132]
			355.9	[62, 116]

(continued)

Table 4.2 (continued)

Characteristics	Symbol	Unit	Value	Reference
Molar enthalpy (heat) of melting (at the melting point)	ΔH_m	kJ mol^{-1}	92	[5, 132]
Specific enthalpy (heat) of melting (at the melting point)		kJ kg^{-1}	868	[5, 132]
Molar enthalpy (heat) of vaporization (dissociation) ^a	$\Delta \hat{H}_v$	kJ mol^{-1}	630–790 ^f	[67, 160]
Melting point	T_m	K (°C)	3660 ± 20 (3390 ± 20) 3750 (3480) 3755 ± 50 (3485 ± 50) 3760 (3490) 3770 ± 100 (3500 ± 100) ^u 3775 ± 75 (3505 ± 75) ^u 3800 ± 35 (3530 ± 35) 3870 ± 50 (3600 ± 50) ^{o,v} 3880 (3610) ^w 3885 ± 25 (3615 ± 25) ^{x,y}	[1] [62, 63, 110] [146] [119] [64, 104, 117, 159, 295, 338, 720, 752] [58] [120] [2, 5–7, 71, 84, 121, 123, 721, 808, 905] [3, 130] [67, 137, 144, 145, 552, 751]
Boiling point	T_b	K (°C)	4570 (4300) 4770 (4500) 5275 (5000)	[64, 117, 130] [62, 63, 67, 118, 138] [751]

^aEnthalpy (heat) of complete dissociation (atomization) from solid state at 298.15 K ($-\Delta_{at}H^\circ_{298}$, kJ mol^{-1}): 1537 ± 9 [1], 1649 [748], 1598 [749], 1674 [750], 1580 ± 10 [1023]

^bCarbon content – 47.7 at. %

^cCarbon content – 48.6 at. %

^dCarbon content – 49.7 at. %

^eCarbon content – 49.5 at. %

^fOn the basis of several sources

^gData extrapolated to the stoichiometric composition of monocarbide

^hMolar entropy S°_T (at 1200 K), $\text{J mol}^{-1} \text{K}^{-1}$, for NbC_{1-x} phases with different deviations from the stoichiometry: 101.61 ($x = 0$), 99.96 ($x = 0.05$), 96.17 ($x = 0.20$), 95.29 ($x = 0.25$) and 94.61 ($x = 0.30$) [128]

ⁱCarbon content – 42.8 at. %

^jMolar heat capacity $c_{p,T}$ (at 1200 K), $\text{J mol}^{-1} \text{K}^{-1}$, for NbC_{1-x} phases with different deviations from the stoichiometry: 55.44 ($x = 0$), 53.89 ($x = 0.05$), 50.34 ($x = 0.20$), 49.52 ($x = 0.25$) and 48.88 ($x = 0.30$) [128]

^kDisordered structure with carbon content – 44.8 at. %

^lCarbon content – 41.2 at. %

^mOrdered structure with carbon content – 44.8 at. %

ⁿDisordered structure with carbon content – 45.4 at. %

^oOrdered structure with carbon content – 45.4 at. %

^pDisordered structure with carbon content – 46.8 at. %

(continued)

Table 4.2 (continued)^qOrdered structure with carbon content – 46.8 at.%^rCarbon content – 49.9 at.%^sEnthalpy (heat) of sublimation of metallic Nb at 298.15 K, $\Delta_{s,me}H^\circ_{298} = 723.1 \text{ kJ mol}^{-1}$ [1024]^tFor the process of NbC_{1-x} (crystal) = NbC_{1-x-y} (crystal) + $y\text{C}$ (gas) at 2800 K (2530 °C)^uCarbon content – ~ 46 at.%^vCarbon content – ~ 50 at.%^wFor $\text{NbC}_{0.78 \pm 0.03}$ composition^xCarbon content – 44.0 ± 1.0 at. % [67, 137, 145]^yCarbon content – 45.0 ± 1.0 at. % [144]**Table 4.3** General thermodynamic properties of near-stoichiometric niobium semicarbide $\text{Nb}_{2 \pm x}\text{C}$

Characteristics	Symbol	Unit	Value	Reference
Standard heat of formation (at 298.15 K) ^a		$-\Delta H^\circ_{298} \text{ kJ mol}^{-1}$	156.5 ^b	[10, 82, 115]
			180.3 ^c	[111]
			188.3	[1]
			190.0	[67, 114]
			190.2	[118]
			195.0 ± 5.0	[6, 7, 84, 108, 111, 112, 140, 753]
Standard molar entropy (at 298.15 K and 100 kPa)		$S^\circ_{298} \text{ J mol}^{-1} \text{ K}^{-1}$	59.80	[63, 82]
			63.50	[132]
			63.80 ± 0.24	[140]
			64.01 ± 0.42	[67, 114, 142]
			64.10	[1, 6, 7, 122]
			73.14	[125]
Standard molar heat capacity (at 298.15 K and 100 kPa)		$c^\circ_{p,298} \text{ J mol}^{-1} \text{ K}^{-1}$	60.52	[125]
			60.67	[67]
			60.72	[62, 63]
			63.51	[1, 6, 7, 114, 122, 125]
			63.56	[2]
			63.56	[2]
Specific heat capacity (at 298.15 K)	c	$\text{J kg}^{-1} \text{ K}^{-1}$	316.0	[62, 116]
Melting point	T_m	K (°C)	2800 ± 20	[144, 147,
			$(2530 \pm 20)^d$	148]
			3200 (2930)	[116]
			3305 ± 20	[7, 67, 137,
			$(3035 \pm 20)^e$	145]
			3350 ± 35	[2, 6, 58, 71,
			$(3080 \pm 35)^f$	84, 130,
			3360 ± 50	146, 751]
$(3090 \pm 50)^f$	[1, 58, 114, 338]			

^aEnthalpy of complete dissociation (atomization) from solid state at 298.15 K ($-\Delta_{at}H^\circ_{298}$): $2348 \pm 14 \text{ kJ mol}^{-1}$ [1]^bCarbon content – 30.1 at. %^cCarbon content – 32.8 at. %^dCarbon content – 29.0 ± 2.0 at. %^eCarbon content – 34.5 at. %^fCarbon content – 33.3 at. %

in the range of temperatures from 1000 to 3000 K [127, 128, 133]

$$c_p = 46.43 + (5.87 \times 10^{-3})T - (9.01 \times 10^5)T^{-2}, \quad (4.11)$$

in the range of temperatures from 1600 to 2400 K [127, 128, 134, 135]

$$c_p = 47.18 + (4.99 \times 10^{-3})T. \quad (4.12)$$

For the specific heat capacity of near-stoichiometric niobium monocarbide NbC_{1-x} $c = f(T, \text{K}), \text{J kg}^{-1} \text{K}^{-1}$, the relationship

$$c = 348.9 + (89.54 \times 10^{-3})T + (326.4 \times 10^6)T^{-2} \quad (4.13)$$

is recommended for the range of temperatures from 700 to 3200 K [127, 128, 136]. The variations of molar heat capacity with temperature for near-stoichiometric niobium carbides $\text{Nb}_{2\pm x}\text{C}$ and NbC_{1-x} are demonstrated in Fig. 4.4 on the basis of

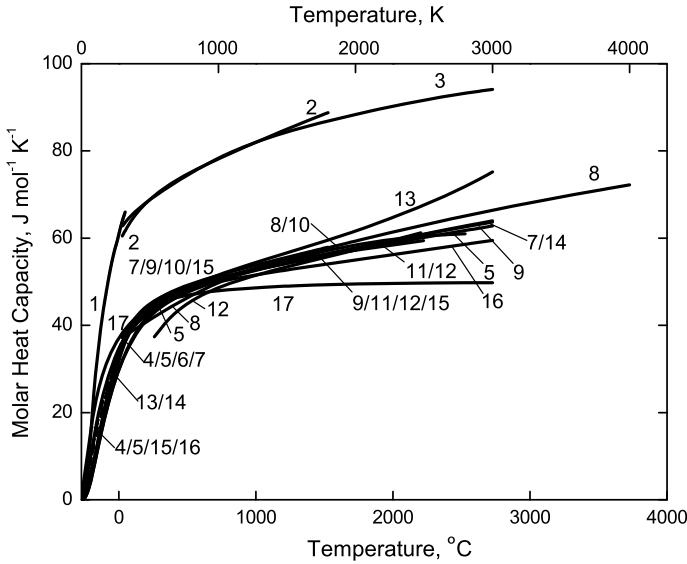


Fig. 4.4 Variation of molar heat capacity (1–14 – at constant pressure, c_p , and 15–17 – at constant volume, c_v) with temperature for near-stoichiometric niobium carbides $\text{Nb}_{2\pm x}\text{C}$ (1 – [122], 2 – summarized [62], 3 – [125]) and NbC_{1-x} (4 – [122], 5 – [80], 6 – [143], 7 – [151–153], 8 – [5, 132], 9 – [6], 10 – [114], 11 – [139], 12 – $\text{NbC}_{0.93}$ [181, 338]); theoretically calculated: 13 – Slater’s approximation and 14 – Dugdale-MacDonald’s approximation on the basis of Debye-Grüneisen model [152], 15 – *ab initio* calculated, based on the mean values between the corresponding generalized gradient approximation (GGA) and local density approximation (LDA) estimations [409], 16 – using the GGA with the Perdew-Wang parameterization (PW91) [356], 17 – using projector augmented-wave (PAW) method within the GGA of the Perdew-Burke-Ernzerhof scheme for ionic solids (PBEsol) [796]; 5, 7–10 – on the basis of several sources)

several sources. For the molar heat capacity of monocarbide NbC_{1-x} phases with various deviations from the stoichiometry the following relationships were recommended in literature:

for $\text{NbC}_{0.75}$ (in the ranges of temperatures from 300 to 1800 K) [125, 127, 128]

$$c_p = 37.45 + (9.43 \times 10^{-3})T - (5.27 \times 10^5)T^{-2}, \quad (4.14)$$

for $\text{NbC}_{0.75}$ (in the ranges of temperatures from 1440 to 2500 K) [128, 139, 156]

$$c_p = 42.22 + (4.76 \times 10^{-3})T + (82.76 \times 10^{10})T^{-2} \exp(-22910/T); \quad (4.15)$$

for $\text{NbC}_{0.86}$ (in the ranges of temperatures from 1270 to 2600 K) [128, 139, 156]

$$c_p = 47.28 + (3.48 \times 10^{-3})T + (31.92 \times 10^9)T^{-2} \exp(-16300/T), \quad (4.16)$$

for $\text{NbC}_{0.87}$ (in the ranges of temperatures from 300 to 1800 K) [125, 127, 128]

$$c_p = 40.58 + (8.33 \times 10^{-3})T - (6.32 \times 10^5)T^{-2}, \quad (4.17)$$

for $\text{NbC}_{0.91}$ (in the ranges of temperatures from 1230 to 2515 K) [128, 139, 156]

$$c_p = 48.14 + (3.85 \times 10^{-3})T + (6.40 \times 10^9)T^{-2} \exp(-14260/T), \quad (4.18)$$

for $\text{NbC}_{0.97}$ (in the ranges of temperatures from 1300 to 2800 K) [127, 128, 131]

$$c_p = 46.50 + (5.38 \times 10^{-3})T, \quad (4.19)$$

for $\text{NbC}_{0.99}$ (in the ranges of temperatures from 1300 to 2500 K) [128, 139, 156]

$$c_p = 48.46 + (4.37 \times 10^{-3})T \quad (4.20)$$

and for NbC_{1-x} (in the ranges of temperatures from 1200 to 2200 K) in general [128, 157]

$$c_p = (1 - 0.83x + 1.07x^2) [48.50 + (4.436 \times 10^{-3})T], \quad (4.21)$$

or

$$c_p = 51.72 + (3.10 \times 10^{-3})T - 32.74x + 36.29x^2, \quad (4.22)$$

where T is temperature, K, and x is the value of index in NbC_{1-x} formula. For the molar heat capacity of niobium semicarbide $\text{Nb}_{2\pm x}\text{C}$ phase ($x = 0$) Geld and Kusenko [125] proposed the relationship as follows

$$c_p = 33.22 + (6.28 \times 10^{-3})T - (4.29 \times 10^5)T^{-2}, \quad (4.23)$$

It should be emphasized specially that all the thermal properties of niobium carbides are very sensitive to the deviation from the stoichiometry in the phases: for the standard heat of formation ΔH_{298}° , kJ mol⁻¹, molar enthalpy difference $H_T^{\circ} - H_{298}^{\circ}$, J mol⁻¹, and molar entropy S_T° , J mol⁻¹ K⁻¹, the following concentration and temperature-concentration dependencies within the homogeneity range of NbC_{1-x} were obtained by the calculations based on experimental data [4, 5, 10, 11, 107, 111, 113, 128, 157, 158, 755, 1021–1023]

$$\Delta H_{298}^{\circ} = 58.58x - 134.69, \quad (4.24)$$

$$\Delta H_{298}^{\circ} = 56.07x - 134.31, \quad (4.25)$$

$$\Delta H_{298}^{\circ} = 27.62 - 297.0(1-x) + 128.7(1-x)^2 \pm 10.0, \quad (4.26)$$

$$H_T^{\circ} - H_{298}^{\circ} = (1 - 0.83x + 1.07x^2) [48.50T + (2.218 \times 10^{-3})T^2 - 19600], \quad (4.27)$$

$$H_T^{\circ} - H_{298}^{\circ} = 51.72T + (1.550 \times 10^{-3})T^2 + 2845x - 32.74xT + 36.29x^2T - 23090, \quad (4.28)$$

$$S_T^{\circ} = 119.11\lg T + (3.100 \times 10^{-3})T - 80.01x\lg T + 83.58x^2\lg T + 211.37x - 218.46x^2 - 268.87, \quad (4.29)$$

where T is temperature, K, and x is the value of index in NbC_{1-x} formula (Eqs. (4.27)–(4.29) were recommended for the range of temperatures from 1200 to 2200 K). The thermodynamic functions of quasi-stoichiometric niobium monocarbide NbC_{0.98} are tabulated by Turchanin et al. [128, 129] and Chase [754] in the range of 0–3000 K, thermodynamic functions of stoichiometric NbC_{~1.0} – by Schick [132] in the range of 0–6000 K, thermodynamic functions of NbC_{0.702}, NbC_{0.825} and NbC_{~1.0} – by Barin [114] in the range of 298.15–1800 K, and thermodynamic functions of NbC_{0.75}, NbC_{0.87} and NbC_{0.98} – by Storms [6] and Toth [7] in the range of 298.15–3000 K. For stoichiometric niobium semicarbide the thermodynamic functions are tabulated by Barin [114] in the range of 298.15–1800 K, by Schick [132] in the range of 0–3363 K, and by Storms [6], Toth [7] and Turchanin A and Turchanin M [128] in the range of 298.15–3000 K (for the composition of niobium semicarbide Nb_{2±x}C with $x = 0$).

During the vaporization processes from the surface of niobium carbides in a vacuum at high and ultra-high temperatures, the composition of the carbide phase (C/Nb ratio) can change significantly. The resulting composition gradient cannot be accurately evaluated, but it was found to become worse as the temperature was increased [6]. The following equations were recommended for niobium (P_{Nb} , Pa) and carbon (P_{C} , Pa) partial pressures over near-stoichiometric monocarbide phase [5, 6, 10, 11, 160] for the range of about 2500–3000 K (2200–2700 °C):

$$\lg P_{\text{Nb}} = -(4.542 \times 10^4)/T + 13.159, \quad (4.30)$$

$$\lg P_{\text{C}} = -(3.276 \times 10^4)/T + 10.302, \quad (4.31)$$

the estimation of niobium partial pressures (P_{Nb} , Pa) in the gaseous phase in the Nb–C system carried out by Kulikov [751] led to such relationships as

for the conditions of $\text{Nb}_{2\pm x}\text{C}$ – NbC_{1-x} phases equilibrium:

at 1000–2740 K (730–2470 °C)

$$\lg P_{\text{Nb}} = -(4.056 \times 10^4)/T + 13.273 \quad (4.32)$$

at 2740–3750 K (2470–3480 °C)

$$\lg P_{\text{Nb}} = -(3.950 \times 10^4)/T + 12.888, \quad (4.33)$$

for the conditions of congruent vaporization of quasi-stoichiometric NbC_{1-x} :

at 1000–2740 K (730–2470 °C)

$$\lg P_{\text{Nb}} = -(4.115 \times 10^4)/T + 13.028, \quad (4.34)$$

at 2740–3750 K (2470–3480 °C)

$$\lg P_{\text{Nb}} = -(4.062 \times 10^4)/T + 12.840, \quad (4.35)$$

at 3750–5000 K (3480–4730 °C)

$$\lg P_{\text{Nb}} = -(3.538 \times 10^4)/T + 11.444, \quad (4.36)$$

for the conditions of NbC_{1-x} –C phases equilibrium:

at 1000–2740 K (730–2470 °C)

$$\lg P_{\text{Nb}} = -(4.479 \times 10^4)/T + 12.836, \quad (4.37)$$

at 2740–3750 K (2470–3480 °C)

$$\lg P_{\text{Nb}} = -(4.331 \times 10^4)/T + 12.298, \quad (4.38)$$

at 3750–5000 K (3480–4730 °C)

$$\lg P_{\text{Nb}} = -(3.726 \times 10^4)/T + 10.685, \quad (4.39)$$

Table 4.4 Parameters of the gaseous phase in the Nb–C system in the conditions of $\text{Nb}_{2\pm x}\text{C}$ – NbC_{1-x} phases equilibrium, congruent vaporization of quasi-stoichiometric NbC_{1-x} and NbC_{1-x}C phases equilibrium calculated on the basis of thermodynamic data [751]

Parameters	Temperature, K (°C)									
	1000 (730)	1500 (1230)	2000 (1730)	2500 (2230)	2740 (2470)	3000 (2730)	3750 (3480)	4000 (3730)	5000 (4730)	
	$\text{Nb}_{2\pm x}\text{C}$ – NbC_{1-x} phases equilibrium									
$\lg P_{\text{Nb}}, \text{Pa}$	-27.282	-13.720	-6.962	-2.933	-1.523	-0.271	2.363	-	-	-
$\lg P_{\Sigma}^{\text{g}}, \text{Pa}$	-27.273	-13.698	-6.929	-2.889	-1.474	-0.210	2.430	-	-	-
C/Nb^{b}	0.021	0.052	0.080	0.106	0.119	0.152	0.172	-	-	-
Contents, vol.%;										
C	2.08	4.91	7.39	9.58	10.53	13.00	13.86	-	-	-
C_2	-	-	-	0.02	0.05	0.10	0.46	-	-	-
Nb	97.92	95.09	92.61	90.40	89.42	86.90	85.68	-	-	-
	Congruent dissociation of quasi-stoichiometric NbC_{1-x}									
$\lg P_{\text{Nb}}, \text{Pa}$	-28.118	-14.363	-7.510	-3.416	-1.979	-0.698	2.017	2.636	4.368	
$\lg P_{\Sigma}^{\text{g}}, \text{Pa}$	-27.818	-14.062	-7.210	-3.117	-1.683	-0.406	2.291	2.908	4.638	
Contents, vol.%;										
C	50.00	50.00	49.92	49.40	48.61	47.48	42.32	41.20	40.19	
C_2	-	-	0.04	0.32	0.65	1.13	3.14	3.76	4.75	
C_3	-	-	0.01	0.08	0.19	0.40	1.39	1.60	1.33	
Nb	50.00	50.00	50.03	50.20	50.55	50.99	53.15	53.44	53.72	
	NbC_{1-x}C phases equilibrium									
$\lg P_{\text{Nb}}, \text{Pa}$	-31.952	-16.951	-9.502	-5.056	-3.504	-2.128	0.757	1.378	3.233	
$\lg P_{\Sigma}^{\text{g}}, \text{Pa}$	-24.287	-11.719	-5.224	-1.156	0.288	1.595	4.358	5.034	6.393	
$\lg(C/\text{Nb})^{\text{c}}$	7.665	4.950	4.568	4.292	4.210	4.154	4.070	4.140	3.627	
Contents, vol.%;										
Nb	-	-	0.005	0.010	0.016	0.019	0.025	0.023	0.069	

^aTotal gas pressure

^bAtomic ratio in gaseous phase

^cLogarithm of atomic ratio in gaseous phase

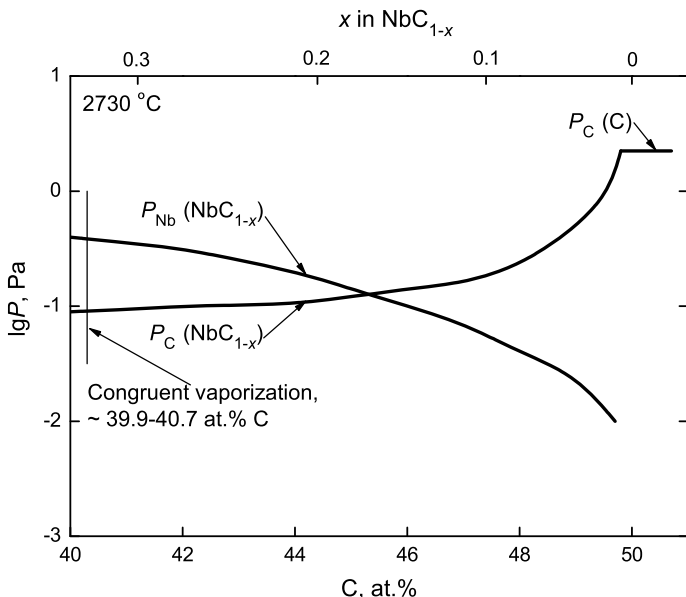


Fig. 4.5 Partial pressures of niobium $P_{\text{Nb}}(\text{NbC}_{1-x})$ and carbon $P_{\text{C}}(\text{NbC}_{1-x})$ over niobium monocarbide NbC_{1-x} phase, and vapour pressure of carbon over pure graphite $P_{\text{C}}(\text{C})$ as functions of monocarbide composition at 3000 K (2730 °C) calculated by Kaufman [5, 7, 10, 11, 161]; an approximate congruently vaporizing composition is marked

where T is temperature, K (see Table 4.4). The partial pressures of niobium and carbon over the monocarbide phase NbC_{1-x} as functions of composition at the fixed temperature 3000 K (2730 °C) are shown in Fig. 4.5 in comparison with the equilibrium pressure of carbon over graphite surface. The presence in the vapour over NbC_{1-x} phase of stable gaseous carbide molecules NbC and NbC_2 as well as carbon clusters $\text{C}_2, \text{C}_3, \dots, \text{C}_7$ becomes noticeable only at temperatures higher than 2700 K (2400 °C) [871, 967]. The vapour phase above carbon-saturated niobium monocarbide NbC_{1-x} in equilibrium with graphite contains atoms of niobium and molecules of carbon plus molecules of NbC_2 , the relative concentration of which is determined at 2500 K (2230 °C) by the ratio $\text{Nb}/\text{NbC}_2 \approx 40$ [147]. The equilibrium pressure should be lower than the pressure observed upon vaporization from an open surface into a vacuum (Langmuir mode). According to Nikolskaya et al. [113, 162, 164, 167] the vapour pressures of niobium (P_{Nb} , Pa) and carbon (P_{C} , Pa) in Langmuir vaporization of niobium monocarbide can be described by the equations

$$\lg P_{\text{Nb}} = 15.16 - (4.148 \times 10^4)/T - (2.3 \times 10^{-4})T + \lg x, \quad (4.40)$$

$$\lg P_{\text{C}} = 11.31 - (4.041 \times 10^4)/T + (1.1 \times 10^{-4})T + \lg[(1-x)/x], \quad (4.41)$$

where x is the value of index in NbC_{1-x} formula and T is temperature, K. The vaporization of NbC_{1-x} in vacuum occurs in a more complex manner than the other transition metal refractory carbides. Fesenko and Bolgar [163, 843] proposed for the evaporation rate of $\text{NbC}_{0.77}$ G , $\text{g cm}^{-2} \text{ s}^{-1}$, as a function of temperature T , K, at 2770–3170 K (2500–2900 °C) the following equation:

$$\lg G = 9.0 - (4.33 \times 10^4)/T, \quad (4.42)$$

the linear evaporation rates of $\text{NbC}_{0.77}$ are $3.8 \times 10^{-10} \text{ sm s}^{-1}$ at 2230 °C and $6.5 \times 10^{-7} \text{ sm s}^{-1}$ at 2830 °C [727]; in vacuum ($\sim 10^{-3}$ Pa) Gusev [966] obtained for the mass evaporation rates of $\text{NbC}_{0.92}$ (content O – 0.27%) at 2150, 2300 and 2400 °C the values of 4.3×10^{-8} , 7.8×10^{-8} and $1.1 \times 10^{-7} \text{ g cm}^{-2} \text{ s}^{-1}$, respectively, and for $\text{NbC}_{0.98}$ (contents: non-combined C – 0.11%, O – 0.09%) at 1800, 2000 and 2300 °C the values of 6.0×10^{-9} , 1.7×10^{-8} and $7.4 \times 10^{-8} \text{ g cm}^{-2} \text{ s}^{-1}$, respectively, and established for the general evaporation rate G , $\text{g cm}^{-2} \text{ s}^{-1}$, at 1900–2700 K (1600–2400 °C) the relationship

$$\lg G = -(2.58 \pm 0.01) - (1.17 \times 10^4)/T. \quad (4.43)$$

In the process of evaporation the lattice parameter on the surface of niobium monocarbide NbC_{1-x} phases gradually decrease, reaching certain constant value for a given temperature [966]. The congruently vaporizing composition of niobium monocarbide shifts significantly in the direction of enrichment of the carbide phase with metal as the temperature increases [10, 11, 113, 162–169, 843]: NbC_{1-x} vaporizes congruently from the composition $\text{NbC}_{0.83}$ at 2450 K (2180 °C) [162] to compositions $\text{NbC}_{0.77}$ at 2770 K (2500 °C) [163], $\text{NbC}_{0.748}$ at 2910 K (2640 °C) [6, 160] and $\text{NbC}_{0.70}$ at 3430 K (3160 °C) [162] – it depends on temperature in the range of 2300–3400 K (2030–3130 °C) according to the following relationship [10, 11, 113, 162]

$$\lg x = 0.1388 - (2.222 \times 10^3)/T, \quad (4.44)$$

where x is the value of index in NbC_{1-x} formula and T is temperature, K. The integral rate of congruent vaporization V , $\text{g cm}^{-2} \text{ s}^{-1}$ of niobium monocarbide NbC_{1-x} at 2480–3430 K (2210–3160 °C) depends on temperature as follows [162, 167]

$$\lg V = 9.406 - (4.127 \times 10^4)/T, \quad (4.45)$$

where T is temperature, K. Niobium semicarbide $\gamma\text{-Nb}_{2\pm x}\text{C}$, when it vaporizes from an open surface into a vacuum preferentially loses the metal; the equilibrium vapour pressure of niobium over the lower carbide is considerably higher than over niobium monocarbide [10, 11].

The values of general thermodynamic properties, vapour pressures and mass/linear vaporization rates for niobium carbides are given in Addendum in comparison with other ultra-high temperature materials in the wide ranges of temperatures.

At room temperature thermal conductivity of near-stoichiometric niobium monocarbide NbC_{1-x} , affected noticeably by porosity, is about $15\text{--}40 \text{ W m}^{-1} \text{ K}^{-1}$ (with thermal diffusivity of around $0.13 \text{ cm}^2 \text{ s}^{-1}$) [1, 2, 7, 10, 11, 62–65, 80, 104, 116, 117, 159, 170–179, 250, 338, 339, 719, 722, 723, 735, 736, 905], for near-stoichiometric niobium semicarbide $\alpha\text{-Nb}_2\text{C}$ the corresponding value is about $12 \text{ W m}^{-1} \text{ K}^{-1}$ [1]. Marmer et al. [170] revealed for NbC_{1-x} materials in the range of $1000\text{--}2400 \text{ }^\circ\text{C}$ the increase of thermal conductivity from $8\text{--}13$ to $11\text{--}17 \text{ W m}^{-1} \text{ K}^{-1}$ with 7% increase of porosity, it should be mentioned especially that the same researchers also found out the similar effect of porosity on TiC_{1-x} and ZrC_{1-x} materials. Within the homogeneity range, as a consequence of conduction electrons scattering on the carbon sublattice vacancies and thermal lattice vibrations, the thermal conductivity of NbC_{1-x} declines with increasing carbon deficit in the phase [10, 11, 171, 172] that is shown in Fig. 4.6. The variations of thermal conductivity with temperature for near- and non-stoichiometric NbC_{1-x} phases on the basis of several sources are given in Figs. 4.7 and 4.8.

At room temperature the mean coefficients of linear thermal expansion of near-stoichiometric semicarbide $\alpha\text{-Nb}_2\text{C}$ and monocarbide NbC_{1-x} phases are $(6.7\text{--}8.1) \times 10^{-6} \text{ K}^{-1}$ and $(5.7\text{--}6.9) \times 10^{-6} \text{ K}^{-1}$, respectively [10, 11, 82, 84, 177,

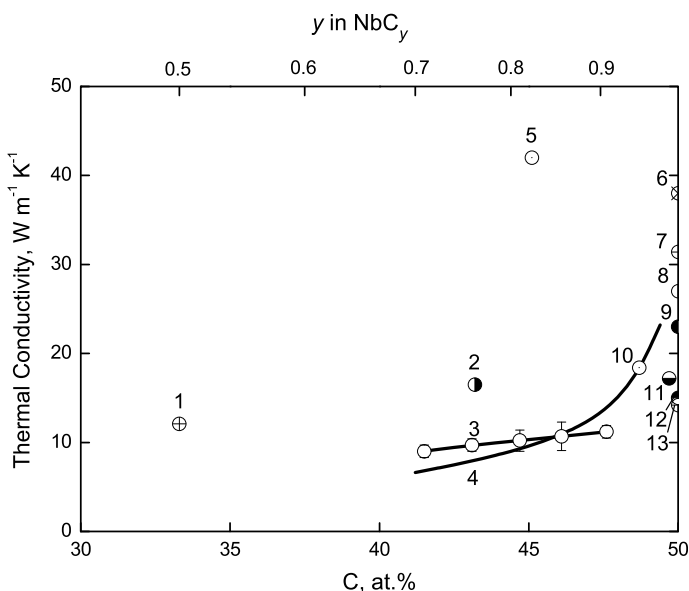


Fig. 4.6 Thermal conductivity at room temperature of niobium semicarbide $\alpha\text{-Nb}_2\text{C}$ (1 – calculated on the basis of Goryachev’s method [1]) and monocarbide NbC_{1-x} (within the homogeneity range: 2 – single crystal [174, 175]; 3 – sintered in vacuum, 5–15% porosity [10, 11, 171]; 4 – hot-pressed at $2730 \text{ }^\circ\text{C}$ and subsequently annealed at $1850\text{--}1950 \text{ }^\circ\text{C}$ in vacuum, corrected to the poreless state [172]; 5 – single crystal [2, 179]; 6 – [170]; 7 – [80]; 8 – [178]; 9 – [65]; 10 – hot-pressed (measured at $0 \text{ }^\circ\text{C}$) [176]; 11 – [173]; 12 – calculated on the basis of Goryachev’s method [1]; 13 – [62–64, 104, 116, 117, 159, 177]) as a function of carbides composition

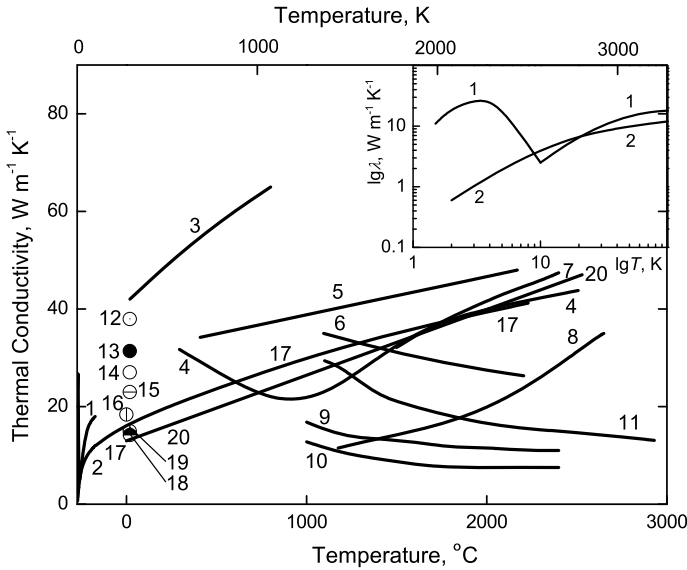


Fig. 4.7 Variation of thermal conductivity λ with temperature for near-stoichiometric (when it is not indicated specially) niobium monocarbide NbC_{1-x} on the basis of several sources: 1 – single crystal, 49.0 at.% C (superconductor with transition at 9.8 K) [182, 183, 194]; 2 – single crystal, 43.2 at.% C [182, 183]; 3 – single crystal, 45.1 at.% C [179]; 4 – heat-soaked at 2480 °C [104, 181]; 5 – sintered in vacuum, ~50 at.% C, corrected to the poreless state [226, 227]; 6 – as-hot-pressed [104, 181]; 7 – vapour deposited, 43.5 at.% C [10, 11, 250]; 8 – hot-pressed [10, 11]; 9 – 27% porosity [170]; 10 – 20% porosity [170]; 11 – hot-pressed, 13–18% porosity, 49.2 at.% C [5, 180, 846]; 12 – [170]; 13 – [80]; 14 – [178, 735, 736]; 15 – [65]; 16 – hot-pressed, 48.7 at.% C [176]; 17 – hot-pressed, 3% porosity, 49.7 at.% C [173]; 18 – [7, 62–64, 104, 116, 117, 159, 177, 719, 722, 723]; 19 – calculated on the basis of Goryachev’s method [1]; 20 – summarized on the basis of various sources [173, 250, 338, 339] (*Inset* – at ultra-low and low temperatures in $\lg \lambda - \lg T$, K scale [182, 183, 194, 711, 852])

178, 195, 1031]; along the main crystallographic directions a and c of Nb_2C , according to Samsonov et al. [10, 67]: $\alpha_{a,m} = 7.0 \times 10^{-6} \text{ K}^{-1}$ and $\alpha_{c,m} = 8.7 \times 10^{-6} \text{ K}^{-1}$. The experimental data collected from the various measurements of thermal expansion of niobium monocarbide NbC_{1-x} are listed in Table 4.5. The approximation function for the temperature dependence of relative thermal linear expansion $\Delta l/l_0 = f(T, K)$, %, of near-stoichiometric NbC_{1-x} was recommended by Touloukian et al. [1031] on the basis of experimental data for pure samples from several sources (accuracy within $\pm 5\%$) for 293–3000 K (20–2730 °C):

$$\Delta l/l_0 = -0.158 + (5.138 \times 10^{-4})T + (1.023 \times 10^{-7})T^2 + (5.718 \times 10^{-13})T^3, \quad (4.46)$$

where T is temperature, K. On the basis of high-temperature X-ray measurements Houska [184] proposed for the average coefficient of linear thermal expansion α_m , K^{-1} , of sintered (in vacuum) $\text{NbC}_{0.98}$ (contents: non-combined C – 0.08%,

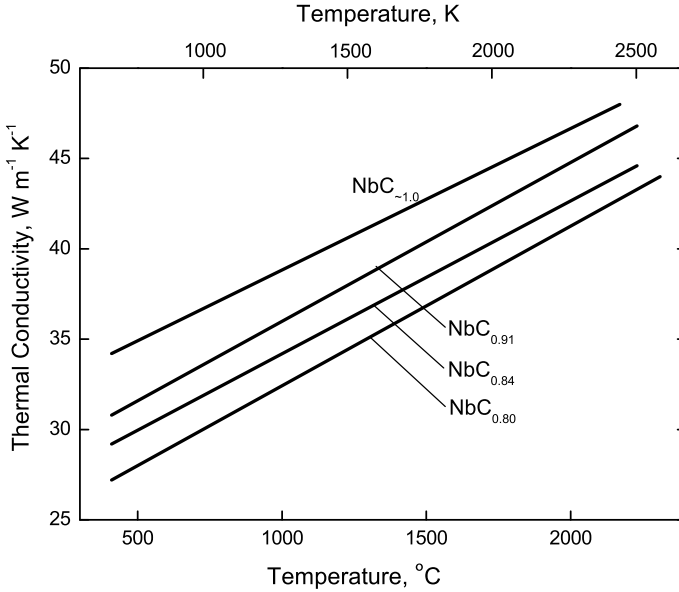


Fig. 4.8 Variations of thermal conductivity with temperature for niobium monocarbide NbC_{1-x} phases having different deviations from the stoichiometry ($x = 0, 0.09, 0.16, 0.20$, corrected to the poreless state [226, 227])

N – 0.03%, O – 0.02%) in the temperature range of 25–2030 °C the following equation:

$$\alpha_m = 6.35 \times 10^{-6} + (0.52 \times 10^{-9})(t - 25), \quad (4.47)$$

for non-stoichiometric phases with x from 0.076 to 0.298 studied by Kempter and Storms [36] in the temperature range of 25–600 °C, the equations modified to the same form could be presented by the following way:

for $\text{NbC}_{0.924}$

$$\alpha_m = 5.22 \times 10^{-6} + (1.76 \times 10^{-9})(t - 25), \quad (4.48)$$

for $\text{NbC}_{0.825}$

$$\alpha_m = 3.30 \times 10^{-6} + (4.77 \times 10^{-9})(t - 25), \quad (4.49)$$

for $\text{NbC}_{0.766}$

$$\alpha_m = 5.11 \times 10^{-6} + (1.58 \times 10^{-9})(t - 25), \quad (4.50)$$

Table 4.5 Average coefficients of linear thermal expansion α_m of near-stoichiometric niobium monocarbide NbC_{1-x} in various temperature ranges

Temperature range, °C	$\alpha_m, 10^{-6} \text{ K}^{-1}$	Reference
20–200	5.93 ^a	[1031]
20–300	6.04 ^a	[1031]
20–400	6.14 ^a	[1031]
20–500	6.25 ^a	[1031]
	6.52	[177, 1032]
	6.65 ^b	[180, 187]
	6.65 ± 0.28 ^c	[86]
20–600	6.23 ^d	[36]
	6.35 ^a	[1031]
	6.70 ^b	[180, 187]
	7.90	[188, 189]
20–700	6.45 ^a	[1031]
	6.76 ^b	[180, 187]
	6.76 ± 0.23 ^c	[86]
20–730	6.52	[880, 881]
20–800	6.56 ^a	[1031]
	8.00	[188, 189]
20–850	6.84 ^b	[180, 187]
	6.84 ± 0.21 ^c	[86]
20–900	5.65 ^e	[699]
	6.66 ^a	[1031]
	6.75 ^d	[59]
20–1000	6.55 ^f	[192]
	6.60	[7, 178]
	6.76 ^a	[1031]
	6.88 ^b	[180, 187]
	7.02	[177]
	7.07	[177, 1032]
	7.10 ^g	[209]
	7.11 ^h	[186]
	8.10	[188, 189]
	8.55	[80]
	9.31	[2]
200–1000	7.77 ⁱ	[190]
20–1100	6.50	[63, 121]
	6.86 ^a	[1031]
20–1200	6.50	[170, 694]
	6.90 ^b	[180, 187]
	6.97 ^a	[1031]
	7.17	[177]
	8.15	[188, 189]
20–1400	6.65	[65, 722]
	6.92 ^b	[180, 187]
	7.18 ^a	[1031]
	7.20	[299]
	7.29	[177]
	7.30	[170]
	8.20	[188, 189]

(continued)

Table 4.5 (continued)

Temperature range, °C	$\alpha_m, 10^{-6} \text{ K}^{-1}$	Reference
25–1450	7.29 ^j	[75, 104]
20–1500	7.28 ^a	[1031]
	7.34 ^f	[192]
	7.46	[177, 1032]
	8.10 ^h	[186]
20–1600	7.15 ^b	[180, 187]
	7.38 ^a	[1031]
	8.30	[188, 189]
20–1730	7.25	[5]
	7.52	[880, 881]
20–1800	7.41 ^b	[180, 187]
	7.58 ^a	[1031]
	8.40	[188, 189]
25–1925	6.30 ^k	[181]
20–2000	7.38 ⁱ	[184]
	7.79 ^a	[1031]
	7.57 ^b	[180, 187]
	7.86 ^f	[192]
	8.27 ^h	[186]
	8.50	[188, 189]
20–2130	7.95	[880, 881]
20–2200	8.01 ^a	[1031]
	8.60	[188, 189]
20–2300	8.12 ^a	[1031]
	7.76 ^b	[180, 187, 727]
20–2400	8.22 ^a	[1031]
	8.37 ^f	[192]
20–2450	8.40 ^l	[193]
20–2500	8.33 ^a	[1031]
	8.75 ^h	[186]
	7.92 ^b	[180, 187]
20–2600	8.43 ^a	[1031]
	8.72 ^f	[192]
	8.54 ^a	[1031]
20–2700	8.99 ^h	[186]
20–2850	8.99 ^h	[186]
20–2900	8.02 ^b	[180, 187]

^aCalculated on the basis of approximation function

^bHot-pressed NbC_{0.97} (13–18% porosity), measured by telemicroscope (dilatation) method in vacuum

^cNbC_{0.88}, measured by high-temperature X-ray diffraction

^dNbC_{0.92}, measured by high-temperature X-ray diffraction

^eNbC_{~1.0}, measured by high-vacuum high-temperature X-ray diffraction

^fHot-pressed NbC_{0.95}, measured by using an optical micrometer in Ar atmosphere

^gHot-pressed NbC_{0.98}, measured by a dilatometric method in Ar atmosphere

^hHot-pressed NbC_{~1.0} (8% porosity), measured by using an optical micrometer in Ar atmosphere

(continued)

Table 4.5 (continued)

ⁱSintered (in vacuum) NbC_{0.93}, measured by high-temperature X-ray diffraction and dilatometric methods

^jNbC_{0.98}, measured by high-temperature X-ray diffraction

^kHot-pressed (2% porosity), measured by a dilatometric method

^lHot-pressed NbC_{0.97}, measured by a dilatometric method

for NbC_{0.702}

$$\alpha_m = 4.98 \times 10^{-6} + (1.59 \times 10^{-9})(t - 25), \quad (4.51)$$

where α_m is the average coefficient of linear thermal expansion, K⁻¹ and t is temperature, °C. The influence of carbon content on the thermal expansion of monocarbide NbC_{1-x} and semicarbide Nb_{2+x}C phases within their homogeneity ranges can be seen in Figs. 4.3 and 4.9. The average values of coefficient of linear thermal expansion of near-stoichiometric niobium semicarbide Nb₂C were evaluated as $(7.0 \pm 0.3) \times 10^{-6}$ K⁻¹ in the range of temperatures from 12 to 190 °C and 6.5×10^{-6} K⁻¹ in the range of 20–1100 °C [62]. On the basis of X-ray measurements Lönnberg and Lundström [47] proposed for α_m , K⁻¹, along the main crystallographic directions of semicarbide modifications the following equations:

for α -Nb₂C (in the temperature range of 25–1200 °C)

$$\alpha_{a,m} = 3.093 \times 10^{-6} + (9.761 \times 10^{-10})(t + 273), \quad (4.52)$$

$$\alpha_{b,m} = 9.424 \times 10^{-6} + (1.551 \times 10^{-9})(t + 273), \quad (4.53)$$

$$\alpha_{c,m} = 5.327 \times 10^{-6} + (1.381 \times 10^{-9})(t + 273), \quad (4.54)$$

for β -Nb_{2+x}C (in the temperature range of 25–1300 °C)

$$\alpha_{a,m} = 4.942 \times 10^{-6} + (1.855 \times 10^{-9})(t + 273), \quad (4.55)$$

$$\alpha_{c,m} = 3.884 \times 10^{-6} + (3.012 \times 10^{-9})(t + 273), \quad (4.56)$$

where $\alpha_{i,m}$ is the average coefficient of linear thermal expansion along the i -th direction, K⁻¹ and t is temperature, °C. The thermal expansion of α -Nb₂C is strongly anisotropic, while that of β -Nb_{2+x}C is nearly isotropic; the volume thermal expansion of the former phase is, however, slightly larger than that of the latter. Some recent works [152, 356, 402, 409, 738, 955] are devoted to the calculations of coefficients of thermal expansion of niobium carbides by means of theoretical modelling.

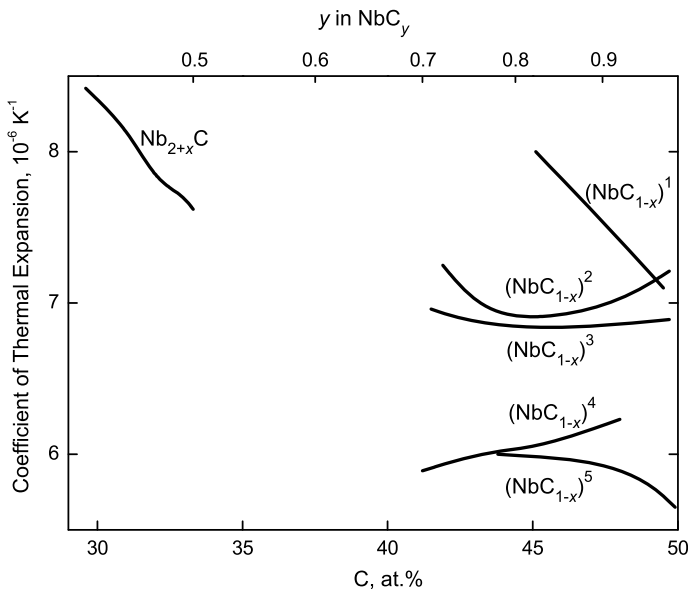


Fig. 4.9 Coefficients of linear thermal expansion in the temperature range of 20–1000 °C (when it is not indicated specially) of niobium monocarbide NbC_{1-x} (1 – hot-pressed, dilatometric method [209]; 2 – [1, 67]; 3 – hot-pressed, 6–10% porosity, content non-combined C \leq 0.16%, dilatometric method [10, 11, 185, 191, 854]; 4 – in the range of 20–600 °C [36]; 5 – in the range of 20–900 °C, high-temperature X-ray diffraction method [699]) and semicarbide Nb_{2+x}C [1, 51, 67] within their homogeneity ranges as functions of carbides composition

In comparison with other ultra-high temperature materials the values of thermal conductivity and thermal expansion of niobium carbides in the wide range of temperatures are summarized in Addendum.

4.3 Electro-magnetic and Optical Properties

At room temperature the value of specific electrical resistance (resistivity) of near-stoichiometric niobium monocarbide NbC_{1-x} lies within the area of 0.2–0.8 $\mu\Omega$ m [1, 5, 62–65, 80, 159, 176–178, 189, 193, 196, 197, 300, 651, 719, 720, 849, 878, 882], and that of near-stoichiometric niobium semicarbide $\alpha\text{-Nb}_2\text{C}$ – within the area of 0.6–1.4 $\mu\Omega$ m [1, 116]. The variation of this property with temperature for near-stoichiometric monocarbide NbC_{1-x} is shown on the basis of several sources in Fig. 4.10. In the wide temperature range from 200–500 °C up to 2600–2900 °C the resistance of monocarbide phase enlarges with increasing temperature, practically in accordance with linear relationship; that is an evidence of mainly metallic type of conduction in NbC_{1-x} [10, 11]. For the temperature range from 20 to 2400 °C the following equation was recommended by Maltseva et al.

[62, 170, 756] for the resistivity of near-stoichiometric niobium monocarbide NbC_{1-x} , ρ , $\mu\Omega \text{ m}$ (corrected to the poreless state):

$$\rho = 0.51 + (4.0 \times 10^{-4})(t - 20), \quad (4.57)$$

where t is temperature, $^{\circ}\text{C}$. Dy and Williams [210] applied to niobium monocarbide phase the empirical equation, which was experimentally determined for ultra-low and low temperature range (4–300 K) by Allison et al. [211] as follows:

for single crystal $\text{NbC}_{0.98}$

$$\rho(T) = 24.0 + (2.2 \times 10^{-2})T + 22.9 \exp(-278/T), \quad (4.58)$$

and for single crystal $\text{NbC}_{0.87}$

$$\rho(T) = 121.6 + (5.0 \times 10^{-3})T + 9.5 \exp(-474/T), \quad (4.59)$$

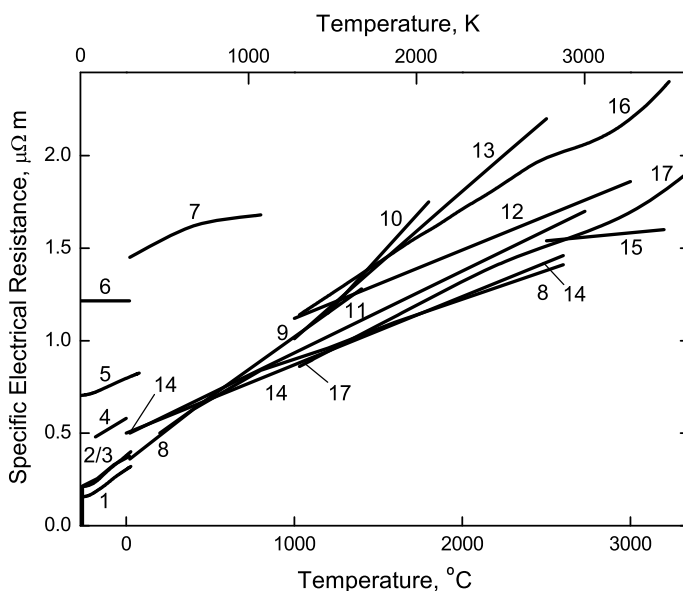


Fig. 4.10 Variation of specific electrical resistance with temperature for niobium monocarbide NbC_{1-x} materials on the basis of several sources: 1 – hot-pressed $\text{NbC}_{0.98}$, 3% porosity [183, 201]; 2 – 14% porosity [177, 189, 200, 1033]; 3 – single crystal $\text{NbC}_{0.975} \langle 100 \rangle$ [971]; 4 – sintered $\text{NbC}_{0.95}$, 23% porosity [176]; 5 – single crystal $\text{NbC}_{0.95}$ [758]; 6 – single crystal $\text{NbC}_{0.84} \langle 100 \rangle$ [971]; 7 – single crystal $\text{NbC}_{0.82}$ [179]; 8 – [10, 11, 199]; 9 – hot-pressed and annealed, almost poreless $\text{NbC}_{0.99}$ [198]; 10 – hot-pressed [67]; 11 – based on several sources [5]; 12 – hot-pressed $\text{NbC}_{0.97}$, 13–18% porosity, corrected to the poreless state [180]; 13 – sintered and annealed in vacuum, 2% porosity [27, 759]; 14 – hot-pressed and annealed $\text{NbC}_{0.87}$ [170, 756]; 15 – [120]; 16 – sintered $\text{NbC}_{0.91-0.97}$, 15–17% porosity, contents: non-combined C – 0.35–0.63%, N \leq 0.26%, O – 0.07–0.21% [243]; 17 – sintered $\text{NbC}_{0.91-0.97}$ (see also 16), corrected for porosity [765] (when it is not indicated specially, data are given for near-stoichiometric compositions)

Table 4.6 Average thermal coefficients of resistivity α_R of niobium monocarbide NbC_{1-x} in various temperature ranges^a

Temperature range, °C	$\alpha_R, 10^{-3} \text{ K}^{-1}$	Reference
(-183)-0	1.14 ^b	[176]
20-1000	~ 1.35	[67, 206]
	$\sim 0.80^c$	[67, 206]
	0.52 ^d	[757]
	$\sim 0.20^e$	[67, 206]
100-1100	1.75	[1, 198, 693]
300-2300	0.86 ^f	[5, 10, 207, 693]

^aWhen it is not indicated specially, value reported is for near-stoichiometric composition

^bSintered materials, 23% porosity, carbon content - 48.7 at.%

^cHot-pressed materials, carbon content - 47.4 at.%, corrected for porosity

^dHot-pressed materials, carbon content - 48.9 at.%, thermal coefficient $\alpha = 1/\rho_\theta \times (d\rho/dT)_\theta$, corresponding to Debye temperature $\theta = 805 \text{ K}$ ($(d\rho/dT)_\theta = 3.5 \times 10^{-4} \mu\Omega \text{ m K}^{-1}$), corrected for porosity

^eHot-pressed materials, carbon content - 42.9 at.%, corrected for porosity

^fHot-pressed materials, $d\rho/dT = 9.0 \times 10^{-4} \mu\Omega \text{ m K}^{-1}$

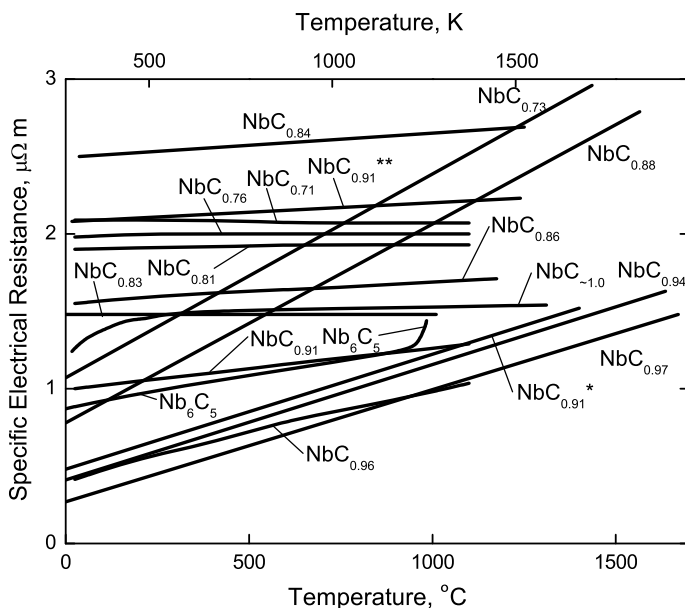


Fig. 4.11 Variations of specific electrical resistance with temperature for the NbC_{1-x} phases having different deviations from the stoichiometry ($x = 0.04, 0.09, 0.14, 0.19, 0.24, 0.29$ [202]; annealed 100 h at 2400 °C, $x = 0.03, 0.06, 0.09^*, 0.12, 0.27$ [5]; $x = 0, 0.09^{**}, 0.16$, corrected to the poreless state [226]; disordered $x = 0.17$ and ordered Nb_6C_5 [74, 210])

where T is temperature, K (the resistivity of single crystal $\text{NbC}_{0.76}$ is nearly constant over 4–300 K temperature range varying only from 1.53 to 1.55 $\mu\Omega \text{ m}$ [211]). In the interval from $T = 0$ to $T = 350$ K the single crystal $\text{NbC}_{0.95}$ resistivity measured by Allison et al. [758] can be described by the Wilson expression (in $\mu\Omega \text{ m}$):

$$\rho(T) = 0.705 + (1.606 \times 10^{-8})T^3 \int_0^{216/T} x^3 / \sinh^2 x dx \quad (4.60)$$

which can be simplified for $T \leq 40\text{--}70$ K up to $\rho(T) = 0.705 + AT^3$, where A is a constant. The data on the thermal coefficients of resistivity α_R of near-stoichiometric NbC_{1-x} in the various temperature ranges are presented in Table 4.6. The variations of resistivity with temperature for the phases having different deviations from the stoichiometry, including the ordered phase Nb_6C_5 as an especial example, are presented in Fig. 4.11 on the basis of several sources. The specific electrical resistance of NbC_{1-x} at the melting point is 2.54 $\mu\Omega \text{ m}$ [62, 159, 177]. Within the homogeneity range the resistivity of Nb_{2+x}C and NbC_{1-x} supplements with increasing carbon deficit in non-metal sublattice, especially the considerable growth of resistivity is inherent for the monocarbide phase, that is shown in Fig. 4.12, where the data from several sources are collected. The variation

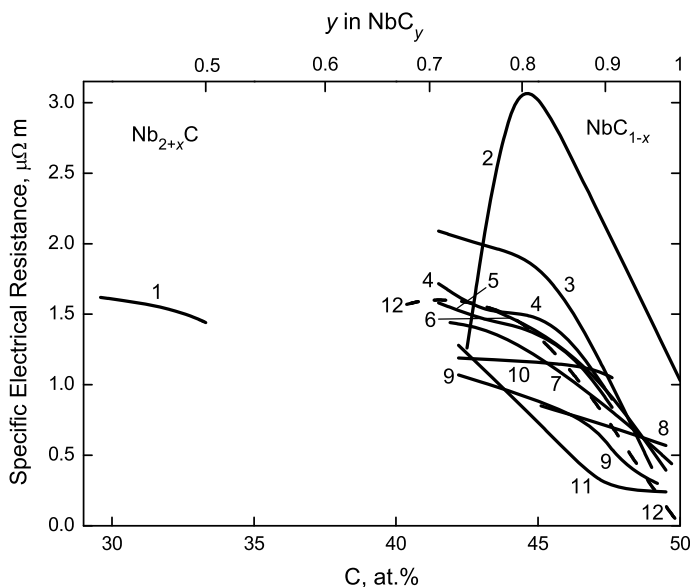


Fig. 4.12 Variations of specific electrical resistance at room temperature within the homogeneity ranges of niobium semicarbide Nb_{2+x}C (1 – sintered [51]) and monocarbide NbC_{1-x} (on the basis of several sources: 2 – [227]; 3 – [204, 215]; 4 – sintered in vacuum, 5–15% porosity [171, 845], 5 – [205]; 6 – single crystals [211]; 7 – [53, 202, 208]; 8 – hot-pressed [209]; 9 – [5]; 10 – hot-pressed and annealed, content non-combined C – 0.15–0.52% [218, 848]; 11 – [203]; in dash: 12 – residual resistivity at ultra-low temperatures, single crystals materials [971])

of $d\rho/dT$ with composition at ambient temperatures is shown in Fig. 4.13; the increase in carbon vacancy concentration in the NbC_{1-x} phase leads to a change not only in absolute resistivity, but also – a regular decrease in $d\rho/dT$ and α_R values [10, 11, 80, 202]. The superconducting transition temperature T_c of near-stoichiometric monocarbide NbC_{1-x} is 6–12 K [84, 92, 183, 212–214, 230–238, 334, 847, 852, 853, 879, 895, 898, 906, 1020, 1036]; it varies with composition considerably, e.g. falling from 11.1 K for $\text{NbC}_{0.98}$ to 1.05 K for $\text{NbC}_{0.83}$. The highest temperature is reached for the most stoichiometric composition, so any deviation therefrom results in a lowering and eventual disappearance (<1.05 K at $x = 0.2-0.3$) of the superconductivity in general [212–214]. The transition temperatures T_c of semicarbide phases: for $\text{Nb}_{2.08}\text{C} < 1.6$ K [213], for $\text{Nb}_{2.0}\text{C} \sim 9.2$ K [212, 933], for $\text{Nb}_{1.96}\text{C} < 2$ K [212, 1035]. At room temperature the Hall and Seebeck coefficients of near-stoichiometric NbC_{1-x} are $R = -(0.8-1.3) \times 10^{-10} \text{ m}^3 \text{ A}^{-1} \text{ s}^{-1}$ and $S = -(3-6) \mu\text{V K}^{-1}$, respectively [1, 7, 10, 11, 67, 82, 216, 217, 760, 849]; the concentration variations of values of these constants within the homogeneity range of niobium monocarbide NbC_{1-x} are presented in Figs. 4.14 and 4.15.

Near-stoichiometric niobium monocarbide NbC_{1-x} is a paramagnetic substance with molar magnetic susceptibility χ_m (SI) $\approx (100-260) \times 10^{-6} \text{ cm}^3 \text{ mol}^{-1}$ at room temperature very slightly varying with temperature in the range from -200 to 900 °C [1, 10, 11, 67, 74, 218–225, 850, 851]. The weak temperature influence and small absolute value of susceptibility indicate that the magnetic properties of

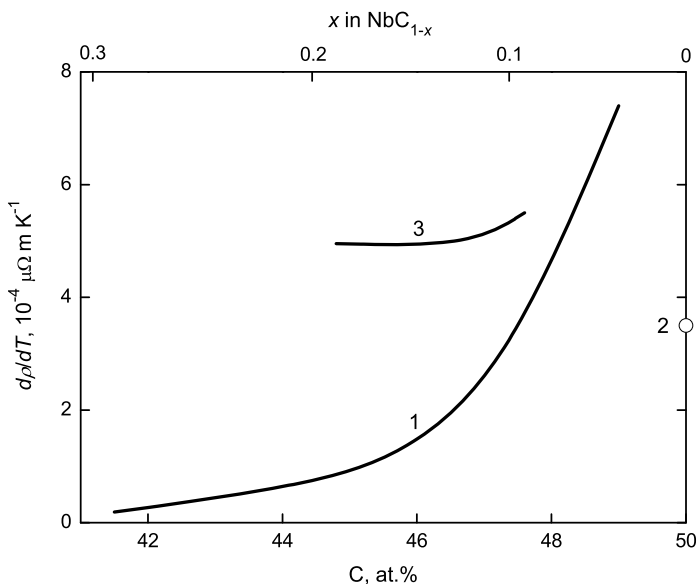


Fig. 4.13 Variation of $d\rho/dT$ (slope of resistivity vs. temperature) at ambient temperatures within the homogeneity range of niobium monocarbide NbC_{1-x} (1 – [10, 11, 202]; 2 – [80]; 3 – hot-pressed, content non-combined C – 0.23–0.52% [218, 848])

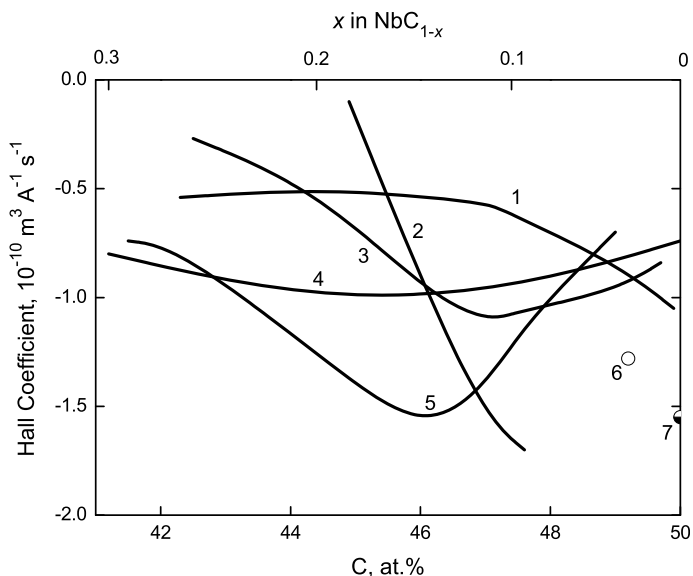


Fig. 4.14 Variations of Hall coefficient at room temperature within the homogeneity range of niobium monocarbide NbC_{1-x} on the basis of several sources (1 – sintered [208, 227]; 2 – hot-pressed, content non-combined C – 0.23–0.52% [218, 848]; 3 – [10, 11]; 4 – single crystal materials [971]; 5 – sintered (in vacuum) [215]; 6 – [760]; 7 – hot-pressed [65, 761, 934, 935])

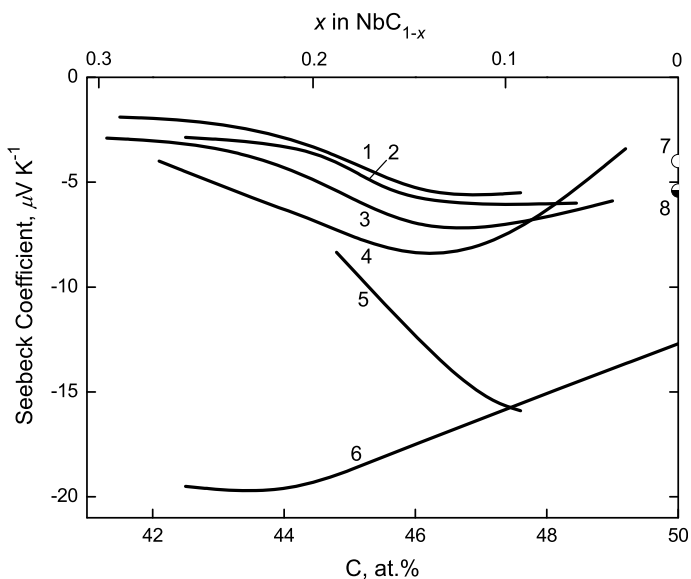


Fig. 4.15 Variations of Seebeck coefficient at room temperature within the homogeneity range of niobium monocarbide NbC_{1-x} on the basis of several sources (1 – sintered in vacuum, 5–15% porosity [171]; 2 – sintered in vacuum, 2–3% porosity [278]; 3 – [215]; 4 – [203]; 5 – hot-pressed, content non-combined C – 0.23–0.52% [218, 848]; 6 – [227]; 7 – hot-pressed [216]; 8 – [761])

monocarbide NbC_{1-x} are determined primarily by conducting electrons [10, 11]. With increasing carbon deficit within the homogeneity range the value of magnetic susceptibility of monocarbide declines and reaches its diamagnetic (negative) minimum at about $-(50-250) \times 10^{-6} \text{ cm}^3 \text{ mol}^{-1}$, corresponding to $\sim \text{NbC}_{0.8}$ composition (see Fig. 4.16), and then it enlarges again proceeding to the paramagnetic region [10, 11, 225]. Gusev and Rempel [74, 222] showed that the minima of χ in niobium monocarbide NbC_{1-x} phases in disordered and ordered states occur for the composition of $\text{NbC}_{0.83}$ at $-(105-125) \times 10^{-6} \text{ cm}^3 \text{ mol}^{-1}$, and for $\text{NbC}_{0.81}$ at $-(200-220) \times 10^{-6} \text{ cm}^3 \text{ mol}^{-1}$, respectively. The temperature coefficient of magnetic susceptibility $d\chi/dT$ changes its sign with composition; it is positive for compositions around $\text{NbC}_{0.78}$ and negative – for near-stoichiometric composition $\text{NbC}_{0.98}$ [10, 11, 228]. According to Caudron et al. [229], niobium semicarbide $\text{Nb}_{2\pm x}\text{C}$ is also a paramagnetic substance with the value of its mass magnetic susceptibility – $\sim 485 \times 10^{-6} \text{ cm}^3 \text{ mol}^{-1}$.

The reflectance spectra from the ultraviolet wavelength region to the mid-infrared band of single crystal monocarbide NbC_{1-x} materials with various carbon content are shown in Fig. 4.17; specular reflectance was measured between 0.025 and 11 eV, and ellipsometry measurements were made at 1.96 eV as well to conclude that HIPed materials had optical and electric properties that were almost identical to those of single crystals with nearly the same composition [211]. Optical constants (refractive index n and extinction coefficient k versus photon energy

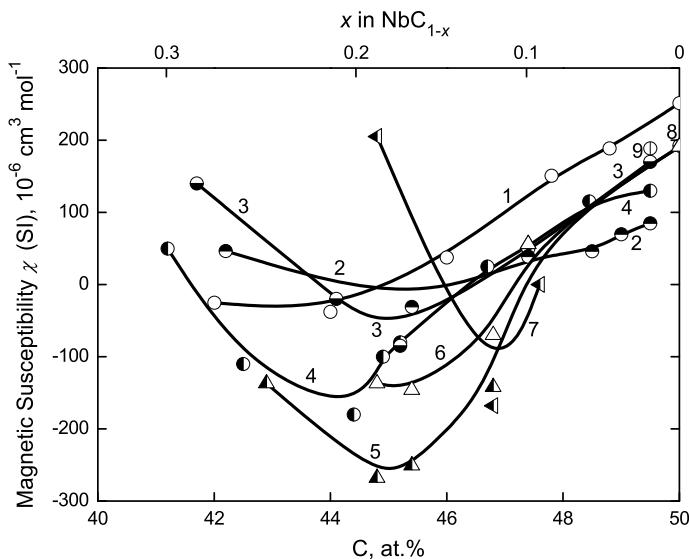


Fig. 4.16 Variation of molar magnetic susceptibility at room temperature within the homogeneity range of niobium monocarbide NbC_{1-x} on the basis of several sources: 1 – from 48.8 to 50 at.% C the values extrapolated [219, 763]; 2 – [220]; 3 – [762]; 4 – [221]; 5 – ordered and 6 – disordered carbide phases [222, 224]; 7 – content non-combined C – 0.23–0.52% [218, 848]; 8 – [761]; 9 – [764]

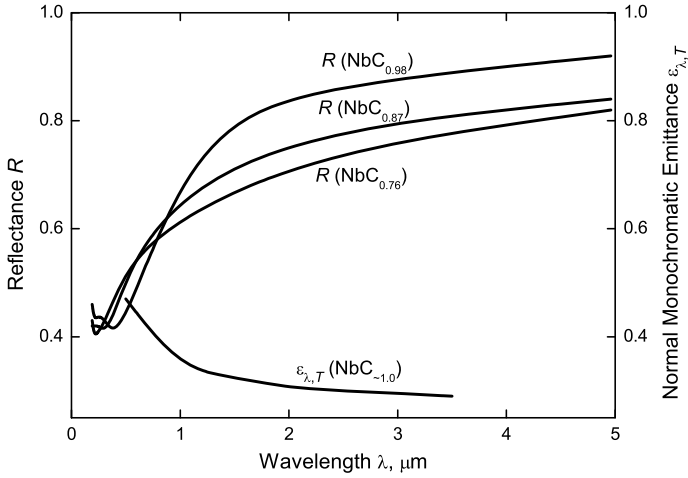


Fig. 4.17 Variations of reflectance R ($\text{NbC}_{0.76}$, $\text{NbC}_{0.87}$ and $\text{NbC}_{0.98}$ single crystal materials [211]) and normal monochromatic emittance $\epsilon_{\lambda,T}$ ($\text{NbC}_{\sim 1.0}$ pyrolytic coating on graphite substrate at 1530–2220 °C [10, 11, 247, 1042]) with wavelength λ .

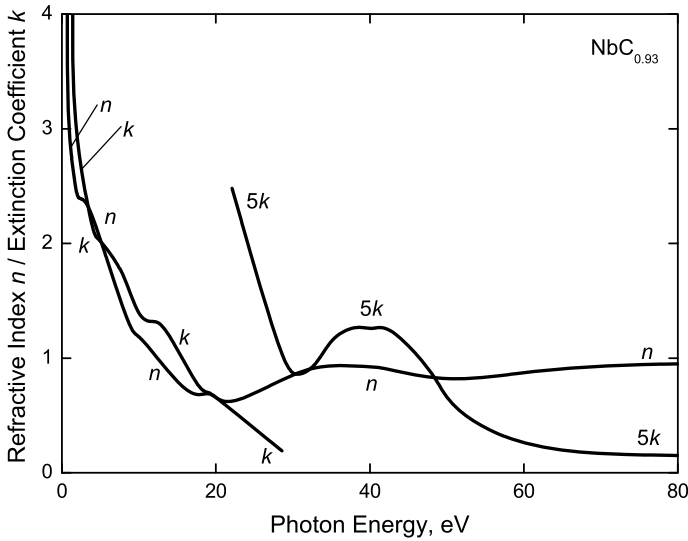


Fig. 4.18 Refractive index n and extinction coefficient k of single crystal $\text{NbC}_{0.93}$ deduced through a Kramers-Kronig analysis of the reflectance spectrum (k is shown in an expanded scale $\times 5$ above 22 eV) [239, 972]

relationships) deduced through a Kramers-Kronig analysis of the reflectance spectrum of single crystal $\text{NbC}_{0.93}$ are presented in Fig. 4.18. Optical spectra of NbC_{1-x} in the infrared (IR) and visible ranges as well as X-ray emission and absorption spectra were considered by Alyamovskii et al. [241], Ramqvist et al. [240], Zhurakovskii et al. [1039–1041], Korsunskii et al. [1038], Kammori et al. [1043] and Upadhyaya [11]. The absorption wave numbers of basic maxima of IR band for niobium carbides are 1100 cm^{-1} (for $\text{NbC}_{0.98}$), 1075 cm^{-1} (for $\text{NbC}_{0.77}$) and 1080 cm^{-1} (for Nb_2C) [241]. At the common conditions the colour of niobium monocarbide NbC_{1-x} powder is light-brown, gray-brown or sometimes gray with a lavender/violet tint, golden-orange colour is more inherent to near-stoichiometric compositions NbC_{1-x} in the compact state [1, 6, 7, 10, 11, 63, 67, 84, 117, 882].

The normal monochromatic emittance (spectral emissivity) $\varepsilon_{\lambda,T}$ of niobium monocarbide NbC_{1-x} falls noticeably with wavelength λ growth (see Fig. 4.17) and only slightly varies with temperature [1, 10, 11, 247, 715]; the linear relationship for $\lambda = 0.65\text{ }\mu\text{m}$

Table 4.7 Normal monochromatic emittance ε_{λ} ($\lambda = 0.630\text{--}0.665\text{ }\mu\text{m}$) of niobium monocarbide NbC_{1-x} materials in various temperature ranges

Monochromatic emittance, ε_{λ}	Temperature range, °C	Reference
0.28	725	[200]
0.35–0.41 ^a	900–1850	[242, 715]
0.42–0.49 ^b	900–3000	[247]
0.55–0.62 ^c	2370–2990	[62, 120]
0.59–0.66 ^d	1000–3200	[243, 246, 765]
0.62–0.66 ^b	1000–2200	[1]
0.71–0.79 ^e	1430–1930	[248]
0.73 ^f	2000–2500	[10]
0.75 ^g	1500–2400	[250]
0.85 ^h	800–1800	[5, 63, 196, 244, 245]

^aArc-melted (via floating zone) polycrystalline $\text{NbC}_{0.83\pm 0.01}$, measured in vacuum $10^{-5}\text{--}10^{-6}$ Pa; ε_{λ} falls with the temperature growth linearly (slope is $\sim 6.6 \times 10^{-5}\text{ K}^{-1}$)

^bSintered materials; ε_{λ} falls with the temperature growth linearly

^c ε_{λ} falls with the temperature growth

^dSintered materials $\text{NbC}_{0.91\text{--}0.97}$ (15–17% porosity, mean grain size $\leq 15\text{--}16\text{ }\mu\text{m}$, contents: non-combined C – 0.35–0.63%, N $\leq 0.26\%$, O – 0.07–0.21%); ε_{λ} falls with the temperature growth linearly

^eFor $\lambda = 0.81\text{ }\mu\text{m}$, sintered materials with 32% porosity, the surface roughness effect on ε_{λ} is very low, after high-temperature exposure in vacuum ε_{λ} gradually decreases from 0.79 and approaches a constant value of 0.71, as a result of exposure to hot H_2 at $1260\text{ }^{\circ}\text{C}$ for 2 h ε_{λ} reduces from 0.79 to 0.72 [249]

^fHot-pressed materials

^gMaterials with composition $\text{NbC}_{0.77}$, deposited from gas phase and annealed in vacuum at $2200\text{ }^{\circ}\text{C}$ for 1 h exposure

^hPowdered materials on tantalum substrate

$$\varepsilon_{\lambda} = 0.4913 - (6.6 \times 10^{-5})(t + 273), \quad (4.61)$$

where t is temperature, °C, was obtained by Mackie et al. [242, 715] for arc-melted (via floating zone) polycrystalline monocarbide $\text{NbC}_{0.83 \pm 0.01}$ in the temperature range 900–1850 °C. For near-stoichiometric NbC_{1-x} Petrov [10, 246] has recommended in the temperature range 1100–3100 °C the equation as follows:

$$\varepsilon_{\lambda} = 0.66 - (2.60 \times 10^{-5})(t - 727), \quad (4.62)$$

where t is temperature, °C. According to the experimental work by Okhremchuk et al. [766], emissivity ε_{λ} of NbC_{1-x} phases decreases from 0.75 to 0.70 with increasing value of index x in NbC_{1-x} formula from 0.02 to 0.18. The data on normal monochromatic emittance ε_{λ} ($\lambda = 0.630\text{--}0.665 \mu\text{m}$) and integral (total) emittance ε_{T} for NbC_{1-x} materials produced by different manufacturing methods and measured at various temperatures are listed in Tables 4.7 and 4.8.

The thermionic emission characteristics (electron work function and Richardson constants) of various niobium carbide phases are given in Table 4.9 and Fig. 4.19. The calculated values of emission current density for near-stoichiometric monocarbide NbC_{1-x} are about 7×10^{-4} , 9×10^{-2} and 0.2 A m^{-2} at 730, 1230 and 1730 °C, respectively [5]. Using the photoemission technique, Lindberg and Johansson [875] revealed that the work function of $\text{NbC}_{0.83}$ (100) increases dramatically with increasing the exposure to O_2 , while only small increases in the work function are observed after the exposure to CO media. A typical brightness characteristic ($U = 75 \text{ kV}$) of niobium monocarbide cathode (thermionic emitter for electron microscopy) is shown in Fig. 4.20. Field emission properties of niobium monocarbide NbC_{1-x} materials were reported in several works [255–257, 776, 811, 1045–1047].

Table 4.8 Integral (total) emittance ε_{T} of near-stoichiometric niobium monocarbide NbC_{1-x} in various temperature ranges

Integral emittance, ε_{T}	Temperature range, °C	Reference
0.40–0.55 ^a	1000–3200	[243, 246, 765]
0.42–0.46 ^b	730–2430	[247]
0.57–0.58 ^c	2000–2500	[1, 10, 11]

^aHemispherical emittance ε_{T} for sintered $\text{NbC}_{0.91\text{--}0.97}$ (15–17% porosity, mean grain size $\leq 15\text{--}16 \mu\text{m}$, contents: non-combined C – 0.35–0.63%, N $\leq 0.26\%$, O – 0.07–0.21%); ε_{T} increases with the temperature growth (from 1000 to 3000 °C the relationship $\varepsilon_{\text{T}} - T$ is linear)

^bNormal emittance ε_{T} for sintered materials; ε_{T} increases with the temperature growth

^cNormal emittance ε_{T} for hot-pressed materials; ε_{T} increases with the temperature growth

Table 4.9 Thermionic emission characteristics (electron work function and Richardson constant) of niobium carbide phases

Composi- tion	Work function ^a , $\varphi = \varphi_0 + (d\varphi/dT)_{av}T$, eV	Richardson constant, A, $10^4 \text{ A m}^{-2} \text{ K}^{-2}$	Temperature range, °C	Remarks ^b	Reference
Nb ₂ C	4.10 ^c	–	1500	TiM, hot-pressed	[271]
	4.12 ^c	–	1500	TiM, hot-pressed	[10, 11, 1044]
	5.20	–	50	–	[824]
	$5.50 - (7.7 \times 10^{-4})T$	–	1200–1800	TiM, hot-pressed	[1, 191, 1044]
NbC _{0.72}	$4.32 - (1.8 \times 10^{-4})T$	–	1200–1750	TiM, hot-pressed	[1, 191]
NbC _{0.75}	4.00 ^c	–	1500	TiM, hot-pressed	[10, 11, 1044]
NbC _{0.81}	$4.45 - (1.7 \times 10^{-4})T$	–	1200–1800	TiM, hot-pressed	[1, 191]
	4.15 ^c	–	1500	TiM, hot-pressed	[10, 11, 1044]
NbC _{0.86}	4.40	–	50	–	[824]
	$4.44 - (1.6 \times 10^{-4})T$	–	1200–1800	TiM, hot-pressed	[1, 191]
	$3.84 (d\varphi/dT = 0)$	–	1000–1700	TiM, single crystal (100), measured in vacuum ($\sim 1.3 \times 10^{-6}$ Pa)	[268, 857, 858]
	$3.90 (d\varphi/dT = 0)$	–	1000–1700	TiM, single crystal (102), measured in vacuum ($\sim 1.3 \times 10^{-6}$ Pa)	[268, 857, 858]
	$3.95 - (6.48 \times 10^{-5})T$	–	≤ 1700	TiM, single crystal (100)	[254, 767]
	$3.95 - (2.93 \times 10^{-5})T$	–	≤ 1700	TiM, single crystal (102)	[254, 767]
	4.0	–	1000–1700	CPDM, single crystal (100), measured in vacuum ($\sim 1.3 \times 10^{-6}$ Pa)	[254, 268, 767]
NbC _{0.88}	4.1	–	25	CPDM, single crystal (102)	[254, 767]
	4.05 ^c	–	1500	TiM, hot-pressed	[10, 11, 1044]
NbC _{0.90}	$4.37 - (1.8 \times 10^{-4})T$	–	1150–1800	TiM, hot-pressed	[1, 191]
	4.05 ^c	–	1400	TiM, sintered	[1, 254]
NbC _{0.91}	$4.30 - (1.7 \times 10^{-4})T$	–	1150–1750	TiM, hot-pressed	[1, 191]
NbC _{0.92}	4.00 ^c	–	1500	TiM, hot-pressed	[10, 11, 1044]
NbC _{0.95}	4.2	–	1600	UPS, single crystal (100)	[257]
	5.2	–	1600	UPS, single crystal (111)	[257]
NbC _{0.99}	3.93 ^c	–	1500	TiM, hot-pressed	[10, 11, 1044]
	4.21 ± 0.05	–	25	CPDM (W), hot-pressed	[1, 261]
NbC _{~1.0}	$4.25 - (1.9 \times 10^{-4})T$	–	1150–1750	TiM, hot-pressed	[1, 191]
	~ 2.24	$\sim 10^{-6}$	–	TiM	[1, 254]
	3.38 ^d	–	–	Single crystal (001), theo- retically evaluated	[395]
	3.50	–	–	TiM, pyrolytic coating	[1, 265]
	3.58 ^c	–	1230	TiM, powder	[1, 258]
	3.66 ^e	–	–	Single crystal (001), theo- retically evaluated	[395]

(continued)

Table 4.9 (continued)

Composi- tion	Work function ^a , $\varphi = \varphi_0 + (d\varphi/dT)_{av}T$, eV	Richardson constant, A, $10^4 \text{ A m}^{-2} \text{ K}^{-2}$	Temperature range, °C	Remarks ^b	Reference
	3.70 ± 0.05^c	–	–	TiM, metal-carburized	[1, 254]
	3.70 ± 0.1	–	–	TiM, metal-carburized	[1, 254]
	3.74^c		1130	TiM, powder	[259]
	3.81^c	418	2130	TiM, metal-carburized wire	[253]
	3.83^c	–	2100	TiM, hot-pressed	[263, 264]
	3.85	–	–	Calculated value (unrelaxed surface)	[949, 950]
	3.95^f	–	–	Single crystal (100), theoretically evaluated	[894]
	4.02^c	–	25	TiM, powder	[259]
	4.07 ± 0.04^c	–	1330	TiM, hot-pressed, plain samples	[1, 262]
	4.10	–	–	UPS, single crystal (100)	[875, 949, 950]
	4.10^c	–	2180	TiM, powder on W	[1, 260]
	$4.10 - (2.5 \times 10^{-4})T^c$	–	1180–1930	TiM, powder	[1, 10, 11, 254]
	4.14 ± 0.05	–	25	CPDM, hot-pressed	[1, 262]
	4.2^g	–	25	FEM, single crystal (001), clean surface	[716, 776, 777, 949, 950]
	4.20^c	72.3	2130	TiM, powder on Ta substrate	[253]
	4.26	–	–	Calculated value (relaxed surface)	[949, 950]
	4.45^h	–	–	Single crystal (100), theoretically evaluated	[894, 949, 950]
	5.0^i	–	25	FEM, single crystal (111), clean surface	[716, 776, 777]
	–	–	–	AeE, cold cathode, $\sim 1 \mu\text{m}$ fibre, 35 A m^{-2} , $6.7 \times 10^{-5} \text{ Pa}$ for $>10^3 \text{ h}$	[1, 255, 256]

^a T is temperature, K

^bMethods applied for the experimental determination of the work function (TiM – thermionic method, UPS – ultraviolet photoemission spectroscopy technique, CPDM – contact potential difference method, second electrode is given in brackets, AeE – autoelectronic emission method) and manufacturing methods for the fabrication of a particular material (or its constitution) are marked

^cThe values of effective electron work function

^dCalculated using the Perdew's generalized gradient approximation (GGA) for the fixed surface model

^eCalculated using the Perdew's GGA for the relaxed surface model

^fCalculated using the full-potential linear-muffin-tin-orbital (FP-LMTO) method

^gFor graphene-covered surface $\varphi = 4.2 \text{ eV}$

^hCalculated using the linear-muffin-tin-orbital with atomic sphere approximation (LMTO-ASA) technique

ⁱFor graphene-covered surface $\varphi = 3.8 \text{ eV}$

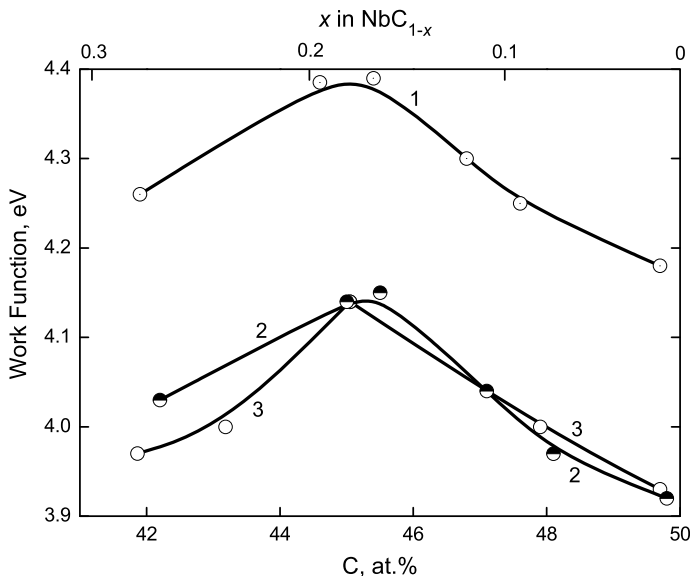


Fig. 4.19 Variations of effective work function of hot-pressed niobium monocarbide NbC_{1-x} materials with carbon content measured by “total current” method: at 50 °C (1 – [824]) and 1530 °C (2 – [854], 3 – [10, 11, 191, 251, 271])

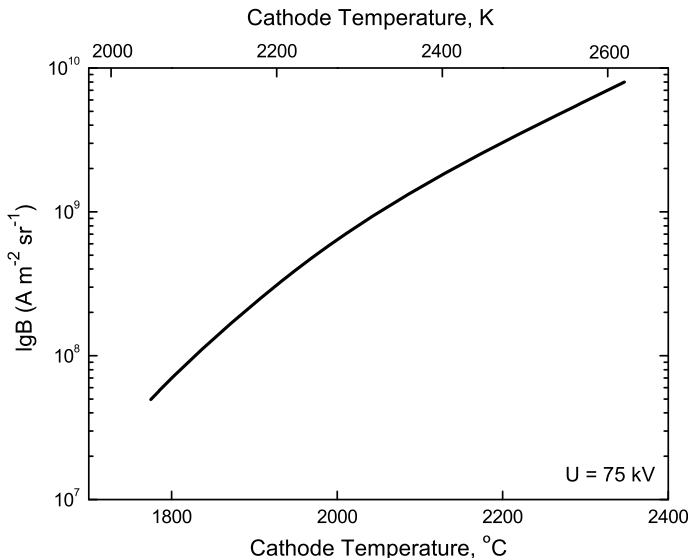


Fig. 4.20 Typical brightness (B) characteristic ($U = 75$ kV) of niobium monocarbide cathode (thermionic emitter with electron work functions $\varphi = 4.07$ eV, $\varphi_{\text{eff}} = 3.81$ eV, Richardson constant $A = 418 \times 10^4$ $\text{A m}^{-2} \text{K}^{-2}$, $T = 2400$ K) produced by the carburization reaction of metal wire/foil with benzene vapour [252, 253]

The recommended values of electrical resistivity, magnetic susceptibility, integral and spectral emittances and thermionic emission characteristics (electron work function and Richardson constant) for niobium carbides are given in the wide range of temperatures in comparison with other ultra-high temperature materials in Addendum.

4.4 Physico-mechanical Properties

The physico-mechanical properties of niobium carbides are very sensitive to the deviations from the stoichiometry, but also to the crystallographic directions in the materials; it has been just marked in Sect. 4.1 concerning the slip systems in NbC_{1-x} . At room temperature the hardness HV , GPa of near-stoichiometric niobium monocarbide NbC_{1-x} is evaluated as 14.3 ± 1.0 (for $\text{NbC}_{0.97}$) [2, 281], 15.0 (for $\text{NbC}_{0.99}$, contents: non-combined C – 0.07%, O – 0.05%, N – 0.45%, porosity – 7%, mean grain size – 12 μm , 1 N load) [1, 2, 361], 15.1 (for $\text{NbC}_{0.96}$, 200 N load) [53], 16.0 [3, 266, 267], 16.7 ± 1.0 (for $\text{NbC}_{0.96}$, content O \leq 0.05%, 1 N load) [2, 282], 17.0 (200 N load) [1, 53], 17.5 ± 0.8 [1], 18.6 ± 1.0 (for $\text{NbC}_{0.97}$, content O + N – 0.1%, 1 N load) [2, 279], 18.9 (for $\text{NbC}_{0.96}$, 200 N load) [53], 19.1 (for NbC_{1-x} monocarbide phase in contact with carbon) [773], 19.2 [65, 170], 19.6 [84, 774], 20.0 [770], 20.2 [64], 20.3 ± 0.5 (1 N load) [775], 20.9–21.6 (for nanostructured $\text{NbC}_{\sim 1.0}$, porosity – 2%, mean grain size – 76 nm, 100 N load) [321, 902], $(21.0\text{--}21.6) \pm (1.2\text{--}2.2)$ [10, 11, 287], 21.1 [882], 21.3 ± 1.3 (for $\text{NbC}_{0.99}$, contents: non-combined C – 0.25%, O – 0.03%, N – 0.01%, 0.5 N load) [1, 67, 772], 21.7 ± 1.3 (0.5 N load) [775], 22.0 (contents: O \leq 0.01%, N \leq 0.01%, porosity – 2%, mean grain size – 10 μm) [27], 23.0 ± 1.5 (contents: O \leq 0.1%, N \leq 0.1%, porosity – 2%, mean grain size – 10 μm) [27], 23.5 (for $\text{NbC}_{0.99}$, 0.5 N load) [769], 23.5 (0.5–1 N load) [5, 177, 189, 286, 716, 771], 24.0 ± 0.95 (0.5 N load) [5, 63] and 24.2 (for $\text{NbC}_{\sim 1.0}$ probably contaminated by W) [333]. The hardness of NbC_{1-x} ($x \approx 0$) in Mohs scale is >9 [67, 159], 9–10 [104, 117, 177, 1052] and in Rockwell scale HRA is 83 kgf mm^{-2} (0.81 GPa) [2, 67, 289], $\sim 90 \text{ kgf mm}^{-2}$ (~ 0.88 GPa) [338], 91 kgf mm^{-2} (0.89 GPa) [177, 189]. The variations of hardness HV/HK and microhardness $H\mu$ at room temperature with deviation from the stoichiometry and indenter orientation (anisotropy) within the homogeneity ranges of niobium semicarbide Nb_{2+x}C and monocarbide NbC_{1-x} are demonstrated in Fig. 4.21. The variations of hardness HV and microhardness $H\mu$ of near-stoichiometric NbC_{1-x} with temperature based on several resources and presented in Fig. 4.22 indicate mainly the linear characteristic hot-hardness behaviour of monocarbide materials on semi-logarithmic plots $HV/HK/H\mu - 1/T$ (or T) [283, 284, 292, 294, 295]. In general, in the temperature range from 0 to 1400 $^{\circ}\text{C}$ the hardness-temperature relationship for NbC_{1-x} materials is described perfectly by the exponential equation [5, 782–784]:

$$HV = 23.5 \exp[-(15.3 \times 10^{-4})t], \quad (4.63)$$

which can be approximated for the lower temperatures (<850 °C) by such linear equation [80] as

$$HV = 29.0 - (2.06 \times 10^{-3})t, \quad (4.64)$$

where HV is Vickers hardness, GPa and t is temperature, °C. Fig. 4.23 demonstrates the microhardness $H\mu$ dependence of single crystal materials on

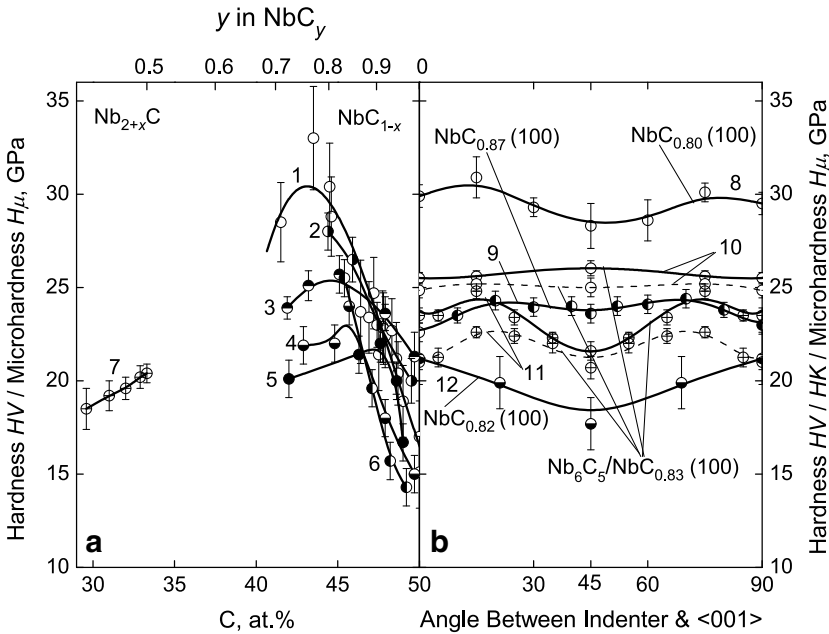


Fig. 4.21 Variations of the hardness HV (1, 8), HK (9–12) and microhardness $H\mu$ (2–7) at room temperature: (a) with deviation from the stoichiometry within the homogeneity ranges of niobium monocarbide NbC_{1-x} (1 – produced by gas carburization and hot-pressing methods, 200 N load [53, 266, 267]; 2 – melted in Ar and annealed in vacuum at 1800–2000 °C, 1.0 N load [277]; 3 – hot-pressed and annealed in vacuum, 6–10% porosity, 0.5 N load [191, 854]; 4 – sintered in vacuum and annealed, porosity – 7–12%, mean grain size – 12–29 μm , contents: non-combined C – 0.05–0.07%, O – 0.05–0.08%, N – 0.27–0.45%, 1.0 N load [1]; 5 – sintered at 2500–2700 °C, 2.0–12.5% porosity, contents: non-combined C \leq 0.01%, O \leq 0.05%, 1.0 N load [282]; 6 – produced by carbon diffusion saturation [281] and semicarbide $Nb_{2+x}C$ phases (7 – sintered in vacuum, 0.5 N load [51]) and (b) with indenter orientation (angle between indenter axis and $\langle 001 \rangle$ direction) on the (100) surface of single crystal materials (8 – $NbC_{0.80}$, produced by radio-frequency floating zone process, 2 N load [283, 284]; 9 – $NbC_{0.87}$, produced by the floating zone technique (zone melted), 5 N load [297, 1048]; 10 – $Nb_6C_5/NbC_{0.83}$, in long-range ordered state (the two curves for different samples), 1.5 N load [296]; 11 – $Nb_6C_5/NbC_{0.83}$, in short-range ordered state (the two curves for different samples), 1.5 N load [296]; 12 – $NbC_{0.82}$, produced by plasma-arc melting, 1 N load [87])

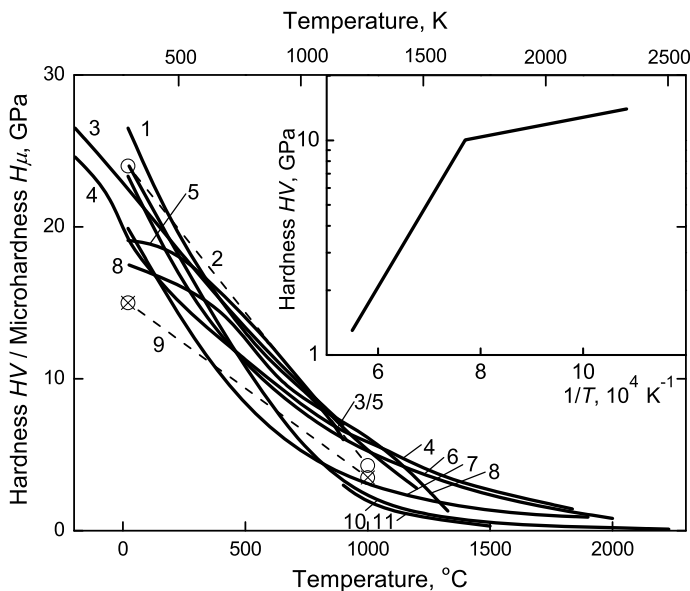


Fig. 4.22 Variations of hardness HV (1, 5–6, 10) and microhardness $H\mu$ (2–4, 7–9) with temperature for near-stoichiometric niobium monocarbide NbC_{1-x} phases based on several sources: 1 – single crystal $NbC_{0.84}$ [268]; 2 – sintered in vacuum and annealed $NbC_{0.84}$, porosity – 10.5%, mean grain size – 18 μm , 1 N load [1]; 3 – single crystal $NbC_{\sim 1.0}$ (001) produced by plasma-arc melting, 1 N load [273]; 4 – hot-pressed and annealed $NbC_{\sim 1.0}$, porosity – 2–4%, 1 N load (<20 °C) and 0.7 N load (>20 °C) [272, 337, 343]; 5 – sintered with temporary metallic binder (in high vacuum), 3 N load [1053]; 6 – sintered $NbC_{0.95}$, porosity – $\sim 10\%$ [1, 270]; 7 – hot-pressed $NbC_{\sim 1.0}$ [1]; 8 – single crystal $NbC_{0.80}$ produced by plasma-arc melting, 9.8 N load [285]; 9 – sintered in vacuum and annealed $NbC_{0.99}$, porosity – 7%, mean grain size – 12 μm , 1.0 N load [1]; 10 – sintered $NbC_{\sim 1.0}$, 0.5 N load [5, 63, 64]; 11 – sintered $NbC_{\sim 1.0}$, porosity – 28%, 1.5 kN load [295] (*Inset* – hardness of single crystal $NbC_{0.87}$ (001) produced by floating zone technique, in $\lg(HV, GPa) - 1/T, K^{-1}$ scale [292])

carbon content [709], and Fig. 4.24 – that of sintered materials with preceding high-temperature plastic deformation in the concentration range from $NbC_{0.74}$ to $NbC_{0.94}$ [278]. The hardness HV , GPa at room temperature of stoichiometric niobium semicarbide Nb_2C produced by gas carburization is 20.5 [53]; for sintered materials with the same composition it is 20.4 ± 0.5 [2, 51, 67] or 20.9 [10, 11, 289]. The data on microhardness $H\mu$ (hardness HK) of niobium monocarbide single crystals and various compositions of niobium semicarbide and monocarbide phases are listed in Tables 4.10–4.11. The hardness of niobium carbide thin films varies considerably, first of all depending on manufacturing methods and compositions: for filtered vacuum cathodic arc deposited films on silicon (thickness 0.5–0.6 μm) a maximum hardness is ~ 45 GPa (5 mN load) [305], for electron beam deposited

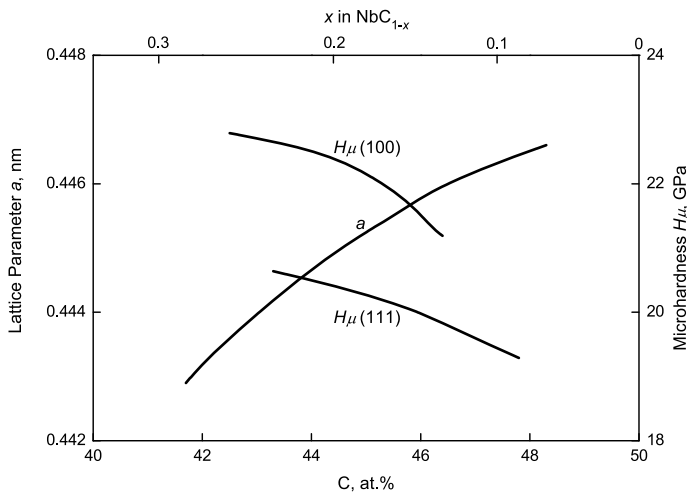


Fig. 4.23 Variations of lattice parameter a and microhardness H_{μ} on the surfaces (100) and (111) of single crystal NbC_{1-x} with carbon content [709]

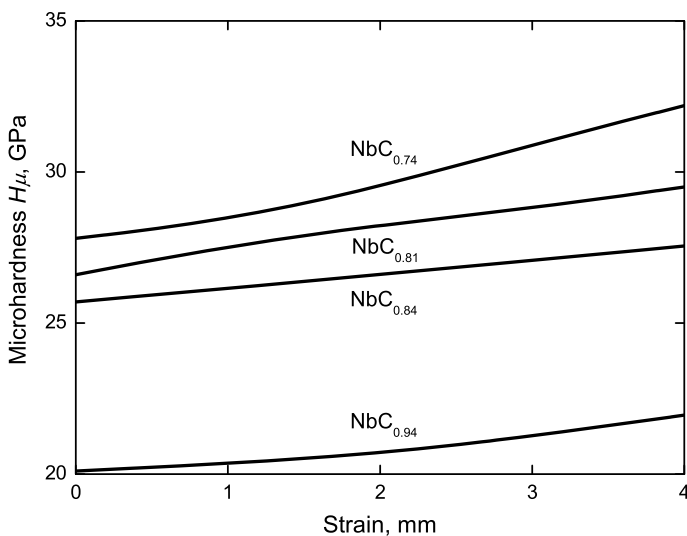


Fig. 4.24 Variations of microhardness H_{μ} (0.5–1.0 N load) at room temperature with preceding high-temperature plastic deformation (strain – bending deflection at 1800–2230 °C, loading time 30 min) for the produced by sintering in vacuum NbC_{1-x} materials (porosity – 2–3%), having different deviations from the stoichiometry [278]

Table 4.10 Microhardness $H\mu$ (HK scale) of niobium monocarbide NbC_{1-x} ($0 < x \leq 0.25$) single crystals at room temperature (1 N load)

Surface	Indentor diagonal direction		Microhardness $H\mu$, GPa	Reference
		$x \approx 0^a$		
(100)	<100>		23.0	[1, 274]
	<110>		23.0	[1, 274]
	<210>		23.0	[1, 274]
(001)	<100>		22.5	[1049, 1050]
	<110>		23.7	[1049, 1050]
		–	23.0 ^{b,c}	[1, 273]
(110)	<100>		22.0	[1, 274]
	<110>		22.0	[1, 274]
	<111>		23.0	[1, 274]
	<112>		23.0	[1, 274]
(111)	<110>		21.0	[1, 274]
	<112>		21.0	[1, 274]
	<123>		21.0	[1, 274]
		$x = 0.025^a$		
(100)	<110>		23.0	[1, 274]
	<210>		23.0	[1, 274]
(110)	<100>		23.0	[1, 274]
	<110>		22.0	[1, 274]
	<111>		23.0	[1, 274]
	<112>		23.0	[1, 274]
(111)	<100>		22.0	[1, 274]
	<110>		21.0	[1, 274]
	<112>		21.0	[1, 274]
	<123>		21.0	[1, 274]
		$x = 0.03\text{--}0.15^a$		
(100)	–		23.1–25.2	[707]
		$x = 0.06$		
(001)	–		27.9 ± 0.5	[1, 275]
	–		27.0 ± 0.5^d	[1, 275]
(110)	–		24.0 ± 0.5	[1, 275]
	–		20.8 ± 0.5^d	[1, 275]
(111)	–		23.8 ± 0.5	[1, 275]
	–		19.9 ± 0.5^d	[1, 275]
		$x = 0.08^e$		
(111)	–		19.8	[1, 276]
		$x = 0.10^{f,g}$		
(100)	<001>		~ 23	[284]
(110)	<001>		~ 24	[284]
(111)	<110>		~ 27	[284]
		$x = 0.13$		
(100)	<100>		17.6 ± 0.8^h	[703]
	<110>		20.0 ± 0.8^h	[703]
	<010>		17.6 ± 0.8^h	[703]
	–		22.2 ^f	[292]

(continued)

Table 4.10 (continued)

Surface	Indenter diagonal direction		Microhardness $H\mu$, GPa	Reference
		$x = 0.14$		
(100)	–		22.0 ^e	[1, 276]
	–		21.6 ± 1.8 ^b	[1, 268]
(102)	–		20.1 ± 1.7 ^b	[1, 268]
(111)	–		20.3 ^e	[1, 276]
		$x = 0.18$		
(100)	<100>		21.2 ± 1.4 ^{b,i}	[87, 179]
	<110>		17.7 ± 1.4 ^b	[87]
	–		22.4 ^e	[1, 276]
		$x = 0.19$		
(100)	<100>		21.7 ± 0.9 ^{b,j}	[2, 87]
(111)	–		20.5 ^e	[1, 276]
		$x = 0.20$		
(100)	<100>		22.4 ± 0.9 ^{b,j}	[2, 87]
	<001>		29.9 ± 0.6 ^f	[283]
	<010>		29.5 ± 0.6 ^f	[283]
	<100>		29.9 ^g	[406]
	<011>		28.3 ± 1.2 ^f	[283]
	<110>		27.9 ^g	[406]
	–		17.5 ^{b,k}	[87, 285]
		$x = 0.21^e$		
(100)	–		22.8	[1, 276]
		$x = 0.22^b$		
(100)	<100>		21.4 ± 0.7 ^l	[2, 87]
		$x = 0.23^e$		
(100)	–		23.0	[1, 276]
(111)	–		21.0	[1, 276]
		$x = 0.25^e$		
(100)	–		23.2	[1, 276]

^aCrystals produced by induction zone melting, contents: non-combined C – 0.05–0.50%, O – 0.05%, N – 0.005%, W – 0.22–0.50%

^bCrystals produced by plasma-arc melting

^c26.5 GPa at –196 °C

^dAnnealed at 2100 °C

^eCrystals produced by arc melting

^fCrystals produced by radio-frequency floating zone process in Ar atmosphere

^g2 N load

^hCrystals produced by diffusion saturation, HV scale, 2 N load

ⁱ HV scale (at 5 N load the measured value is 17.9 ± 0.3 GPa)

^j HV scale (at 5 N load the measured value is 18.3 ± 0.3 GPa)

^k10 N load

^l HV scale (at 5 N load the measured value is 18.1 ± 0.5 GPa)

films $\text{NbC}_{\sim 1.0}$ on titanium (thickness $\sim 0.2 \mu\text{m}$) intrinsic hardness HV is $(18\text{--}21) \pm 1 \text{ GPa}$ (0.1–20 N load) [306], for nanocrystalline films deposited by nonreactive unbalanced DC-magnetron sputtering (thickness 0.5–0.7 μm , mean grain size 12 nm) a maximum hardness is 23 GPa (corresponds to 50 at.% C content) [97] and for films deposited using reactive DC-magnetron sputtering in discharging a mixture of CH_4 and Ar it is $\sim 37 \text{ GPa}$ [98].

Table 4.11 Microhardness $H\mu$ of the various compositions of niobium carbide phases at room temperature

Composition	Microhardness $H\mu$, GPa	Remarks	Reference
$\text{Nb}_{2.38}\text{C}$	18.5 ± 1.1	0.5 N load, sintered in vacuum	[1, 51, 67]
$\text{Nb}_{2.22}\text{C}$	19.2 ± 0.8	0.5 N load, sintered in vacuum	[1, 51, 67]
$\text{Nb}_{2.13}\text{C}$	19.6 ± 0.6	0.5 N load, sintered in vacuum	[1, 51, 67]
$\text{Nb}_{2.04}\text{C}$	20.2 ± 0.6	0.5 N load, sintered in vacuum	[1, 51, 67]
$\text{Nb}_{2.00}\text{C}$	20.4 ± 0.5	0.5 N load, sintered in vacuum	[1, 51, 67]
$\text{Nb}_{\sim 2.0}\text{C}$	26.8	DFT-estimated value	[1097]
	25.8 ± 4.1	Produced by metal carbidization in vacuum	[288]
	24.6 ± 3.1	8 mN load, angular inclusions in U-Nb alloys	[1098]
	20.8 ± 2.0	–	[63, 82]
	20.6	–	[195]
$\text{NbC}_{0.70}$	27.0 ± 1.2	1.0 N load, melted in Ar and annealed in vacuum at 2000 °C for 4 h	[1, 277]
$\text{NbC}_{0.72}$	23.9 ± 0.6	0.5 N load, hot-pressed and annealed in vacuum, porosity – 6–10%, contents: non-combined C – 0.11%	[67, 191]
	20.1	1.0 N load, sintered at 2500–2700 °C, porosity – 10%, contents: non-combined C $\leq 0.01\%$, O $\leq 0.05\%$	[2, 282]
$\text{NbC}_{0.73}$	18.8	0.5 N load, hot-pressed and annealed in vacuum, content non-combined C – 0.15%	[848]
$\text{NbC}_{0.74}$	27.8	0.5–1.0 N load, sintered in vacuum, porosity – 2%	[1, 278]
$\text{NbC}_{0.75}$	21.9 ^a	1.0 N load, sintered in vacuum and annealed, mean grain size – 29 μm , contents: non-combined C – 0.05%, N – 0.27%	[1]
$\text{NbC}_{0.76}$	29.1	The maximal value on cross-section of stock materials	[735, 736, 907]
	25.1 ± 0.8	0.5 N load, hot-pressed and annealed in vacuum, porosity – 6–10%, contents: non-combined C – 0.13–0.19%, O – 0.006%, N – 0.05%	[1, 67, 191]
$\text{NbC}_{0.80}$	28.0 ± 1.0	1.0 N load, melted in Ar and annealed in vacuum at 2000 °C	[1, 277]

(continued)

Table 4.11 (continued)

Composition	Microhardness $H\mu$, GPa	Remarks	Reference
NbC _{0.81}	26.6	0.5–1.0 N load, sintered in vacuum, porosity – 2%	[278]
	22.0	1.0 N load, sintered in vacuum and annealed, porosity – 12%, mean grain size – 14 μm , contents: non-combined C – 0.05%, O – 0.07%, N – 0.38%	[1]
	20.0	0.5 N load, hot-pressed and annealed in vacuum, content non-combined C – 0.23%	[848]
NbC _{0.82}	25.2 \pm 1.0	0.5 N load, hot-pressed and annealed in vacuum, porosity – 6–10%, contents: non-combined C – 0.15–0.18%, O – 0.10%, N – 0.03%	[1, 67, 191, 209]
NbC _{0.83}	25.5	Produced by carbon diffusion saturation	[2, 281]
NbC _{0.84}	25.7	0.5–1.0 N load, sintered in vacuum, porosity – 3%	[278]
	24.0 ^b	1.0 N load, sintered in vacuum and annealed, porosity – 11%, mean grain size – 18 μm , contents: non-combined C – 0.05%, O – 0.08%, N – 0.39%	[1]
NbC _{0.85}	26.5 \pm 1.2	1.0 N load, melted in Ar and annealed in vacuum at 1800 °C	[1, 277]
NbC _{0.86}	21.4	1.0 N load, sintered at 2500–2700 °C, porosity – 12.5%, contents: non-combined C \leq 0.01%, O \leq 0.05%	[2, 282]
NbC _{0.87}	21.0 \pm 2.2	0.2–1.5 N load, hot-pressed and annealed at 1800 °C for 3 h, porosity – 18%, content: non-combined C – 0.09%	[289, 290]
NbC _{0.88}	24.5	0.5 N load, hot-pressed and annealed in vacuum, content non-combined C – 0.19%	[848]
NbC _{0.89}	19.2 \pm 0.9	Produced by carbon diffusion saturation	[82, 281]
NbC _{0.90}	23.0 \pm 1.2	1.0 N load, melted in Ar and annealed in vacuum at 1800 °C	[1, 277]
NbC _{0.91}	26.5	0.5 N load, hot-pressed and annealed in vacuum, content non-combined C – 0.52%	[848]
	24.8 \pm 1.0	0.5 N load, hot-pressed and annealed in vacuum, porosity – 6–10%	[209]
	22.0	1.0 N load, sintered at 2500–2700 °C, porosity – 2%, contents: non-combined C \leq 0.01%, O \leq 0.05%	[2, 282]
NbC _{0.92}	23.6 \pm 0.9	0.5 N load, hot-pressed and annealed in vacuum, porosity – 6–10%, contents: non-combined C – 0.18%, O – 0.10%, N – 0.03%	[1, 67, 191]
	18.0 ^c	1.0 N load, sintered in vacuum and annealed, porosity – 7%, mean grain size – 12 μm , contents: non-combined C – 0.05%, O – 0.07%, N – 0.32%	[1]
NbC _{0.93}	15.7	Produced by carbon diffusion saturation	[2, 281]
NbC _{0.94}	20.1	0.5–1.0 N load, sintered in vacuum, porosity – 3%	[1, 278]
NbC _{0.95}	21.1	1.0 N load, sintered at 2400 °C, porosity \sim 10–30%, contents: non-combined C – 0.35%, O – 0.05%, N – 0.005%, W – 0.22%	[707]
	20.0	1.0 N load, sintered at 2500–2700 °C, porosity – 6%, contents: non-combined C \leq 0.01%, O \leq 0.05%	[2, 282]

(continued)

Table 4.11 (continued)

Composition	Microhardness $H\mu$, GPa	Remarks	Reference
NbC _{0.96}	16.7 ± 1.0	1.0 N load, sintered at 2500–2700 °C, porosity – 10%, contents: non-combined C ≤ 0.01%, O ≤ 0.05%	[2, 282]
NbC _{0.97}	18.6 ± 1.0	1.0 N load, produced by carbon diffusion saturation (carbideization) of pure metal, contents: O – 0.05%, N – 0.06%	[1, 2, 279]
NbC _{0.98}	14.3 ± 1.0	Produced by carbon diffusion saturation	[2, 281]
	21.2	Deposited from gas phase	[1, 280]
	20.0 ± 1.2	1.0 N load, melted in Ar and annealed in vacuum at 1800 °C	[1, 277]
NbC _{0.99}	20.0 ± 1.0	0.5 N load, hot-pressed and annealed in vacuum, porosity – 6–10%	[209]
	13.8 ± 0.8	Pyrolytic materials	[779]
	23.5	Sintered materials	[769]
	21.3 ± 1.3	0.5 N load, hot-pressed and annealed in vacuum, porosity – 6–10%, contents: non-combined C – 0.25%, O – 0.03%, N – 0.01%	[1, 67, 191]
NbC _{~1.0}	15.0 ^d	1.0 N load, sintered in vacuum and annealed, porosity – 7%, mean grain size – 12 μm, contents: non-combined C – 0.07%, O – 0.05%, N – 0.45%	[1]
	24.5	Recommended value	[295, 778]
	24.2 ^e	The highest value for materials sintered in vacuum (with fugitive binder), porosity – 1–5%	[177, 333]
	24.1	Derived from first principles calculations	[154]
	24.0	–	[7, 722, 724]
	23.5	0.5–1.0 N load	[104, 177, 189, 286]
	23.0 ^f	Nanocrystalline coatings deposited by dual DC magnetron sputtering, thickness – 0.5–0.7 μm, ~15% amorphous carbon phase	[97]
	~23 ^g	1.0 N load, arc-cast	[294]
	22.7 ± 3.3	Produced by metal carbideization in vacuum	[288]
	22.5	Calculated theoretically on the basis of Gao's model	[301, 780]
	21.9	First-principles calculated	[955]
	(21.0–21.6) ± (1.2–2.2)	–	[10, 287]
	20.1	–	[1051]
20.0	–	[64, 726, 905]	
19.6	Averaged on the basis of several sources	[84, 110, 291, 293]	
19.2	0.3 N load	[65, 170]	
19.1 ^h	In contact with graphite phase	[773]	
18.7	Calculated theoretically on the basis of Šimůnek model	[301, 781]	

(continued)

Table 4.11 (continued)

Composition	Microhardness $H\mu$, GPa	Remarks	Reference
	18.6 ⁱ	0.6–0.8 N load, hot-pressed, porosity – 7%	[343]
	(18.0–21.0) \pm 1.0	0.1–19.6 N load, electron beam deposited thin films on Ti substrate, thickness – 0.2 μ m	[306]
	18.0	–	[178, 299]
	18.3	Calculated theoretically on the basis of Šimůnek-Vackář's model	[302, 304]
	17.6–19.6	–	[301, 302]
	17.5 \pm 0.8	Produced by metal fibre carbidization	[1]
	16.8 \pm 0.9	2.0 N load, hot-pressed, porosity <2%	[322, 323]
	16.1	Calculated theoretically on the basis of Tian's model	[301–303]
	14.9 ^j	0.2–10 N load, hot-pressed, porosity <5%	[702]
	12.7 (?)	–	[725]

^a3.9 GPa – at 1000 °C

^b4.3 GPa – at 1000 °C

^c3.7 GPa – at 1000 °C

^d3.5 GPa – at 1000 °C

^eKnoop measurement (HK)

^fNanoindentation with a depth set to 50 nm and loading rate – 3mN min⁻¹

^gFor 10 N load with boron carbide indenter: 4.0 GPa – at 1000 °C and 0.8 GPa – at 1800 °C

^hDiamond pyramid hardness measurement (DPH)

ⁱ5.3 GPa at – 1000 °C and 2.0 GPa – at 1700 °C

^jDetermined in accordance with the formula: $H\mu = 18.18P/d^2$, where P is the load on the indenter, N and d is the diagonal of the indentation, μ m; the values of other micromechanical characteristics: microbrittleness $\gamma_\mu = (D^2 - d^2)/d^2 = 0.75$, where D is the average size of the damageability zone, μ m and brittle microstrength $\sigma_\mu = P/D^2 = 4.6$ GPa [702]

On the basis of several sources the variations of ultimate tensile σ_t , flexural (bending) σ_f and compressive σ_c strengths of niobium monocarbide NbC_{1-x} materials with temperature and carbon content within the homogeneity range are shown in Figs. 4.25–4.28. The compressive strength of $NbC_{\sim 1.0}$ crystallites is at least 24 ± 4 GPa at a confining pressure of 57 ± 0.5 GPa [379]. The approximate relationship of $\sigma_t : \sigma_f : \sigma_c = 1 : (1.5\text{--}2.0) : (8\text{--}10)$ can be recommended for the general estimations of the strength characteristics of NbC_{1-x} materials [727, 732, 736]. At ambient temperatures niobium monocarbide NbC_{1-x} materials exhibit fracture toughness K_{IC} of 6.0–8.6 MPa m^{1/2} (for hot-pressed nanostructured materials $NbC_{\sim 1.0}$, porosity – 2%, mean grain size – 76 nm) [321, 902], 4.0 MPa m^{1/2} (for sintered $NbC_{0.96}$, contents: O \leq 0.05%, N – 0.05%, W – 0.2–0.3%) [731] and 3.5–3.8 (for $NbC_{\sim 1.0}$ single crystals) [1, 2, 273, 317]; apparently fracture toughness of single crystals decreases with carbon content decreasing within the homogeneity range as for single crystal $NbC_{0.80}$ (001) it is 2.8 MPa m^{1/2} [1, 2, 87, 285]. Toughness K_{IC} declines with the temperature growth to

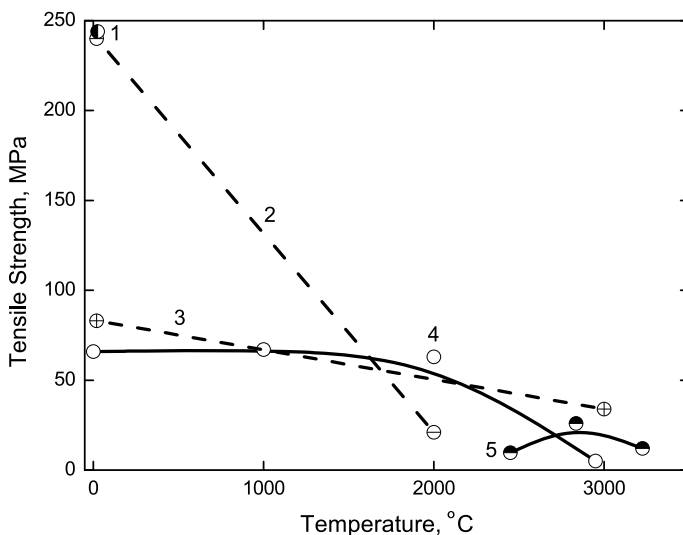


Fig. 4.25 Variation of tensile strength of near-stoichiometric niobium monocarbide NbC_{1-x} with temperature on the basis of several sources: 1 – [338, 340]; 2 – [170, 311]; 3 – [10, 11]; 4 – sintered, 30% porosity [1, 2, 67, 309]; 5 – sintered, corrected to the poreless state [310] (the value of first-principles calculated ideal tensile strength for quasi-stoichiometric NbC_{1-x} is 72.5 GPa [955])

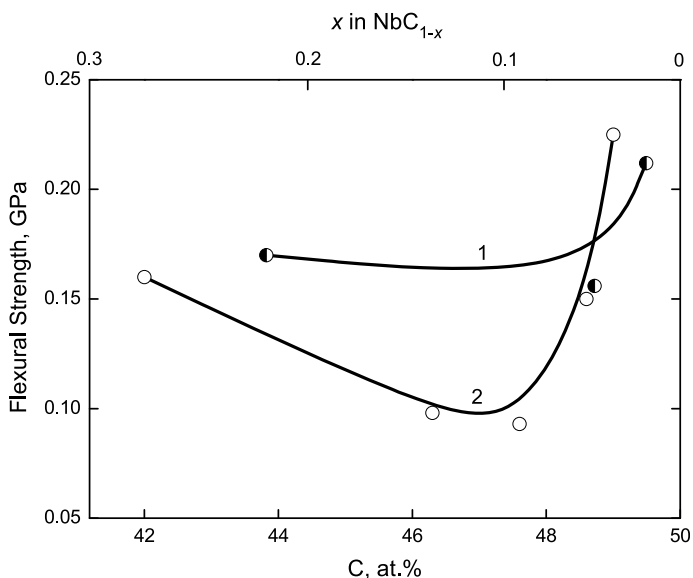


Fig. 4.26 Variation of the flexural (bending) strength at room temperature of sintered niobium monocarbide NbC_{1-x} materials with deviation from the stoichiometry within the homogeneity range: 1 – porosity 6–24%, mean grain size 8–23 μm , content non-combined C 0.05–1.0% [315]; 2 – porosity 2–13%, content O < 0.05% [2, 282]

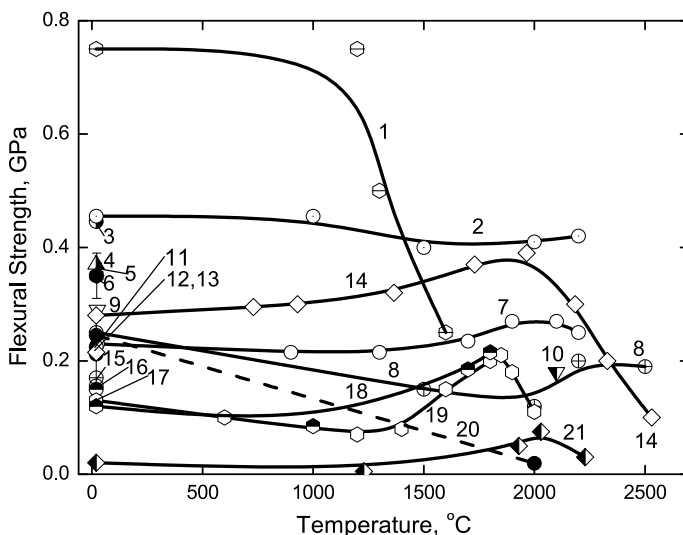


Fig. 4.27 Variation of flexural (bending) strength of near-stoichiometric niobium monocarbide NbC_{1-x} materials with temperature on the basis of several sources: 1 – $\text{NbC}_{0.84}$, single crystal materials produced by plasma-arc melting and cut off along the $\langle 100 \rangle$ axis, 3-point bending scheme, measured in vacuum ($\leq 1.3 \times 10^{-2}$ Pa) [1, 268, 273]; 2 – $\text{NbC}_{0.97}$ produced by metal right-through saturation in Ar atmosphere, cylinder specimen with 0.6 mm diameter, 3-point bending scheme [1, 313]; 3 – $\text{NbC}_{0.97}$ produced by metal carburization (saturation), mean grain size – 350–450 μm , contents: O + N – 0.1% [2, 279]; 4 – [336]; 5 – sintered materials, porosity – 3–5% [1, 314]; 6 – hot-pressed materials, porosity < 2%, 4-point bending scheme (Weibull modulus $m = 9$) [322, 323]; 7 – sintered materials, porosity – 8–10% [2, 312]; 8 – $\text{NbC}_{0.97}$ produced by metal right-through saturation in Ar atmosphere, $0.6 \times 20 \times 25$ mm plate, 3-point bending scheme [1, 313]; 9 – porosity 7–15%, 3-point bending scheme [200, 338]; 10 – [335]; 11 – sintered $\text{NbC}_{0.96}$, porosity – 6%, content O < 0.05% [2, 282]; 12 – sintered $\text{NbC}_{0.98}$, porosity – 6%, mean grain size – 8 μm , contents: non-combined C – 1% [2, 315]; 13 – sintered materials, porosity – 8%, mean grain size – 15 μm , cylinder 3 mm diameter, 4-point bending scheme with 80 mm base (Weibull modulus $m = 3.8$) [727]; 14 – sintered materials [735, 736]; 15 – sintered $\text{NbC}_{0.76}\text{O}_{0.02}\text{N}_{0.01}$, porosity – 20%, mean grain size – 23 μm , content non-combined C – 0.05% [2, 315]; 16 – sintered $\text{NbC}_{0.96}\text{O}_{0.02}$, porosity – 24%, mean grain size – 17 μm , content non-combined C – 0.24% [2, 315]; 17 – sintered $\text{NbC}_{0.945}$, porosity – 5%, content: O < 0.05% [2, 282]; 18 – sintered materials, annealed at 2000 °C for 10 min [1, 316]; 19 – sintered materials, non-annealed [1, 316]; 20 – sintered materials, porosity – 4% [177]; 21 – hot-pressed (low-porous) materials [785, 786] (the values of first-principles calculated ideal tensile and shear strengths for quasi-stoichiometric NbC_{1-x} are 72.5 and 82 GPa, respectively [955])

3.2 $\text{MPa m}^{1/2}$ at 500 °C [273] and up to 1.8–2.0 $\text{MPa m}^{1/2}$ at 900 °C [1, 2]. The first-principles calculated ideal fracture toughness K_{IC} of quasi-stoichiometric NbC_{1-x} is ~ 5.0 $\text{MPa m}^{1/2}$ [955]. The reported values for ductile-to-brittle transition temperatures of NbC_{1-x} phases with various deviations from the stoichiometry are listed in Table 4.12. The values of prolonged strength are very important for the evaluation of operational time of components at high and ultra-high temperatures. The tensile and flexural (bending) steady-state creep isotherms of sintered niobium

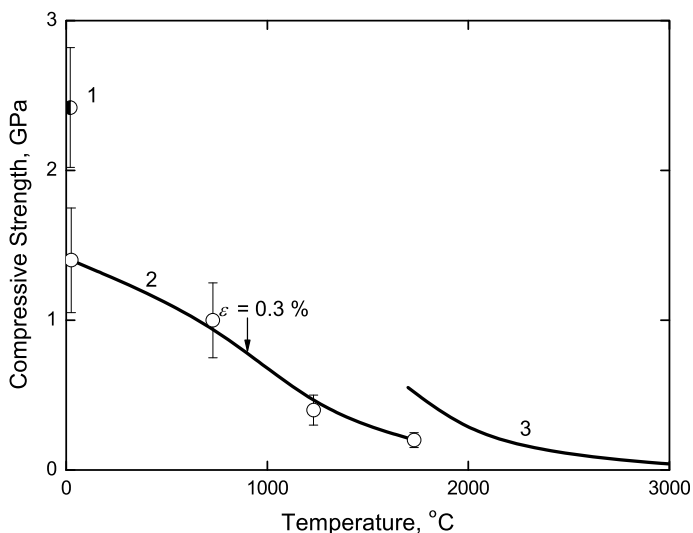


Fig. 4.28 Variation of compressive strength of near-stoichiometric niobium monocarbide NbC_{1-x} materials with temperature: 1 – low-porous $\text{NbC}_{\sim 1.0}$ [1, 2, 10, 11, 63, 67, 170, 338], 2 – $\text{NbC}_{\sim 1.0}$ [5], 3 – $\text{NbC}_{0.94}$ [10, 11] (approximate compression fracture deformation ε is indicated at 900 °C)

Table 4.12 Ductile-to-brittle transition temperatures of niobium monocarbide phases NbC_{1-x} ^{a,b}

Composition	Temperature, K (°C)	Characteristics	Reference
$\text{NbC}_{\sim 1.0}$	1470 (1200)	Single crystals ^c	[273]
$\text{NbC}_{0.95}$	1750 (1480)	Hot-pressed and annealed (porosity $\sim 7.5\%$)	[2, 318]
$\text{NbC}_{0.84}$	1470 (1200)	Single crystals	[1, 268]
$\text{NbC}_{0.77}$	1270–1320 (1000–1050)	Single crystals	[320]
$\text{NbC}_{0.76}$	1270–1370 (1000–1100)	Single crystals ^d	[319, 410]
	1470 (1200)	Single crystals	[2, 268]

^aFor near-stoichiometric NbC_{1-x} the following average values were estimated: Peierls stress $\tau_p = 6.3$ GPa, shear modulus – Peierls stress ratio $\tau_p/G = 0.037$ and slip activation energy barrier $q = 1.5$ eV [739]

^bAccording to Lanin [727, 732], with increasing porosity from 7 to 60% the ductile-to-brittle transition temperatures of NbC_{1-x} materials enlarge by 400 K at flexural (bending) testing and by 600–700 K at compression testing

^cBased on flexural (bending) strength testing

^dBased on compression strength testing

monocarbide NbC_{1-x} materials within the homogeneity range are given in Fig. 4.29, the examples of intermediate-, high- and ultra-high temperature steady-state creep rate $d\epsilon/dt$ variations for near-stoichiometric niobium monocarbide NbC_{1-x} materials with applied stress and temperature are demonstrated in Figs. 4.30 and 4.31; steady-state creep activation energies Q and exponent constants n (see Eq. (I-3.17)) for various NbC_{1-x} phases are listed in Table 4.13. Approximately, the following main dominating creep mechanisms can be established in some overlapping parametric ranges for niobium monocarbide NbC_{1-x} materials with certain changes within the homogeneity range [328, 330, 787–789]:

- vacancy-diffusional (or Nabarro-Herring) mechanism controlled by the bulk diffusion of metal in carbide (at temperatures from 2300 to 3000 °C and applied stresses from 7 to 30 MPa, with $Q \approx 450\text{--}550 \text{ kJ mol}^{-1}$ and $n = 1$);
- dislocation-diffusional mechanism controlled by the bulk diffusion of metal in carbide (at 2300–3000 °C and 30–70 MPa, with $Q \approx 450\text{--}550 \text{ kJ mol}^{-1}$ and $n \approx 3\text{--}4$);
- viscous dislocation sliding mechanism controlled by the bulk diffusion of carbon in carbide (at 1800–2200 °C and 50–200 MPa, with $Q \approx 330\text{--}350 \text{ kJ mol}^{-1}$ and $n \approx 2.5\text{--}3.5$).

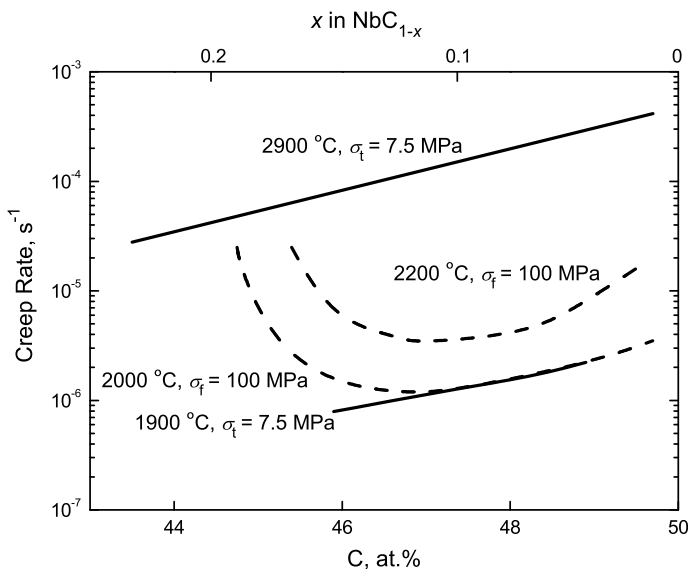


Fig. 4.29 Tensile and flexural (bending) steady-state creep isotherms of sintered niobium monocarbide NbC_{1-x} materials with deviation from stoichiometry within the homogeneity range at various temperatures and stresses [1, 3, 269, 281, 324, 330]

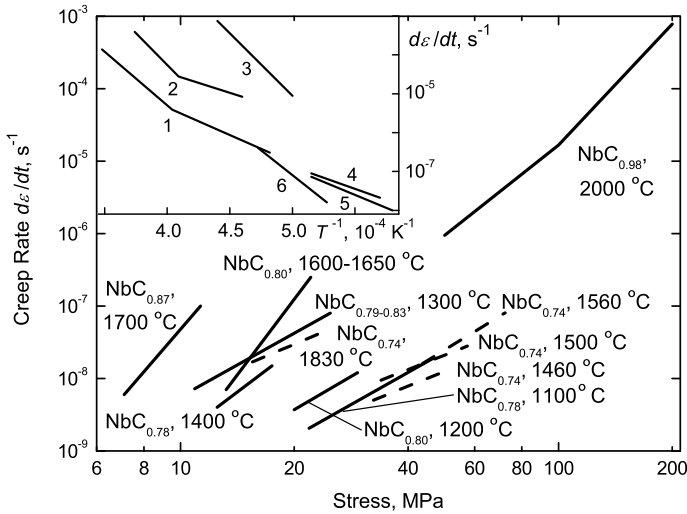


Fig. 4.30 Intermediate- and high-temperature steady-state creep rate $d\varepsilon/dt$ variations of near-stoichiometric niobium monocarbide NbC_{1-x} materials with applied stress on the basis of several sources: $\text{NbC}_{0.74}$ isostatically hot-pressed, porosity $\sim 0.5\%$, mean grain size $\sim 25 \mu\text{m}$, under compressive load at 1460, 1500, 1560 and 1830 °C [342]; $\text{NbC}_{0.78}$, $\text{NbC}_{0.79-0.83}$, $\text{NbC}_{0.80}$ and $\text{NbC}_{0.87}$ single crystals produced by floating zone technique, contents: Ta $\sim 0.08\%$, other impurities (in total) $\sim 0.005\%$, density of dislocations $\sim 2.6 \times 10^9 \text{ m}^{-2}$, under compressive load at 1100, 1200, 1300, 1400, 1600–1650 and 1700 °C [320]; $\text{NbC}_{0.98}$ sintered, porosity $\sim 2\%$, mean grain size $\sim 20 \mu\text{m}$, contents: non-combined C $\sim 0.08\%$, O $\sim 0.05\%$, N $\sim 0.01\%$, W $\sim 0.55\%$, under compressive load at 2000 °C [327, 328] (Inset – variations with temperature: $\text{NbC}_{0.98}$ sintered, porosity $\sim 2\%$, mean grain size $\sim 20 \mu\text{m}$, contents: non-combined C $\sim 0.08\%$, O $\sim 0.05\%$, N $\sim 0.01\%$, W $\sim 0.55\%$, under compressive load of: 1 – 60, 2 – 100 and 3 – 200 MPa [327, 328] and $\text{NbC}_{0.74}$ isostatically hot-pressed, porosity $\sim 0.5\%$, mean grain size $\sim 25 \mu\text{m}$, under compressive load of: 4 – 54, 5 – 48 and 6 – 64 MPa [342]; in $d\varepsilon/dt, \text{ s}^{-1} - 1/T, \text{ K}^{-1}$ scale)

At room temperature the values of Young's E , Coulomb's (shear) G and bulk (compression) K moduli, volume compressibility κ and Poisson's ratio ν of sub- and near-stoichiometric niobium monocarbide NbC_{1-x} materials lie within the areas: $E = 280\text{--}580 \text{ GPa}$ [1–3, 28, 84, 193, 282, 338, 346, 350–352, 741], $G = 140\text{--}250 \text{ GPa}$ [2, 3, 84, 193, 282, 338, 346–348, 351, 352, 893], $K = 300\text{--}380 \text{ GPa}$ [2, 3, 193, 338, 346, 348, 349, 351], $\kappa = 3.26\text{--}3.38 \text{ TPa}^{-1}$ [1–3, 353] and $\nu = 0.21\text{--}0.24$ [2, 3, 193, 282, 338, 348, 351, 352] (see also Table 4.14); while for near-stoichiometric niobium semicarbide $\text{Nb}_{2\pm x}\text{C}$ the estimated value of E is 410 GPa [1, 345], the mean elastic modulus E of angular inclusions of Nb_2C in U-Nb alloys measured by nanoindentation was $247 \pm 24 \text{ GPa}$ [1098], the DFT-calculated moduli for $\alpha\text{-Nb}_2\text{C}$ ($Pnma$) are $E = 307 \text{ GPa}$, $K = 226 \text{ GPa}$, $G = 121 \text{ GPa}$ and $\nu = 0.27$ [154], or $E = 427 \text{ GPa}$, $K = 236 \text{ GPa}$, $G = 178 \text{ GPa}$ and $\nu = 0.19$ [1097], for $\alpha\text{-Nb}_2\text{C}$ (Pm) the values are $E = 221 \text{ GPa}$, $G = 84 \text{ GPa}$, $K = 203 \text{ GPa}$ and $\nu = 0.31$ [405], for $\beta\text{-Nb}_{2+x}\text{C}$ ($P(-3)m1$): $E = 310 \text{ GPa}$, $K = 229 \text{ GPa}$, $G = 122 \text{ GPa}$ and $\nu = 0.27$ [405], and the values of K estimated by Abderrahim et al. [358] for α -, β - and γ -modifications of niobium semicarbide are

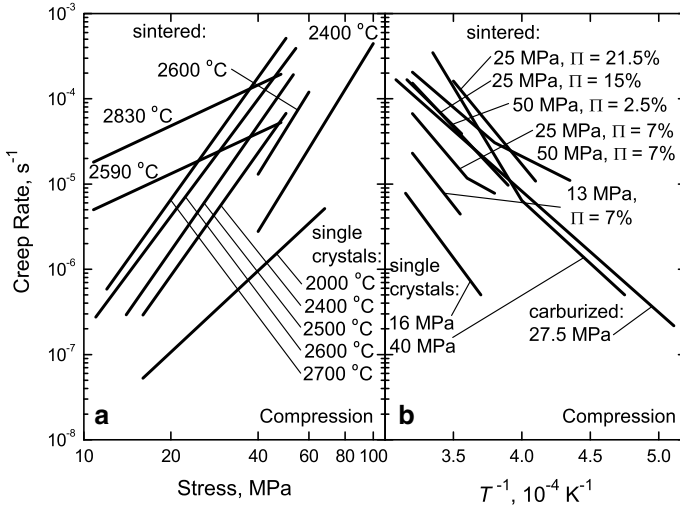


Fig. 4.31 High- and ultra-high temperature steady-state creep rate variations of near-stoichiometric niobium monocarbide NbC_{1-x} materials on the basis of several sources: (a) – with applied stress ($\text{NbC}_{0.90-0.94}$ sintered in vacuum, porosity – 7%, mean grain size – 15 μm , rate after 10 min testing under compressive load at 2590 and 2830 $^{\circ}\text{C}$ [329]; $\text{NbC}_{0.98}$ sintered, porosity – 2%, mean grain size – 20 μm , contents: non-combined C – 0.08%, O – 0.05%, N – 0.01%, W – 0.55%, under compressive load at 2400 and 2600 $^{\circ}\text{C}$ [327, 328]; $\text{NbC}_{\sim 1.0}$ single crystal materials, steady-state creep along the $\langle 110 \rangle$ direction under compressive load at 2000, 2400, 2500, 2600 and 2700 $^{\circ}\text{C}$ [326]) and (b) – with temperature ($\text{NbC}_{0.90-0.94}$ sintered in vacuum with porosity – 2.5–21.5% and mean grain size – 8–36 μm , rate after 10–30 min testing under compressive load of 13, 25 and 50 MPa [329, 332]; $\text{NbC}_{\sim 1.0}$ single crystal materials, steady-state creep along the $\langle 110 \rangle$ direction under compressive load of 16 and 40 MPa [326]; $\text{NbC}_{\sim 1.0}$ metal-carburized materials under compressive load of 27.5 MPa [338, 341])

Table 4.13 Formal creep characteristics (activation energy Q , stress exponent constant n) of niobium monocarbide phases NbC_{1-x} at various temperature and applied stress ranges

Composition	Load type ^a	Temperature range, $^{\circ}\text{C}$	Applied stress range, MPa	Activation energy ^b , Q , kJ mol^{-1}	Exponent constant ^b , n	Reference
$\text{NbC}_{\sim 1.0}$	–	Low temp.	–	~ 360	3.0	[893]
	–	High temp.	–	~ 500	4.8	[893]
$\text{NbC}_{0.89-0.98}^c$	T, F, C ^d	<2350	–	330–345	2.8–3.2	[324, 325]
$\text{NbC}_{0.925}^c$	T, F, C ^d	>2350	$\sigma < \sigma_{\text{th}}^e$	525	1 ^f	[324, 325]
	T, F, C ^d	>2350	$\sigma > \sigma_{\text{th}}^e$	525	3.4–3.7	[324, 325]
$\text{NbC}_{0.98}^g$	C	1700–2200	60–100	240	3.7	[327, 328]
	C	1700–2000	200	~ 600	5.4	[327, 328]
	C	2200–2600	60–200	~ 600	5.4	[327, 328]
$\text{NbC}_{0.97}^h$	T	2500–2900	1.5–8.5	450 ± 20	1	[2, 281]
$\text{NbC}_{0.93}^h$	T	2500–2900	1.5–8.5	450 ± 20	1	[2, 281]
$\text{NbC}_{0.89}^h$	T	2500–2900	1.5–8.5	590 ± 30	1	[2, 281]
$\text{NbC}_{0.83}^h$	T	2500–2900	1.5–8.5	420	1	[2, 281]
$\text{NbC}_{0.96}$	T	2600–2900	–	565	1	[281, 344]
$\text{NbC}_{0.90-0.94}^i$	C	2430–2930	51	345 ± 15	1.66	[329]
	C	2430–2930	25	390 ± 15	1.66	[329]
	C	2430–2930	13	500 ± 15	1.66	[329]

(continued)

Table 4.13 (continued)

Composi- tion	Load type ^a	Temperature range, °C	Applied stress range, MPa	Activation energy ^b , Q , kJ mol ⁻¹	Exponent constant ^b , n	Reference
NbC _{0.92-0.93} ^j	C	2300–3000	7–40	520	1	[2, 330]
	C	2300–3000	40–70	520	3.7	[2, 330]
	F	1800–2200	50–200	340	2.9	[330]
NbC _{0.92} ^k	C	2550–3100	20–100	360 ± 20	–	[331, 332]
NbC _{0.89} ^l	C	1800–2200	12–80	335 ± 35	3.3 ± 0.1	[326, 330]
	C	2200–2700	12–80	500 ± 40	4.8 ± 0.3	[326, 330]
NbC _{0.78-0.80} ^m	C	1100–1200	20–40	–	3.0–3.2	[320, 710]
NbC _{0.78-0.83} ⁿ	C	1300–1400	10–25	290	3.0–4.5	[320, 710]
NbC _{0.78-0.87} ^m	C	1400–1700	7–25	~550	6.2–6.8	[320, 710]
NbC _{0.74} ⁿ	C	1450–1830	16–55	230–250	2	[342, 691]
	C	1560–1830	55–70	470	3.2	[342, 691]
NbC _{0.90} ^o	H	1000–1500	–	320–420	3.2–4.7	[283, 284]
NbC _{0.80} ^p	H	1000–1500	–	380	3.9	[283, 284]
NbC _{0.98} ^q	F	1800–2200	50–200	335	2.8	[330]
NbC _{0.98}	F	2465–2685	10	645	–	[657, 658]
NbC _{0.91}	F	2430–2775	10	580	–	[657, 658]
NbC _{0.89} ^r	F	1800–2200	50–200	330	3.1	[330]
NbC _{0.86}	F	2305–2775	10	475	–	[657, 658]
NbC _{0.81}	F	2305–2775	10	515	–	[657, 658]
NbC _{0.76}	F	2250–2685	10	410	–	[657, 658]
NbC _{0.71}	F	2190–2580	10	350	–	[657, 658]

^aDenoted: T – tension, F – flexure (bending), C – compression, H – hot hardness (measurement)

^bFor Q and n see Eq. (I-3.17) and consideration in [893]

^cPorosity – 3–4%, mean grain size $L = 12$ – 20 μm

^dNo effect of the character of loading on the creep mechanism and rate

^e σ_{th} – threshold value of stress

^fCreep rate $d\epsilon/dt \sim 1/L^2$

^gSintered, porosity – 2%, mean grain size – 20 μm, contents: non-combined C – 0.08%, O – 0.05%, N – 0.01%, W – 0.55%

^hProduced by metal right-through saturation, mean grain size $L = 130$ μm

ⁱSintered in vacuum, porosity – 7–15%, mean grain size $L = 7$ – 12 μm ($n = 2.3$ for samples with porosity – 21.5%, mean grain size $L = 8$ μm and $n = 2.5$ for samples with porosity – 32.5%, mean grain size $L = 3$ – 4 μm)

^jSintered in vacuum, porosity 3–4%, mean grain size $L = 20$ μm

^kSintered in vacuum, porosity – 2%, mean grain size $L = 36$ μm, contaminated with 1.4% WC

^lSingle crystals produced by zone refining, contents: non-combined C ≤ 0.05%, N – 0.01%, Si – 0.03%

^mSingle crystals produced by floating zone technique, contents: Ta – ~0.08%, other impurities (in total) – ~0.005%, density of dislocations – ~ 2.6×10^9 m⁻²

ⁿIsostatically hot-pressed (HIP), porosity – ~0.5%, mean grain size $L = 25$ μm

^oSingle crystal prepared by floating-zone process, data summarized from plane directions (100) <001>, (110) <001> and (111) <110>

^pSingle crystal prepared by floating-zone process, plane direction – (100) <001>

^qSintered, porosity 3–4%, mean grain size $L = 12$ μm

^rSintered, porosity 3–4%, mean grain size $L = 18$ μm

Table 4.14 Elastic properties (stiffness coefficients c_{11} , c_{12} and c_{44} , Young's modulus E , bulk (compression) modulus K , Poisson's ratio ν)^a of niobium monocarbide phases NbC_{1-x}

Composition	Stiffness coefficients c_{ij}			Young's modulus E , GPa	Bulk modulus K , GPa	Poisson's ratio ν	Reference
	c_{11} , GPa	c_{12} , GPa	c_{44} , GPa				
$\text{NbC}_{0.72}^{\text{b}}$	–	–	–	330	–	–	[1, 360]
$\text{NbC}_{0.73}$	–	–	–	342 ^c	189 ^c	–	[2]
$\text{NbC}_{0.75}$	–	–	–	372 ^{b,d}	–	0.21	[2, 282]
	–	–	–	365 ± 7 ^e	–	–	[1, 361]
	542 ^f	–	148 ^f	–	–	–	[369]
	512 ^g	150 ^g	109 ^g	345 ^{g,h}	270 ^{g,h}	–	[393]
	–	–	–	–	227	–	[883]
$\text{NbC}_{0.77}$	–	–	–	385 ^{b,i}	231 ⁱ	–	[1, 2, 360]
	–	–	–	360 (320) ^j	–	–	[1, 352]
$\text{NbC}_{0.80}$	–	–	–	363 ^{b,k}	–	0.23	[2, 282]
	–	–	–	–	225	–	[883]
$\text{NbC}_{0.81}^{\text{l}}$	–	–	–	367 ± 7	221	0.22	[2, 361]
$\text{NbC}_{0.83}^{\text{b}}$	–	–	–	430 ^m	273 ^m	–	[1, 2, 360]
$\text{NbC}_{0.84}^{\text{n}}$	–	–	–	377 ± 7	298	0.245	[1, 2, 361]
$\text{NbC}_{0.86}$	–	–	–	333 ^{b,o}	–	0.23	[2, 282]
	–	–	–	366 ^b	206	0.23	[704]
	–	–	–	–	210	–	[883]
$\text{NbC}_{0.865}^{\text{f}}$	566	117	153	438 ^p	267 ^p	0.23	[369, 394]
$\text{NbC}_{0.875}^{\text{g}}$	608	126	153	452 ^q	287 ^q	–	[393]
$\text{NbC}_{0.88}^{\text{b}}$	–	–	–	368 ^r	–	0.24	[2, 282]
$\text{NbC}_{0.885}$	–	–	–	540	–	–	[59]
$\text{NbC}_{0.90}^{\text{b}}$	–	–	–	466 ^r	300 ^r	–	[1, 2, 360]
$\text{NbC}_{0.90}^{\text{s}}$	413	111	206	–	–	–	[370]
$\text{NbC}_{0.91}$	–	–	–	450 (440) ^{h,j}	–	–	[1, 352]
	–	–	–	428 ^b	255	0.23	[704]
	–	–	–	–	260	–	[883]
$\text{NbC}_{0.92}$	–	–	–	348 ± 7 ^t	217 ^t	0.23	[2, 361]
	–	–	–	435 (395) ^j	–	–	[1, 352]
$\text{NbC}_{0.95}$	–	–	–	475 ^{b,u}	–	0.22	[2, 282]
	–	–	–	478 ^v	–	–	[355]
	–	–	–	500 ^w	–	–	[1, 352]
$\text{NbC}_{0.96}$	–	–	–	489 ^x	303 ^x	0.23	[348, 351]
	–	–	–	494 ^{b,y}	–	0.22	[2, 282]
	–	–	–	500 ^b	302	–	[1, 7, 905]
	–	–	–	370 ^z	–	–	[731]
	–	–	–	–	300	–	[883]

(continued)

Table 4.14 (continued)

Composition	Stiffness coefficients c_{ij}			Young's modulus E , GPa	Bulk modulus K , GPa	Poisson's ratio ν	Reference
	c_{11} , GPa	c_{12} , GPa	c_{44} , GPa				
NbC _{0.97}	–	–	–	504 ^{a1}	296 ^{a1}	0.22	[193, 353]
	–	–	–	505 (460) ^j	–	–	[1, 352]
	–	–	–	518 ^{a2}	301 ^{a2}	0.21	[346, 353]
	–	–	–	495 ^b	–	–	[1, 360]
NbC _{0.98}	–	–	–	510 (490) ^{b,j}	–	0.21 (0.23) ^j	[1, 7, 357]
	–	–	–	477 ^{a5}	312 ^{a5}	0.24	[2, 3, 360]
NbC _{0.99}	–	–	–	470 ^{a5}	305 ^{a5}	0.24	[2, 364]
	–	–	–	469 ± 8 ^{a6}	300 ^{a6}	0.24	[1, 2, 361]
NbC _{~1.0}	–	–	–	421 ^{a7}	–	–	[1, 27]
	–	–	–	569 ^{a8}	–	–	[362, 408]
	–	–	–	338 ^{a9}	–	–	[7, 363, 374, 724, 1054]
	–	–	–	539–540 ^{a9}	–	0.10 (?)	[5, 346, 350]
	–	–	–	274 ^{b1}	–	–	[170]
	–	–	–	340	–	0.22	[80, 722]
	–	–	–	333	–	–	[195]
	–	–	–	580	–	–	[299]
	–	–	–	–	320	–	[365]
	620 ^{b2}	200 ^{b2}	150 ^{b2}	441	302	0.28	[366, 367, 396, 398]
	–	–	–	–	376 ^{b3}	–	[349]
	–	–	–	–	296 ^{b4}	–	[349]
	–	–	–	–	326 ^{b5}	–	[371]
	–	–	–	340	–	–	[178]
	667 ^{b6}	163 ^{b6}	161 ^{b6}	484 ^{b6}	332 ^{b6,b7}	0.26	[375, 396]
	627 ^{b8}	159 ^{b8}	151 ^{b8}	–	326 ^{b8}	–	[376]
	587 ^{b9}	121 ^{b9}	142 ^{b9}	–	–	–	[376]
	627 ^{b8}	179 ^{b8}	220 ^{b8}	–	328 ^{b8}	–	[377]
	546 ^g	167 ^g	224 ^g	–	293 ^g	–	[377]
	640 ^{c1}	180 ^{c1}	140 ^{c1}	–	332 ^{c1}	–	[377, 378]
	–	–	–	419 ^{e2,e3}	285 ^{e2,e3}	0.19 ^{e2}	[152]
	–	–	–	–	274 ± 3 ^{c4}	–	[379]
	–	–	–	–	335 ^{b8}	–	[380]
	–	–	–	–	319 ^{c5}	–	[380]
	–	–	–	–	301 ^{c6}	–	[381, 383]
	–	–	–	–	315 ^{c7}	–	[380, 382]
	–	–	–	–	324 ^{c8}	–	[382]
	–	–	–	–	294 ^{c9}	–	[384]
	–	–	–	–	299 ^{d1}	–	[384]
	648 ^{d2}	109 ^{d2}	109 ^{d2}	617 ^{d2,d3}	288 ^{d2,d3}	0.16 ^{d2}	[385, 386]
	597 ^g	152 ^g	167 ^g	–	301 ^g	–	[380, 390]

(continued)

Table 4.14 (continued)

Composition	Stiffness coefficients c_{ij}			Young's modulus E , GPa	Bulk modulus K , GPa	Poisson's ratio ν	Reference
	c_{11} , GPa	c_{12} , GPa	c_{44} , GPa				
–	–	–	–	–	333 ^{d4}	–	[389]
–	–	–	–	–	357 ^g	–	[391]
–	–	–	–	–	360 ^{d5}	–	[391]
–	–	–	295 ^{d6}	–	–	–	[97]
–	–	–	–	–	333 ^{d7}	–	[395]
–	–	–	–	–	290 ^{d8}	–	[395]
651 ^{d9}	125 ^{d9}	161 ^{d9}	484 ^{d9,e1}	484 ^{d9,e1}	301 ^{d9,e1}	0.23 ^{d9}	[396, 401]
–	–	–	–	–	293 ^{e2}	–	[397]
617 ^{e3}	199 ^{e3}	159 ^{e3}	520 ^{e3,e4}	520 ^{e3,e4}	338 ^{e3,e4}	0.24 ^{e3}	[399]
460 ^{e5}	159 ^{e5}	103 ^{e5}	378 ^{e5,e6}	378 ^{e5,e6}	259 ^{e5,e6}	0.26 ^{e5}	[399]
–	–	–	–	–	333–340 ^{c7,e7}	–	[400]
–	–	–	477 ^{e8}	–	–	–	[322, 323]
630 ^{b5,e5}	200 ^{b5,e5}	161 ^{b5,e5}	461 ^{b5,e5,e9}	461 ^{b5,e5,e9}	343 ^{b5,e5,e9}	0.28 ^{b5,e5}	[402, 403]
556 ^{e5,f1}	184 ^{e5,f1}	140 ^{e5,f1}	402 ^{e5,f1,f2}	402 ^{e5,f1,f2}	308 ^{e5,f1,f2}	0.28 ^{e5,f1}	[402, 403]
604 ^{f3}	146 ^{f3}	179 ^{f3}	486 ^{f3,f4}	486 ^{f3,f4}	299 ^{f3,f4}	0.23 ^{f3}	[154]
–	–	–	–	–	298 ^{b5,f5}	–	[356]
557 ^g	163 ^g	147 ^g	484 ^{g,f6}	484 ^{g,f6}	294 ^{g,f6}	0.23 ^g	[404, 405]
644 ^g	129 ^g	166 ^g	–	–	302 ^{g,f7}	–	[393]
646 ^{f8}	127 ^{f8}	192 ^{f8}	406–604 ^{f8}	406–604 ^{f8}	300 ^{f8}	–	[409]
593 ^{f9}	140 ^{f9}	176 ^{f9}	365–539 ^{f9}	365–539 ^{f9}	291 ^{f9}	–	[409]
–	–	–	–	–	311–336 ^{g1}	–	[409]
–	–	–	310 ^{g2}	–	–	–	[727]
593 ^{g3}	126 ^{g3}	132 ^{g3}	428 ^{g3,g4}	428 ^{g3,g4}	281 ^{g3,g4}	0.24 ^{g3}	[738, 739]
–	–	–	–	–	303 ^{g5}	–	[790]
–	–	–	–	–	327 ^{b8}	–	[791]
–	–	–	–	–	300 ^{b9}	–	[791]
656 ^{g6}	169 ^{g6}	163 ^{g6}	–	–	338 ^{g6}	–	[792]
–	–	–	494 ^{g7,g8}	–	311 ^{g7,g8}	0.235 ^{g7}	[793]
–	–	–	–	–	300 ^{g9}	–	[794]
667 ^g	117 ^g	168 ^g	632 ^{g,h1}	632 ^{g,h1}	300 ^{g,h1}	0.15 ^{h1}	[795]
699 ^{h2}	130 ^{h2}	170 ^{h2}	515 ^{h2,h3}	515 ^{h2,h3}	320 ^{h2,h3}	0.231 ^{h2}	[796]
–	–	–	300 ^{h4}	–	–	–	[731]
–	–	–	495 ^{h5}	–	–	–	[860]
–	–	–	–	–	571 ^{h6}	–	[867]
–	–	–	–	–	305–332 ^{h7}	–	[888]
–	–	–	392 ^{h8}	–	340 ^{h8}	–	[904]
–	–	–	–	–	282 ^{d9}	–	[910]
650 ^{h9}	126 ^{h9}	173 ^{h9}	500 ^{h9,i1}	500 ^{h9,i1}	301 ^{h9,i1}	0.22 ^{h9}	[926]
–	–	–	–	–	285 ⁱ²	–	[926]
629 ⁱ³	129 ⁱ³	161 ⁱ³	475 ^{i3,i4}	475 ^{i3,i4}	296 ^{i3,i4}	–	[955]
–	–	–	–	–	295 ^{i5,i6}	–	[387]
–	–	–	500	–	–	–	[372, 373]
–	–	–	–	–	318 ^{b8}	–	[1078]

(continued)

Table 4.14 (continued)

- ^aFor isotropic (or quasi-isotropic) materials [3]: $E = 2G(1 + \nu)$, $E = 3K(1 - 2\nu)$, $K = c_{12} + 2c_{44}/3$, $G = c_{44}$; the condition for the isotropy is given in Eq. (I-2.18)
- ^bSintered, porosity – 4–12%, corrected to the poreless state
- ^c $G = 142$ GPa
- ^d $G = 153$ GPa
- ^eSintered in vacuum and annealed, porosity – 20%, mean grain size – 29 μm , contents: non-combined C – 0.05%, O – 0.05%, N – 0.27%
- ^fSingle crystal produced by a molten zone technique, contents: O – 0.008%, N < 0.0005%, Al – 0.005%, Fe < 0.005%, W – 0.02%, Zr – 0.085%
- ^gCalculated on the basis of density-functional theory (DFT) with generalized gradient approximation (GGA) using the Perdew-Burke-Ernzerhof (PBE) functional
- ^hCalculated value of $G = 134$ GPa
- ⁱ $G = 162$ GPa
- ^jSintered, corrected to the poreless state (measured values are given in brackets)
- ^k $G = 148$ GPa
- ^lSintered in vacuum and annealed, porosity – 12%, mean grain size – 14 μm , contents: non-combined C – 0.05%, O – 0.07%, N – 0.38%; measured experimentally value of $G = 149$ GPa
- ^m $G = 177$ GPa
- ⁿSintered in vacuum and annealed, porosity – 11%, mean grain size – 18 μm , contents: non-combined C – 0.05%, O – 0.08%, N – 0.39%; measured experimentally value of $G = 140$ GPa
- ^o $G = 136$ GPa
- ^p $G = 178.5$ GPa
- ^qCalculated value of $G = 181$ GPa
- ^r $G = 188$ GPa
- ^sSingle crystal materials
- ^tSintered in vacuum and annealed, porosity – 27%, mean grain size – 12 μm , contents: non-combined C – 0.05%, O – 0.07%, N – 0.32%; measured experimentally value of $G = 141$ GPa
- ^u $G = 195$ GPa
- ^vHot-pressed, porosity – 2%, contents: non-combined C – 0.34%, O – 0.03%, N – 0.02%; measured experimentally value of $G = 197$ GPa
- ^wSintered, corrected to the poreless state
- ^xHot-pressed and annealed (sintered additionally), porosity – 8%, corrected to the poreless state; $G = 198$ GPa and $\kappa = 3.26$ TPa⁻¹
- ^y $G = 202$ GPa
- ^zSintered, porosity – 4%, contents: O \leq 0.05%, N – 0.05%, W – 0.2–0.3%
- ^{a1}Hot-pressed, porosity – 4–8%, corrected to the poreless state; measured experimentally values of $G = 206$ GPa and $\kappa = 3.38$ TPa⁻¹
- ^{a2}Sintered in vacuum, corrected to the poreless state; measured experimentally values of $G = 217$ GPa and $\kappa = 3.32$ TPa⁻¹
- ^{a3}Hot-pressed, corrected to the poreless state; measured experimentally values of $G = 181$ GPa and $\kappa = 3.97$ TPa⁻¹
- ^{a4}Calculated value of $G = 192$ GPa
- ^{a5} $G = 189$ GPa
- ^{a6}Sintered in vacuum and annealed, porosity – 7%, mean grain size – 12 μm , contents: non-combined C – 0.27%, O – 0.05%, N – 0.45%; measured experimentally value of $G = 189$ GPa
- ^{a7}Sintered, porosity – 2%, mean grain size – 10 μm
- ^{a8}Metal-carburized materials
- ^{a9}Extrapolated to zero porosity
- ^{b1}Sintered, porosity – 18%

(continued)

Table 4.14 (continued)

- ^{b2} Estimation from phonon dispersion curves (c_{11} is extrapolated from neutron data)
- ^{b3} Calculated on the basis of high pressure experiments by Champion and Drickamer [368]
- ^{b4} Calculated on the basis of thermal experiments
- ^{b5} At 0 K
- ^{b6} Estimated theoretically by means of density-functional perturbation theory (DFPT) calculations
- ^{b7} $G = 161$ GPa
- ^{b8} Calculated on the basis of DFT with local density approximation (LDA)
- ^{b9} Calculated on the basis DFT with GGA
- ^{c1} Calculated on the basis of DFT with LDA using linearized augmented-plane-wave (LAPW) method
- ^{c2} Calculated using the Debye–Grüneisen model combined with *ab initio* calculations
- ^{c3} Calculated value of $G = 167$ GPa
- ^{c4} Derived from the compression data under quasi-hydrostatic high pressure conditions
- ^{c5} Calculated on the basis of DFT with Wu-Cohen GGA exchange-energy functional
- ^{c6} Calculated on the basis of DFPT
- ^{c7} Summarized value on the basis of critical review of available experimental data
- ^{c8} Calculated on the basis of linearized method of “muffin-tin” orbitals (LMTO)
- ^{c9} Calculated on the basis of linear combination of atomic orbitals (LCAO) method using Perdew-Wang (PW) potential
- ^{d1} Calculated on the basis of LCAO method using Perdew potential
- ^{d2} Calculated on the basis of interionic potential theory with modified ionic charge
- ^{d3} Calculated value of $G = 173$ GPa
- ^{d4} Calculated on the basis of DFT with LDA using full-potential linearized augmented-plane-wave (FP-LAPW) method and PW potential
- ^{d5} Calculated on the basis of DFT with LDA using Ceperley-Alder (CA) type parametrization
- ^{d6} For nanocrystalline coatings deposited by dual DC magnetron sputtering, thickness – 0.5–0.7 μm , ~ 15% amorphous carbon phase; data obtained from nano-indentation measurements
- ^{d7} Calculated on the basis of DFT with GGA using Perdew’s functional
- ^{d8} Calculated on the basis of DFT with GGA using the revised version of the Perdew-Burke-Ernzerhof (RPBE) functional
- ^{d9} Calculated on the basis of DFT with GGA using FP-LAPW method and Perdew potential
- ^{e1} Calculated value of $G = 196$ GPa
- ^{e2} Calculated on the basis of DFT with GGA using the plane-wave pseudopotential code Dacapo and Perdew’s functional
- ^{e3} Calculated on the basis of three body force potential (TBFP) model
- ^{e4} Calculated values of $G = 179$ GPa and $\kappa = 2.96$ TPa^{-1}
- ^{e5} From *ab initio* calculations
- ^{e6} Calculated values of $G = 120$ GPa and $\kappa = 3.86$ TPa^{-1}
- ^{e7} Corresponding value $G = 171$ – 172 GPa
- ^{e8} Hot-pressed, porosity <2%
- ^{e9} Calculated value of $G = 181$ GPa
- ^{f1} At ~ 300 K
- ^{f2} Calculated value of $G = 157$ GPa
- ^{f3} From first principles calculations
- ^{f4} Calculated value of $G = 198$ GPa
- ^{f5} Calculated on the basis of DFT with GGA using PW parametrization
- ^{f6} Calculated value of $G = 193$ GPa
- ^{f7} Calculated value of $G = 196$ GPa
- ^{f8} Calculated on the basis of DFT with LDA using the Ceperley-Alder-Perdew-Zunger (CAPZ) functional (upper and lower values of E are realized for the external stress applied along one of the crystallographic axes and for the stress along any of the bisector direction in each of the coordinate planes, respectively)

(continued)

Table 4.14 (continued)

- ^{f9}Calculated on the basis of DFT with GGA using PBE functional (upper and lower values of E are realized for the external stress applied along one of the crystallographic axes and for the stress along any of the bisector direction in each of the coordinate planes, respectively)
- ^{g1}Calculated on the basis of Murnaghan equation of state (upper and lower values are given to refer to the results obtained using LDA and GGA, respectively)
- ^{g2}Sintered materials, porosity – 12%, measured at 330 °C
- ^{g3}Calculated on the basis of a modified interaction potential model with covalency (MIPMC_v)
- ^{g4}Calculated value of $G = 172$ GPa
- ^{g5}On the basis of interconsistency of the physical properties of transition metal monocarbides
- ^{g6}Calculated on the basis of DFT using full-potential (linear) augmented-plane-wave plus local orbitals (FP-LAPW + LO) method with PW LDA
- ^{g7}Spark plasma sintered, porosity – 1%
- ^{g8} $G = 200$ GPa
- ^{g9}By means of extended Hückel tight-binding band electronic structure calculations
- ^{h1}Calculated value of $G = 205$ GPa
- ^{h2}Calculated on the basis of DFT by projector augmented wave (PAW) method with GGA using PBE functional
- ^{h3}Calculated value of $G = 209$ GPa
- ^{h4}Sintered, porosity – 4%, non-combined C (graphite) – 1.0%, contents: O \leq 0.05%, N – 0.05%, W – 0.2–0.3%
- ^{h5}Experimentally measured by the method of continuous impression of an indenter
- ^{h6}Calculated on the basis of linearized method of “muffin-tin” orbitals using atomic-sphere approximation (LMTO-ASA)
- ^{h7}Calculated by all-electron pseudopotentials with pseudo-wave functions
- ^{h8} $G = 150$ GPa
- ^{h9}Calculated on the basis of DFT using PBE functional with GGA by FP-LAPW method
- ⁱ¹ $G = 204$ GPa
- ⁱ²Calculated on the basis of DFT using PBE functional with GGA by plane wave pseudo-potential (PPPW) method
- ⁱ³From first principles calculations based on virtual crystal approximation
- ⁱ⁴ $G = 192$ GPa
- ⁱ⁵Calculated on the basis of DFT with GGA using PBE functional for zero temperature and pressure conditions
- ⁱ⁶ $G = 198$ GPa

253, 174 and 251 GPa, respectively. The experimentally measured velocities of ultrasonic waves propagated in niobium monocarbide phases NbC_{1-x} are

for single crystal NbC_{0.75} [369]:

$$\begin{aligned} \text{longitudinal velocity (along } \langle 001 \rangle) V_S, \text{ m s}^{-1} & 8381, \\ \text{transversal velocity (along } \langle 100 \rangle) V_T, \text{ m s}^{-1} & 4376, \\ \text{transversal velocity (along } \langle 010 \rangle) V_T, \text{ m s}^{-1} & 4377; \end{aligned}$$

for single crystal NbC_{0.865} [369]:

$$\begin{aligned} \text{longitudinal velocity (along } \langle 110 \rangle) V_S, \text{ m s}^{-1} & 8003, \\ \text{transversal velocity (along } \langle 001 \rangle) V_T, \text{ m s}^{-1} & 4452, \\ \text{transversal velocity (along } \langle 1\bar{1}0 \rangle) V_T, \text{ m s}^{-1} & 5394; \end{aligned}$$

for $\text{NbC}_{\sim 1.0}$ (summarized on the basis of several sources) [382, 867]

average velocity V_m , m s^{-1} 6450;

and theoretically calculated sound velocities for near-stoichiometric niobium monocarbide $\text{NbC}_{\sim 1.0}$ are

by *ab initio* calculations (for zero pressure):

longitudinal velocity V_S , m s^{-1} 8600 [396], 8562 [366, 396, 398], 8698 [375, 396], 8918 (0 K) [402], 7738 (~ 300 K) [402], 7320 [399], 8440–8570 [409], 8152 [404], 8861 [926];

transversal velocity V_T , m s^{-1} 5119 [396], 4722 [366, 396, 398], 5013 [375, 396], 4960 (0 K) [402], 4261 (~ 300 K) [402], 3920 [399], 5020–5200 [409], 4615 [404], 5420 [926];

average velocity V_m , m s^{-1} 5662 [396], 5258 [366, 396, 398], 5562 [375, 396], 4370 [399], 5560–5740 [409], 5133 [404], 5975 [926];

by LMTO (linearized method of “muffin-tin” orbitals) calculations [382]:

average velocity V_m , m s^{-1} 6380;

by LMTO-ASA (linearized method of “muffin-tin” orbitals using atomic-sphere approximation) calculations [867]:

average velocity V_m , m s^{-1} 8470;

by TBFP (three body force potential) modeling calculations [399]:

longitudinal velocity V_S , m s^{-1} 8720;

transversal velocity V_T , m s^{-1} 4850;

average velocity V_m , m s^{-1} 5400.

The variations of the elastic properties of niobium monocarbide phases NbC_{1-x} with temperature are shown in Figs. 4.32 and 4.33; for $\text{NbC}_{\sim 1.0}$ the average rate of decay of the elastic modulus with temperature $1/E_{298\text{K}} \times dE/dT = -1.4 \times 10^{-4} \text{ K}^{-1}$ [739]; the temperature dependence of Young’s modulus E of polycrystalline NbC_{1-x} follows Wachtman’s equation, and was expressed by Brenton et al. [193] for materials with $x = 0.03$ in the range from 12 to 2000 °C as

$$E = 460.4 - (5.729 \times 10^{-2})T \exp(-200.5/T), \quad (4.65)$$

while the similar dependence of Coulomb’s (shear) modulus G for the same materials and temperature ranges is linear:

$$G = 192.9 - (2.484 \times 10^{-2})T, \quad (4.66)$$

where T is temperature, K; for bulk (compression) modulus K of quasi-stoichiometric niobium monocarbide NbC_{1-x} Ajami and MacCrone [349] proposed the equation similar to Wachtman’s for the wide temperature range as well:

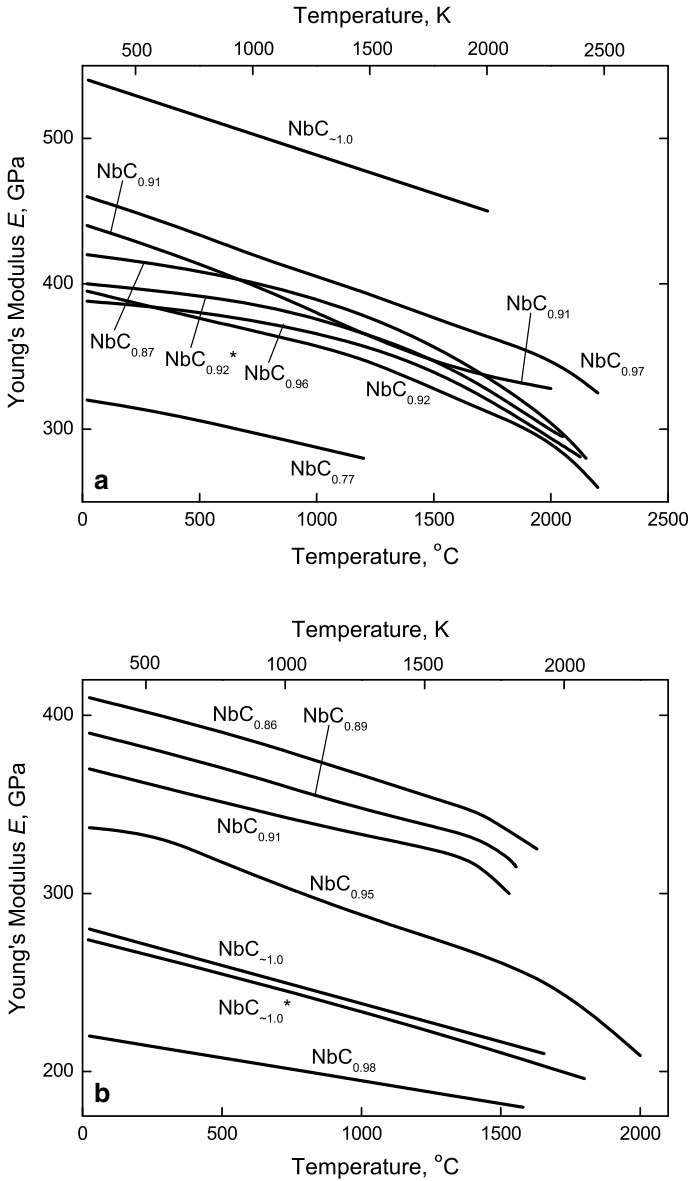


Fig. 4.32 Variations of Young's modulus E with temperature of niobium monocarbide NbC_{1-x} phases: **(a)** – $\text{NbC}_{\sim 1.0}$ (recommended for the poreless state by Kotelnikov et al. [5]); $\text{NbC}_{0.97}$, $\text{NbC}_{0.92}$, $\text{NbC}_{0.91}$ and $\text{NbC}_{0.77}$ sintered, no porosity correction (measured by Baranov et al. [352]); $\text{NbC}_{0.96}$, $\text{NbC}_{0.92}^*$ and $\text{NbC}_{0.87}$ sintered, porosity – 7–27%, mean grain size – 10–29 μm , contents: non-combined C – 0.05–0.27%, O – 0.05–0.08%, N – 0.27–0.45%, no porosity correction (measured by Bukatov et al. [28, 361]); **(b)** – $\text{NbC}_{\sim 1.0}$, $\text{NbC}_{0.98}$, $\text{NbC}_{0.91}$, $\text{NbC}_{0.89}$ and $\text{NbC}_{0.86}$ sintered in vacuum (measured by Avgustinik et al. [354]); $\text{NbC}_{0.95}$ (calculated on the basis of hardness-elasticity relationship by Travushkin et al. [270]); $\text{NbC}_{\sim 1.0}^*$ sintered, 18% porosity (measured by Kashtalyan [1054] and recommended by Marmar et al. [170])

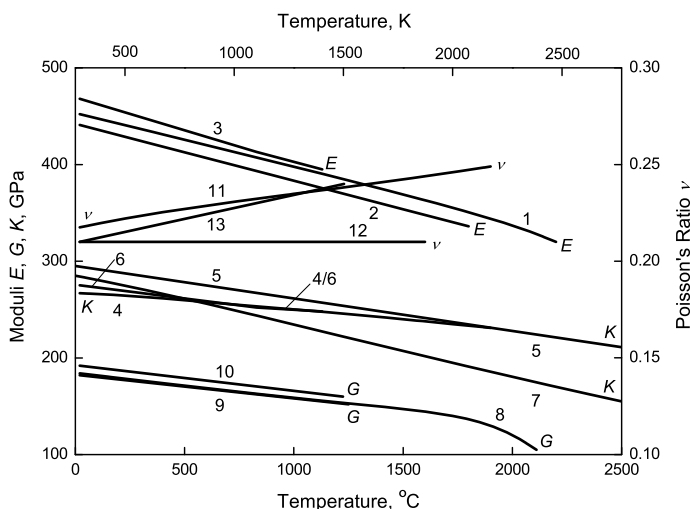


Fig. 4.33 Variations of elastic properties (1–3 – Young’s modulus E , 4–7 – bulk (compression) modulus K , 8–10 – Coulomb’s (shear) modulus G and 11–13 – Poisson’s ratio ν) of near-stoichiometric monocarbide NbC_{1-x} materials with temperature: 1, 4, 8, 11 – hot-pressed $\text{NbC}_{0.97}$, 4% porosity (measured by Brenton et al. [193]); 2, 9, 12 – $\text{NbC}_{0.97}$, 6% porosity (measured by Speck and Miccioli [7, 357]); 3, 6, 10, 13 – hot-pressed $\text{NbC}_{0.95}$, 4% porosity (measured by Jun and Shaffer [355]); 5 – $\text{NbC}_{\sim 1.0}$ (first-principles calculated by Cao et al. [356]); 7 – $\text{NbC}_{\sim 1.0}$ (first-principles calculated by Hua and Li [955])

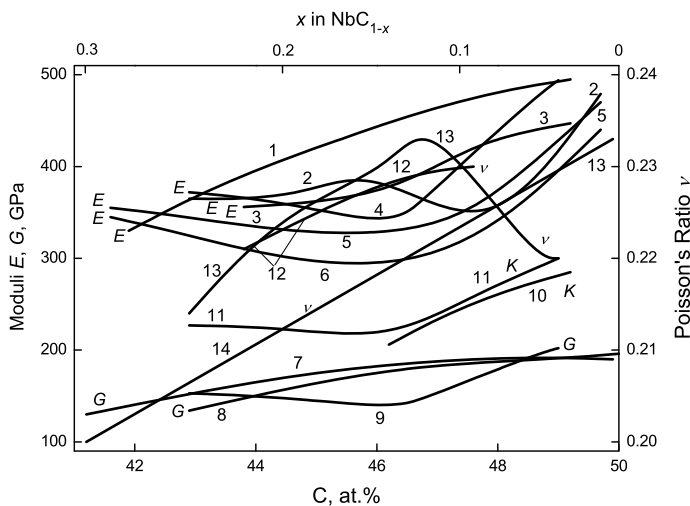


Fig. 4.34 Variations of elastic properties (1–6 – Young’s modulus E , 7–9 – Coulomb’s (shear) modulus G , 10–11 – bulk (compression) modulus K and 12–14 – Poisson’s ratio ν) of niobium monocarbide NbC_{1-x} materials with deviation from stoichiometry within the homogeneity range: 1 – sintered, porosity – 5–10%, corrected to the poreless state [1, 360]; 2 – sintered in vacuum and annealed, porosity – 7–27%, mean grain size – 10–29 μm , contents: non-combined C – 0.05–0.27%, O – 0.05–0.08%, N – 0.27–0.45% [1, 361]; 3, 10, 12 – sintered (in vacuum), E corrected to the poreless state, K and ν calculated [704]; 4, 9, 13 – sintered, porosity – 2.2–12.5%, content O < 0.05% [1, 282]; 5–6 – sintered (5 – 20 $^{\circ}\text{C}$, 6 – 1000 $^{\circ}\text{C}$) [2, 28]; 7, 14 – summarized on the basis of several sources [359]; 8 – DFT-calculated [393]; 11 – calculated [883]

$$K = 269 - (1.87 \times 10^{-2})T \exp(-278/T). \tag{4.67}$$

The variations of the elastic properties of niobium monocarbide NbC_{1-x} with deviation from stoichiometry within the homogeneity range are presented in Fig. 4.34. According to Kurlov and Gusev [359], the concentration dependences of Coulomb’s (shear) modulus G and Poisson’s ratio ν at room temperature have the following forms

$$G = 189.2 + 102.5x - 1001x^2, \tag{4.68}$$

$$\nu = 0.2335 - 0.1169x, \tag{4.69}$$

where x is the value of index in NbC_{1-x} formula. The elastic properties (stiffness coefficients c_{ij} and moduli E , K and Poisson’s ratio ν) of various niobium monocarbide NbC_{1-x} phases are listed in Table 4.14; the DFT-calculated stiffness coefficients c_{ij} for $\alpha\text{-Nb}_2\text{C}$ ($Pnma$) are $c_{11} = 424$, $c_{22} = 431$, $c_{33} = 410$, $c_{44} = 74$, $c_{55} = 137$, $c_{66} = 117$, $c_{12} = 128$, $c_{13} = 141$, $c_{23} = 113$ (in GPa) [154], or $c_{11} = 390$, $c_{22} = 405$, $c_{33} = 390$, $c_{44} = 76$, $c_{55} = 119$, $c_{66} = 122$, $c_{12} = 157$, $c_{13} = 129$, $c_{23} = 136$ (in GPa) [1097] and for $\beta\text{-Nb}_{2+x}\text{C}$ ($P(-3)m1$) the values are $c_{11} = 426$, $c_{33} = 526$, $c_{44} = 79$, $c_{12} = 129$, $c_{13} = 108$ (in GPa) [405]. The theoretically calculated variations of the elastic moduli E , G and K and Poisson’s ratio ν of

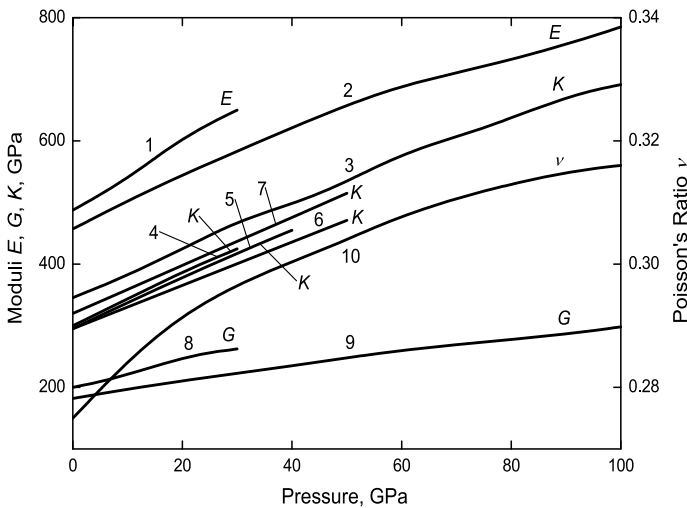


Fig. 4.35 Variations of elastic properties (1–2 – Young’s modulus E , 3–7 – bulk (compression) modulus K , 8–9 – Coulomb’s (shear) modulus G and 10 – Poisson’s ratio ν) of near-stoichiometric niobium monocarbide NbC_{1-x} with higher pressure (computed): 1, 4, 8 – by Soni et al. [396]; 2–3, 9–10 – by Varshney and Shriya [402]; 5 – by Cao et al. [356]; 6 – by Krasnenko and Brik [409] and 7 – by Gautam and Kumar [796]

Table 4.15 Thermal shock/stress resistance (thermal strength) testing data on single phase niobium monocarbide NbC_{1-x} materials

Materials and its characterization	Specimen shape and dimensions, mm	Method of thermal loading (testing)	Experimental (or calculated) results ^a	Reference
NbC _{~1.0} , gas-phase deposited, contents: O + N ≤ 0.3%	Hollow cylinder: wall thickness – 0.8–1.2, height – 20	Direct resistance heating with 400 K s ⁻¹ , cooling by inert gas blow, cycle time – 3 min	Disintegration during the first heating-cooling cycle from 2400 to 50 °C	[2, 280]
NbC _{~1.0} , sintered, porosity 12%	Hollow cylinder: outer diameter – 48, wall thickness – 0.75	Steady-state heating	$R = 43 \text{ K}^{\text{b,c}}$	[727]
NbC _{~1.0} , sintered, porosity – 8%, mean grain size – 15 μm	Rod: diameter – 3, length – 100	Steady-state heating	$R = 70 \text{ K}^{\text{b}}$	[727]
NbC _{0.93} , sintered, porosity 10–12%, non-combined C – 0.2%	Ring-shaped disk: outer diameter – 50, inner diameter – 44, height – 10	Steady-state heating along the outer surface	$R = 40\text{--}50 \text{ K}$ (calculated), $R' = 1.9 \pm 0.3 \text{ kJ m}^{-1} \text{ s}^{-1}$ (experimental)	[2, 3, 728]
NbC _{0.96} , sintered, porosity – 4%, contents: O ≤ 0.05%, N – 0.05%, W – 0.2–0.3%	Disks with a central hole: inner diameter – 5	Unsteady-state heating along the lateral surface of central hole in molten tin	$R = 48 \text{ K}$, $R' = 1.2 \text{ kJ m}^{-1} \text{ s}^{-1}$, $R'' = 3.9 \text{ MPa}^{-1}$, $R''' = 0.07 \text{ mm}$	[731]
NbC _{~1.0} , sintered, porosity – 4%, non-combined C (graphite) – 1.0%, contents: O ≤ 0.05%, N – 0.05%, W – 0.2–0.3%	Disks with a central hole: inner diameter – 5	Unsteady-state heating along the lateral surface of central hole in molten tin	$R = 38 \text{ K}$, $R' = 1.0 \text{ kJ m}^{-1} \text{ s}^{-1}$, $R'' = 7.6 \text{ MPa}^{-1}$, $R''' = 0.11 \text{ mm}$	[731]
NbC _{~1.0} , sintered, porosity – 8%, non-combined C (non-graphitized) – 1.0%, contents: O ≤ 0.05%, N – 0.05%, W – 0.2–0.3%	Disks with a central hole: inner diameter – 5	Unsteady-state heating along the lateral surface of central hole in molten tin	$R = 61 \text{ K}$, $R' = 1.3 \text{ kJ m}^{-1} \text{ s}^{-1}$, $R'' = 4.0 \text{ MPa}^{-1}$, $R''' = 0.13 \text{ mm}$	[731]
NbC _{~1.0} , sintered	–	–	Estimated average values: $R = 45 \text{ K}$, $R' = 1.12 \text{ kJ m}^{-1} \text{ s}^{-1}$	[735, 736]

(continued)

Table 4.15 (continued)

Materials and its characterization	Specimen shape and dimensions, mm	Method of thermal loading (testing)	Experimental (or calculated) results ^a	Reference
NbC _{~1.0}	Linear dimension <30 (area of the beam spot – 100 mm ²)	Thermal pulsed electron beam (energy – 10 keV) with power density – up to 18 kW cm ⁻² and pulse length – up to 1 s	Limiting thermal flux (experimentally determined for thermo-mechanical fracture, recalculated for the initial temperature of 20 °C and pulse length of 0.5 s) – 1.2 kW cm ⁻²	[1055]

^aFigures-of-merit (criteria) of thermal shock/stress resistance [2, 3, 729, 730, 797]: $R = \sigma_t(1 - \nu)/\alpha E$, $R' = \sigma_t \lambda(1 - \nu)/\alpha E$, $R'' = E/\sigma_t^2(1 - \nu)$, $R''' = \gamma E/\sigma_t^2(1 - \nu)$, where σ_t is tensile strength, ν is Poisson's ratio, α is thermal expansion coefficient, E is Young's modulus, λ is thermal conductivity and γ is fracture surface energy

^bThe distribution of R values measured on a representative number of samples (at least 70–90) is characterized by the exponential Weibull relationship; the coefficient of variation agrees closely with similar values obtained from mechanical strength testing

^cSee also Table 4.17

near-stoichiometric niobium monocarbide NbC_{1-x} with higher pressure (up to 100 GPa) are shown in Fig. 4.35.

The testing data on thermal shock/stress resistance (thermal strength) of single phase niobium monocarbide NbC_{1-x} materials are given in Table 4.15.

The magnitudes of physico-mechanical (strength, elasticity) properties of near-stoichiometric niobium carbides in the wide range of temperatures are summarized in Addendum in comparison with other ultra-high temperature materials.

4.5 Nuclear Physical Properties

The comprehensive lists of isotopes for niobium Nb and carbon C elements are presented in Tables I-8.4 and I-2.12, respectively. The nuclear physical properties of the elements, including isotopic mass range, total number of isotopes, thermal neutron macroscopic cross sections, moderating ability and capture resonance integral, are given in Table I-A.8.

The thermal neutron macroscopic cross sections Σ_i (see Eq. 2.53) of near-stoichiometric niobium carbides NbC_{1-x}/Nb_{2+x}C (for 2200 m s⁻¹ neutrons) [5]:

$$\begin{array}{ll} \text{cross section of capture (absorption)} \Sigma_a, \text{ cm}^{-1} & 0.052/0.055, \\ \text{cross section of scattering} \Sigma_s, \text{ cm}^{-1} & \sim 0.49/\sim 0.41. \end{array}$$

For the estimation of probable damage of niobium monocarbide materials exposed to various types of radiation the parameters of formation and migration of lattice point defects (vacancies and interstitial atoms) are given in Table 4.16. An example of such damage (swelling) produced by fast neutrons ($E > 1$ MeV) in the range of moderate temperatures is shown in Fig. 4.36. The damage produced by fast neutrons fluence up to $(2.5\text{--}5.0) \times 10^{21}$ cm⁻² at 130–355 °C results in the

slight failure of near-stoichiometric NbC_{1-x} hot-pressed (or sintered) materials, which is accompanied by ~0.2% relative change of lattice parameter [413]. Lanin [727] has summarized some data on the resistance to irradiation damage of NbC_{1-x} materials in the modeling nuclear rocket engine reactor environment (Table 4.17), which were obtained by testing in reactor IVG-1 [733] and measurements of physical properties after the irradiation. While the geometric volume and shape of the NbC_{1-x} samples are retaining, the irradiation leads to an appreciable growth of the lattice parameter and electrical resistivity accompanied by a minor change of strength and elastic characteristics [314, 727, 734]. According to Dew-Hughes and Jones [799], a neutron ($E \geq 1$ MeV) irradiation dose ($1.5 \times 10^{20} \text{ cm}^{-2}$) causes the reduction in superconducting critical temperature T_c of ~6–27%, which is much less than that for the similarly irradiated superconductors of other types. The effect of earlier stages (< 30 s) of nuclear reactor irradiation with neutron flux $\varphi = \sim 1.0 \times 10^{14} \text{ cm}^{-2} \text{ s}^{-1}$ and gamma quanta dose of $2.58 \times 10^6 \text{ C kg}^{-1}$ on the heat capacity and electrical resistivity of NbC_{~1.0} materials, when the gamma quanta influence dominates, was studied by Taubin [800]. Gusev et al. [945] conclude that at other equal conditions NbC_{1-x} phases with a larger deficit on

Table 4.16 Parameters of formation and migration of lattice point defects (vacancies and interstitial atoms) in near-stoichiometric niobium monocarbide^a

Defect	Metal sublattice				Non-metal sublattice			
	E_f , eV	E_m , eV	S_f/k_B	S_m/k_B	E_f , eV	E_m , eV	S_f/k_B	S_m/k_B
Vacancy ^b [411, 944]	4.09 ^c	3.41	4.89	4.08	1.36	5.44	1.63	6.52
Vacancy ^d [706, 944]	3.64 ^c	3.19	4.37	3.82	1.06	2.98	1.27	3.57
Vacancy ^e [393]	4.10 ^c	–	–	–	-0.42 ^f	3.60 ^g	–	–
Vacancy ^h [938]	1.94	–	–	–	–	–	–	–
Vacancy ⁱ [3]	1.98	–	–	–	–	–	–	–
Interstitial atom ^b [411]	19.72	0.68	23.63	0.81	6.12	0.68	7.33	0.81

^aDenoted: E_f – defect formation energy, E_m – defect migration energy, S_f – defect formation entropy, S_m – defect migration entropy, k_B – Boltzmann constant

^bCalculated on the basis of bonding model (relaxation displacement of atoms surrounding a defect is not taking into account)

^cAccording to Ordanyan et al. [76] the values of vacancy formation energy decreases with increasing defectiveness of the non-metal sublattice from 4.8 eV for NbC_{~1.0} to 3.6 eV for NbC_{0.72}, Storms et al. [147] determined 2.62 eV for NbC_{0.75} and Yu and Davis [630] – 3.30 eV for NbC_{0.77}

^dCalculated on the basis of elastic continuum model

^e*Ab initio* simulation computed from the largest super-cell on the basis of the PAW pseudopotential using the PBE formulation

^fThe computed values of vacancy formation energy on the basis of the *ab initio* pseudopotential approach for NbC_{0.875} and NbC_{0.75} are -0.13 and -0.51 eV, respectively [678]

^gThe calculated value of activation energy for carbon self-diffusion in niobium monocarbide $E_A = 350 \text{ kJ mol}^{-1}$ (see also Sect. 4.6, Table 4.21)

^hCalculated on the basis of data on the yield strength determined through hardness and elasticity measured experimentally

ⁱExperimentally determined

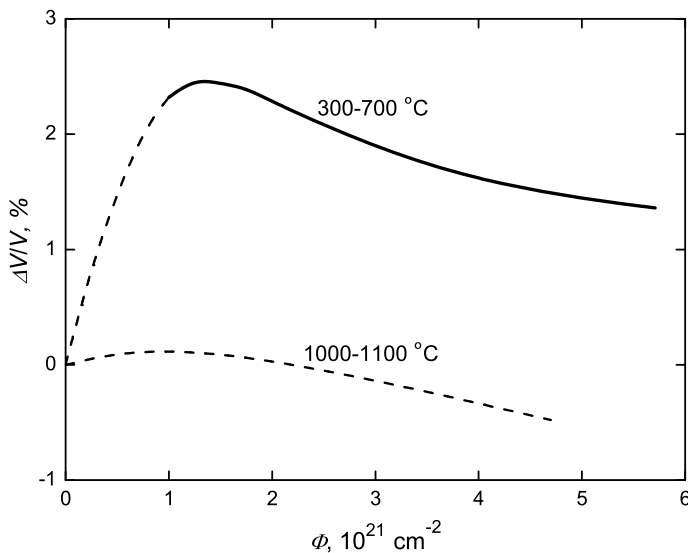


Fig. 4.36 The change in macroscopic volume (swelling/shrinkage) with fast neutron (>1 MeV) fluence Φ for produced by ceramic technologies (hot-pressed, slip-cast, explosion-pressed) near-stoichiometric niobium monocarbide NbC_{1-x} materials irradiated at different temperatures [411, 413, 798, 1056, 1057]

carbon are more radiation resistant. Deb et al. [1059] used 59.5 keV gamma radiation from ^{241}Am source for the measurement of Compton profile of niobium monocarbide NbC_{1-x} .

At room temperature the damage produced on quasi-stoichiometric monocarbide reactively sputtered films (thickness $\sim 0.2 \mu\text{m}$) by 600 keV Ar ions and 200 keV He ions irradiations in the fluence range of 0.01–100 dpa (or 10^{13} – 10^{17} cm^{-2} and 10^{15} – 10^{19} cm^{-2} for Ar and He ions, respectively) leads to the lattice expansion at the first irradiation state (maximum value of expansion 0.4% and maximum static atomic displacement of metal atoms 8 pm are corresponding to the fluence of ~ 0.4 dpa), which is mainly attributed to interstitial metal defects including antisite defects, and subsequent contraction at the second irradiation state (minimum value of -0.5% corresponding to ~ 40 dpa), which is attributed to the clustering or precipitation of the interstitial metal defects; 200 keV He irradiated $\text{NbC}_{0.98}$ single crystal showed the similar behaviour and was characterized at the first irradiation state by small displacements in the metal sublattice and considerable disorder of the non-metal sublattice [414–416]. The superconducting transition temperature T_c of quasi-stoichiometric monocarbide thin films decreases continuously from above 11 K to around 4 K and saturates in the fluence range of 10–100 dpa. The effects of both 600 keV Ar ions and 200 keV He ions irradiations on the changes of the lattice parameter and T_c depressions are nearly the same at 0.01–100 dpa. During

Table 4.17 Structural and physico-mechanical properties of near-stoichiometric niobium monocarbide NbC_{1-x} materials before and after irradiation exposure at different temperatures [2, 727]

Characteristics	Unit	Measured values		
		Initial samples		Irradiated samples ^a
		20 °C	150 °C	1100 °C
Density	g cm ⁻³	7.40	7.40	7.40
Lattice parameter	nm	0.4471	0.4488	0.4472
Electrical resistivity	μΩ m	0.50	0.90	0.50
Flexural strength:				
average	MPa	340	340	380
minimal	MPa	290	300	330
maximal	MPa	400	380	400
Young's modulus	GPa	480	465	490
Microhardness	GPa	13.7	24.5	15.7
load ^b	N	1.18	0.98	–
Thermal stress resistance criterion R ^c	K	70	130	135

^aThe neutron flux – 10¹²–10¹⁵ cm⁻² s⁻¹

^bThe minimum load during the microhardness tests, at which all the indentations were cracking

^cSee notes to Table 4.15

the annealing process of NbC_{~1.0} films irradiated at the first state, stacking fault formation is inferred around 250 °C and recovery of the displacements of the metal atoms has been observed around 700 °C [237, 414]. Employing a positron annihilation method for the studies of atomic defects in the irradiated refractory carbides at low temperatures, Rempel et al. [945, 1058] proved that the recombination of interstitial niobium atoms and vacancies in NbC_{0.84} and NbC_{0.98} occurred at temperatures below 85 K.

Nuclear physical properties of niobium carbides in comparison with other ultra-high temperature materials are also given in Addendum.

4.6 Chemical Properties and Materials Design

The comprehensive data on the chemical properties, compatibility (in the connection with both environmental resistance and composite materials design) and interaction behaviour of niobium mono- and semicarbide phases at elevated, high and ultra-high temperatures with elements (metals, non-metals) are summarized in Table 4.18, with refractory compounds – in Table 4.19 and with gaseous media – in Table 4.20. The data on the oxidation resistance of niobium monocarbide materials listed there are also accompanied by the graphic information in Figs. 4.37 and 4.38; the isothermal oxidation kinetics of near-stoichiometric NbC_{1-x} materials given there can be considered in the context of the ridge-effect model proposed by

Table 4.18 Chemical interaction and/or compatibility of niobium carbide phases with elements (metals, non-metals) at elevated, high and ultra-high temperatures, including solid matters and molten media (reaction systems are given mainly in alphabetical order)^a

System	Atmosphere	Temperature range, °C	Interaction character, products and/or compatibility	Reference
NbC _{1-x} -Ag-Cu			See Table 4.21	
NbC _{1-x} -Al	-	700-800	No chemical interaction	[417-422,
	-	900	Weak interaction	561, 569,
	-	-	Formation of Nb ₂ AlC, α/β -Nb ₄ AlC _{3-x} and Nb ₅ AlC ₄ (M _{n+1} AX _n -phases) and Nb ₃ Al ₂ C	589, 900, 901, 912, 914, 915, 919, 948, 984, 992, 1016, 1081-1083]
			See also section NbC _{1-x} -Al ₄ C ₃ in Table 4.19	
			See also Table 4.21	
			See also section C-Al-Nb in Table I-2.14	
NbC _{1-x} -Al-Co	Ar	1350	Formation of η -Nb ₃ (Co,Al) ₃ C _{1±x} phases	[1084]
NbC _{1-x} -Al-Cr	Ar	1350	Formation of η -Nb ₃ (Cr,Al) ₃ C _{1±x} phases	[1084]
NbC _{1-x} -Al-Cu	Ar	1350	Formation of η -Nb ₃ (Cu,Al) ₃ C _{1±x} phases	[1084]
NbC _{1-x} -Al-Fe	-	1000	Particles of NbC _{1-x} are rather stable in the Fe - 15-26 at.% Al alloys during long-term exposures, although the formation of ε -(Fe,Al) _{2±x} Nb was observed; the solubility of Fe in NbC _{1-x} varies from 0.9 to 5.0 at.% and that of Al is very low	[1011, 1025, 1026, 1084]
	Ar	1350	Formation of η -Nb ₃ (Fe,Al) ₃ C _{1±x} phases	
	Vacuum, 4 Pa	1420	The liquid-phase sintering of powdered NbC _{~1.0} (mean particle size - 1.2 μ m) with 12% addition of Fe - 25 at.% Al alloy (mean particle size <40 μ m) as a metallic binder leads to the formation of hard alloy system	
NbC _{1-x} -Al-Mg	-	800-1000	Most of NbC _{1-x} particles decompose in molten Al - 1 mas.% Mg alloy	[1004]
NbC _{1-x} -Al-Mn	Ar	1350	Formation of η -Nb ₃ (Mn,Al) ₃ C _{1±x} phases	[875]
NbC _{1-x} -Al-Ni	Ar	1350	Formation of η -Nb ₃ (Ni,Al) ₃ C _{1±x} phases	[875]
NbC _{1-x} -Al-V	Ar	1350	Formation of η -Nb ₃ (V,Al) ₃ C _{1±x} phases	[875]
NbC _{1-x} -Al-Zn	Ar	1350	Formation of η -Nb ₃ (Zn,Al) ₃ C _{1±x} phases	[875]
β -Nb _{2+x} C-Al	-	700-800	No chemical interaction	[417-419,
	-	900	Weak interaction	569]
			See also section C-Al-Nb in Table I-2.14	
NbC _{1-x} -SiC-TiC _{1-x} -Al	-	-	Formation of solid solutions (Ti _{1-x} Nb _x) ₃ (Si _{1-x} Al _x)C ₂ based on Ti ₃ SiC ₂	[903]
			See also section NbC _{1-x} -Al ₄ C ₃ -SiC-TiC _{1-x} in Table 4.19	

(continued)

Table 4.18 (continued)

System	Atmo- sphere	Temperature range, °C	Interaction character, products and/or compatibility	Reference
NbC _{1-x} -TiC _{1-x} - Al	-	-	Formation of (Nb,Ti) ₂ AlC, (Nb,Ti) ₄ AlC ₃ and (Nb,Ti) ₅ AlC ₄ (M _{n+1} AX _n -phase solid solutions); (Nb _{0.5} Ti _{0.5}) ₂ AlC, (Nb _{0.5} Ti _{0.5}) ₅ AlC ₄ , (Nb _{1-x} Ti _x) ₃ AlC and (Nb _{1-x} Ti _x) ₄ AlC ₃ (0 ≤ x ≤ 0.3) were synthesized <i>See also</i> section NbC _{1-x} -Al ₄ C ₃ -TiC _{1-x} in Table 4.19 <i>See also</i> section C-Al-Nb-Ti in Table I-2.14	[421, 422, 561, 573, 912-914, 954, 984, 1016, 1061]
NbC _{1-x} -VC _{1-x} - Al	-	-	Formation of (Nb,V) ₂ AlC and (Nb,V) ₄ AlC ₃ (M _{n+1} AX _n -phase solid solutions); composi- tions (Nb _{0.5} V _{0.5}) ₂ AlC and (Nb _{0.5} V _{0.5}) ₄ AlC ₃ were synthesized <i>See also</i> section C-Al-Nb-V in Table I-2.14	[421, 422, 573, 912, 1016]
NbC _{1-x} -ZrC _{1-x} - Al	-	-	Formation of (Nb,Zr) ₂ AlC (M _{n+1} AX _n -phase solid solution); (Nb _{0.6} Zr _{0.4}) ₂ AlC and (Nb _{0.8} Zr _{0.2}) ₂ AlC were synthesized <i>See also</i> section C-Al-Nb-Zr in Table I-2.14	[419, 421, 422, 573, 912, 1014- 1016]
NbC _{1-x} -As	-	-	Formation of Nb ₂ AsC (M _{n+1} AX _n -phase) <i>See also</i> section C-As-Nb in Table I-2.14	[421, 422]
NbC _{1-x} -Au NbC _{1-x} -β-B	-	>2250	Formation of NbB _{2±x} <i>See also</i> section C-B-Nb in Table I-2.14 <i>See</i> section C-B-Nb in Table I-2.14	[1, 5, 473, 474]
β-Nb _{2+x} C-β-B NbC _{1-x} -Be	Vacuum	1500	Formation of the terminal monocarbide (cubic) solid solutions of substitutional- interstitial type <i>See</i> Table 4.21	[985-987]
NbC _{1-x} -Bi NbC _{1-x} -C	Vacuum	<3150	NbC _{1-x} is compatible in contact with C (graphite) parts and articles Eutectic NbC _{1-x} -C (graphite) <i>See also</i> section C-Nb in Table I-2.13	[1, 5, 58, 146, 335, 566, 567, 810, 874, 916, 922, 1077]
NbC _{1-x} -C-Fe NbC _{1-x} -C-Fe- Mn			<i>See</i> Table 4.21 <i>See</i> Table 4.21	

(continued)

Table 4.18 (continued)

System	Atmo- sphere	Temperature range, °C	Interaction character, products and/or compatibility	Reference
NbC _{1-x} - α/ε -Co	–	1100	Formation of η -Nb ₄ C ₂ O ₂ C, or η -Nb ₃ Co ₃ C	[1, 5, 69, 81, 423, 554, 999, 1011, 1012, 1076, 1085]
		1250	The max. solid solubility of NbC _{1-x} in α -Co is ~3–6 mol.% (?)	
	–	1350–1400	Metallic Co on NbC _{1-x} plate instantaneously penetrates into the carbide and forms a eutectic (the process is identical in the case of both sintered and fused carbide materials)	
		~ 1360–1380	Eutectic NbC _{1-x} - α -Co; the max. solubility of NbC _{1-x} in α -Co is ~ 1.5 mol.% and that of Co in NbC _{1-x} is 8 mol.%	
	Vacuum, 4 Pa	1420	The liquid-phase sintering (1 h exposure) of powdered NbC _{~1.0} (mean particle size – 1.2 μ m) – 20 mol.% Co (mean particle size – 0.6 μ m) composition leads to the formation of hard alloy based on (Nb _{0.99±0.01} Co _{0.01±0.005})C _{0.89} phase with (Co _{0.86} Nb _{0.03±0.03} Co _{0.11}) binder	
	–	1400–1500	Intensive interaction (in the contact zone carbide has a changed lattice parameter)	
	–	~ 1400	The max. solubility of NbC _{1-x} in molten Ni is 5.0 mol.%	
–	1450	The solubility of Nb in Co-based binder phase in equilibrium with C is 3.5–4.0% <i>See also Table 4.21</i> <i>See also section C–Co–Nb in Table I-2.14</i> <i>See Table 4.21</i>		
NbC _{1-x} -Co–Si			<i>See section HfC_{1-x}–NbC_{1-x}–Co in Table 3.19</i> <i>See also section C–Co–Hf–Nb in Table I-2.14</i>	
NbC _{1-x} -HfC _{1-x} -Co				
NbC _{1-x} - β -Mo _{2±x} C–Co	Vacuum, 4 Pa	1420	The liquid-phase sintering (1 h exposure) of powdered NbC _{~1.0} (1.2 μ m) – 2.5 mol.% β -Mo _{2±x} C (1.2 μ m) – 20 mol.% Co (0.6 μ m) composition (mean particle sizes are given in brackets) leads to the formation of a hard alloy with core-rim microstructures and approximate compositions of hard phase – (Nb _{0.95±0.04} Mo _{0.04} Co _{0.01})C _{1.06±0.06} and metallic binder phase – (Co _{0.81±0.03} Mo _{0.05} Nb _{0.01} Co _{0.13±0.03})	[1011]
NbC _{1-x} - β -Mo _{2±x} C–Ti(C,N) _{1-x} - δ -TiN _{1±x} - δ -WC _{1±x} -Co–Ni	Ar	1360	Formation of (Nb,Ti,W,Mo)(C,N) _{1-x} -Ti(C,N) _{1-x} -(Co,Ni,Mo,Nb) quasi-three-phase system with core-rim microstructures; the solubility of Nb in (Nb,Ti,W,Mo)(C,N) _{1-x} is limited, so the redundant amounts of Nb dissolves in the metallic binder	[1072]
NbC _{1-x} -TaC _{1-x} -Co			<i>See section TaC_{1-x}–NbC_{1-x}–Co in Table 2.21</i> <i>See also section C–Co–Nb–Ta in Table I-2.14</i>	

(continued)

Table 4.18 (continued)

System	Atmo- sphere	Temperature range, °C	Interaction character, products and/or compatibility	Reference
NbC _{1-x} -TaC _{1-x} -TiC _{1-x} δ-WC _{1±x} -Co			See section TaC _{1-x} -NbC _{1-x} -TiC _{1-x} - δ-WC _{1±x} -Co in Table 2.21 See also section C-Co-Nb-Ta-Ti-W in Table I-2.14	
NbC _{1-x} -TaC _{1-x} -TiC _{1-x} δ-TiN _{1±x} -Co			See section TaC _{1-x} -NbC _{1-x} -TiC _{1-x} - δ-TiN _{1±x} -Co in Table 2.21	
NbC _{1-x} -TaC _{1-x} -TiC _{1-x} δ-TiN _{1±x} -Co-Ni			See section TaC _{1-x} -NbC _{1-x} -TiC _{1-x} - δ-TiN _{1±x} -Co-Ni in Table 2.21	
NbC _{1-x} -TaC _{1-x} -TiC _{1-x} δ-TiN _{1±x} δ-WC _{1±x} -Co			See section TaC _{1-x} -NbC _{1-x} -TiC _{1-x} - δ-TiN _{1±x} -δ-WC _{1±x} -Co in Table 2.21	
NbC _{1-x} -TaC _{1-x} -TiC _{1-x} δ-TiN _{1±x} -VC _{1-x} -δ-WC _{1±x} -Co -Ni-Mo			See section TaC _{1-x} -NbC _{1-x} -TiC _{1-x} - δ-TiN _{1±x} -VC _{1-x} -δ-WC _{1±x} -Co-Ni-Mo in Table 2.21	
NbC _{1-x} -TiC _{1-x} -Co	-	~ 1390–1410	Eutectic (Nb,Ti)C _{1-x} (x = 0.10–0.14)-α-Co	[423, 803, 1003]
			See also section C-Co-Nb-Ti in Table I-2.14	
NbC _{1-x} -VC _{1-x} Co	-	~ 1310–1350	Eutectic (Nb,V)C _{1-x} (x = 0.18)-(V,Nb) C _{1-x} (x = 0.12)-α-Co	[10, 424, 425, 1011]
	Vacuum, 4 Pa	1420	Liquid-phase sintering (1 h exposure) of powdered NbC _{~1.0} (1.2 μm) – 7.5 mol.% VC _{1-x} (1.2 μm) – 19 mol.% Co (0.6 μm) composition (mean particle sizes are given in brackets) leads to the formation of hard alloy based on (Nb _{0.92±0.02} V _{0.07±0.02} Co _{0.01})C _{0.92} phase with (Co _{0.80±0.01} V _{0.04} Nb _{0.02±0.01} C _{0.14±0.01}) binder	
NbC _{1-x} -VC _{1-x} δ-WC _{1±x} -Co	-	1400	See also section C-Co-Nb-V in Table I-2.14 The formation of Co _{3+x} W _{3-x} C is suppressed by the presence of NbC _{1-x} and VC _{1-x}	[977]
NbC _{1-x} δ-WC _{1±x} -Co	-	1200–1450	General considerations of the (Nb,W)C _{1-x} - δ-(W,Nb)C _{1±x} -α-Co system are presented	[426, 427, 838, 952,
	-	1400	The solid solubility of Nb in η ₂ -(Co,W) ₆ C is corresponding to Co _{3.04} W _{2.81} Nb _{0.16} C composition	977, 978, 1011]
	Vacuum, 4 Pa	1420	Liquid-phase sintering (1 h exposure) of powdered NbC _{~1.0} (1.2 μm) – 2.5 mol.% δ-WC _{1±x} (50 nm) – 20 mol.% Co (0.6 μm) composition (mean particle sizes are given in brackets) leads to the formation of hard alloy based on (Nb _{0.96} W _{0.02} Co _{0.02})C _{1.07} phase with (Co _{0.79±0.03} W _{0.03} C _{0.18±0.03}) binder	
			See also section C-Co-Nb-W in Table I-2.14	

(continued)

Table 4.18 (continued)

System	Atmosphere	Temperature range, °C	Interaction character, products and/or compatibility	Reference
NbC _{1-x} -ZrC _{1-x} -Co	-	~ 1380-1410	Eutectic (Nb,Zr)C _{1-x} ($x = 0.18-0.19$)- α -Co	[423]
β -Nb _{2+x} C-Co			<i>See also</i> section C-Co-Nb-Zr in Table I-2.14	
NbC _{1-x} -Cr	-	1050	<i>See</i> section C-Co-Nb in Table I-2.14 The max. solubility of Cr in NbC _{1-x} is <5 at.%; NbC _{1-x} is in equilibrium with all Cr carbides and intermetallide and metallic Cr	[52, 69, 429-432, 465, 553, 932]
		1640	Eutectic NbC _{1-x} -Cr; the max. solubility of Cr in NbC _{1-x} is ~ 3-9 mol.% and that of NbC _{1-x} in Cr is ~ 2 mol.%	
	-	≥1640	Eutectic (Nb,Cr)C _{1-x} ($x \approx 0.1-0.2$)-(Cr _y Nb _z) ($y = 0.98, z = 0.02$)	
NbC _{1-x} -Cr-Fe-Ni	Vacuum, 4 Pa	1420	<i>See also</i> section C-Cr-Nb in Table I-2.14 The liquid-phase sintering of powdered NbC _{~1.0} (mean particle size-1.2 μ m) with 12% addition of Fe - 16-18% Cr - 10-14% Ni - 2-3% Mo stainless steel (mean particle size - 22 μ m) as a metallic binder leads to the formation of hard alloy (cermet) system	[1011]
α -Nb ₂ C-Cr	-	1050	The max. solubility of Cr in β -Nb _{2+x} C is 6 at.% (?); α -Nb ₂ C phase is in equilibrium with λ_2 -NbCr _{2±x} , NbC _{1-x} and metallic Nb and Cr	[52, 553, 585, 932]
β -Nb _{2+x} C-Cr	-	1660-1690	<i>See also</i> section C-Cr-Nb in Table I-2.14 The max. solubility of Cr in β -Nb _{2+x} C is ~ 2 at.%; β -Nb _{2+x} C phase is in equilibrium with λ_1/λ_2 -NbCr _{2±x} , NbC _{1-x} and metallic Nb	[52, 428, 431, 553, 585, 932]
NbC _{1-x} - β -Mo _{2±x} C-TiC _{1-x} -VC _{1-x} -Cr-Ni	Vacuum	1470-1550	The formation of two-phase (Ti,Nb,V,Mo,Cr)C _{1-x} -(Ni,Cr,Mo,Ti) hard alloys (cermets)	[1074]
NbC _{1-x} -Cs	Cs vapour, ~13 Pa	~ 2000	No effect upon structural characteristics of NbC _{1-x} and its thermionic emission parameters (some tens of hours exposure)	[260, 262, 555]
	Cs vapour	-	Chemical reaction with deposited by vacuum evaporation carbide layers (composition and structure uncontrolled) is reported	
NbC _{1-x} -Cu	-	1100-1300	No chemical interaction	[1, 447]
NbC _{1-x} -Cu-Nb			<i>See also</i> Table 4.21	
NbC _{1-x} -Cu-Nb-W			<i>See</i> Table 4.21	

(continued)

Table 4.18 (continued)

System	Atmosphere	Temperature range, °C	Interaction character, products and/or compatibility	Reference
NbC _{1-x} - $\alpha/\gamma/\delta$ -Fe	-	~ 1150	Eutectic NbC _{1-x} - γ -Fe-C	[1, 5, 67,
	-	1250	The max. solid solubility of NbC _{1-x} in γ -Fe is ~ 1–2 mol. %	69, 81,
	-	≤ ~ 1370	NbC _{1-x} is in equilibrium with ϵ -Fe _{2±x} Nb and γ/δ -Fe	436–439,
	-	1390–1440	Metallic Fe on NbC _{1-x} plate instantaneously penetrates into the carbide and forms a eutectic (the process is identical in the case of both sintered and fused carbide materials)	442, 554,
	-	~ 1400–1450	Eutectic NbC _{1-x} - δ -Fe	819, 836,
	-	1450–1550	Intensive interaction (in the contact zone carbide has a changed lattice parameter)	956, 979,
	-	-	DFT calculated semicoherent interfacial energy at relaxed interface – 0.32 J m ⁻² <i>See also</i> Table 4.21 <i>See also</i> section C–Fe–Nb in Table I-2.14	1029, 1078]
NbC _{1-x} -Fe–Mn	-	-	General consideration of the system <i>See also</i> Table 4.21	[980–982]
NbC _{1-x} -Fe–Ni	-	-	General consideration of the system <i>See also</i> Table 4.21	[802]
NbC _{1-x} - δ -NbN _{1-x} - TiC _{1-x} - δ -TiN _{1±x} - -Fe	-	1000–1200	Miscibility gap in the NbC _{1-x} -TiC _{1-x} - δ -NbN _{1-x} - δ -TiN _{1±x} system in the presence of Fe is determined <i>See also</i> section C–Fe–N–Nb–Ti in Table I-2.14	[494, 817, 899]
	-	-	(Nb _{0.23} Ti _{0.77})(C _{0.42–0.50} N _{0.48–0.50}) – 25–55% Fe – 30–60% Ni – 2–17% Cr – 2–17% Mo hard metals (cermets) were designed on the basis of wettability/interaction measurements	[1062–1066]
NbC _{1-x} - δ -NbN _{1-x} - TiC _{1-x} - δ -TiN _{1±x} - -Fe–Ni	-	1200	General consideration of the (Nb,Ti)(C,N) _{1-x} - δ -TiN _{1±x} -Fe system <i>See also</i> section C–Fe–N–Nb–Ti in Table I-2.14	[434]
NbC _{1-x} -TiC _{1-x} - -VC _{1-x} -Fe	-	1000–1200	Miscibility gap in the NbC _{1-x} -TiC _{1-x} - VC _{1-x} system in the presence of Fe is determined	[494, 817, 899]
NbC _{1-x} -VC _{1-x} - Fe	-	~ 1000–1600	Miscibility gap in the NbC _{1-x} -VC _{1-x} system in the presence of Fe is determined	[435, 493, 494, 801,
	-	1350–1450	Eutectic (Nb,V)C _{1-x} - δ -Fe <i>See also</i> section C–Fe–Nb–V in Table I-2.14	899]
NbC _{1-x} - δ -NbN _{1-x} - δ -VN _{1-x} - -VC _{1-x} - -Fe	-	1000–1200	Miscibility gap in the NbC _{1-x} -VC _{1-x} - δ -NbN _{1-x} - δ -VN _{1-x} system in the presence of γ -Fe is determined; monocarbonitride phases (Nb _{0.12–0.88} V _{0.14–0.91})(C _{0.43–0.97} N _{0.03–0.57}) were revealed experimentally	[493, 494, 899, 983]

(continued)

Table 4.18 (continued)

System	Atmo- sphere	Temperature range, °C	Interaction character, products and/or compatibility	Reference
NbC _{1-x} - δ-NbN _{1-x} - δ-TiN _{1±x} -VC _{1-x} - -δ-VN _{1-x} -Fe	-	1000	General consideration of the (Nb,Ti,V)(C,N) _{1-x} -(V,Nb,Ti)(C,N) _{1-x} - γ-Fe system <i>See also</i> section C-Fe-N-Nb-Ti-V in Table I-2.14	[435]
NbC _{1-x} - δ-NbN _{1-x} -Fe	-	-	General consideration of the Nb(C,N) _{1-x} - γ/δ-Fe system <i>See also</i> section C-Fe-N-Nb in Table I-2.14	[433]
NbC _{1-x} - δ-NbN _{1-x} - δ-TiN _{1±x} -γ-Fe	-	1200	General consideration of the (Nb,Ti)(C,N) _{1-x} - -γ-Fe system <i>See also</i> section C-Fe-N-Nb-Ti in Table I-2.14 <i>See</i> section C-Fe-Nb in Table I-2.14	[434]
β-Nb _{2+x} C- α/γ/δ-Fe				
NbC _{1-x} -Fe ₃ Al	Vacuum	1420	The components are compatible to each other as cermet/hardmetal constituents	[1011, 1012]
NbC _{1-x} -Ga	-	-	Formation of Nb ₂ GaC (M _{n+1} AX _n -phase), or Nb ₅ GaC _x (x < 1, ?) <i>See also</i> Table 4.21 <i>See also</i> section C-Ga-Nb in Table I-2.14 <i>See</i> Table 4.21	[81, 421, 422, 564, 747]
NbC _{1-x} -Ge				
NbC _{1-x} -Hf				
β-Nb _{2+x} C- α/β-Hf	-	1200-2050	The max. solid solubility of Hf in β-Nb _{2+x} C is ~ 5 at.% <i>See also</i> section C-Hf-Nb in Table I-2.14	[5, 69, 476-478]
NbC _{1-x} -In	-	-	Formation of Nb ₂ InC (M _{n+1} AX _n -phase) <i>See also</i> Table 4.21 <i>See also</i> section C-In-Nb in Table I-2.14	[421, 422, 456]
NbC _{1-x} -Ir	-	1500	NbC _{1-x} is in equilibrium with Ir _{3±x} Nb and (Nb,Ir) alloy <i>See also</i> section C-Ir-Nb in Table I-2.14 <i>See</i> section C-Ir-Nb in Table I-2.14	[69]
β-Nb _{2+x} C-Ir				
NbC _{1-x} -K	K vapour	~2000	No chemical reaction observed, no effect upon structural characteristics of NbC _{1-x} and its thermionic emission parameters (some tens of hours exposure)	[262, 555, 806]
NbC _{1-x} - α/β/γ/δ-Mn	-	700-1000	NbC _{1-x} is in equilibrium with metallic Mn, intermetallide Mn _{2±x} Nb and all Mn carbides	[1, 585]
	-	1350	Formation of eutectic alloys and solid solutions (in the contact zone carbide has a changed lattice parameter) <i>See also</i> Table 4.21 <i>See also</i> section C-Mn-Nb in Table I-2.14	

(continued)

Table 4.18 (continued)

System	Atmosphere	Temperature range, °C	Interaction character, products and/or compatibility	Reference
NbC _{1-x} -Mo	-	1600	Under pressure 5 MPa the diffusion welded joint between NbC _{1-x} and Mo parts is produced (5–15 min exposure)	[1, 5, 57, 69, 82, 170, 441, 442, 464, 465, 565, 697]
	Vacuum	1700–1800	The initiation of reaction between powdered NbC _{1-x} and compact metallic Mo (exposure 5 h) with the formation of Mo-C solid solution, β-Mo _{2±x} C and β-Nb _{2+x} C	
	Vacuum, 0.01 Pa	1800	The initiation of reaction between sintered dense NbC _{1-x} (x ≈ 0) and compact metallic Mo (exposure 2 h)	
	-	1900	The max. solid solubility of Mo is ~ 45 at.%	
	Vacuum	2000–2200	Intensive contact interaction (exposure >2 h) between powdered NbC _{1-x} and compact metallic Mo <i>See also</i> section C-Mo-Nb in Table I-2.14	
β-Nb _{2+x} C-Mo	-	1900	The max. solid solubility of Mo is ~ 3 at.%. <i>See also</i> section C-Mo-Nb in Table I-2.14	[54, 57, 441]
NbC _{1-x} -TiC _{1-x} -Mo-Ni	Vacuum, 0.05 Pa	1300–1450	The interaction of Nb _{0.24} Ti _{0.76} C _{0.96} phase with Ni – 20% Mo melt is characterized by its dissolution and subsequent precipitation of Nb _{~0.30} Ti _{0.45–0.50} Mo _{0.20–0.25} C _{1-x} (from the melt saturated with Nb, Ti and C)	[815, 989, 1075, 1088, 1089]
NbC _{1-x} -TiC _{1-x} -δ-TiN _{1±x} -Mo-Ni	Vacuum, 0.01 Pa	1450	The interaction of complex carbonitrides Nb _{0.03–0.40} Ti _{0.60–0.97} C _{0.35–0.60} N _{0.40–0.65} with molten Ni – 20% Mo alloys leads to the accelerated incongruent dissolution of the components, preferentially – C and Nb; after the cooling metallic melts contain primary precipitates of (Nb _{0.73} Mo _{0.16} Ti _{0.11})(C,N) _{1-x} and intermetallide Ni _{3±x} Nb phases	[1068]
NbC _{1-x} -Mo-Re	Vacuum	2450	No interaction in the contact zone (1 h exposure) between Mo – 40 mas.% Re alloy and dense carbide materials	[451]
	Vacuum	2600	Interaction in the contact zone (10 min. exposure) between the compact dense materials	
	Vacuum or He	>2625	Being absorbed into the pores molten alloy dissolves (>25 vol.%) in NbC _{1-x} (17% porosity) materials completely <i>See also</i> sections C-Mo-Nb and C-Nb-Re in Table I-2.14	
NbC _{1-x} -Na	Na vapour	-	Adsorption of Na on the single crystal surface NbC _{1-x} (111) was studied	[807]
NbC _{1-x} -Nb	-	1300	Under pressure 5 MPa the diffusion welded joint between NbC _{1-x} and Nb parts is produced (5–15 min exposure).	[1, 5, 6, 67, 82, 170, 458, 463, 465, 929]
	Vacuum	1300–2200	The interaction of powdered carbide with metal results in the formation of Nb-C solid solutions and β-Nb _{2+x} C (5 h exposure) <i>See also</i> section C-Nb in Table I-2.13	
β-Nb _{2+x} C-Nb		~ 2340–2360	Eutectic β-Nb _{2+x} C-Nb <i>See also</i> section C-Nb in Table I-2.13	[2, 4–6, 67, 69]

(continued)

Table 4.18 (continued)

System	Atmosphere	Temperature range, °C	Interaction character, products and/or compatibility	Reference
NbC _{1-x} -Ni	-	1100	Formation of η -Nb ₄ Ni ₂ C _{1-x} , or η -Nb ₃ Ni ₃ C _{1-x} , or η -Nb ₆ Ni ₆ C _{1-x}	[1, 5, 67, 69, 81, 443-448, 554, 802, 809, 812-816, 827, 996, 999, 1069, 1070, 1085]
	Vacuum	1120	Formation of new phases initiates in the contact zone between the bulk solid components	
	-	1200	The max. solid solubility of Ni in near-stoichiometric NbC _{1-x} is ~2-3 mol.%; it increases with growth of C deficit in a carbide phase and inhibits order-disorder phase transformations (stabilizes NaCl structure in a carbide)	
	-	1250	The max. solid solubility of NbC _{1-x} in metallic Ni is ~2-3 mol.%	
	-	1300-1350	Metallic Ni on NbC _{1-x} plate instantaneously penetrates into the carbide and forms a eutectic (the process is identical in the case of both sintered and fused carbide materials)	
	-	~1320-1350	Eutectic NbC _{1-x} -Ni; the max. solid solubility of NbC _{1-x} in Ni is ~2-3 mol.% and that of Ni in NbC _{1-x} is ~9 mol.%	
	-	1325-1335	Formation of a liquid phase in the NbC _{0.97} -Ni powdered mixture with mean grain size ~50 μ m	
	-	~1400	The max. solubility of NbC _{1-x} in molten Ni is 4.0 mol.% <i>See also Table 4.21</i>	
NbC _{1-x} - β -Mo _{2\pmx} C- TiC _{1-x} - δ -TiN _{1\pmx} -Ni	-	1000-1300	Formation of (Nb,Mo,Ti)(C,N) _{1-x} complex monocarbonitride (cubic) phase	[990, 1067]
	-	1480	Powdered TiC _{0.75} N _{0.25} - 2-8 vol.% NbC _{1-x} - 7 vol.% β -Mo _{2\pmx} C - 8 vol.% Ni compositions were heat-treated to form cermets	
NbC _{1-x} -TaC _{1-x} -Ni			<i>See section TaC_{1-x}-NbC_{1-x}-Ni in Table 2.21</i>	
NbC _{1-x} -TaC _{1-x} -TiC _{1-x} - δ -TiN _{1\pmx} -Ni			<i>See also section C-Nb-Ni-Ta in Table I-2.14</i> <i>See section TaC_{1-x}-NbC_{1-x}-TiC_{1-x}-δ-TiN_{1\pmx}-Ni in Table 2.21</i>	
NbC _{1-x} -TiC _{1-x} -Ni	-	-	The cast alloys crystallize in a metastable state, when the carbide phase does not decompose into two solid solutions even after long-term annealing	[812-814, 943, 1003, 1008, 1009, 1069, 1070, 1075]
	Vacuum, 0.01 Pa	1450	The interaction of Nb _{0.24} Ti _{0.76} C _{0.96} phase with Ni melt leads to the dissolution of double carbide (preferentially C and Nb are transferred into the melt), phase separation (stratification) and formation of core-rim microstructures; Nb atoms diffuses from the core to the rim phase (~Nb _{0.40} Ti _{0.60} C _{1-x})	

(continued)

Table 4.18 (continued)

System	Atmosphere	Temperature range, °C	Interaction character, products and/or compatibility	Reference
NbC _{1-x} -TiC _{1-x} -δ-TiN _{1±x} -Ni	Vacuum, 0.01 Pa	1450	The interaction of complex carbonitrides Nb _{0.03-0.40} Ti _{0.60-0.97} C _{0.35-0.60} N _{0.40-0.65} with molten Ni leads to the incongruent dissolution of the components, preferentially – C and Nb; after the cooling metallic melts have a hypoeutectic structure with the primary precipitates of Ni based phase and intermetallide Ni _{3±x} Nb (carbonitride constituents of eutectics is enriched with Nb)	[953, 993–996, 1000, 1068, 1073]
	Vacuum	1500–1510	Formation of (Ti,Nb)(C,N) _{1-x} -Ti(C,N) _{1-x} -Ni cermets with core-rim microstructures, the absent of the core can be caused by the high lattice mismatch at the core – inner rim interface; addition of NbC _{1-x} leads to the enhancement of wettability due to diffusion (dissolution) of Nb atoms into Ni phase	
NbC _{1-x} -TiC _{1-x} -δ-TiN _{1±x} - TiO _{1±x} -Ni	Vacuum, 0.1 Pa	1450	The interaction of Nb _{0.40} Ti _{0.60} C _{0.50} N _{0.40} O _{0.10} oxycarbonitride phase with molten Ni is considered	[953]
NbC _{1-x} -TiC _{1-x} -δ-TiN _{1±x} - δ-WC _{1±x} -Ni	–	1300	Formation of (Nb,W,Ti)(C,N) _{1-x} complex monocarbonitride (cubic) phase based cermet system	[990]
NbC _{1-x} -TiC _{1-x} -VC _{1-x} - δ-WC _{1±x} -Ni- Cr	Vacuum, ~1 Pa	1350–1450	Formation of (Nb,Ti,V,W,Cr)C _{1-x} complex monocarbide (cubic) phases with core-rim microstructures, including elementary carbides, (Nb,Ti)C _{1-x} binary monocarbide phase and Ni-based metallic alloy (binder)	[998]
NbC _{1-x} -VC _{1-x} - Ni	–	~1285–1315	Eutectic (Nb,V)C _{1-x} (x = 0.1)–(V,Nb)C _{1-x} (x ≈ 0.1)–Ni; the max. solubility of NbC _{1-x} in VC _{1-x} is ~15 mol.% and in Ni is ~3 mol.%, and that of VC _{1-x} in NbC _{1-x} is ~20 mol.% and in Ni is ~3 mol.%, and that of Ni in NbC _{1-x} is ~9 mol.% and in VC _{1-x} is ~4 mol.% <i>See also</i> section C–Nb–Ni–V in Table I-2.14	[446]
NbC _{1-x} -ZrC _{1-x} -Ni	–	~1290–1330	Eutectic (Zr,Nb)C _{1-x} -Ni (in the cast state due to the probable formation of a metastable ternary eutectic the alloys begin to melt at 80–100 °C lower than the equilibrium values); the max. solubility of (Zr,Nb)C _{1-x} in Ni is ~2–3 mol.% and that of Ni in (Zr,Nb)C _{1-x} is ~6 mol.% <i>See also</i> section C–Nb–Ni–Zr in Table I-2.14	[448, 1017]
β-Nb _{2+x} C–Ni NbC _{1-x} -Ni–Cr	–	–	<i>See</i> section C–Nb–Ni in Table I-2.14 Porous NbC _{1-x} is impregnated perfectly with the Ni-9.5% Cr alloy <i>See also</i> sections C–Cr–Nb and C–Nb–Ni in Table I-2.14	[1]

(continued)

Table 4.18 (continued)

System	Atmo- sphere	Temperature range, °C	Interaction character, products and/or compatibility	Reference
NbC _{1-x} -Os	-	1500	The solubility of Os in NbC _{1-x} is low <i>See also</i> section C-Nb-Os in Table I-2.14	[69]
β -Nb _{2+x} C-Os			<i>See</i> section C-Nb-Os in Table I-2.14	
NbC _{1-x} -P	-	-	Formation of Nb ₂ PC (M _{n+1} AX _n -phase) <i>See also</i> section C-Nb-P in Table I-2.14	[421, 422]
NbC _{1-x} -Pb			<i>See</i> Table 4.21	
NbC _{1-x} -Pd	-	1200-1500	The formation of (Pd,Nb) solid solutions and failure of NbC _{1-x} are occurred (8 h exposure); NbC _{1-x} is in equilibrium with (Pd _{0.85} Nb _{0.15}) alloy <i>See also</i> section C-Nb-Pd in Table I-2.14	[1, 5, 69, 449]
β -Nb _{2+x} C-Pd			<i>See</i> section C-Nb-Pd in Table I-2.14	
NbC _{1-x} -Pt	-	1200-1500	The formation of (Pt,Nb) solid solutions and the failure of NbC _{1-x} are occurred (8 h exposure); NbC _{1-x} is in equilibrium with α -Pt _{3±x} Nb <i>See also</i> section C-Nb-Pt in Table I-2.14	[1, 5, 69, 449]
β -Nb _{2+x} C-Pt			<i>See</i> section C-Nb-Pt in Table I-2.14	
NbC _{1-x} -Pu			<i>See</i> section C-Nb-Pu in Table I-2.14	
β -Nb _{2+x} C-Pu			<i>See</i> section C-Nb-Pu in Table I-2.14	
NbC _{1-x} -Re	-	2000-2100	The solubility of Re in carbide is ~ 1.5 at.%; non-stoichiometric carbides are in equilibrium with χ -NbRe _{3±x}	[1, 69, 450, 451, 468-470, 570, 951]
	-	-	Stable and compatible with each other as cermet components	
	-	2210-2240	Eutectic NbC _{1-x} -Re; the max. solid solubility of Re in NbC _{1-x} is ~ 1.5-2.0 mol.% and that of NbC _{1-x} in Re is negligible too	
	He	2500	No interaction in the contact zone (1 h exposure) between the compact dense materials was observed (?) <i>See also</i> section C-Nb-Re in Table I-2.14	
β -Nb _{2+x} C-Re	-	1800-2000	The mutual solid solubilities of the components are very low <i>See also</i> section C-Nb-Re in Table I-2.14	[69, 450]
NbC _{1-x} -Rh	-	≥1500	The interaction results in the formation of Rh _{3±x} Nb and C (graphite) <i>See also</i> section C-Nb-Rh in Table I-2.14	[69]
β -Nb _{2+x} C-Rh			<i>See</i> section C-Nb-Rh in Table I-2.14	
NbC _{1-x} -Ru	-	~ 1600	The interaction of non-stoichiometric NbC _{1-x} results in the formation of NbRu ₃ C _{1-x} (x ≈ 0.6); quasi-stoichiometric phases are in equilibrium with Ru <i>See also</i> section C-Nb-Ru in Table I-2.14	[69]

(continued)

Table 4.18 (continued)

System	Atmo- sphere	Temperature range, °C	Interaction character, products and/or compatibility	Reference
β -Nb _{2+x} C–Ru			See section C–Nb–Ru in Table I-2.14	
NbC _{1-x} –S	–	–	Formation of Nb ₂ SC _{1-x} ($x = 0.6$, M _{n+1} AX _n -phase), α/β -Nb ₂ CS ₂ (?) See also section C–Nb–S in Table I-2.14	[421, 422]
NbC _{1-x} –Sb			See Table 4.21	
NbC _{1-x} –Si	Vacuum, <10 ⁻⁴ Pa	600–700	No interdiffusion; no silicides or any other chemical species are formed (up to 1 h exposure) in the multilayers system of components	[5, 145, 421, 422, 452–455, 575, 584, 700, 701]
	Vacuum, 1.3 Pa	1100	Interaction in powdered equimolar mixture NbC _{0.98} + Si (1 h exposure) leads to the formation of 4.7% NbSi ₂ and 0.7% β -SiC	
	Vacuum, 10 ⁻³ Pa	1300	Under pressure (1 MPa) two-phase (NbSi ₂ + SiC) layer is formed with silicide matrix and carbide discontinuous particles in the contact zone between the bulk components	
	Vacuum, 1.3 Pa	1300	Interaction in powdered equimolar mixture NbC _{0.98} + Si (1 h exposure) leads to the formation of NbSi ₂ (28.5%) and β -SiC (6.6%)	
	–	>1300	Formation of SiC and Nb silicides (or ternary phases, including M _{n+1} AX _n -phases, ?)	
	Vacuum, 1.3 Pa	1500	Interaction in powdered equimolar mixture NbC _{0.98} + Si (1 h exposure) leads to the formation of 35.7% NbSi ₂ and 10.2% β -SiC	
	Vacuum, 1.3 Pa	1700–1900	Interaction in equimolar powdered mixture NbC _{0.98} + Si (1 h exposure) leads to the formation of 16–31% NbSi ₂ and 5–10% β -SiC See also Table 4.21	
β -Nb _{2+x} C–Si			See also section C–Nb–Si in Table I-2.14	
NbC _{1-x} –Sn	–	–	Formation of Nb _{2±x} Sn _{1±y} C _{1-z} (M _{n+1} AX _n -phase with homogeneity range from Nb _{2.20} Sn _{0.80} C _{0.93} to Nb _{1.92} Sn _{1.08} C _{0.91}); the solubility of Sn in NbC _{1-x} is extremely low See also Table 4.21	[421, 422, 456, 457]
β -Nb _{2+x} C–Sn	–	–	See also section C–Nb–Sn in Table I-2.14 The solubility of Sn in β -Nb _{2+x} C is extremely low See also section C–Nb–Sn in Table I-2.14	[457]

(continued)

Table 4.18 (continued)

System	Atmo- sphere	Temperature range, °C	Interaction character, products and/or compatibility	Reference
NbC _{1-x} -Ta	-	≤1600	No interaction in the contact zone (2–5 h exposure) between the materials	[1, 5, 82, 145, 170, 442, 458, 463]
	-	1700	Under pressure 5 MPa the diffusion welded joint between NbC _{1-x} and Ta is produced (5–15 min exposure)	
	Vacuum	1700–2200	Formation of Ta-C, Ta _{2+x} C-Nb _{2+x} C and TaC _{1-x} -NbC _{1-x} solid solutions in the contact zone between the bulk materials <i>See also</i> section C-Nb-Ta in Table I-2.14 <i>See</i> section C-Nb-Ta in Table I-2.14 <i>See</i> section C-Nb-Tc in Table I-2.14 <i>See</i> section C-Nb-Th in Table I-2.14	
β-Nb _{2+x} C-Ta				
NbC _{1-x} -Tc				
NbC _{1-x} -Th				
β-Nb _{2+x} C-Th				
NbC _{1-x} -α/β-Ti	Vacuum, <7 × 10 ⁻⁴ Pa	1750	Molten Ti reacts extensively with NbC _{1-x} crucibles resulting in the formation of an alloy, which soaks into carbide materials; a new phase is apparently formed as a distinct layer based on TiC _{1-x} between carbide and metal Ti <i>See also</i> section C-Nb-Ti in Table I-2.14	[689]
β-Nb _{2+x} C-α/β-Ti	-	≤2280	The max. solid solubility of Ti varies from ~5 to ~9 at.% <i>See also</i> section C-Nb-Ti in Table I-2.14	[46, 69, 145, 459]
γ-Nb _{2+x} C-α/β-Ti	-	2600	The max. solid solubility of Ti in γ-Nb _{2+x} C is ~1 at.% <i>See also</i> section C-Nb-Ti in Table I-2.14	[46, 69, 145, 459]
NbC _{1-x} -Ti			<i>See</i> Table 4.21	
NbC _{1-x} -U			<i>See</i> section C-Nb-U in Table I-2.14	
β-Nb _{2+x} C-U			<i>See</i> section C-Nb-U in Table I-2.14	
NbC _{1-x} -V			<i>See</i> section C-Nb-V in Table I-2.14	
β-Nb _{2+x} C-V			<i>See</i> section C-Nb-V in Table I-2.14	
NbC _{1-x} -W	-	1800	Under pressure 5 MPa the diffusion welded joint between NbC _{1-x} and W parts is produced (5–15 min exposure)	[1, 5, 67, 82, 170, 451, 458, 461, 465–467, 697]
	-	2000	The weak interaction between NbC _{1-x} and metallic W with formation of δ-WC _{1±x}	
	Vacuum	2200	The weak interaction between powdered NbC _{1-x} and metallic W (2 h exposure) with the formation of β-(Nb,W) _{2+x} C; practically, no interaction (exposure 5 h) between the bulk dense materials	
	Vacuum, 0.01 Pa	2200	The initiation of reaction between sintered dense NbC _{1-x} (x = 0.11–0.27) and compact metallic W (exposure 2 h)	
	Vacuum, 0.01 Pa	2300	The initiation of reaction between sintered dense NbC _{1-x} (x ≈ 0) and compact metallic W (exposure 2 h)	
	Vacuum	2500	No interaction in the contact zone (4 h exposure) between the compact materials (?) <i>See also</i> section C-Nb-W in Table I-2.14	

(continued)

Table 4.18 (continued)

System	Atmosphere	Temperature range, °C	Interaction character, products and/or compatibility	Reference
β -Nb _{2+x} C–W	–	2000	The max. solid solubility of W in β -Nb _{2+x} C is ~ 8 at. % <i>See also</i> section C–Nb–W in Table I-2.14	[69, 145, 460, 461]
γ -Nb _{2±x} C–W	–	2500	The max. solid solubility of W is ~ 8 at. %	[69, 145, 460, 461]
	–	2690	The max. solid solubility of W is ~ 2 at. % <i>See also</i> section C–Nb–W in Table I-2.14	
NbC _{1-x} –Zn	–	–	Formation of related to η -carbide type Nb ₂ ZnC _{1-x} phase	[81, 563]
NbC _{1-x} – α/β -Zr	Vacuum	750–1500	Interaction in the powdered mixtures (mean grain size – 1–2 μ m) of components leads to the formation of highly non-stoichiometric ZrC _{~0.6} phase <i>See also</i> section C–Nb–Zr in Table I-2.14	[816, 827]
β -Nb _{2+x} C– α/β -Zr	–	–	The solubility of Zr in β -Nb _{2+x} C is low <i>See also</i> section C–Nb–Zr in Table I-2.14	[69, 145, 462]

^aThe parameters of wettability of niobium monocarbide phases by liquid metals at various temperatures are listed in Table 4.21

Table 4.19 Chemical interaction and/or compatibility of niobium carbide phases with refractory compounds at elevated, high and ultra-high temperatures (reaction systems are given mainly in alphabetical order)

System	Atmosphere	Temperature range, °C	Interaction character, products and/or compatibility	Reference
NbC _{1-x} – α -Al ₂ O ₃	CO ₂ , 1.4 × 10 ⁻¹⁵ Pa Ar flow	1000 1650–1750	Calculated equilibrium pressure of the interaction between the components No chemical interaction between the powdered components; no intermediate (amorphous or crystalline) phases at the intergranular interfaces	[576–580, 890]
α -Nb ₂ C– α -Al ₂ O ₃	CO ₂ , 2.2 × 10 ⁻¹⁸ Pa	1000	Calculated equilibrium pressure of the interaction between the components	[576, 577]
NbC _{1-x} –Al ₄ C ₃	–	Up to ~ 2000	No mutual solid solubilities Formation of Nb ₂ AlC, α/β -Nb ₄ AlC ₃ (M _{n+1} AX _n -phases) <i>See also</i> section NbC _{1-x} –Al in Table 4.18 <i>See also</i> section C–Al–Nb in Table I-2.14	[417–419, 559, 561, 569, 589, 900, 901, 948]
NbC _{1-x} –Al ₄ C ₃ –SiC–TiC _{1-x}	–	–	Formation of solid solutions (Ti _{1-x} Nb _x) ₃ (Si _{1-x} Al _x)C ₂ based on Ti ₃ SiC ₂ <i>See also</i> section NbC _{1-x} –SiC–TiC _{1-x} –Al in Table 4.18	[903]

(continued)

Table 4.19 (continued)

System	Atmosphere	Temperature range, °C	Interaction character, products and/or compatibility	Reference
NbC _{1-x} -Al ₄ C ₃ -TiC _{1-x}	-	-	Formation of (Nb,Ti) ₂ AlC, (Nb,Ti) ₄ AlC ₃ and (Nb,Ti) ₅ AlC ₄ (M _{n+1} AX _n -phase solid solutions); (Nb _{0.5} Ti _{0.5}) ₂ AlC, (Nb _{0.5} Ti _{0.5}) ₅ AlC ₄ and (Nb _{1-x} Ti _x) ₄ AlC ₃ (0 ≤ x ≤ 0.3) were synthesized <i>See also</i> section NbC _{1-x} -TiC _{1-x} -Al in Table 4.18 <i>See also</i> section C-Al-Nb-Ti in Table I-2.14	[421, 422, 561, 573, 912-914, 954]
NbC _{1-x} -Al ₄ C ₃ -VC _{1-x}	-	-	Formation of (Nb,V) ₂ AlC and (Nb,V) ₄ AlC ₃ (M _{n+1} AX _n -phase solid solutions); compositions (Nb _{0.5} V _{0.5}) ₂ AlC and (Nb _{0.5} V _{0.5}) ₄ AlC ₃ were synthesized <i>See also</i> section NbC _{1-x} -VC _{1-x} -Al in Table 4.18 <i>See also</i> section C-Al-Nb-V in Table I-2.14	[421, 422, 573, 912, 1016]
NbC _{1-x} -Al ₄ C ₃ -ZrC _{1-x}	-	-	Formation of (Nb,Zr) ₂ AlC (M _{n+1} AX _n -phase solid solution); (Nb _{0.6} Zr _{0.4}) ₂ AlC and (Nb _{0.8} Zr _{0.2}) ₂ AlC were synthesized <i>See also</i> section NbC _{1-x} -ZrC _{1-x} -Al in Table 4.18 <i>See also</i> section C-Al-Nb-Zr in Table I-2.14	[419, 421, 422, 573, 912, 1014-1016]
NbC _{1-x} -B _{4±x} C	-	> ~ 1500	Formation of NbB _{2±x} and C <i>See also</i> section C-B-Nb in Table I-2.14	[5, 67, 472-474]
NbC _{1-x} -B _{4±x} C-α-BN	-	≤ 2100	No contact reaction between powdered NbC _{1-x} and compact dense B _{4±x} C-α-BN composition <i>See also</i> section C-B-N-Nb in Table I-2.14	[804]
β-Nb _{2+x} C-B _{4±x} C NbC _{1-x} -α-BN	-	≥ 2250	Formation of NbB _{2±x} <i>See also</i> section C-B-N-Nb in Table I-2.14	[5, 475]
NbC _{1-x} -CeN _{1±x}	-	-	Terminal mutual solid solubilities between the components, ?	[5]
NbC _{1-x} -CeP _{1±x}	-	-	Terminal mutual solid solubilities between the components, ?	[5]
NbC _{1-x} -CeS _{1±x}	-	-	Terminal mutual solid solubilities between the components, ?	[5]
NbC _{1-x} -Cr ₃ C _{2-x}	-	1740-1820	The max. solubility of "imaginary" phase 'CrC _{1-x} ' in NbC _{1-x} is ~ 26-29 mol.%; NbC _{1-x} phase is in equilibrium with C (graphite) and Cr carbides <i>See also</i> section C-Cr-Nb in Table I-2.14	[431, 585, 588, 932]

(continued)

Table 4.19 (continued)

System	Atmosphere	Temperature range, °C	Interaction character, products and/or compatibility	Reference
NbC _{1-x} -Cr ₇ C _{3±x}	-	1050-1750	The max. solubility of “imaginary” phase ‘CrC _{1-x} ’ in NbC _{1-x} is ~25-28 mol.%; NbC _{1-x} phase is in equilibrium with all Cr carbides and intermetallide and metallic Cr	[52, 69, 429, 431, 553, 585, 588, 932]
	-	1580-1610	The max. solubility of NbC _{1-x} in Cr ₇ C _{3±x} is corresp. to compos. ~ (Cr _{>0.99} Nb _{<0.006}) ₇ C _{3±x}	
	-	~ 1685	Eutectic NbC _{1-x} -Cr ₇ C _{3±x} ; the max. solubility of Cr ₇ C _{3±x} in NbC _{1-x} is corresponding to composition ~ (Nb _{0.90} Cr _{0.10})C _{1-x} and that of NbC _{1-x} in Cr ₇ C _{3±x} - to composition ~ (Cr _{0.99} Nb _{0.01}) ₇ C _{3±x} <i>See also</i> section C-Cr-Nb in Table I-2.14	
NbC _{1-x} -Cr ₂₃ C _{6±x}	-	1550	The max. solubility of NbC _{1-x} in Cr ₂₃ C _{6±x} is corresponding to composition ~ (Cr _{0.98-0.99} Nb _{0.01-0.02}) ₂₃ C _{6±x} <i>See also</i> section C-Cr-Nb in Table I-2.14	[431, 585-588, 932]
β-Nb _{2+x} C-Cr ₃ C _{2-x} -Cr ₇ C _{3±x} -Cr ₂₃ C _{6±x}	-	1600-1680	The max. solubility of Cr carbides in β-Nb _{2+x} C is corresp. to composition ~ (Nb _{0.95-0.99} Cr _{0.01-0.05}) _{2+x} C; β-Nb _{2+x} C phase is in equilibrium with λ ₁ /λ ₂ -NbCr _{2±x} , NbC _{1-x} and metallic Nb <i>See also</i> section C-Cr-Nb in Table I-2.14	[431, 585, 932]
NbC _{1-x} -Cr ₂ O ₃	CO ₂ , 1.2 × 10 ⁻⁶ Pa	1000	Calculated equilibrium pressure of the interaction between the components	[576, 577]
α-Nb ₂ C-Cr ₂ O ₃	CO ₂ , 1.8 × 10 ⁻⁹ Pa	1000	Calculated equilibrium pressure of the interaction between the components	[576, 577]
NbC _{1-x} -DyN _{1±x}	-	-	Monocarbonitride (cubic) continuous solid solution (complete solubility in the system?)	[5]
NbC _{1-x} -ErN _{1±x}	-	-	Monocarbonitride (cubic) continuous solid solution (complete solubility in the system?)	[5]
NbC _{1-x} -EuN _{1±x}	-	-	Terminal mutual solid solubilities between the components (?)	[5]
NbC _{1-x} -EuO	-	-	Terminal mutual solid solubilities between the components (?)	[5]
NbC _{1-x} -Fe ₃ C	-	-	Not (or very slightly) soluble in each other in solid state <i>See also</i> section C-Fe-Nb in Table I-2.14	[69, 81]
NbC _{1-x} -Fe ₂ O ₃	CO ₂ , 1.2 Pa	1000	Calculated equilibrium pressure of the interaction between the components	[576, 577]
α-Nb ₂ C-Fe ₂ O ₃	CO ₂ , 1.8 × 10 ⁻³ Pa	1000	Calculated equilibrium pressure of the interaction between the components	[576, 577]
NbC _{1-x} -Fe _{3+x} Al	Vacuum, 4 Pa	1420	The liquid-phase sintering of powdered NbC _{~1.0} (mean particle size - 1.1 μm) - 7 mol.% Fe _{3+x} Al (mean particle size <40 μm) composition leads to the formation of NbC _{1-x} - (Fe,Al,C) hard alloy (cermet) system	[1011]

(continued)

Table 4.19 (continued)

System	Atmosphere	Temperature range, °C	Interaction character, products and/or compatibility	Reference
NbC _{1-x} -GdN _{1±x}	-	-	Terminal mutual solid solubilities between the components (?)	[5]
NbC _{1-x} -HfC _{1-x}			See section HfC _{1-x} -NbC _{1-x} in Table 3.20 See also section C-Hf-Nb in Table I-2.14	
β-Nb _{2+x} C- HfC _{1-x}			See section HfC _{1-x} -β-Nb _{2+x} C in Table 3.20 See also section C-Hf-Nb in Table I-2.14	
NbC _{1-x} -HfC _{1-x} -TaC _{1-x}			See section TaC _{1-x} -HfC _{1-x} -NbC _{1-x} in Table 2.22	
NbC _{1-x} -HfC _{1-x} -ThC _{1±x}			See section HfC _{1-x} -NbC _{1-x} -ThC _{1±x} in Table 3.20	
NbC _{1-x} -HfC _{1-x} -TiC _{1-x}			See section HfC _{1-x} -NbC _{1-x} -TiC _{1-x} in Table 3.20	
NbC _{1-x} -HfC _{1-x} -UC _{1±x}			See section HfC _{1-x} -NbC _{1-x} -UC _{1±x} in Table 3.20 See also section C-Hf-Nb-U in Table I-2.14	
NbC _{1-x} -HfC _{1-x} -VC _{1-x}			See section HfC _{1-x} -NbC _{1-x} -VC _{1-x} in Table 3.20 See also section C-Hf-Nb-V in Table I-2.14	
NbC _{1-x} -HfC _{1-x} -δ-WC _{1±x}			See section HfC _{1-x} -NbC _{1-x} -δ-WC _{1±x} in Table 3.20	
NbC _{1-x} -HfC _{1-x} -ZrC _{1-x}			See section HfC _{1-x} -NbC _{1-x} -ZrC _{1-x} in Table 3.20	
NbC _{1-x} - δ-NbN _{1-x} - HfC _{1-x}			See section HfC _{1-x} -NbC _{1-x} -δ-NbN _{1-x} in Table 3.20	
NbC _{1-x} -HfN _{1±x}	-	1600-2200	Monocarbonitride (cubic) continuous solid solution (complete solubility in the system)	[5, 479]
NbC _{1-x} -HoN _{1±x}	-	-	Monocarbonitride (cubic) continuous solid solution (complete solubility in the system?)	[5]
NbC _{1-x} -LaN _{1±x}	-	-	Terminal mutual solid solubilities between the components (?)	[5]
NbC _{1-x} -LaB _{6±x}	Ar	1700	The powdered components interact with the formation of NbB _{2±x} and C; complete decomposition of carbide (6 h exposure)	[911]
NbC _{1-x} -LaP _{1±x}	-	-	Terminal mutual solid solubilities between the components (?)	[5]
NbC _{1-x} -LaS _{1-x}	-	-	Terminal mutual solid solubilities between the components (?)	[5]
NbC _{1-x} -LuN _{1±x}	-	-	Monocarbonitride (cubic) continuous solid solution (complete solubility in the system?)	[5]

(continued)

Table 4.19 (continued)

System	Atmosphere	Temperature range, °C	Interaction character, products and/or compatibility	Reference
NbC _{1-x} -MgO	Vacuum 0.01-0.1 Pa	1300	The powdered mixtures of the components lose mass with the release of volatile products (metallic Mg and CO) and formation C-depleted NbC _{1-x} phases	[1, 5, 82, 480, 481, 550]
	Vacuum	1800-2300	Interaction with the formation of metallic Nb and NbC _x O _y oxycarbide phases in the contact zone of compact bulk materials <i>See also</i> section C-Mg-Nb-O in Table I-2.14	
NbC _{1-x} -Mn ₅ C ₂ , Mn ₇ C ₃	-	700-1000	Not (or very slightly) soluble in each other at solid state; NbC _{1-x} phase is in equilibrium with all Mn carbides and intermetallide and metallic Mn <i>See also</i> section C-Mn-Nb in Table I-2.14	[81, 585]
NbC _{1-x} - α-MoC _{1-x}	-	1900-2000	Extended monocarbide solid solution based on NbC _{1-x} - up to composition ~Nb _{0.10-0.15} Mo _{0.85-0.90} C _{1-x} ; the max. solubility of Nb in α-MoC _{1-x} is ~2 at. %	[5, 54, 57, 69, 81, 440, 441, 482, 568, 946, 988]
	-	~2000-2600	Monocarbide (cubic) continuous solid solution <i>See also</i> section C-Mo-Nb in Table I-2.14	
NbC _{1-x} - α-MoC _{1-x} - UC _{1±x}	-	2000	Extended monocarbide (cubic) solid solution based on NbC _{1-x} -UC _{1±x} continuous solid solution; the solubility of α-MoC _{1-x} in NbC _{1-x} is >90 mol. % (the solubilities of NbC _{1-x} and UC _{1±x} in α-MoC _{1-x} are ~1-3 mol. %)	[484]
	-	1900-2000	Extended monocarbide (cubic) solid solution based on NbC _{1-x} -ZrC _{1-x} continuous solid solution; the solubility of α-MoC _{1-x} in NbC _{1-x} and ZrC _{1-x} are >90 mol. % and >80 mol. %, respectively (the solubilities of NbC _{1-x} and ZrC _{1-x} in α-MoC _{1-x} are low)	[27, 484, 759]
NbC _{1-x} - α-MoC _{1-x} - ZrC _{1-x}	-	>2000	Monocarbide (cubic) continuous solid solution (complete solubility in the system) <i>See also</i> section C-Mo-Nb-Zr in Table I-2.14	
	-	~2000	The max. solubility of Nb in β-Mo _{2±x} C corresponds to ~ (Mo _{0.6} Nb _{0.4}) _{2±x} C composition <i>See also</i> section C-Mo-Nb in Table I-2.14	[54, 57, 69, 441, 946]
α-Nb ₂ C- α-Mo _{2+x} C	-	1200	Semicarbide (orthorhombic) solid solution based on α-Nb ₂ C <i>See also</i> section C-Mo-Nb in Table I-2.14	[562]
β-Nb _{2+x} C- β-Mo _{2±x} C	-	1750	Semicarbide (hexagonal) solid solution based on β-Nb _{2+x} C; the max. solubility of Mo is ~3 at. % <i>See also</i> section C-Mo-Nb in Table I-2.14	[54, 57, 69, 441, 562]

(continued)

Table 4.19 (continued)

System	Atmo- sphere	Temperature range, °C	Interaction character, products and/or compatibility	Reference
β -Nb _{2+x} C– β -Mo _{2±x} C– α -Ta _{2+x} C			See section α -Ta _{2+x} C– β -Mo _{2±x} C– β -Nb _{2+x} C in Table 2.22 See also section C–Mo–Nb–Ta in Table I-2.14	
NbC _{1-x} – δ -NbN _{1-x}	–	1250–2130	Monocarbonitride (cubic) continuous solid solution (the variation of lattice parameter <i>a</i> , nm with composition for Nb(C _{1-x} N _x) phases (0 ≤ <i>x</i> ≤ 1) is linear: <i>a</i> = 0.4470 – 0.0080 <i>x</i>)	[5, 34, 69, 485–487, 494, 495, 508, 842, 899, 1030, 1090–1092]
β -Nb _{2+x} C– β -Nb _{2±x} N	–	1250–1450	See also section C–N–Nb in Table I-2.14 Semicarbonitride continuous solid solution	[69, 485]
NbC _{1-x} – δ -NbN _{1-x} –NbO	–	–	See also section C–N–Nb in Table I-2.14 Formation of NbC _{1-x} N _y O _z oxycarbonitride phase ^a based on NbC _{1-x} – δ -NbN _{1-x} (cubic) continuous solid solution	[34, 59]
NbC _{1-x} – δ -NbN _{1-x} – δ -WC _{1±x}	–	–	General consideration of the system	[427, 428]
NbC _{1-x} – δ -NbN _{1-x} – HfN _{1±x}	Pure N ₂	1200–2500	See also section C–N–Nb–W in Table I-2.14 Monocarbonitride (cubic) continuous solid solution (complete solubility in the system)	[34]
NbC _{1-x} – δ -NbN _{1-x} – δ -TiN _{1±x}	Pure N ₂	1200–2500	Monocarbonitride (cubic) continuous solid solution (complete solubility in the system)	[34, 1090– 1092]
NbC _{1-x} – δ -NbN _{1-x} – δ -TiN _{1±x} –ZrN _{1±x}	Pure N ₂	1200–2500	Monocarbonitride (cubic) continuous solid solution (complete solubility in the system)	[34]
NbC _{1-x} – δ -NbN _{1-x} – δ -VN _{1-x}	Pure N ₂	1200–2500	Monocarbonitride (cubic) continuous solid solution (complete solubility in the system)	[34]
NbC _{1-x} –NbB _{2±x}	–	≤2000	The components are compatible and virtually insoluble in each other	[2, 5, 473, 474, 488]
	–	~2600–2900 (?)	Eutectic NbC _{1-x} –NbB _{2±x} ; the max. solid solubility of NbB _{2±x} in NbC _{1-x} is ~7 mol.% and that of NbC _{1-x} in NbB _{2±x} is ~1–2 mol.% See also section C–B–Nb in Table I-2.14	
NbC _{1-x} –NbB _{1±x}	–	~2800	Eutectic NbC _{1-x} –NbB _{1±x}	[5, 473, 474]
β -Nb _{2+x} C– NbB _{1±x}			See also section C–B–Nb in Table I-2.14 See section C–B–Nb in Table I-2.14	

(continued)

Table 4.19 (continued)

System	Atmosphere	Temperature range, °C	Interaction character, products and/or compatibility	Reference
NbC _{1-x} - β-Nb ₂ O ₅	Vacuum 10 Pa	1200–1500	Decrease of the content of carbon in NbC _{1-x} and formation of new phases (β-Nb _{2+x} C, traces NbO) in the powdered mixtures (1 h exposure)	[1, 59, 82, 481, 505–507, 550, 742–744, 868]
	CO, 0.01–101 kPa	1300–2000	Formation of NbC _{1-x} O _y (NbC _{1-x} –‘NbO’ oxycarbide (cubic) solid solution) with approximate homogeneity limits: ~NbC _{0.70} –~NbC _{0.50} O _{0.15} –~NbC _{0.35} O _{0.45} –~NbC _{0.35} O _{0.65} –~NbC _{0.99}	
	Vacuum 10 Pa	1600–1900	Formation of β-Nb _{2+x} C and metallic Nb (1 h exposure)	
	Vacuum, Ar Vacuum >1900 <10 Pa	1900	Formation of oxycarbide (cubic) phase NbC _{0.24–0.71} O _{0.05–0.62} (0.65 ≤ 1-x+y ≤ 1.12) In the powdered mixtures with general O/C ratio = 1.01–1.05 the only product is metallic Nb with some O and C contaminations <i>See also</i> section C–Nb–O in Table I-2.14	
β-Nb _{2+x} C– β-Nb ₂ O ₅	CO, 0.01–101 kPa	1300–2000	Formation of Nb ₂ C _x O _y oxycarbide (hexagonal) solid solution based on β-Nb _{2+x} C with approximate homogeneity composition limits: Nb _{2.5} C–Nb ₂ (C _{0.3} O _{0.3})–Nb ₂ (C _{0.15} O _{0.7})–Nb ₂ (C _{0.35} O _{0.8})–Nb _{2.0} C	[59, 742–744, 868]
	Vacuum, Ar	1900	Formation of oxycarbide (hexagonal) phase Nb ₂ C _{0.33–0.34} O _{0.08–0.17} (0.42 ≤ x+y ≤ 0.50) <i>See also</i> section C–Nb–O in Table I-2.14	
NbC _{1-x} –NbO	Ar, 0.1 MPa	1400	Formation of oxycarbide (cubic) phases NbC _x O _y	[5, 743, 868]
	Vacuum, 0.13 Pa	1600–1700	Decomposition of oxycarbide (cubic) phases NbC _x O _y	
	–	–	Terminal mutual solid solubilities between the components, ? <i>See also</i> section C–Nb–O in Table I-2.14	
β-Nb _{2+x} C–NbO	Ar, 0.1 MPa	1400	Formation of oxycarbide (hexagonal) phases Nb ₂ C _x O _y	[743, 868]
	Vacuum, 0.13 Pa	1600–1700	Decomposition of oxycarbide (hexagonal) phases Nb ₂ C _x O _y <i>See also</i> section C–Nb–O in Table I-2.14	
NbC _{1-x} –NbSi ₂	–	~ 1880–1920	Eutectic (degenerated) NbC _{1-x} –NbSi ₂ ; no mutual solubilities between the components <i>See also</i> section C–Nb–Si in Table I-2.14 <i>See</i> section C–Nb–Si in Table I-2.14	[2, 5, 123, 452–454]
β-Nb _{2+x} C– NbSi ₂	–	–	Terminal mutual solid solubilities between the components (?)	[5]

(continued)

Table 4.19 (continued)

System	Atmo- sphere	Temperature range, °C	Interaction character, products and/or compatibility	Reference
NbC _{1-x} - Nd ₂ Fe ₁₄ B	Pure Ar	1000	The solubility of NbC _{1-x} in complex boride phase is ~8 mol.%	[1007]
NbC _{1-x} -NpC _{1-x}	-	-	Terminal mutual solid solubilities between the components (?)	[5]
NbC _{1-x} -NpN _{1±x}	-	-	Monocarbonitride (cubic) continuous solid solution (complete solubility in the system?)	[5]
NbC _{1-x} -PrN _{1±x}	-	-	Terminal mutual solid solubilities between the components (?)	[5]
NbC _{1-x} -PuC _{1-x}	-	>1600	Monocarbide (cubic) continuous solid solution (complete solubility in the system) <i>See also</i> section C-Nb-Pu in Table I-2.14	[5, 69]
NbC _{1-x} -PuN _{1±x}	-	-	Terminal mutual solid solubilities between the components (?)	[5]
NbC _{1-x} -PuP _{1±x}	-	-	Terminal mutual solid solubilities between the components (?)	[5]
NbC _{1-x} -PuS _{1±x}	-	-	Terminal mutual solid solubilities between the components (?)	[5]
NbC _{1-x} -ScC _{1-x}	-	-	Monocarbide (cubic) continuous solid solution (complete solubility in the system)	[5, 556]
NbC _{1-x} -ScN _{1±x}	-	-	Monocarbonitride (cubic) continuous solid solution (complete solubility in the system?)	[5]
NbC _{1-x} - α/β -SiC	-	-	Compatible with each other within the temperature range of the thermal stabilities of the phases <i>See also</i> section C-Nb-Si in Table I-2.14	[5, 452- 454]
β -Nb _{2+x} C-SiC	-	-	<i>See</i> section C-Nb-Si in Table I-2.14	
NbC _{1-x} - α/β -Si ₃ N ₄	-	~1400-1600	Interaction leads to the formation of Nb silicide phases and SiC	[1005, 1006]
NbC _{1-x} -SiO ₂ - Al ₂ O ₃ -CaO- Fe ₂ O ₃ (basalt)	-	1400	NbC _{1-x} is not stable in molten basalt (SiO ₂ - 15% Al ₂ O ₃ - 13% CaO - 13% Fe ₂ O ₃) at short-term exposure (0.5-1 h) with average dissolution rate ~0.2 g cm ⁻² h ⁻¹	[1027]
NbC _{1-x} -SmN _{1±x}	-	-	Terminal mutual solid solubilities between the components (?)	[5]
NbC _{1-x} -TaC _{1-x}	-	-	<i>See</i> section TaC _{1-x} -NbC _{1-x} in Table 2.22 <i>See also</i> section C-Nb-Ta in Table I-2.14	
NbC _{1-x} -TaC _{1-x} - -ThC _{1±x}	-	-	<i>See</i> section TaC _{1-x} -NbC _{1-x} -ThC _{1±x} in Table 2.22	
NbC _{1-x} -TaC _{1-x} - -TiC _{1-x}	-	-	<i>See</i> section TaC _{1-x} -NbC _{1-x} -TiC _{1-x} in Table 2.22 <i>See also</i> section C-Nb-Ta-Ti in Table I-2.14	
NbC _{1-x} -TaC _{1-x} - - δ -TaN _{1-x} - TiC _{1-x}	-	-	<i>See</i> section TaC _{1-x} - δ -TaN _{1-x} -NbC _{1-x} - TiC _{1-x} in Table 2.22	
NbC _{1-x} -TaC _{1-x} - -UC _{1±x}	-	-	<i>See</i> section TaC _{1-x} -NbC _{1-x} -UC _{1±x} in Table 2.22	

(continued)

Table 4.19 (continued)

System	Atmosphere	Temperature range, °C	Interaction character, products and/or compatibility	Reference
NbC _{1-x} -TaC _{1-x} -VC _{1-x}			See section TaC _{1-x} -NbC _{1-x} -VC _{1-x} in Table 2.22	
NbC _{1-x} -TaC _{1-x} -δ-WC _{1±x}			See section TaC _{1-x} -NbC _{1-x} -δ-WC _{1±x} in Table 2.22 See also section C-Nb-Ta-W in Table I-2.14	
NbC _{1-x} -TaC _{1-x} -ZrC _{1-x} β-Nb _{2+x} C- α-Ta _{2+x} C			See section TaC _{1-x} -NbC _{1-x} -ZrC _{1-x} in Table 2.22 See section α-Ta _{2+x} C-β-Nb _{2+x} C in Table 2.22 See also section C-Nb-Ta in Table I-2.14	
β-Nb _{2+x} C- α-Ta _{2+x} C- γ-W _{2±x} C			See section α-Ta _{2+x} C-β-Nb _{2+x} C-γ-W _{2±x} C in Table 2.22 See also section C-Nb-Ta-W in Table I-2.14	
NbC _{1-x} - δ-TaN _{1-x}	N ₂ , 3 MPa	1800	Monocarbonitride (cubic) continuous solid solution (complete solubility in the system)	[42]
NbC _{1-x} - ε-TaN _{1-x}	N ₂	-	The max. solid solubility of cubic NbC _{1-x} in hexagonal ε-TaN _{1-x} is much lower (practically negligible) than that of ε-TaN _{1-x} in NbC _{1-x}	[5, 159]
NbC _{1-x} -TbN _{1±x}	-	-	Monocarbonitride (cubic) continuous solid solution (complete solubility in the system?)	[5]
NbC _{1-x} -TcC _{1-x}	-	-	Monocarbide continuous solid solution (complete solubility in the system?) See also section C-Nb-Tc in Table I-2.14	[546, 931]
β-Nb _{2+x} C- TcC _{1-x}			The mutual solid solubilities of the components are low (?) See also section C-Nb-Tc in Table I-2.14	[546, 931]
NbC _{1-x} -ThC _{1±x} (α-Th, γ-ThC _{2-x})	-	1500	Compatible with each other (mutual solid solubilities are very low) See also section C-Nb-Th in Table I-2.14	[5, 69, 490]
NbC _{1-x} -ThC _{1±x} -TiC _{1-x}	-	>2000	Practically, no mutual solubilities between NbC _{1-x} -TiC _{1-x} monocarbide continuous solid solution and ThC _{1±x}	[5, 477]
NbC _{1-x} -ThC _{1±x} -UC _{1±x}	-	>2000	Monocarbide continuous solid solution with great miscibility gap because of low mutual solubilities in the NbC _{1-x} -ThC _{1±x} system	[5, 477]
NbC _{1-x} -ThC _{1±x} -VC _{1-x}	-	>2000	Practically, no mutual solubilities between NbC _{1-x} -VC _{1-x} monocarbide continuous solid solution and ThC _{1±x}	[5, 477]
NbC _{1-x} -ThC _{1±x} -ZrC _{1-x}	-	> 2000	Practically, no mutual solubilities between NbC _{1-x} -ZrC _{1-x} monocarbide (cubic) continuous solid solution and ThC _{1±x}	[5, 477]

(continued)

Table 4.19 (continued)

System	Atmosphere	Temperature range, °C	Interaction character, products and/or compatibility	Reference
β -Nb _{2+x} C–ThC _{1±x}	–	1500	Mutual solid solubilities are very low <i>See also</i> section C–Nb–Th in Table I-2.14	[69, 490]
NbC _{1-x} – γ -ThC _{2-x}	–	1500	Compatible with each other (mutual solid solubilities are very low) <i>See also</i> section C–Nb–Th in Table I-2.14 <i>See</i> section C–Nb–Th in Table I-2.14	[5, 69, 490]
β -Nb _{2+x} C– γ -ThC _{2-x}	–	–	Extended monocarbonitride (cubic) solid solutions (terminal solubility?)	[5]
NbC _{1-x} –ThN _{1±x}	–	–	Terminal mutual solid solubilities between the components (?)	[5]
NbC _{1-x} –ThP _{1±x}	–	–	Terminal mutual solid solubilities between the components (?)	[5]
NbC _{1-x} –ThS _{1±x}	–	–	Terminal mutual solid solubilities between the components (?)	[5]
NbC _{1-x} –TiC _{1-x}	–	~ 0	Monocarbide extended solid solutions; the miscibility gap ranges from ~Nb _{0.15} Ti _{0.85} C _{1-x} to ~Nb _{0.7} Ti _{0.3} C _{1-x} (theoretically calculated)	[5, 46, 69, 145, 332, 459, 491, 492, 571, 572, 581, 817, 856, 876, 897, 920, 946, 955, 973–975, 988, 1001, 1002, 1030, 1087, 1093, 1094, 1100]
	–	~ 50–3100	Monocarbide continuous solid solution (the variation of lattice parameter <i>a</i> , nm with composition for (Nb _{1-y} Ti _y)C _{1-x} phases ($x \approx 0$, $0 \leq y \leq 1$) is linear: $a = 0.4470 - 0.0141y$); critical point of the miscibility gap is corresponding to ~50 °C and ~Nb _{0.40} Ti _{0.60} C _{1-x} composition (theoretically calculated)	[5, 46, 69, 145, 332, 459, 491, 492, 571, 572, 581, 817, 856, 876, 897, 920, 946, 955, 973–975, 988, 1001, 1002, 1030, 1087, 1093, 1094, 1100]
	–	1700–2000	No complete homogenization is achieved (1 h exposure) for two-phase carbide mixture prepared by carbothermal reduction of metal oxides	[1001, 1002, 1030, 1087, 1093, 1094, 1100]
	–	–	Formation of (Nb _{0.8} Ti _{0.2}) ₄ C ₃ T _x (MXene, 2D-Nb ₄ C ₃ -based solid solution, where T _x is a surface termination) <i>See also</i> section C–Nb–Ti in Table I-2.14	
β -Nb _{2+x} C–TiC _{1-x}	–	≤2280	The max. solubility of Ti in β -Nb _{2+x} C varies from ~5 to ~9 at.% <i>See also</i> section C–Nb–Ti in Table I-2.14	[69, 145, 459, 492]
γ -Nb _{2±x} C–TiC _{1-x}	–	2600	The max. solubility of Ti in γ -Nb _{2±x} C is ~1 at.% (?) <i>See also</i> section C–Nb–Ti in Table I-2.14	[69, 145, 459, 492]
NbC _{1-x} – δ -NbN _{1-x} –TiC _{1-x}	Pure N ₂	1200–2500	Monocarbonitride (cubic) continuous solid solution (complete solubility in the system)	[34, 571, 572, 1030]
NbC _{1-x} – δ -NbN _{1-x} –TiC _{1-x} – δ -TiN _{1±x}	–	1000–1500	Monocarbonitride (cubic) continuous solid solution (complete solubility in the system, the variation of lattice parameter <i>a</i> , nm with composition for (Nb _{1-y} Ti _y)(C _{1-x} N _x) phases ($0 \leq x \leq 1$, $0 \leq y \leq 1$): $a = 0.4470 - 0.0080x - 0.0141y - 0.0002xy$)	[1, 494, 571, 572, 899, 997, 1030, 1071]

(continued)

Table 4.19 (continued)

System	Atmosphere	Temperature range, °C	Interaction character, products and/or compatibility	Reference
NbC _{1-x} -TiC _{1-x} -UC _{1±x}	-	2000-2050	Monocarbide continuous solid solution with great miscibility gap because of low mutual solubilities in the TiC _{1-x} -UC _{1±x} system <i>See also</i> section C-Nb-Ti-U in Table I-2.14	[5, 69, 477]
NbC _{1-x} -TiC _{1-x} -VC _{1-x}	-	1000	Monocarbide continuous solid solution with the miscibility gap as the mutual solubilities in the NbC _{1-x} -VC _{1-x} system are ~ 10 mol.%	[5, 81, 435, 477, 493, 494, 817, 899]
	-	1600-2000	Monocarbide (cubic) continuous solid solution (complete solubility in the system) <i>See also</i> section C-Nb-Ti-V in Table I-2.14	
NbC _{1-x} -TiC _{1-x} -δ-WC _{1±x}	-	1450	Extended solid solution based on NbC _{1-x} -TiC _{1-x} monocarbide continuous solid solution; the solubilities of δ-WC _{1±x} in NbC _{1-x} and TiC _{1-x} are ~ 10 and ~ 35 mol.%, respectively (the solubilities of NbC _{1-x} and TiC _{1-x} in δ-WC _{1±x} are very low)	[5, 81, 145, 477, 489]
	-	1900-2000	Extended solid solution based on NbC _{1-x} -TiC _{1-x} monocarbide continuous solid solution; the solubilities of δ-WC _{1±x} in NbC _{1-x} and TiC _{1-x} are ~ 35 and ~ 60 mol.%, respectively (the solubilities of NbC _{1-x} and TiC _{1-x} in δ-WC _{1±x} are very low) <i>See also</i> section C-Nb-Ti-W in Table I-2.14	
NbC _{1-x} -TiC _{1-x} -ZrC _{1-x}	-	1900-2000	Monocarbide (cubic) continuous solid solution (complete solubility in the system)	[5, 81, 477]
NbC _{1-x} - δ-TiN _{1±x}	-	~ 2600	Monocarbonitride continuous solid solution (complete solubility in the system)	[5, 495, 571, 572, 1030]
NbC _{1-x} -TiO _{1±x}	-	-	Terminal mutual solid solubilities between the components (?)	[5]
NbC _{1-x} -UC _{1±x}	-	1200-1800	Monocarbide extended solid solutions (?)	[5, 69, 81, 477, 484, 496-498, 727, 937]
		1900-2100	Monocarbide continuous solid solution (a spacing-composition curve in the system is almost linear) <i>See also</i> section C-Nb-U in Table I-2.14	
NbC _{1-x} -UC _{1±x} - VC _{1-x}	-	1900-2050	Monocarbide continuous solid solution with great miscibility gap because of low mutual solubilities in the UC _{1±x} -VC _{1-x} system <i>See also</i> section C-Nb-U-V in Table I-2.14	[5, 69, 477]
NbC _{1-x} -UC _{1±x} - δ-WC _{1±x}	-	1900-2000	The solubility of δ-WC _{1±x} in NbC _{1-x} -UC _{1±x} monocarbide (cubic) continuous solid solution increases with increasing content of Nb from low values up to ~ 30-35 mol.%	[5]

(continued)

Table 4.19 (continued)

System	Atmosphere	Temperature range, °C	Interaction character, products and/or compatibility	Reference
NbC _{1-x} -UC _{1±x} ZrC _{1-x}	-	1400–1800	Monocarbide (cubic) continuous solid solution with a miscibility gap because of lower mutual solubilities in the NbC _{1-x} -UC _{1±x} system; the miscibility gap shortens noticeably with increasing temperature, mainly due to increasing the solubility of NbC _{1-x} in UC _{1±x}	[5, 69, 81, 477, 484, 727, 940–942, 947, 1099]
	-	1900–2050	Monocarbide (cubic) continuous solid solution (complete solubility in the system)	
	-	~2400	(Nb,Zr,U)C _{1+x} hyper-stoichiometric mixed carbide phase based on ZrC _{~1.0} with 5–10 mol.% UC _{1+x} is formed from powdered individual carbides mixture (exposure >20 min)	
	-	>2530	(Nb,Zr,U)C _{1-x} hypo-stoichiometric mixed carbide phase ($x = 0.05$) based on ZrC _{~1.0} with 5–10 mol.% U carbide is formed from the powdered mixture of Zr and Nb carbides with UH ₃ and C addition <i>See also</i> section C–Nb–U–Zr in Table I-2.14	
β -Nb _{2+x} C–UC _{1±x}			<i>See</i> section C–Nb–U in Table I-2.14	
NbC _{1-x} - ζ -U ₂ C ₃			<i>See</i> section C–Nb–U in Table I-2.14	
NbC _{1-x} - α -UC _{2-x}	-	1700	The components are compatible; no solubility of NbC _{1-x} in α -UC _{2-x} <i>See also</i> section C–Nb–U in Table I-2.14	[465, 498]
β -Nb _{2+x} C– α -UC _{2-x}			<i>See</i> section C–Nb–U in Table I-2.14	
NbC _{1-x} -UN _{1-x}	-	-	Monocarbonitride (cubic) continuous solid solution (complete solubility in the system?)	[5]
NbC _{1-x} -UP _{1±x}	-	-	Terminal mutual solid solubilities between the components (?)	[5]
NbC _{1-x} -US _{1±x}	-	-	Terminal mutual solid solubilities between the components (?)	[5]
NbC _{1-x} -VC _{1-x}	-	1300	Monocarbide extended solid solutions; the miscibility gap ranges from ~Nb _{0.80} V _{0.20} C _{1-x} to ~Nb _{0.15} V _{0.85} C _{1-x}	[5, 69, 81, 145, 446, 476, 493,
	-	1500	Monocarbide extended solid solutions; the miscibility gap ranges from ~Nb _{0.60} V _{0.40} C _{1-x} to ~Nb _{0.22} V _{0.78} C _{1-x}	494, 499, 817, 818, 892, 897,
	-	From 1600–1700 (or ~1450, ?) up to 2700	Monocarbide (cubic) continuous solid solution (the variation of lattice parameter a , nm with composition for (Nb _{1-y} V _y)C _{1-x} phases ($x \approx 0, 0 \leq y \leq 1$) is non-linear: $a = 0.4470 - 0.0216y - 0.0082y^2$); critical point of the miscibility gap is cor- resp. to ~1600–1700 °C (or 1400–1480 °C ?) and ~Nb _{0.35–0.45} V _{0.55–0.65} C _{1-x} composition <i>See also</i> section C–Nb–V in Table I-2.14	899, 939, 1030, 1094]

(continued)

Table 4.19 (continued)

System	Atmosphere	Temperature range, °C	Interaction character, products and/or compatibility	Reference
NbC _{1-x} -VC _{1-x} - δ-VN _{1-x}	-	-	Monocarbonitride (cubic) continuous solid solution (complete solubility in the system, the variation of lattice parameter <i>a</i> , nm with composition for (Nb _{1-y} V _y)(C _{1-x} N _x) phases ($0 \leq x \leq 1, 0 \leq y \leq 1$): $a = 0.4470 - 0.0080x - 0.0298y + 0.0044xy$)	[34, 159, 899, 1030]
NbC _{1-x} -VC _{1-x} - δ-WC _{1±x}	-	-	Extended solid solution based on NbC _{1-x} -VC _{1-x} monocarbide continuous solid solution; the max. solubilities of δ-WC _{1±x} in NbC _{1-x} and VC _{1-x} are ~30 and ~60 mol.%, respectively (the solubilities of NbC _{1-x} and VC _{1-x} in δ-WC _{1±x} are very low)	[5, 477]
NbC _{1-x} -VC _{1-x} - ZrC _{1-x}	-	1900–2050	Monocarbide (cubic) continuous solid solution with the great miscibility gap limited by ~(<i>V</i> _{0.99} Zr _{0.01})C _{1-x} ~ (<i>V</i> _{0.03} Zr _{0.97})C _{1-x} ~ (Nb _{0.50} V _{0.30} Zr _{0.20})C _{1-x} compositions	[5, 81, 477]
NbC _{1-x} - VC _{1-x} -δ-NbN _{1-x} - δ-VN _{1-x} - NbC _{1-x} -δ-VN _{1-x}	-	1000–1200	General consideration of the system	[494, 899]
β-Nb _{2+x} C- β-V _{2±x} C	-	1400–2200	Semicarbide (hexagonal) continuous solid solution	[145, 476, 499]
	-	2200–2450	Extended solid solution based on β-Nb _{2+x} C; the max. solubility of V in it decreases with temperature growth from ~48 to ~20 at.%. <i>See also</i> section C–Nb–V in Table I-2.14	
γ-Nb _{2±x} C- β-V _{2±x} C	-	2450	Extended solid solution based on γ-Nb _{2±x} C; the max. solubility of V is ~1 at.%	[145, 499]
	-	2530–2650	Extended solid solution based on γ-Nb _{2±x} C; the max. solid solubility of V varies from 10 to 15 at.%. <i>See also</i> section C–Nb–V in Table I-2.14	
NbC _{1-x} - β-W ₂ B _{5-x}	-	2250	Eutectic NbC _{1-x} -β-W ₂ B _{5-x}	[908]
NbC _{1-x} - γ-WC _{1-x}	-	~2550–2850	Monocarbide (cubic) continuous solid solution <i>See also</i> section C–Nb–W in Table I-2.14	[5, 69, 145, 440, 460, 461]
NbC _{1-x} - δ-WC _{1±x}	-	1700–2000	The max. solid solubility of W in NbC _{1-x} corresponds to ~(<i>Nb</i> _{0.65–0.70} <i>W</i> _{0.30–0.35})C _{1-x} composition and that of Nb in δ-WC _{1±x} is ~2 at.%; the solubility of W increases with increasing value of <i>x</i> index in NbC _{1-x}	[5, 81, 441, 460, 461, 837]
	-	2300–2500	Solubility of δ-WC _{1±x} in NbC _{1-x} is <1 mol.%	
	-	~2500	The max. solubility of W in NbC _{1-x} corresponds to compos. ~(<i>Nb</i> _{0.05–0.30} <i>W</i> _{0.70–0.95})C _{1-x} and that of Nb in δ-WC _{1±x} is ~1.5 at.%	
	-	2690	The max. solid solubility of Nb in δ-WC _{1±x} is ~2 at.%	
	-	2860	The max. solubility of W in NbC _{1-x} corresponds to compos. ~(<i>Nb</i> _{0.25} <i>W</i> _{0.75})C _{1-x} <i>See also</i> section C–Nb–W in Table I-2.14	

(continued)

Table 4.19 (continued)

System	Atmosphere	Temperature range, °C	Interaction character, products and/or compatibility	Reference
NbC _{1-x} - δ-WC _{1±x} -ZrC _{1-x}	-	-	Extended solid solution based on NbC _{1-x} -ZrC _{1-x} monocarbide (cubic) continuous solid solution; the max. solubilities of δ-WC _{1±x} in NbC _{1-x} and ZrC _{1-x} are ~30–35 mol.% (the solubilities of NbC _{1-x} and ZrC _{1-x} in δ-WC _{1±x} are very low)	[5, 477]
NbC _{1-x} - α-W _{2+x} C	-	1700	The max. solid solubility of Nb in α-W _{2+x} C is ~18 at.%; the effects of semicarbide phase transitions on phase equilibrium and solubility are not determined <i>See also</i> section C–Nb–W in Table I-2.14	[5, 441, 460, 461]
NbC _{1-x} - γ-W _{2±x} C	-	2490–2690	The max. solubility of Nb in γ-W _{2±x} C varies from ~23 to ~25 at.%; <i>See also</i> section C–Nb–W in Table I-2.14	[5, 441, 460, 461]
β-Nb _{2+x} C- α/β-W _{2+x} C	-	1700–2490	The max. solubility of W in β-Nb _{2+x} C is ~1–2; the effects of semicarbide phase transitions on phase equilibrium and solubility are not determined <i>See also</i> section C–Nb–W in Table I-2.14	[441, 460, 461]
γ-Nb _{2±x} C- γ-W _{2±x} C	-	2690	The solubility of W in γ-Nb _{2±x} C is very low; the effects of semicarbide phase transitions on phase equilibrium and solubility are not determined <i>See also</i> section C–Nb–W in Table I-2.14	[441, 460, 461]
NbC _{1-x} -YC _{1±x}	-	-	Terminal mutual solid solubilities between the components (?)	[5]
NbC _{1-x} -YN _{1±x}	-	-	Terminal mutual solid solubilities between the components (?)	[5]
NbC _{1-x} -YbN _{1±x}	-	-	Monocarbonitride (cubic) continuous solid solution (complete solubility in the system?)	[5]

(continued)

Table 4.19 (continued)

System	Atmosphere	Temperature range, °C	Interaction character, products and/or compatibility	Reference
NbC _{1-x} -ZrC _{1-x}	-	300	Monocarbide extended solid solutions; the miscibility gap ranges from ~Nb _{0.3} Zr _{0.7} C _{1-x} to ~Nb _{0.9} Zr _{0.1} C _{1-x} (theoretically calculated)	[5, 27, 69, 145, 209, 412, 441, 463, 476,
	-	~410–3400 (or 1600–3400, ?)	Monocarbide (cubic) continuous solid solution (the variation of lattice parameter <i>a</i> , nm with composition for (Nb _{1-y} Zr _y)C _{1-x} phases ($x \approx 0, 0 \leq y \leq 1$) is linear: $a = 0.4470 + 0.0230y$); the critical point of the miscibility gap is corresponding to ~410–570 °C and ~Nb _{0.55-0.65} Zr _{0.35-0.45} C _{1-x} composition	482, 484, 491, 500–502, 522, 557, 558, 583, 759, 808, 817, 844, 887,
	-	>940	The homogeneity region limits of monocarbide (cubic) continuous solid solution phase are ZrC _{0.60} -NbC _{0.70} -NbC _{~1.0} -ZrC _{0.98} compositions	889, 892, 920, 939, 991, 1013, 1018, 1028, 1030, 1086, 1094, 1100]
	-	<1900	No solid solution is formed (1 h exposure) for a two carbides powdered mixture treated by hot pressing	
	Ar, >0.1 MPa	1900–2000	Additions of NbC _{1-x} have no contribution to ZrC _{1-x} hot-pressing densification process, as the formation of solid solutions requires higher temperatures and longer time	
	-	-	Formation of (Nb _{0.8} Zr _{0.2}) ₄ C ₃ T _x (MXene, 2D-Nb ₄ C ₃ -based solid solution, where T _x is a surface termination) <i>See also</i> section C-Nb-Zr in Table I-2.14	
β-Nb _{2+x} C-ZrC _{1-x}	-	1500–1800	The solid solubility of Zr in β-Nb _{2+x} C is low <i>See also</i> section C-Nb-Zr in Table I-2.14	[5, 69, 145, 441, 476]
NbC _{1-x} -ZrC _{1-x} -ZrN _{1±x}	-	-	Monocarbonitride (cubic) continuous solid solution (complete solubility in the system, the variation of lattice parameter <i>a</i> , nm with composition for (Nb _{1-y} Zr _y)(C _{1-x} N _x) phases ($0 \leq x \leq 1, 0 \leq y \leq 1$): $a = 0.4470 - 0.0080x + 0.0230y - 0.0045xy$)	[407, 495, 842, 1030]
NbC _{1-x} -ZrN _{1±x}	-	2450	Monocarbonitride (cubic) continuous solid solution (complete solubility in the system)	[5, 30, 407, 495, 842]
NbC _{1-x} -ZrP _{1±x}	-	-	Terminal mutual solid solubilities between the components (?)	[5]

(continued)

Table 4.19 (continued)

System	Atmosphere	Temperature range, °C	Interaction character, products and/or compatibility	Reference
NbC _{1-x} - β/γ-ZrO _{2-x}	-	>1300	Formation of mixed (complex) oxides and carbides in the contact zone between the compact dense NbC _{1-x} and powdered ZrO _{2-x}	[1, 5, 480, 481, 503, 504, 560, 582, 737]
	Vacuum 0.1–1 Pa	~1400–2100	Mass loss in the powdered mixtures with a simultaneous decrease of the content of combined carbon in them and formation of mixed phases Nb _{1-z} Zr _z C _{1-x} and Zr _{1-y} Nb _y O _{2-y}	
	Ar	1600–1650	No new phases are formed in NbC _{1-x} + β-ZrO _{2-x} powdered (2.3 and 0.8 μm mean grain sizes, respectively) mixtures treated by hot pressing (up to 1 h exposure)	
	Vacuum 10 Pa	≥2100	The formation of intermediate phases in the contact zone between the compact dense materials <i>See also section C–Nb–O–Zr in Table I-2.14</i>	

^aPractically, due to the serious difficulties in manufacturing transition metal carbide materials non-contaminated in any degree by O and N, all the materials labeled in literature as NbC_{1-x} with the appropriate certification more likely would have to be considered as NbC_{1-x}N_yO_z with low or very low values of y and z indexes

Table 4.20 Chemical interaction of niobium carbide phases with gaseous media at elevated, high and ultra-high temperatures (reaction systems are given in alphabetical order)

System	Atmosphere	Temperature range, °C	Interaction character, products and/or compatibility	Reference
NbC _{1-x} -CO	CO	-	Formation of oxycarbide phases NbC _{1-x} O _y (extended substitution solid solution based on NbC _{1-x} with approximate homogeneity limits: ~NbC _{0.70} ~NbC _{0.50} O _{0.15} ~NbC _{0.35} O _{0.45} ~NbC _{0.35} O _{0.65} ~NbC _{0.99}) <i>See also section C–Nb–O in Table I-2.14</i>	[59, 828]
NbC _{1-x} -CO ₂	CO ₂	-	Formation of oxycarbide phases NbC _{1-x} O _y (extended substitution solid solution based on NbC _{1-x} with approximate homogeneity limits: ~NbC _{0.70} ~NbC _{0.50} O _{0.15} ~NbC _{0.35} O _{0.45} ~NbC _{0.35} O _{0.65} ~NbC _{0.99}) and subsequent formation of oxide scales <i>See also section C–Nb–O in Table I-2.14</i>	[59, 828]

(continued)

Table 4.20 (continued)

System	Atmosphere	Temperature range, °C	Interaction character, products and/or compatibility	Reference	
NbC _{1-x} -Cl ₂	Cl ₂	400–800	The interaction leads to the volatilization of NbCl ₅ and formation of surface porous graphite or carbonaceous “cinder” layer growing in the accordance with linear law (apparent activation energy $E = 38 \text{ kJ mol}^{-1}$): $\text{NbC}_{1-x} + 2\frac{1}{2}\text{Cl}_2 = \text{NbCl}_5 \uparrow + (1-x)\text{C}$; at higher temperatures the diffusion resistance of the layer is more considerable, so the reaction rate at 600 °C is higher than at 800 °C due to some changes in the carbide-derived carbon layer structure ^a	[5, 64, 510, 511, 896]	
		700–900	Powdered NbC _{1-x} decomposes easily; remaining carbon presents the ordered structure, which is composed of concentric wavy graphene layers intermediate between onion-like carbon and carbon blacks (<i>see</i> Table I-2.3) with high surface area (up to $\sim 1300 \text{ m}^2 \text{ g}^{-1}$)		
NbC _{1-x} -H ₂	H ₂ , 0.1 MPa	25–1000	The solubility of H in NbC _{1-x} amounts to 5 at.% (?)	[5, 17, 44, 83, 177,	
		H ₂ , 0.1 MPa	700–1000	Formation of cubic carbohydride phases NbC _x H _y ($0.64 \leq x \leq 0.92$, $0 \leq y \leq 0.47$, ?)	210, 249, 542–545,
		H ₂ , 0.1 MPa	730–1330	The mass loss of compact NbC _{1-x} (32% porosity) observed in the range of ~ 0.1 –2% (1 h exposure) is a consequence of the formation and subsequent decomposition of the oxide phases due to residual O ₂ ; in comparison with vacuum ($<1.5 \text{ Pa}$) H ₂ promotes the mass loss of NbC _{1-x} due to the formation of NbH _x (?) and its subsequent decomposition	574, 727, 805, 824–826, 835, 1037]
	H ₂	2000–2500	Weak interaction with the minimally determined mass changes (?)		
	H ₂ (0.07–0.1% O ₂)	2180	Transformation of monocarbide phase into semicarbide after the exposure of 100 min; the gradient of C concentration is insignificant, though Nb _{2+x} C grains are observed all over the cross-section		
	H ₂ ($\sim 0.1\%$ O ₂)	2230	Active growth of Nb _{2+x} C grains is observed at the surface layers of materials		
	H ₂	2700	High resistance (if there is no gas flow or low gas exchange rate?)		
	H ₂ (0.07–0.1% O ₂)	2710–2730	Intensive decarburization with the formation of CH ₄ and damage of bulk parts; materials loss $-2 \times 10^{-2} \text{ g cm}^{-2}$ (exposure – 100 min) ^b		
	H ₂ (0.07–0.1% O ₂)	2830	Decarburization causes inhomogeneous concentration of C, changes in structure, decrease in the density and reduction in the strength (exposure – 17 min)		
				Data available in literature are very controversial <i>See also</i> section C–H–Nb in Table I-2.14	

(continued)

Table 4.20 (continued)

System	Atmosphere	Temperature range, °C	Interaction character, products and/or compatibility	Reference
α/β -Nb _{2+x} C-H ₂	H ₂ , 0.1 MPa	25–1000	The solubility of H in α/β -Nb _{2+x} C amounts to 11 at.% (?)	[83, 542–545, 855]
	H ₂ , 0.1–100 kPa	400–600	Equilibrium H ₂ pressures for the solid solutions containing from 1 to 10 at.% H	
	H ₂ , 0.1 MPa	1000	Formation of hexagonal carbonyl phases NbC _x H _y ($x \approx 0.5$, $0 \leq y \leq 0.6$, ?) <i>See also</i> section C–H–Nb in Table I-2.14	
NbC _{1-x} -N ₂	N ₂ , 0.1 MPa	1100–1400	Formation of NbC _{0.97} N _{0.02–0.03} carbonitride phase (15–24 h exposure)	[1, 5, 69, 82, 159, 170, 177, 485–487, 533, 548]
	N ₂ , 0.1–30 MPa	1100–1800	Formation of various carbonitride NbC _x N _z phases	
	N ₂	1250–1450	Formation of various carbonitride NbC _x N _z and δ -NbN _{1-x} nitride phases (15 h exposure)	
	N ₂	2400–2500	No interaction	
	N ₂	~3500	Noticeable decarbonization of carbide phases <i>See also</i> section C–N–Nb in Table I-2.14	
β -Nb _{2+x} C-N ₂	N ₂	1250–1450	Formation of various semicarbonitride Nb ₂ C _x N _z phases <i>See also</i> section C–N–Nb in Table I-2.14	[69, 485]
NbC _{1-x} -NH ₃	NH ₃	1000–1200	The formation of carbonitride and nitride phases	[82, 514]
NbC _{1-x} -O ₂ ^d	O ₂ (~0.8 Pa) ^e -Ar	20–800	The oxidation of small pieces (irregular shape, uniform thickness ~0.8 mm, mass ~0.1–1 mg) of single crystal NbC _{0.96} (100) in gaseous mixture stream (4.5 ppm O ₂) with heating rate ~10 K min ⁻¹ leads to the maximal reaction rate 1.35×10^{-10} mol s ⁻¹ at 425 °C with subsequent rate decline up to $\sim 0.4 \times 10^{-10}$ mol s ⁻¹ at 800 °C; the reactivity of (<i>hkl</i>) planes correlates with C occupancy in the unit cell of NbC _{1-x}	[5, 63, 67, 82, 93, 159, 177, 515–531, 547, 712, 717, 727, 743, 745, 746, 829–831]
	O ₂ (~0.8 Pa) ^e -Ar	180–360	In this temperature range the oxidation of sintered NbC _{~1.0} in gas mixture flow (5 ppm O ₂) with heating rate ~0.25 K min ⁻¹ leads to the maximal reaction rate 1.3×10^{-10} mol cm ⁻² s ⁻¹ at 250 °C with subsequent rate decline to $\sim 5 \times 10^{-12}$ mol cm ⁻² s ⁻¹ at >300 °C; after prolonged exposition (350 °C, 8 ppm O ₂) the ratio of O/C = $\sim 1.5 \times 10^{-3}$ was achieved in solid	
	Air	350–550	Powdered nanocrystalline NbC _{0.99} (average size of agglomerates ~60 nm) heating in the gas flow oxidizes with max. mass gain ~15% (maximum oxidation rate is at 480–550 °C)	

(continued)

Table 4.20 (continued)

System	Atmosphere	Temperature range, °C	Interaction character, products and/or compatibility	Reference
	Air	400–550	The oxidation of hot-pressed NbC _{1-x} (1–2% porosity) initiates by the formation of oxycarbide phases NbC _{1-x} O _y (extended substitutional solid solution based on NbC _{1-x} with approximate homogeneity limits: NbC _{0.7} –NbC _{0.5} O _{0.15} –NbC _{0.35} O _{0.45} –NbC _{0.35} O _{0.65} –NbC _{0.99}) with the subsequent occurrence of pentoxide α -Nb ₂ O ₅ C _x (with dissolved carbon in it, ?) and separation of carbon ^f (sometimes metallic Nb and suboxides NbO _x were determined in the scale as well, ?); oxide scales have good adherence with substrate and oxidation kinetics is described by linear law at long-term stages (the oxidation resistance of NbC _{1-x} is higher than that of pure Nb)	
	O ₂ , 0.5–2.8 kPa	400–800	Isothermal/isobaric oxidation kinetics of bulk materials NbC _{0.98} is described by linear-parabolic laws at the initial stages and linear law at the later stages, the effect of temperature is described by apparent activation energy $E \approx 50$ – 70 kJ mol^{-1} and effect of oxygen pressure – by power (exponent) index $m = 1$ with increasing at the later stages to $m = 1.5$	
	O ₂ /Ar, 4–16/ 36–24 kPa	420–600	Isothermal/isobaric oxidation kinetics of powdered NbC _{0.92–0.96} (mean grain size – 0.6 – $3.4 \text{ }\mu\text{m}$, surface area – 0.97 – $2.2 \text{ m}^2 \text{ g}^{-1}$) is described by Jander's equation and $E = 160 \pm 15 \text{ kJ mol}^{-1}$; β -Nb ₂ O _{5-x} and NbO form oxide scale slightly cracked at the initial stages and largely fractured with further oxidation	
	Air	450	The oxidation mass gain of NbC _{1-x} is 1.4 mg cm^{-2} and 5.0 mg cm^{-2} for 1 h and 2 h exposure, respectively	
	O ₂ /Ar, 20/80 kPa	515–540	Powdered NbC _{0.92–0.96} (mean grain size – 0.6 – $3.4 \text{ }\mu\text{m}$, surface area – 0.97 – $2.2 \text{ m}^2 \text{ g}^{-1}$) heated from $350 \text{ }^\circ\text{C}$ with $5 \text{ }^\circ\text{C min}^{-1}$ rate performs instantaneous self-heating and combustion (sudden $\sim 100\%$ oxidation mass increase and CO ₂ release marked with great/narrow exothermic DTA peak)	
	Air, flow	550–1000	Nanocrystalline NbC _{0.99} preliminarily oxidized at 350 – $550 \text{ }^\circ\text{C}$ (relative degree of oxidation is $\sim 60\%$) performs high gas corrosion resistance as its mass remains almost constant during further heating up to $1000 \text{ }^\circ\text{C}$	

(continued)

Table 4.20 (continued)

System	Atmosphere	Temperature range, °C	Interaction character, products and/or compatibility	Reference
	O ₂ /Ar, 20/80 kPa	580–880	Single crystal NbC _{0.95–0.97} (100) 0.05–2 mm in size heated with 5 °C min ⁻¹ rate performs gradual mass gain increase with increasing temperature (broad exothermic DTA peak with maximum around 800 °C)	
	Air	600	The oxidation mass gain of NbC _{1-x} is 11.7 mg cm ⁻² (1 h exposure)	
	Air	600–700	The oxidation of hot-pressed (1–2% porosity) NbC _{1-x} evolves by the formation of oxide scales containing α-Nb ₂ O ₅ C _x (with dissolved carbon in it, ?), α-NbO _{2±x} and dispersed carbon phase burning-off gradually (sometimes metallic Nb was determined in the scale as well, ?); oxide scales have no good adherence with substrate and oxidation kinetics is described by linear law at the initial stages and parabolic law at the later stages (the oxidation resistance of NbC _{1-x} is lower than that of pure metal Nb)	
	O ₂ , 5 × 10 ⁻⁴ Pa	600–700	The oxidation of synthetically grown NbC _{1-x} film (thickness 50 nm) gives the oxide scale (thickness 4.7–5.6 nm for 45 min exposure) containing γ-NbO _{2-x} , α-NbO ₂ , β-Nb ₂ O _{5-x} and α-Nb ₂ O ₅ (the reactivity of NbC _{1-x} film is lower than that of pure metallic Nb film under the same conditions)	
	O ₂ , 0.03–13 kPa	600–900	The oxidation of sintered NbC _{0.94} (1–5% porosity, mean grain size ~ 50–100 μm) leads to the formation of single phase α-Nb ₂ O ₅ scale (the only traces of β-Nb ₂ O _{5-x} at 800 °C and 6.7 kPa, carbon burning-off in the scale is incomplete); oxidation kinetics is described by quasi-linear law with apparent activation energy $E = 92 \pm 8 \text{ kJ mol}^{-1}$ and power (exponent) index $m = 1.4 \pm 0.1$ (limiting stage is oxygen adsorption)	
	O ₂ /Ar, 0.8/~10 ⁵ Pa	700–900	The effect of temperature on the oxygen consumption of sintered NbC _{1-x} (~40% porosity) is described by apparent activation energy $E = 96 \pm 5 \text{ kJ mol}^{-1}$	
	Air	700–900	The oxidation rate of hot-pressed NbC _{1-x} (1–2% porosity) grows sharply, the oxide scale containing α-NbO _{2±x} , α-Nb ₂ O ₅ and stabilized by carbon (?) β-Nb ₂ O _{5-x} loses its protective properties completely and crumbles away from the surface of samples; oxidation kinetics is described by linear law	

(continued)

Table 4.20 (continued)

System	Atmosphere	Temperature range, °C	Interaction character, products and/or compatibility	Reference
	Air flow, $\sim 5 \text{ cm s}^{-1}$	800	Oxidation mass gain of hot-pressed NbC_{1-x} (porosity $\sim 4\%$) is 57 mg cm^{-2} (0.5 h exposure)	
	O_2 , 0.5–2.8 kPa	800–1100	The effect of temperature on the oxidation rate of sintered NbC_{1-x} is described by negative apparent activation energy and effect of oxygen pressure – by power (exponent) index $m = 1$ (0.5–1 kPa) and $m \approx 1/5$ (1–2.8 kPa)	
	O_2 , 1.3 kPa	800–1100	The effect of temperature on the oxidation rate of arc-cast $\text{NbC}_{\sim 1.0}$ with 3 mas.% non-combined carbon is described by negative apparent activation energy	
	O_2 , 0.03 kPa	900–1300	The oxidation mass gain of sintered $\text{NbC}_{0.94}$ (1–5% porosity, mean grain size – 50–100 μm) raises from 4.0 to 6.5 mg cm^{-2} (20 min exposure) with temperature growth	
	Air	1000–1200	The intensive (catastrophic) oxidation of hot-pressed NbC_{1-x} (1–2% porosity) accompanied with cracking and splitting of the oxide scales containing $\beta\text{-Nb}_2\text{O}_{5-x}$ and $\alpha\text{-NbO}_{2\pm x}$; porous samples are disintegrated completely	
	Air	1100–1400	Severe oxidation of materials	
	O_2 , 0.03–13 kPa	1000–1400	The oxidation of sintered $\text{NbC}_{0.94}$ (1–5% porosity, mean grain size – 50–100 μm) leads to the formation of scale containing dense (more sintered) $\beta\text{-Nb}_2\text{O}_{5-x}$ and $\alpha\text{-NbO}_{2\pm x}$ (the only traces of $\alpha\text{-Nb}_2\text{O}_5$ at 1000 °C, carbon content in the oxide scale is <0.2 mas.%, as an evidence of stoichiometric burning-off); oxidation kinetics is described by parabolic law with apparent activation energy $E \approx 60\text{--}80 \text{ kJ mol}^{-1}$ and power (exponent) index $m \approx 1/2$ (limiting stage is solid state diffusion through $\alpha\text{-NbO}_{2\pm x}$ dense layer)	
	O_2 , 0.05–13 kPa	1500–1600	The oxidation process of sintered $\text{NbC}_{0.94}$ (1–5% porosity) is described by linear law (limiting stage is oxygen adsorption on the outer surface of liquid oxide)	
	O_2 , $\sim 10^{-5}$ Pa	1700–1800	Treatment (annealing) of $\text{NbC}_{0.97}$ and $\text{NbC}_{0.74}$ powders (1 h exposure) leads to their severe decarburization and conversion of monocarbide phases into semicarbide $\beta\text{-Nb}_{2+x}\text{C}$ or metallic Nb phases, respectively	

(continued)

Table 4.20 (continued)

System	Atmosphere	Temperature range, °C	Interaction character, products and/or compatibility	Reference
	O ₂ , 0.1–0.001 Pa	1730–2230	During the oxidation of hot-pressed NbC _{1-x} a metallic surface layer (formed by CO release) simultaneously reacts with O ₂ forming volatile metal oxides; steady-state layer thickness is reached, if the rates of layer growth and metal evaporation are equal in the ablation <i>See also</i> section C–Nb–O in Table I-2.14	
α/β -Nb _{2+x} C–O ₂	Air	300	Formation of a new carbide phase with lower carbon content <i>See also</i> section C–Nb–O in Table I-2.14	[48, 82, 743]

^aSimilar to the ridge-effect phenomenon discovered by Shabalin [512, 513] in the oxidation process of carbide containing materials

^bThe total rate of materials loss V is maximal at the first moments of exposure; the effect of exposure time t , s and temperature T , K at 2550–3000 K is expressed by the following equation V ($\text{g cm}^{-2} \text{s}^{-1}$) = $0.058 \exp(-0.15 \times 10^{-3}t) \exp[(-54,000 + 3.00 \times 10^{-3}t)/RT]$, where R is the gas constant [727]

^cFine niobium carbide powders are pyrophoric [514]

^dFor near-stoichiometric NbC_{1-x} the value of the Pilling-Bedworth ratio $\alpha = M_O d_C / M_C d_O = 2.22$, where M_O is molecular mass of the oxide phase formed on the oxidation of 1 mol of carbide phase, M_C is molecular mass of carbide phase, d_C and d_O are the densities of carbide and oxide phases, respectively [694]

^ePartial pressure

^fDuring O₂ consumption and oxide (scale) formation at temperatures <500–550 °C in NbC_{1-x} dense materials C does not oxidize

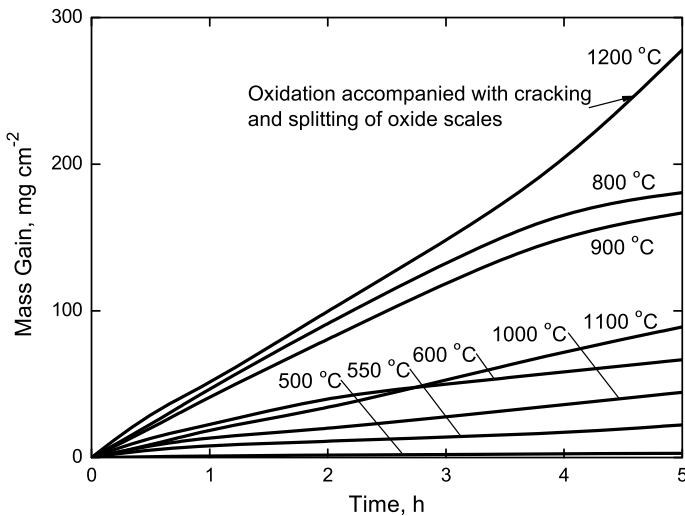


Fig. 4.37 Isothermal oxidation kinetics curves for 8 mm diameter disk-like samples of hot-pressed and subsequently annealed near-stoichiometric niobium monocarbide materials (porosity 1–2%) in air [518–520]

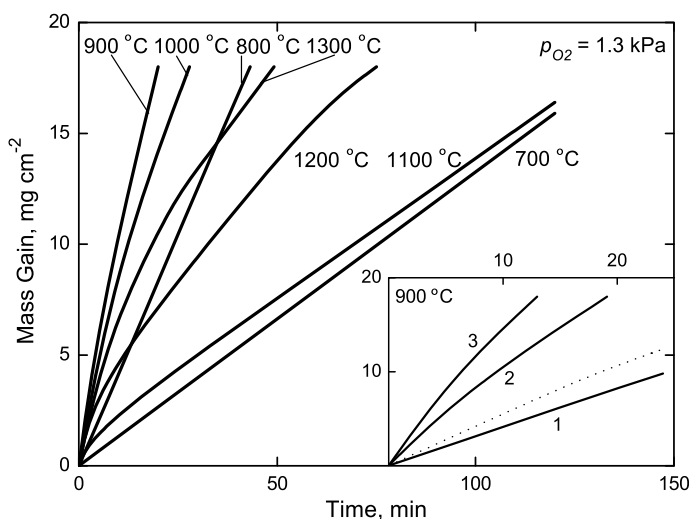


Fig. 4.38 Isothermal oxidation kinetics curves for flat-plate samples of sintered $\text{NbC}_{0.94}$ materials (porosity 1–5%) in oxygen gas flow at pressure of 1.33 kPa (*Inset* – carbon burning-off from the carbide phase: 1 – carbon loss curve (observed experimentally); 2 – thermogravimetric curve (measured directly); 3 – genuine (complete) mass gain due to the oxide formation (calculated); the dotted line corresponds to the stoichiometric oxidation of metal and carbon in the carbide phase, i.e. complete carbon burning-off in the oxide scale) [522, 523, 525]

Table 4.21 The parameters of wettability of niobium monocarbide phases with some liquid metals and alloys (melts)^a

Melt (purity)	Atmosphere	Temp., °C	Time, s	γ_{l-g} , mJ m^{-2}	W_a , mJ m^{-2}	W_m^b , kJ mol^{-1}	θ , degree	Reference
Cu	Vacuum	1100	–	$\text{NbC}_{0.66}$ –	–	–	~70	[67, 540, 549]
Cu	Ar	1150	–	$\text{NbC}_{0.73}^c$ –	–	–	145 ± 3	[551]
Cu	Vacuum	1100	–	$\text{NbC}_{0.75}$ –	–	–	~90	[67, 540, 549]
Cu (99.99%)	Ar	1130	900	$\text{NbC}_{0.80}$ ~1350	230	–	146 ± 3	[1, 534]
Cu	Ar	1150	–	$\text{NbC}_{0.81}^c$ –	–	–	146 ± 3	[551]

(continued)

Table 4.21 (continued)

Melt (purity)	Atmosphere	Temp., °C	Time, s	γ_{1-g} , mJ m^{-2}	W_a , mJ m^{-2}	W_m^b , kJ mol^{-1}	θ , degree	Reference
Cu	Vacuum	1100	–	NbC _{0.82} –	–	–	~85	[67, 540, 549]
Cu	Ar	1150	–	NbC _{0.91} –	–	–	150 ± 3	[551]
Cu (99.99%)	Ar	1130	900	NbC _{0.92} ~1350	315	–	140 ± 3	[1, 534]
Fe (C-4.0, Mn-1.4, Si-2.5, S-0.1%)	Pure Ar	1400–1450	900	NbC _{0.95} –	–	–	~0	[1, 195, 541]
Fe (C-3.1, Mn-0.4, Si-1.6, S-0.02%)	Pure Ar	1400–1450	900	–	–	–	~0	[1, 195, 541]
Fe (C-2.7, Mn-0.4, Si-1.2, S-0.2%)	Pure Ar	1400–1450	900	–	–	–	~0	[1, 195, 541]
Fe (C-2.6, Mn-1.0, Si-1.0, Cr-0.3%)	Pure Ar	1400–1450	900	–	–	–	~0	[1, 195, 541]
Fe (C-1.0, Cr-1.4, Mn-0.4, Si-0.3%)	Pure Ar	1500–1550	900	–	–	–	~0	[1, 195, 541]
Fe (C-1.0, Cr-1.4, Mn-1.1, Si-0.6%)	Pure Ar	1500–1550	900	–	–	–	~0	[1, 195, 541]
Fe (C-0.8, Mn-0.2, Si-0.2, S-0.03%)	Pure Ar	1500–1550	900	–	–	–	~0	[1, 195, 541]
Fe (C-0.2, Cr-14.5, Ni-2.7, Mn-0.5%)	Pure Ar	1500–1550	900	–	–	–	~0	[1, 195, 541]
Cu (0.2% Ag)	Vacuum	1100	900	NbC _{0.97} 1250	1675	–	70	[1, 67, 535, 1080]
Cu (0.2% Ag)	Vacuum	1150	900	1255	1845	–	62	[1, 535]
Cu (0.2% Ag)	Vacuum	1200	900	1240	2070	–	48	[1, 67, 535, 549]
Cu (0.2% Ag)	Vacuum	1300	60	1360	2560	–	28	[1, 535]
Cu (0.2% Ag)	Vacuum	1300	600	1360	2655	–	18	[1, 535]
Cu (0.2% Ag)	Vacuum	1300	900	1360	2685	–	13	[1, 535]
Cu (0.2% Ag)	Vacuum	1300	1200	1360	2710	–	6	[1, 535]

(continued)

Table 4.21 (continued)

Melt (purity)	Atmosphere	Temp., °C	Time, s	γ_{1-g} , mJ m^{-2}	W_a , mJ m^{-2}	W_m^b , kJ mol^{-1}	θ , degree	Reference
				$\text{NbC}_{\sim 1.0}$				
Al	Vacuum	900	900	914	257	12.6	136 ± 0.3	[67, 195, 534, 536]
Al (99.97%)	Vacuum	920–1000	60–1200	914	155–166	–	145–146	[1, 534]
Al (99.97%)	Vacuum	1000	900	914	279	–	134 ± 3	[67, 195, 534, 549]
Al (99.97%)	Vacuum	1150	60–1200	914	155–355	–	127–146	[1, 534]
Au (99.999%)	–	~ 1065	1800	1140	1710	–	60	[1, 67, 540, 549]
Bi (99.999%)	Vacuum	320	900	390	114	5.9	135 ± 4	[1, 195, 534, 536]
Co (Si-0.3, Fe-0.3, Ni-0.2, Al-0.1%)	Vacuum	1420	300	1910	3760	–	11–14	[1, 67, 195, 535, 549]
Co (99.98%)	Vacuum, Ar	1450–1500	900	1805	>3610	–	~ 0	[1, 67, 195, 534, 536, 549]
Co ^e	Vacuum	1500	1200	1805	3665	–	11	[1, 537, 538]
Cu (99.99%)	Vacuum	1130–1300	900	1351	396	20.1	135	[1, 534, 536]
Cu	Vacuum	1100	–	–	–	–	~ 40	[67, 540]
Cu	Vacuum	1100	–	–	–	–	70	[67, 535]
Cu ^f	Vacuum, 1.3 mPa	1150	3600	2400	–	–	58	[1079]
Cu	Vacuum	1200	–	–	–	–	48	[67, 535]
Cu (Nb – 1.45%) ^f	Vacuum, 1.3 mPa	1150	3600	–	–	–	65	[1079]
Cu (Nb – 1.45, W – 2.8%) ^f	Vacuum, 1.3 mPa	1150	3600	–	–	–	56	[1079]
Fe (C-0.003, Si-0.3, Mg-0.3, Cu-0.2%)	Vacuum	1490	60	1900	3620	–	25	[1, 195, 535, 549]
Fe (99.999%)	Vacuum, Ar	1550	900	1780	>3560	–	~ 0	[1, 67, 195, 534, 536, 549]
Ga (99.99999%)	Vacuum	800	900	707	490	24.3	108 ± 0.3	[1, 195, 534, 536]
Ge (99.9999%)	Vacuum	1000	900	600	90	4.4	148 ± 2	[1, 195, 534, 536]
In (99.9995%)	Vacuum	250	900	559	70	3.4	151 ± 1	[1, 195, 260, 345]

(continued)

Table 4.21 (continued)

Melt (purity)	Atmosphere	Temp., °C	Time, s	γ_{l-g} , mJ m ⁻²	W_a , mJ m ⁻²	W_m^b , kJ mol ⁻¹	θ , degree	Reference
Mn (99.8%)	Vacuum, Ar	1300	900	1750	>3500	–	~0	[1, 534, 536]
Ni (Fe-1.0, Al-0.3, Mg-0.2, Ag-0.2%)	Vacuum	1380	300	1810	3530	–	18	[1, 67, 195, 535]
Ni ^e	Vacuum	1400	900	1835	3550	–	21	[1, 539]
Ni	Vacuum	1450	–	–	–	–	21	[217, 832]
Ni (99.99%)	Vacuum, Ar	1450	900	1700	3400	–	~0	[1, 195, 534, 536]
Pb (99.98%)	Vacuum	400	900	480	73	3.6	148 ± 1	[1, 195, 534, 536]
Sb (99.999%)	Vacuum	700	900	384	246	12.1	111 ± 1	[1, 195, 534, 536]
Si (99.9999%)	Vacuum	1500	900	860	>1720	–	~0	[1, 195, 534, 536]
Sn (99.999%)	Vacuum	300	900	554	198	9.6	130 ± 1	[1, 195, 534, 536]
Tl (99.999%)	Vacuum	400	900	490	237	11.7	121 ± 1	[1, 195, 534, 536]

^aThe parameters of wettability are given in accordance with Young-Dupré equation $W_a = \gamma_{l-g} \times (1 + \cos\theta)$ and Young's equation $\gamma_{s-l} = \gamma_{s-g} - \gamma_{l-g}\cos\theta$, where W_a is the work of adhesion, γ_{l-g} is the liquid-vapour interfacial energy (surface tension), γ_{s-l} is solid-liquid interfacial energy, γ_{s-g} is the solid-vapour interfacial energy and θ is the wetting contact angle [1]; compositions of melts are given in mass (weight) percentage

^b $W_m = W_a(M/d)^{2/3}N_A^{1/3}$, where W_m is the molar work of adhesion, M is the molecular mass and d is the density of chemical compound, N_A is the Avogadro constant [1060]

^cPorosity ≤ 15%

^dSintered materials (porosity – 12–16%)

^e $\gamma_{s-l} = 480 \text{ mJ m}^{-2}$

^fSintered materials (porosity – ≤ 2%, contents: non-combined C – 0.40%, O – 0.01%, N – 0.26%, Ti – 0.03%)

^f $\gamma_{s-l} = 1290 \pm 390 \text{ mJ m}^{-2}$

Shabalin [512, 513] with ridge temperatures nearby 800–900 °C. Data on the catalytic activities of niobium carbides are given in several works [1, 483, 590–603, 820–822, 865, 866, 870, 976, 1010]; the electrochemical behaviour of niobium carbides in various media such as salt melts and aqueous solutions is described in [603–606, 688, 708, 823]. The parameters of wettability of niobium monocarbide phases with some liquid metals (melts) are listed in Table 4.21, the diffusion rates for the systems containing niobium carbide phases are presented in species pairs within the various ranges of temperatures in the Table 4.22. The characters of chemical interaction of niobium monocarbide with some common chemicals (acids, alkalis and salts in aqueous solutions) are summarized in Table 4.23.

Table 4.22 Diffusion rates and related parameters in the systems containing niobium, carbon and niobium carbides phases at various temperatures^a

Species pair	Temperature dependence of the diffusion coefficient (diffusivity) $D = D_0 \exp[-E_A/R/T]$, $\text{cm}^2 \text{s}^{-1}$	Temperature range, K (°C)	Remarks on materials characteristics and measurement method	Reference
C → Nb	$10^{-2} \exp(-17,100/T)$	400–2610 (130–2340)	Combined data from several sources	[607, 608, 615, 616, 662]
	$1.09 \times 10^{-5} \exp(-16,000/T)$	1170–1470 (900–1200)	¹⁴ C radiometric method, sectioning technique	[5, 10, 11, 618, 623]
	$9.32 \times 10^{-3} \exp(-17,500/T)$	1370–1870 (1100–1600)	¹⁴ C radiometric method, sectioning technique	[5, 617, 622]
	$3.3 \times 10^{-3} \exp(-19,100/T)$	1200–2070 (930–1800)	Radiotracer ¹⁴ C with mechanical sectioning	[10, 11, 619]
	$2.6 \times 10^{-2} \exp(-19,000/T)$	2190–2610 (1920–2340)	Radiotracer ¹⁴ C with mechanical sectioning	[10, 11, 608, 621]
	$3.61 \times 10^{-2} \exp(-32,700/T)$	1370–1770 (1100–1500)	Radiometric method based on the formation of NbC _{1-x} layer	[1]
	$1.5 \times 10^{-2} \exp(-13,600/T)$	320–430 (50–160)	From the measurements of internal friction with the torsion pendulum	[611, 612]
	$4.5 \times 10^{-3} \exp(-13,700 \pm 40)/T)$	330–430 (60–160)	From the measurements of internal friction	[5, 614]
	$(4.0 \pm 0.7) \times 10^{-3} \exp(-16,600 \pm 90)/T)$	400–550 (130–280)	From the measurements of internal friction	[10, 11, 614, 623]
	$[(3.8-5.0) \pm (0.5-5.0)] \times 10^{-3} \times \exp\{[-(16,600-16,800) \pm (50-500)]/T\}$	410–530 (140–260)	Determined by the various methods of internal friction measurements	[611, 613, 614]
	$1.94 \times 10^{-6} \exp(-8,300/T), ?$	1270–2270 (1200–2000)	Calculation based on the thickness of NbC _{1-x} layer	[5, 63, 609]

(continued)

Table 4.22 (continued)

Species pair	Temperature dependence of the diffusion coefficient (diffusivity) $D = D_0 \exp[-E_a/R/T]$, $\text{cm}^2 \text{s}^{-1}$	Temperature range, K (°C)	Remarks on materials characteristics and measurement method	Reference
C \rightarrow NbC _{1-x}	$0.183 \exp(-36,100/T)$	1570–1870 (1300–1600)	Calculation based on the growth of NbC _{1-x} phase layer	[1, 67, 620]
	$3.14 \times 10^4 \exp(-9,500 \pm 2,900/T)$, ?	1270–2270 (1000–2000)	Calculation based on the growth of β -Nb _{2+x} C phase layer	[609–611]
	$9.6 \times 10^{-2} \exp(-35,400/T)$	1570–1870 (1300–1600)	Calculation based on the growth of β -Nb _{2+x} C phase layer	[1, 67, 620]
	$(0.45^{+0.13}_{-0.10}) \exp(-39,500 \pm 1,200/T)$	1770–2370 (1500–2100)	Reaction diffusion coefficients, forward finite differences (FFD) method	[663]
	$0.86 \exp(-44,000/T)$	2070–2470 (1800–2200)	Polycrystalline NbC _{1-x} ($x = 0.05$), ¹⁴ C radiotracer method	[2, 624]
	$8.8 \times 10^{-6} \exp(-17,800/T)$	1870–2270 (1600–2000)	Polycrystalline sintered NbC _{1-x} ($x = 0.25$, ~10–15% porosity), ¹⁴ C radiotracer	[1, 10, 11, 644, 695]
	$10^{-6} \exp(-16,300/T)$	1870–2270 (1600–2000)	Polycrystalline sintered NbC _{1-x} ($x = 0.02$, ~10–15% porosity), ¹⁴ C radiotracer	[10, 11, 644, 695]
	$(0.11^{+0.003}_{-0.1}) \exp(-47,300 \pm 900/T)$	2670–3070 (2400–2800)	Polycrystalline (hot-pressed and annealed) NbC _{1-x} ($x \approx 0.03$, Nb(C _{0.95} N _{0.04} O _{0.1}) _{0.97} , porosity <5%), ¹⁴ C radiotracer method	[2, 3, 625, 646, 727]
	6.62×10^{-10} 5.25×10^{-9} 3.24×10^{-8}	2500 (2230) 2800 (2530) 3100 (2830)	Calculated on the basis of developed statistic and thermodynamic theory of interstitial phases for NbC _{1-x} ($x = 0.03$)	[727]
	$(0.19^{+0.18}_{-0.16}) \exp(-48,100 \pm 1800/T)$	2670–3070 (2400–2800)	Polycrystalline (hot-pressed and annealed) NbC _{1-x} ($x \approx 0.085$, Nb(C _{0.998} N _{0.001} O _{0.015} , porosity <5%), ¹⁴ C radiotracer method	[10, 11, 625, 656]
$(0.21^{+0.18}_{-0.10}) \exp(-48,600 \pm 1800/T)$	2670–3070 (2400–2800)	Polycrystalline (hot-pressed and annealed) NbC _{1-x} ($x \approx 0.085$, Nb(C _{0.965} N _{0.032} O _{0.003}) _{0.915} , porosity <5%), ¹⁴ C radiotracer method	[2, 625, 646, 656, 945]	
$(1.47^{+0.52}_{-0.38}) \exp(-50,400 \pm 900/T)$	2670–3070 (2400–2800)	Polycrystalline (hot-pressed and annealed) NbC _{1-x} ($x \approx 0.22$, Nb(C _{0.94} N _{0.056} O _{0.004}) _{0.78} , porosity <5%), ¹⁴ C radiotracer method	[2, 625, 646, 656, 945]	

(continued)

Table 4.22 (continued)

Species pair	Temperature dependence of the diffusion coefficient (diffusivity) $D = D_0 \exp[-E_a/R]/T]$, $\text{cm}^2 \text{s}^{-1}$	Temperature range, K (°C)	Remarks on materials characteristics and measurement method	Reference
	2.61×10^{-9}	2500 (2230)	Calculated on the basis of developed statistic and thermodynamic theory of interstitial phases for NbC_{1-x} ($x = 0.21$)	[727]
	2.27×10^{-8}	2800 (2530)		
	1.31×10^{-7}	3100 (2830)		
	$0.5 \exp[-51,400 \pm 5,100/T]$	2570–3070 (2300–2800)	Polycrystalline (hot-pressed and annealed) NbC_{1-x} ($x \approx 0.03$, $\text{Nb}(\text{C}_{0.95}\text{N}_{0.04}\text{O}_{0.01})_{0.97}$, 250–270 μm grain size, porosity <5%), ^{14}C radiotracer method	[2, 626, 637, 656, 945]
	$1.49 \times 10^{-2} \exp(-38,600/T)$	1900–3100 (1630–2830)	Polycrystalline NbC_{1-x} ($x \approx 0$, porosity $\leq 5\%$, $\text{O} + \text{N} \leq 0.32\%$), ^{14}C radiotracer method	[2, 627]
	$(2.59^{+1.82}_{-1.07}) \exp[-50,600 \pm 1,100/T]$	1900–2315 (1630–2045)	Single crystal NbC_{1-x} ($x \approx 0.13$), plane (110), ^{14}C radiotracer method ^b	[2, 628, 629, 646, 661, 664]
	$(7.44^{+9.36}_{-4.14}) \exp[-52,900 \pm 1,700/T]$	1900–2315 (1630–2045)	Single crystal NbC_{1-x} ($x \approx 0.17$), plane (100), ^{14}C radiotracer method ^b	[2, 628, 629, 646, 661, 664]
	$(2.22^{+1.98}_{-1.04}) \times 10^{-2} \exp[-38,300 \pm 1,400/T]$	1900–2315 (1630–2045)	Single crystal NbC_{1-x} ($x \approx 0.23$), plane (110), ^{14}C radiotracer method ^b	[2, 628, 629, 646, 664, 869]
	$7.6 \exp(-44,600/T)$	1970–2370 (1700–2100)	Calculation based on the experimental investigations of solid-state $\text{NbC}_{1-x}\text{-Nb}$ diffusion welding processes	[1, 636]
	$7.6 \exp(-44,400/T)$	1970–2570 (1700–2300)	Calculation based on the experimental investigations of the reaction between metallic Nb and C (graphite)	[639, 647, 666, 695]
	$0.35 \exp[-37,300 \pm 1,400/T]$	1970–2470 (1700–2200)	Action based on the growth of NbC_{1-x} phase layer during the reaction between metallic Nb and C (graphite)	[1, 67, 634, 646]
	$17.6 \exp(-48,400/T)$	1970–2570 (1700–2300)	Parameters of temperature variation of NbC_{1-x} layer growth rate constant upon contact saturation of solid metallic Nb by C	[10, 11, 639]
	$1.08 \exp(-41,800/T)$	2170–2570 (1900–2300)	Parameters of temperature variation of NbC_{1-x} layer growth rate constant upon contact saturation of solid metallic Nb by C	[10, 11, 640]
	$(0.265^{+0.29}_{-0.24}) \exp[-37,600 \pm 1,400/T]$	1670–1970 (1400–1700)	Parameters of temperature variation of NbC_{1-x} layer growth rate constant upon contact saturation of solid metallic Nb by C	[665]

(continued)

Table 4.22 (continued)

Species pair	Temperature dependence of the diffusion coefficient (diffusivity) $D = D_0 \exp(-E_a/R)/T$, $\text{cm}^2 \text{s}^{-1}$	Temperature range, K (°C)	Remarks on materials characteristics and measurement method	Reference
	$7.8 \exp(-42,300/T)$	1520–2150 (1250–1880)	Parameters of temperature variation of NbC _{1-x} layer growth rate constant upon surface carburization of Nb by pure C ₃ H ₈	[672]
	$(4.5^{+1.5}_{-1.5}) \times 10^{-5} \exp(-19,700 \pm 600)/T$	1070–1770 (800–1500)	Parameters of temperature variation of NbC _{1-x} layer growth rate constant upon contact saturation of solid metallic Nb by C (in thin layers) ^c	[667–670]
	$6.84 \times 10^{-7} \exp(-11,000/T)$	1070–1270 (800–1000)	Parameters of temperature variation of NbC _{1-x} + β -Nb _{2-x} C layer growth rate constant upon surface treatment of AISI 1040 steels in Nb containing powder mixtures (in thin layers) ^c	[675]
	$3.61 \times 10^{-2} \exp(-32,500/T)$	1370–1770 (1100–1500)	Parameters of reaction-chemical diffusion, contact saturation of solid Nb in mixture of C (graphite) and BaCO ₃ rich in ¹⁴ C, radiometric method	[10, 11, 641]
	$0.102 \exp(-36,600 \pm 1,500)/T$	1700–2100 (1425–1825)	Parameters of reaction-chemical diffusion, contact saturation of solid Nb (1 wt.% Zr) with C (graphite); metallography method	[10, 11, 642, 695]
	2.1×10^{-11}	1700 (1430)	Parameters of reaction-chemical diffusion, contact saturation of solid Nb (1 wt.% Zr) with C (graphite); metallography method	[642]
	$\sim 8.0 \times 10^{-7}$	2940 (2670)	Evaluation made from vaporization behaviour investigations	[160, 647, 695]
	$\sim \exp(-38,000/T)$	2770–2970 (2500–2700)	Initial composition NbC _{0.64} ; mass loss method, evaluation made from vaporization behaviour investigations	[165, 166, 647]
	$\sim \exp(-34,100 \pm 300)/T$	1670–1970 (1400–1700)	Parameters of reaction-chemical diffusion, contact saturation of solid metallic Nb with C; metallography method ^d	[676]
	$1.2 \exp(-39,800/T)$	2170–2570 (1900–2300)	Parameters of reaction-chemical diffusion, contact saturation of solid metallic Nb with C; metallography method	[10, 11, 640, 646, 647, 695]
	$2.65 \times 10^{-2} \exp(-32,700/T)$	2470–2810 (2200–2540)	Parameters of reaction-chemical diffusion during the formation of NbC _{1-x} (x = 0.13) obtained by precipitation from gas phase onto surface of graphite; X-ray method	[10, 11, 643]

(continued)

Table 4.22 (continued)

Species pair	Temperature dependence of the diffusion coefficient (diffusivity) $D = D_0 \exp[-E_A/R/T]$, $\text{cm}^2 \text{ s}^{-1}$	Temperature range, K ($^{\circ}\text{C}$)	Remarks on materials characteristics and measurement method	Reference
	$5.9 \exp(-46,700/T)$	2420–3290 (2150–3015)	Parameters of chemical diffusion, decarburization of NbC_{1-x} materials	[10, 11, 645, 647]
	$0.66 \exp(-37,000/T)$	2170–2800 (1900–2530)	Chemical diffusion coefficients calculated on the basis of experiments on deposition of non-stoichiometric carbide NbC_{1-x} ($0.10 \leq x \leq 0.36$, porosity $\leq 10\%$) from $\text{CH}_4 + \text{H}_2$ gas phase ^e ($0.10 \leq x \leq 0.36$, porosity $\leq 10\%$) in homogeneity range	[1, 67, 635]
	$16.6 \exp(-48,800/T)$	2570–3570 (2300–3300)	Averaged calculation for NbC_{1-x} in homogeneity range ($0.025 \leq x \leq 0.36$)	[635, 657, 658]
	$3.84 \times 10^{-5} \exp(23.24x) \exp(-28,450 \pm 850/T)$	1670–1970 (1400–1700)	Interdiffusion coefficients as a function of composition, bulk diffusion couples method based on electron probe microanalysis	[665]
	$10^{(3.6-9.8x)} \exp[-(3.6 - 5.6x) \times 23,000/T]$	2570–3570 (2300–3300)	Averaged calculation for NbC_{1-x} ($0.025 \leq x \leq 0.36$) on the basis of steady state creep behaviour data	[635, 657, 658, 666]
	$(0.4^{+0.4}_{-0.2}) \exp(-44,800 \pm 1,500/T)$	1770–2370 (1500–2100)	Reaction diffusion coefficients, profile fitting method (high concentrations)	[663]
	$(0.12^{+0.4}_{-0.2}) \exp(-38,900 \pm 2,300/T)$	1770–2370 (1500–2100)	Reaction diffusion coefficients, profile fitting method (low concentrations)	[663]
	$(2.3^{+3.0}_{-1.3}) \exp(-46,100 \pm 1,600/T)$	1770–2370 (1500–2100)	Reaction diffusion coefficients, forward finite differences (FFD) method	[663]
	$6.5 \times 10^{-2} \exp(-41,000/T)$	–	The values of chemical diffusion coefficients summarized on the basis of several works	[178]
	$\sim \exp(-41,600 \pm 600/T)$	2000–2500 (1730–2230)	Parameters of reaction-chemical diffusion measured by diffusion couples method	[839]
	$\sim 5 \times 10^{-8}$	3170 (2900)	Polycrystalline (hot-pressed and annealed) NbC_{1-x} ($x = 0.04$), ¹⁴ C radiotracer method	[637, 834]
	–	2470–2570 (2200–2300)	Non-isothermal parameters of temperature variation of NbC_{1-x} layer growth rate constant upon surface carburization of Nb by pure CH_4 ; mass gain, layer thickness growth and heat release rate methods ^f	[677]

(continued)

Table 4.22 (continued)

Species pair	Temperature dependence of the diffusion coefficient (diffusivity) $D = D_0 \exp[-E_A/(R)/T]$, $\text{cm}^2 \text{ s}^{-1}$	Temperature range, K ($^{\circ}\text{C}$)	Remarks on materials characteristics and measurement method	Reference
C \rightarrow $\beta\text{-Nb}_{2+x}\text{C}$	$5.7 \times 10^6 \exp(-15,000/T)$	1870–2270 (1600–2000)	Polycrystalline sintered $\beta\text{-Nb}_{2+x}\text{C}$ ($\sim 17\%$ porosity), ^{14}C radio-tracer method	[10, 11, 644]
	$2.3 \times 10^{-3} \exp(-20,100 \pm 2000)/T$	1970–2470 (1700–2200)	Calculation based on the growth of $\beta\text{-Nb}_{2+x}\text{C}$ phase layer during the reaction between metallic Nb and C (graphite)	[1, 67, 634, 646, 666]
	$0.3 \exp(-40,600/T)$	1970–2570 (1700–2300)	Parameters of temperature variation of $\beta\text{-Nb}_{2+x}\text{C}$ layer growth rate constant upon contact saturation of solid metallic Nb by C	[10, 11, 639]
	$40.2 \exp(-30,700/T)$	2170–2570 (1900–2300)	Parameters of temperature variation of $\beta\text{-Nb}_{2+x}\text{C}$ layer growth rate constant upon contact saturation of solid metallic Nb by C	[10, 11, 640]
	$(0.157_{-0.13}^{+0.19}) \exp(-36,400 \pm 3,100)/T$	1670–1970 (1400–1700)	Parameters of temperature variation of $\beta\text{-Nb}_{2+x}\text{C}$ layer growth rate constant upon contact saturation of solid metallic Nb by C	[665]
	$0.10 \exp(-36,100/T)$	1520–2150 (1250–1880)	Parameters of temperature variation of $\beta\text{-Nb}_{2+x}\text{C}$ layer growth rate constant upon surface carburization of Nb by pure C_3H_8	[672]
	$(3.7_{-2}^{+10}) \times 10^{-4} \exp(-22,900 \pm 1800)/T$	1070–1470 (800–1200)	Parameters of temperature variation of $\beta\text{-Nb}_{2+x}\text{C}$ layer growth rate constant upon contact saturation of solid metallic Nb by C (in thin layers) ^c	[667–670]
	$\sim \exp(-34,600 \pm 1,500)/T$	1700–2100 (1425–1825)	Parameters of reaction-chemical diffusion, contact saturation of solid Nb (1 wt.% Zr) with C (graphite); metallography method	[10, 11, 642]
	$\sim \exp(-40,600/T)$	1970–2570 (1700–2300)	Parameters of temperature variation of $\beta\text{-Nb}_{2+x}\text{C}$ layer growth rate constant upon contact saturation of solid metallic Nb by C	[10, 11, 639]
	$\sim \exp(-36,000 \pm 500)/T$	1670–1970 (1400–1700)	Parameters of reaction-chemical diffusion, contact saturation of solid metallic Nb with C; metallography method ^d	[676]
	$(2.9_{-1.3}^{+2.3}) \exp(-45,800 \pm 1,200)/T$	1770–2370 (1500–2100)	Reaction diffusion coefficients, forward finite differences (FFD) method	[178, 663]
	$(2.04 \pm 0.57) \exp(-35,500 \pm 2,200)/T$	1670–1970 (1400–1700)	Interdiffusion coefficients, bulk diffusion couples method based on electron probe microanalysis	[665]
	$\sim \exp(-35,500 \pm 600)/T$	2000–2500 (1730–2230)	Parameters of reaction-chemical diffusion measured by diffusion couples method	[839]

(continued)

Table 4.22 (continued)

Species pair	Temperature dependence of the diffusion coefficient (diffusivity) $D = D_0 \exp[-E_A/R/T]$, $\text{cm}^2 \text{ s}^{-1}$	Temperature range, K (°C)	Remarks on materials characteristics and measurement method	Reference
C → (Nb _{1-y} Zr _y)C _{1-x}	—	2470–2570 (2200–2300)	Non-isothermal parameters of temperature variation of β -Nb _{2+x} C layer growth rate constant upon surface carburization of Nb by CH ₄ ; mass gain, layer thickness growth and heat release rate methods ^f	[677]
	$(2.28^{+0.47}_{-0.30}) \exp[-48,600 \pm 1,300/T]$	2770–3470 (2500–3200)	Polycrystalline (Nb _{1-y} Zr _y)C _{1-x} ($x = 0.03$, $y = 0.48$), ¹⁴ C radio-tracer method	[2, 727]
	8.26×10^{-9}	2500 (2230)	Calculated on the basis of developed statistic and thermodynamic theory of 3-component interstitial phases for	[727]
	6.72×10^{-8}	2800 (2530)	(Nb _{1-y} Zr _y)C _{1-x} ($x = 0.10$, $y = 0.48$)	
	3.56×10^{-7}	3100 (2830)		
	$(0.84^{+0.47}_{-0.30}) \exp[-50,600 \pm 1,700/T]$	2770–3470 (2500–3200)	Polycrystalline (Nb _{1-y} Zr _y)C _{1-x} ($x = 0.18$, $y = 0.48$), ¹⁴ C radio-tracer method	[2, 727]
	1.36×10^{-9}	2500 (2230)	Calculated on the basis of developed statistic and thermodynamic theory of 3-component interstitial phases for	[727]
	1.20×10^{-8}	2800 (2530)	(Nb _{1-y} Zr _y)C _{1-x} ($x = 0.20$, $y = 0.48$)	
	6.91×10^{-8}	3100 (2830)		
Nb → NbC _{1-x}	$(0.11^{+0.28}_{-0.08}) \exp[-64,000 \pm 3,500/T]$	2670–3070 (2400–2800)	Polycrystalline hot-pressed NbC _{1-x} ($0.03 \leq x \leq 0.22$, porosity <5%), ⁹⁵ Nb radiotracer ^g	[2, 3, 10, 11, 625, 646, 727] [727]
	8.73×10^{-13}	2500 (2230)	Calculated on the basis of developed statistic and thermodynamic theory of interstitial phases for NbC _{1-x} ($0.03 \leq x \leq 0.21$)	
	1.32×10^{-11}	2800 (2530)		
	1.23×10^{-10}	3100 (2830)		
	$0.7 \exp(-64,400/T)$	2770–3270 (2500–3000)	Polycrystalline hot-pressed NbC _{1-x} ($x \approx 0.03$, Nb(C _{0.95} N _{0.04} O _{0.01}) _{0.97} , porosity <5%), ⁹⁵ Nb radiotracer method	[10, 11, 637]
	$1.7 \exp(-57,900/T)$	2670–3170 (2400–2900)	Polycrystalline hot-pressed NbC _{1-x} ($x \approx 0.18$, porosity <5%), ⁹⁵ Nb radiotracer method	[10, 11, 637]
	$(4.54^{+2.85}_{-1.75}) \exp[-70,500 \pm 1,200/T]$	2370–2660 (2100–2390)	Single crystal NbC _{1-x} ($0.13 \leq x \leq 0.23$), ⁹⁵ Nb radiotracer method ^g	[2, 630, 631, 646, 661, 664] (continued)

Table 4.22 (continued)

Species pair	Temperature dependence of the diffusion coefficient (diffusivity) $D = D_0 \exp(-E_A/R)/T$, $\text{cm}^2 \text{ s}^{-1}$	Temperature range, K (°C)	Remarks on materials characteristics and measurement method	Reference
	$5.5 \times 10^{-6} \exp(-27,700/T)$	1970–2370 (1700–2100)	Polycrystalline sintered NbC_{1-x} ($0.02 \leq x \leq 0.25$, ~17% porosity), ^{95}Nb radiotracer method ^g	[1, 67, 644, 695]
	$\sim 10^{-9}$	3170 (2900)	Polycrystalline (hot-pressed and annealed) NbC_{1-x} ($x = 0.04$), ^{14}C radiotracer method	[637, 834]
	$1.25 \exp(-54,300/T)$	–	Values calculated on the theoretical basis	[1, 67, 638]
	$\sim \exp(-67,000/T)$	–	Estimated on the basis of LeClaire's relation (connected with phase melting point)	[695]
$\text{Nb} \rightarrow (\text{Nb}_{1-y}\text{Zr}_y)\text{C}_{1-x}$	$(0.51^{+1.33}_{-0.50}) \times 10^2 \exp(-77,100 \pm 4900/T)$	2770–3470 (2500–3200)	Polycrystalline $(\text{Nb}_{1-y}\text{Zr}_y)\text{C}_{1-x}$ ($0.03 \leq x \leq 0.18$, $y = 0.48$), ^{95}Nb radiotracer method ^g	[2, 727]
	2.12×10^{-12}	2500 (2230)	Calculated on the basis of developed statistic and thermodynamic theory of 3-component interstitial phases for $(\text{Nb}_{1-y}\text{Zr}_y)\text{C}_{1-x}$ ($0.10 \leq x \leq 0.20$, $y = 0.48$)	[727]
	5.71×10^{-11}	2800 (2530)		
	8.26×10^{-10}	3100 (2830)	Sintered $(\text{Nb}_{0.5}\text{Ti}_{0.5})\text{C}_{1-x}$ ($x = 0.15$), ^{95}Nb radiotracer method	[654, 655, 695]
$\text{Nb} \rightarrow (\text{Nb}_{0.5}\text{Ti}_{0.5})\text{C}_{1-x}$	$4.7 \times 10^2 \exp(-60,400/T)$	–		
$\text{Pm} \rightarrow \text{NbC}_{1-x}$	$(1.08^{+0.327}_{-0.98}) \times 10^6 \exp(-61,400 \pm 4,500/T)$	2270–2820 (2000–2550)	Polycrystalline hot-pressed NbC_{1-x} ($x \approx 0.03$ – 0.22), ^{147}Pm radiotracer method ^g	[2, 633]

^aThe chemical diffusion coefficient concentration and temperature dependencies can be represented by an equation of the form $D' = D'_0 \exp(\beta x) \exp(-E'_A/R)/T$, where β is the concentration factor and x is the value of index in NbC_{1-x} formula (for the ranges of $x = 0.01$ – 0.60 and $T = 1730$ – 3030 °C the recommended values are $D'_0 = 6.26 \times 10^{-2} \text{ cm}^2 \text{ s}^{-1}$, $\beta = 10$ and $E'_A = 326 \text{ kJ mol}^{-1}$ [647]), and the discrepancy between chemical and self-diffusivities may be estimated on the basis of the thermodynamical relationship: $D' = D \times [1 + (d\ln\gamma_C/d\ln N_C)]$, where γ_C is the activity coefficient of carbon and N_C is the atomic fraction of carbon (evaluated at 2000 °C in NbC_{1-x} : at $x = 0.01$, $d\ln\gamma_C/d\ln N_C = 141$ and at $x = 0.20$, $d\ln\gamma_C/d\ln N_C = 15$ [652]); the approximate values of apparent activation energy for some diffusion controlled processes in NbC_{1-x} and $\beta\text{-Nb}_{2+x}\text{C}$: (a) collective recrystallization of loosely-poured powders – 160 kJ mol^{-1} ($\text{NbC}_{0.77}$, 1600–2000 °C) [653], 175 kJ mol^{-1} ($\text{NbC}_{0.82}$, 1600–2000 °C) [653], 195 kJ mol^{-1} ($\text{NbC}_{0.95}$, 1600–2000 °C) [653], 245 kJ mol^{-1} ($\text{NbC}_{0.99}$, 1600–2000 °C) [653]; (b) recrystallization (grain growth) – 300 kJ mol^{-1} (sintered after bulk deformation $\text{NbC}_{\sim 1.0}$, ≤ 2000 °C) [648, 660], 245 kJ mol^{-1} (hot-pressed $\text{NbC}_{0.99}$, 1600–2000 °C) [649], 275 kJ mol^{-1} (sintered $\text{NbC}_{0.80}$, 1600–2950 °C) [650]; (c) powder sintering densification – 265 – 320 kJ mol^{-1} ($\text{NbC}_{0.72}$, specific surface area 0.55 – $4.4 \text{ m}^2 \text{ g}^{-1}$, 1330 – 2150 °C) [659, 671], 260 – 310 kJ mol^{-1} ($\text{NbC}_{0.92}$, specific surface area 0.65 – $4.8 \text{ m}^2 \text{ g}^{-1}$, 1330 – 2150 °C) [659, 671], 290 – 310 kJ mol^{-1} ($\text{NbC}_{\sim 1.0}$ with carbon excess, 1300 – 1400 °C) [727, 731], 500 – 560 kJ mol^{-1} ($\text{NbC}_{\sim 1.0}$ with carbon excess, 2400 – 2700 °C) [727, 731]; (d) powder hot-pressing densification – 175 kJ mol^{-1} ($\text{Nb}_2\text{C}_{\sim 1.0}$, mean particle size 10 – $25 \mu\text{m}$, 2300 °C) [833], 255 kJ mol^{-1} (continued)

Table 4.22 (continued)

(NbC_{0.72}, mean particle size 10–25 μm, 2300 °C) [833], 295 kJ mol⁻¹ (NbC_{0.82}, mean particle size 10–25 μm, 2300 °C) [833], 325 kJ mol⁻¹ (NbC_{0.92}, mean particle size 10–25 μm, 2300 °C) [833], 360 kJ mol⁻¹ (NbC_{0.99}, mean particle size 10–25 μm, 2300 °C) [833]; (e) internal friction peaks characteristics (Max-Wert formula) – 380 kJ mol⁻¹ (sintered NbC_{0.91}, 1700 °C) [705]; data on creep – see Sect. 4.4 (Table 4.13), see *also* Sect. 4.5 (Table 4.16)

^bOn the near-surface effect in ¹⁴C self-diffusion in NbC_{1-x} see [632]

^cThere are several evidences else that the layer growth rates of mono- and semicarbide phases in the deposited niobium as well as some other metallic thin films (coatings) are far greater (lower activation energy values) than those in ordinary bulk metals; more likely it occurs due to the greater contribution of grain-boundary diffusion as fine grain sizes, microporosity and higher dislocation density are inherent to the deposited films (coatings) [673, 674]

^dThe growth rate constants increase significantly in the presence of pulsed DC current with approximate density ~0.7 kA cm⁻², while the activation energies of formation of the NbC_{1-x} and β-Nb_{2+x}C layers are independent on the presence of the current [676]

^eThe parameters probably contain significant contribution of surface and grain-boundary diffusion due to the rather high porosity of the materials

^fAt heating rates >10,000 K s⁻¹ the sharp increase of carbidization rate occurs; it is caused by the formation of non-equilibrium liquid phase at temperatures noticeably lower than the melting point of the lowest eutectic in Nb-C system [677]

^gTemperature dependences of the diffusion coefficients are the same for all the values of *x* in the indicated interval

Table 4.23 The interaction of near-stoichiometric niobium monocarbide NbC_{1-x} materials with some common chemical reagents in aqueous solutions [1, 62–64, 67, 82, 217, 514, 533, 684–687, 696]

Reagent, formula (density or concentration of aqueous solution) ^a	Treatment conditions		Character of interaction ^b
	Temperature, °C	Exposure time, h	
HCl (1:1) ^c	20	24	No decomposition
	110–112	2	Decomposes up to ~1%
HCl (<i>d</i> = 1.19)	20	24	No decomposition
	120	2	Decomposes up to ~4%
0.05M H ₂ SO ₄	20	1–600	Corrosion rate (coatings on steel) – 2.1 × 10 ⁻⁵ mg cm ⁻² s
H ₂ SO ₄ (1:4)	20	24	No decomposition
	112–115	2	Decomposes up to ~2%
H ₂ SO ₄ (<i>d</i> = 1.84)	20	24	No decomposition
	260	2	Decomposes up to ~93% (36.3% amorphous C) with the formation of stable oxysulfates; composition of released gases: CO ₂ 79.0, CO 19.7 and H ₂ 1.3 mol.% (CO ₂ and CO are products of the oxidation of amor- phous C) ^d
	265	1.5	Decomposes up to ~81% (13.0% amorphous C) with the formation of stable oxysulfates; composition of released gases: CO ₂ 92.3, CO 5.4 and H ₂ 2.3 mol.% (CO ₂ and CO are products of the oxidation of amor- phous C) ^d
	280	1.5	Decomposes up to ~92% (47.0% amorphous C) with the formation of stable oxysulfates; composition of released gases: CO ₂ 73.8, CO 24.3 and H ₂ 1.9 mol.% (CO ₂ and CO are products of the oxidation of amor- phous C) ^d
	290–310	1	Decomposes completely with the formation of stable oxysulfates; composition of released gases: CO ₂ 82.9, CO 13.7 and H ₂ 3.4 mol.% (CO ₂ and CO are products of the oxidation of amorphous C, solution is transparent finally) ^d
HNO ₃ (1:1)	20	24	Partial dissolution (deposition of salts, partial hydrolysis)
	105	2	Partial dissolution (deposition of salts, partial hydrolysis)
HNO ₃ (<i>d</i> = 1.43)	20	24	No decomposition
	110–120	2	Partial dissolution (deposition of salts, partial hydrolysis)

(continued)

Table 4.23 (continued)

Reagent, formula (density or concentration of aqueous solution) ^a	Treatment conditions		Character of interaction ^b
	Tempera- ture, °C	Exposure time, h	
HF ($d = 1.15$)	20	24	Decomposes
H ₃ PO ₄ (1:3)	20	24	Decomposes up to ~10%
	≥100	2	Decomposes up to ~1%
H ₃ PO ₄ ($d = 1.70$)	20	24	No decomposition
	120–300	2	Decomposes very slightly
H ₂ C ₂ O ₄ ^c (saturated solution)	20	24	Decomposes up to ~1%
	100–104	2	Decomposes up to ~1%
NaOH (10%)	20	24	Decomposes up to ~1%
NaOH (20%)	20	24	Decomposes up to ~1%
	110	2	No decomposition
NaCl (3%)	20	1–600	Corrosion rate (coatings on steel) – 2.1×10^{-6} mg cm ⁻² s ⁻¹
Na ₂ CO ₃ (10%)	20	1–600	Corrosion rate (coatings on steel) – 2.7×10^{-7} mg cm ⁻² s ⁻¹
KOH (30%)	20	1–600	Corrosion rate (coatings on steel) – 4.0×10^{-7} mg cm ⁻² s ⁻¹
H ₂ O (technical)	20	1–600	Corrosion rate (coatings on steel) – 1.0×10^{-6} mg cm ⁻² s ⁻¹
H ₂ O ₂ (30%) ^f	110	1.0–1.5	Decomposes completely
NH ₄ F (5%)	–	–	Decomposes up to ~8%
(NH ₄) ₂ S ₂ O ₈ (20–25%)	110	1	Decomposes up to ~10–15%
HCl (1:1) + H ₂ SO ₄ (1:4)	110	1	No decomposition
3HCl (1:1) + HNO ₃ (1:2)	110	1	No decomposition
3HCl ($d = 1.19$) + HNO ₃ ($d = 1.43$)	20	24	Decomposes up to ~8%
	105	2	Complete dissolution with hydrolysis
HCl ($d = 1.19$) + H ₂ O ₂ (30%)	110	1	Decomposes up to ~12–15%
HCl ($d = 1.19$) + (NH ₄) ₂ S ₂ O ₈ (25%)	110	1	Decomposes up to ~3–5%
HCl ($d = 1.19$) + Br ₂ (HBrO, HBr) (saturated solution)	–	–	Decomposes up to ~12%
H ₂ SO ₄ ($d = 1.84$) + HNO ₃ ($d = 1.43$)	20	24	No decomposition
	140	2	Decomposes up to ~78%
H ₂ SO ₄ (1:4) + H ₃ PO ₄ (1:3)	≥150	2	Decomposes up to ~1%
H ₂ SO ₄ ($d = 1.84$) + H ₃ PO ₄ ($d = 1.70$)	20	24	Decomposes up to ~9%
	240	2	Decomposes completely
H ₂ SO ₄ (1:4) + H ₂ C ₂ O ₄ ^c (saturated solution)	20	24	No decomposition
	180	2	Decomposes up to ~5%
H ₂ SO ₄ ($d = 1.84$) + H ₂ C ₂ O ₄ ^c (saturated solution)	20	24	No decomposition
	≥100	2	Decomposes up to ~5%

(continued)

Table 4.23 (continued)

Reagent, formula (density or concentration of aqueous solution) ^a	Treatment conditions		Character of interaction ^b
	Tempera- ture, °C	Exposure time, h	
H ₂ SO ₄ (1:4) + H ₂ O ₂ (30%)	110	1	Decomposes up to ~80–87%
H ₂ SO ₄ (1:4) + (NH ₄) ₂ S ₂ O ₈ (25%)	110	1	Decomposes up to ~35–55%
H ₂ SO ₄ (1:1) + (NH ₄) ₂ S ₂ O ₈ (25%)	110	1	Decomposes up to ~78%
(1–4)HNO ₃ (<i>d</i> = 1.43) + HF (<i>d</i> = 1.15) ^g	20	24	Decomposes completely
	110	0.5–2.0	Decomposes completely
HNO ₃ (<i>d</i> = 1.43) + NH ₄ F (5%)	110–120	0.5	Decomposes completely; composition of released gases: CO ₂ 95–97, CO (traces) and H ₂ 2–3 mol.% (no precipitated C, solution is transparent)
H ₂ O ₂ (30%) + H ₂ C ₂ O ₄ ^c (50%)	110	1	Decomposes completely
H ₂ O ₂ (30%) + H ₂ C ₄ H ₄ O ₆ ^h (50%)	110	1	Decomposes completely
H ₂ O ₂ (30%) + H ₃ C ₆ H ₅ O ₇ ⁱ (50%)	110	1	Decomposes completely
H ₂ O ₂ (30%) + H ₄ C ₁₀ H ₁₂ N ₂ O ₈ ^j (saturated solution)	110	1	Decomposes completely
(NH ₄) ₂ S ₂ O ₈ + H ₄ C ₁₀ H ₁₂ N ₂ O ₈ ^k	–	–	Decomposes up to ~2%
(NH ₄) ₂ S ₂ O ₈ + NH ₄ F	–	–	Decomposes up to ~20%
4NaOH (20%) + Br ₂ (HBrO, HBr)	20	24	No decomposition
	105	2	Decomposes up to ~16% (partial dissolution with hydrolysis)
4NaOH (20%) + H ₂ O ₂ (30%)	20	24	Decomposes up to ~29%
	112	2	Decomposes up to ~12%
4NaOH (20%) + K ₃ [Fe(CN) ₆] (10%)	20	24	Partial dissolution (hydrolysis)
	110	2	Partial dissolution (hydrolysis)

^aAll the ratios are given in volume fractions

^bWhen it is not indicated specially, the character reported is related to the powders with mean particle size of 40–50 μm

^cAnodic oxidation in hydrochloric acid HCl results in the partial oxidation of carbon in the carbide with the formation of gaseous products CO and CO₂ and simultaneous release of hydrogen peroxide H₂O₂; the latter one participates in the formation of water-soluble complexes of Nb, which destabilize the protective oxide (with residual carbon) film on the carbide anode [688]

^dRepresented by the reaction equation: 2NbC_{1-x} + 4H₂SO₄ + 5SO₃ = Nb₂O(SO₄)₄ + 2(1 - x)C + 5SO₂ + 4H₂O

^eOxalic acid

^fIn the mixtures of H₂O₂ (30%) with citric acid H₃C₆H₅O₇, oxalic acid H₂C₂O₄, tartaric acid H₂C₄H₄O₆, ethylenediaminetetraacetic acid C₁₀H₁₆N₂O₈ (EDTA) and ammonium fluoride NH₄F decomposes completely in 20 min [533]

^gRecommended chemical etching agents for NbC_{1-x}: (a) 10 ml HNO₃ (*d* = 1.43) + 3 ml HF (*d* = 1.15) with 0.5–1.0 min exposure at room temperature (for cleavage planes and rough surfaces) [679]; (b) 50 ml H₂SO₄ (*d* = 1.84) + 20 ml HNO₃ (*d* = 1.43) + 10 ml HF (*d* = 1.15) with 5 min exposure at 0 °C (for the electrochemical treatment (anodization) of polished sections, cathode – graphite or Pt, voltage – 30 V, current density – 0.8–1.0 A mm⁻², continuing addition of HF solution, followed by chemical etching in accordance to a) [679]; (c) 10 g K₃[Fe(CN)₆] + 2–10 g KOH/NaOH + 100 ml H₂O (Murakami's reagent for metallographic analysis) [683, 692]; (d) boiling mixture of H₂SO₄ (*d* = 1.84) + (NH₄)₂S₂O₈ [680]; (e) H₂NSO₃H (20% sulfamic acid) with 1 min exposure (for thin films on different substrates) [681, 682]; (f) HF (*d* = 1.15) + 40% NH₄F (BHF solution) with 4 s exposure (for thin films on different substrates) [681, 682]; (g) 50 ml HCl (*d* = 1.19) + 5 ml HNO₃

(continued)

Table 4.23 (continued)

(*d* = 1.43) + 50 ml H₂O (V2A etchant) with 1 min exposure at 40 °C [683]; (h) 40 ml HCl (*d* = 1.19) + 10 ml HNO₃ (*d* = 1.43) + 1 ml HF (*d* = 1.15) with 4 min exposure at 70 °C (for dislocation etching) [297]; (i) HNO₃ (*d* = 1.43) + 2–3% Na₂SiF₆ with 4 min exposure at room or cooler temperatures [692]; (j) 1 ml HNO₃ (*d* = 1.43) + 1 ml HF (*d* = 1.15) + 6 ml H₂O with 4 s exposure (for dislocation electroetching) [297]

^hTartaric acid

ⁱCitric acid

^jEthylenediaminetetraacetic acid (EDTA)

In comparison with other ultra-high temperature materials the summarized data on the chemical behaviour of niobium carbides are given in Addendum.

References

1. Kosolapova TYa, ed (1990) Handbook of high-temperature compounds: properties, production and applications. Hemisphere, New York
2. Andrievskii RA, Spivak II (1989) Prochnost tugoplavkikh soedinenii i materialov na ikh osnove (Strength of refractory compounds and materials based on them). Metallurgiya, Chelyabinsk (in Russian)
3. Andrievskii RA, Lanin AG, Rymashevskii GA (1974) Prochnost tugoplavkikh soedinenii (Strength of refractory compounds). Metallurgiya, Moscow (in Russian)
4. Gusev AI, Rempel AA, Magerl AJ (2001) Disorder and order in strongly nonstoichiometric compounds. Springer, Berlin
5. Kotelnikov RB, Bashlykov SN, Galiakbarov ZG, Kashtanov AI (1968) Osobo tugoplavkie elementy i soedineniya (Extra-refractory elements and compounds). Metallurgiya, Moscow (in Russian)
6. Storms EK (1967) The refractory carbides. Academic Press, New York, London
7. Toth LE (1971) Transition metal carbides and nitrides. Academic Press, New York, London
8. Wei S, Guo BC, Deng HT, Kerns K, Purnell J, Buzza S, Castleman AW (1994) Formation of metcars and face-centered cubic structures: thermodynamically or kinetically controlled? J Am Chem Soc 116:4475–4476
9. Massalski TB, Subramanian PR, Okamoto H, Kacprzak L, eds (1990) Binary alloy phase diagrams, 2nd edn. ASM International, Metals Park, Ohio
10. Samsonov GV, Upadhyaya GS, Neshpor VS (1974) Fizicheskoe materialovedenie karbidov (Physical materials science of carbides). Naukova Dumka, Kyiv (in Russian)
11. Upadhyaya GS (1996) Nature and properties of refractory carbides. Nova Science, Commack, New York
12. Demyashev GM (2010) Review: transition metal-based nanolamellar phases. Prog Mater Sci 55:629–674
13. Yvon K, Parthe E (1970) On the crystal chemistry of the close packed transition metal carbides. I. The crystal structure of the ζ-V, Nb and Ta carbides. Acta Crystallogr B 26(2):149–153
14. Gusev AI, Rempel AA (1986) Order-disorder phase transition channel in niobium carbide. Phys Stat Sol A 93(1):71–80
15. Crane RL, Ostermann F (1971) An X-ray diffraction analysis of the ε phase in dilute Nb-C alloys. Metall Mater Trans B 2(12):3487–3488

16. Rempel AA, Gusev AI, Zubkov VG, Shveikin GP (1984) Struktura uporyadochennogo karbida niobiya Nb_6C_5 (The structure of the ordering niobium carbide Nb_6C_5). Doklady AN SSSR 275:883–887 (in Russian)
17. Skripov AV, Wu H, Udovic TJ, Huang Q, Hempelmann R, Soloninin AV, Rempel AA, Gusev AI (2009) Hydrogen in nonstoichiometric cubic niobium carbides: neutron vibrational spectroscopy and neutron diffraction studies. *J Alloy Compd* 478(1–2):68–74
18. Nakamura K, Yashima M (2008) Crystal structure of NaCl-type transition metal monocarbides MC ($M = V, Ti, Nb, Ta, Hf, Zr$), a neutron powder diffraction study. *Mater Sci Eng B* 148:69–72
19. Khaenko BV, Gnitetskii OA (1993) Crystal structure of Nb_2C carbide low temperature ordered modification. *Crystallogr Rep* 38:741–743
20. Khaenko BV, Sivak OP (1990) Structure of the ordering niobium monocarbide. *Phys Crystallogr* 35:653–655
21. Lönnberg B, Lundström T (1988) Crystal growth of solid solutions of the group IV–VI transition metal monocarbides from molten aluminium. *Chem Scripta* 28:25–32
22. Will G, Platzbecker R (2001) Crystal structure and electron density distribution in niobium carbide. *Z Anorg Allg Chem* 627:2207–2210
23. Landesman JP, Christensen AN, De Novion CH, Lorenzelli N, Convert P (1985) Order-disorder transition and structure of the ordered vacancy compound Nb_6C_5 : powder neutron diffraction studies. *J Phys C* 18:809–823
24. Turchanin AG, Babaenko SA, Gusev AI, Marunya MS (1985) Thermodynamic properties of complex carbide nitrides in the quasi-binary $ZrN-NbC$ system at 298–1500 K. *Russ J Phys Chem* 59:1136–1137
25. Dubrovskaya LB, Nazarova SZ, Prekul AF (1982) Superconducting and normal properties of solid solutions $Nb_{1-x}Ta_xC_y$. *Phys Stat Sol A* 69:167–172
26. Matsumoto O, Yaguchi Y, Shiota Y, Kanzaki Y (1983) Formation of cubic solid solutions in the Mo–Nb–C and Mo–Ta–C systems by the carbonization of oxides in the plasma arc. *High Temp Sci* 16:243–250
27. Funke VF, Pshenichnyi IV, Zubarev PV, Pliner LA, Lyakhov DM, Golomazov VM (1977) Some physicommechanical properties of $ZrC-NbC-MoC_{1-x}$ alloys. *Powder Metall Met Ceram* 16(12):968–973
28. Bukatov VG, Knyazev VI, Korostin OS, Baranov VM (1975) Temperature dependence of the Young modulus of metallic carbides. *Inorg Mater* 11(2):310–312
29. Birla NC, Hoch M (1975) The age hardening characteristics of Nb-base alloys containing carbon and/or silicon. I. Nb – 15 at.% Hf. *Metall Trans A* 6(8):1631–1643
30. Gusev AI, Shveikin GP (1974) Solid solutions in the system $ZrN-NbC$. *Inorg Mater* 10:1087–1089
31. Samsonow GW, Morozow WW (1971) Carbohydride der Übergangsmetallen (Carbohydrides of the transition metals). *Monatsh Chem* 102(6):1667–1678 (in German)
32. Samsonov GV, Timofeeva II (1970) Rentgenograficheskoe issledovanie dinamicheskikh kharakteristik kristallicheskikh reshetok nekotorykh faz vnedreniya (X-ray diffraction study of dynamic characteristics of crystal lattices of some interstitial phases). *Dopov Akad Nauk Ukr RSR Ser A Fiz Mat Tekh Nauki* 32:831–833 (in Russian)
33. Kieffer R, Nowotny HN, Ettmayer P, Dufek G (1972) Neue Untersuchungen über die Mischbarkeit von Übergangsmetallnitride und -karbiden (New studies on the miscibility of transition metal nitrides and carbides). *Metall* 26:701–708 (in German)
34. Pessall N, Gold RE, Johansen HA (1968) A study of superconductivity in interstitial compounds. *J Phys Chem Solids* 29:19–38
35. Yvon K, Nowotny HN, Kieffer R (1967) Die Kristallstruktur der Subcarbide von Übergangsmetallen (The crystal structure of the subcarbides of transition metals). *Monatsh Chem* 98(1):34–44 (in German)
36. Kempter CP, Storms EK (1967) Thermal expansion of some niobium carbides. *J Less-Common Met* 13:443–447

37. Askarova LK, Zhilyaev VA (1994) High-temperature oxidation of vanadium and niobium carbides at low air pressures. *Russ J Inorg Chem* 39(7):1054–1056
38. Zhilyaev VA, Askarova LK (1985) Interaction of niobium carbide with nickel oxide. *Russ J Inorg Chem* 30(11):1568–1571
39. Shveikin GP, Tskhai VA, Mitrofanov BV (1987) Dependence of microhardness on the parameters of the electronic structure of cubic carbides and nitrides of group IV-VI transition metals. *Inorg Mater* 23(6):837–841
40. Mitrokhin VA, Yurkova RS (1981) Unit cell periods of solid solutions of zirconium carbide in niobium carbide. *Inorg Mater* 17(12):1701–1702
41. Korolev LA, Taubin ML (1977) Thermophysical properties of NbC_x. *Inorg Mater* 13(1):50–53
42. Gatterer J, Dufek G, Etmayer P, Kieffer R (1975) Kubisch Tantal Mononitrid (B1) und seine Mischbarkeit mit isotypische Mononitride und Monokarbidene der Gruppe 4a und 5a Gruppenmetalle (Cubic tantalum mononitride (B1) and its miscibility with isotypic mononitrides and monocarbides of 4a group and 5a group metals). *Monatsh Chem* 106(5):1137–1147 (in German)
43. Gusev AI, Dubrovskaya LB, Shveikin GP (1975) Magnetic susceptibility and electrical resistivity of solid solutions ZrN-NbC. *Inorg Mater* 11(6):981–982
44. May CE, Hoekstra PD (1961) Stability of refractory compounds in hydrogen between 4500 and 5000 °F and their compatibility with tungsten. Technical report NASA-TN-D-844. National Aeronautics and Space Administration, Washington, DC, pp. 1–18
45. Christensen AN (1985) Vacancy order in Nb₆C₅. *Acta Chem Scand A* 39:803–804
46. Ono K, Moriyama J (1981) The phase relationships in the Nb-Ti-C system. *J Less-Common Met* 79:255–260
47. Lönnberg B, Lundström T (1985) Thermal expansion and phase analytical studies of Nb₂C. *J Less-Common Met* 113(2):261–268
48. Alyamovskii SI, Shveikin GP, Geld PV (1963) On the oxidation of niobium and its lower carbide. *Russ J Inorg Chem* 8(8):1042–1043
49. Rempel AA, Gusev AI (1985) Order-disorder phase transition in nonstoichiometric niobium carbide. *Phys Crystallogr* 30(6):648–650
50. Savitskii EM, Efimov YV, Mikhailov BP, Moroz EA (1979) Reaction of silicides, germanides and other phases of the A15 structural type with carbon. *Inorg Mater* 15(4):515–518
51. Samsonov GV, Timofeeva II, Naumenko VYa, Bazhenova LN, Rud BM (1975) Properties of Nb₂C and V₂C in the region of homogeneity. *Inorg Mater* 11(1):50–52
52. Fedorov TF, Popova NM, Gorshkova LV, Skolozdra RV, Kuzma YuB (1968) Phase equilibria in the systems vanadium-chromium-carbon, niobium-chromium-carbon and tantalum-chromium-carbon. *Powder Metall Metall Ceram* 7(3):193–197
53. Ramqvist L (1968) Variation of hardness, resistivity and lattice parameter with carbon content of group 5b metal carbides. *Jernkontoret Ann* 152(9):465–475
54. Rudy E, Brukl CE, Windisch S (1967) Constitution of niobium (columbium) – molybdenum – carbon alloys. *Trans Metall Soc AIME* 239(11):1796–1808
55. Stecher P, Benesovsky F, Neckel A, Nowotny H (1964) Untersuchungen in den Systemen Titan (Zirkonium, Hafnium) – Niob – Kohlenstoff (Investigations in the systems titanium (zirconium, hafnium) – niobium – carbon). *Monatsh Chem* 95(6):1630–1645 (in German)
56. Rudy E, Benesovsky F, Toth L (1963) Untersuchung der Dreistoffsysteme der Va-Metalle und VIa-Metalle mit Bor und Kohlenstoff (An investigation of the ternary systems of the Va metals and VIa metals with boron and carbon). *Z Metallkd* 54(6):345–353 (in German)
57. Rudy E, Benesovsky F, Sedlatschek K (1961) Untersuchungen im system Niob-Molybdän-Kohlenstoff (Studies in the system niobium-molybdenum-carbon). *Monatsh Chem* 92(4):841–855 (in German)
58. Storms EK, Krikorian NH (1960) The niobium – niobium carbide system. *J Phys Chem* 64:1471–1477

59. Alyamovskii SI, Zainulin YuG, Shveikin GP (1981) Oksikarbidy i oksinitridy metallov IVA i VA podgrupp (Oxycarbides and oxynitrides of IVA and VA subgroups metals). Nauka, Moscow (in Russian)
60. Parthe E, Yvon K (1970) On the crystal chemistry of the close packed transition metal carbides. II. A proposal for the notation of the different crystal structures. *Acta Crystallogr B* 26(2):153–163
61. Rudy E, Brukl CE (1967) Lower-temperature modifications of Nb₂C and V₂C. *J Am Ceram Soc* 50(5):265–268
62. Krzhizhanovskii RE, Shtern ZYu (1977) Teplofizicheskie svoistva nemetallicheskih materialov (karbidy) (Thermophysical properties of non-metallic materials (carbides)). Energiya, Leningrad (in Russian)
63. Samsonov GV (1964) Refractory transition metal compounds. Academic Press, New York
64. Samsonov GV, Umanskii YaS (1957) Tverdye soedineniya tugoplavkikh metallov (Hard compounds of refractory metals). Metallurgizdat, Moscow (in Russian)
65. Samsonov GV, Paderno VN (1963) Poluchenie i svoistva nekotorykh tugoplavkikh karbidnykh splavov (Preparation and properties of certain carbide alloys). *Zh Prikl Khim* 36(12):2759–2762 (in Russian)
66. Nagakura S, Oketani S (1968) Structure of transition metal carbides. *Trans Iron Steel Inst Jpn* 8:265–294
67. Samsonov GV, Vinitkii IM (1980) Handbook on refractory compounds. IFI/Plenum, New York
68. Kempter CP, Storms EK, Fries RJ (1960) Lattice dimensions of NbC as a function of stoichiometry. *J Chem Phys* 33(6):1873–1874
69. Holleck H (1984) Binäre und ternäre Carbid- und Nitridsysteme der Übergangsmetalle (Binary and ternary carbide and nitride systems of the transition metals). Gebrüder Bornträger, Berlin, Stuttgart (in German)
70. Terao N (1964) Structure des carbures de niobium (Structure of niobium carbides). *Jpn J Appl Phys* 3(2):104–111 (in French)
71. Kimura H, Sasaki Y (1961) The phase diagram of the niobium-carbon system. *Trans Jpn Inst Met* 2(2):98–104
72. Storms EK, Krikorian NH (1959) The variation of lattice parameter with carbon content of niobium carbide. *J Phys Chem* 63(10):1747–1749
73. Lipatnikov VN, Rempel AA, Gusev AI (1990) Effect of nonstoichiometry and ordering on the basal structural parameters of the monocarbides of niobium and tantalum. *Inorg Mater* 26(12):2171–2175
74. Rempel AA (1996) Atomic and vacancy ordering in nonstoichiometric carbides. *Phys Usp* 39(1):31–56
75. Mauer FA, Bolz LH (1955) Measurement of thermal expansion of cermet components by high-temperature X-ray diffraction. Report WADC-TR-55-473, Contracts AF33(616)-56-5 and AF33(616)-53-12. US Air Force, Wright Air Development Centre, Ohio, pp. 1–57
76. Ordanyan SS, Avgustinik AI, Kudryasheva LV (1968) Densification of nonstoichiometric niobium carbide phases. *Powder Metall Met Ceram* 7(8):612–618
77. Smith JF, Carlson ON, De Avillez RR (1987) The niobium-carbon system. *J Nucl Mater* 148:1–16
78. Alyamovskii SI, Shveikin GP, Geld PV, Volkova NM (1967) Orthorhombic β' -phases of niobium and vanadium carbides. *Russ J Inorg Chem* 12:301–303
79. Epicier T (1990) Crystal chemistry of transition metal hemicarbides. In: Freer R (ed) *The physics and chemistry of carbides, nitrides and borides*. Kluwer Academic, Dordrecht, pp. 215–248
80. Krajewski A, D'Alessio L, De Maria G (1998) Physico-chemical and thermophysical properties of cubic binary carbides. *Cryst Res Technol* 33(3):341–374
81. Goldschmidt HJ (1967) *Interstitial alloys*. Butterworths, London
82. Kosolapova TYa (1971) *Carbides: properties, production and applications*. Plenum Press, New York

83. Antonova MM, Bazhenova LN, Timofeeva II (1974) The production and some properties of carbohydrides of titanium, vanadium and niobium. In: Samsonov GV (ed) *Refractory carbides*. Consultants Bureau, New York, London, pp. 47–57
84. Pierson HO (1996) *Handbook of refractory carbides and nitrides*. Noyes Publications, Westwood, New Jersey
85. Brauer G, Lesser R (1959) Karbidenphasen des Niobs (Carbide phases of niobium). *Z Metallkd* 50(1):8–10 (in German)
86. Elliott RO, Kempter CP (1958) Thermal expansion of some transition metal carbides. *J Phys Chem* 62(5):630–631
87. Grigorev ON, Sinelnikova VS (1981) Structure and some properties of niobium carbide single crystals. *Powder Metall Met Ceram* 20(12):894–898
88. Lieber CM, Wong EW, Dai H, Maynor BW, Burns LD (1996) Growth and structure of carbide nanorods. *Mater Res Soc Symp (Proc. 1995 Fall MRS symp., Boston, Massachusetts)* 410:103–111
89. Xu G-Y, Li J-B, Huang Y, Xie Z-P (1999) Fabrication and morphology of different color NbC_x Whiskers. *J Cryst Growth* 200:143–147
90. Xu G-Y, Li J-B, Huang Y, Yang W-Y, Xie Z-P (1999) The fabrication and morphology of niobium carbide crystal with solid cage shape. *Mater Sci Eng B* 60:185–188
91. Fukunaga A, Chu S, McHenry ME, Nagumo M (1999) Synthesis, structure and superconducting properties of NbC nanorods and nanoparticles. *Mater Trans JIM* 40(2):118–122
92. Shi L, Gu Y, Chen L, Yang Z, Ma J, Qian Y (2005) Synthesis and characterisation of superconducting NbC nanotubes. *Carbon* 43:195–213
93. Shi L, Gu Y, Chen L, Yang Z, Ma J, Qian Y (2005) Synthesis and oxidation behaviour of nanocrystalline niobium carbide. *Solid State Ionics* 176:841–843
94. Andrievski RA (2005) Nanomaterials based on high-melting carbides, nitrides and borides. *Russ Chem Rev* 74(12):1061–1072
95. Ma J, Wu M, Du Y, Chen S, Jin W, Fu L, Yang Q, Wen A (2009) Formation of nanocrystalline niobium carbide (NbC) with a convenient route at low temperature. *J Alloy Compd* 475:415–417
96. Li X, Westwood A, Brown A, Brydson R, Rand B (2009) A convenient general synthesis of carbide nanofibres via templated reactions on carbon nanotubes in molten salt media. *Carbon* 47:201–208
97. Nedfors N, Tengstrand O, Lewin E, Firian A, Eklund P, Hultman L, Jansson U (2011) Structural, mechanical and electrical-contact properties of nanocrystalline-NbC/ amorphous-C coatings deposited by magnetron sputtering. *Surf Coat Technol* 206:354–359
98. Zhang K, Wen M, Meng QN, Hu CQ, Li X, Liu C, Zheng WT (2012) Effects of substrate bias voltage on the microstructure, mechanical properties and tribological behaviour of reactive sputtered niobium carbide films. *Surf Coat Technol* 212:185–191
99. Zhang K, Wen M, Cheng G, Li X, Meng QN, Lian JS, Zheng WT (2014) Reactive magnetron sputtering deposition and characterization of niobium carbide films. *Vacuum* 99:233–234
100. Chen K, Bao Z (2012) Synthesis and characterisation of carbide nanosheets by a template-confined reaction. *J Nanopart Res* 14(9):1141
101. Kobayashi K, Kitaura R, Wang Q, Wakamori I, Shinohara H, Anada S, Nagase T, Saito T, Kiyomiya M, Yasuda H (2014) Synthesis of refractory conductive niobium carbide nanowires within the inner space of carbon nanotube templates. *Appl Phys Express* 7(1):015101
102. Mashtalir O, Naguib M, Mochalin VN, Dall'Agnesse Y, Heon M, Barsoum MW, Gogotsi Y (2013) Intercalation and delamination of layered carbides and carbonitrides. *Nature Commun* 4:1716
103. Naguib M, Gogotsi Y (2014) Synthesis of two-dimensional materials by selective extraction. *Acc Chem Res* 48(1):128–135

104. Hague JR, Lynch JF, Rudnick A, Holden FC, Duckworth WH (1964) Refractory ceramics for aerospace. Battelle Memorial Institute, The American Ceramic Society, Columbus, Ohio
105. Storms EK (1964) A critical review of refractories. Report LA-TR-2942, Contract W-7405-ENG-36. Los Alamos Scientific Laboratory, New Mexico, pp. 1–255
106. Lyakishev NP, ed (1996) Diagrammy sostoyaniya dvoynikh metallicheskich sistem (Phase diagrams of binary metallic systems), Vol. 1. Mashinostroenie, Moscow (in Russian)
107. Kornilov AN, Zaikin ID, Skuratov SM, Shveikin GP (1966) Standard heats of formation of niobium carbides present in NbC phase. *Russ J Phys Chem* 40(5):576–582
108. Mah AD, Boyle BG (1955) Heats of formation of niobium carbide and zirconium carbide from combustion calorimetry. *J Am Chem Soc* 77(24):6512–6513
109. Kornilov AN, Leonidov VYa, Skuratov SM (1962) Standartnye teploty obrazovaniya vysshikh karbidov niobiya i tantalala (The standard heats of formation of higher niobium and tantalum carbides). *Vestn Mosk Univ Ser II Khim* (6):48–50 (in Russian)
110. Samsonov GV, Paderno VN (1965) Preparation of solid solution alloys of hafnium carbide with carbides of titanium, zirconium, niobium and tantalum and determination of their physical properties. *Russ Metall* (1):119–126
111. Huber EJ, Jr, Head EL, Holley CE, Jr, Storms EK, Krikorian NH (1961) The heats of combustion of niobium carbides. *J Phys Chem* 65(10):1846–1849
112. Kusenko FG, Geld PV (1960) Teploty obrazovaniya oksidov i karbidov niobiya (Heats of formations of niobium oxides and carbides). *Izv Sib Otd AN SSSR* (2):46–52 (in Russian)
113. Nikolskaya TA, Avarbe RG, Vil'k YuN (1968) Temperature and concentration dependence of thermodynamic functions of niobium and tantalum carbides. *Russ J Phys Chem* 42(3):337–340
114. Barin I (1995) Thermochemical data of pure substances, 3rd edn. Vol. 1–2. VCH, Weinheim, New York
115. Zaikin ID, Kornilov AN (1966) Dependence of heats of formation of carbides on composition over range of homogeneity. *Russ J Phys Chem* 40(9):1099–1104
116. Chirkin VS (1968) Teplofizicheskie svoystva materialov yadernoi tekhniki (Thermophysical properties of nuclear materials). Atomizdat, Moscow (in Russian)
117. Shepline VM, Runck RJ (1956) Carbides. In: Campbell IE (ed) High temperature technology. Wiley, Chapman and Hall, New York, London, pp. 114–130
118. Zefirov AP (ed), Veryatin UD, Mashirev VP, Ryabtsev NG, Tarasov VI, Rogozkin BD, Korobov IV (1965) Termodinamicheskie svoystva neorganicheskikh veschestv (Thermodynamic properties of inorganic substances). Atomizdat, Moscow (in Russian)
119. Goldsmith A, Waterman T, Hirschorn HJ (1961) Handbook of thermophysical properties of solid materials. Pergamon Press, Oxford, London
120. Fesenko VV, Bolgar AS (1963) O kompleksnom izmerenii fiziko-khimicheskikh svoystv tugoplavkikh soedinenii pri vysokikh temperaturakh (On the complex measurement of physico-chemical properties of refractory compounds at high temperatures). In: Budnikov PP (ed) Silikaty i oksidy v khimii vysokikh temperatur (Silicates and oxides in the chemistry of high temperatures). Metallurgizdat, Moscow, pp. 135–148 (in Russian)
121. Chirkin VS (1959) Teplofizicheskie svoystva materialov (Thermophysical properties of materials). Fizmatgiz, Moscow (in Russian)
122. Sandenaw TA, Storms EK (1966) Heat capacities of NbC_{0.702}, NbC_{0.825}, NbC_{0.980} and Nb₂C below 320 K. *J Phys Chem Solid* 27(1):217–218
123. Stepanenko EK, Dogadaeva IM, Ordanyan SS (1982) Reactions in the NbC-NbSi₂ and NbB₂-NbSi₂ systems. *Powder Metall Met Ceram* 21(7):568–570
124. Pankratz LB, Weller WW, Kelley KK (1964) Thermodynamic data for columbium (niobium) carbide. Report BM-RI-6446. Bureau of Mines, US Department of the Interior, Washington, DC, pp. 1–9
125. Geld PV, Kusenko FG (1960) Teplosoderzhanie i teploemkost oksidov i karbidov niobiya pri vysokikh temperaturakh (The enthalpy and heat capacity of niobium oxides and carbides at high temperatures). *Izv AN SSSR OTN Metall Toplivo* (2):79–86 (in Russian)

126. Kantor PB, Fomichev EN (1967) Enthalpy and specific heat of niobium and zirconium carbides in temperature range 500 to 2400 K. *High Temp* 5(1):41–44
127. Bolgar AS, Turchanin AG, Fesenko VV (1973) Termodinamicheskie svoistva karbidov (Thermodynamic properties of carbides). *Naukova Dumka, Kyiv* (in Russian)
128. Turchanin AG, Turchanin MA (1991) Termodinamika tugoplavkikh karbidov i karbonitridov (Thermodynamics of refractory carbides and carbonitrides). *Metall, Moscow* (in Russian)
129. Turchanin AG, Guseva EA, Fesenko VV (1971) Thermodynamic properties of refractory carbides in the temperature range 0–3000 K. II. Niobium carbide. *Powder Metall Met Ceram* 10(11):890–891
130. Lide DR, ed (2010) *Handbook of chemistry and physics*, 90th edn. CRC Press, Boca Raton, New York
131. Levinson LS (1963) High-temperature heat content of niobium carbide and tantalum carbide. *J Chem Phys* 39(6):1550–1551
132. Schick HL, ed (1966) *Thermodynamics of certain refractory compounds*, Vol. 1–2. Academic Press, New York, London
133. Sheindlin AE, Chekhovskoy VYa, Shpilrain EE (1970) Research on thermophysical properties of solids at high temperatures at the Institute for High Temperatures of the USSR Academy of Sciences. *High Temp High Press* 2(1):1–6
134. Petrova II, Chekhovskoi VYa (1978) True heat capacity of zirconium, niobium and tantalum carbides by a pulse method. *High Temp* 16(6):1045–1050
135. Petrova II, Chekhovskoi VYa (1981) Application of a minicomputer in studies of the specific heats of refractory compounds by the pulse method. *High Temp* 19(3):444–448
136. Sheindlin AE, Belevich IS, Kozhevnikov IG (1973) Study of enthalpy and specific heat of materials based on niobium carbide at high temperatures. *High Temp* 11(1):75–78
137. Hörz G (1973) Carbonisierung und Entkohlung von Niob und Tantal (Carburization and decarburization of niobium and tantalum). *Metall* 27(7):680–687 (in German)
138. Bolgar AS, Verkhoglyadova TS, Samsonov GV (1961) Davlenie para i skorost ispareniiya nekotorykh tugoplavkikh soedinenii v vakuume pri vysokikh temperaturakh (The vapour pressure and vaporization rate of certain refractory compounds in vacuum at high temperatures). *Izv AN SSSR OTN Metall Toplivo* (1):142–146 (in Russian)
139. Turchanin AG, Ordanyan SS, Fesenko VV (1967) Enthalpy and specific heat of niobium carbide in its homogeneity region over the temperature range 1300–2500 K. *Powder Metall Met Ceram* 6(12):702–705
140. Coltters RG (1985) Thermodynamics of binary metallic carbides: a review. *Mater Sci Eng* 76(1–2):1–50
141. Worrell WL, Chipman J (1964) The free energies of formation of the niobium, niobium and tantalum carbides. *J Phys Chem* 68(4):860–866
142. Kubaschewski O, Alcock CB (1979) *Metallurgical thermochemistry*, 5th edn. Pergamon Press, Oxford, New York
143. Gusev AI, Rempel AA, Lipatnikov VN (1996) Heat capacity of niobium and tantalum carbides NbC_y and TaC_y in disordered and ordered states below 300 K. *Phys Status Sol B* 194:467–482
144. Huang W (1990) Thermodynamic evaluation of Nb-C system. *Mater Sci Technol* 6:687–694
145. Rudy E (1969) Compendium of phase diagram data. In: *Ternary phase equilibria in transition metal-boron-carbon-silicon systems*. Report AFML-TR-65-2, Contracts USAF 33(615)-1249 and USAF 33(615)-67-C-1513, Part 5. Air Force Materials Laboratory, Wright-Patterson Air Force Base, Ohio, pp. 1–689
146. Nadler MR, Kempter CP (1960) Some solidus temperatures in several metal-carbon systems. *J Phys Chem* 64(10):1468–1471
147. Storms EK, Calkin B, Yencha A (1969) The vaporization behaviour of the defect carbides. Part I: The Nb-C system. *High Temp Sci* 1(4):430–455

148. Brizes WF, Brody HD (1972) Modification of the Nb-C phase diagram. *J Am Ceram Soc* 55(5):277–278
149. Billingham J, Bell PS, Lewis MH (1972) Vacancy short-range order in substoichiometric transition metal carbides and nitrides with the NaCl structure. I. Electron diffraction studies of short-range ordered compounds. *Acta Crystallogr A* 28(6):602–606
150. Rempel AA, Gusev AI (1983) Uporyadochenie v nestekhiometricheskom monokarbide niobiya (Ordering in nonstoichiometric niobium monocarbide). Ural Scientific Centre, USSR Academy of Sciences, Sverdlovsk (in Russian)
151. Huang W, Selleby M (1997) Thermodynamic assessment of the Nb-W-C system. *Z Metallkd* 88(1):55–62
152. Lu X-G, Selleby M, Sundman B (2007) Calculations of thermophysical properties of cubic carbides and nitrides using the Debye-Grüneisen model. *Acta Mater* 55:1215–1226
153. Rathod N, Gupta SD, Gupta SK, Jha PK (2011) First-principles study of structural, electronic, elastic, phonon and thermodynamical properties of niobium carbide. *Solid State Phenom* 171:67–77
154. Wu L, Wang Y, Yan Z, Zhang J, Xiao F, Liao B (2013) The phase stability and mechanical properties of Nb-C system: using first-principles calculations and nano-indentation. *J Alloy Compd* 561:220–227
155. Zubkov VG, Dubrovskaya LB, Geld PV, Tskhai VA, Dorofeev YuA (1969) Neutron-difraktsionnoe issledovanie uporyadocheniya nestekhiometricheskikh kubicheskikh karbidov perekhodnykh metallov V gruppy (Neutron diffraction study of the ordering of non-stoichiometric cubic carbides of group V transition metals). *Dokl AN SSSR* 184:874–876 (in Russian)
156. Turchanin AG, Fesenko VV (1969) Thermodynamic characteristics of refractory carbides in their homogeneity regions. *Powder Metall Met Ceram* 8(6):466–469
157. Turchanin AG (1982) Equations for temperature-concentration function of enthalpy and heat capacity of niobium carbide in the homogeneity region. *Inorg Mater* 18(7):962–964
158. Turchanin AG (1986) Thermodynamic properties of group V transition metal carbides of variable composition over the temperature range 1200–2500 K. *Inorg Mater* 22(1):49–52
159. Kieffer R, Schwarzkopf P (1953) *Hartstoffe und Hartmetalle* (Refractory hard metals). Springer, Vienna (in German)
160. Fries RJ (1962) Vaporization behaviour of niobium carbide. *J Chem Phys* 37(2):320–327
161. Kaufman L (1964) Thermodynamic factors controlling the stability of solid phases at high temperatures. In: Waber JT, Chiotti P, Miner WN (eds) *Compounds of interest in nuclear reactor technology*. Metallurgical Society of American Institute of Mining Engineers, New York, pp. 193–225
162. Nikolskaya TA, Avarbe RG, Vilk YuN (1970) Determination of rate of vaporization of congruently vaporizing compositions of monocarbide phase of niobium. *High Temp* 8(1):72–75
163. Fesenko VV, Bolgar AS (1969) Study of evaporation rates of carbides of titanium, zirconium, hafnium, niobium and tantalum at high temperatures. *High Temp* 7(2):226–233
164. Nikolskaya TA, Avarbe RG (1971) Nekotorye zakonomernosti ispareniya karbidov perekhodnykh metallov IV-V podgrupp v vakuume (Some regularities of transition metals of IV-V subgroups carbides evaporation in a vacuum). In: Kornilov II, Matveeva NM (eds) *Metallidy – stroenie, svoystva, primeneniye* (Metallides – structure, properties, application). Nauka, Moscow, pp. 127–134 (in Russian)
165. Vlasov VK, Golubtsov IV (1968) Evaporation of niobium carbide from an open surface into a vacuum. *Russ J Phys Chem* 42(3):328–334
166. Vlasov VK, Golubtsov IV, Nesmeyanov AN (1968) Measurement of rates of evaporation of refractory carbides from a free surface into a vacuum. *Russ J Phys Chem* 42(3):420–426
167. Nikolskaya TA, Vilk YuN, Avarbe RG (1968) Investigation of laws governing high-temperature vaporization from an open surface in a vacuum of monocarbide phases of transition metals of IV-V groups. 1. Behaviour of monocarbide phase of niobium with vaporization from an open surface in a vacuum in temperature interval 2453–3428 K. *High Temp* 6(1):161–164

168. Avarbe RG, Vil'k YuN (1964) Calculation of temperature and concentration dependences of some thermodynamic functions of NbC_x phases. *High Temp* 2(3):370–374
169. Fesenko VV, Bolgar AS (1966) *Isparenie tugoplavkikh soedinenii* (Evaporation of refractory compounds). Metallurgiya, Moscow (in Russian)
170. Marmer ÉN, Gurvich OS, Maltseva LF (1967) *Vysokotemperaturnye materialy* (High-temperature materials). Metallurgiya, Moscow (in Russian)
171. Neshpor VS, Ordanyan SS, Avgustinik AI, Khusidman MB (1964) Vliyanie khimicheskogo sostava na elektro- i teplofizicheskie svoistva karbidov tsirkoniya i niobiya v oblasti ikh gomogenosti (The effect of the chemical composition of zirconium and niobium carbides in the homogeneity region on their electrical and thermal properties). *Zh Prikl Khim* 37(11):2375–2382 (in Russian)
172. Storms EK, Wagner P (1973) Thermal conductivity of substoichiometric ZrC and NbC. *High Temp Sci* 5(6):454–462
173. Morrison BH, Sturgess LL (1970) Thermal diffusivity and conductivity of zirconium carbide and niobium carbide from 100 to 2500 K. *Rev Int Hautes Temp Refract* 7(4):351–358
174. Radosevich LG, Williams WS (1969) Phonon scattering by conduction electrons and by lattice vacancies in carbides of the transition metals. *Phys Rev* 181(3):1110–1117
175. Radosevich LG, Williams WS (1970) Thermal conductivity of transition metal carbides. *J Am Ceram Soc* 53(1):30–33
176. Sakurai J, Hayashi J, Mekata M, Tsuchida T, Takagi H (1961) Thermal conductivities of monocarbides of transition metals. *J Jpn Inst Met Mater* 25(4):289–292 (in Japanese)
177. Shaffer PTB (1964) *Handbooks of high-temperature materials: No. 1 – Materials index*. Plenum Press, Springer Science, New York
178. Lengauer W (2000) Transition metal carbides, nitrides and carbonitrides. In: Riedel R (ed) *Handbook of ceramic hard materials*. Wiley-VCH, Weinheim, pp. 202–252
179. Sinelnikova VS, Grebenkina VG (1982) Electrophysical properties of niobium carbide single crystals. *Powder Metall Met Ceram* 21(10):804–806
180. Paderno YuB, Barantseva IG, Yupko VL (1965) *Izmerenie teploprovodnosti i elektroprotivleniya ZrC, HfC, NbC i TaC pri vysokikh temperaturakh* (Measurement of thermal conductivity and electrical resistance of ZrC, HfC, NbC and TaC at high temperatures). In: Grigoreva VV, Eremenko VN, Nazarchuk TN, Samsonov GV, Fedorchenko IM, Frantsevich IN (eds) *Vysokotemperaturnye neorganicheskie soedineniya* (High-temperature inorganic compounds). Naukova Dumka, Kyiv, pp. 199–204 (in Russian)
181. Neel DS, Pears CD, Oglesby S, Jr (1962) The thermal properties of thirteen solid materials to 5000 °F or their destruction temperatures. Technical report WADD-TR-60–924, Contract USAF 33(616)-6312. Southern Research Institute, University of Alabama, Birmingham, USA, pp. 1–216
182. Radosevich LG, Williams WS (1969) Lattice thermal conductivity of superconducting niobium carbide. *Phys Rev* 188(2):770–773
183. Williams WS (1971) Transition-metal carbides. *Prog Solid State Chem* 6(C):57–118
184. Houska CR (1964) Thermal expansion of certain group IV and group V carbides at high temperatures. *J Am Ceram Soc* 47(6):310–311
185. Samsonov GV, Naumenko VYa (1970) Thermal expansion of transition metal carbides IV-V groups in their homogeneity regions. *High Temp* 8(5):1022–1024
186. Miccioli BR, Shaffer PTB (1964) High-temperature thermal expansion behaviour of refractory materials. I. Selected monocarbides and binary carbides. *J Am Ceram Soc* 47(7):351–356
187. Paderno YuB, Dudnik EM, Andreeva TV, Barantseva IG, Yupko VL (1965) *Izmerenie koeffitsientov termicheskogo rasshireniya ZrC, HfC, NbC i TaC pri vysokikh temperaturakh* (Measurement of the coefficients of thermal expansion of ZrC, HfC, NbC and TaC at high temperatures). In: Grigoreva VV, Eremenko VN, Nazarchuk TN, Samsonov GV, Fedorchenko IM, Frantsevich IN (eds) *Vysokotemperaturnye neorganicheskie soedineniya* (High-temperature inorganic compounds). Naukova Dumka, Kyiv, pp. 293–296 (in Russian)

188. Neel DS, Pears CD (1962) Progress in international research on thermodynamic and transport properties. Academic Press, New York
189. Portnoi KI, Chubarov VM (1967) Svoistva tugoplavkikh metallov i soedinenii (The properties of refractory metals and compounds). In: Tumanov AT, Portnoi KI (eds) Tugoplavkie materialy v mashinostroenii (Refractory materials in machinery construction). Mashinostroenie, Moscow, pp. 7–124 (in Russian)
190. Khatsinskaya IM, Chaporova IN, Cheburaeva RF, Samoilov AI, Logunov AV, Ignatova IA, Dodonova LP (1983) Structure and thermal expansion of NbC base complex carbides. Powder Metall Met Ceram 22(11):952–956
191. Samsonov GV, Naumenko VY, Okhremchuk LN (1971) Herstellung und Eigenschaften von Karbiden der Übergangsmetalle in ihren Homogenitätsbereichen (Synthesis and properties of carbides of transition metals in their homogeneity range). Phys Status Sol A 6(1):201–211 (in German)
192. Jun CK, Shaffer PTB (1971) Thermal expansion of niobium carbide, hafnium carbide and tantalum carbide at high temperatures. J Less-Common Met 24(3):323–327
193. Brenton RF, Saunders CR, Kempter CP (1969) Elastic properties and thermal expansion of niobium monocarbide to high temperatures. J Less-Common Met 19(3):273–278
194. Williams WS (1993) Thermal conductivity peaks in old and new ceramic superconductors. Solid State Commun 87(4):355–358
195. Samsonov GV, Épik AP (1973) Tugoplavkie pokrytiya (Refractory coatings). Metallurgiya, Moscow (in Russian)
196. Samsonov GV, Portnoi KI (1961) Splavy na osnove tugoplavkikh soedinenii (The alloys on the basis of refractory compounds). Oborongiz, Moscow (in Russian)
197. Samsonov GV (1956) The electrical conductivity of certain compounds of the transitional metals with boron, carbon and nitrogen and the electrical conductivity of alloys of these compounds. Sov Phys Tech Phys 1(4):695–701
198. Kolomoets NV, Neshpor VS, Samsonov GV, Semenkovich SA (1958) Thermoelectrical properties of some metal-like compounds. Sov Phys Tech Phys 3(11):2186–2193
199. Samsonov GV, Sinelnikova VS (1962) Vysokotemperaturnye metallokeramicheskie materialy (High-temperature sintered metal-powder materials). UkrSSR Academy of Sciences, Kyiv (in Russian)
200. Lowrie R (1963) Research on physical and chemical principles affecting high temperature materials for rocket nozzles. Quarterly progress report, Contract DA 30-069-ORD-2787. Union Carbide Research Institute, Tarrytown, New York, pp. 1–50
201. Clinard FW Jr, Kempter CP (1968) Low-temperature electrical properties of some transition metals and transition-metal carbides. J Less-Common Met 15:59–73
202. Neshpor VS, Airapetyants SV, Ordanyan SS, Avgustinik AI (1966) Effect of the chemical composition of the monocarbides of group IV and V transition metals in the homogeneity range on the temperature dependence of their resistivity and thermo-e.m.f. Inorg Mater 2(5):728–730
203. Samsonov GV, Panasyuk AD (1966) Some electrophysical properties of niobium and zirconium carbides in their homogeneous regions. High Temp 4(2):203–208
204. Golikova OA, Matveeva NN, Avgustinik AI, Ordanyan SS (1967) Electrical conductivity and thermo-e.m.f. of niobium carbide between 20 and 2000 °C. High Temp 5(6):894–896
205. Neshpor VS, Samsonov GV (1964) Thermoelectric efficiency of monocarbides and mononitrides of transitional metals as related to their atomic characteristics. Doklady AN SSSR 157(4):834–836
206. Grebenkina VG, Denbnovetskaya EN (1974) Thermal coefficient of the electrical resistivity of carbides and their solid solutions. In: Samsonov GV (ed) Refractory carbides. Consultants Bureau, New York, London, pp. 269–274
207. Samsonov GV, Sinelnikova VS (1962) The resistivity of refractory compounds at high temperatures. Powder Metall Met Ceram 1(4):272–274

208. Borukhovich AS, Geld PV, Tskhai VA, Dubrovskaya LB, Matveenko II (1971) Conduction band of IVa and Va subgroup transition metal monocarbides. II. *Phys Status Sol B* 45(1):179–187
209. Samsonov GV, Naumenko VYa, Ryabokon LP, Verkhoturov AD (1975) Some properties of alloys of zirconium and niobium carbides in their homogeneity ranges. *Powder Metall Met Ceram* 14(1):44–46
210. Dy LC, Williams WS (1982) Resistivity, superconductivity and order-disorder transformations in transition metal carbides and hydrogen-doped carbides. *J Appl Phys* 53(12):8915–8927
211. Allison CY, Modine FA, French RH (1987) Optical and electrical properties of niobium carbide. *Phys Rev B* 35(6):2573–2582
212. Giorgi AL, Szklarz EG, Storms EK, Bowman AL, Matthias BT (1962) Effect of composition on the superconducting transition temperature of tantalum carbide and niobium carbide. *Phys Rev* 125(3):837–838
213. Roberts BW (1972) Properties of selected superconductive materials. NBS Technical note 724, National Bureau of Standards, US Government Printing Office, Washington, DC
214. Roberts BW (1978) Properties of selected superconductive materials. Report NBS-TN-983/NBS-TN-825, Accession PB-287013/7, N79-74281. National Technical Information Service, Washington, DC, pp. 1–103
215. Avgustinik AI, Golikova OA, Neshpor VS, Ordanyan SS (1967) Mechanism of conductivity in NbC with defects. *Inorg Mater* 3(2):256–259
216. Lvov SN, Nemchenko VF, Samsonov GV (1960) Nekotorye zakonomernosti v elektricheskikh svoistvakh boridov, karbidov i nitridov perekhodnykh metallov IV-VI grupp periodicheskoi sistemy (Some regularities in the electric properties of borides, carbides and nitrides of transition metals within the IV-VI groups of the periodic system). *Doklady AN SSSR* 135(3):577–580 (in Russian)
217. Samsonov GV (1964) Handbooks of high-temperature materials: No. 2 – Properties index. Plenum Press, Springer Science, New York
218. Samsonov GV, Upadhyaya GS (1969) Physical properties of the monocarbides of the transition metals in their homogeneity regions. I. TiC_{1-x} and NbC_{1-x} . *Powder Metall Met Ceram* 8(5):394–398
219. Bittner H, Goretzki H (1962) Magnetische Untersuchungen der Carbide TiC, ZrC, HfC, VC, NbC und TaC (Magnetic studies of the TiC, ZrC, HfC, VC, NbC and TaC carbides) *Monatsh Chem* 93(5):1000–1004 (in German)
220. Samsonov GV, Kuchma AYa (1968) Magnetic susceptibility of zirconium, hafnium and niobium monocarbides. *Inorg Mater* 4(8):1195–1197
221. Matveenko II, Dubrovskaya LB, Geld PV, Tretnikova MG (1965) Magnitnaya vospriimchivost karbida niobiya (Magnetic susceptibility of niobium carbide). *Izv AN SSSR Neorg Mater* 1(7):1062–1064 (in Russian)
222. Gusev AI, Rempel AA (1984) A study of the atomic ordering in the niobium carbide using the magnetic susceptibility method. *Phys Stat Sol A* 84(2):527–534
223. Borukhovich AS, Dubrovskaya LB, Matveenko II, Geld PV (1969) Magnetic susceptibility of niobium and tantalum monocarbides at low temperatures. *Phys Solid State* 11(3):681–682
224. Nazarova SZ, Gusev AI (2001) Magnetic susceptibility as a method of investigation of short-range ordering in highly nonstoichiometric carbides. *J Struct Chem* 42(3):470–484
225. Gusev AI, Nazarova SZ (2005) Magnetic susceptibility of nonstoichiometric compounds of transition d-metals. *Phys Usp* 48(7):651–673
226. Korshunov IG, Zinovev VE, Geld PV, Borukhovich AS, Chernyaev VS, Shveikin GP (1977) Thermophysical properties of cubic carbides of zirconium and niobium at high temperatures. *High Temp* 15(3):439–444
227. Borukhovich AS (1978) Kinetic properties of IVa and Va subgroup transition metal monocarbides. *Phys Stat Sol A* 46(1):11–37

228. Dubrovskaya LB, Matveenko II (1965) Magnetic properties of cubic tantalum carbide. *Phys Met Metallogr* 19(2):142–146
229. Caudron R, Ducastelle F, Costa P (1970) Chaleur spécifique électronique et susceptibilité magnétique des carbures de transition hexagonaux de formule M_2C (Specific electronic heat and magnetic susceptibility of transition metal hexagonal carbides with formula M_2C). *J Phys Chem Solids* 31(2):291–297 (in French)
230. Allen PB, Cohen ML (1972) Superconductivity and phonon softening. *Phys Rev Lett* 29(24):1593–1596
231. Klein BM, Papaconstantopoulos DA (1974) Electron-phonon interaction and superconductivity in transition metals and transition metal carbides. *Phys Rev Lett* 32(21):1193–1195
232. Haufe U, Kerker G, Benneman KH (1975) Calculations of the superconducting transition temperature T_c for metals with phonon-anomalies. *Solid State Commun* 17(3):321–325
233. Wada H, Tachikawa K, Ohasa M (1977) A study on niobium carbide dispersed superconducting tapes. *J Less-Common Met* 56(1):1–8
234. Pflüger J, Fink J (1985) Electronic structure of unoccupied states of stoichiometric ZrN, NbC and NbN as determined by high-energy electron energy loss spectroscopy. *Solid State Commun* 55(8):675–677
235. Pflüger J, Fink J, Weber W, Bohnen KP, Creelius G (1985) Dielectric properties of ZrN, NbC and NbN as determined by electron energy loss spectroscopy. *Phys Rev B* 31(3):1244–1247
236. Niculescu D, Cruceanu E (1985) Superconducting transition temperature of ion bombarded niobium surface layers. *J Mater Sci* 20(2):467–470
237. Kobayashi N, Linker G, Meyer O (1987) Structural disorder and superconducting transition temperature of ion-irradiated NbC. *J Phys F* 17(7):1491–1509
238. Gusev AI, Rempel AA (1989) Superconductivity in disordered and ordered niobium carbide. *Phys Status Sol B* 151(1):211–224
239. Koide T, Shidara T, Fukutani H, Fujimori A, Otani S, Ishizawa Y (1993) Optical constants of $TiC_{0.95}$, $VC_{0.86}$ and $NbC_{0.93}$ from 0.8 to 80 eV. *Jpn J Appl Phys* 1 32(3A):1130–1134
240. Ramqvist L, Ekstig B, Källne E, Noreland E, Manne R (1971) X-ray emission spectra of VC_x , NbC_x , TaC_x and ZrC_x . *J Phys Chem Solid* 32(1):149–157
241. Alyamovskii SI, Shveikin GP, Geld PV (1966) Infrazrasnye spektry pogloshcheniya karbidov i nizshikh okislov vanadiya, niobiya i tantala (The infrared absorption spectra of vanadium, niobium and tantalum carbides and lower oxides). *Zh Neorg Khim* 12(7):1738–1742 (in Russian)
242. Mackie WA, Carleson P, Fillion J, Hinrichs CH (1991) Normal spectral emittance of crystalline transition metal carbides. *J Appl Phys* 69(10):7236–7239
243. Petrov VA, Chekhovskoi VYa, Sheindlin AE, Nikolaeva VA, Fomina LP (1967) Total hemispherical emissive power monochromatic ($\lambda = 0.65 \mu m$), emissive power and specific electrical resistivity of zirconium and niobium carbides in temperature range 1200–3500 K. *High Temp* 5(6):889–893
244. Samsonov GV, Fomenko VS, Paderno YuB (1962) Spectral emittance of the powders of some high-melting compounds. *Refract Ind Ceram* 3(1–2):35–37
245. Samsonov GV, Podchernyaeva IA, Fomenko VS (1969) Emission coefficient of high-melting compounds. *Powder Metall Met Ceram* 8(5):374–379
246. Petrov VA (1969) Izluchatel'naya sposobnost vysokotemperaturnykh materialov (The emissivity of high-temperature materials). Nauka, Moscow (in Russian)
247. Rakov AM, Khrustalev BA (1979) Experimental determination of high-temperature radiative properties of solids. *Heat Transfer Sov Res* 11(4):121–126
248. Ozaki Y, Zee RH (1995) Investigation of thermal and hydrogen effects on emissivity of refractory metals and carbides. *Mater Sci Eng A* 202(1–2):134–141
249. Cohron J, Ozaki Y, Chin B, Zee R (1994) Reactivity of refractory carbides with hot hydrogen. *AIP Conf Proc* 301:939

250. Fridlender BA, Neshpor VS, Ermakov BG, Sokolov VV (1973) Thermal diffusivity and conductivity of pyrolytic titanium carbide, columbium carbide and titanium nitride at high temperatures. *J Eng Phys* 24(2):210–212
251. Fomenko VS, Naumenko VYa, Okhremchuk LN, Podchernyaeva IA, Samsonov GV (1970) Glühemissionseigenschaften der Monokarbid von Übergangsmetallen der IV und V Gruppe im Homogenitätsbereich (The thermionic emission properties of transition metals monocarbides of groups IV and V in the homogeneity range). *Phys Status Sol A* 2(3):K181–K184 (in German)
252. Yada K, Shimoyama H (1985) Brightness characteristics of carbide emitters for electron microscopy. *J Electron Microsc* 34:147–155
253. Yada K, Masaoka H, Shoji Y, Tanji T (1989) Studies of refractory carbides, nitrides and borides as the thermionic emitters for electron microscopy. *J Electron Microsc Techn* 12:252–261
254. Fomenko VS (1981) Emissionnye svoystva materialov (The thermionic emission properties of materials). Naukova Dumka, Kyiv (in Russian)
255. Stewart D, Rivlin VG, Wilson PD (1981) Field emission cold cathode devices based on eutectic systems. Final technical report RADC-TR-81-170, Contract/Grant AFOSR-77-3292, A1-A15. Rome Air Development Center, Air Force Systems Command, Griffis Air Force Base, New York, pp. 1–89
256. Stewart D, Wilson PD, Latham RV, Allen NK (1981) Energy spectra of electrons field emitted from a broad area composite cathode of tantalum carbide. *J Mater Sci* 16(1):111–117
257. Ishizawa Y, Aizawa T, Otani S (1993) Stable field emission and surface evaluation of surface-processed NbC <110> tips. *Appl Surf Sci* 67:36–42
258. Samsonov GV, Fomenko VS, Paderno YuB (1963) Termoemisiini vlastivosti deyakikh tugoplavkikh spoluk (The thermionic properties of certain refractory compounds). *Ukr Fiz Zh* 8(6):700–702 (in Ukrainian)
259. Samsonov GV (ed), Fomenko VS (1966) Handbook of thermionic properties. Plenum Press, New York
260. Bolshov VG (1966) Work function of carbides of refractory metals in cesium vapour. *Sov Phys Tech Phys* 11(2):239–245
261. Okhremchuk LN, Podchernyaeva IA, Podgrushko NF, Fomenko VS (1972) Voprosy raboty vykhoda perekhodnykh metallov (Problems of transition metals work function). *Radiotekh Elektron* 17(1):205–206 (in Russian)
262. Samsonov GV, Siman NI, Podchernyaeva IA, Fomenko VS (1976) Issledovanie energii adsorbtsii Cs i K na poverkhnosti tugoplavkikh karbidov (Study of Cs and K adsorption energies on surface of high-melting carbides). *Zh Tekh Fiz* 46(2):393–397 (in Russian)
263. Samsonov GV, Paderno YuB, Fomenko VS (1967) Thermionic emission characteristics of transition metals and their compounds. *Sov Phys Tech Phys* 11(8):1070–1083
264. Samsonov GV, Fomenko VS, Paderno VN, Rud BM (1964) Thermoemission characteristics of alloys of isomorphous carbides. *High Temp* 2(5):656–661
265. Hojo H, Nakayama K (1976) Coated emitters of transition metal carbides for vacuum measurement. *J Vac Soc Jpn* 19(9):312–317 (in Japanese)
266. Ramqvist L (1969) Preparation, properties and electronic structure of refractory carbides and related compounds. *Jernkontoret Ann* 153(4):159–179
267. Ramqvist L (1971) Electronic structure of cubic refractory carbides. *J Appl Phys* 42(5):2113–2127
268. Sinelnikova VS, Gurin VN (1979) Monokrystally tugoplavkikh soedinenii perekhodnykh metallov (Monocrystals of high-melting compounds of transition metals). *Zh Vsesoyuz Khim Obshchestva Im D I Mendeleev* 24(3):266–269 (in Russian)
269. Andrievskii RA (1979) Prochnost tugoplavkikh soedinenii (Strength of high-melting compounds). *Zh Vsesoyuz Khim Obshchestva Im D I Mendeleev* 24(3):258–262 (in Russian)

270. Travushkin GG, Knyazev VI, Belov VS, Rymashevskii GA (1973) Temperature threshold of brittle failure in interstitial phases. *Strength Mater* 5(5):639–641
271. Samsonov GV, Okhremchuk LN, Upadhyaya GS, Naumenko VYA (1970) Work function of titanium and niobium carbides in homogeneity region. *High Temp* 8(4):870–871
272. Kovalchenko MS, Dzhemelinskii VV, Skuratovskii VN, Tkachenko YuG, Yurchenko DZ, Alekseev VI (1971) Microhardness of some carbides at various temperatures. *Powder Metall Met Ceram* 10(8):665–668
273. Gridneva IV, Milman YuV, Sinelnikova VS, Chugunova SI (1982) Effect of temperature on the mechanism of failure and mechanical properties of niobium carbide single crystals. *Phys Met* 4(5):940–947
274. Funke VF, Pshenichnyi IV, Kruglov VN (1973) Substruktura i kharakter razrusheniya monokristallov karbidov tsirkoniya i niobiya (The substructure and character of fracture of single crystal zirconium and niobium carbides). *Izv AN SSSR Neorg Mater* 9(12):2151–2155 (in Russian)
275. Vahldiek FW, Mersol SA (1977) Slip and microhardness of IVa to VIa refractory materials. *J Less-Common Met* 55(2):265–278
276. Kosolapova TYa, Sinelnikova VS (1977) Poluchenie i svoystva monokristallov tugoplavkikh soedinenii (Preparation and properties of single crystals of refractory compounds). In: Dutchak YaI (ed) *Konfiguratsionnye predstavleniya elektronogo stroeniya v fizicheskom materialovedenii* (Configuration conception of the electron structure in the physical materials science). *Naukova Dumka, Kyiv*, pp. 98–100 (in Russian)
277. Ordanyan SS, Kudryashova LV, Avgustinik AI (1971) Mikrotverdost nestekhiometrichnykh tverdykh rastvorov na osnove karbidov tsirkoniya i niobiya (Microhardness of the non-stoichiometric solid solutions based on zirconium and niobium carbides). *Izv AN SSSR Neorg Mater* 7(12):2179–2182 (in Russian)
278. Bychkov AKh, Neshpor VS, Oradanyan SS (1974) Effect of plastic deformation on some properties of niobium monocarbide in its homogeneity range. *Powder Metall Met Ceram* 13(7):560–565
279. Fedotov MA, Yanchur VP, Maksimov VP (1976) Strength of carbide specimens prepared by impregnation through saturation. *Inorg Mater* 12(1):40–43
280. Khusainov MA (1979) Termoprochnost tugoplavkikh materialov, poluchennykh gazofaznym osazhdeniem (Thermal strength of refractory materials manufactured by gas-phase deposition). *Leningrad State University, Leningrad* (in Russian)
281. Andrievskii RA, Spivak II, Tsulin AE (1969) Otkloneniya ot stekhiometricheskogo sostava kak opredelyayushchie diffuzionno-kontroliruemye protsessy v fazakh vnedreniya (Deviations from stoichiometric composition as influencing diffusion-controlled processes in interstitial phases). *Doklady AN SSSR* 185(4):792–794 (in Russian)
282. Spivak II, Baranov VM, Knyazev VI, Rystsov VN, Fedotov MA (1975) Physicomechanical properties of zirconium nitride and niobium carbide within the range of homogeneity. *Strength Mater* 7(9):1097–1100
283. Kumashiro Y, Sakuma E (1980) The Vickers micro-hardness of non-stoichiometric niobium carbide and vanadium carbide single crystals up to 1500 °C. *J Mater Sci* 15(5):1321–1324
284. Kumashiro Y, Nagai Y, Kato H (1982) The Vickers micro-hardness of NbC, ZrC and TaC single crystals up to 1500 °C. *J Mater Sci Lett* 1(2):49–52
285. Grigorev ON, Trefilov VI, Shatokhin AM (1983) Influence of temperature on the failure of brittle materials in concentrated loading. *Powder Metall Met Ceram* 22(12):1028–1033
286. Weber WP, Quirk JF, Lemmon AW, Jr, Filbert RB, Jr (1957) Properties of beryllium oxide and carbides of beryllium, molybdenum, niobium, tantalum and titanium. Report BMI-1165, Contract W-7405-eng-92. Battelle Memorial Institute, Columbus, Ohio, pp. 1–37
287. Bazhenova LN, Ivanko AA (1969) Microhardness of carbides of certain transition metals. *Inorg Mater* 5(12):1763–1767

288. Zhunkovskii GL (1974) The vacuum carburization of transition metals of groups IV and V. In: Samsonov GV (ed) *Refractory carbides*. Consultants Bureau, New York, pp. 107–115
289. Ivanko AA (1968) *Tverdost (The hardness)*. Naukova Dumka, Kyiv (in Russian)
290. Ivanko AA (1974) The microhardness of transition-metal carbides. In: Samsonov GV (ed) *Refractory carbides*. Consultants Bureau, New York, London, pp. 367–370
291. Artamonov AYa, Bovkun GA (1974) Some aspects of the abrasive wear of transition-metal carbides. In: Samsonov GV (ed) *Refractory carbides*. Consultants Bureau, New York, London, pp. 371–376
292. Kohlstedt DL (1973) The temperature dependence of microhardness of the transition-metal carbides. *J Mater Sci* 8(6):777–786
293. Santhanam AT (1996) Application of transition metal carbides and nitrides in industrial tools. In: Oyama ST (ed) *The chemistry of transition metal carbides and nitrides*. Chapman & Hall, London, Glasgow, pp. 28–52
294. Koester RD, Moak DP (1967) Hot hardness of selected borides, oxides and carbides to 1900 °C. *J Am Ceram Soc* 50(6):290–296
295. Atkins AG, Tabor D (1966) Hardness and deformation properties of solids at very high temperatures. *Proc Roy Soc Lond A* 292(1431):441–459
296. Morgan G, Lewis MH (1974) Hardness anisotropy in niobium carbide. *J Mater Sci* 9(3):349–358
297. Hannink RHJ, Kohlstedt DL, Murray MJ (1972) Slip system determination in cubic carbides by hardness anisotropy. *Proc Roy Soc Lond A* 326(1566):409–420
298. Hannink RHJ, Murray MJ (1978) Comment on “Slip and microhardness of IVa to VIa refractory materials”. *J Less-Common Met* 60(1):143–145
299. Holleck H (1986) Material selection for hard coatings. *J Vac Sci Technol A* 4(6):2661–2669
300. Williams WS (1999) Electrical properties of hard materials. *Int J Refract Met Hard Mater* 17(1):21–26
301. Guo X, Li L, Liu Z, Yu D, He J, Liu R, Xu B, Tian Y, Wang H-T (2008) Hardness of covalent compounds: roles of metallic component and d-valence electrons. *J Appl Phys* 104(2):023503
302. Tian Y, Xu B, Zhao Z (2012) Microscopic theory of hardness and design of novel superhard crystals. *Int J Refract Met Hard Mater* 33:93–106
303. Gao F, He J, Wu E, Liu S, Yu D, Li D, Zhang S, Tian Y (2003) Hardness of covalent crystals. *Phys Rev Lett* 91(1):015502
304. Šimůnek A, Vackář J (2006) Hardness of covalent and ionic crystals: first-principle calculations. *Phys Rev Lett* 96(8):085501
305. Bendavid A, Martin PJ, Kinder TJ, Preston EW (2003) The deposition of NbN and NbC thin films by filtered vacuum cathodic arc deposition. *Surf Coat Technol* 163–164:347–352
306. Ferro D, Rau JV, Generosi A, Rossi-Albertini V, Latini A, Barinov SM (2008) Electron beam deposited VC and NbC thin films on titanium: hardness and energy-dispersive X-ray diffraction study. *Surf Coat Technol* 202:2162–2168
307. Kurlov AS, Gusev AI (2017) Density and particle size of cubic niobium carbide NbC_y nanocrystalline powders. *Phys Solid State* 59(1):184–190
308. Kurlov AS, Gusev AI, Kuznetsov VS, Bobrikov IA, Balagurov AM, Rempel AA (2017) Time-of-flight neutron diffraction of nanocrystalline powders of nonstoichiometric niobium carbide NbC_{0.77}. *Phys Solid State* 59(3):607–612
309. Hivert A, Poulignier J (1968) Mechanical properties at high temperatures of some ultra-refractory carbides. *Rev Int Hautes Temp Refract* 5(1):55–61
310. Kislyi PS (1979) *Poluchenie izdelii iz tugoplavkikh soedinenii metodami poroshkovoi metallurgii (The manufacture of articles from refractory compounds by powder metallurgy methods)*. *Zh Vsesoyuz Khim Obshch Im D I Mendeleev* 24(3):270–276 (in Russian)
311. Ramke WG, Latva JD (1963) *Refractory ceramics and intermetallic compounds*. *Aerospace Eng* 22(1):76–84

312. Ordanyan SS, Stepanenko EK, Sokolov IV (1984) Prochnost spechennykh kompozitnykh materialov NbC-NbB₂ (Strength of sintered compound materials NbC-NbB₂). *Izv Vyssh Uchebn Zaved Khim Kh Technol* 27(10):1201–1203 (in Russian)
313. Fedotov MA, Yanchur VP (1976) Temperature-dependence of strength and plasticity of carbides obtained by right-through saturation. *Inorg Mater* 12(3):364–367
314. Andrievskii RA, Vlasov KP, Shevchenko AS, Lanin AG, Pritchkin SA, Klyushin VV, Kurushin SP, MaskaeV AS (1978) Influence of reactor irradiation on physicomechanical properties of zirconium and niobium carbides. *Inorg Mater* 14(4):530–533
315. Deryavko II, Lanin AG, MaskaeV AS (1984) An X-ray diffraction study of the temporary microstresses in sintered carbides. *Powder Metall Met Ceram* 23(10):810–812
316. Kharchenko VK (1980) High-temperature strength of refractory materials. *Strength Mater* 12(10):1284–1294
317. Trefilov VI, Milman YuV, Gridneva IV (1984) Mechanical properties of covalent crystals. *Inorg Mater* 20(6):833–841
318. Kelly A, Rowcliffe DJ (1967) Deformation of polycrystalline transition metal carbides. *J Am Ceram Soc* 50(5):253–256
319. Williams WS (1964) Influence of temperature, strain rate, surface conditions and composition on the plasticity of transition metal carbides. *J Appl Phys* 35(4):1329–1338
320. Chevacharenkul S, Davis RF (1989) Dislocation mechanisms, diffusional processes and creep behaviour in NbC_x. *Acta Metall* 37(2):417–427
321. Kim B-R, Woo K-D, Yoon J-K, Doh J-M, Shon I-J (2009) Mechanical properties and rapid consolidation of binderless niobium carbide. *J Alloy Compd* 481:573–576
322. Woydt M, Mohrbacher H (2013) Friction and wear of binderless niobium carbide. *Wear* 306:126–130
323. Woydt M, Mohrbacher H (2014) Tribological profile of binderless niobium carbide. *Ceram Eng Sci Proc* 34(2):189–193
324. Zubarev PV, Dementev LN (1977) Creep of carbides of transition metals of groups IV-V in region of homogeneity. *Inorg Mater* 13(7):988–991
325. Zubarev PV, Dementev LN (1977) Osnovnye zakonomernosti vysokotemperaturnoi polzuchesti karbidov tsirkoniya i niobiya (Basic regularities of high-temperature creep of zirconium and niobium carbides). *Doklady AN SSSR* 232(6):1373–1375 (in Russian)
326. Dementev LN, Zubarev PV, Turchin VN, Kharkhardin YeD (1978) High-temperature creep of monocrystalline niobium carbide. *Phys Met Metallogr* 46(3):142–146
327. Vlasov NM, Zubarev PV (1983) Osobennosti plasticheskogo techeniya vaz vnedreniya (Peculiarities of plastic yield of the interstitial phases). *Fiz Met Metalloved* 56(2):361–365 (in Russian)
328. Zubarev PV, Kuraev AB (1992) Creep of monocarbides of transition metals of IV, V groups. III. Creep of hafnium, niobium and tantalum carbides. *Phys Met Metallogr* 73(6):649–653
329. Kats SM, Ordanyan SS, Gorin AI, Kudryasheva LV (1973) Effect of porosity on the creep of niobium carbide and other materials during monoaxial loading. *Strength Mater* 5(7):858–862
330. Zubarev PV (1985) Zharoprochnost faz vnedreniya (The heat-resistance of interstitial alloys). *Metallurgiya*, Moscow (in Russian)
331. Kats SM, Ordanyan SS (1983) Extremal character of concentration dependence of creep rate of solid solutions of carbides in the M^{IV}C-M^VC system. *Inorg Mater* 19(2):196–201
332. Kats SM, Ordanyan SS (1984) Creep in sintered polycrystalline niobium carbide and niobium carbide – based solid solutions. *Powder Metall Met Ceram* 23(5):414–418
333. Foster LS, Forbes LW, Jr, Friar LB, Moody LS, Smith WH (1950) Sintering carbides by means of fugitive binders. *J Am Ceram Soc* 33(1):27–33
334. Vallance SR, Round DM, Ritter C, Cussen EJ, Kingman S, Gregory DH (2009) Ultrarapid microwave synthesis of superconducting refractory carbides. *Adv Mater* 21:4502–4504

335. Harada Y (1968) Metal carbide – graphite composites. Report IITRI-G6003-06 (NASA-CR-92723), Contract NASr-65(09). IIT Research Institute, Chicago, Illinois, pp. 1–35
336. Merryman RG, Robertson RH, Dietz RJ (1966) The room temperature flexural strength of some metal carbide – carbon composites hot-pressed by CMB-6. Report LASL-N-1-1824. Los Alamos Scientific Laboratory, New Mexico, pp. 1–12
337. Kovalchenko MS, Dzhemelinskii VV, Skuratovskii VN, Tkachenko YuG (1973) Temperaturaya zavisimost mikrotverdosti karbidov perekhodnykh metallov (Temperature dependence of the microhardness of transition metal carbides). *Izv AN SSSR Neorg Mater* 9(10):1525–1528 (in Russian)
338. Lynch JF (1979) Engineering property data on selected ceramics, Vol. 2 – Carbides. Report MCIC-HB-07. Metals and Ceramics Information Centre, Battelle Columbus Laboratories, Ohio, pp. 1–136
339. Buravoi SE, Taubin ML (1974) Thermophysical properties of carbides of titanium, zirconium, hafnium and niobium at 50–1000 °C. *Inorg Mater* 10(2):319–321
340. Sinelnikova VS, Gurin VN (1975) Single-crystal refractory carbides: state of the art and prospects. *High Temp High Press* 7:507–515
341. Brizes WF (1970) Deformation of the groups IVB and VB monocarbides. Report NASA-CR-110189, Contract N70-28729. Space Research Coordination Centre, University of Pittsburgh, Pennsylvania, pp. 1–132
342. Nixon RD, Chevachroenkul S, Davis RF (1987) Steady-state creep behaviour of hot isostatically pressed niobium carbide. *Mat Res Bull* 22(9):1233–1240
343. Skuratovskii VN, Tkachenko YuG, Borisenko VA (1969) A technique for the investigating the microhardness of refractory compounds within a wide temperature range. *Strength Mater* 1(4):393–396
344. Zubarev PV, Dementev LN (1971) Relation between the activation energies of high-temperature creep and diffusion in transition metal carbides. *Strength Mater* 3(9):1058–1061
345. Frantsevich IN (ed), Gnesin GG, Kurdyumov AV, Karyuk GG, Bochko AV, Semenenko NP (1980) *Sverkhтвердые материалы (Superhard materials)*. Naukova Dumka, Kyiv (in Russian)
346. Frantsevich IN, Zhurakovskii EA, Lyashchenko AB (1967) Elastic constants and characteristics of the electron structure of certain classes of refractory compounds obtained by the metal-powder method. *Inorg Mater* 3(1):6–12
347. Gropyanov VM, Sobolev VG (1967) Sintering and properties of solid solutions of carbides. *Powder Metall Met Ceram* 6(4):277–279
348. Brown HL, Armstrong PE, Kempter CP (1966) Elastic properties of some polycrystalline transition-metal monocarbides. *J Chem Phys* 45(2):547–549
349. Ajami FI, MacCrone RK (1974) Thermal expansion, Debye temperature and Gruneisen constant of carbides and nitrides. *J Less-Common Met* 38(2–3):101–110
350. Frantsevich IN, Lyashchenko AB (1966) Young's moduli of the carbides of some transition metals. *Powder Metall Met Ceram* 5(7):573–574
351. Chang YA, Toth LE, Tyan YS (1971) On the elastic and thermodynamic properties of transition metal carbides. *Metall Trans* 2(1):315–320
352. Baranov VM, Knyazev VI, Korostin OS (1975) Elastic properties of nonstoichiometric niobium carbides in the range 20–2000 °C. *Inorg Mater* 11(3):375–378
353. Frantsevich IN, Voronov FF, Bakuta SA (1982) Uprugie postoyannye i moduli uprugosti metallov i nemetallov (The elastic constants and elasticity moduli of metals and non-metals). *Naukova Dumka, Kyiv* (in Russian)
354. Avgustinik AI, Ordanyan SS, Fishchev VN (1974) Temperature dependence of the elastic moduli of cubic carbides in the Zr-Nb-C system. *Inorg Mater* 10(9):1399–1402
355. Jun CK, Shaffer PTB (1971) Elastic moduli of niobium carbide and tantalum carbide at high temperature. *J Less-Common Met* 23(4):367–373

356. Cao Y, Zhu J, Liu Y, Long Z (2013) Thermodynamic properties of MC (M = V, Nb, Ta): first principles calculations. *Modern Phys Lett B* 27(19):1341035 (7 pp.)
357. Speck DA, Miccioli BR (1968) Advanced ceramic systems for rocket nozzle applications. Technical report. The Carborundum Company, Niagara Falls, New York, pp. 1–80
358. Abderrahim FZ, Faraoun HI, Ouahrani T (2012) Structure, bonding and stability of semi-carbides M_2C and sub-carbides M_4C (M = V, Cr, Nb, Mo, Ta, W): a first principles investigation. *Phys B Condens Matter* 407:3833–3838
359. Kurlov AS, Gusev AI (2013) Accounting for nonstoichiometry of niobium carbide NbC_y upon milling to a nanocrystalline state. *Phys Solid State* 55(12):2522–2530
360. Avgustinik AI, Ordanyan SS, Fishchev VN, Kudryashova LV (1973) Elastic properties of zirconium and niobium carbides in their homogeneity regions. *Inorg Mater* 9(7):1039–1041
361. Bukatov VG (1979) Issledovanie fiziko-mekhanicheskikh svoystv karbidov tugoplavkikh metallov i nekotorykh splavov na ikh osnove (Studies of physico-mechanical properties of refractory metal carbides and some alloys on their basis). PhD thesis, Moscow Institute of Steels and Alloys (in Russian)
362. Portnoi KI, Mukoseev AA, Gribkov VN, Levinskii YuV, Prokofev SA (1971) Modul uprugosti tugoplavkikh nitridov, karbidov i boridov (Elastic modulus of refractory nitrides, carbides and borides). In: Kornilov II, Matveeva NM (eds) *Metallidy – stroenie, svoystva, primenenie* (Metallides – structure, properties, application). Nauka, Moscow, pp. 123–126 (in Russian)
363. Köster W, Rauscher W (1948) Beziehung Zwischen dem Elastizitätsmodul von Zweistofflegierung und ihren Aufbau (The relation between the modulus of elasticity and chemical composition of some binary alloys). *Z Metallkd* 39(4):111–120 (in German)
364. Ordanyan SS, Fishchev VN (1976) Porosity as a factor in the elastic modulus of zirconium and niobium monocarbides. *Refract Ind Ceram* 17(1–2):111–113
365. Drickamer HG, Lynch RW, Clendenen RL, Perez-Albuerne EA (1966) X-ray diffraction studies of the lattice parameters of solids under very high pressures. *Solid State Phys* 19:135–228
366. Weber W (1973) Lattice dynamics of transition-metal carbides. *Phys Rev B* 8(11):5082–5092
367. Yadav RB, Thakur KC (1984) Lattice dynamics of niobium carbide. *Solid State Commun* 49(6):601–603
368. Champion AR, Drickamer HG (1965) The effect of high pressure on the compressibility of four cubic carbides. *J Phys Chem Solids* 26:1973–1975
369. Ledbetter HM, Chevacharoenkul S, Davis RF (1986) Monocrystal elastic constants of NbC. *J Appl Phys* 60(5):1614–1617
370. Kumashiro Y, Tokumoto H, Sakuma E, Itoh A (1977) The elastic constants of TiC, VC and NbC single crystals. In: Hasiguti RR, Mikoshiba N (eds) *Internal friction and ultrasonic attenuation in solids*. Proc. 6th Int. conf. on internal friction and ultrasonic attenuation in solids, Tokyo, 4–7 July 1977. International Union of Pure and Applied Physics, University Press, Tokyo, pp. 395–399
371. Singh DJ, Klein BM (1992) Electronic structure, lattice stability and superconductivity of CrC. *Phys Rev B* 46(23):14969–14974
372. Ettmayer P, Lengauer W (1994) Transition metal solid-state chemistry: carbides. In: *Encyclopedia of inorganic chemistry*. Wiley, New York, pp. 519–531
373. Kral C, Lengauer W, Rafaja D, Ettmayer P (1998) Critical review on the elastic properties of transition metal carbides, nitrides and carbonitrides. *J Alloy Compd* 265:215–233
374. Neshpor VS, Samsonov GV (1957) Brittleness in metallic compounds. *Phys Met Metallogr* 4(1):147–148
375. Wu Z, Chen X-J, Struzhkin VV, Cohen RE (2005) Trends in elasticity and electronic structure of transition-metal nitrides and carbides from first principles. *Phys Rev B* 71(21):214103
376. Zaoui A, Bouhafs B, Ruterana P (2005) First-principles calculations on the TiC_xN_{1-x}, Zr_xNb_{1-x}C and HfC_xN_{1-x} alloys. *Mater Chem Phys* 91:108–115

377. Amriou T, Bouhafs B, Aourag H, Khelifa B, Bresson S, Mathieu C (2003) FP-LAWT investigations of electronic structure and bonding mechanism of NbC and NbN compounds. *Phys B* 325:46–56
378. Chen J, Boyer LL, Krakauer H, Mehl MJ (1988) Elastic constants of NbC and MoN: instability of B_1 -MoN. *Phys Rev B* 37(7):3295–3298
379. Liermann HP, Singh AK, Somayazulu M, Saxena SK (2007) Compression behaviour of NbC under nonhydrostatic conditions to 57 GPa. *Int J Refract Met Hard Mater* 25:386–391
380. Tran F, Laskowski R, Blaha P, Schwarz K (2007) Performance on molecules, surfaces and solids of the Wu-Cohen GGA exchange-correlation energy functional. *Phys Rev B* 75(11):115131 (14 pp.)
381. Isaev EI, Ahuja R, Simak SI, Lichtenstein AI, Vekilov YuKh, Johansson B, Abrikosov IA (2005) Anomalously enhanced superconductivity and *ab initio* lattice dynamics in transition metal carbides and nitrides. *Phys Rev B* 72(6):064515 (5 pp.)
382. Gubanov VA, Ivanovsky AL, Zhukov VP (1994) Electronic structure of refractory carbides and nitrides. Cambridge University Press, Cambridge, New York
383. Isaev EI, Simak SI, Abrikosov IA, Ahuja R, Vekilov YuKh, Katsnelson MI, Lichtenstein AI, Johansson B (2007) Phonon related properties of transition metals, their carbides and nitrides: a first principles study. *J Appl Phys* 101:123519 (18 pp.)
384. Joshi KB, Paliwal U (2009) First-principles study of structural and bonding properties of vanadium carbide and niobium carbide. *Phys Scripta* 80:055601 (6 pp.)
385. Singh A, Aynyas M, Sanyal SP (2009) High pressure behaviour and structural properties of transition metal carbides. *Phase Transit* 82(8):576–586
386. Singh A, Aynyas M, Sanyal SP (2009) Phase transition and high pressure behaviour of zirconium and niobium carbides. *Central Eur J Phys* 7(1):102–107
387. Zhao Z, Zhou X-F, Wang L-M, Xu B, He J, Liu Z, Wang H-T, Tian Y (2011) Universal phase transitions of B1-structured stoichiometric transition metal carbides. *Inorg Chem* 50:9266–9272
388. Storms EK, Krikorian NH, Kempter CP (1960) Niobium monocarbide. *Anal Chem* 32(12):1722
389. Zaoui A, Kacimi S, Zaoui M, Bouhafs B (2009) Vacancy effects on structural and electronic properties of 4d transition-metal carbides. *Comput Mater Sci* 44:1071–1075
390. Feng W-X, Cui S-X, Hu H-Q, Zhang G-Q, Lv Z-T (2011) Electronic structure and elastic constants of TiC_xN_{1-x} , $Zr_xNb_{1-x}C$ and HfC_xN_{1-x} alloys: a first-principles study. *Phys B* 406:3631–3635
391. Srivastava A, Chauhan M, Singh RK (2011) High-pressure phase transitions in transition metal carbides XC (X = Ti, Zr, Hf, V, Nb, Ta): a first-principle study. *Phase Transit* 84(1):58–66
392. Shukoor VA, Thakre V, Singh S (2013) Study of structural properties of NbC at high temperatures. In: Proc. Int. conf. on recent trends in applied physics and materials science (RAM 2013), Bikaner, Rajasthan, India, 1–2 Feb 2013. *AIP Conf Proc* 1536:893–894
393. Yu X-X, Thompson GB, Weinberger CR (2015) Influence of carbon vacancy formation on the elastic constants and hardening mechanisms in transition metal carbides. *J Eur Ceram Soc* 35:95–103
394. Friedrich A, Winkler B, Juarez-Arellano EA, Bayarjargal L (2011) Synthesis of binary transition metal nitrides, carbides and borides from the elements in the laser-heated diamond anvil cell and their structure-property relations. *Mater* 4:1648–1692. <https://doi.org/10.3390/ma4101648>
395. Viñes F, Sousa C, Liu P, Rodriguez JA, Illas F (2005) A systematic density functional theory study of the electronic structure of bulk and (001) surface of transition-metals carbides. *J Chem Phys* 122:174709 (11 pp.)
396. Soni P, Pagare G, Sanyal SP (2011) Structural, high pressure and elastic properties of transition metal monocarbides: a FP-LAPW study. *J Phys Chem Solids* 72:810–816
397. Vojvodic A, Ruberto C (2010) Trends in bulk electron-structural features of rocksalt early transition-metal carbides. *J Phys Condens Matter* 22:375501 (10 pp.)

398. Weber W (1984) First principles lattice dynamics of transition metals. In: Phariseau P, Temmerman WM (eds) *The electronic structure of complex systems*. Plenum Press, New York, London, pp. 345–462
399. Srivastava A, Diwan BD (2012) Elastic and thermodynamic properties of divalent transition metal carbides MC (M = Ti, Zr, Hf, V, Nb, Ta). *Can J Phys* 90:331–338
400. Chen X-Q, Niu H, Li D, Li Y (2011) Modeling hardness of polycrystalline materials and bulk metallic glasses. *Intermetallics* 19:1275–1281
401. Soni P, Pagare G, Sanyal SP, Rajagopalan M (2012) A comparative study of electronic structure and bonding in transition metal monocarbides. *J Phys Chem Solids* 73:873–880
402. Varshney D, Shriya S (2013) Elastic, mechanical and thermodynamic properties at high pressures and temperatures of transition metal monocarbides. *Int J Refract Met Hard Mater* 41:375–401
403. Varshney D, Shriya S, Singh N (2013) Mechanical stiffening of transition metal carbides: XC (X = Ti, Zr, Nb, Hf, Ta). In: Proc. 57th DAE solid state physics symp., Bombay, Mumbai, India, 3–7 Dec 2012. *AIP Conf Proc* 1512:1016–1017
404. Liu Y-Z, Jiang Y-H, Zhou R, Feng J (2014) First principles study the stability and mechanical properties of MC (M = Ti, V, Zr, Nb, Hf and Ta) compounds. *J Alloy Compd* 582:500–504
405. Gao X-P, Jiang Y-H, Liu Y-Z, Zhou R, Feng J (2014) Stability and elastic properties of Nb_xC_y compounds. *Chin Phys B* 23(9):097704
406. McCollm IJ (1990) *Ceramic hardness*. Plenum Press, New York, London
407. Gusev AI (2013) Elastic and thermal properties of Zr_zNb_{1-z}C_xN_y solid solutions. *Phys Solid State* 55(7):1557–1561
408. Portnoi KI, Mukoseev AA, Gribkov VN, Levinskii YuV, Prokofev SA (1971) Modulus of elasticity of some refractory compounds. *Powder Metall Met Ceram* 7(3):185–186
409. Krasnenko V, Brik MG (2012) First-principles calculations of hydrostatic pressure effects on the structural, elastic and thermodynamic properties of cubic monocarbides XC (X = Ti, V, Cr, Nb, Mo, Hf). *Solid State Sci* 14:1431–1444
410. Rowcliffe DJ (1984) Plastic deformation of transition metal carbides. In: Tressler RE, Bradt RC (eds) *Deformation of ceramic materials II*. Plenum Press, New York and London, pp. 49–71
411. Kovalchenko MS, Ogorodnikov VV, Rogovoi YuI, Krainii AG (1979) *Radiatsionnoe povrezhdenie tugoplavkikh soedinenii* (The radiation damage of refractory compounds). Atomizdat, Moscow (in Russian)
412. Emelyanov VS, Godin YuG, Suchkov II, Yastrebkov AA (1979) *Issledovanie splavov sistemy Zr-Nb-C* (A study of alloys of the Zr-Nb-C system). In: Emelyanov VS, Yevstyukhin AI (eds) *Metallurgiya i metallovedenie chistykh metallov* (Metallurgy and metallography of pure metals), Vol. 6. Atomizdat, Moscow, pp. 92–100 (in Russian)
413. Keilholtz GW, Moore RE, Osborne MF (1968) Fast-neutron effects on the carbides of titanium, zirconium, tantalum, niobium and tungsten. *Nucl Appl* 4:330–336
414. Kobayashi N, Kaufmann R, Linker G (1985) Ion irradiation and annealing studies of NbC thin films. *J Nucl Mater* 133–134:732–735
415. Smith CJ, Weinberger CR, Thompson GB (2018) Phase stability and microstructural formations in the niobium carbides. *J Eur Ceram Soc* 38:4850–4866
416. Kobayashi N, Tanoue H, Linker G (1988) Defect structure and superconducting transition temperature of ion-irradiated refractory metal carbides and nitrides. *Nucl Inst Meth Phys Res B* 33(1–4):795–798
417. Monteiro WA (1990) The Al-C-Nb (aluminium-carbon-niobium) system. *Ternary Alloy VCH* 3:515–517
418. Savitskii EM, Efimov YV, Myasnikova EA, Bodak OI, Ryabtsev LA (1981) The niobium-aluminium-carbon system and the critical temperatures of the alloys (summary). *Sov Non-Ferrous Met Res* 9:342–343
419. Schuster JC, Nowotny H (1980) Investigations of the ternary systems (Zr,Hf,Nb,Ta)-Al-C and studies on complex carbides. *Z Metallkd* 71:341–346

420. Sun ZM (2011) Progress in research and development on MAX phases: a family of layered ternary compounds. *Int Mater Rev* 56(3):143–166
421. Barsoum MW (2010) The $M_{n+1}AX_n$ phases and their properties. In: Riedel R, Chen I-W (eds) *Ceramics science and technology*, Vol. 2 – Properties. Wiley-VCH, Weinheim, pp. 299–347
422. Barsoum MW (2013) *MAX phases*. Wiley-VCH Verlag, Weinheim
423. Shurin AK, Dmitrieva GP, Cherepova TS (1996) Phase equilibria in Co – Me'C – Me''C alloys. 1. Systems with three-phase eutectic equilibria. *Powder Metall Met Ceram* 35(11–12):615–620
424. Shurin AK, Dmitrieva GP, Cherepova TS (1997) Phase equilibria in Co – Me'C – Me''C alloys. 2. Systems with four-phase eutectic equilibrium. *Powder Metall Met Ceram* 36(3–4):193–196
425. Dmitrieva GP, Krasnokutskaya ZB, Belyavina NN, Shurin AK (1989) Phase diagram of the Co-VC-NbC system. *Powder Metall Met Ceram* 28(3):233–238
426. Kruse O, Jansson B, Frisk K (2001) Experimental study of invariant equilibria in the Co-W-C and Co-W-C-Me (Me = Ti, Ta, Nb) systems. *J Phase Equilib* 22(5):552–555
427. Frisk K, Dumitrescu L, Ekroth M, Jansson B, Kruse O, Sundman B (2001) Development of a database for cemented carbides: thermodynamic modelling and experiments. *J Phase Equilib* 22(6):645–655
428. Huang W (1997) Thermodynamic properties of the Nb-W-C-N system. *Z Metallkd* 84:63–68
429. Bondar AA, Velikanova TYa (1996) Aspects of construction diagrams of ternary systems formed by chromium with carbon and *d*-transition metals. *Powder Metall Met Ceram* 35(7–8):484–496
430. Dovbenko OI, Bondar AA, Velikanova TYa, Sleptsov SV (2000) The (Cr) + (NbC) quasibinary eutectic in the Cr-Nb-C system. *Powder Metall Met Ceram* 39(5–6):256–261
431. Velikanova TYa, Dovbenko OI, Grytsiv AV, Bondar AA (2001) Metallochemistry of chromium with *d*-metals and carbon. *J Alloy Compd* 320:341–352
432. Velikanova TYa, Bondar AA (2002) Melting diagram for the Cr – Nb – C system in the (Cr) – (Nb) – (NbC) region. *Powder Metall Met Ceram* 41(11–12):620–626
433. Raghavan V (2003) The C-Fe-N-Nb (carbon-iron-nitrogen-niobium) system. *J Phase Equilib* 24(1):73–74
434. Raghavan V (2003) The C-Fe-N-Nb-Ti (carbon-iron-nitrogen-niobium-titanium) system. *J Phase Equilib* 24(1):77–78
435. Raghavan V (2003) The C-Fe-N-Nb-Ti-V (carbon-iron-nitrogen-niobium-titanium-vanadium) system. *J Phase Equilib* 24(1):79–81
436. Raghavan V (2003) The C-Fe-Nb (carbon-iron-niobium) system. *J Phase Equilib* 24(1):57–61
437. Cornish L, Watson A (2008) Carbon – iron – niobium system. In: Effenberg G, Ilyenko S (eds) *Ternary alloy systems*. Subvol. D, Part 2. Springer, Berlin, Heidelberg, pp. 184–199
438. Fedorov TF, Kuzma YuB, Skolozdra RV, Popova NM (1965) Phase equilibria in the ternary systems Zr-Co-C and Nb-Fe-C. *Powder Metall Met Ceram* 4(12):1010–1014
439. Das RC, Jha R, Mukherjee T (1986) The carbon – iron – niobium system. *J Alloy Phase Diagrams* 2(2):131–140
440. Eremenko VN, Velikanova TY, Shabanova SV, Artyukh LV (1973) Continuous series of solid solutions of carbides with NaCl structure in the ternary systems Mo(W)-Me^{IV,V}-C. *Powder Metall Met Ceram* 12(11):909–912
441. Velikanova TYa, Eremenko VN (1974) Phase equilibria in the ternary systems formed by molybdenum and tungsten with the groups IV and V transition metals and carbon. *Powder Metall Met Ceram* 13(4):293–297
442. Huang W (1990) A thermodynamic evaluation of the Fe-Nb-C system. *Z Metallkd* 81(6):397–404
443. Stadelmaier HH, Fiedler ML (1975) The ternary system nickel-niobium-carbon. *Z Metallkd* 66(4):224–225

444. Gridnev VN, Barabash OM, Legkaya TN (1985) Termodinamicheskii raschet i eksperimentalnoe issledovanie poverkhnosti likvidusa i solidusa v troinnoi sisteme nikel-niobii-uglerod (Thermodynamic calculation and experimental study of liquidus and solidus surfaces in the nickel-niobium-carbon ternary system). In: Ageev NV (ed) Raschety i eksperimentalnye metody postroeniya diagramm sostoyaniya (Calculation and experimental methods of plotting phase diagrams). Nauka, Moscow, pp. 130–133 (in Russian)
445. Gridnev VN, Barabash OM, Legkaya TN (1985) Phase equilibria and structure of directionally crystallized alloys of the Ni-Nb-C system. *Russ Metall* (6):199–204
446. Shurin AK, Dmitrieva GP, Razumova NA, Khandros EL (1987) The phase diagram of the Ni-VC-NbC system. *Powder Metall Met Ceram* 26(8):658–660
447. Ichikawa K, Achikita M (1993) Electric conductivity and mechanical properties of carbide dispersion-strengthened copper prepared by compocasting. *Mater Trans JIM* 34(8):718–724
448. Shurin AK, Dmitrieva GP, Razumova NA, Khandros EL (1987) State diagram of Ni-ZrC-NbC. *Russ Metall* (6):205–207
449. Raub E, Falkenburg G (1964) Reactionen zwischen Karbide und Platin oder Palladium während des Sinterns bei hohen Temperaturen (The reactions between carbides and platinum or palladium during sintering at high temperatures). *Z Metallkd* 55(4):190–192 (in German)
450. Gorshkova LV, Fedorov TF, Kuzma YuB (1967) Ternary systems niobium-rhenium-carbon and tantalum-rhenium-carbon. *Powder Metall Met Ceram* 6(4):287–290
451. Manning C, Stoops R (1968) High-temperature cermets: 1. Compatibility. *J Am Ceram Soc* 51(8):411–415
452. Savitskii EM, Efimov YuV, Bodak OI, Kharchenko OI, Myasnikova EA (1981) The niobium-silicon-carbon system. *Inorg Mater* 17(12):1649–1652
453. Brukl CE (1965) The Ti-Si-C, Nb-Si-C, and W-Si-C systems. In: Ternary phase equilibria in transition metal-boron-carbon-silicon systems. Report AFML-TR-65-2, Contract USAF 33(615)–1249, Part 2, Vol. 7. Air Force Materials Laboratory, Wright-Patterson Air Force Base, Ohio, pp. 1–57
454. Cacciamani G, Riani P (2010) Carbon – niobium – silicon system. In: Effenberg G, Ilyenko S (eds) Ternary alloy systems, Subvol E, Part 2. Springer, Berlin, Heidelberg, pp. 560–566
455. Ghebouli MA, Ghebouli B, Bouhemadou A, Fatmi M (2011) Theoretical study of the structural, elastic, electronic and thermal properties of the MAX phase Nb₂SiC. *Solid State Commun* 151:382–387
456. Jeitschko W, Nowotny H, Benesovsky F (1964) Die H-phasen Ti₂TiC, Ti₂PbC, Nb₂InC, Nb₂SnC und Ta₂GaC (The H-phases Ti₂TiC, Ti₂PbC, Nb₂InC, Nb₂SnC and Ta₂GaC). *Monatsh Chem* 95(2):431–435 (in German)
457. Barsoum MW, Ganguly A, Seifert HJ, Aldinger F (2002) The 1300 °C isothermal section in the Nb-Sn-C ternary phase diagram. *J Alloy Compd* 337:202–207
458. Samsonov GV, Strashinskaya LV, Shiller EA (1962) Kontaktnoe vzaimodeistvie metallopodobnykh karbidov, nitridov i boridov s tugoplavkimi metallami pri vysokikh temperaturakh (The contact reaction of metallic carbides, nitrides and borides with refractory metals at elevated temperatures). *Izv AN SSSR OTN Metall Toplivo* (5):167–180 (in Russian)
459. Rudy E (1970) The phase diagram of the systems Ti-Nb-C, Ti-Ta-C and Ti-Mo-C. In: Phase equilibria investigations of binary, ternary and higher order systems. Report AFML-TR-69-117, Contract USAF 33(615)-67-C-1513, Part 1. Air Force Materials Laboratory, Wright-Patterson Air Force Base, Ohio, pp. 1–132
460. Rudy E (1966) Constitution of niobium-tungsten-carbon alloys. In: Ternary phase equilibria in transition metal-boron-carbon-silicon systems. Report AFML-TR-65-2, Contract USAF 33(615)-1249, Part 2, Vol. 18. Air Force Materials Laboratory, Wright-Patterson Air Force Base, Ohio, pp. 1–61
461. Perrot P, Lebrun N (2010) Carbon – niobium – tungsten system. In: Effenberg G, Ilyenko S (eds) Ternary alloy systems. Subvol. E, Part 2. Springer, Berlin, Heidelberg, pp. 567–578

462. Tan Y, Ma CL, Kasama A, Tanaka R, Mishima Y, Hanada S, Yang J-M (2003) Effect of alloy composition on microstructure and high temperature properties of Nb-Zr-C ternary alloys. *Mater Sci Eng A* 341:282–288
463. Borisova AL, Borisov YuS (1977) A thermodynamic evaluation of the effect of nonstoichiometry of compounds on the course of their solid-phase reactions. *Powder Metall Met Ceram* 16(6):440–447
464. Zakharov AM (1974) Sovmestnaya rastvorimost C i Nb v Mo v tverdom sostoyanii (The joint solubility of C and Nb in Mo). *Izv Vyssh Uchebn Zaved Tsvetn Metall* (1):129–132 (in Russian)
465. Borisova AL (1985) Sovmestimost tugoplavkikh soedinenii s metallami i grafitom (The compatibility of refractory compounds with metals and graphite). *Naukova Dumka, Kyiv* (in Russian)
466. Vil'k YuN, Avarbe RG, Neshpor VS, Ryzhkova TP, Omelchenko YuA (1964) Interaction of niobium carbide with tungsten. *High Temp* 2(2):241–245
467. Vil'k YuN, Avarbe RG, Neshpor VS, Ryzhkova TP, Omelchenko YuA (1965) K voprosu o vzaimodeistvii karbida niobiya s volframom (On the problem of the interaction of niobium carbide with tungsten). In: Grigoreva VV, Eremenko VN, Nazarchuk TN, Samsonov GV, Fedorchenko IM, Frantsevich IN (eds) *Vysokotemperaturnye neorganicheskie soedineniya* (High-temperature inorganic compounds). *Naukova Dumka, Kyiv*, pp. 219–236 (in Russian)
468. Ordanyan SS, Vil'k YuN, Avgustinik AI (1972) Nekotorye dannye o stroenii splavov pri 2000 °C v troinoi sisteme Nb-C-Re (Some data on the structure of alloys at 2000 °C in the ternary system Nb-C-Re). *Izv AN SSSR Neorg Mater* 8(2):383–384 (in Russian)
469. Vil'k YuN, Ordanyan SS, Muravev AA, Miroshnichenko AG, Omelchenko YuA (1974) The NbC-Re polythermal section in the niobium-rhenium-carbon system. In: Samsonov GV (ed) *Refractory carbides*. Consultants Bureau, New York, pp. 165–171
470. Kuzma YuB, Gladyshevskii EI, Gorshkova LV, Fedorov TF (1968) Troinye sistemy reniya s perekhodnymi tugoplavkimi metallami i uglerodom (Ternary systems of rhenium with transition refractory metals and carbon). In: Savitskii EM (ed) *Diagrammy sostoyaniya metallicheskih sistem* (Phase diagrams of metallic systems). *Nauka, Moscow*, pp. 185–191 (in Russian)
471. Ghidui M, Naguib M, Shi C, Mashtalir O, Pan LM, Zhang B, Yang J, Gogotsi Y, Billinge SJL, Barsoum MW (2014) Synthesis and characterization of two-dimensional Nb₄C₃ (MXene). *Chem Commun* 50:9517–9520
472. Glaser FW (1952) Contribution to the metal-carbon-boron systems. *J Metal* 4(4):391–396
473. Rogl P (1998) The system boron – carbon – niobium. In: Effenberg G (ed) *Phase diagrams of ternary metal-boron-carbon systems*. ASM International, Materials Park, Ohio, pp. 197–213
474. Rogl P, Korniyenko K, Velikanova T (2009) Boron – carbon – niobium system. In: Effenberg G, Ilyenko S (eds) *Ternary alloy systems, Subvol. E, Part 1*. Springer, Berlin, Heidelberg, pp. 347–366
475. Schwarzkopf P, Glaser FW (1953) Struktur und chemische Eigenschaften der Boride der Übergangsmetalle der vierten, fünften und sechsten Gruppe (Structure and chemical properties of the transition metal borides of the fourth, fifth and sixth groups). *Z Metallkd* 44(8):353–358 (in German)
476. Fedorov TF, Gladyshevskii EI (1965) Phase equilibria in ternary systems of transition metals of groups IV and V and carbon. *Powder Metall Met Ceram* 4(1):27–29
477. Benesovsky F, Rudy E (1960) Pseudoternary carbide systems. *Metall* (9):875–876
478. Rudy E, Nowotny H, Benesovsky F, Kieffer R, Neckel A (1960) Über Hafniumkarbid enthaltende Karbidsysteme (On hafnium carbide containing carbide system). *Monatsh Chem* 91(1):176–187 (in German)
479. Nowotny H, Benesovsky F, Rudy E (1960) Hochschmelzende Systeme mit Hafniumkarbid und –nitrid (Refractory systems with hafnium carbide and nitride). *Monatsh Chem* 91(2):348–356 (in German)

480. Samsonov GV, Burykina AL, Strashinskaya LV, Pugach ÉA (1964) Reactions between magnesium oxide or zirconium dioxide and refractory compounds at high temperatures under vacuum. *Russ Metall* 4(4):70–77
481. Krylov YuI, Balakir ÉA (1976) Karbidno-okisnye sistemy (Carbide-oxide systems). *Metallurgiya*, Moscow (in Russian)
482. Eremenko VN, Velikanova TYa (1983) Use of the phase diagrams of ternary transition metal systems containing carbides in the development of heat-resisting hard alloys. *Powder Metall Met Ceram* 22(12):1010–1021
483. Ramanathan S, Da Silva VLST, Oyama ST (1994) New catalysts for hydroprocessing: transition metal carbides and nitrides. *Am Chem Soc Div Petroleum Chem Prep* 39(4):618–620
484. Funke VF, Pshenichnyi IV, Pliner LA, Loktionov YuD (1983) Phase fields and initial melting diagrams of the pseudoquaternary system UC-MoC_{1-x}ZrC-NbC. *Powder Metall Met Ceram* 22(2):110–116
485. English JJ (1961) Binary and ternary phase diagrams of columbium, molybdenum, tantalum and tungsten. Report DMIC-152, Contract AF-33(616)-7747. Defence Metals Information Center, Battelle Memorial Institute, Columbus, Ohio, pp. 1–226
486. Sudarikov MV, Zhikharev VM (1988) The niobium carbide – nitride *p-T-x*-diagram. *Inorg Mater* 24(2):176–179
487. Sudarikov MV, Zhikharev VM, Lykasov AA (2001) Gibbs energy of formation of cubic NbC_xN_y. *Inorg Mater* 37(3):243–247
488. Ordanyan SS, Stepanenko EK, Unrod VI (1977) Reactions in the system NbC-NbB₂. *Inorg Mater* 13(2):312–314
489. Chatfield C (1986) The γ -WC solubility boundary in the quaternary TiC-NbC-TaC-WC system at 1723 K. *J Mater Sci* 21(2):577–582
490. Holleck H (1977) Zum Aufbau der Systeme Thorium – (Zirkon, Niob, Ruthenium, Rhodium) – Kohlenstoff (The structure of thorium – (zirconium, niobium, ruthenium, rhodium) – carbon systems). *J Nucl Mater* 66(3):273–282 (in German)
491. Gusev AI (1985) Phase diagrams of the pseudo-binary TiC – NbC, TiC – TaC, ZrC – NbC, ZrC – TaC and HfC – TaC carbide systems. *Russ J Phys Chem* 59(3):336–340
492. Bandyopadhyay D, Sharma RC, Chakraborti N (2000) The C-Nb-Ti (carbon-niobium-titanium) system. *J Phase Equilib* 21(1):102–104
493. Kieffer R, Nowotny H, Neckel A, Etmayer P, Usner L (1968) Zur Entmischung von kubischen Mehrstoffcarbiden (On the miscibility of multicomponent cubic carbides). *Monatsh Chem* 99(3):1020–1027 (in German)
494. Inoue K, Ishikawa N, Ohnuma I, Ohtani H, Ishida K (2001) Calculation of phase equilibria between austenite and (Nb,Ti,V)(C,N) in microalloyed steels. *ISIJ Int* 41(2):175–182
495. Duwez P, Odell F (1950) Phase relationships in the binary systems of nitrides and carbides of zirconium, columbium, titanium and vanadium. *J Electrochem Soc* 97(10):299–304
496. Brownlee LD (1958) The pseudo-binary systems of uranium carbide with zirconium carbide, tantalum carbide and niobium carbide. *J Inst Met* 87(2):58–61
497. Benesovsky F (1964) The importance of powder metallurgy for developing and producing new types of nuclear fuel materials. *Powder Metall Met Ceram* 3(3):248–255
498. Benesovsky F, Rudy E (1961) Zur Kenntnis der System Uran – Zirkonium (Hafnium, Niob, Tantal) – Kohlenstoff (To the knowledge of the uranium – zirconium (hafnium, niobium, tantalum) – carbon systems). *Planseeber Pulvermetall* 9(1/2):65–76 (in German)
499. Chang YA (1967) V-Nb-C system. In: Ternary phase equilibria in transition metal-boron-carbon-silicon systems. Report AFML-TR-65-2, Contract USAF 33(615)-1249, Part 2, Vol. 16. Air Force Materials Laboratory, Wright-Patterson Air Force Base, Ohio, pp. 1–54
500. Gusev AI (1985) Prognoz i raschety fazovykh diagramm psevdobinarykh system na osnove tugoplavkikh soedinenii perekhodnykh metallov (Prediction and calculation of phase diagrams of pseudobinary systems based on high-melting transition metal compounds). In: Ageev NV (ed) *Raschety i eksperimentalnye metody postroeniya diagramm sostoyaniya* (Calculation and experimental methods of plotting phase diagrams). Nauka, Moscow, pp. 42–47 (in Russian)

501. Rempel SV, Gusev AI (2001) ZrC segregation to the surface of dilute solid solutions of zirconium carbide in niobium carbide. *Inorg Mater* 37(10):1024–1029
502. Gusev AI, Rempel SV (2003) X-ray diffraction study of the nanostructure resulting from decomposition of $(\text{ZrC})_{1-x}(\text{NbC})_x$ solid solutions. *Inorg Mater* 39(1):43–46
503. Avgustinik AI, Gropyanov VM, Drozdetskaya GV, Vigdergauz VSh (1964) The interaction of some refractory carbides and zirconium dioxide. *Refract Ind Ceram* 5(11–12):611–616
504. Kosolapova TYa, Fedorus VB, Kuzma YuB, Kotlyar ÉÉ (1966) Kharakter vzaimodeistviya dnuokisi tsirkoniya s karbidami titana, niobiya i khroma (Character of the interaction of zirconium dioxide with titanium, niobium and chromium carbides). *Izv AN SSSR Neorg Mater* 2(8):1521–1523 (in Russian)
505. Kosolapova TYa, Fedorus VB, Kuzma YuB (1966) Vzaimodeistvie karbidov perekhodnykh metallov s ikh oksislami (Interaction of carbides of transition metals and their oxides). *Izv AN SSSR Neorg Mater* 2(8):1516–1520 (in Russian)
506. Ueda Y, Ono K, Moriyama J (1980) Thermodynamic study of the Nb-C-O solid solutions at 2073–2273 K. *J Jpn Inst Met Mater* 44(9):1069–1075 (in Japanese)
507. Krishnamurthy N, Venkataramani R, Garg SP (1979) A study on the high temperature reaction of niobium pentoxide with niobium carbide and titanium carbide. *Mater Res Bull* 14:993–1000
508. Brauer G, Lesser R (1959) Karbonitride des Niobs (Carbonitrides of niobium). *Z Metallkd* 50(8):487–492 (in German)
509. Grove DE, Gupta U, Castleman AW, Jr (2010) Effect of hydrocarbons on the morphology of synthesized niobium carbide nanoparticles. *Langmuir* 26(10):16517–16521
510. Kirillova GF, Meerson GA, Zelikman AN (1960) Kinetika khlorirovaniya karbidov titana i niobiya (Kinetics of chlorination of titanium and niobium carbides). *Izv Vyssh Uchebn Zaved Tsvetn Metall* (3):90–96 (in Russian)
511. Yushin G, Nikitin A, Gogotsi Y (2006) Carbide-derived carbon. In: Gogotsi Y (ed) *Nanomaterials handbook*. CRC Press, Boca Raton, London, New York, pp. 240–283
512. Shabalin IL (2008) “Ridge effect” in oxidation kinetics of hetero-modulus ceramics based on titanium carbide. *Powder Metall Met Ceram* 47(1–2):137–150
513. Shabalin IL (2009) Oxidation behaviour of hetero-modulus ceramics based on titanium carbide. In: Lin H-T, Koumoto K, Kriven WM, Norton DP, Garsia E, Reimanis IE (eds) *Developments in strategic materials. Ceramic engineering and science proceedings*, Vol. 29 (10), Wiley, New York, pp. 261–278
514. Samsonov GV (1962) Analiz tugoplavkikh soedinenii (The analysis of refractory compounds). *Metallurgizdat*, Moscow (in Russian)
515. Alabushev VA (1974) Okislenie karbidov urana, niobiya i tverdykh rastvorov UC-NbC (Oxidation of uranium carbide, niobium carbide and UC-NbC solid solutions). PhD thesis, Ural Polytechnic Institute, Sverdlovsk (in Russian)
516. Vlasov VG, Alabushev VA, Beketov AR (1975) Oxidation of solid solutions of uranium and niobium monocarbides. *Atom Energy* 38(6):539–542
517. Vlasov VG, Alabushev VA, Beketov AR (1975) Okislenie karbida niobiya v intervale temperatur 400–600 °C (Oxidation of niobium carbide in the range of temperatures 400–600 °C). *Izv Vyssh Uchebn Zaved Tsvetn Metall* (6):117–119 (in Russian)
518. Voitovich RF, Pugach ÉA (1975) Vysokotemperaturnoe okislenie karbidov perekhodnykh metallov IV-VI grupp (High temperature oxidation of transition metals IV-VI groups carbides). In: Samsonov GV (ed) *Vysokotemperaturnye karbidy* (High-temperature carbides). *Naukova Dumka*, Kyiv, pp. 143–156 (in Russian)
519. Voitovich RF, Pugach ÉA (1976) Nekotorye osobennosti protsessa okisleniya karbidov metallov IV-VI grupp (The certain features of the oxidation process of metals IV-VI groups carbides). In: Samsonov GV, Kosolapova TYa, Gnesin GG, Fedorus VB, Domasevich LG (eds) *Karbidy i splavy na ikh osnove* (Carbides and alloys based on them). *Naukova Dumka*, Kyiv, pp. 233–234 (in Russian)

520. Voitovich RF (1981) Okislenie karbidov i nitridov (Oxidation of carbides and nitrides). Naukova Dumka, Kyiv (in Russian)
521. Shevchenko AS, Lyutikov RA, Andrievskii RA, Terekhova VA (1980) Oxidation of zirconium and niobium carbides. Powder Metall Met Ceram 19(1):48–52
522. Afonin YuD, Shalaginov VN, Beketov AR, Alyamovskii SI (1980) Vysokotemperaturnoe okislenie slozhnykh karbidov niobiya i tsirkoniya pri nizkikh davleniyakh kisloroda (High-temperature oxidation of niobium and zirconium complex carbides at low oxygen pressures). Izv Vyssh Uchebn Zaved Tsvetn Metall (2):81–85 (in Russian)
523. Afonin YuD, Shalaginov VN, Beketov AR (1981) Vysokotemperaturnoe okislenie karbidno-uglerodnykh materialov sistem NbC-C, NbC-TiC-C (High-temperature oxidation of carbide-carbon materials of NbC-C, NbC-TiC-C systems). Zh Prikl Khim 54(4):776–780 (in Russian)
524. Szoekfalvi-Nagy A, Jehn H (1984) High-temperature oxidation of NbC and TaC at low oxygen pressures. Z Metallkd 75(5):389–394
525. Afonin YuD, Shalaginov VN, Beketov AR (1985) High-temperature oxidation of niobium monocarbide. Russ J Appl Chem 58(3/1):423–427
526. Shimada S, Inagaki M (1993) A kinetic study on oxidation of niobium carbide. Solid State Ionics 63–65(C):312–317
527. Shimada S (1994) A kinetic and thermoanalytical study on oxidation of powder and single-crystal samples of niobium carbide. Oxid Met 42(5/6):357–373
528. Gozzi D, Montozzi M, Cignini PL (1999) Apparent oxygen solubility in refractory carbides. Solid State Ionics 123(1):1–10
529. Gozzi D, Montozzi M, Cignini PL (1999) Oxidation kinetics of refractory carbides at low oxygen partial pressures. Solid State Ionics 123(1):11–18
530. Miller CF, Simmons GW, Wei RP (2000) High temperature oxidation of Nb, NbC and Ni_3Nb and oxygen enhanced crack growth. Scripta Mater 42:227–232
531. Xu G, Li J, Huang Y, Cai S (2001) Oxidation characters of NbC_x -C three-dimensional netted fibers. Corros Sci Protect Technol 13(1):16–20
532. Tao X, Li Y, Du J, Xia Y, Yang Y, Huang H, Gan Y, Zhang W, Li X (2011) A generic bamboo-based carbothermal method for preparing carbide (SiC , B_4C , TiC , TaC , NbC , $Ti_xNb_{1-x}C$ and $Ta_xNb_{1-x}C$) nanowires. J Mater Chem 21(25):9095–9102
533. Kotlyar EE, Nazarchuk TN (1966) O nekotorykh khimicheskikh svoistvakh karbidov perekhodnykh metallov IV, V grupp periodicheskoi sistemy (On certain chemical properties of the transition metal carbides of IV, V groups of the periodic table). Izv AN SSSR Neorg Mater 2(10):1778–1780 (in Russian)
534. Kozina GK (1970) Issledovanie kontaktnogo vzaimodeistviya tugoplavkikh karbidov i materialov na ikh osnove s zhidkimi metallami i splavami (A study of the contact interaction of refractory carbides and materials on their basis with liquid metals and alloys). PhD thesis, Institute for Problems of Materials Science, Ukrainian SSR Academy of Sciences, Kyiv (in Russian)
535. Ramqvist L (1965) Wettability of metallic carbides by liquid Cu, Ni, Co and Fe. Int J Powder Metall 1(4):2–21
536. Samsonov GV, Panasyuk AD, Kozina GK (1968) Wetting of refractory carbides with liquid metals. Powder Metall Met Ceram 7(11):874–878
537. Warren R (1980) Solid-liquid interfacial energies in binary and pseudo-binary systems. J Mater Sci 15(10):2489–2496
538. Warren R, Waldron MB (1972) Surface and interfacial energies in systems of certain refractory metal monocarbides with liquid cobalt. Nature Phys Sci 235(56):73–74
539. Tumanov VA, Funke FV, Belenkaya LI (1962) Nekotorye dannye po smachivaemosti oksida aliuminiya i karbidov metallami gruppy zheleza (Some data on the wettability of aluminium oxide and carbides with iron group metals). Zh Fiz Khim 36(7):1574–1577 (in Russian)

540. Goretzki H, Exner HE, Scheuermann W (1971) Electronic structure of refractory carbides and its relation to wetting. In: Hausner HH (ed) *Modern developments in powder metallurgy*, Vol. 4 – Processes, Plenum Press, New York, pp. 327–337
541. Samsonov GV, Kozina GK, Panasyuk AD, Bondarchuk SN (1974) The reaction of refractory carbides with molten steels and cast irons. In: Samsonov GV (ed) *Refractory carbides*. Consultants Bureau, New York, London, pp. 433–440
542. Samsonov GV, Antonova MM, Morozov VV (1970) Ternary systems Me-C-H and Me-N-H. *Powder Metall Met Ceram* 9(4):318–327
543. Yvon K, Nowotny H, Kieffer R (1967) Zur Kristallstruktur der Carbohydride von Übergangsmetallen (Crystal structure of transition metal carbohydrides). *Monatsh Chem* 98(6):2164–2172 (in German)
544. Pavlov IE, Alyamovskii SI, Shveikin GP (1978) Solid solutions of hydrogen formed in the systems M(IV-V)-C-N-O-H. *Inorg Mater* 14(9):1319–1322
545. Pavlov IE, Alyamovskii SI, Shveikin GP (1978) Solubility of hydrogen in niobium oxides, carbides and oxycarbides. *Inorg Mater* 14(12):1718–1721
546. Eremenko VN, Velikanova TYa, Bondar AA (1989) Phase equilibria at the solidus surface of the equilibrium diagram of ternary systems of technetium with carbon and d-transition metals of groups III-VII. *Powder Metall Met Ceram* 28(11):868–873
547. Voitovich RF, Pugach ÉA (1968) Okislenie tugoplavkikh soedinenii (Oxidation of refractory compounds). *Naukova Dumka, Kyiv* (in Russian)
548. Kieffer R, Nowotny H, Eitmayer P, Freudhofmeier M (1970) Über die Beständigkeit von Übergangsmetallcarbiden gegen Stickstoff bis zu 300 at (On the stability of transition metal carbides in nitrogen up to 300 atm). *Monatsh Chem* 101(1):65–82 (in German)
549. Vishnyakov LR, Grudina TV, Kadyrov VKh, Karpinos DM, Oleynik VI, Sapozhnikova AB, Tuchinskii LI (1985) Kompozitsionnye materialy (Composite materials). *Naukova Dumka, Kyiv* (in Russian)
550. Samsonov GV, ed (1973) *The oxide handbook*. IFI/Plenum, New York
551. Samsonov GV, Upadhyaya GS, Kozina GK (1970) Wettability of titanium and niobium carbides and their alloys in the homogeneity range by copper. *Mater Sci* 6(4):518–519
552. Rudy E, Progulski J (1967) A Pirani furnace for the precision determination of the melting temperatures of refractory metallic substances. *Planseeber Pulvermetall* 15:13–45
553. Rassaerts H, Benesovsky F, Nowotny H (1965) Untersuchungen in den systemen Nb- und Ta-Cr-C (Studies in the systems Nb- and Ta-Cr-C). *Planseeber Pulvermetall* 13(3):199–206 (in German)
554. Samsonov GV, Panasyuk AD, Kozina GK, Dyakonova LV (1972) Contact reaction of refractory compounds with liquid metals. 2. Reaction of carbides of subgroup Va and VIa metals with liquid transition metals. *Powder Metall Met Ceram* 11(8):629–631
555. Samsonov GV, Podchernyaeva IA, Siman NI, Fomenko VS (1976) Behaviour of refractory compounds in alkali metal media. *Powder Metall Met Ceram* 15(2):122–127
556. Velikanova TYa, Eremenko VN, Artyukh LV, Bondar AA, Gordiichuk OV (1989) Phase diagrams of Sc-M(IV-VII)-C systems. *Powder Metall Met Ceram* 28(9):711–718
557. Rempel SV, Rempel AA, Gusev AI (2000) Latent decomposition regions in the model of subregular solutions: the ZrC-NbC system. *Russ J Phys Chem A* 74(3):341–346
558. Ordanyan SS, Avgustinik AI, Vigdergauz VS (1966) Stroenie splavov sistemy Zr-C-Nb (The structure of alloys of the Zr-C-Nb system). *Zh Prikl Khim* 39(2):312–317 (in Russian)
559. Li D, Ma S, Li WF, Wu B, Zhang ZD (2007) Disorder and the electronic transport behaviours of NbC-Al₄C₃-C composite. *J Mater Sci* 42:6929–6934
560. Klimov DA, Myktybekov B, Nizovtsev VE, Ukhov PA (2011) Perspektivy primeneniya nanostrukturnykh kompozitsionnykh materialov na osnove karbidov i oksidov tugoplavkikh metallov dlya aviakosmicheskikh obektov (Perspectives of the application of nanostructured composite materials based on carbides and oxides of refractory metals for aerospace facilities). *Trudy MAI* 46, 9 pp (in Russian) <http://www.mai.ru/upload/iblock/1a1/1a1493319c8c15a70decf28b0a51172d.pdf>. Accessed 10 Feb 2015

561. Bentzel GW, Lane NJ, Vogel SC, An K, Barsoum MW, Caspi EN (2015) A high-temperature neutron diffraction study of Nb₂AlC and TiNbAlC. *J Am Ceram Soc* 98(3):940–947
562. Ostermann F, Kibbey EE (1970) Molybdenum in Nb-C alloys. *Metall Trans* 1(8):2257–2263
563. Jeitschko W, Nowotny H, Benesovsky F (1964) Ternäre Carbide und Nitride in Systemen: Übergangsmetall – Metametal – Kohlenstoff (Stickstoff) (Ternary carbides and nitrides in systems: transition metal – meta metal – carbon (nitrogen)). *Monatsh Chem* 95(1):156–157 (in German)
564. Jeitschko W, Nowotny H, Benesovsky F (1964) Die H-Phasen: Ti₂CdC, Ti₂GaC, Ti₂GaN, Ti₂InN, Zr₂InN und Nb₂GaC (The H-phases: Ti₂CdC, Ti₂GaC, Ti₂GaN, Ti₂InN, Zr₂InN and Nb₂GaC). *Monatsh Chem* 95(1):178–179 (in German)
565. Samsonov GV, Yasinskaya GA, Shiller EA (1961) Interaction of certain oxides, carbides and high-melting metals at high temperatures. *Refract Ind Ceram* 2(7–8):274–277
566. Adelsberg LM, Cadoff LH, Tobin JM (1966) Group IVB and VB metal carbide – carbon eutectic temperatures. *J Am Ceram Soc* 49(10):573–574
567. Portnoi KI, Levinskii YuV, Fadeeva VI (1961) Vzaimodeistvie s uglerodom nekotorykh tugoplavkikh karbidov i ikh tverdykh rastvorov (Reaction with carbon of some refractory carbides and their solid solutions). *Izv AN SSSR OTN Metallurgiya Toplivo* (2):147–149 (in Russian)
568. Denbnovetskaya EN (1967) Physical properties of NbC-Mo₃C₂ solid solutions. *Powder Metall Met Ceram* 6(4):300–302
569. Karpinos DM, Zilberberg VG, Épik AP, Batalin GI, Beloborodova EA (1969) Use of diffusion and plasma coatings for increasing the durability of electrodes in molten aluminium. *Powder Metall Met Ceram* 8(11):907–910
570. Ordanyan SS (1975) Reactions of rhenium and other refractory metals with some metal-like compounds. *Powder Metall Met Ceram* 14(2):125–129
571. Ordanyan SS, Maskhuliya LG, Panteleev IB, Samodurov AA (1981) Physicomechanical properties of Ti_{1-x}Nb_xC_{0.5}N_{0.5} complex solid solutions. *Powder Metall Met Ceram* 20(10):744–746
572. Ordanyan SS, Maskhuliya LG, Panteleev IB (1982) Effect of annealing conditions on grain growth in the complex Ti_{1-x}Nb_xC_{0.5}N_{0.5} solid solutions. *Powder Metall Met Ceram* 21(5):398–401
573. Nowotny H, Rogl P, Schuster JC (1982) Structural chemistry of complex carbides and related compounds. *J Solid State Chem* 44:126–133
574. Cohron J, Zee R, Chin B (1994) Degradation of refractory metal carbides by hot hydrogen. *J Nucl Mater* 212–215:1488–1491
575. Kao CR, Woodford J, Chang YA (1996) Reactive diffusion between silicon and niobium carbide: application to the synthesis of a silicon carbide – niobium disilicide composite. In: *Proc. 125th TMS annual meeting, Anaheim, California, 4–8 Feb 1996*, pp. 3–14
576. Loshak MG (1984) Prochnost i dolgovechnost tverdykh splavov (The strength and durability of hard alloys). *Naukova Dumka, Kyiv* (in Russian)
577. VorobeV YuP (2004) Karbidy v stalyakh (Carbides in steels). *Izv Chelyabinsk Nauch Tsentr* (2):34–60 (in Russian)
578. Pasotti RMR, Bressiani AHA, Bressiani JC (1998) Sintering of alumina – niobium carbide composites. *Int J Refract Met Hard Mater* 16(4–6):423–427
579. Acchar W, Greil P, Martinelli AE, Cairo CAA, Bressiani AHA, Bressiani JC (2000) Sintering behaviour of alumina – niobium carbide composites. *J Eur Ceram Soc* 20:1765–1769
580. Acchar W, Cairo CAA, Segadães AM (2005) TEM Study of a hot-pressed Al₂O₃-NbC composite material. *Mater Res* 8(1):109–112
581. Kud IV, Likhoded LS, Eremenko LI, Makarenko GN, Fedorus VB, Prilutskii ÉV (2006) Features of (Ti, Me)C solid solution formation. *Powder Metall Met Ceram* 45(1–2):14–19

582. Santos C, Maeda LD, Cairo CAA, Acchar W (2008) Mechanical properties of hot-pressed ZrO_2 -NbC ceramic composites. *Int J Refract Met Hard Mater* 26:14–18
583. Wang X-G, Liu J-X, Kan Y-M, Zhang G-J (2012) Effect of solid solution formation on densification of hot-pressed ZrC ceramics with MC (M = V, Nb and Ta) additions. *J Eur Ceram Soc* 32:1795–1802
584. Modi MH, Rai SK, Idir M, Schaefers F, Lodha GS (2012) NbC/Si multilayer mirror for next generation EUV light sources. *Optics Express* 20(14):15114–15120
585. Khvan AV, Hallstedt B, Chang K (2012) Thermodynamic assessment of Cr-Nb-C and Mn-Nb-C systems. *Calphad* 39:54–61
586. Rutkowski P, Stobierski L, Bućko MM (2008) Zmiany strukturalne i fazowe w tworzywach $NbC_{0.95}$ - $Cr_{23}C_6$ (The microstructural and phase changes of $NbC_{0.95}$ - $Cr_{23}C_6$ materials). *Mater Ceram* 60(4):249–253 (in Polish)
587. Rutkowski P, Stobierski L (2009) Ewolucja mikrostruktury tworzyw kompozytowych z węglików metali przejściowych (Microstructure evolution of composite materials based on transition metal carbides). *Mater Ceram* 61(2):140–145 (in Polish)
588. Rutkowski P (2013) Sintering of $NbC_{0.95}$ - Cr_yC_z composite materials. *Int J Refract Met Hard Mater* 41:614–621
589. He X, Bai Y, Zhu C, Sun Y, Li M, Barsoum MW (2010) General trends in the structural, electronic and elastic properties of the M_3AlC_2 phases (M = transition metal): a first-principle study. *Comput Mater Sci* 49:691–698
590. Lavrenko VA (1973) Rekombinatsiya atomov vodoroda na poverkhnostyakh tverdykh tel (The recombination of hydrogen atoms on the surfaces of solid bodies). *Naukova Dumka, Kyiv* (in Russian)
591. Buchner H, Gutjahr MA, Gross K, Beccu KD (1973) Über das Verhalten unterstöchiometrischer Übergangsmetallcarbide als Katalysatoren in Dehydrierungsprozessen (On the behaviour of under-stoichiometric transition metal carbides as catalysts in dehydrogenation processes). *Monatsh Chem* 104(1):160–165 (in German)
592. Samsonov GV, Zhidkova TG, Klimak ZA (1975) O kataliticheskikh svoystvakh karbidov perekhodnykh metallov (On the catalytic properties of transition metal carbides). In: Samsonov GV (ed) *Vysokotemperaturnye karbidy* (High-temperature carbides). *Naukova Dumka, Kyiv*, pp. 76–81 (in Russian)
593. Samsonov GV, Zhidkova TG (1975) Vliyanie defektnosti uglerodnoi podreshetki na kataliticheskie svoystva karbidov titana i niobiya (The influence of carbon sublattice on the catalytic properties of titanium and niobium carbides). In: Samsonov GV (ed) *Vysokotemperaturnye karbidy* (High-temperature carbides). *Naukova Dumka, Kyiv*, pp. 82–84 (in Russian)
594. Rafal AN (1983) Kinetika reaktsii s uchastiem vodoroda na beskisorodnykh tugoplavlykh soedinenii perekhodnykh metallov IV-VI grupp periodicheskoi sistemy (Kinetics of reactions involving hydrogen on oxygen-free refractory compounds of periodic system IV-VI groups transition metals). PhD thesis, Institute for Problems of Materials Science, Ukrainian SSR Academy of Sciences, Kyiv (in Russian)
595. Samsonov GV, Kharlamov AI (1975) Catalytic properties of refractory compound powders (survey). *Powder Metall Met Ceram* 14(9):699–707
596. Chebotareva NP, Ilichenko NI, Golodets GI (1976) Kinetics and mechanism of oxidation of hydrogen on carbides of transition metals of groups IV-VI. *Theor Exp Chem* 12(2):154–162
597. Kharlamov AI, Kirillova NV, Yatsimirskii VK (1981) The catalytic properties of transition element carbides and nitrides in the oxidation of carbon monoxide. *Theor Exp Chem* 17(2):168–179
598. Kharlamov AI, Kirillova NV (1983) Catalytic properties of powdered refractory compounds of transition elements. Carbides and nitrides – a review. *Powder Metall Met Ceram* 22(2):123–134
599. Ledoux MJ, Pham-Huu C (1992) High specific area carbides of silicon and transition metals for catalysis. *Catal Today* 15(2):263–284

600. Oyama ST (1992) Preparation and catalytic properties of transition metal carbides and nitrides. *Catal Today* 15(2):179–200
601. Ledoux MJ, Pham-Huu C, Chianelli RR (1996) Catalysis with carbides. *Cur Opin Solid I*(1):96–100
602. Ilchenko NI, Pyatnitsky YuI (1996) Carbides of transition metals as catalysts for oxidation reactions. In: Oyama ST (ed) *The chemistry of transition metal carbides and nitrides*. Chapman & Hall, London, Glasgow, pp. 311–327
603. Ham DJ, Lee JS (2009) Transition metal carbides and nitrides as electrode materials for low temperature fuel cells. *Energies* 2:873–899. <https://doi.org/10.3390/en20400873>
604. Ivanovskii LE, Plekhanov AF (1968) Behaviour of niobium carbide anodes during electrolysis of chloride melts. *Electrochem Molten Solid Electrolytes* 6:82–86
605. Semenov-Kobzar AA, Obolonchik VA, Akinina ZS (1969) Stability of transition metal carbides under anodic polarization conditions. *Powder Metall Met Ceram* 8(5):399–402
606. Tomás-García AL, Jensen JO, Bjerrum NJ, Li Q (2014) Hydrogen evolution activity and electrochemical stability of selected transition metal carbides in concentrated phosphoric acid. *Electrochim Acta* 137:639–646
607. Gale WF, Totemeir TC, eds (2004) *Smithells metals reference book*, 8th edn. Elsevier Butterworth Heinemann, ASM International Materials Information Society, Amsterdam, Boston
608. Schmidt FA, Carlson ON (1972) Electrotransport of carbon in niobium and tantalum. *J Less-Common Met* 26(2):247–253
609. Samsonov GV, Latysheva VP (1956) Issledovanie diffuzii bora i ugleroda v nekotorye metally perekhodnykh grupp (A study of the diffusion of boron and carbon into certain transition groups metals). *Fiz Met Metalloved* 2(2):309–319 (in Russian)
610. Samsonov GV, Latysheva VP (1956) Diffuziya bora, ugleroda i azota v perekhodnye metally IV, V i VI grupp periodicheskoi sistemy (The diffusion of boron, carbon and nitrogen into transition metals of the IV, V and VI groups of the periodic system). *Doklady AN SSSR* 109(3):582–585 (in Russian)
611. Peterson NL (1960) Diffusion in refractory metals. Technical Report WADD-TR-60-793, Contract AF 33(616)-7382. US Air Force, Wright-Patterson Air Force Base, Ohio, pp. 1–164
612. Wert CA (1950) Measurements on the diffusion of interstitial atoms in b.c.c. lattices. *J Appl Phys* 21(11):1196–1197
613. Powers RW, Doyle MV (1957) Some internal friction studies in columbium. *Trans AIME* 209:1285–1288
614. Powers RW, Doyle MV (1959) Diffusion of interstitial solutes in the group V transition metals. *J Appl Phys* 30(4):514–524
615. Mehrer H (2007) *Diffusion in solids*. Springer, Berlin, Heidelberg
616. Le Claire AD (1990) Diffusion of C, N and O in metals. In: Mehrer H (ed) *Diffusion in solid metals and alloys*. Crystal and solid state physics, Vol. 26. Springer, Berlin, Heidelberg, pp. 471–485
617. Nakonechnikov AI, Pavlinov LV, Bykov VN (1966) Diffusion of carbon in refractory metals with a bcc lattice. *Phys Met Metallogr* 22(2):73–77
618. Geld PV, Lyubimov VD (1963) Mobility activation energy of Nb and C in metallic niobium and its carbides. *Powder Metall Met Ceram* 2(4):313–315
619. Son P, Ihara S, Miyake M, Sano T (1969) Diffusion of carbon in vanadium. *J Jpn Inst Met Mater* 33(1):1–3 (in Japanese)
620. Zhunkovskii GL (1969) Issledovanie protsessov diffuzionnogo nasyscheniya tugo-plavkikh metallov uglerodom i borom v vakuume (A study of the processes of diffusion saturation of refractory metals with carbon and boron in vacuum). PhD thesis, Institute for Problems of Materials Science, Ukrainian SSR Academy of Sciences, Kyiv (in Russian)
621. Hörz G, Lindenmaier K (1972) Kinetik der Entkohlung Niob in strömendem Sauerstoff zu bilden Kohlenmonoxid (Kinetics of decarburization of niobium in flowing oxygen to form carbon monoxide). *Z Metallkd* 63(5):240–247 (in German)

622. Samsonov GV, ed (1976) *Svoistva elementov (Properties of elements)*, Vol. 1, 2nd edn. Metallurgiya, Moscow (in Russian)
623. Bokshstein SZ, Bronfin MB, Kishkin ST (1967) Diffuzionnye kharakteristiki tugoplavkikh metallov ispolzuemykh pri vysokikh temperaturah (The diffusion characteristics of refractory metals applied at high temperatures). In: Tumanov AT, Portnoi KI (eds) *Tugoplavkie materialy v mashinostroenii (Refractory materials in machinery construction)*. Mashinostroenie, Moscow, pp. 151–176 (in Russian)
624. Kokon H, Son P, Miyake M, Sano T (1973) Self-diffusion of carbon in the monocarbide of niobium. *J Jpn Inst Met Mater* 37(10):1065–1068 (in Japanese)
625. Andrievskii RA, Khromov YuF, Alekseeva IS (1971) Self-diffusion of carbon and metal atoms in zirconium and niobium carbides. *Phys Met Metallogr* 32(3):228–231
626. Dergunova VS, Levinskii YuV, Shurshakov AN, Kravetskii GA (1974) *Vzaimodeistvie ugleroda s tugoplavkimi metallami (Interaction of carbon with refractory metals)*. Metallurgiya, Moscow (in Russian)
627. Meshcheryakov GYa, Zagryazkin VN (1971) Self-diffusion of carbon in monocarbides of transition metals. *Phys Met Metallogr* 32(4):217–220
628. Yu BB, Davis RF (1979) Self-diffusion of ¹⁴C in single crystals of NbC_x. *J Phys Chem Solids* 40(12):997–1006
629. Yu BB, Davis RF (1979) Self-diffusion of ¹⁴C in NbC_x. *Am Ceram Soc Bull* 58(3):348
630. Yu BB, Davis RF (1979) Self-diffusion of ⁹⁵Nb in NbC_x. *Am Ceram Soc Bull* 59(3):359
631. Yu BB, Davis RF (1981) Self-diffusion of ⁹⁵Nb in single crystals of NbC_x. *J Phys Chem Solids* 42(2):83–87
632. Yu BB, Davis RF (1979) Near-surface effect in self-diffusion in NbC_x. *Phys Status Sol A* 51(1):261–267
633. Khromov YuF, Zhmurov SA, Svistunov DE (1982) Samodiffuziya ¹⁴⁷Pm v karbidakh tsirkoniya i niobiya (Self-diffusion of ¹⁴⁷Pm in zirconium and niobium carbides). *Fiz Met Metalloved* 54(6):1223–1225 (in Russian)
634. Fujikawa Y, Son P, Miyake M, Sano T (1970) Diffusion of carbon in the carbides of niobium. *J Jpn Inst Met Mater* 34(12):1259–1263 (in Japanese)
635. Vilks YuN, Nikolskii SS, Avarbe RG (1967) Temperature dependence of diffusion coefficient of carbon in nonstoichiometric zirconium, niobium and tantalum carbides. *High Temp* 5(4):545–548
636. Borisova AL, Evtushenko OV (1979) Diffusional processes in the welding of some refractory carbides to metals. *Powder Metall Met Ceram* 18(7):481–487
637. Andrievskii RA, Klimenko VV, Khromov YuF (1969) Samodiffuziya ugleroda v karbidakh perekhodnykh metallov IV i V grupp (The self-diffusion of carbon in transition metals IV and V groups carbides). *Fiz Met Metalloved* 28(2):298–303 (in Russian)
638. Zagryazkin VN (1969) O mekhanizme diffuzii v monokarbidakh perekhodnykh metallov (On the mechanism of diffusion in transition metals monocarbides). *Fiz Met Metalloved* 28(2):292–297 (in Russian)
639. Brizes WF, Cadoff LH, Tobin JM (1966) Carbon diffusion in the carbides of niobium. *J Nucl Mater* 20(1):57–67
640. Resnick R, Steinitz R, Seigle L (1965) Determination of diffusivity of carbon in tantalum and columbium carbides by layer-growth measurements. *Trans Met Soc AIME* 233(10):1915–1920
641. Shcherbedinskaya AV, Minkevich AN (1965) Diffuziya ugleroda v karbidakh niobiya i titana (Diffusion of carbon in the carbides of niobium and titanium). *Izv Vyssh Uchebn Zaved Tsvetn Metall* 4:123–125 (in Russian)
642. Bornstein NS, Hirakis EC, Friedrich LA (1966) Diffusivity data on the formation of niobium carbide surface films. *J Less-Common Met* 10(3):200–205
643. Ambartsumyan RS, Babich BN (1970) Ob obrazovanii karbidov niobiya i tantalata pri termicheskoi dissotsiatsii khloridov na grafitovoi podlozhke (On the formation of niobium and tantalum carbides at the thermal dissociation of chlorides on graphite substrate). *Izv AN SSSR Neorg Mater* 6(7):1224–1227 (in Russian)

644. Geld PV, Lyubimov VD (1961) Diffuziya niobiya i ugleroda v niobii i ego karbidakh (Diffusion of niobium and carbon in niobium and its carbides). *Izv AN SSSR OTN Metall Toplivo* (6):119–126 (in Russian)
645. DePoorter GL, Wallace TC (1971) Diffusion in binary carbides. In: Eyring L (ed) *Advances in high temperature chemistry*, Vol. 4. Academic Press, New York, pp. 107–135
646. Matzke Hj, Rondinella VV (1999) Diffusion in carbides, nitrides, hydrides and borides. In: Beke DL (ed) *Diffusion in non-metallic solids*, Subvol. B, Part 1. Springer, Berlin, Heidelberg, pp. 5/1–5/29
647. Wallace TC, Sr, Butt DP (1996) Review of diffusion and vaporization of group 4 and 5 transition metal carbides. In: Oyama ST (ed) *The chemistry of transition metal carbides and nitrides*. Chapman & Hall, London, Glasgow, pp. 53–90
648. Samsonov GV, Kushtalova IP (1973) Issledovanie protsessov deformatsii i rekristallizatsii tugoplavkikh soedinenii (A study of the deformation and recrystallization processes of refractory compounds). *Izv AN SSSR Neorg Mater* 9(1):46–47 (in Russian)
649. Spivak II, Klimenko VV (1973) Densification kinetics in the hot pressing and recrystallization of carbides. *Powder Metall Met Ceram* 12(11):883–887
650. Ordanyan SS, Avgustinik AI (1966) Temperature dependence of the grain size of NbC_{0.80}. *Powder Metall Met Ceram* 5(9):718–721
651. Rudy E, Benesovsky F (1960) Über die elektrische Leitfähigkeit von hochschmelzenden harten Karbiden und Karbidmischkristallen (On the electrical conductivity of refractory hard carbides and carbide mixed crystals). *Planseeber Pulvermetall* 8:72–77 (in German)
652. Brizes WF, Salkovitz EI (1969) Comparison of the chemical and self-diffusivities in the transition metal monocarbides. *Scripta Metall* 3(9):659–662
653. Samsonov GV, Bozhko SA (1969) Recrystallization during the sintering of niobium and titanium carbide powders. *Powder Metall Met Ceram* 8(7):542–546
654. Baskin ML, Tretyakov VI, Chaporova IN (1961) Diffuziya niobiya v karbide titana i tverdom rastvore TiC-NbC ekvimolyarnogo sostava (Diffusion of niobium in titanium carbide and TiC-NbC equimolar solid solution). *Fiz Met Metalloved* 12(6):860–864 (in Russian)
655. Sarian S, Dalton JT (1973) Diffusion of ⁹⁵Nb in TiC_{0.95}. *Solid State Commun* 13(8):1229–1234
656. Khromov YuF, Alekseeva IS (1976) Diffusion mobility of carbon and metal atoms in the range of homogeneity of niobium and zirconium carbides and their solid solutions. *Phys Met Metallogr* 42(1):96–102
657. Vilk YuN, Ordanyan SS (1977) Temperature and composition dependence of the effective diffusion coefficient of niobium carbide in its homogeneity range. *Powder Metall Met Ceram* 16(10):761–766
658. Ordanyan SS, Avgustinik AI (1972) Nekotorye kharakteristiki vysokotemperaturnoi polzuchesti monokarbidnykh faz tsirkoniya i niobiya v oblasti ikh gomogennosti (Some characteristics of the high-temperature creep behaviour of zirconium and niobium monocarbide phases in their homogeneity ranges). In: *Short communications of Lensovet Leningrad Technological Institute scientific-technical conf.* Lensovet LTI, Leningrad, pp. 34–35 (in Russian)
659. Ordanyan SS, Kravchik AE, Neshpor VS (1978) Sintering kinetics of niobium carbide powders of nonstoichiometric composition. *Powder Metall Met Ceram* 17(5):368–370
660. Kushtalova IP, Ristic MM (1984) Recrystallization of refractory materials. II. Kinetics of recrystallization. *Sci Sinter* 16:115–117
661. Matzke Hj (1984) Point defects and transport properties in carbides. *Solid State Ionics* 12:25–45
662. Uz M, Rehbein DK, Carlson ON (1986) Thermotransport of carbon in two-phase V-C and Nb-C alloys. *Metall Trans A* 17(11):1955–1966

663. Rafaja D, Lengauer W, Wiesenberger H, Joguet M (1998) Combined refinement of diffusion coefficients applied on the Nb-C and Nb-N systems. *Metall Mater Trans A* 29(2):439–446
664. Matzke Hj (1990) Mass transport in carbides and nitrides. In: Freer R (ed) *The physics and chemistry of carbides, nitrides and borides*. Kluwer Academic, Dordrecht, pp. 357–383
665. Woodford J, Chang YA (1998) Interdiffusion in the carbides of the Nb-C system. *Metall Mater Trans A* 29(11):2717–2726
666. Murch GE, Bruff CM (1999) Chemical diffusion in bulk inhomogeneous nonmetallic compounds. In: Beke DL (ed) *Diffusion in non-metallic solids*, Subvol. B, Part I. Springer, Berlin, Heidelberg, pp. 10/1–10/62
667. Barzilai S, Raveh A, Frage N (2005) Annealing of niobium coatings deposited on graphite. *Vacuum* 79:171–177
668. Barzilai S, Weiss M, Frage N, Raveh A (2005) Structure and composition of Nb and NbC layers on graphite. *Surf Coat Technol* 197:208–214
669. Barzilai S, Raveh A, Frage N (2006) Interdiffusion of carbon into niobium coatings deposited on graphite. *Thin Solid Films* 496:450–456
670. Barzilai S, Frage N, Raveh A (2006) Niobium layers on graphite: growth parameters and thermal annealing effects. *Surf Coat Technol* 200:4646–4653
671. Kravchik AE, Ordanyan SS (2005) Isothermal sintering of inorganic powders. *Refract Ind Ceram* 46(6):423–431
672. Takeshita H, Miyake M, Sano T (1978) Surface carburization of niobium with propane. *J Nucl Mater* 78(1):77–82
673. Miyake M, Hirooka Y, Imoto R, Sano T (1979) Chemical vapour deposition of niobium on graphite. *Thin Solid Films* 63(2):303–308
674. Isobe Y, Son P, Miyake M (1989) Carbide layer growth behaviour in a molybdenum coating on graphite at elevated temperatures. *J Less-Common Met* 147(2):261–268
675. Sen U (2004) Kinetics of niobium carbide coating produced on AISI 1040 steel by thermo-reactive deposition technique. *Mater Chem Phys* 86(1):189–194
676. Kondo T, Yasuhara M, Kuramoto T, Kodera Y, Ohyanagi M, Munir ZA (2008) Effect of pulsed DC current on atomic diffusion of Nb-C diffusion couple. *J Mater Sci* 43:6400–6405
677. Adamyantsa, Kharatyan SL (2010) On the singularity of high temperature carbidization of niobium. *J Alloy Compd* 496:418–422
678. Jhi S-H, Louie SG, Cohen ML, Ihm J (2001) Vacancy hardening and softening in transition metal carbides and nitrides. *Phys Rev Lett* 86(15):3348–3351
679. Turchin VN, Rymashevskii GA (1970) Vyyavlenie dislokatsii v karbide niobiya (Etching of dislocations in niobium carbide). *Kristallografiya* 15(1):193–194 (in Russian)
680. Markhasev BI, Pior NCh, Shumilova RG (1979) Travitel dlya vyyavleniya mikrostruktury materialov na osnove karbidov niobiya, tantala i gafniya (An etching agent for revealing microstructure of materials on the base of niobium, tantalum and hafnium carbides). *Zavod Lab* 45(6):543–545 (in Russian)
681. Walker P, Tarn WH (1991) *CRC handbook of metal etchants*. CRC Press, Boca Raton, Boston, London
682. Hockman AJ, Feigelson RS (1983) Low temperature electrosynthesis of tantalum and niobium carbides. *J Electrochem Soc* 130(1):221–224
683. Scheibe M, Binkowski S, Benemann S, Saliwan-Neumann R (2015) Comparing different preparation techniques for the characterisation of niobium carbides. *Bundesanstalt für Materialforschung und -prüfung*, Berlin, pp. 1–12. http://www.struers.com/resources/alias/Artikel_BAM_ENG.pdf. Accessed 21 Mar 2015
684. Kopylova VP (1961) Khimicheskaya ustoichivost karbidov perekhodnykh elementov IV, V i VI grupp (The chemical stability of transition element carbides IV, V and VI groups). *Zh Prikl Khim* 34(9):1936–1939 (in Russian)
685. Umanskii YaS (1947) *Karbidy tverdykh splavov (Carbides of hard alloys)*. Metallurgizdat, Moscow (in Russian)

686. Lukashenko TA, Tikhonov KI (1998) Korroziionnaya stoikost ryada karbidov i nitridov perekhodnykh metallov 4-6 grupp v kontsentrirrovannykh rastvorakh sernoi i fosfornoj kislot (Corrosion resistance of a number of carbides and nitrides of group 4-6 transition metals in concentrated solutions of sulfuric and phosphoric acids). *Zh Prikl Khim* 71(12):2017–2020 (in Russian)
687. Kopylova VP, Kornilova VI, Nazarchuk TN, Fedorus VB (1980) Reactions of powders of zirconium and niobium carbides in their homogeneity with some acids. *Powder Metall Met Ceram* 19(1):9–12
688. Lesnikova KP, Rybina GL, Freid MKh (1987) Behaviour of niobium carbide in hydrochloric acid solutions. *Protect Met* 23(3):335–337
689. Chapin EJ, Friske WH (1954) A metallurgical evaluation of refractory compounds for containing molten titanium. Part II – Carbon, graphite and carbides. Report NRL-4467. Naval Research Laboratory, Washington, DC, pp. 1–22
690. Rowcliffe DJ, Hollox GE (1971) Hardness anisotropy, deformation mechanisms and brittle-to-ductile transition in carbide. *J Mater Sci* 6(10):1270–1276
691. Davis RF (1985) Kinetics and mechanisms of creep in sintered alpha silicon carbide and niobium carbide. Technical report ARO-18434.8-MS (NSF-DMR-812–0804). North Carolina State University, Raleigh, pp. 1–56
692. Samsonov GV, Kovalchenko MS (1962) Goryachee pressovanie (Hot pressing). UkrSSR State Engineering Literature Publishing House, Kyiv (in Russian)
693. Samsonov GV, Sinelnikova VS (1964) Electrical resistance of refractory compounds at high temperatures. In: Samsonov GV (ed) *Refractory transition metal compounds and high temperature cermets*. Academic Press, New York, London, pp. 172–177
694. Samsonov GV, Épik AP (1966) Coatings of high-temperature materials. Some properties of high-temperature compounds. In: Hausner HH (ed) *Coatings of high-temperature materials*. Springer, Plenum Press, New York, pp. 7–111
695. Harrod DL, Fleischer LR (1968) On the role of diffusion in the plastic deformation of transition metal carbides. In: Vahldiek FW, Mersol SA (eds) *Anisotropy in single-crystal refractory compounds*, Vol. 1. Springer, Plenum Press, New York, pp. 341–356
696. Kotlyar EE, Nazarchuk TN (1972) Interaction of the carbides of group IV and V transition metals with various acids. In: Samsonov GV (ed) *Chemical properties and analysis of refractory compounds*. Consultants Bureau, New York, London, pp. 1–5
697. Etinger IA, Maltseva LF, Savranskaya LA, Marmer EN, Kindysheva VS, Nikolaeva VA, Dubovik TV (1974) The reaction of highly refractory oxides, refractory carbides and boron carbonitride with molybdenum and tungsten under the operating conditions in high-temperature vacuum electric furnaces. In: Samsonov GV (ed) *Refractory carbides*. Consultants Bureau, New York, London, pp. 449–461
698. Chin GY (1975) Slip and twinning systems in ceramic crystals. In: Bradt RC, Tressler RE (eds) *Deformation of ceramic materials*. Plenum Press, New York, London, pp. 25–59
699. Samsonov GV, Klochkov LA, Timofeeva II (1975) Termicheskoe rasshirenie TiC, ZrC i NbC v oblastiakh ikh gomogenosti (Thermal expansion of TiC, ZrC and NbC in the ranges of their homogeneities). In: Samsonov GV (ed) *Vysokotemperaturnye karbidy (High-temperature carbides)*. Naukova Dumka, Kyiv, pp. 46–48 (in Russian)
700. Kutysheva ÉV, Kuzma YuB (1975) O vzaimodeistvii poroshkov karbida niobiya i kremniya (On the interaction of niobium carbide and silicon powders). In: Samsonov GV (ed) *Vysokotemperaturnye karbidy (High-temperature carbides)*. Naukova Dumka, Kyiv, pp. 135–139 (in Russian)
701. Kutysheva ÉV (1975) Vzaimodeistvie karbidov perekhodnykh metallov IV-VI grupp periodicheskoi sistemy elementov s kremniem (The interaction of carbides of transition metals IV-VI groups periodic system of elements with silicon). In: Samsonov GV (ed) *Vysokotemperaturnye karbidy (High-temperature carbides)*. Naukova Dumka, Kyiv, pp. 139–142 (in Russian)

702. Samsonov GV, Tkachenko YuG, Berdikov VF, Bovkun GA (1976) Mikrotverdst, mikrohrupkost i khrupkaya mikroprochnost karbidov perekhodnykh metallov (Microhardness, microbrittleness and brittle microstrength of transition metal carbides). In: Samsonov GV, Kosolapova TYa, Gnesin GG, Fedorus VB, Domasevich LG (eds) Karbidy i splavy na ikh osnove (Carbides and alloys based on them). Naukova Dumka, Kyiv, pp. 98–104 (in Russian)
703. Turchin VN, Knyazev VI, Evstyukhin NA, Fursov YuD (1976) Nekotorye voprosy issledovaniya deformatsii monokristallov karbidov perekhodnykh metallov pri vdavlivanii (Some research problems of single crystal transition metal carbides deformation at the indentation). In: Samsonov GV, Kosolapova TYa, Gnesin GG, Fedorus VB, Domasevich LG (eds) Karbidy i splavy na ikh osnove (Carbides and alloys based on them). Naukova Dumka, Kyiv, pp. 104–107 (in Russian)
704. Bukatov VG, Knyazev VI, Korostin OS, Baranov VM (1976) Izmenenie uprugikh kharakteristik v oblasti gomogennosti nekotorykh karbidov perekhodnykh metallov (Change of elastic characteristics in the range of homogeneity of some transition metal carbides). In: Samsonov GV, Kosolapova TYa, Gnesin GG, Fedorus VB, Domasevich LG (eds) Karbidy i splavy na ikh osnove (Carbides and alloys based on them). Naukova Dumka, Kyiv, pp. 111–114 (in Russian)
705. Knyazev VI, Bukatov VG, Korostin OS (1976) Vnutrennee trenie nekotorykh monokarbidov perekhodnykh metallov v diapazone temperatur 20–2000 °C (The internal friction of some transition metal carbides in the temperature range of 20–2000 °C). In: Samsonov GV, Kosolapova TYa, Gnesin GG, Fedorus VB, Domasevich LG (eds) Karbidy i splavy na ikh osnove (Carbides and alloys based on them). Naukova Dumka, Kyiv, pp. 114–121 (in Russian)
706. Ogorodnikov VV, Rogovoi YuI (1976) Tochechnye defekty v kubicheskikh monokarbidakh (Point defects in cubic monocarbides). In: Samsonov GV, Kosolapova TYa, Gnesin GG, Fedorus VB, Domasevich LG (eds) Karbidy i splavy na ikh osnove (Carbides and alloys based on them). Naukova Dumka, Kyiv, pp. 129–137 (in Russian)
707. Kharkhardin ED, Kruglov VN, Poltoratskii NI, Rymashevskii GA, Kiparisov SS (1976) Issledovanie struktury monokristallov karbidov tsirkoniya i niobiya poluchennykh induktsionnoi zonnoi plavkoi (A study of the structure of single crystal zirconium and niobium carbides obtained by induction zone melting). In: Samsonov GV, Kosolapova TYa, Gnesin GG, Fedorus VB, Domasevich LG (eds) Karbidy i splavy na ikh osnove (Carbides and alloys based on them). Naukova Dumka, Kyiv, pp. 137–140 (in Russian)
708. Knyazheva VM, Kolotyrkin YaM, Pancheshnaya VP, Neiman CN, Klyueva VV, Plaskeev AV (1976) Korroziionno-elektrokhimicheskie svoistva i perspektivy primeneniya nekotorykh karbidov v kachestve korroziionostoikikh materialov (The corrosion-electrochemical properties and application prospects of some carbides as corrosion-resistant materials). In: Samsonov GV, Kosolapova TYa, Gnesin GG, Fedorus VB, Domasevich LG (eds) Karbidy i splavy na ikh osnove (Carbides and alloys based on them). Naukova Dumka, Kyiv, pp. 209–221 (in Russian)
709. Savitskii EM, Sinelnikova VS, Burkhanov GS, Kuzmishchev VA, Kosolapova TYa, Matsera VE, Nekrasov IA, Sdobyrev VV (1977) Issledovanie protsessa rosta monokristallov NbC (A study of the growth process of single crystal NbC). In: Tananaev IV, Savitskii EM, Burkhanov GS, Ottenberg EV, Kirillova VM (eds) Monokristally tugoplavkikh i redkikh metallov, splavov i soedinenii (Single crystals of refractory and less-common metals, alloys and compounds). Nauka, Moscow, pp. 32–36 (in Russian)
710. Davis RF, Carter CH, Jr, Chevacharoenkul S, Bentley J (1984) The occurrence and behaviour of dislocations during plastic deformation of selected transition metal and silicon carbides. In: Tressler RE, Bradt RC (eds) Deformation of ceramic materials II. Plenum Press, New York and London, pp. 97–124
711. Williams WS (1990) Thermal conductivity of transition metal carbides. In: Freer R (ed) The physics and chemistry of carbides, nitrides and borides. Kluwer Academic, Dordrecht, pp. 625–637

712. Loskutov VF, Khizhnyak VG, Kunitskii YuA, Kindrachuk MV (1991) Diffuzionnye karbidnye pokrytiya (Diffusion carbide coatings). Tekhnika, Kyiv (in Russian)
713. Kumashiro Y (2000) Survey of refractory metalloids: transition metal carbides, nitrides and diborides. In: Kumashiro Y (ed) Electric refractory materials. Marcel Dekker, New York, Basel, pp. 7–17
714. Dai H, Wong EW, Lu YZ, Fan S, Lieber CM (1995) Synthesis and characterization of carbide nanorods. *Nature* 375(6534):769–772
715. Kumashiro Y (2000) High-temperature characteristics. In: Kumashiro Y (ed) Electric refractory materials. Marcel Dekker, New York, Basel, pp. 191–222
716. Ishizawa Y (2000) Transition metal carbide field emitters. In: Kumashiro Y (ed) Electric refractory materials. Marcel Dekker, New York, Basel, pp. 269–287
717. Pomytkin AP (1976) Kinetika vysokotemperaturnogo okisleniya karbidov titana, niobiya, khroma, bora i kremniya v kislorode (Kinetics of high-temperature oxidation of titanium, niobium, chromium, boron and silicon carbides in oxygen). PhD thesis, Institute for Problems of Materials Science, Ukrainian SSR Academy of Sciences, Kyiv (in Russian)
718. Pearson WB (1958) Lattice spacings and structures of metals and alloys. Pergamon Press, London
719. Berg G, Friedrich C, Broszeit E, Berger C (2000) Data collection of properties of hard materials. In: Riedel R (ed) Handbook of ceramic hard materials. Wiley-VCH, Weinheim, pp. 965–995
720. Haefler RA (1987) Oberflächen- und Dünnschichttechnologie. Teil 1 – Beschichtung von Oberflächen (Surface and thin film technology. Part 1 – Coating surfaces). Springer, Berlin (in German)
721. Rühle M (1982) Zum technischen Stand der Dispersionshärtung. Teil 1 (State of the art dispersion hardening. Part 1). *Metall* 36(12):1280–1287 (in German)
722. Kieffer R, Benesovsky F (1963) Hartstoffe (Hard materials). Springer, Vienna (in German)
723. Frey H, Kienel G (1987) Dünnschichttechnologie (Thin film technology). VDI-Verlag, Düsseldorf (in German)
724. Schedler W (1988) Hartmetall für den Praktiker (Hard metal for the practitioner). VDI-Verlag, Düsseldorf (in German)
725. Habig K-H (1980) Verschleiß und Härte von Werkstoffen (Wear and hardness of materials). Hanser, München (in German)
726. Steffens H-D, Brandl W (1992) Moderne Beschichtungsverfahren (Modern surface technology). Lehrstuhl für Werkstofftechnologie der Universität Dortmund (in German)
727. Lanin A (2013) Nuclear rocket engine reactor. Springer, Berlin, Heidelberg
728. Popov VP, Lanin AG, Manyukhin VP (1973) Calorimetric determination of the heat resistance of ring-shaped samples of brittle electric conductors. *Strength Mater* 5(10):1260–1263
729. Hasselman DPH (1978) Figures-of-merits for the thermal stress resistance of high-temperature brittle materials: a review. *Ceramurg Int* 4(4):147–150
730. Shabalin IL, Wang Y, Krynkina AV, Umnova OV, Vishnyakov VM, Shabalin LI, Churkin VK (2010) Physico-mechanical properties of ultra-high temperature hetero-modulus ceramics based on group 4 transition metal carbides. *109(7):405–415*
731. Lanin AG, Popov VP, Maskaev AS, Sokolov VA, Turchin VN (1981) Strength of carbide-graphite composites with force and thermal loading. *Strength Mater* 13(12):1534–1539
732. Lanin AG (1998) Prochnost i termostoikost konstruktsionnoi keramiki (Strength and thermal stress resistance of structural ceramics). Moscow Engineering Physics Institute, Moscow (in Russian)
733. Deryavko II, Perepelkin IG, Pivovarov OS, Storozhenko AN (2001) Ekspressnye metodiki dlya poslereaktornogo issledovaniya bezobolocheknykh sterzhnevnykh karbidnykh tvelov (Express methods for postreactor research of cladding-free rod carbide fuel pins). *Nat Nucl Centre Rep Kaz* (4):88–94 (in Russian)

734. Vlasov NM, Fedik II (2001) Teplovydelyayushchie elementy yadernykh raketnykh dvigatelei (Fuel elements of nuclear rocket engines). TsNIIAtominform, Moscow (in Russian)
735. Lanin A, Fedik I (2005) Termoprochnost materialov (Thermal strength of materials). Scientific Research Institute of Scientific Industrial Association "Luch", Podolsk, Moscow Area (in Russian)
736. Lanin A, Fedik I (2008) Thermal stress resistance of materials. Springer, Berlin, Heidelberg, New York
737. Zhang G-J, Liu H-T, Wu W-W, Zou J, Ni D-W, Guo W-M, Liu J-X, Wang X-G (2014) Reactive processes for diboride-based ultra-high temperature ceramics. In: Fahrenholtz WG, Wuchina EJ, Lee WE, Zhou Y (eds) Ultra-high temperature ceramics. Wiley, Hoboken, New Jersey, pp. 33–59
738. Bhardwaj P, Singh S (2012) Structural phase stability and elastic properties of refractory carbides. *Int J Refract Met Hard Mater* 35:115–121
739. Wang J, Vandeperre LJ (2014) Deformation and hardness of UHTCs as a function of temperature. In: Fahrenholtz WG, Wuchina EJ, Lee WE, Zhou Y (eds) Ultra-high temperature ceramics. Wiley, Hoboken, New Jersey, pp. 236–266
740. Guo Z, Zhu L, Zhou J, Sun Z (2015) Microscopic origin of MXenes derived from layered MAX phases. *RSC Adv* 5(32):25403–25408
741. Hampshire S (2014) Fundamental aspects of hard ceramics. In: Sarin VK, Llanes L, Mari D (eds) *Comprehensive hard materials*, Vol. 2 – Ceramics. Elsevier, Amsterdam, Oxford, pp. 3–28
742. Zainulin YuG, Dyachkova TV, Alyamovskii SI, Shveikin GP, Shilyaeva OI (1978) Oblast gomogennosti i izmenenie prirody stepeni slozhnosti v elementaroi yacheike oksikarbidov niobiya (Homogeneity region and change nature of degree of complicity in elementary cell of niobium oxycarbides). *Zh Neorg Khim* 23(11):2898–2901 (in Russian)
743. Shveikin GP, Geld PV, Alyamovskii SI (1963) Usloviya obrazovaniya oksikarbidov niobiya (Conditions governing the formation of niobium oxycarbides). *Zh Neorg Khim* 8(3):689–696 (in Russian)
744. Lapitskii AV, Simanov YuP, Artamonova EP (1957) Ob obrazovanii nizshikh okislov niobiya i tantala v nekotorykh reaktsiyakh vosstanovleniya i okisleniya (On the formation of lower niobium and tantalum oxides in some reduction and oxidation reactions). *Zh Neorg Khim* 2(1):80–83 (in Russian)
745. Gozzi D, Guzzardi G, Montozzi M, Cignini PL (1997) Kinetics of high temperature oxidation of refractory carbides. *Solid State Ionics* 101–103(1):1243–1250
746. Gozzi D, Cascino G, Loreti S, Minarini C, Shimada S (2001) Weak interaction of oxygen with some refractory carbides. *J Electrochem Soc* 148(4):J15–J24
747. Bouhemadou A, Khenata R (2007) Prediction study of structural and elastic properties under pressure effect of M_2GaC ($M = Ti, V, Nb, Ta$). *J Appl Phys* 102(4):043528
748. Ormont BF (1959) Energii atomizatsii i teploty obrazovaniya nekotorykh karbidov i nitridov i naibolee veroyatnye znacheniya dlya energii dissotsiatsii azota i energii sublimatsii ugleroda (Atomization energies and heats of formation of some carbides and nitrides and the most probable values for the dissociation energy of nitrogen and sublimation energy of carbon). *Zh Fiz Khim* 33(7):1455–1460 (in Russian)
749. Fujishiro S (1961) Thermodynamic properties of transition metal carbides and their periodicity. *J Jpn Soc Powder Metall* 8(2):73–76
750. Oshcherin BN (1965) Nekotorye voprosy termodinamiki karbidnykh faz vnedreniya v oblasti gomogennosti (The certain problems of thermodynamics of carbide interstitial phases within the homogeneity ranges). In: Grigoreva VV, Eremenko VN, Nazarchuk TN, Samsonov GV, Fedorchenko IM, Frantsevich IN (eds) *Vysokotemperaturnye neorganicheskie soedineniya* (High-temperature inorganic compounds). Naukova Dumka, Kyiv, pp. 157–165 (in Russian)
751. Kulikov IS (1988) Termodinamika karbidov i nitridov (Thermodynamics of carbides and nitrides). *Metallurgiya, Chelyabinsk* (in Russian)

752. Kaufman L, Bernstein H (1968) Thermodynamic properties of refractory transition metal compounds. In: Vahldiek FW, Mersol SA (eds) Anisotropy in single-crystal refractory compounds, Vol. 1. Springer, New York, pp. 269–297
753. Bowman AL, Krikorian NH (1976) Interstitial phases. In: Hannay NB (ed) Treatise on solid state chemistry, Vol. 3. Crystalline and noncrystalline solids. Plenum Press, New York, London, pp. 253–292
754. Chase MW, Jr, ed (1998) NIST-JANAF thermochemical tables, 4th edn. J Phys Chem Ref Data. Monograph No. 9. American Institute of Physics, New York
755. Fesenko VV, Turchanin AG, Ordanyan SS (1974) A study of the dependence of some thermodynamic properties of niobium and zirconium carbides on temperature and composition. In: Samsonov GV (ed) Refractory carbides. Consultants Bureau, New York, London, pp. 323–328
756. Maltseva LF, Lapshov YuK, Marmer ÉN, Samsonov GV (1965) High-temperature heaters of niobium and zirconium carbides. Powder Metall Met Ceram 4(11):942–946
757. Samsonov GV, Grebenkina VG (1968) Temperature coefficient of electroresistance of some high-melting compounds. Powder Metall Met Ceram 7(2):107–111
758. Allison CY, Finch CB, Foegelle MD, Modine FA (1988) Low-temperature resistivity of transition-metal carbides. Solid State Commun 68(4):387–390
759. Funke VF, Pshenichnyi IV, Pliner LA, Lyakhov DM, Golomazov VM, Zubarev PV (1980) Thermal conductivity and electrical resistivity of Mo₃C₂-ZrC-NbC solid solutions. Powder Metall Met Ceram 19(10):722–727
760. Tsuchida T, Mekata M, Nakamura Y, Sakurai J, Takaki H (1961) Hall effect in carbides of transition metals. J Phys Soc Jpn 16(12):2453–2456
761. Samsonov GV, Paderno VN (1964) Über die Herstellung von Karbidmischkristallen und die Untersuchung ihrer physikalischen Eigenschaften (The production of mixed crystals of carbides and investigation of their physical properties). Planseeber Pulvermetall 12(1):19–31 (in German)
762. Genkin YaE, Milovanova IA, Lyakutkin AV (1976) Magnitnaya vospriimchivost nekotorykh soedinenii niobiya s borom, uglerodom i azotom (Magnetic susceptibility of some niobium compounds with boron, carbon and nitrogen). Izv AN Kaz SSR Ser Fiz Mat 2:12–16 (in Russian)
763. Goretzki H (1963) Untersuchung der magnetischen, elektrischen und thermoelektrischen Eigenschaften der Karbide und Nitride der 4a- und 5a-Gruppen Übergangsmetalle (A study of magnetic, electrical and thermoelectrical properties of carbides and nitrides of 4a and 5a groups transition metals). PhD thesis, Wien Universität (in German)
764. Geballe TH, Matthias BT, Remeika JP, Clogston AM, Compton VB, Maita JP, Williams HJ (1966) High temperature *sp*-band superconductors. Phys 2(6):293–310
765. Petrov VA, Chekhovskoi VYa, Sheindlin AE, Kashekhlebova II, Nikolaeva VA, Fomina LP (1974) Emissive power and specific electrical resistivity of zirconium and niobium carbides at high temperatures. In: Samsonov GV (ed) Refractory carbides. Consultants Bureau, New York, London, pp. 231–238
766. Okhremchuk LN, Podchernyaeva IA, Upadhyaya GS, Fomenko VS (1969) Izluchatel'naya sposobnost monokarbidov titana, niobiya i ikh splavov v oblasti gomogenosti (Emissivity of monocarbides of titanium, niobium and their alloys in the range of homogeneity). Izv Vyssh Uchebn Zaved Fiz (11):126–132 (in Russian)
767. Simon NI (1977) Emissionno-adsorbtsionnye svoistva tugoplavkikh uglerodsoderzhashchikh elektrodnykh materialov (Emission and adsorption properties of refractory carbon-containing electrode materials). PhD thesis, Institute for Problems of Materials Science, Ukrainian SSR Academy of Sciences, Kyiv (in Russian)
768. Kovalchenko MS, Samsonov GV (1961) Oblast NbC-C diagramy systemy niobii-vuglets (Section NbC-C of the diagram of the niobium-carbon system). Dopov Akad Nauk Ukr RSR Ser A Fiz Mat Tekh Nauki 23(11):1478–1481 (in Ukrainian)
769. Kieffer R, Kölbl F (1949) Tungsten carbide – free hard metals. Powder Metall Bull 4(1):4–17

770. Kovalskii AE, Petrova LA (1951) Mikrotverdst dvoinykh tugoplavkikh karbidov (Microhardness of binary refractory carbides). In: Khrushchov MM (ed) Mikrotverdst (Microhardness). AN SSSR, Moscow, pp. 170–186 (in Russian)
771. Shaffer PTB, Watts RL (1961) Development of ultra refractory materials. Summary Report, Contract NOrd-17175. The Carborundum Company, Niagara Falls, New York, pp. 1–40
772. Naumenko VYa (1971) Tekhnologiya polucheniya i issledovanie nekotorykh svoistv karbidov perekhodnykh metallov IV-V grupp v oblastiakh ikh gomogenosti (Production technology and investigation of some properties of transition metal carbides IV-V groups in the regions of their homogeneity). PhD thesis, Institute for Problems of Materials Science, Ukrainian SSR Academy of Sciences, Kyiv (in Russian)
773. Jones T (1956) The metallography of certain hot-pressed carbides possessing high melting points. In: Technical papers of the metallographic group meeting held at Bridgeport Brass Company, 7–8 Nov 1956, TID-7567, Part 1. US Atomic Energy Commission, Washington DC, pp. 32–45
774. Stern KH (1996) Electrodeposition of refractory compounds from molten salts – borides, carbides and silicides. In: Stern KH (ed) Metallurgical and ceramic protective coatings. Chapman & Hall, London, Weinheim, New York, pp. 54–73
775. Weimer AW, ed (1997) Carbide, nitride and boride materials synthesis and processing. Chapman & Hall, London, Weinheim, New York
776. Ishizawa Y, Koizumi M, Oshima C, Otani S (1987) Field emission properties of <110>-oriented carbide tips. J Phys Colloq C-6 48(11):9–14
777. Nagashima A, Nuka K, Satoh K, Itoh H, Ichinokawa T, Oshima C, Otani S (1993) Electronic structure of monolayer graphite on some transition metal carbide surfaces. Surf Sci 287–288(2):609–613
778. Jhi S-H, Ihm J, Louie SG, Cohen ML (1999) Electronic mechanism of hardness enhancement in transition-metal carbonitrides. Nature 399(6732):132–134
779. Khusainov MA (1989) Mechanical properties and special features of failure of carbides and nitrides of metals of groups IV-V deposited from the gas phase. Powder Metall Met Ceram 28(7):551–555
780. Gao F (2006) Theoretical model of intrinsic hardness. Phys Rev B 73(13):132104
781. Šimůnek A (2007) How to estimate hardness of crystals on a pocket calculator. Phys Rev B 75(17):172108
782. Mukhopadhyay A, Raju GB, Basu B (2013) Ultra-high temperature ceramics: processing, properties and applications. In: Low IM, Sakka Y, Hu CF (eds) MAX phases and ultra-high temperature ceramics for extreme environments. IGI Global, Hershey, Pennsylvania, pp. 49–99
783. Wang HL, Hon MH (1999) Temperature dependence of ceramics hardness. Ceram Int 25(3):267–271
784. Kramer BM, Judd PK (1985) Computational design of wear coatings. J Vac Sci Technol A 3(6):2439–2444
785. Samsonov GV, Kharchenko VK, Struk LI (1968) Static strength of refractory compounds at high temperatures. Powder Metall Met Ceram 7(3):206–209
786. Struk LI (1969) Issledovanie protsessa pressovaniya i nekotorykh fiziko-mekhanicheskikh svoistv tugoplavkikh soedinenii (A study of pressing procedure and some physico-mechanical properties of refractory compounds). PhD thesis, Institute for Problems of Materials Science, Ukrainian SSR Academy of Sciences, Kyiv (in Russian)
787. Hollox GE (1968/69) Microstructure and mechanical behaviour of carbides. Mater Sci Eng 3(3):121–137
788. Cannon WR, Langdon TG (1983) Creep of ceramics. 1. Mechanical characteristics. J Mater Sci 18(1):1–50
789. Cannon WR, Langdon TG (1988) Creep of ceramics. 2. An examination of flow mechanisms. J Mater Sci 23(1):1–20

790. Ogorodnikov VV, Rogovoi Yul (1993) Rules of change in elastic, thermal and energy properties in a number of cubic transition metal monocarbides. *Powder Metall Met Ceram* 32(5):445–449
791. Korir KK, Amolo GO, Makau NW, Joubert DP (2011) First-principle calculations of the bulk properties of $4d$ transition metal carbides and nitrides in the rocksalt, zincblende and wurtzite structures. *Diamond Relat Mater* 20:157–164
792. Zaoui A, Kacimi S, Boukourt A, Bouhafs B (2010) *Ab initio* studies of structural, elastic and electronic properties of $Zr_xNb_{1-x}C$ and $Zr_xNb_{1-x}N$ alloys. *Phys B* 405:153–157
793. Nino A, Tanaka A, Sugiyama S, Taimatsu H (2010) Indentation size effect for the hardness of refractory carbides. *Mater Trans* 51(9):1621–1626
794. Kang D-B (2013) Effect of valence electron concentration on elastic properties of $4d$ transition metal carbides MC ($M = Y, Zr, Nb$ and Rh). *Bull Korean Chem Soc* 34(7):2171–2175
795. Sun X-W, Zhang X-Y, Zhang S-H, Zhu Y, Wang L-M, Zhang S-L, Ma M-Z, Liu R-P (2013) The structural, elastic and electronic properties of $Zr_xNb_{1-x}C$ alloys from first principle calculations. *Chin Phys B* 22(10):107105 (5 pp.)
796. Gautam GS, Kumar KCH (2014) Elastic, thermochemical and thermophysical properties of rock salt – type transition metal carbides and nitrides: a first principles study. *J Alloy Compd* 587:380–386
797. Shabalin IL (2014) TSR of hetero-modulus ceramics. In: Hetnarski RB (ed) *Encyclopedia of thermal stresses*, Vol. 11. Springer, Dordrecht, New York, London, pp. 6250–6255
798. Patriarca P, Rucker DJ (1970) Fuels and materials development program. Technical Report ORNL-4480, Contract W-7405-ENG-26. Oak Ridge National Laboratory, Tennessee, pp. 1–255
799. Dew-Hughes D, Jones R (1980) The effect of neutron irradiation upon the superconducting critical temperature of some transition metal carbides, nitrides and carbonitrides. *Appl Phys Lett* 36(10):856–859
800. Taubin ML (1990) Some radiation effects in ZrC, NbC and ZrN interstitial phases. *Atom Energy* 69(3):765–767
801. Dmitrieva GP, Shurin AK (1980) Constitution diagram of the quasiternary system Fe-VC-NbC. *Powder Metall Met Ceram* 19(10):699–702
802. Dmitrieva GP, Shurin AK, Polotnyuk VV, Zolkina SV (1982) Alloys of the quasi-ternary Fe-Ni-NbC system. *Phys Met* 3(6):1046–1052
803. Dmitrieva GP, Cherepova TS, Shurin AK (1992) Co-TiC_{0.86}-NbC_{0.9} of the equilibrium diagram of Co-Ti-Nb-C system. *Powder Metall Met Ceram* 31(4):349–352
804. Oshchipko IS, Burykina AL (1969) Study of the reactions between boron carbonitride and refractory metals and compounds. *Powder Metall Met Ceram* 8(6):499–501
805. Skripov AV, Udovic TJ, Cook JC, Hempelmann R, Rempel AA, Gusev AI (2009) Quasi-elastic neutron scattering study of hydrogen motion in NbC_{0.71}H_{0.28}. *J Phys Condens Matter* 21(17):175410
806. Ozawa K, Ishikawa S, Miyazaki E, Edamoto K, Kato H, Otani S (1997) Potassium adsorption on the polar NbC (111) surface: angle-resolved photoemission study. *Surf Sci* 375(2–3):250–256
807. Ozawa K, Ishikawa S, Edamoto K, Kato H, Otani S (1999) Na adsorption on the polar NbC (111) surface. *Surf Sci* 419(2–3):226–235
808. Gusev AI, Rempel SV (2000) Phase diagram for the Zr-Nb-C System. *Dokl Phys Chem* 375(4–6):249–253
809. Leiderman GM, Nikolaeva VA (1973) Vzaimodeistvie NbC i ZrC s Ni (Interaction of NbC and ZrC with Ni). *Izv AN SSSR Neorg Mater* 9(10):1721–1723 (in Russian)
810. Evtushok TM, Burykina AL (1968) Issledovanie vzaimodeistviya grafita s tugoplavkimi soedineniyami i zhidkimi metallami (A study of the interaction of graphite with refractory compounds and liquid metals). In: Samsonov GV (ed) *Vzaimodeistvie materialov vysokotemperaturnogo naznacheniya so sredoi* (Interaction of high-temperature appropriated materials with environment). Naukova Dumka, Kyiv, pp. 221–228 (in Russian)

811. Xu NS, Huq SE (2005) Novel cold cathode materials and applications. *Mater Sci Eng R* 48:47–189
812. Zhilyaev VA, Patrakov EI (2006) Mekhanizm zhidkofaznogo vzaimodeistviya dvoynykh karbidov (Ti,Me)C s nikelom (The mechanism of liquid-phase interaction of double carbides (Ti,Me)C with nickel). *Konstruk Kompoz Mater* 4:199–201 (in Russian)
813. Zhilyaev VA, Patrakov EI (2015) Regularities of the contact interaction of double carbides (Ti_{1–n}Me_n)C with nickel. *Russ J Non-Ferr Met* 56(3):329–332
814. Zhilyaev VA (2015) Regularities of reactions of group IV, V transition metal carbides with nickel. *Russ J Non-Ferr Met* 56(5):575–579
815. Zhilyaev VA, Patrakov EI (2006) Osobennosti vzaimodeistviya dvoynykh karbidov (Ti,Me)C s Ni-Mo raspalvom (The particularities of the interaction of double carbides (Ti,Me)C with Ni-Mo melt). *Konstruk Kompoz Mater* 4:196–199 (in Russian)
816. Zhilyaev VA (2006) Zakonomernosti tverdogaznykh reaktzii s uchastiem tugoplavkikh faz vnedreniya (The regularities of solid-phase reactions with the participation of refractory interstitial phases). *Konstruk Kompoz Mater* 4:192–196 (in Russian)
817. Markström A, Andersson D, Frisk K (2008) Combined *ab initio* and experimental assessment of A_{1–x}B_xC mixed carbides. *Calphad* 32(4):615–623
818. Cuppari MGDV, Santos SF (2016) Physical properties of the NbC carbide. *Met* 6(10):250 (17 pp.). doi:[10.3390/met6100250](https://doi.org/10.3390/met6100250).
819. Jung W-S, Chung S-H (2010) *Ab initio* calculation of interfacial energies between transition metal carbides and fcc iron. *Model Simul Mater Sci Eng* 18(7):075008
820. Schaidle JA, Thompson LT (2015) Fischer-Tropsch synthesis over early transition metal carbides and nitrides: CO activation and chain growth. *J Catal* 329:325–334
821. Christensen JM, Duchstein LDL, Wagner JB, Jensen PA, Temel B, Jensen AD (2012) Catalytic conversion of syngas into higher alcohols over carbide catalysts. *Ind Eng Chem Res* 51(11):4161–4172
822. Stottlemyer AL, Kelly TG, Meng Q, Chen JG (2012) Reactions of oxygen-containing molecules on transition metal carbides: surface science insight into potential applications in catalysis and electrocatalysis. *Surf Sci Rep* 67:201–232
823. Knyazheva VM, Babich SG, Kolotyркиn VI, Kozhevnikov VV (1991) Metallopodobnye soedineniya kak vtorichnye fazy, korrozionnostoikie materialy i zashchitnye pokrytiya (Metal-like compounds as excessive phases, corrosion-resistant materials and protective coatings). *Khim Neftekhim Mashin* (10):16–20 (in Russian)
824. Samsonov GV, Podchernyaeva IA, Fomenko VS, Lavrenko VA, Okhremchuk LN, Protsenko TG (1972) Correlation between the work functions of transition metal carbides in their homogeneity regions and surface recombination of hydrogen atoms. *Powder Metall Met Ceram* 11(5):389–392
825. Aizawa T, Hayami W, Souda R, Otani S, Ishizawa Y (1997) Hydrogen adsorption on transition metal carbide (111) surfaces. *Surf Sci* 381:157–164
826. Tuffias RH, Duffy AJ, Arrieta VM, Abrams WM, Benander RE (1997) Materials and fabrication processes for operation in hot hydrogen. *AIP Conf Proc* 387:1613–1618
827. Zhilyaev VA (2012) Vzaimosvyaz sostava, struktury i khimicheskikh svoystv tugoplavkikh faz vnedreniya. I. Zakonomernosti reaktzii tugoplavkikh faz vnedreniya s tverdymi reagentami (Interrelation of composition, structure and chemical properties of refractory interstitial phases. I. Regularities of reactions of refractory interstitial phases with solid reagents). *Vestn Perm Nats Issl Politekh Univ Mashin Mater* 14(3):7–21 (in Russian)
828. Ouensanga A (1986) Thermodynamic study of the reduction of diniobium pentoxide and of niobium dioxide by graphite in the temperature range 1100–1300 K. *J Less-Common Met* 119(2):189–197
829. Alabushev VA, Sychev AG, Shalaginov VN (1976) Okislenie monokarbida niobiya v oblasti 300–1000 °C (Oxidation of niobium monocarbide in the range 300–1000 °C). In: Samsonov GV (ed) *Elektronnaya struktura i fiziko-khimicheskie svoystva splavov i soedinenii perekhodnykh metallov* (Electronic structure and physico-chemical properties of transition metal alloys and compounds). Naukova Dumka, Kyiv, pp. 123–127 (in Russian)

830. Zhilyaev VA (2013) Vzaimosvyaz sostava, struktury i khimicheskikh svoystv tugoplavkikh faz vnedreniya. III. Zakonomernosti proyavleniya khimicheskoi aktivnosti tugoplavkikh faz vnedreniya v vozdushno-vakuumnykh i gazovykh sredakh (Interrelation of composition, structure and chemical properties of refractory interstitial phases. III. The regularities of manifestation of refractory interstitial phases chemical activity in air-vacuum and gaseous media). *Vestn Perm Nats Issl Politekh Univ Mashin Mater* 15(1):7–19 (in Russian)
831. Watt W, Cockett GH, Hall AR (1953) Sintering of zirconium carbide by hot-pressing: some results of preliminary tests on oxidation resistance of carbides. *Metaux Corros Ind* 28:222–237
832. Tumanov VI, Funke VF, Belenkaya LI (1963) The wetting of CbC-VC and CbC-TiC carbide alloys by nickel. *Powder Metall Met Ceram* 2(5):376–378
833. Samsonov GV, Kovalchenko MS, Petrykina RYa, Naumenko VYa (1970) Hot-pressing of the transition metals and their carbides in their homogeneity regions. *Powder Metall Met Ceram* 9(9):713–716
834. Andrievskii RA (1973) Thermodynamic approach to the analysis of diffusion-controlled processes in interstitial phases. *Powder Metall Met Ceram* 12(2):149–153
835. May CE, Koneval D, Fryburg GC (1959) Stability of ceramics in hydrogen between 4000 °F and 4500 °F. NASA Memorandum 3-5-59E. National Aeronautics and Space Administration, Washington, DC, pp. 1–18
836. Goldshtein MI, Panfilova LM, Syreishchikova VI, Zeldovich ÉS, Fedorus VB (1975) Rastvorimost karbidov elementov IV-V grupp v austenite stalei razlichnogo sostava (The solubility of carbides of IV-V groups elements in austenite of steels different in composition). In: Samsonov GV (ed) *Vysokotemperaturnye karbidy* (High-temperature carbides). Naukova Dumka, Kyiv, pp. 119–121 (in Russian)
837. Kindysheva VS, Maltseva LF, Fedorus VB (1975) O nekotorykh svoystvakh splavov sistemy NbC-WC (On certain properties of the NbC-WC system alloys). In: Samsonov GV (ed) *Vysokotemperaturnye karbidy* (High-temperature carbides). Naukova Dumka, Kyiv, pp. 173–176 (in Russian)
838. Wang X-Z, Wang H-B, Liu X-M, Yang T, Song X-Y (2017) Grain growth inhibitor on the WC-Co cemented carbide coating. *J Inorg Mater* 32(8):813–818 (in Chinese)
839. Lengauer W, Wiesenberger H, Joguét M, Rafaja D, Ettmayer P (1996) Chemical diffusion in transition metal – carbon and transition metal – nitrogen systems. In: Oyama ST (ed) *The chemistry of transition metal carbides and nitrides*. Chapman & Hall, London, pp. 91–106
840. Wiesenberger H, Lengauer W, Ettmayer P (1998) Reactive diffusion and phase equilibria in the V-C, Nb-C, Ta-C and Ta-N systems. *Acta Mater* 46(2):651–666
841. Rohmer M-M, Benard M, Poble J-M (2000) Structure, reactivity and growth pathways of metallocarbohedrenes M_3C_{12} and transition metal/carbon clusters and nanocrystals: a challenge to computational chemistry. *Chem Rev* 100:495–542
842. Bittner H, Goretzki H, Benesovsky F, Nowotny H (1963) Über einige Monocarbide-Mononitrid-Systeme und deren magnetische Eigenschaften (On some monocarbide-mononitride systems and their magnetic properties). *Monatsh Chem* 94(3):518–526 (in German)
843. Fesenko VV, Bolgar AS (1963) Evaporation rate and vapour pressure of carbides, silicides, nitrides and borides. *Powder Metall Met Ceram* 2(1):11–17
844. Panasyuk AD, Samsonov GV (1963) Termopary s termoelektrodami iz tugoplavkikh karbidov dlya izmereniya temperatur do 3000 °C (Thermocouples with temperature electrodes made from refractory carbides for the measurement of temperatures up to 3000 °C). *Teplofiz Vysok Temp* 1(1):136–140 (in Russian)
845. Kuchma AY, Samsonov GV (1966) Obrazovanie stabilnykh elektronnykh konfiguratsii i nekotorye fizicheskie svoystva karbidov i nitridov perekhodnykh metallov v oblasti ikh gomogenosti (Formation of stable electron configurations and some physical properties of carbides and nitrides of transition metals in the range of their homogeneity). *Izv AN SSSR Neorg Mater* 2(11):1970–1974 (in Russian)

846. Paderno YuB, Andreeva TV, Barantseva IG, Goryachev YuM (1965) Nature of the thermal conductivity in the carbides of some transition metals of groups IV and V. *Powder Metall Met Ceram* 4(2):131–134
847. Willens RH, Buehler E, Matthias BT (1967) Superconductivity of the transition metal carbides. *Phys Rev* 159(2):327–330
848. Samsonov GV, Upadhyaya GS (1968) Properties of alloys of niobium and titanium carbides in their homogeneity region. *Powder Metall Met Ceram* 7(9):723–726
849. Dubrovskaya LB, Matveenko II (1970) Elektricheskoe soprotivlenie i effekt Kholla monokarbida niobiya (Electrical resistance and Hall effect of niobium carbide). In: Shveikin GP, Geld PV (eds) *Issledovaniya soedinenii redkikh elementov. Trudy Instituta khimii* (Studies of less-common element compounds. Proc. Institute of chemistry), Vol. 18. USSR Academy of Sciences Ural Filial, Sverdlovsk, pp. 124–125 (in Russian)
850. Borukhovich AS, Dubrovskaya LB, Matveenko II, Geld PV (1970) Issledovanie magnitnoi vospriimchivosti kubicheskikh karbidov niobiya i tantala v oblasti nizkikh temperatur (A study of the magnetic susceptibility of cubic niobium and tantalum carbides in the low temperature range). In: Shveikin GP, Geld PV (eds) *Issledovaniya soedinenii redkikh elementov. Trudy Instituta khimii* (Studies of less-common element compounds. Proc. Institute of chemistry), Vol. 20. USSR Academy of Sciences Ural Filial, Sverdlovsk, pp. 71–73 (in Russian)
851. Dubrovskaya LB, Borukhovich AS, Geld PV, Matveenko II, Kudryashova LV, Ordanyan SS (1970) Magnetic susceptibility of solid solutions of zirconium and niobium monocarbides. *Phys Solid State* 11(10):2451–2453
852. Shacklette LW, Radosevich LG, Williams WS (1971) Gap energy of superconducting niobium carbide. *Phys Rev B* 4(1):84–87
853. Savitskii EM, Baron VV, Efimov YuV, Bychkova MI, Myzenkova LF (1973) Superconducting materials. Plenum Press, New York, London
854. Samsonov GV, Fomenko VS, Podchernyaeva IA, Okhremchuk LN (1974) Thermionic emission properties of refractory compounds and materials based on them (a review). *Powder Metall Met Ceram* 13(10):836–842
855. Franzen HF, Khan AS, Peterson DT (1976) Thermodynamics of solid solution of hydrogen in M_2C type carbides of vanadium and niobium. *J Solid State Chem* 19:81–85
856. Samsonov GV, Voronkin MA (1976) Properties of double carbides of titanium and group Va metals. *Powder Metall Met Ceram* 15(4):296–299
857. Goryachev YuM, Podchernyaeva IA, Siman NI, Sinelnikova VS, Timofeeva II (1978) Anizotropiya raboty vykhoda elektrona monokristallov ZrC_x i NbC_x (Electron work function of ZrC_x and NbC_x single crystals). *Sci Sinter* 10(Spec. Issue):119–128 (in Russian)
858. Goryachev YuM, Podchernyaeva IA, Siman NI, Sinelnikova VS, Timofeeva II, Burkhanov GS (1978) Work function of ZrC_x and NbC_x single crystals. *Sov Phys Tech Phys* 23(3):321–324
859. Khaenko BV (1978) Phase transitions in Me_2X -type carbides and nitrides of groups V and VI metals. *Powder Metall Met Ceram* 17(1):55–58
860. Kovalchenko MS, Bovkun GA, Tkachenko YuG, Ragozin IP (1983) Deformation properties of monocarbides of transition metals by the method of continuous impression of an indenter. *Powder Metall Met Ceram* 22(12):1034–1037
861. Moisy-Maurice V, De Novion CH, Lorenzelli N, Christensen AN (1983) Neutron scattering studies of the defect structures in TiC_{1-x} and NbC_{1-x} . In: Viswanadham RK, Rowcliffe DJ, Gurland J (eds) *Science of hard materials*. Plenum Press, New York, London, pp. 83–101
862. De Novion CH, Maurice V (1977) Order and disorder in carbides and nitrides. In: Proc. Int. symp. of the CNRS, Paris, 4–8 July 1977. *J Phys Colloq C-7* 38(12):211–220
863. Anderson JS (1984) Non-stoichiometric compounds: a critique of current structural views. *Proc Indian Acad Sci (Chem Sci)* 93(6):861–904

864. De Novion CH, Landesman JP (1985) Order and disorder in transition metal carbides and nitrides: experimental and theoretical aspects. *Pure Appl Chem* 57(10):1391–1402
865. Wesner D, Krummacher S, Strongin M, Carr R, Sham TK, Eberhardt W, Weng SL (1984) Synchrotron radiation studies of the formation of niobium carbide layers on niobium. *Phys Rev B* 30(2):855–860
866. Kojima I, Orita M, Miyazaki E (1985) Adsorption of O₂, CO and CH₃OH on NbC (100) and (111) single crystal surfaces by ultraviolet photoelectron spectroscopy. *Surf Sci* 160(1):153–163
867. Zhukov VP, Gubanov VA, Jarlborg T (1985) Study of energy-band structures, some thermomechanical properties and chemical bonding for a number of refractory metal carbides by the LMTO-ASA method. *J Phys Chem Solids* 46(10):1111–1116
868. Begrambekov LB, Nikolskii MV, Retnikov NN, Telkovskii VG, Fedorov YuV, Chuzhko RK, Sharapov VM (1986) Decomposition of metal carbides in the presence of ion irradiation in high-temperature conditions. *Atom Energy* 61(6):1004–1010
869. Matzke Hj (1989) Point defects and transport properties in carbides and nitrides. In: Johanneson Ø, Andersen AG, Kofstad P (eds) *Selected topics in high-temperature chemistry: defect chemistry of solids*. Elsevier, Amsterdam, New York, pp. 353–384
870. Simões JAM, Beauchamp JL (1990) Transition metal – hydrogen and metal – carbon bond strengths: the keys to catalysis. *Chem Rev* 90(4):629–688
871. Gupta SK, Gingerich KA (1981) Mass-spectrometric study of the stabilities of gaseous carbides of vanadium, niobium and molybdenum. *J Chem Phys* 74(6):3584–3590
872. Luo Y-R (2007) *Comprehensive handbook of chemical bond energies*. CRC Press, Boca Raton, London, New York
873. Simard B, Presunka PI, Loock HP, Bérces A, Launila O (1997) Laser spectroscopy and density functional calculations on niobium monocarbide. *J Chem Phys* 107(2):307–318
874. Hwang Y, Aizawa T, Hayami W, Otani S, Ishizawa Y (1992) Charge transfer between monolayer graphite and NbC single crystal substrates. *Solid State Commun* 81(5):397–400
875. Lindberg PAP, Johansson LI (1988) Work function and reactivity of some crystal faces of substoichiometric transition metal carbides. *Surf Sci* 194(1–2):199–204
876. MacInnes AN, Barron AR, Li JJ, Gilbert TR (1994) Reaction bonded refractory metal carbide/carbon composites. *Polyhedron* 13(8):1315–1327
877. Teresiak A, Kubsch H (1995) X-ray investigations of high energy ball milled transition metal carbides. *NanoStruct Mater* 6(5–8):671–674
878. Wang CC, Akbar SA, Chen W, Patton VD (1995) Electrical properties of high-temperature oxides, borides, carbides and nitrides. *J Mater Sci* 30:1627–1641
879. Shabanova NP, Krasnosvobotsev SI, Nozdrin VS, Pechen EV, Varlashkin AV, Antonenko SV, Zhabrev GI, Golovashkin AI (1996) Upper critical magnetic fields of NbC from clean to dirty limit. In: *Proc. 21st Int. conf. on low temperature physics*, Prague, 8–14 Aug 1996. *Czechoslovak J Phys* 46(S2):853–854
880. Singh M, Wiedemeier H (1997) Estimation of thermal expansion behaviour of some refractory carbides and nitrides. *J Mater Sci* 32(21):5749–5751
881. Eckerlin P, Kandler H (1971) *Structural data for elements and intermetallic phases*. Springer, Berlin
882. Williams WS (1997) Transition metal carbides, nitrides and borides for electronic applications. *J Miner Met Mater Soc (JOM)* 49(3):38–42
883. Rogovoi YuI (1999) Effect of structural vacancies on the nature of metal-metal and metal-carbon bonds in cubic monocarbides. *Powder Metall Met Ceram* 38(1–2):44–50
884. Johansson M (2000) Synthesis and characterization of NbC whiskers. *J Mater Sci Lett* 19:1571–1574
885. Hugosson HW, Jansson U, Johansson B, Eriksson O (2001) Phase stability diagrams of transition metal carbides, a theoretical study. *Chem Phys Lett* 333:444–450
886. Hugosson HW, Eriksson O, Jansson U, Johansson B (2001) Phase stabilities and homogeneity ranges in 4d transition metal carbides: a theoretical study. *Phys Rev B* 63(13):134108 (11 pp.)

887. Rempel SV, Gusev AI (2001) Phase equilibria in the Zr-Nb-C ternary system. *Russ J Phys Chem A* 75(9):1413–1419
888. Šimůnek A, Vackář J (2001) Correlation between core-level shift and bulk modulus in transition metal carbides and nitrides. *Phys Rev B* 64(23):2351151–2351156
889. Rempel SV, Gusev AI (2002) Surface segregation of ZrC from a carbide solid solution. *Phys Solid State* 44(1):68–74
890. Acchar W, Wolff DMB, Dantas AC da S (2003) Sintering behaviour of alumina – niobium carbide ceramics from polymer-filler mixtures. *Mater Sci Forum* 416–418:499–504
891. Gueorguiev GK, Pacheco JM (2003) Shapes of cage-like metal clusters: first principles calculations. *Phys Rev B* 68(24):2414011–2414014
892. Gusev AI (2003) Analysis of surface segregation and solid-phase decomposition of substitutional solid solutions. *Dokl Phys Chem* 392(1–3):235–239
893. Siethoff H (2003) Correspondence of the plasticity of rocksalt structure ceramics and tetrahedrally coordinated semiconductors. *J Appl Phys* 94(5):3128–3134
894. Hugosson HW, Eriksson O, Jansson U, Ruban AV, Souvatzis P, Abrikosov IA (2004) Surface energies and work functions of the transition metal carbides. *Surf Sci* 557(1–3):243–254
895. Maksimov EG, Magnitskaya MV, Ebert SV, Savrasov SYu (2004) *Ab initio* calculations of the superconducting transition temperature for NbC at various pressures. *JETP Lett* 80(8):548–551
896. Ávila-Brande D, Katcho NA, Urones-Garrote E, Gómez-Herrero A, Landa-Cánovas AR, Otero-Díaz LC (2006) Nano-structured carbon obtained by chlorination of NbC. *Carbon* 44:753–761
897. Gusev AI (2006) Short-range order and diffuse scattering in nonstoichiometric compounds. *Phys Usp* 49(7):693–718
898. Li D, Li WF, Ma S, Zhang ZD (2006) Electronic transport properties of NbC(C)-C nanocomposites. *Phys Rev B* 73(19):1934021–1934024
899. Frisk K (2008) Thermodynamic modelling of multicomponent cubic Nb, Ti and V carbides/carbonitrides. *Calphad* 32:326–337
900. Wang J, Wang J, Zhou Y, Lin Z, Hu C (2008) *Ab initio* study of polymorphism in layered ternary carbides M_4AlC_3 ($M = V, Nb$ and Ta). *Scripta Mater* 58:1043–1046
901. Wang J, Wang J, Zhou Y, Lin Z, Hu C (2008) Phase stability, electronic structure and mechanical properties of ternary layered carbide Nb_4AlC_3 : an *ab initio* study. *Acta Mater* 56:1511–1518
902. Kim B-R, Moon M-S, Woo K-D, Shon I-J (2009) Properties and rapid consolidation of binderless nanostructured NbC by pulsed current activated sintering. *Electron Mater Lett* 5(3):119–122
903. Wan D-T, He L-F, Zheng L-L, Zhang J, Bao Y-W, Zhou Y-C (2010) A new method to improve the high-temperature mechanical properties of Ti_3SiC_2 by substituting Ti with Zr, Hf or Nb. *J Am Ceram Soc* 93(6):1749–1753
904. Jiang X, Zhao J, Jiang X (2011) Correlation between hardness and elastic moduli of the covalent crystals. *Comput Mater Sci* 50(7):2287–2290
905. Lanin AG, Fedik II (2011) Selecting and using materials for a nuclear rocket engine reactor. *Phys Usp* 54(3):305–318
906. Jha R, Awana VPS (2012) Vacuum encapsulated synthesis of 11.5 K NbC superconductor. *J Supercond Nov Magn* 25:1421–1425
907. Lanin AG (2012) Effect of residual stresses on the strength of ceramic materials (review). *Russ Metall* (4):307–322
908. Ordanyan SS, Orekhov AN, Vikhman SV (2012) Interaction of W_2B_5 with $Me^{IV,V}C$ carbides. *Russ J Non-Ferr Met* 55(1):91–94
909. Khazaei M, Arai M, Sasaki T, Chung C-Y, Venkataramanan NS, Estili M, Sakka Y, Kawazoe Y (2013) Novel electronic and magnetic properties of two-dimensional transition metal carbides and nitrides. *Adv Funct Mater* 23(17):2185–2192

910. Rahim GPA, Rodríguez JA (2013) Structural and electronic properties of ScC and NbC: a first principles study. *Solid State Phenom* 194:276–279
911. Kondrashov AI (1974) Reactions of lanthanum hexaboride with carbides and borides of refractory metals. *Powder Metall Met Ceram* 13(11):911–913
912. Naguib M, Bentzel GW, Shah J, Halim J, Caspi EN, Lu J, Hultman L, Barsoum MW (2014) New solid solution MAX phases: $(\text{Ti}_{0.5}\text{V}_{0.5})_3\text{AlC}_2$, $(\text{Nb}_{0.5}\text{V}_{0.5})_2\text{AlC}$, $(\text{Nb}_{0.5}\text{V}_{0.5})_4\text{AlC}_3$ and $(\text{Nb}_{0.8}\text{Zr}_{0.2})_2\text{AlC}$. *Mater Res Lett* 2(4):233–240
913. Zheng L, Wang J, Lu X, Li F, Wang J, Zhou Y (2010) $(\text{Nb}_{0.5}\text{Ti}_{0.5})_5\text{AlC}_4$: a new layered compound belonging to MAX phases. *J Am Ceram Soc* 93(10):3068–3071
914. Salama I, El-Raghy T, Barsoum MW (2002) Synthesis and mechanical properties of Nb_2AlC and $(\text{Ti}, \text{Nb})_2\text{AlC}$. *J Alloy Compd* 347:271–278
915. Hu C, Li F, Zhang J, Wang J, Wang J, Zhou Y (2007) Nb_4AlC_3 : a new compound belonging to the MAX phases. *Scripta Mater* 57:893–896
916. Kizuka T, Koizumi H (2014) Interface structure of niobium carbide – encapsulating carbon nanocapsules studied by high-resolution transmission electron microscopy. *J Nanosci Nanotechnol* 14(4):3228–3232
917. Kurlov AS, Bobrikov IA, Balagurov AM, Gusev AI (2014) Neutron diffraction study of nanocrystalline $\text{NbC}_{0.93}$ powders and the anisotropy of deformation distortions. *JETP Lett* 100(10):629–634
918. Sun D, Hu Q, Chen J, Zhou A (2014) First principles calculations of the relative stability, structure and electronic properties of two-dimensional metal carbides and nitrides. In: Proc. 8th Int. conf. on high-performance ceramics (CICC 2013), Chongqing, China, 4–7 Nov 2013. *Key Eng Mater* 602–603:527–531
919. Zhang H, Hu T, Wang X, Li Z, Hu M, Wu E, Zhou Y (2015) Discovery of carbon vacancy ordering in $\text{Nb}_4\text{AlC}_{3-x}$ under the guidance of first principles calculations. *Sci Rep* 5:14192 (10 pp.)
920. Yang J, Naguib M, Ghidui M, Pan L-M, Gu J, Nanda J, Halim J, Gogotsi Y, Barsoum MW (2016) Two-dimensional Nb-based M_4C_3 solid solutions (MXenes). *J Am Ceram Soc* 99(2):660–666
921. Yate L, Coy LE, Wang G, Beltrán M, Díaz-Barriga E, Saucedo EM, Ceniceros MA, Zaleski K, Llarena I, Möller M, Ziolo RF (2014) Tailoring mechanical properties and electrical conductivity of flexible niobium carbide nanocomposite thin films. *RSC Adv* 4:61355–61362
922. Zou Z, Fu L, Song X, Zhang Y, Liu Z (2014) Carbide-forming groups IVB-VIB metals: a new territory in the periodic table for CVD growth of graphene. *Nano Lett* 14:3832–3839
923. Anasori B, Xie Y, Beidaghi M, Lu J, Hosler BC, Hultman L, Kent PRC, Gogotsi Y, Barsoum MW (2015) Two-dimensional ordered double transition metals carbides (MXenes). *ACS Nano* 9(10):9507–9516
924. Mashtalir O, Lukatskaya MR, Zhao M-Q, Barsoum MW, Gogotsi Y (2015) Amine-assisted delamination of Nb_2C MXene for Li-ion energy storage devices. *Adv Mater* 27(23):3501–3506
925. Halim J, Cook KM, Naguib M, Eklund P, Gogotsi Y, Rosen J, Barsoum MW (2015) X-ray photoelectron spectroscopy of select multi-layered transition metal carbides (MXenes). *Appl Surf Sci* 362:406–417
926. Chauhan M, Gupta DC (2015) Electronic, mechanical, phase transition and thermo-physical properties of TMC (TM = V, Nb and Ta): high pressure *ab initio* study. *Phase Transit* 88(12):1193–1212
927. Kurlov AS, Gusev AI (2015) Milling of nonstoichiometric niobium carbide powder to a nanocrystalline state. *Inorg Mater* 51(1):29–37
928. Naguib M, Come J, Dyatkin B, Presser V, Taberna P-L, Simon P, Barsoum MW, Gogotsi Y (2012) MXene: a promising transition metal carbide anode for lithium-ion batteries. *Electrochem Commun* 16(1):61–64
929. Salehinia I, Shao S, Wang J, Zbib HM (2015) Interface structure and the inception of plasticity in Nb/NbC nanolayered composites. *Acta Mater* 86:331–340

930. Yu X-X, Weinberger CR, Thompson GB (2016) *Ab initio* investigations of the phase stability in group IVB and VB transition metal carbides. *Comput Mater Sci* 112:318–326
931. Wang Q, German KE, Oganov AR, Dong H, Feya OD, Zubavichus YaV, Murzin VYu (2016) Explaining stability of transition metal carbides – and why TeC does not exist. *RSC Adv* 6(20):16197–16202
932. Peng Y, Zhou P, Bu M, Zhang W, Du Y (2016) A thermodynamic evaluation of the C-Cr-Nb system. *Calphad* 53:10–19
933. Hardy GF, Hulm JK (1954) The superconductivity of some transition metal compounds. *Phys Rev* 93(5):1004–1016
934. Piper J (1964) Electrical properties of some transition metal carbides and nitrides. Technical Report TR-C-21, Contracts DA-30-069-ORD-2787, NP-13944. Union Carbide Corporation Research Institute, Tarrytown, New York, pp. 1–34
935. Neuberger MS, Grigsby DL, Veazie WH, Jr (1972) Niobium alloys and compounds. Springer Science, IFI/Plenum Data Corporation, New York, Washington
936. Li B, Xu G-Y, Sun E-Y, Huang Y, Becher PF (1998) Synthesis and morphology of niobium monocarbide whiskers. *J Am Ceram Soc* 81(6):1689–1691
937. Arabei BG, Levinskii YuV, Markov YuM, Portnoi KI (1978) Effect of alloying of uranium carbide on its interaction with carbon. *Atom Energy* 44(3):288–290
938. Balankin SA, Loshmanov LP, Skorov DM, Sokolov VS (1979) Raschet energii obrazovaniya vakansii v fazakh vnedreniya po dannym mekhanicheskikh svoistv (Calculation of vacancy formation energy in interstitial phases through mechanical properties data). In: Sobolev ND, Beskorovainyi NM, Morozov EM, Kulbakh AA, Markochev VM, Sapunov VT (eds) *Fizika i mekhanika deformatsii i razrusneniya* (Physics and mechanics of deformation and fracture), Vol. 7. Atomizdat, Moscow, pp. 8–12 (in Russian)
939. Fedorov ÉM, Andrievskii RA (1979) Thermodynamic stability of carbide solid solutions. *Inorg Mater* 15(3):357–360
940. Godin YuG, Suchkov II, Yevstyukhin AI (1979) Struktura splavov sistemy UC-ZrC-NbC (Structure of UC-ZrC-NbC alloys). In: Emelyanov VS, Yevstyukhin AI (eds) *Metallurgiya i metallovedenie chistyykh metallov* (Metallurgy and metallography of pure metals), Vol. 13. Atomizdat, Moscow, pp. 77–84 (in Russian)
941. Lanin AG, Zubarev PV, Vlasov KP (1992) Osnovnye kharakteristiki materialov ispolzuemykh v teplovydelayayushchikh sborkakh vysokotemperaturnykh gazoohlazhdaemykh reaktorov (Main characteristics of materials for fuel elements of gas cooled high-temperature reactors). In: Volkova YuV, Porodnova VI (eds) *Proc. 3rd interindustry conf. on reactor materials science*, Dimitrovgrad, Russian Federation, 27–30 Oct 1992, pp. 40–41 (in Russian)
942. Lanin AG, Zubarev PV, Vlasov KP (1992) Mechanical and thermophysical properties of materials in HTGR fuel bundles. *Atom Energy* 74(1):40–44
943. Dmitrieva GP, Razumova NA, Shurin AK, Khandros EL (1986) Phase equilibria in alloys of the Ni-TiC-MeC (Me: Zr, Hf, Nb, Ta) systems. *Russ Metall* (1):210–215
944. Ogorodnikov VV, Rogovoi YuI (1992) Simulating point defects in cubic monocarbides. *Inorg Mater* 28(5):763–767
945. Gusev AI, Rempel AA, Shveikin GP (1997) Nestekhiometriya i radiatsionnaya stoikost konstruksionnykh materialov (analiz dannyykh) (Nonstoichiometry and structural materials resistance to radiation damage (data analysis)). *Doklady AN SSSR* 357(4):490–494 (in Russian)
946. Cherkashenko VM, Nazarova SZ, Gusev AI, Ivanovskii AL (2001) Electronic structure, chemical bonding and properties of binary carbides $M_xM_yC_z$ in the crystalline and molecular states: XES, XPS and quantum-chemical studies. *J Struct Chem* 42(6):1002–1024

947. Knight TW, Anghaie S (2001) Fuels for space nuclear power systems. 1. Tri-carbide nuclear fuel processing and characterization for space nuclear applications. In: Proc. American nuclear society annual meeting, Milwaukee, Wisconsin, 17–21 June 2001. *Trans Am Nucl Soc* 84:149–150
948. Wang J, Zhou Y (2009) Recent progress in theoretical prediction, preparation and characterization of layered ternary transition metal carbides. *Annu Rev Mater Res* 39:415–443
949. Yoshitake M (2012) Examination of work function of transition metal carbides and nitrides. *J Vac Soc Jpn* 55(7):349–353 (in Japanese)
950. Yoshitake M (2014) Generic trend of work functions in transition metal carbides and nitrides. *J Vac Sci Technol A* 32(6):061403
951. Ordanyan SS, Udalov YuP (2015) On the structure of the $\text{SiC-Mo(W)Si}_2\text{-Me}^d\text{B}_2$ systems and prospective development of refractory materials based on these systems. In: Ordanyan SS (ed) *Aktualnye problemy tekhnologii proizvodstva sovremennykh keramicheskikh materialov* (Current problems of the modern technology of ceramic materials). Polytechnic University Publishing House, Saint Petersburg, pp. 7–16 (in Russian)
952. Konyashin I, Lengauer W (2016) Sintering mechanisms of functionally graded cemented carbides. *Mater Sci Forum* 835:116–198
953. Zhilyaev VA, Patravok EI (2016) Influence of alloying titanium carbonitride by transition metals of groups IV–VI on the interaction with nickel melt. *Russ J Non-Ferr Met* 57(2):141–147
954. Gu J, Pan L, Yang J, Yu L, Zhang H, Zou W, Xu C, Hu C, Qiu T (2016) Mechanical properties and oxidation behaviour of Ti-doped Nb_4AlC_3 . *J Eur Ceram Soc* 36:1001–1008
955. Hua G, Li D (2015) A first principles study on the mechanical and thermodynamic properties of $(\text{Nb}_{1-x}\text{Ti}_x)\text{C}$ complex carbides based on virtual crystal approximation. *RSC Adv* 5(125):103686–103694
956. Lekakh SN, Medvedeva NI (2015) *Ab initio* study of Fe adsorption on the (001) surface of transition metal carbides and nitrides. *Comput Mater Sci* 106:149–154
957. Khazaei M, Arai M, Sasaki T, Ranjbar A, Liang Y, Yunoki S (2015) OH-terminated two-dimensional transition metal carbides and nitrides as ultra-low work function materials. *Phys Rev B* 92(7):075411 (10 pp.)
958. Kostenko MG, Rempel AA, Sharf SV, Lukoyanov AV (2015) Short-range order in disordered transition metal oxides, carbides and nitrides with the B1 structure. *Phys Solid State* 57(4):637–651
959. Rudy E, Windisch S, Brukl CE (1968) Revision of the vanadium-carbon and niobium-carbon systems. *Planseeber Pulvermetall* 16(1):3–33
960. Kikuchi M, Nagakura S, Oketani S (1971) Crystal structures of transition metal carbides. *J Iron Steel Inst Jpn* 57(6):1009–1053 (in Japanese)
961. Rempel AA, Gusev AI, Zhdanov YuI (1987) Statistical crystal lattice distortion in disordered niobium carbide. *Inorg Mater* 23(1):48–51
962. Gusev AI (1989) Structural stability boundaries for nonstoichiometric compounds. *Phys Stat Sol A* 111(2):443–450
963. Gusev AI (1991) Disorder and long-range order in non-stoichiometric interstitial compounds. *Phys Stat Sol B* 163(1):17–54
964. Gusev AI, Rempel AA (1997) Phase diagrams of metal-carbon and metal-nitrogen systems and ordering in strongly nonstoichiometric carbides and nitrides. *Phys Stat Sol A* 163(2):273–304
965. Li PG, Lei M, Tang WH (2008) Route to transition metal carbide nanoparticles through cyanamide and metal oxide. *Mater Res Bull* 43:3621–3626
966. Gusev AI (1993) Vaporization of cubic carbides of vanadium, niobium and tantalum. *High Temp* 31(2):248–254
967. Sasaki N, Kubo K, Asano M (1974) Thermal ion emission from some transition metal carbides heated on graphite filament. *J Chem Phys* 60(4):1545–1557

968. Naumenko VYa (1970) Preparation of carbides of the IV-V groups transition metals in their homogeneity regions. *Powder Metall Met Ceram* 9(10):799–801
969. Carlsson M, Johnsson M, Nygren M (1999) Synthesis and characterization of $Ti_{0.33}Ta_{0.33}Nb_{0.33}C$ and $Ti_{0.33}Ta_{0.33}Nb_{0.33}C_xN_{1-x}$ whiskers. *J Am Ceram Soc* 82(8):1969–1976
970. Johnsson M (2004) Synthesis of boride, carbide and carbonitride whiskers. *Solid State Ionics* 172:365–368
971. Ishizawa Y, Otani S, Nozaki H, Tanaka T (1992) Carbon-vacancy concentration dependences of electrical properties of NbC_x single crystals. *J Phys Condens Matter* 4:8593–8598
972. Koide T, Shidara T, Fukutani H, Fujimori A, Miyahara T, Kato H, Otani S, Ishizawa Y (1990) Optical study of the stoichiometry-dependent electronic structure of TiC_x , VC_x and NbC_x . *Phys Rev B* 42(8):4979–4995
973. Nan CW, Yuan RZ, Yang ZL (1991) Percolation phenomena in niobium-doped TiC_{1-x} . *Mater Sci Eng B* 7:283–286
974. Samsonov GV, Upadhyaya GS, Nemchenko VF (1969) Temperature dependence of the electrical resistivity and thermal e.m.f. of niobium and titanium carbide alloys in their homogeneity range. *High Temp* 7(3):408–410
975. Min XM, Cai KF, Nan CW, Yuan RZ (1996) Structure, properties and quantum chemistry studies on non-stoichiometric compounds of $(Nb_yTi_{1-y})C_x$. *Ceram Int* 22:193–196
976. Neylon MK, Choi S, Kwon H, Curry KE, Thompson LT (1999) Catalytic properties of early transition metal nitrides and carbides: *n*-butane hydrogenolysis, dehydrogenation and isomerisation. *Appl Catal A* 183:253–263
977. Xiao D-H, He Y-H, Luo W-H, Song M (2009) Effect of VC and NbC additions on microstructure and properties of ultra-fine WC-10Co cemented carbides. *Trans Nonferrous Met Soc China* 19:1520–1525
978. Morton CW, Wills DJ, Stjernberg K (2005) The temperature ranges for maximum effectiveness of grain growth inhibitors in WC-Co alloys. *Int J Refract Met Hard Mater* 23:287–293
979. Taylor KA (1995) Solubility products for titanium, vanadium and niobium carbides in ferrite. *Scripta Metall Mater* 32(1):7–12
980. Raghavan V (1996) C-Fe-Mn-Nb (carbon-iron-manganese-niobium) system. In: *Phase diagrams of quaternary iron alloys*. Indian Institute of Metals, Calcutta, pp. 229–231
981. Khvan AV, Hallstedt B (2012) Thermodynamic description of the Fe-Mn-Nb-C system. *Calphad* 39:62–69
982. Raghavan V (2013) Phase diagram updates and evaluations of the Al-Fe-P-Zn, Al-Fe-V-Zn, C-Fe-Mn-Nb and C-Fe-N-Ti-V systems. *J Phase Equilib Diff* 34(3):244–250
983. Gorbachev II, Popov VV (2011) Thermodynamic simulation of the Fe-V-Nb-C-N system using the CALPHAD method. *Phys Met Metallogr* 111(5):495–502
984. Barsoum MW, Salama I, El-Raghy T, Golczewski J, Porter WD, Wang H, Seifert HJ, Aldinger F (2002) Thermal and electrical properties of Nb_2AlC , $(Ti,Nb)_2AlC$ and Ti_2AlC . *Metall Mater Trans A* 33:2775–2779
985. Zainulin YuG, Alyamovskii SI, Shveikin GP, Shchetnikov EN, Geld PV (1969) Vzaimodeistvie kubicheskikh karbidov titana, vanadiya, niobiya i tantala s berilliem (Interaction of cubic titanium, vanadium, niobium and tantalum carbides with beryllium). *Zh Prikl Khim* 42(3):693–695 (in Russian)
986. Ivanovskii AI, Anisimov VI, Kurmaev ÉZ, Gubanov VA (1988) Electronic structure of titanium and niobium carbides with beryllium impurity. *Theor Exp Chem* 24(3):332–337
987. Ivanovskii AL, Novikov DL, Anisimov VI, Gubanov VA (1988) The influence of structural defects on the electronic properties of interstitial alloys. III. Non-metal substitutional impurities. *J Phys Chem Solids* 49(5):487–497
988. Ivanovskii AL, Anisimov VI, Lichtenstein AI, Gubanov VA (1988) The influence of structural defects on the electronic properties of interstitial alloys. II. Metal substitutional impurities. *J Phys Chem Solids* 49(5):479–486

989. Samsonov GV, Vitryanyuk VK, Voronkin MA, Lomakin GK (1973) Effect of niobium carbide on the properties of tungsten-free hard alloys. *Powder Metall Met Ceram* 12(9):757–760
990. Park S, Kang YJ, Kwon HJ, Kang S (2006) Synthesis of $(\text{Ti}, \text{M}_1, \text{M}_2)(\text{CN})$ – Ni nanocrystalline powders. *Int J Refract Met Hard Mater* 24:115–121
991. Kellie JLF, Davies P, Retelsdorf HJ (1984) Production of zirconium hafnium and zirconium niobium carbides. *Int J Refract Met Hard Mater* 3(3):136–141
992. Misra PS, Upadhyaya GS (1984) Bonding in sintered aluminium – refractory carbides composites – an electronic and microstructural evidence. In: Upadhyaya GS (ed) *Sintered metal-ceramic composites*. Elsevier Science, Amsterdam, pp. 255–257
993. Kumar BVM, Basu B, Kang S, Ramkumar J (2006) Erosion wear behaviour of TiCN-Ni cermets containing secondary carbides (WC/NbC/TaC). *J Am Ceram Soc* 89(12):3827–3831
994. Kumar BVM, Balasubramaniam R, Basu B (2007) Electrochemical behaviour of TiCN-Ni-based cermets. *J Am Ceram Soc* 90(1):205–210
995. Kumar BVM, Basu B (2008) Fretting wear properties of TiCN-Ni cermets: influence of load and secondary carbide addition. *Metall Mater Trans A* 39:539–550
996. Liu N, Chen M, Xu Y, Zhou J, Shi M (2005) Effect of various carbides on the wettability in Ni/Ti(C, N) system. *J Wuhan Univ Technol* 20(3):35–39
997. Borrell A, Salvador MD, Garsía-Rocha V, Fernández A, Chicardi E, Gotor FJ (2012) Spark plasma sintering of $\text{Ti}_y\text{Nb}_{1-y}\text{C}_x\text{N}_{1-x}$ monolithic ceramics obtained by mechanically induced self-sustaining reaction. *Mater Sci Eng A* 543:173–179
998. Marinenko SYu, Bodrova LG, Kramar GM, Lazaryuk VV (2009) Special features of structure formation in polycarbide based hard alloys. *J Superhard Mater* 31(2):89–96
999. Ettmayer P, Kolaska H, Lengauer W, Dreyer K (1995) Ti(C,N) cermets – metallurgy and properties. *Int J Refract Met Hard Mater* 13:343–351
1000. Qi F, Kang S (1998) A study on microstructural changes in Ti(C, N)-NbC-Ni cermets. *Mater Sci Eng A* 251:276–285
1001. Tsurekawa S, Nakashima M, Murata A, Kurishita H, Yoshinaga H (1991) Solid solution hardening of titanium carbide by niobium and zirconium at high temperatures. *J Jpn Inst Met* 55(4):390–397 (in Japanese)
1002. Ehm VT, Tashmetov MYu (1992) Структуры упорядочения и фазовые превращения в карбидках $\text{Ti}_{1-y}\text{Ta}_y\text{C}_{0.63}$ и $\text{Ti}_{1-z}\text{Nb}_z\text{C}_{0.6}$ (Ordering structures and phase transformations in $\text{Ti}_{1-y}\text{Ta}_y\text{C}_{0.63}$ and $\text{Ti}_{1-z}\text{Nb}_z\text{C}_{0.6}$ carbides). *Fiz Met Metalloved* (3):112–116 (in Russian)
1003. Dmitrieva GP, Cherepova TS (1992) Phase equilibria and properties of alloys of Co(Ni)-TiC-NbC systems. *Russ Metall* (6):136–137
1004. Kobashi M, Harata M, Choh T (1993) Dispersion behaviour of several carbides into molten aluminium and mechanical properties of TiC/Al composite. *J Jpn Inst Light Met* 43(10):522–527 (in Japanese)
1005. Grigorev ON, Chugunova SI, Shatokhin AM, Yaroshenko VP (1981) Mechanical properties of silicon nitride composite materials. *Powder Metall Met Ceram* 20(7):502–505
1006. Gogotsi YuG (1994) Review. Particulate silicon nitride – based composites. *J Mater Sci* 29:2541–2556
1007. Branagan DJ, Kramer MJ, McCallum RW (1996) Transition metal carbide formation in the $\text{Nd}_2\text{Fe}_{14}\text{B}$ system and potential as alloying additions. *J Alloy Compd* 244:27–39
1008. Cai KF, Nan CW, Yuan RZ, Min XM (1996) The flexural strength at high temperature and oxidation behaviour of (Nb,Ti)C-Ni composite. *Ceram Int* 22:167–170
1009. Cai KF, Nan CW, Min XM (1997) The microstructure of (Nb,Ti)C-35Ni(Y_2O_3) cermet. *Mater Res Bull* 32(10):1327–1332
1010. Kitchin JR, Nørskov JK, Barteau MA, Chen JG (2005) Trends in the chemical properties of early transition metal carbide surface: a density functional study. *Catal Today* 105:66–73
1011. Huang SG, Vanmeensel K, Mohrbacher H, Woydt M, Vleugels J (2015) Microstructure and mechanical properties of NbC-matrix hardmetals with secondary carbide addition and different metal binders. *Int J Refract Met Hard Mater* 48:418–426

1012. Woydt M, Mohrbacher H (2014) The tribological and mechanical properties of niobium carbides (NbC) bonded with cobalt or Fe₃Al. *Wear* 321:1–7
1013. Gladyshevskii EI, Popova NM, Fedorov TF (1963) Mutual solubility of zirconium, niobium and hafnium carbides. *Russ J Inorg Chem* 8(8):1040–1041
1014. Emmerlich J, Music D, Houben A, Dronskowski R, Schneider JM (2007) Systematic study on the pressure dependence of M₂AlC phases (M = Ti, V, Cr, Zr, Nb, Mo, Hf, Ta, W). *Phys Rev B* 76:224111
1015. Ivanovskii AL, Gusev AI, Shveikin GP (1996) Kvantovaya khimiya v materialovedenii: troinye karbidy i nitridy perekhodnykh metallov i elementov IIIb, IVb podgrupp (Quantum chemistry in materials science: ternary carbides and nitrides of transition metals and subgroup IIIb, IVb elements). *Uralskoe Otdelenie Rossiiskoi Akademii Nauk, Yekaterinburg* (in Russian)
1016. Barsoum MW (2000) The M_{N+1}AX_N phases: a new class of solids. *Prog Solid St Chem* 28:201–281
1017. Shurin AK, Dmitrieva GP, Razumova NA (1988) Phase equilibria in ternary nickel-carbide alloys. *Russ Metall* (6):63–69
1018. Fedorov TV, Popova NM, Gladyshevskii EI (1965) Ternary Hf-Nb-C, Zr-Nb-C and Ti-Nb-C systems. *Russ Metall* (3):72–76 (in Russian)
1019. Naguib M, Halim J, Lu J, Cook KM, Hultman L, Gogotsi Yu, Barsoum MW (2013) New two-dimensional niobium and vanadium carbides as promising materials for Li-ion batteries. *J Am Chem Soc* 135:15966–15969
1020. Toth LE, Ishikawa M, Chang YA (1968) Low temperature heat capacity of superconducting niobium and tantalum carbides. *Acta Mater* 16(9):1183–1187
1021. Gusev AI, Rempel AA (2001) Nestekhiometriya, besporyadok i poryadok v tverdom tele (Nonstoichiometry, disorder and order in solids). *Ural Division of the Russian Academy of Sciences, Yekaterinburg* (in Russian)
1022. Gusev AI (2007) Nestekhiometriya, besporyadok, blizhnii i dalnii poryadok v tverdom tele (Nonstoichiometry, disorder short-range and long-range order in solids). *Nauka Fizmatlit, Moscow* (in Russian)
1023. Kurlov AS, Gusev AI (2014) High-energy milling of nonstoichiometric carbides: effect of nonstoichiometry on particle size of nanopowders. *J Alloy Compd* 582:108–118
1024. Glushko VP, Gurvich LV, eds (1982) *Termodinamicheskie svoystva individualnykh veshchestv* (Thermodynamic properties of individual substances), Vol. IV, Parts 1–2. *Nauka, Moscow* (in Russian)
1025. Schneider A, Falat L, Sauthoff G, Frommeyer G (2003) Constitution and microstructures of Fe-Al-M-C (M = Ti, V, Nb, Ta) alloys with carbides and Laves phase. *Intermetallics* 11:443–450
1026. Falat L, Schneider A, Sauthoff G, Frommeyer G (2005) Mechanical properties of Fe-Al-M-C (M = Ti, V, Nb, Ta) alloys with strengthening carbides and Laves phase. *Intermetallics* 13:1256–1262
1027. Burykina AL, Struk LI, Manzhumet KV (1967) Stability of refractory compounds in fused basalt. *Powder Metall Met Ceram* 6(2):122–123
1028. Barantseva IG, Paderno VN, Paderno YuB (1967) Some physical properties of alloys of the systems ZrC-NbC and TaC-HfC. *Powder Metall Met Ceram* 6(2):139–141
1029. Ohtani H, Hasebe M, Nishizawa T (1989) Calculation of the Fe-C-Nb ternary phase diagram. *Calphad* 13(2):183–204
1030. Senczyk D (1984) The lattice parameters of MeC-type carbides, nitrides and carbonitrides of transition metals of IV and V groups of the periodic system. In: *Proc. 11th conf. on applied crystallography*, Vol. 1. Kozubnik, Poland, pp. 234–240
1031. Touloukian YS, Kirby RK, Taylor RE, Lee TYR (1977) *Thermophysical properties of matter*, Vol. 13 – Thermal expansion – nonmetallic solids. *IFI/Plenum Data Corporation, New York, Washington*
1032. Krikorian OH (1960) Thermal expansion of high-temperature materials. Report UCRL-6132. *University of California Radiation Laboratory, Berkeley, California*, pp. 1–7

1033. Pessall N, Hulm JK, Walker MS (1967) Superconducting behaviour of alloyed interstitial compounds with the NaCl crystal structure. Technical Report AFML-TR-67-168, Contract AF33(615)-2729. Westinghouse Research Laboratories, Pittsburgh, Pennsylvania, pp. 1–14
1034. Woydt M, Mohrbacher H, Vleugels J, Huang S (2017) Tailoring the functional properties of niobium carbide. In: Ohji T, Halbig M, Moon KI, Singh M (eds) Advanced processing and manufacturing technologies for nanostructured and multifunctional materials III. Proc. 40th Int. conf. on advanced ceramics and composites (ICACC 2016), Daytona Beach, Florida, 24–29 Jan 2016. Ceram Eng Sci Proc 37(5):101–113
1035. Giorgi AL, Szklarz EG, Storms EK, Bowman AL (1963) Investigation of Ta₂C, Nb₂C and V₂C for superconductivity. Phys Rev 129(4):1524–1525
1036. Samsonov GV (1965) Superconductivity of refractory compounds. In: Savitskii EM, Baron VV (eds) Metal science and physics of superconductors. Nauka, Moscow, pp. 65–71 (in Russian)
1037. Soloninin AV, Skripov AV, Stepanov AP, Kozhanov VN, Rempel AA, Gusev AI (2002) Spin-lattice relaxation of ¹³C and ¹H in hydrogenated niobium and titanium carbides. Phys Met Metallogr 94(1):40–46
1038. Korsunskii MI, Genkin YaE, Lifshits VG (1974) An X-ray spectral study of some compounds of niobium and carbon. In: Samsonov GV (ed) Refractory carbides. Consultants Bureau, New York, London, pp. 175–178
1039. Vainstein EE, Zhurakovskii EA (1959) O nekotorykh rezultatakh rentgenospektralnogo issledovaniya fizicheskoi prirody faz vnedreniya (On some results of X-ray spectral study of physical nature of interstitial phases). Zh Neorg Khim 4(1):245–246 (in Russian)
1040. Zhurakovskii EA (1969) X-ray K_α-emission band of carbon in the monocarbides of transition metals belonging to groups IV and V. Phys Dokl 14:168–172
1041. Zhurakovskii EA, Vasilenko NN (1974) The state of the carbon atom in transition metal carbides. In: Samsonov GV (ed) Refractory carbides. Consultants Bureau, New York, London, pp. 179–185
1042. Khrustalev BA, Rakov AM (1968) Izluchatelnye svoistva tantala, molibdena, niobiya, grafita i karbida niobiya pri vysokikh temperaturakh (Emissivity of tantalum, molybdenum, niobium, graphite and niobium carbide at high temperatures). In: Kutateladze SS (ed) Teploobmen, gidrodinamika i teplofizicheskie svoistva veshchestv (Thermoexchange, hydrodynamics and thermophysical properties of matters). Nauka, Moscow, pp. 198–205 (in Russian)
1043. Kammori Ō, Sato K, Kurosawa F (1968) Infrared absorption spectra of metal carbides, nitrides and sulfides. Jpn Analyst 17(10):1270–1273 (in Japanese)
1044. Fomenko WS, Lawrenko WA, Ochremtschuk LN, Podtschernjaeva IA, Prozenko TG, Samsonow GW (1971) Korrelation von Abtrennungsarbeit von Übergangsmetall Karbide in Homogenitätsbereich mit Oberflächenrekombination von Wasserstoffatomen (Correlation of work function of transition metal carbides in homogeneity region with surface recombination of hydrogen atoms). Rev Int Hautes Temp 8(3–4):315–318 (in German)
1045. Mackie WA, Cabe GL, Southall LA, Xie TB, McClelland PH (2001) Materials deposition and emission characteristics of NbC/Nb field emitter array cathodes. In: Proc. 14th IEEE Int. vacuum microelectronics conf. (IVMC), Davis, California, 12–16 Aug 2001. Institute of Electrical and Electronics Engineers, New York, pp. 97–98
1046. Mackie WA, Southall LA, Xie TB, Cabe GL, McClelland PH (2003) Emission characteristics of NbC/Nb field emitter array cathodes. J Vac Sci Technol B 21(1 Spec):422–426
1047. Charbonnier F, Southall L, Mackie WA (2003) Emission characteristics of NbC/Nb field emitters. In: Proc. 16th Int. vacuum microelectronics conf. (IVMC 2003), Osaka, Japan, 07–11 July 2003. Institute of Electrical and Electronics Engineers, New York, pp. 5–6

1048. Hannink RHJ, Kohlstedt DL, Murray MJ (1971) Brittle-region slip systems in the transition metal carbides. *Phys Stat Sol A* 6:K25–K28
1049. Brookes CA, O'Neill JB, Redfern BAW (1971) Anisotropy in hardness of single crystals. *Proc R Soc Lond A* 322(1548):73–88
1050. Sirdeshmukh DB, Sirdeshmukh L, Subhadra KG (2006) *Micro- and macro-properties of solids*. Springer, Berlin, Heidelberg
1051. Meerson GA, Umanskii YaS (1953) O tverdsti tugoplavkikh karbidov (On the hardness of refractory carbides). *Izv Sektora Fiz Khim Analiza AN SSSR* 22:104–110 (in Russian)
1052. Plendl JN, Gielisse PJ (1962) Hardness of nonmetallic solids on an atomic basis. *Phys Rev* 125(3):828–832
1053. Miyoshi A, Hara A (1965) High-temperature hardness of WC, TiC, TaC, NbC and their mixed carbides. *J Jpn Soc Powder Metall* 12(2):78–84
1054. Kashtalyan YuA (1970) Kharakteristiki uprugosti materialov pri vysokikh temperaturakh (Elasticity characteristics of materials at high temperature). *Naukova Dumka, Kyiv* (in Russian)
1055. Ulrickson M (1979) Material studies related to TFTR limiters and wall armour. *J Nucl Mater* 85–86:231–235
1056. Patriarca P, Harms WO, Rucker DJ (1969) Fuels and materials development program. Quarterly Progress Report ORNL-4350, Contract W-7405-ENG-26. Oak Ridge National Laboratory, Tennessee, pp. 1–320
1057. Patriarca P, Rucker DJ (1969) Fuels and materials development program. Quarterly Progress Report ORNL-4420, Contract W-7405-ENG-26. Oak Ridge National Laboratory, Tennessee, pp. 1–270
1058. Rempel AA, Schaefer H-E, Forster M, Girka AI (1994) Atomic defects in transition metal carbides and SiC studied by positron annihilation. In: Barron AR, Fishman GS, Fury MA, Hepp AF (eds) *Covalent ceramics II: non-oxides*. Materials Research Society, Pittsburgh, Pennsylvania, pp. 299–304
1059. Deb A, Saha SK, Guin R, Chatterjee AK (1998) Compton scattering studies on niobium carbide and vanadium carbide. *Radiat Phys Chem* 51(4–6):517–518
1060. Samsonov GV, Panasyuk AD, Kozina GK, Dyakonova LV (1976) Kontaknoe vzaimodistvie karbida tsirkoniya s nikelievymi splavami (The contact interaction of zirconium carbide with nickel alloys). In: Samsonov GV, Kosolapova TYa, Gnesin GG, Fedorus VB, Domasevich LG (eds) *Karbidy i splavy na ikh osnove* (Carbides and alloys based on them). *Naukova Dumka, Kyiv*, pp. 56–59 (in Russian)
1061. Cam G, Flower HM, West DRF (1991) Solid state transformations in Ti-Al-C and Ti-Al-Nb-C alloys. *Mater Sci Technol* 7(7):587–591
1062. Ordanyan SS, Maskhuliya LG, Panteleev IB, Zhukov VA (1983) Structure and some physico-mechanical characteristics of Fe-Ni-Cr-Mo alloys. *Powder Metall Met Ceram* 22(3):196–199
1063. Ordanyan SS, Maskhuliya LG, Panteleev IB, Litvinov VF (1984) Wettability of a solid solution of titanium-niobium carbonitride by iron and nickel base alloy. *Powder Metall Met Ceram* 23(3):240–242
1064. Ordanyan SS, Maskhuliya LG, Panteleev IB, Persinin SA (1984) Mechanical properties of titanium-niobium carbonitride – Fe (Ni, Cr, Mo) cermets. *Powder Metall Met Ceram* 23(7):521–524
1065. Maskhuliya LG, Serebryakov YuA, Semenov OV, Zakharov VM, Panteleev IB, Ordanyan SS (1986) Tungstenless hard alloy for tools. *Chem Petrol Eng* 22(9):415–417
1066. Lukovkin IV, Ordanyan SS, Samodurov AA, Maskhuliya LG (1988) Properties of cermets based on complex titanium-niobium (vanadium) carbonitrides. *Powder Metall Met Ceram* 27(11):873–875
1067. Ueki M, Saito Ts, Saito Ta, Kitamura K, Suzuki H (1988) Properties of TiC-TiN-Mo₂C-Ni alloy affected mainly by additional tantalum or tungsten carbide. *J Jpn Soc Powder Metall* 35(1):27–32 (in Japanese)

1068. Zhilyaev VA, Patrakov EI, Pelts AD (1990) Kontaktnoe vzaimodeistvie legirovannykh karbonitridov titana s rasplavami na osnove nikelya (The contact interaction of alloyed titanium carbonitrides with nickel based melts). In: Nauch. soobshcheniya 7-oi Vsesoyuznoi konf. po strukture i svoistvam metallicheskih i shlakovykh rasplavov (Proc. 7th All-Union conf. on structure and properties of metallic and slag melts), Vol. 3, Part 3. Chelyabinsk Polytechnical Institute, Chelyabinsk, pp. 232–235 (in Russian)
1069. Cai KF, Nan CW, Yuan R, Ye N (1994) Microstructure and mechanical properties of (Nb,Ti)C-Ni composite. *J Wuhan Univ Technol Mater Sci Ed* 9(3):15–18
1070. Cai KF, Nan CW, Min XM (1998) Microstructure and mechanical properties of (Nb,Ti)C-Ni base superalloy. *Trans Nonferrous Met Soc China* 8(2):275–276
1071. Zalite I, Ordanyan S, Ivanov I, Maskhulia L (2000) Effect of highly dispersed titanium-niobium carbonitride powders on the formation of single-phase materials and cermets. *J Adv Mater* 32(4):3–9
1072. Wang J, Liu Y, Feng Y, Ye J, Tu M (2009) Effect of NbC on the microstructure and sinterability of Ti(C_{0.7}N_{0.3})-based cermets. *Int J Refract Met Hard Mater* 27:549–551
1073. Kim S, Zuo J-M, Kang S (2010) Effect of WC or NbC addition on lattice parameter of surrounding structure in Ti(C_{0.7}N_{0.3})-Ni cermets investigated by TEM/CBED. *J Eur Ceram Soc* 30:2131–2138
1074. Grebenok TP, Dubovik TV, Kovalchenko MS, Klochkov LA, Rogozinskaya AA, Subbotin VI (2016) Structure and properties of titanium carbide based cermets with additives of other carbides. *Powder Metall Met Ceram* 55(1–2):48–53
1075. Zhilyaev VA, Patrakov EI (2016) Regularities of the contact interaction of double carbides (Ti_{1–n}Me_n^{IV,V})C with the Ni-Mo melt. *Russ J Non-Ferr Met* 57(6):610–617
1076. Andersson G, Jansson B (2001) The solubility of cubic carbide formers in liquid cobalt. In: Kneringer G, Röthhammer P, Wildner H (eds) Proc. 15th Int. Plansee seminar, Vol. 2. Plansee Holding AG, Reutte, Tyrol, Austria, pp. 662–676
1077. Harada Y, Bortz SA (1967) Properties of hot-pressed TaC-C & NbC-C composites. Report NASA-CR-85164. IIT Research Institute, Chicago, Illinois, pp. 1–27
1078. Jang JH, Lee C-H, Heo Y-U, Suh D-W (2012) Stability of (Ti,M)C (M = Nb, V, Mo and W) carbide in steels using first principles calculations. *Acta Mater* 60:208–217
1079. Mortimer DA, Nicholas MG (1973) The wetting of carbon and carbides by copper alloys. *J Mater Sci* 8:640–648
1080. Eustathopoulos N, Nicholas MG, Drevet B (1999) Wettability at high temperatures. Elsevier Science, Oxford
1081. Jeitschko W, Nowotny H, Benesovsky F (1963) Kohlenstoffhaltige ternäre Phasen (Nb₃Al₂C und Ta₃Al₂C) (Carbonaceous ternary phases (Nb₃Al₂C and Ta₃Al₂C)). *Monatsh Chem* 94(1):332–333 (in German)
1082. Jeitschko W, Nowotny H, Benesovsky F (1963) Kohlenstoffhaltige ternäre Verbindungen (H-Phase) (Carbonaceous ternary compounds (H-phase)). *Monatsh Chem* 94(4):672–676 (in German)
1083. Johnston J, Toth L, Kennedy K, Parker ER (1964) Superconductivity of Mo₃Al₂C. *Solid State Commun* 2(4):123
1084. Reiffenstein E, Nowotny H, Benesovsky F (1965) Einige neue η -Carbide (Some new η -carbides). *Monatsh Chem* 96(5):1543–1546 (in German)
1085. Holleck H, Thümmel F (1967) Ternäre Komplex-carbide, -nitride und -oxide mit teilweise aufgefüllter Ti₂Ni-Struktur (Ternary complex carbides, nitrides and oxides with partial filled Ti₂Ni structure). *Monatsh Chem* 98(1):133–134 (in German)
1086. Hoch M (1968) Non-stoichiometry and bonding in refractory monocarbides. In: Vahldiek FW, Mersol SA (eds) Anisotropy in single-crystal refractory compounds, Vol. 1. Springer, New York, pp. 163–175
1087. Vitryanyuk VK, Arbuзов EA (1972) Manufacture of high-porosity materials from complex carbides. *Powder Metall Met Ceram* 11(3):216–219

1088. Samsonov GV, Voronkin MA, Bronshtein DKh (1976) Tungsten-free hard alloys based on binary carbides. I. Preparation of alloys and characteristics of formation of their structure during sintering. *Powder Metall Met Ceram* 15(11):844–847
1089. Samsonov GV, Voronkin MA, Linnikov AP, Loktionov VA (1976) Tungsten-free hard alloys based on binary carbides. II. Physico-mechanical properties of alloys. *Powder Metall Met Ceram* 15(12):927–931
1090. Tkachenko YuG, Ordanyan SS, Yulyugin VK, Yurchenko DZ, Pantelev IB, Maskhuliya LG (1984) High-temperature antifricition properties of $Ti_{1-x}Nb_xC_{0.5}N_{0.5}$ alloys. *Powder Metall Met Ceram* 23(8):645–648
1091. Ordanyan SS, Maskhuliya LG, Pavlyuk ÉG, Pantelev IB, Persinin SA (1985) X-ray diffraction characteristics of $Ti_{1-x}Nb_xC_{0.5}N_{0.5}$ solid solutions. *Powder Metall Met Ceram* 24(12):933–937
1092. Churbanov ED, Moiseev VF, Nechaev VP, Taubkin BL, Maskhuliya LG, Petrov NV (1991) Wettability of refractory compounds by intermetallic compounds. *Chem Petrol Eng* 27(10):602–605
1093. Cui W, Lei M (1998) Calculations for electronic structure of TiC, TiC_{1-x} and $(Ti_{1-x}Nb_x)C$. *Acta Phys Chim Sin* 14(3):198–203 (in Chinese)
1094. Gusev AI (2000) Order-disorder transformations and phase equilibria in strongly nonstoichiometric compounds. *Phys Usp* 43(1):1–37
1095. Vishwanadh B, Krishna KVM, Upadhyay A, Banerjee R, Arya A, Tewari R, Fraser HL, Dey GK (2016) Formation mechanism of the Nb_2C phase in the Nb-1Zr-0.1C (wt.%) alloy and interrelation between γ , β and α - Nb_2C carbide phases. *Acta Mater* 108:186–196
1096. Vishwanadh B, Murthy TSRCh, Arya A, Tewari R, Dey GK (2016) Synthesis and phase transformation mechanism of Nb_2C carbide phases. *J Alloy Compd* 671:424–434
1097. Sha X, Xiao N, Guan Y, Yi X (2017) Structural, mechanical and electronic properties of Nb_2C : first principles calculations. *RSC Adv* 7:33402–33407
1098. Chen D, Li R, Lang D, Wang Z, Su B, Zhang X, Meng D (2017) Determination of the mechanical properties of inclusions and matrices in α -U and aged U-5.5Nb alloy by nanoindentation measurements. *Mater Res Express* 4:116516 (10 pp.)
1099. Chernetsov MV (2017) Integral materials studies of nuclear fuel at Institute of Reactor Materials. *Atom Energy* 121(4):255–258
1100. Gusev AI (2004) Solid-state decomposition and surface segregation in carbide solid solutions. *Russ J Phys Chem A* 78(3):357–363

Chapter 5

Zirconium Monocarbide



5.1 Structures

Practically zirconium forms with carbon the only one chemical compound (see also section C–Zr in Table I-2.13) – zirconium monocarbide ZrC_{1-x} with extremely broad homogeneity range, apart from low-temperature (<860–1080 °C) ordered structures of $Zr_{2\pm x}C$ ($Fd(-3)m$, $R(-3)m$, $Pnma$, $P3m1$, $I4_1/amd$, $Pbcn$, $P4/mmm$), $Zr_3C_{2\pm x}$ ($C2/m$, $P(-3)m1$, $I4/mmm$, $Immm$), $Zr_4C_{3\pm x}$ ($C2/c$, $P(-3)m1$, $Pm(-3)m$), $Zr_5C_{4\pm x}$ ($P(-1)$, $C2/m$, $I4/m$), $Zr_6C_{5\pm x}$ ($C2/m$, $C2/c$, $P3_112$), $Zr_7C_{6\pm x}$ ($R(-3)$) and $Zr_8C_{7\pm x}$ ($P4_332$, $Fm(-3)m$) as well as molecular clusters Zr_8C_{12} , $Zr_{13}C_{22}$, $Zr_{14}C_{23}$, $Zr_{18}C_{29}$, $Zr_{22}C_{35}$, including endohedral $C@Zr_8C_{12}$, which are not confirmed sufficiently in literature [1–14, 696, 702, 1029, 1080, 1143, 1376, 1391, 1408, 1409, 1420]. The ordered structures should be in thermodynamic equilibrium with disordered monocarbide phase; however, the latter one can exist as a metastable phase for an infinitely long time because the diffusion rate at lower temperatures is extremely small [2, 8]. A high-temperature partial variant of zirconium–carbon phase diagram is given in Fig. 5.1, and the structural features of zirconium monocarbide ZrC_{1-x} are presented in Table 5.1. The C/Zr radii ratio, calculated on the basis of Pauling’s atomic size of Zr (0.1597 nm, CN = 12) is 0.483 [11, 74]; the ratio of Zr radii (in nm) in Me/MeC is 0.161/0.166 (2.8% expansion of Zr atoms in carbide) [17]. The phase transformation of ZrC_{1-x} from NaCl type ($Fm(-3)m$) to CsCl type ($Pm(-3)m$) structure under very high pressures (~100–500 GPa) was predicted theoretically [18–25, 466, 716, 1372].

The variation of the lattice parameter of zirconium monocarbide ZrC_{1-x} phases with carbon content (or deviation from the stoichiometry) within the homogeneity range is shown in Fig. 5.2; in a modified form the following equation described this relationship was proposed by Senczyk (for $0 \leq x \leq 0.5$) [1476]:

$$a = 0.4701 - 0.00665x - 0.00185x^2, \quad (5.1)$$

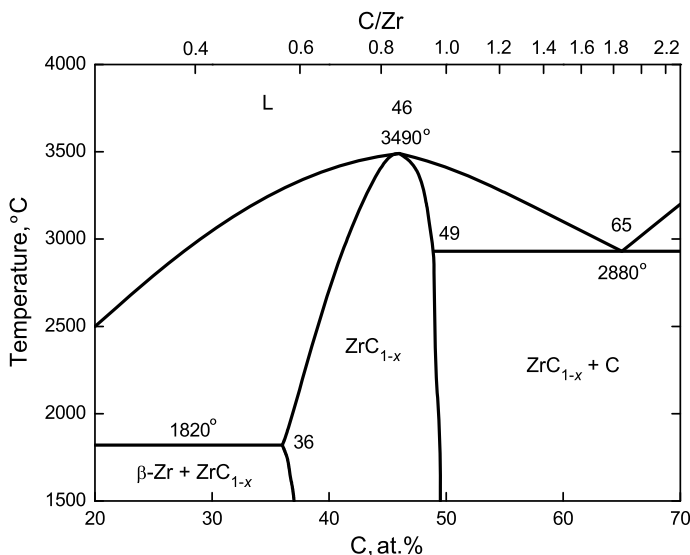


Fig. 5.1 High-temperature partial variant of zirconium – carbon equilibrium phase diagram [2, 4, 8, 10, 11, 15, 16, 26, 27, 43, 72–76, 80, 96–99, 105, 146, 201, 267–269, 600, 1388, 1389, 1450, 1539]

and Gusev (for $x \leq 0.355$) [160]:

$$a = 0.46965 + 0.00697x - 0.02018x^2, \quad (5.2)$$

where a is lattice parameter, nm and x is the value of index in ZrC_{1-x} formula. The wide spread of data available in literature for the relationships between the lattice parameter and composition of ZrC_{1-x} mainly could be explained by some difficulties in the contamination control of phase composition; the considerable solubilities of oxygen and nitrogen, which are always present in ZrC_{1-x} , result in the formation of oxycarbide $ZrC_{1-x}O_y$, carbonitride $ZrC_{1-x}N_z$ and more commonly oxycarbonitride $ZrC_{1-x}N_zO_y$ phases (*see also* sections C–N–Zr, C–N–O–Zr and C–O–Zr in Table I-2.14) with various deviations from the stoichiometry and noticeable decrease in the magnitude of lattice parameter observed due to the direct substitution of carbon for oxygen and/or nitrogen [26, 27, 44, 151, 161–166, 598, 1077]. On the basis of various literature values for a range of oxygen and/or nitrogen impurity contents Mitrokhin et al. [71] established the quantitative relationship between lattice parameter and composition for zirconium monocarbide (oxycarbonitride in practice) $ZrC_{1-x}(N,O)_y$ phases, which looks in a modified form as

$$a = 0.4696 + 0.0074x - 0.0208x^2 - 0.080xy, \quad (5.3)$$

Table 5.1 Structural properties (crystal structure, density) of zirconium monocarbide phase

Formula	Crystal structure					Density ^c , g cm ⁻³	Reference
	System	Type	Space group	Lattice parameter ^a <i>a</i> , nm	Z ^b		
ZrC _{1-x}	Cubic	NaCl	<i>Fm</i> (-3) <i>m</i>	0.4652 ^d	4	–	[79]
				0.4656 ^e	4	–	[78]
				0.4665 ^f	4	–	[44, 162]
				0.4669	4	6.74	[150]
				0.4670	4	6.73	[148]
				0.4670	4	6.47	[36, 139]
				0.4673	4	–	[37]
				0.4675 ^g	4	–	[146]
				0.4676 ^h	4	–	[44, 162]
				0.4677 ⁱ	4	–	[61]
				0.4680 ^{j,k}	4	–	[57, 153]
				0.4681 ^l	4	–	[44, 161]
				0.4682 ^{m,n}	4	–	[53, 72, 155]
				0.4683 ^o	4	6.66	[32, 47, 100]
				0.4683	4	6.65	[130]
				0.4683	4	6.64	[127, 128]
				0.4683 ^p	4	6.31	[154]
				0.4683 ^q	4	–	[78, 237]
				0.4686	4	6.66	[140]
				0.4687	4	6.66	[41, 143, 236]
				0.4688	4	–	[30, 31, 42, 45]
				0.4688 ^{r,s,t}	4	–	[44, 62, 81, 163]
				0.4689 ^{u,v}	4	–	[38, 39, 62, 68]
				0.4690 ^{q,w}	4	–	[40, 78, 844]
				0.4691	4	6.64	[141]
				0.4691 ^x	4	6.33	[10]
				0.4691 ^x	4	6.29	[43]
				0.4691 ^{q,y}	4	–	[66, 242, 243]
				0.4692 ^{q,z}	4	–	[77, 88]
				0.4692 ^q	4	6.64	[117]
				0.4692	4	6.52	[131]
				0.4693 ^{a1,a2,a3}	4	–	[54, 65, 83, 89]
				0.4693 ^{o,a4}	4	–	[91, 132, 153]
0.4693	4	6.63	[124, 133, 147]				
0.4693	4	6.60	[136]				
0.4693	4	6.56	[135]				
0.4693 ^{a5}	4	6.46	[844]				

(continued)

Table 5.1 (continued)

Formula	Crystal structure			Lattice parameter ^a <i>a</i> , nm	<i>Z</i> ^b	Density ^c , g cm ⁻³	Reference
	System	Type	Space group				
				0.4694 ^{a3,a6,a7}	4	–	[57, 72, 101, 102]
				0.4694 ^{a8}	4	6.63	[111, 122, 129]
				0.4694 ^{a9}	4	6.62	[844]
				0.4694 ^{b1}	4	6.61	[109]
				0.4694 ^{b2}	4	6.35	[85]
				0.4694 ^q	4	–	[146, 1482]
				0.4695 ^{a6,b3,b4}	4	–	[26, 27, 69, 94]
				0.4695 ^{b5}	4	6.62	[844]
				0.4695	4	6.60	[106–108]
				0.4695 ^{b6}	4	6.50	[844]
				0.4695 ^{b7}	4	–	[156]
				0.4696 ^{b8,b9}	4	–	[44, 60, 71, 95]
				0.4696	4	6.62	[145, 149]
				0.4696 ^{a6}	4	6.60	[120, 121]
				0.4697 ^{c1}	4	6.73	[1, 3, 4, 26–29]
				0.4697 ^{c2,c3,c4}	4	–	[59, 64, 84]
				0.4697 ^{o,c5,c6}	4	–	[91, 97–99, 200]
				0.4697 ^{c7}	4	6.62	[110, 116, 126]
				0.4697	4	6.59	[91, 118, 132]
				0.4697	4	6.58	[123]
				0.4698	4	6.73	[63, 67]
				0.4698 ^{c8}	4	6.66	[2, 10, 33–35, 52]
				0.4698 ^{c9}	4	6.62	[58]
				0.4698 ^{b3}	4	6.59	[11, 48, 55, 112]
				0.4698 ^{d1}	4	6.57	[43, 46, 53, 72]
				0.4698 ^{d2}	4	6.56	[56]
				0.4698 ^{d3}	4	6.55	[87]
				0.4698 ^{d4}	4	6.51	[58]
				0.4698	4	6.50	[119]
				0.4698 ^{q,d5,d6}	4	–	[89, 152, 156]
				0.4698 ^{d5,d7}	4	–	[157, 186]
				0.4699 ^{d8,d9}	4	–	[49, 50, 61, 62]
				0.4699 ^q	4	6.61	[77, 114, 115]
				0.4699 ^{e1,e2,e3}	4	–	[83, 84, 88]
				0.4699 ^{e4}	4	6.60	[85]
				0.4699	4	6.59	[142]
				0.4699 ^{p,e5,e6}	4	–	[90, 92, 200]
				0.4699	4	6.54	[125]
				0.4700	4	6.60	[113, 144]
				0.4700 ^{e7}	4	6.58	[82]
				0.4700 ^{e8,e9}	4	–	[51, 81, 86]

(continued)

Table 5.1 (continued)

Formula	Crystal structure			Lattice parameter ^a <i>a</i> , nm	<i>Z</i> ^b	Density ^c , g cm ⁻³	Reference
	System	Type	Space group				
				0.4700 ^{f1}	4	–	[156]
				0.4701 ^{e7,f2,f3}	4	–	[88, 89, 152]
				0.4701 ^{f4}	4	–	[415]
				0.4701	4	6.58	[134]
				0.4701 ^{a4}	4	6.56	[154]
				0.4702 ^{f5,f6,f7}	4	–	[10, 70, 81, 84]
				0.4702 ^{f8}	4	6.50	[85]
				0.4702 ^{f9,g1}	4	–	[93, 200]
				0.4703	4	6.52	[137, 138]
				0.4708 ^{g2}	4	–	[175]
				0.475–0.478 ^{g3}	4	–	[103, 104, 191]

^aWhen it is not indicated specially, value reported is for near-stoichiometric composition

^bNumber of formula units per lattice cell

^cCalculated from XRD or neutron diffraction patterns

^dCarbon content – 36.6 at.%

^eCarbon content – 27.6 at.% (?)

^fTaking into account O contamination, it is corresponding to ZrC_{0.65}O_{0.03}

^gCarbon content – 35.0 at.%

^hTaking into account O contamination, it is corresponding to ZrC_{0.90}O_{0.04}

ⁱHigh purity materials with carbon content – 42.5 at.%

^jCarbon content – 39.4 at.%

^kCarbon content – 37.5 at.%

^lTaking into account O contamination, it is corresponding to ZrC_{0.64}O_{0.05}

^mCarbon content – 35.9 at.% (in equilibrium with α -Zr)

ⁿCarbon content – 36.5 at.%

^oCarbon content – 49.0 at.%

^pCarbon content – 36.7 at.%

^qCarbon content – ~50 at.%

^rCarbon content – 49.7 at.% (combined), non-combined C – 0.2%, O – 0.1%, N – 0.1%

^sCarbon content – 41.9 at.%, O – 0.77%

^tTaking into account O contamination, it is corresponding to ZrC_{0.90}O_{0.05}

^uCarbon content – 40.5 at.% (combined), non-combined C – absent, O – 0.3%, N – 0.1%

^vCalculated by all-electron full-potential linearized augmented plane-wave (FLAPW) method

^wPrepared by self-propagating high-temperature synthesis (SHS) with charged C/Zr ratio – 0.7, carbon content – 37.5 at.%

^xCarbon content – 35.5–36.7 at.% (in equilibrium with α -Zr)

^yInteratomic distances: Zr–Zr and C–C – 0.33171 nm, Zr–C – 0.23455 nm

^zCarbon content – 35.5 at.%

^{a1}Reported thermal increment is $6.8 \times 10^{-6} \text{ K}^{-1}$

^{a2}Carbon content – 38.7 at.%, O – 0.32%, N – 0.014%

^{a3}Carbon content – 38.5 at.%

^{a4}Carbon content – 39.0 at.%

^{a5}Prepared by SHS with charged C/Zr ratio – 0.8, carbon content – 41.5 at.%

^{a6}Carbon content – 49.2 at.%

^{a7}Related to the carbide phase (contents O – 0.6–1.0%, N – 0.3–0.5%) in equilibrium with graphite in two phase carbide-carbon compositions

^{a8}99.9% purity materials, carbon content 49.8 at.%

(continued)

Table 5.1 (continued)

- ^{a9}Prepared by SHS with charged C/Zr ratio – 2.0, carbon content – 49.7 at. %
- ^{b1}Carbon content – 49.5 at. %, O – 0.15%, Hf – 2.5%
- ^{b2}Carbon content – 39.0 at. %, O – 0.13%
- ^{b3}Carbon content – 38.3 at. %
- ^{b4}Calculated on the basis of density-functional theory (DFT) with generalized gradient approximation (GGA)
- ^{b5}Prepared by SHS with charged C/Zr ratio – 1.5, carbon content – 49.7 at. %
- ^{b6}Prepared by SHS with charged C/Zr ratio – 1.0, carbon content – 45.7 at. %
- ^{b7}Experimental data extrapolated from $\text{ZrC}_{0.79}\text{O}_{0.19}$ measurements to an oxygen-free phase
- ^{b8}Carbon content – 48.7 at. %
- ^{b9}Experimental data extrapolated to $x = y = 0$ for $\text{ZrC}_{1-x}(\text{O},\text{N})_y$ compounds
- ^{c1}Carbon content – 49.2–49.7 at. %; minimal interatomic distances: Zr–Zr and C–C – 0.332 nm, Zr–C – 0.235 nm
- ^{c2}Experimental data extrapolated to $y = 1$ for $\text{ZrC}_y\text{N}_{1-y}$ compounds
- ^{c3}For nanoparticles; taking into account O contamination, it is corresponding to $\text{ZrC}_{0.93}\text{O}_{0.02}$
- ^{c4}Carbon content – 38.3 at. %, O – 0.005%
- ^{c5}Carbon content – 45.1–46.8 at. %
- ^{c6}Related to the carbide phase (O – 0.5%, N < 0.001%) in equilibrium with graphite (lattice parameter increases after the melting procedure of two phase carbide-carbon composition by 0.0002–0.0013 nm)
- ^{c7}Carbon content – 46.2 at. %
- ^{c8}Carbon content – 49.2 at. % (in equilibrium with graphite)
- ^{c9}Taking into account N and O contaminations, it is corresponding to $\text{ZrC}_{0.88}\text{N}_{0.04}\text{O}_{0.02}$
- ^{d1}Carbon content – 48.7–49.5 at. % (in equilibrium with graphite)
- ^{d2}Experimental data extrapolated from $(\text{Zr}_{0.992}\text{Hf}_{0.008})\text{C}_{0.937}$ (contents: non-combined C – 0.26%, O < 0.15%, N < 0.01%) measurements to a Hf-free stoichiometric phase; minimal interatomic distance Zr–C – 0.2349 nm
- ^{d3}Single crystal materials, carbon content – 48.7 at. %
- ^{d4}Taking into account N and O contaminations, it is corresponding to $\text{ZrC}_{0.73}\text{N}_{0.03}\text{O}_{0.02}$
- ^{d5}Chemical vapour deposited whiskers, carbon content – 40.3 at. %, O – 0.05%
- ^{d6}Experimental data extrapolated from $\text{ZrC}_{0.83}\text{O}_{0.15}$ measurements to an oxygen-free phase
- ^{d7}Nanoparticles with average size ~7 nm, carbon content – 49.9 at. %
- ^{d8}High purity materials with carbon content – 49.5 at. %
- ^{d9}Carbon content – 47.6 at. % (combined), non-combined C – absent, O – 0.1%, N – 0.1%
- ^{e1}Carbon content – 49.5 at. % (combined), non-combined C – 0.5%, O – 0.04%, N – 0.003%
- ^{e2}Carbon content – 49.7 at. %, O – 0.02%
- ^{e3}Carbon content – 47.9 at. %
- ^{e4}Carbon content – ~50 at. %, O – 0.05%
- ^{e5}Carbon content – 48.2 at. %
- ^{e6}Carbon content – 40.0 at. %
- ^{e7}Carbon content – 49.1 at. % (combined), non-combined C – 0.4%, O – 0.07–0.09%, N – 0.1%
- ^{e8}Carbide phase in equilibrium with graphite (content O – 0.36%)
- ^{e9}Carbon content – 49.3 at. % (combined), non-combined C – 0.15%, O – 0.62%, N – 0.018%
- ^{f1}Experimental data extrapolated from $\text{ZrC}_{0.87-0.89}\text{O}_{0.007-0.070}$ measurements to an oxygen-free phase
- ^{f2}Carbon content – 43.5 at. %
- ^{f3}Chemical vapour deposited whiskers, carbon content – 43.8–45.3 at. %, O – 0.05%
- ^{f4}Thin films (2 μm thickness) prepared by activated reactive evaporation
- ^{f5}Carbon content – 47.6 at. %, O – 0.04%
- ^{f6}Carbon content – 45.1–46.6 at. %, O – 0.02–0.07%, N – 0.004–0.005%
- ^{f7}Carbon content – 45.4 at. %; the maximal value measured for the phase lattice parameters in homogeneity region
- ^{f8}Carbon content – 46.5 at. %, O – 0.06%
- ^{f9}Carbon content – 47.4 at. %
- ^{g1}Carbon content – 45.0 at. %
- ^{g2}Powders with nanoscale dimensions ~5 nm
- ^{g3}Related to nanocrystalline phase (~2–12 nm grains) in contact with amorphous carbon

where a is lattice parameter, nm and x is the value of index in ZrC_{1-x} (or oxy-carbonitride $ZrC_{1-x}(N,O)_y$) formula ($0 < x \leq 0.38$) and y is the $(O + N)/Zr$ atomic ratio ($y < 0.3$). Some examples of the effects of temperatures and oxygen impurity atoms on the lattice parameters of ZrC_{1-x} monocarbide phases are demonstrated in Figs. 5.3 and 5.4; the examples of impurities effect on the completeness of metal and non-metal sublattices in ZrC_{1-x} ($ZrC_{1-x}N_zO_y$) are given in Table 5.2.

Like most other transition metal carbides, metal and carbon atoms in the zirconium monocarbide ZrC_{1-x} lattice are bound by ionic and covalent (C–Zr) and metallic (Zr–Zr) bonds; the latter bonds are known to be significantly weaker than metal-to-carbon bonds. Although ZrC_{1-x} is a polar covalent compound with considerable charge transfer from metal to carbon atoms [167, 168], namely the strong covalent character of chemical bonding in ZrC_{1-x} determines the high value of C–Zr bond energy (enthalpy), which is about 5.81 ± 0.3 eV [96, 1384], or 5.14 ± 0.4 eV [746, 1385, 1386].

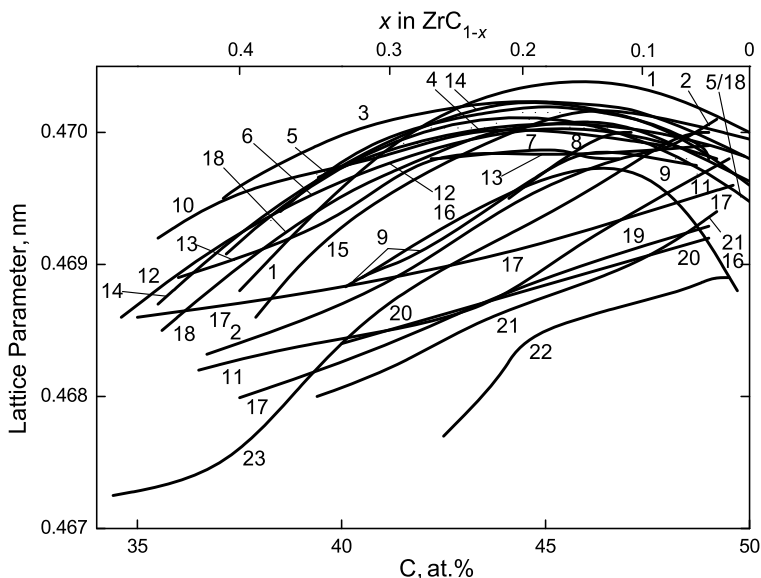


Fig. 5.2 Lattice parameter of ZrC_{1-x} as a function of phase composition: 1 – [160], 2 – synthesized from elements [154], 3 – arc-melted and annealed in vacuum [84], 4 – chemical vapour deposited whiskers [152], 5 – polynomial approximation [26, 27], 6 – synthesized by reacting Zr hydride with carbon and annealed [80], 7 – $ZrC_{1-x}N_{0.02-0.04}O_{0.02-0.03}$ synthesized from elements in H_2 [58], 8 – measurement extrapolation to oxygen free phases [156], 9 – [53], 10 – [88], 11 – [155], 12 – [10], 13 – arc-melted and annealed [158], 14 – polynomial approximation extrapolated to oxygen free phases [71, 74], 15 – [75], 16 – contents O – 0.1–0.3%, N – 0.1% [62, 1311], 17 – prepared by the carbothermal reduction of Zr oxide [98], 18 – synthesized by different methods [546, 1449], 19 – [153], 20 – [159], 21 – synthesized from elements in vacuum [57, 513, 877, 1308], 22 – contents O, N – 0.05–0.15% [61], 23 – [1477, 1478] (1, 5, 11, 13–14, 18 – on the basis of several sources)

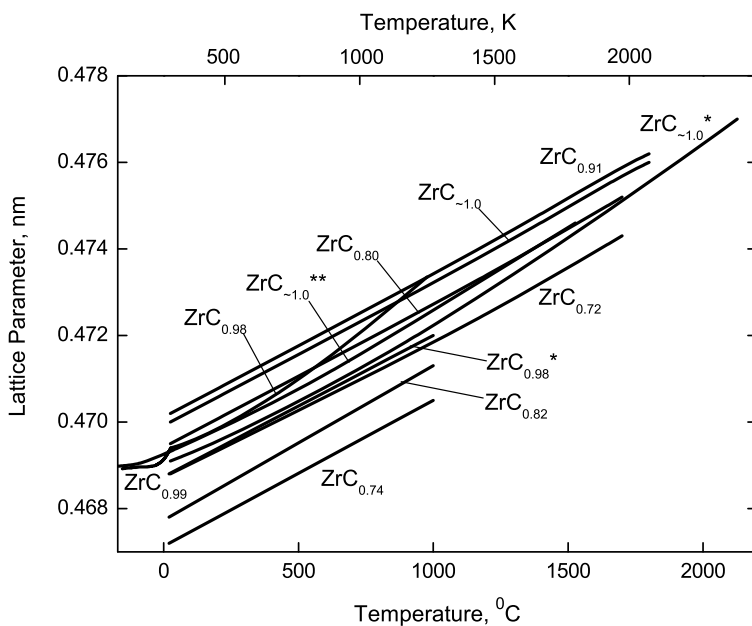


Fig. 5.3 Lattice parameter of ZrC_{1-x} as a function of temperature for the phases having different deviations from the stoichiometry ($x \approx 0$ (in equilibrium with carbon), $x = 0.09$, $x = 0.20$ and $x = 0.28$, synthesized by the reaction of Zr hydride with carbon in vacuum, content O – 0.04–0.77% [81]; $x \approx 0^*$, on the basis of several sources [242]; $x \approx 0^{**}$, prepared by the carbothermic reduction of Zr oxide, content O < 0.01%, measured by neutron diffraction [362]; $x = 0.01$, 99.9% purity [111]; $x = 0.02^*$, contents: O – 0.15%, Hf – 2.5% [109]; $x = 0.02^*$, $x = 0.18$ and $x = 0.26$ [1350])

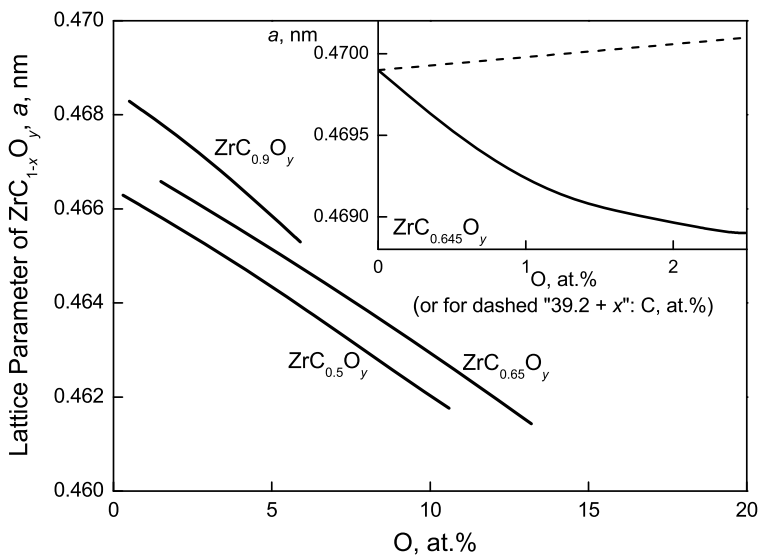


Fig. 5.4 Effect of oxygen atoms on the lattice parameter of $ZrC_{1-x}O_y$ oxycarbide phases formed: $ZrC_{0.9}O_y$, $ZrC_{0.65}O_y$ and $ZrC_{0.5}O_y$ [26, 27] (Inset – for $ZrC_{0.645}O_y$ phase, the dashed line shows the change of parameter if carbon atoms were added to the vacancies instead of oxygen [83, 84])

Table 5.2 The completeness of zirconium monocarbide (oxycarbonitride) ZrC_{1-x} ($ZrC_{1-x}N_zO_y$) sublattices (with various impurity contents) [3, 44, 58, 151, 1445]

Phase composition	Fraction of structural defects in sublattices	
	metal	non-metal
$ZrC_{0.88}N_{0.04}O_{0.02}$	–	0.06
$ZrC_{0.85}O_{0.15}$	0.015	0.015
$ZrC_{0.79}O_{0.21}$	0.0225	0.025
$ZrC_{0.74}N_{0.04}O_{0.02}$	–	0.20
$ZrC_{0.74}O_{0.26}$	0.035	0.035
$ZrC_{0.73}O_{0.19}$	0.025	0.1025
$ZrC_{0.70}O_{0.24}$	0.0325	0.09
$ZrC_{0.63}O_{0.33}$	0.055	0.0925
$ZrC_{0.54}O_{0.19}$	0.02	0.2825
$ZrC_{0.50}O_{0.09}$	0	0.41
$ZrC_{0.50}O_{0.21}$	0.075	0.3425

Table 5.3 The DFT-calculated values of unstable stacking fault energies and total energies required to shear for the crystals of near-stoichiometric zirconium monocarbide ZrC_{1-x} along different slip systems [174]

Slip system	Unstable stacking fault energy ^a , eV nm ⁻²	Shear total energy ^b , eV nm ⁻³
(0 0 1) <110>	16.4	77
(1 $\bar{1}$ 0) <110>	14.1	331
(1 $\bar{1}$ 1) <110>	15.6	305

^aResistance to dislocation nucleation processes [182]^bMeasure of ideal shear stress

It was determined mainly by the hardness measurements on single crystal materials that the preferred slip systems for near-stoichiometric ZrC_{1-x} phases are (110)<1 $\bar{1}$ 0> – at moderate temperatures, (100)<1 $\bar{1}$ 0>, (110)<1 $\bar{1}$ 0> and (111)<1 $\bar{1}$ 0> – at elevated and higher temperatures, and the combination of (110)<1 $\bar{1}$ 0> and (111)<1 $\bar{1}$ 0> systems – for the intermediate regions [11, 26, 27, 169–173, 572, 658, 671, 672, 1470, 1503, 1504]. However, Kiani et al. [174, 1407], using *in situ* electron microscopy based nanomechanical testing under compression jointly with density functional theory calculations, identified the (001) <110> slip system at quasi-room temperature as an active system operating in ZrC (111) single-crystalline nanopillars; the energy values, DFT-calculated by them, which characterize several different possible slip systems in near-stoichiometric ZrC_{1-x} , are given in Table 5.3. The minimal Burgers vector of near-stoichiometric monocarbide ZrC_{1-x} ($\frac{1}{2}$ <110>) $b = 0.332$ – 0.334 nm [4, 52, 659]. For parameters of formation and migration of lattice point defects (vacancies and interstitial atoms) in ZrC_{1-x} see Sect. 5.5 (Table 5.19).

Recently, due to massive progress in nanotechnology, many nanostructures based on ZrC_{1-x} , including various (in types) nanopowders and nanoparticles (with

mean sizes from 5 to 500 nm) [64, 148, 175–181, 185–188, 375, 987, 1547], nanofibres (40–700 nm in diameter, few micrometers in length) [183, 184, 194], whiskers (1–20 μm diameter, 0.1–7 mm length) grown along $\langle 100 \rangle$ and $\langle 110 \rangle$ crystal directions [152, 157, 878, 1464, 1548], various nanocrystalline thin films/coatings (up to 0.6 nm in thickness) [103, 104, 144, 193, 198, 580, 581, 663, 729, 1060, 1491, 1493, 1495], have been synthesized; 2D-molecular $\text{Zr}_{n+1}\text{C}_n$ (or Zr_2CT_x , where T are functional groups OH, O, F) MXenes [189–192, 195–197, 1398, 1406, 1441, 1442] were synthesized and examined using first principles calculations too.

According to Storms [10], the X-ray density of zirconium monocarbide ZrC_{1-x} phase changes from 6.33 g cm^{-3} for $\text{ZrC}_{0.58}$ to 6.59 g cm^{-3} for $\text{ZrC}_{0.97}$. For the bulk density of poreless ZrC_{1-x} single-phase materials with various deviations from the stoichiometry Katoh et al. [96] proposed the following approximation function:

$$d = 6.61 - 0.88x + 0.32x^2, \quad (5.4)$$

where d is the bulk mass density, g cm^{-3} and x is the value of index in ZrC_{1-x} formula ($0 < x \leq 0.4$). The recommended value for the density of pure poreless near-stoichiometric zirconium monocarbide ZrC_{1-x} materials at room temperature is $6.60\text{--}6.65 \text{ g cm}^{-3}$ [1, 4, 30, 32, 33, 37, 45, 199].

5.2 Thermal Properties

Zirconium monocarbide ZrC_{1-x} has one of the highest melting points of all the solid substances available. Within the homogeneity range of ZrC_{1-x} the melting point of the phase varies (*see* Fig. 5.1); the maximum temperature is pertaining to the nonstoichiometric composition $\text{ZrC}_{0.82 \pm 0.03}$ [2–4, 10, 11, 15, 16, 72–80, 98, 200, 201]. The general thermodynamic properties of near-stoichiometric zirconium monocarbide are summarized in Table 5.4. For the molar heat capacity of near-stoichiometric zirconium monocarbide ZrC_{1-x} $c_p = f(T, \text{K})$, $\text{J mol}^{-1} \text{K}^{-1}$, the following relationships were recommended in the literature:

in the range of temperatures from 40 to 1380 K [54]

$$c_p = 58.58 \exp(-132.1/T), \quad (5.5)$$

in the range of temperatures from 300 to 1200 K [250]

$$c_p = 47.70 + (5.941 \times 10^{-3})T - (7.811 \times 10^5)T^{-2}, \quad (5.6)$$

in the range of temperatures from 300 to 3300 K [31, 42, 207]

$$c_p = 54.81 + (2.218 \times 10^{-3})T - (1.105 \times 10^7)T^{-2}, \quad (5.7)$$

Table 5.4 General thermodynamic properties of near-stoichiometric zirconium monocarbide ZrC_{1-x}

Characteristics	Symbol	Unit	Value	Reference
Standard heat of formation (at 298.15 K) ^a	$-\Delta H^\circ_{298}$	kJ mol^{-1}	171.5	[230]
			182.9 ^b	[376]
			184.5 ± 6.3	[31, 35, 46, 207, 217, 218, 223, 375, 635]
			190.0	[37]
			196.6 ± 13.0	[1, 208, 221, 224, 225, 241, 260, 272]
			198.4 ± 4.0	[264]
			198.7 ± 6.3	[231]
			199.4 ± 12.6	[32, 39, 42, 47, 48]
			200.0 ± 6.3	[219, 220, 251, 381]
			200.8 ± 20.9	[30, 33, 211, 229]
			201.1 ± 2.5	[261]
			202.0 ± 2.5^c	[83, 262, 273]
			206.6 ± 10.0^d	[2, 83, 240, 1466–1468]
			207.0 ± 6.0	[16, 274]
			209.2	[232]
			222.0 ± 8.4	[212]
Standard molar entropy ^e (at 298.15 K and 100 kPa)	S°_{298}	$\text{J mol}^{-1} \text{K}^{-1}$	33.05 ± 2.09	[244]
			33.15	[202]
			33.17 ^c	[10, 11, 217]
			33.32	[1, 33, 208, 211, 222, 224, 241]
			33.80 ^f	[249]
			35.56 ± 6.28	[32, 35, 42, 207, 223, 235]
			37.66	[247]
			38.91 ± 1.26	[248]
			5.607 ^f	[249]
			5.832 ^c	[10, 11, 222]
Molar enthalpy difference	$H_{298} - H_0$	kJ mol^{-1}	5.841	[202]
			5.862	[208, 211, 224]
			36.34	[207]
			37.72 ^c	[4, 10, 11, 48]
			37.82	[202]
Standard molar heat capacity ^g (at 298.15 K and 100 kPa)	$c^\circ_{p,298}$	$\text{J mol}^{-1} \text{K}^{-1}$	37.90 ± 1.20	[1, 32, 33, 208, 211, 222, 224, 241, 244]
			38.07	[208, 209, 257, 266]
			40.68	[250]

(continued)

Table 5.4 (continued)

Characteristics	Symbol	Unit	Value	Reference
Specific heat capacity ^h (at 298.15 K)	c	$\text{J kg}^{-1} \text{K}^{-1}$	352.0	[45]
			367.1	[33, 798]
			368.0	[222, 325, 341–343]
			458.0	[31, 199]
Molar enthalpy (heat) of melting (at 298.15 K)	ΔH_m°	kJ mol^{-1}	79.5	[224, 241, 1471]
Molar enthalpy (heat) of melting (at the melting point)	ΔH_m	kJ mol^{-1}	83.7	[33, 211, 235]
			113	[1507, 1508]
Specific enthalpy (heat) of melting (at the melting point)		kJ kg^{-1}	814	[33]
			850	[279]
Molar enthalpy (heat) of vaporization (at 298.15 K) ^j	ΔH_v°	kJ mol^{-1}	1100 ⁱ	[1507, 1508]
			608 ^k	[74]
Molar enthalpy (heat) of vaporization (dissociation) ^l	$\Delta \hat{H}_v$	kJ mol^{-1}	805	[229]
Melting point	T_m	$\text{K (}^\circ\text{C)}$	1515	[10]
			1520 ^m	[219, 251]
			3400 ± 50	[215]
			(3130 ± 50)	
			3450 ± 50	[35, 246, 319]
			(3175 ± 50)	
			3670 (3400)	[704]
			3690 ± 20	[4, 10, 11, 33,
			(3420 ± 20) ^{n,o,p}	45, 48, 72, 80,
				211, 238, 263,
				380, 1032]
			3700 (3430) ^q	[16, 267, 269,
				279]
			3710 (3440) ^f	[3, 256]
			3720 ± 25	[75, 271, 382,
			(3450 ± 25) ^{r,s}	635, 1009]
			3750 ± 35	[216]
			(3475 ± 35)	
			3755 (3480)	[227, 228]
			3775 (3500)	[377, 378]
3800 ± 50	[1, 30–32, 37,			
(3530 ± 50) ^t	42, 46, 47, 208,			
	213, 214, 223,			
	381, 659, 1412]			
3805 ± 125	[224, 226, 241,			
(3532 ± 125)	285, 477]			
3810 ± 70	[149, 201, 218]			
(3535 ± 70)				
3815 (3540) ^u	[15, 149, 1471]			
3830 (3560)	[63, 252, 259]			
4010 (3735)	[207]			
4015 (3740)	[270]			

(continued)

Table 5.4 (continued)

Characteristics	Symbol	Unit	Value	Reference
Boiling point	T_b	K (°C)	5130 (4860)	[238]
			5370 (5100)	[30, 32, 37, 39, 42, 45, 199, 207, 1471]
			5920 (5650)	[31]

^aFor liquid state: $-\Delta H^\circ_{298} = 118.8 \text{ kJ mol}^{-1}$ [224], $110.0 \text{ kJ mol}^{-1}$ [211]; in gaseous state: $-\Delta H^\circ_{298} = 1484 \text{ kJ mol}^{-1}$ [208]; enthalpy (heat) of complete dissociation (atomization) from solid state at 298,15 K ($-\Delta_{at}H^\circ_{298}$, kJ mol^{-1}): 1523 ± 7 [1, 232], 1506 [32], 1512 [233], 1565 [234], 1520 ± 10 [1468] (for ZrC_{1-x} phases with different deviations from the stoichiometry: 1489 ± 9 ($x = 0.04$), 1437 ± 9 ($x = 0.10$), 1350 ± 8 ($x = 0.20$), 1263 ± 9 ($x = 0.30$), 1180 ± 10 ($x = 0.40$) [1]; 1509 ($x = 0.04$), 1359 ($x = 0.20$) [276])

^bFirst principles calculated with generalized gradient approximation (GGA) using the Perdew-Burke-Ernzerhof (PBE) functional

^cCarbon content – 49.0 at.%

^dExtrapolated to the stoichiometric composition

^eMolar entropy S°_T (at 1200 K), $\text{J mol}^{-1} \text{K}^{-1}$, for ZrC_{1-x} phases with different deviations from the stoichiometry: 89.51 ($x = 0$), 88.54 ($x = 0.05$), 87.57 ($x = 0.10$), 86.60 ($x = 0.15$), 85.64 ($x = 0.20$), 84.67 ($x = 0.25$), 83.70 ($x = 0.30$), 82.73 ($x = 0.35$) and 81.76 ($x = 0.40$) [202]

^fCalculated by means of the Lindemann equation using a method similar to that utilized for TiB_2

^gMolar heat capacity $c_{p,T}$ (at 1200 K), $\text{J mol}^{-1} \text{K}^{-1}$, for ZrC_{1-x} phases with different deviations from the stoichiometry: 48.75 ($x = 0$), 47.53 ($x = 0.05$), 46.30 ($x = 0.10$), 45.08 ($x = 0.15$), 43.56 ($x = 0.20$), 42.63 ($x = 0.25$), 41.40 ($x = 0.30$), 40.18 ($x = 0.35$) and 38.96 ($x = 0.40$) [202]

^hSpecific heat capacity c , $\text{J kg}^{-1} \text{K}^{-1}$, at elevated and high temperatures for ZrC_{1-x} phases with different deviations from the stoichiometry: $\text{ZrC}_{-1.0} - 630$ (2230 °C) [74, 105]; $\text{ZrC}_{0.95} - 477$ (1130 °C), 515 (1530 °C), 552 (1930 °C), 594 (2330 °C); $\text{ZrC}_{0.85} - 502$ (1130 °C), 561 (1530 °C), 623 (1930 °C), 682 (2330 °C) [239]

ⁱFor $\text{ZrC}_{0.95}$ (temperatures of solidus – 3450 (3180) K (°C) and liquidus – 3850 (3580) K (°C))

^jEnthalpy (heat) of sublimation of metallic Zr at 298,15 K, $\Delta_{\text{SMC}}H^\circ_{298} = 599.3 \text{ kJ mol}^{-1}$ [1469]

^kBased on Knudsen mode measurements

^lThe sum of average partial enthalpies (heats) of vaporization of C_1 (gas) and Zr (gas) from $\text{ZrC}_{-1.0}$ calculated in accordance to the second law of thermodynamics

^mBased on Langmuir mode measurements

ⁿCarbon content – 44.4 at.% [10]

^oCarbon content – 49.2 at.% [11]

^pCarbon content of ~46 at.% is corresponding to the maximal melting temperature; for 49.9 at.% of carbon composition: solidus and liquidus temperatures are ~3375 and ~3410 °C, respectively [72]

^qCarbon content – 46 at.%

^rCarbon content – 44–46 at.%

^sCarbon content – 44.1 at.%

^tCarbon content – 48.7 at.%

^uCarbon content – 46.5 at.%

in the range of temperatures from 300 to 3700 K (up to melting point) [211]

$$c_p = 47.43 + (9.234 \times 10^{-3})T - (1.092 \times 10^6)T^{-2}, \quad (5.8)$$

in the range of temperatures from 300 to 3800 K (up to melting point) [224]

$$c_p = 51.03 + (3.686 \times 10^{-3})T - (1.990 \times 10^{-7})T^2 + (2.893 \times 10^{-11})T^3 - (1.304 \times 10^6)T^{-2}, \quad (5.9)$$

in the range of temperatures from 500 to 2870 K [245]

$$c_p = 73.21 - (3.591 \times 10^{-2})T + (1.348 \times 10^{-5})T^2, \quad (5.10)$$

in the range of temperatures from 1000 to 3000 K [202, 204]

$$c_p = 45.99 + (4.841 \times 10^{-3})T + (8.368 \times 10^5)T^{-2}, \quad (5.11)$$

in the range of temperatures from 1400 to 2800 K [54]

$$c_p = 38.50 + (0.962 \times 10^{-2})T, \quad (5.12)$$

in the range of temperatures from 1400 to 2800 K [54]

$$c_p = 80.64 \exp(-641.5/T), \quad (5.13)$$

in the range of temperatures from 1600 to 2300 K [202, 205]

$$c_p = 38.41 + (0.839 \times 10^{-2})T. \quad (5.14)$$

in the range of temperatures from 3800 to 6000 K (in liquid state) [224]

$$c_p = 62.76 - (2.984 \times 10^{-10})T + (5.524 \times 10^{-14})T^2 - (3.538 \times 10^{-18})T^3 - 0.8337T^{-2}, \quad (5.15)$$

For the molar heat capacity $c_p = f(T, \text{K})$, $\text{J mol}^{-1} \text{K}^{-1}$, of zirconium monocarbide phases with various deviations from the stoichiometry, the following relationships were recommended in literature:

for $\text{ZrC}_{0.58}$ (in the range of temperatures from 700 to 2500 K) [4, 210]

$$c_p = 28.7 + (1.06 \times 10^{-3})T, \quad (5.16)$$

for $\text{ZrC}_{0.69}$ (in the range of temperatures from 1200 to 2500 K) [4, 202, 208, 1465]

$$c_p = 33.71 + (8.067 \times 10^{-3})T + (31.90 \times 10^{12})T^{-2} \exp(-31400/T), \quad (5.17)$$

for $\text{ZrC}_{0.76}$ (in the range of temperatures from 1200 to 2500 K) [4, 202, 208, 1465]

$$c_p = 32.48 + (9.824 \times 10^{-3})T + (13.85 \times 10^{10})T^{-2} \exp(-19960/T), \quad (5.18)$$

for $\text{ZrC}_{0.80}$ (in the range of temperatures from 700 to 2500 K) [4, 210]

$$c_p = 25.1 + (1.26 \times 10^{-3})T, \quad (5.19)$$

for $\text{ZrC}_{0.96}$ (in the range of temperatures from 300 to 2500 K) [31, 96, 203, 207]

$$c_p = 36.44 + (9.540 \times 10^{-3})T - (2.636 \times 10^5)T^{-2}, \quad (5.20)$$

for $\text{ZrC}_{0.96}$ (in the range of temperatures from 300 to 3200 K) [74, 84]

$$c_p = 56.86 - (10.90 \times 10^{-3})T + (5.586 \times 10^{-6})T^2 - (1.456 \times 10^6)T^{-2}, \quad (5.21)$$

for $\text{ZrC}_{0.96}$ (in the range of temperatures from 1300 to 2800 K) [94, 202]

$$c_p = 41.50 + (0.954 \times 10^{-3})T, \quad (5.22)$$

for $\text{ZrC}_{0.96}\text{N}_{0.04}$ (in the range of temperatures from 300 to 1100 K) [278]

$$c_p = 48.18 + (5.35 \times 10^{-3})T - (1.851 \times 10^{-6})T^2 - (1.202 \times 10^6)T^{-2}, \quad (5.23)$$

for $\text{ZrC}_{0.97}$ (in the range of temperatures from 700 to 2500 K) [4, 210]

$$c_p = 24.5 + (0.80 \times 10^{-3})T, \quad (5.24)$$

for $\text{ZrC}_{0.98}$ (in the range of temperatures from 1200 to 2500 K) [202, 203]

$$c_p = 25.18 + 0.183T, \quad (5.25)$$

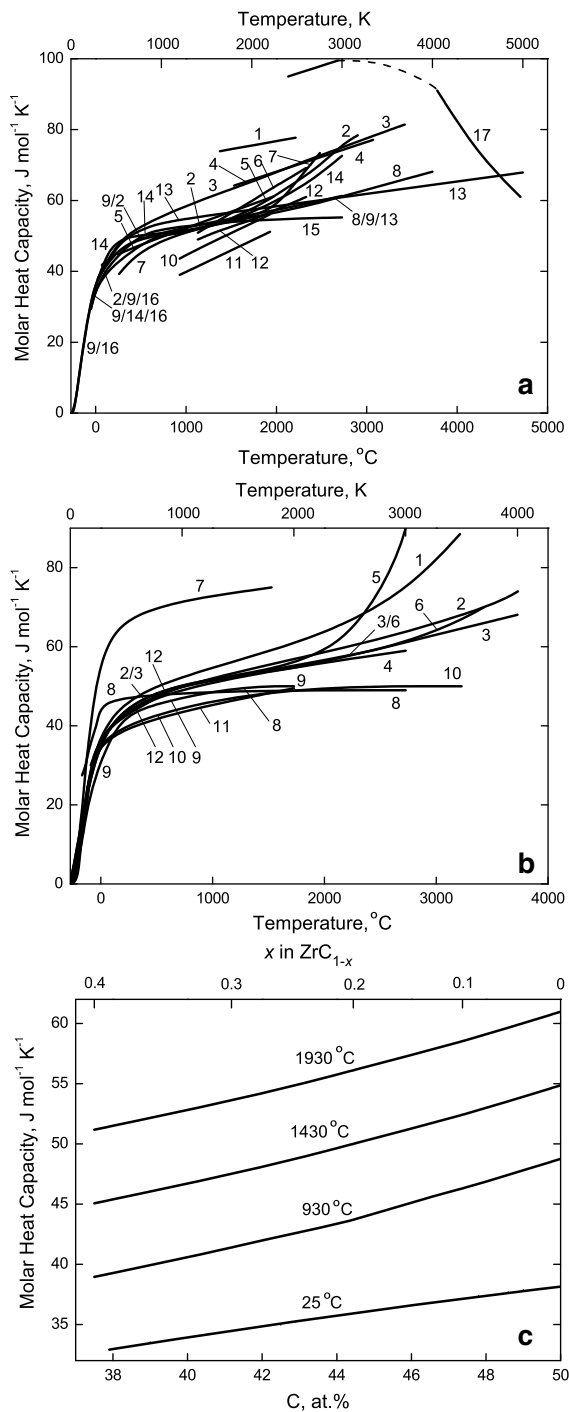


Fig. 5.5 (see caption on page 439)

◀**Fig. 5.5** Variations of molar heat capacity c of zirconium carbide ZrC_{1-x} phases with temperature (a–b) and carbon content within the homogeneity range at various temperatures (c): (a) – experimental data at constant pressure, c_p (1 – $ZrC_{0.94}$, contents: O – 1.21%, N – 1.03%, Hf – 0.78% [254]; 2 – $ZrC_{0.96}$, on the basis of several sources [84, 94, 255, 265, 278]; 3 – $ZrC_{\sim 1.0}$, recommended on the basis of several sources [211]; 4 – $ZrC_{\sim 1.0}$ [275]; 5 – plasma-sprayed $ZrC_{0.95}$, non-combined C – 0.67% [253]; 6 – $ZrC_{0.85}$ [239]; 7 – $ZrC_{0.92-0.94}$, contents: O < 0.1%, N – 0.5% [245]; 8 – $ZrC_{\sim 1.0}$, assessment based on thermodynamical calculations [16], experimentally confirmed [204, 205]; 9 – $ZrC_{\sim 1.0}$, 10 – $ZrC_{0.80}$ and 11 – $ZrC_{0.60}$, calculated on the basis of experimental data [202, 208, 257, 258]; 12 – $ZrC_{0.95}$ [239]; 13 – $ZrC_{\sim 1.0}$, recommended on the basis of several sources [224, 241]; 14 – $ZrC_{0.96}$, on the basis of several sources [10]; 15 – $ZrC_{\sim 1.0}$, recommended on the basis of several sources [272]; 16 – $ZrC_{0.95}$, contents: O – 0.005%, N – 0.067% [222] and 17 – $ZrC_{0.95}$, from experimental data on pulsed electrical heating with microsecond duration around solidus (3180 °C) and liquidus (3580 °C) temperatures with uncertainties ± 60 K for solid and ± 110 K for liquid states [1507, 1508]); (b) – theoretically calculated values for stoichiometric $ZrC_{\sim 1.0}$ at constant pressure, c_p (1 – Slater’s approximation and 2 – Dugdale-MacDonald’s approximation on the basis of Debye-Grüneisen model [280], 3 – thermodynamical assessment [16], 4 – on the basis of the projector augmented-wave (PAW) method within the generalized gradient approximation (GGA) [284], 5 – on the basis of two-stage upsampled thermodynamic integration using Langevin dynamics (TU-TILD) approach within GGA and 6 – same, within local density approximation (LDA) [698]) and at constant volume, c_v , on the basis of density functional theory (DFT) (7 – [69], 8 – [285], 9 – [284], 10 – [281], 11 – using GGA of the Perdew-Burke-Ernzerhof (PBE) scheme, lattice heat capacity [282] and 12 – [283]); (c) – experimental data at constant pressure, c_p (at 25 °C, based on several sources [84, 85, 222]; at 930, 1430 and 1930 °C, statistical-mathematical treatment of experimental temperature-concentration functions [202, 206, 208, 209, 257, 258]); when it is not indicated specially, data given are for quasi-stoichiometric composition

for $ZrC_{0.99}$ (in the range of temperatures from 1200 to 2500 K) [4, 202, 208, 1465]

$$c_p = 30.66 + (13.92 \times 10^{-3})T \quad (5.26)$$

and for ZrC_{1-x} in general (in the range of temperatures from 1200 to 2200 K, for $0 < x \leq 0.31$) [202, 206]

$$c_p = (1 - 0.427x) [30.765 + (14.108 \times 10^{-3})T], \quad (5.27)$$

or

$$c_p = 34.077 + (12.288 \times 10^{-3})T - 24.483x, \quad (5.28)$$

where T is temperature, K, and x is the value of index in ZrC_{1-x} formula (*note*: Eq. (5.28) for $0 < x \leq 0.05$ can be applied in the extended interval at higher temperatures – up to 2500 K); for the specific heat capacity of zirconium monocarbide ZrC_{1-x} in the homogeneity range ($0 < x < 0.35$) at ~ 300 K the equation $c = f(T, K)$, $J kg^{-1} K^{-1}$, is given by Katoh et al. [96] as

$$c = 373.2 - 355.6x + 686.0x^2 - 335.3x^3. \quad (5.29)$$

The variations of molar heat capacity c with temperature for zirconium monocarbide ZrC_{1-x} phases are demonstrated on the basis of several sources in Fig. 5.5. The thermal properties of ZrC_{1-x} are very sensitive to the deviation from the stoichiometry: for the standard heat of formation ΔH_{298}° , kJ mol⁻¹, molar enthalpy difference $H_T^{\circ} - H_{298}^{\circ}$, J mol⁻¹, and molar entropy S_T° , J mol⁻¹ K⁻¹, the following concentration and temperature-concentration dependencies within the homogeneity range of ZrC_{1-x} were calculated on the basis of experimental data [2, 202, 206, 208, 209, 240, 257, 258, 286, 292, 1466–1468]:

$$\Delta H_{298}^{\circ} = -206.7 + 154.04x, \quad (5.30)$$

$$\Delta H_{298}^{\circ} = 27.97 - 347.4(1 - x) + 112.8(1 - x)^2 \pm 10.0, \quad (5.31)$$

$$H_T^{\circ} - H_{298}^{\circ} = (1 - 0.427x) [30.765T + (7.054 \times 10^{-3})T^2 - 3230], \quad (5.32)$$

$$H_T^{\circ} - H_{298}^{\circ} = 12,713x - 24.488xT + 34.077T + (6.114 \times 10^{-3})T^2 - 6198 \quad (5.33)$$

$$S_T^{\circ} = 74.48 \lg T + (12.228 \times 10^{-3})T + 151.21x - 55.40x \lg T - 154.50, \quad (5.34)$$

where T is temperature, K, and x is the value of index in ZrC_{1-x} formula (in general Eqs. (5.32–5.34) were recommended for the range of temperatures from 1200 to 2200 K, but for carbon-rich compositions ($0 \leq x \leq 0.05$) the interval of reliable usage expands up to 2500 K). The thermodynamic functions of stoichiometric zirconium carbide are tabulated by Turchanin et al. [202, 208, 257] in the range of 0–3000 K, by Schick [211] and Chase [224] in the range of 0–6000 K, and by Barin [241] in the range of 298.15–4000 K, the thermodynamic functions of $ZrC_{0.96}$ in the range of 298.15–3000 K – by Storms [10] and Toth [11].

During the vaporization processes from the surface of zirconium monocarbide at high and ultra-high temperatures in vacuum, the composition of the carbide phase (C/Zr ratio) can change noticeably. The following equation was recommended for zirconium (P_{Zr} , Pa) partial pressure over near-stoichiometric monocarbide phase, which is in equilibrium with carbon ($ZrC_{1-x} + C$), by Storms [10] for 2520–2820 K (2245–2545 °C):

$$\lg P_{Zr} = -(4.161 \times 10^4)/T + 12.592, \quad (5.35)$$

the estimation of zirconium (P_{Zr} , Pa) and carbon (P_C , Pa) partial pressures in the gaseous phase in the Zr–C system carried out by Kulikov [238] led to such relationships as

for the conditions of congruent vaporization of quasi-stoichiometric ZrC_{1-x} :

at 1000–2125 K (730–1850 °C)

$$\lg P_{Zr} = -(3.948 \times 10^4)/T + 12.888, \quad (5.36)$$

at 2125–3690 K (1850–3420 °C)

$$\lg P_{Zr} = -(3.933 \times 10^4)/T + 12.819, \quad (5.37)$$

at 3690–5000 K (3420–4730 °C)

$$\lg P_{Zr} = -(3.379 \times 10^4)/T + 11.319, \quad (5.38)$$

for the monoatomic gases of Zr and C over ZrC_{1-x} in the monocarbide homogeneity range:

at 2000 K (1730 °C)

$$\lg P_{Zr} = -0.935 - 7.420(1 - x)^2, \quad (5.39)$$

$$\lg P_C = -12.792 + 7.420(1 - x)^2, \quad (5.40)$$

at 3000 K (2730 °C)

$$\lg P_{Zr} = 3.236 - 5.069(1 - x)^2, \quad (5.41)$$

$$\lg P_C = -3.971 + 5.069(1 - x)^2, \quad (5.42)$$

at 5000 K (4730 °C)

$$\lg P_{Zr} = 5.467 - 1.904(1 - x)^2, \quad (5.43)$$

$$\lg P_C = 3.473 + 1.904(1 - x)^2, \quad (5.44)$$

for the conditions of ZrC_{1-x} -C phases equilibrium:

at 1000–2125 K (730–1850 °C)

$$\lg P_{Zr} = -(4.143 \times 10^4)/T + 12.534, \quad (5.45)$$

at 2125–3690 K (1850–3420 °C)

$$\lg P_{\text{Zr}} = -(4.057 \times 10^4)/T + 12.122, \quad (5.46)$$

at 3690–5000 K (3420–4730 °C)

$$\lg P_{\text{Zr}} = -(3.430 \times 10^4)/T + 10.423, \quad (5.47)$$

where T is temperature, K and x is the value of index in ZrC_{1-x} (see Tables 5.5 and 5.6). Within the homogeneity range of ZrC_{1-x} the vapour pressure of metal over the carbide surface increases rapidly, e.g. from $\sim 4.1 \times 10^{-8}$ Pa for $\text{ZrC}_{\sim 1.0} + \text{C}$ to $\sim 2.0 \times 10^{-3}$ Pa for $\text{ZrC}_{0.58} + \text{Zr}$ at 2100 K (1830 °C), or from $\sim 9.1 \times 10^{-2}$ Pa up to ~ 20 Pa for the similar compositions at 3000 K (2730 °C), while the average partial enthalpy (heat) of vaporization of zirconium decreases from ~ 820 – 840 kJ mol $^{-1}$ for $\text{ZrC}_{\sim 1.0}$ to ~ 570 – 590 kJ mol $^{-1}$ for $\text{ZrC}_{0.58}$ (the sharpest drop in this value is observed for compositions within $0 < x < 0.1$ interval) [10, 26, 27, 84, 294, 1377]. The partial pressures of zirconium and carbon over the monocarbide phase as functions of composition at the fixed temperature 3000 K (2730 °C) are shown in Fig. 5.6 in comparison with the equilibrium pressure of carbon over pure graphite surface. The vapour phase above carbon-saturated zirconium monocarbide in equilibrium with graphite contains atoms of zirconium and molecules of carbon [293], plus molecules of ZrC_2 , observed at 2660 K (2390 °C) by Starostina et al. [289]. The equilibrium pressure should be lower than the pressure observed upon vaporization from an open surface into a vacuum (Langmuir mode). According to Nikolskaya et al. [290, 291] the vapour pressures of zirconium (P_{Zr} , Pa) and carbon (P_{C} , Pa) in Langmuir vaporization of zirconium monocarbide in the temperature range of 2300–3100 K (2030–2830 °C) can be described by the equations

$$\lg P_{\text{Zr}} = 11.26 - (3.147 \times 10^4)/T - (7.2 \times 10^{-5})T + \lg x, \quad (5.48)$$

$$\lg P_{\text{C}} = 14.76 - (4.759 \times 10^4)/T + (1.2 \times 10^{-5})T + \lg[(1-x)/x], \quad (5.49)$$

where x is the value of index in ZrC_{1-x} formula and T is temperature, K. For the general evaporation rate G , g cm $^{-2}$ s $^{-1}$, as a function of temperature T , K, the following equations were proposed by Fesenko and Bolgar [26, 27, 208, 288] with the measurements from an open surface into a vacuum for $\text{ZrC}_{0.95}$ in the range of temperatures from 2770 K (2500 °C) to 3170 K (2900 °C):

$$\lg G = (8.9 \pm 0.2) - [(4.11 \pm 0.04) \times 10^4]/T \quad (5.50)$$

and by Vlasov et al. [295] for $\text{ZrC}_{0.97}$ (lost mainly carbon during the initial heating) in the range of temperatures from 2500 K (2230 °C) to 3270 K (3000 °C)

Table 5.5 Parameters of the gaseous phase in the Zr-C system in the conditions of Zr-ZrC_{1-x} phases equilibrium, congruent dissociation of quasi-stoichiometric ZrC_{1-x} and ZrC_{1-x}-C phases equilibrium calculated on the basis of thermodynamic data [238]

Parameters	Temperature, K (°C)									
	1000 (730)	1500 (1230)	2125 (1850)	2500 (2230)	3000 (2730)	3690 (3420)	4000 (3730)	4645 (4370)	5000 (4730)	
	Zr-ZrC _{1-x} phases equilibrium									
lgP _{Zr} , Pa	-18.885	-8.582	-2.504	-0.396	1.580	3.416	4.021	5.025	-	-
lgP _Σ ^a , Pa	-18.885	-8.582	-2.504	-0.396	1.580	3.417	4.024	5.031	-	-
lg(C/Zr) ^b	-15.412	-9.862	-6.245	-4.942	-3.655	-2.469	-2.180	-1.857	-	-
Contents, vol.%,										
C	-	-	-	-	0.02	0.21	0.39	0.77	-	-
C ₂	-	-	-	-	-	-	0.005	0.01	-	-
Zr	100.0	100.0	100.0	100.0	99.97	99.66	99.34	98.63	-	-
ZrC ^c	-	-	-	-	0.007	0.13	0.26	0.59	-	-
	Congruent dissociation of quasi-stoichiometric ZrC _{1-x}									
lgP _{Zr} , Pa	-26.591	-13.416	-5.691	-2.908	-0.282	2.168	2.918	4.052	4.560	
lgP _Σ ^a , Pa	-26.291	-13.115	-5.393	-2.617	-0.005	2.427	3.178	4.322	4.833	
Contents, vol.%,										
C	50.00	49.94	49.18	47.20	42.76	37.18	34.83	35.28	35.21	
C ₂	-	0.01	0.31	0.93	2.30	4.28	5.00	5.46	5.72	
C ₃	-	0.003	0.17	0.67	1.84	3.21	3.37	2.47	2.20	
Zr	50.00	50.05	50.33	51.16	52.84	55.09	54.95	53.76	53.30	
ZrC ^c	-	-	0.01	0.04	0.26	1.25	1.84	3.01	3.55	

(continued)

Table 5.5 (continued)

Parameters	Temperature, K (°C)									
	1000 (730)	1500 (1230)	2125 (1850)	2500 (2230)	3000 (2730)	3690 (3420)	4000 (3730)	4645 (4370)	5000 (4730)	
$\lg P_{\text{Zr}}, \text{Pa}$	-28.896	-15.067	-6.972	-4.068	-1.357	1.135	1.857	3.038	3.563	
$\lg P_{\Sigma}^{\text{g}}, \text{Pa}$	-24.286	-11.719	-4.044	-1.154	1.596	4.156	5.035	6.012	6.394	
$\lg(C/\text{Zr})^{\text{b}}$	4.610	3.426	3.250	3.161	3.357	3.388	3.521	3.252	3.076	
Contents, vol.%,										
C	99.88	89.72	42.12	23.51	12.75	7.28	5.58	7.76	9.61	
C ₂	0.01	0.82	5.08	6.66	8.15	9.28	9.21	12.97	15.52	
C ₃	0.11	9.41	52.66	69.23	77.34	75.05	71.36	63.36	59.28	
C ₄	-	-	0.01	0.04	0.26	1.25	2.04	3.16	3.62	
C ₅	-	-	0.02	0.20	1.38	7.02	11.71	12.58	11.72	
Zr	0.003	0.05	0.12	0.12	0.11	0.10	0.07	0.11	0.15	
ZrC ^c	-	-	-	0.002	0.007	0.02	0.03	0.06	0.10	

^aTotal gas pressure^bLogarithm of atomic ratio in gaseous phase^cGaseous molecule

Table 5.6 Calculated parameters of the gaseous phase over zirconium monocarbide ZrC_{1-x} in its homogeneity range on the basis of thermodynamic data [238]

Parameters	Phase composition, x															
	0.01	0.04	0.10	0.11	0.125	0.15	0.17	0.19	0.20	0.25	0.30	0.35	0.40	0.42		
$\lg P_{Zr}$, Pa	-8.207	-	-	-6.839	-6.613	-6.296	-	-	-	-5.109	-	-4.070	-	-3.431		
$\lg P_{\Sigma}$, Pa	-5.223	-	-	-6.561	-6.494	-6.265	-	-	-	-5.109	-	-4.070	-	-3.431		
Contents, vol.%;																
C	50.52	-	-	47.07	23.97	6.83	-	-	-	0.03	-	-	-	-		
C ₂	4.04	-	-	0.16	0.05	0.007	-	-	-	-	-	-	-	-		
C ₃	45.34	-	-	0.08	0.01	0.001	-	-	-	-	-	-	-	-		
Zr	0.10	-	-	52.69	75.97	93.16	-	-	-	99.97	-	100.0	-	100.0		
$\lg P_{Zr}$, Pa	-	-1.436	-0.870	-	-	-	-0.291	-0.071	-0.008	-	0.752	-	1.411	-		
$\lg P_{\Sigma}$, Pa	-	1.577	0.370	-	-	-	-0.046	0.021	0.069	-	0.755	-	1.411	-		
Contents, vol.%;																
C	-	12.99	58.18	-	-	-	40.01	21.59	15.99	-	0.57	-	0.03	-		
C ₂	-	8.29	10.08	-	-	-	1.83	0.62	0.15	-	0.002	-	-	-		
C ₃	-	78.63	25.99	-	-	-	1.24	0.27	0.13	-	-	-	-	-		
Zr	-	0.09	5.75	-	-	-	56.92	77.52	87.73	-	99.43	-	99.97	-		

^aTotal gas pressure

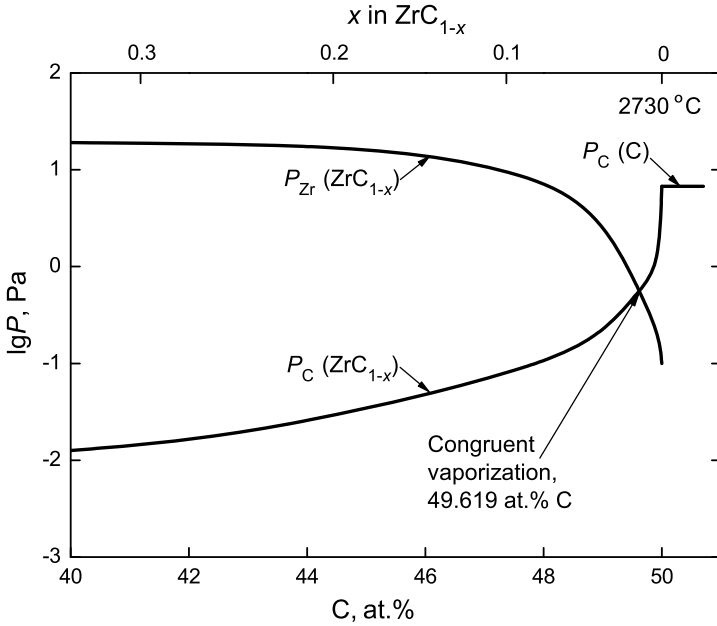


Fig. 5.6 Partial pressures of zirconium $P_{Zr}(\text{ZrC}_{1-x})$ and carbon $P_C(\text{ZrC}_{1-x})$ over zirconium carbide ZrC_{1-x} phase, and vapour pressure of carbon over pure graphite $P_C(\text{C})$ as functions of carbide composition at 3000 K (2730 °C) calculated by Kaufman [11, 33, 231, 287]; a congruently vaporizing composition is marked

$$\lg G = (3.2 \pm 0.5) - [(2.26 \pm 0.24) \times 10^4]/T \quad (5.51)$$

and for $\text{ZrC}_{0.88}$ (demonstrated the constancy of the composition irrespectively of the duration of heating) at 2600–3030 K (2330–2760 °C)

$$\lg G = (8.1 \pm 1.2) - [(3.92 \pm 0.35) \times 10^4]/T, \quad (5.52)$$

where T is temperature, K. Through a large part of the homogeneity range of ZrC_{1-x} the vapour phase should receive metallic atoms mainly, although in a certain area of compositions congruent vaporization may occur [26, 27, 296]. According to Kaufman and Sarney [287, 294], Coffman et al. [229] and Fesenko and Bolgar et al. [288, 1474], the congruently vaporizing composition of zirconium monocarbide phase at temperatures above 2500 K (2230 °C) corresponds to $\text{ZrC}_{\sim 1.0}$ ($x \approx 0$). However, at temperatures about 3000 K (2730 °C) Storms [10] showed that this carbide composition is located at around of $0.13 \leq x \leq 0.18$; the similar data, which could be described by the following equation for the congruently vaporizing composition of ZrC_{1-x} :

$$\lg x = -0.1696 - (1.633 \times 10^3)/T, \quad (5.53)$$

where x is the value of index in ZrC_{1-x} formula and T is temperature, K, were presented by Nikolskaya et al. [290, 291] for the temperature range from 2270 K (2000 °C) to 3070 K (2800 °C), where the composition vaporizing congruently shifts from $\text{ZrC}_{0.87}$ to $\text{ZrC}_{0.80}$ with temperature growth, while the rate of congruent vaporization V , $\text{g cm}^{-2} \text{ s}^{-1}$, was estimated by them in the temperature interval of 2390–3100 K (2120–2830 °C) as

$$\lg V = 8.555 - (3.813 \times 10^4)/T, \quad (5.54)$$

where T is temperature, K. Also it should be mentioned that Andrievskii et al. [231, 298] demonstrated that the value of congruently vaporizing composition of ZrC_{1-x} phase at temperatures about 2300 K (2030 °C) ranges within the limited interval of $0.08 \leq x \leq 0.09$ and depends very little on temperature; while Zotov and Kotelnikov [1473], who studied volatilization of various compositions of zirconium monocarbide from $\text{ZrC}_{0.72}$ to $\text{ZrC}_{0.98}$ in high vacuum ($3 \times 10^{-2} - 5 \times 10^{-3}$ Pa) at 2770–3100 K (2500–2830 °C), revealed that the interval of congruently vaporizing compositions in above mentioned conditions is around $0.12 \leq x \leq 0.14$ and a decrease in carbon content in ZrC_{1-x} increases vaporization rate of the materials noticeably [320].

The values of some general thermodynamic properties, vapour pressures and mass/linear vaporization rates for zirconium monocarbide are given in Addendum in comparison with other ultra-high temperature materials in the wide ranges of temperatures.

At room temperature the thermal conductivity of near-stoichiometric zirconium monocarbide ZrC_{1-x} is around $15\text{--}40 \text{ W m}^{-1} \text{ K}^{-1}$ (with thermal diffusivity of about $0.07\text{--}0.15 \text{ cm}^2 \text{ s}^{-1}$) [1, 26, 27, 30, 32, 35, 37, 39, 45, 46, 53, 85, 199, 213, 278, 299–301, 306, 308, 319, 320, 325, 328, 331–337, 341, 342, 377, 378, 380, 721]; it is affected by the incoherent boundaries and porosity in carbide materials noticeably [96], e.g. the thermal conductivity of ZrC_{1-x} fibrous materials with 70–75% porosity at 300–900 °C is $0.5\text{--}2.0 \text{ W m}^{-1} \text{ K}^{-1}$ [336–339]. Marmer et al. [213] revealed for ZrC_{1-x} materials in the range of 1200–2700 °C the increase of thermal conductivity from 9–10 to 19–38 $\text{W m}^{-1} \text{ K}^{-1}$ with 12–20% increase of porosity, it should be mentioned especially that the same researchers also found out the similar effect of porosity on NbC_{1-x} and TiC_{1-x} materials. Within the homogeneity range, as a consequence of conduction electrons scattering on the carbon sublattice vacancies and thermal lattice vibrations, the thermal conductivity of ZrC_{1-x} declines with increasing carbon deficit (value of x) in the phase [33, 344] that is demonstrated perfectly in Fig. 5.7; while Wagner [345] proposed that the electronic contribution to the thermal conductivity at room temperature, which is $\sim 37\%$ for a material with composition in the range of $0.15 \leq x \leq 0.35$, diminishes as x approaches zero. Storms and Wagner [85] gave an empirical equation ($0 < x \leq 0.4$)

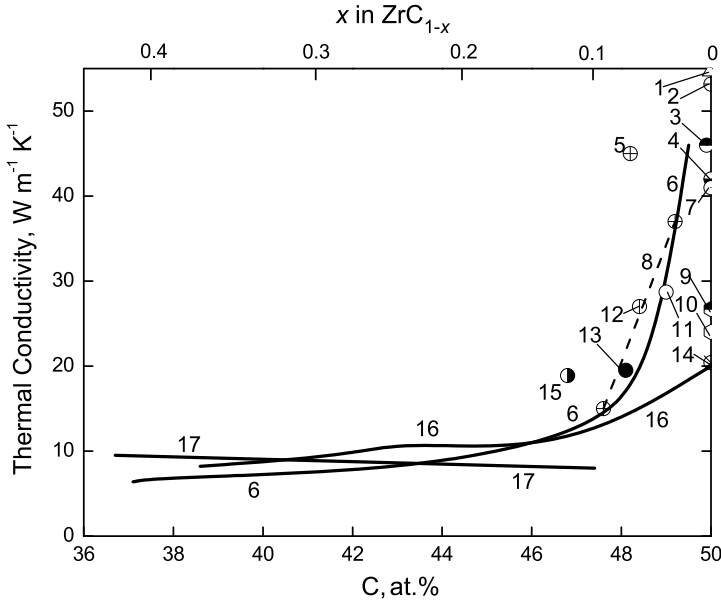


Fig. 5.7 Thermal conductivity λ of zirconium monocarbide ZrC_{1-x} materials at room temperature as a function of carbide composition within the homogeneity range: 1 – [30, 213]; 2 – at 300 °C [45, 306]; 3 – pyrolytic [301]; 4 – at 0 °C [53]; 5 – sintered, porosity 6–8%, contents: non-combined C – 0.5%, W – 0.2% [411]; 6 – hot-pressed, content O – 0.015–0.090%, corrected to porosity [85, 325]; 7 – at 50 °C, hot-pressed rods, corrected to porosity [308]; 8 – sintered, porosity 13–19% [297]; 9 – hot-pressed, porosity 1% [341, 342]; 10 – extrapolated value [328]; 11 – pyrolytic, content N – 0.03–0.08% [300]; 12 – hot-pressed, corrected to porosity [326]; 13 – hot-pressed, content O – 0.6% [90]; 14 – at 0–500 °C [35, 37, 46]; 15 – single crystal, contents: O < 0.01%, N < 0.01% [302, 303]; 16 – sintered in vacuum, corrected to porosity [1, 26, 27, 32, 299]; 17 – sintered in vacuum, content N – 0.05% [137]

$$\lambda = 1.05 \times 10^3 \left[3.82 \times 10^{-3} + (55 + 950x)^{-1} \right] + 0.07x^{-2}, \quad (5.55)$$

where x is the value of index in ZrC_{1-x} formula, to represent the relationship between the thermal conductivity λ and composition within the homogeneity range of monocarbide. However, the effect of an increase in the deviation from the stoichiometry was proposed by Avgustinik et al. [137] to reduce the connectivity of the monocarbide lattice while introducing vacancies and increasing the concentration of non-localized electrons, as they found out the decline of thermal conductivity from $\sim 9 \text{ W m}^{-1} \text{ K}^{-1}$ for $ZrC_{0.60}$ to $\sim 6 \text{ W m}^{-1} \text{ K}^{-1}$ for $ZrC_{0.90}$ employing the high-purity zirconium monocarbide materials. The variations of thermal conductivity with temperature for near-stoichiometric ZrC_{1-x} materials on

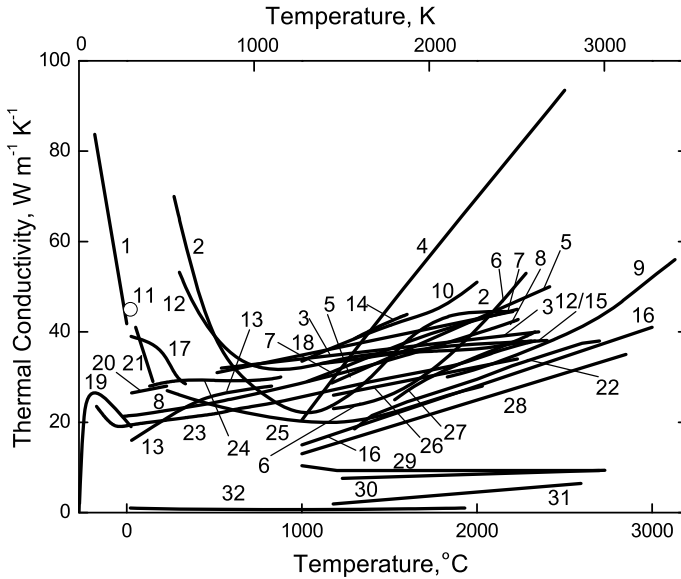


Fig. 5.8 Variation of thermal conductivity λ with temperature for near-stoichiometric zirconium monocarbide ZrC_{1-x} materials on the basis of several sources: 1 – $ZrC_{\sim 1.0}$, porosity 2% [321]; 2 – $ZrC_{0.92}$, sintered and annealed at 2200–2500 °C, porosity 7.5% and 3 – same, without annealing [245, 319]; 4 – $ZrC_{\sim 1.0}$, sintered and annealed in vacuum, porosity 10% [117, 329]; 5 – $ZrC_{0.96}$, porosity 5% [330]; 6 – $ZrC_{\sim 1.0}$, porosity 6% [337]; 7 – $ZrC_{0.97}$, sintered and annealed in vacuum, corrected to porosity, content N – 0.04% [210, 305]; 8 – [304, 320]; 9 – $ZrC_{0.96}$, porosity 12–16% [311]; 10 – pyrolytic $ZrC_{0.99}$ [314]; 11 – sintered $ZrC_{0.93}$, porosity 6–8%, contents: non-combined C – 0.5%, W – 0.2% [411]; 12 – [45, 306]; 13 – hot-pressed $ZrC_{0.96}N_{0.04}$, porosity 1% [278]; 14 – hot-pressed $ZrC_{0.93-0.99}$, content non-combined C – 0–0.8%, radial diffusivity method [322, 323]; 15 – $ZrC_{0.95}$ [239]; 16 – recommended on the basis of several sources [33]; 17 – hot-pressed $ZrC_{\sim 1.0}$ spheres, corrected to porosity [308]; 18 – hot-pressed $ZrC_{0.93-0.99}$, content non-combined C – 0–0.8, steady-state method [307]; 19 – single crystal $ZrC_{0.88}$, contents: O < 0.01%, N < 0.01% [302, 303]; 20 – [327]; 21 – hot-pressed $ZrC_{\sim 1.0}$ rods, corrected to porosity [308]; 22 – hot-pressed $ZrC_{0.93}$, porosity 19–24% [310, 324]; 23 – hot-pressed $ZrC_{0.92}$, porosity 5%, content O – 0.6% [90]; 24 – $ZrC_{0.79}$, porosity 5–12%, content non-combined C – 1.1% [312]; 25 – sintered $ZrC_{0.98}$, porosity 3–7% [313]; 26 – hot-pressed (in vacuum) $ZrC_{\sim 1.0}$, corrected to porosity and thermal expansion, contents: non-combined C – 0.18–0.30%, O – 0.001–0.09% [77]; 27 – pyrolytic $ZrC_{0.99}$ [309, 318]; 28 – hot-pressed $ZrC_{\sim 1.0}$ [26, 27]; 29 – sintered $ZrC_{0.98}$, porosity 5–7% [213]; 30 – sintered $ZrC_{0.98}$, corrected to porosity [315–317]; 31 – $ZrC_{\sim 1.0}$, porosity 63% [330]; 32 – unwoven felt $ZrC_{\sim 1.0}$, mean filament diameter 16 μm , porosity $\sim 80\%$ [338] (when it is not indicated specially, data are given for near-stoichiometric compositions)

the basis of several sources are shown in Fig. 5.8. The thermal conductivity λ of hot-pressed (in vacuum) $ZrC_{0.97}$ (contents: non-combined C – 0.3%, O – 0.09%) in the range of temperatures from 1230 to 2130 °C Grossman [77] described by the following equation (with accuracy $\pm 10\%$):

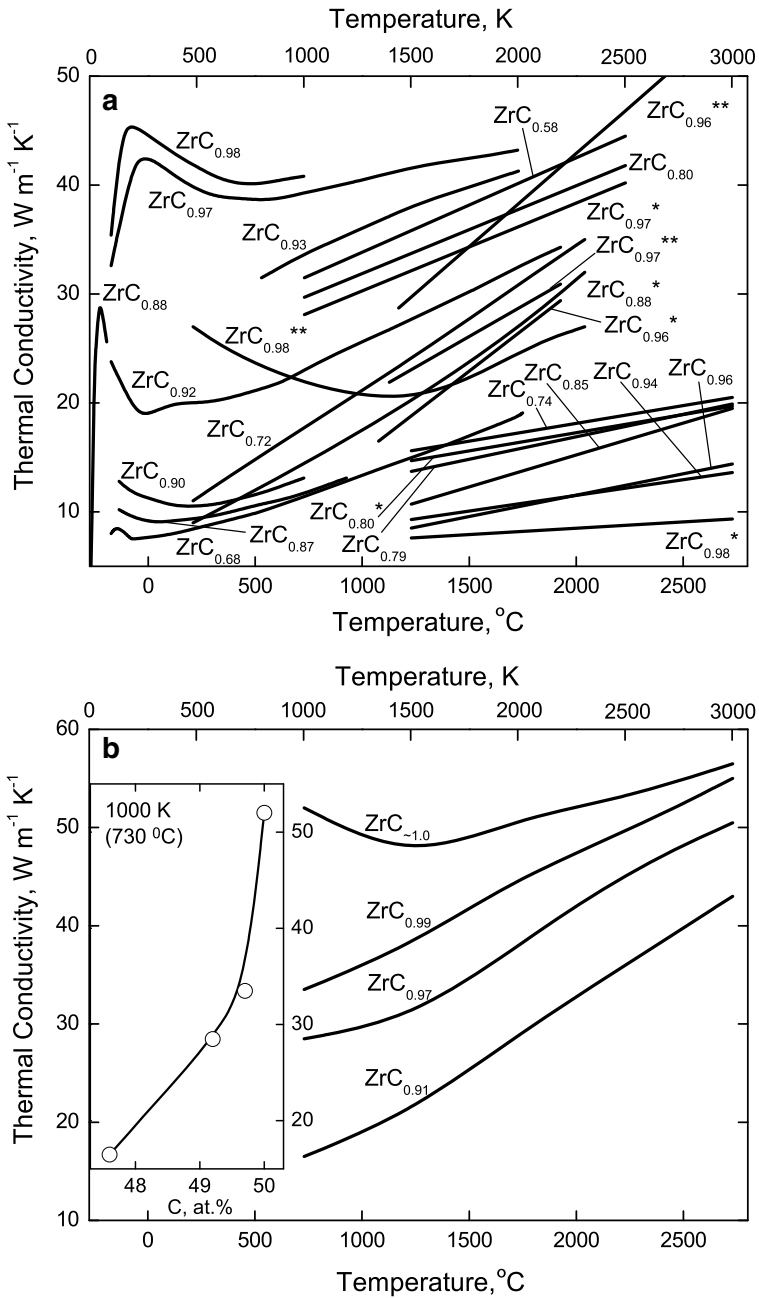


Fig. 5.9 (see caption on page 451)

◀**Fig. 5.9** Thermal conductivity λ of ZrC_{1-x} as a function of temperature for the phases having different deviations from the stoichiometry: **(a)** – experimental data (hot-pressed at 2730 °C, data corrected to 100% dense materials, content O – 0.015–0.1%, $x = 0.02, 0.03, 0.10, 0.13, 0.32$ [325]; sintered in vacuum, corrected to porosity, $x = 0.03^*, 0.20, 0.42$ [210, 305, 409]; high purity materials sintered in vacuum at 2230 °C, corrected to porosity, content O + N – 0.1–0.3%, $x = 0.02^*, 0.04, 0.06, 0.15, 0.20^*, 0.26$ [61, 315–317]; hot-pressed, corrected to porosity, $x = 0.07$ [326]; single crystals, contents O, N < 0.01%, $x = 0.12$ [302, 303]; hot-pressed, porosity 5%, content O – 0.6%, $x = 0.08$ [90]; hot-pressed in vacuum, porosity 8.5%, contents: non-combined C – 0.3%, O – 0.09%, $x = 0.03^{**}$ [77]; hot-pressed, porosity 20%, $x = 0.04^*$ [310]; porosity 5%, $x = 0.04^{**}$ [330]; $x = 0.02^{**}, 0.12^*, 0.28$ [313]) and **(b)** – values calculated by empirical potential molecular dynamics (vibrational part) and density functional theory (electronic part) for $x = 0, 0.01, 0.03, 0.09$ (*Inset* – calculated relationship between thermal conductivity and carbon content in carbide for $0 \leq x \leq 0.09$ at 730 °C) [340]

$$\lambda = 16.7 + (7.11 \times 10^{-3})(t + 273), \quad (5.56)$$

and for the experimental data fit of thermal conductivity λ of $\text{ZrC}_{0.96}\text{N}_{0.04}$ phase Lengauer et al. [278] obtained the following polynomial expression for the range of 300–1100 K (25–830 °C):

$$\lambda = 22.11 + (7.224 \times 10^{-3})(t + 273) - (0.804 \times 10^{-6})(t + 273)^2 - (6.600 \times 10^5)/(t + 273)^2, \quad (5.57)$$

where t is temperature, °C. The experimentally measured and theoretically calculated thermal conductivities as functions of temperature for the various ZrC_{1-x} phases having different deviations from the stoichiometry are presented in Fig. 5.9.

At room temperature the mean coefficient of linear thermal expansion of near-stoichiometric zirconium monocarbide ZrC_{1-x} is $(4.0\text{--}7.4) \times 10^{-6} \text{ K}^{-1}$ [47, 60, 63, 96, 199, 346, 357, 380, 452, 797, 887, 1480]. Usually, as it was confirmed by experiments, the porosity of materials has no significant effect on this property [345, 374, 384]. The experimental data collected from the various measurements of thermal expansion of zirconium monocarbide are listed in Table 5.7. The approximation functions for the temperature dependence of relative thermal linear expansion $\Delta l/l_0 = f(T, \text{K})$, %, of near-stoichiometric ZrC_{1-x} was recommended by Touloukian et al. [357] on the basis of experimental data for pure samples from several sources (accuracy within $\pm 5\%$ at $T < 2200 \text{ K}$ and within $\pm 10\%$ at $T > 2200 \text{ K}$):

for 293–1500 K (20–1230 °C):

$$\Delta l/l_0 = -0.080 + (1.280 \times 10^{-4})T + (5.372 \times 10^{-7})T^2 - (1.392 \times 10^{-10})T^3, \quad (5.58)$$

Table 5.7 Average coefficients of linear thermal expansion α_m of zirconium monocarbide ZrC_{1-x} in various temperature ranges

Temperature range, °C	$\alpha_m, 10^{-6} K^{-1}$	Reference
(-190)–(+20)	1.9 ± 0.8^a	[47, 142]
	3.5 ± 0.4^b	[47, 142]
	3.7 ± 0.4^c	[47, 142]
(-170)–(+100)	4.51^d	[134]
(-150)–(+30)	6.22^e	[111]
(-20)–(+80)	6.2	[199]
(-20)–(+400)	8.1	[199]
20–100	4.57^f	[357]
	5.45^d	[134]
20–200	4.83^f	[357]
	5.73^g	[308]
	6.0	[45]
	7.2	[49]
20–300	5.17^f	[357]
30–330	7.0^h	[277]
20–400	5.47^f	[357]
	6.0	[45]
	6.55^g	[308]
20–500	5.75^f	[357]
	6.73 ± 0.32^i	[100]
	6.74	[246]
20–550	$6.7\text{--}6.8^j$	[213, 320, 349, 350]
20–600	6.02^f	[357]
	6.66	[45]
	6.80^i	[100]
	6.94^g	[308]
20–700	6.25^f	[357]
	6.86 ± 0.22^i	[100]
20–730	6.35	[242, 243]
20–800	6.47^f	[357]
	6.7^k	[37]
	6.75	[45]
	6.9^l	[359]
	7.16^g	[308]
20–850	6.93^i	[100]
20–900	6.65^f	[357]
	6.89^m	[1350]
	7.42^n	[1350]
	7.68^o	[1350]

(continued)

Table 5.7 (continued)

Temperature range, °C	$\alpha_m, 10^{-6} \text{ K}^{-1}$	Reference
20–950	6.60 ^p	[133]
	7.50 ^q	[361]
20–1000	6.3 ^r	[363]
	6.57 ± 0.08 ^s	[57]
	6.72 ^t	[60, 346, 635]
	6.80 ^f	[357]
	6.87 ^u	[130]
	6.9 ^v	[356]
	6.91 ^w	[348]
	6.99 ± 0.16 ⁱ	[100]
	7.00	[45]
	7.01 ^s	[1, 32, 364]
	7.05 ^x	[384]
	7.14 ^y	[373]
	7.33 ^g	[308]
	7.79 ^z	[372]
8.73 ^{a1}	[4, 91, 132]	
9.66 ^u	[4, 91, 132]	
20–1100	6.73	[30, 31, 378]
	6.93 ^f	[357]
20–1130	7.00	[242, 243]
20–1200	6.53 ^{a2}	[352, 365]
	7.00	[45]
20–1300	7.06 ^f	[357]
	7.45 ^g	[308]
	7.50 ^{a3}	[51, 59, 469]
	6.91 ^{a4}	[362]
	7.17 ^f	[357]
20–1350	7.20 ^{a5}	[347, 358]
20–1350	7.49 ^g	[308, 369]
20–1400	6.70	[351, 355]
	6.77 ^{a2}	[367]
20–1500	7.15	[45]
	7.29 ^f	[357]
	7.40 ^d	[357]
	7.43 ^{a5}	[347, 358]
800–1500	9.15 ^w	[348]
20–1600	8.43 ^{a6}	[371]
	7.12	[45]
20–1700	7.51 ^f	[357]
	7.16	[74, 81]
	7.60 ^f	[357]
	7.70 ^{a5}	[347, 358]

(continued)

Table 5.7 (continued)

Temperature range, °C	$\alpha_m, 10^{-6} \text{ K}^{-1}$	Reference
900–1700	7.4 ± 0.2^{a7}	[81]
20–1730	7.0	[33]
20–1800	7.22	[45]
	7.70^f	[357]
20–1900	7.78^f	[357]
	8.10^{a5}	[347, 358]
20–2050	7.04^{a8}	[366]
20–2000	6.90	[45]
	7.56^t	[60, 346]
	7.7^{a9}	[360, 383]
	7.87^f	[357]
	8.0^l	[359]
	9.05^{b1}	[368]
	9.77^w	[348]
20–2100	4.63^{b2}	[245]
	7.94^f	[357]
1000–2100	9.13^{b3}	[320, 354]
20–2130	7.98	[242, 243]
20–2200	7.45	[45]
	8.02^f	[357]
20–2300	8.03^{b4}	[370]
	8.10^f	[357]
	8.77^{a2}	[347, 358]
1000–2300	11.8^{b5}	[319, 354]
20–2400	7.50	[45]
	8.17^f	[357]
	8.65^v	[356]
	10.34^w	[348, 369]
20–2500	8.23^f	[357]
20–2600	7.54	[45]
	8.30^f	[357]
	9.30^{a5}	[347]
20–2700	7.56 ± 0.20^{b6}	[95, 320, 353]
	8.37^f	[357]
	9.85^{b7}	[326]
20–2900	9.61^{a4}	[347]

^aPowdered $\text{ZrC}_{0.80}$, measured by low-temperature X-ray diffraction method

^bPowdered $\text{ZrC}_{0.97}$, measured by low-temperature X-ray diffraction method

^cPowdered $\text{ZrC}_{0.95}$, measured by low-temperature X-ray diffraction method

^dSintered (in high vacuum) $\text{ZrC}_{0.97}$ (10–20% porosity), measured by dilatometric method

^ePowdered $\text{ZrC}_{0.99}$, measured by low-temperature X-ray diffraction method

^fCalculated on the basis of approximation function

^gHot-pressed $\text{ZrC}_{-1.0}$ (9% porosity), measured (perpendicular to the direction of pressing) by dilatometric method in inert atmosphere

^hSintered (in vacuum) $\text{ZrC}_{0.98}$ (contents: non-combined C – 0.15–0.20%, O – 0.10–0.18%), measured by dilatometric method

ⁱPowdered $\text{ZrC}_{0.96}$ (content non-combined C – 0.5%), measured by high-temperature X-ray diffraction method

(continued)

Table 5.7 (continued)

- ^jHot-pressed $\text{ZrC}_{0.83-0.85}$ (content non-combined C – 4.0%), measured using a dilatation interferometer
- ^kHot-pressed materials
- ^lPyrolytic $\text{ZrC}_{0.99}$
- ^mPowdered $\text{ZrC}_{0.98}$, measured by high-temperature X-ray diffraction method
- ⁿPowdered $\text{ZrC}_{0.82}$, measured by high-temperature X-ray diffraction method
- ^oPowdered $\text{ZrC}_{0.74}$, measured by high-temperature X-ray diffraction method
- ^pPowdered $\text{ZrC}_{0.91}$ (contents: non-combined C – 1.0%, N – 0.34%, O – 0.23%), measured by high-temperature X-ray diffraction method
- ^qHot-pressed materials, measured by telemicroscope (dilatation) method
- ^rPyrolytic $\text{ZrC}_{-1.0}$
- ^sHot-pressed $\text{ZrC}_{0.97}$, measured by dilatometric method in inert atmosphere
- ^tSintered $\text{ZrC}_{0.95}$ (contents: non-combined C – 0.14%, N – 0.26%, O – 0.11%), measured by high-temperature X-ray diffraction method
- ^uSintered (in vacuum) $\text{ZrC}_{0.96}$
- ^vHot-pressed $\text{ZrC}_{0.85}$ (contents: non-combined C – 1.4%, N – 0.94%, O – 0.18%), measured by dilatometric method
- ^wHot-pressed $\text{ZrC}_{0.95}$ (11% porosity, content non-combined C – 0.26%), measured by dilatometric method
- ^xHot-pressed and annealed (in vacuum) $\text{ZrC}_{0.98}$, measured using a high-sensitivity quartz dilatometer in inert (Ar) atmosphere
- ^yMeasured by dilatometric method
- ^zPlasma sprayed materials, measured by dilatometric method
- ^{a1}Sintered (in vacuum) $\text{ZrC}_{0.92}$
- ^{a2}Powdered $\text{ZrC}_{-1.0}$ (content non-combined C – 1.3%), measured by high-temperature X-ray diffraction method
- ^{a3}Extrapolated to $\text{ZrC}_{1.0}$ composition
- ^{a4}Hot-pressed $\text{ZrC}_{-1.0}$ (content O < 0.01%), measured by high-temperature neutron diffraction method
- ^{a5}Hot-pressed $\text{ZrC}_{0.94}$ (19–24% porosity), measured by dilatometric method
- ^{a6}Measured by high-temperature X-ray diffraction method in high vacuum
- ^{a7}Same for all the compositions: $\text{ZrC}_{0.72}$, $\text{ZrC}_{0.80}$, $\text{ZrC}_{0.91}$ and $\text{ZrC}_{-1.0}$ (content O – 0.77%, 0.76%, 0.04%, 0.36%, respectively), measured by high-temperature X-ray diffraction method
- ^{a8}Carburized materials, measured by telemicroscope method in inert (He) atmosphere
- ^{a9}Pyrolytic $\text{ZrC}_{0.8-1.0}$
- ^{b1}Measured by dilatometric method in inert atmosphere
- ^{b2}Sintered $\text{ZrC}_{0.94}$ (content N – 0.5%), measured by dilatometric method
- ^{b3}Hot-pressed $\text{ZrC}_{-1.0}$ (3% porosity), measured by telemicroscope (dilatation) method
- ^{b4}Powdered (annealed in vacuum) $\text{ZrC}_{-1.0}$ (contents: N – 0.01%, O – 0.05%), measured by high-temperature neutron diffraction method
- ^{b5}Hot-pressed and annealed $\text{ZrC}_{-1.0}$ (3% porosity), measured by telemicroscope (dilatation) method
- ^{b6}Grains of monocarbide phase in the arc-cast carbide-carbon eutectics in the presence of graphite flakes, measured by high-temperature X-ray diffraction method using (111) reflections
- ^{b7}Hot-pressed $\text{ZrC}_{-1.0}$ in the presence of non-combined carbon

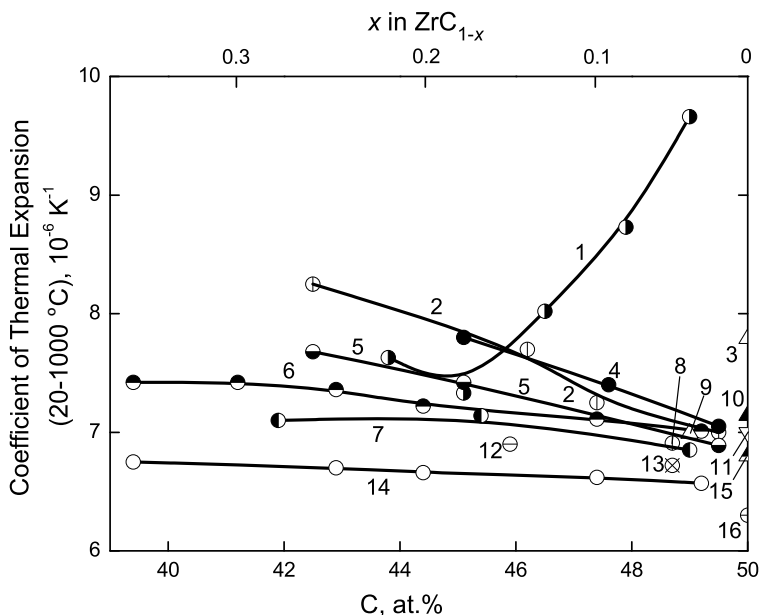


Fig. 5.10 Coefficients of linear thermal expansion in the temperature range of 20–1000 °C (when it is not indicated specially) of zirconium monocarbide ZrC_{1-x} materials (within the homogeneity range) as a function of carbide composition on the basis of several sources (1 – sintered in vacuum [4, 91, 132]; 2 – in the range of 30–330 °C, sintered in vacuum, contents: non-combined C – 0.15–0.20%, O – 0.10–0.18%, dilatometric method [277]; 3 – plasma sprayed, dilatometric method [372]; 4 – hot-pressed and annealed in vacuum, dilatometric method [384]; 5 – in the range of 20–900 °C, powdered, high-temperature X-ray diffraction method [1350]; 6 – hot-pressed, dilatometric method in inert atmosphere [1, 32, 509]; 7 – sintered in vacuum [130]; 8 – hot-pressed, dilatometric method [348]; 9 – powdered, high-temperature X-ray diffraction method [100]; 10 – [373]; 11 – [45]; 12 – hot-pressed, dilatometric method [356]; 13 – sintered, high-temperature X-ray diffraction method [60, 346]; 14 – hot-pressed, 6–10% porosity, dilatometric method in inert atmosphere [57, 364, 516]; 15 – calculated on the basis of approximation function [357]; 16 – pyrolytic [363])

and for 1500–3000 K (1230–2730 °C):

$$\Delta l/l_0 = -0.358 + (7.355 \times 10^{-4})T + (4.859 \times 10^{-8})T^2 - (6.327 \times 10^{-13})T^3, \quad (5.59)$$

where T is temperature, K. On the basis of high-temperature X-ray measurements in the temperature range of 25–2040 °C Houska [60, 346] proposed for the average coefficient of linear thermal expansion α_m , K^{-1} , of annealed (in vacuum) $ZrC_{0.95}$ (contents: non-combined C – 0.14%, N – 0.26%, O – 0.11%, Ti – 0.22%, B – 0.22%, Fe – 0.18%) the following equation:

$$\alpha_m = 6.26 \times 10^{-6} + (0.44 \times 10^{-9})(t - 25), \quad (5.60)$$

a similar linear equation for α_m , K^{-1} , of $\text{ZrC}_{0.95-0.96}$ in the temperature range of 25–2130 °C was also proposed by Katoh et al. [96]:

$$\alpha_m = 5.65 \times 10^{-6} + (1.30 \times 10^{-9})(t + 273), \quad (5.61)$$

where t is temperature, °C; according to Eq. (5.61) the coefficient of thermal expansion of monocarbide phase increases from $6.0 \times 10^{-6} \text{ K}^{-1}$ at room temperature to $7.3 \times 10^{-6} \text{ K}^{-1}$ at 1000 °C. The extrapolation of the relationship, obtained by Aigner et al. [59] for the range of 25–1200 °C, to hypothetical $\text{ZrC}_{1.0}$ phase gives the following expression for its coefficient of linear thermal expansion α , K^{-1} :

$$\alpha = \frac{2.1168 \times 10^{-6} + 1.6488 \times 10^{-9}T}{0.46896 + 2.1168 \times 10^{-6}T + 0.8247 \times 10^{-9}T^2}, \quad (5.62)$$

where T is temperature, K. The influence of carbon content on the thermal expansion of ZrC_{1-x} phase within the homogeneity range can be seen in Fig. 5.10.

The first principles calculated thermophysical properties of zirconium monocarbide materials under higher pressures are reported by Fu et al. [69], Zhu et al. [281], Varshney and Shriya [283] and Rathod et al. [379]. Some recent works [69, 167, 280, 281, 283, 284, 466] are devoted to the calculations of coefficients of thermal expansion of zirconium monocarbide by means of theoretical modelling.

In comparison with other ultra-high temperature materials the values of thermal conductivity and thermal expansion of zirconium carbide in the wide range of temperatures are summarized in Addendum.

5.3 Electro-magnetic and Optical Properties

At room temperature the values of specific electrical resistance (resistivity) of near-stoichiometric zirconium monocarbide ZrC_{1-x} lie within the area of 0.40–0.75 $\mu\Omega \text{ m}$ [26, 27, 31–33, 74, 77, 96, 213, 307, 635, 1481]. The variations of specific electrical resistance with temperature for near-stoichiometric ZrC_{1-x} on the basis of several sources are shown in Fig. 5.11. In the wide temperature range from 0–300 °C up to 2700–3000 °C the resistance of monocarbide phase enlarges with increasing temperature, practically in accordance with linear relationship; that is an evidence of mainly metallic type of conduction in ZrC_{1-x} [26, 27]. For the temperature range of 20–2700 °C the following simple equation was recommended by Maltseva et al. [31, 213, 390] for the resistivity of near-stoichiometric zirconium monocarbide ZrC_{1-x} , ρ , $\mu\Omega \text{ m}$, prepared by sintering (corrected to the poreless state):

$$\rho = 0.50 + (9.0 \times 10^{-4})(t - 20), \quad (5.63)$$

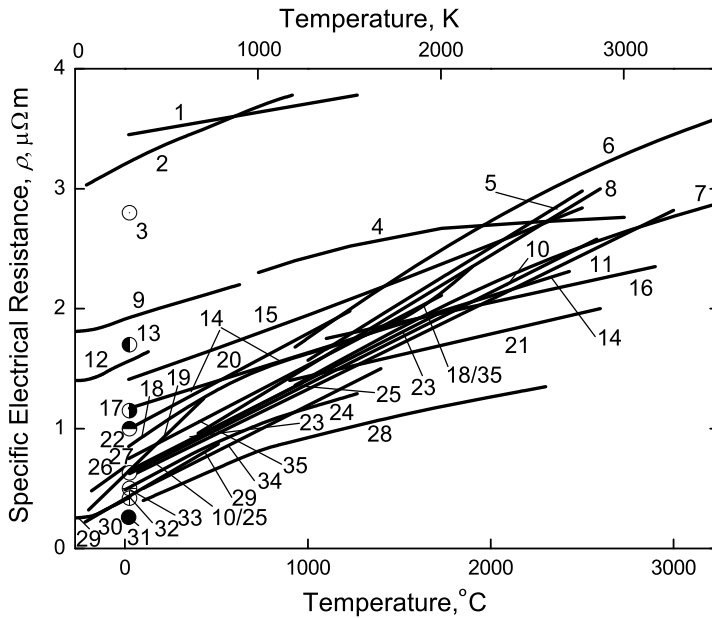


Fig. 5.11 Variation of specific electrical resistance (resistivity) with temperature for zirconium monocarbide ZrC_{1-x} materials on the basis of several sources: 1 – sintered (in vacuum) $ZrC_{0.97}$, corrected to porosity [210]; 2 – sintered and annealed (in vacuum) $ZrC_{0.97}$, corrected to porosity [405, 406]; 3 – reactively sputtered thin film, thickness $0.42 \mu m$ [414, 472]; 4 – single crystal $ZrC_{0.93}$ [396]; 5 – sintered and annealed (in vacuum) $ZrC_{\sim 1.0}$, porosity 10%, contents: non-combined C – 0.05–0.1%, N < 0.1%, O < 0.1% [117, 329]; 6 – sintered $ZrC_{\sim 1.0}$, porosity 12–13%, mean grain size – 10–20 μm , contents: non-combined C – 0.48–1.14%, N – 0.23–0.72%, O – 0.06–0.41% [397]; 7 – sintered $ZrC_{\sim 1.0}$ (see 6), corrected to porosity [479]; 8 – hot-pressed and annealed, content non-combined C – 1.2–1.4% [390]; 9 – single crystal $ZrC_{0.93}$ [394, 395]; 10 – hot-pressed $ZrC_{\sim 1.0}$, corrected to porosity and thermal expansion, contents: non-combined C – 0.18–0.30%, O – 0.001–0.09% [77]; 11 – recommended [33]; 12 – single crystal $ZrC_{0.98}$ [395]; 13 – sintered $ZrC_{0.98}N_{0.02}$, corrected to porosity [412]; 14 – pyrolytic $ZrC_{0.962}N_{0.035}O_{0.071}$ [413]; 15 – sintered $ZrC_{0.94}$, porosity 4%, contents: N – 0.2–0.4%, O – 0.2–0.4% [61]; 16 – hot-pressed $ZrC_{\sim 1.0}$, corrected to porosity [310, 358]; 17 – sintered (in vacuum) $ZrC_{0.96}$, porosity 5%, content N – 0.15% [399]; 18 – pyrolytic $ZrC_{0.92}$, content N – 0.8% [300]; 19 – hot-pressed $ZrC_{0.98}$, porosity 24%, contents: non-combined C – 0.3%, O – 0.05% [325]; 20 – sintered $ZrC_{\sim 1.0}$, content non-combined C – 0.3% [137]; 21 – hot-pressed $ZrC_{0.98}$, corrected to porosity [384, 387, 388]; 22 – sintered (in vacuum) $ZrC_{0.6-0.9}$, porosity 5–15%, content N – 1.4% [299]; 23 – hot-pressed $ZrC_{0.93}$, corrected to porosity [326]; 24 – sintered (in vacuum) $ZrC_{\sim 1.0}$, content N – 0.05% [398]; 25 – hot-pressed $ZrC_{0.93}$, porosity 5%, [307]; 26 – sintered, porosity 2% [321]; 27 – [35, 37, 46, 63, 407, 416]; 28 – hot-pressed $ZrC_{\sim 1.0}$, corrected to porosity [386, 402]; 29 – hot-pressed $ZrC_{0.98}$, corrected to porosity [393]; 30 – hot-pressed $ZrC_{0.97}$, porosity 9%, content O – 0.1% [325]; 31 – sintered $ZrC_{0.93}$, porosity 6–8%, content non-combined C – 0.5% [411]; 32 – [328, 392]; 33 – hot-pressed $ZrC_{\sim 1.0}$, porosity 5–7% [30, 213, 214, 382, 385, 401, 417]; 34 – hot-pressed $ZrC_{0.99}$, porosity 6%, content non-combined C – 0.12% [31, 389]; 35 – obtained from the experimental data for $ZrC_{1-x}C$ materials by the extrapolation to the pure carbide composition [1482] (when it is not indicated specially, data are given for near-stoichiometric compositions)

which looks similar to the proposed by Zapadaeva et al. [470]

$$\rho = 0.543 + (5.63 \times 10^{-4})(t + 273), \quad (5.64)$$

and

$$\rho = 0.393 + (7.67 \times 10^{-4})(t + 273), \quad (5.65)$$

determined by Taylor [307] for hot-pressed $\text{ZrC}_{0.93}$ and Grossman [77] for hot-pressed $\text{ZrC}_{\sim 1.0}$ materials (contents: non-combined C – 0.18–0.30%, O – 0.001–0.09%, corrected to porosity and thermal expansion) at 25–2580 °C, and also given by Katoh et al. [96] in their special review:

$$\rho = 0.372 + (8.28 \times 10^{-4})(t + 273), \quad (5.66)$$

where t is temperature, °C. At lower temperatures the resistivity of ZrC_{1-x} is perfectly described by the empirical equation

$$\rho(T) = \rho_0 + AT + B \exp(-T_0/T), \quad (5.67)$$

where T is temperature, K, ρ_0 , A , B and T_0 are the constants, which were determined by Modine et al. [420] for the single crystals of $\text{ZrC}_{0.89}$ as following: $\rho_0 = 1.915 \mu\Omega \text{ m}$, $A = 2.5 \times 10^{-4} \mu\Omega \text{ m K}^{-1}$, $B = 0.265 \mu\Omega \text{ m}$ and $T_0 = 495 \text{ K}$ ($\rho(300 \text{ K}) = 2.04 \mu\Omega \text{ m}$) (the same equation was also employed by Hinrichs et al. [396, 469] at elevated and higher temperatures (730–2730 °C) – with the values of constants: $\rho_0 = 1.765 \mu\Omega \text{ m}$, $A = 5.52 \times 10^{-4} \mu\Omega \text{ m K}^{-1}$, $B = 6.50 \mu\Omega \text{ m}$ and $T_0 = 6900 \text{ K}$); or also by the Bloch-Grüneisen classical expression [395]

$$\rho(T) = \rho_0 + 4\rho_1 T(T/\theta)^4 J_n(\theta/T), \quad (5.68)$$

where T is temperature, K, and $J_n(\theta/T)$ is the transport integral defined by

$$J_n(\theta/T) = 2^{n-1} \int_0^{\theta/2T} x^n / \sinh^2 x dx \quad (5.69)$$

with $n = 5$; for the range of temperatures from –270 to +80 °C (4–350 K), the following values of ρ_0 , $\mu\Omega \text{ m}$, ρ_1 , $\mu\Omega \text{ m K}^{-1}$, and θ , K parameters were obtained by Modine et al. [395] from the measurements of ZrC_{1-x} single crystals with various deviations from the stoichiometry, respectively:

- for $\text{ZrC}_{0.98}$: 1.397, 6.74×10^{-4} , 539;
- for $\text{ZrC}_{0.93}$: 1.808, 4.90×10^{-4} , 570;
- for $\text{ZrC}_{0.89}$: 1.938, 4.25×10^{-4} , 574;

at ultra-low temperatures ($T < 35\text{--}50\text{ K}$) the simpler expression [394]:

$$\rho(T) = \rho_0 + AT^n, \quad (5.70)$$

where A and n are constants, can be employed with $n = 4.0\text{--}4.8$ (the lower values of exponent n is corresponding to higher temperatures). Savvatimskiy et al. [1508] measured electrical resistance of $\text{ZrC}_{0.95}$ in the wide range of ultra-high temperatures by pulsed heating method with microsecond duration: referred to the initial linear dimensions the resistivity at $2730\text{ }^\circ\text{C}$ amounted to $\sim 3.2 \pm 0.2\ \mu\Omega\ \text{m}$, at solidus ($3180\text{ }^\circ\text{C}$) and liquidus ($3580\text{ }^\circ\text{C}$) temperatures it was $\sim 2.9 \pm 0.2\ \mu\Omega\ \text{m}$ and $\sim 2.5 \pm 0.2\ \mu\Omega\ \text{m}$, respectively; with further temperature growth the resistivity of liquid zirconium carbide increased monotonically to $\sim 3.1 \pm 0.2\ \mu\Omega\ \text{m}$ at $4730\text{ }^\circ\text{C}$. The experimental data collected from the various measurements of

Table 5.8 Average values of thermal coefficients of resistivity α_R of zirconium monocarbide ZrC_{1-x} in various temperature ranges^a

Temperature range, $^\circ\text{C}$	$\alpha_R, 10^{-3}\ \text{K}^{-1}$	Reference
(-195)–0	9.31 ^b	[400]
(-183)–0	2.28 ^c	[321]
(-190)–(+20)	3.22	[387]
20–950	1.23	[387]
20–1000	$\sim 1.55^{\text{d}}$	[32, 391]
	$\sim 0.90^{\text{e}}$	[32, 391]
	0.88^{f}	[404]
	$\sim 0.50^{\text{g}}$	[32, 391]
	0.18^{h}	[415]
	$\sim 0.15^{\text{i}}$	[32, 391]
100–1100	0.79	[389, 402, 1344]
20–1250	1.05	[387]
20–1700	0.90	[387]
20–1730	1.20	[33, 77]
400–2000	0.60	[403]
20–2150	0.79	[387]
300–2300	0.95	[26, 27, 386, 402, 1344]
20–2350	0.75	[387]
20–2700	0.90	[213]

^aWhen it is not indicated specially, value reported is for near-stoichiometric composition

^bMaterials deposited from gas phase

^cSintered materials, porosity 2%

^dHot-pressed materials, carbon content $\sim 50\text{ at.}\%$, corrected to porosity

^eHot-pressed materials, carbon content $\sim 47.4\text{ at.}\%$, corrected to porosity

^fHot-pressed materials, carbon content $\sim 48.6\text{ at.}\%$, corrected to porosity; thermal coefficient $\alpha = 1/\rho_\theta \times (d\rho/dT)_\theta$ corresponds to Debye temperature $\theta = 780\text{ K}$ ($(d\rho/dT)_\theta = 6.6 \times 10^{-4}\ \mu\Omega\ \text{m}\ \text{K}^{-1}$)

^gHot-pressed materials, carbon content $\sim 44.4\text{ at.}\%$, corrected to porosity

^hThin films ($2\ \mu\text{m}$ thickness) prepared by activated reactive evaporation

ⁱHot-pressed materials, carbon content $\sim 37.5\text{ at.}\%$, corrected to porosity

thermal coefficient of resistivity for near-stoichiometric zirconium monocarbide are listed in Table 5.8. For the phases having different deviations from the stoichiometry the variations of resistivity with temperature are presented in Fig. 5.12. The published experimental data on the resistivity of ZrC_{1-x} within the homogeneity range (Fig. 5.13) show the effect of carbon content on it as multivalued completely. Various authors [57, 85, 299, 358, 398, 408, 419] have found a decrease in resistivity values with a decrease in carbon deficit in non-metal sublattice, so Storms and Wagner [85] fit these data to the equation ($0 < x \leq 0.5$)

$$\rho = [0.382 + (0.55 + 9.50x)^{-1}]^{-1}, \quad (5.71)$$

where ρ is specific electrical resistance (resistivity), $\mu\Omega$ m and x is the value of index in ZrC_{1-x} formula (corresponding to curve 11 in Fig. 5.13); whereas other researchers [61, 134, 137, 210, 405, 406] have revealed the opposite trend in the resistivity versus carbon content relationships. However, Taylor and Storms [325] proposed later this relationship to be a dome-shaped curve with the maximum in resistivity ($\sim 2.3 \mu\Omega$ m) at around $ZrC_{0.80-0.85}$ composition. In some works [61, 316, 317] it was shown that the resistivity of high-purity ZrC_{1-x} sintered materials

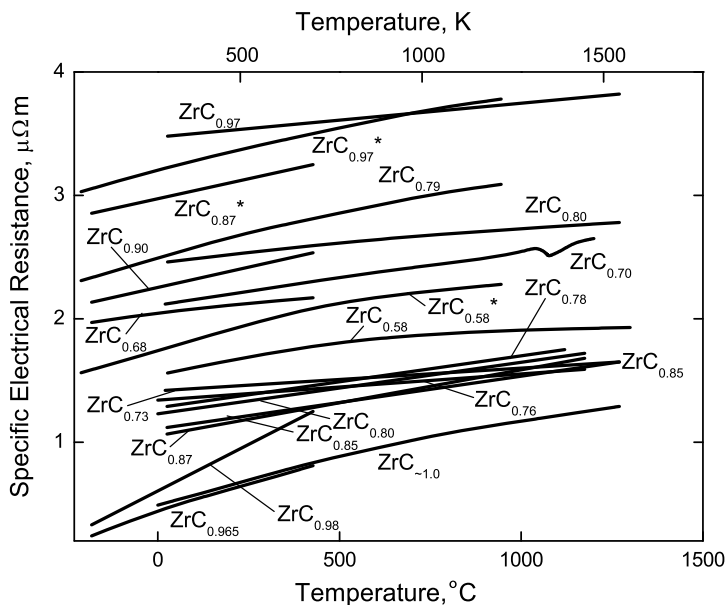


Fig. 5.12 Variations of specific electrical resistance with temperature for the ZrC_{1-x} phases having different deviations from the stoichiometry (materials sintered in vacuum, $x = 0.00, 0.13, 0.15, 0.20, 0.22, 0.24, 0.27$ [398]; sintered in vacuum, data corrected to porosity, $x = 0.03, 0.20, 0.42$ [210]; sintered in vacuum, corrected to porosity, $x = 0.03^*, 0.21, 0.42^*$ [405, 406]; hot-pressed, $x = 0.02$ (contents: non-combined C – 0.30%, O – 0.05%), 0.035 (content O – 0.10%), 0.10 (O – 0.015%), 0.13* (O – 0.064%), 0.32 (O – 0.084%) [325]; arc-melted with order-disorder transition (superlattice formation) at 1060–1080 °C, $x = 0.30$ [5])

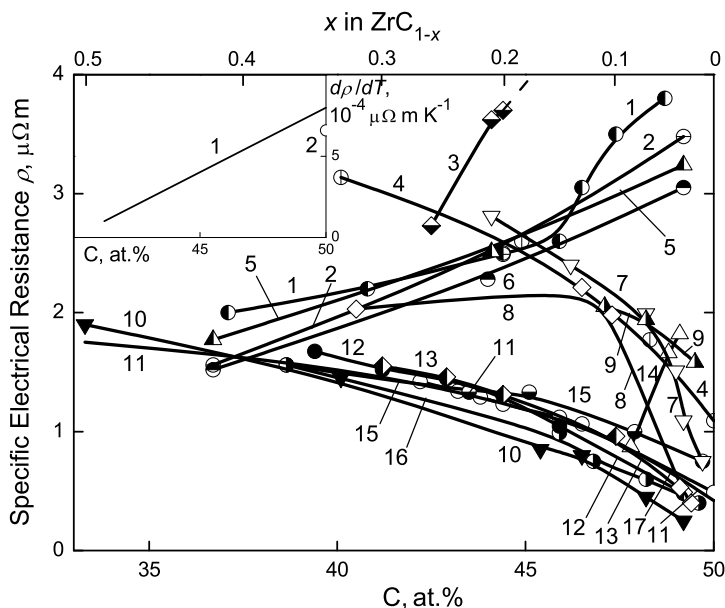


Fig. 5.13 Variations of specific electrical resistance (resistivity) at room temperature with carbon content within the homogeneity range of zirconium monocarbide ZrC_{1-x} : 1 – sintered [137]; 2 – sintered in vacuum, corrected to porosity [210]; 3 – sintered, high purity materials, 16–26% porosity [61]; 4 – hot-pressed [418]; 5 – sintered in vacuum, corrected to porosity [405, 406]; 6 – sintered in vacuum, corrected to porosity [134]; 7 – pyrolytic materials, annealed at 3000 °C [26, 27]; 8 – hot-pressed, content O – 0.015–0.10% [325]; 9 – single crystals [395]; 10 – [358]; 11 – on the basis of several sources [85]; 12 – hot-pressed [419]; 13 – hot-pressed, corrected to porosity [57]; 14 – pyrolytic, content N – 0.03–0.8% [300]; 15 – sintered, porosity 5–15%, content N > 1% [299]; 16 – [408]; 17 – [398] (Inset – variation of $d\rho/dT$ (slope of resistivity vs. temperature) at ambient temperatures with carbon content within the homogeneity range based on: 1 – [398], 2 – [391])

(with introduced corrections for porosity) decreases, but the resistivity of materials commercially purified increases – with the growth of vacancies in non-metal sublattice. This observation could be linked with the conclusion of independence of resistivity of carbide phases on atomic defect concentrations (carbon vacancies and atomic substitutions), which was made earlier by Golikova et al. [138, 423–425] and Avgustinik et al. [137, 426, 427]. The variation of $d\rho/dT$ (slope of resistivity vs. temperature) with ZrC_{1-x} composition at ambient temperatures is shown in the inset to Fig. 5.13. The superconducting transition temperature T_c of near-stoichiometric ZrC_{1-x} is 1.1–2.3 K [1, 421, 452, 1381]. According to Nikitin et al. [155] and Neshpor et al. [422], in the temperature range from 0.8 to 4.2 K for the ZrC_{1-x} compositions with $x < 0.36$ the temperature has little effect on the electrical conductivity, but a superconductive state was observed for materials with $x > 0.42$. At room temperature the Hall and Seebeck coefficients of near-stoichiometric zirconium monocarbide are $R = -(9-19) \times 10^{-10} \text{ m}^3 \text{ A}^{-1} \text{ s}^{-1}$ and $S = -(10-16) \mu\text{V K}^{-1}$, respectively [26, 27, 30, 131, 137, 299, 401, 405, 406, 408–410, 430, 1378]; the

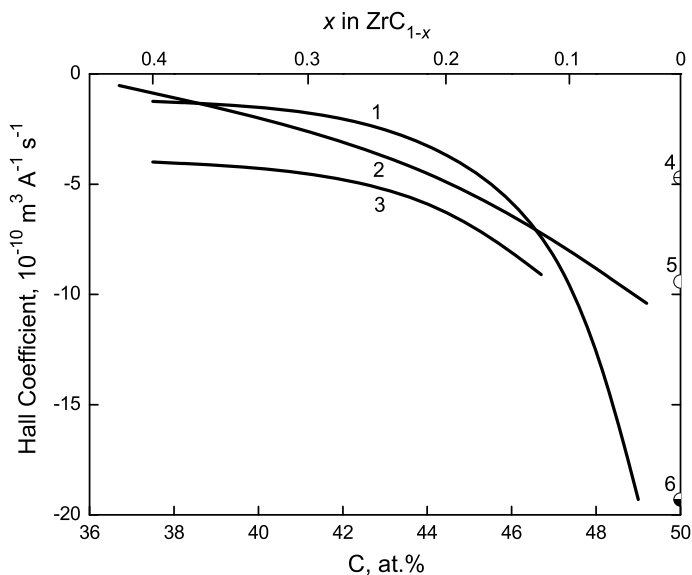


Fig. 5.14 Variations of Hall coefficient at room temperature within the homogeneity range of zirconium monocarbide ZrC_{1-x} (1 – sintered (in vacuum) materials [137]; 2 – sintered (in vacuum), corrected to porosity [1, 32, 405, 406, 409]; 3 – [131]; 4 – [432, 433]; 5 – hot-pressed [30, 401, 428, 430, 431]; 6 – [429])

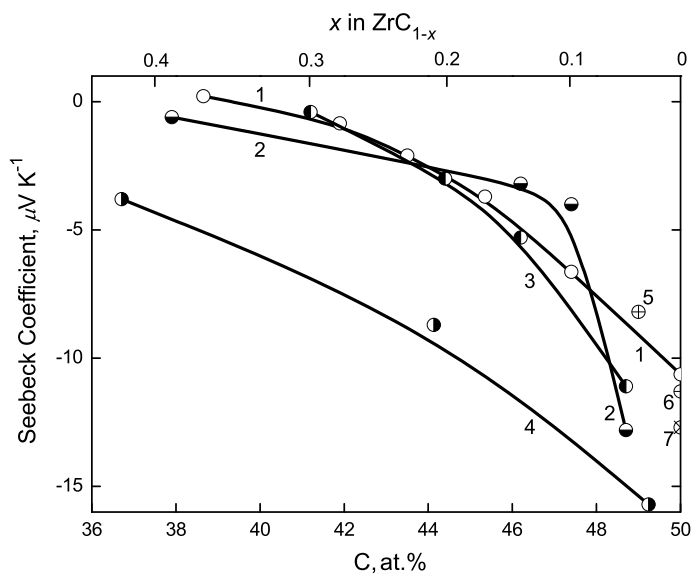


Fig. 5.15 Variations of Seebeck coefficient at room temperature within the homogeneity range of zirconium monocarbide ZrC_{1-x} (1 – sintered materials [299]; 2 – sintered (in vacuum) [137]; 3 – [408]; 4 – sintered (in vacuum) [405, 406, 409]; 5 – pyrolytic, content N – 0.03–0.08% [300]; 6 – [430]; 7 – hot-pressed [401, 428])

experimental data obtained by several researchers for these coefficients varying within the homogeneity range of ZrC_{1-x} are presented in Figs. 5.14 and 5.15.

Near-stoichiometric zirconium monocarbide ZrC_{1-x} is a diamagnetic substance with molar magnetic susceptibility χ_m (SI) $\approx -(30\text{--}300) \times 10^{-6} \text{ cm}^3 \text{ mol}^{-1}$ at room temperature slightly increasing with temperature in the range from 20 to 1000 °C [26, 27, 154, 437–439]. However, an increase in carbon deficit (value of x) in ZrC_{1-x} results in changing in the magnetic properties of zirconium monocarbide phase from diamagnetic to paramagnetic, so the maximum of molar magnetic susceptibility χ_m (SI) $\approx (740\text{--}770) \times 10^{-6} \text{ cm}^3 \text{ mol}^{-1}$ is corresponding to the lowest carbon content in the homogeneity range, and χ_m (SI) ≈ 0 – to the composition of $\sim\text{ZrC}_{0.8\text{--}0.9}$, as it is shown in Fig. 5.16.

The room-temperature reflectance spectrum of sintered near-stoichiometric ZrC_{1-x} (1% porosity, mean surface roughness $R_a = 23 \pm 2 \text{ nm}$, distance between the highest peak and the lowest valley $R_t = 0.68 \pm 0.08 \mu\text{m}$) from the ultraviolet wavelength region to the mid-infrared band is shown in Fig. 5.17. The reflectance of single-crystalline $\text{ZrC}_{0.98}$ in the interval of 0.025–6.5 eV was measured by Modine et al. [420], and that of hot-pressed $\text{ZrC}_{\sim 1.0}$ in the interval of 1.0–8.0 eV – by Alward et al. [1486] and reactively sputtered $\text{ZrC}_{\sim 1.0}$ thin films – by Bonnot et al. [414, 472]. The soft X-ray reflectivity data of thin films deposited by ion beam sputtering were reported by Singh et al. [198, 1430]; there it was shown that the presence of non-combined carbon and oxygen contamination lower the reflectivity

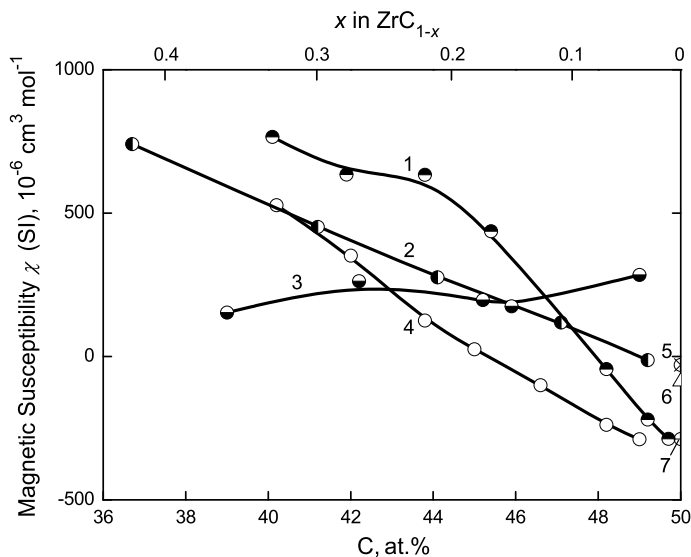


Fig. 5.16 Variation of molar magnetic susceptibility at room temperature within the homogeneity range of zirconium monocarbide ZrC_{1-x} on the basis of several sources: 1 – [434]; 2 – contents: N – 0.04%, Fe – 0.02% [154]; 3 – [136]; 4 – [159]; 5 – [409, 436–439]; 6 – extrapolated value [154]; 7 – [433, 435]

performance of ZrC_{1-x} . Delin et al. [1487] presented the results of *ab initio* calculations of optical properties for quasi-stoichiometric zirconium monocarbide. Optical spectra in the infrared (IR) and visible ranges as well as X-ray emission and absorption spectra of ZrC_{1-x} were considered by Zhurakovskii et al. [442, 443], Ramqvist et al. [444], Kosolapova et al. [163], Guerrero et al. [445] and Kammori et al. [1488] and summarized by Upadhyaya [27]. The absorption wave numbers of basic maxima of IR band for zirconium monocarbide ZrC_{1-x} are 1078 cm^{-1} (for $\text{ZrC}_{0.96}$) [163], 1055 cm^{-1} (for $\text{ZrC}_{0.70}$) [163] and 776, 1332, 1383 and 1634 cm^{-1} (for $\text{ZrC}_{\sim 1.0}$) [445]; the latter 4 baselines are used for the FTIR quantitative determination of ZrC_{1-x} phase in ceramic materials. At the common conditions the colour of zirconium monocarbide ZrC_{1-x} materials is dark-grey in the dispersed state (powdered) or steel/silver-grey with characteristic metallic glitter in the compact state [1, 11, 30–32, 63, 452]; this is related to the broad selection of possible electron transitions in the entire spectral range of visible light and the small area of the free Fermi surface corresponding to non-localized electrons. Such “absence” of colour is inherent for ZrC_{1-x} in the entire homogeneity region, although near its lower boundary the materials take on a lighter (more silvery) colour; it occurs due to the increasing overlap of the valency band with the conduction band and the increase in free Fermi surface, which causes some selectivity of reflections [26, 27].

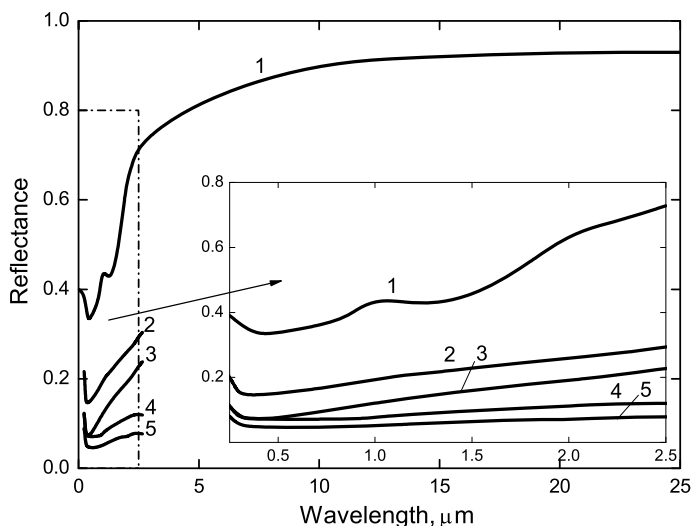


Fig. 5.17 Room-temperature normal reflectance spectrum of near-stoichiometric ZrC_{1-x} from the ultraviolet wavelength region to the mid-infrared band: 1 – sintered materials (1% porosity, mean surface roughness $R_a = 23 \pm 2 \text{ nm}$, distance between the highest peak and the lowest valley $R_l = 0.68 \pm 0.08 \text{ μm}$) [440, 441]; 2 – powder, cold-pressed [468]; 3 – powder, cold-pressed and heated at 700 °C , 0.5 h [468]; 4 – powder, cold-pressed and heated at 900 °C , 1 h [468]; 5 – powder, cold-pressed and heated at 900 °C , 0.5 h [468]

Table 5.9 Normal monochromatic emittance ε_λ ($\lambda = 0.650\text{--}0.665 \mu\text{m}$) of near-stoichiometric zirconium monocarbide ZrC_{1-x} materials in various temperature ranges

Monochromatic emittance, ε_λ	Temperature range, °C	Reference
0.43–0.56 ^a	1050–2100	[467]
0.49	2300–2500	[275]
0.50–0.70 ^b	1600–2500	[26, 454]
0.51 ^c	2600–3300	[450]
0.51–0.54 ^d	2200–3100	[465]
0.51–0.83	1500–3300	[459]
(0.53 ± 0.05)–(0.55 ± 0.05) ^e	2200–3200	[453]
(0.55 ± 0.05)–(0.68 ± 0.06) ^f	900–2200	[453]
0.55–0.72 ^g	1700–2600	[455]
0.58 ^h	900–2700	[1, 446]
0.58–0.90 ⁱ	900–3100	[479]
0.59–0.61 ^j	2000–2600	[470]
0.60–0.65	800–2100	[460]
0.62–0.65 ^k	730–2230	[33]
0.63 ± 0.02 ^l	800–2100	[77]
0.63–0.88	1100–3200	[449]
0.64–0.80	1400	[461]
0.69–0.91 ^m	850–3100	[26]
0.69–0.94 ⁿ	900–3200	[397, 447]
0.71 ^o	2000–2900	[26]
0.75–0.79 ^p	800–2000	[30–32, 451]
0.75–0.85 ^q	1300–2800	[465]
0.76–0.86 ^r	1500–2100	[275]
0.78 ^s	1500	[478]
0.79–0.80 ^t	1100–1700	[26]
0.80–0.83 ^c	1500	[450]
0.81–0.85 ^d	1300–1900	[465]
0.90 ^u	1400–1900	[473]
0.97	700–1800	[448]

^aArc-melted (via floating zone) polycrystalline $\text{ZrC}_{0.92\pm 0.02}$, measured in vacuum $10^{-5}\text{--}10^{-6}$ Pa; ε_λ falls with the temperature growth linearly (slope is $\sim 1.2 \times 10^{-4} \text{ K}^{-1}$)

^bSintered materials; ε_λ falls with the temperature growth linearly

^cHot-pressed $\text{ZrC}_{0.98}$ (porosity $\leq 10\%$); with a hysteresis effect of ~ 400 °C, depending to some extent of the heating/cooling rate, observed from 1500 to 2600 °C (probably due to the surface oxidation and/or nitridation)

^dSintered $\text{ZrC}_{0.95}$ (contents before measurement: non-combined C < 0.1%, O < 0.05%), measured in high-purity He; ε_λ falls with the temperature growth linearly

^eAnalyzed on the basis of several sources: measurements from polished and stabilized surfaces, ε_λ falls very slightly with the temperature growth (almost linearly)

^fAnalyzed on the basis of several sources: measurements from polished and stabilized surfaces, ε_λ falls with the temperature growth (almost linearly)

^g ε_λ falls with the temperature growth

^hPyrolytic $\text{ZrC}_{0.86\text{--}0.99}$ coating (contents: non-combined C – traces, N $\leq 1\%$, O – 0.2–0.4%)

ⁱSintered $\text{ZrC}_{\geq 0.99}$ (13% porosity, mean grain size – 10–20 μm , contents: non-combined C – 0.48–1.14%, N – 0.23–0.72%, O – 0.06–0.41%) measured in vacuum and Ar multiply; ε_λ falls with the temperature growth

^jPyrolytic $\text{ZrC}_{0.99}$ (contents: non-combined C – 0.03%, N – 0.15%, O – 0.28%)

^kRecommended for high-temperature technological applications

(continued)

Table 5.9 (continued)^lHot-pressed (in vacuum) $ZrC_{-1.0}$ (contents: non-combined C – 0.18–0.30%, O – 0.001–0.09%)^mSintered materials; ε_λ falls with the temperature growth linearlyⁿSintered $ZrC_{-1.0}$ (12–13% porosity, contents: non-combined C – 0.3–1.1%, N – 0.5–0.7%, O – 0.4%); ε_λ falls with the temperature growth linearly^oHot-pressed materials^pPowdered materials (coatings); ε_λ increases slightly with the temperature growth^qSintered $ZrC_{0.95}$ (contents before measurement: non-combined C < 0.1%, O < 0.05%), measured in commercial He; ε_λ falls with the temperature growth linearly^r ε_λ falls with the temperature growth^sPowdered materials (coatings) on tantalum substrate^tHot-pressed materials; ε_λ falls with the temperature growth^uFor $\lambda = 0.81 \mu\text{m}$, the value is constant and rather independent on surface roughness and thermal treatment in vacuum and hot hydrogen

The normal monochromatic emittance (spectral emissivity) ε_λ of zirconium monocarbide ZrC_{1-x} materials slightly varies with temperature, the linear relationship for $\lambda = 0.65 \mu\text{m}$

$$\varepsilon_\lambda = 0.715 - (1.174 \times 10^{-4})(t + 273), \quad (5.72)$$

was obtained by Mackie et al. [467, 469] for arc-melted (via floating zone) polycrystalline monocarbide $ZrC_{0.92 \pm 0.02}$ by vacuum (10^{-5} – 10^{-6} Pa) measurements in the temperature range 1050–2100 °C. Similar equations were proposed by Naumenko [513] for 730–2200 °C

$$\varepsilon_\lambda = 0.80 - (2.86 \times 10^{-5})(t - 727) \quad (5.73)$$

and by Rithof et al. [454] for 1600–2500 °C

$$\varepsilon_\lambda = 0.90 - (2.29 \times 10^{-4})(t - 727), \quad (5.74)$$

where t is temperature, °C. At the ZrC_{1-x} -C eutectic temperature (~ 2880 °C) the normal monochromatic emittance ε_λ ($\lambda = 0.65 \mu\text{m}$) of zirconium monocarbide $ZrC_{\sim 1.0}$ phase is close to 0.6 [99]. For the integral (total) hemispherical emittance ε_T of hot-pressed (in vacuum) $ZrC_{\sim 1.0}$ (8.5% porosity), Grossman [77] also proposed the linear equation (for 1200–2100 °C)

$$\varepsilon_T = 0.772 - (9.0 \times 10^{-5})(t + 273), \quad (5.75)$$

where t is temperature, °C. According to the experimental works by Naumenko [513], emissivity ε_λ of ZrC_{1-x} phases decreases from 0.78 to 0.72 with increasing value of index x in ZrC_{1-x} formula from 0.03 to 0.30. The data on normal monochromatic emittance ε_λ ($\lambda = 0.650$ – $0.665 \mu\text{m}$) and integral (normal and hemispherical) emittances ε_T for ZrC_{1-x} materials produced by different manufacturing methods and measured in various temperature intervals are listed in

Table 5.10 Integral (total) emittance ε_T of near-stoichiometric zirconium monocarbide ZrC_{1-x} in various temperature ranges

Integral emittance, ε_T	Temperature range, °C	Reference
0.25–0.72 ^a	800–1150	[476]
0.35–0.51 ^b	900–2700	[1, 446]
0.37–0.40 ^c	950–1400	[26, 1489]
0.38–0.55 ^d	900–2600	[463, 464]
0.38–0.56 ^e	1000–3000	[479]
0.38–0.83 ^f	900–2700	[456, 471]
0.40–0.47 ^g	2000–2600	[470, 477]
0.41–0.57 ^h	900–3100	[449]
0.42–0.46 ⁱ	1650–2200	[457]
0.43–0.44 ^j	2000–2500	[454]
0.43–0.45 ^k	1800–2600	[458]
0.43–0.46 ^l	2000–2500	[455]
0.50 ^l	2000–3100	[275]
0.50–0.68 ^m	730–2730	[33]
0.55–0.57 ⁿ	2000–2900	[26]
0.56–0.64 ^o	1200–2100	[77]
0.58–0.62 ^p	1250–2100	[460]
0.59 ^q	3530	[477]
0.64–0.85 ^r	900–3100	[397]
0.70–0.87 ^s	600–1400	[480, 481]
0.89–0.91 ^t	1100	[474, 475]

^aHemispherical emittance ε_T for hot-pressed $ZrC_{-1.0}$ (porosity < 2%, mean grain size – 10–20 μm , contains non-combined C); ε_T increases with the temperature growth (almost linearly)

^bHemispherical emittance ε_T for pyrolytic $ZrC_{0.86-0.99}$ coating (contents: non-combined C – traces, N \leq 1%, O – 0.2–0.4%); ε_T increases with the temperature growth

^cHemispherical emittance ε_T for sintered materials; ε_T falls with the temperature growth

^dHemispherical emittance ε_T for pyrolytic materials (content O after the measurement dropped from 0.06 to 0.04%); ε_T increases with the temperature growth linearly

^eHemispherical emittance ε_T for Sintered $ZrC_{\geq 0.99}$ (13% porosity, mean grain size – 10–20 μm , contents: non-combined C – 0.48–1.14%, N – 0.23–0.72%, O – 0.06–0.41%) measured in vacuum and Ar multiply; curve $\varepsilon_T - T$ with the minimum at ~ 1400 °C and maximum at ~ 2500 °C

^fNormal emittance ε_T for sintered materials, measured in Ar; ε_T increases slightly with the temperature growth up to ~ 1900 °C and then falls sharply with further temperature increase

^gNormal emittance ε_T for pyrolytic $ZrC_{0.99}$ (contents: non-combined C – 0.03%, N – 0.15%, O – 0.28%); ε_T increases with the temperature growth (almost linearly)

^hHemispherical emittance ε_T for sintered materials; curve $\varepsilon_T - T$ with the minimum at ~ 1400 °C and maximum at ~ 2500 °C

ⁱNormal emittance ε_T for hot-pressed and polished materials, measured in Ar, integrated from spectral data; ε_T increases with the temperature growth

^jNormal emittance ε_T for sintered materials; ε_T increases with the temperature growth linearly

^kNormal emittance ε_T for $ZrC_{-1.0}$ with content non-combined C \geq 2.5%, integrated from spectral data; ε_T increases with the temperature growth

^lHemispherical emittance ε_T

^mRecommended for high-temperature technological applications; ε_T falls with the temperature growth

ⁿNormal emittance ε_T for hot-pressed; ε_T increases with the temperature growth

^oHemispherical emittance ε_T for hot-pressed (in vacuum) $ZrC_{-1.0}$ (8.5% porosity, contents: non-combined C – 0.18–0.30%, O – 0.001–0.09%); ε_T falls with the temperature growth linearly

(continued)

Table 5.10 (continued)

^pHemispherical emittance ε_T for hot-pressed $\text{ZrC}_{-1.0}$ (10% porosity, contents: non-combined C $\geq 0.16\%$, O $< 0.002\%$), measured in vacuum $\sim 10^{-4}$ Pa; ε_T falls with the temperature growth

^qTheoretically calculated normal emittance ε_T for stoichiometric composition

^rHemispherical emittance ε_T for sintered $\text{ZrC}_{-1.0}$ (12–13% porosity, contents: non-combined C – 0.3–1.1%, N – 0.5–0.7%, O – 0.4%); ε_T falls with the temperature growth from 0.82 up to the minimum at ~ 2700 °C (almost linearly) and then increases to the maximum with the further temperature growth

^sHemispherical emittance ε_T for sintered pigmented coating, measured in vacuum $< 7 \times 10^{-4}$ Pa; ε_T increases with the temperature growth

^tHemispherical emittance ε_T for 25–50 μm thickness vacuum-plasma sprayed coating (after annealing ε_T falls to 0.72–0.86 depending on substrate compositions)

Tables 5.9 and 5.10. The variations of normal monochromatic emittance $\varepsilon_{\lambda,T}$ with wavelength and temperature for ZrC_{1-x} are shown in Fig. 5.18. Thermodynamics of thermal radiation for stoichiometric zirconium monocarbide was considered in details by Fisenko et al. [477, 1490]; the same authors studied thermal radiation of solid and liquid zirconium monocarbide [1428] on the basis of experimental data for the normal spectral emissivity in a visible-near infrared range ($0.55 \mu\text{m} \leq \lambda < 0.90 \mu\text{m}$) at melting (eutectic) point obtained by Manara et al. [99].

The thermionic emission characteristics (electron work function and Richardson constants) of various zirconium monocarbide ZrC_{1-x} phases are given in Table 5.11 and Fig. 5.19. The calculated values of emission current density for near-stoichiometric monocarbide ZrC_{1-x} are about 56, 1.5×10^3 and 1.9×10^5 A m^{-2} at 730, 1230 and 1730 °C, respectively [33]. The work functions found for ZrC_{1-x} thin films in cesium vapour are 0.9–1.1 eV higher than those given in literature due to

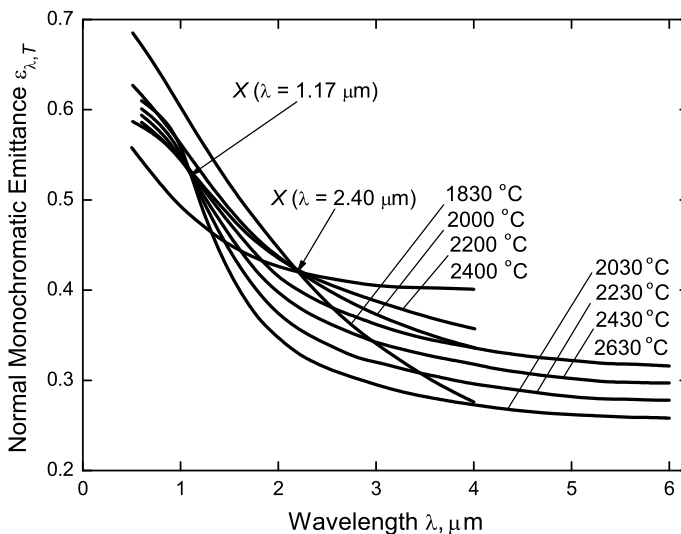


Fig. 5.18 Variations of normal monochromatic emittance $\varepsilon_{\lambda,T}$ with wavelength λ for zirconium monocarbide materials: sintered $\text{ZrC}_{-1.0}$ (96% purity, contains non-combined C) – at 1830, 2000, 2200 and 2400 °C [454, 462]; pyrolytic $\text{ZrC}_{0.99}$ (contents: non-combined C – 0.03%, N – 0.15%, O – 0.28%) – at 2030, 2230, 2430 and 2630 °C [470] (for the families of $\varepsilon - \lambda$ curves X-points or isosbestic points, where $[1/\varepsilon_{\lambda,T} \times d\varepsilon_{\lambda,T}/dT]_{\lambda=X} = 0$, are marked specially)

Table 5.11 Thermionic emission characteristics (electron work function and Richardson constant) of zirconium monocarbide ZrC_{1-x} phases

Composition	Work function ^a , $\varphi = \varphi_0 + (d\varphi/dT)_{av}T$, eV	Richardson constant, A, $10^4 \text{ A m}^{-2} \text{ K}^{-2}$	Temperature range, °C	Remarks ^b	Reference
ZrC _{0.70}	3.88 ^c	–	1500	TiM, hot-pressed	[26, 27, 513]
	$5.10 - (6.8 \times 10^{-4})T$	–	1350–1800		[1, 485]
ZrC _{0.74}	4.0 ^d	–	–	PhES, nanocrystalline thin films	[1491]
ZrC _{0.75}	3.95 ^c	–	1500	TiM, hot-pressed	[26, 27, 513]
	$5.10 - (6.6 \times 10^{-4})T$	–	1300–1800	TiM, hot-pressed	[1, 485]
ZrC _{0.80}	3.97 ^c	–	1500	TiM, hot-pressed	[26, 27, 513]
	$5.17 - (6.7 \times 10^{-4})T$	–	1300–1800	TiM, hot-pressed	[1, 485]
ZrC _{0.84}	3.40 ($d\varphi/dT = 0$)	–	1000–1700	CPDM, single crystal (102), non-combined C – 0.8%, measured in vacuum ($\sim 1.3 \times 10^{-6}$ Pa)	[482, 483, 521, 522, 563]
	3.49 ^c	–	1200–1500	CPDM, single crystal (100), non-combined C – 0.8%	[521, 522]
	3.50 ($d\varphi/dT = 0$)	–	1000–1700	TiM, single crystal (102), non-combined C – 0.8%, measured in vacuum ($\sim 1.3 \times 10^{-6}$ Pa)	[563]
	$3.54 - (2.45 \times 10^{-5})T$	–	≤ 1700	TiM, single crystal (100), non-combined C – 0.8%	[482, 483, 521, 522]
ZrC _{0.88}	4.39 ^c	–	1500	TiM, hot-pressed	[1, 141]
ZrC _{0.90}	4.00 ^c	–	1500	TiM, hot-pressed	[26, 27, 513]
	$5.10 - (6.0 \times 10^{-4})T$	–	1300–1800	TiM, hot-pressed	[1, 485]
ZrC _{0.91±0.02}	3.25	–	–	Single crystal (210), theoretically calculated	[526]
	3.26	–	–	Single crystal (110), theoretically calculated	[526]
	3.26–3.49	–	1600–2100	TiM, single crystal, (210) plane within 6°	[523, 524]
	3.32 ^c	–	1300	TiM (projection microscope), single crystal (210)	[526]
	3.33–3.34 ^c	–	1700	TiM, single crystal (210)	[523, 525, 526]
	3.35	–	1400–1700	TiM, single crystal (100)	[523, 524]
	3.46 ^c	–	1300	TiM (projection microscope), single crystal (110)	[526]

(continued)

Table 5.11 (continued)

Composition	Work function ^a , $\varphi = \varphi_0 + (d\varphi/dT)_{av}T$, eV	Richardson constant, A, $10^4 \text{ A m}^{-2} \text{ K}^{-2}$	Temperature range, °C	Remarks ^b	Reference
	3.48–3.62	–	1600–1900	TiM, single crystal (100), cleaned surface	[523, 524]
	3.50 ^c	–	–	TiM, single crystal, aver- age value	[526]
	3.53	–	–	Single crystal (100), theo- retically calculated	[526]
	3.56–3.61	–	1800–2100	TiM, single crystal (100)	[523, 524]
	3.59	–	1800	TiM, single crystal, (311) plane, ~7° off axis	[523, 524]
	3.59 ^c	–	1500	FEM, single crystal (100)	[527]
	3.60 ^c	–	1700	TiM, single crystal (100)	[523, 525]
	3.61–3.77	–	1700–2250	TiM, single crystal (100)	[523, 524]
	3.63 ^c	–	1300	TiM (projection micro- scope), single crystal (100)	[526]
	3.80	–	–	Single crystal (111), theoretically calculated	[526]
	3.85 ^c	–	1300	TiM (projection micro- scope), single crystal (111)	[526]
ZrC _{0.94}	3.72 ^c	–	1400	TiM, contents: non-com- bined C – 1.15%, N – 1.48%, O > 0.4%	[1, 482, 497, 498]
ZrC _{0.96-0.97}	$4.82 - (4.3 \times 10^{-4})T$	–	–	TiM, pyrolytic, textured surface with (100) prefer- ential orientation	[482, 484]
ZrC _{0.97}	3.95 ± 0.04	–	1700	TiM, hot-pressed	[484, 485]
	4.07 ^c	–	1500	TiM, hot-pressed	[26, 27, 513]
	4.28 ± 0.05 ^e	–	25	CPDM, hot-pressed	[484, 485]
	4.43 ± 0.04	–	25	TiM, hot-pressed	[484, 485]
	$4.52 - (2.8 \times 10^{-4})T$	–	1300–1750	TiM, hot-pressed	[1, 484, 485]
ZrC _{~1.0}	1.60	–	–	TiM, in the presence of Cs vapour	[26, 27, 495, 500]
	2.10 ^c	–	–	TiM, powder	[1, 486]
	2.10 ^c	–	900–1200	TiM, on W substrate, in the presence of Cs vapour	[504, 529]
	2.16	–	–	TiM, powder on W sub- strate	[507, 508, 529]
	2.18	–	–	TiM	[1, 482]
	2.18 ^c	0.31	900–1700	TiM, powder on W substrate	[1, 487, 529]
	2.30	0.20	–	TiM, powder on Ta substrate	[1, 488]

(continued)

Table 5.11 (continued)

Composition	Work function ^a , $\varphi = \varphi_0 + (d\varphi/dT)_{av}T$, eV	Richardson constant, A, $10^4 \text{ A m}^{-2} \text{ K}^{-2}$	Temperature range, °C	Remarks ^b	Reference
	2.60 ^c	1.12	1400–1700	TiM, in the presence of Cs vapour	[1, 33, 489, 529]
	2.70	0.15	–	TiM, powder on Ta substrate	[1, 482, 490]
	2.86	88.15	1200–2200	TiM	[1, 482]
	2.95 ^c	–	25	FEM, thin films on Mo substrate, measured in vacuum ($\sim 3 \times 10^{-8}$ Pa)	[529, 531, 1493]
	2.96	14	–	TiM, powder on Ta substrate	[1, 33, 482]
	3.00	0.7	–	TiM, powder on Ta substrate with MoSi ₂ under-layer	[1, 482, 490]
	3.00	–	–	TiM, pyrolytic coating on Ta wire	[1, 259, 482]
	3.10	36	–	TiM, hot-pressed	[1, 482]
	3.1 ± 0.1	0.5 ± 0.1	–	TiM, melted in Ar	[1, 482]
	3.15 ^c	–	25	On Si substrate, measured in vacuum ($\sim 3 \times 10^{-8}$ Pa)	[529, 531]
	3.2 ± 0.1	3 ± 2	–	TiM, sintered, 8% porosity	[1, 482]
	3.2 ± 0.1	8 ± 2	–	TiM, sintered, 15% porosity	[1, 482]
	3.20 ^c	–	800	Measured in vacuum ($\sim 5 \times 10^{-5}$ Pa of O ₂)	[529]
	3.24 + (2.0 × 10 ⁻⁴)T	–	1000–1700	TiM, powder	[1, 482]
	3.24 + (2.0 × 10 ⁻⁴)T	–	1000–2500	TiM, pyrolytic coating on W substrate	[1, 33, 482, 491]
	3.30 ^c	–	1700	TiM	[1, 482]
	3.32	17	1300–1800	TiM	[1, 482]
	3.4 ± 0.1	16 ± 6	–	TiM, sintered, 44% porosity	[1, 482]
	3.49 ^c	–	1500	TiM, powder on Ta substrate	[1, 33, 482]
	3.50	–	–	AeE	[1, 482, 1422, 1426]
	3.5 ^c	–	–	FEM, single crystal tips (field emitters)	[1493]
	3.54 ^c	–	25	FEM, thin films on W substrate, measured in vacuum ($\sim 3 \times 10^{-8}$ Pa)	[529, 531, 532, 1493]
	3.56 ^c	181	2200	TiM, powder on Ta substrate	[535]
	3.58 ^c	–	2100	TiM, hot-pressed	[1, 492]
	3.58 ^c	–	25	On Mo substrate, measured in vacuum ($\sim 3 \times 10^{-8}$ Pa)	[529, 532]

(continued)

Table 5.11 (continued)

Composition	Work function ^a , $\varphi = \varphi_0 + (d\varphi/dT)_{av}T$, eV	Richardson constant, A, $10^4 \text{ A m}^{-2} \text{ K}^{-2}$	Temperature range, °C	Remarks ^b	Reference
	3.60 ^c	–	1900	TiM, powder on W substrate	[1, 482, 493]
	3.6 ^c	–	–	TiM, sintered, average value accepted	[526]
	3.62 ± 0.01 ^c	–	25	CPDM (Mo), electro-phoretic coating on Ta substrate, measured in vacuum ($\sim 10^{-7}$ – 10^{-8} Pa)	[1, 33, 482, 494, 529]
	3.64 ^c	–	1700	TiM, powder on W substrate	[1, 482]
	3.66	–	1700	TiM, sintered	[523, 524]
	3.67 ^c	–	1000–1300	Measured in vacuum ($\leq 4 \times 10^{-7}$ Pa)	[517, 519, 529]
	3.70 ^c	–	2050	TiM, powder on Ta substrate	[1, 482]
	3.70 ^c	–	2050	TiM, melted	[1, 482]
	3.70	32	–	TiM, pressed	[1, 482]
	3.70	–	–	TiM, cleaned surface in the presence of Cs vapour	[1, 482, 495]
	3.70 ± 0.04 ^c	–	1100–1200	TiM, high purity materials, measured in vacuum ($\sim 10^{-7}$ Pa)	[1, 495, 496, 529]
	3.70–3.95	–	700–1100	TiM, high purity materials, measured in vacuum ($\sim 10^{-7}$ Pa)	[496, 529]
	3.73 ^f	–	–	Single crystal (001), theoretically evaluated	[710]
	3.74 ± 0.07	–	–	Recommended as the most probable value for essentially clean surfaces	[529]
	3.75 ^c	–	1000–1700	TiM, sintered, 15% porosity	[1, 482, 529]
	~3.75	–	1700	TiM, hot-pressed, 5–9% porosity	[1379]
	3.78 ^c	–	1000–1700	TiM, sintered, 8–45% porosity	[1, 26, 27, 482, 529]
	3.80	134	1300–1700	TiM, melted	[1, 33, 499, 529]
	3.80	–	–	TiM, sintered rod	[1, 500]
	3.80	–	830–1130	TiM	[1, 501]
	3.80	–	1700	TiM, carbide-graphite hypereutectic alloy	[1, 482, 502]
	3.82 – (6.35 × 10 ⁻⁴)T	–	700–1300	Measured in vacuum ($\leq 10^{-7}$ Pa)	[529, 533]
	3.85 ^c	–	–	TiM, single crystal (100) film on W (100) substrate	[528]
	3.90 ^c	–	2100	TiM, powder on Ta substrate	[1, 482, 500]

(continued)

Table 5.11 (continued)

Composition	Work function ^a , $\varphi = \varphi_0 + (d\varphi/dT)_{av}T$, eV	Richardson constant, A, $10^4 \text{ A m}^{-2} \text{ K}^{-2}$	Temperature range, °C	Remarks ^b	Reference
	3.90 ^c	–	2200	TiM, powder on W substrate	[1, 482, 503]
	3.94	–	–	Calculated value (unrelaxed surface)	[1422, 1426]
	3.95 ± 0.04 ^c	–	1300	TiM, hot-pressed, measured in vacuum (<10 ⁻⁶ Pa)	[482, 504, 529]
	3.97 ^c	–	1700	TiM	[516]
	3.97 ^g	–	–	Single crystal (001), theoretically evaluated	[710]
	4.00 ^c	140	–	TiM, melted, measured in vacuum (~10 ⁻⁵ Pa)	[1, 33, 505, 529]
	4.00 ^c	–	1500	TiM, on Mo/Ta substrates	[1, 482, 529]
	4.0 ^h	–	25	FEM, single crystal (001), clean surface	[557–560, 1492]
	4.01 ± 0.05 ^c	–	25	CPDM, hot-pressed, plain, measured in vacuum (<3 × 10 ⁻⁷ Pa)	[482, 504, 529]
	4.02 ^c	–	1650	TiM, melted in Ar	[1, 26, 27, 482]
	4.09 ^{c,i}	–	–	Single crystal (100), theoretically evaluated	[529, 530]
	4.19 ^c	–	25	FEM, thin films on Si substrate, measured in vacuum (~3 × 10 ⁻⁸ Pa)	[529, 532, 1493]
	4.20	360	1100–1800	TiM, electrophoretic coating on W filament	[1, 482, 506]
	4.30	–	–	Calculated value (relaxed surface)	[1422, 1426]
	4.30 ^c	–	800	Measured in vacuum (~10 ⁻³ Pa of O ₂)	[529]
	4.39 ^c	–	1500	–	[26, 27, 141]
	4.40–4.80	–	–	TiM, single crystal (111) film on W (110) substrate	[528]
	4.45 ^{c,j}	–	–	Single crystal (100), theoretically evaluated	[529, 530, 1422, 1426]
	4.48 ^c	–	1300–1600	–	[529, 534]
	4.52	–	–	FEM, thin films on W substrate, clean surface	[1493]
	4.60	–	–	FEM, thin films on Mo substrate, clean surface	[1493]
	4.7 ^k	–	25	FEM, single crystal (111), clean surface	[557–560]

(continued)

Table 5.11 (continued)

Composition	Work function ^a , $\varphi = \varphi_0 + (d\varphi/dT)_{av}T$, eV	Richardson constant, A, $10^4 \text{ A m}^{-2} \text{ K}^{-2}$	Temperature range, °C	Remarks ^b	Reference
	4.82	–	–	FEM, thin films on Si substrate, clean surface	[1493]
	–	–	1700	TiM, powder on Ta, current density: 10^4 A m^{-2} (constant mode) and $5 \times 10^4 \text{ A m}^{-2}$ (impulse mode)	[1, 482, 488]
	–	–	–	FEM, current density: $(1.2\text{--}6.2) \times 10^4 \text{ A m}^{-2}$ (impulse mode)	[527]

^a T is temperature, K

^bMethods applied for the experimental determination of the work function (TiM – thermionic method, AeE – autoelectron emission, FEM – field emission microscopy, PhES – photoelectron spectroscopy, CPDM – contact potential difference method, second electrode is given in brackets) and manufacturing methods for the fabrication of a particular material (or its constitution) are marked

^cValues of effective electron work function

^dThe presence of amorphous C and/or metallic Zr is very probable

^eFor materials with additions of 0.5–1.0% Y $\varphi = 5.3\text{--}5.6 \text{ eV}$

^fFirst principles calculated using the Perdew's generalized gradient approximation (GGA) for the fixed surface model

^gFirst principles calculated using the Perdew's GGA for the relaxed surface model

^hFor graphene-covered surface $\varphi = 4.2 \text{ eV}$

ⁱCalculated using the full-potential linear-muffin-tin-orbital (FP-LMTO) method

^jCalculated using the linear-muffin-tin-orbital with atomic sphere approximation (LMTO-ASA) technique

^kFor graphene-covered surface $\varphi = 4.3 \text{ eV}$

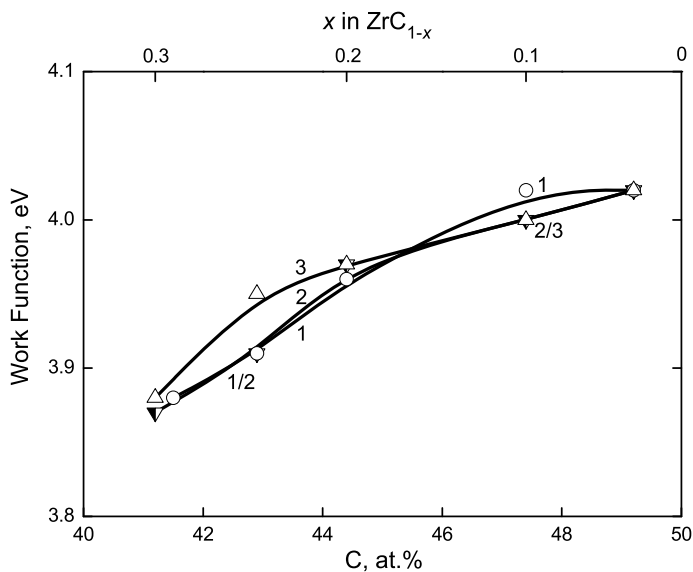


Fig. 5.19 Variation of effective work function of hot-pressed zirconium monocarbide ZrC_{1-x} materials with carbon content measured by “total current” method at 1530 °C: 1 – [482, 485, 516], 2 – [57, 510–512, 514, 515, 1502], 3 – [26, 27, 513]

uncontrolled impurity gases containing oxygen [517–519]. Using the photoemission technique, Lindberg and Johansson [1387] revealed that the work function of $\text{ZrC}_{0.92}$ (100) increases dramatically with increasing the exposure to O_2 , while only small increases in the work function are observed after the exposure to CO media. Similar to some other transition metal carbides, single crystal ZrC_{1-x} materials show the following relationships between effective thermionic work functions of different crystallographic planes: $\varphi_{(210, 310)} < \varphi_{(100)} \approx \varphi_{(110)} \gg \varphi_{(111)}$ [527]. Field emission properties of ZrC_{1-x} single crystal tips and thin films (coatings) were reported in several works [527, 531, 532, 558, 1491, 1493–1501]. Secondary ion emission of hot-pressed ZrC_{1-x} materials was studied by Cherepin et al. [520].

The recommended values of electrical resistivity, magnetic susceptibility, integral and spectral emittances and thermionic emission characteristics (electron work function and Richardson constant) for zirconium monocarbide are given in the wide range of temperatures in comparison with other ultra-high temperature materials in Addendum.

5.4 Physico-mechanical Properties

The physico-mechanical properties of zirconium monocarbide ZrC_{1-x} are sensitive to the deviations from the stoichiometry, but also to the crystallographic directions in the materials. At room temperature the hardness HV , GPa of near-stoichiometric zirconium monocarbide ZrC_{1-x} is evaluated as $(17\text{--}20) \pm (2\text{--}3)$ [581], $17.9\text{--}28.7$ [63], $(17.9\text{--}18.0) \pm (0.6\text{--}1.0)$ (9.8 N load, mean grain size – 5 μm) [441, 587, 588], $19.6\text{--}27.5$ [540], $20\text{--}34$ [74], 20.5 (porosity – 3–5%, 0.5 N load) [538, 556], 21.0 (for $\text{ZrC}_{0.98}$, porosity 9%, mean grain size – 50 μm) [537], $(21.6\text{--}22.6) \pm (1.7\text{--}2.2)$ [1, 26, 27, 547, 548], 21.7 (contents: non-combined C – 0.05–1.0%, O \leq 0.01%, N \leq 0.01%, porosity – 10%, mean grain size – 10 μm) [117], $22.7\text{--}24.7$ (0.5 N load) [553], 22.8 (contents: non-combined C – 0.05–1.0%, O \leq 0.1%, N \leq 0.1%, porosity – 10%, mean grain size – 10 μm) [117], 23.5 (1.2 N load) [213], 24.0 (for $\text{ZrC}_{0.96}$, 1 N load) [1, 4, 132], 24.5 [1, 539], 24.5 (for $\text{ZrC}_{0.79}$) [104], 25.0 ± 1.5 (for $\text{ZrC}_{0.96}$, contents: O – 0.01%, N – 0.46%) [4, 545], 25.4 (0.5 N load) [213], 25.5 (0.5–2.0 N load) [43, 46, 214, 218, 384, 550, 552], 25.5 (for $\text{ZrC}_{0.98}$, 200 N load) [28, 546], 25.7 (for $\text{ZrC}_{0.96}$) [554], 25.9 [452], 26.5 [557], $26.5\text{--}28.4$ [47], 27.0 (porosity – 7%, mean grain size – 10–14 μm) [541], 27.5 (2 N load) [48], $27.5\text{--}30.9$ [103], 27.8 ± 0.9 [35, 542, 549], $27.8\text{--}34.1$ (1 N load) [39, 550], 28.0 [351, 536], 28.6 ± 1.8 (0.3 N load) [30, 33, 213], 28.7 [30, 47, 213], 28.9 ± 1.2 (for $\text{ZrC}_{0.97}$, 0.5 N load) [32, 513], 29.3 [555] and 32.9 (for $\text{ZrC}_{0.92}$) [300]; hardness HK , GPa is 17.9 (1 N load) [319, 543, 544], 21.0 [39, 551] and 25.5 (0.5 N load) [319, 543]. The hardness of near-stoichiometric zirconium monocarbide ZrC_{1-x} in Mohs scale is >8 [63], $8\text{--}9$ [32, 43, 547, 1511], or 9 [46], and in Rockwell scale HRA it is 87 kgf mm^{-2} (0.85 GPa) [4, 30, 33, 48, 547], $88\text{--}94 \text{ kgf mm}^{-2}$ (0.86–0.92 GPa) [46], or 92.5 kgf mm^{-2} (0.91 GPa) [39]. According to the data available in literature within the homogeneity region the microhardness $H\mu$ of ZrC_{1-x} enlarges almost linearly from low-carbon to high-carbon phase boundaries in the range from 18.7 to 26.5 GPa (0.5 N load) [79], or from 19.6 to 28.4 GPa [1506]. The variations of hardnesses HVI/HK and microhardness $H\mu$ with carbon content within the homogeneity range of ZrC_{1-x} ,

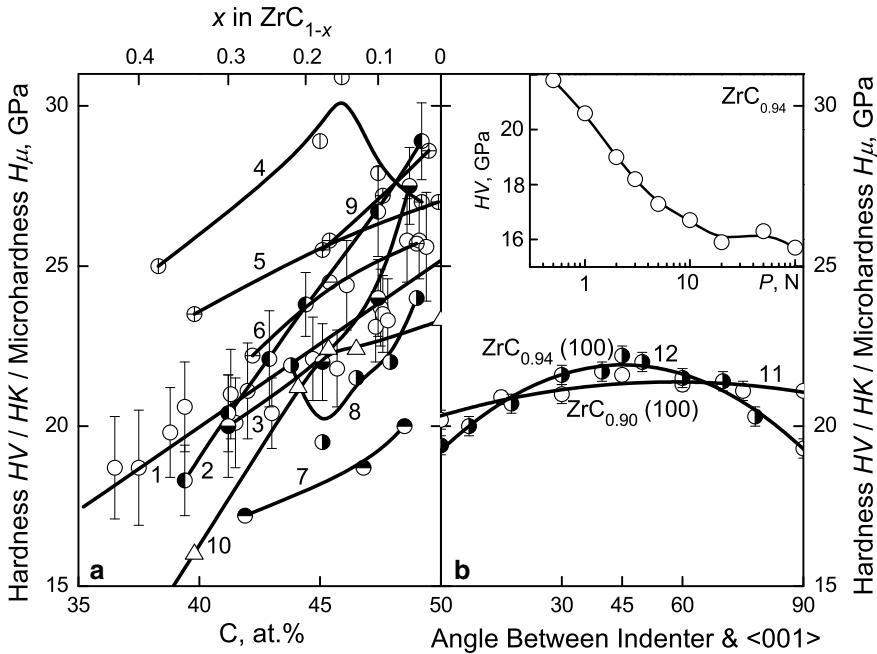


Fig. 5.20 Variations of the hardnesses HV (1, 10–11), HK (4, 12) and microhardness $H\mu$ (2–3, 5–9, 11) at room temperature for prepared by various methods zirconium monocarbide ZrC_{1-x} materials: (a) with deviation from the stoichiometry within the homogeneity range (1 – 200 N load [28, 546]; 2 – sintered (in vacuum) materials, contents: O – 0.08–0.17%, N – 0.01–0.09%, 0.5 N load [32, 513, 516]; 3 – fused (in Ar) materials, 1 N load [561]; 4 – thin films prepared by tri-ion beam-assisted deposition [103]; 5 – carburized coatings on graphite produced by soaking graphite in liquid metal, 0.5 N load [615]; 6 – fused (in Ar) materials [554]; 7 – hot-pressed, 0.2 N load [562, 590]; 8 – sintered (in vacuum) materials, porosity – 6–30%, mean grain size – 10–18 μm , contents: non-combined C – 0.10–0.55%, O – 0.13–0.72%, N – 0.01–0.30%, 1 N load [132]; 9 – hot-pressed (annealed in vacuum) materials, 0.5 N load [384]; 10 – DFT-estimated [696]) and (b) with indenter orientation (angle between indenter axis and <001> direction) on the (100) surface of single crystal materials grown by floating-zone processes (11 – $ZrC_{0.90}$, 2 N load [93]; 12 – $ZrC_{0.94}$, 5 N load [171, 1503, 1504]); *Inset* – variation of hardness with test force loading for spark plasma sintered $ZrC_{0.94}$, porosity – 1%, contents: non-combined C – 0.28%, O – 0.79%, N – 0.52%, Fe – 0.02% in HV , GPa – $\lg P$, N scale [726]

indenter orientation (for the (100) surface of $ZrC_{0.90}$ and $ZrC_{0.94}$ single crystals) and test force loading are demonstrated in Fig. 5.20. In the wide temperature range from 0 to 1400 °C the hardness of ZrC_{1-x} materials can be expressed by the following exponential temperature dependency [591–593]:

$$HV = 29.4 \exp[-(16.4 \times 10^{-4})t], \quad (5.76)$$

where HV is Vickers hardness, GPa and t is temperature, °C, which is approximated at lower and moderate temperatures (<600 °C) by the linear equation [54]:

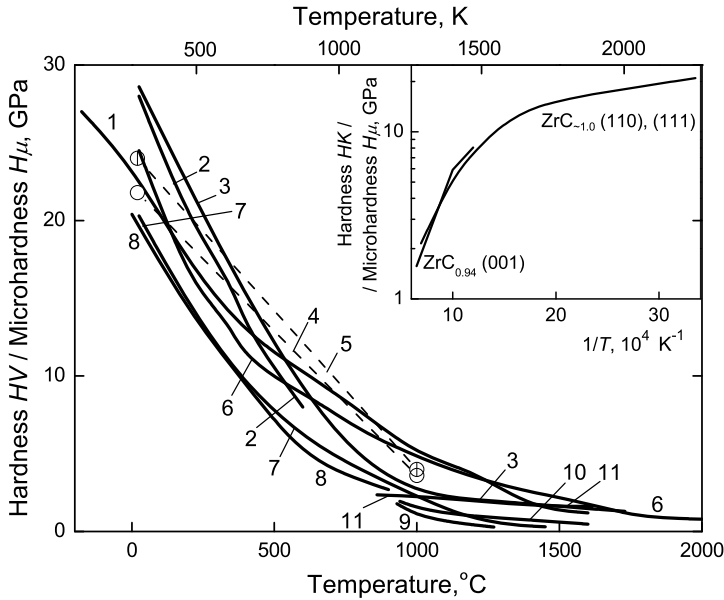


Fig. 5.21 Variations of the hardness HV (3, 6, 8–10) and microhardness $H\mu$ (1–2, 4–5, 7) of zirconium monocarbide ZrC_{1-x} materials with temperature: 1 – $ZrC_{0.95}$, zone melted single crystal (100), contents: non-combined C – 0.05%, O – 0.01%, N – 0.03%, W – 0.46%, 1.15 N load [537]; 2 – $ZrC_{\sim 1.0}$, sintered [536]; 3 – recommended for near-stoichiometric compositions by Kotelnikov et al. [33]; 4 – $ZrC_{0.78}$, sintered (in vacuum) and annealed, porosity – 21%, mean grain size – 18 μm , contents: non-combined C – 0.1%, O – 0.26%, N – 0.20%, 1 N load [132]; 5 – $ZrC_{0.96}$, sintered (in vacuum) and annealed, porosity – 6%, mean grain size – 10 μm , contents: non-combined C – 0.55%, O – 0.13%, N – 0.07%, 1 N load [132]; 6 – $ZrC_{\sim 1.0}$, hot-pressed and annealed (in H_2), porosity – 1–2%, content non-combined C – 0.54%, 9.8 N load [573–575, 595]; 7 – $ZrC_{0.90}$, grown by radio-frequency floating-zone process (zone melted) single crystal (100), 2 N load [172]; 8 – $ZrC_{\sim 1.0}$, [567]; 9 – $ZrC_{0.75}$, fused (in Ar) [568]; 10 – $ZrC_{0.82}$, fused (in Ar) [568]; 11 – $ZrC_{\sim 1.0}$, sintered, porosity – 7%, 1.5 kN load [1412] (*Inset* – single crystal materials: $ZrC_{0.94}$ (001), grown by the floating-zone technique, 5 N load in $\lg(HK) - 1/T$, K scale [572] and $ZrC_{\sim 1.0}$ (110), (111) in $\lg(H\mu) - 1/T$, K scale [333])

$$HV = 34.9 - (3.53 \times 10^{-3})t. \quad (5.77)$$

The variations of the hardness HV and microhardness $H\mu$ of near-stoichiometric zirconium monocarbide with temperature on the basis of several sources are presented in Fig. 5.21. The data on microhardness $H\mu$ of zirconium monocarbide single crystals and various polycrystalline materials are listed in Tables 5.12 and 5.13.

On the basis of several sources the variations of ultimate tensile strength σ_t (some data on σ_t are supplied with corresponding elongation δ and reduction in area ψ values) with temperature of near-stoichiometric zirconium monocarbide ZrC_{1-x} , which were determined on materials manufactured by various techniques, are shown in Fig. 5.22 (not given in the figure, the highest value of tensile strength of ZrC_{1-x} materials ~ 0.7 GPa (at room temperature) [1] was revealed for carbide polycrystalline fibre prepared by the impregnation of viscose rayon with zirconium chloride solution followed by the heat treatment). For ZrC_{1-x} materials the stress-strain diagrams (at moderate strain rates $\leq 10^{-3} \text{ s}^{-1}$) under tension and compression are linear up to 1200 and 2000 $^\circ\text{C}$, respectively; at higher strain rate ($\geq 10^{-1} \text{ s}^{-1}$) ZrC_{1-x}

Table 5.12 Microhardness $H\mu$ of zirconium monocarbide ZrC_{1-x} ($0 < x \leq 0.16$) single crystals at room temperature

Surface	Indenter diagonal direction	Microhardness $H\mu$, GPa	Reference
		$x \approx 0$	
(100) ^a	<100>	26.0	[1, 564]
	<110>	25.0	[1, 564]
	<210>	27.0	[1, 564]
(110) ^a	<100>	25.0	[1, 564]
	<110>	24.0	[1, 564]
	<111>	26.0	[1, 564]
	<112>	25.5	[1, 564]
(001)	<100>	19.4	[1470, 1505]
	<110>	22.1	[1470, 1505]
		$x = 0.04^b$	
(100)	<110>	25.0	[1, 564]
	<210>	27.0	[1, 564]
(110)	<100>	26.0	[1, 564]
	<110>	24.0	[1, 564]
	<111>	26.0	[1, 564]
	<112>	25.5	[1, 564]
(111)	<100>	25.0	[1, 564]
	<110>	23.0	[1, 564]
	<112>	24.0	[1, 564]
	<123>	25.0	[1, 564]
			$x = 0.05^c$
(100)	–	24.0	[1, 537]
		$x = 0.06$	
(100)	<100>	19.8 ^d	[171]
		19.4 ± 0.3^e	[171]
	<110>	20.9 ^d	[171]
		22.2 ± 0.3^e	[171]
	<010>	19.3 ± 0.3^e	[171]
	< $\bar{1}00$ >	19.6 ± 0.3^e	[171]
	< $\bar{1}10$ >	22.1 ± 0.3^e	[171]
	–	21.2 ^d	[572]
		$x = 0.08-0.11^f$	
(100)	–	24.0–26.0	[571]
		$x = 0.10$	
(100)	<100>	17.2 ± 0.8^g	[570]
	<001>	20.3 ^h	[4, 93]
	<010>	17.2 ± 0.8^g	[570]
		20.6 ^h	[4, 93]
	<110>	18.7 ± 0.8^g	[570]
	<011>	21.6 ^h	[4, 93]
	–	26.0	[566]

(continued)

Table 5.12 (continued)

Surface	Indentor diagonal direction	Microhardness $H\mu$, GPa	Reference
(110)	<001>	18.8 ^h	[172]
(111)	<110>	17.4 ^h	[172]
		$x = 0.11$	
(001)	–	25.0 ± 0.5 ⁱ	[565]
	–	24.6 ± 0.5 ^j	[565, 577]
(110)	–	22.9 ± 0.5 ^j	[565, 577]
	–	22.8 ± 0.5 ⁱ	[565]
(111)	–	23.8 ± 0.5 ⁱ	[565]
	–	23.5 ± 0.5 ^j	[565, 577]
		$x = 0.16^k$	
(100)	–	24.2 ± 2.9	[1, 563]

^aCrystals produced by induction zone melting, 1 N load, Knoop measurement (*HK*)

^bCrystals produced by induction zone melting, contents: non-combined C – 0.05%, O – 0.01%, N – 0.01%, 1 N load, Knoop measurement (*HK*)

^cCrystals grown by controlled solidification from the melt, contents: non-combined C – 0.05%, O – 0.01%, N – 0.03%, W – 0.46%, 1.15 N load

^dCrystals grown by the floating zone technique, 5 N load

^eCrystals grown by the floating zone technique, 5 N load, Knoop measurement (*HK*)

^fCrystals produced by induction zone melting, contents: non-combined C – 0.05–0.59%, O – 0.01–0.95%, N – 0.02–0.12%, W – 0.45–0.52%, 1 N load

^gCrystals produced by zone melting, 2 N load

^hHigh-purity crystals grown by radio-frequency floating-zone process, 2 N load

ⁱCrystals grown by controlled solidification from the melt, 1 N load, Knoop measurement (*HK*)

^jCrystals grown by controlled solidification from the melt, annealed at 2050 °C, 1 N load, Knoop measurement (*HK*)

^kCrystals produced by plasma-arc melting, content: non-combined C – 0.8%

Table 5.13 Microhardness $H\mu$ of the various compositions of zirconium monocarbide ZrC_{1-x} phase at room temperature

Composition	Microhardness $H\mu$, GPa	Remarks	Reference
ZrC _{0.54}	18.2	0.5 N load, sintered	[35, 79]
ZrC _{0.65}	23.5	0.5 N load, carbidized coating on graphite produced by soaking graphite in liquid metal	[615]
	18.3 ± 1.1	0.5 N load, sintered in vacuum, contents: O – 0.14%, N – 0.08%	[32, 513]
ZrC _{0.66}	16.0	DFT-estimated	[696]
ZrC _{0.70}	20.4 ± 1.2	0.5 N load, sintered in vacuum, contents: O – 0.13%, N – 0.06%	[32, 513]
	20.0 ± 1.6	1 N load, fused in Ar	[1, 561]
ZrC _{0.72}	17.2	0.2 N load, hot-pressed	[1, 562]

(continued)

Table 5.13 (continued)

Composi- tion	Microhardness $H\mu$, GPa	Remarks	Reference
ZrC _{0.75}	22.1 ± 1.5	0.5 N load, sintered in vacuum, contents: O – 0.12%, N – 0.09%	[32, 513]
ZrC _{0.77}	27.8 ± 0.9	0.2–1.5 N load, hot-pressed and annealed, porosity – 12%, contents: non-combined C – 0.2%	[35, 542, 549]
ZrC _{0.78}	21.9 ^a	1 N load, sintered in vacuum and annealed, porosity – 21%, mean grain size – 18 μm, contents: non-combined C – 0.1%, O – 0.26%, N – 0.20%	[1, 4, 132]
ZrC _{0.79}	24.5 ^b	Reactive magnetron sputtered thin films, thickness <3 μm, mean grain size – 10–13 nm, hardness values were taken at ~0.1–0.2 μm depth	[104]
	21.2	DFT-estimated	[696]
ZrC _{0.79} O _{0.02}	27.0	0.3 kN load, hot-pressed, porosity <0.5%, mean grain size – ~0.1 μm	[175, 179]
ZrC _{0.79} O _{0.13}	21.0 ± 1.4 ^b	Spark plasma sintered, porosity < 1%, mean grain size – 5.2 ± 0.2 μm	[630]
ZrC _{0.80}	23.8 ± 1.0	0.5 N load, sintered in vacuum, contents: O – 0.17%, N – 0.07%	[32, 513]
ZrC _{0.82}	22.0 ± 1.2 19.5 ^c	1 N load, fused in Ar 1 N load, sintered in vacuum and annealed, porosity – 30%, mean grain size – 12 μm, contents: non-combined C – 0.47%, O – 0.72%, N – 0.30%	[1, 561] [1, 4, 132]
ZrC _{0.83}	25.8	0.5 N load, carbidized coating on graphite produced by soaking graphite in liquid metal	[615]
	22.4	DFT-estimated	[696]
ZrC _{0.87}	22.4	DFT-estimated	[696]
	21.5	1 N load, sintered in vacuum and annealed, porosity – 15%, mean grain size – 15 μm, contents: non-combined C – 0.10%, O – 0.62%, N – 0.01%	[1, 132]
ZrC _{0.88}	18.7	0.2 N load, hot-pressed	[1, 562]
ZrC _{0.89}	24.1	0.5 N load, sintered	[79]
ZrC _{0.90}	26.7 ± 1.4	0.5 N load, sintered in vacuum, contents: O – 0.11%, N – 0.03%	[32, 513]
	24.0 ± 1.2	1 N load, fused in Ar	[1, 561]
	(17.8–18.5) ± (0.4–0.5)	9.8 N load, reactive hot-pressed, porosity – ~1%, mean grain size – 50–100 μm	[1425]
ZrC _{0.92}	32.9	Pyrolytic materials, in the parallel direction to the chemical vapour deposition surface	[4, 300]
	22.0	1 N load, sintered in vacuum and annealed, porosity – 14%, mean grain size – 11 μm, contents: non-combined C – 0.10%, O – 0.50%, N – 0.01%	[1, 4, 132]
ZrC _{0.93±0.01}	16.0 ^d	2 N load, hot-pressed, porosity – 7%, mean grain size – 4 μm, contents: non-combined C – 0.85%, O – 0.56%, N – 0.32%, Hf – 1.0%	[356, 634]
ZrC _{0.94}	20.0	0.2 N load, hot-pressed	[1, 562]
ZrC _{0.94} O _{0.05}	28.3 ± 1.0 ^b	Spark plasma sintered, porosity <1%, mean grain size – 4.7 ± 0.2 μm	[630]

(continued)

Table 5.13 (continued)

Composi- tion	Microhardness $H\mu$, GPa	Remarks	Reference
ZrC _{0.95}	27.5 ± 1.2	1 N load, fused in Ar	[1, 561]
	24.7 ± 1.0	0.5 N load, hot-pressed and work-hardened by grinding, porosity – 2–3%, contents: non-combined C – 0.91%, Fe – 0.30%	[553]
	22.0	0.5 N load, extruded, presintered and sintered non-isothermally, porosity – 14%, mean grain size – 11 μm, contents: non-combined C – 0.04%, O – 0.33%, N – 0.03%, W – 0.4%	[623]
	20.5 ± 1.0	0.5 N load, hot-pressed and recrystallized at 1680 °C, porosity – 2–3%, contents: non-combined C – 0.91%, Fe – 0.30%	[553]
	18.0	0.5 N load, extruded, presintered and sintered non-isothermally, porosity – 4–8%, mean grain size – 16–30 μm, contents: non-combined C – 0.04%, O – 0.33%, N – 0.03%, W – 0.4%	[623]
ZrC _{0.96}	25.7	Fused materials	[554]
	25.0 ± 1.5	1 N load, produced by carbidization through metal saturation, contents: O – 0.01%, N – 0.46%	[1, 4, 545]
	24.0°	1 N load, sintered in vacuum and annealed, porosity – 6%, mean grain size – 10 μm, contents: non-combined C – 0.55%, O – 0.13%, N – 0.07%	[1, 4, 132]
	(14.4–16.2) ± (0.3–0.9)	9.8 N load, reactive hot-pressed, porosity < 2%, mean grain size – 5–10 μm, trace amount of non-combined C	[1425]
ZrC _{0.97}	28.9 ± 1.2	0.5 N load, sintered in vacuum, contents: O – 0.08%, N – 0.01%	[32, 513]
ZrC _{0.98}	27.2 ^b	Hot-pressed, mean grain size – 5–20 μm	[703]
	26.5 ± 0.6	Pyrolytic materials	[579]
	23.2	Hot-pressed, mean grain size – 5–20 μm	[703]
	21.0	Sintered materials, porosity – 9%, mean grain size – 50 μm	[537]
ZrC _{~1.0}	48 ± 3 ^b	5–750 μN load, pulsed laser deposited thin films, mean grain size – 19 nm, microstrain – 1.6%, content O < 0.5%	[729]
	41 ± 2 ^b	5–750 μN load, pulsed laser deposited thin films, mean grain size – 12 nm, microstrain – 1.7%, content O < 0.5%	[729]
	29.3	Hot-pressed materials	[555]
	28.7	–	[30, 213]
	28.6 ± 1.8	0.3 N load	[30, 33]
	28.4	Value extrapolated to the stoichiometric composition (high-carbon ZrC _{1-x} phase boundary)	[35, 1506]
	28.0	–	[351, 536]
	27.9–28.4	–	[635]
	27.8–34.1	1 N load	[39, 550]
	27.8	0.5 N load, sintered	[35, 542, 1509]

(continued)

Table 5.13 (continued)

Composition	Microhardness $H\mu$, GPa	Remarks	Reference
	27.5–30.9	Thin films prepared by tri-ion beam-assisted deposition	[103]
	27.5	2 N load	[48]
	27.0	0.5 N load, carbided coating on graphite produced by soaking graphite in liquid metal	[336, 615]
	26.5–28.4	–	[47]
	26.5	0.5 N load, sintered, porosity – 7%, mean grain size – 10–14 μm	[1, 541, 557]
	26.5	Value extrapolated to the stoichiometric composition (high-carbon ZrC_{1-x} phase boundary)	[35, 79]
	26.2–30.5	Calculated on the basis of hardness-elasticity correlation	[578, 586]
	26.0 ^f	0.2–10 N load, hot-pressed and annealed, porosity <5%	[547, 569, 589, 591]
	26.0	Value summarized on the basis of critical review of available experimental data	[65]
	26.0 (24.0 ^d)	Electron beam deposited thin films on Ti substrate, thickness – 0.51 \pm 0.02 μm , mean grain size <0.2 μm	[580]
	25.8	–	[719]
	25.5	0.5–2.0 N load	[43, 46, 54, 260, 550, 552]
	25.5 ^d	0.5 N load	[319, 543, 1412]
	25.4	0.5 N load	[213]
	25.2 \pm 1.4 ^b	Spark plasma sintered, porosity – 1–2%, mean grain size – 5–13 μm	[588]
	25.0–25.9	On the basis of several sources	[582]
	24.5	Pyrolytic materials	[1, 539]
	23.7	4.9 N load, spark plasma sintered, porosity <3%, mean grain size – ~30 μm	[1431]
	23.5	1.2 N load	[213]
	23.3	DFT-estimated	[696]
	23.0	Pyrolytic materials	[363]
	22.9	4.9 N load, spark plasma sintered, porosity <4%, mean grain size – 15 μm	[1431]
	22.8	Sintered materials, porosity – 10%, mean grain size – 10 μm , contents: non-combined C – 0.05–1.0%, O \leq 0.1%, N \leq 0.1%	[117]
	22.3 ^g	High-pressure hot-pressed, porosity – 6%	[576]
	22.2	Hot-pressed, porosity – 1–2%, content non-combined C – 0.54%	[573, 574]
	21.8	0.5 N load, spark plasma sintered, porosity – 1%	[726]
	21.7	Sintered materials, porosity – 10%, mean grain size – 10 μm , contents: non-combined C – 0.05–1.0%, O \leq 0.01%, N \leq 0.01%	[117]

(continued)

Table 5.13 (continued)

Composition	Microhardness $H\mu$, GPa	Remarks	Reference
	21.6 ^h	–	[1510]
	21.3	4.9 N load, spark plasma sintered, porosity <5%, mean grain size – ~10 μm	[1431]
	21.0 ^d	–	[39, 551]
	21.0	Calculated theoretically on the basis of Tian's model	[582, 584, 585]
	20.9	–	[721]
	20.6	1 N load, spark plasma sintered, porosity – 1%	[726]
	20.5	0.5 N load, sintered, porosity – 3–5%	[1, 538]
	20 \pm 1 ^b	5–750 μN load, pulsed laser deposited thin films, mean grain size – 6 nm, microstrain – 2.0%, content O < 0.5%	[729]
	19.6–27.5	Pyrolytic materials, carbide is in contact with carbon	[540]
	19.3	Calculated on the basis of Gao's model	[582, 583]
	19.0	2 N load, spark plasma sintered, porosity – 1%	[726]
	18.6 ⁱ	1.5 load, sintered and annealed (in Ar), grain size from 10 to 60 μm	[616]
	18.0 \pm 0.4	9.8 N load, hot-pressed, porosity – 2%	[1479]
	(17.9–18.0) \pm (0.6–1.0)	9.8 N load, spark plasma sintered, porosity – 1–2%, mean grain size – 5–13 μm	[441, 587, 588]
	17.9–28.7	General estimation	[63]
	17.9 ^d	1 N load	[319, 543, 544]
	17.3	4.9 N load, spark plasma sintered, porosity – 1%	[726]
	(17–20) \pm (2–3)	Pulsed laser ablation deposited thin films on Ti substrate, thickness – 0.59–0.60 μm , approximate grain size – 10–100 nm	[581]
	16.7	9.8 N load, spark plasma sintered, porosity – 1%	[726]
	16.3 \pm 1.6	0.1 kN load, reactive spark plasma sintered materials, porosity – 4%, mean grain size <10 μm	[594]
	15.7	0.1 kN load, spark plasma sintered, porosity – 1%	[726]
	15.6	DFT-estimated	[376]

^a3.6 GPa – at 1000 °C

^bEvaluated by nanoindentation with a diamond tip

^c3.9 GPa – at 1000 °C

^dKnoop measurement (HK)

^e4.0 GPa – at 1000 °C

^fDetermined in accordance with the formula: $H\mu = 18.18P/d^2$, where P is the load on the indenter, N and d is the diagonal of the indentation, μm ; the values of other micromechanical characteristics: microbrittleness $\gamma_\mu = (D^2 - d^2)/d^2 = 6.0$, where D is the average size of the damageability zone, μm and brittle microstrength $\sigma_\mu = P/D^2 = 2.1$ GPa [569]

^gDepth-sensing indentation measurement

^hDiamond pyramid hardness measurement (DPH)

ⁱIndependent on grain size and annealing temperature

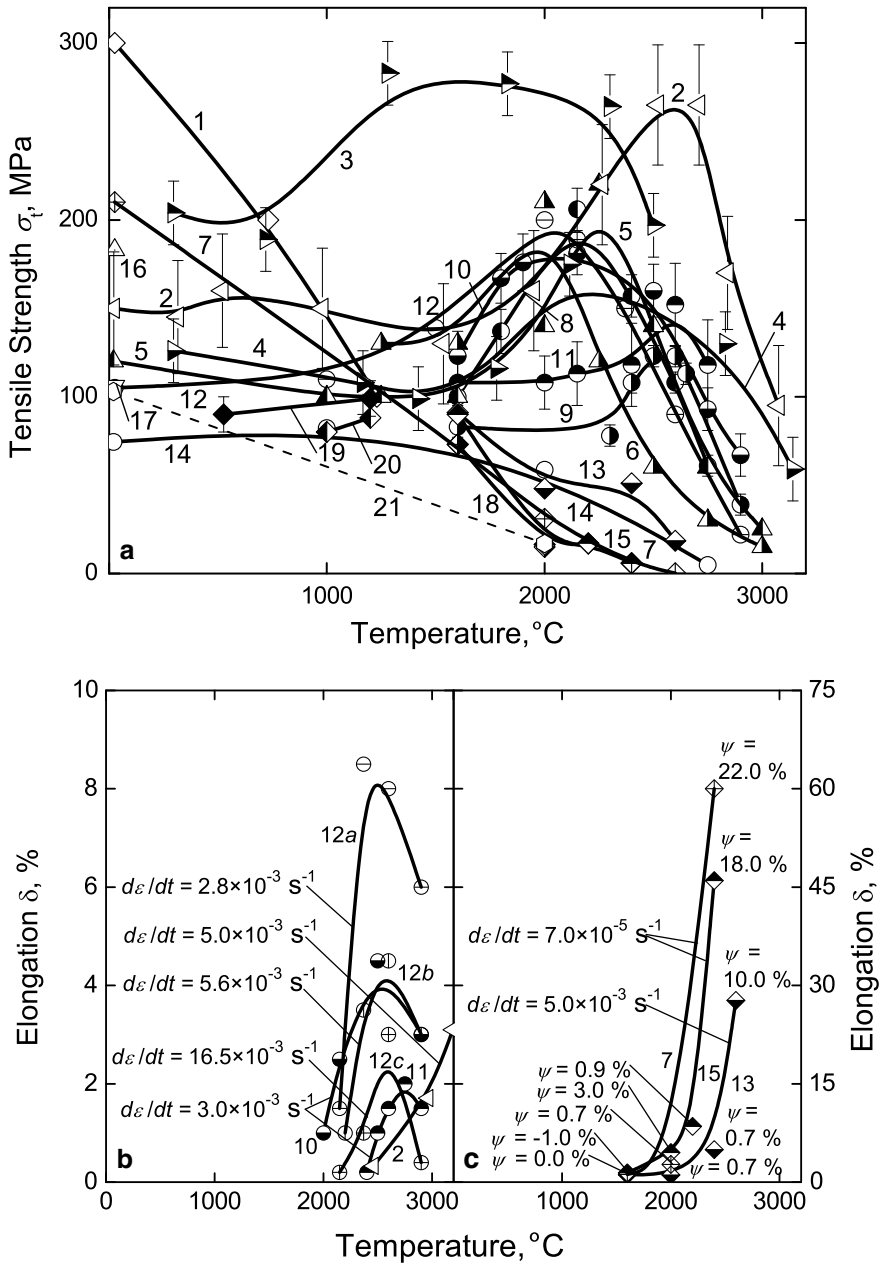


Fig. 5.22 (see caption on page 486)

◀**Fig. 5.22** Variation of (a) ultimate tensile strength σ_t , (b, c) elongation δ and (c) reduction in area ψ at fracture with temperature for zirconium monocarbide ZrC_{1-x} materials on the basis of several sources: 1 – sintered $ZrC_{\sim 1.0}$, porosity – 9% [30, 33, 607]; 2 – sintered $ZrC_{\sim 1.0}$, porosity – 5%, strain rate $d\epsilon/dt = 5 \times 10^{-3} s^{-1}$ [333, 336]; 3 – sintered and treated thermomechanically $ZrC_{0.97}$, porosity – 5% [632, 633]; 4 – same, without special thermomechanical treatment [632, 633]; 5 – sintered $ZrC_{0.95}$, porosity – 7%, mean grain size – 8 μm , contents: O + N – 0.14%, $d\epsilon/dt = 3 \times 10^{-3} s^{-1}$ [4, 645]; 6 – same, $d\epsilon/dt = 3 \times 10^{-5} s^{-1}$ [4, 645]; 7 – hot-pressed $ZrC_{0.83}$, porosity – 9%, mean grain size – 6 μm , contents: non-combined C – 1.40%, O – 0.18%, N – 0.94%, $d\epsilon/dt = 7 \times 10^{-5} s^{-1}$ [356, 634]; 8 – cold-rolled and sintered $ZrC_{0.94}$, porosity – 14%, mean grain size – 12 μm , contents: non-combined C – 0.10%, O – 0.08%, N – 0.02%, W – 0.20, $d\epsilon/dt = 3 \times 10^{-3} s^{-1}$ [597]; 9 – cold-rolled and sintered $ZrC_{0.95}$ (zonal segregation structured), porosity – 6%, mean grain size – 10 μm , contents: non-combined C – 0.10%, O – 0.20%, W – 0.20, $d\epsilon/dt = 3 \times 10^{-3} s^{-1}$ [597]; 10 – cold-pressed and sintered $ZrC_{0.95}$, porosity – 7%, mean grain size – 8 μm , contents: non-combined C – 0.10%, O – 0.12%, N – 0.02%, W – 0.40, $d\epsilon/dt = 3 \times 10^{-3} s^{-1}$ [597]; 11 – cold-pressed and sintered $ZrC_{0.98}$ (zonal segregation structured), porosity – 6%, mean grain size – 12 μm , contents: non-combined C – 0.60%, O – 0.08%, N – 0.008%, W – 0.30, $d\epsilon/dt = 3 \times 10^{-3} s^{-1}$ [597]; 12 – sintered $ZrC_{\sim 1.0}$, porosity – 5%, mean grain size – 15–25 μm , $d\epsilon/dt = 2.8 \times 10^{-3} s^{-1}$ [601, 620, 645]; 13 – hot-pressed and annealed $ZrC_{0.83}$, porosity – 9%, mean grain size – 6 μm , contents: non-combined C – 1.40%, O – 0.18%, N – 0.94%, $d\epsilon/dt = 5 \times 10^{-3} s^{-1}$ [356, 634]; 14 – sintered $ZrC_{\sim 1.0}$, porosity – 30% [32, 596]; 15 – hot-pressed $ZrC_{0.93\pm 0.01}$, porosity – 7%, mean grain size – 4 μm , contents: non-combined C – 0.85%, O – 0.56%, N – 0.32%, $d\epsilon/dt = 7 \times 10^{-5} s^{-1}$ [356, 634]; 16 – sintered $ZrC_{\sim 1.0}$ [319, 613]; 17 – $ZrC_{\sim 1.0}$ [614, 635]; 18 – hot-pressed $ZrC_{0.77-0.84}$, porosity – 1–5%, content non-combined C – 1.6–2.5% [356]; 19 – $ZrC_{\sim 1.0}$ [213]; 20 – hot-pressed $ZrC_{0.84\pm 0.01}$, porosity – 2%, content non-combined C – 4.1–4.3% [350]; 21 – $ZrC_{\sim 1.0}$ [351] (b: curves 12a, 12b and 12c are corresponding to the various values of strain rate $d\epsilon/dt$; c: reduction in area ψ is indicated for curves 7, 13 and 15, for all the curves $\psi = 0$ at 1600 °C)

continues to be brittle even at around 2700 °C [335]. The examples of tensile stress-strain graphic diagrams (curves) of ZrC_{1-x} materials for various temperatures, strain rates and microstructural characteristics (mean grain size) are given in Fig. 5.23. The variations of flexural (bending) strength σ_f with carbon content within the homogeneity range and temperature within the wide range from room to ultra-high temperatures are presented in Figs. 5.24 and 5.25. The effect of surface conditions on the flexural (bending) strength σ_f at room temperature for the materials with various porosity is demonstrated by data given in Table 5.14. The data on compressive strength σ_c of near-stoichiometric ZrC_{1-x} materials are summarized in Fig. 5.26. For the relationships between strength characteristics and microstructural factors (porosity $P \leq 30$ –35% and mean grain size L , 3–24 μm) of ZrC_{1-x} materials Bulychev et al. [4, 86] proposed the following equations:

$$\sigma_f = 540(1 - 2.8P), \quad (5.78)$$

$$\sigma_f = 1490L^{-0.45}, \quad (5.79)$$

$$\sigma_c = 1830(1 - 3.3P), \quad (5.80)$$

while Kruglov et al. [610] for the flexural (bending) strength σ_f proposed the modified expression (for the structures with mean grain size L in the range from 8 to 60 μm)

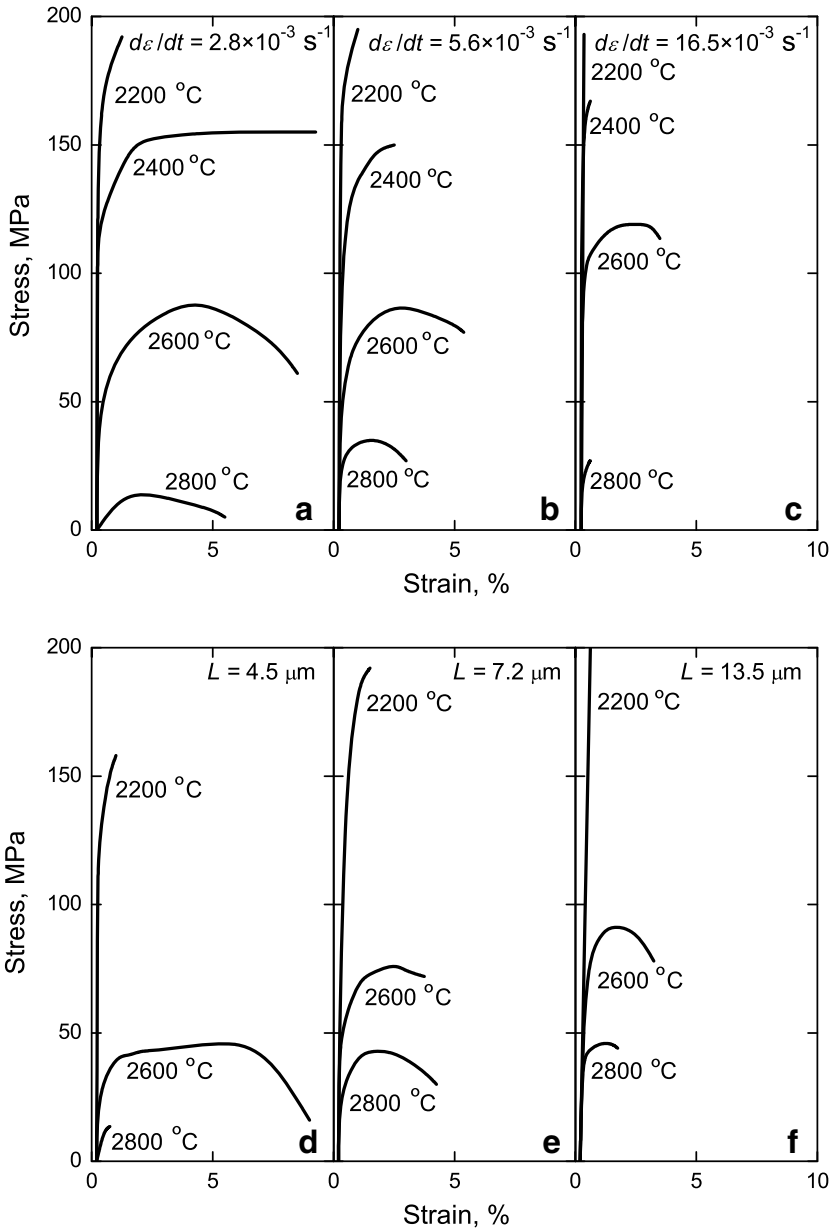


Fig. 5.23 The examples of tensile stress-strain graphic diagrams (curves) of sintered $\text{ZrC}_{\sim 1.0}$ materials with the various values of strain rates $d\varepsilon/dt$ (**a**, **b**, **c**) and mean grain sizes L (**d**, **e**, **f**) at high and ultra-high temperatures [601]

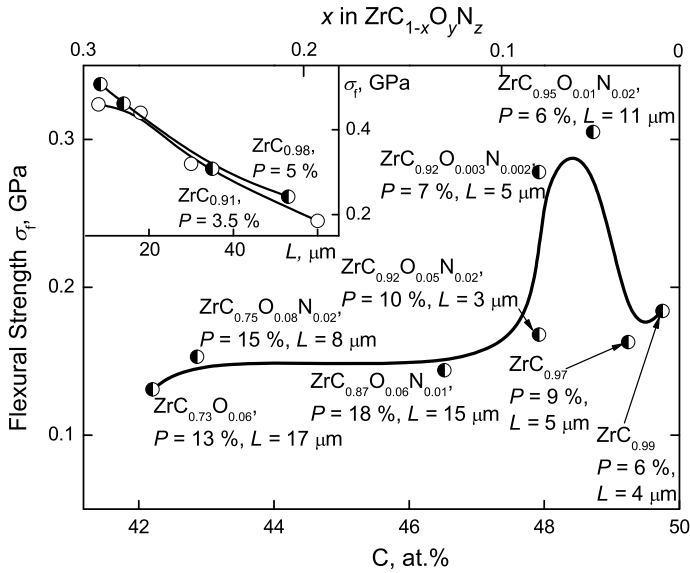


Fig. 5.24 Variation of the flexural (bending) strength σ_f at room temperature of sintered zirconium monocarbide $ZrC_{1-x}O_yN_z$ (contents of oxygen and nitrogen determined and marked; content non-combined carbon – 1.3% ($x = 0.01$), 2.2% ($x = 0.03$), 0.22% ($x = 0.05$), 0.15% ($x = 0.08$, $y = 0.003$), 0.05% ($x = 0.08$, $y = 0.05$; $x = 0.13$; $x = 0.25$; $x = 0.27$)) materials with deviation from the stoichiometry within the homogeneity range; porosity P and mean grain size L are indicated for all the compositions [606] (Inset – for sintered (in Ar) $ZrC_{0.91}$ (contents: non-combined C – 0.02%, O < 0.05%) [610] and sintered $ZrC_{0.98}$ [333], porosity indicated, in σ_f , GPa – L , μm scale)

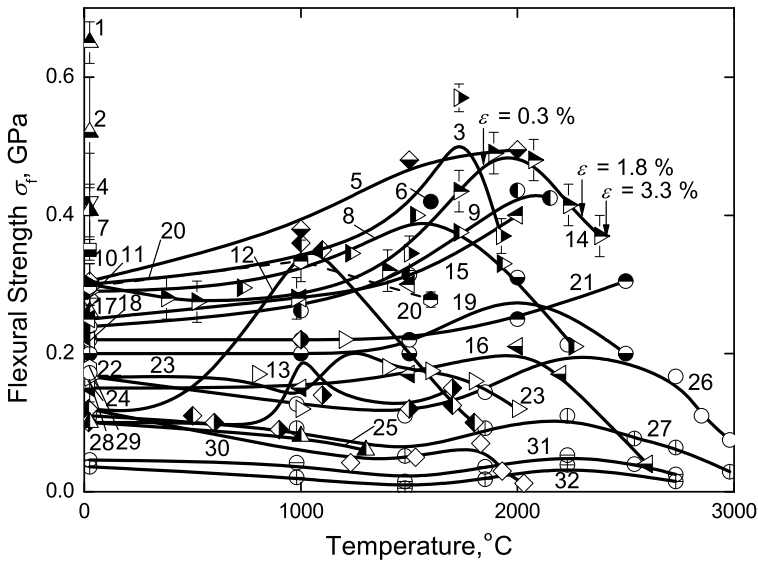


Fig. 5.25 (see caption on page 489)

◀**Fig. 5.25** Variation of flexural (bending) strength σ_f of near-stoichiometric zirconium monocarbide ZrC_{1-x} materials with temperature on the basis of several sources: 1 – sintered non-isothermally $ZrC_{0.95}$, porosity – 8%, mean grain size – 12–18 μm , contents: non-combined C – 0.04%, O – 0.33%, N – 0.03%, W – 0.40%, 3-point bending scheme [623]; 2 – sintered $ZrC_{0.96-1.00}$, porosity – 2–3%, mean grain size – 1–10 μm [86]; 3 – sintered $ZrC_{\sim 1.0}$, porosity – 5%, mean grain size – 6–16 μm , contents: non-combined C – 0.30%, O – 0.08%, N – 0.01%, W – 0.90%, $2.75 \times 2.75 \times 60$ mm bar, 4-point bending scheme [625–627]; 4 – sintered $ZrC_{\sim 1.0}$, porosity – 3–7%, mean grain size – 3–14 μm [440, 441, 536, 541, 605]; 5 – pyrolytic $ZrC_{\sim 1.0}$ [363]; 6 – sintered (in Ar) $ZrC_{\sim 1.0}$, porosity – 10–12%, mean grain size – 1–2 μm [1, 612]; 7 – spark plasma sintered $ZrC_{\sim 1.0}$, porosity – 1–2%, mean grain size – $13 \pm 1 \mu m$, $0.8 \times 1.0 \times 10$ mm bar, 3-point bending scheme [587, 588, 591]; 8 – sintered $ZrC_{\sim 1.0}$, porosity – 6%, mean grain size – 8 μm [330]; 9 – sintered $ZrC_{\sim 1.0}$, porosity – 5% [601]; 10 – sintered $ZrC_{\sim 1.0}$, porosity < 2%, mean grain size – 6 μm , $2 \times 3 \times 15$ mm bar, 3-point bending scheme [631]; 11 – sintered $ZrC_{0.96}$, porosity – 6%, contents: O \leq 0.05%, N – 0.05%, W – 0.2–0.3%, $2.5 \times 2.5 \times 30$ mm bar, 3-point bending scheme [617]; 12 – sintered $ZrC_{0.95}$, porosity – 2.5%, mean grain size – 10 μm , thickness – 1 mm, 4-point bending scheme [537]; 13 – same, thickness – 2 mm, 4-point bending scheme [537]; 14 – sintered $ZrC_{\sim 1.0}$, porosity – 5%, $d\epsilon/dt = 5 \times 10^{-3} s^{-1}$ [333, 336]; 15 – $ZrC_{0.96}$ obtained by metal right-through saturation (in Ar), mean grain size – 250 μm , $0.8 \times 1.5 \times 20$ mm bar, 3-point bending scheme [611]; 16 – same, $0.6 \times 2.0 \times 20$ mm bar, 3-point bending scheme [611]; 17 – sintered and annealed materials (Weibull modulus $m = 6.0$) [3]; 18 – sintered $ZrC_{0.93}$, porosity – 4–8%, mean grain size – 66 μm , contents: non-combined C – 0.5%, W – 0.2%, 3-point bending scheme (measured values at the temperature of liquid nitrogen proved to be practically equal to the corresponding values at 20 °C) [411, 624, 628, 687]; 19 – sintered $ZrC_{0.95}$, porosity – 6%, contents: O + N – 0.69%, $d\epsilon/dt = 2.8 \times 10^{-3} s^{-1}$ [4, 645]; 20 – hot-pressed $ZrC_{\sim 1.0}$, porosity – 2%, content O – 0.36% [1479]; 21 – sintered $ZrC_{0.95}$, porosity – 6%, contents: O + N – 0.69%, $d\epsilon/dt = 16.5 \times 10^{-3} s^{-1}$ [4, 645]; 22 – metal carbidized $ZrC_{0.96}$ [545]; 23 – hot-pressed $ZrC_{\sim 1.0}$, porosity – 4%, $6.3 \times 12.7 \times 76$ mm bar, loaded in perpendicular direction to hot-pressing axis, 3-point bending scheme for room temperature and 4-point bending scheme for high temperatures, calculated strain at fracture at room temperature – 0.04% [308]; 24 – metal carbidized $ZrC_{\sim 1.0}$, mean grain size – 200–300 μm , contents: O + N < 0.56% [545]; 25 – sintered $ZrC_{0.98}$, porosity – 9%, mean grain size – 50 μm , 4-point bending scheme [537]; 26 – slip-cast and sintered $ZrC_{0.93}$, porosity – 14%, mean grain size – 16–18 μm , content non-combined C – 0.3% [603]; 27 – cold-pressed and sintered $ZrC_{0.93}$, porosity – 10%, content non-combined C – 0.3% [603]; 28 – sintered $ZrC_{0.97}$, $1.7 \times 4.2 \times 30$ mm bar, 3-point bending scheme [618]; 29 – sintered and annealed (in Ar) $ZrC_{\sim 1.0}$, $0.8 \times 2.0 \times 13$ mm bar, 3-point bending scheme [616]; 30 – hot-pressed (low-porous) materials [608, 609]; 31 – slip-cast and sintered $ZrC_{0.93}$, porosity – 40%, mean grain size – 8–10 μm , content non-combined C – 0.3% [603]; 32 – cold-pressed and sintered $ZrC_{0.93}$, porosity 37%, content non-combined C – 0.3% [603] (bending strain values ϵ are indicated for curve 14 at corresponding temperatures)

$$\sigma_f = K(1/L - 1/L_0)^{1/2}, \quad (5.81)$$

where K is a constant and L_0 is a critical grain size determined by the scale factor and stressed state. In the insets to Figs. 5.24 and 5.26 the effect of mean grain size magnitude of ZrC_{1-x} materials on the strength characteristics is demonstrated specially. The approximate general relationship $\sigma_f : \sigma_c \approx 1 : (1.5-3) : (7-12)$ can be recommended for the common estimations of the strength characteristics of monocarbide ZrC_{1-x} materials [3, 33, 86, 330, 604, 619, 629]. According to Lanin et al. [411, 617, 660, 661], at room temperature sintered $ZrC_{0.93}$ (porosity – 4–8%, mean grain size – 66 μm , contents: non-combined C – 0.5%, W – 0.2%) has the fracture toughness $K_{IC} = 3.5$ MPa $m^{1/2}$ and sintered $ZrC_{0.96}$ (porosity 7%, mean grain size 20 μm , contents: non-combined C – 0.1%, O – 0.1%, N – 0.04%) – 2.8 MPa $m^{1/2}$ (with the ratio $K_{IA}/K_{IC} = 0.94$, scattered from 0.89 to 0.99); earlier for sintered $ZrC_{0.95}$ (porosity 8%) Warren [662] estimated K_{IC} to be in the range from 1.1 ± 0.1 to 2.3 ± 0.3 MPa $m^{1/2}$

Table 5.14 The effect of surface condition/treatment on the flexural (bending) strength at room temperature for sintered $\text{ZrC}_{0.90}$ materials with various porosity [602]

Porosity, %	Treatment character	Variations of ultimate flexural (bending) strength, MPa for the different efficiency of spark cutting treatment, $10^{-6} \text{ m}^2 \text{ min}^{-1}$			
		0.8	1.6	5.0	18.0
3	SCT ^a	279	230	204	204
	SCT + BCP ^b	330	319	286	281
8	SCT	–	176	141	132
	SCT + BCP	–	225	221	222
18	SCT	–	118	114	106
	SCT + BCP	–	169	171	170

^aSCT – spark cutting treatment^bSCT + BCP – spark cutting treatment with subsequent polishing by boron carbide powder

with the average fracture surface energy variation from 1.7 to 7.7 J m⁻². Katoh et al. [96] employing different methods for the K_{IC} determination of high-purity zone-refined $\text{ZrC}_{0.93}$ got $1.40 \pm 0.02 \text{ MPa m}^{1/2}$ measured by Vickers indentation technique and $2.7 \pm 0.3 \text{ MPa m}^{1/2}$ – by chevron-notched beam flexure method (ASTM C1421); Wang et al. [1425] by direct crack measurements – $(1.9\text{--}3.0) \pm (0.4\text{--}0.8) \text{ MPa m}^{1/2}$ for hot-pressed $\text{ZrC}_{0.90}$ (porosity – 1–2%, mean grain size – 50–100 μm). Fracture toughness K_{IC} of magnetron-sputtered nanocrystalline $\text{ZrC}_{0.80\text{--}1.0}$ films (thickness – 0.15–0.20 μm) was also reported in the range of 1.5–2.5 $\text{MPa m}^{1/2}$ [74, 663], and the value of K_{IC} for quasi-stoichiometric $\text{ZrC}_{\sim 1.0}$ recommended by Mukhopadhyay et al. [591] is around 2 $\text{MPa m}^{1/2}$. The fracture toughness K_{IC} of spark-plasma sintered $\text{ZrC}_{\sim 1.0}$ (porosity – 16%) is $2.5 \pm 0.2 \text{ MPa m}^{1/2}$; for the same materials post-annealed $K_{IC} = 3.1 \pm 0.2 \text{ MPa m}^{1/2}$ [697]. For hot-pressed $\text{ZrC}_{\sim 1.0}$ materials (porosity – 2%) Zhao et al. [1479] determined $K_{IC} = 2.62 \pm 0.05 \text{ MPa m}^{1/2}$ by calculating indentation crack length. The highest values of fracture toughness were reported for reactive hot-pressed $\text{ZrC}_{0.96}$ (porosity < 2%, mean grain size – 5–10 μm , trace amount of non-combined C) $K_{IC} = (4.0\text{--}4.7) \pm 0.4 \text{ MPa m}^{1/2}$ (direct crack measurements) [1425]. The particularities of fatigue behaviour of ZrC_{1-x} materials were studied and analyzed in the works by Lanin with co-authors [333–335, 660, 661, 666, 667, 745].

The reported values for ductile-to-brittle transition temperatures of ZrC_{1-x} phases with various deviations from the stoichiometry are listed in Table 5.15. At the temperatures above ~1900–2000 °C yield strength $\sigma_{0.2}$ of ZrC_{1-x} is ruled by the Hall-Petch law [333]:

$$\sigma_{0.2} = \sigma_0 + k_y L^{-1/2}, \quad (5.82)$$

where σ_0 is the Peierl's stress, k_y is the coefficient, which characterizes the energy consumption for sliding transfer through the grain boundaries and L is the mean grain size; for sintered $\text{ZrC}_{0.98}$ (porosity – 3–4%, mean grain size – 5–8 μm , contents: non-combined C – 0.07%, O – 0.05%) under compression $\sigma_{0.2}$ falls off with temperature rise from 536 MPa at 1900 °C up to 278 MPa at 2200 °C (strain rate $de/dt = 10^{-2} \text{ s}^{-1}$) [742]. For practical applications of ultra-high temperature materials the values of prolonged strength (creep resistance) are of great importance. The examples of creep (deformation) kinetics of sintered and annealed zirconium

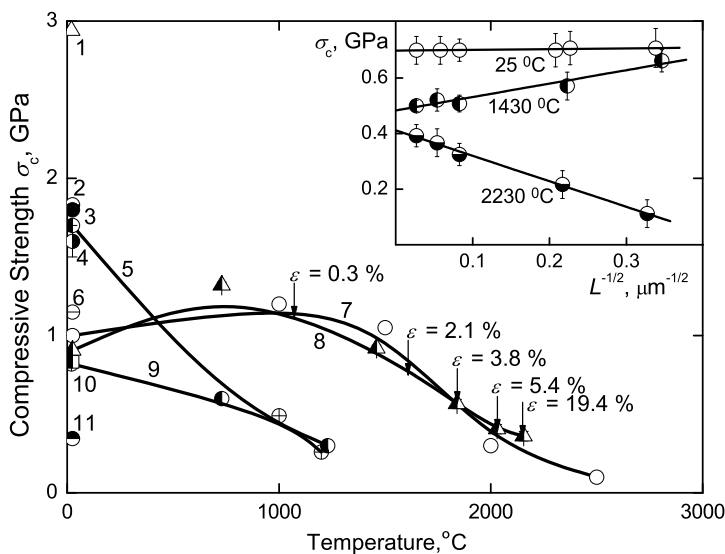


Fig. 5.26 Variation of compressive strength σ_c of near-stoichiometric zirconium monocarbide ZrC_{1-x} materials with temperature on the basis of several sources: 1 – $\text{ZrC}_{\sim 1.0}$, corrected to the poreless state [30, 213, 320, 635]; 2 – sintered $\text{ZrC}_{0.96}$, mean grain size – 3–10 μm , corrected to the poreless state [86]; 3 – sintered $\text{ZrC}_{0.97}$, porosity – 5%, mean grain size – 15–20 μm , $d\epsilon/dt = 3.7 \times 10^{-3} \text{ s}^{-1}$ [1]; 4 – sintered $\text{ZrC}_{\sim 1.0}$, porosity – 6%, mean grain size – 3 μm [37, 63, 319, 536, 567, 635, 636]; 5 – recommended for near-stoichiometric compositions [30, 33, 607]; 6 – $\text{ZrC}_{\sim 1.0}$ [3, 604]; 7 – sintered $\text{ZrC}_{0.95}$, porosity – 7%, mean grain size – 8 μm , contents: O + N – 0.14%, $d\epsilon/dt = 3.0 \times 10^{-3} \text{ s}^{-1}$ [4, 645]; 8 – sintered $\text{ZrC}_{\sim 1.0}$, $d\epsilon/dt = 3.0 \times 10^{-3} \text{ s}^{-1}$ [333, 336]; 9 – hot-pressed $\text{ZrC}_{\sim 1.0}$, porosity < 1% [1, 32, 608]; 10 – [1512]; 11 – pyrolytic $\text{ZrC}_{\sim 1.0}$ [363]; compression strain values ϵ are indicated for curve 8 at corresponding temperatures (Inset – for sintered $\text{ZrC}_{0.98}$, porosity – 5% [333, 621, 622], Hall-Petch relationships in σ_c , GPa – $L^{-1/2}$, $\mu\text{m}^{-1/2}$ scale)

Table 5.15 Ductile-to-brittle transition temperatures of zirconium monocarbide phases ZrC_{1-x}^a

Composition	Temperature, K ($^{\circ}\text{C}$)	Characteristics	Reference
$\text{ZrC}_{\sim 1.0}$	2470 (2200)	Sintered, polycrystalline	[3]
$\text{ZrC}_{0.98}$	1420 (1150)	Sintered, polycrystalline ^b	[654–656]
$\text{ZrC}_{0.95}$	1370 (1100)	Single crystal ^c	[170]
$\text{ZrC}_{0.94}$	1470 (1200)	Arc-melted and annealed, polycrystalline ^d	[652]
$\text{ZrC}_{0.93}$	2270–2670 (2000–2400)	Sintered, polycrystalline ^e	[603]
$\text{ZrC}_{0.87-0.90}$	1170–1370 (900–1100)	Single crystal ^f	[657, 658]

^aFor near-stoichiometric ZrC_{1-x} the following average values were estimated: Peierls stress $\tau_p = 6.0 \text{ GPa}$, shear modulus – Peierls stress ratio $\tau_p/G = 0.036$ and slip activation energy barrier $q = 1.6 \text{ eV}$ [52]

^bMaterials with mean grain sizes from 10 to 1000 μm , deformed under uniaxial compression

^cMaterials with contents: O – 0.005%, N – 0.067%

^dMaterials with content O – 0.04%, deformed under compression

^eMaterials with porosity – 14%, mean grain size – 16–18 μm , content non-combined C – 0.3%, deformed under flexure (bending) loading

^fCompression testing

monocarbide ZrC_{1-x} materials are given in Fig. 5.27; the variations of long-term rupture strength σ_r for sintered $ZrC_{0.98}$ materials with time-to-rupture and temperature (1-, 10- and 100-h strength characteristics) are demonstrated in Fig. 5.28. Similar to some other ceramics and metals, the time-to-rupture τ_r of ZrC_{1-x} materials is related with applied stress σ exponentially [638]:

$$\tau_r = B\sigma^{-m}\exp(U/RT), \quad (5.83)$$

where T is temperature, K, R is the gas constant, U is the activation energy of long-term rupture, B and m are pre-exponential and exponent constants, respectively, and the effect of temperature on σ_r is well described by the Ito-Shishokin equation:

$$\sigma_r = C\exp(-\alpha T), \quad (5.84)$$

where C and α are constants. High- and ultra-high temperature steady-state creep rate $d\varepsilon/dt$ characteristics for the various compositions of ZrC_{1-x} materials are shown in Fig. 5.29. Creep rate variations of sintered ZrC_{1-x} materials with deviation from the stoichiometry within the homogeneity range are shown in Fig. 5.30. On the basis of all the previous research Frost and Ashby [659] plotted first stress–temperature (plasticity and creep deformation mechanism) and strain-rate–stress maps/diagrams for transition metal carbide materials, in particular for $ZrC_{0.95}$ of grain size 10 μm , followed later by Zubarev [638], who constructed similar map/diagram for $ZrC_{0.93}$ with mean grain size 15 μm (the diagrams are not given in the reference book); Fig. 5.31 has the special form of the detailed normalized shear stress – homologous temperature map/diagram for sintered $ZrC_{\sim 1.0}$ materials (mean grain size – 14 μm), which was constructed by Zubarev et al. [643, 644] on the basis of latest precise investigations. The formal creep characteristics (activation

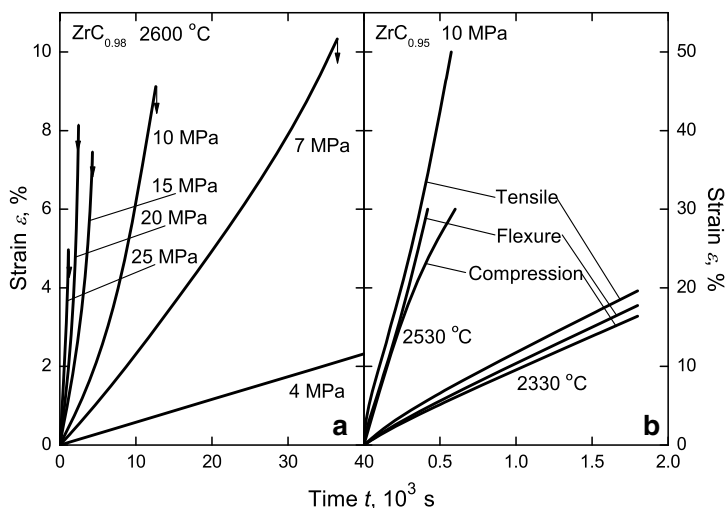


Fig. 5.27 High- and ultra-high temperature creep of sintered and annealed zirconium monocarbide ZrC_{1-x} materials: (a) tensile characteristics of $ZrC_{0.98}$ (porosity – 3%, mean grain size – 15 μm , contents: non-combined C – 0.40%, O – 0.07%, N – 0.025%) at 2600 °C and 4–25 MPa and (b) tensile, flexure (bending) and compression characteristics of $ZrC_{0.95}$ (porosity – 15–17%, mean grain size – 4.5 μm) at 2330–2530 °C and 10 MPa [637, 638]

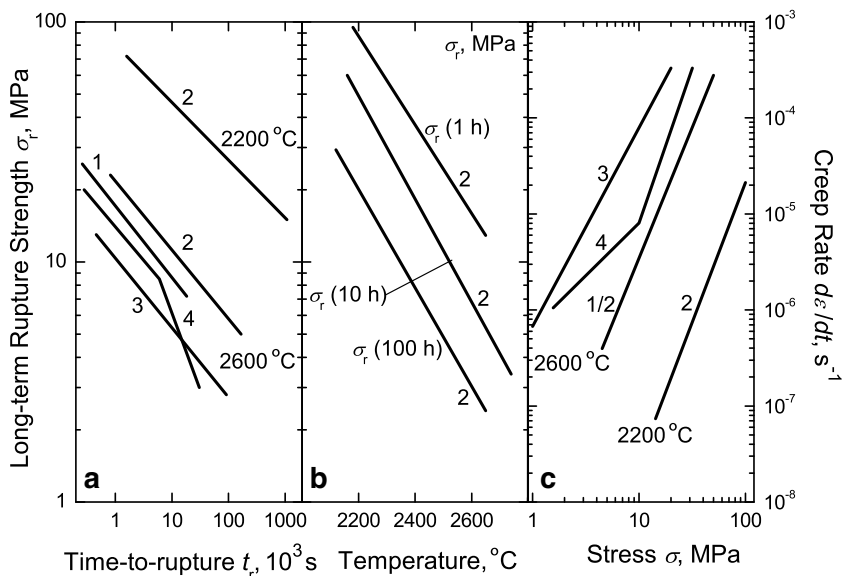


Fig. 5.28 Variations of long-term rupture strength σ_r with time-to-rupture (a) and temperature (for 1-, 10- and 100-hour strength characteristics) (b), and variation of steady-state creep rate $d\epsilon/dt$ with applied stress σ (c) of sintered and annealed $\text{ZrC}_{0.98}$ materials with various compositions and structures: 1 – contents: non-combined C – 0.35%, O – 0.08%, N – 0.05%, W – 0.21% (porosity – 4%, mean grain size – 15 μm); 2 – contents: non-combined C – 0.40%, O – 0.07%, N – 0.025% (porosity – 3%, mean grain size – 15–20 μm); 3 – contents: non-combined C – 1.0%, O – 0.08%, N – 0.04%, W – 0.21% (porosity – 4–5%, mean grain size – 5–6 μm); 4 – contents: non-combined C – 1.1%, O – 0.10%, N – 0.04% (porosity – 3–4%, mean grain size – 15–20 μm) [638–640]

energy Q , exponent constant n) of zirconium monocarbide phases ZrC_{1-x} at various temperature and stress ranges are listed in Table 5.16. Approximately, the following main dominating creep mechanisms can be established in some overlapping parametric ranges for zirconium monocarbide ZrC_{1-x} materials with certain changes within the homogeneity range [638–644, 646, 668, 669]:

- vacancy-diffusional (or Nabarro-Herring) mechanism controlled by the bulk diffusion of metal in carbide (at temperatures from 2400 to 3000 °C and applied stresses from 5 to 60 MPa, with $Q \approx 660\text{--}820 \text{ kJ mol}^{-1}$ and $n \approx 1.0\text{--}1.9$);
- dislocation-diffusional mechanism controlled by the bulk diffusion of metal in carbide (at 2200–3000 °C and 30–100 MPa, with $Q \approx 660\text{--}840 \text{ kJ mol}^{-1}$ and $n \approx 3\text{--}8$);
- viscous dislocation sliding mechanism controlled by the bulk diffusion of carbon in carbide (at 1800–2200 °C and 60–280 MPa, with $Q \approx 370\text{--}470 \text{ kJ mol}^{-1}$ and $n \approx 3.0\text{--}4.5$).

Some other plasticity and creep mechanisms of sintered $\text{ZrC}_{\sim 1.0}$ and their parametric ranges, including the comparison with single crystal materials, are indicated in the graphic scheme and legend of Fig. 5.31. Darolia and Archbold have found out that arc-melted and annealed $\text{ZrC}_{0.94}$ materials can undergo dynamic recrystallization at 1800 °C during the creep compression testing with strain rate of $\sim 3 \times 10^{-4} \text{ s}^{-1}$ [1310]. The particularities of the irradiation induced creep of ZrC_{1-x} materials were considered by Katoh et al. [757].

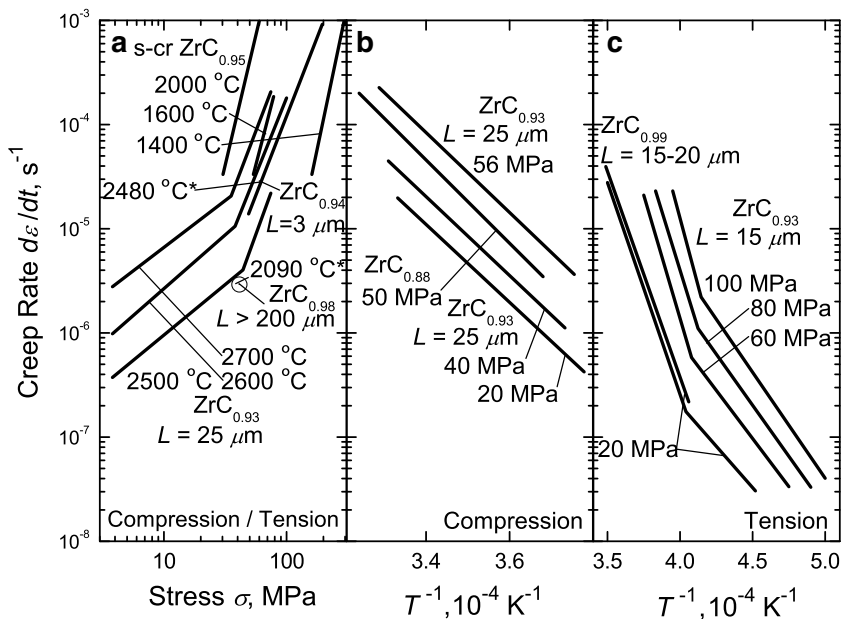


Fig. 5.29 High- and ultra-high temperature steady-state creep rate $d\varepsilon/dt$ variations of single crystal $ZrC_{0.95}$ (contents: O – 0.005%, N – 0.067%) at 1400–2000 °C [170], arc-fused and cast $ZrC_{0.98}$ (mean grain size > 200 μm) at 2090 °C* [320, 653], sintered $ZrC_{0.99}$ (porosity – 3%, mean grain size – 15–20 μm , contents: non-combined C – 0.38%, O – 0.06%, N – 0.025%, Fe – 0.09%) at 20 MPa [639, 640], sintered and annealed $ZrC_{0.94}$ (porosity – 15–20%, mean grain size – 3 μm , contents: non-combined C – 0.17%, O – 0.17%, N – 0.03%, Fe – 0.11%) at 2480 °C* [639, 640], sintered $ZrC_{0.93}$ (porosity – 2–4%, mean grain size – 15 μm and 25 μm) at 2500–2700 °C and 20–100 MPa [638, 641, 642] and sintered $ZrC_{0.88}$ materials at 50 MPa [119]: (a) with applied stress under compression/tension (tension temperature marked with asterisk), (b) with reciprocal temperature under compression and (c) with reciprocal temperature under tension

At room temperature the values of Young's E , Coulomb's (shear) G and bulk (compression) K moduli, volume compressibility κ and Poisson's ratio ν of sub- and near-stoichiometric zirconium monocarbide ZrC_{1-x} materials lie within the areas: $E = 300\text{--}500$ GPa [1, 3, 4, 11, 26, 27, 30, 32, 33, 39, 42, 46–49, 52, 54, 74, 82, 96, 101, 452, 466, 677, 678, 684, 692, 706], $G = 120\text{--}200$ GPa [3, 4, 11, 39, 49, 69, 82, 125, 132, 277, 284, 466, 659, 675–678, 703], $K = 170\text{--}340$ GPa [3, 4, 11, 49, 82, 125, 466, 675–678, 684, 706], $\kappa = 4.25\text{--}4.75$ TPa $^{-1}$ [1, 3, 4, 54, 725, 1372, 1514] and $\nu = 0.16\text{--}0.26$ [3, 4, 11, 39, 49, 82, 123, 132, 277, 308, 670, 677, 678, 684, 686, 689, 696, 706] (see also Table 5.17); the experimentally measured velocity of ultrasonic waves propagated in quasi-stoichiometric zirconium monocarbide $ZrC_{\sim 1.0}$ (summarized on the basis of several sources) [736]:

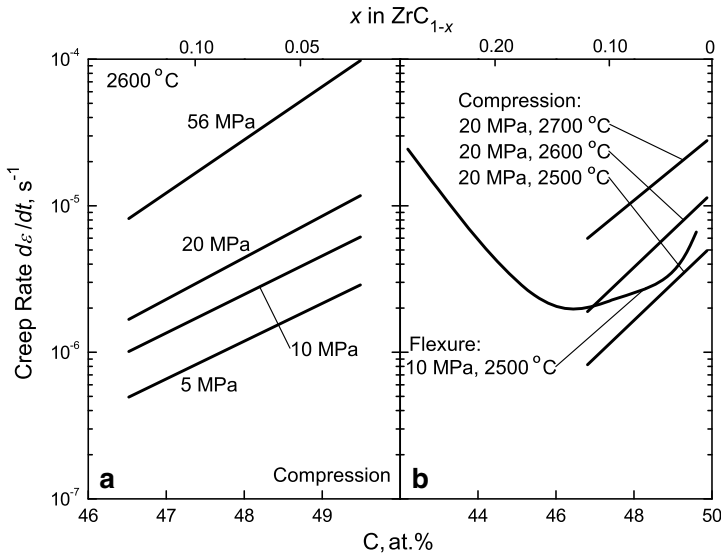


Fig. 5.30 Creep rate $d\epsilon/dt$ variations of zirconium monocarbide ZrC_{1-x} materials with deviation from the stoichiometry within the homogeneity range: (a, b) under compression (sintered materials, porosity – 2–5%, mean grain size – 25 μm [118, 638]) and (b) under flexure (hot-pressed materials, porosity – 4–6%, mean grain size – 20–70 μm , non-combined C – 0.10%, O – 0.03–0.47%, N – 0.01–0.23% [599]) loading (temperatures and applied stresses are marked)

average velocity V_m , $m s^{-1}$ 6270,
 and theoretically calculated sound velocities for near-stoichiometric zirconium monocarbide $ZrC_{\sim 1.0}$ are

- by *ab initio* and similar theoretical calculations (for zero pressure):
 - longitudinal velocity V_S , $m s^{-1}$ 13560
 [701], 8850 [725, 1372], 8194 [24], 8641 (0 K) [283], 7981 (~ 300 K) [283], 7984 [376];
 - transversal velocity V_T , $m s^{-1}$ 4500 [701],
 5280 [725], 4968 [24], 5254 (0 K) [283], 4662 (~ 300 K) [283], 4788 [376];
 - average velocity V_m , $m s^{-1}$ 5129 [701],
 5840 [725], 5481 [24], 5297 [376];
- by LMTO (linearized method of “muffin-tin” orbitals) calculations [736]:
 - average velocity V_m , $m s^{-1}$ 5970;
- by TBFP (three body force potential) modeling calculations [725]:
 - longitudinal velocity V_S , $m s^{-1}$ 8170;
 - transversal velocity V_T , $m s^{-1}$ 5020;
 - average velocity V_m , $m s^{-1}$ 5540.

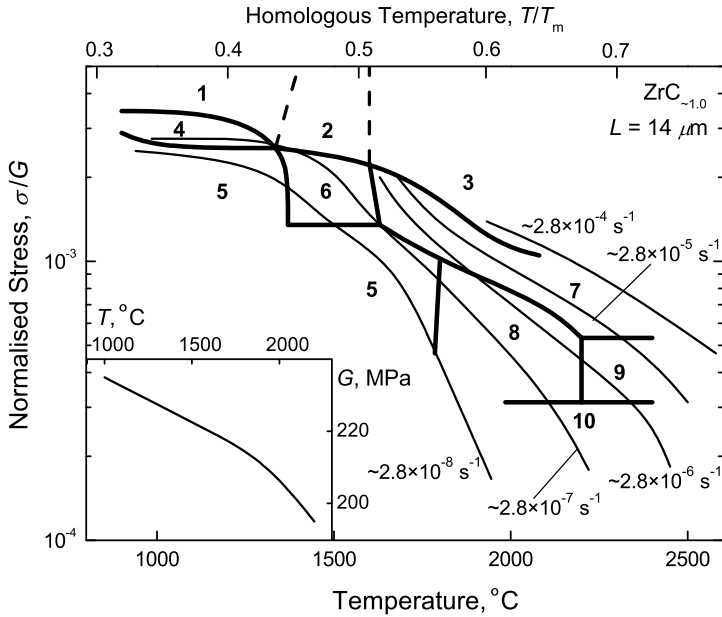


Fig. 5.31 A normalized shear stress σ/G – homologous (to melting point) temperature T/T_m map (creep mechanism diagram) for quasi-stoichiometric sintered $ZrC_{\sim 1.0}$ materials (mean grain size – 14 μm , contents: non-combined C – 0.07%, O – 0.06%, N – 0.03%) under compression loading ($2.7 \times 2.7 \times 8.0$ mm bar) in He atmosphere, demarcated areas with different creep mechanisms: 1 – quasi-brittle fracture ($< \sim 1400$ °C); 2 – applied stress exceeds the yield strength (~ 1350 – 1650 °C, creep characteristic: activation energy $Q = 210$ – 435 kJ mol^{-1} , maximal values of yield strength); 3 – applied stress exceeds the yield strength ($> \sim 1650$ °C, $Q = 210$ – 435 kJ mol^{-1} , highest creep rates); 4 – interaction with forest dislocations (presence of long-term non-steady-state creep stages with $\varepsilon \approx 0.1$, $< \sim 1350$ – 1400 °C, $Q = \sim 15$ kJ mol^{-1}); 5 – generation of dislocations ($< \sim 1800$ °C, $Q = 480$ – 1270 kJ mol^{-1}); 6 – cross-gliding of dislocations (~ 1350 – 1650 °C, > 200 MPa, creep characteristics for polycrystalline materials with grain size 14– 1000 μm : $Q = 270$ – 365 kJ mol^{-1} , exponent constant $n = 4$ – 7 ; creep characteristics for single crystal materials: $Q = 405$ kJ mol^{-1}); 7 – climb of dislocations by means of bulk (lattice) diffusion (dislocation-diffusional mechanism, > 1600 °C, polycrystalline materials: $Q = 815$ – 835 kJ mol^{-1} , $n = 8.0$; single crystal: $Q = 930$ kJ mol^{-1} , $n = 5.8$ – 6.3); 8 – climb of dislocations by means of diffusion through dislocation core (nucleus) or Burgers (screw) dislocation gliding (polycrystalline materials: $Q = 440$ – 470 kJ mol^{-1} , $n = 4.2$ – 4.4 ; single crystal: $Q = 365$ kJ mol^{-1} , $n = 1.6$); 9 – grain boundary sliding (> 2200 °C, $Q = 795$ – 835 kJ mol^{-1} , $n = 4.0$ – 4.3); 10 – diffusion mass transfer (Nabarro-Herring (vacancy-diffusional) creep mechanism, $Q = 795$ – 815 kJ mol^{-1} , $n = 1.4$ – 1.9); for some areas the comparison of characteristics with single crystal $ZrC_{0.94}$ under compression loading ($2.0 \times 2.0 \times 6.0$ mm bar (100) faced) along $\langle 100 \rangle$ direction is given above, isolines of creep rate $d\varepsilon/dt$ from $\sim 2.8 \times 10^{-4} \text{ s}^{-1}$ up to $\sim 2.8 \times 10^{-8} \text{ s}^{-1}$ are indicated; (Inset – variation of Coulomb's (shear) modulus G of $ZrC_{\sim 1.0}$ with temperature) [643, 644]

Table 5.16 Formal creep characteristics (activation energy Q , stress exponent constant n) of zirconium monocarbide phases ZrC_{1-x} at various temperature and stress ranges

Composition	Load type ^a	Temperature range, °C	Stress range ^b , MPa	Activation energy ^b , Q , kJ mol ⁻¹	Exponent constant ^b , n	Reference
ZrC _{~1.0} ^c	C	1350–1400	450–900	15	–	[643, 644]
	C	1000–1800	200–600	480–1270	–	[643, 644]
	C	1350–1650	280–680	270–365	4.0–7.0	[643, 644]
	C	1350–1650	680–1100	210–435	–	[643, 644]
	C	1650–2100	200–680	210–435	–	[643, 644]
	C	1600–2400	90–680	815–835	8.0	[643, 644]
	C	2200–2400	50–90	795–835	4.0–4.3	[643, 644]
	C	1800–2200	70–200	440–470	4.2–4.4	[643, 644]
	C	2000–2400	20–70	795–815	1.4–1.9	[643, 644]
ZrC _{~1.0} ^d	C	1700–2000	–	580	–	[646, 650]
ZrC _{~1.0} ^d	H	700–1660	–	45	–	[573, 574]
	H	1660–2650	–	200	–	[573, 574]
ZrC _{~1.0} ^e	R	~1700	–	95	3.2	[335]
ZrC _{0.99} ^f	T	2200–2750	2–75	710 ± 40	2.3–3.1	[639, 640]
ZrC _{0.99} ^g	T	2600	2–10	–	1	[639, 640]
ZrC _{0.98} ^h	F	2400–2700	0–15	760 ± 50	1	[3, 4, 599]
ZrC _{0.98}	T,F,C	1800–3000	<σ _{1c}	660	1	[118, 647]
	F	<2400	>σ _{1c}	370–440	2.8–3.2	[118, 647]
ZrC _{0.98} ⁱ	F	1800–2200	120–280	370	3.4	[638]
ZrC _{0.97}	F	1800–2300	120–210	335	3	[642, 646]
ZrC _{0.97} ^k	C	2200–2600	6.5–55	690 ± 60	1	[4, 649]
ZrC _{0.97} ^l	C	2200–2600	6.5–55	540 ± 40	1	[4, 649]
ZrC _{0.96} ^m	F	2400–2700	0–15	700 ± 40	1	[3, 4, 599]
ZrC _{0.96} ⁿ	C	2500–2700	5–20	660	1	[4, 638]
ZrC _{0.96}	F	>2400	>σ _{1c}	660–720	3.4–3.7	[118, 647]
ZrC _{0.95} ^o	–	1400–2000	40–270	460	5	[170, 707]
ZrC _{0.95} ^p	T	2180–2540	3.5–20	485 ± 75	1	[646, 651]
ZrC _{0.94–0.95} ^q	T,F,C	2150–2630	2–20	520 ± 40	1.0–1.1	[118, 637]
ZrC _{0.94} ^r	C	1800–2000	140–200	405	–	[643, 644]
	C	2000–2200	20–140	365	1.6	[643, 644]
	C	2200–2400	20–140	930	5.8–6.3	[643, 644]
ZrC _{0.94} ^s	C	2200–2600	3–60	680	1	[638]
ZrC _{0.94} ^t	C	2500–2750	1–30	710 ± 40	1	[638, 646]
	C	2500–2750	30–75	710 ± 40	2.3–3.7	[638, 646]
ZrC _{0.94} ^u	F	1800–2200	70–240	385	3.3	[638]
ZrC _{0.94} ^v	C	1200–1800	–	500 ± 20	3.8–6.5	[646, 652]
ZrC _{0.94} O _{0.05} ^w	C	1500–1600	60–100	–	0.7 ± 0.4	[664, 665]
	C	1500–1600	100–140	690 ± 40	≥3.3 ± 0.4	[664, 665]

(continued)

Table 5.16 (continued)

Compo- sition	Load type ^a	Temperature range, °C	Stress range ^b , MPa	Activation energy ^b , Q , kJ mol ⁻¹	Exponent constant ^b , n	Reference
ZrC _{0.93±0.01} ^x	T	1800–2250	2.5–35	315	3	[356, 634]
	T	2150–2500	2.5–35	840	3	[356, 634]
ZrC _{0.93} ^y	T	2200–2600	20–60	680	1	[638]
	C	2400–2700	5–50	700	1	[638, 641]
	T	2200–2400	60–100	720	3.1	[638]
	C	2500–2700	50–80	700	3.4	[638, 641]
	T	1800–2200	60–120	400	3.2	[638]
ZrC _{0.93} ^z	C	2400–2700	5–40	680–695	1	[4, 638]
	C	2500–2700	35–80	680	3.1	[638]
ZrC _{0.93} ^{a1}	C	2200–2700	5–40	690 ± 40	1	[4, 638]
	C	2200–2700	40–690	690 ± 40	3.4	[4, 638]
ZrC _{0.93}	F	2600	> σ_{lc}	660–720	3.4–3.7	[118, 647]
ZrC _{0.92} ^j	T	2200–3000	3–80	750	2.5	[3, 642]
ZrC _{0.92} ^{a2}	C	2200–2700	5–45	660	1	[638, 646]
	C	2200–2700	55–70	660	3.4	[638, 646]
ZrC _{0.92} ^r	F	1900–2200	80–240	440	3.2	[638]
ZrC _{0.92}	F	>2400	> σ_{lc}	660–720	3.4–3.7	[118, 647]
	F	<2400	> σ_{lc}	370–440	2.8–3.2	[118, 647]
ZrC _{0.90} ^{a3}	H	900–1500	–	310–330	3.8–4.1	[93, 172]
ZrC _{0.89} ⁿ	C	2500–2700	5–20	740	1	[4, 638]
ZrC _{0.89}	T,F,C	1800–3000	< σ_{lc}	740	1	[118, 647]
ZrC _{0.88} ^{a4}	F	2400–2700	0–15	730 ± 40	1	[3, 4, 599]
ZrC _{0.88} ^{a5}	C	2450–3100	10–70	770	–	[119, 648]
ZrC _{0.85} ^{a6}	F	2400–2700	0–15	680 ± 40	1	[3, 4, 599]
ZrC _{0.81} ^{a7}	F	2400–2700	0–15	660 ± 40	1	[3, 4, 599]
ZrC _{0.79} O _{0.13} ^{a8}	C	1500–1600	60–100	–	0.8 ± 0.4	[664, 665]
	C	1500–1600	100–140	–	≥2.7 ± 0.4	[664, 665]
	C	1500–1600	100	740 ± 30	–	[664, 665]
	C	1500–1600	140	480 ± 30	–	[664, 665]
ZrC _{0.73} ^{a9}	F	2400–2700	0–15	580 ± 30	1	[3, 4, 599]
ZrC _{0.72} ^{b1}	F	2400–2700	0–15	510 ± 30	1	[3, 4, 599]
ZrC _{0.63–0.90} ^{b2}	F	–	–	380–690 ($Q = 801-1143x$)	–	[26, 27, 1277]

^aDenoted: T – tension, F – flexure (bending), C – compression, H – hot hardness (measurement), R – relaxation

^b $\sigma_{lc} = AL^{-0.388}$, where σ_{lc} is the ultimate linear stress, L is the mean grain size and A is a constant [4, 118, 647]; for Q and n see the Eq. (I-3.17) and consideration in [707]

^cSintered, mean grain size – from 14 to 1000 μm , contents: non-combined C – 0.07%, O – 0.06%, N – 0.03%

^dHot-pressed and annealed, porosity – 1–2%, mean grain size – ~50 μm , content non-combined C – 0.54%

^eNumerical calculation of residual stresses for the relaxation rate in the complex field of thermal stresses

^fSintered, porosity – 3%, mean grain size – 15–20 μm , contents: non-combined C – 0.38–0.40%, O – 0.06–0.07%, N – 0.025%, Fe – 0.09%

^gSintered, porosity – 3–4%, mean grain size – 15–20 μm , contents: non-combined C – 1.1%, O – 0.10%, N – 0.04%

(continued)

Table 5.16 (continued)

- ^hHot-pressed, porosity – 4–6%, mean grain size – 30 μm , contents: non-combined C – 0.10%, O – 0.03%, N – 0.01%
- ⁱSintered, porosity – 3–4%, mean grain size – 30 μm
- ^jSintered materials
- ^kSintered, porosity – 0.3–5.0%, mean grain size – 5–7 μm , contents: O + N – 0.15%
- ^lSintered, porosity – 19%, mean grain size – 7 μm , contents: O + N – 0.15%
- ^mHot-pressed, porosity – 4–6%, mean grain size – 8–17 μm , contents: non-combined C – 0.10%, O – 0.05%, N – 0.01%
- ⁿSintered, porosity – 3–4%, mean grain size – 25 μm , contents: non-combined C – 0.25%, O + N – 0.07–0.14%
- ^oSingle crystal (direction – $\langle 111 \rangle$), contents: O – 0.005%, N – 0.067%
- ^pSintered, porosity – 7%, mean grain size – 3–5 μm , contents: non-combined C – 0.25%, O – 0.12%, N – 0.03%, Fe – 0.04%
- ^qSintered, porosity – 15–17%, mean grain size – 4.5 μm , contents: non-combined C – 0.17%, O – 0.08%, N – 0.02%
- ^rSingle crystal (plane/direction – (100) $\langle 100 \rangle$), contents: non-combined C – 0.05%, O – 0.10%, N – 0.02%
- ^sSintered, porosity – 3–4%, mean grain size – 6 μm
- ^tSintered, porosity – 3–4%, mean grain size – 5–45 μm
- ^uSintered, porosity – 3–4%, mean grain size – 14 μm
- ^vArc-melted, mean grain size – 250 μm , content O – 0.04%
- ^wSpark plasma sintered, fully dense, mean grain size – 5–20 μm
- ^xHot-pressed, porosity – 7%, mean grain size – 4 μm , contents: non-combined C – 0.85%, O – 0.56%, N – 0.32%, Hf – 1.0%
- ^ySintered, porosity – 3–4%, mean grain size – 15 μm
- ^zSintered, porosity – 2–3%, mean grain size – 25 μm , contents: O + N – 0.12%
- ^{a1}Sintered, porosity – 5%, mean grain size – 20 μm
- ^{a2}Sintered, porosity – 2–4%, mean grain size – 6–45 μm
- ^{a3}Single crystal (plane/direction – (100) $\langle 001 \rangle$, (110) $\langle 001 \rangle$ and (111) $\langle 110 \rangle$)
- ^{a4}Hot-pressed, porosity – 4–6%, mean grain size – 6–65 μm , contents: non-combined C – 0.10%, O – 0.05%, N – 0.09%
- ^{a5}Sintered, porosity – 4–9%, mean grain size – 23 μm
- ^{a6}Hot-pressed, porosity – 4–6%, mean grain size – 16 μm , contents: non-combined C – 0.10%, O – 0.47%, N – 0.23%
- ^{a7}Hot-pressed, porosity – 4–6%, mean grain size – 20 μm , contents: non-combined C – 0.10%, O – 0.29%, N – 0.06%
- ^{a8}Spark plasma sintered, fully dense, mean grain size – 5 μm
- ^{a9}Hot-pressed, porosity – 4–6%, mean grain size – 70 μm , contents: non-combined C – 0.10%, O – 0.29%, N – 0.06%
- ^{b1}Hot-pressed, porosity – 4–6%, mean grain size – 45 μm , contents: non-combined C – 0.10%, O – 0.08%, N – 0.03%
- ^{b2}For sintered ZrC_{1-x} ($0.10 \leq x \leq 0.37$) materials Q is described by the given equation

Table 5.17 Elastic properties (stiffness coefficients c_{11} , c_{12} and c_{44} , Young's modulus E , bulk (compression) modulus K , Poisson's ratio ν)^a of zirconium monocarbide phases ZrC_{1-x}

Composition	Stiffness coefficients c_{ij}			Young's modulus E , GPa	Bulk modulus K , GPa	Poisson's ratio ν	Reference
	c_{11} , GPa	c_{12} , GPa	c_{44} , GPa				
ZrC _{0.66} ^b	–	–	–	266 ^c	166 ^c	0.23	[696]
ZrC _{0.75}	–	–	–	342 ^{d,e}	200 ^{d,e}	0.22 ^d	[125, 675, 676]
	403 ^b	105 ^b	105 ^b	301 ^{b,f}	204 ^{b,f}	–	[735]
ZrC _{0.77}	–	–	–	282 ^g	–	0.21 ^g	[123, 670, 689]
	–	–	–	353 ± 1 ^h	–	–	[356, 634]
ZrC _{0.78} ⁱ	–	–	–	300 ^j	173 ^j	0.21	[4, 132]
ZrC _{0.79}	–	–	–	305 ^{k,l}	147 ^{k,l}	0.16 ^k	[685]
	–	–	–	330 ^{b,m}	187 ^{b,m}	0.21 ^b	[696]
ZrC _{0.80}	–	–	–	301 ⁿ	–	0.20 ⁿ	[123, 670, 689]
	–	–	–	–	225 ^o	–	[276]
	–	–	–	–	188 ^p	–	[699]
ZrC _{0.83} ^b	–	–	–	347 ^q	196 ^q	0.21	[696]
ZrC _{0.84}	–	–	–	353 ± 1 ^b	–	–	[356, 634]
	–	–	–	346 ^{r,s}	174 ^{r,s}	0.17 ^r	[685]
ZrC _{0.85}	–	–	–	369 ^{d,t}	265 ^{d,t}	–	[125, 675, 676]
	–	–	–	347 ^u	–	0.20 ^u	[123, 670, 689]
ZrC _{0.87}	–	–	–	365 ^{v,w}	203 ^{v,w}	0.20 ^v	[4, 132]
	–	–	–	402 ± 4 ^x	–	–	[96, 681]
	–	–	–	355 ^{b,y}	203 ^{b,y}	0.21 ^b	[696]
ZrC _{0.88} ^b	460	104	139	374 ^z	223 ^z	–	[735]
ZrC _{0.89} ^{a1}	468	100	157	–	223	–	[49, 705, 706]
ZrC _{0.90}	–	–	–	387 ^{a2,a3}	258 ^{a2,a3}	0.25 ^{a2}	[277]
	–	–	–	–	195 ^p	–	[699]
ZrC _{0.91}	–	–	–	385 ^{d,a4}	312 ^{d,a4}	–	[125, 675, 676]
	–	–	–	382 ^{a5}	–	–	[679]
ZrC _{0.92}	–	–	–	385 ^{a6,a7}	225 ^{a6,a7}	0.22 ^{a6}	[4, 132]
	–	–	–	403 ^{a8}	–	–	[575]
ZrC _{0.93}	–	–	–	390 ^{a9}	–	–	[624]
	–	–	–	328 ^{b1}	–	0.24 ^{b1}	[411]
	–	–	–	320 ^{a9}	–	0.20 ^{a9}	[741]
ZrC _{0.94} ^{a1}	472	99	159	407 ^{b2}	223 ^{b2}	0.19	[11, 49, 684, 706]
ZrC _{0.95}	–	–	–	400 ^{d,b3}	339 ^{d,b3}	–	[125, 675, 676]
	–	–	–	400 ^{b4,b5}	–	0.20 ^{b4}	[96, 662]
ZrC _{0.96}	–	–	–	386 ^{b6,b7}	207 ^{b6,b7}	0.19 ^{b6}	[11, 82]
	–	–	–	393 ^{b8,b9}	240 ^{b8,b9}	0.23 ^{b8}	[4, 132]
	–	–	–	390 ^{c1}	272 ^{c1}	0.23 ^{c1}	[123, 670, 689]
	–	–	–	320 ^{c2}	–	–	[617]
	–	–	–	–	275 ^o	–	[276]

(continued)

Table 5.17 (continued)

Composition	Stiffness coefficients c_{ij}			Young's modulus E , GPa	Bulk modulus K , GPa	Poisson's ratio ν	Reference
	c_{11} , GPa	c_{12} , GPa	c_{44} , GPa				
ZrC _{0.97} ^b	484	108	146	394 ^{c3}	234 ^{c3}	–	[735]
ZrC _{0.98}	–	–	–	452 ^{x,c4}	270 ^{x,c4}	0.22 ^x	[277]
	–	–	–	–	275 ^{c5}	–	[276]
	–	–	–	394 ^{c6,c7}	222 ^{c6,c7}	–	[703]
ZrC _{-1.0}	428 ^{e8}	41 ^{c8}	146 ^{c8}	369 ^{e9}	168 ^{e9}	0.13 ^{e9}	[49, 82, 677, 678]
	–	–	–	495 ^{d1}	–	–	[3]
	–	–	–	410 ± 3 ^{d2,d3}	–	0.17 ^{d3}	[308]
	–	–	–	475 ^{d4}	–	–	[673]
	–	–	–	392 ^{d1}	–	–	[680]
	522 ^{d5}	110 ^{d5}	160 ^{d5}	–	247 ^{d5,d6}	–	[682]
	470 ^{d7}	100 ^{d7}	160 ^{d7}	–	223 ^{d7}	–	[683, 713]
	–	–	–	375 ^{d8}	–	–	[576]
	–	–	–	345 ± 7	–	–	[246]
	–	–	–	310 ^{d9}	–	–	[41]
	–	–	–	475	–	0.17	[686]
	–	–	–	394 ^{e1}	–	–	[117]
	–	–	–	–	216 ^{e2}	–	[688]
	–	–	–	–	218 ^{e3}	–	[688]
	–	–	–	–	230 ^{e4}	–	[690]
	–	–	–	350	–	–	[691, 692]
	–	–	–	348 ^{d1}	–	–	[693, 1515]
	–	–	–	318 ^{e5,e6}	214 ^{e5,e6}	0.26 ^{e5}	[39]
	–	–	–	388	–	–	[694]
	–	–	–	400 ^{e7}	–	–	[628]
	–	–	–	–	237 ^{e8}	–	[695]
	496 ^b	109 ^b	151 ^b	408 ^{b,e9}	238 ^{b,e9,f1}	0.21 ^b	[696]
	–	–	–	222 ^{f2}	–	–	[697]
	–	–	–	–	221 ^{p,f3}	–	[699]
	272 ^{e8}	134 ^{e8}	429 ^{e8}	–	232 ^{e8}	–	[68]
	–	–	–	506 ^{e9,f4,f5}	–	0.14 ^{e9,f4,f5}	[68]
	–	–	–	473 ^{e8,f6,f7}	–	0.16 ^{e8,f6,f7}	[68]
	452 ^b	102 ^b	154 ^b	390 ^{b,f8}	219 ^{b,f8}	0.20 ^b	[700]
	428 ^{e8}	118 ^{e8}	119 ^{e8}	332 ^{e8,f9}	222 ^{e8,f9}	0.25 ^{e8}	[701]
	477 ^{g1}	98 ^{g1}	162 ^{g1}	–	–	–	[705]
	472 ^{g2}	105 ^{g2}	135 ^{g2}	–	–	–	[705]
	480 ^{g3}	102 ^{g3}	170 ^{g3}	–	–	–	[705]
	381 ^{g4}	121 ^{g4}	178 ^{g4}	–	–	–	[167]

(continued)

Table 5.17 (continued)

Composition	Stiffness coefficients c_{ij}			Young's modulus E , GPa	Bulk modulus K , GPa	Poisson's ratio ν	Reference
	c_{11} , GPa	c_{12} , GPa	c_{44} , GPa				
441	60	151	384 ^{g5}	187 ^{g5}	0.16	[708, 1369]	
—	—	—	216–325 ^{g6}	—	—	[663]	
—	—	—	—	222 ^{d5}	—	[709, 713]	
—	—	—	—	227 ^{g7}	—	[710]	
—	—	—	—	214 ^{g8}	—	[710]	
643 ^{g2}	95 ^{g2}	128 ^{g2}	—	239 ^{g2}	—	[711]	
512 ^{g3}	73 ^{g3}	121 ^{g3}	—	—	—	[711]	
—	—	—	—	248 ^{g2}	—	[712]	
—	—	—	—	236 ^{g9}	—	[712]	
—	—	—	—	222 ^b	—	[712]	
—	—	—	—	250 ^{h1}	—	[714]	
—	—	—	312 ^{h2,h3}	217 ^{h2,h3}	0.19 ^{h2}	[280]	
—	—	—	390–445 ^{h4,h4}	265 ^{h4,h5}	0.19 ^{h4}	[65, 712]	
457 ^{g3}	115 ^{g3}	150 ^{g3}	—	278 ^{g3}	—	[715]	
—	—	—	464 ± 22 ^{h6}	—	—	[588]	
548 ^{h7}	87 ^{h7}	87 ^{h7}	525 ^{h7,h8}	265 ^{h7,h8}	0.13 ^{h7}	[18, 716]	
504 ^{g2}	90 ^{g2}	173 ^{g2}	438 ^{f4,g2,h9,i1}	228 ^{g2,i1}	0.18 ^{f4,g2,i2}	[69]	
504 ^{g2}	90 ^{g2}	173 ^{g2}	436 ^{f6,g2,h9,i3}	228 ^{g2,i3}	0.18 ^{f6,g2,i3}	[69]	
499 ^{g3}	93 ^{g3}	170 ^{g3}	436 ^{f4,g4,h9,i4}	225 ^{g3,i4}	0.18 ^{f4,g3,i2}	[69]	
499 ^{g3}	93 ^{g3}	170 ^{g3}	434 ^{f6,g3,h9,i5}	225 ^{g3,i5}	—	[69]	
455 ⁱ⁶	116 ⁱ⁶	152 ⁱ⁶	408 ^{i6,i7}	229 ^{i6,i7}	0.21 ⁱ⁶	[717]	
471 ⁱ⁸	91 ⁱ⁸	156 ⁱ⁸	—	218 ⁱ⁸	—	[281]	
—	—	—	—	258 ⁱ⁹	—	[718]	
—	—	—	350–440	—	—	[452]	
462 ^b	102 ^b	154 ^b	—	224 ^b	0.20 ^b	[19]	
—	—	—	387 ⁱ¹	223 ⁱ¹	—	[719]	
—	—	—	—	245 ^{g2}	—	[720]	
—	—	—	—	220 ^{g3}	—	[720]	
458 ^{e8,j2}	101 ^{e8,j2}	156 ^{e8,j2}	—	218 ^{e8,j2}	—	[20]	
—	—	—	—	281 ^b	—	[21]	
—	—	—	—	220 ^b	—	[282]	
—	—	—	407 ⁱ³	223 ⁱ³	0.20 ⁱ³	[721]	
452 ^{j4}	92 ^{j4}	112 ^{j4}	341 ^{j4,j5}	212 ^{j4,j5}	0.22 ^{j4}	[52, 722]	
455 ^{h2}	101 ^{h2}	150 ^{h2}	387 ^{h2,j6}	219 ^{h2,j6}	—	[724]	
457 ^b	98 ^b	157 ^b	395 ^{b,j7}	224 ^{b,j7}	—	[22]	
468 ⁱ⁸	100 ⁱ⁸	159 ⁱ⁸	433 ^{i8,j9}	222 ^{i8,j9}	0.18 ⁱ⁸	[725]	
483 ^{k1}	109 ^{k1}	142 ^{k1}	443 ^{k1,k2}	234 ^{k1,k2}	0.18 ^{k1}	[725]	
468 ^{k3}	102 ^{k3}	148 ^{k3}	390 ^{k3,c3}	224 ^{k3,c3}	0.21 ^{k3}	[24]	
—	—	—	400 ^{k4}	—	0.20	[54]	
—	—	—	415 ^{k5,k6}	234 ^{k5,k6}	0.21 ^{k5}	[726]	
557 ^{k7}	95 ^{k7}	155 ^{k7}	—	248 ^{k7}	—	[727]	

(continued)

Table 5.17 (continued)

Composition	Stiffness coefficients c_{ij}			Young's modulus E , GPa	Bulk modulus K , GPa	Poisson's ratio ν	Reference
	c_{11} , GPa	c_{12} , GPa	c_{44} , GPa				
446 ^b	103 ^b	153 ^b	–	–	217 ^b	–	[728]
–	–	–	–	240 ± 10 ^{k8}	–	–	[729]
–	–	–	–	290 ± 13 ^{k9}	–	–	[729]
–	–	–	–	320 ± 17 ^{l1}	–	–	[729]
–	–	–	–	–	220 ^{l2}	–	[730]
458 ^b	104 ^b	152 ^b	–	420 ^{b,13}	222 ^{b,13}	0.19 ^b	[731]
488 ^{j2,14}	108 ^{j2,14}	160 ^{j2,14}	–	413 ^{j2,14,15}	235 ^{j2,14,15}	0.21 ^{j2,14}	[283, 732]
375 ^{l4,16}	204 ^{l4,16}	253 ^{l4,16}	–	406 ^{l4,16,17}	261 ^{l4,16,17}	0.24 ^{l4,16}	[283, 732]
–	–	–	–	–	222 ^{l8}	–	[284]
482 ^{l8}	113 ^{l8}	146 ^{l8}	–	392 ^{i6,18}	236 ^{i6,18}	0.22 ^{l8}	[285]
503 ^{l9}	99 ^{l9}	171 ^{l9}	–	–	234 ^{l9}	–	[733]
438 ^b	93 ^b	161 ^b	–	–	208 ^b	–	[733]
446 ^b	104 ^b	138 ^b	–	407 ^{b,m1}	218 ^{b,m1}	0.19 ^b	[376]
452 ^{m2}	105 ^{m2}	150 ^{m2}	–	385 ^{m2,m3}	221 ^{m2,m3}	0.21 ^{m2}	[734]
–	–	–	–	377 ^{m4,m5}	216 ^{m4,m5}	–	[734]
487 ^{m6}	107 ^{m6}	152 ^{m6}	–	403 ^{m6,g5}	234 ^{m6,g5}	0.21 ^{m6}	[734]
–	–	–	–	395 ^{f8,m7}	229 ^{f8,m7}	–	[734]
511 ^{m8}	111 ^{m8}	156 ^{m8}	–	418 ^{m8,m9}	244 ^{m8,m9}	0.22 ^{m8}	[734]
–	–	–	–	399 ^{l7,n1}	233 ^{l7,n1}	–	[734]
490 ^b	112 ^b	147 ^b	–	–	238 ^{b,c7}	–	[735]
–	–	–	–	310 ⁿ²	–	–	[617]
–	–	–	–	380–407 ⁿ³	–	–	[666]
–	–	–	–	–	231 ^{l8}	–	[808]
–	–	–	–	405 ⁿ⁴	–	–	[1382]
–	–	–	–	–	233–253 ⁿ⁵	–	[1390]
–	–	–	–	398 ^{n6,n7,n8}	–	0.19	[1479]
513 ^{l9}	113 ^{l9}	163 ^{l9}	–	428 ^{l9,n9}	246 ^{l9,n9}	0.21 ^{l9}	[1516]
452 ^b	107 ^b	155 ^b	–	391 ^{b,o1}	222 ^{b,o1}	0.21 ^b	[1516]
433 ^{g8}	104 ^{g8}	155 ^{g8}	–	382 ^{g8,o2}	214 ^{g8,o2}	0.20 ^{g8}	[1516]
475 ^{g7}	134 ^{g7}	156 ^{g7}	–	398 ^{g7,o3}	247 ^{g7,o3}	0.23 ^{g7}	[1516]
–	–	–	–	–	210 ^{b,o2}	–	[1517]
–	–	–	–	549–550 ^{d1}	–	0.10	[33, 365, 674, 692]

^aFor isotropic (or quasi-isotropic) materials [3]: $E = 2G(1 + \nu)$, $E = 3K(1 - 2\nu)$, $K = c_{12} + 2c_{44}/3$, $G = c_{44}$; the condition for the isotropy is given in Eq. (I-2.18)

^bCalculated on the basis of density-functional theory (DFT) with generalized gradient approximation (GGA) using the Perdew-Burke-Ernzerhof (PBE) functional

^cCalculated value of $G = 108$ GPa

^dSintered, corrected to the poreless state (true porosity – 5–10%)

^eMeasured experimentally $G = 142$ GPa

^fCalculated value of $G = 120$ GPa

^gSintered, porosity – 12%, contents: non-combined C < 0.10%, O – 1.20%, N – 0.22%, W – 0.35%; sonic velocity measurement method

^hHot-pressed, porosity <4%, content non-combined C – 1.6–2.5%

ⁱSintered (in vacuum) and annealed, porosity – 21%, mean grain size – 18 μm , contents: non-combined C – 0.01%, O – 0.26%, N – 0.20%

(continued)

Table 5.17 (continued)

- ^jMeasured experimentally $G = 125$ GPa
- ^kSintered, porosity – 8–10%
- ^l $G = 132$ GPa
- ^mCalculated value of $G = 137$ GPa
- ⁿSintered, porosity – 10%, contents: non-combined C < 0.10%, O – 1.60%, N – 0.035%, W – 0.35%; sonic velocity measurement method
- ^oTheoretical estimation; for $ZrC_{0.80}$ the same values determined by Zr–Zr and Zr–C bonds are 74 GPa and 610 GPa, respectively, and for $ZrC_{0.96-0.98}$ the same values determined by Zr–Zr and Zr–C bonds are 110 GPa and 623 GPa, respectively
- ^pCalculated on the basis of DFT by the means of the exact muffin-tin orbitals within coherent potential approximation (EMTO-CPA) method using GGA for the total energies evaluation
- ^qCalculated value of $G = 144$ GPa
- ^rSintered, porosity – 4–6%
- ^s $G = 148$ GPa
- ^tMeasured experimentally $G = 146$ GPa
- ^uSintered, porosity – 7%, contents: non-combined C < 0.10%, O – 1.00%, N – 0.03%, W – 0.20%; sonic velocity measurement method
- ^vSintered (in vacuum) and annealed, porosity – 15%, mean grain size – 15 μm , contents: non-combined C – 0.01%, O – 0.62%, N – 0.01%
- ^wMeasured experimentally $G = 151$ GPa
- ^xZone refined materials
- ^yCalculated value of $G = 147$ GPa
- ^zCalculated value of $G = 147$ GPa
- ^{a1}Single crystal materials; sonic resonance method
- ^{a2}Sintered in vacuum, contents: non-combined C – 0.15–0.20%, O – 0.10–0.18%
- ^{a3} $G = 155$ GPa
- ^{a4}Measured experimentally $G = 150$ GPa
- ^{a5}Sintered, extrapolated to zero porosity
- ^{a6}Sintered (in vacuum) and annealed, porosity – 14%, mean grain size – 11 μm , contents: non-combined C – 0.10%, O – 0.50%, N – 0.01%
- ^{a7}Measured experimentally $G = 158$ GPa
- ^{a8}Sintered, porosity – 10%
- ^{a9}Sintered, porosity – 4–5%, content non-combined C < 0.1%
- ^{b1}Sintered, porosity 6–8%, contents: non-combined C – 0.5%, W – 0.2%
- ^{b2}Calculated values: $G = 172$ GPa (isotropic), $E_{001} = 438$ GPa, $E_{011} = 398$ GPa, $E_{111} = 386$ GPa, $G_{001} = 159$ GPa, $G_{011} = 172$ GPa, $G_{111} = 177$ GPa, $2c_{44}/(c_{11} - c_{12}) = 0.85$
- ^{b3}Measured experimentally $G = 154$ GPa (according to Frost and Ashby [659]; $G = 173$ GPa)
- ^{b4}Hot-pressed, corrected to the poreless state (true porosity – 8%); calculated from the data on Hertizan indentation measurements
- ^{b5} $G = 167$ GPa (according to Frost and Ashby [659]; $G = 173$ GPa)
- ^{b6}Hot-pressed, contents: non-combined C – 0.40%, O – 0.07–0.09%, N – 0.10%, Fe – 0.1%, corrected to the poreless state (true porosity – 3%); sonic resonance method
- ^{b7}Measured experimentally $G = 162$ GPa
- ^{b8}Sintered (in vacuum) and annealed, porosity – 6%, mean grain size – 10 μm , contents: non-combined C – 0.55%, O – 0.13%, N – 0.07%
- ^{b9}Measured experimentally $G = 160$ GPa
- ^{c1}Sintered, porosity – 6%, contents: non-combined C – 0.13%, O – 0.08%, N – 0.01%, W – 0.01%; sonic velocity measurement method
- ^{c2}Sintered, porosity – 6%, contents: O \leq 0.05%, N – 0.05%, W – 0.2–0.3%
- ^{c3}Calculated value of $G = 161$ GPa
- ^{c4} $G = 185$ GPa
- ^{c5}Theoretical estimation; the same values for Zr–Zr and Zr–C bonds are 110 GPa and 623 GPa, respectively

(continued)

Table 5.17 (continued)

- ^{c6}Hot-pressed, corrected to the poreless state (true porosity – up to 12%), mean grain size – 5–20 μm ; ultrasonic wave velocity measurements
- ^{c7} $G = 163$ GPa
- ^{c8}Single crystal materials, Bernstein's data
- ^{c9}Calculated by Brown and Kempter using Kröner's averaging technique for Voigt-Reuss calculations, calculated value of $G = 163$ GPa
- ^{d1}Corrected to the poreless state
- ^{d2}Hot-pressed, porosity – 3%
- ^{d3}Measured experimentally $G = 170$ GPa
- ^{d4}Extrapolated to stoichiometric pure carbide phase from the experimental data on compositions containing non-combined carbon
- ^{d5}Estimated by means of density-functional perturbation theory (DFPT) calculations
- ^{d6} $G = 161$ GPa
- ^{d7}Estimation from phonon dispersion curves
- ^{d8}Hot-pressed, porosity – 6%; calculated from depth-sensing indentation (DSI) measurements
- ^{d9}Hot-pressed, porosity – 8%; determined by acoustic method
- ^{e1}Sintered, porosity – 10%, mean grain size – 10 μm
- ^{e2}Calculated from thermal experimental measurements of elastic constants
- ^{e3}Calculated from high-pressure experiments of Champion and Drickamer [723]
- ^{e4}On the basis of interconsistency of the physical properties of transition metal monocarbides
- ^{e5}Porosity – 8%
- ^{e6} $G = 124$ GPa
- ^{e7}Sintered, porosity ~5%
- ^{e8}Calculated on the basis of DFT using full-potential linearized augmented-plane-wave (FP-LAPW) method with GGA
- ^{e9}Calculated value of $G = 168$ GPa
- ^{f1}Zero temperature, zero pressure
- ^{f2}Spark-plasma sintered, porosity – 16% (for the same post-annealed material $E = 236$ GPa)
- ^{f3}At 0 K (at 2000 K: $K = 193$ GPa)
- ^{f4}Assuming uniform strain throughout the polycrystalline single-phase materials
- ^{f5}Calculated value of $G = 223$ GPa
- ^{f6}Assuming uniform stress throughout the polycrystalline single-phase materials
- ^{f7}Calculated value of $G = 204$ GPa
- ^{f8}Calculated value of $G = 163$ GPa
- ^{f9}Calculated value of $G = 132$ GPa
- ^{g1}Extrapolated to the stoichiometric composition from the experimental data obtained by Chang and Graham [49]
- ^{g2}Calculated on the basis of DFT using local density approximation (LDA)
- ^{g3}Calculated on the basis of DFT using using plane-wave pseudopotential (PWPP) method GGA
- ^{g4}Calculated on the basis of DFT using empirical (force-based many-body interatomic) potential
- ^{g5}Calculated values of $G = 166$ GPa
- ^{g6}Magnetron-sputtered nanocrystalline films
- ^{g7}Calculated on the basis of DFT with GGA using Perdew's functional
- ^{g8}Calculated on the basis of DFT with GGA using the revised version of the Perdew-Burke-Ernzerhof (RPBE) functional
- ^{g9}Calculated on the basis of DFT with Wu-Cohen GGA exchange-energy functional
- ^{h1}Calculated on the basis of DFT using FP-LAPW method with LDA
- ^{h2}Calculated using the Debye-Grüneisen model combined with *ab initio* calculations
- ^{h3}Calculated value of $G = 124$ GPa
- ^{h4}Summarized values on the basis of critical review of available experimental data
- ^{h5} $G = 165$ GPa

(continued)

Table 5.17 (continued)

- ^{h6} Spark plasma sintered, porosity – 1–2%, mean grain size – 5–13 μm ; from nanoindentation measurements
- ^{h7} Calculated on the basis of interionic potential theory with modified ionic charge
- ^{h8} Calculated value of $G = 144$ GPa
- ^{h9} Calculated value of isotropic $E = 435$ GPa
- ⁱ¹ Calculated value of $G = 186$ GPa
- ⁱ² For isotropic structure calculated value of $\nu = 0.18$
- ⁱ³ Calculated value of $G = 185$ GPa
- ⁱ⁴ Calculated value of $G = 185$ GPa
- ⁱ⁵ Calculated value of $G = 184$ GPa
- ⁱ⁶ Calculated on the basis of linear combination of atomic orbitals (LCAO) method using GGA and Perdew-Wang potential
- ⁱ⁷ Calculated value of $G = 170$ GPa
- ⁱ⁸ Calculated using the quasi-harmonic Debye model combined with *ab initio* calculations
- ⁱ⁹ Calculated on the basis of DFT with GGA using the plane-wave pseudopotential code Dacapo and Perdew-Wang functional
- ^{j1} $G = 160$ GPa
- ^{j2} At zero temperature and pressure conditions
- ^{j3} $G = 170$ GPa
- ^{j4} Calculated on the basis of a modified interaction potential model with covalency (MIPMC_v)
- ^{j5} Calculated value of $G = 140$ GPa
- ^{j6} Calculated value of $G = 160$ GPa
- ^{j7} Calculated value of $G = 165$ GPa
- ^{j8} Calculated on the basis of three body force potential (TBFP) model
- ^{j9} Calculated values of $G = 169$ GPa and $\kappa = 4.5$ TPa⁻¹
- ^{k1} From *ab initio* calculations
- ^{k2} Calculated values of $G = 159$ GPa and $\kappa = 4.3$ TPa⁻¹
- ^{k3} Calculated on the basis of DFT using full-potential linearized augmented plane-wave plus local orbital (FP-LAPW+LO) method with GGA and PBE functional
- ^{k4} $\kappa = 4.50$ TPa⁻¹
- ^{k5} Spark plasma sintered, porosity – 1%
- ^{k6} $G = 172$ GPa
- ^{k7} Calculated on the basis of DFT using FP-LAPW+LO method with the Perdew-Wang LDA
- ^{k8} Pulsed laser deposited thin films, mean grain size – 6 nm, microstrain – 2.0%, content O < 0.5%; calculated from nanoindentation measurements
- ^{k9} Pulsed laser deposited thin films, mean grain size – 12 nm, microstrain – 1.7%, content O < 0.5%; calculated from nanoindentation measurements
- ^{l1} Pulsed laser deposited thin films, mean grain size – 19 nm, microstrain – 1.6%, content O < 0.5%; calculated from nanoindentation measurements
- ^{l2} By means of extended Hückel tight-binding band electronic structure calculations
- ^{l3} Calculated value of $G = 162$ GPa
- ^{l4} Calculated by formulating effective interatomic interaction potential
- ^{l5} Calculated value of $G = 171$ GPa
- ^{l6} At ~300 K
- ^{l7} Calculated value of $G = 164$ GPa
- ^{l8} Calculated on the basis of DFT by PAW method with GGA using PBE functional
- ^{l9} Calculated on the basis of DFT with LDA using Ceperley-Alder-Perdew-Zunger (CAPZ) functional
- ^{m1} Calculated value of $G = 150$ GPa
- ^{m2} Calculated on the basis of DFT with GGA using the PBE parametrization from the stress-strain relationship
- ^{m3} Calculated value of $G = 159$ GPa
- ^{m4} Calculated on the basis of DFT with GGA using the PBE parametrization from the energy-volume fitting

(continued)

Table 5.17 (continued)

- ^{m5}Calculated values of $G = 156$ GPa
^{m6}Calculated on the basis of DFT with GGA-PBE exchange correlations for solids from the stress-strain relationship
^{m7}Calculated on the basis of DFT with GGA-PBE exchange correlations for solids from the energy-volume fitting
^{m8}Calculated on the basis of DFT using LDA from the stress-strain relationship
^{m9}Calculated value of $G = 172$ GPa
ⁿ¹Calculated on the basis of DFT using LDA from the energy-volume fitting
ⁿ²Sintered, porosity – 7%, contents: non-combined C (graphite) – 0.9%, O \leq 0.05%, N – 0.05%, W – 0.2–0.3%
ⁿ³Sintered, porosity – 4–6%, contents: non-combined C – 0.5%, O – 0.05–0.07%, N – 0.02–0.07%, W < 0.05%, Fe < 0.01%
ⁿ⁴Experimentally measured by the method of continuous impression of an indenter
ⁿ⁵Calculated by all-electron pseudopotentials with pseudo-wave functions
ⁿ⁶Hot-pressed, porosity – 2%, content O – 0.36%; measured by an impulse excitation technique
ⁿ⁷At 1300 °C: $E = 313$ GPa
ⁿ⁸Measured experimentally $G = 167$ GPa
ⁿ⁹Calculated value of $G = 177$ GPa
^{o1}Calculated value of $G = 162$ GPa
^{o2}Calculated value of $G = 159$ GPa
^{o3}Calculated value of $G = 161$ GPa

The variations of Young's E , Coulomb's (shear) G and bulk (compression) K moduli and Poisson's ratio ν with temperature for the ZrC_{1-x} phases with different deviations from the stoichiometry are shown in Fig. 5.32 and the variations with carbon content – in Fig. 5.33; the elastic properties (stiffness coefficients c_{ij} and moduli E , K and Poisson's ratio ν) of various ZrC_{1-x} materials are listed in Table 5.17. For $\text{ZrC}_{\sim 1.0}$ the approximate average rate of decay of Young's modulus with temperature $1/E_{298\text{K}} \times dE/dT = -1.2 \times 10^{-4} \text{K}^{-1}$ [52], that is a bit different to the data presented earlier [33, 365, 674, 692] by the following equation (corrected to porosity)

$$E = 550 [1 - (7.0 \times 10^{-5})t], \quad (5.85)$$

where t is temperature, °C. However, as it was reported by Baranov et al. [670], the temperature dependence of Young's modulus E of polycrystalline ZrC_{1-x} materials with various deviations from stoichiometry is more complicated: below ~ 1700 °C it is fairly well represented by Wachtman's equation:

$$E = E_0 - BT \exp(-T_0/T), \quad (5.86)$$

where E_0 is the value of E at $T = 0$ K, B and T_0 are constants affected by the composition of materials (T_0 decreases as the composition deviates further from the stoichiometry) and T is temperature, K, and at the temperatures above ~ 1700 °C there is the deviation of dependence graph from the logarithmic linearity, which can be representing by adding to the above equation an exponential term [670]:

$$E = E_0 - BT \exp(-T_0/T) - C \exp(-H_a/RT), \quad (5.87)$$

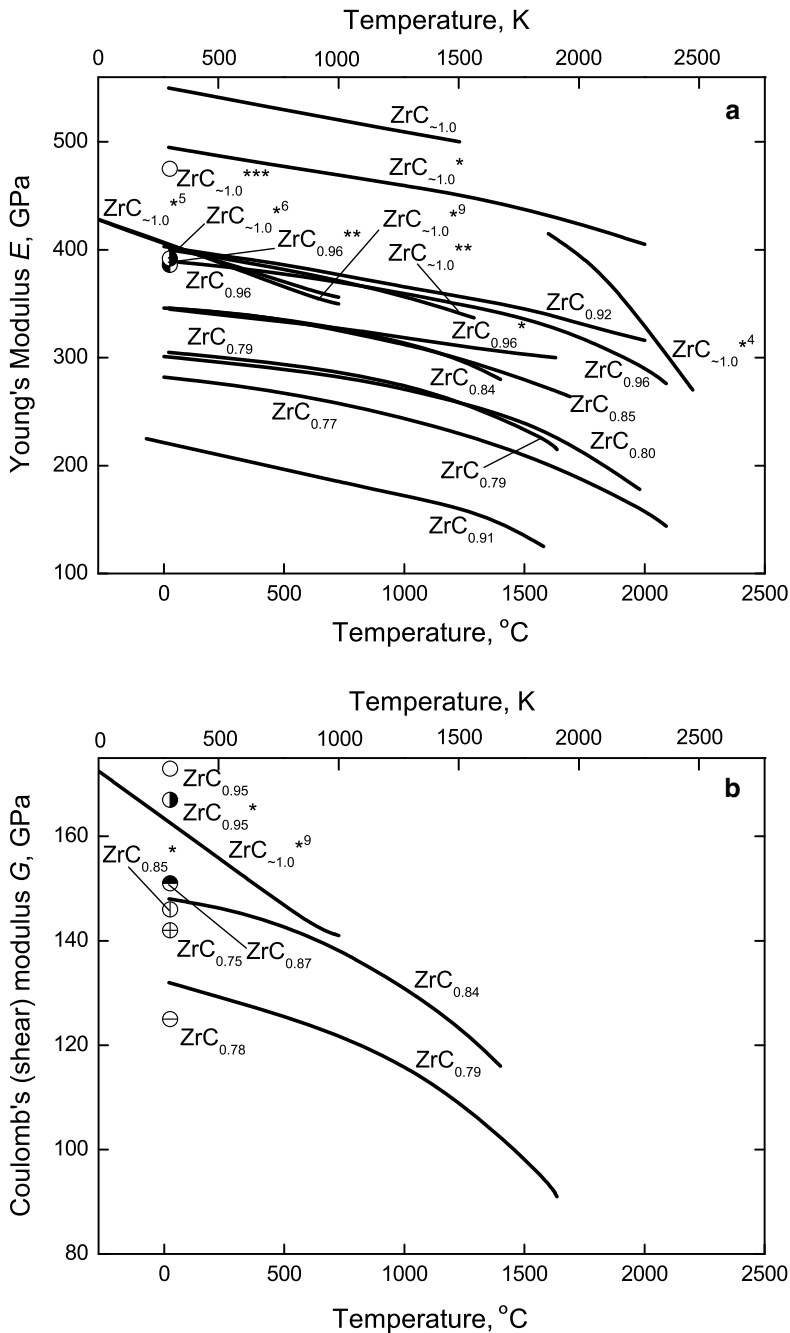


Fig. 5.32 (continued)

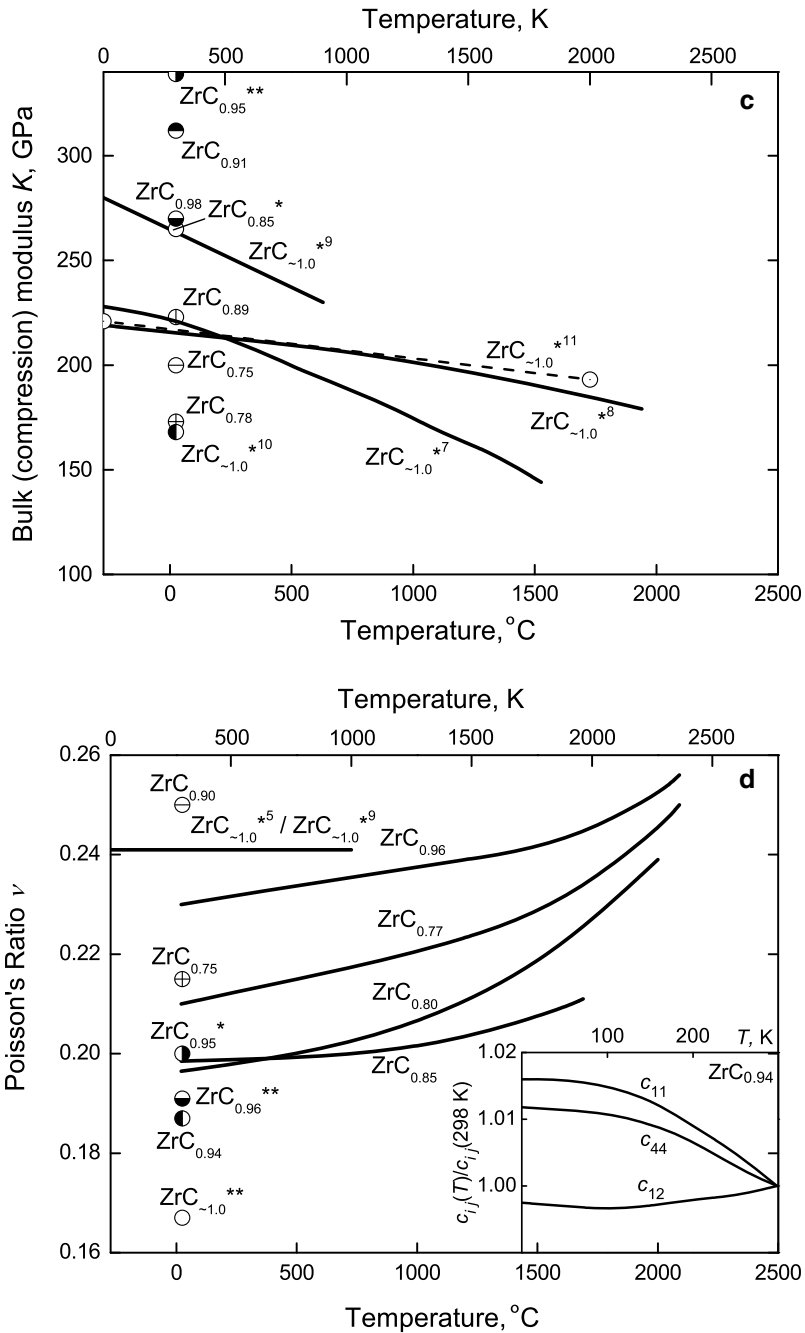


Fig. 5.32 (see caption on page 510)

◀**Fig. 5.32** Variations of Young's modulus E (a), Coulomb's (shear) modulus G (b), bulk (compression) modulus K (c) and Poisson's ratio ν (d) of zirconium carbide ZrC_{1-x} materials with temperature: sintered $ZrC_{0.75}$, $ZrC_{0.85}^*$ and $ZrC_{0.95}^{**}$ (porosity – 5–10%), corrected to the poreless state [125, 675, 676]; sintered $ZrC_{0.77}$ (porosity – 12%, contents: non-combined C < 0.10%, O – 1.20%, N – 0.22%, W – 0.35%), $ZrC_{0.80}$ (porosity – 10%, contents: non-combined C < 0.10%, O – 1.60%, N – 0.035%, W – 0.35%), $ZrC_{0.85}$ (porosity – 7%, contents: non-combined C < 0.10%, O – 1.00%, N – 0.03%, W – 0.20%) and $ZrC_{0.96}$ (porosity – 6%, contents: non-combined C – 0.13%, O – 0.08%, N – 0.01%, W – 0.01%) [123, 670, 689]; sintered (in vacuum) and annealed $ZrC_{0.78}$ (porosity – 21%, mean grain size – 18 μm , contents: non-combined C – 0.01%, O – 0.26%, N – 0.20%) [4, 132]; sintered $ZrC_{0.79}$ (porosity – 8–10%) and $ZrC_{0.84}$ (porosity – 4–6%) [685]; sintered (in vacuum) and annealed $ZrC_{0.87}$ (porosity – 15%, mean grain size – 15 μm , contents: non-combined C – 0.01%, O – 0.62%, N – 0.01%) [4, 132]; single crystal $ZrC_{0.89}$ [49, 705, 706]; sintered (in vacuum) $ZrC_{0.90}$ (contents: non-combined C – 0.15–0.20%, O – 0.10–0.18%) [277]; sintered (in vacuum) $ZrC_{0.91}$ (porosity – 18%) [125, 675, 676]; sintered $ZrC_{0.92}$ (porosity – 10%) [575]; single crystal $ZrC_{0.94}$ [49]; $ZrC_{0.95}$ (mean grain size – 10 μm) [659]; hot-pressed $ZrC_{0.95}^*$, (porosity – 8%), calculated from the data on Hertzian indentation measurements, corrected to porosity [96, 662]; sintered $ZrC_{0.96}^*$ (porosity – 7%, content O – 0.04%) [4]; hot-pressed $ZrC_{0.96}^{**}$ (porosity – 3%, contents: non-combined C – 0.40%, O – 0.07–0.09%, N – 0.10%, Fe – 0.1%), corrected to the poreless state [82]; zone refined $ZrC_{0.98}$ [277]; sintered $ZrC_{\sim 1.0}$, corrected to the poreless state [33, 365, 674]; $ZrC_{\sim 1.0}^*$, corrected to porosity [3]; hot-pressed $ZrC_{\sim 1.0}^{**}$ (porosity – 4%) [308]; $ZrC_{\sim 1.0}^{***}$, extrapolated to stoichiometric pure carbide phase from the experimental data on compositions containing non-combined carbon [673]; die-extruded and sintered $ZrC_{\sim 1.0}^{*4}$, calculated from stress relaxation tests [625–627]; $ZrC_{\sim 1.0}^{*5}$, *ab initio* calculated [283]; $ZrC_{\sim 1.0}^{*6}$, extrapolated to zero porosity [680]; $ZrC_{\sim 1.0}^{*7}$, theoretically calculated on the basis of linear combination of atomic orbitals (LCAO) method [69]; $ZrC_{\sim 1.0}^{*8}$, theoretically calculated using the Debye–Grüneisen model combined with *ab initio* calculations [724]; $ZrC_{\sim 1.0}^{*9}$, *ab initio* calculated [283]; $ZrC_{\sim 1.0}^{*10}$, calculated [49, 82, 677, 678]; $ZrC_{\sim 1.0}^{*11}$, calculated on the basis of DFT by the means of the exact muffin-tin orbitals within coherent potential approximation (EMTO-CPA) method [699] (*Inset in d* – variations of normalized elastic constants of single crystal $ZrC_{0.94}$ with low- and ultra-low temperatures in $c_{ij}(T)/c_{ij}(298\text{ K}) - T$, K scale [49])

where T is temperature, K, C is the constant, which varies from 3.9×10^3 GPa for $ZrC_{0.77}$ to 4.9×10^5 GPa for $ZrC_{0.96}$, R is the gas constant and H_a is a quantity with the significance of the effective activation energy of the thermally activated processes, which gives a more than linear fall of the modulus and varies from 85.4 kJ mol^{-1} for $ZrC_{0.77}$ to 198 kJ mol^{-1} for $ZrC_{0.96}$. Ajami and MacCrone [688] proposed Wachtman's equation for bulk (compression) K modulus of quasi-stoichiometric zirconium monocarbide $ZrC_{\sim 1.0}$ in the wide temperature range:

$$K = 256 - (1.94 \times 10^{-2})T \exp(-257/T), \quad (5.88)$$

where T is temperature, K. According to the calculations on the basis of DFT with LDA produced by Krasnenko and Brik [733] bulk (compression) modulus K of $ZrC_{\sim 1.0}$ arises at elevated hydrostatic pressures p (up to 50 GPa) linearly

$$K = 238.0 + 3.65p. \quad (5.89)$$

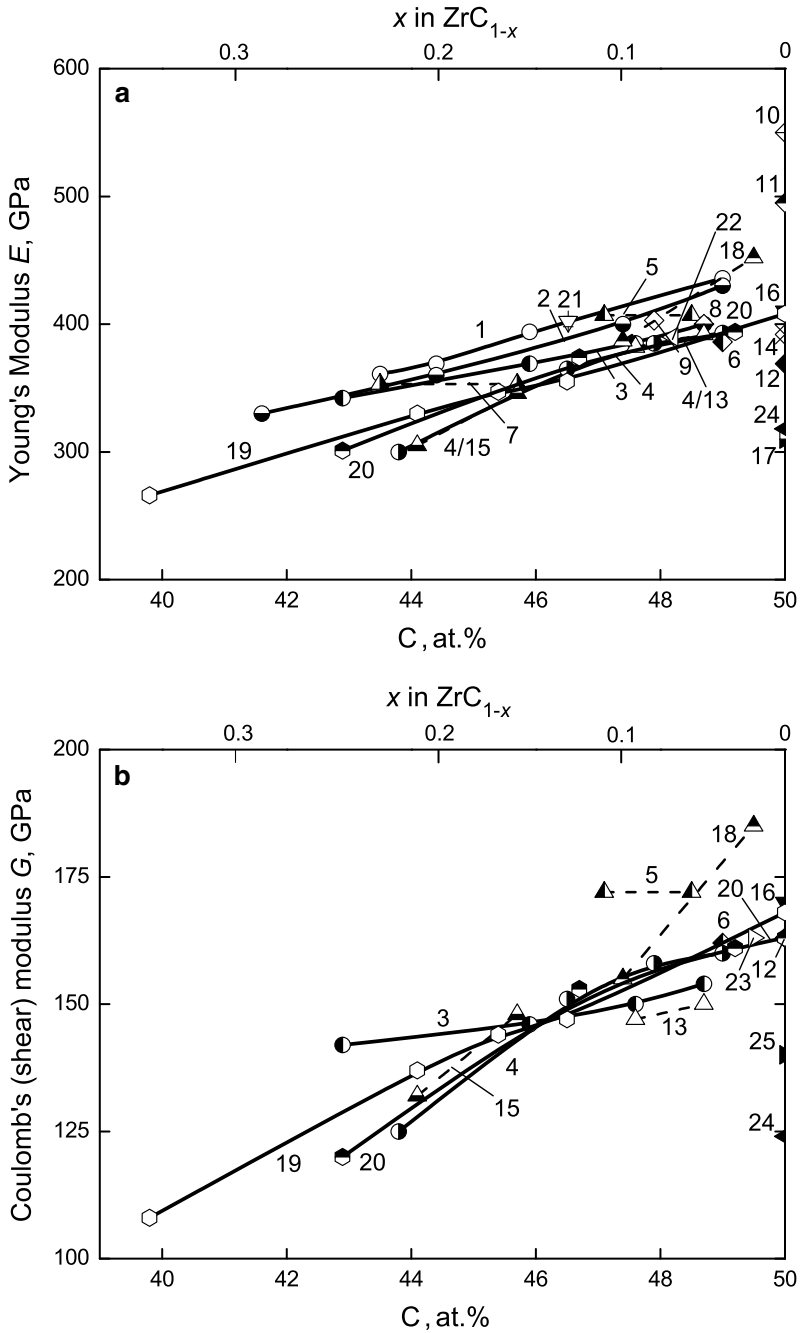


Fig. 5.33 (continued)

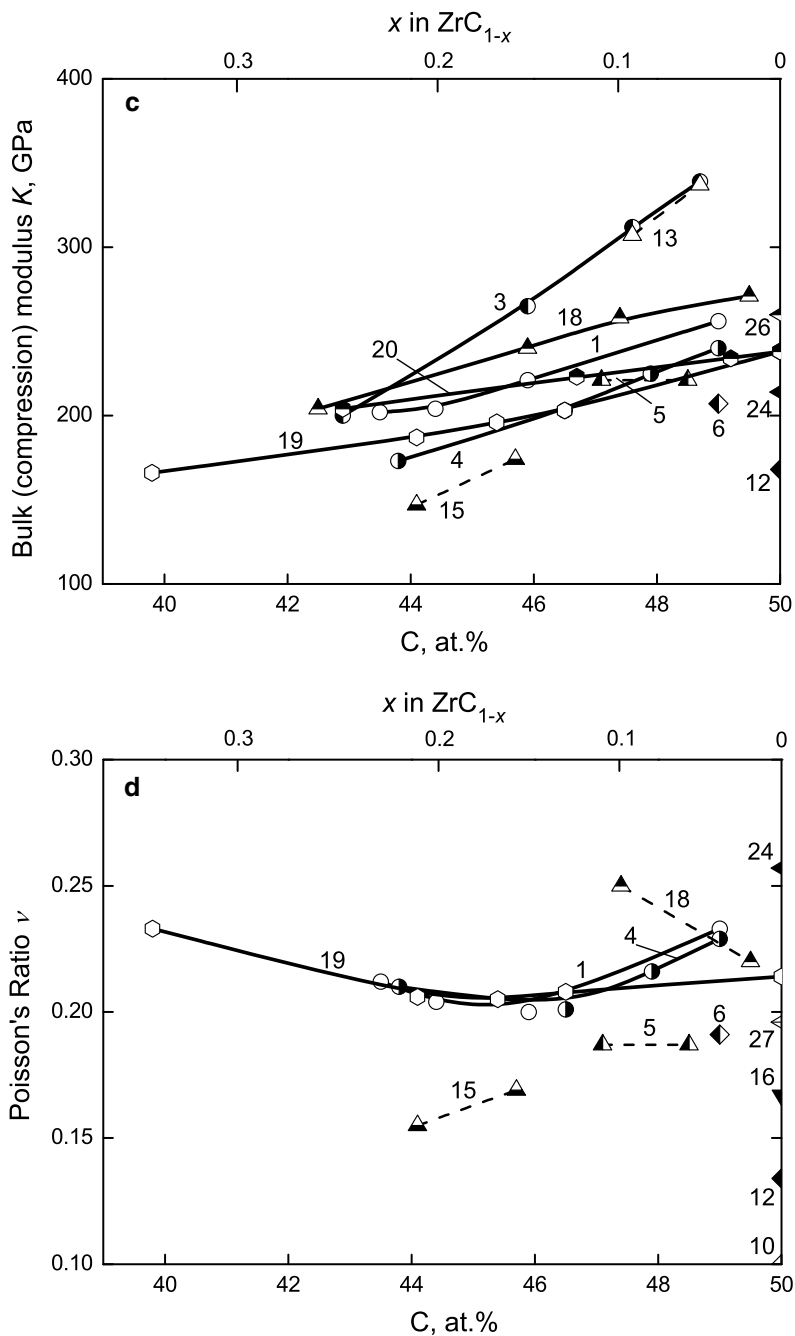


Fig. 5.33 (see caption on page 513)

◀**Fig. 5.33** Variations of Young's modulus E (a), Coulomb's (shear) modulus G (b), bulk (compression) modulus K (c) and Poisson's ratio ν (d) of zirconium carbide ZrC_{1-x} with deviation from the stoichiometry within the homogeneity range at ambient temperatures: 1 – sintered materials, corrected to porosity [123, 670, 689]; 2 – sintered materials [1]; 3 – sintered materials, corrected to the poreless state (true porosity – 5–10%) [125, 675, 676]; 4 – sintered (in vacuum) and annealed materials, porosity – 6–21%, mean grain size – 10–18 μm , contents: non-combined C – 0.10–0.55%, O – 0.13–0.79%, N – 0.01–0.03% [4, 132]; 5 – single crystal materials, calculated on the basis of elastic constants [11, 49]; 6 – hot-pressed materials, corrected to the poreless state (true porosity – 3%) [11, 82]; 7 – hot-pressed materials, porosity <4%, contents: non-combined C – 1.6–2.5% [356, 634]; 8 – sintered materials, porosity – 8% [662]; 9 – sintered materials, porosity – 10% [575]; 10 – sintered materials, corrected to porosity [33, 365, 674]; 11 – corrected to porosity [3]; 12 – single crystal materials [49, 82, 677, 678]; 13 – sintered materials, extrapolated to zero porosity [679]; 14 – extrapolated to zero porosity [680]; 15 – sintered materials, porosity – 4–10% [685]; 16 – hot-pressed materials, porosity – 3% [308]; 17 – hot-pressed materials, porosity – 8% [41]; 18 – sintered (in vacuum) materials, contents: non-combined C – 0.15–0.20%, O – 0.10–0.18% [277]; 19 – calculated on the basis of density-functional theory (DFT) [696]; 20 – calculated on the basis of DFT [735]; 21 – zone refined materials [96, 681]; 22 – sintered materials, porosity – 4–5% [624]; 23 – hot-pressed, corrected to the poreless state (true porosity – up to 12%), mean grain size – 5–20 μm [703]; 24 – [39]; 25 – calculated on the basis of a modified interaction potential model with covalency (MIPMC_v) [722]; 26 – calculated on the basis of DFT [715]; 27 – [721]

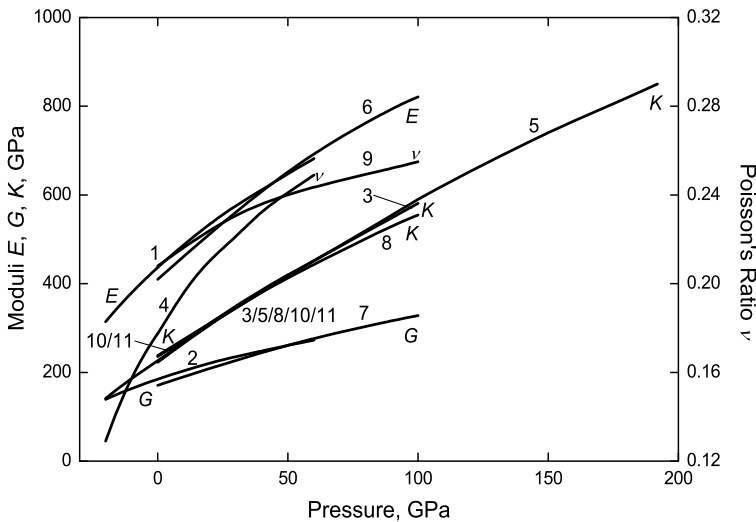


Fig. 5.34 Variations of elastic properties (1, 6 – Young's modulus E ; 2, 7 – Coulomb's (shear) modulus G ; 3, 5, 8, 10–11 – bulk (compression) modulus K and 4, 9 – Poisson's ratio ν) of quasi-stoichiometric zirconium monocarbide $ZrC_{\sim 1.0}$ with higher pressure based on *ab initio* and other theoretical calculations: 1–4 – by Fu et al. [69], 5 – by Zhu et al. [281], 6–9 – by Varshney et al. [283, 732], 10 – by Gautam and Kumar [285], 11 – by Krasnenko and Brik [733]

Table 5.18 Thermal shock/stress resistance (thermal strength) testing data on single phase zirconium monocarbide ZrC_{1-x} materials

Materials and its characterization	Specimen shape and dimensions, mm	Method of thermal loading (testing)	Experimental (or calculated) results ^a	Reference
$ZrC_{0.83-0.85}$, hot-pressed, porosity – 2%, content non-combined C – 4.1–4.3%	Disks: diameter – 50.8, thickness – 6.35	Quenching in air stream ($\sim 76 \text{ m s}^{-1}$) in parallel direction to the flat surfaces, full cycle time – 15 min	No disintegration after 22 heating-cooling cycles from 980 to 30 °C (excessive oxidation was noted)	[349, 350]
$ZrC_{0.93}$, sintered, porosity – 10%, contents: non-combined C – 0.2%, N – 0.04%, W – 0.3%	Ring-shaped disks: outer diameter – 50, inner diameter – 44, height – 10	Steady-state heating along the outer surface	$R = 40\text{--}50 \text{ K}$ (calculated), $R' = 2.3 \pm 0.4 \text{ kJ m}^{-1} \text{ s}^{-1}$ (experimental)	[3, 4, 740]
$ZrC_{0.93}$, sintered	Rods: diameter – 3, length – 30	Quenching in water	$R = 60 \text{ K}$	[334, 335, 629]
$ZrC_{0.93}$, sintered	Disks: diameter – 25, height – 3	Quenching in water	$R = 50 \text{ K}$	[334, 335, 629]
$ZrC_{0.93}$, sintered	Disks: diameter – 35, height – 2.5	Unsteady-state heating in molten tin	$R = 61 \text{ K}$	[334, 335, 617, 629]
$ZrC_{0.93}$, sintered	Disks: diameter – 20, height – 1	Surface electron-beam heating	$R = 65 \text{ K}$	[334, 335, 629, 687]
$ZrC_{0.93-0.95}$, sintered, porosity – 4–5%, content non-combined C < 0.1%	Disks: diameter – 24–26, thickness – 1–2.4; rods: diameter – 2.2, length – 50–80	Surface electron-beam heating with the usage of special diaphragms	At 50 °C: $R = 65 \text{ K}$, $R' = 1.3 \text{ kJ m}^{-1} \text{ s}^{-1}$; in cryogenic conditions: at –170 °C: $R = 106 \text{ K}$, $R' = 2.6 \text{ kJ m}^{-1} \text{ s}^{-1}$	[334, 335, 624, 687, 741]
$ZrC_{0.93-0.96}$, sintered, porosity – 4–80%	–	–	Extrapolated to zero porosity: $R = 45 \text{ K}$, $R' = 1.9 \text{ kJ m}^{-1} \text{ s}^{-1}$; (for samples with 80% porosity: $R = 70 \text{ K}$, $R' = 0.08 \text{ kJ m}^{-1} \text{ s}^{-1}$)	[330, 334, 335]
$ZrC_{0.94}$, sintered	Cylinders: diameter – 15, height – 45	Induction heating	$R = 50 \text{ K}$	[334, 335, 629]

(continued)

Table 5.18 (continued)

Materials and its characterization	Specimen shape and dimensions, mm	Method of thermal loading (testing)	Experimental (or calculated) results ^a	Reference
ZrC _{0.95} , sintered, porosity – 5%, non-combined C < 0.1%	Cylinders: diameter – 55, height – 50	Unsteady-state radiative heating	Variation of σ_o^b from 34 to 81 MPa	[3, 4]
ZrC _{0.95} , sintered, porosity – 10%	Continuous and ring-shaped disks: outer diameter – 16–52, ratio of inner diameter to outer diameter – 0–0.9	Unsteady-state heating in molten tin, cooling in water	$R = 40\text{--}70$ K (complete disintegration during heating), $R = 40$ K (appearance of surface cracks during cooling)	[3, 4, 739, 744]
ZrC _{0.95–0.97} , sintered, porosity – 4–6%, contents: O – 0.05–0.07%, N – 0.02–0.07%, W < 0.05%, Fe < 0.01%	Ring-shaped disks: inner diameter – 4–6, ratio of inner diameter to outer diameter – 0.16	Unsteady-state heating in molten tin	$R' = 1.9$ kJ m ⁻¹ s ⁻¹	[666]
ZrC _{0.96} , sintered, porosity – 8%	Cylinders: diameter – 20, height – 50	Unsteady-state radiative heating	$R = 30$ K ($R_1 = 40$ K ^c , $\sigma_z = 96$ MPa ^d)	[3, 4]
ZrC _{0.96} , sintered, porosity – 6%, contents: O ≤ 0.05%, N – 0.05%, W – 0.2–0.3%	Disks with a central hole: inner diameter – 5	Unsteady-state heating along the lateral surface of central hole in molten tin	$R = 49$ K, $R' = 1.4$ kJ m ⁻¹ s ⁻¹ , $R''' = 4.2$ MPa ⁻¹ , $R'''' = 0.05$ mm	[334, 335, 617]
ZrC _{0.96} , sintered	Cylinders: diameter – 15, height – 45	Unsteady-state radiative heating	$R = 57$ K	[334, 335, 629, 743]
ZrC _{-1.0} , hot-pressed, porosity – 9%	Spheres: diameter – 50.8	Unsteady-state (transient) state radiative heating	Observed experimentally temperature required to initiate fracture – 1450 °C	[308]
ZrC _{-1.0} , gas-phase deposited, contents: O + N ≤ 0.3%	Hollow cylinders: wall thickness – 0.8–1.2, height – 20	Direct resistance heating with 400 K s ⁻¹ , cooling by inert gas blow, cycle time – 3 min	No disintegration after 16 heating-cooling cycles from 2000 to 50 °C, disintegration during the first heating-cooling cycle from 2400 to 50 °C	[4, 539]
ZrC _{-1.0} , gas-phase deposited, contents: non-combined C – 1.0%, O + N ≤ 0.3%	Hollow cylinders: wall thickness – 0.8–1.2, height – 20	Direct resistance heating with 400 K s ⁻¹ , cooling by inert gas blow, cycle time – 3 min	Disintegration during 4 heating-cooling cycles from 2400 to 50 °C	[4, 539]

(continued)

Table 5.18 (continued)

Materials and its characterization	Specimen shape and dimensions, mm	Method of thermal loading (testing)	Experimental (or calculated) results ^a	Reference
ZrC _{-1.0} , sintered, porosity – 7%, contents: non-combined C (graphite) – 0.9%, O ≤ 0.05%, N – 0.05%, W – 0.2–0.3%	Disks with a central hole: inner diameter – 5	Unsteady-state heating along the lateral surface of central hole in molten tin	$R = 25 \text{ K}$, $R' = 0.6 \text{ kJ m}^{-1} \text{ s}^{-1}$, $R''' = 15.5 \text{ MPa}^{-1}$, $R'''' = 0.17 \text{ mm}$	[617]
ZrC _{-1.0} , sintered, porosity – 4–6%, contents: non-combined C – 0.5%, O – 0.05–0.07%, N – 0.02–0.07%, W < 0.05%, Fe < 0.01%	Ring-shaped disks: inner diameter – 4–6, ratio of inner diameter to outer diameter – 0.16	Unsteady-state heating in molten tin	$R' = 3.2\text{--}3.9 \text{ kJ m}^{-1} \text{ s}^{-1}$	[666]
ZrC _{-1.0} , sintered, porosity – 5%	Hollow cylinders: outer diameter – 48, wall thickness – 0.75	–	$R = 50 \text{ K}^c$	[336]
ZrC _{-1.0} , sintered, porosity – 75%	Hollow cylinders: outer diameter – 52, wall thickness – 2.2	–	$R = 68 \text{ K}$	[336]
ZrC _{-1.0}	Linear dimension < 30 (area of the beam spot – 100 mm ²)	Thermal pulsed electron beam (energy – 10 keV) with power density – up to 18 kW cm ⁻² and pulse length – up to 1 s	Limiting thermal flux (experimentally determined for thermo-mechanical fracture, recalculated for the initial temperature of 20 °C and pulse length of 0.5 s) – 2.0 kW cm ⁻²	[1518]

^aFigures-of-merit (criteria) of thermal shock/stress resistance [3, 4, 101, 737, 738]: $R = \sigma_t(1 - \nu)/\alpha E$, $R' = \sigma_t \lambda(1 - \nu)/\alpha E$, $R''' = E/\sigma_t^2(1 - \nu)$, $R'''' = \gamma E/\sigma_t^2(1 - \nu)$, where σ_t is tensile strength, ν is Poisson's ratio, α is thermal expansion coefficient, E is Young's modulus, λ is thermal conductivity and γ is fracture surface energy

^bValues of maximal tangential stresses

^cFor the convenience of comparison the experimental values are normalized to the corresponding disk-shaped samples

^dValues of maximal axial stresses

^eSee also Table 5.22

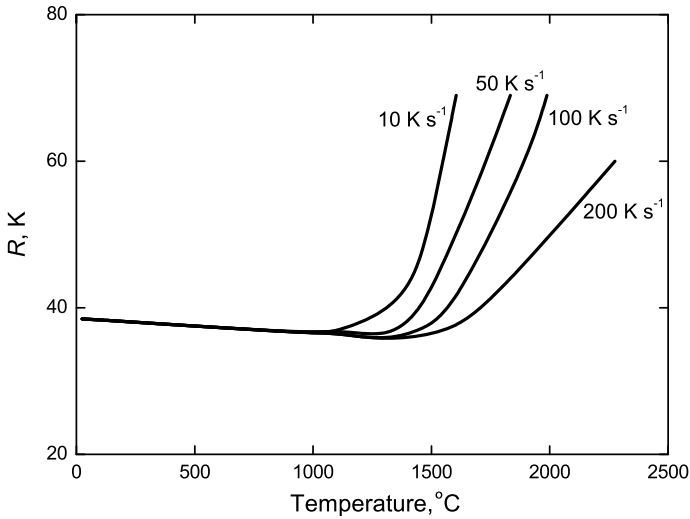


Fig. 5.35 Temperature dependence of thermal shock/stress resistance (thermal strength) R of sintered $ZrC_{\sim 1.0}$ materials at various heating rates [334, 335]

The variations of the elastic characteristics with higher pressure (up to 200 GPa) for quasi-stoichiometric zirconium monocarbide $ZrC_{\sim 1.0}$ based on *ab initio* calculations are shown in Fig. 5.34.

The experimental and calculated data on thermal shock/stress resistance (thermal strength) of single phase zirconium monocarbide ZrC_{1-x} materials are given in Table 5.18 and its temperature dependence – in Fig. 5.35.

The magnitudes of physico-mechanical (strength, elasticity) properties of near-stoichiometric zirconium monocarbide ZrC_{1-x} materials in the wide range of temperatures are summarized in Addendum in comparison with other ultra-high temperature materials.

5.5 Nuclear Physical Properties

Zirconium monocarbide ZrC_{1-x} is a material of special interest for the next-generation of nuclear engineering projects [74, 96, 798]; so, this trend makes its nuclear properties to be very important. The isotopes of elemental zirconium Zr (standard atomic mass – 91.224 u) from ^{78}Zr to ^{110}Zr , including metastable isomers (^{85m}Zr , ^{87m}Zr , ^{89m}Zr , $^{90m1-2}Zr$, ^{91m}Zr), and their general characteristics are summarized in Table 5.19; neutron nuclear physical properties of the isotopes of zirconium are given in Table 5.20. The comprehensive list of isotopes of element carbon C is presented in Table I-2.12 and its nuclear physical properties, including isotopic mass range, total number of isotopes, thermal neutron macroscopic cross sections, moderating ability and capture resonance integral, are given in Table I-A.8.

Table 5.19 General characteristics of the isotopes of zirconium [746–750]

Isotope	Mass, u	Abundance, %	Half-life period	Decay mode, excitation (radiation) energy, MeV
⁹⁰ Zr ^a	89.904704	51.45	–	–
⁹⁴ Zr ^{a,b}	93.906315	17.38	–	–
⁹² Zr ^{a,c}	91.905041	17.15	–	–
⁹¹ Zr ^a	90.905646	11.22	–	–
⁹⁶ Zr ^{a,d}	95.908273	2.80	2.0 × 10 ¹⁹ y	β [−] β [−]
⁹³ Zr ^e	92.906476	–	1.53 × 10 ⁶ y	β [−] , 0.063
⁸⁸ Zr	87.910227	–	83.4 d	K-capture; γ, 0.395
⁹⁵ Zr ^a	94.908043	–	64.032 d	β [−] , 0.364 (54%), 0.396 (43%), 0.883 (3%); γ, 0.235, 0.722, 0.754
⁸⁹ Zr	88.908890	–	3.267 d	β ⁺
⁹⁷ Zr	96.910953	–	16.744 h	β [−] , 1.91; γ, 0.75
⁸⁶ Zr	85.91647	–	16.5 h	β ⁺
⁸⁷ Zr	86.914816	–	1.68 h	β ⁺
⁸⁴ Zr	83.92325	–	25.9 min	β ⁺
⁸⁵ Zr	84.92147	–	7.86 min	β ⁺
^{89m} Zr	–	–	4.161 min	Isomer (93.77%), γ, 0.588; β ⁺ (6.23%), 0.85 (71%), 2.43 (29%)
⁸³ Zr	82.92865	–	41.6 s	β ⁺ (>99.9%), β ⁺ , p (<0.1%)
⁸² Zr	81.93109 (?)	–	32 s	β ⁺
⁹⁸ Zr	97.912735	–	30.7 s	β [−]
^{87m} Zr	–	–	14.0 s	Isomer, γ, 0.336
^{85m} Zr	–	–	10.9 s	Isomer (92%), γ, 0.292; β ⁺ (8%)
¹⁰⁰ Zr	99.91776	–	7.1 s	β [−]
⁸¹ Zr	80.93721	–	5.5 s	β ⁺ (>99.9%), β ⁺ , p (<0.1%)
⁸⁰ Zr	79.9404	–	4.6 s	β ⁺
¹⁰² Zr	101.92298	–	2.9 s	β [−]
¹⁰¹ Zr	100.92114	–	2.3 s	β [−]
⁹⁹ Zr	98.916512	–	2.1 s	β [−]
¹⁰³ Zr	102.92660	–	1.3 s	β [−]
¹⁰⁴ Zr	103.92878 (?)	–	1.2 s	β [−]
^{90m1} Zr	–	–	0.8 s	Isomer, γ, 2.319
¹⁰⁵ Zr	104.93305 (?)	–	0.6 s	β [−] (>99.9%), β [−] , n (<0.1%)
¹⁰⁶ Zr	105.93591 (?)	–	0.2 s (?)	β [−]
¹⁰⁷ Zr	106.94075 (?)	–	0.15 s (?)	β [−]
¹⁰⁸ Zr	107.94396 (?)	–	80 ms (?)	β [−]
¹⁰⁹ Zr	108.94924 (?)	–	60 ms (?)	β [−]
⁷⁹ Zr	78.94916 (?)	–	56 ms	β ⁺ , p; β ⁺
⁷⁸ Zr	77.95523 (?)	–	50 ms (?)	?
¹¹⁰ Zr	109.95287 (?)	–	30 ms (?)	?
^{91m} Zr	–	–	4.35 μs	Isomer, γ, 3.167
^{90m2} Zr	–	–	131 ns	Isomer, γ, 3.589

^aFission product^bBelieved to decay by β[−]β[−] to ⁹⁴Mo with a half-life over 1.1 × 10¹⁷ y^cHeaviest theoretically stable nuclide^dPrimordial radionuclide, a half-life is longer than the age of the universe (nearly stable), theorized to also undergo β[−] decay to ⁹⁶Nb^eLong-lived fission product

Table 5.20 Neutron nuclear physical properties of the isotopes of zirconium [751–754]

Isotope	Microscopic thermal neutron cross sections ^{a, b}		Macroscopic thermal neutron cross sections ^{a, cm⁻¹}		Resonance integral for neutron capture I_γ , b
	capture (absorption) σ_a	scattering ^b σ_s	capture (absorption) Σ_a	scattering ^b Σ_s	
Zr ^c	0.185 ± 0.003	6.46 ± 0.14	0.00775	0.340	0.93 ± 0.15
⁹⁰ Zr	0.011 ± 0.005	5.10 ± 0.20	–	–	0.13 ± 0.02
⁹⁴ Zr	0.050 ± 0.002	8.40 ± 0.40	–	–	0.27 ± 0.03
⁹² Zr	0.22 ± 0.06	6.90 ± 0.40	–	–	0.63 ± 0.02
⁹¹ Zr	1.24 ± 0.25	9.70 ± 0.20	–	–	5.20 ± 0.70
⁹⁶ Zr	0.020 ± 0.001	3.80 ± 0.10	–	–	5.60 ± 0.20

^aFor 2200 m s⁻¹ neutrons^bTotal bound scattering cross sections^cOccurred naturally

The thermal neutron macroscopic cross sections Σ_i (see Eq. 2.53) of near-stoichiometric zirconium monocarbide ZrC_{1-x} (for 2200 m s⁻¹ neutrons) [33]:

$$\begin{aligned} \text{cross section of capture (absorption) } \Sigma_a, \text{ cm}^{-1} & 7.27 \times 10^{-3} \\ \text{cross section of scattering } \Sigma_s, \text{ cm}^{-1} & \sim 0.43 \end{aligned}$$

On the basis of the previous data on lattice dynamics and elastic constants [705] double differential (coherent elastic and incoherent inelastic) neutron scattering cross sections of the ZrC_{~1.0} crystal were calculated by Difilippo and Renier [790].

For the estimation of probable damage of zirconium monocarbide materials exposed to various types of radiation the parameters of formation and migration of lattice point defects (vacancies, antisites and interstitial atoms and clusters) are given in Table 5.21.

An example of such damage (swelling) produced by fast neutrons ($E > 1$ MeV) in the range of moderate temperatures is shown in Fig. 5.36. Severe fracturing of the sintered and hot-pressed materials is observed at moderate temperatures (130–355 °C) for fluences $> (2.5\text{--}3.0) \times 10^{21}$ cm⁻² (dpa > 1.6) [758, 764]; with a fluence of 2.4×10^{21} cm⁻² at elevated temperatures (1000–1100 °C) swelling was lower with relative expansion $\Delta V/V < 1\%$ [765, 775]. The severe fracturing is corresponding to the doses led to the maximal expansion of a ZrC_{1-x} phase lattice parameter [795]. The effect of irradiation with a fast neutrons fluence of 1.5×10^{20} cm⁻² on ZrC_{0.98} sintered materials at 150 and 1100 °C leads to the expansion of lattice parameter and decrease of density, which are not correlated with each other, as despite a lesser degree of lattice parameter expansion at higher temperatures, intergranular porosity increases and accelerates the process of swelling in general [538]. The behaviour of ZrC_{1-x} materials irradiated with fast neutrons ($E \geq 0.85$ MeV, $\Phi = 1.0 \times 10^{19}$ cm⁻², 140 °C) varies noticeably with a deviation from the stoichiometry, e.g. in irradiated ZrC_{0.94} the relative expansion of lattice parameter is ~ 8 times higher than that of ZrC_{0.73} treated at the same conditions; this difference in the behaviour, according to Andrievskii et al. [766], is connected with the possibility of induced displacements of carbon atoms into tetrahedral sites, which exists in

Table 5.21 Parameters of formation and migration of lattice point defects (vacancies, antisites and interstitial atoms and clusters) in near-stoichiometric zirconium monocarbide^a

Defect	Metal sublattice				Non-metal sublattice			
	E_f , eV	E_m , eV	S_f/k_B	S_m/k_B	E_f , eV	E_m , eV	S_f/k_B	S_m/k_B
Vacancy ^b [755, 756, 1419]	3.95	3.29	4.95	4.12	1.32	5.28	1.65	6.60
Vacancy ^c [756, 1419]	3.59	3.08	4.51	3.87	0.98	3.16	1.23	3.97
Vacancy ^d [735]	9.4	–	–	–	0.28	4.3 ^e	–	–
Vacancy ^f [167]	8.89	–	–	–	1.16	–	–	–
Vacancy ^g [167]	5.80	–	–	–	1.51	4.86	–	–
Vacancy ^h [805]	8.92	–	–	–	1.20	–	–	–
Vacancy ⁱ [805]	8.81	–	–	–	0.95	–	–	–
Vacancy ⁱ [806]	8.83	–	–	–	0.93	–	–	–
Vacancy ⁱ [808]	8.89	–	–	–	0.93	–	–	–
Vacancy ⁱ [809]	7.19	5.44	–	–	0.93	4.41	–	–
Vacancy ^j [1287, 1401]	7.81	5.67	–	–	0.23	–	–	–
Vacancy ^k [1414]	4.72	–	–	–	–	–	–	–
Di-vacancy ^j [1287, 1401]	6.49	4.05 ^l	–	–	6.49	4.05 ^l	–	–
Di-vacancy ^j [1521]	6.97	–	–	–	6.97	–	–	–
Antisite ^h [805]	13.16	–	–	–	9.92	–	–	–
Antisite ^l [805]	12.97	–	–	–	9.65	–	–	–
Antisite ⁱ [806]	13.00	–	–	–	9.56	–	–	–
Interstitial atom ^b [755, 756]	19.14	0.66	24.06	0.83	5.94	0.66	7.47	0.83
Interstitial atom ^{i,m} [809]	10.36	0.47	–	–	3.56	0.27	–	–
Interstitial atom ⁱ [808]	17.69	–	–	–	4.54	–	–	–
Frenkel pairs ^j [1287, 1401]	18.61	–	–	–	5.27	–	–	–
Interstitial dimer cluster along $\langle 100 \rangle^{h,n}$ [805]	–	–	–	–	4.43	–	–	–
Interstitial dimer cluster along $\langle 100 \rangle^{i,n}$ [805]	–	–	–	–	4.39	–	–	–
Interstitial dimer cluster along $\langle 100 \rangle^{i,n}$ [806]	10.66	–	–	–	4.43	–	–	–
Interstitial dimer cluster along $\langle 110 \rangle^{h,o}$ [805]	–	–	–	–	4.54	–	–	–
Interstitial dimer cluster along $\langle 110 \rangle^{i,o}$ [805]	–	–	–	–	4.52	–	–	–

(continued)

Table 5.21 (continued)

Defect	Metal sublattice				Non-metal sublattice			
	E_f , eV	E_m , eV	S_f/k_B	S_m/k_B	E_f , eV	E_m , eV	S_f/k_B	S_m/k_B
Interstitial dimer deviates 8° from $\langle 100 \rangle^{h,p}$ [805]	–	–	–	–	4.27	–	–	–
Interstitial dimer deviates 8° from $\langle 100 \rangle^{i,p}$ [805]	–	–	–	–	4.12	–	–	–
Interstitial trimer cluster along $\langle 101 \rangle^{h,q}$ [805]	–	–	–	–	3.71	–	–	–
Interstitial trimer cluster along $\langle 101 \rangle^{i,p}$ [805]	–	–	–	–	3.52	–	–	–
Interstitial trimer cluster along $\langle 101 \rangle^{i,q}$ [806]	–	–	–	–	3.56	–	–	–
Interstitial trimer cluster (nonlinear) ^{h,r} [805]	–	–	–	–	3.66	–	–	–
Interstitial trimer cluster (nonlinear) ^{i,r} [805]	–	–	–	–	3.51	–	–	–
Interstitial trimer cluster (nonlinear) ^{i,s} [806]	–	–	–	–	3.56	–	–	–
Interstitial tetrahedron ^{h,t} [805]	–	–	–	–	3.98	–	–	–
Interstitial tetrahedron ^{i,t} [805]	–	–	–	–	3.78	–	–	–
Interstitial (along $\langle 111 \rangle$) tetrahedron ⁱ [806]	8.72 ^u	–	–	–	3.82 ^t	–	–	–
Interstitial tetrahedron ^{i,v} [808]	8.80	–	–	–	3.61	–	–	–
Interstitial dimer cluster along $\langle 101 \rangle^{i,w}$ [806]	9.96	–	–	–	–	–	–	–
Interstitial dimer cluster aligned to $\langle 111 \rangle^{i,x}$ [806]	9.29	–	–	–	–	–	–	–
Interstitial dimer cluster aligned to $\langle 111 \rangle^{i,y}$ [806]	9.24	–	–	–	–	–	–	–
V _{Zr} -(VC) ₆ -cluster ^j [1287, 1401]	2.92	4.54 ^z	–	–	2.92	4.54 ^z	–	–

(continued)

Table 5.21 (continued)

- ^aDenoted: E_f – defect formation energy, E_m – defect migration energy, S_f – defect formation entropy, S_m – defect migration entropy, k_B – Boltzmann constant
- ^bCalculated on the basis of bonding model (relaxation displacement of atoms surrounding a defect is not taking into account)
- ^cCalculated on the basis of elastic continuum model
- ^d*Ab initio* simulation computed from the largest super-cell on the basis of the PAW pseudopotential using the PBE formulation
- ^eCalculated value of activation energy for carbon self-diffusion in zirconium monocarbide $E_A = 440$ kJ mol⁻¹ (see also Sect. 5.6, Table 5.29)
- ^fCalculated using the Vienna *Ab initio* Simulation Package (VASP) [788, 789]
- ^gCalculated using ultrasoft pseudopotential
- ^hCalculated on the basis of the Vanderbilt-type ultrasoft pseudopotential with GGA exchange-correlation function
- ⁱCalculated on the basis of the projector-augmented plane-wave (PAW) method with PBE exchange-correlation function
- ^jCalculated on the basis of PAW (using VASP) within GGA and nudged elastic band (NEB) methods
- ^kCalculated on the basis of data on the yield strength determined by hardness and elasticity experimental measurements
- ^lCalculated value of activation energy for metal self-diffusion in zirconium monocarbide (di-vacancy mechanism) $E_A = 1020$ kJ mol⁻¹ (see also Sect. 5.6, Table 5.29)
- ^mDefect formation and defect migration entropies are set to zero; calculated activation energies E_A of diffusion for defects: C vacancy – 515 kJ mol⁻¹, C interstitial – 370 kJ mol⁻¹, Zr vacancy – 1220 kJ mol⁻¹ and Zr interstitial – 1050 kJ mol⁻¹
- ⁿDumbbell structure cluster, interatomic distances: C–C – 0.124 nm, Zr–Zr – 0.176 nm
- ^oDumbbell structure cluster, interatomic distance C–C – 0.139 nm
- ^pDumbbell structure cluster, interatomic distance C–C – 0.125 nm
- ^qInteratomic distances C–C–C – 0.139 nm
- ^rInteratomic distances C–C – 0.146 nm with 139° angle between C–C pairs
- ^sInteratomic distances C–C – 0.141 nm
- ^tInteratomic distances C–C – 0.161 nm with 117° angle between C–C pairs
- ^uZr-centred double tetrahedron, interatomic distance Zr–Zr – 0.212 nm
- ^vCalculated E_f of isolated Frenkel pairs for Zr atoms – 17.69 eV and C atoms – 4.54 eV and that of a Schottky defect – 8.14 eV
- ^wInteratomic distance Zr–Zr – 0.184 nm
- ^xPerturbed <100>, interatomic distance Zr–Zr – 0.1849 nm
- ^yPerturbed <101>, interatomic distance Zr–Zr – 0.1854 nm
- ^zCalculated value of activation energy for metal self-diffusion in zirconium monocarbide (cluster mechanism) $E_A = 720$ kJ mol⁻¹ (see also Sect. 5.6, Table 5.29)

near-stoichiometric compositions, while in carbon-deficient compositions carbon atoms may be displaced to already vacant octahedral sites. Some data on the resistance of ZrC_{1-x} materials to fast neutron irradiation damage, based on the measurements of their physical properties after the irradiation, are summarized in Table 5.22; the data, including the results obtained by materials testing in reactor IVG-1 for modeling nuclear rocket engine reactor environment, show that the irradiation leads to appreciable changes of density and electrical resistivity accompanied by minor changes of strength, hardness and elastic characteristics [337, 761, 762]. The fast neutron irradiation ($E > 0.18$ MeV, $\Phi = 5 \times 10^{21}$ cm⁻², 1200 °C) behaviour of ZrC_{~1.0} chemically vapour deposited coatings (thickness – 45–52 μm) on the

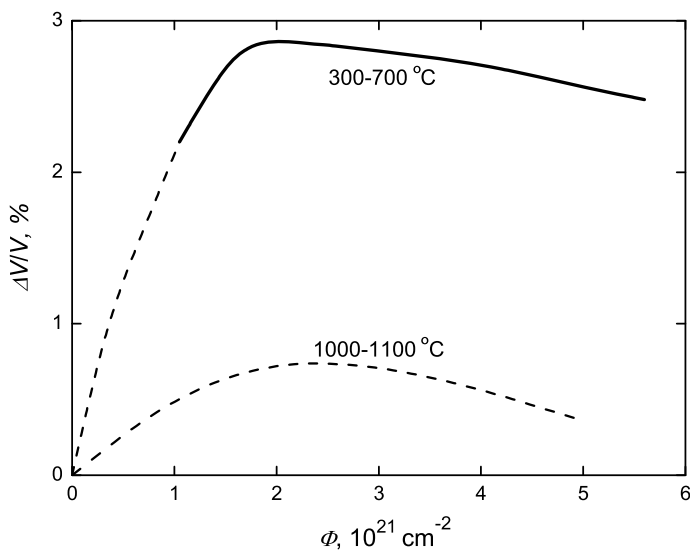


Fig. 5.36 The change in macroscopic volume (swelling) with fast neutron (>1 MeV) fluence Φ for produced by ceramic technologies (hot-pressed, slip-cast, explosion-pressed) near-stoichiometric zirconium monocarbide ZrC_{1-x} materials irradiated at different temperatures [755, 758, 764, 765, 1519]

Table 5.22 Structural, electrical and physico-mechanical properties of $\text{ZrC}_{0.98}$ sintered materials before and after fast neutron irradiation ($\Phi = 1.5 \times 10^{20} \text{ cm}^{-2}$) exposure at different temperatures [4, 337, 538]

Characteristics	Unit	Measured values		
		Initial samples 20 °C	Irradiated samples ^a	
			150 °C	1100 °C
Density	g cm^{-3}	6.40	6.29	6.27
Lattice parameter	nm	0.4692	0.4714	0.4698
Electrical resistivity	$\mu\Omega \text{ m}$	0.43	2.50	0.65
Flexural strength:				
average	MPa	245	315	255
minimal	MPa	215	235	235
maximal	MPa	300	340	290
Young's modulus	GPa	400	405	400
Microhardness	GPa	20.1	22.5	21.6
load ^b	N	0.98	0.39	–
Thermal stress resistance criterion R^c	K	45	75	75

^aThe neutron flux – 10^{12} – $10^{15} \text{ cm}^{-2} \text{ s}^{-1}$

^bThe minimum load during the microhardness tests, at which all the indentations were cracking

^cSee notes to Table 5.18

experimental fuel particles was studied by Reynolds et al. [767]; at something similar irradiation conditions, but at rather higher temperatures Fukuda et al. ($E > 0.18$ MeV, $\Phi = 1.4 \times 10^{21} \text{ cm}^{-2}$, 1260 °C) [781], Ogawa et al. ($E > 0.18$ MeV, $\Phi = (1.0\text{--}2.2) \times 10^{21} \text{ cm}^{-2}$, 900–1600 °C) [768, 782–785] and Minato et al. ($E > 0.18$ MeV, $\Phi = 1.2 \times 10^{21} \text{ cm}^{-2}$, 1400–1650 °C) [769–773] also confirmed good mechanical and environmental stability of $\text{ZrC}_{\sim 1.0}$ coatings on the fuel particles. High purity zone refined $\text{ZrC}_{0.93}$ materials were fast neutron irradiated by Snead et al. ($E > 0.1$ MeV, $\Phi = (1.0\text{--}10.0) \times 10^{21} \text{ cm}^{-2}$, 640–1500 °C) [681], measurements of lattice parameter indicated a lack of significant crystalline strain due to irradiation, only modest changes in the physico-mechanical properties of fracture toughness, hardness and elastic modulus and slight reduction of thermal conductivity near 1000 °C irradiation (though the parameter was essentially unchanged at higher temperatures) were observed; so, the general finding of the studies was that the materials are quite stable under neutron irradiation in the testing conditions.

The damage produced by thermal neutrons fluences up to $1.5 \times 10^{20} \text{ cm}^{-2}$ at ~ 50 °C results in the slight failure of hot-pressed $\text{ZrC}_{0.98}$ materials, which is accompanied by $\sim 0.3\%$ relative change of lattice parameter, but $\sim 190\%$ relative change of specific electrical resistance (Table 5.23), while the accumulated energy in the materials corresponding to these irradiation conditions amounts to 12.7 kJ mol^{-1} [755, 759, 760, 794]. By *in situ* property measurements Taubin et al. [774] found out only minor changes in heat capacity, thermal conductivity, thermal expansion and electrical resistivity in $\text{ZrC}_{0.96}$ irradiated below 400 °C with mixed fission neutrons ($\Phi = \sim 1.0 \times 10^{16} \text{ cm}^{-2}$). According to Markin et al. [786] the damage ability of monocarbide ZrC_{1-x} materials under the action of neutron irradiation in the part of magnetic susceptibility only weakly depends on the deviation from the

Table 5.23 The effect of thermal neutron irradiation on the structure and physical properties of zirconium monocarbide ZrC_{1-x} hot-pressed materials [755, 759, 760, 763, 794, 1520]

Characteristics	Unit	Temperature, °C	Initial values	After irradiation with different thermal neutron fluences Φ , 10^{19} cm^{-2}			
				1.0	3.7	7.5	15
			$\text{ZrC}_{\sim 1.0}$				
Flexural strength	MPa	80–100	200	158	155	153	–
			$\text{ZrC}_{0.98}$				
Lattice parameter	nm	~ 50	0.4679	0.4681	0.4683	0.4689	0.4694
Electrical resistivity	$\mu\Omega \text{ m}$	~ 50	0.56	0.68	0.95	1.37	1.63
relative change	%	~ 50	0	+23	+70	+145	+191
Microhardness	GPa	~ 50	26.4	26.0	25.5	27.2	30.1
relative change	%	~ 50	0	–1.5	–3.4	+3.0	+14
Accumulated energy ^a							
per gram	J g^{-1}	~ 50	0	18	32	75	123
per mole	kJ mol^{-1}	~ 50	0	1.86	3.34	7.70	12.7
Effective temperature ^a	K	~ 50	–	80	140	310	490

^aFor additional information

stoichiometry of monocarbide phase. The effect of earlier stages (< 30 s) of nuclear reactor irradiation with neutron flux $\varphi = \sim 1.0 \times 10^{14} \text{ cm}^{-2} \text{ s}^{-1}$ and gamma quanta dose of $2.58 \times 10^6 \text{ C kg}^{-1}$ on the heat capacity, thermal conductivity and electrical resistivity of $\text{ZrC}_{\sim 1.0}$ materials, when the gamma quanta influence dominates, was studied by Taubin [787]. A study of the primary damage due to neutron irradiation created by a high energy collision cascade (50 keV) in single crystal stoichiometric zirconium monocarbide was conducted by Van Brutzel and Crocombette [791] by means of classical molecular dynamics simulation.

To simulate high irradiation damage rate in near-stoichiometric zirconium monocarbide Gan et al. [776] conducted Kr ion irradiation ($E = 1 \text{ MeV}$, $\Phi = 2.5 \times 10^{15} - 1.75 \times 10^{16} \text{ cm}^{-2}$, corresponding to 10–70 dpa) of hot-pressed $\text{ZrC}_{\sim 1.0}$ materials (porosity $< 1\%$, contents: O – 0.21%, N – 0.61%, Hf – 1.90%, Ti – 0.19%) at room temperature (10 and 30 dpa) and 800°C (10 and 70 dpa) with a damage rate $\sim 3.0 \times 10^{-3} \text{ dpa s}^{-1}$; as a result no radiation induced amorphization was found, and the maximal lattice expansion of $\sim 7\%$ was observed at higher irradiation intensity and higher temperature. The same $\text{ZrC}_{\sim 1.0}$ materials were also irradiated with protons ($E = 2.6 \text{ MeV}$, $\Phi = 2.75 \times 10^{19} \text{ cm}^{-2}$, corresponding to 0.7–1.8 dpa) at 800°C [777]; in comparison to Kr ion irradiation (10 dpa) mentioned above, proton irradiated materials show less damage to the lattice structure and exhibit faulted dislocation loops on (111) planes, which were not observed in the Kr ion irradiated materials. To irradiate the same materials to doses 0.7 and 1.5 dpa, Yang et al. [778, 792] also used a 2.6 MeV proton beam at $600\text{--}900^\circ\text{C}$ to doses up to 1.75 dpa and found out the lattice expansion at $600\text{--}800^\circ\text{C}$ and slight lattice contraction at 900°C , which were in good agreement with the earlier reported results from neutron irradiation; the hardness and the fracture toughness of materials both increase with increasing the radiation dose: for 1.5 dpa dose the relative increases were 10–15 and 50–100%, respectively. Jensen et al. [341–342, 799–800] reported about $\sim 66\%$ degradation of thermal conductivity (up to $11.9 \text{ W m}^{-1} \text{ K}^{-1}$) in the $\sim 50 \mu\text{m}$ deep zone of hot-pressed $\text{ZrC}_{\sim 1.0}$ materials proton-irradiated ($E = 2.6 \text{ MeV}$, 1.75 dpa, 600°C). In the range of doses from 1 to 3 dpa in the zone refined ZrC_{1-x} materials with $0 < x \leq 0.1$ and non-combined C content – up to 2.3%, which were irradiated with protons ($E = 2.0 \text{ MeV}$, $\varphi = 1.0 \times 10^{18} \text{ cm}^{-2} \text{ s}^{-1}$, dose rate at the depth of $5\text{--}20 \mu\text{m} - 4.7 \times 10^{-5} \text{ dpa s}^{-1}$, $800 \pm 10^\circ\text{C}$), the following parameters of irradiation-induced defects were characterized and estimated: average size of dislocation loops – from 7 to 28 nm and density of dislocation loops from $1.5 \times 10^{15} \text{ cm}^{-3}$ to $7.5 \times 10^{15} \text{ cm}^{-3}$ [803]. In the similar materials ($0 < x \leq 0.16$ and non-combined C content – up to 1.9%) irradiated with protons ($E = 2.0 \text{ MeV}$, $\Phi = 2.0 \times 10^{19} \text{ cm}^{-2}$ corresponding to ~ 2 dpa for $\text{ZrC}_{1.0}$, dose rate at the depth of $10\text{--}15 \mu\text{m} - 1.8 \times 10^{-5} \text{ dpa s}^{-1}$, 1125°C) Yang et al. [804] identified the dislocation loops as interstitial type perfect loops with average size from 9.85 nm (for $\text{ZrC}_{0.95}$) to 53 nm (for $\text{ZrC}_{\sim 1.0}$ with content non-combined

C – 1.9%); it was indirectly proved that the dislocation loop core likely consists of carbon atoms, and graphite precipitates in the super-stoichiometric compositions are detrimental, as the dramatic increases in the size of and density of dislocation loops were observed in the vicinity of these precipitates in monocarbide phases. Proton irradiation induced faceted voids were only observed in a near-stoichiometric composition, which is attributed to the pre-existing dislocation lines as biased sinks for vacancies.

Sintered $\text{ZrC}_{\sim 1.0}$ materials were irradiated with fast and energetic Kr ions ($E = 25.8 \text{ MeV}$, $\Phi = (1.0\text{--}6.0) \times 10^{16} \text{ cm}^{-2}$); the study considered two domains produced by the inelastic and the elastic collisions that occurred during the process of ion irradiation, significant thermal conductivity degradation in both domains was observed, elastic collisions were shown to degrade the thermal properties of $\text{ZrC}_{\sim 1.0}$ more strongly, reducing thermal conductivity from $20 \text{ W m}^{-1} \text{ K}^{-1}$ before irradiation to less than $1 \text{ W m}^{-1} \text{ K}^{-1}$ [331, 332]. Floating-zone refined $\text{ZrC}_{0.80}$ and $\text{ZrC}_{0.90}$ were also irradiated with Kr ions ($E = 1 \text{ MeV}$, $\varphi = 6.25 \times 10^{11} \text{ cm}^{-2} \text{ s}^{-1}$, maximal dose from 3.9 to 12.8 dpa, -253 to $800 \text{ }^\circ\text{C}$), no long-range migration of the visible defects or dynamic defect creation and elimination were observed during the irradiation, but some coarsening of the microstructure with the formation of dislocation loops was observed at higher temperatures; the irradiated microstructure was found to be only weakly dependent on the stoichiometry [807]. Gosset et al. [779, 780] performed low energy Au ions ($\Phi = 1.0 \times 10^{12} \text{--} 5.0 \times 10^{15} \text{ cm}^{-2}$, corresponding to 7–35 dpa) irradiation of hot-pressed $\text{ZrC}_{0.95}$ and $\text{ZrC}_{0.85}\text{O}_{0.08}$ at room temperature, high sensitivity to oxidation was observed with the formation of oxide precipitates during the irradiation process; three stages of damage could be classified: at lower fluences ($\Phi < 1.0 \times 10^{12} \text{ cm}^{-2}$) – low oxide modifications (*see also* Table 5.26) are formed, at intermediate fluences ($1.0 \times 10^{12} \text{ cm}^{-2} < \Phi < 1.0 \times 10^{14} \text{ cm}^{-2}$) – high micro-strains appear jointly with small faulted dislocation loops and at higher fluences ($\Phi > 1.0 \times 10^{14} \text{ cm}^{-2}$) – the micro-strains saturate and the loops coalesce to form a dense dislocation network. The materials showed the moderate lattice increase up to 0.6 vol.%, which saturates at $\Phi = \sim 1.0 \times 10^{14} \text{ cm}^{-2}$. No amorphization was observed in (001)-oriented single crystal $\text{ZrC}_{\sim 0.9}$ (99.99% purity) irradiated with Au ions beam ($E = 1.2 \text{ MeV}$, $\Phi = 3.0 \times 10^{13} \text{--} 3.0 \times 10^{16} \text{ cm}^{-2}$, $25 \text{ }^\circ\text{C}$) as well, with increasing fluence the irradiation damage was found to spread in the materials deeper than the depth of direct damaging by the ion beam [801, 802, 810, 929]. Jiang et al. [811] showed that the metal sublattice in zirconium monocarbide remains structurally stable against carbon sublattice displacements up to the highest dose of 1.0 dpa; consequently, ZrC_{1-x} cannot be amorphized by the accumulations of Frenkel pairs of carbon atoms like it is occurred with covalent carbides. A comparative study of ZrC_{1-x} materials with micro- and nano-sized grains irradiated with low energy heavy ions concluded that the resulting damaged surface area of the materials has a 0.1–0.2 μm thickness, both

materials with micro- and nano-sized grains showed high internal distortions, for micro-sized-grain materials a linear volume swelling in the range of 20–40 Zr dpa was observed [180]. Spark-plasma sintered $\text{ZrC}_{0.95}\text{O}_{0.05}$ materials were implanted with Xe ions ($E = 0.8$ MeV, $\Phi = 1.0 \times 10^{15}$ and $\Phi = 1.0 \times 10^{16}$ cm⁻², 25 °C), in the as-implanted samples Xe bubbles were not formed at both fluences and the point defects as vacancies, interstitials and Xe-substitutions were predominant, the higher fluence led to thinner damaged layer; the post-implantation annealing of the samples treated with higher fluence caused formation of Xe bubbles, and the concentration of bubbles increased with the time of the high vacuum ($5 \times 10^{-4} - 5 \times 10^{-5}$ Pa) annealing at 1800 °C indicating good Xe retention, while the annealing of samples treated with lower fluence at first caused clustering of defects, and only after more than 8 h of annealing led to the formation of Xe bubbles [793]. It was also shown that the presence of residual oxide inclusions ($\sim 2\%$) and some free carbon ($\sim 0.15\%$) induces a plate-like damaging of the materials surface whereas pure Xe-implanted $\text{ZrC}_{0.95}\text{O}_{0.05}$ materials display a less damaged surface after vacuum annealing procedure [796]. First principles calculations were employed to study the diffusion behaviour of He impurities in ZrC_{1-x} materials; it was revealed that Zr-vacancy assisted mechanism plays a dominant role in it with a small energy barrier of 0.70 eV. He is likely trapped in Zr pre-existing vacancies, which may impact on the mechanical properties and dimensional stability of ZrC_{1-x} materials [808].

The details of radiochemical compatibility of ZrC_{1-x} materials with some fission products and diffusion parameters of these products in ZrC_{1-x} phases are given in Table 5.27. Nuclear physical properties of zirconium monocarbide ZrC_{1-x} in comparison with other ultra-high temperature materials are also given in Addendum.

5.6 Chemical Properties and Materials Design

The comprehensive data on the chemical properties, compatibility (in the connection with both environmental resistance and composite materials design) and interaction behaviour of zirconium monocarbide at elevated, high and ultra-high temperatures with elements (metals, non-metals) are summarized in Table 5.24, with refractory compounds – in Table 5.25 and with gaseous media – in Table 5.26. The data on the oxidation resistance of zirconium monocarbide materials listed there are also accompanied by the graphic information in Figs. 5.37 and 5.38; the isothermal oxidation kinetics of near-stoichiometric ZrC_{1-x} materials can be considered in the context of ridge-effect model proposed by Shabalin [984, 985] with ridge temperatures at lower oxygen pressures: nearby ~ 900 °C – for denser materials (with lower porosity) and around ~ 550 °C – for highly porous (or more active chemically) materials. The details of radiochemical compatibility of ZrC_{1-x} materials with some fission products and diffusion parameters of these products in

Table 5.24 Chemical interaction and/or compatibility of zirconium monocarbide with elements (metals, non-metals) at elevated, high and ultra-high temperatures, including solid matters and molten media (reaction systems are given mainly in alphabetical order)^a

System	Atmosphere	Temperature range, °C	Interaction character, products and/or compatibility	Reference
ZrC _{1-x} -Ag			See Tables 5.27 and 5.28	
ZrC _{1-x} -Ag-Pd	-	1230	Formation of ZrPd ₃	[1014]
ZrC _{1-x} -Al	-	<1000	No chemical interaction; the partial dissolution of Zr from ZrC _{1-x} into Al melt was observed	[1, 30, 32, 33, 42, 45, 48, 63, 812-839, 906, 907, 911-913, 934, 1011, 1025, 1026, 1071, 1082, 1090, 1091, 1233, 1366, 1375, 1404]
	-	1000	The contact interaction is weak (5 h exposure)	
	Ar	1000-1250	Weak interaction during 0.2 h exposure	
	He	1000-1400	Formation of Al ₄ C ₃	
	-	≥1250	Intensive interaction and formation of Al solid solutions in carbide	
	-	1700	Intensive interaction with Al vapour and formation of new refractory phases	
	-	-	Formation of Zr ₃ Al ₃ C ₅ , Zr ₃ Al ₄ C ₆ , Zr ₂ Al ₃ C ₅ , Zr ₅ Al ₃ C, Zr ₂ Al ₃ C ₄ , Zr ₂ Al ₄ C ₅ , ZrAl ₈ C ₇ , ZrAl ₃ C ₃ , ZrAl ₄ C ₄ , ZrAlC _{2-x} , Zr ₃ AlC ₂ and Zr ₂ AlC	
	-	-	Hexagonal ZrC _{1-x} platelets are formed via self-propagating high-temperature synthesis from Al-Zr-C powder mixtures	
	-	-	The effect of Al as an additive for hot-pressing process was studied	
			Data on chemical resistance in molten Al available in literature are controversial	
			See also section ZrC _{1-x} -Al ₄ C ₃ in Table 5.25	
			See also Table 5.28	
			See also section C-Al-Zr in Table I-2.14	
ZrC _{1-x} -Al-Cu	Vacuum	550	Particles of ZrC _{1-x} (0.3-6 μm) are compatible with Al - 4 mas.% Cu matrix alloy	[946]
ZrC _{1-x} -Al-Mg	-	750	Particles of ZrC _{1-x} (1-3 μm) show high stability and uniform distribution in molten Al - 1% Mg alloy, even though minute amounts of Al ₃ Zr were observed	[1044]
ZrC _{1-x} -Al-Zr	-	-	Formation of Zr ₃ Al ₃ C ₅ , Zr ₃ Al ₄ C ₆ , Zr ₂ Al ₃ C ₅ , Zr ₅ Al ₃ C, Zr ₂ Al ₃ C ₄ , Zr ₂ Al ₄ C ₅ , ZrAl ₈ C ₇ , ZrAl ₃ C ₃ , ZrAl ₄ C ₄ , ZrAlC _{2-x} , Zr ₃ AlC ₂ and Zr ₂ AlC	[814-825, 828, 829, 834-839, 906, 907, 911-913, 1011, 1090, 1091, 1366, 1404]

(continued)

Table 5.24 (continued)

System	Atmosphere	Temperature range, °C	Interaction character, products and/or compatibility	Reference
ZrC _{1-x} -Al ₂ O ₃ -Al	-	-	Compatible as components of metal matrix composites	[1363]
ZrC _{1-x} -NbC _{1-x} -Al	-	-	See section NbC _{1-x} -ZrC _{1-x} -Al in Table 4.18 See also section C-Al-Nb-Zr in Table I-2.14	
ZrC _{1-x} -SiC-Al	-	-	Formation of Zr(Al _{1-x} Si _x) ₈ C ₇ , Zr(Al _{1-x} Si _x) ₄ C ₄ , Zr ₂ (Al _{1-x} Si _x) ₄ C ₅ and Zr ₃ (Al _{1-x} Si _x) ₄ C ₆ See also section ZrC _{1-x} -Al ₄ C ₃ -Si in this table See also section ZrC _{1-x} -Al ₄ C ₃ -SiC in Table 5.25	[826, 827, 831-833, 904, 1082]
ZrC _{1-x} -SiC-TiC _{1-x} -Al	-	-	Formation of (Ti,Zr) ₃ (Si,Al)C ₂ (M _{n+1} AX _n -phase solid solution) See also section ZrC _{1-x} -Al ₄ C ₃ -SiC-TiC _{1-x} in Table 5.25	[834, 838]
ZrC _{1-x} -β-B	-	1500 - 2000-2600	Solubility of B in ZrC _{1-x} is very low Formation of ZrB _{2±x}	[1, 33, 46, 76, 200, 840-845, 914, 1030, 1403, 1462]
ZrC _{1-x} -B _{4±x} C-β-B	Chamber of anvil type	1600-2000 (0.015-5 GPa)	See also section C-B-Zr in Table I-2.14 Formation of ZrB _{2±x} ; the addition of B favours the reaction between ZrC _{1-x} and B _{4±x} C going to completion	[1030, 1462]
ZrC _{1-x} -Ba	-	-	See also section C-B-Zr in Table I-2.14 See Table 5.27	
ZrC _{1-x} -Be	-	-	The effect of Be as an additive for hot-pressing process was studied	[33]
ZrC _{1-x} -Bi	Ar	280-320	No chemical interaction during 10 h exposure	[1, 30, 32, 33, 42, 45, 48, 63]
	Air	375	Traces of Zr were revealed in liquid metal after 10 h exposure See also Table 5.28	
ZrC _{1-x} -Bi-Pb	-	1100	Testing materials (content non-combined C-4.1%) in dynamic conditions (24 h exposure) showed disintegration rate - 5.25 μm h ⁻¹ , pitting type of attack was observed	[33, 846]
ZrC _{1-x} -C	-	<2750	ZrC _{1-x} is compatible in contact with any C (graphite) parts and articles	[1, 30, 33, 99, 102, 559, 841, 847, 848, 901, 920, 995, 1049, 1089, 1395, 1534]
	-	~2850-2930	Eutectic ZrC _{1-x} -C (graphite)	

See also section C-Zr in Table I-2.13

(continued)

Table 5.24 (continued)

System	Atmo- sphere	Temperature range, °C	Interaction character, products and/or compatibility	Reference
ZrC _{1-x} -TiC _{1-x} - δ-WC _{1±x} -C	-	1300-1800	Isothermal sections with miscibility gaps determined	[1074]
ZrC _{1-x} -VC _{1-x} - δ-WC _{1±x} -C	-	1300-1500	Isothermal sections with miscibility gaps determined	[1074]
ZrC _{1-x} -C-Fe			See Table 5.28	
ZrC _{1-x} -C-Fe-Mn			See Table 5.28	
ZrC _{1-x} -C-Ni			See Table 5.28	
ZrC _{1-x} -Cd	Air	450	The contact interaction is very weak: after 10 h exposure the content of Zr in the melt achieved 0.01%	[30, 32, 33, 42, 45, 48, 63]
ZrC _{1-x} -Ce			See Table 5.27	
ZrC _{1-x} -α/ε-Co	-	800	ZrC _{1-x} is in equilibrium with all Zr intermet- allides, α-Zr and α-Co; the solid solubility of Co in ZrC _{1-x} is negligible	[1, 4, 32, 33, 42, 45, 48, 63, 200, 849- 855, 901, 1226, 1230, 1233]
	-	~1340-1410	Eutectic ZrC _{1-x} -α-Co, the mutual solubili- ties between the components are low; the eutectic structure is plate-like mainly	
	-	1500	Liquid metal penetrates into bulk ZrC _{1-x} (two-phase contact zone) with formation of solid solutions; the contact interaction is very intensive (5 h exposure), mutual ex- change (dissolution) between the solid and liquid phases was observed	
	N ₂ + CO	1550	Noticeable interaction between the compo- nents (0.2 h exposure)	
	-	>1550	ZrC _{1-x} materials are corroded by liquid Co and Co containing melts See also Table 5.28 See also section C-Co-Zr in Table I-2.14	
ZrC _{1-x} -Co-Ni			See Table 5.28	
ZrC _{1-x} -Co-Ni-W			See Table 5.28	
ZrC _{1-x} -HfC _{1-x} - Co			See section HfC _{1-x} -ZrC _{1-x} -Co in Table 3.19 See also section C-Co-Hf-Zr in Table I-2.14	
ZrC _{1-x} -NbC _{1-x} - Co			See section NbC _{1-x} -ZrC _{1-x} -Co in Table 4.18 See also section C-Co-Nb-Zr in Table I-2.14	
ZrC _{1-x} -TaC _{1-x} - Co			See section TaC _{1-x} -ZrC _{1-x} -Co in Table 2.21 See also section C-Co-Ta-Zr in Table I-2.14	
ZrC _{1-x} -TiC _{1-x} - Co	-	1320	Eutectic (Zr,Ti)C _{1-x} (x = 0.19)-(Ti,Zr)C _{1-x} (x = 0.20)-α-Co See also section C-Co-Ti-Zr in Table I-2.14	[855, 1074]

(continued)

Table 5.24 (continued)

System	Atmosphere	Temperature range, °C	Interaction character, products and/or compatibility	Reference
ZrC _{1-x} -TiC _{1-x} -VC _{1-x} -δ-WC _{1±x} -Co	-	1200-1800	General consideration of the system	[1074]
ZrC _{1-x} -TiC _{1-x} -δ-WC _{1±x} -Co	-	1300-1500	General consideration of the system; a miscibility gap in the ZrC _{1-x} -TiC _{1-x} system in the presence of Co is determined; spinodal decomposition during the sintering process of alloys with Zr/Ti ratios 3:7 and 5:5 and 10-30 mol.% of W carbide was revealed	[1074, 1375, 1526]
ZrC _{1-x} -VC _{1-x} -Co	-	1300	Eutectic (Zr,V)C _{1-x} (x = 0.19)-(V,Zr)C _{1-x} (x = 0.17)-α-Co <i>See also</i> section C-Co-V-Zr in Table I-2.14	[855, 1074]
ZrC _{1-x} -VC _{1-x} -δ-WC _{1±x} -Co	-	1300-1500	General consideration of the system; a miscibility gap in the ZrC _{1-x} -VC _{1-x} system in the presence of Co is determined	[1074]
ZrC _{1-x} -Cr	-	1120-1140 (?)	Eutectic ZrC _{1-x} (x = 0.03)-Cr; the max. solubility of Cr in ZrC _{1-x} is 2.3-8.5 mol.% (?) and that of ZrC _{1-x} in Cr is ≤ 0.1 mol.%	[1, 4, 30, 32, 33, 42, 45, 48, 63, 200, 856-864, 901, 995, 1059, 1429, 1523]
	Vacuum, 10 ⁻³ Pa	1200-1300	Almost no interaction between the components was observed during 100 h exposure	
	Vacuum, 10 ⁻³ Pa	1400	Formation of Cr ₂₃ C _{6±x} (the impurities contained in metallic Cr were found to affect the interaction in the system considerably)	
	Vacuum, Ar	1730-1805	Eutectic ZrC _{1-x} (x = 0.10)-Cr; the max. solubility of Cr in ZrC _{1-x} is ~1.5-3.0 mol.% and that of ZrC _{1-x} in Cr is 1.3 mol.%; ZrC _{1-x} is in equilibrium with all Cr carbides and intermetallide and metallic Cr	
	-	-	Stable and compatible with each other as cermet components	
	-	1830	The contact interaction is intensive (5 h exposure)	
	Ar (pure)	~1860	ZrC _{1-x} is resistant to Cr melts (contact zone thickness <0.5 mm, at long-term exposures)	
	N ₂ + CO	1900	No chemical interaction during 0.2 h exposure	
	-	>1900	ZrC _{1-x} materials are corroded by liquid Cr and Cr containing melts Data available in literature are controversial <i>See also</i> section C-Cr-Zr in Table I-2.14 <i>See</i> Table 5.28	
	ZrC _{1-x} -Cr-Cu-Fe			

(continued)

Table 5.24 (continued)

System	Atmosphere	Temperature range, °C	Interaction character, products and/or compatibility	Reference
ZrC _{1-x} -Cr-Fe			See Table 5.28	
ZrC _{1-x} -Cr-Ni			See Table 5.28	
ZrC _{1-x} -Cr ₂₃ C _{6±x} -Cr	-	1575	Eutectic ZrC _{1-x} -Cr ₂₃ C _{6±x} -Cr	[860-863, 917-919]
			See also section ZrC _{1-x} -Cr ₂₃ C _{6±x} in Table 5.25	
			See also section C-Cr-Zr in Table I-2.14	
ZrC _{1-x} -Cs	Cs vapour	1100-1800	Solubility of Cs in ZrC _{1-x} decreases with increasing temperature from ~5 × 10 ⁻² mol.% at 1100 °C to ~7 × 10 ⁻⁵ mol.% at 1800 °C	[33, 96, 489, 495, 500, 504, 865-867]
	Cs vapour	~1300-1700	Only adsorption interaction was observed on the surface of carbide powder (exposure for many hours)	
	Cs vapour	1400	Surface carbide composition unchanged after many hours of heating exposure	
	Cs vapour, ~13 Pa	~2000	No effect upon structural characteristics of ZrC _{1-x} and its thermionic emission parameters (some tens of hours exposure), adsorption character of interaction	
	Cs vapour	-	Chemical reaction with deposited by vacuum evaporation carbide layers (composition and structure uncontrolled) is reported	
	-	-	The interaction with Cs as a fission product and O released during fission is predicted to form Cs ₂ ZrO ₃	
			See also Table 5.27	
			See also section C-Cs-Zr in Table I-2.14	
ZrC _{1-x} -Cu	Vacuum	300-800	Nanocrystalline ZrC _{1-x} films (mean grain size <5 nm) grown on Si(100) thermally stable in contact with Cu (0.5 h exposure)	[1, 33, 48, 850, 868, 944, 989, 1060, 1233, 1527]
	-	1100	Weak contact interaction (5 h exposure); the partial dissolution of ZrC _{1-x} in Cu melt was observed	
	-	>1100	ZrC _{1-x} materials migrate into molten Cu	
	Vacuum, 0.3 Pa	1100-1300	Formation of Zr _x Cu _y C _z (?) in the presence of W and/or δ-WC _{1±x}	
	Ar	<1150	No chemical interaction	
			See also Table 5.28	
			See also section C-Cu-Zr in Table I-2.14	
ZrC _{1-x} -Cu-Fe-Si			See Table 5.28	
ZrC _{1-x} -Cu-Ni			See Table 5.28	
ZrC _{1-x} -Cu-V-Zr			See Table 5.28	
ZrC _{1-x} -Cu-Zr			See Table 5.28	
ZrC _{1-x} -Eu			See Table 5.27	

(continued)

Table 5.24 (continued)

System	Atmosphere	Temperature range, °C	Interaction character, products and/or compatibility	Reference
ZrC _{1-x} -α/γ/δ-Fe	-	1100	Formation of Zr ₃ Fe ₃ C _{1-x} , solubility of ZrC _{1-x} in γ-Fe is ≤ 0.5 mol.%; ZrC _{1-x} is in equilibrium with Fe and Fe-Zr intermetallides	[1, 4, 32, 33, 48, 63, 168, 200, 850, 869, 873, 901,
	-	1200	Formation of a new phase in the contact zone between ZrC _{1-x} powder and compact Fe	1025, 1026,
	-	1400	Formation of a liquid phase in the contact zone between ZrC _{1-x} powder and compact Fe	1076, 1226,
	-	~1380–1480	Eutectic ZrC _{1-x} -δ-Fe, the max. solid solubility of ZrC _{1-x} in δ-Fe is ≤ ~1 mol.%; eutectics structure is the complex system of colonies, which consists of the carbide plates (less rarely – filaments) located in the metallic matrix, in the hypereutectic alloys primary carbide crystals have predominantly cubic forms (along with them dendrite crystals are also observed)	1230, 1233, 1439, 1531]
	Vacuum	1550	Liquid Fe penetrates into the bulk dense carbide (depth of penetration – ~300 μm) and forms solid solutions (in the contact zone carbide has a changed lattice parameter); mutual exchange (dissolution) between the solid and liquid phases was observed	
	Ar	1550	Liquid Fe penetrates into the bulk dense carbide (depth of penetration – ~40 μm) and forms solid solutions	
	-	>1550	ZrC _{1-x} materials are corroded by liquid Fe and Fe containing melts	
	-	1560	The contact interaction is very intensive (5 h exposure)	
	-	-	According to DFT calculations the ZrC _{-1,0} (100)/ Fe (110) interface is well lattice-matched (~1.7%) producing a fairly smooth interface with little structural relaxation; semicoherent interfacial energy at relaxed interface – 0.66 J m ⁻²	
	-	-	See also Table 5.28 See also section C-Fe-Zr in Table I-2.14	
ZrC _{1-x} -Fe-Ni			See Table 5.28	
ZrC _{1-x} -Fe-Si			See Table 5.28	
ZrC _{1-x} -Ga	Ar	<800	No chemical interaction	[1, 850]
			See also Table 5.28	
ZrC _{1-x} -Ge	Ar	<1000	No chemical interaction	[1, 850]
			See also Table 5.28	
ZrC _{1-x} -Al ₄ C ₃ -Ge	-	-	Formation of Zr ₂ Al ₃ (Al,Ge)C ₅ and Zr ₃ Al ₃ (Al,Ge)C ₆ (intergrowth structures, consisting of Zr _m C _{m+1} (NaCl-type) slabs separated by (Al ₄₋₂ Ge ₂)C ₄ (Al ₄ C ₃ -type) layers)	[905]

(continued)

Table 5.24 (continued)

System	Atmosphere	Temperature range, °C	Interaction character, products and/or compatibility	Reference
ZrC _{1-x} -Hf			See section C-Hf-Zr in Table I-2.14	
ZrC _{1-x} -In	Ar	<250	No chemical interaction	[1, 836-839, 850, 1530]
	-	-	Formation of Zr ₂ InC (M _{n+1} AX _n -phase) See also Table 5.28	
			See also section C-In-Zr in Table I-2.14	
ZrC _{1-x} -TiC _{1-x} -In	-	-	Formation of (Zr,Ti) ₂ InC (M _{n+1} AX _n -phase solid solution); (Zr _{0.5} Ti _{0.5}) ₂ InC was synthesized	[837, 838, 1404, 1405]
ZrC _{1-x} -Ir	-	-	In the reaction with metallic Ir carbide is decomposed to form graphite and intermetallic ZrIr _{3-x} (with defective ordered structure)	[200, 990, 991, 1374]
	-	1500-2000	ZrC _{1-x} is in equilibrium with ZrIr _{3±x} and (Zr,Ir) alloys	
	-	~2030-2130	Eutectic (estimated) ZrC _{1-x} (x ≈ 0.18)-Ir See also section C-Ir-Zr in Table I-2.14	
ZrC _{1-x} -K	-	~2000	No chemical reaction observed, no effect upon structural characteristics of ZrC _{1-x} and its thermionic emission parameters (some tens of hours exposure)	[504, 866, 1031, 1052]
ZrC _{1-x} -ZrB _{2±x} -La	Vacuum	~1800	The addition of La was found to be a very effective aid for spark-plasma sintering, but not useful for the conventional sintering process, because of the intensive evaporation of La in those conditions	[1453, 1457]
ZrC _{1-x} -Li	-	-	The results of screening tests on ZrC _{1-x} for molten Li are given	[1024, 1025]
ZrC _{1-x} -Mg	-	>650	ZrC _{1-x} materials migrate into Mg melts	[48, 63, 989, 995]
	-	700-800	Weak contact interaction (2 h exposure)	
	-	>800	ZrC _{1-x} materials were corroded intensively by liquid Mg and Mg containing melts	
ZrC _{1-x} -α/β/γ/δ-Mn	Vacuum, Ar	1250	The mutual exchange (dissolution) between the solid (ZrC _{1-x}) and liquid (Mn) phases was observed in the contact zone	[1, 33, 48, 63, 850, 1233]
	-	1270-1300	Intensive contact interaction with formation of eutectic alloys and solid solutions (5 h exposure)	
	-	>1300	ZrC _{1-x} materials are corroded by liquid Mn and Mn containing melts intensively	
	-	-	The effect of Mn as an additive for hot-pressing process was studied See also Table 5.28	
			See also section C-Mn-Zr in Table I-2.14	

(continued)

Table 5.24 (continued)

System	Atmosphere	Temperature range, °C	Interaction character, products and/or compatibility	Reference
ZrC _{1-x} -Mo	-	1100	ZrC _{1-x} layer (thickness – 4 μm) on Mo wire is intact (compatible) after 150 h exposure	[1, 4, 30, 32, 33, 63,
	-	1250	The max. solid solubility of ZrC _{1-x} in Mo is ~0.6 mol.%	158, 200, 213, 377,
	-	1300	Under pressure 5 MPa a diffusion welded joint between ZrC _{1-x} and Mo parts is produced (5–15 min exposure)	870–872, 885, 901, 922, 1037–
	Vacuum	1900–2000	The initiation of interaction between powdered (or sintered) carbide and compact dense metal with the formation of Mo solid solution in ZrC _{1-x} (2–5 h exposure)	1043, 1051, 1058, 1230,
	-	1970	The max. solid solubility of ZrC _{1-x} in Mo is ~1.0 mol.%	1243, 1429, 1460, 1463, 1523, 1541]
	-	2000–2200	Compact dense Mo and ZrC _{1-x} are compatible with each other; only weak diffusion interaction is observed (2–5 h exposure)	
	-	2200	No interaction between dispersed ZrC _{1-x} inclusions (up to 10%) with Mo matrix	
	-	-	Stable and compatible with each other as cermet components	
	-	>2200	The noticeable interaction of powdered carbide with compact dense metal is observed	
	-	~2240–2310	Eutectic ZrC _{1-x} -Mo; the max. solid solubility of Mo in ZrC _{1-x} is >10 mol.% and that of ZrC _{1-x} in Mo is ~3.2 mol.%	
-	>2650	ZrC _{1-x} materials are corroded by liquid Mo and Mo containing melts		
ZrC _{1-x} -Mo-Ni	Vacuum, 0.1 Pa	1450	<i>See also</i> section C-Mo-Zr in Table I-2.14 The contact interaction of compact dense ZrC _{1-x} (x = 0.04) with Ni – 25% Mo melt leads to the preferential dissolution of C; after cooling the needle-like isolations based on β-Mo _{2±x} C (hexagonal) phase, surrounded by metal-semicarbide eutectics, are formed in the metal melt (Ni _{1-0.91} Mo _{0.08} Zr _{0.004} C _{<0.005}) in parallel with Ni-ZrNi _{5±x} eutectics	[1525]
ZrC _{1-x} -Mo-Re	Vacuum	2450	No interaction in the contact zone (1 h exposure) between compact dense ZrC _{1-x} materials and Mo – 40% Re alloy	[993]
	He	2500	Interaction in the contact zone (15 min. exposure) between the compact dense materials	
ZrC _{1-x} -Mo-W	-	1200–2000	The solubility of ZrC _{1-x} in the Mo-W solid solution decreases with fall in temperature; homogeneity range of the solid solution steadily decreases with rise in W content	[943, 1429]
	-	-	Stable and compatible with each other as cermet components <i>See also</i> section C-Mo-W-Zr in Table I-2.14	

(continued)

Table 5.24 (continued)

System	Atmosphere	Temperature range, °C	Interaction character, products and/or compatibility	Reference
ZrC _{1-x} -TiC _{1-x} -Mo-Ni	Vacuum, 0.05 Pa	1450	The interaction of Zr _{0.25} Ti _{0.75} C _{0.96} phase with Ni – 20–25% Mo melt is characterized by preferential dissolution of C and subsequent precipitation of Zr _{0.01} Ti _{0.60} Mo _{0.40} C _{1-x} (from the melt saturated with Zr, Ti and C); the interaction of the compositions, having higher Zr content in them, with Ni-Mo melts such as Zr _{0.50} Ti _{0.50} C _{0.96} and Zr _{0.76} Ti _{0.24} C _{0.95} , does not vary considerably, but after cooling in these cases the bulk content of ZrNi _{5±x} intermetallide in solidified eutectics increases	[1066, 1525]
ZrC _{1-x} -TiC _{1-x} -δ-TiN _{1±x} -Mo-Ni	Vacuum, 0.01 Pa	1450	The interaction of complex carbonitrides Zr _{0.06-0.20} Ti _{0.80-0.94} C _{0.50-0.80} N _{0.20-0.50} with Ni – 20% Mo melt leads to the accelerated incongruent dissolution of the components, such as C and Zr, preferentially; during the cooling procedure at the ceramic-metal interface, primary eutectic precipitates on the basis of β-Mo _{2±x} C (hexagonal) and (Ti,Mo)(C,N) _{1-x} (cubic) phases and ZrNi _{5±x} and TiNi ₃ intermetallides are formed (Zr is mainly concentrated in the metallic solid solutions and intermetallides)	[1524]
ZrC _{1-x} -UC _{1±x} -Mo	–	~2000	(Zr _{0.50} U _{0.50})C _{1±x} reacts vigorously with metallic Mo	[928]
ZrC _{1-x} -Nb	Vacuum	900–1500	Interaction in the powdered mixtures (mean grain size – 1–2 μm) of components leads to the formation of β-Nb _{2+x} C	[1, 30, 32, 33, 42, 63, 213, 377, 901, 922, 1005, 1033–1036, 1067, 1150, 1230]
	–	1400	Under pressure 5 MPa a diffusion welded joint between ZrC _{1-x} and Nb is produced (5–15 min exposure)	
	Vacuum	1400–1600	The weak interaction of powdered carbide with compact dense metallic Nb is observed (5 h exposure); the formation of solid solutions of C in Nb in the contact zone between the dense compact components	
	–	1600–1800	The weak interaction of powdered carbide with compact dense metallic Nb results in the formation of ZrC _{1-x} -NbC _{1-x} solid solutions	
	–	2000–2200	The noticeable interaction with the formation of ZrC _{1-x} -NbC _{1-x} solid solutions; the max. solid solubility of Nb in ZrC _{1-x} is ~20–40 mol.%	
	Vacuum	2120	Eutectic ZrC _{1-x} -Nb	
	–	>2470	ZrC _{1-x} materials are corroded by liquid Nb and Nb containing melts	
			See also Table 5.27	
			See also section C–Nb–Zr in Table I-2.13	

(continued)

Table 5.24 (continued)

System	Atmosphere	Temperature range, °C	Interaction character, products and/or compatibility	Reference
ZrC _{1-x} -UC _{1±x} -Nb	-	~2000	(Zr _{0.50} U _{0.50})C _{1±x} reacts vigorously with metallic Nb <i>See also</i> section C-Nb-U-Zr in Table I-2.14	[928]
ZrC _{1-x} -Ni	-	700	The max. solid solubility of ZrC _{1-x} in Ni is ~0.6 mol.%	[1, 4, 30, 32, 33, 42,
	-	1100	Formation of a liquid phase in the contact zone between a carbide powder and compact dense Ni; the max. solid solubility of ZrC _{1-x} in Ni is ~1 mol.%	45, 48, 63, 200, 850, 874-880, 901, 1002,
	Ar	1160-1185	Formation of a liquid phase in the ZrC _{1-x} -Ni powdered mixture with mean grain size ~50 μm	1003, 1025, 1026, 1063-1065, 1150,
	-	~1210-1350	Eutectic ZrC _{1-x} -Ni; the max. solid solubility of ZrC _{1-x} in Ni is ~3.5 mol.% and that of Ni in ZrC _{1-x} is ~5 mol.%	1226, 1230, 1233, 1351, 1525]
	-	1250	The max. solid solubility of ZrC _{1-x} in Ni is ~1.7 mol.%	
	Vacuum	~1280	Eutectic ZrC _{1-x} -Ni (C = 0.7-7.2%); the contact reaction leads to the penetration of eutectic alloy into the carbide substrate, the depth of penetration decreases with increasing C content in Ni-C alloy	
	-	1350-1400	The max. solid solubility of Ni in ZrC _{1-x} is ~3.5-4.3 mol.%; the addition of C (up to 7%) to Ni inhibits the penetration of Ni into the bulk ZrC _{1-x} and reduces the depth of the resultant diffusion zone in the contact, the interfacial reaction leads to the formation of Ni-based solid solutions, carbide-metal eutectics and intermetallide ZrNi _{5±x} phase (the variation of Ni concentration between the boundary of a grain and its core obeys a parabolic law)	
	-	1450-1460	The contact interaction is very intensive (5 h exposure); the mutual exchange (dissolution) between the solid (ZrC _{1-x}) and liquid (Ni) phases was observed in the contact zone	
	N ₂ + CO	1500	Intensive interaction with the dissolution of Ni and formation solid solutions (in the contact zone carbide has a changed lattice parameter) after 0.2 h exposure	
-	>1500	ZrC _{1-x} materials are corroded by liquid Ni and Ni containing melts Data available in literature are controversial <i>See also</i> Table 5.28 <i>See also</i> section C-Ni-Zr in Table I-2.14		

(continued)

Table 5.24 (continued)

System	Atmo- sphere	Temperature range, °C	Interaction character, products and/or compatibility	Reference
ZrC _{1-x} -Ni-P			See Table 5.28	
ZrC _{1-x} -Ni-W			See Table 5.28	
ZrC _{1-x} -HfC _{1-x} - Ni			See section HfC _{1-x} -ZrC _{1-x} -Ni in Table 3.19	
ZrC _{1-x} - β -Mo _{2±x} C- TiC _{1-x} -Ni	Vacuum	1250	See also section C-Hf-Ni-Zr in Table I-2.14 The effect of ZrC _{1-x} addition on cermet sintering was studied	[1023]
ZrC _{1-x} -NbC _{1-x} - Ni			See section NbC _{1-x} -ZrC _{1-x} -Ni in Table 4.18	
ZrC _{1-x} -TaC _{1-x} - Ni			See also section C-Nb-Ni-Zr in Table I-2.14 See section TaC _{1-x} -ZrC _{1-x} -Ni in Table 2.21	
ZrC _{1-x} -TiC _{1-x} - Ni	-	~1160-1190	Eutectic (Zr,Ti)C _{1-x} -(Ti,Zr)C _{1-x} -Ni (cast alloys show a tendency to the crystallization in metastable state when the carbide phase does not decompose into two solid solutions)	[876, 880, 1063-1065, 1535]
	Ar	1230	Formation of a liquid phase in the powdered mixture Zr _{0.25} Ti _{0.75} C _{1-x} -Ni	
	Vacuum, 0.01-0.1 Pa	1450	Zr _{0.25} Ti _{0.75} C _{1-x} phase has a higher dissolu- tion rate in molten Ni; preferentially C and Zr are transferred into the melt, when attain- ing composition Zr _{0.06} Ti _{0.94} C _{<0.96} the dissolution becomes congruent	
ZrC _{1-x} -TiC _{1-x} - δ -TiN _{1±x} -Ni	Vacuum, 0.01-0.1 Pa	1450	The interaction of complex carbonitrides Zr _{0.06-0.20} Ti _{0.80-0.94} C _{0.50-0.80} N _{0.20-0.50} with molten Ni leads to the incongruent dissolution of the components, preferentially - C and Zr; so the outer layers of complex carbonitride grains are enriched with N and Ti - up to Zr _{0.01-0.02} Ti _{0.98-0.99} C _{0.05-0.15} N _{0.85-0.95} and delaminated, the metallic melts have a hypoeutectic structure with primary precipitates of Ni based phase and ternary eutectics (no intermetallic phases were observed)	[1435, 1524]
ZrC _{1-x} -TiC _{1-x} - δ -TiN _{1±x} - δ -WC _{1±x} -Ni	Vacuum	1450	The formation of complex monocarbo- nitride (Zr,Ti,W)(C,N) _{1-x} phases with core-rim microstructures	[945]
ZrC _{1-x} -TiC _{1-x} - δ -TiN _{1±x} -TiO _{1±x} - Ni	Vacuum, 10 ⁻¹ Pa	1450	The interaction of Zr _{0.05} Ti _{0.95} C _{0.50} N _{0.40} O _{0.10} oxycarbonitride phase with Ni is considered	[1435]
ZrC _{1-x} - δ -WC _{1±x} - Ni	-	1000	General consideration of the system; regions of solid solutions based on the individual components are not large (~6-8 mol.%) See also section C-Ni-W-Zr in Table I-2.14	[875]

(continued)

Table 5.24 (continued)

System	Atmosphere	Temperature range, °C	Interaction character, products and/or compatibility	Reference
ZrC _{1-x} -UC _{1±x} -Ni	-	-	The effect of Ni as an additive for hot-pressing process was studied	[1357]
ZrC _{1-x} -ZrB _{2±x} -Ni	-	-	Plasma-sprayed coatings were fabricated and studied; the positive effect of Ni on the densification during reactive hot-pressing process was observed	[886, 1416, 1458, 1459]
ZrC _{1-x} -Os	-	1500	ZrC _{1-x} is in equilibrium with metal Os; the mutual solid solubilities of ZrC _{1-x} and Os are low, η -Zr ₄ Os ₂ C _{1-x} is formed	[200, 990, 991, 1531]
	-	-	ZrC _{1-x} is decomposed to form graphite and solid solution of Zr in metallic Os <i>See also</i> section C-Os-Zr in Table I-2.14	
ZrC _{1-x} -Pb	Ar	≤400	No chemical interaction (10 h exposure)	[1, 30, 32, 33, 42, 45, 48, 63, 836-839, 850]
	Air	450	Traces of Zr were revealed in liquid metal after 10 h exposure	
	-	-	Formation of Zr ₂ PbC (M _{n+1} AX _n -phase) <i>See also</i> Table 5.28 <i>See also</i> section C-Pb-Zr in Table I-2.14	
ZrC _{1-x} -Pd	-	≥1300	The interaction with Pd results in the formation of ordered ZrPd ₃ intermetallide phase and C (graphite) precipitation <i>See also</i> Table 5.27 <i>See also</i> section C-Pd-Zr in Table I-2.14	[200, 1014]
ZrC _{1-x} -Pt	-	≥1500	The interaction with Pt results in the formation of ordered ZrPt _{3±x} intermetallide phase and C (graphite) precipitation <i>See also</i> section C-Pt-Zr in Table I-2.14	[200, 990, 991]
ZrC _{1-x} -Pu	-	-	<i>See</i> section C-Pu-Zr in Table I-2.14 ZrC _{1-x} -UC _{1±x} -Pu <i>See</i> section C-Pu-U-Zr in Table I-2.14	
ZrC _{1-x} -Rb	-	-	ZrC _{1-x} materials are stable in liquid and vapourized Rb in the wide temperature range	[63]
ZrC _{1-x} -Re	-	1900	The solubility of Re in carbide is ~3 mol.% and that of ZrC _{1-x} in Re is <0.5 mol.%	[1, 200, 872, 881, 882, 901, 993, 1033, 1047, 1429]
	Vacuum	2500	No interaction in the contact zone between the compact dense materials (1 h exposure)	
	-	-	Stable and compatible with each other as cermet components	
	-	~2540-2670	Eutectic ZrC _{1-x} -Re; the max. solid solubility of Re in ZrC _{1-x} is 1.7 mol.% Data available in literature are controversial <i>See also</i> section C-Re-Zr in Table I-2.14	
ZrC _{1-x} -UC _{1±x} -Re	-	2100	(Zr _{0.5} U _{0.5})C _{1±x} is compatible with metallic Re (up to ~0.5 h exposure) <i>See also</i> section C-Re-U-Zr in Table I-2.14	[928]

(continued)

Table 5.24 (continued)

System	Atmosphere	Temperature range, °C	Interaction character, products and/or compatibility	Reference
ZrC _{1-x} -Rh	-	≥1500	The interaction results in the formation of ZrRh _{3±x} (or ZrRh ₃ C _x) and C (graphite); practically, no solubility of Rh in ZrC _{1-x} <i>See also</i> section C-Rh-Zr in Table I-2.14	[200]
ZrC _{1-x} -Ru	-	≥1500	The interaction of non-stoichiometric ZrC _{1-x} results in the formation of ZrRu ₃ C _{1-x} ($x \approx 0.3$); quasi-stoichiometric phases are in equilibrium with Ru	[200]
	-	~1800	Eutectic ZrC _{1-x} -Ru <i>See also</i> Table 5.27	
	-	-	<i>See also</i> section C-Ru-Zr in Table I-2.14	
ZrC _{1-x} -S	-	-	Formation of Zr ₂ SC (M _{n+1} AX _n -phase) <i>See also</i> section C-S-Zr in Table I-2.14	[836-838]
ZrC _{1-x} -Sb	Ar	<700	No chemical interaction <i>See also</i> Table 5.28	[1, 850]
ZrC _{1-x} -Sc			<i>See</i> section C-Sc-Zr in Table I-2.14	
ZrC _{1-x} -Si	Vacuum	300-800	Nanocrystalline ZrC _{1-x} films (mean grain size < 5 nm) thermally stable (0.5 h exposure) in contact with Si substrate	[1, 30, 32, 33, 42, 45, 48, 63, 76, 883, 884, 902, 995, 1025, 1026, 1060, 1083, 1233, 1245]
	Ar	800-1000	Weak interaction in the powdered mixtures of components with the formation of ZrSi ₂ (1 h exposure, growing from 1.2 to 12.1% with increasing temperature)	
	Ar	1100	The interaction in the powdered mixtures results in the formation of α -ZrSi (17%) and small amounts of β -SiC (1%)	
	Ar	1400-1700	The intensive interaction in the powdered mixtures results in the formation of α/β -ZrSi and β -SiC (0.2-1.0 h exposure, no non-combined Si in the products)	
		1410	The mutual exchange (dissolution) between the solid (ZrC _{1-x}) and liquid (Si) phases was observed in the contact zone	
	-	>1450-1500	ZrC _{1-x} materials are corroded by liquid Si and Si containing melts intensively <i>See also</i> Table 5.28 <i>See also</i> section C-Si-Zr in Table I-2.14	
ZrC _{1-x} -Al ₄ C ₃ -Si	-	-	Formation of Zr(Al _{1-x} Si _x) ₈ C ₇ , Zr(Al _{1-x} Si _x) ₄ C ₄ , Zr ₂ (Al _{1-x} Si _x) ₄ C ₅ and Zr ₃ (Al _{1-x} Si _x) ₄ C ₆ <i>See also</i> section ZrC _{1-x} -SiC-Al in this table <i>See also</i> section ZrC _{1-x} -Al ₄ C ₃ -SiC in Table 5.25	[826, 827, 831-833, 904, 1072, 1082]

(continued)

Table 5.24 (continued)

System	Atmosphere	Temperature range, °C	Interaction character, products and/or compatibility	Reference
ZrC _{1-x} -Sn	Air -	≤350 -	No chemical interaction (10 h exposure) Formation of Zr ₂ SnC (M _{n+1} AX _n -phase) and Zr ₅ Sn ₃ C (?) <i>See also Table 5.28</i> <i>See also section C-Sn-Zr in Table I-2.14</i> <i>See Table 5.27</i>	[1, 30, 32, 33, 45, 48, 63, 836-839, 850, 1529]
ZrC _{1-x} -Sr ZrC _{1-x} -Ta	- - - Vacuum -	1600-2000 1900 2000-2200 >2200 >3000	No interaction in the contact zone between the compact dense materials (2 h exposure) Under pressure 5 MPa a diffusion welded joint between ZrC _{1-x} and Ta is produced (5-15 min exposure) Weak interaction in the contact zone between the compact dense materials (2-5 h exposure) The interaction of powdered carbide with compact dense metal results in the formation of ZrC _{1-x} -TaC _{1-x} solid solutions ZrC _{1-x} materials are corroded by liquid Ta and Ta containing melts <i>See also section C-Ta-Zr in Table I-2.14</i>	[1, 32, 33, 42, 63, 76, 200, 213, 886-888, 901, 922, 995, 1044, 1045, 1081, 1230]
ZrC _{1-x} -UC _{1±x} -Ta	-	~2100	(Zr _{0.50} U _{0.50})C _{1±x} is compatible with metallic Ta for periods of up to 35 min <i>See also section C-Ta-U-Zr in Table I-2.14</i>	[928]
ZrC _{1-x} -Tc ZrC _{1-x} -α/β-Th	-	1500	ZrC _{1-x} is in equilibrium with both α-Th and β-Th metal modifications; the mutual solid solubilities of the components are low <i>See also section C-Th-Zr in Table I-2.14</i>	[200, 950-952, 1006]
ZrC _{1-x} -α/β-Ti	- Vacuum, < 7 × 10 ⁻⁴ Pa	1730 1850	The contact interaction is very intensive (5 h exposure) ZrC _{1-x} materials are highly soluble in the melt Ti-Zr-C alloys formed at the interface (powerful solvent action of liquid Ti) <i>See also section C-Ti-Zr in Table I-2.14</i>	[48, 200, 888-893]
ZrC _{1-x} -Tl	Ar -	<400 -	No chemical interaction Formation of Zr ₂ TlC (M _{n+1} AX _n -phase) <i>See also Table 5.28</i> <i>See also section C-Tl-Zr in Table I-2.14</i>	[1, 836-839, 850]
ZrC _{1-x} -α/β/γ-U	-	>1150	ZrC _{1-x} materials are corroded by liquid U and U containing melts <i>See also section C-U-Zr in Table I-2.14</i>	[63]

(continued)

Table 5.24 (continued)

System	Atmosphere	Temperature range, °C	Interaction character, products and/or compatibility	Reference
ZrC _{1-x} -V	-	1685	Eutectic (Zr,V)C _{1-x} -(V,Zr)	[4, 48, 63, 1429, 1523]
	-	1730	Contact interaction is very intensive (5 h exposure)	
	-	>1900	ZrC _{1-x} materials are corroded by liquid V and V containing melts	
	-	-	Stable and compatible with each other as cermet components <i>See also</i> section C-V-Zr in Table I-2.14	
ZrC _{1-x} -W	-	1600-2000	No interaction between powdered ZrC _{1-x} and compact dense metallic W	[1, 4, 32, 33, 200, 213, 377, 576, 871, 894-899, 901, 922, 993, 1041, 1046, 1230, 1243, 1362, 1429, 1523, 1549]
	-	1800	Under pressure 5 MPa a diffusion welded joint between ZrC _{1-x} and W parts is produced (5-15 min exposure)	
	Vacuum	2200	The interaction between powdered (or sintered) ZrC _{1-x} and compact dense metal leads to the formation of W-C solid solutions (2-5 h exposure)	
	-	-	Stable and compatible with each other as cermet components	
	He	2500	No interaction in the contact zone between the compact dense materials (2 h exposure)	
	-	~2630-2800	Eutectic ZrC _{1-x} -W; the max. solubility of W in ZrC _{1-x} is ~7 mol.% <i>See also</i> section C-W-Zr in Table I-2.14	
ZrC _{1-x} -UC _{1±x} -W	-	~2100	(Zr _{0.50} U _{0.50})C _{1±x} is compatible with metallic W for periods of up to 35 min <i>See also</i> section C-U-W-Zr in Table I-2.14	[928]
ZrC _{1-x} -γ-W _{2±x} C-W	-	2620	Eutectic ZrC _{1-x} -γ-W _{2±x} C-W	[894, 896, 899]
ZrC _{1-x} -Zn	Ar	550	<i>See also</i> section C-W-Zr in Table I-2.14 The interaction is weak: after 6 h exposure the content of Zr in the melt achieved 0.02%	[30, 32, 33, 42, 45, 48, 63]
	-	>550	ZrC _{1-x} materials are corroded by liquid Zn and Zn containing melts slightly	
ZrC _{1-x} -α/β-Zr	-	940	Weak contact interaction (170 h exposure)	[1, 10, 48, 126, 600, 900, 901, 1005, 1057, 1085, 1370, 1371, 1375]
	-	1300-1700	The formation of solid solutions of C in Zr in the contact zone (the microhardness of carbide decreases and that of metal increases)	
	-	1805-1835	Eutectic ZrC _{1-x} -β-Zr with actual compositions ZrC _{0.49-0.57} -Zr(C _{-0.02})	
	-	1950	The contact interaction is very intensive (5 h exposure)	
-	~2000	The molten metallic Zr caused a very limited dissolution of ZrC _{1-x} <i>See also</i> section C-Zr in Table I-2.13		

(continued)

Table 5.24 (continued)

System	Atmosphere	Temperature range, °C	Interaction character, products and/or compatibility	Reference
ZrC _{1-x} -ZrN _{1±x} - α/β -Zr	-	1150	Monocarbonitride phases with \sim ZrC _{0.56} - \sim ZrC _{0.33} N _{0.23} compositions are in the equilibrium with metallic solid solutions ranged from β -Zr(C _{-0.01}) to β -Zr(C _{-0.01} ,N _{-0.02}), while monocarbonitride phases with \sim ZrC _{0.33} N _{0.23} - \sim ZrN _{0.56} compositions are in the equilibrium with metallic solid solutions ranged from α -Zr(C _{-0.02} ,N _{-0.14}) to α -Zr(N _{-0.30}) <i>See also</i> section C-N-Zr in Table I-2.14	[126, 962, 994]
ZrC _{1-x} -UC _{1±x} - U-Zr	-	1700	The composition of (Zr,U)C _{1±x} in the equilibrium with Zr-U alloy varies with increasing U content rapidly from ZrC _{0.62} to (Zr,U)C _{0.88} and remains constant up to UC _{0.88} <i>See</i> section C-U-Zr in Table I-2.14	[958]
ZrC _{1-x} -ZrB _{2±x} - α/β -Zr	-	~1615-1650	Eutectic ZrC _{1-x} -ZrB _{2±x} - β -Zr <i>See also</i> section C-B-Zr in Table I-2.14	[200, 840, 843, 845, 1086]

^aThe parameters of wettability of ZrC_{1-x} phases by liquid metals at various temperatures are listed in Table 5.28

Table 5.25 Chemical interaction and/or compatibility of zirconium carbide phases with refractory compounds at elevated, high and ultra-high temperatures (reaction systems are given mainly in alphabetical order)

System	Atmosphere	Temperature range, °C	Interaction character, products and/or compatibility	Reference
ZrC _{1-x} -Al ₄ C ₃	-	up to 2200	No mutual solid solubilities between the components Formation of Zr ₃ Al ₃ C ₅ , Zr ₂ Al ₃ C ₅ , Zr ₅ Al ₃ C, Zr ₂ Al ₃ C ₄ , ZrAl ₈ C ₇ , ZrAl ₄ C ₄ and ZrAlC _{2-x} <i>See also</i> section ZrC _{1-x} -Al in Table 5.24 <i>See also</i> section C-Al-Zr in Table I-2.14	[814-835, 904-913, 1011]
ZrC _{1-x} -Al ₄ C ₃ - SiC	-	-	Formation of intergrowth structures, consisting of Zr _m C _{m+1} (NaCl-type) slabs separated by (Al ₁₋₂ Si _z) ₈ C ₇ (Al ₄ C ₃ -type) layers, such as Zr(Al _{1-x} Si _x) ₈ C ₇ (0 ≤ x ≤ 0.07), Zr(Al _{1-x} Si _x) ₄ C ₄ (0 ≤ x ≤ 0.04), Zr ₂ (Al _{1-x} Si _x) ₄ C ₅ (0 ≤ x ≤ 0.11) and Zr ₃ (Al _{1-x} Si _x) ₄ C ₆ (0 ≤ x ≤ 0.11) <i>See also</i> section ZrC _{1-x} -SiC-Al in Table 5.24 <i>See also</i> section ZrC _{1-x} -Al ₄ C ₃ -Si in Table 5.24	[826, 827, 831-833, 904, 910, 1082]
ZrC _{1-x} -Al ₄ C ₃ - SiC-TiC _{1-x}	-	-	Formation of (Ti,Zr) ₃ (Si,Al)C ₂ (M _{n+1} AX _n -phase solid solution) <i>See also</i> section ZrC _{1-x} -SiC-TiC _{1-x} -Al in Table 5.24	[834, 838]

(continued)

Table 5.25 (continued)

System	Atmosphere	Temperature range, °C	Interaction character, products and/or compatibility	Reference
ZrC _{1-x} -Al ₄ C ₃ - YC _{1±x} /β-YC _{2±x}	-	-	Formation of (Zr,Y)Al ₄ C ₄ and (Zr,Y) ₂ Al ₄ C ₅	[908, 909]
ZrC _{1-x} - α-Al ₂ O ₃	CO ₂ , 1.4 × 10 ⁻¹⁷ Pa	1000	Calculated equilibrium pressure of the interaction between the components	[381, 903, 1015]
	-	1530	Interaction between the components during a hot-pressing procedure was studied	
ZrC _{1-x} -B _{4±x} C	-	1400–1500	Formation of ZrB _{2±x} and C (via a stage of intermediate phase formation)	[33, 42, 200, 840, 841, 843–845, 1030, 1462]
	Chamber of anvil type	1600–2000 (15 MPa) 1750–1950 (5 GPa)	Formation of ZrB _{2±x} Formation of ZrB _{2±x} ; as the temperature increases, the ratio between the ZrC (remain) and ZrB ₂ (product) phases alters in a such way that the ZrB ₂ content increases <i>See also</i> section C–B–Zr in Table I-2.14	
ZrC _{1-x} -B _{4±x} C- α-BN	-	≤ 2100	No contact reaction between powdered ZrC _{1-x} and compact dense B _{4±x} C-α-BN composite	[915, 916, 996]
ZrC _{1-x} -B _{4±x} C- SiB _{3±x}	Chamber of anvil type	1600–2000 (0.015–5 GPa)	Formation of ZrB _{2±x} ; the addition of SiB _{3±x} favours the reaction between ZrC _{1-x} and B _{4±x} C going to its completion <i>See also</i> section C–B–Si–Zr in Table I-2.14	[1030]
ZrC _{1-x} -α-BN	-	≥ 2400	Formation of ZrB _{2±x}	[33, 914–916]
ZrC _{1-x} -CaO	Vacuum	1245	The rate of the following reaction (confirmed experimentally for $x = 0.04$ and 0.09) ZrC _{1-x} + (4 - x)CaO = CaZrO ₃ + (3-x)Ca↑ + (1 - x)CO↑ is controlled by diffusion of reactant ions through the product layer of CaZrO ₃	[997]
ZrC _{1-x} -β-CeC _{2±x}	-	1600	No mutual solubilities <i>See also</i> section C–Ce–Zr in Table I-2.14	[200]
ZrC _{1-x} - β-CeC _{2±x} -UC _{1±x}	-	-	The solubility of “imaginary” phase ‘CeC’ in (U,Zr,Ce)C _{1±x} mixed carbide decreases sharply with increasing content of Zr <i>See also</i> section C–Ce–U–Zr in Table I-2.14	[200]
ZrC _{1-x} -CeN _{1±x}	-	-	Terminal mutual solid solubilities between the components, ?	[33]
ZrC _{1-x} -CeP _{1±x}	-	-	Terminal mutual solid solubilities between the components, ?	[33]
ZrC _{1-x} -CeS _{1±x}	-	-	Terminal mutual solid solubilities between the components, ?	[33]

(continued)

Table 5.25 (continued)

System	Atmosphere	Temperature range, °C	Interaction character, products and/or compatibility	Reference
ZrC _{1-x} -Cr ₃ C _{2-x}	-	1300-1800	The max. solubility of "imaginary" phase 'CrC _{1-x} ' in ZrC _{1-x} is ~1.5-3.0 mol.% and that of ZrC _{1-x} in Cr ₃ C _{2-x} is very low; ZrC _{1-x} phase is in equilibrium with C (graphite) and Cr ₃ C _{2-x} <i>See also section C-Cr-Zr in Table I-2.14</i>	[33, 200, 552, 856, 860-863, 995]
ZrC _{1-x} -Cr ₇ C _{3±x}	-	1750	Eutectic ZrC _{1-x} -Cr ₇ C _{3±x} ; ZrC _{1-x} phase is in equilibrium with all Cr carbides, intermetallic and metallic Cr, the max. solubility of Cr in ZrC _{1-x} is ~1.5-3.0 mol.% and that of Zr in Cr ₇ C _{3±x} is very low <i>See also section C-Cr-Zr in Table I-2.14</i>	[200, 856, 860-863, 917]
ZrC _{1-x} -Cr ₃ C _{2-x} -Cr ₇ C _{3±x}	-	1730	Eutectic ZrC _{1-x} -Cr ₃ C _{2-x} -Cr ₇ C _{3±x} <i>See also section C-Cr-Zr in Table I-2.14</i>	[860-863, 917]
ZrC _{1-x} -Cr ₂₃ C _{6±x}	-	-	ZrC _{1-x} phase is in equilibrium with all Cr carbides and intermetallic and metallic Cr, the max. solid solubility of Cr in ZrC _{1-x} is ~1.5-3.0 mol.% and that of Zr in Cr ₂₃ C _{6±x} is very low <i>See also section ZrC_{1-x}-Cr₂₃C_{6±x}-Cr in Table 5.24</i>	[200, 860-863, 917-919]
ZrC _{1-x} -Cr ₃ C _{2-x} -TiC _{1-x}	-	1550	<i>See also section C-Cr-Zr in Table I-2.14</i> The addition of ZrC _{1-x} into Cr ₃ C _{2-x} matrix suppresses the recrystallization due to the formation of (Ti,Cr)C _{1-x} in the presence of TiC _{1-x} , because of the difference in lattice parameters between TiC _{1-x} and the mixed (solid solution) monocarbide is diminished by forming (Ti,Cr,Zr)C _{1-x} carbide phase	[1538]
ZrC _{1-x} -Cr ₂ O ₃	CO ₂ , 6.5 × 10 ⁻⁹ Pa	1000	Calculated equilibrium pressure of the interaction between the components	[381, 903]
ZrC _{1-x} -DyN _{1±x}	-	-	Monocarbonitride (cubic) continuous solid solution (complete solubility in the system?)	[33]
ZrC _{1-x} -Dy ₂ O ₃	Vacuum, ~3 Pa	1500-1700	The effect of Dy ₂ O ₃ as an additive for spark plasma sintering process was studied	[1394]
ZrC _{1-x} -ErN _{1±x}	-	-	Monocarbonitride (cubic) continuous solid solution (complete solubility in the system?)	[33]
ZrC _{1-x} -EuN _{1±x}	-	-	Monocarbonitride (cubic) continuous solid solution (complete solubility in the system?)	[33]
ZrC _{1-x} -EuO	-	-	Terminal mutual solid solubilities between the components (?)	[33]
ZrC _{1-x} -Fe ₃ C	-	-	Not (or very slightly) soluble in each other in solid state <i>See also section C-Fe-Zr in Table I-2.14</i>	[43, 200]

(continued)

Table 5.25 (continued)

System	Atmo- sphere	Temperature range, °C	Interaction character, products and/or compatibility	Reference
ZrC _{1-x} -Fe ₂ O ₃	Vacuum	800–900	Interaction leads to the formation of C-depleted ZrC _{1-x} phases, α-ZrO ₂ , Fe ₃ O ₄ and α-Fe	[381, 903, 925]
	CO ₂ , 6.8 × 10 ⁻³ Pa	1000	Calculated equilibrium pressure of the interaction between the components	
ZrC _{1-x} -GdN _{1±x}	–	–	Monocarbonitride (cubic) continuous solid solution (complete solubility in the system?)	[33]
ZrC _{1-x} -HfC _{1-x}			<i>See</i> section HfC _{1-x} -ZrC _{1-x} in Table 3.20	
ZrC _{1-x} -HfC _{1-x} - NbC _{1-x}			<i>See</i> section HfC _{1-x} -NbC _{1-x} -ZrC _{1-x} in Table 3.20	
ZrC _{1-x} -HfC _{1-x} - TaC _{1-x}			<i>See</i> section TaC _{1-x} -HfC _{1-x} -ZrC _{1-x} in Table 2.22	
ZrC _{1-x} -HfC _{1-x} - ThC _{1±x}			<i>See</i> section HfC _{1-x} -ThC _{1±x} -ZrC _{1-x} in Table 3.20	
ZrC _{1-x} -HfC _{1-x} - TiC _{1-x}			<i>See</i> section HfC _{1-x} -TiC _{1-x} -ZrC _{1-x} in Table 3.20	
ZrC _{1-x} -HfC _{1-x} - UC _{1±x}			<i>See</i> section HfC _{1-x} -UC _{1±x} -ZrC _{1-x} in Table 3.20	
ZrC _{1-x} -HfC _{1-x} - VC _{1-x}			<i>See also</i> section C-Hf-U-Zr in Table I-2.14 <i>See</i> section HfC _{1-x} -VC _{1-x} -ZrC _{1-x} in Table 3.20	
ZrC _{1-x} -HfC _{1-x} - δ-WC _{1±x}			<i>See</i> section HfC _{1-x} -δ-WC _{1±x} -ZrC _{1-x} in Table 3.20	
ZrC _{1-x} -HfN _{1±x}	–	1600–2200	Monocarbonitride (cubic) continuous solid solution (complete solubility in the system)	[33, 147]
ZrC _{1-x} -HoN _{1±x}	–	–	Monocarbonitride (cubic) continuous solid solution (complete solubility in the system?)	[33]
ZrC _{1-x} -LaN _{1±x}	–	–	Terminal mutual solid solubilities between the components (?)	[33]
ZrC _{1-x} -LaB _{6±x}	Vacuum	1900	Interaction between the powders (exposure – 0.5 h) leads to the formation of ZrB _{2±x} and some (La,Zr) _x (C,B) _y unidentified phases; no changes in ZrC _{1-x} stoichiometry	[1457]
ZrC _{1-x} -LaB _{6±x} - SiC	Vacuum	1900	Interaction between the powders ZrC _{1-x} and LaB _{6±x} (exposure – 0.5 h) leads to the formation of ZrB _{2±x} ; SiC powder is almost inert to other ingredients of the composition	[1457]
ZrC _{1-x} -LaP _{1±x}	–	–	Terminal mutual solid solubilities between the components (?)	[33]
ZrC _{1-x} -LaS _{1-x}	–	–	Terminal mutual solid solubilities between the components (?)	[33]
ZrC _{1-x} -LuN _{1±x}	–	–	Monocarbonitride (cubic) continuous solid solution (complete solubility in the system?)	[33]
ZrC _{1-x} -MgO	Vacuum	2000–2300	Interaction of compact dense materials results in the formation of ZrC _x O _y oxycarbide phases and MgC (?) in the contact zone; also other products (metallic Mg, graphite C) were observed	[1, 33, 923–925]
			<i>See also</i> section C-Mg-O-Zr in Table I-2.14	

(continued)

Table 5.25 (continued)

System	Atmo- sphere	Temperature range, °C	Interaction character, products and/or compatibility	Reference
ZrC _{1-x} -Mn ₅ C ₂ , Mn ₇ C ₃	-	700-1000	Not (or very slightly) soluble in each other at solid state <i>See also</i> section C-Mn-Zr in Table I-2.14	[43]
ZrC _{1-x} - α -MoC _{1-x}	-	1900-2000	Extended monocarbide (cubic) solid solution based on ZrC _{1-x}	[33, 117, 158, 200,
	-	~2000-2600	Monocarbide (cubic) continuous solid solution	329, 870, 871, 882, 926, 927, 930]
ZrC _{1-x} - α -MoC _{1-x} -NbC _{1-x}			<i>See also</i> section C-Mo-Zr in Table I-2.14 <i>See</i> section NbC _{1-x} - α -MoC _{1-x} -ZrC _{1-x} in Table 4.19 <i>See also</i> section C-Mo-Nb-Zr in Table I-2.14	
ZrC _{1-x} - α -MoC _{1-x} - UC _{1±x}	-	2000	Extended monocarbide (cubic) solid solution based on ZrC _{1-x} -UC _{1±x} continuous solid solution; the solubility of α -MoC _{1-x} in ZrC _{1-x} is >80 mol.% (the solubilities of ZrC _{1-x} and UC _{1±x} in α -MoC _{1-x} are low) <i>See also</i> section C-Mo-U-Zr in Table I-2.14	[927]
ZrC _{1-x} - β -Mo _{2±x} C	-	1400-2100	Solubility of Zr in β -Mo _{2±x} C is very low	[33, 158, 200, 870, 871, 930]
ZrC _{1-x} -MoSi ₂	Ar	1900-1950	<i>See also</i> section C-Mo-Zr in Table I-2.14 Interaction in powder mixtures leads to the formation of (Mo,Zr) ₅ Si _{3±x} and SiC	[476, 587, 588, 1181- 1183, 1410, 1411]
ZrC _{1-x} -NbC _{1-x}			<i>See also</i> section C-Mo-Si-Zr in Table I-2.14	
ZrC _{1-x} -NbC _{1-x}			<i>See</i> section NbC _{1-x} -ZrC _{1-x} in Table 4.19	
-TaC _{1-x}			<i>See</i> section TaC _{1-x} -NbC _{1-x} -ZrC _{1-x} in Table 2.22	
ZrC _{1-x} -NbC _{1-x}			<i>See</i> section NbC _{1-x} -ThC _{1±x} -ZrC _{1-x} in Table 4.19	
-ThC _{1±x}				
ZrC _{1-x} -NbC _{1-x}			<i>See</i> section NbC _{1-x} -TiC _{1-x} -ZrC _{1-x} in Table 4.19	
-TiC _{1-x}				
ZrC _{1-x} -NbC _{1-x}			<i>See</i> section NbC _{1-x} -UC _{1±x} -ZrC _{1-x} in Table 4.19	
-UC _{1±x}			<i>See also</i> section C-Nb-U-Zr in Table I-2.14	
ZrC _{1-x} -NbC _{1-x}			<i>See</i> section NbC _{1-x} -VC _{1-x} -ZrC _{1-x} in Table 4.19	
-VC _{1-x}				

(continued)

Table 5.25 (continued)

System	Atmo- sphere	Temperature range, °C	Interaction character, products and/or compatibility	Reference
ZrC _{1-x} -NbC _{1-x} -δ-WC _{1±x}			See section NbC _{1-x} -δ-WC _{1±x} -ZrC _{1-x} in Table 4.19	
ZrC _{1-x} - β-Nb _{2+x} C			See section β-Nb _{2+x} C-ZrC _{1-x} in Table 4.19	
ZrC _{1-x} - δ-NbN _{1-x}	N ₂ , >0.1 MPa	1500	Monocarbonitride (cubic) continuous solid solution (complete solubility in the system)	[33, 140, 1532]
ZrC _{1-x} -NbO	-	-	Terminal mutual solid solubilities between the components (?) See also section C-Nb-O-Zr in Table I-2.14	[33]
ZrC _{1-x} -NdN _{1±x}	-	-	Monocarbonitride (cubic) continuous solid solution (complete solubility in the system?)	[33]
ZrC _{1-x} - Nd ₂ Fe ₁₄ B	Pure Ar	1000	The solubility of ZrC _{1-x} in complex boride phase is ~6 mol.%	[1055]
ZrC _{1-x} -NiO	-	-	Interaction between the components is determined by the carbide composition: ZrC _{0.97} primarily reacts to form C oxides, then as the carbide phase is depleted of C, γ-ZrO _{2-x} is formed, while C is precipitated in non- combined form; but ZrC _{0.77} reacts only through the preferential formation of Zr oxide (no oxycarbide phases were revealed in these conditions)	[1016]
ZrC _{1-x} -NpC _{1-x}	-	-	Monocarbide (cubic) continuous solid solution (complete solubility in the system?)	[33]
ZrC _{1-x} -NpN _{1±x}	-	-	Monocarbonitride (cubic) continuous solid solution (complete solubility in the system?)	[33]
ZrC _{1-x} -PrN _{1±x}	-	-	Monocarbonitride (cubic) continuous solid solution (complete solubility in the system?)	[33]
ZrC _{1-x} -PuC _{1-x}	-	1250-1500	Max. terminal solid solubility of ZrC _{1-x} in PuC _{1-x} is 23 mol.% and that of PuC _{1-x} in ZrC _{1-x} is 24 mol.%	[33, 116, 200, 936- 939]
	-	>1600	Monocarbide (cubic) continuous solid solution (complete solubility in the system) See also section C-Pu-Zr in Table I-2.14	
ZrC _{1-x} -PuC _{1-x} - UC _{1±x}	-	-	Monocarbide (cubic) continuous solid solution (in the regions with lower PuC _{1-x} content) See also section C-Pu-U-Zr in Table I-2.14	[200, 1019, 1355, 1356]
ZrC _{1-x} -Pu ₂ C _{3-x}	-	1250-1600	Terminal solid solubility of ZrC _{1-x} is low	[200, 936- 939]
ZrC _{1-x} -PuN _{1±x}	-	-	See also section C-Pu-Zr in Table I-2.14 Monocarbonitride (cubic) continuous solid solution (complete solubility in the system)	[33]

(continued)

Table 5.25 (continued)

System	Atmosphere	Temperature range, °C	Interaction character, products and/or compatibility	Reference
ZrC _{1-x} -PuP _{1±x}	-	-	Terminal mutual solid solubilities between the components (?)	[33]
ZrC _{1-x} -PuS _{1±x}	-	-	Terminal mutual solid solubilities between the components (?)	[33]
ZrC _{1-x} -ScC _{1-x}	-	1500-1900	Monocarbide (cubic) continuous solid solution (complete solubility in the system) <i>See also</i> section C-Sc-Zr in Table I-2.14	[33, 940, 941]
ZrC _{1-x} -ScN _{1±x}	-	-	Monocarbonitride (cubic) continuous solid solution (complete solubility in the system?)	[33]
ZrC _{1-x} -α/β-SiC	Vacuum, 10 ⁻³ Pa	1300	A transition zone formed on the ZrC _{1-x} side between compact dense components during diffusion welding procedure (loading time - 20 min), while annealing procedure (50 h exposure) the zone stratified forming a solid solution of Si in ZrC _{1-x} with SiC inclusions	[33, 76, 883, 884, 929, 935, 942, 1050, 1059, 1364, 1365, 1535]
	-	-	Practically, the pure components are compatible with each other within the temperature range of their thermal stability <i>See also</i> section C-Si-Zr in Table I-2.14	
ZrC _{1-x} -α/β-SiC-δ-WC _{1±x}	-	1800	Hot-pressing of powdered δ-WC _{1.01} (mean particle size - 0.75 μm, contents: non-combined C - 0.04%, Fe - 0.05%) - 1-6 mol.% β-SiC (mean particle size - 0.4-0.6 μm, contents: O - 1.80%, Fe - 0.05%) - 2-14 mol.% ZrC _{0.95} (mean particle size - 2 μm, contents: non-combined C - 0.25%, O - 0.62%, N - 0.68%, Fe - 0.01%) mixtures led to the formation of (Zr,W)C _{1-x} solid solution and small amounts of W _{2±x} C and ZrO _{2-x}	[1550]
ZrC _{1-x} -SiC-ZrB _{2±x}	-	1800-2000	The components are compatible to each other as constituents of composites	[1050, 1068, 1427, 1542, 1543]
ZrC _{1-x} -α/β-Si ₃ N ₄	-	~1400-1600	Interaction with the formation of Zr silicides, β-SiC and monocarbonitride (cubic) phase with the composition close to ~ZrC _{0.4} N _{0.6} ; carbide phase inhibits α → β nitride transformation	[1013, 1045, 1053, 1054, 1472]
ZrC _{1-x} -β-Si ₃ N ₄ -Al ₂ O ₃	-	1650-1700	Interaction with the formation of β-SiC, monocarbonitride (cubic) phase with the composition close to ~ZrC _{0.4} N _{0.6} , Si ₃ N ₄ -Al ₂ O ₃ solid solutions and glasses of Al ₂ O ₃ ·SiO ₂ type	[1053, 1054]
ZrC _{1-x} -β-Si ₃ N ₄ -MgO	-	1650-1700	Interaction with the formation of β-SiC, monocarbonitride (cubic) phase with the composition close to ~ZrC _{0.4} N _{0.6} , MgSiO ₄ , Mg ₂ SiO ₃ and glasses of MgO·SiO ₂ type	[1053, 1054]
ZrC _{1-x} -SiO ₂ -Al ₂ O ₃ -CaO-Fe ₂ O ₃ (basalt)	-	1400	ZrC _{1-x} (8-12% porosity) is not stable in molten basalt (SiO ₂ - 15% Al ₂ O ₃ - 13% CaO - 13% Fe ₂ O ₃) at short-term exposure (0.5-1 h) with average dissolution rate ~0.2 g cm ⁻² h ⁻¹	[1475]

(continued)

Table 5.25 (continued)

System	Atmo- sphere	Temperature range, °C	Interaction character, products and/or compatibility	Reference
ZrC _{1-x} -SmN _{1±x}	-	-	Monocarbonitride (cubic) continuous solid solution (complete solubility in the system?)	[33]
ZrC _{1-x} -TaC _{1-x}			<i>See</i> section TaC _{1-x} -ZrC _{1-x} in Table 2.22	
ZrC _{1-x} -TaC _{1-x} - ThC _{1±x}			<i>See</i> section TaC _{1-x} -ThC _{1±x} -ZrC _{1-x} in Table 2.22	
ZrC _{1-x} -TaC _{1-x} - TiC _{1-x}			<i>See</i> section TaC _{1-x} -TiC _{1-x} -ZrC _{1-x} in Table 2.22	
ZrC _{1-x} -TaC _{1-x} - UC _{1±x}			<i>See</i> section TaC _{1-x} -UC _{1±x} -ZrC _{1-x} in Table 2.22 <i>See also</i> section C-Ta-U-Zr in Table I-2.14	
ZrC _{1-x} -TaC _{1-x} - VC _{1-x}			<i>See</i> section TaC _{1-x} -VC _{1-x} -ZrC _{1-x} in Table 2.22	
ZrC _{1-x} -TaC _{1-x} - δ-WC _{1±x}			<i>See</i> section TaC _{1-x} -δ-WC _{1±x} -ZrC _{1-x} in Table 2.22	
ZrC _{1-x} - α-Ta _{2+x} C			<i>See</i> section α-Ta _{2+x} C-ZrC _{1-x} in Table 2.22 <i>See also</i> section C-Ta-Zr in Table I-2.14	
ZrC _{1-x} - β-Ta _{2±x} C			<i>See</i> section β-Ta _{2±x} C-ZrC _{1-x} in Table 2.22 <i>See also</i> section C-Ta-Zr in Table I-2.14	
ZrC _{1-x} - δ-TaN _{1-x}	N ₂ , 3 MPa	1800	Monocarbonitride (cubic) continuous solid solution (complete solubility in the system)	[122]
ZrC _{1-x} - ε-TaN _{1-x}	N ₂ , >0.1 MPa	1500	Terminal mutual solid solubilities between the components; the max. solid solubility of ε-TaN _{1-x} (hexagonal) in ZrC _{1-x} amounts to ~80 mol.%	[33, 140]
ZrC _{1-x} -TaSi ₂	Vacuum (~0.1 kPa)	1700	The interaction between the components leads to the formation of (Zr,Ta)C _{1-x} , Zr ₂ Si, ZrSi ₂ and SiC	[1423]
ZrC _{1-x} -TbN _{1±x}	-	-	Monocarbonitride (cubic) continuous solid solution (complete solubility in the system?)	[33]
ZrC _{1-x} -TcC _{1-x}	-	-	Terminal mutual solid solubilities between the components (?) <i>See also</i> section C-Tc-Zr in Table I-2.14	[947, 1409]
ZrC _{1-x} -ThC _{1±x} (α-Th)	-	1000	Compatible with each other (practically, no solid solubility of ZrC _{1-x} in ThC _{1±x} , 120 h exposure)	[33, 200, 948-952, 1006]
	-	1100-1500	Compatible with each other (the solid solubilities of metallic Th and Th carbides in ZrC _{1-x} and those of ZrC _{1-x} in metallic Th and Th carbides are very low)	
	-	1500	ZrC _{1-x} is in equilibrium with both ThC _{1±x} and γ-ThC _{2-x} carbides	
	-	1950-2150	The max. solid solubility of ZrC _{1-x} in ThC _{1±x} is ≤3 mol.% and that of ThC _{1±x} in ZrC _{1-x} is noticeably lower <i>See also</i> section C-Th-Zr in Table I-2.14	

(continued)

Table 5.25 (continued)

System	Atmosphere	Temperature range, °C	Interaction character, products and/or compatibility	Reference
ZrC _{1-x} -ThC _{1±x} -TiC _{1-x}	-	>2000	The mutual solubilities between ZrC _{1-x} -TiC _{1-x} monocarbide (cubic) continuous solid solution and ThC _{1±x} are very low (the max. solubility of ThC _{1±x} in ZrC _{1-x} is a bit higher than it is in TiC _{1-x} , those of ZrC _{1-x} and TiC _{1-x} in ThC _{1±x} are noticeably lower)	[33, 921]
ZrC _{1-x} -ThC _{1±x} -UC _{1±x}	-	>2000	Monocarbide (cubic) continuous solid solution with great miscibility gap because of low mutual solubilities in the ZrC _{1-x} -ThC _{1±x} system <i>See also</i> section C-Th-U-Zr in Table I-2.14	[33, 200, 948, 949]
ZrC _{1-x} -ThC _{1±x} -VC _{1-x}	-	>2000	The mutual solubilities between all the components are extremely low	[33, 921]
ZrC _{1-x} - γ-ThC _{2-x}	-	1500	Compatible with each other (mutual solid solubilities are very low) <i>See also</i> section C-Th-Zr in Table I-2.14	[33, 200, 951, 952]
ZrC _{1-x} -ThN _{1±x}	-	-	Monocarbonitride (cubic) continuous solid solution (complete solubility in the system?)	[33]
ZrC _{1-x} -ThP _{1±x}	-	-	Terminal mutual solid solubilities between the components (?)	[33]
ZrC _{1-x} -ThO _{2-x}	Vacuum 0.1 Pa	≥1700	The initiation of interaction in the powdered ZrC _{1-x} and ThO _{2-x} mixtures (preliminarily cold-pressed), noticeable mass loss is observed	[42, 925, 963]
ZrC _{1-x} -ThO _{2-x} -UO _{2+x}	He flow	1850-2550	Chemical vapour deposited ZrC _{1-x} coatings (20 μm thickness) are compatible with ThO _{2-x} -UO _{2+x} solid solutions substrate (intact after heating procedure for 1 h)	[785]
ZrC _{1-x} -ThS _{1±x}	-	-	Terminal mutual solid solubilities between the components (?)	[33]
ZrC _{1-x} -TiC _{1-x}	-	1500	Monocarbide (cubic) extended solid solutions; the miscibility gap ranges in homogeneity area from ~Zr _{0.05-0.20} Ti _{0.80-0.95} C _{0.96} to ~Zr _{0.80} Ti _{0.20} C _{0.96} and from ~Zr _{0.20} Ti _{0.80} C _{0.50} to ~Zr _{0.60} Ti _{0.40} C _{0.56} (experimentally determined and theoretically calculated)	[33, 144, 193, 200, 887, 888, 890-893, 931, 953-955, 988, 1010, 1020, 1056, 1069, 1070, 1073, 1074, 1084, 1087, 1088, 1092, 1314, 1347, 1348, 1400, 1436-1438, 1443, 1444, 1447, 1448, 1476, 1484, 1485, 1533, 1536, 1537, 1539, 1540, 1541, 1546]
	-	~2000-2400	Critical point of the miscibility gap is corresponding to ~Zr _{0.35-0.45} Ti _{0.55-0.65} C _{1-x} composition (experimentally determined and theoretically calculated)	
	-	~2100-2900	Monocarbide (cubic) continuous solid solution (complete solubility in the system, the variation of lattice parameter <i>a</i> , nm with composition for (Zr _{1-y} Ti _y)C _{1-x} phases (<i>x</i> ≈ 0, 0 ≤ <i>y</i> ≤ 1) is linear: <i>a</i> = 0.4700 - 0.0371 <i>y</i>)	
	-	2400	Sintering process of the equimolar mixture of components was studied	

(continued)

Table 5.25 (continued)

System	Atmosphere	Temperature range, °C	Interaction character, products and/or compatibility	Reference
	–	~2880–2900	Min. melting point corresponding to $\sim\text{Zr}_{0.25-0.35}\text{Ti}_{0.65-0.75}\text{C}_{1-x}$ composition (experimentally determined and theoretically calculated) <i>See also</i> section C–Ti–Zr in Table I-2.14	
$\text{ZrC}_{1-x}\text{-TiC}_{1-x}$ $\delta\text{-TiN}_{1\pm x}$	Vacuum, <0.1 Pa	1300–2100	Monocarbonitride (cubic) continuous solid solution (complete solubility in the system, the variation of lattice parameter a , nm with composition for $(\text{Zr}_{1-y}\text{Ti}_y)(\text{C}_{1-x}\text{N}_x)$ phases ($0 \leq x \leq 1, 0 \leq y \leq 1$): $a = 0.4700 - 0.0125x - 0.0371y + 0.0043xy$)	[1476, 1545]
$\text{ZrC}_{1-x}\text{-TiC}_{1-x}$ $\text{UC}_{1\pm x}$	–	2000–2050	Monocarbide (cubic) continuous solid solution with great miscibility gap because of very low mutual solubilities in the $\text{TiC}_{1-x}\text{-UC}_{1\pm x}$ system <i>See also</i> section C–Ti–U–Zr in Table I-2.14	[33, 200, 921]
$\text{ZrC}_{1-x}\text{-TiC}_{1-x}$ VC_{1-x}	–	1900–2000	Monocarbide (cubic) continuous solid solution with great miscibility gap because of very low mutual solubilities in the $\text{ZrC}_{1-x}\text{-VC}_{1-x}$ system	[921, 1074]
$\text{ZrC}_{1-x}\text{-TiC}_{1-x}$ $\delta\text{-WC}_{1\pm x}$	–	1900–2000	Extended solid solution based on $\text{ZrC}_{1-x}\text{-TiC}_{1-x}$ monocarbide (cubic) continuous solid solution; the solubilities of $\delta\text{-WC}_{1\pm x}$ in ZrC_{1-x} and TiC_{1-x} are ~30 and ~60 mol.%, respectively (the solubilities of ZrC_{1-x} and TiC_{1-x} in $\delta\text{-WC}_{1\pm x}$ are very low)	[921, 1074]
$\text{ZrC}_{1-x}\text{-TiC}_{1-x}$ $\delta\text{-NbN}_{1-x}$	Pure N_2	1200–2500	Monocarbonitride (cubic) continuous solid solution (complete solubility in the system)	[1532]
ZrC_{1-x} $\delta\text{-TiN}_{1\pm x}$	–	~2600	Monocarbonitride (cubic) continuous solid solution (complete solubility in the system)	[33, 46, 1476, 1484, 1545]
$\text{ZrC}_{1-x}\text{-TiB}_{2\pm x}$	–	2620–2700	Eutectic ZrC_{1-x} ($x \approx 0$) – $\text{TiB}_{2\pm x}$ ($x \approx 0$)	[1081, 1359, 1397, 1456]
$\text{ZrC}_{1-x}\text{-TiO}_{1\pm x}$	–	–	Terminal mutual solid solubilities between the components, ?	[33]
$\text{ZrC}_{1-x}\text{-UC}_{1\pm x}$	–	~1200–2500	Monocarbide (cubic) continuous solid solution (a spacing-composition curve in the system is almost linear, complete solubility in the system)	[33, 43, 149, 200, 260, 337, 370, 901, 927, 928, 948–950, 956–961, 1007, 1021, 1022, 1048, 1357, 1358, 1413, 1417, 1418, 1421, 1552]

See also section C–U–Zr in Table I-2.14

(continued)

Table 5.25 (continued)

System	Atmosphere	Temperature range, °C	Interaction character, products and/or compatibility	Reference
ZrC _{1-x} -UC _{1±x} -UN _{1-x}	-	~1200-2100	Monocarbonitride (cubic) continuous solid solution <i>See also</i> section C-N-U-Zr in Table I-2.14	[1551]
ZrC _{1-x} -UC _{1±x} -VC _{1-x}	-	1900-2000	Low mutual solubilities between ZrC _{1-x} -UC _{1±x} monocarbide (cubic) continuous solid solution and VC _{1-x}	[921]
ZrC _{1-x} -UC _{1±x} -δ-WC _{1±x}	-	1900-2000	The solubility of δ-WC _{1±x} in ZrC _{1-x} -UC _{1±x} monocarbide (cubic) continuous solid solution increases with increasing content of Zr from very low values up to ~30 mol.%	[33]
ZrC _{1-x} -UC _{1±x} -αβ-UC _{2-x}	-	1700-2000	The composition of ZrC _{1-x} -UC _{1±x} monocarbide (cubic) continuous solid solution in the equilibrium with UC _{2-x} , shifts from ~Zr _{0.60-0.65} U _{0.35-0.40} C _{1-x} (at 1700 °C) to ~Zr _{0.70-0.80} U _{0.20-0.30} C _{1-x} (at 1900-2000 °C)	[901, 958, 961]
	-	~2400	Quasi-eutectic (Zr,U)C _{1-x} -β-(U,Zr)C _{2-x} -C <i>See also</i> section C-U-Zr in Table I-2.14	
ZrC _{1-x} -UC _{1±x} -US _{1±x}	-	1650	The solubility of US _{1±x} in ZrC _{1-x} -UC _{1±x} monocarbide (cubic) continuous solid solution is ~5 mol.% (independent on (Zr,U)C _{1±x} composition); solubilities of ZrC _{1-x} and UC _{1±x} in US _{1±x} are ~15 and ~40 mol.%, respectively	[1352]
	-	2100	The solubility of US _{1±x} in ZrC _{1-x} -UC _{1±x} monocarbide (cubic) continuous solid solution is ~7.5 mol.% (independent on (Zr,U)C _{1±x} composition); solubilities of ZrC _{1-x} and UC _{1±x} in US _{1±x} are ~18 and ~40 mol.%, respectively	
	-	>2100	The solubility of US _{1±x} in ZrC _{1-x} -UC _{1±x} monocarbide (cubic) continuous solid solution is ~10-20 mol.%; solubilities of ZrC _{1-x} and UC _{1±x} in US _{1±x} are ~21 and ~42 mol.%, respectively	
ZrC _{1-x} -β-UC _{2-x}	-	~2400	Quasi-eutectic ZrC _{1-x} -β-UC _{2-x} ; the max. solubility of Zr in β-UC _{2-x} is corresponding to ~(U _{0.94} C _{0.06})C _{1.94} composition <i>See also</i> section C-U-Zr in Table I-2.14	[33, 901, 961]
ZrC _{1-x} -UN _{1-x}	-	-	Monocarbonitride (cubic) continuous solid solution (complete solubility in the system)	[33, 798]
ZrC _{1-x} -UP _{1±x}	-	-	Terminal mutual solid solubilities between the components (?)	[33]
ZrC _{1-x} -UO _{2+x}	-	1500	Chemical vapour deposited ZrC _{1-x} coatings are compatible with UO _{2+x}	[1211, 1225]

(continued)

Table 5.25 (continued)

System	Atmosphere	Temperature range, °C	Interaction character, products and/or compatibility	Reference
ZrC _{1-x} -UO _{2+x} -ThO _{2-x}	He flow	1850–2550	Chemical vapour deposited ZrC _{1-x} coatings (20 μm thickness) are compatible with UO _{2+x} -ThO _{2-x} solid solution substrate (intact after heating procedure for 1 h)	[785]
ZrC _{1-x} -US _{1±x}	–	1300	The max. solid solubility of ZrC _{1-x} in US _{1±x} is ~13 mol.% and that of US _{1±x} in ZrC _{1-x} is ~3 mol.%	[33, 1004, 1352, 1353]
		2470	The following peritectic reaction is observed: L + ZrC _{1-x} (US _{1±x}) solid solution → US _{1±x} (ZrC _{1-x}) solid solution with the max. solid solubility of ZrC _{1-x} in US _{1±x} – 21.5–22.5 mol.% and that of US _{1±x} in ZrC _{1-x} – ~19 mol.%	
ZrC _{1-x} -VC _{1-x}	Ar, >0.1 MPa	1900	Additions of VC _{1-x} (3.5–13.5 mol.%), higher than the max. solid solubility of VC _{1-x} in ZrC _{1-x} (1.8 mol.%), effectively promote the hot-pressing densification process (up to nearly poreless state)	[33, 38, 144, 193, 200, 888, 953, 1061, 1062, 1070, 1074, 1078, 1539]
		2100	Terminal monocarbide (cubic) solid solutions; the solid solubility of ZrC _{1-x} in VC _{1-x} is ~1.0 mol.% and that of VC _{1-x} in ZrC _{1-x} is ~5.0 mol.%	
		~2460–2530	Eutectic VC _{1-x} (x = 0.12) – ZrC _{1-x} (x ≈ 0); the solid solubility of ZrC _{1-x} in VC _{1-x} is ~2.5–5.0 mol.% and that of VC _{1-x} in ZrC _{1-x} is ~8.0–8.5 mol.% <i>See also</i> section C–V–Zr in Table I-2.14	
ZrC _{1-x} -VC _{1-x} -δ-WC _{1±x}	–	~1900–2000	The max. solubility of δ-WC _{1±x} in cubic carbides ZrC _{1-x} and VC _{1-x} corresponds to ~(Zr _{0.3} W _{0.7})C _{1±x} and ~(V _{0.4} W _{0.6})C _{1-x} compositions, respectively; the max. mutual solubilities of carbides ZrC _{1-x} and VC _{1-x} corresponds to ~(Zr _{0.95} V _{0.05})C _{1-x} and ~(V _{0.99} Zr _{0.01})C _{1-x} compositions, respectively, and with increasing V content in (Zr,V)C _{1-x} the max. solubility of W decreases there	[33, 921, 1074]
ZrC _{1-x} -δ-VN _{1-x}	–	–	Terminal solid solutions with negligible mutual solubilities (?)	[33, 46]
ZrC _{1-x} -γ-WC _{1-x}	–	~2500–2800	Monocarbide (cubic) continuous solid solution <i>See also</i> section C–W–Zr in Table I-2.14	[33, 200, 896, 899, 926, 1093]

(continued)

Table 5.25 (continued)

System	Atmosphere	Temperature range, °C	Interaction character, products and/or compatibility	Reference
ZrC _{1-x} - δ-WC _{1±x}	-	1500	No solubility of Zr in δ-WC _{1±x}	[33, 200,
	-	1600	The max. solid solubility of W in ZrC _{1-x} corresponds to ~($Zr_{0.80-0.85}W_{0.15-0.20}$)C _{1-x} composition	373, 871, 882, 894, 899, 901,
	-	1950–2000	The max. solid solubility of W in ZrC _{1-x} corresponds to ~($Zr_{0.60-0.70}W_{0.30-0.40}$)C _{1-x} composition	1046, 1093, 1380, 1479]
	-	≥2100	The max. solid solubility of W in ZrC _{1-x} corresponds to ($Zr_{0.04-0.40}W_{0.60-0.96}$)C _{1-x} composition <i>See also section C–W–Zr in Table I-2.14</i>	
ZrC _{1-x} - αβ/γ-W _{2±x} C	-	-	The max. solid solubility of Zr in γ-W _{2±x} C is ~3.5 at.% <i>See also section C–W–Zr in Table I-2.14</i>	[33, 899, 1093]
ZrC _{1-x} - β-W ₂ B _{5-x}	-	2240	Eutectic ZrC _{1-x} -β-W ₂ B _{5-x}	[1399]
ZrC _{1-x} -YC _{1±x}	-	-	Monocarbide (cubic) continuous solid solution (complete solubility in the system?)	[33]
ZrC _{1-x} -YN _{1±x}	-	-	Monocarbonitride (cubic) continuous solid solution (complete solubility in the system?)	[33]
ZrC _{1-x} -YbN _{1±x}	-	-	Monocarbonitride (cubic) continuous solid solution (complete solubility in the system?)	[33]
ZrC _{1-x} -ZrN _{1±x}	-	1100–2000	Monocarbonitride (cubic) continuous solid solution (complete solubility in the system, the variation of lattice parameter <i>a</i> , nm with composition for Zr(C _{1-x} N _x) phases (0 ≤ <i>x</i> ≤ 1) is linear: <i>a</i> = 0.4700 – 0.0125 <i>x</i>) with the homogeneity range within ~ZrC _{0.56-0.59} – ~ZrC _{0.95} – ~ZrN _{0.54-0.56} – ~ZrN _{1.04} compositions <i>See also section C–N–Zr in Table I-2.14</i>	[33, 46, 51, 59, 110, 124, 126, 200, 278, 328, 472, 576, 703, 962, 992, 994, 1201, 1434, 1446, 1476, 1483, 1484]
ZrC _{1-x} -ZrN _{1±x} - ZrB _{2±x}	-	-	Quasi-binary eutectic system Zr(C,N) _{1-x} -ZrB _{2±x}	[1079]
ZrC _{1-x} -ZrN _{1±x} - ‘ZrO’	-	-	Formation of ZrC _{1-x} N _y O _z oxycarbonitride phase ^a based on of monocarbonitride (cubic) ZrC _{1-x} -ZrN _{1±x} continuous solid solution	[44, 124, 165, 962, 994, 1027, 1415]
	-	1600	Homogeneity range limits of ZrC _x N _y O _z phase are ~ZrC _{0.45} O _{0.55} and ~ZrN _{0.65} O _{0.35}	
	-	2000	Homogeneity range limits of ZrC _x N _y O _z phase are ~ZrC _{0.25} O _{0.75} and ~ZrN _{0.45} O _{0.55} <i>See also section C–N–O–Zr in Table I-2.14</i>	
ZrC _{1-x} -ZrP _{1±x}	-	-	Terminal mutual solid solubilities between the components, ?	[33]

(continued)

Table 5.25 (continued)

System	Atmosphere	Temperature range, °C	Interaction character, products and/or compatibility	Reference
ZrC _{1-x} -ZrB _{2±x}	-	2360	Eutectic ZrC _{1-x} -ZrB _{2±x} -C	[33, 200,
	-	~2620-2850	Eutectic ZrC _{1-x} (x = 0.03-0.12)-ZrB _{2±x} (x ≈ 0); the max. solid solubility of ZrB _{2±x} in ZrC _{1-x} is ~1-5 mol.% and that of ZrC _{1-x} in ZrB _{2±x} is <2 mol.%	840, 842, 843, 845, 967-969, 995, 1008, 1012, 1081,
	-	2815-2845	Eutectic ZrC _{1-x} (x ≈ 0)-ZrB _{2±x} (x ≈ 0)	1359, 1397, 1416, 1453-1459, 1462, 1544]
ZrC _{1-x} -β/γ-ZrO _{2-x}	Vacuum, 0.1-1.0 Pa	1400-1450	<i>See also</i> section C-B-Zr in Table I-2.14 The initiation of interaction in the powdered ZrC _{1-x} and β/γ-ZrO _{2-x} mixtures (preliminarily cold-pressed)	[14, 33, 42, 44, 63, 74, 124, 130,
		1500-2000	Formation of ZrC _{1-x} O _y oxycarbide (cubic) phases, extended solid solutions based on ZrC _{1-x} with ~ZrC _{0.60} - ~ZrC _{0.50} O _{0.20} - ~ZrC _{0.40-0.60} O _{0.30-0.55} - ~ZrC _{0.80} O _{0.20} - ZrC _{0.99} approximate homogeneity limits	151, 161-164, 230, 923, 924, 963-966, 970-979,
	Vacuum, 1.0 Pa	≥1800	Formation of intermediate ZrC _y O _δ oxycarbide (cubic) phases (with shortened lattice parameter) in the powdered mixtures of components in accordance with the following reactions: $aZrC_{1-x} + bZrO_{2-z} = (a + b)ZrC_yO_\delta + [a(1 - x) - y(a + b)]CO \uparrow$, where $\delta = [b(2 - z) + y(a + b) - a(1 - x)] / (a + b)$, or in experimental practice: $4ZrC + ZrO_2 = 5ZrC_{0.7}O_{-0.3} + \frac{1}{2}CO$ (determined for powdered mixture 80 mol.% ZrC _{-1.0-20} mol.% ZrO _{-2.0} vacuum heat treatment, resulting in the formation of single-phase products)	986, 997-1001, 1017, 1018, 1027, 1028, 1075, 1077, 1154, 1170, 1171, 1197-1204, 1392, 1393, 1396, 1402, 1415, 1432, 1433, 1445, 1452, 1513]
		2000	In the equimolar powdered ZrC _{1-x} and β/γ-ZrO _{2-x} mixture carbon content loss (difference between initial and final carbon contents) amounts to 2% (2 h exposure)	
	Vacuum, 0.1 Pa	2050-2150	In the conditions of high vacuum and long-term exposures (up to 24 h), the formation of metallic solid solutions α-Zr(C,O) with ZrC _{0.02-0.03} and ZrO _{0.41-0.54} solubility limits was observed	
	-	>2200	The initiation of interaction in the contact zone between compact dense materials (formation of intermediate phases)	
	-	~2700	ZrC _{1-x} materials are chemically resistant to molten ZrO _{2-x}	

(continued)

Table 5.25 (continued)

System	Atmosphere	Temperature range, °C	Interaction character, products and/or compatibility	Reference
	Ar ($p_{O_2} \approx 1$ Pa)	≥ 3300	ZrC _{0.82} C _{0.14} surface heating leads to ZrC _{0.75} formation; O releases in the form of the gaseous species ZrO (?), while the grains of oxycarbide, converted into the carbide, grew from 2 to 20 μ m	
	–	–	Formation of carbon-stabilized (cubic) γ -ZrO _{2-x} C _z oxide (solid solution, ?) and ZrO ₂ C _x phase (?) <i>See also</i> section C–O–Zr in Table I-2.14	

^aPractically, due to the serious difficulties in manufacturing carbides non-contaminated in any degree by O and N, which are dissolved at higher temperatures easily, all the materials labeled as ZrC_{1-x} would have to be considered as ZrC_{1-x}N_yO_z with low or very low values of y and z indexes

Table 5.26 Chemical interaction of zirconium carbide phases with gaseous media at elevated, high and ultra-high temperatures (reaction systems are given in alphabetical order)

System	Atmosphere	Temperature range, °C	Interaction character, products and/or compatibility	Reference
ZrC _{1-x} -Br ₂	–	20	No interaction with Br ₂ dissolved in CCl ₄ (200 h exposure)	[452, 1331]
ZrC _{1-x} -CO ^a	Br ₂	>500	Reacts readily	
	CO	–	Formation of ZrC _{1-x} O _y oxycarbide phases (extended substitution solid solution based on ZrC _{1-x} with approximate homogeneity limits: ~ZrC _{0.60} ~ZrC _{0.50} O _{0.20} ~ ~ZrC _{0.40-0.60} O _{0.30-0.55} ~ZrC _{0.80} O _{0.20} ~ ~ZrC _{0.99})	[10, 33, 44, 74, 124, 1001, 1131, 1199, 1200, 1204, 1209–1211, 1342, 1343, 1402, 1445, 1513]
	CO	1150–1250	For the “imaginary” reaction ZrC _{-1.0} + 2CO (gas) \leftrightarrow ZrO _{-2.0} + 3C (graphite) (not taking into account the formation of oxycarbide phases) near-equilibrium pressure p_{CO} , Pa measured experimentally by torsion effusion method is obeyed the following rule $\lg p_{CO} = 11.55 - 16,100/T$, where T is temperature, K	
	CO	1600–1950	For the “imaginary” reaction ZrC _{-1.0} + 2CO (gas) \leftrightarrow ZrO _{-2.0} + 3C (graphite) (not taking into account the formation of oxycarbide phases) near-equilibrium pressure p_{CO} , Pa measured experimentally by manometric method is obeyed the following rule $\lg p_{CO} = 13.59 - 16,580/T$, where T is temperature, K <i>See also</i> section C–O–Zr in Table I-2.14	

(continued)

Table 5.26 (continued)

System	Atmosphere	Temperature range, °C	Interaction character, products and/or compatibility	Reference
ZrC _{1-x} -CO ₂ ^a	CO ₂	–	Formation of ZrC _{1-x} O _y oxycarbide phases (extended substitution solid solution based on ZrC _{1-x} with approximate homogeneity limits: ~ZrC _{0.60} ~ZrC _{0.50} O _{0.20} ~ZrC _{0.40-0.60} O _{0.30-0.55} ~ZrC _{0.80} O _{0.20} ~ZrC _{0.99}) and subsequent formation of oxide scales	[33, 44, 74, 124, 1001, 1131, 1152, 1199, 1200, 1209, 1210, 1402, 1513]
	CO ₂	–	The selective character of interaction is inherent for ZrC _{1-x} materials, it is described by the following reactions: ZrC _{1-x} + yCO ₂ = ZrC _{1-x-y} + 2yCO↑ (for x ≈ 0, accompanied with mass loss), ZrC _{1-x} + yCO ₂ = ZrO _{2-z} + (3 - x - y - z)C + (2y + z - 2)CO↑ (for x >> 0, accompanied with mass gain) See also section C–O–Zr in Table I-2.14	
ZrC _{1-x} -Cl ₂	Cl ₂	~0–250	The preferential reaction under equilibrium conditions (in accordance with thermodynamic analysis): ZrC _{1-x} + (4 - 2x)Cl ₂ = ZrCl ₄ + (1 - x)CCl ₄ ↑	[32, 35, 46, 223, 452, 1130, 1132, 1133, 1135–1137]
	Cl ₂	~200–250	The initiation of interaction between powdered ZrC _{1-x} and gaseous Cl ₂ observed experimentally	
	Cl ₂	>250	Powdered ZrC _{1-x} burns in Cl ₂ or Cl ₂ -rich atmosphere	
	Cl ₂	~250–750	The interaction leads to the volatilization of ZrCl ₄ and formation of carbon: ZrC _{1-x} + (3 - x)Cl ₂ = ZrCl ₄ ↑ + [(1 - x)/2]C + [(1 - x)/2]CCl ₄ ↑ via the chemical reaction, which is preferential under equilibrium conditions (in accordance with thermodynamic analysis)	
	Cl ₂	400	Powdered ZrC _{1-x} is easily attacked by Cl ₂	
	Cl ₂	450–650	The chlorination rate is linear (apparent activation energy E ≈ 60 kJ mol ⁻¹)	
	Cl ₂	550	ZrC _{1-x} powder (850 mg) are chlorinated completely after 4 h exposure ^b	
	Cl ₂	650–950	The chlorination rate is linear (apparent activation energy E ≈ 10 kJ mol ⁻¹)	
	Cl ₂	700–800	Powdered ZrC _{1-x} decomposes easily and completely	
	Cl ₂	~700–1200	The preferential reaction under equilibrium conditions (in accordance with thermodynamic analysis): ZrC _{1-x} + 2Cl ₂ = ZrCl ₄ ↑ + (1 - x)C; in steady-flow chlorination, the gas flow rate was shown to have a significant influence on the reaction rate, a decrease in Cl ₂ gas pressure creates a local atmosphere near the ZrC _{1-x} surface causing the reaction rate to drop	

(continued)

Table 5.26 (continued)

System	Atmosphere	Temperature range, °C	Interaction character, products and/or compatibility	Reference
ZrC _{1-x} -F ₂	F ₂	>25	Powdered ZrC _{1-x} burns in F ₂ or F ₂ -rich atmosphere	[46, 223, 452, 1134, 1136, 1137, 1207]
	F ₂	~250–300	Electron-beam melted ZrC _{-1.0} burns in F ₂ or F ₂ -rich atmosphere	
	F ₂ (4.1 kPa), He	280–410	The formation of soft and fluffy uniform ZrF ₄ scales with poor adhesion, the reaction rate is linear (mass gain with 0.1–3.7 mg cm ⁻² min ⁻¹ , $E = 92 \pm 7$ kJ mol ⁻¹ , the rate is approximately proportional to $p_{F_2}^{1/2}$)	
	F ₂ (0.4 kPa), He	720–970	Since ZrF ₄ is very volatile in this temperature range, practically no scales is formed on ZrC _{1-x} surface, the reaction rate is linear (mass loss with 0.91–1.05 mg cm ⁻² min ⁻¹ , practically $E \approx 0$, the rate is approximately proportional to $p_{F_2}^{3/2}$), the rate-determining process is the diffusion of F to the reaction surface through the gaseous products	
ZrC _{1-x} -H ₂	H ₂	–	Coefficients of surface recombination of H atoms (measured experimentally by “mobile overlapping sample” technique) are 0.056 for ZrC _{0.80} and 0.030 for ZrC _{0.99} phases	[33, 223, 260, 319, 336, 337, 452, 515, 517, 762, 1021, 1022, 1138–1152, 1249]
	H ₂	–	Formation of carbohydride phases ZrC _x H _y ($x = 0.30$ – 0.65 , $y = 0.30$ – 1.25 , including Zr ₂ CH _x and Zr ₃ CH _x) ^c	
	H ₂ (pure)	800	The total content of carbon in powdered ZrC _{0.97} after 2 h exposure decreases from 11.5% to 11.1% (content of non-combined carbon from 0.1% drops to zero)	
	H ₂ (flow)	1250	Powdered ZrC _{1-x} interacts (or burns) intensively	
	H ₂ , C ₂ H ₂	1730–2730	For the following reaction ZrC _{1-x} (solid) + [(1 - x)/2]H ₂ (gas) = Zr(gas) + [(1 - x)/2]C ₂ H ₂ (gas), calculated equilibrium partial pressures $p_{C_2H_2}$ are 10^{-9} – 5×10^{-3} Pa for ZrC _{0.60} and 50 – 2×10^4 Pa for ZrC _{0.99}	
	H ₂ , CH ₄	1730–2730	For the following reaction ZrC _{1-x} (solid) + 2(1 - x)H ₂ (gas) = Zr(gas) + (1 - x)CH ₄ (gas), calculated equilibrium partial pressures p_{CH_4} are 10^{-4} – 10^{-2} Pa for ZrC _{0.60} and 50 – 10 Pa for ZrC _{0.99}	
	H ₂	2000–2500	Weak interaction with the minimal determined mass change	
	H ₂	2200–2480	Powdered ZrC _{1-x} is stable in static conditions (2 h exposure)	

(continued)

Table 5.26 (continued)

System	Atmosphere	Temperature range, °C	Interaction character, products and/or compatibility	Reference
	H ₂	~2800	The exposure of ZrC _{1-x} materials in H ₂ for 1–2 h results in inhomogeneous carbon concentration in bulk, but also leads to the change of microstructure, decrease of density and five-fold drop of strength	
	H ₂	~3100	The mass loss of ZrC _{~1.0} materials amounts up to $\sim 4 \times 10^{-2} \text{ g cm}^{-2}$ (1½ h exposure) <i>See also</i> section C–H–Zr in Table I-2.14	
ZrC _{1-x} –‘ZrO’–H ₂	H ₂	–	Formation of ZrO _{0.6} C _{0.2} H _x	[1138]
ZrC _{1-x} –H ₂ O ^a	H ₂ O, 100 MPa	200–400	<i>See also</i> section C–H–O–Zr in Table I-2.14 The hydrothermal oxidation reaction $\text{ZrC}_{1-x} + (2-y)\text{H}_2\text{O} = \text{ZrO}_{2-y} + (1-x)\text{CH}_4 + (2x-y)\text{H}_2$ of powdered ZrC _{0.98} (mean particle size – 3.2 μm, contents: non-combined C – 0.24%, O – 0.11%, N – 0.25%, H – 0.002%, Fe – 0.01%) converts it into α-ZrO _{2-x} (completely at >270 °C and exposure >10 h, or at >340 °C and exposure >3 h); the process is controlled by phase boundary reactions with apparent activation energy $E \approx 80\text{--}100 \text{ kJ mol}^{-1}$ (protective oxide layer does not form)	[10, 33, 46, 1131, 1138, 1155–1157, 1193, 1210]
	H ₂ O	300–400	Bulk ZrC _{1-x} materials are stable in water steam	
	H ₂ O	315	Non-stoichiometric ZrC _{1-x} phases are more reactive than near-stoichiometric phase	
	H ₂ O/O ₂ . 21–42/ >0.5 kPa	450–580	Water vapour accelerates the oxidation surface reaction of powdered ZrC _{1-x}	
	H ₂ O, He	500–950	The main hydrolytic reactions in superheated steam are: $\text{ZrC}_{1-x} + 2(1-x)\text{H}_2\text{O} = \text{ZrO}_{2-2x} + (1-x)\text{CH}_4$, $\text{ZrC}_{1-x} + (4-b)\text{H}_2\text{O} = \text{ZrO}_{2-x(b-2)} + b(1-x)\text{CO} + (1-b)(1-x)\text{CO}_2 + (4-b)\text{H}_2$, while the contribution of the reaction $\text{ZrC}_{1-x} + 2(1-x)\text{H}_2\text{O} = \text{ZrO}_{2-2x} + (1-x)\text{C} + 2(1-x)\text{H}_2$ is rather negligible; powdered ZrC _{0.99} (contents: non-combined C – 0.28%, O – 0.25%, N – 0.19%) converts into β-ZrO _{2-x} at ≤800 °C and α-ZrO _{2-x} – at ≥800 °C, with temperature growth the evolution of H ₂ increases monotonously from 7.1 to 28.5 mol kg ⁻¹ and molar ratio of CO:CO ₂ :CH ₄ (a conversion rate is given in brackets) varies from 1.0:0.5:0.6 (2.1%) at 500 °C to 1.0:2.5:0.03 (77.2%) at 800 °C, and 1.0:0.7:0.004 (93.3%) at 950 °C	

(continued)

Table 5.26 (continued)

System	Atmosphere	Temperature range, °C	Interaction character, products and/or compatibility	Reference
	H ₂ O	–	Formation of ZrO _{0.6} C _{0.2} H _x oxycarbonyhydride phases <i>See also</i> section C–H–O–Zr in Table I-2.14	
ZrC _{1-x} –ZrN _{1±x}	H ₂ O, He –H ₂ O	500–950	Hydrolysis of ZrC _x N _y monocarbonitride phases leads to the evolution of H ₂ (larger amounts of H ₂ evolves in the phases richer in C), CO, CO ₂ (delayed in release), CH ₄ (small amounts, the phases richer in N are more productive of it), NH ₃ and N ₂ , and precipitation of C (converted thereafter into CO ₂ and H ₂); the residue consists of α/β-ZrO _{2-x} mixture at lower temperatures and α-ZrO _{2-x} phase at higher temperatures	[1156]
ZrC _{1-x} –HX (X = F, Cl, Br, I)	HX	–	Powdered ZrC _{1-x} decomposes by gaseous hydrogen halides easily <i>See</i> Tables 5.27 and 5.29	[223]
ZrC _{1-x} –He				
ZrC _{1-x} –I ₂	I ₂	500–800	Powdered ZrC _{1-x} burns in I ₂ or I ₂ -rich atmosphere	[223, 452, 1354]
	I ₂	780–800	The ZrI ₄ yield of the following reaction ZrC _{1-x} + 2I ₂ = ZrI ₄ + (1 - x)C is 97% (15 h exposure) <i>See</i> Table 5.27	
ZrC _{1-x} –Kr				
ZrC _{1-x} –N ₂	N ₂	>800	Formation of various monocarbonitride ZrC _x N _z (0.54 ≤ x + z ≤ 1.04) and mononitride ZrN _{1±x} phases	[1, 32, 33, 39, 42, 46, 47, 51, 59, 124, 126, 200, 213, 223, 278, 691, 692, 703, 962, 992, 994, 1153, 1158, 1201]
	N ₂	1150	Formation of monocarbonitride (cubic) continuous solid solution with the homogeneity range within ~ZrC _{0.56-0.59} – ~ZrC _{0.95} –~ZrN _{0.54-0.56} –~ZrN _{1.04} compositions	
	N ₂ , 0.1–30 MPa	1400	Treatment of porous ZrC _{1-x} in N ₂ leads to the formation of ZrC _{0.48} N _{0.52} at p _{N2} = 0.1 MPa and ZrC _{0.28} N _{0.72} at p _{N2} = 30.0 MPa (36–37 h exposure)	
	N ₂	>1500	Formation of mononitride ZrN _{1±x} phases	
	N ₂	1500–2500	Formation of various monocarbonitride ZrC _x N _z and mononitride ZrN _{1±x} phases	
	N ₂ , 0.1–30 MPa	1800	Treatment of porous ZrC _{1-x} in N ₂ leads to the formation of ZrC _{0.69} N _{0.31} at p _{N2} = 0.1 MPa and ZrC _{0.39} N _{0.61} at p _{N2} = 30.0 MPa (8 h exposure) Data available in literature are controversial <i>See also</i> section C–N–Zr in Table I-2.14	

(continued)

Table 5.26 (continued)

System	Atmosphere	Temperature range, °C	Interaction character, products and/or compatibility	Reference
ZrC _{1-x} -NH ₃	NH ₃	<400–500	No interaction	[223]
ZrC _{1-x} -O ₂ ^{a,d,e}	Air, O ₂	–	Formation of ZrC _{1-x} O _x oxycarbide (cubic) phases, extended solid solutions based on ZrC _{1-x} with ~ZrC _{0.60} ~ZrC _{0.50} O _{0.20} ~ZrC _{0.40-0.60} O _{0.30-0.55} ~ZrC _{0.80} O _{0.20} ~ZrC _{0.99} approximate homogeneity limits	[1, 14, 30–33, 35, 37, 42, 46, 74, 92, 96, 106–108, 124, 223, 250, 265, 319, 452, 519, 630, 932, 971, 972, 977, 980–983, 986, 999–1001, 1075, 1077, 1152, 1154, 1159–1224, 1248, 1264, 1265, 1322–1327, 1332, 1373, 1383, 1402, 1423, 1424, 1445, 1451, 1452, 1551]
	O ₂ , 10 ⁻⁸ Pa	20–30	The single crystal ZrC _{0.93} (111) clean surface (prepared in a vacuum chamber by flashing at <i>T</i> > 1500 °C) adsorbs O ₂ dissociatively (chemisorption bonding)	
	O-plasma, 6.7 Pa	20–30	No oxidation of ZrC _{1-x} coating and powders (exposure – up to 4 h)	
	Air	250–400	During the heat treatment of ZrC _{0.60} the diffusion of O is significantly facilitated through the ordered C vacancies with the formation of ordered ZrC _{0.60} C _{0.40} oxycarbide; at > 350 °C metastable β-ZrO _{2-x} nanocrystals are gradually developed	
	Air	200–450	The oxidation of hot-pressed ZrC _{-1.0} leads to the formation of oxycarbide ZrC _{1-x} O _x outer layer, which keeps little change with time while <i>x</i> attains 0.58; the electrical resistance of outer layer increases from ~0.4 to ~7 μΩ m	
	Air	280–290	TG-curves and DTA-peaks indicate onset of oxidation of nanopowdered ZrC _{-1.0} (mean grain size – 40 nm)	
	Flow O ₂ (5–50 kPa), Ar	320–1000	The non-isothermal oxidation kinetics of powdered ZrC _{-1.0} (surface area 0.7 m ² g ⁻¹) (with heating rates varied from 5 to 15 K min ⁻¹) is described by Ginstling-Brounstein's equation with apparent activation energies <i>E</i> ≈ 140 kJ mol ⁻¹ (<i>p</i> _{O₂} = 5 kPa), <i>E</i> ≈ 110–125 kJ mol ⁻¹ (<i>p</i> _{O₂} = 10 kPa) and <i>E</i> ≈ 100 kJ mol ⁻¹ (<i>p</i> _{O₂} = 50 kPa); the conversion of carbide to oxides is controlled by O diffusion through the formation of oxycarbide as the intermediate, γ-ZrO _{2-x} (stabilized by C) and α-ZrO _{2-x} are present in the oxide scales at <i>T</i> < 800 °C, while only α-ZrO _{2-x} is in the scales at <i>T</i> > 800 °C	
	O ₂ (1–40 kPa), Ar	380–400	TG-curves and DTA-peaks indicate onset of oxidation of powdered ZrC _{-1.0} (grain size – 1–10 μm, surface area – 1.7 m ² g ⁻¹ , contents: non-combined C < 0.5%, O – ~2.0%)	

(continued)

Table 5.26 (continued)

System	Atmo- sphere	Temperature range, °C	Interaction character, products and/or compatibility	Reference
	O ₂ /Ar, 1.3–7.9/ 32–38 kPa	380–550	The oxidation kinetics of powdered ZrC _{-1.0} (mean grain size – 3.3 μm, surface area – 0.7 m ² g ⁻¹) is described by Jander's equation with apparent activation energy $E \approx 140 \text{ kJ mol}^{-1}$ (<470 °C) and $E \approx 180 \text{ kJ mol}^{-1}$ (>470 °C); the oxidation process is determined by O diffusion through compact quasi-amorphous γ -ZrO _{2-x} layer (<470 °C), or faster O diffusion along the grain boundaries in crystallized γ -ZrO _{2-x} (>470 °C)	
	Air (circulated)	385	A TG-curve indicates onset of oxidation (mass gain) of powdered ZrC _{0.70} (mean particle size – 70–80 μm)	
	O ₂ , 1.3 Pa –2.7 kPa	400–600	Oxidation of sintered ZrC _{0.86} (porosity – 5 and 30%, contents: non-combined C – 0.1%, O ≤ 0.05%, N ≤ 0.05%) leads to the increase of content of non-combined C, it is dispersed in ZrC _{1-x} O _y solid solutions (at 400–500 °C) and in γ -ZrO _{2-x} (at 600 °C)	
	Air (circulated)	400–600	The formation of ZrO ₂ C _x phase (?) with interplanar spacings slightly different from those of β -ZrO _{2-x}	
	Air (flow)	400–900	Powdered ZrC _{1-x} (mean particle size – 1.5 μm, specific surface area – 0.59 m ² g) is oxidized 22% at 400 °C, 90% at 500 °C and complete at >500 °C, no change in the surface area at 400 °C, but the max. increase is up to 15.2 m ² g at 500 °C (or from 16.7 m ² g after 0.25 h to 3.2 m ² g after 20 h) and smaller increases are 9.9 m ² g (at 600 °C) and 5.3 m ² g (at 700 °C) due to sintering of the oxide scales, the data not indicated specially are for 1 h exposure ($E = 14.6 \pm 0.3 \text{ kJ mol}^{-1}$); the oxidation products are oxycarbide/suboxide intermediates (only at 400–500 °C and in traces, with a new phase (111) topotactically produced from (200) of initial carbide lattice), γ -ZrO _{2-x} (at 400–600 °C), γ -ZrO _{2-x} and α -ZrO _{2-x} (at >600 °C, with increasing amounts of α -ZrO _{2-x} at higher temperatures)	
	O ₂ , 13 kPa	400–1000	The effect of temperature on the oxidation of ZrC _{1-x} is estimated by activation energy $E \approx 290 \text{ kJ mol}^{-1}$ for diffusion controlled mechanism (at lower temperatures) and $E \approx 190 \text{ kJ mol}^{-1}$ for phase boundary controlled mechanism (at higher temperatures)	
	Air	450	The oxidation mass gain of ZrC _{-1.0} is ~20 mg cm ⁻² (1 h exposure) and ~60 mg cm ⁻² (2 h exposure)	

(continued)

Table 5.26 (continued)

System	Atmosphere	Temperature range, °C	Interaction character, products and/or compatibility	Reference
	O ₂ , 6.5 Pa – 0.7 MPa	450–580	Oxidation kinetics of powdered ZrC _{1-x} is controlled by two parallel processes: surface reaction of γ -ZrO _{2-x} formation (mostly accounted, kinetics is directly proportional to p_{O_2} (at $p_{O_2} < 10$ kPa) and described by linear law, apparent activation energy $E \approx 190$ kJ mol ⁻¹) and O diffusion forming oxycarbide solid solution ZrC _{1-x} O _y ($E \approx 220$ kJ mol ⁻¹); the initial process of O chemisorption on ZrC _{1-x} surface is characterized by $E = 54$ kJ mol ⁻¹	
	Flow O ₂ , 0.13 Pa– 13 kPa	450–700	The oxidation of powdered ZrC _{1-x} leads to the formation of γ -ZrO _{2-x} stabilized by the presence of C; no oxycarbide phases were detected	
	Air	450–800	The oxidation of ZrC _{1-x} powders is detectable from 450 °C, both α -ZrO _{2-x} and β -ZrO _{2-x} phases coexist in the oxide scales at 550–800 °C; β -ZrO _{2-x} is stabilized at lower temperatures on smaller particles, at $T > 650$ °C the formation of α -ZrO _{2-x} is favoured	
	O ₂	~480	A TG-DSC-curve indicates onset of oxidation (mass gain) of fine-dispersed ZrC _{-1.0} (mean particle size – 0.8 μ m, specific surface area – 1.3 m ² g ⁻¹)	
	Flow O ₂ (20 kPa), Ar	485–530	The isothermal oxidation kinetics of powdered ZrC _{-1.0} (surface area – 0.7 m ² g ⁻¹) is described by Ginstling-Brounstein equation with activation energy $E \approx 130$ kJ mol ⁻¹	
	O ₂ (1–40 kPa), Ar	500–540	MS-curves indicate onset of C burning-off (CO ₂ evolution) in powdered ZrC _{-1.0} (grain size – 1–10 μ m, surface area – 1.7 m ² g ⁻¹ , contents: non-combined C < 0.5%, O – ~2.0%); the current rate of oxidation (dependent on p_{O_2}), defined for the complete carbide-oxide conversion, reaches 20–40%	
	O ₂ , 6.7 Pa –1.3 kPa	500–600	At earlier stages (0.5–30 min exposure) the oxidation of ZrC _{1-x} phases is accompanied with release of CO (for $x \leq 0.03$) or a CO ₂ + CO mixture with ratio CO ₂ : CO > 1 (for $x \geq 0.23$, the ratio increases with growth of value x) in accordance with the following reactions: $\text{ZrC}_{1-x} + y/2 \text{O}_2 = \text{ZrC}_{1-x-y} + y\text{CO}\uparrow$ (for $x \leq 0.03$, accompanied with mass loss), $\text{ZrC}_{1-x} + (2-z)/2 \text{O}_2 = \text{ZrO}_{2-z} + (1-x)\text{C}$ $\text{C} + (m+n/2)\text{O}_2 = m\text{CO}_2\uparrow + n\text{CO}\uparrow$ (for $x \geq 0.23$, $m/n > 1$, accompanied with mass gain)	

(continued)

Table 5.26 (continued)

System	Atmosphere	Temperature range, °C	Interaction character, products and/or compatibility	Reference
	O ₂ (2.6 kPa), Ar	500–600	The oxidation of single crystal ZrC _{0.97} (100) leads to the formation of the oxide scale divided into inner (poreless amorphous ZrO _{2-x} containing γ -ZrO _{2-x} particles in the regions remote from the reaction surface and 14–23 at.% of residual (unoxidized) C) and outer (aggregated γ -ZrO _{2-x} particles containing 7–10 at.% of residual C) zones; the thickness of inner zone increases parabolically reaching a constant value of 2–3 μ m (at 500 °C, 240 h exposure) in contrast to that of outer zone, which increases linearly with time	
	Air	500–850	In the initial stage of the oxidation of ZrC _{0.95} powder the effect of temperature is estimated by $E \approx 170 \text{ kJ mol}^{-1}$	
	Air	500–850	The oxidation of powdered ZrC _{0.98} (mean particle size – 10–40 μ m, contents: non-combined C – 0.30%, O – 0.08%, N – 0.01%) is described by the transitional between parabolic and linear laws kinetics (<750 °C) or approximately linear kinetics (>750 °C), oxide scales consist of γ -ZrO _{2-x} with noticeable amount of elemental C in it (<750 °C) or α -ZrO _{2-x} (>750 °C); at $T < 750 \text{ }^\circ\text{C}$ oxide scales on carbide are protective, max. content of elemental C in the scales coincides with the beginning of their destruction as a result of the disturbance produced by CO release	
	O ₂	~500–900	Both ZrC _{1-x} powders and single crystals start to interact with O ₂ in the accordance with the following reaction: $\text{ZrC}_{1-x} + (y/2 + z)\text{O}_2 = \text{ZrC}_{1-x-z}\text{O}_y + z\text{CO}_2 \uparrow,$ as the process proceeds the oxycarbide-gas interface becomes saturated in O, forming the oxide scale: $\text{ZrC}_{1-x-z}\text{O}_y + (2 - y - \delta)/2 \text{O}_2 = \text{ZrO}_{2-\delta} + (1 - x - z)\text{C},$ this layer is dense and protective, which results in parabolic kinetics, and contain some residual elemental C in amorphous state; once this layer reaches 1–10 μ m in thickness, the stresses in it leads to crack formation, which results in linear kinetics, with the dense layer maintaining a constant thickness as new scale layer growth occurs, while the outer portions continue to crack forming pathways for O ingress to oxidize C in the oxide scale (the evolution of C oxides also contributes to additional crack and pore formation in the outer (non-protective) layer	

(continued)

Table 5.26 (continued)

System	Atmo- sphere	Temperature range, °C	Interaction character, products and/or compatibility	Reference
	Air	500–1000	The oxidation of hot-pressed $ZrC_{-1.0}$ leads to the formation of intermediate Zr_2O (?), which almost completely transferred to ZrO_2 phases at higher temperatures	
	Air, static conditions	500–1200	At earlier stages (5 min exposure) oxidation of hot-pressed $ZrC_{-1.0}$ (porosity $\leq 1\%$) results in the formation of the oxide scale, which consists mainly of γ - ZrO_{2-x} with C inclusions (at ≤ 900 °C metallic Zr and at ≥ 1000 °C α - ZrO_{2-x} were observed too); after 6 h exposure the scale composition is shifted to α/γ - ZrO_{2-x} – $ZrN_{1\pm x}$ mixture accompanied with a well-defined C layer (at ≤ 800 °C metallic Zr was observed too), the max. mass gain (up to 100 mg cm^{-2}) is observed at 800 °C ^f	
	O ₂ , 0.13– 27 kPa	500–1200	At earlier oxidation stages (5–10 min exposure) of sintered $ZrC_{0.99}$ (porosity – 30%, contents: non-combined C – 0.20%, O \leq 0.05%, N \leq 0.05%) the effect of temperature is estimated by $E \approx 170 \text{ kJ mol}^{-1}$ and effect of oxygen pressure – by power (exponent) index $m = 1/3$	
	O ₂ (0.02– 2.0 kPa), Ar	500–1500	The isothermal oxidation (1–20 h exposure) of single crystal $ZrC_{0.97}$ (200), (220) leads to the formation of the oxide scale divided into outer layer (cracked and porous, growing linearly and formed by preferentially oriented α - ZrO_{2-x} and β - ZrO_{2-x} crystals containing 5–10 at.% C) and inner film (almost poreless, growing parabolically to finally attain a constant thickness and formed by amorphous (at < 1100 °C) or relatively ordered (at > 1100 °C) elemental (non-combined) C (up to 25 at.% with dispersed γ - ZrO_{2-x} and α/β - ZrO_{2-x} particles in it, all of them – 1–10 nm in size); a considerable amount of C concentrated at the interface between carbide and inner film and gradient of O concentration both in carbide and inner film are observed, γ - ZrO_{2-x} crystallites are formed directly at the interface on the ZrC_{1-x} lattice while maintaining the above preferred orientation	
	O ₂ , 0.9–2.7 kPa	550–600	Oxidation of ZrC_{1-x} ($0.13 \leq x \leq 0.34$) phases is accompanied with the precipitation of elemental carbon, which is more intensive for the phases with less carbon deficit	

(continued)

Table 5.26 (continued)

System	Atmosphere	Temperature range, °C	Interaction character, products and/or compatibility	Reference
	O ₂ , 0.01–0.1 MPa	550–650	Oxidation kinetics of powdered ZrC _{1-x} is described by linear law with activation energy $E = 70 \pm 7 \text{ kJ mol}^{-1}$; porous oxide scales formed on carbide are not protective	
	O ₂ , 0.13–27 kPa	550–1200	At earlier oxidation stages (5 min exposure) of sintered ZrC _{0.66} (porosity – 5%, contents: non-combined C – 0.1%, O ≤ 0.05%, N ≤ 0.05%) the effect of temperature is estimated by $E = 160 \text{ kJ mol}^{-1}$ and effect of oxygen pressure – by power (exponent) index $m = 1/4$	
	O ₂ , 0.13–27 kPa	550–1200	Oxidation kinetics of arc-melted ZrC _{-1.0} (content non-combined C – 5.0%) is described by parabolic law, the effect of temperature is estimated by $E \approx 135 \text{ kJ mol}^{-1}$ and effect of oxygen pressure – by power (exponent) index $m = 1/3$ (at 550–700 °C) and $m = 1/10$ (at 800–1200 °C); at $T \leq 1000 \text{ °C}$ formed oxide scales are adherent to substrate only at earlier stages of oxidation	
	Air	575	A DTA-peak indicates onset of oxidation of Zr in powdered ZrC _{0.98} (mean particle size – 10–40 μm, contents: non-combined C – 0.30%, O – 0.08%, N – 0.01%)	
	O ₂ (0.5 kPa), Ar	580–900	The oxidation rate of powdered ZrC _{1-x} is proportional to p_{O_2} , but virtually independent of T , as oxidation kinetics is controlled by the rate of O arrival at the reaction surface; $\gamma\text{-ZrO}_{2-x}$ is the major oxidation product, though $\alpha\text{-ZrO}_{2-x}$ is observed too	
	O ₂ (2.6 kPa), Ar	600	The oxidation of single crystal ZrC _{0.97} (100) occurs through the dissolution of O accompanied with the precipitation of C: $\text{ZrC}_{1-x} + y/2 \text{ O}_2 = \text{ZrC}_{1-x-z}\text{O}_y + z\text{C}$, and subsequent formation of oxygen-deficit $\gamma\text{-ZrO}_{2-x}$ oxide scale: $\text{ZrC}_{1-x-z}\text{O}_y + (2 - y - \delta)/2 \text{ O}_2 = \text{ZrO}_{2-\delta} + (1 - x - z)\text{C}$; high C concentration (up to 25 at.%) is observed at the carbide-oxide interface and in the oxide scale after 1 h exposure	
	O ₂ /Ar, ~20/80 kPa	600–700	Pure (single-phase) ZrC _{1-x} ceramics is oxidized completely during continuous heating with 20 °C min^{-1} rate	
	Air, static conditions	600–1000	At earlier stages (4–30 min exposure) of oxidation of arc-melted ZrC _{0.61–0.83} materials the dissolution of O ₂ and N ₂ and formation of ZrC _{1-x} N _y O _z oxycarbonitride phase is observed; the oxidation process of ZrC _{1-x} phases with greater deviation from the stoichiometry starts earlier	

(continued)

Table 5.26 (continued)

System	Atmosphere	Temperature range, °C	Interaction character, products and/or compatibility	Reference
	Air	600–1200	The rate of oxidation of arc-melted $ZrC_{0.61-0.96}$ materials (content non-combined C – 0.12–0.20%) increases with a decrease in the carbon content of monocarbide phases, the formed oxide scales consist of γ - ZrO_{2-x} and α - ZrO_{2-x} phases at all the temperatures, on the boundary of the scales and carbide phases an elemental C layer is formed by the reaction $ZrC_{1-x} + (2 - \delta)/2 O_2 = ZrO_{2-\delta} + (1 - x)C$ followed by the formation of C oxides	
	Air (flow)	600–1200	Oxidation kinetics of powdered ZrC_{1-x} (mean grain size – 1.5 μm , specific surface area – 0.59 $m^{-2} g$) is $2/3$ -ordered (plots of the mass of remaining carbide, fraction unoxidized, is linear with time); the oxidation leads to the formation of γ - ZrO_{2-x} and α - ZrO_{2-x} with increasing amounts of α - ZrO_{2-x} at higher temperatures, and appearance of β - ZrO_{2-x} at $T \geq 1200$ °C	
	Air	650–700	The oxidation of CVD- ZrC_{1-x} coating leads to the formation of α - ZrO_{2-x} (mainly) and β - ZrO_{2-x} phases	
	Flow O_2/Ar , 0.8 Pa/0.16 MPa	675	During the non-isothermal oxidation of sintered $ZrC_{-1.0}$ (porosity $\sim 30\%$) with heating rate 10 $K min^{-1}$, the current reactivity of $\sim 7 \times 10^{-3} nmol cm^{-2} s^{-1}$ for carbide interaction with O_2 was detected	
	Air	700–800	Both γ - ZrO_{2-x} and α - ZrO_{2-x} phases are detected in the oxide scale formed on powdered $ZrC_{0.98}$ (mean particle size – 10–40 μm , contents: non-combined C – 0.30%, O – 0.08%, N – 0.01%); the attainment of max. content of non-combined C in the oxide scale coincides with the beginning of its destruction	
	O_2 , 1.3–2.7 kPa	700–1000	Oxidation kinetics of sintered $ZrC_{0.92}$ (porosity $\leq 5\%$) is described by linear law, the effect of temperature is described by $E \approx 60 kJ mol^{-1}$ and effect of oxygen pressure – by power (exponent) index $m = 1.3$ (oxidation process is controlled by a surface reaction at the α - ZrO_{2-x} - $ZrC_{1-x}O_3$ phase boundary)	
	O_2 (0.08–80 kPa), Ar	700–1500	The isothermal oxidation of single crystal $ZrC_{0.97}$ (200), (220) is described by linear kinetics, the duplex oxide scale consists of outer zone (cracked and porous, 6–11 at.% of elemental C) growing linearly and inner zone (poreless, 20–25 at.% of elemental C) growing parabolically	

(continued)

Table 5.26 (continued)

System	Atmosphere	Temperature range, °C	Interaction character, products and/or compatibility	Reference
	Air	725	A DTA-peak indicates onset of oxidation of C in powdered $\text{ZrC}_{0.98}$ (mean particle size – 10–40 μm , contents: non-combined C – 0.30%, O – 0.08%, N – 0.01%)	
	Air flow, $\sim 5 \text{ cm s}^{-1}$	800	Oxidation mass gain of hot-pressed ZrC_{1-x} (porosity $\sim 5\%$) is 20–50 mg cm^{-2} (exposure – 0.5–5.0 h)	
	Air	800–900	CVD- ZrC_{1-x} coating is oxidized completely; the oxide scale consists of $\alpha\text{-ZrO}_{2-x}$ only phase (1 h exposure)	
	Air, static conditions	800–1200	Recession rates (determined from the change in dimensions after the removal of oxide scale for 15 min exposure) of hot-pressed $\text{ZrC}_{-1.0}$ are 28, 97 and 114 nm s^{-1} at 800, 1000 and 1200 °C, respectively ($E \approx 70 \text{ kJ mol}^{-1}$)	
	Air, O_2	800–1200	The “Maltese cross” oxidation mechanism of dense ZrC_{1-x} cuboids comprised 3 steps: delamination of sample edges, crack formation at corners and crack propagation towards the inner core with formation of microcracks parallel to the interface that increase the accessible surface area followed by a drastic volume expansion; the reaction interface comprises an amorphous C layer (thickness $< 2 \mu\text{m}$) with $\alpha\text{-ZrO}_{2-x}$ nanocrystals ($< 5 \text{ nm}$) embedded in it	
	O_2/Ar , 10–13 Pa/ 0.1 MPa	810–820	The oxidation of single crystal $\text{ZrC}_{0.98}$ (content O $< 0.002\%$) leads to the formation of $\gamma\text{-ZrO}_{2-x}$ and $\alpha\text{-ZrO}_{2-x}$ phases containing elemental C (the latter one is in the amorphous state); during the cooling treatment, due to crack formation attributed to thermal expansion mismatch between carbide and oxides, a relatively small fraction of C is burnt with CO and CO_2 formation	
	O_2 (0.3–44 kPa), He (flow rate $\sim 1 \text{ cm}^3 \text{ s}^{-1}$)	850–1900	Oxidation kinetics of zone-refined $\text{ZrC}_{0.96}$ (contents: O – 0.005%, N – 0.067%) is described by linear law with non-preferential interaction (i.e. Zr is oxidized at the same rate as C), the oxidation process is controlled by the rate of O_2 arrival at the surface, only $\alpha\text{-ZrO}_{2-x}$ phase was detected in oxide scales, while both CO and CO_2 were present in gaseous reaction products (materials disintegration due to the growth of oxide in pre-existing cracks and grain boundaries is observed at $T = 850\text{--}1300 \text{ }^\circ\text{C}$, the average oxidation mass gain is $\sim 25\text{--}30 \text{ mg cm}^{-2}$ for 2 h exposure at $T = 1600\text{--}1900 \text{ }^\circ\text{C}$ and $p_{\text{O}_2} = 1.2 \text{ kPa}$)	

(continued)

Table 5.26 (continued)

System	Atmosphere	Temperature range, °C	Interaction character, products and/or compatibility	Reference
	O ₂	~870	The penetration of O into the bulk ZrC _{1-x} materials is 175 μm (100 h exposure)	
	Air	900	The oxidation mass gain of ZrC _{1-x} hot-pressed materials is 25–46 mg cm ⁻² (exposure – 1–5 h)	
	Air	900–1000	Hot-pressed ZrC _{1-x} materials are oxidized considerably	
	O ₂ , 0.03 kPa	900–1300	The oxidation mass gain of sintered ZrC _{0.92} (1–5% porosity, grain size – 50–100 μm) is 12–13 mg cm ⁻² (20 min exposure)	
	Air	980	Thickness of oxide scale on ZrC _{1-x} materials: 87.5 μm (50 h exposure) and 175 μm (100 h exposure)	
	Air	1000	The oxidation mass gain of ZrC _{1-x} hot-pressed materials is ~20 mg cm ⁻² (5 h exposure)	
	O ₂ , 4 × 10 ⁻³ – 4 × 10 ⁻⁷ Pa	1000–1200	Surface of ZrC _{1-x} materials is covered by a layer of O atoms adsorbed on a ZrC _{1-x} O _y monolayer	
	Air	1100–1200	The oxidation mass gain of ZrC _{1-x} hot-pressed materials is ~55–60 mg cm ⁻² (5 h exposure)	
	O ₂ , 3 Pa– 2.7 kPa	1100–1500	Oxidation kinetics of sintered ZrC _{0.92} (porosity ≤5%) is described by parabolic law °C and effect of oxygen pressure – by power (exponent) index $m = 0.3$ (1200 °C), “Maltese cross” dense oxide scales consist of inner (γ-ZrO _{2-x} ($x \approx 0.14$ at 1200 °C) stabilized by dissolved C (or ZrO ₂ C _x) and dispersed C) and outer (α-ZrO _{2-x}) layers; only ~70% of C remove from solids to gases to form CO ₂ , CO is observed in gaseous products only at $p_{O_2} < 13$ Pa (oxidation process is controlled by diffusion of O to the γ-ZrO _{2-x} -ZrC _{1-x} O _y phase boundary)	
	O ₂ , ~10 ⁻⁵ Pa	1200–1800	At earlier stages the oxidation of ZrC _{1-x} phases is accompanied with release of CO (for $x \approx 0$) or a CO ₂ + CO mixture (for $x \gg 0$) in accordance with the following reactions: $\text{ZrC}_{1-x} + y/2 \text{O}_2 = \text{ZrC}_{1-x-y} + y\text{CO}\uparrow$ (for $x \approx 0$, accompanied with mass loss), $\text{ZrC}_{1-x} + [(2-z) + (1-x)(1+m)]/2$ $\text{O}_2 = \text{ZrO}_{2-z} + m(1-x)\text{CO}_2\uparrow +$ $(1-m)(1-x)\text{CO}\uparrow$ (for $x \gg 0$, $m \gg 1/2$, accompanied with mass gain)	

(continued)

Table 5.26 (continued)

System	Atmosphere	Temperature range, °C	Interaction character, products and/or compatibility	Reference
	Air flow, 41.5 m s ⁻¹ (0.72 d m ³ s ⁻¹)	1600–2200	Average recession rates (determined from the change in dimensions for 5 min exposure) of hot-pressed ZrC _{-1.0} are 0.5, 1.2 and 2.2 μm s ⁻¹ at 1600, 2000 and 2200 °C, respectively ($E \approx 70 \text{ kJ mol}^{-1}$)	
	O ₂ /C ₂ H ₂ torch	~2000–3000 (heat fluxes 0.24–0.42 kW cm ⁻²)	The CVD ZrC _{-1.0} coating (thickness ~75–85 μm) is oxidized forming transitional ZrC _{1-x} O _y (thickness ~8–25 μm) and outer ZrC _{-2.0} layers, which act as a good O diffusion barrier and exhibit efficacious mechanical denudation resistance	
	O ₂ /C ₂ H ₂ torch	≤~2800	The supersonic plasma-sprayed ZrC _{1-x} coating (thickness ~200 μm, contaminated with Zr oxides) has linear ablating rate ~0.9 μm s ⁻¹ and mass gain rate ~2.0 mg s ⁻¹ (30 s exposure); during the ablation process the reaction ZrC _{1-x} + [2 + (1 + m)(1 - x)]/2 O ₂ = ZrO ₂ + m(1 - x)CO ₂ ↑ + (1 - m)(1 - x)CO↑ produce the liquid oxide layer, which acts as a thermal barrier and reduces the diffusion of O into the bulk material	
	O ₂ /C ₂ H ₂ torch	≤~2800	The CVD ZrC _{0.70} coating (thickness > 200 μm) has ablating rates: linear ~0.3 μm s ⁻¹ and mass ~0.1 mg cm ² s ⁻¹ (4 min exposure)	
	O ₂ (~1 Pa), Ar	≥3300 (laser heating, ~25 kW cm ⁻²)	The surface heat treatment of ZrC _{0.82} O _{0.14} leads to the evolution of O in the form of the gaseous species ZrO and conversion of oxycarbide into the pure carbide phase of ZrC _{0.75} , while the grains of solids grow considerably; the traces of O ₂ present in the treatment cell react with the carbide surface also giving ZrO gas, and do not form any oxidised solid phases (oxide scales) See also section C–O–Zr in Table I-2.14 See Table 5.27	

ZrC_{1-x}-Xe

^aUnder the conditions simulated rocket combustion gases at the surface temperatures of ~2250 °C sintered ZrC_{1-x} was oxidized according to a parabolic law owing to the formation of an adherent oxide film (scale) [932]

^bIn this temperature range the chlorination can be also carried out in molten salts (e.g. LiCl-KCl melts) by means of electrochemical procedures (both dissolved chlorine and chlorine gas bubbles react with ZrC_{1-x})

^cThe analogous Ti₂CH and Hf₂CH phases were synthesized via hydrogen dissolution in non-stoichiometric carbides (dehydrogenation leads to the starting carbides again) by Goretzki et al. [1142, 1143]

^dFine zirconium carbide powders are pyrophoric and susceptible to oxidation at room temperature [39, 46, 96]

^eFor near-stoichiometric ZrC_{1-x} the value of the Pilling-Bedworth ratio $\alpha = M_O d_C / M_C d_O = 1.43$, where M_O is molecular mass of the oxide phase formed on the oxidation of 1 mol of carbide phase, M_C is molecular mass of carbide phase, d_C and d_O are the densities of carbide and oxide phases, respectively [1253]

^fTermed as a ridge temperature in accordance with Shabalin's "ridge effect" model [984, 985]

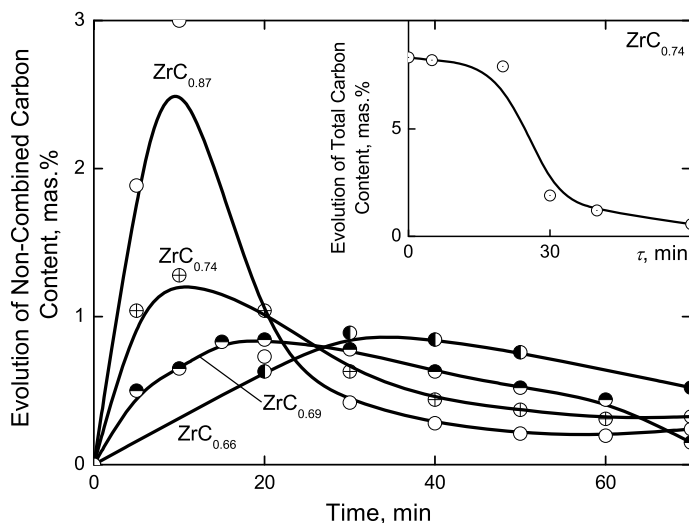


Fig. 5.37 Evolution of non-combined carbon content during the isobaric-isothermal oxidation of flat-plate samples of sintered ZrC_{1-x} materials with various deviations from the stoichiometry (porosity in the range of 5–15%) in the gas flow of oxygen with pressure of 2.67 kPa at temperature of 600 °C (*Inset* – evolution of total carbon content (corresponding to the total burning-off of carbon) in $ZrC_{0.74}$ during the oxidation process at the same conditions) [983]

ZrC_{1-x} phases are given in Table 5.27. Data on the catalytic activities of zirconium carbide are given in several works [1, 515, 710, 1089, 1094–1122, 1384, 1461, 1502]; the electrochemical behaviour of zirconium monocarbide materials in various media is described elsewhere [933, 1120–1130, 1345, 1346]. The parameters of wettability of ZrC_{1-x} phases with some liquid metals (melts) are listed in Table 5.28, the diffusion rates for the systems containing zirconium carbide phases are presented in species pairs within the various ranges of temperatures in the Table 5.29. The characters of chemical interaction of ZrC_{1-x} and $ZrC_{1-x}O_y$ phases with some common chemicals (acids, alkalies and salts in aqueous solutions and melts) are summarized in Tables 5.30 and 5.31.

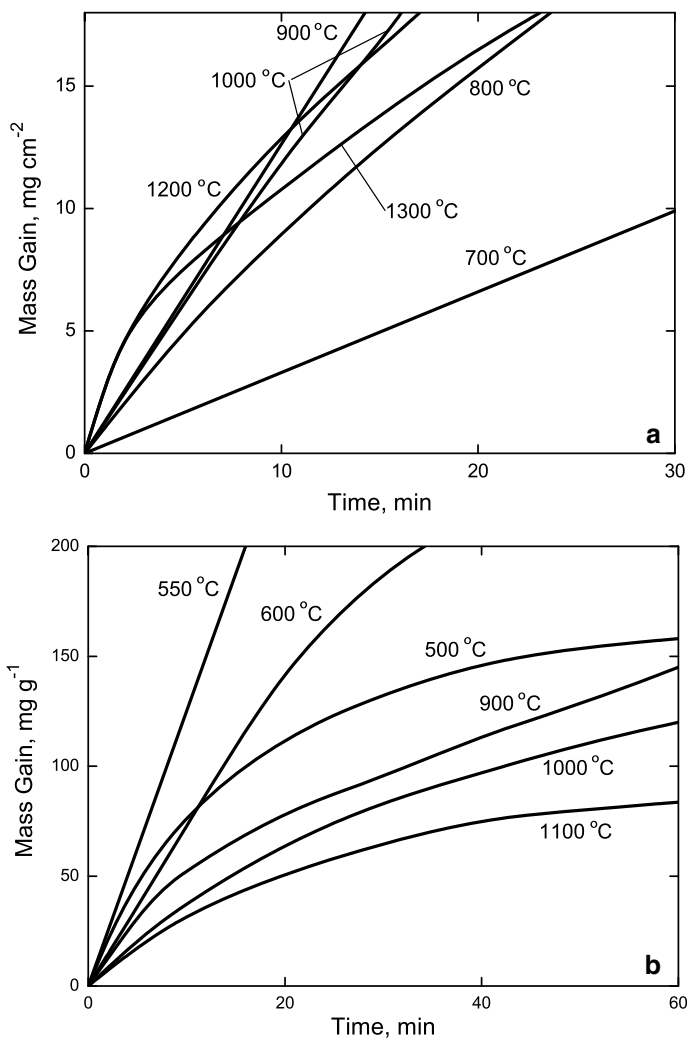


Fig. 5.38 Isothermal-isobaric oxidation kinetics curves for the flat-plate samples of sintered ZrC_{1-x} materials in gas flow at lower oxygen pressure p_{O_2} : (a) $ZrC_{0.92}$ (open porosity $\leq 5\%$), $p_{O_2} = 1.33$ kPa [980, 981]; (b) $ZrC_{0.99}$ (porosity – 30%, content non-combined C – 0.2%), $p_{O_2} = 0.40$ kPa [982]

Table 5.27 The radiochemical compatibility of ZrC_{1-x} materials with some fission products (in alphabetical order) and diffusion parameters of these products in carbide phases at irradiation and/or annealing temperatures

Fission product	Carbide phase composition	Temperature range, °C	Temperature range, Neutron irradiation fluence, cm^{-2}	Diffusion coefficient, $cm^2 s^{-1}$	Activation energy, $kJ mol^{-1}$	Release %	Reference
^{110m}Ag	$ZrC_{-1.0}$	900 ^a /1500(10 ⁴ h) ^b	3.4×10^{25} (fast)	—	—	— ^c	[96, 1211]
	$ZrC_{-1.0}$	1200 ^a /1500(10 ⁴ h) ^b	6.5×10^{25} (fast)	—	—	—	[96, 1211]
	$ZrC_{-1.0}$	~1200–1700	—	—	~80 ^d and ~225 ^e	—	[96, 1225]
	$ZrC_{-1.0}$	900 ^a	1.2×10^{25} (fast)	—	—	Good retention	[770, 773]
	$ZrC_{-1.0}$	~1200–1700	—	—	~290	—	[96, 1225]
	$ZrC_{-1.0}$	1400(220 h)	—	10^{-13} – 10^{-14}	—	Good retention	[96, 1227]
^{144}Ce	$ZrC_{-1.0}$ (content non-combined C ~ 3.4%)	1260(1040 h) ^a / 1600 ^b	1.4×10^{21} (fast)	~ 2.0×10^{-12}	—	<0.01 ^f	[4, 96, 781]
	$ZrC_{-1.0}$	900 ^a /1500(10 ⁴ h) ^b	3.4×10^{25} (fast)	—	—	Good retention	[96, 1211]
^{134}Cs / ^{137}Cs	$ZrC_{-1.0}$	1200 ^a /1500(10 ⁴ h) ^b	6.5×10^{25} (fast)	—	—	Good retention	[96, 1211]
	$ZrC_{-1.0}$	1200 ^a	5.0×10^{21} (fast)	—	—	Good retention	[96, 767]
	$ZrC_{-1.0}$	—	—	—	—	Good retention	[96, 1229]
	$ZrC_{-1.0}$	900 ^a	1.2×10^{25} (fast)	—	—	2 ^g	[770, 773]
	$ZrC_{-1.0}$	1600(4500 h) ^b	1.2×10^{25} (fast)	$(1-5) \times 10^{-14}$	—	0.03	[96, 770, 773]
	$ZrC_{-1.0}$	1800(3000 h) ^b	1.2×10^{25} (fast)	1×10^{-13} – 2×10^{-14}	—	0.04	[96, 770, 772]
^{137}Cs	$ZrC_{-1.0}$	2000(100 h) ^b	1.2×10^{25} (fast)	—	—	10	[770, 772]
	$ZrC_{-1.0}$	1200 ^a	5.0×10^{21} (fast)	—	—	— ^c	[96, 767]
	$ZrC_{0.98}$	~1200–1600	—	1.4×10^{-12} – 3.1×10^{-14}	~50	—	[96, 867]
	$ZrC_{-1.0}$ (content non-combined C ~ 3.4%)	1260(1040 h) ^a /1500– 1600 ^b	1.4×10^{21} (fast)	6.0×10^{-14} / 4.0×10^{-12} – 6.0×10^{-13} , or $D = 2.3 \times 10^{-3} \times \exp(-38,200/T)$ (see also Table 5.29)	~310–320	—	[4, 96, 781]
$ZrC_{-1.0}$	$ZrC_{-1.0}$	900 ^a /1500(10 ⁴ h) ^b	3.4×10^{25}	—	—	Good retention	[96, 1211]
	$ZrC_{-1.0}$	1200 ^a /1500(10 ⁴ h) ^b	6.5×10^{25}	—	—	Good retention	[96, 1211]

(continued)

Table 5.27 (continued)

Fission product	Carbide phase composition	Temperature range, °C	Neutron irradiation fluence, cm ⁻²	Diffusion coefficient, cm ² s ⁻¹	Activation energy, kJ mol ⁻¹	Release %	Reference
¹⁵⁴ Eu	ZrC _{-1.0}	900 ^a /1500(10 ⁴ h) ^b	3.4 × 10 ²⁵	—	—	Good retention	[96, 1211]
	ZrC _{-1.0}	1200 ^a /1500(10 ⁴ h) ^b	6.5 × 10 ²⁵	—	—	Good retention	[96, 1211]
	ZrC _{-1.0}	1600 ^b	1.2 × 10 ²⁵ (fast)	—	—	>0.03 (4500 h)?	[96, 773]
	ZrC _{-1.0}	1600 ^b	1.2 × 10 ²⁵ (fast)	—	—	>0.03 (4500 h)?	[96, 773]
¹⁵⁵ Eu (^{3, 4})He	ZrC _{0.92±0.0}	1000–1600 ^b	—	—	74 ± 8 (see also Table 5.29)	—	[1360]
	ZrC _{-1.0}	-70–1730	—	5.13 × 10 ⁻⁷ exp(-9.050/T) (see also Table 5.29) ⁱ	75	—	[808, 1361]
⁸⁸ Kr	ZrC _{-1.0}	900 ^a	1.2 × 10 ²⁵ (fast)	—	—	(2–4) × 10 ⁻⁵	[768, 770]
⁹⁵ Nb (¹⁰⁷)Pd	ZrC _{-1.0}	1400	—	10 ⁻¹⁴	—	—	[96, 1227]
	ZrC _{-1.0}	1550–1850 ^b	—	—	~300 ^j	—	[96, 1014]
	ZrC _{-1.0}	1200–1500 ^b	—	—	~210–270 ^j	—	[1284]
	ZrC _{-1.0}	1400	—	10 ⁻¹²	—	—	[96, 1227]
¹⁰³ Ru ¹⁰⁶ Ru	ZrC _{-1.0}	1600(500 h) ^b	1.2 × 10 ²⁵ (fast)	3 × 10 ⁻¹²	—	0.4	[96, 770]
	ZrC _{-1.0}	1600(4500 h) ^b	1.2 × 10 ²⁵ (fast)	—	—	13	[96, 770, 773]
	ZrC _{-1.0}	1800(3000 h) ^b	1.2 × 10 ²⁵ (fast)	—	—	86	[96, 770, 773]
⁸⁵ Sr	ZrC _{-1.0}	1400	—	~2 × 10 ⁻¹⁴	—	—	[96, 1227]
⁹⁰ Sr	ZrC _{-1.0} (content non-combined C – 3.4%)	1260(1040 h) ^g /1600 ^b	1.4 × 10 ²¹ (fast)	~1.5 × 10 ⁻¹¹	—	—	[4, 96, 781]

(continued)

Table 5.27 (continued)

Fission product	Carbide phase composition	Temperature range, °C	Neutron irradiation fluence, cm ⁻²	Diffusion coefficient, cm ² s ⁻¹	Activation energy, kJ mol ⁻¹	Release %	Reference
¹³³ Xe (~1.0 × 10 ⁻⁷ at%)	ZrC _{0.58-0.64} (content O -0.67%) ^k	~1200–1650 ^b	1.0 × 10 ¹³ cm ⁻² s ⁻¹ (thermal) ^k	10 ⁻⁴ –10 ⁻⁶	~240–330	75 (465 h)	[1228]
	ZrC _{0.58-0.64} (content O -0.67%) ^k	~1200–1800 ^b	1.0 × 10 ¹³ cm ⁻² s ⁻¹ (thermal) ^k	–	–	84 (790 h)	[1228]
	ZrC _{0.76-0.79} (content O -0.64%) ^k	~1200–1800 ^b	1.0 × 10 ¹³ cm ⁻² s ⁻¹ (thermal) ^k	10 ³ –10 ⁴	~660	30 (700 h)	[1228]
	ZrC _{0.83-0.85} (content O -0.31%) ^k	~1250–1850 ^b	1.0 × 10 ¹³ cm ⁻² s ⁻¹ (thermal) ^k	10 ⁵ –10 ⁶	~790	30 (760 h)	[1228]
	ZrC _{0.91-0.92} (content O -0.04%) ^k	~1300–1900 ^b	1.0 × 10 ¹³ cm ⁻² s ⁻¹ (thermal) ^k	10 ³ –10 ⁴	~770	23 (770 h)	[1228]
	ZrC _{0.91-0.92} (content O -0.04%) ^k	~1200–1900 ^b	1.0 × 10 ¹³ cm ⁻² s ⁻¹ (thermal) ^k	–	–	30 (570 h)	[1228]
	ZrC _{-1.0} (content O -0.05%) ^k	1200–1500 ^b	1.0 × 10 ¹³ cm ⁻² s ⁻¹ (thermal) ^k	10 ⁻⁶	~340	49 (650 h) ^l	[1228]
	ZrC _{-1.0} (content O -0.05%) ^k	1500–1700 ^b	1.0 × 10 ¹³ cm ⁻² s ⁻¹ (thermal) ^k	5.0 × 10 ⁻³	~460	49 (650 h) ^l	[1228]
	ZrC _{-1.0} (content O -0.05%) ^k	1650–1850 ^b	1.0 × 10 ¹³ cm ⁻² s ⁻¹ (thermal) ^k	10	~610	49 (650 h) ^l	[1228]
	ZrC _{0.80-0.95} O _{0.05-0.20}	1600–1800 ^b	–	–	–	Xe migration is enhanced in O-rich phases	[1322]

^aIrradiation temperature^bPost-irradiation heat treatment temperature^cRelease is below the detectable limit^dFor migration along the short circuit paths^eFor migration in the grain volumes^fMostly through grain boundaries with some contribution from volume diffusion^gThe value compared to the concentration in the kernel^hAnnealing temperatureⁱObtained from first-principles total energy and phonon frequency calculations on the basis of the transition state theory (TST)^jThe value of the activation energy of ZrPd₃ formation^kThe value of thermal neutron flux^lSummarized for the temperature range from 1200 to 1850 °C

Table 5.28 The parameters of wettability of zirconium monocarbide ZrC_{1-x} phases with some liquid metals and alloys (melts)^a

Melt (purity)	Atmosphere	Temperature, °C	Time, s	γ_{l-g} , mJ m ⁻²	W_{ad} , mJ m ⁻²	W_m^b , kJ mol ⁻¹	θ , degree	Reference
Cu	Vacuum	1100	1200	ZrC _{0.60} 1357	2385	–	~40	[1, 32, 1240]
Cu	Vacuum	1100	1200	ZrC _{0.72} 1351	1585	–	~80	[1, 32, 1240]
Cu	Ar	1130	900	ZrC _{0.78} 1351	270	–	143 ± 2	[1, 1231]
Cu	–	~1100	–	ZrC _{0.86} –	–	–	141	[1241, 1244]
Cu	Vacuum	1100	900	ZrC _{0.88} 1352	780	–	~115	[1, 32, 1240]
Cu	Ar	1130	900	1351	365	–	137 ± 1	[1, 1231]
Cu	Ar	1130	900	ZrC _{0.90} 1351	332	–	139 ± 1	[1, 1231]
Cu	–	~1100	–	–	–	–	141	[1241, 1244]
Cu	–	~1100	–	ZrC _{0.92} –	–	–	142	[1241, 1244]
Cu ^c	Vacuum, 1.3 mPa	1150	3600	1000	–	–	128	[1527]
Cu (Zr – 1.4%) ^c	Vacuum, 1.3 mPa	1150	3600	–	–	–	138	[1527]
Cu (Zr – 1.4, V – 0.8%) ^c	Vacuum, 1.3 mPa	1150	3600	–	–	–	112.5	[1527]
Ni ^d	Vacuum	1450	1500	–	–	–	25	[1351]
Ni (C-0.7%) ^{d,e}	Vacuum	1450	1500	–	3100	159	35	[1, 1351, 1522]
Ni (C-1.0%) ^d	Vacuum	1450	1500	–	–	–	60	[1, 1351, 1532]
Ni (C-1.4%) ^{d,f}	Vacuum	1450	1500	–	2300	117	68	[1, 1351, 1522]
Ni (C-1.8%) ^d	Vacuum	1450	1500	–	–	–	70	[1, 1351, 1522]
Ni (C-2.8%) ^{d,g}	Vacuum	1450	1500	–	2000	105	80	[1, 1351, 1522]
Ni (C-3.5%) ^{d,h}	Vacuum	1450	1500	–	1700	88	91	[1, 1351, 1522]
Ni (C-7.2%) ^{d,i}	Vacuum	1450	1500	–	1300	67	103	[1, 1351, 1522]
Cu	–	~1100	–	ZrC _{0.96} –	–	–	143	[1241, 1244]

(continued)

Table 5.28 (continued)

Melt (purity)	Atmosphere	Temperature, °C	Time, s	γ_{1-g} , mJ m^{-2}	W_a , mJ m^{-2}	W_m^b , kJ mol^{-1}	θ , degree	Reference
$\text{ZrC}_{0.97}$								
Co ^j	Vacuum	1500	900	1805	3260	152	36	[1, 851]
Cu	Ar	1130	900	1351	332	–	139 ± 2	[1, 1231]
Fe ^k	Vacuum	1550	900	1780	2940	155	49	[1, 851]
Fe (C-4.0,	Pure Ar	1450	900	–	–	–	125	[1, 48, 1242]
Mn-1.4, Si-	Pure Ar	1450	1200	–	–	–	111	[1, 1242]
2.5, S-0.1%) ^l	Pure Ar	1450	2400	–	–	–	95	[1, 1242]
	Pure Ar	1450	3600	–	–	–	85	[1, 1242]
	Pure Ar	1450	7200	–	–	–	83	[1, 1242]
Fe (C-3.1,	Pure Ar	1400–	900	–	–	–	100	[1, 48, 1242]
Mn-0.4, Si-		1450						
1.6, S-0.02%) ^l								
Fe (C-2.7,	Pure Ar	1400–	900	–	–	–	122	[1, 48, 1242]
Mn-0.4, Si-		1450						
1.2, S-0.2%) ^l								
Fe (C-2.6,	Pure Ar	1400–	900	–	–	–	132	[1, 48, 1242]
Mn-1.0, Si-		1450						
1.0, Cr-0.3%) ^l								
Fe (C-1.2,	Pure Ar	1550	900	–	–	–	110	[1, 1242]
Mn-0.2, Si-								
0.2, P-0.03, S-								
0.02%) ^l								
Fe (C-1.0, Cr-	Pure Ar	1500	900	–	–	–	122	[1, 48, 1242]
1.4, Mn-0.4,								
Si-0.3%) ^l								
Fe (C-1.0, Cr-	Pure Ar	1500–	900	–	–	–	145	[1, 48, 1242]
1.4, Mn-1.1,		1550						
Si-0.6%) ^l								
Fe (C-1.0,	Pure Ar	1550	900	–	–	–	119	[1, 1242]
Mn-0.2, Si-								
0.2, P-0.03, S-								
0.02%) ^l								
Fe (C-0.8,	Pure Ar	1500	900	–	–	–	131	[1, 48, 1242]
Mn-0.2, Si-								
0.2, S-0.03%) ^l								
Fe (C-0.5,	Pure Ar	1500–	900	–	–	–	128	[1, 1242]
Mn-0.6, Si-		1550						
0.2, P-0.03, S-								
0.03%) ^l								
Fe (C-0.5,	Pure Ar	1500–	900	–	–	–	135	[1, 1242]
Mn-0.6, Si-		1550						
0.2, P-0.03, S-								
0.035%) ^l								
Fe (C-0.5,	Pure Ar	1500–	900	–	–	–	110	[1, 1242]
Mn-0.6, Si-		1550						
0.2, P-0.03, S-								
0.07%) ^l								

(continued)

Table 5.28 (continued)

Melt (purity)	Atmosphere	Temperature, °C	Time, s	γ_{1-g} , mJ m^{-2}	W_a , mJ m^{-2}	W_m^b , kJ mol^{-1}	θ , degree	Reference
Fe (C-0.5, Mn-0.6, Si-0.2, P-0.03, S-0.11%) ^l	Pure Ar	1500–1550	900	–	–	–	90	[1, 1242]
Fe (C-0.5, Mn-0.6, Si-0.2, P-0.03, S-0.13%) ^l	Pure Ar	1500–1550	900	–	–	–	76	[1, 1242]
Fe (C-0.2, Cr-14.5, Ni-2.7, Mn-0.5%) ^l	Pure Ar	1500–1550	900	–	–	–	102	[1, 48, 1242]
Fe (C-0.2, Mn-0.4, Si-0.06, S-0.03, P-0.03%) ^l	Pure Ar	1550	900	–	–	–	130	[1, 1242]
Ni ^m	Vacuum	1450	900	1700	3240	151	25	[1, 851]
				ZrC _{-1.0}				
Ag	He	1100	1200	910	495	–	117 ± 2	[1, 1239]
Ag	He	1200	1200	910	510	–	116 ± 2	[1, 1239]
Ag	He	1300	1200	910	510	–	116 ± 2	[1, 1239]
Ag	He	1400	1200	910	705	–	103 ± 2	[1, 1239]
Ag	He	1500	1200	910	880	–	92 ± 2	[1, 1239]
Ag	He	1600	1200	910	1005	–	84 ± 2	[1, 1239]
Al (99.97%)	Vacuum	900–1000	900	914	122	6.5	150 ± 1	[1, 32, 48, 1231, 1232]
Al	Vacuum, Ar	1000	900	914	803	–	97	[1, 1233]
Al ⁿ	He	1000	900	914	430	–	122 ± 3	[1, 812]
Al ⁿ	He	1200	900	865	485	–	116 ± 3	[1, 812]
Al ⁿ	He	1400	900	865	1297	–	60 ± 3	[1, 812]
Au	Vacuum	–	1800	1140	143	–	151	[1, 32, 1230, 1240]
Bi (99.99%)	Vacuum	320–1200	900	390 ± 1	87	5	141 ± 1	[1, 32, 48, 1231, 1232]
Co (99.99%) ^d	Vacuum	1500	900	1805	3260	175	36	[1, 851, 1231, 1235]
Co (99.99%)	Ar	1500	900	1805	3550	186	15	[1, 32, 48, 1230, 1232]
Co	Vacuum, Ar	1495	–	–	–	–	86	[32, 48, 1230, 1233]
Co ^o	Vacuum	1420	300	1910	3460	–	36	[1, 32, 1230, 1234]
Cu (99.99%)	Vacuum	1130	900	1351	315	17	140 ± 1	[1, 48, 1231]
Cu (99.99%)	Ar	1370	900	1351	315	–	140	[1, 1230–1232]
Cu (99.99%)	Ar	1500	900	1351	395	–	135	[1, 1231, 1232]
Cu	Vacuum, Ar	1100	–	–	–	–	135	[31, 42, 1233, 1246]

(continued)

Table 5.28 (continued)

Melt (purity)	Atmosphere	Temperature, °C	Time, s	γ_{1-g} , mJ m^{-2}	W_a , mJ m^{-2}	W_m^b , kJ mol^{-1}	θ , degree	Reference
Cu	Ar	1100	900	1351	315	–	~140	[1, 31, 32, 48, 1238, 1240]
Cu	Ar	1500	900	1351	715	–	118	[1, 31, 32, 48, 1230, 1238]
Cu ^P	Vacuum	1100	900	1270	505	–	127	[1, 1234, 1528]
Cu ^P	Vacuum	1150	900	1255	525	–	126	[1, 1234]
Cu ^P	Vacuum	1200	900	1240	540	–	124	[1, 1234]
Cu (Ni-0.01%)	Vacuum, Ar	1200	1200	–	–	–	96	[1, 30, 31, 42, 1238, 1246]
Cu (Ni-0.05%)	Vacuum, Ar	1200	1200	–	–	–	70	[1, 30, 31, 42, 1238, 1246]
Cu (Ni-0.1%)	Vacuum, Ar	1200	1200	–	–	–	63	[1, 30, 31, 42, 1238, 1246]
Cu (Ni-0.25%)	Vacuum, Ar	1200	1200	–	–	–	54	[1, 30, 31, 42, 1246]
Fe (99.99%) ^k	Vacuum	1550	900	1780	2950	155	49	[1, 32, 851, 1230–1232]
Fe (99.99%)	Ar	1550	900	1780	420	32	140	[1, 32, 851, 1230–1232]
Fe	Vacuum, Ar	1535	–	–	–	–	50	[32, 48, 1230, 1233]
Fe ^q	Vacuum	1490	<60	1900	3245	–	45	[1, 32, 1230, 1234]
Fe (C-0.5%) ^r	Vacuum	1550	–	–	–	–	78	[1]
Fe (C-1.0%) ^r	Vacuum	1550	–	–	–	–	82	[1]
Fe (C-2.0%) ^r	Vacuum	1550	–	–	–	–	85	[1]
Fe (C-3.0%) ^r	Vacuum	1550	–	–	–	–	92	[1]
Fe (C-4.0%) ^r	Vacuum	1550	–	–	–	–	123	[1]
Fe (C-3.1–3.4, Si-1.7–2.1, Mn-0.8–1.2%)	Vacuum	1550	–	–	492	–	121	[1]
Fe (C-0.2, Mn-0.3, Si-0.2, W-0.07%)	Pure Ar	1550	–	–	–	–	~50	[1328]
	Pure Ar	1600	–	–	–	–	~40	[1328]
Fe (C-0.32–0.40, Mn-0.4–0.9, Si-0.20–0.52%)	Vacuum	1550	1200	–	1385	–	81	[1]
Fe–Cr ^s (Cu-3%) ^t	Vacuum	1200	900	–	–	–	42	[1, 1247]
Fe–Cr ^s (Cu-10%) ^t	Vacuum	1200	900	–	–	–	83	[1, 1247]
Fe–Cr ^s (Cu-25%) ^t	Vacuum	1200	900	–	–	–	83	[1, 1247]
Fe–Cr ^s (Cu-40%) ^t	Vacuum	1200	900	–	–	–	60	[1, 1247]

(continued)

Table 5.28 (continued)

Melt (purity)	Atmosphere	Temperature, °C	Time, s	γ_{l-g} , mJ m^{-2}	W_a , mJ m^{-2}	W_m^b , kJ mol^{-1}	θ , degree	Reference
Fe–Cr ^s (Cu-60%) ^t	Vacuum	1200	900	–	–	–	56	[1, 1247]
Fe–Cr ^s (Cu-70%) ^t	Vacuum	1200	900	–	–	–	56	[1, 1247]
Fe–Cr ^s (Cu-75%) ^t	Vacuum	1200	900	–	–	–	45	[1, 1247]
Fe–Cr ^s (Cu-90%) ^t	Vacuum	1200	900	–	–	–	61	[1, 1247]
Fe (Ni-2.5%)	Vacuum	1550	1200	–	–	–	39	[1, 1237]
Fe (Ni-5%)	Vacuum	1550	1200	–	–	–	30	[1, 1237]
Fe (Ni-25%)	Vacuum	1550	1200	–	–	–	21	[1, 1237]
Fe (Ni-30%)	Vacuum	1550	1200	–	–	–	27	[1, 1237]
Fe–Si ^t	Vacuum	1200	900	–	–	–	84	[1, 1247]
Fe–Si ^u (Cu-2%) ^t	Vacuum	1200	900	–	–	–	45	[1, 1247]
Fe–Si ^u (Cu-25%) ^t	Vacuum	1200	900	–	–	–	90	[1, 1247]
Fe–Si ^u (Cu-50%) ^t	Vacuum	1200	900	–	–	–	40	[1, 1247]
Fe–Si ^u (Cu-60%) ^t	Vacuum	1200	900	–	–	–	62	[1, 1247]
Fe–Si ^u (Cu-70%) ^t	Vacuum	1200	900	–	–	–	52	[1, 1247]
Fe–Si ^u (Cu-75%) ^t	Vacuum	1200	900	–	–	–	38	[1, 1247]
Fe–Si ^u (Cu-90%) ^t	Vacuum	1200	900	–	–	–	66	[1, 1247]
Ga (99.999%)	Ar	1300	900	707	225	–	138	[1, 1231]
Ga (99.99%)	Vacuum, Ar	800	900	707	215	11	134 ± 1	[1, 32, 48, 1230, 1232]
Ge (99.999%)	Vacuum	1000	–	–	–	–	135	[32, 48, 1230]
Ge	Ar	1100	900	700	176	10	135 ± 1	[1, 1231, 1232]
Ge	Ar	1300	900	700	176	10	133 ± 1	[1, 1231, 1232]
In (99.99%)	Vacuum, Ar	250–700	900	559	113	6	143 ± 3	[1, 32, 48, 1230–1232]
Mn (99.8%)	Vacuum	1300	900	1750	2405	130	68	[1, 1231]
Mn (99.8%)	Ar	1300	900	1750	2200	116	75	[1, 1231, 1232]
Mn	Vacuum, Ar	1245	–	–	–	–	70	[32, 48, 1230, 1233]
Ni (99.99%) ^m	Vacuum	1450	900	1700	3240	170	25	[1, 851, 1231]
Ni (99.99%)	Ar	1450	900	1700	3240	165	32	[1, 32, 48, 1230–1232]

(continued)

Table 5.28 (continued)

Melt (purity)	Atmosphere	Temperature, °C	Time, s	γ_{1-g} , mJ m^{-2}	W_a , mJ m^{-2}	W_m^b , kJ mol^{-1}	θ , degree	Reference
Ni (99.98%) ^v	Ar (99.999%)	1480	–	1700	–	–	73 ± 0.5	[1440]
Ni (99.98%) ^v	Ar (99.999%)	1480	400	1700	–	–	32 ± 0.8	[1440]
Ni	Vacuum	1380	–	–	–	–	24	[32, 1230, 1533]
Ni	Vacuum, Ar	1455	–	1700	–	–	43	[32, 48, 1230, 1233]
Ni ^w	Vacuum	1500	900	1700	3240	–	32	[1, 1232]
Ni ^x	Vacuum	1500	900	1700	3395	–	5	[1, 1232]
Ni	Vacuum	1550	1200	1700	3170	–	30	[1, 1237]
Ni ^y	Vacuum	1380	300	1810	3460	–	24	[1, 32, 1234, 1236]
Ni (P-0.1%)	Vacuum	1450	1200	–	–	–	15	[1]
Ni (P-1.5%)	Vacuum	1450	1200	–	–	–	6	[1]
Ni (P-2.5%)	Vacuum	1450	1200	–	–	–	4	[1]
Ni (P-4.8%)	Vacuum	1450	1200	–	–	–	2	[1]
Ni (P-7.2%)	Vacuum	1450	1200	–	–	–	33	[1]
Ni (P-12.0%)	Vacuum	1450	1200	–	–	–	82	[1]
Ni (P-20.0%)	Vacuum	1450	1200	–	–	–	95	[1]
Ni (Co-10, W-10, Cr-9.5, Al-5.5, Ti-2.5, Mo-2%) ^z	Vacuum, ~6.7 mPa	1450	60	–	–	–	110	[1]
	Vacuum, ~6.7 mPa	1450	300	–	–	–	60	[1]
	Vacuum, ~6.7 mPa	1450	600	–	–	–	52	[1]
	Vacuum, ~6.7 mPa	1450	1200	–	–	–	46	[1]
	Vacuum, ~6.7 mPa	1450	1800	–	–	–	46	[1]
Ni (W-9.5–11.0, Co-9.0–10.5, Cr-8.0–9.5%) ^z	He	1400	1200	–	2760	–	46	[1]
Ni (Cr-9.5–12.0, Al-5.0–6.0, W-4.5–5.5%) ^z	He	1350	1200	–	840	–	30	[1]
Ni (Co-10.0–15.0, Cr-8.5–10.5, Al-5.0–5.7%) ^z	He	1350	1200	–	1770	–	78	[1]
Ni (Cr-13.0–16.0, Mo-2.8–3.2, Al-1.3–1.7%) ^z	He	1380	1200	–	1660	–	90	[1]
Pb (99.99%)	Vacuum	400–1200	900	480	77	4	147 ± 1	[1, 32, 48, 1230–1232]

(continued)

Table 5.28 (continued)

Melt (purity)	Atmosphere	Temperature, °C	Time, s	γ_{l-g} , mJ m ⁻²	W_a , mJ m ⁻²	W_m^b , kJ mol ⁻¹	θ , degree	Reference
Sb (99.999%)	Vacuum	700–920	900	384	260	13	110 ± 7	[1, 32, 48, 1230–1232]
Si (99.999%)	Vacuum, Ar	1500	900	860	1655	87.1	22 ± 1	[1, 32, 48, 1231, 1232]
Si	Vacuum, Ar	1410	–	–	–	–	57	[32, 48, 1233]
Sn (99.99%)	Vacuum, Ar	300–1200	900	554	74	4	150 ± 1	[1, 32, 48, 1230–1232]
Tl (99.99%)	Vacuum	400	900	490	188	10	128 ± 2	[1, 32, 48, 1230–1232]

^aThe parameters of wettability are given in accordance with Young-Dupré equation $W_a = \gamma_{l-g} \times (1 + \cos\theta)$ and Young's equation $\gamma_{s-l} = \gamma_{s-g} - \gamma_{l-g}\cos\theta$, where W_a is the work of adhesion, γ_{l-g} is the liquid-vapour interfacial energy (surface tension), γ_{s-l} is solid-liquid interfacial energy, γ_{s-g} is the solid-vapour interfacial energy and θ is the wetting contact angle [1]; compositions of melts are given in mass (weight) percentage

^b $W_m = W_a(M/d)^{2/3}N_A^{1/3}$, where W_m is the molar work of adhesion, M is the molecular mass and d is the density of chemical compound, N_A is the Avogadro constant [1351]

^cSintered materials (porosity – ≤ 2.0%, contents: non-combined C – 0.30%, O – 0.015%, N – 0.27%, Fe – 0.10%)

^dPorosity ≤ 5%, content non-combined C – 0.3%

^e $\gamma_{s-l} = 1300$ mJ m⁻²

^f $\gamma_{s-l} = 2000$ mJ m⁻²

^g $\gamma_{s-l} = 2400$ mJ m⁻²

^h $\gamma_{s-l} = 2700$ mJ m⁻²

ⁱ $\gamma_{s-l} = 3000$ mJ m⁻²

^j $\gamma_{s-l} = 1200$ mJ m⁻²

^k $\gamma_{s-l} = 1490$ mJ m⁻²

^lSintered materials (porosity – 3–8%, content non-combined C – 0.50%)

^m $\gamma_{s-l} = 1130$ mJ m⁻²

ⁿPlasma-sprayed carbide coatings

^oMetal impurities: Si-0.8%, Fe-0.3%, Ni-0.2%, Al-0.1%, Mg-0.1%, Ca-0.1%, Cu-0.1%, Ag-0.1%

^pMetal impurities: Ag-0.2, Fe-0.1, Si-0.1, Mg-0.1%, Pb-0.1%

^qMetal impurities: Si-0.3%, Mg-0.3%, Cu-0.2%, Ni-0.2%, Mn-0.2%, Ag-0.1%, C-0.003%, N-0.001%, O-0.001%

^rAlloys prepared by refusion of carbonyl iron and graphite with spectral purity

^sFe–Cr alloy: Cr-65%, Fe-29%, C-6%

^tPorosity ≤ 4%

^uFe–Si alloy: Si-75%, Fe-25%

^vPorosity < 4%, impurities < 2 mas.%

^wPorosity – 4–8%

^xPorosity – 23%

^yMetal impurities: Fe-1.0%, Al-0.3%, Mg-0.2%, Ag-0.2%, Ca-0.1%, Cu-0.1%

^zHot-pressed materials, poreless

Table 5.29 Diffusion rates and related parameters in the systems containing zirconium, carbon and zirconium carbides/carbonylides phases at various temperatures^{a,b}

Species pair	Temperature dependence of the diffusion coefficient (diffusivity) $D = D_0 \exp(-E_N/RT)$, $\text{cm}^2 \text{s}^{-1}$	Temperature range, K ($^{\circ}\text{C}$)	Remarks on materials characteristics and measurement method	Reference
C \rightarrow α -Zr	$7.90 \times 10^{-4} \exp(-15,350/T)$	870–1070 (600–800)	Polycrystalline Zr, ^{14}C radiometric method	[26, 27, 1262]
	$(2.00 \pm 0.37) \times 10^{-3} \exp(-18,200 \pm 300/T)$	870–1120 (600–850)	Polycrystalline Zr (~2 mm grain size), ^{14}C radiometric (thin layer residual activity) method	[1, 1285, 1286]
	$3.51 \times 10^{-5} \exp(-15,500/T)$	870–1070 (600–800)	Polycrystalline Zr, ^{14}C radiometric method	[1, 32]
	$6.0 \times 10^{-5} \exp(-16,400/T)$	890–1010 (620–740)	Polycrystalline Zr, ^{14}C radiometric method	[1, 1288]
	$5.0 \times 10^{-8} \exp(-46,200/T)$	1010–1100 (740–830)	Polycrystalline Zr, ^{14}C radiometric method	[1, 1288]
C \rightarrow β -Zr	$6.02 \times 10^{-3} \exp(-23,400/T)$	700–1100 (430–830)	Calculated by using kinetic Monte-Carlo simulations	[1283]
	$(8.90 \pm 1.60) \times 10^{-2} \exp(-16,000 \pm 200/T)$	1140–1520 (870–1250)	Polycrystalline Zr (~2 mm grain size), ^{14}C radiometric (thin layer residual activity) method	[1, 1285, 1286]
	$3.57 \times 10^{-2} \exp(-17,200/T)$	1370–1870 (1100–1600)	Polycrystalline 99.6%-purity Zr (contents: C – 0.01%, O – 0.1%, N – 0.035%, Fe – 0.22%, Hf – 0.015%), ^{14}C radiometric method	[1, 26, 27, 1259, 1260]
	$4.80 \times 10^{-3} \exp(-13,500/T)$	1170–1570 (900–1300)	Polycrystalline 99.9%-purity Zr (contents: N – 0.014%, Si – 0.05%, Fe – 0.04%, Hf – 0.07%), ^{14}C radiometric (diffusion couple) method ^c	[1, 26, 27, 1260, 1263, 1286, 1304]
	$1.30 \times 10^{-4} \exp(-12,700/T)$	1240–1820 (970–1550)	Polycrystalline Zr, metallography method	[1, 1289]

(continued)

Table 5.29 (continued)

Species pair	Temperature dependence of the diffusion coefficient (diffusivity) $D = D_0 \exp(-E_N/RT)$, $\text{cm}^2 \text{s}^{-1}$	Temperature range, K (°C)	Remarks on materials characteristics and measurement method	Reference
$\text{C} \rightarrow \text{ZrC}_{1-x}$	$3.44 \times 10^{-2} \exp(-20,700 \pm 4,800/T)$	1170–1570 (900–1300)	Parameters of reaction-chemical diffusion, contact saturation of solid Zr with C (graphite), metallography method (determination of the concentration gradient by microhardness) ^c	[1, 26, 27, 32, 42, 48, 1252, 1253, 1291]
	$4.52 \times 10^3 \exp(-9000 \pm 2,800/T)$	1270–1870 (1000–1600)	Parameters of reaction-chemical diffusion, contact saturation of solid Zr with C (graphite), metallography method	[1250, 1251, 1254, 1294]
	$1.4 \times 10^{-6} \exp(-15,200/T)$	1370–1970 (1100–1700)	—	[1, 32, 1290]
	$10^2 \exp(-44,500/T)$	1470–1670 (1200–1400)	Parameters of the diffusion saturation of solid Zr with C in vacuum	[1, 32, 1292]
	$1.6 \times 10^{-2} \exp(-34,600/T)$	1570–1770 (1300–1500)	Parameters of reaction-chemical diffusion, contact saturation of solid Zr with C (graphite)	[1, 1289]
	$2.4 \times 10^{-6} \exp(-20,100/T)$	1570–1820 (1300–1550)	Parameters of reaction-chemical diffusion, contact saturation of solid high-purity Zr (prepared by iodide method) with C	[1, 1289]
	$1.5 \times 10^{-6} \exp(-19,100/T)$	1570–1870 (1300–1600)	Parameters of reaction-chemical diffusion, contact saturation of solid Zr (prepared by arc-melting) with C	[1, 1289]
	$1.32 \times 10^2 \exp(-57,200/T)$ (for volume diffusion) $1.6 \exp(-45,300/T)$ (for short-circuit diffusion)	1620–2420 (1350–2150)	Single crystal and polycrystalline ($0.2 \times 0.2 \times 3$ mm columnar grains) ZrC_{1-x} ($x = 0.03$, contents: non-combined C – 0.02%, Hf – 2.5%), ^{14}C radiometric method	[1, 4, 26, 27, 298, 1273, 1295, 1309, 1316–1318]
	$(3.3 \pm 0.6) \times 10^2 \exp(-57,400 \pm 3,000/T)$	1870–2370 (1600–2100)	Polycrystalline (hot-pressed and annealed) ZrC_{1-x} ($x = 0.04$, porosity $\leq 5\%$, content non-combined C – 0.65%), ^{14}C radiometric method	[4, 26, 27, 298, 841, 1254, 1259, 1261, 1274]
	$56.4 \exp(-62,400 \pm 6,200/T)$	2520–3010 (2250–2740)	Polycrystalline (hot-pressed and annealed) ZrC_{1-x} ($x = 0.19$, 110–130 μm grain size, porosity – 3%, contents: O + N $\leq 0.6\%$), ^{14}C radiometric method	[1, 4, 26, 27, 32, 298, 841, 1261]
	$(14.1^{+15.5}_{-12.7}) \exp(-54,800 \pm 3,000/T)$	2670–3070 (2400–2800)	Polycrystalline (hot-pressed and annealed) ZrC_{1-x} ($x = 0.03$, $\text{Zr}(\text{C}_{0.97}\text{N}_{0.02}\text{O}_{0.01})_{0.97}$, 100–300 μm grain size, porosity 1–3%), ^{14}C radiometric (with sectioning technique) method	[1, 4, 26, 27, 298, 1272, 1316–1318]

(continued)

Table 5.29 (continued)

Species pair	Temperature dependence of the diffusion coefficient (diffusivity) $D = D_0 \exp(-E_N/RT)$, $\text{cm}^2 \text{s}^{-1}$	Temperature range, K (°C)	Remarks on materials characteristics and measurement method	Reference
	4.26×10^{-9}	2500 (2230)	Calculated on the basis of developed statistic and thermodynamic theory of interstitial phases for ZrC_{1-x} ($x = 0.03$)	[337]
	4.35×10^{-8}	2800 (2530)		
	2.88×10^{-7}	3100 (2830)		
	$(19.5^{+40.5}_{-13.0}) \exp(-60,200 \pm 3,100/T)$	2670–3070 (2400–2800)	Polycrystalline (hot-pressed and annealed) ZrC_{1-x} ($x = 0.07$, porosity 1–3%), ^{14}C radiometric (with sectioning technique) method	[1, 4, 26, 27, 298, 1272]
	$(61.2^{+45.2}_{-54.0}) \exp(-64,200 \pm 6,000/T)$	2670–3070 (2400–2800)	Polycrystalline (hot-pressed and annealed) ZrC_{1-x} ($x = 0.12$, porosity 1–3%), ^{14}C radiometric (with sectioning technique) method	[1, 4, 26, 27, 298, 1272]
	$(2.64^{+4.26}_{-1.63}) \times 10^2 \exp(-67,000 \pm 4,200/T)$	2670–3070 (2400–2800)	Polycrystalline (hot-pressed and annealed) ZrC_{1-x} ($x = 0.15$, porosity 1–3%), ^{14}C radiometric (with sectioning technique) method	[1, 4, 26, 27, 298, 1272]
	$(3.16^{+8.80}_{-2.32}) \times 10^2 \exp(-69,200 \pm 3,800/T)$	2670–3070 (2400–2800)	Polycrystalline (hot-pressed and annealed) ZrC_{1-x} ($x = 0.16$, porosity 1–3%), ^{14}C radiometric (with sectioning technique) method	[1, 4, 26, 27, 298, 1272]
	$(2.8^{+5.0}_{-2.0}) \times 10^4 \exp(-82,600 \pm 2,600/T)$	2770–3270 (2500–3000)	Polycrystalline (hot-pressed and annealed) ZrC_{1-x} ($x = 0.30$, porosity 1–3%), ^{14}C radiometric method	[4, 1295, 1298]
	$6.3 \times 10^3 \exp(-N_C) \exp(-35,600/T)$	1570–2020 (1300–1750)	Chemical diffusion coefficient as a function of the atomic fraction of C (N_C) and temperature determined by diffusion couple technique through electron-probe microanalysis	[1319, 1320]
	$8.3 \times 10^{-3} \exp(9.2\gamma) \exp(-36,600 \pm 3,700/T)$	1570–2020 (1300–1750)	Parameters of chemical diffusion ($0 < x \leq 0.49$) determined by diffusion couple technique through electron-probe microanalysis	[1295, 1296]
	$2.94 \times 10^2 \exp(-54,700/T)$	1670–1870 (1400–1600)	^{14}C radiometric method	[1, 1289]
	$3.32 \exp(-57,600/T)$	1870–2350 (1600–2080)	Parameters of chemical diffusion during solid-phase welding of pairs of $\text{Zr}-\text{ZrC}_{1-x}$ materials	[1, 1293]

(continued)

Table 5.29 (continued)

Species pair	Temperature dependence of the diffusion coefficient (diffusivity) $D = D_0 \exp(-E_N/RT)$, $\text{cm}^2 \text{s}^{-1}$	Temperature range, K (°C)	Remarks on materials characteristics and measurement method	Reference
	1.40×10^{-10}	2500 (2230)	Calculated on the basis of developed statistic and thermodynamic theory of interstitial phases for ZrC_{1-x} ($x = 0.30$)	[337]
	5.09×10^{-9}	2800 (2530)		
	8.10×10^{-8}	3100 (2830)		
	$-\exp(-46,000/T)$	2070–2570 (1800–2300)	Rate of carburization of Zr obtained by the precipitation from gas phase on the surface of graphite	[26, 27, 1254, 1255]
	$5 \times 10^2 \exp(-39,800/T)$	1920–2270 (1650–2000)	Rate of carburization of Zr obtained by the precipitation from gas phase on the surface of graphite; X-ray method	[26, 27, 1254, 1256, 1271]
	$0.95 \exp(-39,600/T)$	2270–3130 (2000–2860)	Parameters of temperature variation of ZrC_{1-x} layer growth rate constant upon C saturation of liquid Zr in graphite crucible, photomicrography of longitudinal sections ^c	[26, 27, 1254, 1257, 1258, 1304]
	$1.83 \exp(-42,400/T)$	2270–3070 (2000–2800)	Parameters of temperature variation of ZrC_{1-x} layer growth rate constant upon C saturation of liquid Zr in graphite crucible and ZrC_{1-x} recrystallization (solid-state grain growth); metallography method	[26, 27, 1266–1269]
	$0.37 \exp(-38,400/T)$	1570–2070 (1300–1800)	Parameters of reaction-chemical diffusion, contact saturation of solid Zr with C (graphite); metallography method	[26, 27, 1270]
	$0.34 \exp(-34,700/T)$	2170–2800 (1900–2530)	Chemical diffusion coefficients calculated on the basis of experiments on deposition of non-stoichiometric carbide ZrC_{1-x} ($0 < x \leq 0.44$, porosity $\leq 10\%$) from $\text{CH}_4 + \text{H}_2$ gas phase ^d	[1, 26, 27, 32, 1275]
	$0.92 \exp(-40,500/T)$	2510–2720 (2240–2450)	Chemical diffusion coefficients calculated on the basis of mass change measurements for the initial composition of ZrC_{1-x} with $x = 0.44$	[296]
	$0.167 \exp(-41,700/T)$	–	The values of chemical diffusion coefficients summarized on the basis of several works	[51, 296]
C → $(\text{Zr}_{1-y}\text{Nb}_y)\text{C}_{1-x}$	$(2.28^{+0.47}_{-0.30}) \exp(-48,600 \pm 1,300/T)$	2770–3470 (2500–3200)	Polycrystalline $(\text{Zr}_{1-y}\text{Nb}_y)\text{C}_{1-x}$ ($x = 0.03$, $y = 0.52$), ¹⁴ C radio-tracer method	[4, 337, 1295, 1298]
	8.26×10^{-9}	2500 (2230)	Calculated on the basis of developed statistic and thermodynamic theory of 3-component interstitial phases for $(\text{Zr}_{1-y}\text{Nb}_y)\text{C}_{1-x}$ ($x = 0.10$, $y = 0.52$)	[337]
	6.72×10^{-8}	2800 (2530)		
	3.56×10^{-7}	3100 (2830)		

(continued)

Table 5.29 (continued)

Species pair	Temperature dependence of the diffusion coefficient (diffusivity) $D = D_0 \exp(-E_N/R/T)$, $\text{cm}^2 \text{s}^{-1}$	Temperature range, K ($^{\circ}\text{C}$)	Remarks on materials characteristics and measurement method	Reference
	$(0.84^{+0.47}_{-0.30}) \exp(-50,600 \pm 1,700/T)$	2770–3470 (2500–3200)	Polycrystalline $(\text{Zr}_{1-y}\text{Nb}_y)\text{C}_{1-x}$ ($x = 0.18$, $y = 0.52$), ^{14}C radio-tracer method	[4, 337, 1295, 1298] [337]
	1.36×10^{-9}	2500 (2230)	Calculated on the basis of developed statistic and thermodynamic theory of 3-component interstitial phases for $(\text{Zr}_{1-y}\text{Nb}_y)\text{C}_{1-x}$ ($x = 0.20$, $y = 0.52$)	
	1.20×10^{-8}	2800 (2530)		
	6.91×10^{-8}	3100 (2830)		
$\text{C} \rightarrow$ $(\text{Zr}_{1-y}\text{U}_y)\text{C}_{1-x}$	$9.0 \times 10^{-3} \exp(-32,200/T)$	2170–2570 (1900–2300)	Polycrystalline $(\text{Zr}_{1-y}\text{U}_y)\text{C}_{1-x}$ ($x = 0.06$, $y = 0.79$), ^{14}C radio-tracer method	[1295, 1297]
	$2.4 \times 10^{-2} \exp(-36,200/T)$	2170–2570 (1900–2300)	Polycrystalline $(\text{Zr}_{1-y}\text{U}_y)\text{C}_{1-x}$ ($x = 0.07$, $y = 0.49$), ^{14}C radio-tracer method	[1295, 1297]
	$10^{-2} \exp(-39,200/T)$	2170–2570 (1900–2300)	Polycrystalline $(\text{Zr}_{1-y}\text{U}_y)\text{C}_{1-x}$ ($x = 0.10$, $y = 0.28$), ^{14}C radio-tracer method	[1295, 1297]
$\text{C} \rightarrow \text{ZrN}_{1+x}$	$(1.59^{+0.27}_{-0.22}) \times 10^{-3} \exp(-46,400/T)$	2300–2960 (2030–2690)	Polycrystalline (nitrided through metal saturation) $\text{ZrN}_{0.95}$ (no porosity, content $\text{O} \leq 0.015\%$), ^{14}C radiometric method	[4, 26, 27, 1280]
$\text{Cs} \rightarrow \text{ZrC}_{1-x}$	$2.3 \times 10^{-3} \exp(-38,200/T)$	1470–1870 (1200–1600)	Polycrystalline $\text{ZrC}_{1.0}$ (content non-combined $\text{C} - 3.4\%$) coating (thickness – 45 μm) on 500 μm nuclear fuel particles (see also Table 5.27)	[4, 96, 781]
$\text{He} \rightarrow \text{ZrC}_{1-x}$	$\sim \exp(-8900 \pm 900/T)$	1270–1870 (1000–1600)	Polycrystalline ZrC_{1-x} ($x = 0.08 \pm 0.02$, 1–5 μm grain size, porosity 1%), resonant $^3\text{He}(\text{d},\text{p})^4\text{He}$ nuclear reaction in as-implanted (3 MeV $^3\text{He}^+$) and thermally annealed materials	[1360]
	$5.13 \times 10^{-7} \exp(-9,050/T)$	200–2000 (–70–1730)	Parameters obtained from first-principles total energy and phonon frequency calculations (including the all atoms) on the basis of transition state theory (TST)	[808, 1361]
$\text{Nb} \rightarrow \text{ZrC}_{1-x}$	$(1.81^{+3.30}_{-1.63}) \times 10^2 \exp(-84,600 \pm 4,300/T)$	2770–3470 (2500–3200)	Polycrystalline (hot-pressed and annealed) ZrC_{1-x} ($x = 0.30$, $\text{Zr}(\text{C}_{0.98}\text{Nb}_{0.01}\text{O}_{0.01})_{0.70}$, porosity 1–3%), ^{95}Nb radiotracer method	[4, 1279, 1295, 1298]
$\text{Nb} \rightarrow$ $(\text{Zr}_{1-y}\text{Nb}_y)\text{C}_{1-x}$	$(0.51^{+1.33}_{-0.50}) \times 10^2 \exp(-77,100 \pm 4,900/T)$	2770–3470 (2500–3200)	Polycrystalline $(\text{Nb}_{1-y}\text{Zr}_y)\text{C}_{1-x}$ ($0.03 \leq x \leq 0.18$, $y = 0.52$), ^{95}Nb radiotracer method ^e	[4, 337, 1298]

(continued)

Table 5.29 (continued)

Species pair	Temperature dependence of the diffusion coefficient (diffusivity) $D = D_0 \exp(-E_N/RT)$, $\text{cm}^2 \text{s}^{-1}$	Temperature range, K (°C)	Remarks on materials characteristics and measurement method	Reference
	2.12×10^{-12}	2500 (2230)	Calculated on the basis of developed statistic and thermodynamic theory of 3-component interstitial phases for	[337]
	5.71×10^{-11}	2800 (2530)		
	8.26×10^{-10}	3100 (2830)	$(\text{Nb}_{1-y}\text{Zr}_y)\text{C}_{1-x}$ ($0.10 \leq x \leq 0.20$, $y = 0.52$)	
Pm \rightarrow ZrC _{1-x}	$(1.26^{+7.96}_{-1.10}) \times 10^2 \exp(-83,600 \pm 5,000/T)$	2270–2820 (2000–2550)	Polycrystalline hot-pressed ZrC _{1-x} ($0.03 \leq x \leq 0.30$, contents: O + N $\approx 0.5\%$, ¹⁴⁷ Pm radiotracer ^e)	[4, 1282]
U \rightarrow (Zr _{1-y} U _y)C _{1-x}	$4.6 \times 10^{-2} \exp(-52,800/T)$	2170–2570 (1900–2300)	Polycrystalline (Zr _{1-y} U _y)C _{1-x} ($x = 0.06$, $y = 0.79$), ²³⁵ U radio-tracer method	[1295, 1297]
	$1.6 \exp(-62,900/T)$	2170–2570 (1900–2300)	Polycrystalline (Zr _{1-y} U _y)C _{1-x} ($x = 0.07$, $y = 0.49$), ²³⁵ U radio-tracer method	[1295, 1297]
	$9.6 \exp(-68,000/T)$	2170–2570 (1900–2300)	Polycrystalline (Zr _{1-y} U _y)C _{1-x} ($x = 0.10$, $y = 0.28$), ²³⁵ U radio-tracer method	[1295, 1297]
W \rightarrow ZrC _{1-x}	$(2.0^{+8.3}_{-1.6}) \times 10^4 \exp(-82,600 \pm 4,000/T)$	2270–2820 (2000–2550)	Polycrystalline hot-pressed ZrC _{1-x} ($x \approx 0$, porosity $\approx 5\%$, contents: O + N $\approx 0.5\%$), ¹⁸⁵ W radiotracer method	[4, 1281]
Zr \rightarrow ZrC _{1-x}	$(1.03^{+6.03}_{-0.88}) \times 10^2 \exp(-86,600 \pm 5,400/T)$	2520–2920 (2250–2650)	Polycrystalline hot-pressed ZrC _{1-x} ($0.03 \leq x \leq 0.30$, porosity $\approx 1\text{--}3\%$, contents: O + N $\leq 1.5\text{--}2.0\%$), ⁹⁵ Zr radiotracer method ^e	[1, 4, 26, 27, 1272, 1279, 1295]
	$6.67 \times 10^2 \exp(-81,700/T)$	–	Calculated on the basis of general theoretical approach on diffusion processes in transition metal monocarbides	[1, 32, 1278]
	9.93×10^{-13}	2500 (2230)	Calculated on the basis of developed statistic and thermodynamic theory of interstitial phases (for $0.03 \leq x \leq 0.30$)	[337]
	3.83×10^{-11}	2800 (2530)		
	7.62×10^{-10}	3100 (2830)		
	$2.4 \times 10^{10} \exp(-105,700/T)$	2670–3520 (2400–3250)	Effective diffusion coefficients calculated on the basis of sintering kinetics data of ZrC _{1-x} ($x = 0.18$) spherical particles	[26, 27, 1276, 1295]
	$10^{5.2-11.9x} \exp[-(96,400 - 137600x)/T]$	–	Effective diffusion coefficients calculated on the basis of data on several diffusion-controlled processes in sintered ZrC _{1-x} materials (steady-state creep in flexure for $0.10 \leq x \leq 0.37$, decarburization for $x = 0.38$ and carburization for $x = 0.44$) ^r	[26, 27, 1277]

(continued)

Table 5.29 (continued)

$\text{mol}^{-1}(\text{ZrC}_{0.96})$, mean particle size 10–18 μm , 2000–2300 °C) [1308], 170 $\text{kJ mol}^{-1}(\text{ZrC}_{0.96})$, mean particle size 3–5 μm , specific surface area 0.5 $\text{m}^2 \text{g}^{-1}$, 1700–2400 °C) [1321], 190 $\text{kJ mol}^{-1}(\text{ZrC}_{-1.0})$, mean particle size 10–18 μm , 2000–2300 °C) [1308]; (e) powder spark-plasma sintering densification – 690–770 $\text{kJ mol}^{-1}(\text{ZrC}_{0.94}\text{O}_{0.05})$, mean particle size $\sim 0.5 \mu\text{m}$, specific surface area 1.15 $\text{m}^2 \text{g}^{-1}$, 1900–2200 °C) [630, 1075]; (f) internal friction peaks characteristics (Marx-Wert formula) – 390 kJ mol^{-1} (sintered $\text{ZrC}_{0.94}$, 1730 °C) [1329], data on creep – see Sect. 5.4 (Table 5.16), see also Sect. 5.5 (Table 5.21)

^cThe diffusion coefficients were assumed to be independent on concentration

^dThe parameters probably contain significant contribution of surface and grain-boundary diffusion due to the rather high porosity of the materials

^eTemperature dependences of the diffusion coefficients are the same for all the values of x in the indicated interval

^fThe given equation shows that in these processes the diffusion flows of both metallic and carbon components of ZrC_{1-x} phases contribute: the metallic component contribution is more considerable for near-stoichiometric compositions, the carbon component contribution – for the phases with higher values of x formula index; the difference in the effective diffusion coefficients for various ZrC_{1-x} phases decreases with an increase of temperature, it agrees with the assumption [1278] of approximate equality of the self-diffusion coefficients for the both components near carbide-graphite eutectic point

Table 5.30 The interaction of near-stoichiometric zirconium monocarbide ZrC_{1-x} materials with some common chemical reagents in aqueous solutions or molten states [1, 10, 11, 30–32, 35, 39, 42, 47, 96, 213, 223, 452, 607, 781, 979, 1124, 1158, 1330, 1331, 1333–1337, 1346, 1367, 1368]

Reagent, formula (density or concentration of aqueous solution) ^a	Treatment conditions		Character of interaction ^b
	Temperature, °C	Exposure time, h	
HCl (1:1)	20	24	Decomposes up to 2%
	100	1	Decomposes up to 1%
	110	2	Decomposes up to 5%
HCl ($d = 1.19$)	20	24	Decomposes up to 2%
	100–110	1	Decomposes up to 2–4%
6M HCl	100	40	Very slight interaction
0.05M H_2SO_4	20	1–600	Corrosion rate (coatings on steel) – $2.1 \times 10^{-5} \text{ mg cm}^{-2} \text{ s}$
H_2SO_4 (1:4)	20	24	Decomposes up to 2%
	100	1	Decomposes up to 5%
	140	1	Decomposes up to 24%
H_2SO_4 ($d = 1.84$)	20	24	Decomposes up to 3%
	100	1	Decomposes up to 9%
	200–235	1.5	Decomposes completely with the formation of oxysulfates and amorphous C; composition of released gases: CH_4 71, CO_2 26.5, H_2 2.5 mol.% and SO_2 (deposition of amorphous C – 7%) ^c
	260	1	Decomposes completely with the formation of oxysulfates and amorphous C; composition of released gases: CH_4 48, CO_2 48, H_2 3 mol.% and SO_2 (deposition of amorphous C – 14%) ^c
HNO_3 (1:1)	20	24	Decomposes up to 24%
	100	1	Decomposes up to 18%
	110	1–2	Decomposes with the formation of soluble nitrates up to 94%; composition of released gases: CO_2 95–97, H_2 2–3 mol.% and NO/NO_2 (no precipitated C, solution is transparent) ^d
HNO_3 ($d = 1.37$)	100	1	Decomposes up to 56%
HNO_3 ($d = 1.43$)	20	24	Decomposes up to 17%
	110–120	0.5	Decomposes completely with the formation of soluble nitrates; composition of released gases: CO_2 95–97, H_2 2–3 mol.%, CH_4 – traces and NO/NO_2 (no precipitated C, solution is transparent) ^d

(continued)

Table 5.30 (continued)

Reagent, formula (density or concentration of aqueous solution) ^a	Treatment conditions		Character of interaction ^b
	Temperature, °C	Exposure time, h	
HF ($d = 1.15$)	20	24	Decomposes completely
10M HF	100	~50	Decomposes, composition of released gases: CH ₄ 92, H ₂ 6, C ₂ H ₆ 0.6 and CO ₂ 0.35 mol.% ^{e,f}
H ₃ PO ₄ (1:3)	20	24	Decomposes up to 4%
	≥100	2	Decomposes up to 12%
H ₃ PO ₄ ($d = 1.70$)	20	24	Decomposes up to 2%
	250–255	1	Decomposes completely with the formation (or deposition) of ZrO(H ₂ PO ₄) ₂ ; composition of released gases: CH ₄ 91.4, CO ₂ 7.8 and H ₂ 0.8 mol.% ^g
	260–270	1	Decomposes completely with the formation (or deposition) of ZrO(H ₂ PO ₄) ₂ ; composition of released gases: CH ₄ 87.3, CO ₂ 12 and H ₂ 0.7 mol.% ^g
HClO ₄ (1:3)	20	24	Decomposes up to 1%
	≥100	2	Decomposes up to 16%
HClO ₄ ($d = 1.35$)	20	24	Decomposes up to 3%
	≥100	2	Decomposes up to 98%
H ₂ C ₂ O ₄ ^h (saturated solution)	20	24	Decomposes up to 2%
	100–104	2	Decomposes up to 8%
Other organic acids	110	1	No decomposition
NaOH (10%)	20	24	Decomposes up to 9%
	≥100	2	No decomposition
NaOH (20%)	20	24	No decomposition
	100	1	No decomposition
	110	2	No decomposition
4 M NaOH	100	20	No reaction
NaCl (3%)	20	1–600	Corrosion rate (coatings on steel) – $2.6 \times 10^{-6} \text{ mg cm}^{-2} \text{ s}^{-1}$
Na ₂ CO ₃ (10%)	20	1–600	Corrosion rate (coatings on steel) – $2.4 \times 10^{-7} \text{ mg cm}^{-2} \text{ s}^{-1}$
KOH (30%)	20	1–600	Corrosion rate (coatings on steel) – $4.0 \times 10^{-7} \text{ mg cm}^{-2} \text{ s}^{-1}$
H ₂ O (technical)	20	1–600	Corrosion rate (coatings on steel) – $1.0 \times 10^{-6} \text{ mg cm}^{-2} \text{ s}^{-1}$
NaOH (fused)	650	–	Decomposes
Na ₂ CO ₃ (fused)	850	–	Decomposes
KOH (fused)	500	5	Decomposes, composition of released gases: H ₂ 86, CH ₄ 9, O ₂ 0.5, CO ₂ 0.10, CO 0.07 and C ₂ H ₂ 0.02 mol.% (He gas carrier) ^{e,i}

(continued)

Table 5.30 (continued)

Reagent, formula (density or concentration of aqueous solution) ^a	Treatment conditions		Character of interaction ^b
	Tempera- ture, °C	Exposure time, h	
KClO ₃ (fused)	360	–	Decomposes easily
KNO ₃ (fused)	340	–	Decomposes easily
K ₂ MnO ₄ (fused)	190	–	Decomposes easily
NaCl + BaCl ₂ (fused)	1100	–	Weak interaction
H ₂ O ₂ (30%)	100	1	Decomposes up to 1%
	110	2	Decomposes up to 3%
NH ₄ F (5%)	110	2	Decomposes up to 24%
NH ₄ F (10%)	100	1	Decomposes up to 7%
(NH ₄) ₂ S ₂ O ₈ (25%)	100–110	1	Decomposes up to ~60–80% (C deficient phases decomposes completely)
HCl (1:1) + H ₂ SO ₄ (1:4)	110	1	Decomposes partially
3HCl (1:1) + HNO ₃ (1:2)	110	1	Decomposes up to ~90%
3HCl (<i>d</i> = 1.19) + HNO ₃ (<i>d</i> = 1.43)	20	24	Decomposes up to 86%
	100–105	1–2	Decomposes up to 94% (C deficient phases decomposes completely)
HCl (<i>d</i> = 1.19) + H ₂ O ₂ (30%)	110	1	Decomposes up to ~50–60%
HCl (<i>d</i> = 1.19) + (NH ₄) ₂ S ₂ O ₈ (25%)	110	1	Decomposes up to ~50–60%
HCl (<i>d</i> = 1.19) + Br ₂ (HBrO, HBr) (saturated solution)	–	–	Decomposes up to ~90%
H ₂ SO ₄ (<i>d</i> = 1.84) + HNO ₃ (<i>d</i> = 1.43)	20	24	Decomposes up to 98%
	140	2	Decomposes completely
H ₂ SO ₄ (1:4) + H ₃ PO ₄ (1:3)	20	24	Decomposes partially with hydrolysis and salt depositions
	≥150	2	Decomposes partially with hydrolysis and salt depositions
H ₂ SO ₄ (<i>d</i> = 1.84) + H ₃ PO ₄ (1:1)	20	2	Decomposes up to 3%
	≥150	2	Decomposes partially
H ₂ SO ₄ (<i>d</i> = 1.84) + H ₃ PO ₄ (<i>d</i> = 1.70)	20	24	Decomposes up to 3%
	240	2	Mainly decomposes with the formation of salt depositions
H ₂ SO ₄ (1:4) + H ₂ C ₂ O ₄ ^h (saturated solution)	20	24	Decomposes up to 4%
	180	2	Decomposes up to 9%
H ₂ SO ₄ (<i>d</i> = 1.84) + H ₂ C ₂ O ₄ ^h (saturated solution)	20	24	Decomposes up to 4%
	≥100	2	Decomposes completely
H ₂ SO ₄ (1:4) + H ₂ O ₂ (30%)	110	1	Decomposes up to 99% ^j
H ₂ SO ₄ (1:4) + (NH ₄) ₂ S ₂ O ₈ (25%)	100–110	1	Decomposes up to 96% (C deficient phases decomposes completely)
H ₂ SO ₄ (1:1) + (NH ₄) ₂ S ₂ O ₈ (25%)	110	1	Decomposes up to 98%
6M H ₂ SO ₄ + 0.5M CrO ₃	100	~50	Decomposes, composition of released gases: CO ₂ 94, CO 4, O ₂ 1, H ₂ 0.08 and CH ₄ 0.04 mol.% ^{e,k}

(continued)

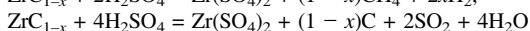
Table 5.30 (continued)

Reagent, formula (density or concentration of aqueous solution) ^a	Treatment conditions		Character of interaction ^b
	Tempera- ture, °C	Exposure time, h	
1M H ₂ SO ₄ + 1M H ₂ O ₂	20	~200	Decomposes, composition of re- leased gases: O ₂ 95, CO 3, CO ₂ 1, CH ₄ 0.4, H ₂ 0.07 and C ₂ H ₂ 0.03 mol.% ^c
0.5M H ₂ SO ₄ + 1M CuSO ₄	20	200	No reaction
HNO ₃ (<i>d</i> = 1.43) + HF (<i>d</i> = 1.15) ^l	20	24	Decomposes completely
	110	0.5	Decomposes completely
4HNO ₃ (<i>d</i> = 1.43) + HF (<i>d</i> = 1.15)	20	24	Decomposes completely
	110	0.5	Decomposes completely
HNO ₃ (<i>d</i> = 1.43) + NH ₄ F (5%)	110–120	0.5	Decomposes
H ₂ O ₂ (30%) + H ₂ C ₂ O ₄ ^h (50%)	110	1	Hydrolysis
H ₂ O ₂ (30%) + H ₂ C ₄ H ₄ O ₆ ^m (50%)	110	1	Decomposes up to 4%
H ₂ O ₂ (30%) + H ₃ C ₆ H ₅ O ₇ ⁿ (50%)	110	1	Decomposes up to 5%
H ₂ O ₂ (30%) + H ₄ C ₁₀ H ₁₂ N ₂ O ₈ ^o (satu- rated solution)	110	1	Decomposes up to 2%
H ₂ O ₂ (30%) + NH ₄ F	–	–	Decomposes completely
(NH ₄) ₂ S ₂ O ₈ + H ₄ C ₁₀ H ₁₂ N ₂ O ₈ ^o	–	–	Decomposes up to 2%
(NH ₄) ₂ S ₂ O ₈ + NH ₄ F	–	–	Decomposes up to 99%
4NaOH (20%) + Br ₂ (HBrO, HBr)	20	24	Decomposes up to ~2–7%
	105	2	Decomposes up to 13%
4NaOH (20%) + H ₂ O ₂ (30%)	20	24	Decomposes up to 47%
	112	2	Decomposes up to 97%
4NaOH (20%) + K ₃ [Fe(CN) ₆] (10%)	20	24	Decomposes up to 18%
	110	2	Decomposes up to 63%
CCl ₄ + Br ₂ ^p	20	200	No reaction

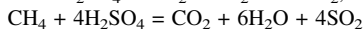
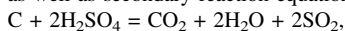
^aAll the ratios are given in volume fractions and percents in mass (weight)

^bWhen it is not indicated specially, the character reported is related to the powders with mean particle size of 40–50 μm

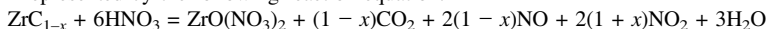
^cThe decomposition of ZrC_{1-x} starts at 200–220 °C, at 230–250 °C the dissolution is very energetical and decomposition, accompanied by the release of amorphous finely-dispersed C, mainly finishes in 30–40 min; it is represented by the main reaction equations:



as well as secondary reaction equations:

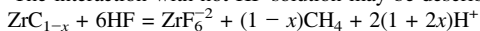


^dRepresented by the following reaction equation:

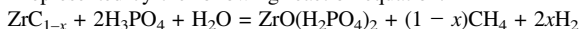


^eSintered cylinders (diameter 12.7 mm, height 6.4 mm)

^fThe interaction with hot HF solution may be described by the equation

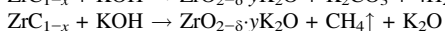
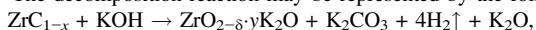


^gRepresented by the following reaction equation:



^hOxalic acid

ⁱThe decomposition reaction may be represented by the following schemes:

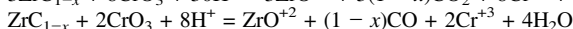
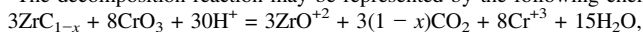


(continued)

Table 5.30 (continued)

^jThe resistance of ZrC_{1-x} phases in similar solvents increases with increasing their deviation from the stoichiometry

^kThe decomposition reaction may be represented by the following chemical equations:



^lRecommended chemical etching (dissolving) agents for ZrC_{1-x} : (a) 25–50 ml HNO_3 ($d = 1.43$) + 0.25–1.0 ml HF ($d = 1.15$) + 50 ml H_2O at 60–80 °C (for the SEM observation of materials with excess carbon) [781, 1337]; (b) 7 ml HF ($d = 1.15$) + 3 ml HNO_3 ($d = 1.43$) [785]; (c) 3 ml HNO_3 ($d = 1.43$) + 2.0 ml HF ($d = 1.15$) + 95 ml H_2O (for the SEM observation of materials) [1338]; (d) 1 ml HF ($d = 1.15$) + 1 ml HNO_3 ($d = 1.43$) + 2 ml H_2O with 1 min exposure at room temperature (for cleavage planes) [1339, 1340]; (e) the same with 1–10 s exposure (for electroetching with voltage – 1–10 V) [1339]; (f) 25 ml HNO_3 ($d = 1.43$) + 25 ml $HClO_4$ ($d = 1.35$) (for the SEM observation of materials with excess carbon) [1337]; (g) 2 ml HNO_3 ($d = 1.43$) + 1 ml HCl ($d = 1.19$) + 1 ml H_2O with HF (<5%) traces at a constant temperature <35 °C (for the electrochemical treatment of carbide emitters, cathode – Ta wire, DC voltage in pulsed operation – 15–30 V) [525]; (h) 2 ml HNO_3 ($d = 1.43$) + 0.5 ml NaF (0.1 N solution) + 3 ml H_2O at a constant temperature <35 °C (for the electrochemical treatment of carbide emitters, cathode – Ta wire, DC voltage in continuous or pulsed operation – 30 V) [525]; (i) 3 ml HNO_3 ($d = 1.43$) + 1 ml HCl ($d = 1.19$) + ~2 ml H_2O at a constant temperature <35 °C (for the electrochemical treatment of carbide emitters, cathode – Ta wire, DC voltage in continuous operation initially and pulsed operation just before drop-off – 25–35 V) [525]; (j) 10 g $K_3[Fe(CN)_6]$ + 2–10 g KOH/NaOH + 100 ml H_2O (Murakami's reagent for metallographic analysis) [879]; (k) 5% Br_2 solution in CH_3OH (methanol) (for the separation of carbide phases from metal-carbide alloys) [879]; (l) boiling H_2SO_4 ($d = 1.84$) [171]; (m) HNO_3 ($d = 1.43$) + 2–3% Na_2SiF_6 with 5 min exposure at room or cooler temperatures [1341]

^mTartaric acid

ⁿCitric acid

^oEthylenediaminetetraacetic acid (EDTA)

^pOrganic solutions

Table 5.31 The interaction of zirconium oxycarbide $ZrC_{1-x}O_y$ phases (powdered materials with mean particle size of 15–20 μm , treated at 100 °C, 1 h exposure) with some common chemical reagents in aqueous solutions [979]

Reagent, formula (density or concentration of aqueous solution) ^a	Decomposition, %		
	$ZrC_{0.82}O_{0.12}^b$	$ZrC_{0.77}O_{0.16}^b$	$ZrC_{0.70}O_{0.24}^b$
HCl (1:1)	0	2	2
HCl ($d = 1.19$)	2	2	3
H_2SO_4 (1:4)	8	21	67
H_2SO_4 ($d = 1.84$)	13	24	66
HNO_3 (1:1)	10	6	3
HNO_3 ($d = 1.37$)	17	12	4
3HCl (1:1) + HNO_3 (1:1)	100	44	16
$(NH_4)_2S_2O_8$ (25%)	97	70	3
H_2SO_4 (1:4) + $(NH_4)_2S_2O_8$ (25%)	100	100	98
NH_4F (10%)	23	38	86
H_2O_2 (30%)	1	4	3
NaOH (20%)	1	0	0

^aAll the ratios are given in volume fractions and percents in mass (weight)

^bNon-combined C is not detected

In comparison with other ultra-high temperature materials the summarized data on the chemical behaviour of zirconium monocarbide are given in Addendum.

References

1. Kosolapova TYa, ed (1990) Handbook of high-temperature compounds: properties, production and applications. Hemisphere, New York
2. Gusev AI, Rempel AA, Magerl AJ (2001) Disorder and order in strongly nonstoichiometric compounds. Springer, Berlin
3. Andrievskii RA, Lanin AG, Rymashevskii GA (1974) Prochnost tugoplavkikh soedinenii (Strength of refractory compounds). Metallurgiya, Moscow (in Russian)
4. Andrievskii RA, Spivak II (1989) Prochnost tugoplavkikh soedinenii i materialov na ikh osnove (Strength of refractory compounds and materials based on them). Metallurgiya, Chelyabinsk (in Russian)
5. Obata N, Nakazawa N (1976) Superlattice formation in zirconium-carbon system. *J Nucl Mater* 60:39–42
6. Khaenko BV (1979) Order in cubic carbides and nitrides of transition metals of groups IV and V. *Inorg Mater* 15:1535–1543
7. Karimov I, Ėm VT, Latergaus IS, Khidirov I, Myasishcheva TM, Khvatinskaya DYa, Borovinskaya IP, Prokudina VK (1976) Neutron diffraction investigation of zirconium carbides. *Phys Met Metallogr* 41(5):175–178
8. Gusev AI (1991) Fizicheskaya khimiya nestekhiometricheskikh tugoplavkikh soedinenii (Physical chemistry of non-stoichiometric refractory compounds). Nauka, Moscow (in Russian)
9. Guo BC, Wei S, Purnell J, Buzza S, Castleman AW (1992) Metallo-carbohedrenes [M₈C₁₂ (M = V, Zr, Hf and Ti)]: a class of stable molecular cluster ions. *Science* 256:515–516
10. Storms EK (1967) The refractory carbides. Academic Press, New York, London
11. Toth LE (1971) Transition metal carbides and nitrides. Academic Press, New York, London
12. Xia HB, Tian DC, Jin ZZ, Wang LL (1994) First-principles calculation of the electronic structure of Ti₈C₁₂ and Zr₈C₁₂. *J Phys Condens Matter* 6:4269–4276
13. De Novion CH, Landesman JP (1985) Order and disorder in transition metal carbides and nitrides: experimental and theoretical aspects. *Pure Appl Chem* 57(10):1391–1402
14. Hu W, Tian Y, Liu Z (2013) Carbon vacancy ordered non-stoichiometric ZrC_{0.6}: synthesis, characterization and oxidation at low temperature. In: Low IM, Sakka Y, Hu CF (eds) MAX phases and ultra-high temperature ceramics for extreme environments. IGI Global, Hershey, Pennsylvania, pp. 478–508
15. Massalski TB, Subramanian PR, Okamoto H, Kacprzak L, eds (1990) Binary alloy phase diagrams, 2nd edn. ASM International, Metals Park, Ohio
16. Guillermet AF (1995) Analysis of thermochemical properties and phase stability in the zirconium-carbon system. *J Alloys Compd* 217:69–89
17. Rowcliffe DJ, Hollox GE (1971) Hardness anisotropy, deformation mechanisms and brittle-to-ductile transition in carbide. *J Mater Sci* 6(10):1270–1276
18. Singh A, Aynyas M, Sanyal SP (2009) Phase transition and high pressure behaviour of zirconium and niobium carbides. *Cent Eur J Phys* 7(1):102–107
19. Hao A, Zhou T, Zhu Y, Zhang X, Liu R (2011) First-principles investigations on electronic, elastic and thermodynamic properties of ZrC and ZrN under high pressure. *Mater Chem Phys* 129:99–104
20. Lv Z, Hu H, Wu C, Cui S, Zhang G, Feng W (2011) First-principles study of structural stability, electronic and elastic properties of ZrC compounds. *Phys B* 406(14):2750–2754

21. Srivastava A, Chauhan M, Singh RK (2011) High-pressure phase transitions in transition metal carbides XC (X = Ti, Zr, Hf, V, Nb, Ta): a first-principle study. *Phase Transit* 84(1):58–66
22. Rathod N, Gupta SK, Jha PK (2012) Dynamical stability and phase transition of ZrC under pressure. *Phase Transit* 85(12):1060–1069
23. Ivashchenko VI, Turchi PEA, Shevchenko VI (2013) Phase transformation B1 to B2 in TiC, TiN, ZrC and ZrN under pressure. *Condens Matter Phys* 16(3):1–9
24. Chauhan M, Gupta DC (2013) Electronic, mechanical, phase transition and thermo-physical properties of TiC, ZrC, HfC: high pressure computational study. *Diam Relat Mater* 40:96–106
25. Diwan BD (2014) Structural phase transition of refractory metal carbides at high pressure. *Can J Phys* 92:415–419
26. Samsonov GV, Upadhyaya GS, Neshpor VS (1974) *Fizicheskoe materialovedenie karbidov* (Physical materials science of carbides). Naukova Dumka, Kyiv (in Russian)
27. Upadhyaya GS (1996) *Nature and properties of refractory carbides*. Nova Science, Commack, New York
28. Ramqvist L (1968) Variation of lattice parameter and hardness with carbon content of group 4b metal carbides. *Jernkontoret Ann* 152(10):517–523
29. Ramqvist L (1971) Electronic structure of cubic refractory carbides. *J Appl Phys* 42(5):2113–2127
30. Samsonov GV (1964) *Refractory transition metal compounds*. Academic Press, New York
31. Krzhizhanovskii RE, Shtern ZYu (1977) *Teplofizicheskie svoistva nemetallicheskih materialov (karbidy)* (Thermophysical properties of non-metallic materials (carbides)). Energiya, Leningrad (in Russian)
32. Samsonov GV, Vinitkii IM (1980) *Handbook on refractory compounds*. IFI/Plenum, New York
33. Kotelnikov RB, Bashlykov SN, Galiakbarov ZG, Kashtanov AI (1968) *Osobo tugoplavkie elementy i soedineniya* (Extra-refractory elements and compounds). Metallurgiya, Moscow (in Russian)
34. Duwez P, Odell F (1950) Phase relationships in the binary systems of nitrides and carbides of zirconium, columbium, titanium and vanadium. *J Electrochem Soc* 97(10):299–304
35. Samsonov GV, Umanskii YaS (1957) *Tverdye soedineniya tugoplavkikh metallov* (Hard compounds of refractory metals). Metallurgizdat, Moscow (in Russian)
36. Samsonov GV (1953) *Fizicheskie svoistva nekotorykh faz vnedreniya* (Physical properties of certain interstitial phases). *Doklady AN SSSR* 93(4):689–692 (in Russian)
37. Shepline VM, Runck RJ (1956) Carbides. In: Campbell IE (ed) *High-temperature technology*. Wiley, New York, pp. 114–130
38. Norton JT, Mowry AL (1949) Solubility relationships of the refractory monocarbides. *Trans AIME* 185(2):133–136
39. Shaffer PTB (1964) *Handbooks of high-temperature materials: No. 1 – Materials index*. Plenum Press, Springer, New York
40. Thielke NR (1950) Application of crystal chemistry to the search for new refractories. *J Am Ceram Soc* 33(10):304–309
41. Lang SM (1960) *Properties of high-temperature ceramics and cermets: elasticity and density at room temperature*. Monograph No. 6. National Bureau of Standards, US Department of Commerce, Washington, DC
42. Samsonov GV (1964) *Handbooks of high-temperature materials: No. 2 – properties index*. Plenum Press, Springer, Science, New York
43. Goldschmidt HJ (1967) *Interstitial alloys*. Butterworths, London
44. Alyamovskii SI, Zainulin YuG, Shveikin GP (1981) *Oksikarbidy i oksinitridy metallov IVA i VA podgrupp* (Oxycarbides and oxynitrides of IVA and VA subgroups metals). Nauka, Moscow (in Russian)

45. Portnoi KI, Chubarov VM (1967) Svoistva tugoplavkikh metallov i soedinenii (The properties of refractory metals and compounds). In: Tumanov AT, Portnoi KI (eds) *Tugoplavkie materialy v mashinostroenii* (Refractory materials in machinery construction). Mashinostroenie, Moscow, pp. 7–124 (in Russian)
46. Kieffer R, Schwarzkopf P (1953) *Hartstoffe und Hartmetalle* (Refractory hard metals). Springer, Vienna (in German)
47. Kosolapova TYa (1971) *Carbides: properties, production and applications*. Plenum Press, New York
48. Samsonov GV, Épik AP (1973) *Tugoplavkie pokrytiya* (Refractory coatings). Metallurgiya, Moscow (in Russian)
49. Chang R, Graham LJ (1966) Low-temperature elastic properties of ZrC and TiC. *J Appl Phys* 37(10):3778–3783
50. Politis C (1975) Zur thermischen Gitterdilatation einiger Übergangsmetallverbindungen (On the thermal dilatation of lattice of some transition metal compounds). KFK 2168. Institut für Material- und Festkörperforschung, Gesellschaft für Kernforschung MBH, Karlsruhe (in German)
51. Lengauer W (2000) Transition metal carbides, nitrides and carbonitrides. In: Riedel R (ed) *Handbook of ceramic hard materials*. Wiley-VCH, Weinheim, New York, pp. 202–252
52. Wang J, Vandeperre LJ (2014) Deformation and hardness of UHTCs as a function of temperature. In: Fahrenholtz WG, Wuchina EJ, Lee WE, Zhou Y (eds) *Ultra-high temperature ceramics*. Wiley, Hoboken, New Jersey, pp. 236–266
53. Eisenmann B, Schäfer H (1988) Carbides. In: Hellwege K-H, Hellwege AM (eds) *Structure data of elements and intermetallic phases*, Subvol. A. Springer, Berlin, Heidelberg, pp. 197–318
54. Krajewski A, D’Alessio L, De Maria G (1998) Physico-chemical and thermophysical properties of cubic binary carbides. *Cryst Res Technol* 33(3):341–374
55. Tullhoff H (2005) Carbides. In: *Ullmann’s encyclopedia of industrial chemistry*. Wiley, Weinheim
56. Kempter CP, Fries RJ (1960) Crystallographic data. Zirconium carbide. *Anal Chem* 32(4):570
57. Samsonov GV, Naumenko VY, Okhremchuk LN (1971) Herstellung und Eigenschaften von Karbiden der Übergangsmetalle in ihren Homogenitätsbereichen (Synthesis and properties of carbides of transition metals in their homogeneity range). *Phys Stat Sol A* 6(1):201–211 (in German)
58. Shevchenko AS, Andrievskii RA, Kalinin VP, Lyutikov RA (1970) X-ray diffraction and pycnometric determinations of the density of zirconium-base interstitial phases. *Powder Metall Met Ceram* 9(1):71–73
59. Aigner K, Lengauer W, Rafaja D, Ettmayer P (1994) Lattice parameters and thermal expansion of $Ti(C_xN_{1-x})$, $Zr(C_xN_{1-x})$, $Hf(C_xN_{1-x})$ and TiN_{1-x} from 298 to 1473 K as investigated by high-temperature X-ray diffraction. *J Alloys Compd* 215:121–126
60. Houska CR (1964) Thermal expansion and atomic vibration amplitudes for TiC, TiN, ZrC, ZrN and pure tungsten. *J Phys Chem Solids* 25(4):359–366
61. Vishnevetskaya IA, Kudryasheva LV, Ordanyan SS, Petrov VA (1983) The effect of processing factors on the thermal and electrical conductivity of zirconium carbides at high temperatures. In: Larsen DC (ed) *Thermal conductivity – 16*. Proc. 16th Int. conf. on thermal conductivity, IIT Research Institute, Chicago, 7–9 Nov 1979. Plenum Press, New York, pp. 351–365
62. Kravchik AE, Ordanyan SS (2005) Isothermal sintering of inorganic powders. *Refract Indust Ceram* 46(6):423–431
63. Warlimont H (2005) Ceramics. In: Martienssen W, Warlimont H (eds) *Springer handbook of condensed matter and materials data*. Springer, Berlin, Heidelberg, pp. 431–476
64. Dolle M, Gosset D, Bogicevic C, Karolak F, Simeone D, Baldinozzi G (2007) Synthesis of nanosized zirconium carbide by a sol-gel route. *J Eur Ceram Soc* 27:2061–2067

65. Kalin BA (ed), Platonov PA, Chernov II, Shtrombakh YaI (2008) *Fizicheskoe materialovedenie* (Physical materials science). Vol. 6, Part 1 – Konstruktsionnyye materialy yadernoi tekhniki (Structural materials of nuclear engineering). National Research Nuclear University MEPhI, Moscow (in Russian)
66. Nakamura K, Yashima M (2008) Crystal structure of NaCl-type transition metal monocarbides MC (M = V, Ti, Nb, Ta, Hf, Zr), a neutron powder diffraction study. *Mater Sci Eng, B* 148:69–72
67. Birch F (1947) Finite elastic strain of cubic crystals. *Phys Rev* 71(11):809–824
68. Cheng D, Wang S, Ye H (2004) First-principles calculations of the elastic properties of ZrC and ZrN. *J Alloys Compd* 377(1–2):221–224
69. Fu H, Peng W, Gao T (2009) Structural and elastic properties of ZrC under high pressure. *Mater Chem Phys* 115:789–794
70. Silva GWC, Kercher AA, Hunn JD, Martin RC, Jellison GE, Meyer HM (2012) Characterization of zirconium carbides using electron microscopy, optical anisotropy, Auger depth profiles, X-ray diffraction and electron density calculated by charge flipping method. *J Solid State Chem* 194:91–99
71. Mitrokhin VA, Lyutikov RA, Yurkova RS (1975) Change in the lattice constant of zirconium carbide in the region of homogeneity. *Inorg Mater* 11(6):978–980
72. Sara RV, Dolloff RT, Kroenke WJ, Ruggiero JD, Lowell CE, Forgeng WD, Shaler AJ, Beodray FJ, Weigel J (1962) Research study to determine the phase equilibrium relations of selected metal carbides at high temperatures. Report WADD-TR-60-143, Contracts AF33(616)-6286 and AF33(657)-8025, Part 3. Research Laboratory of National Carbon Company, Union Carbide Corporation, Parma, Ohio, pp. 1–31
73. Storms EK (1964) A critical review of refractories. Report LA-TR-2942, Contract W-7405-ENG-36. Los Alamos Scientific Laboratory, New Mexico, pp. 1–255
74. Jackson HF, Lee WE (2012) Properties and characteristics of ZrC. In: Konings RJM, Allen TR, Stoller RE, Yamanaka S (eds) *Comprehensive nuclear materials*, Vol. 2 – Materials properties, oxide fuels for light water reactors and fast neutron reactors. Elsevier, Amsterdam, Oxford, pp. 339–372
75. Rudy E, Harmon DP, Brukl CE (1965) Ti-C and Zr-C system. In: Ternary phase equilibria in transition metal-boron-carbon-silicon systems. Report AFML-TR-65-2, Contract USAF 33(615)-1249, Part 1, Vol. 2. Air Force Materials Laboratory, Wright-Patterson Air Force Base, Ohio, pp. 1–51
76. Rudy E (1969) Compendium of phase diagram data. In: Ternary phase equilibria in transition metal-boron-carbon-silicon systems. Report AFML-TR-65-2, Contracts USAF 33(615)-1249 and USAF 33(615)-67-C-1513, Part 5. Air Force Materials Laboratory, Wright-Patterson Air Force Base, Ohio, pp. 1–689
77. Grossman LN (1965) High-temperature thermophysical properties of zirconium carbide. *J Am Ceram Soc* 48(5):236–242
78. Umanskii YaS (1947) *Karbidy tverdykh splavov* (Carbides of hard alloys). Metallurgizdat, Moscow (in Russian)
79. Kovalskii AE, Makarenko PG (1951) Izmerenie mikrotverdosti karbida tsirkoniya v zavisimosti ot sodержaniya ugleroda (Microhardness measurement of zirconium carbide depending on carbon content). In: Khrushchov MM (ed) *Mikrotverdest* (Microhardness). AN SSSR, Moscow, pp. 187–188 (in Russian)
80. Sara RV (1965) The system zirconium-carbon. *J Am Ceram Soc* 48(5):243–247
81. Aronson S, Cisney E, Auskern AB (1966) Thermal expansion of nonstoichiometric zirconium carbides. *J Am Ceram Soc* 49(8):456
82. Brown HL, Kempter CP (1966) Elastic properties of zirconium carbide. *Phys Stat Sol B* 18(1):K21–K23
83. Baker FB, Storms EK, Holley CE Jr (1969) Enthalpy of formation of zirconium carbide. *J Chem Eng Data* 14(2):244–246
84. Storms EK, Griffin J (1973) The vaporization behaviour of the defect carbides. IV. The zirconium-carbon system. *High Temp Sci* 5(4):291–310

85. Storms EK, Wagner P (1973) Thermal conductivity of sub-stoichiometric ZrC and NbC. *High Temp Sci* 5(6):454–462
86. Bulychev VP, Andrievskii RA, Nezhevenko LB (1977) The sintering of zirconium carbide. *Powder Metall Met Ceram* 16(4):273–276
87. Christensen AN (1990) A neutron diffraction investigation on single crystals of titanium oxide, zirconium carbide and hafnium nitride. *Acta Chem Scand* 44(8):851–852
88. Henney J, Jones JWS (1964) Ternary phases in the zirconium-carbon-oxygen system. Report AERE-R-4619. Atomic Energy Research Establishment, Harwell, UK, pp. 1–17
89. Nickel H, Inanc Ö, Lücke K (1968) Beitrag zum System Zirconium-Kohlenstoff (Contribution to zirconium-carbon system). *Z Metallkd* 59(12):935–940 (in German)
90. Morrison BH, Sturgess LL (1970) Thermal diffusivity and conductivity of zirconium carbide and niobium carbide from 100 to 2500 K. *Res Int Hautes Temp Refract* 7(4):351–358
91. Bukatov VG, Rymashevskii GA, Fedorov VB (1971) Thermal expansion of nonstoichiometric zirconium carbides. *Inorg Mater* 7(3):457–458
92. Shevchenko AS, Lyutikov RA, Andrievskii RA, Terekhova VA (1980) Oxidation of zirconium and niobium carbides. *Powder Metall Met Ceram* 19(1):48–52
93. Kumashiro Y, Nagai Y, Kato H, Sakuma E, Watanabe K, Misawa S (1981) The preparation and characteristics of ZrC and TaC single crystals using an r.f. floating-zone process. *J Mater Sci* 16(10):2930–2933
94. Levinson LS (1965) High-temperature heat contents of TiC and ZrC. *J Chem Phys* 42(8):2891–2892
95. Richardson JH (1965) Thermal expansion of three group IVA carbides to 2700 °C. *J Am Ceram Soc* 48(10):497–499
96. Katoh Y, Vasudevamurthy G, Nozawa T, Snead LL (2013) Properties of zirconium carbide for nuclear fuel applications. *J Nucl Mater* 441:718–742
97. Jackson HF, Jayaseelan DD, Lee WE, Reece MJ, Inam F, Manara D, Perinetti-Casoni C, De Bruycker F, Boboridis K (2010) Laser melting of spark plasma-sintered zirconium carbide: thermophysical properties of a generation IV very high-temperature reactor material. *Int J Appl Ceram Technol* 7(3):316–326
98. Jackson HF, Jayaseelan DD, Manara D, Perinetti-Casoni C, Lee WE (2011) Laser melting of zirconium carbide: determination of phase transitions in refractory ceramic systems. *J Am Ceram Soc* 94(10):3561–3569
99. Manara D, Jackson HF, Perinetti-Casoni C, Boboridis K, Welland MJ, Luzzi L, Ossi PM, Lee WE (2013) The ZrC-C eutectic structure and melting behaviour: a high-temperature radiance spectroscopy study. *J Eur Ceram Soc* 33:1349–1361
100. Elliott RO, Kempter CP (1958) Thermal expansion of some transition metal carbides. *J Phys Chem* 62(5):630–631
101. Shabalin IL, Wang Y, Krynkin AV, Umnova OV, Vishnyakov VM, Shabalin LI, Churkin VK (2010) Physico-mechanical properties of ultra-high temperature hetero-modulus ceramics based on group 4 transition metal carbides. *Adv Appl Ceram* 109(7):405–415
102. Gorinskii SG, Shabalin IL, Korshunov IG, Beketov AR, Kokorin AF (1979) Thermophysical properties of hot-pressed TiC-C and ZrC-C composite materials at high temperatures. *Powder Metall Met Ceram* 18(4):266–269
103. He X-M, Shu L, Li H-B, Li H-D, Lee S-T (1998) Structural characteristics and hardness of zirconium carbide films prepared by tri-ion beam-assisted deposition. *J Vac Sci Technol A* 16(4):2337–2344
104. Meng QN, Wen M, Mao F, Nedfors N, Jansson U, Zheng WT (2013) Deposition and characterization of reactive magnetron sputtered zirconium carbide films. *Surf Coat Technol* 232:876–883
105. Kondratyev A, Muboyajan S, Onufriev S, Savvatimskiy A (2015) The application of the fast pulse heating method for investigation of carbon-rich side of Zr-C phase diagram under high temperatures. *J Alloys Compd* 631:52–59

106. Zhilyaev VA, Askarova LK (1992) Regularities of redox reactions in the mixtures of carbides and nitrides of metals 4A-5A groups. *Russ J Inorg Chem* 37(1):1–4
107. Askarova LK, Zhilyaev VA (1993) Low-temperature oxidation of cubic carbides M(IV,V) C in air. *Russ J Inorg Chem* 38(12):1811–1814
108. Askarova LK, Zhilyaev VA (1994) High-temperature oxidation of titanium and zirconium carbides under lower air pressures. *Russ J Inorg Chem* 39(5):710–713
109. Čapková P, Merisalo M, Laitinen M, Valvoda V, Dobiášová L (1988) Thermal vibrations and thermal expansion of $ZrC_{0.98}$ studied by X-ray diffraction. *Phys Stat Sol A* 106(1):107–114
110. Kosukhin VV, Funke VF, Minashkin VI, Smirnov VS, Efremov YuP (1987) Zirconium nitride and carbonitride coatings obtained by the method of gas-phase metallurgy. *Inorg Mater* 23(1):52–56
111. Rahimzadeh E, Joshi NR, Singh S (1984) Thermal expansion of ZrC from 120 to 300 K by an X-ray powder method. *J Am Ceram Soc* 67(7):C139–C140
112. Mitrokhin VA, Yurkova RS (1981) Unit cell periods of solid solutions of zirconium carbide in niobium carbide. *Inorg Mater* 17(12):1701–1702
113. Matsumoto O, Yaguchi Y, Kajiwara T, Konuma M, Kanzaki Y (1981) Preparation and properties of a ternary cubic solid solution in the Mo-Zr-C system. *High Temp Sci* 14(3):161–169
114. Lesnaya MI, Nemchenko VF, Savin VI (1979) Some properties of solid solutions TiC-ZrC. *Inorg Mater* 15(1):61–64
115. Ivashina GA, Lesnaya MI, Nemchenko VF, Savin VI (1979) Physical and electrochemical properties of solid solutions TiC-ZrC and TiC-VC. *Inorg Mater* 15(4):546–549
116. Benedict U, Richter K, Walker CT (1978) Solubility study in the systems PuC-ZrC and PuC-TaC. *J Less-Common Met* 60(1):123–133
117. Funke VF, Pshenichnyi IV, Zubarev PV, Pliner LA, Lyakhov DM, Golomazov VM (1977) Some physicommechanical properties of $ZrC-NbC-MoC_{1-x}$ alloys. *Powder Metall Met Ceram* 16(12):968–973
118. Zubarev PV, Dementev LN (1977) Creep of carbides of transition metals of groups IV-V in region of homogeneity. *Inorg Mater* 13(7):988–991
119. Kats SM, Ordanyan SS (1977) High-temperature creep of solid solutions ZrC-TaC. *Inorg Mater* 13(10):1426–1428
120. Gusev AI, Ivanov NA, Shveikin GP, Geld PV (1976) Some properties of solutions of systems $ZrC_{0.97}-NbN_{0.93}$ and $Zr_{0.5}Nb_{0.5}C_xNb_{0.98-x}$. *Inorg Mater* 12(8):1149–1153
121. Gusev AI, Dubrovskaya LB, Shveikin GP (1975) Magnetic susceptibility and zone structure of solid solutions of systems $ZrN-NbC$ and $Zr_{0.5}Nb_{0.5}C_xN_{1-x}$. *Inorg Mater* 11(10):1520–1522
122. Gatterer J, Dufek G, Ettmayer P, Kieffer R (1975) Das kubische Tantalmononitrid (B1-Typ) und seine Mischbarkeit mit den isotypen Übergangsmetallnitriden und -carbiden (The cubic tantalum mononitride (B1 type) and its miscibility with the isotypic transition metal nitrides and carbides). *Monatsh Chem* 106(5):1137–1147 (in German)
123. Bukatov VG, Knyazev VI, Korostin OS, Baranov VM (1975) Temperature dependence of the Young's modulus of metalline carbides. *Inorg Mater* 11(2):310–312
124. Constant K, Kieffer R, Ettmayer P (1975) Über das pseudoternäre System "ZrO"-ZrN-ZrC (On the pseudoternary system "ZrO"-ZrN-ZrC). *Monatsh Chem* 106(4):823–832 (in German)
125. Avgustinik AI, Ordanyan SS, Fishchev VN (1974) Temperature dependence of the elastic moduli of cubic carbides in the Zr-Nb-C system. *Inorg Mater* 10(9):1399–1402
126. Danisina IN, Vil'k YuN, Avarbe RG, Omelchenko YuA, Ryzhkova TP (1968) Phase diagram of the system zirconium – zirconium nitride – zirconium carbide. *Russ J Appl Chem* 41(3):478–486
127. Tskhai VA, Alyamovskii SI, Shveikin GI, Geld PV (1972) Kонтсentrационная зависимость периодов решетки монокарбидов переходных металлов IV и V групп (The concentration dependence of lattice periods of transition metal monocarbides of IV and V groups). *Zh Neorg Khim* 17(3):602–604 (in Russian)

128. Alyamovskii SI, Zainulin YuG, Tskhai VA, Shveikin GP, Geld PV (1972) Thermal expansion of titanium oxycarbides and oxynitrides with a NaCl-type structure. *Inorg Mater* 8(10):1558–1560
129. Kieffer R, Ettmayer P, Nowotny H, Dufek G (1972) Neue Ermittlungen zur Mischbarkeit von Übergangsmetallnitride und -carbide (New investigations concerning miscibility of transition metal nitrides and carbides). *Metall* 26(7):701–708 (in German)
130. Zainulin YuG, Shveikin GP, Alyamovskii SI, Geld PV (1971) Coefficients of thermal expansion of cubic (NaCl type) oxycarbides and oxynitrides of zirconium and hafnium. *High Temp* 9(3):496–499
131. Samsonow GW, Morozow WW (1971) Carbohydride der Übergangsmetallen (Carbohydrides of the transition metals). *Monatsh Chem* 102(6):1667–1678 (in German)
132. Bukatov VG (1979) Issledovanie fiziko-mekhanicheskikh svoystv karbidov tugoplavkikh metallov i nekotorykh splavov na ikh osnove (Studies of physico-mechanical properties of refractory metal carbides and some alloys on their basis). PhD thesis, Moscow Institute of Steels and Alloys (in Russian)
133. Stuart H, Ridley N (1970) Thermal expansion of some carbides and tessellated stresses in steels. *J Iron Steel Inst* 208(12):1087–1092
134. Borukhovich AS, Matveenko II, Zainulin YuG, Alyamovskii SI, Geld PV (1970) The nature of the bond and electrical conductivity of cubic zirconium carbides and oxycarbides. *Inorg Mater* 6(12):1866–1870
135. Samsonov GV, Timofeeva II (1970) Rentgenograficheskoe issledovanie dinamicheskikh kharakteristik kristallicheskikh reshetok nekotorykh faz vnedreniya (X-ray diffraction study of dynamic characteristics of crystal lattices of some interstitial phases). *Dopov Akad Nauk Ukr RSR Ser A Fiz Mat Tekh Nauki* 32(9):831–833 (in Russian)
136. Samsonov GV, Kuchma AYu (1968) Magnetic susceptibility of zirconium, hafnium and niobium monocarbides. *Inorg Mater* 4(8):1195–1197
137. Avgustinik AI, Golikova OA, Klimashin GM, Neshpor VS, Ordanyan SS, Snetkova VA (1966) Some electrical and thermophysical properties of zirconium monocarbide as functions of carbon content over the homogeneous range. *Inorg Mater* 2(8):1230–1233
138. Golikova OA, Avgustinik AI, Klimashin GM, Kozlovskii LV, Ordanyan SS, Snetkova VA (1966) Electrical properties of carbides of transition metals in group 4. *Sov Phys Solid State* 7(12):2995–3002
139. Stecher P, Benesovsky F, Neckel A, Nowotny H (1964) Untersuchungen in den Systemen Titan (Zirkonium, Hafnium) – Niob – Kohlenstoff (Investigations in the systems titanium (zirconium, hafnium) – niobium – carbon). *Monatsh Chem* 95(6):1630–1645 (in German)
140. Bittner H, Goretzki H, Benesovsky F, Nowotny H (1963) Über einige Monocarbide-Mononitrid-Systeme und deren magnetische Eigenschaften (On some monocarbide-mononitride systems and their magnetic properties). *Monatsh Chem* 94(3):518–526 (in German)
141. Ingold JH (1963) Thermionic properties of some refractory metal carbides. *J Appl Phys* 34(7):2033–2039
142. Krikorian NH, Wallace TC, Anderson JL (1963) Low-temperature thermal expansion of the group 4a carbides. *J Electrochem Soc* 110(6):587–588
143. Smith DK, Cline CF (1963) An X-ray investigation of polymorphism in ZrC. *J Am Ceram Soc* 46(11):566
144. Brock WF, Krzanowski JE, Leuchtner RE (1997) Nanocomposite thin films of transition metal carbides fabricated using pulsed laser deposition. *Mater Res Soc Symp Proc* 457:419–424
145. Rudy E, Benesovsky F (1963) Zur Kenntnis der Stabilität des Urandicarbids und der Kohlenstoff-stabilen Bereiche in den Partialsystemen von UC mit ZrC, HfC, NbC und TaC (To the knowledge of uranium dicarbide stability and carbon stable areas in the partial systems of UC with ZrC, HfC, NbC and TaC). *Monatsh Chem* 94(1):204–224 (in German)

146. Benesovsky F, Rudy E (1960) Beitrag zum Aufbau des Systeme Zr-C und Hf-C (Contributions to the construction of the systems Zr-C and Hf-C). *Planseeber Pulvermetall* 8:66–71 (in German)
147. Nowotny H, Benesovsky F, Rudy E (1960) Hochschmelzende Systeme mit Hafniumkarbid und -nitrid (Refractory systems with hafnium carbide and nitride). *Monatsh Chem* 91(2):348–356 (in German)
148. Bandow S, Saito Y (1993) Encapsulation of ZrC and V_4C_3 in graphite nanoballs via arc-burning of metal carbides/graphite composites. *Jpn J Appl Phys* 32(11B): L1677–L1680
149. Brownlee LD (1958) The pseudo-binary systems of uranium carbide with zirconium carbide, tantalum carbide and niobium carbide. *J Inst Met* 87(2):58–61
150. Nowotny H, Kieffer R (1947) Roentgenographische Untersuchungen von Karbidsystemen (X-ray investigations of carbide systems). *Z Metallkd* 38:257–265 (in German)
151. Alyamovskii SI, Zainulin YuG, Shveikin GP, Geld PV (1971) Kontsenratsionnaya oblast ustoiichivosti kubicheskogo (tipa NaCl) oksikarbida tsirkoniya i stepen zapolneniya ego elementarnoi yacheiki (The concentration region of the stability of cubic (NaCl type) zirconium oxycarbide and degree of filling of its unit cell). *Zh Neorg Khim* 16(1):7–11 (in Russian)
152. Naito K, Kamegashira N, Fujiwara N (1978) Synthesis of nonstoichiometric zirconium carbide whiskers by chemical vapour deposition. *J Cryst Growth* 45:506–510
153. Timofeeva II, Klochkov LA (1974) Variation in the lattice parameters and static distortions in the homogeneity range of transition metal monocarbides. In: Samsonov GV (ed) *Refractory carbides*. Consultants Bureau, New York, London, pp. 239–245
154. Borukhovich AS, Dubrovskaya LB, Matveenko II, Geld PV (1969) Magnetic susceptibility and energy band structure of zirconium monocarbide. *Phys Stat Sol* 36(1):97–102
155. Nikitin VP, Novikov VI, Neshpor VS, Popov VV (1975) Superconductivity of zirconium-carbon alloys. *Phys Solid State* 17(11):2229–2231
156. Rymashevskii GA, Gurevich BD, Kosykh VG, Kutyreva GA (1972) The effect of oxygen impurity on the value of the lattice parameter of zirconium carbide. *Inorg Mater* 8(5):952–954
157. Tamari N, Kato A (1978) Catalytic effect of nickel on the growth of zirconium carbide whiskers by chemical vapour deposition. *J Less-Common Met* 58(2):147–160
158. Wallace TC, Gutierrez CP, Stone PL (1963) The molybdenum-zirconium-carbon system. *J Phys Chem* 67(4):796–801
159. Bittner H, Goretzki H (1962) Magnetische Untersuchungen der Carbide TiC, ZrC, HfC, VC, NbC und TaC (Magnetic studies of the TiC, ZrC, HfC, VC, NbC and TaC carbides). *Monatsh Chem* 93(5):1000–1004 (in German)
160. Gusev AI (1989) Structural stability boundaries for nonstoichiometric compounds. *Phys Stat Sol A* 111(2):443–450
161. Zhelankin VI, Kutsev VS, Ormont BF (1958) Issledovanie ravnovesiya v reaktsiyakh vosstanovleniya ZrO_2 i V_2O_3 uglerodom pri vysokikh temperaturakh (A study of equilibrium in the reactions of ZrO_2 and V_2O_3 reduction by carbon at high temperatures). *Zh Neorg Khim* 3(5):1237–1240 (in Russian)
162. Klimashin GM, Kozlovskii LV, Tsyu AK (1971) Oblast obrazovaniya oksikarbidnoi fazy v sisteme Zr-C-O (Region of oxycarbide phase occurrence in Zr-C-O system). *Zh Prikl Khim* 44(7):1644–1646 (in Russian)
163. Kosolapova TYa, Fedorus VB, Panasyuk AD, Kozina GK (1972) Conditions of formation and some properties of zirconium oxycarbides. *Powder Metall Met Ceram* 11(1):47–50
164. Sarkar SK, Miller AD, Mueller JI (1972) Solubility of oxygen in ZrC. *J Am Ceram Soc* 55(12):628–630
165. Zainulin YuG, Alyamovskii SI, Mitrofanov BV, Lyubimov VD, Shveikin GP (1976) Cubic titanium and zirconium oxycarbonitrides. *Inorg Mater* 12(9):1296–1299

166. Jayaseelan DD, Xin Y, Vandeperre L, Brown P, Lee WE (2015) Development of multi-layered thermal protection system (TPS) for aerospace applications. *Composites B* 79:392–405
167. Li J, Liao D, Yip S, Najafabadi R, Ecker L (2003) Force-based many-body interatomic potential for ZrC. *J Appl Phys* 93(11):9072–9085
168. Arya A, Carter EA (2004) Structure, bonding and adhesion at the ZrC(100)/Fe(110) interface from first principles. *Surf Sci* 560:103–120
169. Williams WS (1964) Influence of temperature, strain rate, surface condition and composition on the plasticity of transition metal carbide crystals. *J Appl Phys* 35(4):1329–1338
170. Lee DW, Haggerty JS (1969) Plasticity and creep in single crystals of zirconium carbide. *J Am Ceram Soc* 52(12):641–647
171. Hannink RHJ, Kohlstedt DL, Murray MJ (1972) Slip system determination in cubic carbides by hardness anisotropy. *Proc R Soc Lond A* 326:409–420
172. Kumashiro Y, Nagai Y, Kato H (1982) The Vickers micro-hardness of NbC, ZrC and TaC single crystals up to 1500 °C. *J Mater Sci Lett* 1(2):49–52
173. Perry AJ, Jagner M (1989) Residual stress in physically vapour deposited films: a study of deviations from elastic behaviour. *Thin Solid Films* 171:197–216
174. Kiani S, Ratsch C, Minor AM, Kodambaka S, Yang J-M (2015) Orientation- and size-dependent room-temperature plasticity in ZrC crystals. *Philos Mag* 95(9):985–997
175. Mahday AA, El-Eskandarany MS, Ahmed HA, Amer AA (2000) Mechanically induced solid state carburization for fabrication of nanocrystalline ZrC refractory material powder. *J Alloys Compd* 299(1–2):244–253
176. Hu Z, Sacks MD, Staab GA, Wang C-A, Jain A (2002) Solution-based processing of nanocrystalline ZrC. *Ceram Eng Sci Proc* 23(4):711–717
177. Li C, Yang X, Zhao Z, Qian Y (2002) A co-reduction carburization route to synthesize nanocrystalline ZrC. *Chem Lett* (11):1088–1089
178. Sacks MD, Wang C-A, Yang Z, Jain A (2004) Carbothermal reduction synthesis of nanocrystalline zirconium carbide and hafnium carbide powders using solution-derived precursors. *J Mater Sci* 39:6057–6066
179. Andrievskii RA (2005) Nanomaterials based on high-melting carbides, nitrides and borides. *Russ Chem Rev* 74(12):1061–1072
180. Dollé M, Gosset D, Bogicevic C, Baldinozzi G, Karolak F, Simeoni D (2005) Nano-sized zirconium carbides: synthesis, characterisation and irradiation. *Mater Res Soc Symp Proc* 908:13–17
181. Combemale L, Leconte Y, Portier X, Herlin-Boime N, Reynaud C (2009) Synthesis of nanosized zirconium carbide by laser pyrolysis route. *J Alloys Compd* 483:468–472
182. Rice JR (1992) Dislocation nucleation from a crack tip – an analysis based on the Peierls concept. *J Mech Phys Solids* 40(2):239–271
183. Li X, Westwood A, Brown A, Brydson R, Rand B (2009) A convenient general synthesis of carbide nanofibres via template reactions on carbon nanotubes in molten salt media. *Carbon* 47:201–208
184. Nam YS, Cui XM, Jeong L, Lee JY, Park WH (2009) Fabrication and characterization of zirconium carbide (ZrC) nanofibers with thermal storage property. *Thin Solid Films* 517:6531–6538
185. Tao X, Qiu W, Li H, Zhao T (2010) Synthesis of nanosized zirconium carbide from preceramic polymers by the facile one-pot reaction. *Polym Adv Technol* 21:300–304
186. Xiang JY, Liu SC, Hu WT, Zhang Y, Chen CK, Wang P, He JL, Yu DL, Xu B, Lu YF, Tian YJ, Liu ZY (2011) Mechanochemically activated synthesis of zirconium carbide nanoparticles at room temperature: a simple route to prepare nanoparticles of transition metal carbides. *J Eur Ceram Soc* 31:1491–1496
187. Reddy RS, Kamaraj M, Mudali UK, Chakravarthy SR, Sarathi R (2012) Generation and characterization of zirconium carbide nanoparticles by wire explosion process. *Mater Trans* 53(8):1420–1424

188. Tao X, Qui W, Li H (2012) Synthesis of nanosized zirconium carbide (ZrC) by a polymeric precursor route. *Adv Mater Res* 393–395:373–376
189. Naguib M, Mashtalir O, Carle J, Presser V, Lu J, Hultman L, Gogotsi Y, Barsoum MW (2012) Two-dimensional transition metal carbides. *ACS Nano* 6(2):1322–1331
190. Naguib M, Come J, Dyatkin B, Presser V, Taberna P-L, Simon P, Barsoum MW, Gogotsi Y (2012) MXene: a promising transition metal carbide anode for lithium-ion batteries. *Electrochem Commun* 16:61–64
191. Tang Q, Zhou Z (2013) Graphene-analogous low-dimensional materials. *Prog Mater Sci* 58:1244–1315
192. Khazaei M, Arai M, Sasaki T, Chung C-Y, Venkataramanan NS, Estili M, Sakka Y, Kawazoe Y (2013) Novel electronic and magnetic properties of two-dimensional transition metal carbides and nitrides. *Adv Funct Mater* 23(17):2185–2192
193. Jansson U, Lewin E (2013) Sputter deposition of transition metal carbide films – a critical review from a chemical perspective. *Thin Solid Films* 536:1–24
194. Li F, Kang Z, Huang X, Zhang G-J (2014) Fabrication of zirconium carbide nanofibers by electrospinning. *Ceram Int* 40:10137–10141
195. Sun D, Hu Q, Chen J, Zhou A (2014) First principles calculations of the relative stability, structure and electronic properties of two-dimensional metal carbides and nitrides. In: Proc. 8th Int. conf. on high-performance ceramics (CICC 2013), Chongqing, China, 4–7 Nov 2013. *Key Eng Mater* 602–603:527–531
196. Zhao S, Kang W, Xue J (2014) Manipulation of electronic and magnetic properties of M₂C (M = Hf, Nb, Sc, Ta, Ti, V, Zr) monolayer by applying mechanical strains. *Appl Phys Lett* 104:133106 (4 pp.)
197. Guo Z, Zhu L, Zhou J, Sun Z (2015) Microscopic origin of MXenes derived from layered MAX phases. *RSC Adv* 5(32):25403–25408
198. Singh A, Modi MH, Sinha AK, Dhawan R, Lodha GS (2015) Study of structural and optical properties of zirconium carbide (ZrC) thin films deposited by ion beam sputtering for soft X-ray optical applications. *Surf Coat Technol* 272:409–414
199. Chirkin VS (1968) *Teplofizicheskie svoistva materialov yadernoi tekhniki* (Thermophysical properties of nuclear materials). Atomizdat, Moscow (in Russian)
200. Holleck H (1984) *Binäre und ternäre Carbide- und Nitridsysteme der Übergangsmetalle* (Binary and ternary carbide and nitride systems of the transition metals). Gebrüder Bornträger, Berlin, Stuttgart (in German)
201. Zotov YuP, Kotelnikov RB (1975) Solidus temperature of zirconium carbide in homogeneous region. *Russ Metall* (1):148–150
202. Turchanin AG, Turchanin MA (1991) *Termodinamika tugoplavkikh karbidov i karbonitridov* (Thermodynamics of refractory carbides and carbonitrides). Metallurgiya, Moscow (in Russian)
203. Bolgar AS, Guseva EA, Fesenko VV (1967) Thermodynamic properties of zirconium and hafnium carbides in the range 298–2500 K. *Powder Metall Met Ceram* 6(1):31–33
204. Sheindlin AE, Chekhovskoi VYa, Spilrain EE (1970) Research on thermophysical properties of solids at high temperatures at the Institute for High Temperatures of the USSR Academy of Sciences. *High Temp High Press* 2(1):1–6
205. Petrova II, Chekhovskoi VYa (1978) True heat-capacity of zirconium, niobium and tantalum carbides by a pulse method. *High Temp* 16(6):1045–1050
206. Turchanin AG (1981) Temperature-concentration dependence of the enthalpy and heat capacity of zirconium carbide in the homogeneity region. *Inorg Mater* 17(2):183–185
207. Zefirov AP (ed), Vertyatin UD, Mashirev VP, Ryabtsev NG, Tarasov VI, Rogozkin BD, Korobov IV (1965) *Termodinamicheskie svoistva neorganicheskikh veschestv* (Thermodynamic properties of inorganic substances). Atomizdat, Moscow (in Russian)
208. Bolgar AS, Turchanin AG, Fesenko VV (1973) *Termodinamicheskie svoistva karbidov* (Thermodynamic properties of carbides). Naukova Dumka, Kyiv (in Russian)
209. Turchanin AG, Fesenko VV (1968) Enthalpy and thermal capacity of zirconium carbide in the homogeneous range of 1300–2500 K. *Powder Metall Met Ceram* 7(1):67–68

210. Korshunov IG, Zinovev VE, Geld PV, Borukhovich AS, Chernyaev VS, Shveikin GP (1977) Thermophysical properties of cubic carbides of zirconium and niobium at high temperatures. *High Temp* 15(3):439–444
211. Schick HL, ed (1966) Thermodynamics of certain refractory compounds, Vol. 1–2. Academic Press, New York, London
212. Reznitskii LA (1966) Approximate estimates of heats of formation of certain compounds of transition metals of groups IV and V. *Russ J Phys Chem* 40(1):68–72
213. Marmer ÉN, Gurchich OS, Maltseva LF (1967) Vysokotemperaturnye materialy (High-temperature materials). Metallurgiya, Moscow (in Russian)
214. Samsonov GV, Paderno VN (1963) Poluchenie i svoistva nekotorykh tugoplavkikh karbidnykh splavov (Preparation and properties of certain refractory carbide alloys). *Zh Prikl Khim* 36(12):2759–2762 (in Russian)
215. Hansen M, Anderko K (1958) Constitution of binary alloys, 2nd edn. McGraw-Hill, New York, London
216. Fesenko VV, Bolgar AS (1963) O kompleksnom izmerenii fiziko-khimicheskikh svoistv tugoplavkikh soedinenii pri vysokikh temperaturakh (On the complex measurement of physico-chemical properties of refractory compounds at high temperatures). In: Budnikov PP (ed) Silikaty i oksidy v khimii vysokikh temperatur (Silicates and oxides in the chemistry of high temperatures). Metallurgizdat, Moscow, pp. 135–148 (in Russian)
217. Mah AD, Boyle BJ (1955) Heats of formation of niobium carbide and zirconium carbide from combustion calorimetry. *J Am Chem Soc* 77(24):6512–6513
218. Kieffer R, Benesovsky F (1968) Hartstoffe (Hard materials). Springer, Vienna (in German)
219. Pollock BD (1961) The vaporization behaviour and thermodynamic stability of zirconium carbide at high temperature. *J Phys Chem* 65(5):731–735
220. Fesenko VV, Bolgar AS (1965) Isparenie tugoplavkikh soedinenii (Vaporization of refractory compounds). Metallurgiya, Moscow (in Russian)
221. Mah AD (1964) Heats of formation of zirconium carbide and hafnium carbide. Report BM-RI-6518. US Bureau of Mines, US Department of the Interior, Washington, DC, pp. 1–8
222. Westrum EF, Jr, Feick G (1963) Zirconium carbide: heat capacity and thermodynamic properties from 5 to 350 K. *J Chem Eng Data* 8(2):176–178
223. Samsonov GV (1962) Analiz tugoplavkikh soedinenii (The analysis of refractory compounds). Metallurgizdat, Moscow (in Russian)
224. Chase MW, Jr, ed (1998) NIST-JANAF thermochemical tables, 4th edn. *J Phys Chem Ref data monograph No. 9*. American Institute of Physics, New York (*see also* <http://webbook.nist.gov/chemistry>). Accessed 21 Oct 2016
225. Vidale GL (1961) The measurement of the vapour pressure of atomic species from spectrophotometric measurements of the absorption of resonance lines. V. The free energy of formation of TiC and ZrC. Report R61SD147, Contract AF33(616)-6841. Missile and Space Vehicle Department, General Electric Company, Philadelphia, Pennsylvania, pp. 1–20
226. Agte C, Alterthum H (1930) Forschungen auf Systemen mit Carbide bei hohen Schmelzpunkt und Beiträge für das Problem der Kohlenstoff Fusion (Researches on systems with carbides at high melting point and contributions to the problem of carbon fusion) *Z Tech Physik* 11:182–191 (in German)
227. Worrell WL (1964) Estimation of the entropy of formation at 298 K for some refractory metal carbides. *J Phys Chem* 68(4):954–955
228. Storms EK (1962) Selected properties of group 4a, 5a and 6a carbides. In: A critical review of refractories. Report LA-TR-2674, Contract W-7405-eng-36, Part 1. Los Alamos Scientific Laboratory, New Mexico, pp. 1–93
229. Coffman JA, Kibler GM, Lyon TF, Acchione BD (1963) Carbonization of plastics and refractory materials research. Report WADD-TR-60-646, Contract AF-33(616)-6841, Part 2. Directorate of Materials and Processes Aeronautical Systems Division, Wright-Patterson Air Force Base, Ohio, pp. 1–183

230. Kutsev VS, Ormont BF, Epelbaum VA (1955) Issledovanie ravnovesiya v sisteme ZrO_2-C pri vysokikh temperaturakh (A study of equilibrium in the ZrO_2-C system at high temperatures). Doklady AN SSSR 104(4):567–570 (in Russian)
231. Andrievskii RA, Alekseeva IS, Khromonozhkin VV, Khromov YuF, Mitrokhin VA (1972) Partzialnye termodinamicheskie svoystva karbida tsirkoniya v oblasti gomogenosti (Partial thermodynamic properties of zirconium carbide in region of homogeneity). Doklady AN SSSR 206(4):896–898 (in Russian)
232. Ormont BF (1959) Energii atomizatsii i teploty obrazovaniya nekotorykh karbidov i nitridov i naibolee veroyatnye znacheniya dlya energii dissotsiatsii azota i energii sublimatsii ugleroda (Atomization energies and heats of formation of some carbides and nitrides and the most probable values for the dissociation energy of nitrogen and sublimation energy of carbon). Zh Fiz Khim 33(7):1455–1460 (in Russian)
233. Fujishiro S (1961) Thermodynamic properties of transition metal carbides and their periodicity. J Jpn Soc Powder Metall 8(2):73–76
234. Oshcherin BN (1965) Nekotorye voprosy termodinamiki karbidnykh faz vnedreniya v oblasti gomogenosti (The certain problems of thermodynamics of carbide interstitial phases within the homogeneity ranges). In: Grigoreva VV, Eremenko VN, Nazarchuk TN, Samsonov GV, Fedorchenko IM, Frantsevich IN (eds) Vysokotemperaturnye neorganicheskie soedineniya (High-temperature inorganic compounds). Naukova Dumka, Kyiv, pp. 157–165 (in Russian)
235. Kubaschewski O, Evans EL (1958) Metallurgical thermochemistry. Pergamon Press, London, New York
236. Ormont BF (1950) Struktury neorganicheskikh veshchestv (Structure of inorganic substances). Gosizdat Tekhniko-Teoreticheskoi Literatury, Moscow, Leningrad (in Russian)
237. Gorshkov VS, Savelev VG, Fedorov NF (1988) Fizicheskaya khimiya silikatov i drugikh tugoplavkikh soedinenii (Physical chemistry of silicates and other refractory compounds). Vysshaya Shkola, Moscow (in Russian)
238. Kulikov IS (1988) Termodinamika karbidov i nitridov (Thermodynamics of carbides and nitrides). Metallurgiya, Chelyabinsk (in Russian)
239. Mebed MM, Yurchak RP, Korolev LA (1973) Thermophysical properties of zirconium carbide in high-temperature region. High Temp 11(2):380–381
240. Kornilov AN, Chelovskaya NV, Zhelankin VI (1975) Heat of formation of zirconium carbides. Russ J Phys Chem 49(5):792–798
241. Barin I (1995) Thermochemical data of pure substances, Vol. 1-2. 3rd edn. VCH, Weinheim, New York
242. Singh M, Wiedemeier H (1997) Estimation of thermal expansion behaviour of some refractory carbides and nitrides. J Mater Sci 32(21):5749–5751
243. Eckerlin P, Kandler H (1971) Structural data for elements and intermetallic phases. Springer, Berlin
244. Krikorian OH (1962) Estimation of high-temperature heat capacities of carbides. Report UCRL-6785. University of California Radiation Laboratory, Berkeley, California, pp. 1–5
245. Neel DS, Pears CD, Oglesby S, Jr (1962) The thermal properties of thirteen solid materials to 5000 °F or their destruction temperatures. Technical report WADD-TR-60-924, Contract USAF 33(616)-6312. Southern Research Institute, University of Alabama, Birmingham, USA, pp. 1–216
246. Neshpor VS, Samsonov GV (1957) Brittleness in metallic compounds. Phys Met Metallogr 4(1):147–148
247. Kaufman L, Bernstein H, Sarney A (1962) Thermodynamics of interstitial solid solutions and refractory compounds. Technical Report ASD-TR-61-445, Contract AF33(657)-9826, Part 2. Air Force Materials Laboratory, Wright-Patterson Air Force Base, Ohio, pp. 1–88
248. Kelley KK, King EG (1961) Contributions to data on theoretical metallurgy. XIV. Entropies of the elements and inorganic compounds. US Bur Mines Bull 592:1–149

249. Krestovnikov AN, Vendrikh MS (1959) Termodinamika diborida titana (Thermodynamics of titanium diboride). *Izv Vyssh Uchebn Zaved Tsvet Metall* (2):54–57 (in Russian)
250. McClaine LA, ed (1964) Thermodynamic and kinetic studies for a refractory materials program. Technical Report ASD-TDR-62-204, Contract AF33(616)-7472, Part 3. Air Force Materials Laboratory, Wright-Patterson Air Force Base, Ohio, pp. 1–236
251. Pollock BD (1961) The vaporization behaviour and thermodynamic stability of zirconium carbide at high temperature. Report NAA-SR-5439. US Atomic Energy Commission, Atomic International, Canoga Park, California, pp. 1–22
252. Engelke JL, Halden FA, Farley EP (1960) Synthesis of new high-temperature materials. Report WADC-TR-59-654, Contract AF33(616)-5888. Stanford Research Institute, Menlo Park, California, pp. 1–45
253. Levinstein MA (1962) Properties of plasma sprayed materials. Report ASD-TDR-62-201, Contract AF33(616)-6376. General Electric Company, Evendale, Ohio, pp. 1–93
254. Barriault RJ, Bender SL, Dreikorn RE, Einwohner TH, Feber RC, Gannon RE, Hanst PL, Ilnat ME, Phaneuf JP, Schick HL, Ward CH (1962) Thermodynamics of certain refractory compounds. Report ASD-TR-61-260, Part 1, Vol. 1. Air Force Materials Laboratory, Wright-Patterson Air Force Base, Ohio, pp. 1–404
255. Mezaki R, Tilleux EW, Jambois TF, Margrave JL (1965) High-temperature thermodynamic functions for refractory compounds. In: Gratch S (ed) *Advances in thermophysical properties at extreme temperatures and pressures*. Papers of 3rd ASME symp., American Society of Mechanical Engineers, Lafayette, Indiana, pp. 138–145
256. Kaufman L, Bernstein H (1968) Thermodynamic properties of refractory transition metal compounds. In: Vahldiek FW, Mersol SA (eds) *Anisotropy in single-crystal refractory compounds*, Vol. 1. Springer, New York, pp. 269–297
257. Turchanin AG, Guseva EA, Fesenko VV (1973) Thermodynamic properties of refractory carbides in the temperature range 0–3000 K. III. Zirconium carbide. *Powder Metall Met Ceram* 12(3):215–217
258. Turchanin AG, Fesenko VV (1973) Thermodynamic properties of refractory carbides in the homogeneity region at high temperatures. *Heat Transfer Res* 5(5):23–28
259. Hojo H, Nakayama K (1976) Coated emitters of transition metal carbides for vacuum measurement. *J Vac Soc Jpn* 19(9):312–317 (in Japanese)
260. Bowman AL, Krikorian NH (1976) Interstitial phases. In: Hannay NB (ed) *Treatise on solid state chemistry*, Vol. 3. Crystalline and noncrystalline solids. Plenum Press, New York, London pp. 253–292
261. Coltters RG (1985) Thermodynamics of binary metallic carbides: a review. *Mater Sci Eng* 76(1–2):1–50
262. Kubaschewski O, Alcock CB (1983) *Metallurgical thermochemistry*, 5th edn. Pergamon Press, Oxford
263. Butt DP, Wantuck PJ, Rehse SJ, Wallace TC, Sr (1994) Vaporization behaviour of non-stoichiometric refractory carbide materials and direct observations of the vapour phase using laser diagnostics. In: Nickel KG (ed) *Corrosion of advanced ceramics*. Kluwer Academic, Springer, Dordrecht, pp. 363–374
264. Maslov VM, Neganov AS, Borovinskaya IP, Merzhanov AG (1978) Self-propagating high-temperature synthesis as a method for determination of the heat formation of refractory compounds. *Combust Explo Shock Waves* 14(6):759–766
265. McClaine LA, ed (1963) Thermodynamic and kinetic studies for a refractory materials program. Technical report ASD-TDR-62-204, Contract AF33(616)-7472, Part 2. Air Force Materials Laboratory, Wright-Patterson Air Force Base, Ohio, pp. 1–142
266. Kantor PB, Fomichev EN (1967) Enthalpy and specific heat of niobium and zirconium carbides in temperature range 500 to 2400 K. *High Temp* 5(1):41–44
267. Kubaschewski - Von Goldbeck O (1976) Phase diagrams. In: Kubaschewski O (ed) *Zirconium. Physico-chemical properties of its compounds and alloys*. Atomic Energy Review, Special Issue N 6. International Atomic Energy Agency, Vienna, pp. 67–140

268. Elliott RP (1965) Constitution of binary alloys (first supplement). McGraw-Hill, New York
269. Shunk FA (1969) Constitution of binary alloys (second supplement). McGraw-Hill, New York
270. Paderno VN (1964) Poluchenie i fizicheskie svoistva karbidov i karbidnykh splavov nekotorykh perekhodnykh metallov (Preparation and physical properties of carbides and carbide alloys of some transition metals). PhD thesis, Institute of Metal Ceramics and Special Alloys, Ukrainian SSR Academy of Sciences, Kyiv (in Russian)
271. Rudy E, Progulski J (1967) A Pirani furnace for the precision determination of the melting temperatures of refractory metallic substances. *Planseeber Pulvermetall* 15:13–45
272. Hultgren R, Desai PD, Hawkins DT, Gleiser M, Kelley KK, Wagman DD (1973) Selected values of the thermodynamic properties of binary alloys. American Society for Metals, Metals Park, Ohio
273. Alcock CB, Jakob KT, Zador S (1976) Thermodynamic properties. In: Kubaschewski O (ed) Zirconium. Physico-chemical properties of its compounds and alloys. Atomic Energy Review, Special Issue N 6. International Atomic Energy Agency, Vienna, pp. 7–66
274. Guillermet AF, Häglund J, Grimvall G (1992) Cohesive properties of 4d-transition-metal carbides and nitrides in the NaCl-type structure. *Phys Rev B* 45(20):11557–11567
275. Kolesnichenko AN, Pustogarov AV (1975) Determination of thermophysical properties of zirconium carbide at high temperatures. *High Temp* 13(6):1108–1112
276. Rogovoi Yul (1999) Effect of structural vacancies on the nature of metal-metal and metal-carbon bonds in cubic monocarbides. *Powder Metall Met Ceram* 38(1–2):44–50
277. Kiparisov SS, Nuzhdin AA (1988) Thermal expansion of titanium and zirconium carbides in the area of their homogeneity. *Powder Metall Met Ceram* 27(4):307–310
278. Lengauer W, Binder S, Aigner K, Etmayer P, Guillou A, Debuigne J, Grobth G (1995) Solid state properties of group IVb carbonitrides. *J Alloys Compd* 217:137–147
279. Knyazkov AM, Kurbakov SD, Savvatimskiy AI, Sheindlin MA, Yanchuk VI (2011) Melting of carbides by electrical pulse heating. *High Temp High Press* 40:349–358
280. Lu X-G, Selleby M, Sundman B (2007) Calculations of thermophysical properties of cubic carbides and nitrides using the Debye-Grüneisen model. *Acta Mater* 55:1215–1226
281. Zhu J, Zhu B, Qu J-Y, Gou Q-Q, Chen F (2009) Thermodynamic properties of cubic ZrC under high pressure from first-principles calculations. *Sci China Series G Phys Mech Astron* 52(7):1039–1042
282. Li H, Zhang L, Zeng Q, Ren H, Guan K, Liu Q, Cheng L (2011) First-principles study of the structural, vibrational, phonon and thermodynamic properties of transition metal carbides TMC (TM = Ti, Zr, Hf). *Solid State Commun* 151:61–66
283. Varshney D, Shriya S (2013) Elastic, mechanical and thermodynamic properties at high pressures and temperatures of transition metal monocarbides. *Int J Refract Met Hard Mater* 41:375–401
284. Abdollahi A (2013) First-principle calculations of thermodynamic properties of ZrC and ZrN at high pressures and high temperatures. *Phys B* 410:57–62
285. Gautam GS, Kumar KCH (2014) Elastic, thermochemical and thermophysical properties of rock salt – type transition metal carbides and nitrides: a first principles study. *J Alloys Compd* 587:380–386
286. Turchanin AG (1986) Thermodynamics of cubic refractory carbides of group IV transition metals of variable composition in the range 1200–2500 K. *Inorg Mater* 22(8):1136–1139
287. Kaufman L (1964) Thermodynamic factors controlling the stability of solid phases at high temperatures. In: Waber JT, Chiotti P, Miner WN (eds) Compounds of interest in nuclear reactor technology. Metallurgical Society of American Institute of Mining Engineers, New York, pp. 193–225
288. Fesenko VV, Bolgar AS (1969) Study of evaporation rates of carbides of titanium, zirconium, hafnium, niobium and tantalum at high temperatures. *High Temp* 7(2):226–233
289. Starostina TS, Sidorov LN, Akishin PA, Karasev NM (1967) Mass-spektrometricheskoe issledovanie sostava para nad sistemami TiC-C i ZrC-C (A mass-spectrometric study of vapour composition over TiC-C and ZrC-C systems). *Izv AN SSSR Neorg Mater* 3(4):727 (in Russian)

290. Nikolskaya TA, Avarbe RG (1971) Nekotorye zakonomernosti ispareniya karbidov perekhodnykh metallov IV-V podgrupp v vakuume (Some regularities of transition metals of IV-V subgroups carbides evaporation in a vacuum). In: Kornilov II, Matveeva NM (eds) Metallidy – stroenie, svoistva, primeneniye (Metallides – structure, properties, application). Nauka, Moscow, pp. 127–134 (in Russian)
291. Nikolskaya TA, Avarbe RG, Vil'k YuN (1974) Temperature dependence of the congruently evaporated compositions of the zirconium monocarbide phase and their evaporation rates. In: Samsonov GV (ed) Refractory carbides. Consultants Bureau, New York, London, pp. 329–334
292. Fesenko VV, Turchanin AG, Ordanyan SS (1974) A study of the dependence of some thermodynamic properties of niobium and zirconium carbides on temperature and composition. In: Samsonov GV (ed) Refractory carbides. Consultants Bureau, New York, London, pp. 323–328
293. Torshina VV, Smolina GN, Dobyshin SL, Avarbe RG, Vil'k YuN (1974) Mass-spectrometric study of the evaporation of zirconium carbide at high temperatures. In: Samsonov GV (ed) Refractory carbides. Consultants Bureau, New York, London, pp. 335–339
294. Kaufman L, Sarney A (1964) Thermodynamic properties of transition metal monocarbides. In: Waber JT, Chiotti P, Miner WN (eds) Compounds of interest in nuclear reactor technology. Metallurgical Society of American Institute of Mining Engineers, New York, pp. 267–283
295. Vlasov VK, Golubtsov IV, Nesmeyanov AN (1968) Measurement of rates of evaporation of refractory carbides from a free surface into a vacuum. *Russ J Phys Chem* 42(3):420–426
296. Wallace TC, Sr, Butt DP (1996) Review of diffusion and vaporization of group 4 and 5 transition metal carbides. In: Oyama ST (ed) The chemistry of transition metal carbides and nitrides. Chapman & Hall, London, Glasgow, pp. 53–90
297. Buravoi SE, Taubin ML (1974) Thermophysical properties of carbides of titanium, zirconium, hafnium and niobium at 50–1000 °C. *Inorg Mater* 10(2):319–321
298. Andrievskii RA, Spivak II, Khromov YuF, Khromonozhkin VV (1975) Issledovanie partialnykh termodinamicheskikh i diffuzionnykh kharakteristik nekotorykh karbidov perekhodnykh metallov (Study of partial thermodynamic and diffusion characteristics of some transition metal carbides). In: Proc. symp. on thermodynamics of nuclear materials, Vienna, 21–25 Oct 1974, Vol. 1. International Atomic Energy Agency, Vienna, pp. 409–414 (in Russian)
299. Neshpor VS, Ordanyan SS, Avgustinik AI, Khusidman MB (1964) The effect of the chemical composition of zirconium and niobium carbides in the homogeneity region on their electrical and thermal properties. *Russ J Appl Chem* 37(11):2349–2354
300. Neshpor VS, Davydov VS, Ermakov BG, Mogilevich BV (1967) Some properties of pyrolytic carbides and nitrides of group IV metals. *Powder Metall Met Ceram* 6(2):135–138
301. Sklarew S, Albom MJ (1963) Pyrolytically derived refractory materials. Report NASA-CR-50404. The Marquardt Corporation, Van Nuys, California, pp. 1–36
302. Radosevich LG, Williams WS (1969) Phonon scattering by conduction electrons and by lattice vacancies in carbides of the transition metals. *Phys Rev* 181(3):1110–1117
303. Radosevich LG, Williams WS (1970) Thermal conductivity of transition metal carbides. *J Am Ceram Soc* 53(1):30–33
304. Powell RW, Tye RP (1969) Thermal and electrical conductivities of some metallic compounds. In: Ho CY, Taylor RE (eds) Proc. 8th conf. on thermal conductivity. Plenum Press, New York, pp. 575–583
305. Korshunov IG, Zinov'ev VE, Geld PV, Chernyaev VS, Borukhovich AS, Shveikin GP (1973) Thermal diffusivity and thermal conductivity of titanium and zirconium carbides at high temperatures. *High Temp* 11(4):803–805
306. Neel DS, Pears CD (1962) High temperature thermal property measurement to 5000 °F. In: Masi JF, Tsai DH (eds) Progress in international research on thermodynamic and transport properties. Proc. 2nd symp. on thermophysical properties, Princeton University, New Jersey, 24–26 Jan 1962. Academic Press, New York, pp. 461–475

307. Taylor RE (1962) Thermal conductivity of zirconium carbide at high temperatures. *J Am Ceram Soc* 45(7):353–354
308. Shaffer PTB, Hasselman DPH (1962) Factors affecting thermal shock resistance of polyphase ceramic bodies. Report WADD-TR-60-749, Contract AF33(616)-6806, Part 2. The Carborundum Company, Research and Development Division, Niagara Falls, New York, pp. 1–167
309. Fridlender BA, Neshpor VS (1970) Thermal diffusivity of pyrolytic zirconium carbide. *High Temp* 8(4):750–753
310. Paderno YuB, Barantseva IG, Yupko VL (1965) Izmerenie teploprovodnosti i elektrosoprotivleniya ZrC, HfC, NbC i TaC pri vysokikh temperaturakh (Measurement of thermal conductivity and electrical resistance of ZrC, HfC, NbC and TaC at high temperatures). In: Grigoreva VV, Eremenko VN, Nazarchuk TN, Samsonov GV, Fedorchenko IM, Frantsevich IN (eds) *Vysokotemperaturnye neorganicheskie soedineniya (High-temperature inorganic compounds)*. Naukova Dumka, Kyiv, pp. 199–204 (in Russian)
311. Fedorov VB, Aleinikov IN (1971) Thermal conductivity of zirconium carbide at high temperatures (2100 to 3400 K). *High Temp* 9(5):984–985
312. Lvov SN, Lesnaya MI, Vinitskii IM, Naumenko VYa (1972) Thermal conductivity of some refractory carbides and borides. *High Temp* 10(6):1196–1198
313. Zotov YuP, Kotelnikov RB, Kakushadze LE, Migunov LV, Galiakbarov ZG (1974) Some physical properties of zirconium carbide. *Russ Metall* (6):59–64
314. Fridlender BA, Sokolov VV (1981) Thermal and temperature conductivity at high temperatures of binary alloys of the ZrC-C system obtained by chemical vapour deposition. *High Temp* 19(5):702–706
315. Vishnevetskaya IA, Petrov VA (1977) Method of investigation and experimental device for measuring of thermal conductivity of refractory compounds. *High Temp* 15(6):1076–1081
316. Vishnevetskaya IA, Kudryasheva LV, Ordanyan SS, Petrov VA (1980) Thermal conductivity and electrical resistance of zirconium carbides in the region of homogeneity with high temperatures. *High Temp* 18(3):414–421
317. Vishnevetskaya IA, Kudryasheva LV, Ordanyan SS, Petrov VA (1980) Effect of degree of dispersion of initial powder on thermal and electrical conductivity of sintered zirconium carbide. *High Temp* 18(4):586–589
318. Fridlender BA (1974) *Issledovaniya teplofizicheskikh svoystv tugoplavkikh materialov poluchennykh khimicheskim osazhdeniem iz gazovoi fazy (Studies on the thermophysical properties of refractory materials produced by chemical vapour deposition)*. PhD thesis, State Institute of Applied Chemistry, Leningrad (in Russian)
319. Hague JR, Lynch JF, Rudnick A, Holden FC, Duckworth WH (1964) Refractory ceramics for aerospace. Battlle Memorial Institute, The American Ceramic Society, Columbus, Ohio
320. Lynch JF (1979) Engineering property data on selected ceramics, Vol. 2 – Carbides. Report MCIC-HB-07. Metals and Ceramics Information Centre, Battelle Columbus Laboratories, Ohio, pp. 1–136
321. Sakurai J, Hayashi J, Mekata M, Tsuchida T, Takagi H (1961) Thermal conductivities of monocarbides in transition metals. *J Jpn Inst Met* 25(4):289–292
322. Taylor RE, Morreale J (1964) Thermal conductivity of titanium carbide, zirconium carbide and titanium nitride at high temperatures. *J Am Ceram Soc* 47(2):69–73
323. Williams WS (1966) High-temperature thermal conductivity of transition metal carbides and nitrides. *J Am Ceram Soc* 49(3):156–159
324. Paderno YuB, Andreeva TV, Barantseva IG, Goryachev YuM (1965) Nature of the thermal conductivity in the carbides of some transition metals of groups IV and V. *Powder Metall Met Ceram* 4(2):131–134
325. Taylor RE, Storms EK (1976) Thermal transport in refractory carbides. In: Klemens PG, Chu TK (eds) *Thermal conductivity – 14*. Proc. 14th Int. conf. on thermal conductivity, University of Connecticut, Storrs, 2–4 June 1975. Plenum Press, New York, pp. 161–174

326. Taylor RE, Nakata MM (1963) Thermal properties of refractory materials. Report WADD-TR-60-581, Contract AF 33(616)-6794, Part 4. Air Force Materials Laboratory, Wright-Patterson Air Force Base, Ohio, pp. 1–109
327. Powell RW, Tye RP (1965) The thermal conductivities of some electrically conducting compounds. In: Popper P (ed) *Special ceramics*. Proc. British ceramic society symp., Academic Press, London, New York, pp. 243–257
328. Grebenkina VG, Lesnaya MI (1977) Electro- and thermophysical properties of alloys of the ZrC-ZrN system. *Powder Metall Met Ceram* 16(6):448–451
329. Funke VF, Pshenichnyi IV, Pliner LA, Lyakhov DM, Golomazov VM, Zubarev PV (1980) Thermal conductivity and electrical resistivity of Mo_3C_2 -ZrC-NbC solid solutions. *Powder Metall Met Ceram* 19(10):722–727
330. Lanin AG, Zubarev PV, Vlasov KP (1993) Mechanical and thermophysical properties of materials in HTGR fuel bundles. *Atom Energy* 74(1):40–44
331. David L, Gomes S, Carlot G, Roger J-P, Fournier D, Valot C, Raynaud M (2008) Characterization of thermal conductivity degradation induced by heavy ion irradiation in ceramic materials. *J Phys D* 41:035502 (11 pp.)
332. Gomes S, David L, Roger J-P, Carlot G, Fournier D, Valot C, Raynaud M (2008) Thermal conductivity degradation induced by heavy ion irradiation at room temperature in ceramic materials. *Eur Phys J Spec Top* 153(1):87–90
333. Lanin AG (1998) Prochnost i termostoikost konstruktsionnoi keramiki (Strength and thermal stress resistance of structural ceramics). Moscow Engineering Physics Institute, Moscow (in Russian)
334. Lanin A, Fedik I (2005) Termoprochnost materialov (Thermal strength of materials). Scientific Research Institute of Scientific Industrial Association “Luch”, Podolsk, Moscow Area (in Russian)
335. Lanin A, Fedik I (2008) Thermal stress resistance of materials. Springer, Berlin, Heidelberg, New York
336. Lanin AG, Fedik II (2011) Selecting and using materials for a nuclear rocket engine reactor. *Phys Usp* 54(3):305–318
337. Lanin AG (2013) Nuclear rocket engine reactor. Springer, Berlin, Heidelberg
338. Gorin AI, Moiseev AM (1970) Thermal conductivity of carbide thermal insulation materials. *High Temp* 8(5):935–937
339. Kats SM, Gorin AI, Semenov MV (1972) Physico-mechanical properties of carbide fiber materials. *Powder Metall Met Ceram* 11(7):585–589
340. Crocombette J-P (2013) Origins of the high-temperature increase of the thermal conductivity of transition metal carbides from atomistic simulations. *J Phys Condens Matter* 25:505501 (8 pp.)
341. Jensen C, Chirtoc M, Horny N, Antoniow JS, Pron H, Ban H (2013) Thermal conductivity profile determination in proton-irradiated ZrC by spatial and frequency scanning thermal wave methods. *J Appl Phys* 114(13):133509 (9 pp.)
342. Jensen C, Chirtoc M, Antoniow JS, Ban H (2013) In-depth thermal-conductivity profile of ion-irradiated zirconium carbide using scanning thermal microscopy. *Int J Thermophys* 34(4):597–608
343. Touloukian YS, Buyco EH (1970) Thermophysical properties of matter. Vol. 5 – Specific heat – nonmetallic solids. IFI/Plenum Data Corporation, New York, Washington
344. Williams WS (1998) The thermal conductivity of metallic ceramics. *J Miner Met Mater Soc (JOM)* 50(6):62–66
345. Wagner P (1973) Research, development and production of substoichiometric ZrC for high-temperature insulation. Report LA-5224. Los Alamos Scientific Laboratory of the University of California, New Mexico, pp. 1–19
346. Houska CR (1964) Thermal expansion of certain group IV and group V carbides at high temperatures. *J Am Ceram Soc* 47(6):310–311

347. Paderno YuB, Dudnik EM, Andreeva TV, Barantseva IG, Yupko VL (1965) Izmerenie koefitsientov termicheskogo rasshireniya ZrC, HfC, NbC i TaC pri vysokikh temperaturakh (Measurement of the coefficients of thermal expansion of ZrC, HfC, NbC and TaC at high temperatures). In: Grigoreva VV, Eremenko VN, Nazarchuk TN, Samsonov GV, Fedorchenko IM, Frantsevich IN (eds) Vysokotemperaturnye neorganicheskie soedineniya (High-temperature inorganic compounds). Naukova Dumka, Kyiv, pp. 293–296 (in Russian)
348. Miccioli BR, Shaffer PTB (1964) High-temperature thermal expansion behaviour of refractory materials. I. Selected monocarbides and binary carbides. *J Am Ceram Soc* 47(7):351–356
349. Gangler JJ, Robards CF, McNutt JE (1949) Physical properties at elevated temperatures of seven hot-pressed ceramics. Technical Report NACA-TN-1911. National Advisory Committee for Aeronautics, Washington, DC, pp. 1–33
350. Gangler JJ (1950) Some physical properties of eight refractory oxides and carbides. *J Am Ceram Soc* 33(12):367–374
351. Ramke WG, Latva JD (1963) Refractory ceramics and intermetallic compounds. *Aerosp Eng* 22(1):76–84
352. Mauer FA, Bolz LH (1955) Measurement of thermal expansion of cermet components by high-temperature X-ray diffraction. Report WADC-TR-55-473, Contracts AF33(616)-56-5 and AF33(616)-53-12. US Air Force, Wright Air Development Centre, Ohio, pp. 1–57
353. Richardson JH (1964) Thermal expansion of titanium, zirconium and hafnium carbides to 2700 °C. Report TDR-469-(5250-10)-3, Contract AF04(695)-469. The Aerospace Corporation, El Segundo, California, pp. 1–19
354. Lehman GW (1960) Thermal properties of refractory materials. Report WADD-TR-60-581, Contract AF33(616)-6794. Atomic International Division North American Aviation, Canoga Park, California, pp. 1–29
355. Latva JD (1962) Selection and fabrication of ceramics and intermetallics. *Met Prog* 82(4):139–144
356. Leipold MH, Nielsen TH (1963) Mechanical and thermal properties of hot-pressed zirconium carbide tested to 2600 °C. Report NASA-TR-32-452. Jet Propulsion Laboratory, Pasadena, California, pp. 1–14
357. Touloukian YS, Kirby RK, Taylor RE, Lee TYR (1977) Thermophysical properties of matter. Vol. 13 – Thermal expansion – nonmetallic solids. IFI/Plenum Data Company, New York, Washington
358. Samsonov GV, Paderno IB, Panasiuk AD (1966) Proprietes electriques et physiques des composes definis et des domaines d'homogeneite des carbures des metaux de transition des groupes 4 et 5 de la classification periodique jusqu'a la temperature de 2500 °C (Physical and electrical properties of certain compositions in the regions of homogeneity of transition metal carbides of periodic system groups 4 and 5 up to the temperature of 2500 °C). *Rev Int Hautes Temp Refract* 3(2):180–184, correction 5(4):316 (in French)
359. Fridlender BA, Neshpor VS (1976) Thermal expansion of carbides of group 4-6 metals (transition class). *High Temp* 14(5):847–850
360. Caputo AJ (1977) Fabrication and characterization of vapour deposited niobium and zirconium carbides. *Thin Solid Films* 40(1):49–55
361. Graham JA (1950) The thermal expansion coefficients of chromium, titanium and zirconium carbides. Report RAE-TN-MET-130. US Atomic Energy Commission, Washington, DC, pp. 1–15
362. Lawson AC, Butt DP, Richardson JW, Li J (2007) Thermal expansion and atomic vibrations of zirconium carbide to 1600 K. *Philos Mag* 87(17):2507–2519
363. Lepie MP (1964) The properties of pyrolytic ZrC. *Trans Brit Ceram Soc* 63(8):431–439
364. Samsonov GV, Naumenko VYa (1970) Thermal expansion of transition metal carbides IV-V groups in their homogeneity regions. *High Temp* 8(5):1022–1024

365. Frantsevich IN, Zhurakovskii EA, Lyashchenko AB (1967) Elastic constants and characteristics of the electron structure of certain classes of refractory compounds obtained by the metal-powder method. *Inorg Mater* 3(1):6–12
366. Brizes WF (1968) Mechanical properties of the groups IVB and VB transition metal monocarbides. Report NASA-CR-95887, Contract N68-30720. Space Research Coordination Centre, University of Pittsburgh, Pennsylvania, pp. 1–45
367. Mauer FA, Bolz LH (1957) Measurement of thermal expansion of cermet components by high-temperature X-ray diffraction. Report WADC-TR-55-473, Supplement 1 – NBS-5837, Contracts AF33(616)-56-5 and AF33(616)-53-12. US Air Force, Wright Air Development Centre, Ohio, pp. 1–47
368. Shaffer PTB, Mark SD (1963) Inert-atmosphere dilatometer for use to 2000 °C. *J Am Ceram Soc* 46(2):104–106
369. Miccioli GR, Julien HP (1965) Refractory materials suitable for use in guided missile propulsion systems. Quarterly Progress Report No. 6. The Carborundum Company, Niagara Falls, New York, pp. 1–27
370. Bowman AL, Krikorian NH, Nereson NG (1972) The variation of lattice parameter of uranium carbide – zirconium carbide solid solutions with temperature and composition. In: Graham MG, Hagy HE (eds) Proc. AIP conf., Vol. 3, “Thermal expansion – 1971”. American Institute of Physics, New York, pp. 119–130
371. Bernstein H (1964) Debye temperatures and thermal properties of hafnium boride, zirconium boride, hafnium carbide and zirconium carbide from X-ray diffraction measurements. In: Waber JT, Chiotti P, Miner WN (eds) Compounds of interest in nuclear reactor technology. Metallurgical Society of American Institute of Mining Engineers, New York, pp. 609–625
372. Zilberberg VG, Kutsenok TG, Sharivker SYu (1970) Fizicheskie svoistva plazmenno-naplyennykh karbidnykh pokrytii (Physical properties of plasma spray-coated carbides). *Fiz Khim Obrab Mater* (4):49–52 (in Russian)
373. Samsonov GV, Grebenkina VG, Klimenko VS (1971) Coefficient of thermal expansion of refractory compounds. *Powder Metall Met Ceram* 10(8):643–647
374. Wagner P (1993) Materials science experience gained from the space nuclear rocket program: insulators. Report LA-12320-MS. Los Alamos National Laboratory, New Mexico, pp. 1–46
375. Teresiak A, Kubsch H (1995) X-ray investigations of high energy ball milled transition metal carbides. *Nanostruct Mater* 6(5–8):671–674
376. Liu Y-Z, Jiang Y-H, Zhou R, Feng J (2014) First principles study the stability and mechanical properties of MC (C = Ti, V, Zr, Nb, Hf and Ta) compounds. *J Alloys Compd* 582:500–504
377. Alekseeva ZM, Ivanov OS (1968) Fiziko-khimicheskoe vzaimodeistvie monokarbidov urana i tsirkoniya s tugoplavkimi metallami (Physico-chemical interaction of uranium and zirconium monocarbides with refractory metals). In: Alekseeva ZM, Ivanov OS (eds) Fiziko-khimiya splavov i tugoplavkikh soedinenii s toriem i uranom (Physical chemistry of alloys and refractory compounds containing thorium and uranium). Nauka, Moscow, pp. 152–160 (in Russian)
378. Simonenko EP, Sevastyanov DV, Simonenko NP, Sevastyanov VG, Kuznetsov NT (2013) Promising ultra-high temperature ceramic materials for aerospace applications. *Russ J Inorg Chem* 58(14):1669–1693
379. Rathod N, Gupta SK, Shinde S, Jha PK (2013) First principles investigation of thermophysical properties of cubic ZrC under high pressure. *Int J Thermophys* 34(10):2019–2026
380. Panda B, Hickman RR, Shah S (2005) Solid solution carbides are the key fuels for future nuclear thermal propulsion. Report to Joint Army – Navy – NASA – Air Force (JANNAF) conf., Monterey, California, 5–8 Dec 2005. NASA Marshall Space Flight Centre, Huntsville, Alabama, pp. 1–7

381. Vorobev YuP (2004) Karbidy v stalyakh (Carbides in steels). *Izv Chelyabinsk Nauch Tsentr* 2:34–60 (in Russian)
382. Williams WS (1997) Transition metal carbides, nitrides and borides for electronic applications. *J Miner Met Mater Soc (JOM)* 49(3):38–42
383. Pelaccio DG, El-Genk MS (1994) A review of nuclear thermal propulsion carbide fuel corrosion and key issues. Technical Document (Report) NASA-CR-197533. University of New Mexico, Albuquerque, pp. 1–66
384. Samsonov GV, Naumenko VYa, Ryabokon LP, Verkhoturov AD (1975) Some properties of alloys of zirconium and niobium carbides in their homogeneity ranges. *Powder Metall Met Ceram* 14(1):44–46
385. Samsonov GV, Paderno VN (1965) Preparation of solid solution alloys of hafnium carbide with carbides of titanium, zirconium, niobium and tantalum and determination of their physical properties. *Russ Metall* (1):119–126
386. Samsonov GV, Sinelnikova VS (1962) Vysokotemperaturnye metallokeramicheskie materialy (High-temperature sintered metal-powder materials). UkrSSR Academy of Sciences, Kyiv (in Russian)
387. Agte C, Moers K (1931) Methoden zur Reindarstellung hochschmelzender Carbide, Nitride und Boride und Beschreibung einiger ihrer Eigenschaften (Methods for the purification of refractory carbides, nitrides and borides and description of some their properties). *Z Anorg Allg Chem* 198(1):233–275 (in German)
388. Strasser A, Koch LJ (1963) Thermal conductivity of carbides. *Nucleonics* 21(11):6–10
389. Kolomoets NV, Neshpor VS, Samsonov GV, Semenkovich SA (1958) Thermoelectrical properties of some metal-like compounds. *Sov Phys Tech Phys* 3(11):2186–2193
390. Maltseva LF, Lapshov YuK, Marmer ÉN, Samsonov GV (1965) High-temperature heaters of niobium and zirconium carbides. *Powder Metall Met Ceram* 4(11):942–946
391. Grebenkina VG, Denbnovetskaya EN (1974) Thermal coefficient of the electrical resistivity of carbides and their solid solutions. In: Samsonov GV (ed) *Refractory carbides*. Consultants Bureau, New York, London pp. 269–274
392. Rudy E, Benesovsky F (1960) Über die elektrische Leitfähigkeit von hochschmelzenden harten Karbiden und Karbidmischkristallen (On the electrical conductivity of refractory hard carbides and carbide mixed crystals). *Planseeber Pulvermetall* 8:72–77 (in German)
393. Clinard FW, Jr, Kempter CP (1968) Low-temperature electrical properties of some transition metals and transition-metal carbides. *J Less-Common Met* 15:59–73
394. Allison CY, Finch CB, Foegelle MD, Modine FA (1988) Low-temperature resistivity of transition-metal carbides. *Solid State Commun* 68(4):387–390
395. Modine FA, Foegelle MD, Finch CY, Allison CY (1989) Electrical properties of transition metal carbides of group IV. *Phys Rev B* 40(14):9558–9564
396. Hinrichs CH, Hinrichs MH, Mackie WA (1990) Electrical resistivity of crystalline ZrC 1000–3000 K. *J Appl Phys* 68(7):3401–3404
397. Petrov VA, Chekhovskoi VYa, Sheindlin AE, Nikolaeva VA, Fomina LP (1967) Total hemispherical emissive power, monochromatic ($\lambda = 0.65 \mu\text{m}$) emissive power and specific electrical resistivity of zirconium and niobium carbides in temperature range 1200–500 K. *High Temp* 5(6):889–893
398. Neshpor VS, Airapetyants SV, Ordanyan SS, Avgustinik AI (1966) Effect of the chemical composition of the monocarbides of group IV and V transition metals in the homogeneity range on the temperature dependence of their resistivity and thermo-e.m.f. *Inorg Mater* 2(5):728–730
399. Neshpor VS, Bychkov AKh, Ordanyan SS, Semenov SS (1976) Influence of high-temperature plastic deformation on the electrical properties of hard refractory compounds. *Powder Metall Met Ceram* 15(5):363–366
400. Meissner W, Franz H, Westerhoff H (1932) Messungen mit Hilfe von flüssigem Helium. XVI. Untersuchungen über die Supraleitfähigkeit von Carbiden, Nitriden, Boriden und Siliciden (Measurements using liquid helium. XVI. Studies on the superconductivity of carbides, nitrides, borides and silicides). *Z Phys* 75(7–8):521–530 (in German)

401. Lvov SN, Nemchenko VF, Samsonov GV (1962) Effect of nonmetallic atoms on the electric properties of high-melting compounds of transition metals. *Powder Metall Met Ceram* 1(4):231–236
402. Samsonov GV, Sinelnikova VS (1962) The resistivity of refractory compounds at high temperatures. *Powder Metall Met Ceram* 1(4):272–274
403. Samsonov GV (1956) The electrical conductivity of certain compounds of the transitional metals with boron, carbon and nitrogen and the electrical conductivity of alloys of these compounds. *Sov Phys Tech Phys* 1(4):695–701
404. Samsonov GV, Grebenkina VG (1968) Temperature coefficient of electroresistance of some high-melting compounds. *Powder Metall Met Ceram* 7(2):107–111
405. Geld PV, Tskhai VA, Borukhovich AS, Dubrovskaya LB, Matveenko II (1970) Conduction band of IVa and Va subgroup transition metal monocarbides. I. *Phys Stat Sol* 42:85–93
406. Borukhovich AS, Geld PV, Tskhai VA, Dubrovskaya LB, Matveenko II (1971) Conduction band of IVa and Va subgroup transition metal monocarbides. II. *Phys Stat Sol B* 45(1):179–187
407. Samsonov GV, Upadkhaya GS (1971) Properties of zirconium carbide – niobium carbide alloys in their homogeneity region. *Powder Metall Met Ceram* 10(2):151–153
408. Samsonov GV, Panasyuk AD (1966) Some electrophysical properties of niobium and zirconium carbides in their homogeneous regions. *High Temp* 4(2):203–208
409. Borukhovich AS (1978) Kinetic properties of IVa and Va subgroup transition metal monocarbides. *Phys Stat Sol A* 46(1):11–37
410. Borukhovich AS, Geld PV, Startsev VE (1973) Galvanomagnitnye svoistva monokarbidov perekhodnykh metallov IVa i Va podgrupp (Galvanomagnetic properties of monocarbides of IVa and Va subgroup transitional metals). *Izv Vyssh Uchebn Zaved Fiz* (5):142–145 (in Russian)
411. Egorov VS, Lanin AG, Fedik II (1981) Fracture of thermally loaded disks of material in elasto-brittle state. *Strength Mater* 13(2):183–189
412. Neshpor VS, Klimashin GM, Nikitin VP (1974) Study of the galvanomagnetic and electrical properties of TiC-TiO, TiN-TiO, TiC-TiN and ZrC-ZrN alloys. In: Samsonov GV (ed) *Refractory carbides*. Consultants Bureau, New York, London, pp. 287–306
413. Gaisanyuk AV, Zapadaeva TE, Petrov VA (1985) Effect of defectiveness of the microstructure on the electrophysical properties of pyrolytic zirconium carbide with a near-stoichio-metric composition. *High Temp* 23(6):842–845
414. Bonnot AM, Belkhir H, Pailharey D, Mathiez P (1986) Reactively sputtered zirconium carbides, carbonitrides and nitrides thin films – optical properties. *Solar Energ Mater* 14:375–384
415. Lei J-F, Okimura H, Brittain JO (1990) The electrical resistance of the group IV transition metal monocarbides and mononitrides in the temperature range 20–1000 °C. *Mater Sci Eng, A* 123:129–140
416. Wang CC, Akbar SA, Chen W, Patton VD (1995) Electrical properties of high-temperature oxides, borides, carbides and nitrides. *J Mater Sci* 30:1627–1641
417. Williams WS (1999) Electrical properties of hard materials. *Int J Refract Met Hard Mater* 17:21–26
418. Goretzki H (1963) Untersuchung der magnetischen, elektrischen und thermoelektrischen Eigenschaften der Karbide und Nitride der 4a- und 5a-Gruppen Übergangsmetalle (A study of magnetic, electrical and thermoelectrical properties of carbides and nitrides of 4a and 5a groups transition metals). PhD thesis, Wien Universität (in German)
419. Kuchma AYa, Samsonov GV (1966) Obrazovanie stabilnykh elektronnykh konfiguratsii i nekotorye fizicheskie svoistva karbidov i nitridov perekhodnykh metallov v oblasti ikh gomogenosti (Formation of stable electron configurations and some physical properties of carbides and nitrides of transition metals in the range of their homogeneity). *Izv AN SSSR Neorg Mater* 2(11):1970–1974 (in Russian)

420. Modine FA, Haywood TW, Allison CY (1985) Optical and electrical properties of single-crystalline zirconium carbide. *Phys Rev B* 32(12):7743–7747
421. Samsonov GV (1965) Superconductivity of refractory compounds. In: Savitskii EM, Baron VV (eds) *Metal science and physics of superconductors*. Nauka, Moscow, pp. 65–71 (in Russian)
422. Neshpor VS, Nikitin VP, Novikov VI, Popov VV (1977) Electrophysical properties of zirconium carbide. *Inorg Mater* 13(4):534–537
423. Golikova OA, Dzhafarov EO, Avgustinik AI, Kudryashova LV, Ordanyan SS (1967) Electrical properties of solid solutions of carbides of transition metals of groups 4 and 5. *Sov Phys Solid State* 9(5):1228–1232
424. Golikova OA, Dzhafarov EO, Avgustinik AI, Klimashin GM (1968) Thermoelectrical power and electrical conductivity of titanium and zirconium monocarbides in temperature range 20–2000 °C. *Sov Phys Solid State* 10(1):124–126
425. Golikova OA, Dzhafarov EO, Avgustinik AI, Klimashin GM (1969) Electric properties of transition metal carbides of group 4. *Sov Phys Semiconduct* 3(4):429–433
426. Avgustinik AI, Golikova OA, Kudryasheva LV, Ordanyan SS, Snetkova VA (1967) Elektricheskie svoystva tverdykh rastvorov ZrC-NbC (The electrical properties of ZrC-NbC solid solutions). *Izv AN SSSR Neorg Mater* 3(10):1823–1827 (in Russian)
427. Avgustinik AI, Golikova OA, Kudryasheva LV, Ordanyan SS, Snetkova VA (1968) Elektricheskie svoystva slozhnykh nestekhiometrichnykh karbidov tsirkoniya i niobiya. (The electrical properties of complex non-stoichiometric carbides of zirconium and niobium). *Izv AN SSSR Neorg Mater* 4(6):904–908 (in Russian)
428. Samsonov GV, Paderno VN (1964) Über die Herstellung von Karbidmischkristallen und die Untersuchung ihrer physikalischen Eigenschaften (The production of mixed crystals of carbides and investigation of their physical properties). *Planseeber Pulvermetall* 12(1):19–31 (in German)
429. Tsuchida T, Mekata M, Nakamura Y, Sakurai J, Takaki H (1961) Hall effect in carbides of transition metals. *J Phys Soc Jpn* 16(12):2453–2456
430. Lvov SN, Nemchenko VF, Samsonov GV (1960) Nekotorye zakonomernosti v elektricheskikh svoystvakh boridov, karbidov i nitridov perekhodnykh metallov IV-VI grupp periodicheskoi sistemy (Some regularities in the electric properties of borides, carbides and nitrides of transition metals within the IV-VI groups of the periodic system). *Doklady AN SSSR* 135(3):577–580 (in Russian)
431. Barantseva IG, Paderno VN, Paderno YuB (1967) Some physical properties of alloys of the systems ZrC-NbC and TaC-HfC. *Powder Metall Met Ceram* 6(2):139–141
432. Borukhovich AS, Dubrovskaya LB, Matveenko II, Ordanyan SS (1973) Kineticheskie kharakteristiki tverdykh rastvorov TiC_xN_{1-x} i $Zr_xNb_{1-x}C$ (The kinetic characteristics of TiC_xN_{1-x} and $Zr_xNb_{1-x}C$ solid solutions). *Izv AN SSSR Neorg Mater* 9(5):791–795 (in Russian)
433. Dubrovskaya LB, Nazarova SZ (1984) Some regularities in the behaviour of the magnetic, electrokinetic and superconducting properties of transition metal monocarbide and mononitride solid solutions. *Phys Stat Sol A* 83(11):11–38
434. Kikuchi M, Nagakura S, Oketani S (1966) Physical properties of metal carbide films. In: *Proc. 6th Int. cong. on electron microscopy, Kyoto, 1966, Vol. 1*. Maruzen, Tokyo, pp. 497–502
435. Dew-Hughes D, Jones R (1980) The effect of neutron irradiation upon the superconducting critical temperature of some transition metal carbides, nitrides and carbonitrides. *Appl Phys Lett* 36(10):856–859
436. Prekul AF (1980) Superconductivity of equilibrium solid solutions. *Phys B + C* 100(3):281–296
437. Gusev AI, Dubrovskaya LB (1976) Tverdye rastvory ZrC-NbN i $Zr_{0.5}Nb_{0.5}C_xN_{1-x}$, ikh magnitnaya vospriimchivost i zonnaya struktura (The solid solutions of ZrC-NbN and $Zr_{0.5}Nb_{0.5}C_xN_{1-x}$, their magnetic susceptibility and zone structure). In: Shveikin GP (ed) *Sintez i svoystva soedinenii redkikh elementov III-V grupp* (Synthesis and properties of less-common elements of III-V groups). Ural Scientific Centre Institute of Chemistry, Sverdlovsk, pp. 16–21 (in Russian)

438. Gusev AI, Nazarova SZ (2005) Magnetic susceptibility of nonstoichiometric compounds of transition *d*-metals. *Phys Usp* 48(7):651–673
439. Dubrovskaya LB, Borukhovich AS, Geld PV, Matveenko II, Kudryashova LV, Ordanyan SS (1970) Magnetic susceptibility of solid solutions of zirconium and niobium monocarbides. *Phys Solid State* 11(10):2451–2453
440. Sani E, Mercatelli L, Sansoni P, Silvestroni L, Sciti D (2012) Spectrally selective ultra-high temperature ceramic absorbers for high-temperature solar plants. *J Renew Sustain Energy* 4(3):033104
441. Sani E, Mercatelli L, Jafrancesco D, Sans J-L, Sciti D (2012) Ultra-high temperature ceramics for solar receivers: spectral and high-temperature emittance characterization. *J Eur Opt Rap Public* 7:12052 (5 pp.)
442. Zhurakovskii EA (1969) X-ray K_{α} -emission band of carbon in the monocarbides of transition metals belonging to groups IV and V. *Phys Dokl* 14:168–172
443. Zhurakovskii EA, Vasilenko NN (1974) The state of the carbon atom in transition metal carbides. In: Samsonov GV (ed) *Refractory carbides*. Consultants Bureau, New York, London pp. 179–185
444. Ramqvist L, Ekstig B, Källne E, Noreland E, Manne R (1971) X-ray emission spectra of VC_x , NbC_x , TaC_x and ZrC_x . *J Phys Chem Solids* 32(1):149–157
445. Guerrero MML, de Torres AG, Alonso EV, Cordero MTS, Pavon JMC (2011) Quantitative determination of ZrC in new ceramic materials by Fourier transform infrared spectroscopy. *Ceram Int* 37:607–613
446. Petrov VA, Radzyukevich TE, Sokolov VV (1977) Emissivity of stoichiometric zirconium carbide. *High Temp* 15(5):832–836
447. Petrov VA (1969) *Izluchatel'naya sposobnost vysokotemperaturnykh materialov* (The emissivity of high-temperature materials). Nauka, Moscow (in Russian)
448. Morgan FH (1951) Spectral emissivity of coatings of thoria and other refractories as a function of temperature. *J Appl Phys* 22(1):108–109
449. Petrov VA, Chekhovskoi VYa, Sheindlin AE (1968) Emissivity and electrical resistivity of some refractory carbides. In: Proc. 4th symp. on thermophysical properties, University of Maryland, College Park, 1968. American Society of Mechanical Engineers, New York, pp. 270–277
450. Shaffer PTB (1963) Evidence for high-temperature forms of zirconium and tantalum monocarbides. *J Am Ceram Soc* 46(4):177–179
451. Samsonov GV, Fomenko VS, Paderno YuB (1962) Spectral emittance of the powders of some high-melting compounds. *Refract Indust Ceram* 3(1–2):35–37
452. Pierson HO (1996) *Handbook of refractory carbides and nitrides*. Noyes Publications, Westwood, New Jersey
453. Touloukian YS, DeWitt DP (1972) *Thermophysical properties of matter. Vol. 8 – Thermal radiative properties – nonmetallic solids*. IFI/Plenum Data Corporation, New York, Washington
454. Riethof T, Acchione BD, Branyan ER (1962) High-temperature spectral emissivity studies on some refractory metals and carbides. In: Herzfeld CM, Dahl AI (eds) *Temperature, its measurement and control in science and industry, Vol. 3, Part 2*. Reinholds, New York, Chapman and Hall, London, pp. 515–522
455. Svet DYa (1964) *Temperaturnoe izluchenie metallov i nekotorykh veshchestv* (Temperature emission of metals and some substances). *Metallurgiya*, Moscow (in Russian)
456. Neel DS, Pears CD, Oglesby S (1963) The thermal properties of twenty-six solid materials to 5000 °F or their destruction temperatures. Report ASD-TDR-62-765, Contract USAF 33(616)-7319. Southern Research Institute, University of Alabama, Birmingham, USA, pp. 1–420
457. Riethof TR, DeSantis VJ (1963) Techniques for measuring normal spectral emissivity of conductive refractory compounds at high temperature. In: Proc. symp. on measurement of thermal radiation properties of solids, Dayton, Ohio, 5–7 Sept 1962. National Aeronautics and Space Administration, Washington, DC, pp. 565–584

458. Kibler GM, Lyon TF, Linevsky MJ, DeSantis VJ (1964) Refractory materials research. Report WADD-TR-60-646, Contract USAF 33(616)-6841, Part 4. Flight Propulsion Laboratory Department, General Electric Company, Cincinnati, Ohio, pp. 1–151
459. Shaffer PTB (1961) Development of ultra-refractory materials. Progress Report No. 25, Contract NOrd-17175. The Carborundum Company, Niagara Falls, New York, pp. 1–4
460. Grossman LN, Hoyt EW, Ingold HH, Kaznoff AJ, Sanderson MJ (1962) Thermionic emitter material properties. Final Technical Summary Report DDC-GEST-2009. General Electric Company, Vallecitos Nuclear Centre, Alameda, California pp. 1–208
461. Grossman LN (1963) On the question of a phase change in zirconium carbide. *J Am Ceram Soc* 46(9):457–458
462. Riethof TR (1961) High temperature spectral emissivity studies. General Electric Company, Missile and Space Vehicle Department, Philadelphia, Pennsylvania
463. Petrov VA, Chekhovskoi VYa, Dymov BK, Kilin VS (1969) Integrated hemispherical emissivity of pyrolytic zirconium carbide. *High Temp* 7(2):239–243
464. Petrov VA, Chekhovskoi VYa, Sheindlin AE, Dymov BK (1973) Integral hemispherical radiativity of pyrolytic silicon and zirconium carbides. *Heat Trans Res* 5(2):65–67
465. Kolesnichenko AN, Krasnoschekov YuA, Nezhevenko LB, Pustogarov AV (1971) High temperature emissivity of zirconium carbide. *High Temp* 9(1):178–180
466. Qian J, Wu C-Y, Gong H-R (2018) Phase transition, thermodynamic and elastic properties of ZrC. *Trans Nonferrous Met Soc China* 28(12):2520–2527
467. Mackie WA, Carleson P, Fillion J, Hinrichs CH (1991) Normal spectral emittance of crystalline transition metal carbides. *J Appl Phys* 69(10):7236–7239
468. Schatz EA, Alvarez GH, Counts CR III, Hoppe MA (1965) High-temperature high-emittance intermetallic coatings. Report AFML-TR-65-217, Part 3. Air Force Materials Laboratory, Wright-Patterson Air Force Base, Ohio, pp. 1–100
469. Kumashiro Y (2000) High-temperature characteristics. In: Kumashiro Y (ed) *Electric refractory materials*. Marcel Dekker, New York, Basel pp. 191–222
470. Zapadaeva TE, Petrov VA, Sokolov VV (1981) Emissivity of stoichiometric zirconium and titanium carbides at high temperatures. *High Temp* 19(2):228–234
471. Pears CD (1963) Some problems in emittance measurements of the higher temperatures and surface characterisation. In: Proc. symp. on measurement of thermal radiation properties of solids, Dayton, Ohio, 5–7 Sept 1962. National Aeronautics and Space Administration, Washington, DC, pp. 541–549
472. Bonnot AM, Belkhir H, Pailharey D, Mathiez P (1985) Reactively sputtered zirconium carbides, carbonitrides and nitrides thin films – optical properties. In: Proc. SPIE (4th conf. on optical materials technology for energy efficiency and solar energy conversion, San Diego, California, 1985) 562:209–224
473. Ozaki Y, Zee RH (1995) Investigation of thermal and hydrogen effects on emissivity of refractory metals and carbides. *Mater Sci Eng A* 202(1–2):134–141
474. Cockeram BV, Measures DP, Mueller AJ (1999) The development and testing of emissivity enhancement coatings for thermophotovoltaic (TPV) radiator applications. *Thin Solid Films* 355–356:17–25
475. Cockeram BV, Hollenbeck JL (2002) The spectral emittance and long-term thermal stability of coatings for thermophotovoltaic (TPV) radiator applications. *Surf Coat Technol* 157:274–281
476. Sani E, Mercatelli L, Francini F, Sans J-L, Sciti D (2011) Ultra-refractory ceramics for high-temperature solar absorbers. *Scripta Mater* 65:775–778
477. Fisenko AI, Lemberg V (2012) Radiative properties of stoichiometric hafnium, titanium and zirconium carbides: thermodynamics of thermal radiation. *Int J Thermophys* 33:513–527
478. Samsonov GV, Podchernyaeva IA, Fomenko VS (1969) Emission coefficient of high-melting compounds. *Powder Metall Met Ceram* 8(5):374–379
479. Petrov VA, Chekhovskoi VYa, Sheindlin AE, Kashekhlebova II, Nikolaeva VA, Fomina LP (1974) Emissive power and specific electrical resistivity of zirconium and niobium carbides at high temperatures. In: Samsonov GV (ed) *Refractory carbides*. Consultants Bureau, New York, London pp. 231–238

480. Cade CM (1961) The thermal emissivity of some materials used in thermionic valve manufacture. *IRE Trans Electron Dev* 8:56–69
481. Touloukian YS, DeWitt DP, Hemicz RS (1972) Thermophysical properties of matter. Vol. 9 – Thermal radiative properties – coatings. IFI/Plenum Data Corporation, New York, Washington
482. Fomenko VS (1981) Emissionnye svoistva materialov (The thermionic emission properties of materials). Naukova Dumka, Kyiv (in Russian)
483. Siman NI (1977) Emissionno-adsorbtsionnye svoistva tugoplavkikh uglerod-soderzhashchikh elektrodnykh materialov (Emission and adsorption properties of refractory carbon-containing electrode materials). PhD thesis, Institute for Problems of Materials Science, Ukrainian SSR Academy of Sciences, Kyiv (in Russian)
484. Samsonov GV, Kalinina NG, Neshpor VS, Okhremchuk LN, Podchernyaeva IA, Skaletskaya NA, Fomenko VS (1975) Thermionic emission characteristics of pure and yttrium-containing zirconium carbide. *Powder Metall Met Ceram* 14(8):661–664
485. Okhremchuk LN (1971) Issledovanie termoemissionnykh svoistv karbidov perekhodnykh metallov IV-V grup v oblastiakh ikh gomogenosti (A study of thermionic emission properties of transition metal carbides of IV-V groups in the regions of their homogeneity). PhD thesis, Institute for Problems of Materials Science, Ukrainian SSR Academy of Sciences, Kyiv (in Russian)
486. Mikhailovskii BI (1964) Elektronnaya i ionnaya emissiya karbida tsirkoniya, gekhsaborida lantana i okisi toriya v parakh tseziya pri nizkom davlenii (Electronic and ionic emission of zirconium carbide, lanthanum hexaboride and thorium oxide in cesium vapour at low pressure). *Izv AN SSSR Ser Fiz* 28(9):1504–1507 (in Russian)
487. Goldwater DL, Haddad RE (1951) Certain refractory compounds as thermionic emitters. *J Appl Phys* 22(1):70–73
488. Wright DA (1953) A survey of present knowledge of thermionic emitters. *Proc IEE Lond* 100(65):125–142
489. Mikhailovskii BI (1962) Elektronna ta ionna emisiya deyakikh materialiv v zvyazku z ykh vykorystanniam v termoelektronnomu peretvoryuvachi energii (Electronic and ionic emissions of certain materials in the connection with their applications in thermionic energy conversion). *Ukr Fiz Zh* 7(1):75–77 (in Ukrainian)
490. Gorbatyi NA, Lvov GV, Perederii VA, Ryabchenko EM, Khashimova SS (1966) Termoelektronnaya emissiya karbidov gafniya i tsirkoniya (Thermoionic emission of hafnium and zirconium carbides). *Izv AN SSSR Ser Fiz* 30(12):1942–1949 (in Russian)
491. Matskevich TL, Krachino TV, Vilk YuN, Davydov VS (1968) Termoemissionnye svoistva piroliticheskikh pokrytii iz karbida tsirkoniya i volframa (Thermionic emission of pyrolytic zirconium carbide and tungsten coatings). *Zh Tekh Fiz* 38(8):1379–1384 (in Russian)
492. Fomenko VS (1965) Termoemissionnye svoistva nekotorykh tugoplavkikh soedinenii (Thermionic emission properties of some refractory compounds). PhD thesis, Institute for Problems of Materials Science, Ukrainian SSR Academy of Sciences, Kyiv (in Russian)
493. Matskevich TL, Krachino TV, Kazantsev AP, Markova LS (1964) Termoemissionnye svoistva nekotorykh tugoplavkikh soedinenii nanesennykh na metallicheskie podlozhki (Thermionic properties of some refractory compounds deposited on the metal substrates). *Zh Tekh Fiz* 34(11):2021–2027 (in Russian)
494. Hopkins BJ, Ross KJ (1962) Work function of zirconium carbide. *Proc Phys Soc Lond B* 79(508):447–448
495. Wilson RG (1968) Electron and ion emission from surfaces originally of TaB₂, ZrC, Mo₂C, MoSi₂, TaSi₂ and WSi₂ in cesium vapour. *J Appl Phys* 39(5):2306–2310
496. Wilson RG, McKee WE (1967) Vacuum thermionic work functions and thermal stability of TaB₂, ZrC, Mo₂C, MoSi₂, TaSi₂ and WSi₂. *J Appl Phys* 38(4):1716–1718
497. Kulvarskaya BS, Rekov AI, Serebrennikova VE, Nikolaeva VA, Kan KhS (1968) Thermionic emission of certain refractory materials and their possible application in devices filled with complex gaseous medium. *Radio Eng Electron Phys* 13(7):1131–1137
498. Kulvarskaya BS, Rekov AI, Serebrennikova VE, Nikolaeva VA, Kan KhS (1969) Thermionic emission of certain refractory materials and possible use as cathodes in gaseous devices. *Sov Phys Tech Phys* 14(1):122–127

499. Pidd RW, Grover GM, Roehling DJ, Salmi EW, Farr JD, Krikorian NH, Witteman WG (1959) Characteristics of UC, ZrC and (ZrC)(UC) as thermionic emitters. *J Appl Phys* 30(10):1575–1578
500. Bolshov VG (1966) Work function of carbides of refractory metals in cesium vapour. *Sov Phys Tech Phys* 11(2):239–245
501. Dyubua BC, Stepanov LA (1965) Thermionic emission of metal-like compounds in barium vapours. *Radio Eng Electron Phys* 10(12):1878–1881
502. Fekhtretinov FA, Belevich IS, Kudintseva GA, Kuznetsova GM (1964) Poluchenie i issledovanie zaevtekticheskogo splava karbida tsirkoniya s grafitom (Preparation and investigation of a hypereutectic alloy of zirconium carbide with graphite). *Izv AN SSSR Neorg Mater* 7(8):1457–1458 (in Russian)
503. Matskevich TL, Krachino TV (1962) Thermoelectron emission of some refractory compounds. *Sov Phys Tech Phys* 7(2):156–159
504. Samsonov GV, Siman NI, Podchernyaeva IA, Fomenko VS (1976) Issledovanie energii adsorbtsii Cs i K na poverkhnosti tugoplavkikh karbidov (Study of Cs and K adsorption energies on surface of high-melting carbides). *Zh Tekh Fiz* 46(2):393–397 (in Russian)
505. Danforth WE, Williams AJ (1961) On thermionic properties of ZrC, UC and ZrC-UC mixture. *J Appl Phys* 32(6):1181–1184
506. Takada Y, Imoto S, Sano T (1962) Thermionic properties of UC, (U,Zr)C and ZrC. *J Atom Energy Soc Jpn* 4(8):525–529 (in Japanese)
507. Haddad RE, Goldwater DL, Morgan FH (1949) Zirconium carbide as a thermionic emitter. *J Appl Phys* 20(9):886
508. Haddad RE, Goldwater DL, Morgan FH (1949) Abstract of zirconium carbide as a thermionic emitter. *J Frankl Inst* 248(5):449
509. Samsonov GV, Bolgar AS, Guseva EA, Klochkov LA, Kovenskaya BA, Serebryakova TI, Timofeeva II, Turchanin AG, Fesenko VV (1973) Thermophysical properties of transition metal carbides and diborides. *High Temp High Press* 5(1):29–33
510. Fomenko VS, Naumenko VYa, Okhremchuk LN, Podchernyaeva IA, Samsonov GV (1970) Glühemissionseigenschaften der Monokarbide von Übergangsmetallen der IV und V Gruppe im Homogenitätsbereich (Thermionic emission properties of monocarbides of transition metals of the IV and V groups in homogeneity region). *Phys Stat Sol A* 2(3):K181–K184 (in German)
511. Samsonow GW, Fomenko WS, Podtschernyaeva IA (1970) Quelques base du développement des matériaux de cathode (Some basis of cathode materials development). *Rev Int Hautes Temp Refract* 7(1):69–75 (in French)
512. Fomenko WS, Lawrenko WA, Ochremtschuk LN, Podtschernjaeva IA, Prozenko TG, Samsonow GW (1971) Korrelation von Abtrennungsarbeit von Übergangsmetall Karbide in Homogenitätsbereich mit Oberflächenrekombination von Wasserstoffatomen (Correlation of work function of transition metal carbides in homogeneity region with surface recombination of hydrogen atoms). *Rev Int Hautes Temp Refract* 8(3–4):315–318 (in German)
513. Naumenko VYa (1971) Tekhnologiya polucheniya i issledovanie nekotorykh svoystv karbidov perekhodnykh metallov IV-V grupp v oblastiakh ikh gomogennosti (Production technology and investigation of some properties of transition metal carbides IV-V groups in the regions of their homogeneity). PhD thesis, Institute for Problems of Materials Science, Ukrainian SSR Academy of Sciences, Kyiv (in Russian)
514. Samsonov GV, Paderno YuB, Fomenko VS (1967) Thermionic emission characteristics of transition metal and their compounds. *Sov Phys Tech Phys* 11(8):1070–1076
515. Samsonov GV, Podchernyaeva IA, Fomenko VS, Lavrenko VA, Okhremchuk LN, Protsenko TG (1972) Correlation between the work functions of transition metal carbides in their homogeneity regions and surface recombination of hydrogen atoms. *Powder Metall Met Ceram* 11(5):389–392
516. Samsonov GV, Fomenko VS, Podchernyaeva IA, Okhremchuk LN (1974) Thermionic emission properties of refractory compounds and materials based on them (a review). *Powder Metall Met Ceram* 13(10):836–842

517. Matskevich TL, Krachino TV (1977) Thermionic emission of zirconium carbide in hydrogen. *Sov Phys Tech Phys* 22(6):710–716
518. Matskevich TL, Krachino TV (1977) Anode work function in a thermionic converter with carbide cathode. *Sov Phys Tech Phys* 22(6):716–719
519. Matskevich TL (1978) Work function of zirconium carbide – oxygen. *Sov Phys Tech Phys* 23(8):972–975
520. Cherepin VT, Kosyachkov AA, Vasilev MA (1978) Secondary ion emission of transition metal carbides. *Phys Stat Sol A* 50:K113–K116
521. Goryachev YuM, Podchernyaeva IA, Siman NI, Sinelnikova VS, Timofeeva II, Burkhanov GS (1978) Work function of ZrC_x and NbC_x single crystals. *Sov Phys Tech Phys* 23(3):321–324
522. Goryachev YuM, Podchernyaeva IA, Siman NI, Sinelnikova VS, Timofeeva II (1978) Anizotropiya raboty vykhoda elektrona monokristallov ZrC_x i NbC_x (Electron work function of ZrC_x and NbC_x single crystals). *Sci Sinter (Spec. Issue)* 10:119–128 (in Russian)
523. Mackie WA (1987) Preparation and surface characterization of zirconium carbide single crystals. PhD thesis, Oregon Graduate Centre, McMinnville
524. Mackie WA, Davis PR (1989) Single-crystal zirconium carbide as a high-temperature thermionic cathode material. In: *Proc. tri-service cathode workshop, Fort Monmouth, New Jersey, 22–24 Mar 1988*. *IEEE Trans Electron Dev* 36(1):220–224
525. Mackie WA, Hinrichs CH, Davis PR (1989) Preparation and characterization of zirconium carbide field emitters. In: *Proc. 1st Int. vacuum microelectronics conf., Williamsburg, Virginia, 1 June 1988*. *IEEE Trans Electron Dev* 36(11/2):2697–2702
526. Mackie WA, Hinrichs CH, Davis PR (1990) Effective work function measurements of advanced cathode materials via a thermionic projection microscope system. *IEEE Trans Electron Dev* 37(12):2568–2574
527. Mackie WA, Hartman RL, Davis PR (1993) High current density field emission from transition metal carbides. *Appl Surf Sci* 67:29–35
528. Tessner TC, Davis PR (1993) Preparation and characterization of crystalline ZrC films. *J Vac Sci Technol, A* 11(1):1–5
529. Kawano H (2008) Effective work functions for ionic and electronic emissions from mono and polycrystalline surfaces. *Prog Surf Sci* 83:1–165
530. Hugosson HW, Eriksson O, Jansson U, Ruban AV, Souvatzis P, Abrikosov IA (2004) Surface energies and work functions of the transition metal carbides. *Surf Sci* 557(1–3):243–254
531. Mackie WA, Xie TB, Davis PR (1995) Field emission from carbide film cathode. In: *Proc. 39th Int. conf. on electron, ion and photon beam technology and nanofabrication (EIPBN), Scottsdale, Arizona, 30 May–2 June 1995*. *J Vac Sci Technol B* 13(6):2459–2463
532. Xie TB, Mackie WA, Davis PR (1996) Field emission from ZrC films on Si and Mo single emitters and emitter arrays. In: *Proc. 8th Int. vacuum microelectronics conf. (IVMC-95), Portland, Oregon, 31 Jul–3 Aug 1995*. *J Vac Sci Technol B* 14(3):2090–2092
533. Wilson RG (1965) Ion thruster electrode surface physics studies. Summary Report NASA-CR-54680/HRL-6278-SR. Hughes Research Laboratories, Malibu, California, pp. 1–626
534. Myatt J (1963) Thermionic emission from zirconium carbide with caesium vapour present. *Adv Energ Convers* 3(1):279–285
535. Yada K, Masaoka H, Shoji Y, Tanji T (1989) Studies of refractory carbides, nitrides and borides as the thermionic emitters for electron microscopy. *J Electron Microscopy Techn* 12:252–261
536. Tkachenko YuG, Ordanyan SS, Yurchenko DS, Yulyugin VK, Bovkun GA, Unrod VI (1979) Strength and anti-friction properties of alloys of the systems $M^{IV}C$ - $M^{IV}B_2$ over a wide range of component concentrations. *Inorg Mater* 15(4):549–553
537. Gridneva IV, Milman YuV, Rymashevskii GA, Trefilov VI, Chugunova SI (1976) Effect of temperature on the strength characteristics of zirconium carbide. *Powder Metall Met Ceram* 15(8):638–645

538. Andrievskii RA, Vlasov KP, Shevchenko AS, Lanin AG, Pritchkin SA, Klyushin VV, Kurushin SP, MaskaeV AS (1978) Influence of reactor irradiation on physicomechanical properties of zirconium and niobium carbides. *Inorg Mater* 14(4):530–533
539. Khusainov MA (1979) Termoprochnost tugoplavkikh materialov, poluchennykh gazofaznym osazhdeniem (Thermal strength of refractory materials manufactured by gas-phase deposition). Leningrad State University, Leningrad (in Russian)
540. Ogawa T, Ikawa K, Iwamoto K (1976) Microhardness and microstructure of chemically vapour deposited ZrC-C alloy. *J Nucl Mater* 62(2–3):322–324
541. Kats SM, Ordanyan SS, Unrod VI (1981) Compressive creep of alloys of the ZrC-ZrB₂ and TiC-TiB₂ systems. *Powder Metall Met Ceram* 20(12):886–890
542. Kovalskii AE, Petrova LA (1951) Mikrotverdost dvoynykh tugoplavkikh karbidov (Microhardness of binary refractory carbides). In: Khrushchov MM (ed) Mikrotverdost (Microhardness). AN SSSR, Moscow, pp. 170–186 (in Russian)
543. Hausner HH, Friedemann HC (1962) High temperature compounds – a data book. General Astrametals Corporation, Yonkers, New York
544. Shaffer PTB, Watts RL (1961) Development of ultra-refractory materials. Summary Report NP-11160, Contract NOrd-17175. The Carborundum Company, Niagara Falls, New York, pp. 1–48
545. Fedotov MA, Yanchur VP, Maksimov VP (1976) Strength of carbide specimens prepared by impregnation through saturation. *Inorg Mater* 12(1):40–43
546. Ramqvist L (1969) Preparation, properties and electronic structure of refractory carbides and related compounds. *Jernkontoret Ann* 153(4):159–179
547. Ivanko AA (1968) Tverdost (The hardness). Naukova Dumka, Kyiv (in Russian)
548. Bazhenova LN, Ivanko AA (1969) Microhardness of carbides of certain transition metals. *Inorg Mater* 5(12):1763–1767
549. Ivanko AA (1974) The microhardness of transition-metal carbides. In: Samsonov GV (ed) Refractory carbides. Consultants Bureau, New York, London pp. 367–370
550. Mott BW (1956) Microindentation hardness testing. Butterworth's, London
551. Calvert ED, Kirk MM, Beall RA (1962) Chemical reactions in the electric arc: reactive metal carbides. Report BM-RI-5951. Bureau of Mines, US Department of the Interior, Washington, DC, pp. 1–13
552. Kieffer R, Kölbl F (1949) Tungsten carbide – free hard metals. *Powder Metall Bull* 4(1):4–17
553. Kushtalova IP, Ivanov AN (1966) Plastic strain of high-melting point compounds. *Powder Metall Met Ceram* 5(9):741–742
554. Samsonov GV, Stepanchuk AN, Pritulyak AS, Shlyuko VYa, Adamovskii AA, Mashonkina TV (1974) Composition dependence of the abrasive properties of fused titanium and zirconium carbide powders. *Powder Metall Met Ceram* 13(9):735–738
555. Artamonov AY, Bovkun GA (1974) Some aspects of the abrasive wear of transition metal carbides. In: Samsonov GV (ed) Refractory carbides. Consultants Bureau, New York, London pp. 371–376
556. Weimer AW, ed (1997) Carbide, nitride and boride materials synthesis and processing. Chapman & Hall, London Weinheim, New York
557. Ishizawa Y (2000) Transition metal carbide field emitters. In: Kumashiro Y (ed) Electric refractory materials. Marcel Dekker, New York, Basel pp. 269–287
558. Fujii K, Zaima S, Adachi H, Otani S, Oshima C, Ishizawa Y, Shibata Y (1983) Basic field emission properties of TiC and ZrC single crystals. *J Vac Soc Jpn* 26(3):251–258 (in Japanese)
559. Hwang Y, Aizawa T, Hayami W, Otani S, Ishizawa Y, Park S-J (1992) Surface phonon and electronic structure of a graphite monolayer formed on ZrC (111) and (001) surfaces. *Surf Sci* 271(1–2):299–307
560. Nagashima A, Nuka K, Satoh K, Itoh H, Ichinokawa T, Oshima C, Otani S (1993) Electronic structure of monolayer graphite on some transition metal carbide surfaces. *Surf Sci* 287–288(2):609–613

561. Ordanyan SS, Kudryashova LV, Avgustinik AI (1971) Mikrotverdost nestekhiometrichnykh tverdykh rastvorov na osnove karbidov tsirkoniya i niobiya (Microhardness of the non-stoichiometric solid solutions on the basis of zirconium and niobium carbides). *Izv AN SSSR Neorg Mater* 7(12):2179–2182 (in Russian)
562. Andrievskii RA, Maksimov VP, Shlykov VI (1977) Micro X-ray-spectral analysis of boundary zones in zirconium carbide. *Inorg Mater* 13(9):1296–1299
563. Sinelnikova VS, Gurin VN (1979) Monokristally tugoplavkikh soedinenii perekhodnykh metallov (Monocrystals of high-melting compounds of transition metals). *Zh Vsesoyuz Khim Obshchestva Im D I Mendeleev* 24(3):266–269 (in Russian)
564. Funke VF, Pshenichnyi IV, Kruglov VN, Kharkhardin ED (1973) Substruktura i kharakter razrusheniya monokristallov karbidov tsirkoniya i niobiya (Substructure and fracture character of single crystals of zirconium and niobium carbides). *Izv AN SSSR Neorg Mater* 9(12):2151–2155 (in Russian)
565. Vahldiek FW, Mersol SA (1977) Slip and microhardness of IVa to VIa refractory materials. *J Less-Common Met* 55(2):265–278
566. Trefilov VI, Milman YuV, Gridneva IV (1984) Mechanical properties of covalent crystals. *Inorg Mater* 20(6):833–841
567. Westbrook JH, Stover ER (1967) Carbides for high-temperature materials. In: Campbell IE, Sherwood EM (eds) *High-temperature materials and technology*. Wiley, New York, pp. 312–348
568. Savitskii EM, Kulbakh AA, Evstyukhin NA (1974) Investigation of the hot hardness of cast zirconium carbide. In: Samsonov GV (ed) *Refractory carbides*. Consultants Bureau, New York, London pp. 361–365
569. Samsonov GV, Tkachenko YuG, Berdikov VF, Bovkun GA (1976) Mikrotverdost, mikrokrupkost i khrupkaya mikroprochnost karbidov perekhodnykh metallov (Microhardness, microbrittleness and brittle microstrength of transition metal carbides). In: Samsonov GV, Kosolapova TYa, Gnesin GG, Fedorus VB, Domasevich LG (eds) *Karbidy i splavy na ikh osnove (Carbides and alloys based on them)*. Naukova Dumka, Kyiv, pp. 98–104 (in Russian)
570. Turchin VN, Knyazev VI, Evstyukhin NA, Fursov YuD (1976) Nekotorye voprosy issledovaniya deformatsii monokristallov karbidov perekhodnykh metallov pri vdavliivanii (Some research problems of single crystal transition metal carbides deformation at the indentation). In: Samsonov GV, Kosolapova TYa, Gnesin GG, Fedorus VB, Domasevich LG (eds) *Karbidy i splavy na ikh osnove (Carbides and alloys based on them)*. Naukova Dumka, Kyiv, pp. 104–107 (in Russian)
571. Kharkhardin ED, Kruglov VN, Poltoratskii NI, Rymashevskii GA, Kiparisov SS (1976) Issledovanie struktury monokristallov karbidov tsirkoniya i niobiya poluchennykh induktsionnoi zonnoi plavkoi (A study of the structure of single crystal zirconium and niobium carbides obtained by induction zone melting). In: Samsonov GV, Kosolapova TYa, Gnesin GG, Fedorus VB, Domasevich LG (eds) *Karbidy i splavy na ikh osnove (Carbides and alloys based on them)*. Naukova Dumka, Kyiv, pp. 137–140 (in Russian)
572. Kohlstedt DL (1973) The temperature dependence of microhardness of the transition-metal carbides. *J Mater Sci* 8(6):777–786
573. Kovalchenko MS, Dzhemelinskii VV, Borisenko VA (1969) Temperature dependence of the hardness of titanium, zirconium and hafnium carbides. *Strength Mater* 1(5):515–518
574. Kovalchenko MS, Dzhemelinskii VV, Skuratovskii VN, Tkachenko YuG (1973) Temperaturnaya zavisimost mikrotverdosti karbidov perekhodnykh metallov (Temperature dependence of the microhardness of transition metal carbides). *Izv AN SSSR Neorg Mater* 9(10):1525–1528 (in Russian)
575. Travushkin GG, Knyazev VI, Belov VS, Rymashevskii GA (1973) Temperature threshold of brittle failure in interstitial phases. *Strength Mater* 5(5):639–641
576. Brozek V, Cübor P, Cheong D-I, Yang S-H, Mastny L, Novak M (2011) Preparation and properties of ultra-high temperature ceramics based on ZrC and HfC. *Solid State Phenom* 170:37–40

577. McCollm IJ (1990) Ceramic hardness. Plenum Press, New York, London
578. Jhi S-H, Ihm J, Louie SG, Cohen ML (1999) Electronic mechanism of hardness enhancement in transition-metal carbonitrides. *Nature* 399(6732):132–134
579. Khusainov MA (1989) Mechanical properties and special features of failure of carbides and nitrides of metals of groups IV-V deposited from the gas phase. *Powder Metall Met Ceram* 28(7):551–555
580. Ferro D, Barinov SM, Rau JV, Latini A, Scandurra R, Brunetti B (2006) Vickers and Knoop hardness of electron beam deposited ZrC and HfC thin films on titanium. *Surf Coat Technol* 200:4701–4707
581. Ferro D, Rau JV, Albertini VR, Generosi A, Teghil R, Barinov SM (2008) Pulsed laser deposited hard TiC, ZrC, HfC and TaC films on titanium: hardness and an energy-dispersive X-ray diffraction study. *Surf Coat Technol* 202:1455–1461
582. Guo X, Li L, Liu Z, Yu D, He J, Liu R, Xu B, Tian Y, Wang H-T (2008) Hardness of covalent compounds: roles of metallic component and *d*-valence electrons. *J Appl Phys* 104(2):023503
583. Gao F (2006) Theoretical model of intrinsic hardness. *Phys Rev B* 73(13):132104
584. Tian Y, Xu B, Zhao Z (2012) Microscopic theory of hardness and design of novel superhard crystals. *Int J Refract Met Hard Mater* 33:93–106
585. Gao F, He J, Wu E, Liu S, Yu D, Li D, Zhang S, Tian Y (2003) Hardness of covalent crystals. *Phys Rev Lett* 91(1):015502
586. Chen X-Q, Niu H, Li D, Li Y (2011) Modeling hardness of polycrystalline materials and bulk metallic glasses. *Intermetallics* 19(9):1275–1281
587. Sciti D, Nygren M (2008) Spark plasma sintering of ultra-refractory compounds. *J Mater Sci* 43:6414–6421
588. Sciti D, Guicciardi S, Nygren M (2008) Spark plasma sintering and mechanical behaviour of ZrC-based composites. *Scripta Mater* 59:638–641
589. Friedrich A, Winkler B, Juarez-Arellano EA, Bayarjargal L (2011) Synthesis of binary transition metal nitrides, carbides and borides from the elements in the laser-heated diamond anvil cell and their structure-property relations. *Mater* 4:1648–1692. <https://doi.org/10.3390/ma4101648>
590. Andrievskii RA, Klimenko VV, Mitrofanov VI, Poltoratskii NI (1977) Effect of structural vacancies in interstitial phases on their sintering shrinkage. *Powder Metall Met Ceram* 16(6):423–426
591. Mukhopadhyay A, Raju GB, Basu B (2013) Ultra-high temperature ceramics: processing, properties and applications. In: Low IM, Sakka Y, Hu CF (eds) MAX phases and ultra-high temperature ceramics for extreme environments. IGI Global, Hershey, Pennsylvania pp. 49–99
592. Wang HL, Hon MH (1999) Temperature dependence of ceramics hardness. *Ceram Int* 25(3):267–271
593. Kramer BM, Judd PK (1985) Computational design of wear coatings. *J Vac Sci Technol, A* 3(6):2439–2444
594. Sun S-K, Zhang G-J, Wu W-W, Liu J-X, Suzuki T, Sakka Y (2013) Reactive spark plasma sintering of ZrC and HfC ceramics with fine microstructures. *Scripta Mater* 69:139–142
595. Dzhemelinskii VV (1970) Issledovanie temperaturnoi zavisimosti tverdsti nekotorykh tugoplavkikh soedinenii (A study of the temperature dependence of hardness of some refractory compounds). PhD thesis, Kyiv Polytechnic Institute (in Russian)
596. Hivert A, Poulignier J (1968) Mechanical properties at high temperatures of some ultra-refractory carbides. *Rev Int Hautes Temp Refract* 5(1):55–61
597. Turchin VN, Emelyanov AB, Rymashevskii GA, Lanin AG (1980) Structural segregation phenomena in dense zirconium carbide. *Powder Metall Met Ceram* 19(1):24–27
598. Zainulin YuG, Alyamovskii SI, Shveikin GP, Geld PV (1970) Solubility of oxygen in zirconium carbide. *Inorg Mater* 6(1):96–97
599. Spivak II, Andrievskii RA, Klimenko VV (1973) Diffusion-controlled processes in the homogeneity range of zirconium carbide. *Powder Metall Met Ceram* 12(3):212–214

600. Vil'k YuN, Ordanyan SS, Avarbe RG, Avgustinik AI, Ryzhkova TP, Omelchenko YuA (1965) Diagramma sostoyaniya sistemy Zr-ZrC (Phase diagram of the Zr-ZrC system). *Zh Prikl Khim* 38:1500–1506 (in Russian)
601. Lanin AG, Fedotov MA, Glagolev VV (1969) Festigkeit und Plastizität von Zirkoniumkarbid (Strength and plasticity of zirconium carbide). In: Benesovsky F (ed) *Hochtemperaturwerkstoffe. Vorträge, gehalten auf dem 6. Plansee seminar, 24–28 Juni 1968, Reutte* (High-temperature materials. Papers presented at the 6th Plansee seminar, 24–28 June 1968, Reutte) Springer, Wien, New York, pp. 105–113. (in German)
602. Lanin AG, Fedotov MA, Glagolev VV (1968) The effect of surface condition on the strength of ceramic specimens. *Powder Metall Met Ceram* 7(5):414–417
603. Ordanyan SS, Drozdetskaya GV (1970) High-temperature strength of TiC and ZrC specimens prepared by different techniques. *Powder Metall Met Ceram* 9(8):665–668
604. Pisarenko GS, Rudenko VN, Tretyachenko GN, Troshchenko VT (1966) Prochnost materialov pri vysokikh temperaturakh (The strength of materials at high temperatures). *Naukova Dumka, Kyiv* (in Russian)
605. Gurevich BD, Nezhevenko LB, Zubarev PV, Bulychev VP, Bragin NN, Kruglov VN, Fedotov MA (1983) Effect of small amounts of tungsten carbide on the strength, creep and brittle-to-ductile transition temperature of zirconium carbide. *Powder Metall Met Ceram* 22(1):35–38
606. Deryavko II, Lanin AG, Maskaev AS (1984) An X-ray diffraction study of the temporary microstresses in sintered carbides. *Powder Metall Met Ceram* 23(10):810–812
607. Samsonov GV, Portnoi KI (1961) *Splavy na osnove tugoplavkikh soedinenii* (The alloys on the basis of refractory compounds). Oborongiz, Moscow (in Russian)
608. Struk LI (1969) *Issledovanie protsessa pressovaniya i nekotorykh fiziko-mekhanicheskikh svoystv tugoplavkikh soedinenii* (A study of pressing procedure and some physico-mechanical properties of refractory compounds). PhD thesis, Institute for Problems of Materials Science, Ukrainian SSR Academy of Sciences, Kyiv (in Russian)
609. Samsonov GV, Kharchenko VK, Struk LI (1968) Static strength of refractory compounds at high temperatures. *Powder Metall Met Ceram* 7(3):206–209
610. Kruglov VN, Gurevich BD, Groshev VI, Nezhevenko LB, Pritchinn SA (1979) Effect of structure and substructure on the strength of sintered zirconium carbide specimens. *Powder Metall Met Ceram* 18(1):47–51
611. Fedotov MA, Yanchur VP (1976) Temperature-dependence of strength and plasticity of carbides obtained by right-through saturation. *Inorg Mater* 12(3):364–367
612. Bulychev VP, Tyurlenev VI (1982) Role of plasticizer in the extrusion of zirconium carbide blanks. *Powder Metall Met Ceram* 21(2):98–102
613. Majumder BI (1953) New materials of construction for heat engines in high-temperature service. *Sci Eng India* 6(2):33–39
614. Ryshkewitch E (1950) Properties and physical constants data of high refractory materials. Technical Report WADC-TR-6330, ATI-92387. US Air Force, Wright Air Development Centre, Ohio, pp. 1–265
615. Burykina AL, Yevtushok TM (1964) Pokrytiya iz karbida titana i tsirkoniya na grafite (Titanium and zirconium carbide coatings on graphite). *Izv AN SSSR Metall Gornoe Delo* (5):147–149 (in Russian)
616. Travushkin GG, Bukatov VG (1972) Effect of high-temperature annealing upon the rupture characteristics of zirconium carbide. *Powder Metall Met Ceram* 11(9):735–736
617. Lanin AG, Popov VP, Maskaev AS, Sokolov VA, Turchin VN (1981) Strength of carbide-graphite composites with force and thermal loading. *Strength Mater* 13(12):1534–1539
618. Gazuko IV, Shesterikov SA, Yumashev MV (1983) Brittle fracture of a ceramic in bending under conditions of impulse heating. *Strength Mater* 15(4):518–523
619. Lanin AG, Bochkov NA, Egorov VS, Sokolov VA (1985) Brittle fracture of materials in compression. *Strength Mater* 17(9):1274–1282

620. Lanin AG, Fedotov MA, Glagolev VV (1969) Prochnost i plastichnost karbida tsirkoniya (The strength and ductility of zirconium carbide). In: Pisarenko GS (ed) Termoprochnost materialov i drugikh konstruktivnykh elementov (Thermal strength of materials and other structural elements), Vol. 5, Naukova Dumka, Kyiv, pp. 306–312 (in Russian)
621. Lanin AG, Turchin VN, Erin ON (1990) Zirconium carbide strength and plasticity. Part 1. Influence of loading parameters. *Int J Refract Met Hard Mater* 9(2):88–91
622. Lanin AG, Turchin VN, Erin ON (1990) Zirconium carbide strength and plasticity. Part 2. ZrC deformation structure. *Int J Refract Met Hard Mater* 9(3):139–142
623. Lanin AG, Marchev EV, Pritchins SA (1991) Non-isothermal sintering parameters and their influence on the structure and properties of zirconium carbide. *Ceram Int* 17(5):301–307
624. Lanin AG (1993) Thermal shock resistance and fracture of ceramic materials. In: Schneider GA, Petzow G (eds) Thermal shock and thermal fatigue behaviour of advanced ceramics. Springer, Dordrecht, pp. 317–330
625. Zubarev PV, Kuraev AB, Maskaev AS, Astakhova EV, Bessarabov AA (1994) Stress relaxation in zirconium carbide. 1. Test method and stress relaxation curves. *Strength Mater* 26(1):63–69
626. Zubarev PV, Kuraev AB (1994) Stress relaxation in zirconium carbide. 2. Mechanisms of stress relaxation. The relationship of the processes of creep and relaxation. *Strength Mater* 26(2):132–136
627. Zubarev PV (1996) Stress relaxation in some refractory metals. *Russ Metall* (6):47–51
628. Lanin AG, Deryavko II (2000) Influence of residual stresses on thermal stress resistance of refractory ceramics. *J Eur Ceram Soc* 20(2):209–213
629. Lanin AG, Tkachev AL (2000) Numerical method of thermal shock resistance estimation by quenching of samples in water. *J Mater Sci* 35(9):2353–2359
630. Gendre M, Maître A, Troiliard G (2011) Synthesis of zirconium oxycarbide (ZrC_xO_y) powders: influence of stoichiometry on densification kinetics during spark plasma sintering and on mechanical properties. *J Eur Ceram Soc* 31(13):2377–2385
631. Zhao L, Jia D, Duan X, Yang Z, Zhou Y (2011) Pressureless sintering of ZrC-based ceramics by enhancing powder sinterability. *Int J Refract Met Hard Mater* 29(4):516–521
632. Lanin AG, Emelyanov AV, Turchin AV (1982) Vliyaniye programmnoy uprochneniya na mekhanicheskie svoystva karbida tsirkoniya (Effect of program hardening on the mechanical properties of zirconium carbide). *Fiz Khim Obrab Mater* (2):88–92 (in Russian)
633. Lanin AG (2012) Effect of residual stresses on the strength of ceramic materials (review). *Russ Metall* (4):307–322
634. Leipold MH, Nielsen TH (1964) Mechanical properties of hot-pressed zirconium carbide tested to 2600°C. *J Am Ceram Soc* 47(9):419–424
635. Juenke EF (1964) A review of recent research on refractory metal carbides and borides. Summary Report GEMP-267, Contract USAEC-AT(40-1)-2847. Nuclear Materials and Propulsion Operation Advanced Technology Services, General Electric, Cincinnati, Ohio, pp. 1–24
636. Steele SR, Pappis J, Schilling H, Simpson J (1968) Chemical vapour deposited materials for electron tubes. Research and Development Technical Report ECOM-0156-1, Contract DAA-B07-68-C-0156. Raytheon Company, Waltham, Massachusetts, pp. 1–88
637. Zubarev PV, Dementev LN (1973) Effect of mode of loading on the high-temperature creep of zirconium carbide. *Strength Mater* 5(8):964–967
638. Zubarev PV (1985) Zharoprochnost faz vnedreniya (The heat-resistance of interstitial alloys). *Metallurgiya*, Moscow (in Russian)
639. Zubarev PV, Shmelev AG (1980) Creep process kinetics and long-term strength of zirconium carbide. 1. *Strength Mater* 12(2):142–148
640. Zubarev PV, Shmelev AG (1980) Creep process kinetics and long-term strength of zirconium carbide. 2. *Strength Mater* 12(3):264–268
641. Dementev LN, Zubarev PV, Nezhevenko LB, Groshev VI (1975) Investigation of the influence of grain size on high-temperature creep of zirconium carbide. *Phys Met Metallogr* 39(3):117–123

642. Zubarev PV, Dementev LN (1971) Relation between the activation energies of high-temperature creep and diffusion in transition metal carbides. *Strength Mater* 3(9):1058–1061
643. Zubarev PV, Kuraev AB (1992) Creep of monocarbides of transition metals of IV, V groups. I. Creep of zirconium carbide. *Phys Met Metallogr* 73(6):643–646
644. Zubarev PV, Kuraev AB, Lanin AG, Turchin VN, Erin ON, Burkhanov GS, Kuzmishchev VD, Sdobyrev VV (1992) Creep of monocarbides of transition metals of IV, V groups. II. Influence of grain size on creep of zirconium carbide. *Phys Met Metallogr* 73(6):647–649
645. Lanin AG, Turchin VN, Fedotov MA (1982) Prochnost i razrushenie karbida tsirkoniya (Strength and fracture of zirconium carbide). *Vopr Atom Nauki Tekhn Ser Atom Mater* (5):12–18 (in Russian)
646. Cannon WR, Langdon TG (1983) Creep of ceramics. 1. Mechanical characteristics. *J Mater Sci* 18(1):1–50
647. Zubarev PV, Dementev LN (1977) Osnovnye zakonomernosti vysokotemperaturnoi polzuchesti karbidov tsirkoniya i niobiya (Basic regularities of high-temperature creep of zirconium and niobium carbides). *Doklady AN SSSR* 232(6):1373–1375 (in Russian)
648. Kats SM, Ordanyan SS (1983) Extremal character of concentration dependence of creep rate of solid solutions of carbides in the $M^{IV}C$ - M^{VC} system. *Inorg Mater* 19(2):196–201
649. Zubarev PV, Dementev LN, Shmelev AG (1980) Vliyanie rezhimov pressovaniya na vysokotemperaturnuyu polzuchest karbidov IV-VI grupp perekhodnykh metallov (Effect of compression mode on the high-temperature creep of transition metal carbides of IV-VI groups). *Fiz Khim Obrab Mater* (3):91–95 (in Russian)
650. Chang R, Bente GG, Ekstrom FE (1962) Some recent studies of the high-temperature mechanical properties of refractory oxides and carbides. In: Marsh DR (ed) *Materials science and technology for advanced applications*. American Society for Metals, Prentice-Hall, Englewood Cliffs, New Jersey pp. 533–563
651. Miloserdin YuV, Naboichenko KV, Laveikin LI, Bortsov AG (1972) The high-temperature creep of zirconium carbide. *Strength Mater* 4(3):302–305
652. Darolia R, Archbold TF (1976) Plastic deformation of polycrystalline zirconium carbide. *J Mater Sci* 11:283–290
653. Aspinall SR (1965) Research on physical and chemical principles affecting high temperature materials for rocket nozzles. Technical Report NP-15514, Contract DA-30-069-ORD-2787, Vol. 2. Union Carbide Corporation Research Institute, Tarrytown, New York, pp. 1–147
654. Britun VF, Erin ON, Lanin AG, Turchin VN (1992) Structure of deformed polycrystalline zirconium carbide. *Powder Metall Met Ceram* 31(12):1054–1058
655. Lanin AG, Turchin VN, Erin ON (1989) Vliyanie velichin nagruzki i razmera zerna na prochnost i deformatsionnye kharakteristiki karbida tsirkoniya (Effect of the parameters of loading and grain size on the strength and deformation characteristics of zirconium carbide). *Metallofiz* 11(3):79–84 (in Russian)
656. Lanin AG, Turchin VN, Erin ON (1989) Kinetika plasticheskoi deformatsii karbida tsirkoniya (Kinetics of plastic deformation of zirconium carbide). *Metallofiz* 11(4):17–21 (in Russian)
657. Rowcliffe DJ (1984) Plastic deformation of transition metal carbides. In: Tressler RE, Bradt RC (eds) *Deformation of ceramic materials II*. Plenum Press, New York and London, pp. 49–71
658. Williams WS (1967) Brittle-ductile behaviour of the transition metal carbides. In: *Propriétés thermodynamiques physiques et structurales des derives semimetalliques*. Centre National de la Recherche Scientifique, Paris, pp. 181–189
659. Frost HJ, Ashby MF (1982) Deformation-mechanism maps. The plasticity and creep of metals and ceramics. Pergamon Press, Oxford
660. Lanin AG, Sokolov VA, Egorov VS (1984) Cyclic cracking resistance of brittle materials in compressive loading. *Strength Mater* 16(1):101–107

661. Lanin AG, Sokolov VA, Bochkov NA (1984) Determination of crack resistance of brittle materials. *Strength Mater* 16(2):161–165
662. Warren R (1978) Measurement of the fracture properties of brittle solids by Hertzian indentation. *Acta Metall* 26(11):1759–1769
663. Chen C-S, Liu C-P, Tsao C-YA (2005) Influence of growth temperature on microstructure and mechanical properties of nanocrystalline zirconium carbide films. *Thin Solid Films* 479(1–2):130–136
664. Antou G, Gendre M, Laborde E, Maître A, Trolliard G (2014) High-temperature compressive creep of spark plasma sintered zirconium (oxy-)carbide. *Mater Sci Eng A* 612:326–334
665. Antou G, Pradeilles N, Gendre M, Laborde E, Maître A (2015) New approach of the evolution of densification mechanisms during spark plasma sintering: application to zirconium (oxy-)carbide ceramics. *Scripta Mater* 101:103–106
666. Gerasimov PV, Egorov VS, Lanin AG, Nezhevenko LB, Sokolov VA (1982) Strength of zirconium carbide composites with disperse carbon inclusions. *Powder Metall Met Ceram* 21(1):59–64
667. Lanin AG (2009) Cyclic cracking resistance of brittle materials under compressive loading. *Strength Mater* 41(1):64–67
668. Cannon WR, Langdon TG (1988) Creep of ceramics. 2. An examination of flow mechanisms. *J Mater Sci* 23(1):1–20
669. Hollox GE (1968/69) Microstructure and mechanical behaviour of carbides. *Mater Sci Eng* 3(3):121–137
670. Baranov VM, Knyazev VI, Korostin OS (1973) The temperature dependence of the elastic constants of nonstoichiometric zirconium carbides. *Strength Mater* 5(9):1074–1077
671. Andrievskii RA, Rymashevskii GA, Sinelnikova VS (1972) Single crystals of refractory compounds – a review. I. *Powder Metall Met Ceram* 11(3):207–215
672. Andrievskii RA, Rymashevskii GA, Sinelnikova VS (1972) Single crystals of refractory compounds – a review. II. *Powder Metall Met Ceram* 11(10):796–809
673. Hasselman DPH (1963) Experimental and calculated Young's moduli of zirconium carbide containing a dispersed phase of graphite. *J Am Ceram Soc* 46(2):103–104
674. Frantsevich IN, Lyashchenko AB (1966) Young's moduli of the carbides of some transition metals. *Powder Metall Met Ceram* 5(7):573–574
675. Avgustinik AI, Ordanyan SS, Fishchev VN (1973) Uprugie svoystva monokarbidov tsirkoniya i niobiya v oblastiakh ikh gomogennosti (The elastic properties of zirconium and niobium monocarbides in their homogeneity regions). *Izv AN SSSR Neorg Mater* 9(7):1169–1171 (in Russian)
676. Avgustinik AI, Ordanyan SS, Kudryashova LV, Fishchev VN (1973) Uprugie svoystva tverdykh rastvorov monokarbidov tsirkoniya i niobiya pri komnatnoi temperature (The elastic properties of solid solutions of zirconium and niobium monocarbides at room temperature). *Izv AN SSSR Neorg Mater* 9(8):1358–1361 (in Russian)
677. Wachtman JB, Jr (1969) Elastic deformation of ceramics and other refractory materials. In: Wachtman JB, Jr (ed) *Mechanical and thermal properties of ceramics*. Proc. symp., Gaithersburg, Maryland. National Bureau of Standards, US Government Printing Office, Washington, DC, pp. 139–168
678. Lowrie R (1962) Research on physical and chemical principles affecting high temperature materials for rocket nozzles. Semiannual Progress Report, Contract DA-30-069-ORD-2787. Union Carbide Corporation Research Institute, Tarrytown, New York, Parma Research Centre, Cleveland, Ohio, pp. 1–64
679. Ordanyan SS, Fishchev VN (1976) Porosity as a factor in the elastic modulus of zirconium and niobium monocarbides. *Refract Indust Ceram* 17(1–2):111–113
680. Kats SM (1972) Elastic modulus of materials with a cellular-porous structure. *Strength Mater* 4(3):291–296
681. Snead LL, Katoh Y, Kondo S (2010) Effects of fast neutron irradiation on zirconium carbide. *J Nucl Mater* 399:200–207

682. Wu Z, Chen X-J, Struzhkin VV, Cohen RE (2005) Trends in elasticity and electronic structure of transition-metal nitrides and carbides from first principles. *Phys Rev B* 71(21):214103
683. Weber W (1973) Lattice dynamics of transition-metal carbides. *Phys Rev B* 8(11):5082–5092
684. Chang YA, Toth LE, Tyan YS (1971) On the elastic and thermodynamic properties of transition metal carbides. *Metall Trans* 2(1):315–320
685. Miloserdin YuV, Baranov VM, Korostin OS (1971) Apparatus for measuring the elastic constants of small samples of isotropic materials at temperatures to 1700 °C. *Strength Mater* 3(1):104–106
686. Onracek G (1978) Zum Zusammenhang zwischen Eigenschaften und Gefügestruktur mehrphasiger Werkstoffe (On the relationship between the properties and the microstructure of multiphase materials). Kernforschungszentrum Karlsruhe, Institut für Material- und Festkörperforschung, Karlsruhe (in German)
687. Popov VP, Lanin AG, Bochkov NA (1984) Method of testing the heat resistance of specimens of brittle electrically conducting materials using electron-beam heating. *Strength Mater* 16(9):1304–1308
688. Ajami FI, MacCrone RK (1974) Thermal expansion, Debye temperature and Gruneisen constant of carbides and nitrides. *J Less-Common Met* 38(2–3):101–110
689. Bukatov VG, Knyazev VI, Korostin OS, Baranov VM (1976) Izmenenie uprugikh kharakteristik v oblasti gomogennosti nekotorykh karbidov perekhodnykh metallov (Change of elastic characteristics in the range of homogeneity of some transition metal carbides). In: Samsonov GV, Kosolapova TYa, Gnesin GG, Fedorus VB, Domasevich LG (eds) *Karbidy i splavy na ikh osnove* (Carbides and alloys based on them). Naukova Dumka, Kyiv, pp. 111–114 (in Russian)
690. Ogorodnikov VV, Rogovoi Yul (1993) Rules of change in elastic, thermal and energy properties in a number of cubic transition metal monocarbides. *Powder Metall Met Ceram* 32(5):445–449
691. Ettmayer P, Lengauer W (1994) Transition metal solid-state chemistry: carbides. In: *Encyclopedia of inorganic chemistry*. Wiley, New York, pp. 519–531
692. Kral C, Lengauer W, Rafaja D, Ettmayer P (1998) Critical review on the elastic properties of transition metal carbides, nitrides and carbonitrides. *J Alloys Compd* 265:215–233
693. Santhanam AT (1996) Application of transition metal carbides and nitrides in industrial tools. In: Oyama ST (ed) *The chemistry of transition metal carbides and nitrides*. Chapman & Hall, London, Glasgow pp. 28–52
694. Kieffer R (1971) *Sondermetalle* (Special metals). Springer, Wien (in German)
695. Méçabih S, Amrane N, Nabi Z, Abbar B, Aourag H (2000) Description of structural and electronic properties of TiC and ZrC by generalized gradient approximation. *Phys A* 285:392–396
696. Xie C, Oganov AR, Li D, Debela TT, Liu N, Dong D, Zeng Q (2016) Effect of carbon vacancies on the structures, mechanical properties and chemical bonding of zirconium carbides: a first principles study. *Phys Chem Chem Phys* 18(17):12299–12306
697. Kim J-H, Park C, Ha D, Kang S (2015) WC-toughened (Zr,W)C solid solution carbides. *J Alloys Compd* 637:183–187
698. Duff AI, Davey T, Korbmacher D, Glensk A, Grabowski B, Neugebauer J, Finnis MW (2015) Improved method of calculating *ab initio* high-temperature thermodynamic properties with application to ZrC. *Phys Rev B* 91(21):214311
699. Razumovskiy VI, Ruban AV, Odqvist J, Dilner D, Korzhavyi PA (2014) Effect of carbon vacancies on thermodynamic properties of TiC-ZrC mixed carbides. *Calphad* 46:87–91
700. Ivashchenko VI, Turchi PEA, Shevchenko VI (2009) First principles study of elastic and stability properties of ZrC-ZrN and ZrC-TiC alloys. *J Phys: Condens Matter* 21(39):395503 (8 pp.)
701. Ramasubramanian S, Rajagoplan M, Thangavel R, Kumar J (2009) *Ab initio* study on elastic and thermodynamic properties of $Ti_{1-x}Zr_xC$. *Eur Phys J B* 69(2):265–268

702. Williams WS (1966) Cubic carbides. *Science* 152:34–42
703. Yang Q, Lengauer W, Koch T, Scheerer M, Smid I (2000) Hardness and elastic properties of $Ti(C_xN_{1-x})$, $Zr(C_xN_{1-x})$ and $Hf(C_xN_{1-x})$. *J Alloys Compd* 309:L5–L9
704. Justin JF, Jankowiak A (2011) Ultra-high temperature ceramics: densification, properties and thermal stability. *J Aerospace Lab* (3):AL03-08 (11 pp.)
705. Jochym PT, Parlinski K (2000) *Ab initio* lattice dynamics and elastic constants of ZrC. *Eur Phys J B* 15:265–268
706. Smith HG, Wakabayashi N, Mostoller M (1976) Phonon anomalies in transition metals, alloys and compound. In: Douglass DH (ed) *Superconductivity in d- and f-band metals*. Plenum Press, New York, London pp. 223–250
707. Siethoff H (2003) Correspondence of the plasticity of rocksalt structure ceramics and tetrahedrally coordinated semiconductors. *J Appl Phys* 94(5):3128–3134
708. Every AG, McCurdy AK (1992) Second and higher order elastic constants. Subvol. A. In: Nelson DF (ed) *High and low frequency properties of dielectric crystals*. Vol. III/29. Springer, Berlin, Heidelberg
709. Isaev EI, Ahuja R, Simak SI, Lichtenstein AI, Vekilov YuKh, Johansson B, Abrikosov IA (2005) Anomalously enhanced superconductivity and *ab initio* lattice dynamics in transition metal carbides and nitrides. *Phys Rev B* 72(6):064515 (5 pp.)
710. Viñes F, Sousa C, Liu P, Rodriguez JA, Illas F (2005) A systematic density functional theory study of the electronic structure of bulk and (001) surface of transition-metals carbides. *J Chem Phys* 122:174709 (11 pp.)
711. Zaoui A, Bouhafs B, Ruterana P (2005) First-principles calculations on the TiC_xN_{1-x} , $Zr_xNb_{1-x}C$ and HfC_xN_{1-x} alloys. *Mater Chem Phys* 91:108–115
712. Tran F, Laskowski R, Blaha P, Schwarz K (2007) Performance on molecules, surfaces and solids of the Wu-Cohen GGA exchange-correlation energy functional. *Phys Rev B* 75(11):115131 (14 pp.)
713. Isaev EI, Simak SI, Abrikosov IA, Ahuja R, Vekilov YuKh, Katsnelson MI, Lichtenstein AI, Johansson B (2007) Phonon related properties of transition metals, their carbides and nitrides: a first principles study. *J Appl Phys* 101:123519 (18 pp.)
714. Hart GLW, Klein BM (2000) Phonon and elastic instabilities in MoC and MoN. *Phys Rev B* 61(5):3151–3154
715. Maouche D, Louail L, Ruterana P, Maamache M (2008) Formation and stability of di-transition-metal carbides $Ti_xZr_{1-x}C$, $Ti_xHf_{1-x}C$ and $Hf_xZr_{1-x}C$. *Comput Mater Sci* 44(2):347–350
716. Singh A, Aynyas M, Sanyal SP (2009) High pressure behaviour and structural properties of transition metal carbides. *Phase Transit* 82(8):576–586
717. Wang J, Zhou Y, Lin Z, Liao T, He LF (2006) First-principles prediction of the mechanical properties and electronic structure of ternary aluminium carbide $Zr_3Al_3C_5$. *Phys Rev B* 73(13):134107
718. Vojvodic A, Ruberto C (2010) Trends in bulk electron-structural features of rocksalt early transition-metal carbides. *J Phys Condens Matter* 22:375501 (10 pp.)
719. Jiang X, Zhao J, Jiang X (2011) Correlation between hardness and elastic moduli of the covalent crystals. *Comput Mater Sci* 50(7):2287–2290
720. Korir KK, Amolo GO, Makau NW, Joubert DP (2011) First-principle calculations of the bulk properties of *4d* transition metal carbides and nitrides in the rocksalt, zincblende and wurtzite structures. *Diamond Relat Mater* 20:157–164
721. Wang J, Zhou Y (2009) Recent progress in theoretical prediction, preparation and characterization of layered ternary transition metal carbides. *Annu Rev Mater Res* 39:415–443
722. Bhardwaj P, Singh S (2012) Structural phase stability and elastic properties of refractory carbides. *Int J Refract Met Hard Mater* 35:115–121
723. Champion AR, Drickamer HG (1965) The effect of high pressure on the compressibility of four cubic carbides. *J Phys Chem Solids* 26(12):1973–1975

724. Kim J, Kang S (2012) First principles investigation of temperature and pressure dependent elastic properties of ZrC and ZrN using Debye-Grüneisen theory. *J Alloys Compd* 540:94–99
725. Srivastava A, Diwan BD (2012) Elastic and thermodynamic properties of divalent transition metal carbides MC (M = Ti, Zr, Hf, V, Nb, Ta). *Can J Phys* 90:331–338
726. Nino A, Tanaka A, Sugiyama S, Taimatsu H (2010) Indentation size effect for the hardness of refractory carbides. *Mater Trans* 51(9):1621–1626
727. Zaoui A, Kacimi S, Boukortt A, Bouhafs B (2010) *Ab initio* studies of structural, elastic and electronic properties of $Zr_xNb_{1-x}C$ and $Zr_xNb_{1-x}N$ alloys. *Phys B* 405:153–157
728. Feng W, Cui S, Hu H, Zhang G, Lv Z (2011) Electronic structure and elastic constants of TiC_xN_{1-x} , $Zr_xNb_{1-x}C$ and HfC_xN_{1-x} alloys: a first-principles study. *Phys B* 406:3631–3635
729. Craciun V, McCumiskey EJ, Hanna M, Taylor CR (2013) Very hard ZrC thin films grown by pulsed laser deposition. *J Eur Ceram Soc* 33:2223–2226
730. Kang D-B (2013) Effect of valence electron concentration on elastic properties of 4d transition metal carbides MC (M = Y, Zr, Nb and Rh). *Bull Korean Chem Soc* 34(7):2171–2175
731. Sun X-W, Zhang X-Y, Zhang S-H, Zhu Y, Wang L-M, Zhang S-L, Ma M-Z, Liu R-P (2013) The structural, elastic and electronic properties of $Zr_xNb_{1-x}C$ alloys from first principle calculations. *Chin Phys B* 22(10):107105 (5 pp.)
732. Varshney D, Shriya S, Singh N (2013) Mechanical stiffening of transition metal carbides: XC (X = Ti, Zr, Nb, Hf, Ta). In: Proc. 57th DAE solid state physics symp., Bombay, Mumbai, India, 3–7 Dec 2012. *AIP Conf Proc* 1512:1016–1017
733. Krasnenko V, Brik MG (2014) First principles calculations of the structural, elastic and electronic properties of MN_xC_{1-x} (M = Ti, Zr, Hf; $0 \leq x \leq 1$) carbonitrides at ambient and elevated pressure. *Solid State Sci* 28:1–8
734. Kim J, Kwon H, Kim J-H, Roh K-M, Shin D, Jang HD (2015) Elastic and electronic properties of partially ordered and disordered $Zr(C_{1-x}N_x)$ solid solution compounds: a first principles calculation study. *J Alloys Compd* 619:788–793
735. Yu X-X, Thompson GB, Weinberger CR (2015) Influence of carbon vacancy formation on the elastic constants and hardening mechanisms in transition metal carbides. *J Eur Ceram Soc* 35:95–103
736. Gubanov VA, Ivanovsky AL, Zhukov VP (1994) Electronic structure of refractory carbides and nitrides. Cambridge University Press, Cambridge, New York
737. Hasselman DPH (1978) Figures-of-merits for the thermal stress resistance of high-temperature brittle materials: a review. *Ceramurg Int* 4(4):147–150
738. Shabalin IL (2014) TSR of hetero-modulus ceramics. In: Hetnarski RB (ed) Encyclopedia of thermal stresses, Vol. 11. Springer, Dordrecht, New York, London pp. 6250–6255
739. Lanin AG, Borunov VV, Egorov VS, Popov VP (1973) Failure under thermal loading of brittle cylindrical solids. *Strength Mater* 5(3):322–326
740. Popov VP, Lanin AG, Manyukhin VP (1973) Calorimetric determination of the heat resistance of ring-shaped samples of brittle electric conductors. *Strength Mater* 5(10):1260–1263
741. Lanin AG, Popov VP, Kolesov VS, Bochkov NA (1986) Failure of ceramic materials in local thermal loading. *Strength Mater* 18(9):1177–1181
742. Lanin AG, Turchin VN, Erin ON, Sulyanov SN (1986) Zirconium carbide recrystallization. *Powder Metall Met Ceram* 25(2):151–156
743. Tkachev AL, Lanin AG, Egorov VS, Koroleva GV (1975) Rupture-end effect in the heating of a brittle cylinder. *Strength Mater* 7(10):1217–1221
744. Lanin AG, Egorov VS (2002) Fracture kinetics of thermally loaded bodies in elastic-brittle state and criterion of thermal stress resistance. In: Bradt RC, Munz D, Sakai M, Shevchenko VYa, White K (eds) Fracture mechanics of ceramics. Vol. 13 – Crack-microstructure interaction, R-curve behaviour, environmental effects in fracture and standartization. Springer, Kluwer Academic, New York, pp. 395–412

745. Konoplenko VP, Lanin AG, Sokolov VA, Glagolev VV (1975) Issledovanie ustalosti karbidnykh i karbidografityovykh materialov (A fatigue study of carbide and carbide-graphite materials). In: Tekhnika radiatsionnogo eksperimenta (Technics of radiation experiment). Atomizdat, Moscow, pp. 92–95 (in Russian)
746. Lide DR, ed (2010) CRC handbook of chemistry and physics, 90th ed. CRC Press, Boca Raton, New York
747. Samsonov GV, ed (1976) Svoistva elementov (Properties of elements), 2nd ed., Vol. 1, Metallurgiya, Moscow (in Russian)
748. Audi G, Wapstra AH, Thibault C, Blachot J, Bersillon O (2003) The NUBASE evaluation of nuclear and decay properties. Nucl Phys A 729:3–128
749. De Laeter JR, Bohlke JK, De Bièvre P, Hidaka H, Peiser HS, Rosman KJR, Taylor PDP (2003) Atomic weights of the elements. Review 2000 (IUPAC Technical report). Pure Appl Chem 75(6):683–800
750. Wieser ME (2006) Atomic weights of the elements 2005 (IUPAC Technical report). Pure Appl Chem 78(11):2051–2066
751. Sears VF (1992) Neutron scattering lengths and cross sections. Neutron News 3(3):26–37
752. Mughabghab SF (1984) Neutron cross sections. Vol. 1 – Neutron resonance parameters and thermal cross sections, Part B – Z = 61–100. Academic Press, Orlando
753. Mughabghab SF (2003) Thermal neutron capture cross sections resonance integral and G-factors. IAEA Nuclear Data Section, Vienna
754. Gordeev NV, Kardashev DA, Malyshev AV (1963) Yaderno-fizicheskie konstanty (Nuclear physics constants). Gosatomizdat, Moscow (in Russian)
755. Kovalchenko MS, Ogorodnikov VV, Rogovoi YuI, Krainii AG (1979) Radiatsionnoe povrezhdenie tugoplavkikh soedinenii (The radiation damage of refractory compounds). Atomizdat, Moscow (in Russian)
756. Ogorodnikov VV, Rogovoi YuI (1976) Tochechnye defekty v kubicheskikh monokarbidakh (Point defects in cubic monocarbides). In: Samsonov GV, Kosolapova TYa, Gnesin GG, Fedorus VB, Domasevich LG (eds) Karbidy i splavy na ikh osnove (Carbides and alloys based on them). Naukova Dumka, Kyiv, pp. 129–137 (in Russian)
757. Katoh Y, Snead LL, Parish CM, Hinoki T (2013) Observation and possible mechanism of irradiation induced creep in ceramics. J Nucl Mater 434:141–151
758. Keilholtz GW, Moore RE, Osborne MF (1968) Fast-neutron effects on the carbides of titanium, zirconium, tantalum, niobium and tungsten. Nucl Appl 4:330–336
759. Kovalchenko MS, Rogovoi YuI (1973) The effect of neutron irradiation on the structure and properties of zirconium carbide. Inorg Mater 9(2):290–292
760. Rogovoi YuI (1973) Issledovanie vliyaniya neitronnogo oblucheniya na strukturu i svoistva karbidov perekhodnykh metallov IV-VI grupp (A study of the effect of neutron irradiation on the structure and properties of transition metal carbides of IV-VI groups). PhD thesis, Institute for Problems of Materials Science, Ukrainian SSR Academy of Sciences, Kyiv (in Russian)
761. Deryavko II, Perepelkin IG, Pivovarov OS, Storozhenko AN (2001) Ekspressnye metodiki dlya poslereaktornogo issledovaniya bezobolocheknykh sterzhnevyykh karbidnykh tvelov (Express methods for postreactor research of cladding-free rod carbide fuel pins). Nat Nucl Centre Rep Kazakhstan (4):88–94 (in Russian)
762. Vlasov NM, Fedik II (2001) Teplovyydelyayushchie elementy yadernykh raketnykh dvigatelei (Fuel elements of nuclear rocket engines). TsNIIAtominform, Moscow (in Russian)
763. Ogorodnikov VV, Murzin LM, Krainii AG (1976) Vliyanie oblucheniya na mekhanicheskie svoistva tugoplavkikh karbidov i boridov (The effect of irradiation on the mechanical properties of refractory carbides and borides). In: Radiatsionnye efekty izmeneniya mekhanicheskikh svoistv konstruksionnykh materialov i metody ikh issledovaniya (Radiation effects of the changes of mechanical properties of structural materials and methods of their investigation). Naukova Dumka, Kyiv, pp. 89–97 (in Russian)

764. Patriarca P, Rucker DJ (1970) Fuels and materials development program. Technical Report ORNL-4480, Contract W-7405-ENG-26. Oak Ridge National Laboratory, Tennessee, pp. 1–255
765. Patriarca P, Harms WO, Rucker DJ (1969) Fuels and materials development program. Quarterly Progress Report ORNL-4350, Contract W-7405-ENG-26. Oak Ridge National Laboratory, Tennessee, pp. 1–320
766. Andrievskii RA, Savin VI, Markin VYu, Spravtsev VT, Shevchenko AS (1978) Effect of reactor irradiation on electrical and magnetic properties of interstitial phases. *Inorg Mater* 14(4):526–529
767. Reynolds GH, Janvier JC, Kaae JL, Morlevat JP (1976) Irradiation behaviour of experimental fuel particles containing chemically vapour deposited zirconium carbide coatings. *J Nucl Mater* 62(1):9–16
768. Ogawa T, Fukuda K, Kashimura S, Tobita T, Kobayashi F, Kado S, Miyanishi H, Takahashi I, Kikuchi T (1992) Performance of ZrC-coated particle fuel in irradiation and postirradiation heating tests. *J Am Ceram Soc* 75(11):2985–2990
769. Minato K, Ogawa T, Sawa K, Ishikawa A, Tomita T, Iida S, Sekino H (2000) Irradiation experiment on ZrC-coated fuel particles for high-temperature gas-cooled reactors. *Nucl Technol* 130(3):272–280
770. Minato K, Ogawa T, Koya T, Sekino H, Tomita T (2000) Retention of fission product caesium in ZrC-coated fuel particles for high-temperature gas-cooled reactors. *J Nucl Mater* 279(2–3):181–188
771. Minato K, Fukuda K, Sekino H, Ishikawa A, Oeda E (1998) Deterioration of ZrC-coated fuel particle caused by failure of pyrolytic carbon layer. *J Nucl Mater* 252(1–2):13–21
772. Minato K, Ogawa T, Fukuda K, Sekino H, Kitagawa I, Mita N (1997) Fission product release from ZrC-coated fuel particles during post-irradiation heating at 1800 and 2000 °C. *J Nucl Mater* 249(2–3):142–149
773. Minato K, Ogawa T, Fukuda K, Nabielek H, Sekino H, Nozawa Y, Takahashi I (1995) Fission product release from ZrC-coated fuel particles during post-irradiation heating at 1600 °C. *J Nucl Mater* 224(1):85–92
774. Taubin ML, Fateev SV, Ivanov MV, Shutov PV (1991) Change of the physical properties of zirconium carbide in a short exposure to a neutron current. *Atom Energy* 70(1):74–76
775. Keilholtz GW, Moore RE (1969) Fast neutron stability of refractory metal carbides at high temperatures. *Trans Am Nucl Soc* 12(1):101–105
776. Gan J, Meyer MK, Birtcher RC, Allen TR (2006) Microstructure evolution in ZrC irradiated with Kr ions. In: Allen TR, Lott RG, Busby JT, Kumar AS (eds) Proc. 22nd Int. symp. on effects of radiation on materials, Boston, Massachusetts, 8–10 June 2004 (ASTM Special Techn Publ, Vol. 1475). American Society for Testing and Materials, West Conshohocken, Pennsylvania, pp. 358–364
777. Gan J, Yang Y, Dickerson C, Allen T (2009) Proton irradiation study of GFR candidate ceramics. *J Nucl Mater* 389(2):317–325
778. Yang Y, Dickerson CA, Swoboda H, Miller B, Allen TR (2008) Microstructure and mechanical properties of proton irradiated zirconium carbide. *J Nucl Mater* 378(3):341–348
779. Gosset D, Dollé M, Simeone D, Baldinozzi G, Thomé L (2008) Structural behaviour of nearly stoichiometric ZrC under ion irradiation. *Nucl Instrum Meth B* 266(12–13):2801–2805
780. Gosset D, Dollé M, Simeone D, Baldinozzi G, Thomé L (2008) Structural evolution of zirconium carbide under ion irradiation. *J Nucl Mater* 373(1–3):123–129
781. Fukuda K, Ikawa K, Iwamoto K (1979) Fission product diffusion in ZrC coated fuel particles. *J Nucl Mater* 87(2–3):367–374
782. Ogawa T, Ikawa K, Fukuda K, Kashimuro S, Iwamoto K (1985) Research and development of ZrC-coated UO₂ particle fuel at the Japan Atomic Energy Research Institute. In: Proc. conf. on nuclear fuel performance, Stratford-upon-Avon, England, code 8933. British Nuclear Energy Society, London

783. Ogawa T, Ikawa K, Iwamoto K (1981) Chemical vapour deposition of ZrC within a spouted bed by bromide process. *J Nucl Mater* 97(1–2):104–112
784. Ogawa T, Ikawa K (1981) Crushing strength of SiC-Triso and ZrC-Triso coated fuel particles. *J Nucl Mater* 98(1–2):18–26
785. Ogawa T, Ikawa K (1981) High-temperature heating experiments on unirradiated ZrC-coated fuel particles. *J Nucl Mater* 99(1):85–93
786. Markin VYu, Savin VI, Shevchenko AS, Andrievskii RA (1982) Effect of reactor irradiation on the magnetic properties of zirconium carbides. *Inorg Mater* 18(1):39–42
787. Taubin ML (1990) Some radiation effects in ZrC, NbC and ZrN interstitial phases. *Atom Energy* 69(3):765–767
788. Kresse G, Hafner J (1993) *Ab initio* molecular dynamics for liquid metals. *Phys Rev B* 47(1):558–561
789. Kresse G, Furthmüller J (1996) Efficient iterative schemes for *ab initio* total-energy calculations using a plane-wave basis set. *Phys Rev B* 54(16):11169–11186
790. Difilippo FC, Renier JP (2007) Double differential neutron scattering cross sections of materials for ultra-high temperature reactors. *Ann Nucl Energy* 34:130–139
791. Van Brutzel L, Crocombette JP (2007) Classical molecular dynamics study of primary damage created by collision cascade in a ZrC matrix. *Nucl Instrum Meth B* 255(1SPEC):141–145
792. Yang Y, Dickerson CA, Allen TR (2009) Radiation stability of proton irradiated zirconium carbide. In: Proc. Int. cong. on advances in nuclear power plants (ICAAP 2009), Shinjuku, Tokyo, 10–14 May 2009, Vol. 3. Atomic Energy Society of Japan, Tokyo, pp. 1932–1939
793. Djourelou N, Gutierrez G, Marinov H, Popov E, Toulhoat N, Moncoffre N, Pipon Y, Nédélec P (2011) Xe-implanted zirconium oxycarbide studied by variable energy positron beam. *Nucl Instrum Meth B* 269(23):2709–2714
794. Ogorodnikov VV, Murzin LM, Krainii AG (1976) Vliyanie oblucheniya na mekhanicheskie svoystva karbidov (The effect of irradiation on the mechanical properties of carbides). In: Samsonov GV, Kosolapova TYa, Gnesin GG, Fedorus VB, Domasevich LG (eds) *Karbidy i splavy na ikh osnove* (Carbides and alloys based on them). Naukova Dumka, Kyiv, pp. 121–126 (in Russian)
795. Gusev AI, Rempel AA, Shveikin GP (1997) Nestekhiometriya i radiatsionnaya stoikost konstruktsionnykh materialov (analiz dannykh) (Nonstoichiometry and structural materials resistance to radiation damage (data analysis)). *Doklady AN SSSR* 357(4):490–494 (in Russian)
796. Gutierrez G, Toulhoat N, Moncoffre N, Pipon Y, Maître A, Gendre M, Perrat-Mabilon A (2011) Thermal behaviour of xenon in zirconium carbide at high temperature: role of residual zirconia and free carbon. *J Nucl Mater* 416(1–2):94–98
797. Kostanovskiy AV, Zeodinov MG, Kostanovskaya ME, Pronkin AA (2018) Thermal expansion of zirconium carbide at 1200–2850 K. *High Temp* 56(6):936–937
798. Castro L, Delgado G, Garcia C, Dominguez DS (2019) Thermal analysis of ceramic nuclear fuels for the HPLWR. *Ann Nucl Energy* 127:227–236
799. Jensen C, Chirtoc M, Antoniow JS, Horny N, Ban H (2013) Photothermal radiometry and scanning thermal microscopy for in-depth thermal conductivity characterization of proton-irradiated ZrC. *Trans Am Nucl Soc* 108:326–327
800. Jensen C, Chirtoc M, Horny N, Antoniow JS, Pron H, Ban H (2013) Thermal wave techniques for thermophysical properties characterization for ion-irradiated studies. *Trans Am Nucl Soc* 109(1):640–641
801. Pellegrino S, Thomé L, Debelle A, Miro S, Trocellier P (2013) Damage production in carbide single crystals irradiated with MeV heavy ions. *Nucl Instrum Meth B* 307:294–298
802. Pellegrino S, Thomé L, Debelle A, Miro S, Trocellier P (2014) Radiation effects in carbides: TiC and ZrC *versus* SiC. *Nucl Instrum Meth B* 327(1):103–107
803. Huang Y, Maier BR, Allen TR (2014) Irradiation-induced effects of proton irradiation on zirconium carbides with different stoichiometries. *Nucl Eng Design* 277:55–63
804. Yang Y, Lo W-Y, Dickerson C, Allen TR (2014) Stoichiometry effect on the irradiation response in the microstructure of zirconium carbides. *J Nucl Mater* 454(1–3):130–135

805. Zhang Y, Wang J, Liu B, Wang J, Zhang H (2014) Understanding the behaviour of native point defects in ZrC by first principles calculations. *J Am Ceram Soc* 97(12):4024–4030
806. Kim S, Szlufarska I, Morgan D (2010) *Ab initio* study of point defect structures and energetics in ZrC. *J Appl Phys* 107(5):053521
807. Ulmer CJ, Motta AT, Kirk MA (2015) *In situ* ion irradiation of zirconium carbide. *J Nucl Mater* 466:606–614
808. Yang X, Lu Y, Zhang P (2015) First principles study of native point defects and diffusion behaviours of helium in zirconium carbide. *J Nucl Mater* 465:161–166
809. Zheng M-J, Szlufarska I, Morgan D (2015) Defect kinetics and resistance to amorphization in zirconium carbide. *J Nucl Mater* 457:343–351
810. Pellegrino S, Crocombette J-P, Debelle A, Jourdan T, Trocellier P, Thomé L (2016) Multi-scale simulation of the experimental response of ion-irradiated zirconium carbide: role of interstitial clustering. *Acta Mater* 102:79–87
811. Jiang C, Zheng M-J, Morgan D, Szlufarska I (2013) Amorphization driven by defect-induced mechanical instability. *Phys Rev Lett* 111(15):155501 (5 pp.)
812. Akhmatov VI, Kostikov VI, Melekhin VF, Stepanyuk VS, Shesterin YuA (1977) Smachivanie plazmennyykh pokrytii zhidkim alyuminiem (The wettability of plasma-sprayed coatings by aluminium). *Izv Vyssh Uchebn Zaved Chern Metall* (5):29–32 (in Russian)
813. Schuster JC, Nowotny H (1980) Investigations of the ternary systems (Zr,Hf,Nb,Ta)-Al-C and studies on complex carbides. *Z Metallkd* 71:341–346
814. Schuster JC (1990) The Al-C-Zr (aluminium-carbon-zirconium) system. *Ternary Alloys VCH* 3:582–586
815. Leela-Adisorn U, Choi SM, Tera N, Takeuchi T, Hashimoto S, Honda S, Awaji H, Hayakawa K, Yamaguchi A (2005) Sintering and mechanical properties of AlZrC₂. *J Ceram Soc Jpn* 113:188–190
816. Schneider JM, Music D, Sun Z (2005) Effect of the valence electron concentration on the bulk modulus and chemical bonding in Ta₂AC and Zr₂AC, A = Al, Si and P. *J Appl Phys* 97:066105
817. Leela-Adisorn U, Choi SM, Hashimoto S, Honda S, Awaji H, Hayakawa K, Yamaguchi A (2006) Sintering and characterization of Zr₂Al₃C₅ monolith. *Key Eng Mater* 317–318:27–30
818. Lin ZJ, Zhuo MJ, He LF, Zhou YC, Li MS, Wang JY (2006) Atomic-scale microstructures of Zr₂Al₃C₄ and Zr₃Al₃C₅. *Acta Mater* 54:3843–3851
819. Leela-Adisorn U, Choi SM, Matsunaga T, Hashimoto S, Honda S, Hayakawa K, Awaji H, Yamaguchi A (2006) AlZrC₂ synthesis. *Ceram Int* 32:431–439
820. He L-F, Zhou Y-C, Bao Y-W, Lin Z-J, Wang J-Y (2007) Synthesis, physical and mechanical properties of bulk Zr₃Al₃C₅ ceramic. *J Am Ceram Soc* 90(4):1164–1170
821. He L-F, Lin Z-J, Wang J-Y, Bao Y-W, Li M-S, Zhou Y-C (2007) Synthesis and characterization of bulk Zr₂Al₃C₄ ceramic. *J Am Ceram Soc* 90(11):3687–3689
822. He L-F, Wang J-Y, Bao Y-W, Zhou Y-C (2007) Elastic and thermal properties of Zr₂Al₃C₄: experimental investigation and *ab initio* calculations. *J Appl Phys* 102(4):043531
823. He L-F, Zhou Y-C, Bao Y-W, Wang J-Y, Li M-S (2007) Synthesis and oxidation of Zr₃Al₃C₅ powders. *Int J Mater Res* 98(1):3–9
824. Emmerlich J, Music D, Houben A, Dronskowski R, Schneider JM (2007) Systematic study on the pressure dependence of M₂AlC phases (M = Ti, V, Cr, Zr, Nb, Mo, Hf, Ta, W). *Phys Rev B* 76:224111
825. Bouhemadou A, Khenata R, Chegaar M (2007) Structural and elastic properties of Zr₂AlX and Ti₂AlX (X = C and N) under pressure effect. *Eur Phys J B* 56:209–215
826. Fukuda K, Hisamura M, Iwata T, Tera N, Sato K (2007) Synthesis, crystal structure and thermoelectric properties of a new carbide Zr₂[Al_{3.56}Si_{0.44}]C₅. *J Solid State Chem* 180(6):1809–1815
827. Fukuda K, Hisamura M, Kawamoto Y, Iwata T (2007) Synthesis, crystal structure and thermoelectric properties of a new layered carbide (ZrC)₃[Al_{3.56}Si_{0.44}]C₃. *J Mater Res* 22(10):2888–2894

828. He L-F, Lin Z-J, Bao Y-W, Li M-S, Wang J-Y, Zhou Y-C (2008) Isothermal oxidation of bulk $Zr_2Al_3C_4$ at 500 to 1000 °C in air. *J Mater Res* 23(2):359–366
829. He L-F, Bao Y-W, Li M-S, Wang J-Y, Zhou Y-C (2008) Improving the high-temperature oxidation resistance of $Zr_2Al_3C_4$ by silicon pack cementation. *J Mater Res* 23(8):2275–2282
830. Lin Z-J, He L-F, Wang J-Y, Li M-S, Bao Y-W, Zhou Y-C (2008) Atomic-scale microstructures and elastic properties of quaternary Zr-Al-Si-C ceramics. *Acta Mater* 56(9):2022–2031
831. He L-F, Bao Y-W, Li M-S, Wang J-Y, Zhou Y-C (2008) Oxidation of $Zr_2[Al(Si)]_4C_5$ and $Zr_3[Al(Si)]_4C_6$ in air. *J Mater Res* 23(12):3339–3346
832. He L-F, Bao Y-W, Wang J-Y, Li M-S, Zhou Y-C (2009) Mechanical and thermophysical properties of Zr-Al-Si-C ceramics. *J Am Ceram Soc* 92(2):445–451
833. He L-F, Lu X-P, Bao Y-W, Wang J-Y, Zhou Y-C (2009) High-temperature internal friction, stiffness and strength of Zr-Al(Si)-C ceramics. *Scripta Mater* 61(1):60–63
834. Wan D-T, He L-F, Zheng L-L, Zhang J, Bao Y-W, Zhou Y-C (2010) A new method to improve the high-temperature mechanical properties of Ti_3SiC_2 by substituting Ti with Zr, Hf or Nb. *J Am Ceram Soc* 93(6):1749–1753
835. He X, Bai Y, Zhu C, Sun Y, Li M, Barsoum MW (2010) General trends in the structural, electronic and elastic properties of the M_3AlC_2 phases (M = transition metal): a first-principle study. *Comput Mater Sci* 49:691–698
836. Barsoum MW (2000) The $M_{N+1}AX_N$ phases: a new class of solids. *Prog Solid St Chem* 28:201–281
837. Barsoum MW (2010) The $M_{n+1}AX_n$ phases and their properties. In: Riedel R, Chen I-W (eds) *Ceramics science and technology, Vol. 2 – Properties*, Wiley-VCH, Weinheim, pp. 299–347
838. Barsoum MW (2013) *MAX phases*. Wiley-VCH Verlag, Weinheim
839. Ivanovskii AL, Gusev AI, Shveikin GP (1996) *Kvantovaya khimiya v materialovedenii: troinye karbidy i nitridy perekhodnykh metallov i elementov IIIb, IVb podgrupp* (Quantum chemistry in materials science: ternary carbides and nitrides of transition metals and subgroup IIIb, IVb elements). *Uralskoe Otdelenie Rossiiskoi Akademii Nauk, Yekaterinburg* (in Russian)
840. Rudy E, Windisch S (1966) Phase diagrams of the systems Ti-B-C, Zr-B-C and Hf-B-C. In: *Ternary phase equilibria in transition metal-boron-carbon-silicon systems*. Report AFML-TR-65-2, Contract USAF 33(615)-1249, Part 2, Vol. 13. Air Force Materials Laboratory, Wright Patterson Air Force Base, Ohio, pp. 1–212
841. Dergunova VS, Levinskii YuV, Shurshakov AN, Kravetskii GA (1974) *Vzaimodeistvie ugleroda s tugoplavkimi metallami* (Interaction of carbon with refractory metals). *Metallurgiya, Moscow* (in Russian)
842. Ordanyan SS (1980) Laws of interaction in the systems $M^{IV.V}C - M^{IV.V}B_2$. *Inorg Mater* 16(8):961–965
843. Duschanek H, Rogl P (1998) The system boron – carbon – zirconium. In: Effenberg G (ed) *Phase diagrams of ternary metal-boron-carbon systems*. ASM International, Materials Park, Ohio, pp. 445–485
844. Shabalin IL, Luchka MV, Shabalin LI (2007) Vacuum SHS in systems with group IV transition metals for production of ceramic compositions. *Phys Chem Solid State* 8(1):159–175
845. Rogl P (2009) Boron – carbon – zirconium system. In: Effenberg G, Ilyenko S (eds) *Ternary alloy systems*. Subvol. E, Part 1. Springer, Berlin, Heidelberg, pp. 450–475
846. Gangler JJ (1954) Resistance of refractories to molten lead-bismuth alloy. *J Am Ceram Soc* 37(7):312–316
847. Portnoi KI, Levinskii YuV, Fadeeva VI (1961) *O kharaktere vzaimodeistviya nekotorykh tugoplavkikh karbidov i ikh tverdykh rastvorov s uglem* (On the character of interaction of some refractory carbides and their solid solutions with carbon). *Izv AN SSSR OTN Metall Toplivo* (2):147–149 (in Russian)
848. Adelsberg LM, Cadoff LH, Tobin JM (1966) Group IVB and VB metal carbide – carbon eutectic temperatures. *J Am Ceram Soc* 49(10):573–574

849. Fedorov TF, Kuzma YuB, Skolozdra RV, Popova NM (1965) Phase equilibria in the ternary systems Zr-Co-C and Nb-Fe-C. *Powder Metall Met Ceram* 4(12):1010–1014
850. Samsonov GV, Panasyuk AD, Kozina GK (1971) Smachivanie tugoplavkikh karbidov rasplavlennymi metallami i splavami (Wetting of refractory carbides by molten metals and alloys). In: Eremenko VN (ed) *Fizicheskaya khimiya poverkhnostnykh yavlenii v rasplavakh* (Physical chemistry of the surface phenomena in melts). Naukova Dumka, Kyiv, pp. 206–208 (in Russian)
851. Samsonov GV, Panasyuk AD, Kozina GK, Dyakonova LV (1972) Contact reaction of refractory compounds with liquid metals. I. Reaction of carbides of subgroup IVa metals with the iron group metals. *Powder Metall Met Ceram* 11(7):568–571
852. Dmitrieva GP, Shurin AK (1973) Fazovye ravnovesiya i struktura splavov Co-ZrC i Co-HfC (The phase equilibria and structure of Co-ZrC and Co-HfC alloys). *Dopov Akad Nauk UkrRSR Ser A Fiz Mat Tekh Nauki* 35(9):845–848 (in Russian)
853. Shurin AK, Dmitrieva GP (1981) Sovremennoe sostoyanie i perspektivy razvitiya issledovaniy kvazibinarykh i kvazitroinykh splavov Fe, Co i Ni s karbidami (Current status and prospects of the research development of quasibinary and quasiternary Fe, Co and Ni alloys with carbides). In: Eremenko VN (ed) *Diagrammy sostoyaniya karbid- i nitrid-soderzhashchikh sistem* (Phase diagrams of carbide and nitride containing systems). Institute for Problems of Materials Science, Ukrainian SSR Academy of Sciences, Kyiv, pp. 28–38 (in Russian)
854. Shurin AK, Dmitrieva GP, Cherepova TS (1996) Phase equilibria in Co – Me'C – Me''C alloys. 1. Systems with three-phase eutectic equilibria. *Powder Metall Met Ceram* 35(11–12):615–620
855. Shurin AK, Dmitrieva GP, Cherepova TS (1997) Phase equilibria in Co – Me'C – Me''C alloys. 2. Systems with four-phase eutectic equilibrium. *Powder Metall Met Ceram* 36(3–4):193–196
856. Fedorov TF, Kuzma YuB (1965) Phase equilibria in the system zirconium-chromium-carbon. *Powder Metall Met Ceram* 4(3):234–237
857. Guha JP, Kolar D (1973) The systems TiC-Cr and ZrC-Cr. *J Less-Common Met* 31(3):337–343
858. Shurin AK, Dmitrieva GP (1974) Diagrammy sostoyaniya sistem Cr-HfC i Cr-ZrC (Phase diagrams of the Cr-HfC and Cr-ZrC systems). *Metallofizika (Akad Nauk Ukr SSR Inst Metallofiz)* (51):105–109 (in Russian)
859. Eremenko VN, ed (1981) *Diagrammy sostoyaniya sistem soderzhashchikh karbidy i nitridy* (The phase diagrams of systems containing carbides and nitrides). Naukova Dumka, Kyiv (in Russian)
860. Eremenko VN, Velikanova TYa, Sleptsov SV, Bondar AA (1990) Diagramma plavkosti sistemy Cr – Zr – C (The meltability diagram of the Cr – Zr – C system). *Dopov Akad Nauk Ukr RSR Ser A Fiz Mat Tekh Nauki* 52(1):70–72 (in Russian)
861. Bondar AA, Velikanova TYa (1996) Aspects of construction diagrams of ternary systems formed by chromium with carbon and *d*-transition metals. *Powder Metall Met Ceram* 35(7–8):484–496
862. Velikanova TYa, Bondar AA, Grytsiv AV, Dovbenko OI (2001) Metallochemistry of chromium with *d*-metals and carbon. *J Alloys Compd* 320:341–352
863. Ivanchenko V, Pryadko T (2010) Carbon – chromium – zirconium system. In: Effenberg G, Ilyenko S (eds) *Ternary alloy systems*. Subvol. E, Part 2. Springer, Berlin, Heidelberg, pp. 397–408
864. Rakitskii AN (1975) The chromium-melt resistance of superduty refractory materials. *Refract Indust Ceram* 16(11–12):780–783
865. Samsonov GV, Podchernyaeva IA, Fomenko VS (1967) Nature of interaction of zirconium carbide with cesium vapour. *High Temp* 5(1):139–141
866. Samsonov GV, Podchernyaeva IA, Siman NI, Fomenko VS (1976) Behaviour of refractory compounds in alkali metal media. *Powder Metall Met Ceram* 15(2):122–127

867. Stark WA, Jr (1978) Cesium solubility, diffusion and permeation in zirconium carbide. *J Nucl Mater* 73:169–179
868. Zhao Y-W, Wang Y-J, Zhou Y, Peng H-X, Song G-M (2011) Ternary phase $Zr_xCu_yC_z$ in reactively infiltrated ZrC/W composite. *J Am Ceram Soc* 94(10):3178–3180
869. Frey H, Holleck H (1975) DTA investigations of high-temperature phase equilibria in ternary transition metal – carbon systems. In: Buzas I (ed) Proc. 4th Int. conf. in thermal analysis, Budapest, 8–13 July 1974, Vol. 1. John Wiley, Chichester, pp. 339–348
870. Savitskii EM, Burkhanov GS (1971) Metallovedenie splavov tugoplavkikh i redkih metallov (Metallography of refractory and less-common metal alloys), 2nd edn. Nauka, Moscow (in Russian)
871. Velikanova TYa, Eremenko VN (1974) Phase equilibria in the ternary systems formed by molybdenum and tungsten with the groups IV and V transition metals and carbon. *Powder Metall Met Ceram* 13(4):293–297
872. Kosterova NV, Ordanyan SS, Neshpor VS, Ostrovskii EK (1980) Thermoionic properties of cermets of eutectic compositions in Me(IV) – (C,B) – (Mo,Re,W) systems. *Powder Metall Met Ceram* 19(1):61–66
873. Shurin AK, Dmitrieva GP (1974) Phase diagrams of iron alloys with zirconium and hafnium carbides. *Metal Sci Heat Treat* 16(7–8):665–667
874. Shurin AK, Dmitrieva GP (1974) Issledovanie fazovykh ravnovesii i struktury splavov Ni-ZrC i Ni-HfC (Examination of phase equilibria and structure of the Ni-ZrC and Ni-HfC alloys). *Metallofizika (Akad Nauk Ukr SSR Inst Metallofiz)* (53):97–100 (in Russian)
875. Raevskaya MV, Tatarkina AL, Kulova LK (1981) Fazovye ravnovesiya v kvazi-troinykh sistemakh nikel – karbid volframa (WC) – karbid tsirkoniya (ZrC) i nikel – karbid volframa (WC) – karbid gafniya (HfC) (Phase equilibria in the nickel – tungsten carbide (WC) – zirconium carbide (ZrC) and nickel – tungsten carbide (WC) – hafnium carbide (HfC) quasiternary systems). In: Drits ME (ed) Fazovye ravnovesiya v metallicheskiykh splavakh (Phase equilibria in metallic alloys). Nauka, Moscow, pp. 273–276 (in Russian)
876. Dmitrieva GP, Razumova NA, Shurin AK, Khandros EL (1986) Phase equilibria in the alloys of the Ni-TiC-MeC (Me: Zr, Hf, Nb, Ta) systems. *Russ Metall* (1):210–215
877. Naumenko VYa (1970) Preparation of carbides of the IV-V groups transition metals in their homogeneity regions. *Powder Metall Met Ceram* 9(10):799–801
878. Xu L, Huang C, Liu H, Zou B, Zhu H, Zhao G, Wang J (2014) Study on the synthesis and growth mechanisms of the refractory ZrC whiskers. *Int J Refract Met Hard Mater* 42:116–119
879. Shurin AK, Dmitrieva GP, Razumova NA, Khandros EL (1987) Phase diagram of the Ni-ZrC-HfC system. *Powder Metall Met Ceram* 26(9):754–757
880. Shurin AK, Dmitrieva GP, Razumova NA (1988) Phase equilibria in ternary nickel-carbide alloys. *Russ Metall* (6):63–69
881. Gorshkova LV, Voroshilov YuV, Fedorov TF (1969) Study of the ternary system zirconium-rhenium-carbon. *Powder Metall Met Ceram* 8(2):146–148
882. Eremenko VN, Velikanova TYa (1983) Use of the phase diagrams of ternary transition metal systems containing carbides in the development of heat-resisting hard alloys. *Powder Metall Met Ceram* 22(12):1010–1021
883. Brukl CE (1966) The Zr-Si-C, Hf-Si-C, Zr-Si-B, and Hf-Si-B systems. In: Ternary phase equilibria in transition metal-boron-carbon-silicon systems. Report AFML-TR-65-2, Contract USAF 33(615)-1249, Part 2, Vol. 10. Air Force Materials Laboratory, Wright-Patterson Air Force Base, Ohio, pp. 1–95
884. Wang YZ, Carim AH (1995) Ternary phase equilibria in the Zr-Si-C system. *J Am Ceram Soc* 78(3):662–666
885. Samsonov GV, Yasinskaya GA, Shiller ÉA (1961) Interaction of certain oxides, carbides and high-melting metals at high temperatures. *Refract Indust Ceram* 2(7–8):274–277
886. Xu J, Zou B, Zhao S, Hui Y, Huang W, Zhou X, Wang Y, Cai X, Cao X (2014) Fabrication and properties of ZrC-ZrB₂/Ni cermet coatings on a magnesium alloy by atmospheric plasma spraying of SHS powders. *Ceram Int* 40:15537–15544
887. Lesnaya MI, Nemchenko VF, Sotnik AA, Sotnik SG (1978) Thermophysical properties of the carbide alloys TiC-ZrC and TiC-VC. *High Temp* 16(3):456–459

888. Fedorov TF, Gladyshevskii EI (1965) Phase equilibria in ternary systems of transition metals of groups IV and V and carbon. *Powder Metall Met Ceram* 4(1):27–29
889. Chapin EJ, Friske WH (1954) A metallurgical evaluation of refractory compounds for containing molten titanium. Part II – Carbon, graphite and carbides. Report NRL-4467. Naval Research Laboratory, Washington, DC, pp. 1–22
890. Brukl CE, Harmon DP (1966) The Ti-Zr-C, Ti-Hf-C and Zr-Hf-C systems. In: Ternary phase equilibria in transition metal-boron-carbon-silicon systems. Report AFML-TR-65-2, Contract USAF 33(615)-1249, Part 2, Vol. 4. Air Force Materials Laboratory, Wright-Patterson Air Force Base, Ohio, pp. 1–78
891. Bandyopadhyay D, Sharma RC, Chakraborti N (2001) The C-Ti-Zr (carbon-titanium-zirconium) system. *J Phase Equilib* 22(1):61–64
892. Voroshilov YuV, Gorshkova LV, Popova AM, Fedorov TF (1967) Ternary systems Ti-Zr-C and Ti-Hf-C. *Powder Metall Met Ceram* 6(5):403–405
893. Voroshilov YuV (1968) Concerning “Ternary systems of titanium-zirconium-carbon and titanium-hafnium-carbon”. *Powder Metall Met Ceram* 7(8):669
894. Kuzma YuB, Fedorov TF, Shvets EA (1965) Phase equilibria in the system Zr-W-C. *Powder Metall Met Ceram* 4(2):106–109
895. Zakharov AM, Naumkin OP, Kurganov GV (1974) Tungsten-rich corner of W-Zr-C and W-Hf-C ternary systems. *Russ Metall* (1):136–139
896. Eremenko VN, Velikanova TYa, Artyukh LV, Aktselrod GM, Vishnevskii AS (1976) Issledovanie splavov troinykh sistem W-HfC-C i W-ZrC-C pri subsolidusnykh temperaturakh (A study of ternary systems W-HfC-C and W-ZrC-C alloys at subsolidus temperatures). *Dopov Akad Nauk Ukr RSR Ser A Fiz Mat Tekh Nauki* 38(1):83–89 (in Russian)
897. Savitsky EM, Povarova KB, Makarov PV, Zavarzina YaK (1977) Phase-Zusammensetzung, Struktur und Eigenschaften von vakuumgeschmolzenem W-C-(Zr,Hf,Nb,Ta,Re) Legierung (Phase composition, structure and properties of vacuum-melted W-C-(Zr,Hf,Nb,Ta,Re) alloys). *Planseeber Pulvermetall* 25(3):168–185 (in German)
898. Savitsky EM, Povarova KB, Makarov PV (1982) Physikalisch-chemische Grundlagen des Legierens von warmfesten Wolframlegierungen (Physical and chemical principles underlying alloying of heat-resistant tungsten alloys). *Z Metallkd* 73(2):92–97 (in German)
899. Xiong W, Du Y, Zhang W, Xu H (2010) Carbon – tungsten – zirconium system. In: Effenberg G, Ilyenko S (eds) Ternary alloy systems. Subvol. E, Part 3. Springer, Berlin, Heidelberg, pp. 31–47
900. Vil'k YuN, Ordanyan SS, Avarbe RG, Avgustinnik AI, Ryzhkova TP, Omelchenko YuA (1965) Diagramma sostoyaniya v sisteme Zr-ZrC (Phase diagram of the Zr-ZrC system). In: Grigoreva VV, Eremenko VN, Nazarchuk TN, Samsonov GV, Fedorchenko IM, Frantsevich IN (eds) Vysokotemperaturnye neorganicheskie soedineniya (High-temperature inorganic compounds). Naukova Dumka, Kyiv, pp. 211–218 (in Russian)
901. Borisova AL (1985) Sovmestimost tugoplavkikh soedinenii s metallami i grafitom (The compatibility of refractory compounds with metals and graphite). Naukova Dumka, Kyiv (in Russian)
902. Kosolapova TYa, Kutysheva ÉV (1969) Reaction between zirconium carbide and silicon powders. *Powder Metall Met Ceram* 8(11):914–917
903. Loshak MG (1984) Prochnost i dolgovechnost tverdykh splavov (The strength and durability of hard alloys). Naukova Dumka, Kyiv (in Russian)
904. Iwata T, Hattori E, Sugiura K, Hashimoto S, Nakano H, Fukuda K (2009) Syntheses and crystal structures of Si-bearing layered carbides $ZrAl_8C_7$ and $ZrAl_4C_4$. *J Ceram Soc Jpn* 117(1):37–41
905. Sugiura K, Iwata T, Sunada N, Hashimoto S, Nakano H, Fukuda K (2009) Syntheses and crystal structures of Ge-bearing layered carbides $Zr_2Al_4C_5$ and $Zr_3Al_4C_6$. *J Ceram Soc Jpn* 117(1):22–26
906. Iwata T, Sugiura K, Hashimoto S, Fukuda K (2008) Synthesis and crystal structure of a new layered carbide $ZrAl_8C_7$. *J Am Ceram Soc* 91(11):3758–3761

907. Zhang J, Wang J-Y, Zhou Y-C (2011) Microstructure evolution of $Zr_2Al_3C_4$ in Cu matrix. *J Mater Res* 26(3):372–383
908. Fukuda K, Hisamura M, Iwata T, Hashimoto S, Nakano H (2008) Synthesis and crystal structure of a new layered carbide $[Zr_{1.97}Y_{0.03}]Al_4C_5$. *J Am Ceram Soc* 91(4):1342–1345
909. Sugiura K, Iwata T, Nakano H, Fukuda K (2009) $[Zr_{0.72}Y_{0.28}]Al_4C_4$: a new member of the homologous series $(MC)_n(T_4C_3)_m$ (M = Zr, Y and Hf, T = Al, Si, Ge). *J Solid State Chem* 182(7):1619–1623
910. Sugiura K, Iwata T, Yoshida H, Hashimoto S, Fukuda K (2008) Syntheses, crystal structures and Si solubilities of new layered carbides $Zr_2Al_4C_5$ and $Zr_3Al_4C_6$. *J Solid State Chem* 181(10):2864–2868
911. Iwata T, Hattori E, Hashimoto S, Fukuda K (2008) Synthesis and crystal structure of a new layered carbide $ZrAl_4C_4$. *J Am Ceram Soc* 91(8):2713–2715
912. Fukuda K, Mori S, Hashimoto S (2005) Crystal structure of $Zr_2Al_3C_4$. *J Am Ceram Soc* 88(12):3528–3530
913. Gesing TM, Jeitschko W (1998) The crystal structures of $Zr_3Al_3C_5$, $ScAl_3C_3$ and UAl_3C_3 and their relation to the structures of $U_2Al_3C_4$ and Al_4C_3 . *J Solid State Chem* 140(2):396–401
914. Schwarzkopf P, Glaser FW (1953) Struktur und chemische Eigenschaften der Boride der Übergangsmetalle der vierten, fünften und sechsten Gruppe (Structure and chemical properties of the transition metal borides of the fourth, fifth and sixth groups). *Z Metallkd* 44(8):353–358 (in German)
915. Sorrell CC, Ruys AJ (1991) Ternary phase equilibria in the system Zr-N-B-C at 1500 °C. *Key Eng Mater* 53–55:92–100
916. Sorrell CC, Ruys AJ (1991) Quaternary phase equilibria in the system Zr-N-B-C at 1500 °C. *Key Eng Mater* 53–55:83–91
917. Eremenko VN, Velikanova TYa, Sleptsov SV, Bondar AA (1992) Phase equilibria at subsolidus temperatures and a scheme for solidification of alloys of the Cr-Zr-C system. *Russ Metall* (5):132–139
918. Ivanchenko VG, Pogorelaya VV (2001) Structure formation in eutectic alloys of chromium with carbide $Cr_{23}C_6$ and with carbides of IVA-group metals. *Met Phys Adv Techn* 19(3):869–874
919. Ivanchenko VG (2001) Phase equilibria and formation of structure and properties in the chromium alloys with interstitial phases. *Met Phys Adv Techn* 19(3):669–710
920. Bittermann H, Rogl P (2002) Critical assessment and thermodynamic calculation of ternary system C-Hf-Zr (carbon-hafnium-zirconium). *J Phase Equilib* 23(3):218–235
921. Benesovsky F, Rudy E (1960) Pseudoternary carbide systems. *Metall* (9):875–876
922. Samsonov GV, Strashinskaya LV, Shiller ÉA (1962) Kontaktnoe vzaimodeistvie metallopodobnykh karbidov, nitridov i boridov s tugoplavkimi metallami pri vysokikh temperaturakh (The contact interaction of metal-like carbides, nitrides and borides with refractory metals at high temperatures). *Izv AN SSSR OTN Metall Toplivo* (5):167–180 (in Russian)
923. Samsonov GV, ed (1973) The oxide handbook. IFI/Plenum, New York, London
924. Samsonov GV, Burykina AL, Strashinskaya LV, Pugach ÉA (1964) Reactions between magnesium oxide or zirconium dioxide and refractory compounds at high temperatures under vacuum. *Russ Metall* (4):70–77
925. Krylov YuI, Balakir ÉA (1976) Karbidno-okisnye sistemy (Carbide-oxide systems). *Metallurgiya*, Moscow (in Russian)
926. Eremenko VN, Velikanova TY, Shabanova SV, Artyukh LV (1973) Continuous series of solid solutions of carbides with NaCl structure in the ternary systems Mo(W)-Me^{IV,V}-C. *Powder Metall Met Ceram* 12(11):909–912
927. Funke VF, Pshenichnyi IV, Pliner LA, Loktionov YuD (1983) Phase fields and initial melting diagrams of the pseudoquaternary system UC-MoC_{1-x}-ZrC-NbC. *Powder Metall Met Ceram* 22(2):110–116
928. Allinson JD, Riviere JC (1965) High temperature short-term compatibility of some refractory metals with the thermoionic fuel UC-ZrC. *J Nucl Mater* 17:97–110

929. Bao W, Liu J-X, Wang X, Zhang H-B, Xue J, Sun S-K, Xu F, Xue J, Zhang G-J (2018) Structural evolution in ZrC-SiC composite irradiated by 4 MeV Au ions. *Nucl Instrum Meth B* 434:23–28
930. Fedorov TF, Kuzma YuB, Gorshkova LV (1965) Phase equilibria in the ternary system zirconium-molybdenum-carbon. *Powder Metall Met Ceram* 4(3):229–233
931. Gusev AI (1985) Prognoz i raschety fazovykh diagramm psevdobinarykh system na osnove tugoplavkikh soedinenii perekhodnykh metallov (Prediction and calculation of phase diagrams of pseudobinary systems based on high-melting transition metal compounds). In: Ageev NV (ed) *Raschety i eksperimentalnye metody postroeniya diagramm sostoyaniya* (Calculation and experimental methods of plotting phase diagrams). Nauka, Moscow, pp. 42–47 (in Russian)
932. Watt W (1958) The oxidation of zirconium carbide in high-temperature combustion gases. *Powder Metall* 1(1–2):227–234
933. Ivashina GA, Lesnaya MI, Nemchenko VF, Savin VI (1979) Electrochemical behaviour and physical properties of binary carbide solutions of titanium and zirconium. *Sov Electrochem* 15(6):708–711
934. Misra PS, Upadhyaya GS (1984) Bonding in sintered aluminium – refractory carbides composites – an electronic and microstructural evidence. In: Upadhyaya GS (ed) *Sintered metal-ceramic composites*. Elsevier Science, Amsterdam, pp. 255–257
935. Li F, Wang X-G, Huang X, Liu J-X, Bao W, Zhang G-J, Wang H (2018) Preparation of ZrC/SiC porous self-supporting monoliths via sol-gel process using polyethylene glycol as phase separation inducer. *J Eur Ceram Soc* 38:4806–4813
936. Korniyenko K (2007) Carbon – plutonium – zirconium system. In: Effenberg G, Ilyenko S (eds) *Ternary alloy systems*. Subvol. C, Part 4. Springer, Berlin, Heidelberg, pp. 160–167
937. Haines HR, Potter PE (1970) Constitutional studies in uranium and plutonium carbide – fission product systems. I. Uranium and plutonium – transition metal – carbon systems. Report AERE-R 6512. UK Atomic Energy Authority, Harwell Laboratory, Oxfordshire, pp. 1–15
938. Kotelnikov RB, Bashlykov SN, Kashtanov AI, Menshikova TS (1978) *Vysokotemperaturnoe yadernoe toplivo* (High-temperature nuclear fuel). Atomizdat, Moscow (in Russian)
939. Holleck H, Kleykamp H (1969) Thermodynamics of multi-component systems containing UC and PuC – a review. *J Nucl Mater* 32(1):1–19
940. Velikanova TYa, Eremenko VN, Artyukh LV, Bondar AA, Gordiichuk OV (1989) Phase diagrams of Sc-M(IV-VII)-C systems. *Powder Metall Met Ceram* 28(9):711–718
941. Artyukh LV, Velikanova TYa, Ilyenko SM (1998) Phase equilibria in the Sc-Zr-C system. *J Alloys Compd* 269:193–200
942. Farr JD (1968) Phase diagrams of selected refractory compounds. In: Hausner HH, Bowman MG (eds) *Fundamentals of refractory compounds*. Plenum Press, New York, pp. 33–48
943. Gorshkova LV (1976) Joint solubility of carbon and zirconium in molybdenum-tungsten solid solutions. *Powder Metall Met Ceram* 15(3):215–216
944. Takahashi T, Hashimoto Y (1989) Mechanical properties of the TiC- and ZrC-dispersion-strengthened coppers prepared by the application of mechanical alloying. *J Jpn Soc Powder Metall* 36(6):688–692 (in Japanese)
945. Kwon WT, Park JS, Kim S-W, Kang S (2004) Effect of WC and group IV carbides on the cutting performance of Ti(C,N) cermet tools. *Int J Machine Tools Manufact* 44:341–346
946. Kaftelen H, Öveçoğlu ML, Henein H, Çimenoglu H (2010) ZrC particle reinforced Al – 4 wt.% Cu alloy composites fabricated by mechanical alloying and vacuum hot pressing: microstructural evaluation and mechanical properties. *Mater Sci Eng A* 527:5930–5938
947. Eremenko VN, Velikanova TYa, Bondar AA (1989) Phase equilibria at the solidus surface of the equilibrium diagram of ternary systems of technetium with carbon and d-transition metals of groups III-VII. *Powder Metall Met Ceram* 28(11):868–873

948. Ivanov OS, Badaeva TA (1959) Diagrammy sostoyaniya nekotorykh troinykh sistem urana i toriya (Phase diagrams of some ternary systems of uranium and thorium). In: Yaderno goryuchee i reaktornye materialy. Trudy 2-oi mezhd. konf. OON po mirnomu ispolzovaniyu atomnoi energii, Zheneva, 1-13 sentyabrya 1958. Raboty sovetskikh uchenykh. (Nuclear fuel and reactor materials. Proc. 2nd UN Int. conf. on the peaceful uses of atomic energy, Geneva, 1–13 Sept 1958. Papers of Soviet scientists.), Vol. 3. Atomizdat, Moscow, pp. 347–369 (in Russian)
949. Ivanov OS, Alekseeva ZM (1961) Issledovaniya stroeniya splavov sistem UC-ZrC, UC-ThC i ThC-ZrC (Structure studies of alloys of the UC-ZrC, UC-ThC and ThC-ZrC systems). In: Ivanov OS (ed) Stroenie splavov nekotorykh sistem s uranom i toriem (The structure of alloys of some systems with uranium and thorium). Gosatomizdat, Moscow, pp. 438–439 (in Russian)
950. Alekseeva ZM (1968) Fazovyi sostav splavov UC-Zr i Zr-ThC i otositelnoe srodstvo ugleroda k Zr, Th i U (The phase composition of UC-Zr and Zr-ThC alloys and relative affinity of carbon to Zr, Th and U). In: Alekseeva ZM, Ivanov OS (eds) Fiziko-khimiya splavov i tugoplavkikh soedinenii s toriem i uranom (Physico-chemistry of alloys and refractory compounds with thorium and uranium). Nauka, Moscow, pp. 136–145 (in Russian)
951. Rudy E, Benesovsky F (1962) Untersuchungen im System Th-Zr-C (Investigations of the system Th-Zr-C). *Monatsh Chem* 93:1279–1283 (in German)
952. Perrot P (2007) Carbon – thorium – zirconium system. In: Effenberg G, Ilyenko S (eds) Ternary alloy systems. Subvol. C, Part 4. Springer, Berlin, Heidelberg, pp. 216–219
953. Gusev AI (1984) Calculations of the phase diagrams of pseudo-binary systems based on titanium, zirconium, hafnium and vanadium carbides. *Inorg Mater* 20(7):976–981
954. Kieffer R, Nowotny H, Neckel A, Ettmayer P, Usner L (1968) Zur Entmischung von kubischen Mehrstoffcarbiden (On the miscibility of multicomponent cubic carbides). *Monatsh Chem* 99(3):1020–1027 (in German)
955. Kieffer R (1969) Preparation and properties of interstitial compounds. *J Inst Met* 97(6):164–172
956. Benesovsky F, Rudy E (1961) Auf der Systeme U-Zr(Hf,Nb,Ta)-C (On the systems U-Zr(Hf,Nb,Ta)-C). *Planseeber Pulvermetall* 9(1/2):65–76 (in German)
957. Benesovsky F (1964) The importance of powder metallurgy for developing and producing new types of nuclear fuel materials. *Powder Metall Met Ceram* 3(3):248–255
958. Nickel H, Oe Inanc, Lücke K (1968) Auf das Wissen der U-Zr-C System (On the knowledge of the U-Zr-C system). *J Nucl Mater* 28:79–92 (in German)
959. Storms EK, Griffin J (1973) Thermodynamics and phase relationships of the zirconium-uranium-carbon system. *High Temp Sci* 5:423–437
960. Butt DP, Wallace TC (1993) The U-Zr-C ternary phase diagram above 2473 K. *J Am Ceram Soc* 76(6):1409–1419
961. Perrot P (2007) Carbon – uranium – zirconium system. In: Effenberg G, Ilyenko S (eds) Ternary alloy systems. Subvol. C, Part 4. Springer, Berlin, Heidelberg, pp. 220–229
962. Binder S, Lengauer W, Ettmayer P, Bauer J, Debuigne J, Bohn M (1995) Phase equilibria in the systems Ti – C – N, Zr – C – N and Hf – C – N. *J Alloys Compd* 217(1):128–136
963. Avgustinik AI, Gropyanov VM, Drozdetskaya GV, Vigdergauz VSh (1964) The interaction of some refractory carbides and zirconium dioxide. *Refract Indust Ceram* 5(11–12):611–616
964. Kosolapova TYa, Fedorus VB, Kuzma YuB (1966) Vzaimodeistvie karbidov perekhodnykh metallov s ikh okoislami (The interaction of transition metal carbides with their oxides). *Izv AN SSSR Neorg Mater* 2(8):1516–1520 (in Russian)
965. Gropyanov VM, Kovalevskaya GA, Yudin BF (1972) Ustoichivost oksikarbidov v sisteme ZrC-ZrO₂ (Stability of oxycarbides in the ZrC-ZrO₂ system). *Izv AN SSSR Neorg Mater* 8(1):88–91 (in Russian)
966. Gropyanov VM, Kovalevskaya GA, Razumovskii SN (1972) Kristallicheskaya struktura oksikarbidov tsirkoniya v sisteme ZrC-ZrO₂ (The crystal structure of zirconium oxycarbides in the ZrC-ZrO₂ system). *Izv AN SSSR Neorg Mater* 8(1):92–95 (in Russian)

967. Ordanyan SS (1993) Rules for the reactions in $B_4C-Me^{IV-VI}B_2$ systems. *Refract Indust Ceram* 34(5–6):268–271
968. Ordanyan SS, Unrod VI (1975) Reactions in the system $ZrC-ZrB_2$. *Powder Metall Met Ceram* 14(5):393–395
969. Ordanyan SS, Unrod VI (2005) Eutectics and their models, sintered composites in the systems of refractory materials. *Refract Industrial Ceram* 46(4):276–281
970. Kotlyar EE, Kosolapova TYa, Nazarchuk TN (1967) Chemical phase analysis of ZrO_2-ZrC and ZrO_2-TiC alloys. *Russ Metall* (1):104–106
971. Guerlet JP, Lehr P (1965) Sur les reactions entre le zirconium et le gaz carbonique aux temperatures elevees (On reactions of zirconium and carbon dioxide at elevated temperatures). *Compt Rend Acad Sci C* 260(3):899–901 (in French)
972. Guerlet JP, Lehr P (1967) Sur l'oxydation du zirconium par l'oxyde carbon (On oxidation of zirconium by carbon monoxide). *Compt Rend Acad Sci C* 264(23):1833–1835 (in French)
973. Zainulin YuG, Alyamovskii SI, Shveikin GP, Geld PV (1973) K voprosu o komplektnosti reshetki kubicheskogo oksikarbida tsirkoniya v oblasti ego gomogennosti (Problem of completeness of cubic zirconium oxycarbide lattice in the region of its homogeneity). *Zh Neorg Khim* 18(7):1986–1987 (in Russian)
974. Zainulin YuG, Alyamovskii SI, Shveikin GP (1975) Mekhanizm formirovaniya tverdykh rastvorov pri vnedrenii kisloroda v reshetku defektykh karbidov (Mechanism of solid solution formation when oxygen is intruding in imperfect carbide lattice). *Doklady AN SSSR* 223(4):904–906 (in Russian)
975. Lyubimov VD, Shveikin GP, Alyamovskii SI (1982) Mekhanizm pryamogo vosstanovleniya okislov tantalata, gafniya i tsirkoniya (Mechanism of the direct reduction of tantalum, hafnium and zirconium oxides). *Zh Neorg Khim* 27(12):3015–3019 (in Russian)
976. Alyamovskii SI, Zainulin YuG, Shveikin GP, Geld PV (1973) Vozmozhnost obrazovaniya stabilizirovannogo ZrO (The possibility of formation of stabilized ZrO). *Izv AN SSSR Neorg Mater* 9(10):1837–1838 (in Russian)
977. Zainulin YG, Zhilyaev VA, Alyamovskii SI, Shveikin GP (1976) Cubic carbon-stabilized low-temperature zirconium dioxide. *Inorg Mater* 12(2):239–240
978. Pavlov IE, Tskhai VA, Alyamovskii SI, Shveikin GP (1976) Solubility of hydrogen in zirconium oxycarbides, oxynitrides and oxycarbonitrides. *Inorg Mater* 12(12):1768–1770
979. Kutysheva ÉV, Fedorus VB (1975) Khimicheskie svoystva oksikarbidov titana i tsirkoniya (Chemical properties of titanium and zirconium oxycarbides). In: Samsonov GV (ed) *Vysokotemperaturnye karbidy* (High-temperature carbides). Naukova Dumka, Kyiv, pp. 176–179 (in Russian)
980. Afonin YuD, Shalaginov VN, Beketov AR (1983) Vysokotemperaturnoe okislenie karbida tsirkoniya pri nizkom davlenii kisloroda (The high-temperature oxidation of zirconium carbide at low oxygen pressure). *Zh Prikl Khim* 56(10):2185–2189 (in Russian)
981. Afonin YuD, Shalaginov VN, Beketov AR, Alyamovskii SI (1980) Vysokotemperaturnoe okislenie slozhnykh karbidov niobiya i tsirkoniya (High-temperature oxidation of niobium and zirconium complex carbides at low oxygen pressures). *Izv Vyssh Uchebn Zaved Tsvetn Metall* (2):81–85 (in Russian)
982. Beketov AR, Vlasov VG, Kuptsov SG, Fedorenko OV, Pykhteev YuP (1978) Okislenie karbida tsirkoniya (The oxidation of zirconium carbide). *Izv Vyssh Uchebn Zaved Tsvetn Metall* (2):99–102 (in Russian)
983. Kuptsov SG, Vlasov VG, Beketov AR, Fedorenko OV, Obabkov NV (1976) Povedenie ugleroda pri okislenii karbida tsirkoniya (Behaviour of carbon in the oxidation of zirconium carbide). *Izv Vyssh Uchebn Zaved Tsvetn Metall* (2):104–105 (in Russian)
984. Shabalin IL (2008) “Ridge effect” in oxidation kinetics of hetero-modulus ceramics based on titanium carbide. *Powder Metall Met Ceram* 47(1–2):137–150
985. Shabalin IL (2009) Oxidation behaviour of hetero-modulus ceramics based on titanium carbide. In: Lin H-T, Koumoto K, Kriven WM, Norton DP, Garsia E, Reimanis IE (eds) *Developments in strategic materials. Ceramic engineering and science proceedings*, Vol. 29(10). Wiley, New York, pp. 261–278

986. Hu W, Xiang J, Liu S, Zhang Y, Chen C, Wang P, Wang H, Wen F, Xu B, He J, Yu D, Tian Y, Liu Z (2012) Low-temperature diffusion of oxygen through ordered carbon vacancies in Zr_2C_x : the formation of ordered $Zr_2C_xO_3$. *Inorg Chem* 51:5164–5172
987. Hu W, Xiang J, Zhang Y, Liu S, Chen C, Wang P, Wang H, Wen F, Xu B, He J, Yu D, Tian Y, Liu Z (2012) Superstructural nanodomains of ordered carbon vacancies in nonstoichiometric $ZrC_{0.61}$. *J Mater Res* 27(9):1230–1236
988. Tsurekawa S, Nakashima M, Murata A, Kurishita H, Yoshinaga H (1991) Solid solution hardening of titanium carbide by niobium and zirconium at high temperatures. *J Jpn Inst Met* 55(4):390–397 (in Japanese)
989. Samsonov GV, Yasinskaya GS (1964) Interaction between high-melting compounds and molten metals. *Powder Metall Met Ceram* 3(5):366–370
990. Krikorian NH, Wallace TC, Krupka MC, Radosevich CL (1967) The reaction of some noble and transition metals with refractory carbides. *J Nucl Mater* 21:236–238
991. Brewer L (1967) A most striking confirmation of the Engel metallic correlation. *Acta Metall* 15(3):553–556
992. Neshpor VS, Vilks YuN, Danisina IN (1967) Change in the electro- and thermophysical properties in pseudobinary alloys along the ray $ZrC_{0.92}$ - $ZrN_{0.85}$ of the zirconium-nitrogen-carbon system. *Powder Metall Met Ceram* 6(1):68–71
993. Manning C, Stoops R (1968) High-temperature cermets: 1. Compatibility. *J Am Ceram Soc* 51(8):411–415
994. Vilks YN, Danisina IN, Omelchenko YuA, Ryzhkova TP (1968) Variations of certain physico-chemical properties in the system zirconium carbide – zirconium nitride. *Russ J Appl Chem* 41(4):873–881
995. Carnahan RD, Janowski KR, Rossi RC (1969) Microstructure of zirconium based ternary carbide alloys. *Metallogr* 2:65–77
996. Oshchipko IS, Burykina AL (1969) Study of the reactions between boron carbonitride and refractory metals and compounds. *Powder Metall Met Ceram* 8(6):499–501
997. Rai JH, Gregory NW (1970) An effusion study of the reaction of zirconium carbide with calcium oxide. *J Phys Chem* 74(5):1076–1082
998. Miller AD (1967) Electronic band structure and oxygen solubility in Zr-C-O. PhD thesis, University of Washington, Seattle
999. Zhilyaev VA, Zainulin YuG, Alyamovskii SI, Shveikin GP (1972) High-temperature oxidation of zirconium and hafnium oxycarbides and oxycarbonitrides. *Powder Metall Met Ceram* 11(8):632–636
1000. Ouensanga A, Dode M (1974) Etude a 1555 °C de la solubilité de l'oxygène dans le carbure de zirconium en présence de carbone libre et dans les conditions d'équilibre thermodynamique (Study of oxygen solubility in zirconium carbide at 1555 °C in the presence of free carbon and under thermodynamic equilibrium conditions). *Rev Int Hautes Temp Refract* 11(1):35–39 (in French)
1001. Ouensanga A, Dode M (1976) Etude thermodynamique et structurale a haute température du système Zr-C-O. Diagramme de phases a 1555 °C. (Thermodynamic and structural study of the Zr-C-O system at high-temperature. Phase diagram at 1555 °C). *J Nucl Mater* 59(1):49–60 (in French)
1002. Samsonov GV, Sharkin OP, Panasyuk AD, Kozina GK, Dyakonova LV (1975) Electron-microprobe investigation of interfacial reactions in systems composed of a refractory compound and a liquid metal. 3. Effects of carbon on the contact reaction in the system ZrC-Ni. *Powder Metall Met Ceram* 14(8):649–653
1003. Leiderman GM, Nikolaeva VA (1973) Vzaimodeistvie NbC i ZrC s Ni (Interaction of NbC and ZrC with Ni). *Izv AN SSSR Neorg Mater* 9(10):1721–1723 (in Russian)
1004. Kokhtev SA, Yevstyukhin AI, Andrievskii RA, Solovyev GI (1976) Pseudobinary system uranium monosulfide – zirconium carbide. *J Nucl Mater* 59:331–332
1005. Borisova AL, Borisov YuS (1977) A thermodynamic evaluation of the effect of non-stoichiometry of compounds on the course of their solid-phase reactions. *Powder Metall Met Ceram* 16(6):440–447

1006. Holleck H (1977) Zum Aufbau der Systeme Thorium – (Zirkon, Niob, Ruthenium, Rhodium) – Kohlenstoff (The structure of thorium – (zirconium, niobium, ruthenium, rhodium) – carbon systems). *J Nucl Mater* 66(3):273–282 (in German)
1007. Godin YuG, Suchkov II, Yevstyukhin AI (1979) Struktura splavov sistemy UC-ZrC-NbC (Structure of UC-ZrC-NbC alloys). In: Emelyanov VS, Yevstyukhin AI (eds) *Metallurgiya i metallovedenie chistykh metallov* (Metallurgy and metallography of pure metals), Vol. 13. Atomizdat, Moscow, pp. 77–84 (in Russian)
1008. Tkachenko YuG, Ordanyan SS, Yulyugin VK, Yurchenko DS, Unrod VI (1979) The role of the boride phase in MeC-MeB₂ alloys when subjected to wear in a vacuum. *J Less-Common Met* 67(2):437–441
1009. Shatynski SR (1979) The thermochemistry of transition metal carbides. *Oxid Met* 13(2):105–118
1010. Mozhzhukhin EI, Kondratev NN (1982) Issledovanie protsessov tverdogaznogo spekaniya karbidov titana, tsirkoniya i gafniya (Study of the processes of solid-phase sintering of titanium, zirconium and hafnium carbides). *Izv Vyssh Uchebn Zaved Chern Metall* (3):12–15 (in Russian)
1011. Nowotny H, Rogl P, Schuster JC (1982) Structural chemistry of complex carbides and related compounds. *J Solid State Chem* 44(1):126–133
1012. Lavrenko VA, Neshpor VS, Pugach ÉA, Shvaiko VV, Ordanyan SS (1983) High-temperature oxidation of a ZrC-ZrB₂ alloy of eutectic composition. *Powder Metall Met Ceram* 22(3):211–214
1013. Lakiza SN (1985) Interaction analysis of systems involving refractory compounds by means of DTA method. *Thermochim Acta* 93:577–580
1014. Ogawa T, Ikawa T (1986) Reactions of Pd with SiC and ZrC. *High Temp Sci* 22(3):179–193
1015. Zambetakis T, Guille JL, Willer B, Daire M (1987) Mechanical properties of pressure-sintered Al₂O₃-ZrC composites. *J Mater Sci* 22(3):1135–1140
1016. Zhilyaev VA, Askarova LKh (1987) Oxidation of zirconium carbide by nickel oxide. *Inorg Mater* 23(5):706–710
1017. Kats SM, Basalaeva TS, Bogin VN, Akimova KP (1987) Sintering behaviour of multilayer ZrO₂/ZrC composites. *Powder Metall Met Ceram* 26(12):961–965
1018. Min-Haga E, Scott WD (1988) Sintering and mechanical properties of ZrC-ZrO₂ composites. *J Mater Sci* 23(8):2865–2870
1019. Arai Y, Ohmichi T, Fukushima S, Handa M (1989) Thermal conductivity of near-stoichiometric (U,Pu,Zr)C solid solutions. *J Nucl Mater* 168:137–143
1020. Knotek O, Barimani A (1989) On spinodal decomposition in magnetron-sputtered (Ti,Zr) nitride and carbide thin films. *Thin Solid Films* 174:51–56
1021. Pellacio D, El-Genk MS, Butt DP (1993) Review of nuclear thermal propulsion carbide reactor fuel corrosion and exhibit. Report LA-UR-93-2174, Contract W-7405-ENG-36. Los Alamos Scientific Laboratory, New Mexico, pp. 1–15
1022. Pellacio D, El-Genk MS (1994) A review of nuclear thermal propulsion carbide fuel corrosion and key issues. Final report NASA-CR-197533, Contracts NAG3-1346 and NGT-40019. University of New Mexico, Albuquerque, pp. 1–58
1023. Terada O, Saito M, Suzuki H (1993) The cause of formation of pores in titanium carbide based cermet with the addition of zirconium carbide. *J Jpn Soc Powder Metall* 40(11):1131–1135 (in Japanese)
1024. Steinmeyer PA, Olson DL, Edwards GR, Matlock DK (1981) Review on corrosion phenomena in molten lithium. *Rev Coat Corros* 4(4):349–434
1025. Sangiorgi R (1994) Corrosion of ceramics by liquid metals. In: Nickel KG (ed) *Corrosion of advanced ceramics*. Springer, Kluwer Academic, Dordrecht, pp. 261–284
1026. Geirmaert G (1975) Ceramiques – metaux liquides. Compatibilites et angles de mouillages. (Ceramics – liquid metals. Compatibilities and angles of wetting) *Bull Soc Fr Ceram* (106):7–50 (in French)
1027. Preiss H, Berger L-M, Szulzewsky K (1996) Thermal treatment of binary carbonaceous/zirconia gels and formation of Zr(C,O,N) solid solutions. *Carbon* 34(1):109–119
1028. Maitre A, Lefort P (1997) Solid state reaction of zirconia with carbon. *Solid State Ionics* 104:109–122

1029. Rempel AA (1996) Atomic and vacancy ordering in nonstoichiometric carbides. *Phys Usp* 39(1):31–56
1030. Bykov AI, Gridneva IV, Makarenko GN, Timofeeva II, Fedorus VB, Chugunova SI (1998) Interactions of boron carbide with titanium and zirconium carbide under pressure. *Powder Metall Met Ceram* 37(1–2):45–47
1031. Ozawa K, Noda T, Nakane T, Yamazaki M, Edamoto K, Otani S (1999) Photoemission study of K adsorption on ZrC (111). *Surf Sci* 433–435:700–704
1032. Ordanyan SS, Avgustinik AI, Vigdergauz VS (1966) Stroenie splavov sistemy Zr-C-Nb (The structure of alloys of the Zr-C-Nb system). *Zh Prikl Khim* 39(2):312–317 (in Russian)
1033. Ordanyan SS (1975) Reactions of rhenium and other refractory metals with some metal-like compounds. *Powder Metall Met Ceram* 14(2):125–129
1034. Fedorov TV, Popova NM, Gladyshevskii EI (1965) Ternary Hf-Nb-C and Zr-Nb-C and Ti-Nb-C systems. *Russ Metall* (3):72–76 (in Russian)
1035. Druzhinin II, Zakharov AM, Novikov II (1972) Fazovye ravovesiya v niobievom uglu sistem Nb-Zr-C i Nb-Ti-C (Phase equilibria in the niobium-rich corner of the Nb-Zr-C and Nb-Ti-C system). *Izv Vyssh Uchebn Zaved Tsvet Metall* (1):118–121 (in Russian)
1036. Emelyanov VS, Godin YuG, Suchkov II, Yastrebkov AA (1979) Issledovanie splavov sistemy Zr-Nb-C (A study of alloys of the Zr-Nb-C system). In: Emelyanov VS, Yevstyukhin AI (eds) *Metallurgiya i metallovedenie chistykh metallov* (Metallurgy and metallography of pure metals), Vol. 6. Atomizdat, Moscow, pp. 92–100 (in Russian)
1037. Zakharov AM, Savitskii EM (1967) Investigation of molybdenum-rich corner of Mo-Zr-C phase diagram. *Russ Metall* (6):101–107
1038. Zakharov AM, Parshikov VG, Novikov II (1970) Investigation of Mo-Zr-C system. *Russ Metall* (6):130–132
1039. Zakharov AM, Novikov II, Parshikov VG (1971) Examination of molybdenum-rich Mo-Ti-Zr-C alloys. *Russ Metall* (4):169–171
1040. Zakharov AM, Kurganov GV, Parshikov VG, Golubev MYu (1981) Phase diagram of the Mo-Zr-Hf-C system. *Russ Metall* (4):215–219
1041. Strashinskaya LV, Stashevskaya IA (1974) An X-ray diffraction study of the reactions of molybdenum and tungsten with disperse inclusions. *Powder Metall Met Ceram* 13(5):420–422
1042. Zakharov AM, Savitskii EM (1969) Vzaimodeistvie molibdena s metallami IVa grupy i ugleterodom (Interaction of molybdenum with the metals of IVa group and carbon). *Izv Vyssh Uchebn Zaved Tsvet Metall* (6):96–103 (in Russian)
1043. Ordanyan SS, Avgustinik AI, Vigdergauz VS (1965) Diagramma sostoyaniya ZrC-Mo (ZrC-Mo phase diagram). In: Budnikov PP (ed) *Issledovaniya v oblasti khimii silikatov i okislov* (Studies in the field of chemistry of silicates and oxides). Nauka, Moscow, Leningrad (in Russian)
1044. Kobashi M, Harata M, Choh T (1993) Dispersion behaviour of several carbides into molten aluminium and mechanical properties of TiC/Al composite. *J Jpn Inst Light Met* 43(10):522–527 (in Japanese)
1045. Gogotsi YuG (1994) Review. Particulate silicon nitride – based composites. *J Mater Sci* 29:2541–2556
1046. Vilks YuN, Ordanyan SS, Avgustinik AI (1972) O vozmozhnom stroenii izotermicheskikh razrezov sistemy Zr-W-C pri 2200 i 2600 °C (On the probable structure of isothermal sections of the Zr-W-C system at 2200 and 2600 °C). *Izv AN SSSR Neorg Mater* 8(7):1245–1248 (in Russian)
1047. Vilks YuN, Danisina IN, Omelchenko YuA (1973) Vzaimodeistvie reniya s karbidom tsirkoniya pri vysokikh temperaturakh (Interaction of rhenium with zirconium carbide at high temperatures). *Izv AN SSSR Neorg Mater* 9(1):145–148 (in Russian)
1048. Gomofov LI, Lyutina ÉM, Makhova VA, Ivanov OS (1971) The composition of the carbide phase in alloys of uranium with zirconium and niobium. *Atom Energy* 31(3):1013–1015

1049. Evtushok TM, Burykina AL (1968) Issledovanie vzaimodeistviya grafita s tugoplavkimi soedineniyami i zhidkimi metallami (A study of the interaction of graphite with refractory compounds and liquid metals). In: Samsonov GV (ed) *Vzaimodeistvie materialov vysokotemperaturnogo naznacheniya so sredoi* (Interaction of high-temperature appropriated materials with environment). Naukova Dumka, Kyiv, pp. 221–228 (in Russian)
1050. Li F, Huang X (2018) Preparation of highly porous ZrB₂/ZrC/SiC composite monoliths using liquid precursors via direct drying process. *J Eur Ceram Soc* 38:1103–1111
1051. Karpinos DM, Fedorenko VK, Listovnichaya SP (1976) Primenenie zashchitnykh pokrytii v kompozitsionnykh materialakh na osnove nikhroma (Application of protective coatings in the composite materials based on nichrome). In: Ageev NV (ed) *Voloknistye i dispersno-uprochnennye kompozitsionnye materialy* (Fibrous and particulate-reinforced composite materials). Nauka, Moscow, pp. 52–57 (in Russian)
1052. Ozawa K, Noda T, Nakane T, Yamazaki M, Edamoto K, Tanaka S, Otani S (2000) Potassium adsorption on the polar ZrC (111) surface: photoemission spectroscopy study. *Surf Sci* 446:229–240
1053. Gnesin GG, Gerbits EI, Shipilova LA, Petrovskii VYa, Kasyanenko AA (1990) A Si₃N₄-ZrC resistive composite. I. Conductivity concentration dependence. *Powder Metall Met Ceram* 29(4):325–328
1054. Gnesin GG, Gerbits EI, Shipilova LA, Petrovskii VYa, Kasyanenko AA (1990) A Si₃N₄-ZrC resistive composite. II. Temperature dependence of electrical conductivity. *Powder Metall Met Ceram* 29(6):483–486
1055. Branagan DJ, Kramer MJ, McCallum RW (1996) Transition metal carbide formation in the Nd₂Fe₁₄B system and potential as alloying additions. *J Alloys Compd* 244:27–39
1056. Gusev AI (2003) Analysis of surface segregation and solid-phase decomposition of substitutional solid solutions. *Dokl Phys Chem* 392(1–3):235–239
1057. McDeavitt SM, Billings GW, Indacochea JE (2002) High temperature interaction behavior at liquid metal – ceramic interfaces. *J Mater Eng Performance* 11(4):392–401
1058. Suzuki T, Matsumoto H, Nomura N, Hanada S (2002) Microstructures and fracture toughness of directionally solidified Mo-ZrC eutectic composites. *Sci Technol Adv Mater* 3:137–143
1059. Pisarenko VA, Rakitskii AN, Samelyuk AV (2003) Diffusion interaction in fiber-reinforced composites of the chromium alloy – silicon carbide system. *Powder Metall Met Ceram* 42(5–6):297–301
1060. Chen C-S, Liu C-P (2005) Characterization of sputtered nano-crystalline zirconium carbide as a diffusion barrier for Cu metallization. *J Electron Mater* 34(11):1408–1413
1061. Umanskii YaS, Fadeeva VI (1965) Diffuznoe rasseyanie rentgenovskikh luchei tverdykh rastvorom HfC-ZrC (Diffuse X-ray scattering of the HfC-ZrC solid solution). *Fiz Met Metalloved* 20(5):719–722 (in Russian)
1062. Gusev AI (2006) Short-range order and diffuse scattering in nonstoichiometric compounds. *Phys Usp* 49(7):693–718
1063. Zhilyaev VA, Patrakov EI (2006) Mekhanizm zhidkofaznogo vzaimodeistviya dvoynykh karbidov (Ti,Me)C s nikelom (The mechanism of liquid-phase interaction of double carbides (Ti,Me)C with nickel). *Konstruk Kompoz Mater* (4):199–201 (in Russian)
1064. Zhilyaev VA, Patrakov EI (2015) Regularities of the contact interaction of double carbides (Ti_{1-n}Me_n)C with nickel. *Russ J Non-Ferr Met* 56(3):329–332
1065. Zhilyaev VA (2015) Regularities of reactions of group IV, V transition metal carbides with nickel. *Russ J Non-Ferr Met* 56(5):575–579
1066. Zhilyaev VA, Patrakov EI (2006) Osobennosti vzaimodeistviya dvoynykh karbidov (Ti,Me)C s Ni-Mo raspalvom (The particularities of the interaction of double carbides (Ti,Me)C with Ni-Mo melt). *Konstruk Kompoz Mater* (4):196–199 (in Russian)
1067. Zhilyaev VA (2006) Zakonomernosti tverdogaznykh reaktsii s uchastiem tugoplavkikh faz vnedreniya (The regularities of solid-phase reactions with the participation of refractory interstitial phases). *Konstruk Kompoz Mater* (4):192–196 (in Russian)
1068. Licheri R, Orrù R, Musa C, Cao G (2008) Combination of SHS and SPS techniques for fabrication of fully dense ZrB₂-ZrC-SiC composites. *Mater Lett* 62:432–435

1069. Kovalskii AE, Vrzheschch EYa (1959) Vzaimnaya rastvorimost izomorfnykh tugoplavkikh karbidov s kubicheskoj kristallicheskoj reshetkoj (Mutual solubility of isomorphic high-melting point carbides with cubic crystal lattice). In: Bashkurov SI (ed) Tverdye splavy. Sbornik trudov VNIITS. (Hard alloys. Proc. of VNIITS). Metallurgizdat, Moscow, pp. 305–319 (in Russian)
1070. Markström A, Andersson D, Frisk K (2008) Combined *ab-initio* and experimental assessment of $A_{1-x}B_xC$ mixed carbides. *Calphad* 32(4):615–623
1071. Song MS, Huang B, Zhang MX, Li JG (2008) Formation and growth mechanism of ZrC hexagonal platelets synthesized by self-propagating reaction. *J Cryst Growth* 310(18):4290–4294
1072. Lin ZJ, He LF, Wang JY, Li MS, Bao YW, Zhou YC (2008) Atomic-scale microstructure and elastic properties of quaternary Zr-Al-Si-C ceramics. *Acta Mater* 56:2022–2031
1073. Adjaoud O, Steinle-Neumann G, Burton BP, Van de Walle A (2009) First principles phase diagram calculations for the HfC-TiC, ZrC-TiC and HfC-ZrC solid solutions. *Phys Rev B* 80(13):134112 (7 pp.)
1074. Markström A, Frisk K (2009) Experimental and thermodynamic evaluation of the miscibility gaps in MC carbides for the C-Co-Ti-V-W-Zr system. *Calphad* 33(3):530–538
1075. Gendre M, Maître A, Trolliard G (2010) A study of the densification mechanisms during spark plasma sintering of zirconium (oxy-)carbide powders. *Acta Mater* 58:2598–2609
1076. Jung W-S, Chung S-H (2010) *Ab initio* calculation of interfacial energies between transition metal carbides and fcc iron. *Model Simul Mater Sci Eng* 18(7):075008
1077. Goutier F, Glandut N, Lefort P (2011) Purification of hot-pressed ZrCO into ZrC by a laser treatment. *J Mater Sci* 46(21):6794–6800
1078. Wang X-G, Liu J-X, Kan Y-M, Zhang G-J (2012) Effect of solid solution on densification of hot-pressed ZrC ceramics with MC (M = V, Nb, Ta) additions. *J Eur Ceram Soc* 32:1795–1802
1079. Cheng EJ, Katsui H, Goto T (2016) ZrB₂-ZrC_xN_{1-x} eutectic composites produced by melt solidification. *J Am Ceram Soc* 99(2):667–673
1080. Hu W, Liu S, Wen B, Xiang J, Wen F, Xu B, He J, Yu D, Tian Y, Liu Z (2013) {111}-specific twinning structures in nonstoichiometric ZrC_{0.6} with ordered carbon vacancies. *J Appl Crystallogr* 46:43–47
1081. Sorrell CC, Beratan HR, Bradt RC, Stubican VS (1984) Directional solidification of (Ti,Zr) carbides – (Ti,Zr) diboride eutectics. *J Am Ceram Soc* 67(3):190–194
1082. Zhou Y-C, He L-F, Lin Z-J, Wang J-Y (2013) Synthesis and structure-property relationships of a new family of layered carbides in Zr-Al(Si)-C and Hf-Al(Si)-C systems. *J Eur Ceram Soc* 33:2831–2865
1083. Aizawa T, Suehara S, Otani S (2014) Silicene on zirconium carbide (111). *J Phys Chem C* 118:23049–23057
1084. Borgh I, Hedström P, Blomqvist A, Ågren J, Odqvist J (2014) Synthesis and phase separation of (Ti,Zr)C. *Acta Mater* 66:209–218
1085. Chakrabarti T, Rangaraj L, Jayaram V (2014) Effect of zirconium on the densification of reactively hot-pressed zirconium carbide. *J Am Ceram Soc* 97(10):3092–3102
1086. Guo S (2014) Densification, microstructure, elastic and mechanical properties of reactive hot-pressed ZrB₂-ZrC-Zr cermets. *J Eur Ceram Soc* 34:621–632
1087. Li Y, Katsui H, Goto T (2014) Consolidation of titanium carbide with zirconium carbide by spark plasma sintering. *Key Eng Mater* 616:52–55
1088. Li Y, Katsui H, Goto T (2015) Spark plasma sintering of TiC-ZrC composites. *Ceram Int* 41(5B):7103–7108
1089. Zou Z, Fu L, Song X, Zhang Y, Liu Z (2014) Carbide-forming groups IVB-VIB metals: a new territory in the periodic table for CVD growth of graphene. *Nano Lett* 14:3832–3839
1090. Lapauw T, Halim J, Lu J, Cabioch T, Hultman L, Barsoum MW, Lambrinou K, Vleugels J (2016) Synthesis of the novel Zr₃AlC₂ MAX phase. *J Eur Ceram Soc* 36(3):943–947
1091. Lapauw T, Lambrinou K, Cabioch T, Halim J, Lu J, Pesach A, Rivin O, Ozeri O, Caspi EN, Hultman L, Eklund P, Rosen J, Barsoum MW, Vleugels J (2016) Synthesis of the new MAX phase Zr₂AlC. *J Eur Ceram Soc* 36(8):1874–1853

1092. Ma T, Hedström P, Ström V, Masood A, Borgh I, Blomqvist A, Odqvist J (2015) Self-organizing nanostructured lamellar (Ti,Zr)C – a superhard mixed carbide. *Int J Refract Met Hard Mater* 51:25–28
1093. Zhou P, Peng Y, Du Y, Wang S, Wen G (2015) Thermodynamic modeling of the C-W-Zr system. *Int J Refract Met Hard Mater* 50:274–281
1094. Buchner H, Gutjahr MA, Gross K, Beccu KD (1973) Über das Verhalten unterstöchiometrischer Übergangsmetallcarbide als Katalysatoren in Dehydrierungsprozessen (On the behaviour of under-stoichiometric transition metal carbides as catalysts in dehydrogenation processes). *Monatsh Chem* 104(1):160–165 (in German)
1095. Rafal AN (1983) Kinetika reaktsii s uchastiem vodoroda na beskislorodnykh tugoplavlykh soedinenii perekhodnykh metallov IV-VI grupp periodicheskoi sistemy (Kinetics of reactions involving hydrogen on oxygen-free refractory compounds of periodic system IV-VI groups transition metals). PhD thesis, Institute for Problems of Materials Science, Ukrainian SSR Academy of Sciences, Kyiv (in Russian)
1096. Samsonov GV, Zhidkova TG, Klimak ZA (1975) O kataliticheskikh svoistvakh karbidov perekhodnykh metallov (On the catalytic properties of transition metal carbides). In: Samsonov GV (ed) *Vysokotemperaturnye karbidy* (High-temperature carbides). Naukova Dumka, Kyiv, pp. 76–81 (in Russian)
1097. Lavrenko VA (1973) Rekombinatsiya atomov vodoroda na poverkhnostyakh tverdykh tel (The recombination of hydrogen atoms on the surfaces of solid bodies). *Naukova Dumka, Kyiv* (in Russian)
1098. Ilchenko NI, Chebotareva NP, Shvidak NV (1976) Oxidation of ammonia on transition metal carbides. *React Kinet Catal Lett* 4(3):343–349
1099. Chebotareva NP, Ilchenko NI, Golodets GI (1976) Kinetics and mechanism of oxidation of hydrogen on carbides of transition metals of groups IV-VI. *Theor Exp Chem* 12(2):154–162
1100. Samsonov GV, Kharlamov AI (1975) Catalytic properties of refractory compound powders (survey). *Powder Metall Met Ceram* 14(9):699–707
1101. Nechiporenko NN, Vasilenko II, Bugai PM (1972) Kataliticheskoe razlozhenie perekisi vodoroda na nekotorykh tugoplavlykh soedineniyakh (Catalytic decomposition of hydrogen peroxide on some refractory compounds). *Ukr Khim Zh* 38(6):547–550 (in Russian)
1102. Kharlamov AI, Rafal AN, Fedorus VB (1983) Katalychnye okyslennya vodnyu na metallopodobnykh karbidakh i nitrydakh z riznimi metal-nemetal spivvidnoshennyamy (Catalytic oxidation of hydrogen on metal-like carbides and nitrides with various metal-nonmetal ratios). *Dopov Akad Nauk Ukr RSR Ser B Geol Khim Biol Nauki* (2):47–51 (in Ukrainian)
1103. Kharlamov AI (1980) The nature of the catalytic action of metal-like compounds of *d*-metals. *Kinet Catal* 21(1):197–202
1104. Kharlamov AI, Kosolapova TYa, Rafal AN, Kirillova NV (1980) Catalytic activity of metal-like carbides in oxidation of carbon monoxide. *Kinet Catal* 21(3):534–539
1105. Kharlamov AI, Kirillova NV, Yatsimirskii VK (1980) Kinetics of CO oxidation over metal-like carbides. *React Kinet Catal Lett* 13(2):105–110
1106. Ilchenko NI, Dolgikh LYa (1985) Factors determining the activities of different chemical types of catalysts in the oxidation of hydrogen. 4. Causes for differences in activities of optimum metallic, carbide and oxide catalysts. *Kinet Catal* 26(4):779–784
1107. Svintsova LG, Shimanovskaya VV, Ilchenko NI, Golodets GI (1982) Oxidation of carbon monoxide on transition metal carbides. *Kinet Catal* 23(2):332–335
1108. Ilchenko NI, Malyshev EM, Pankratev YuD, Golodets GI (1978) Bonding energy of oxygen to surface of transition metal carbides and their catalytic activity in hydrogen and ammonia oxidation reactions. *Kinet Catal* 19(3):505–509
1109. Ilchenko NI (1977) Oxidative catalysis on transition metal carbides. *Kinet Catal* 18(1):126–134
1110. Kharlamov AI, Kirillova NV, Yatsimirskii VK (1981) The catalytic properties of transition element carbides and nitrides in the oxidation of carbon monoxide. *Theor Exp Chem* 17(2):168–179

1111. Ilchenko NI, Pyatnitsky YuI (1996) Carbides of transition metals as catalysts for oxidation reactions. In: Oyama ST (ed) *The chemistry of transition metal carbides and nitrides*. Chapman & Hall, London, Glasgow, pp. 311–327
1112. Posada-Perez S, Vines F, Rodriguez JA, Illas F (2015) Fundamentals of methanol synthesis on metal carbide based catalysts: activation of CO₂ and H₂. *Top Catal* 58(2–3):159–173
1113. Kunkel C, Vines F, Illas F (2016) Transition metal carbides as novel materials for CO₂ capture, storage and activation. *Energy Environ Sci* 9(1):141–144
1114. Kharlamov AI, Kirillova NV (1983) Catalytic properties of powdered refractory compounds of transition elements. Carbides and nitrides – a review. *Powder Metall Met Ceram* 22(2):123–134
1115. Ledoux MJ, Pham-Huu C (1992) High specific area carbides of silicon and transition metals for catalysis. *Catal Today* 15(2):263–284
1116. Raevskaya LN, Pavlovsky FG, Kolotusha BI, Ilchenko NI (1991) Okislitel'naya kondensatsiya metana s uchastiem kisloroda i zakisi azota na karbidakh perekhodnykh metallov (Oxidative condensation of methane with participation of oxygen and nitrous oxide on carbides of transition metals). *Ukr Khim Zh* 57(10):1080–1084 (in Russian)
1117. Oyama ST (1992) Preparation and catalytic properties of transition metal carbides and nitrides. *Catal Today* 15(2):179–200
1118. Ledoux MJ, Pham-Huu C, Chianelli RR (1996) Catalysis with carbides. *Curr Opin Solid State Mater Sci* 1(1):96–100
1119. Regmi YN, Waetzig GR, Duffee KD, Schmuecker SM, Thode JM, Leonard BM (2015) Carbides of group IVA, VA and VIA transition metals as alternative HER and ORR catalysts and support materials. *J Mater Chem A* 3(18):10085–10091
1120. Chen W-F, Muckerman JT, Fujita E (2013) Recent developments in transition metal carbides and nitrides as hydrogen evolution electrocatalysts. *Chem Comm* 49(79):8896–8909
1121. Ham DJ, Lee JS (2009) Transition metal carbides and nitrides as electrode materials for low temperature fuel cells. *Energies* 2:873–899. <https://doi.org/10.3390/en20400873>
1122. Stottlemeyer AL, Kelly TG, Meng Q, Chen JG (2012) Reactions of oxygen-containing molecules on transition metal carbides: surface science insight into potential applications in catalysis and electrocatalysis. *Surf Sci Rep* 67:201–232
1123. Semenov-Kobzar AA, Obolonchik VA, Akinina ZS (1969) Stability of transition metal carbides under anodic polarization conditions. *Powder Metall Met Ceram* 8(5):399–402
1124. Brynza AP, Khmelovskaya SA, Fedorus VB, Silina ZR (1976) Issledovanie khimicheskoi stoikosti i elektrokhimicheskogo povedeniya karbidov (A study of the chemical resistance and electrochemical behaviour of carbides). In: Samsonov GV, Kosolapova TYa, Gnesin GG, Fedorus VB, Domasevich LG (eds) *Karbidy i splavy na ikh osnove* (Carbides and alloys based on them). *Naukova Dumka, Kyiv*, pp. 199–208 (in Russian)
1125. Abdulin IA (1993) Vlyanie rezhimov elektroliza na formirovanie i strukturu kompozitsionnogo elektroliticheskogo pokrytiya (Influence of electrolysis regimes on composite electroplate generation and structure). *Elektron Obrab Mater* (5):75–76 (in Russian)
1126. Nikishanov VV, Shulga AV (1984) Electrochemical isolation of carbide phases from tungsten alloys. *Sov Electrochem* 20(6):915–918
1127. Shulga AV, Nikishanov VV, Ofitserov AV (1987) Electrochemical isolation of intermetallic and carbide phases from nickel-base alloys. *Sov Electrochem* 23(7):915–918
1128. Coughanowr CA, Dissaux BA, Muller RH, Tobias CW (1986) Electrochemical machining of refractory materials. *J Appl Electrochem* 16(3):345–356
1129. Horita T, Sakai N, Kawada T, Yokokawa H, Dokiya M (1995) Investigation of anodes for direct oxidation of carbon in solid oxide fuel cells. *J Electrochem Soc* 142(8):2621–2624
1130. Bourg S, Péron F, Lacquement J (2007) The evaluation of the pyrochemistry for the treatment of Gen IV nuclear fuels – inert matrix chlorination studies in the gas phase or molten chloride salts. *J Nucl Mater* 360:58–63
1131. Boosz H-J (1956) Die Beständigkeit von Hartstoffen gegen Gase (The resistance of hard materials to gases). *Metall* 10(3/4):130–136 (in German)
1132. Dash RK, Yushin G, Gogotsi Y (2005) Synthesis, structure and porosity analysis of microporous and mesoporous carbon derived from zirconium carbide. *Micropor Mesopor Mater* 86:50–57

1133. Orekhov VP, Seryakov GV, Zelikman AN, Starostina TM, Khazanova TI, Petrova KV, Sverchkov PM (1969) Kinetika khlorirovaniya briketov karbida tsirkoniya (Kinetics of chlorination of zirconium carbide briquets). *Zh Prikl Khim* 42(2):251–260 (in Russian)
1134. Kuriakose AK, Margrave JL (1964) Kinetics of the reactions of elemental fluorine with zirconium carbide and zirconium diboride at high temperatures. *J Phys Chem* 68(2):290–295
1135. Babkin OE, Ivakhnyuk GK, Fedorov NF (1984) Porous structure of carbon adsorbents made from zirconium carbide. *J Appl Chem USSR* 57(3):463–467
1136. Yushin G, Nikitin A, Gogotsi Y (2006) Carbide-derived carbon. In: Gogotsi Y (ed) *Nanomaterials handbook*. CRC Press, Boca Raton, London, New York, pp. 240–283
1137. Presser V, Heon M, Gogotsi Y (2011) Carbide-derived carbon – from porous networks to nanotubes and graphene. *Adv Funct Mater* 21(5):810–833
1138. Samsonov GV, Antonova MM, Morozov VV (1970) Ternary systems Me-C-H and Me-N-H. *Powder Metall Met Ceram* 9(4):318–327
1139. Khodosov EF, Andrievskii RA (1967) Studying nuclear magnetic resonance spectra of zirconium and yttrium hydrides. *Powder Metall Met Ceram* 6(8):649–653
1140. Aleksanyan AG, Aghajanyan NN, Dolukhanyan SK, Mnatsakanyan NL, Harutyunyan KhS, Hayrapetyan VS (2002) Thermal-radiation synthesis of zirconium hydridonitrides and carbohydrides. *J Alloys Compd* 330–332:559–563
1141. Samsonov GV, Lavrenko VA, Neshpor VS, Okhremchuk LN, Podchernyaeva IA, Fomenko VS, Chekhovskii AI (1972) Reaction of hydrogen atoms with the surface of yttrium containing zirconium carbide. *Powder Metall Met Ceram* 14(9):751–752
1142. Goretzki H, Bittner H, Nowotny H (1964) Der Einfluß von Wasserstoff auf Titancarbid (The influence of hydrogen on titanium carbide). *Monatsh Chem* 95(6):1521–1526 (in German)
1143. Goretzki H (1967) Neutron diffraction studies on titanium-carbon and zirconium-carbon alloys. *Phys Stat Sol* 20(2):K141–K143
1144. Yvon K, Nowotny H, Kieffer R (1967) Zur Kristallstruktur der Carbohydride von Übergangsmetallen (The crystal structure of carbohydrides of transition metals). *Monatsh Chem* 98(6):2164–2172 (in German)
1145. Aizawa T, Hayami W, Souda R, Otani S, Ishizawa Y (1997) Hydrogen adsorption on transition metal carbide (111) surfaces. *Surf Sci* 381:157–164
1146. Tuffias RH, Duffy AJ, Arrieta VM, Abrams WM, Benander RE (1997) Materials and fabrication processes for operation in hot hydrogen. *AIP Conf Proc* 387:1613–1618
1147. Mireles OR, Anghaie S, Cunningham B, Dooies B (2009) Material performance evaluation of TaC, WC and ZrC under prototypic nuclear thermal propulsion hot hydrogen environment. In: Proc. 3rd topical meeting on nuclear and emerging technologies for space, NETC 2009, Atlanta, Georgia, 14–19 June 2009. American Nuclear Society, Illinois, pp. 99–106
1148. Krivko-Krasko SV, Parshin NYa, Podladchikov YuN, Popov EB, Fedorov ÉM (1993) Raschetno-teoreticheskoe obosnovanie rabotosposobnosti teplovdyeluyushchikh sborok reaktorov yadernykh raketnykh dvigatelei (Calculation and theoretical basis of efficiency of fuel assemblies of nuclear rocket engine reactors). Scientific Research Institute of Industrial Association “Luch”, Podolsk, Moscow Region (in Russian)
1149. Demyanko JG, Konukhov GA, Koroteev AS, Kuzmin EP, Pavelev AA (2001) Yadernye raketnye dvigateli (Nuclear rocket engines). Norm-Inform, Moscow (in Russian)
1150. Zhilyaev VA (2012) Vzaimosvyaz sostava, struktury i khimicheskikh svoystv tugoplavkikh faz vnedreniya. I. Zakonomernosti reaktsii tugoplavkikh faz vnedreniya s tverdymi reagentami (Interrelation of composition, structure and chemical properties of refractory interstitial phases. I. Regularities of reactions of refractory interstitial phases with solid reagents). *Vestn Perm Nats Issl Politekh Univ Mashin Mater* 14(3):7–21 (in Russian)

1151. Zhilyaev VA (2012) Vzaimosvyaz sostava, struktury i khimicheskikh svoystv tugoplavkikh faz vnedreniya. II. Priroda khimicheskoi i elektrokhimicheskoi aktivnosti tugoplavkikh faz vnedreniya v mineralnykh kislotakh (Interrelation of composition, structure and chemical properties of refractory interstitial phases. II. The nature of chemical and electrochemical activity of refractory interstitial phases in mineral acids). *Vestn Perm Nats Issl Politekh Univ Mashin Mater* 14(4):61–72 (in Russian)
1152. Zhilyaev VA (2013) Vzaimosvyaz sostava, struktury i khimicheskikh svoystv tugoplavkikh faz vnedreniya. III. Zakonomernosti proyavleniya khimicheskoi aktivnosti tugoplavkikh faz vnedreniya v vozdušno-vakuumnykh i gazovykh sredakh (Interrelation of composition, structure and chemical properties of refractory interstitial phases. III. The regularities of manifestation of refractory interstitial phases chemical activity in air-vacuum and gaseous media). *Vestn Perm Nats Issl Politekh Univ Mashin Mater* 15(1):7–19 (in Russian)
1153. Kieffer R, Nowotny H, Eitmayer P, Freudhofmeier M (1970) Über die Beständigkeit von Übergangsmetallcarbiden gegen Stickstoff bis zu 300 at (On the stability of transition metal carbides in nitrogen up to 300 atm). *Monatsh Chem* 101(1):65–82 (in German)
1154. Gendre M (2010) Approche des mécanismes de synthèse par carboréduction et de frittage “flash” de l’oxycarbure de zirconium (Approach to the synthesis mechanisms of carboreduction and spark plasma sintering of zirconium oxycarbide). PhD thesis, Université de Limoges (in French)
1155. Kyō B, Uchida K, Imoto S (1973) Hydrolysis of zirconium nitrides and carbides. *J Jpn Inst Met Mater* 37(4):411–416 (in Japanese)
1156. Uchida K, Imoto S, Kyō B (1977) Hydrolysis of titanium and zirconium carbonitrides. *Trans Jpn Inst Met* 18(10):727–734
1157. Yoshimura M, Hayakawa M, Sōmiya S (1988) Reactions between ZrC and ZrN powder and high-temperature – high-pressure water. *J Ceram Soc Jpn* 96(2):193–200 (in Japanese)
1158. Kotlyar EE, Nazarchuk TN (1966) O nekotorykh khimicheskikh svoystvakh karbidov perekhodnykh metallov IV, V grupp periodicheskoi sistemy (On certain chemical properties of the transition metal carbides of IV, V groups of the periodic table). *Izv AN SSSR Neorg Mater* 2(10):1778–1780 (in Russian)
1159. Kuptsov SG, Vlasov VG, Beketov AR, Shabalin IL, Fedorenko OV, Pykhiteev YuP (1975) Mekhanizm nizkotemperaturnogo okisleniya karbida tsirkoniya (Mechanism of low-temperature oxidation of zirconium carbide). In: Prodan AE (ed) *Kinetika i mekhanizm reaktsii v tverdykh telakh* (Kinetics and mechanism of reactions in solid bodies). Lenin Byelorussian State University, Minsk, pp. 182–184 (in Russian)
1160. Berkowitz-Mattuck JB (1967) High-temperature oxidation. IV. Zirconium and hafnium carbides. *J Electrochem Soc* 114(10):1030–1033
1161. Voitovich RF, Pugach ÉA (1973) High-temperature oxidation of ZrC and HfC. *Powder Metall Met Ceram* 12(11):916–920
1162. Voitovich RF, Pugach ÉA (1975) Vysokotemperaturnoe okislenie karbidov perekhodnykh metallov IV-VI grupp (High-temperature oxidation of transition metals IV-VI groups carbides). In: Samsonov GV (ed) *Vysokotemperaturnye karbidy* (High-temperature carbides). Naukova Dumka, Kyiv, pp. 143–156 (in Russian)
1163. Voitovich RF, Pugach ÉA (1976) Nekotorye osobennosti protsessa okisleniya karbidov metallov IV-VI grupp (The certain features of the oxidation process of metals IV-VI groups carbides). In: Samsonov GV, Kosolapova TYa, Gnesin GG, Fedorus VB, Domasevich LG (eds) *Karbidy i splavy na ikh osnove* (Carbides and alloys based on them). Naukova Dumka, Kyiv, pp. 233–234 (in Russian)
1164. Voitovich RF (1981) Okislenie karbidov i nitridov (Oxidation of carbides and nitrides). Naukova Dumka, Kyiv (in Russian)
1165. Stepanchuk AN, Trukhan SG, Shlyuko VYa (1975) The air oxidation resistance of fused titanium and zirconium carbides in their regions of homogeneity. *Refract Indust Ceram* 16(3–4):236–238
1166. Terekhova VA, Bragin NN (1982) Effect of crystalline structural defects on the chemical activity of zirconium carbide. *Inorg Mater* 18(3):330–335 (in Russian)

1167. Trefilov VI, Lavrenko VA, Tikush VL, Stegnii AI, Rogozinskaya AA, Timofeeva II, Shatokhin AM (1989) Oxidation of zirconium diboride and carbide in radiant heating. *Powder Metall Met Ceram* 28(1):61–63
1168. Shimada S, Ishii T (1990) Oxidation kinetics of zirconium carbide at relatively low temperatures. *J Am Ceram Soc* 73(10):2804–2808
1169. Shimada S, Nishisako M, Inagaki M, Yamamoto K (1995) Formation and microstructure of carbon-containing oxide scales by oxidation of single crystals of zirconium carbide. *J Am Ceram Soc* 78(1):41–48
1170. Shimada S, Inagaki M, Suzuki M (1996) Microstructural observation of the ZrC/ZrO₂ interface formed by oxidation of ZrC. *J Mater Res* 11(10):2594–2597
1171. Shimada S (1997) Microstructural observation of ZrO₂ scales formed by oxidation of ZrC single crystals with formation of carbon. *Solid State Ionics* 101–103(1):749–753
1172. Shimada S (1998) TEM observation of the ZrC/ZrO₂ interface formed by oxidation of ZrC single crystals. *J Mater Synth Process* 6(3):191–195
1173. Shimada S, Yoshimatsu M, Inagaki M, Otani S (1998) Formation and characterization of carbon at the ZrC/ZrO₂ interface by oxidation of ZrC single crystals. *Carbon* 36(7–8):1125–1131
1174. Shimada S (2001) Formation and mechanism of carbon-containing oxide scales by oxidation of carbides (ZrC, HfC, TiC). *Mater Sci Forum* 369–372(1):377–384
1175. Shimada S (2001) Oxidation and mechanism of single crystal carbides with formation of carbon. *J Ceram Soc Jpn* 109(3):S33–S42
1176. Gozzi D, Cascino G, Loreti S, Minarini C, Shimada S (2001) Weak interaction of oxygen with some refractory carbides. *J Electrochem Soc* 148(4):J15–J24
1177. Shimada S (2001) Interfacial reaction on oxidation of carbides with formation of carbon. *Solid State Ionics* 141–142:99–104
1178. Shimada S (2002) A thermoanalytical study on the oxidation of ZrC and HfC powders with formation of carbon. *Solid State Ionics* 149(3–4):319–326
1179. Hu W, Tian Y, Liu Z (2014) Carbon vacancy ordered non-stoichiometric ZrC_{0.6}: synthesis, characterization and oxidation at low temperature. In: Khosrow-Pour M, Clarke S, Jennex ME, Becker A, Antiroiko A-V (eds) *Nanotechnology: concepts, methodologies, tools and applications*, Vol. 1–3. IGI Global, Hershey, Pennsylvania, pp. 667–689
1180. Bellucci A, Gozzi D, Kimura T, Noda T, Otani S (2005) Zirconia growth on zirconium carbide single crystals by oxidation. *Surf Coat Technol* 197(2–3):294–302
1181. Charpentier L, Balat-Pichelin M, Sciti D, Silvestroni L (2013) High-temperature oxidation of Zr- and Hf-carbides: influence of matrix and sintering additive. *J Eur Ceram Soc* 33(15–16):2867–2878
1182. Charpentier L, Balat-Pichelin M, Bêche E, Sciti D, Silvestroni L (2013) Microstructural characterization of ZrC-MoSi₂ composites oxidized in air at high temperatures. *Appl Surf Sci* 283:751–758
1183. Pierrat B, Balat-Pichelin M, Silvestroni L, Sciti D (2011) High-temperature oxidation of ZrC-20%MoSi₂ in air for future solar receivers. *Solar Energy Mater Solar Cells* 95(8):2228–2237
1184. Opila EJ, Jacobson NS (2013) Oxidation and corrosion of ceramics. In: Riedel R, Chen I-W (eds) *Ceramics science and technology*. Vol. 4 – Applications. Wiley-VCH, Weinheim, pp. 3–93
1185. Tamura K, Ogawa T, Fukuda K (1990) The oxidation behaviour of ZrC coating and powder studied by laser Raman spectroscopy and X-ray diffraction. *J Nucl Mater* 175(3):266–269
1186. Opeka MM, Talmy IG, Wuchina EJ, Zaykoski JA, Causey SJ (1999) Mechanical, thermal and oxidation properties of refractory hafnium and zirconium compounds. *J Eur Ceram Soc* 19(13–14):2405–2414
1187. Noda T, Yamazaki M, Ozawa K, Edamoto K, Otani S (2000) Oxygen adsorption on a ZrC (111) surface: angle-resolved photoemission study. *Surf Sci* 450:27–33

1188. Wu H, Li H-J, Fu Q-G, Yao D-J, Wang Y-J, Ma C, Wei J-F, Han Z-H (2011) Microstructures and ablation resistance of ZrC coating for SiC-coated carbon/carbon composites prepared by supersonic plasma spraying. *J Therm Spray Technol* 20(6):1286–1291
1189. Shimada T, Imamura K, Edamoto K, Orita H (2009) Electronic structures of the suboxide films formed on TiC(100) and ZrC(100) surfaces: density functional theory studies. *Surf Sci* 603:2340–2344
1190. Sun W, Xiong X, Huang B-Y, Li G-D, Zhang H-B, Chen Z-K, Zheng X-L (2009) ZrC ablation protective coating for carbon/carbon composites. *Carbon* 47:3368–3371
1191. Rao GAR, Venugopal V (1994) Kinetics and mechanism of the oxidation of ZrC. *J Alloys Compd* 206(2):237–242
1192. Hou X-M, Chou K-C (2011) Investigation of the effect of temperature and oxygen partial pressure on oxidation of zirconium carbide using different kinetics models. *J Alloys Compd* 509:2395–2400
1193. Bartlett RW, Wadsworth ME, Cutler IB (1963) Oxidation kinetics of zirconium carbide. *Trans Metall Soc AIME* 227(2):467–472
1194. Kuriakose AK, Margrave JL (1964) The oxidation kinetics of zirconium diboride and zirconium carbide at high temperatures. *J Electrochem Soc* 111(7):827–831
1195. Dufour LC, Simon J, Barret P (1967) Oxydation dechantillons pulverulents de monocarbure de zirconium entre 450 et 700 °C et sous des pressions d'oxygene comprises entre 10^{-3} et 100 torr (Oxidation of powdered samples of zirconium monocarbide between 450 and 700 °C and under oxygen pressure between 10^{-3} and 100 torr). *Compt Rend Hebd Seances Acad Sci Ser C Chim* 265(3):171–174 (in French)
1196. Barnier P, Thevenot F (1988) Une étude comparative de la résistance à l'oxydation du carbure de zirconium et du oxycarbure de zirconium (A comparative study of the oxidation resistance of zirconium carbide and zirconium oxycarbide). *Eur J Solid State Inorg Chem* 25(5–6):495–508 (in French)
1197. Barnier P, Thevenot F (1986) Synthesis and hot-pressing of single-phase ZrC_xO_y and two-phase ZrC_xO_y - ZrO_2 materials. *Int J High Technol Ceram* 2(4):291–307
1198. Henney J, Jones JWS (1964) Phases in the zirconium-carbon-oxygen system. In: Popper P (ed) *Special ceramics*. Academic Press, London, pp. 35–43
1199. Ouensanga A, Vermesse C, Dodé M (1972) Contribution à l'étude thermodynamique du système Zr-O-C à haute température (Contribution to thermodynamic study of the Zr-O-C system at high temperature). *Rev Chim Miner* 9(3):473–481 (in French)
1200. Ouensanga A, Pialoux A, Dodé M (1974) Etude aux rayons X à haute température du système Zr-O-C dans les conditions d'équilibre thermodynamique puis sous vide (High-temperature X-ray study of the Zr-O-C system in thermodynamic equilibrium conditions and in vacuum). *Rev Int Hautes Temp Refract* 11(4):289–293 (in French)
1201. Klimashin GM, Avgustinik AI, Smirnov GV (1972) Karbonitridnye i oksikarbidnye fazy titana i tsirkoniya (Carbonitride and oxycarbide phases of titanium and zirconium). *Izv AN SSSR Neorg Mater* 8(5):843–845 (in Russian)
1202. Fedorus VB, Kosolapova TYa, Kuzma YuB (1969) Interaction of carbides of transition metals of IV-VI groups of the periodic system of elements with zirconium oxide. *Rev Int Hautes Temp Refract* 6(3):193–197
1203. Granov VI, Glazkov AV (1975) Teoreticheskii analiz reaktsii dnuokisi tsirkoniya s karbidom tsirkoniya (Theoretical analysis of the reaction of zirconium dioxide with zirconium carbide). *Izv AN SSSR Neorg Mater* 11(2):226–229 (in Russian)
1204. Ogawa T (1982) Method to assess the equilibrium MO_x -“ MC_y ”-C-CO. The system ZrO_2 -“ZrC”-C-CO. *J Chem Eng Data* 27(2):186–188
1205. Matskevich TL, Kazantsev AP (1982) Issledovanie sistemy Zr-C-O metodom elektronnoi Ozhe spektroskopii (Study of the Zr-C-O system by the electron Auger spectroscopy method). *Zh Tekh Fiz* 52(4):753–758 (in Russian)
1206. Berkowitz-Mattuck J, Larson JT, Quigley RF, Christiansen W (1963) Kinetics of oxidation of refractory metals and alloys at 1000–2000 °C. Report ASD-TDR-62-203, Contract AF33(616)-6154, Part 2. Arthur D. Little Inc., Cambridge, Massachusetts, pp. 1–117

1207. McClaine LA, ed (1962) Thermodynamic and kinetic studies for a refractory materials program. Technical report ASD-TDR-62-204, Contract AF33(616)-7472, Part 1. Air Force Materials Laboratory, Wright-Patterson Air Force Base, Ohio, pp. 1–92
1208. Janowski KR, Carnahan RD, Rossi RC (1966) Static and dynamic oxidation of ZrC. Report TDR-669(6250-10)-3, Contract AF04(695)-669. Laboratory Operations Aerospace Corporation, El Segundo, California, pp. 1–38
1209. Maitre A, Lefort P (1997) Solid state reaction of zirconia with carbon. *Solid State Ionics* 104(1–2):109–122
1210. Minato K, Fukuda K (1995) Thermodynamic analysis of behaviour of HTGR fuel and fission products under accidental air or water ingress conditions. In: Response of fuel, fuel elements and gas cooled reactor cores under accidental air and water ingress conditions (IAEA-TECDOC-784). International Atomic Energy Agency, Vienna, pp. 86–91
1211. Bullock RE, Kaae JL (1983) Performance of coated UO₂ particles gettered with ZrC. *J Nucl Mater* 115:69–83
1212. Stocher J (1961) Remarques sur la stabilisation de la zircone cubique (Notes on the stabilization of cubic zirconia). *Bull Soc Chim France* (1):78–81 (in French)
1213. Dufour LC, Simon J (1967) Cinétique d'oxydation sous faible pression d'oxygène d'échantillons pulvérulents de monocarbures de zirconium et de tungstène et d'hemicarbure de molybdène (Oxidation kinetics of powdered samples of zirconium and tungsten monocarbides and molybdenum semicarbide at low oxygen pressure). *Bull Soc Chim France* (9):3643–3651 (in French)
1214. Simon J, Dufour LC (1968) Oxydation dechantillons pulverulents de monocarbure de zirconium à 450 et 700 °C et sous des pressions d'oxygène 10⁻³-100 torr (Oxidation of powdered samples of zirconium monocarbide at 450-700 °C and under oxygen pressures from 10⁻³ to 100 torr). *Bull Soc Chim France* (10):3591–3597 (in French)
1215. Watt W, Cockett GH, Hall AR (1953) Sintering of zirconium carbide by hot-pressing: some results of preliminary tests on oxidation resistance of carbides. *Metaux Corros Indust* 28:222–237
1216. Beketov AR, Kuptsov SG, Obabkov NV, Fedorenko OV (1976) Okislenie karbida tsirkoniya pri temperaturakh nizhe 1400 °C (Oxidation of zirconium carbide at temperatures below 1400 °C). In: Samsonov GV (ed) *Elektronnaya struktura i fiziko-khimicheskie svoystva splavov i soedinenii perekhodnykh metallov* (Electronic structure and physico-chemical properties of transition metal alloys and compounds). Naukova Dumka, Kyiv, pp. 127–131 (in Russian)
1217. Lyubimov VD, Shveikin GP, Askarova LK, Alyamovskii SI, Zainulin YuG (1976) Kinetics and mechanism of initial stages of carbothermal reduction of ZrO₂. *Inorg Mater* 12(12):1765–1768
1218. Clark JN, Glasson DR, Jayaweera SAA (1987) The oxidation of some transition metal nitrides and carbides. *Rev Chim Miner* 24(6):654–666
1219. Pugach ÉA (1969) High-temperature oxidation of the carbides and borides of the transition metals of group IV–VI of the periodic table. PhD thesis, Institute for Problems of Materials Science, Ukrainian SSR Academy of Sciences, Kyiv (in Russian)
1220. Voitovich RF (1995) High-temperature oxidation of materials. *Powder Metall Met Ceram* 34(7–8):441–445
1221. Gozzi D, Montozzi M, Cignini PL (1999) Apparent oxygen solubility in refractory carbides. *Solid State Ionics* 123(1–4):1–10
1222. Gozzi D, Montozzi M, Cignini PL (1999) Oxidation kinetics of refractory carbides at low oxygen pressures. *Solid State Ionics* 123(1–4):11–18
1223. Rudneva VV, Galevskii GV (2007) Investigation of thermal oxidation resistance of nanopowders of refractory carbides and borides. *Russ J Non-Ferr Met* 48(2):143–147
1224. Rudneva VV, Galevskii GV (2007) Thermooxidative stability of refractory carbide and boride nanopowders. *Steel Transl* 37(4):329–332
1225. Chernikov A, Kosukhin V (2008) Deposition of ZrC coats on UO₂ particles using the chloride process. In: Lohnert G (ed) *Proc. 3rd Int. topical meeting on high-temperature reactor technology (HTR 2006)*, Gauteng, South Africa, 1–4 Oct 2006. *Nucl Eng Design* 238(11):2861–2865

1226. Holleck H, Kleykamp H (1981) The constitution of cemented carbide systems. In: Hausner HH, Antes HW, Smith GD (eds) *Modern developments in powder metallurgy*, Vol. 14. Metal Powder Industry Federation, Princeton, New Jersey, pp. 233–245
1227. Ogawa T, Ikawa K (1982) Diffusion of metal fission products in $ZrC_{1.0}$. *J Nucl Mater* 105(2–3):331–334
1228. Auskern A (1967) Rare gas diffusion in nonstoichiometric zirconium carbide. *J Nucl Mater* 22(3):257–268
1229. Valentine KH, Homan FJ, Long EL, Jr, Tiegs TN, Montgomery BH, Hamner RL, Beatty RL (1977) Irradiation performance of HTGR fuel rods in HFIR experiments HRB-7 and -8. Technical Report ORNL-5228. Oak Ridge National Laboratory, Tennessee, pp. 1–58
1230. Vishnyakov LR, Grudina TV, Kadyrov VKh, Karpinos DM, Oleynik VI, Sapozhnikova AB, Tuchinskii LI (1985) *Kompozitsionnye materialy (Composite materials)*. Naukova Dumka, Kyiv (in Russian)
1231. Kozina GK (1970) *Issledovanie kontaktnogo vzaimodeistviya tugoplavkikh karbidov i materialov na ikh osnove s zhidkimi metallami i splavami (A study of the contact interaction of refractory carbides and materials on their basis with liquid metals and alloys)*. PhD thesis, Institute for Problems of Materials Science, Ukrainian SSR Academy of Sciences, Kyiv (in Russian)
1232. Samsonov GV, Panasyuk AD, Kozina GK (1968) Wetting of refractory carbides with liquid metals. *Powder Metall Met Ceram* 7(11):874–878
1233. Yasinskaya GA (1966) The wetting of refractory carbides, borides and nitrides by molten metals. *Powder Metall Met Ceram* 5(7):557–559
1234. Ramqvist L (1965) Wettability of metallic carbides by liquid copper, nickel, cobalt and iron. *Int J Powder Metall* 1(4):2–21
1235. Warren R (1980) Solid-liquid interfacial energies in binary and pseudo-binary systems. *J Mater Sci* 15(10):2489–2496
1236. Naidich YuV (1972) *Kontaktnye yavleniya v metallicheskikh rasplavakh (Contact phenomena in metallic melts)*. Naukova Dumka, Kyiv (in Russian)
1237. Iksanov BA, Martynov SZ, Minaev YuA, Pavlov YuA (1976) *Rastekanie zhelezonikelevykh po ZrC and nikel-kobaltovykh splavov po ZrN (Spreading of iron-nickel alloys on ZrC and nickel-cobalt alloys on ZrN)*. *Izv Vyssh Uchebn Zaved Chern Metall* (1):12–13 (in Russian)
1238. Eremenko VN, Naidich YuV (1958) *Zmochuvannya ridkymy metallamy poverkhen tugoplavkykh spoluk (The wetting of surface of refractory compounds by rare metals)*. AN UkrRSR, Kyiv (in Ukrainian)
1239. Ukhov VF, Esin OA, Vatolin NA, Dubinin ÉK (1971) *Issledovaniya smachivaemosti tverdykh nemetallicheskikh tel zhidkimi splavami na osnove palladiya (Investigations on the wettability of solid non-metallic bodies by liquid alloys on the basis of palladium)*. In: Eremenko VN (ed) *Fizicheskaya khimiya poverkhnostnykh yavlenii pri vysokikh temperaturakh (Physical chemistry of the surface phenomena at high temperatures)*. Naukova Dumka, Kyiv, pp. 139–142 (in Russian)
1240. Goretzki H, Exner HE, Scheuermann W (1971) Electronic structure of refractory carbides and its relation to wetting. In: Hausner HH (ed) *Modern developments in powder metallurgy*. Vol. 4 – Processes. Plenum Press, New York, pp. 327–337
1241. Upadhyaya GS (1984) Wetting of ceramics by metal melts – an electronic approach. In: Upadhyaya GS (ed) *Sintered metal-ceramic composites*. Elsevier Science, Amsterdam, pp. 41–50
1242. Samsonov GV, Kozina GK, Panasyuk AD, Bondarchuk SN (1974) The reaction of refractory carbides with molten steels and cast irons. In: Samsonov GV (ed) *Refractory carbides*. Consultants Bureau, New York, London, pp. 433–440
1243. Etinger IA, Maltseva LF, Savranskaya LA, Marmer EN, Kindysheva VS, Nikolaeva VA, Dubovik TV (1974) The reaction of highly refractory oxides, refractory carbides and boron carbonitride with molybdenum and tungsten under the operating conditions in high-temperature vacuum electric furnaces. In: Samsonov GV (ed) *Refractory carbides*. Consultants Bureau, New York, London, pp. 449–461

1244. Samsonov GV, Panasyuk AD, Kozina GK (1972) O vzaimodeistvii metallopodobnykh karbidov s zhidkimi perekhodnymi metallami (On the interaction of metal-like carbides with liquid transition metals). In: Eremenko VN, Naidich YV (eds) Smachivaemost i poverkhnostnye svoystva rasplavov i tverdykh tel (Wetting and surface properties of melts and solid bodies). Naukova Dumka, Kyiv, pp. 85–102 (in Russian)
1245. Kutysheva ÉV (1975) Vzaimodeistvie karbidov perekhodnykh metallov IV-VI grupp periodicheskoi sistemy elementov s kremniem (The interaction of transition metal carbides of groups IV-VI of the periodic system of elements with silicon). In: Samsonov GV (ed) Vysokotemperaturnye karbidy (High-temperature carbides). Naukova Dumka, Kyiv, pp. 139–143 (in Russian)
1246. Livey DT, Murray P (1956) The wetting properties of solid oxides and carbides by liquid metals. In: Benesovsky F (ed) Proc. 2nd Plansee seminar on sintered high-temperature and corrosion resistance materials, Reutte, Tyrol, 19–23 June 1955. Metallwerk Plansee AG, Reutte, Tyrol, pp. 375–404
1247. Oreshkin VD, Svetlopol'yanskii VI, Kozina GK, Panasyuk AD (1975) Kontaknoe vzaimodeistvie karbidov s ferrosplavami pri naplavke (The contact interaction of carbides with ferroalloys during surfacing). In: Samsonov GV (ed) Vysokotemperaturnye karbidy (High-temperature carbides). Naukova Dumka, Kyiv, pp. 125–129 (in Russian)
1248. Anthony FM, Pearl HA (1960) Investigation of feasibility of utilizing available heat resistant for hypersonic leading edge applications. Technical Report WADC-TR-59-744, Contract AF 33(616)-6034. Vol. 3 – Screening test results and selection of materials. Bell Aircraft Corporation Materials Laboratory, Buffalo, New York, pp. 1–347
1249. May CE, Koneval D, Fryburg GC (1959) Stability of ceramics in hydrogen between 4000 °F and 4500 °F. NASA Memorandum 3-5-59E. National Aeronautics and Space Administration, Washington, DC, pp. 1–18
1250. Samsonov GV, Latysheva VP (1956) Diffuziya bora, ugleroda i azota v perekhodnye metally IV, V i VI grupp periodicheskoi tablitsy (The diffusion of boron, carbon and nitrogen into transition metals of the IV, V and VI groups of the periodic table). Doklady AN SSSR 109(3):582–585 (in Russian)
1251. Samsonov GV, Latysheva VP (1956) Issledovanie diffuzii bora i ugleroda v nekotorye metally perekhodnykh grupp (A study of the diffusion of boron and carbon into certain metals of transition groups). Fiz Met Metalloved 2(2):309–319 (in Russian)
1252. Samsonov GV, Épik AP (1962) K voprosu o parametrakh reaktsionnoi diffuzii bora i ugleroda v tugoplavkie perekhodnye metally (On the problem of parameters of reaction diffusion into refractory transition metals). Fiz Met Metalloved 14(3):479–480 (in Russian)
1253. Samsonov GV, Épik AP (1966) Coatings of high-temperature materials. Some properties of high-temperature compounds. In: Hausner HH (ed) Coatings of high-temperature materials. Springer, Plenum Press, New York, pp. 7–111
1254. Harrod DL, Fleischer LR (1968) On the role of diffusion in the plastic deformation of transition metal carbides. In: Vahldiek FW, Mersol SA (eds) Anisotropy in single-crystal refractory compounds, Vol. 1. Springer, New York, pp. 341–356
1255. Blocher JM, Jr, Ish CJ, Leiter DP, Jr, Plock LF, Campbell IE (1957) Carbide coatings on graphite. Report BMI-1165, Contract W-7405-eng-92. Battelle Memorial Institute, Columbus, Ohio, pp. 1–23
1256. Gert LM, Babad-Zakhryapin AA (1966) Determination of diffusion coefficient of carbon into zirconium carbide at high temperatures. Indust Lab 32(8):1195–1198
1257. Adelsberg LM, Cadoff LH, Tobin JM (1966) Kinetics of zirconium-carbon reaction at temperatures above 2000 °C. Trans AIME 236(7):972–977
1258. Tobin JM, Adelsberg LM, Cadoff LH, Brizes WF (1966) Carbon diffusion in group IVB and VB transition element monocarbides. Am Ceram Soc Bull 45(4):471–473
1259. Andrievskii RA, Zagryazkin VN, Meshcheryakov GYa (1966) Issledovanie diffuzii ugleroda v tsirkonii i karbide tsirkoniya (A study of the diffusion of carbon in zirconium and zirconium carbide). In: Babad-Zakhryapin AA (ed) Proc. symp. on thermodynamics with emphasis on nuclear materials and atomic transport in solids, Vienna, 22–27 July 1965, Vol. 2. International Atomic Energy Agency, Vienna, pp. 172–180 (in Russian)

1260. Andrievskii RA, Zagryazkin VN, Meshcheryakov GYa (1966) Issledovanie diffuzii ugleroda v β -tsirkonii (A study of the diffusion of carbon in β -zirconium). *Fiz Met Metalloved* 21(1):140–143 (in Russian)
1261. Andrievskii RA, Klimenko VV, Khromov YuF (1969) Samodiffuziya ugleroda v karbidakh perekhodnykh metallov IV i V grupp (The self-diffusion of carbon in transition metals IV and V groups carbides). *Fiz Met Metalloved* 28(2):298–203 (in Russian)
1262. Nakonechnikov AI, Pavlinov LV (1972) Diffuziya ugleroda v fazakh tsirkoniya i titana (Diffusion of carbon in the phases of zirconium and titanium). *Izv AN SSSR Metall* (2):213 (in Russian)
1263. Pavlinov LV, Bykov VN (1965) Diffuziya ugleroda v β -tsirkonii (Diffusion of carbon in β -zirconium). *Fiz Met Metalloved* 19(3):397–400 (in Russian)
1264. Clark JN, Glasson DR, Jayaweera SAA (1986) Oxidation of chromium carbide. *Thermochim Acta* 103(1):193–199
1265. Clark JN (1995) The reactivity of some transition metal carbide and nitride. PhD thesis, University of Plymouth
1266. Tobin JM, Fleischer LR (1968) Preparation and characterization of high-quality single-crystal refractory metal carbides. Technical Report AFML-TR-67-137, Contracts AF33(615)-3982 and WANL-PR(GG)-017, Part 2. Westinghouse Electric Corporation Astronuclear Laboratory, Pittsburgh, Pennsylvania, pp. 1–54
1267. Tobin JM, Fleischer LR (1969) Refractory carbide recrystallization and crystal growth. *Am Ceram Soc Bull* 48(4):392–394
1268. Fleischer LR, Tobin JM (1971) Growth of transition metal carbide single crystals by recrystallization. 1. Preparation of fully-dense transition metal carbide. *J Cryst Growth* 8(3):235–242
1269. Fleischer LR, Tobin JM (1971) Growth of transition metal carbide single crystals by recrystallization. 2. Transition metal carbide recrystallization and crystal growth. *J Cryst Growth* 8(3):243–246
1270. Ushakov BF, Zagryazkin VN, Panov AS (1972) The interaction of graphite with titanium and zirconium. *Inorg Mater* 8(11):1690–1693
1271. Babad-Zakhryapin AA, Gert LM (1966) Osobennosti diffuzionnykh protsessov v kondensatakh obrazovannykh na goryachei podlozhke (The particularities of diffusion processes in the precipitates formed on a heated substrate). In: Babad-Zakhryapin AA (ed) *Proc. symp. on thermodynamics with emphasis on nuclear materials and atomic transport in solids*, Vienna, 22–27 July 1965, Vol. 2. International Atomic Energy Agency, Vienna, pp. 153–161 (in Russian)
1272. Andrievskii RA, Khromov YuF, Alekseeva IS (1971) Self-diffusion of carbon and metal atoms in zirconium and niobium carbides. *Phys Met Metallogr* 32(3):228–231
1273. Sarian S, Criscione JM (1967) Diffusion of carbon through zirconium monocarbide. *J Appl Phys* 38(4):1794–1798
1274. Andrievskii RA, Eremeev VS, Zagryazkin VN, Panov AS (1967) Diffuziya ugleroda v karbidakh perekhodnykh metallov IV-VI grupp periodicheskoi sistemy (Diffusion of carbon in carbides of periodic table IV-VI groups transition metals). *Izv AN SSSR Neorg Mater* 3(12):2158–2164 (in Russian)
1275. Vilks YuN, Nikolskii SS, Avarbe RG (1967) Temperature dependence of diffusion coefficient of carbon in nonstoichiometric zirconium, niobium and tantalum carbides. *High Temp* 5(4):545–548
1276. Andrievskii RA, Spivak II, Chevasheva KL (1968) Effective self-diffusion coefficients in interstitial compounds. *Powder Metall Met Ceram* 7(7):559–562
1277. Vilks YN, Ordanyan SS (1972) Effektivnye koeffitsienty diffuzii monokarbidnykh faz tsirkoniya v oblasti ikh gomogennosti (The effective diffusion coefficients of zirconium monocarbide phases in their homogeneity ranges). In: *Short communications of Lensovet Leningrad Technological Institute scientific-technical conf.*, Lensovet LTI, Leningrad, pp. 37–38 (in Russian)
1278. Zagryazkin VN (1969) O mekhanizme diffuzii v monokarbidakh perekhodnykh metallov (On the mechanism of diffusion in transition metals monocarbides). *Fiz Met Metalloved* 28(2):292–297 (in Russian)

1279. Khromov YuF, Alekseeva IS (1976) Diffusion mobility of carbon and metal atoms in the range of homogeneity of niobium and zirconium carbides and of their solid solutions. *Phys Met Metallogr* 42(1):96–102
1280. Khromov YuF, Yanchur VP, Eremeev VS (1972) Diffuziya ugleroda v nitride tsirkoniya (Diffusion of carbon in zirconium nitride). *Fiz Met Metalloved* 33(3):642–644 (in Russian)
1281. Zagryazkin VN, Ushakov BF (1975) Diffuziya volframa v karbidakh tsirkoniya i tantalata (Diffusion of tungsten in zirconium and tantalum carbides). *Izv AN SSSR Neorg Mater* 11(12):2238–2240 (in Russian)
1282. Khromov YuF, Zhmurov SA, Svistunov DE (1982) Samodiffuziya ^{147}Pm v karbidakh tsirkoniya i niobiya (Self-diffusion of ^{147}Pm in zirconium and niobium carbides). *Fiz Met Metalloved* 54(6):1223–1225 (in Russian)
1283. Xu Y, Roques J, Domain C, Simoni E (2016) Carbon diffusion in bulk hcp zirconium: a multi-scale approach. *J Nucl Mater* 473:61–67
1284. Geng X, Yang F, Liu H, Lu X, Xiao P (2016) Palladium migration through a zirconium carbide coating in TRISO-coated fuel particles. *J Am Ceram Soc* 99(4):1455–1463
1285. Agarwala RP, Paul AR (1975) Diffusion of carbon in zirconium and some of its alloys. *J Nucl Mater* 58(1):25–30
1286. Gale WF, Totemeir TC, eds (2004) *Smithells metals reference book*, 8th ed. Elsevier Butterworth Heinemann, ASM International Materials Information Society, Amsterdam, Boston
1287. Razumovskiy VI, Korzhavyi PA, Ruban AV (2011) *Ab initio* calculations of kinetic properties in ZrC and TiC carbides. *Solid State Phenom* 172–174:990–995
1288. Zotov VS, Tsedilkin AP (1979) Diffuziya ugleroda v $\alpha\text{-Zr}$ (Carbon diffusion in $\alpha\text{-Zr}$). *Fiz Met Metalloved* 47(2):344–348 (in Russian)
1289. Fedorov GB, Zhomov FI, Gusev VN, Paraev SA, Smirnov EA (1973) Diffuziya ugleroda v tsirkonii i karbide tsirkoniya (Diffusion of carbon in zirconium and zirconium carbide). In: Emelyanov VS, Yevstyukhin AI (eds) *Metallurgiya i metallovedenie chistyykh metallov* (Metallurgy and metallography of pure metals), Vol. 10. Atomizdat, Moscow, pp. 58–62 (in Russian)
1290. Suzuki H (1969) Diffusion of carbon in tantalum and zirconium. *Bull Tokyo Inst Technol* 90:105–115
1291. Samsonov GV, Épik AP (1964) O reaktsionnoi diffuzii bora i ugleroda v tugoplavkie perekhodnye metally (On the reactive diffusion of boron and carbon in refractory transition metals). *Dopov Akad Nauk Ukr RSR* 1:67–71 (in Russian)
1292. Zhunkovskii GL (1969) Issledovanie protsessov diffuzionnogo nasyscheniya tugoplavkikh metallov uglerodom i borom v vakuume (A study of the diffusion saturation of refractory metals by carbon and boron in vacuum). PhD thesis, Institute for Problems of Materials Science, Ukrainian SSR Academy of Sciences, Kyiv (in Russian)
1293. Borisova AL, Evtushenko OV (1979) Diffusional processes in the welding of some refractory carbides to metals. *Powder Metall Met Ceram* 18(7):481–487
1294. Peterson NL (1960) Diffusion in refractory metals. Technical Report WADD-60-793, Contract AF33(616)-7382. Wright Air Development Division, Air Research and Development Command USAF, Wright-Patterson Air Force Base, Ohio, pp. 1–164
1295. Matzke Hj, Rondinella VV (1999) Diffusion in carbides, nitrides, hydrides and borides. In: Beke DL (ed) *Diffusion in non-metallic solids*. Subvol. B, Part 1. Springer, Berlin, Heidelberg, pp. 5/1–5/29
1296. Van Loo FJJ, Wakelkamp W, Bastin GF, Metselaar R (1989) Diffusion of carbon in TiC_{1-x} and ZrC_{1-x} . *Solid State Ionics* 32–33(2):824–832
1297. Fedorov GB, Gusev VN, Smirnov EA, Solovev GI, Yankulev SS (1972) Component diffusion in UC-ZrC system. *Atom Energy* 33(1):676–678
1298. Khromov YuF, Alekseeva IS (1976) Self-diffusion mechanism of carbon in certain carbides of transition metals. *Phys Met Metallogr* 41(5):193–195
1299. Brizes WF, Salkovitz EI (1969) Comparison of the chemical and self-diffusivities in the transition metal monocarbides. *Scripta Metall* 3(9):659–662
1300. Spivak II, Klimentko VV (1973) Densification kinetics in the hot pressing and recrystallization of carbides. *Powder Metall Met Ceram* 12(11):883–887

1301. Spivak II, Klimenko VV (1971) Study of diffusion effects on interstitial phases. *Phys Met Metallogr* 32(2):87–92
1302. Samsonov GV, Kushtalova IP (1973) Issledovanie protsessov deformatsii i rekristallizatsii tugoplavkikh soedinenii (A study of the deformation and recrystallization processes of refractory compounds). *Izv AN SSSR Neorg Mater* 9(1):46–47 (in Russian)
1303. Kushtalova IP (1967) Investigation of the sintering of loosely poured titanium carbide and zirconium carbide powders. *Powder Metall Met Ceram* 6(8):604–605
1304. Dragoo AL (1968) Diffusion rates in inorganic nuclear materials. *J Res Nat Bureau Stand A* 72A(2):157–173
1305. Samsonov GV, Bozhko SA (1970) Collective recrystallization in loosely poured zirconium carbide powders. *Powder Metall Met Ceram* 9(3):204–206
1306. Samsonov GV, Bozhko SA, Kushtalova IP (1970) Recrystallization of refractory compounds. In: *Proc. 2nd Int. conf. on powder metallurgy*. High Tatras, Czechoslovakia, pp. 98–104
1307. Samsonov GV, Bozhko SA, Kushtalova IP (1971) Plasticheskaya deformatsiya karbidov pri almaznom shlifovanii (Plastic deformation of carbides during diamond grinding). *Doklady AN SSSR* 198(1):83–85 (in Russian)
1308. Samsonov GV, Kovalchenko MS, Petrykina RYa, Naumenko VYa (1970) Hot-pressing of the transition metals and their carbides in their homogeneity regions. *Powder Metall Met Ceram* 9(9):713–716
1309. Williams WS (1971) Transition metal carbides. *Prog Solid State Chem* 6(C):57–118
1310. Darolia R, Archbold TF (1976) Dynamic recrystallization of zirconium carbide. *Scripta Metall* 10:251–253
1311. Kravchik AE, Savelev GA, Neshpor VS, Ordanyan SS (1977) Recrystallization of niobium and zirconium carbides. *Powder Metall Met Ceram* 16(1):1–4
1312. Kushtalova IP (1974) A study of recrystallization processes in refractory compounds. In: Samsonov GV (ed) *Refractory carbides*. Consultants Bureau, New York, London, pp. 311–313
1313. Ordanyan SS, Kravchik AE, Neshpor VS (1977) Isothermal sintering kinetics of zirconium carbide. *Powder Metall Met Ceram* 16(12):952–955
1314. Andrievskii RA, Spivak II, Mitrokhin VA, Klimenko VV (1979) Effect of changes in structure on the creep parameters of binary carbide composites. *Powder Metall Met Ceram* 18(12):918–923
1315. Kushtalova IP, Ristic MM (1984) Recrystallization of refractory materials. II. Kinetics of recrystallization. *Sci Sinter* 16:115–117
1316. Andrievskii RA, Gurov KP (1975) O samodiffuzii nemetallicheskih atomov v fazakh vnedreniya (On self-diffuzion of non-metallic atoms in interstitial phases). *Fiz Met Metalloved* 39(1):57–61 (in Russian)
1317. Matzke Hj (1984) Point defects and transport properties in carbides. *Solid State Ionics* 12:25–45
1318. Matzke Hj (1989) Point defects and transport properties in carbides and nitrides. In: Johannesen Ø, Andersen AG, Kofstad P (eds) *Selected topics in high-temperature chemistry: defect chemistry of solids*. Elsevier, Amsterdam, New York, pp. 353–384
1319. Van Loo FJJ, Wakelkamp W, Bastin GF, Metselaar R (1989) The diffusion of carbon in titanium carbide and zirconium carbide. In: *Proc. 11th Int. symp. on the reactivity of solids*, Princeton University, New Jersey, 19–24 June 1988. *Solid State Ionics* 26(2):179
1320. Wakelkamp W, Van Loo FJJ, Boelen B, Bastin GF, Metselaar R (1989) The diffusion of carbon in nonstoichiometric carbides. In: Kedves FJ, Beke DL (eds) *Proc. Int. conf. on diffusion in metals and alloys (DIMETA-88)*, Balatonfüred, Hungary, 20–25 Sept 1988. *Defect Diffus Forum* 66–69:1485–1490
1321. Barnier P, Brodhag C, Thevenot F (1986) Hot-pressing kinetics of zirconium carbide. *J Mater Sci* 21(7):2547–2552
1322. Pipon Y, Toulhoat N, Moncoffre N, Gutierrez G, Maître A, Gendre M (2013) Influence of the oxygen content on the thermal migration of xenon in ZrC_xO_{1-x} . *J Nucl Mater* 440(1–3):546–552

1323. Zhang Y, Zhang J, Fu Z (2013) Oxidation resistance analysis of zirconium carbide sintered by hot-pressing. *J Chin Ceram Soc* 41(7):901–904 (in Chinese)
1324. Wang S-L, Li K-Z, Li H-J, Zhang Y-L, Feng T (2014) Structure evolution and ablation behaviour of ZrC coating on C/C composites under single and cyclic oxyacetylene torch environment. *Ceram Int* 40:16003–16014
1325. Wang S-L, Li K-Z, Li H-J, Zhang Y-L, Zhang W-Y (2015) Ablation behaviour of CVD-ZrC coating under oxyacetylene torch environment with different heat fluxes. *Int J Refract Met Hard Mater* 48:108–114
1326. Jia Y, Li H, Feng L, Sun J, Li K, Fu Q (2016) Ablation behaviour of rare-earth La modified ZrC coating for SiC-coated carbon/carbon composites under a oxyacetylene torch. *Corros Sci* 104:61–70
1327. Voitovich RF, Pugach ÉA (1968) Okislenie tugoplavkikh soedinenii (Oxidation of refractory compounds). *Naukova Dumka, Kyiv* (in Russian)
1328. Anikeev AN, Chumanov IV (2015) Study of zirconium carbide contact angle. *Proc Eng* 129:821–824
1329. Knyazev VI, Bukatov VG, Korostin OS (1976) Vnutrennee trenie nekotorykh monokarbidov perekhodnykh metallov v diapazone temperatur 20–2000 °C (The internal friction of some transition metal carbides in the temperature range of 20–2000 °C). In: Samsonov GV, Kosolapova TYa, Gnesin GG, Fedorus VB, Domasevich LG (eds) *Karbidy i splavy na ikh osnove* (Carbides and alloys based on them). *Naukova Dumka, Kyiv*, pp. 114–121 (in Russian)
1330. Kopylova VP (1961) Khimicheskaya ustoichivost karbidov perekhodnykh elementov IV, V i VI grupp (The chemical stability of transition element carbides IV, V and VI groups). *Zh Prikl Khim* 34(9):1936–1939 (in Russian)
1331. Philipp WH (1966) Chemical reactions of carbides, nitrides and diborides of titanium and zirconium and chemical bonding in these compounds. Report NASA-TN-D-3533. National Aeronautics and Space Administration, Washington DC, pp. 1–23
1332. Campbell IE, Powell CF, Nowicki DH, Gonser BW (1949) The vapour-phase deposition of refractory materials. I. General conditions and apparatus. *J Electrochem Soc* 96(5):318–333
1333. Lukashenko TA, Tikhonov KI (1998) Korroziionnaya stoikost ryada karbidov i nitridov perekhodnykh metallov 4-6 grupp v kontsentrirrovannykh rastvorakh sernoi i fosfornoj kislot (Corrosion resistance of a number of carbides and nitrides of group 4-6 transition metals in concentrated solutions of sulfuric and phosphoric acids). *Zh Prikl Khim* 71(12):2017–2020 (in Russian)
1334. Kopylova VP, Kornilova VI, Nazarchuk TN, Fedorus VB (1980) Reactions of powders of zirconium and niobium carbides in their homogeneity with some acids. *Powder Metall Met Ceram* 19(1):9–12
1335. Kotlyar EE, Nazarchuk TN (1972) Interaction of the carbides of group IV and V transition metals with various acids. In: Samsonov GV (ed) *Chemical properties and analysis of refractory compounds*. Consultants Bureau, New York, London, pp. 1–5
1336. Burykina AL, Strashinskaya LV (1965) A study of new materials operating in contact with certain solid and liquid metals and compounds. *Mater Sci* 1(5):385–389
1337. Fukuda K, Ikawa K, Kobayashi F, Iwamoto K (1975) Microstructure of vapour-deposited ZrC-C alloy. *J Nucl Mater* 56:243–245
1338. Nachiappan C, Rangaraj L, Divakar C, Jayaram V (2010) Synthesis and densification of monolithic zirconium carbide by reactive hot pressing. *J Am Ceram Soc* 93(5):1341–1346
1339. Otani S (1984) Study on single crystal growth of group IVa and group Va transition metal carbides by a floating zone technique. PhD thesis, Osaka University
1340. Walker P, Tarn WH (1991) *CRC handbook of metal etchants*. CRC Press, Boca Raton, Boston, London
1341. Samsonov GV, Kovalchenko MS (1962) *Goryachee pressovanie* (Hot pressing). *UkrSSR State Engineering Literature Publishing House, Kyiv* (in Russian)
1342. Prescott CH, Jr (1926) The equilibrium between zirconium oxide and carbon and their reaction products at incandescent temperatures. *J Am Chem Soc* 48(10):2534–2550
1343. Hollahan JR, Gregory NW (1964) A torsion effusion study of the reaction of graphite with oxides of thorium and zirconium. *J Phys Chem* 68(8):2346–2351

1344. Samsonov GV, Sinelnikova VS (1964) Electrical resistance of refractory compounds at high temperatures. In: Samsonov GV (ed) Refractory transition metal compounds and high temperature cermets. Academic Press, New York, London, pp. 172–177
1345. Suchkov AB, Meerson GA, Olesov JG (1968) Elektroliticheskaya ochkistka karbida tsirkoniya (Electrolytic purification of zirconium carbide). *Izv AN SSSR Metall* (3):106–108 (in Russian)
1346. Georgieva GG, Lashko NF, Sorokina KP (1972) Chemical and electrochemical methods of separating the carbides MeC and the carbonitrides Me(C,N) of group IV and V metals. In: Samsonov GV (ed) Chemical properties and analysis of refractory compounds. Consultants Bureau, New York, London, pp. 72–76
1347. Ogorodnikov VV, Sverdlik NN (1975) Teoreticheskii analiz protsessa gomogenizatsii dispersnykh smesei psevdobinarnoi sistemy TiC-ZrC pri spekanii i goryachem pressovanii (Theoretical analysis of the homogenization process of dispersed mixtures of the TiC-ZrC pseudobinary system during sintering and hot-pressing). In: Samsonov GV (ed) Vysokotemperaturnye karbidy (High-temperature carbides). Naukova Dumka, Kyiv, pp. 100–112 (in Russian)
1348. Ogorodnikov VV, Sverdlik NN (1975) Eksperimentalnoe issledovanie protsessa uplotneniya i gomogenizatsii dispersnykh smesei psevdobinarnoi sistemy TiC-ZrC pri spekanii i goryachem pressovanii (An experimental study of the densification and homogenization process of dispersed mixtures of the TiC-ZrC pseudobinary system during sintering and hot-pressing). In: Samsonov GV (ed) Vysokotemperaturnye karbidy (High-temperature carbides). Naukova Dumka, Kyiv, pp. 112–118 (in Russian)
1349. Danisina IN, Avarbe RG (1975) Issledovanie kinetiki rekristallizatsionnogo rosta zerna v karbide tsirkoniya (A kinetics study of the recrystallization grain growth in zirconium carbide). In: Samsonov GV (ed) Vysokotemperaturnye karbidy (High-temperature carbides). Naukova Dumka, Kyiv, pp. 70–73 (in Russian)
1350. Samsonov GV, Klochkov LA, Timofeeva II (1975) Termicheskoe rasshirenie TiC, ZrC i NbC v oblastiakh ikh gomogennosti (Thermal expansion of TiC, ZrC and NbC in the regions of their homogeneity). In: Samsonov GV (ed) Vysokotemperaturnye karbidy (High-temperature carbides). Naukova Dumka, Kyiv, pp. 46–48 (in Russian)
1351. Samsonov GV, Panasyuk AD, Kozina GK, Dyakonova LV (1976) Kontaknoe vzaimod-eistvie karbida tsirkoniya s nikelovymi splavami (The contact interaction of zirconium carbide with nickel alloys). In: Samsonov GV, Kosolapova TYa, Gnesin GG, Fedorus VB, Domasevich LG (eds) Karbidy i splavy na ikh osnove (Carbides and alloys based on them). Naukova Dumka, Kyiv, pp. 56–59 (in Russian)
1352. Kokhtev SA, Yevstyukhin AI, Solovev GI (1979) Diagramma sostoyaniya sistemy monosulfid urana – monokarbid urana – karbid tsirkoniya (Phase diagram of the uranium monosulfide – uranium monocarbide – zirconium monocarbide system). In: Emelyanov VS, Yevstyukhin AI (eds) Metallurgiya i metallovedenie chistyykh metallov (Metallurgy and metallography of pure metals), Vol. 13. Atomizdat, Moscow, pp. 45–59 (in Russian)
1353. Yevstyukhin AI, Kokhtev SA, Andrievskii RA, Solovyev GI (1975) Issledovanie psevdobinarnoi sistemy monosulfid urana – karbid tsirkoniya (Investigation of pseudobinary system uranium monosulfide – zirconium carbide). In: Emelyanov VS, Yevstyukhin AI (eds) Materialy atomnoi tekhniki (Nuclear engineering materials), Vol. 1. Atomizdat, Moscow, pp. 42–47 (in Russian)
1354. Yevstyukhin AI, Barinov IP, Abanin DD (1959) Issledovanie iodidnogo protsessa polucheniya tsirkoniya s ispolzovaniem karbida tsirkoniya v kachestve syrya (The investigation of iodide process of zirconium production with the usage of zirconium carbide as a raw material). In: Emelyanov VS, Yevstyukhin AI (eds) Metallurgiya i metallovedenie chistyykh metallov (Metallurgy and metallography of pure metals), Vol. 1. Moscow Engineering Physics Institute, Moscow, pp. 78–83 (in Russian)

1355. Bocker S (1970) Contribution à l'étude du monocarbure d'uranium et de plutonium avec de faibles additions de zirconium (A contribution to the study of the mixed uranium-plutonium monocarbides containing small quantities of zirconium). Rapport CEA-R-3765(2). Centre d'Etudes Nucléaires de Fontenay-aux-Roses, Commissariat à l'Énergie Atomique, pp. 1–114 (in French)
1356. Bocker S, Boucher R, Lorenzelli R, Milet C (1970) Etude de carbures U-Pu-C-M (M = Zr, Ti, Mo) (A study of U-Pu-C-M (M = Zr, Ti, Mo) carbides). In: Miner WN (ed) Plutonium 1970. Proc. 4th Int. conf. on plutonium and other actinides, Santa Fe, New Mexico, 5–9 Oct 1970, Vol. 2. Metallurgical Society of AIME, New York, pp. 4–13 (in French)
1357. Meerson GA, Kotelnikov RB, Bashlykov SN, Gaevskaya NS (1963) Tverdye rastvory karbid tsirkoniya – karbid urana (Zirconium carbide – uranium carbide solid solutions). In: New nuclear materials including non-metallic fuels. Proc. conf. on new nuclear materials technology including non-metallic fuel elements, Prague, 1–5 July 1963, Vol. 2. International Atomic Energy Agency, Vienna, pp. 19–32 (in Russian)
1358. Barth F, Von der Decken CB, Schifferstein K, Clauss A, Reichel H, Rygaert J, Ruston WR (1963) Release of fission products from UC-ZrC fuel inserts. In: New nuclear materials including non-metallic fuels. Proc. conf. on new nuclear materials technology including non-metallic fuel elements, Prague, 1–5 July 1963, Vol. 2. International Atomic Energy Agency, Vienna, pp. 535–556
1359. Sorrell CC, Stubican VS, Bradt RC (1986) Mechanical properties of ZrC-ZrB₂ and ZrC-TiB₂ directionally solidified eutectics. *J Am Ceram Soc* 69(4):317–321
1360. Agarwal S, Trocellier P, Serruys Y, Vaubailon S, Miro S (2014) Helium mobility in advanced nuclear ceramics. *Nucl Instrum Meth B* 327(1):117–120
1361. Yang X-Y, Lu Y, Zhang P (2015) The temperature-dependent diffusion coefficient of helium in zirconium carbide. *J Appl Phys* 117(16):164903 (5 pp.)
1362. Kim J-H, Zhe G, Lim J, Park C, Kang S (2015) Thermodynamic stability of in situ W-ZrC and W-Zr(CN) composites. *J Alloys Compd* 647:1048–1053
1363. Shamanian M, Mohammadnezhad M, Asgari H, Szpunar J (2015) Fabrication and characterization of Al-Al₂O₃-ZrC composite produced by accumulative roll bonding (ARB) process. *J Alloys Compd* 618:19–26
1364. El-Sheikh SM, Zaki ZI, Ahmed YMZ (2014) *In situ* synthesis of ZrC/SiC nanocomposite via carbothermic reduction of binary xerogel. *J Alloys Compd* 613:379–386
1365. Jiang J, Wang S, Li W, Chen Z, Zhu Y (2014) Preparation of 3D C_f/ZrC-SiC composites by joint processes of PIP and RMI. *Mater Sci Eng A* 607:334–340
1366. Song M, Ran M, Long Y (2013) Synthesis of ultrafine zirconium carbide particles by SHS in an Al-Zr-C system: microstructural evaluation and formation mode. *J Alloys Compd* 564:20–26
1367. Ball MC, Brown DS, Page D, Thurman RRT (1967) The action of alkali on transition metal carbides. *Trans Brit Ceram Soc* 66:307–313
1368. Loskutov VF, Khizhnyak VG, Kunitskii YuA, Kindrachuk MV (1991) Diffuzionnye karbidnye pokrytiya (Diffusion carbide coatings). *Tekhnika*, Kyiv (in Russian)
1369. Grimvall G (2000) Lattice vibrations, heat capacity and related properties. In: Kumashiro Y (ed) *Electric refractory materials*. Marcel Dekker, New York, Basel, pp. 153–172
1370. Chakrabarti T (2013) Study on reactive hot pressing of zirconium carbide. PhD thesis, Indian Institute of Science, Bangalore
1371. Chakrabarti T, Rangaraj L, Jayaram V (2015) Computational modelling of reactive hot-pressing of zirconium carbide. *J Mater Res* 30(12):1876–1886
1372. Diwan BD, Srivastava A (2012) Pressure-induced structural phase transitions in Ti_{1-x}Zr_xC solid solution. In: Proc. 23rd Int. conf. on high pressure science and technology (AIRAPT-23), Mumbai, India, 25–30 Sep 2011. *J Phys Conf Ser* 377(1):012091
1373. Edamoto K, Nagayama T, Ozawa K, Otani S (2007) Angle-resolved and resonant photoemission study of the ZrO-like film on ZrC (100). *Surf Sci* 601(21):5077–5082
1374. Strife JR, Smeggil JG, Worell WL (1990) Reaction of iridium with metal carbides in the temperature range of 1923 to 2400 K. *J Am Ceram Soc* 73(4):838–845

1375. Alekseeva TI, Galevsky GV, Rudneva VV, Galevsky SG (2018) Application of zirconium carbide: assessment, determination of dominant trends and prospects. *IOP Conf Ser Mater Sci Eng* 411:012007 (4 pp.)
1376. Rohrer M-M, Benard M, Poble J-M (2000) Structure, reactivity and growth pathways of metallocarbohedrenes M_8C_{12} and transition metal/carbon clusters and nanocrystals: a challenge to computational chemistry. *Chem Rev* 100:495–542
1377. Fesenko VV, Bolgar AS (1963) Evaporation rate and vapour pressure of carbides, silicides, nitrides and borides. *Powder Metall Met Ceram* 2(1):11–17
1378. Panasyuk AD, Samsonov GV (1963) Termopary s termoelektrodami iz tugoplavkikh karbidov dlya izmereniya temperatur do 3000 °C (Thermocouples with temperature electrodes made from refractory carbides for the measurement of temperatures up to 3000 °C). *Teplotiz Vysok Temp* 1(1):136–140 (in Russian)
1379. Samsonov GV, Fomenko VS, Paderno VN, Rud BM (1964) Thermoemission characteristics of alloys of isomorphous carbides. *High Temp* 2(5):656–661
1380. Grebenkina VG, Sorokin VN, Yusov YuP, Perezentsev AV (1973) Use of refractory carbides in resistors. *Powder Metall Met Ceram* 12(6):502–504
1381. Savitskii EM, Baron VV, Efimov YuV, Bychkova MI, Myzenkova LF (1973) Superconducting materials. Plenum Press, New York, London
1382. Kovalchenko MS, Bovkun GA, Tkachenko YuG, Ragozin IP (1983) Deformation properties of monocarbides of transition metals by the method of continuous impression of an indenter. *Powder Metall Met Ceram* 22(12):1034–1037
1383. Ogawa T, Fukuda K (1990) Quick analysis of free carbon in metal carbides by plasma oxidation. *J Am Ceram Soc* 73(8):2558–2560
1384. Simões JAM, Beauchamp JL (1990) Transition metal – hydrogen and metal – carbon bond strengths: the keys to catalysis. *Chem Rev* 90(4):629–688
1385. Luo Y-R (2007) Comprehensive handbook of chemical bond energies. CRC Press, Boca Raton, London, New York
1386. Sievers MR, Chen Y-M, Armentrout PB (1996) Metal oxide and carbide thermochemistry of Y^+ , Zr^+ , Nb^+ and Mo^+ . *J Chem Phys* 105(15):6322–6333
1387. Lindberg PAP, Johansson LI (1988) Work function and reactivity of some crystal faces of substoichiometric transition metal carbides. *Surf Sci* 194(1–2):199–204
1388. Hugosson HW, Jansson U, Johansson B, Eriksson O (2001) Phase stability diagrams of transition metal carbides, a theoretical study. *Chem Phys Lett* 333:444–450
1389. Hugosson HW, Eriksson O, Jansson U, Johansson B (2001) Phase stabilities and homogeneity ranges in $4d$ transition metal carbides: a theoretical study. *Phys Rev B* 63(13):134108 (11 pp.)
1390. Šimůnek A, Vackář J (2001) Correlation between core-level shift and bulk modulus in transition metal carbides and nitrides. *Phys Rev B* 64(23):235115 (6 pp.)
1391. Gueorguiev GK, Pacheco JM (2003) Shapes of cagelike metal clusters: first principles calculations. *Phys Rev B* 68(24):241401 (4 pp.)
1392. Arun R, Subramanian M, Mehrotra GM (1990) Oxidation behaviour of TiC, ZrC and HfC dispersed in oxide matrices. In: Tressler E, McNallan M (eds) Corrosion and corrosive degradation of ceramics. Ceramic transactions, Vol. 10. The American Ceramic Society, Westerville, Ohio, pp. 211–223
1393. McCauley RA (2004) Corrosion of ceramic and composite materials, 2nd edn. Marcel Dekker, New York, Basel
1394. Ryu HJ, Lee YW, Cha SI, Hong SH (2006) Sintering behaviour and microstructures of carbides and nitrides for the inert matrix fuel by spark plasma sintering. *J Nucl Mater* 352:341–348
1395. Jackson HF, Jayaseelan DD, Clegg WJ, Reece MJ, Inam F, Manara D, Perinetti-Casoni C, Lee WE (2010) Microstructure of laser-melted zirconium carbide ceramics. In: Fox K, Hoffman E, Manjooran N, Pickrell G (eds) Advances in materials science for environmental and nuclear technology. Ceramic transactions, Vol. 222. The American Ceramic Society, Wiley, Hoboken, New Jersey, pp. 113–125

1396. Klimov DA, Myktybekov B, Nizovtsev VE, Ukhov PA (2011) Perspektivy primeneniya nanostrukturnykh kompozitsionnykh materialov na osnove karbidov i oksidov tugoplavlykh metallov dlya aviakosmicheskikh obektov (Perspectives of the application of nanostructured composite materials based on carbides and oxides of refractory metals for aerospace facilities). Trudy MAI 46, 9 pp. (in Russian) <http://www.mai.ru/upload/iblock/1a/1a1493319c8c15a70defc28b0a51172d.pdf>. Accessed 10 Feb 2015
1397. Chen W-T, White RM, Goto T, Dickey EC (2016) Directionally solidified boride and carbide eutectic ceramics. J Am Ceram Soc 99(6):1837–1851
1398. Kurtoglu M, Naguib M, Gogotsi Y, Barsoum MW (2012) First principles study of two-dimensional early transition metal carbides. Mater Res Soc Commun 2:133–137
1399. Ordanyan SS, Orekhov AN, Vikhman SV (2012) Interaction of W_2B_5 with $Me^{IV}VC$ carbides. Russ J Non-Ferrous Met 55(1):91–94
1400. Razumovskiy VI (2012) Thermodynamic and kinetic properties of Fe-Cr and TiC-ZrC alloys from density functional theory. PhD thesis, Kungliga Tekniska Högskolan, Stockholm
1401. Razumovskiy VI, Ruban AV, Odqvist J, Korzhavyi PA (2013) Vacancy-cluster mechanism of metal atom diffusion in substoichiometric carbides. Phys Rev B 87:054203 (7 pp.)
1402. Rejasse F, Rapaud O, Pradeilles N, Maitre A, Trolliard G (2013) Experimental study of group IVB metals oxycarbides. In: David N, Jaubert J-N, Privat R (eds) Proc. 39th joint European days on equilibrium between phases, Nancy, France, 19–21 Mar 2013. MATEC Web Conf 3:01077. <http://dx.doi.org/10.1051/mateconf/20130301077>. Accessed 28 May 2016
1403. Nowotny H, Rudy E, Benesovsky F (1961) Untersuchungen in den Systemen – Hafnium-Bor-Kohlenstoff und Zirkonium-Bor-Kohlenstoff (Investigations in the systems hafnium-boron-carbon and zirconium-boron-carbon). Monatsh Chem 92(2):393–406 (in German)
1404. Naguib M, Bentzel GW, Shah J, Halim J, Caspi EN, Lu J, Hultman L, Barsoum MW (2014) New solid solution MAX phases: $(Ti_{0.5}V_{0.5})_3AlC_2$, $(Nb_{0.5}V_{0.5})_2AlC$, $(Nb_{0.5}V_{0.5})_4AlC_3$ and $(Nb_{0.8}Zr_{0.2})_2AlC$. Mater Res Lett 2(4):233–240
1405. Gupta S, Hoffman EN, Barsoum MW (2006) Synthesis and oxidation of Ti_2InC , Zr_2InC , $(Ti_{0.5}Zr_{0.5})_2InC$ and $(Ti_{0.5}Hf_{0.5})_2InC$ in air. J Alloys Compd 426:168–175
1406. Yang J, Naguib M, Ghidui M, Pan L-M, Gu J, Nanda J, Halim J, Gogotsi Y, Barsoum MW (2016) Two-dimensional Nb-based M_4C_3 solid solutions (MXenes). J Am Ceram Soc 99(2):660–666
1407. Kiani S, Yang J-M, Kodambaka S (2015) Nanomechanics of refractory transition metal carbides: a path to discovering plasticity in hard ceramics. J Am Ceram Soc 98(8):2313–2323
1408. Yu X-X, Weinberger CR, Thompson GB (2016) *Ab initio* investigations of the phase stability in group IVB and VB transition metal carbides. Comput Mater Sci 112:318–326
1409. Wang Q, German KE, Oganov AR, Dong H, Feya OD, Zubavichus YaV, Murzin VYu (2016) Explaining stability of transition metal carbides – and why TcC does not exist. RSC Adv 6(20):16197–16202
1410. Silvestroni L, Sciti D (2010) Sintering behaviour, microstructure and mechanical properties: a comparison among pressureless sintered ultra-refractory carbides. Adv Mater Sci Eng ID835018:1–11. <https://doi.org/10.1155/2010/835018>
1411. Sani E, Mercatelli L, Meucci M, Balbo A, Silvestroni L, Sciti D (2016) Compositional dependence of optical properties of zirconium, hafnium and tantalum carbides for solar absorber applications. Sol Energy 131:199–207
1412. Atkins AG, Tabor D (1966) Hardness and deformation properties of solids at very high temperatures. Proc Royal Soc London Ser A Math Phys Sci 292(1431):441–459
1413. Arabei BG, Levinskii YuV, Markov YuM, Portnoi KI (1978) Effect of alloying of uranium carbide on its interaction with carbon. Atom Energy 44(3):288–290

1414. Balankin SA, Loshmanov LP, Skorov DM, Sokolov VS (1979) Raschet energii obrazovaniya vakansii v fazakh vnedreniya po dannym mekhanicheskikh svoistv (Calculation of vacancy formation energy in interstitial phases through mechanical properties data). In: Sobolev ND, Beskorovainyi NM, Morozov EM, Kulbakh AA, Markochev VM, Sapunov VT (eds) Fizika i mekhanika deformatsii i razrusneniya (Physics and mechanics of deformation and fracture), Vol. 7. Atomizdat, Moscow, pp. 8–12 (in Russian)
1415. Deryavko II, Lanin AG, Maksimov VP, Taubin ML (1979) Rentgenograficheskoe izuchenie dvykhfaznosti v karbide tsirkoniya (An X-ray study of the formation of two phases within bulk zirconium carbide). In: Sobolev ND, Beskorovainyi NM, Morozov EM, Kulbakh AA, Markochev VM, Sapunov VT (eds) Fizika i mekhanika deformatsii i razrusneniya (Physics and mechanics of deformation and fracture), Vol. 7. Atomizdat, Moscow, pp. 47–54 (in Russian)
1416. Rangaraj L, Suresha SJ, Divakar C, Jayaram V (2008) Low-temperature processing of ZrB₂-ZrC composites by reactive hot-pressing. *Metall Mater Trans A* 39:1496–1505
1417. Lanin AG, Zubarev PV, Vlasov KP (1992) Osnovnye kharakteristiki materialov ispolzuemykh v teplovyydelayushchikh sborkakh vysokotemperaturnykh gazoohlazhdaemykh reaktorov (Main characteristics of materials for fuel elements of gas cooled high-temperature reactors). In: Volkova YuV, Porodnova VI (eds) Proc. 3rd interindustry conf. on reactor materials science, Dimitrovgrad, Russian Federation, 27–30 Oct 1992, pp. 40–41 (in Russian)
1418. Lanin AG, Zubarev PV, Vlasov KP (1992) Mechanical and thermophysical properties of materials in HTGR fuel bundles. *Atom Energy* 74(1):40–44
1419. Ogorodnikov VV, Rogovoi YuI (1992) Simulating point defects in cubic monocarbides. *Inorg Mater* 28(5):763–767
1420. Cherkashenko VM, Nazarova SZ, Gusev AI, Ivanovskii AL (2001) Electronic structure, chemical bonding and properties of binary carbides M_xM'_yC_z in the crystalline and molecular states: XES, XPS and quantum-chemical studies. *J Struct Chem* 42(6):1002–1024
1421. Knight TW, Anghaie S (2001) Fuels for space nuclear power systems. 1. Tri-carbide nuclear fuel processing and characterization for space nuclear applications. In: Proc. American nuclear society annual meeting, Milwaukee, Wisconsin, 17–21 June 2001, *Trans Am Nucl Soc* 84:149–150
1422. Yoshitake M (2012) Examination of work function of transition metal carbides and nitrides. *J Vac Soc Jpn* 55(7):349–353 (in Japanese)
1423. Silvestroni L, Sciti D, Balat-Pichelin M, Charpentier L (2013) Zirconium carbide doped with tantalum silicide: microstructure, mechanical properties and high-temperature oxidation. *Mater Chem Phys* 143:407–415
1424. Wang Y, Zhu X, Zhang L, Cheng L (2011) Reaction kinetics and ablation properties of C/C-ZrC composites fabricated by reactive melt infiltration. *Ceram Int* 37:1277–1283
1425. Wang X-G, Guo W-M, Kan Y-M, Zhang G-J, Wang P-L (2011) Densification behaviour and properties of hot-pressed ZrC ceramics with Zr and graphite additives. *J Eur Ceram Soc* 31:1103–1111
1426. Yoshitake M (2014) Generic trend of work functions in transition metal carbides and nitrides. *J Vac Sci Technol A* 32(6):061403
1427. Datye A, Wu K-H, Kulkarni S, Lin HT, Vleugels J (2010) Processing, microstructure and mechanical properties of ultra-high temperature ceramics fabricated by spark-plasma sintering. *Ceram Eng Sci Proc* 30(2):53–65
1428. Fisenko AI, Lemberg V (2015) Polylogarithmic representation of radiative and thermodynamic properties of thermal radiation in a given spectral range: II. Real-body radiation. *Int J Thermophys* 36(10–11):2705–2719

1429. Ordanyan SS, Udalov YuP (2015) On the structure of the SiC-Mo(W)Si₂-Me^dB₂ systems and prospective development of refractory materials based on these systems. In: Ordanyan SS (ed) Aktualnye problemy tekhnologii proizvodstva sovremennykh keramicheskikh materialov (Current problems of the modern technology of ceramic materials). Polytechnic University Publishing House, Saint Petersburg, pp. 7–16 (in Russian)
1430. Singh A, Modi MH, Lodha GS (2015) Optical properties of zirconium carbide in 60–200 Å wavelength region using X-ray reflectivity technique. *Appl Optics* 54(2):253–258
1431. Wei X, Back C, Izhvanov O, Khasanov OL, Haines CD, Olevsky EA (2015) Spark-plasma sintering of commercial zirconium carbide powders: densification behaviour and mechanical properties. *Mater* 8(9):6043–6061. <https://doi.org/10.3390/ma8095289>
1432. David J, Trolliard G, Volklinger C, Loiseau T, Masson O, Maitre A (2016) Study of the reaction mechanisms involved in the formation of zirconium oxycarbide from metal-organic frameworks (MOFs) precursors. *J Alloys Compd* 680:571–585
1433. Veliša G, Mylonas S, Trocellier P, Thomé L, Debelle A, Vaubailion S, Bachelet C (2016) Ion beam synthesis of ZrC_xO_y nanoparticles in cubic zirconia. *J Appl Phys* 119(16):165902
1434. Tsuda K (2016) History of development of cemented carbides and cermets. *SEI Tech Rev* (82):16–20
1435. Zhilyaev VA, Patrakov EI (2016) Influence of alloying titanium carbonitride by transition metals of groups IV–VI on the interaction with nickel melt. *Russ J Non-Ferr Met* 57(2):141–147
1436. Niu B, Zhang F, Ji W, Zhang JY, Fu ZY, Wang WM (2016) Effect of solid solution formation on densification of spark-plasma sintered ZrC ceramics with TiC as sintering aid. *Adv Appl Ceram* 115(1):55–59
1437. Li Y, Katsui H, Goto T (2015) Phase decomposition of TiC-ZrC solid solution prepared by spark plasma sintering. *Ceram Int* 41(10B):14258–14262
1438. Li Y, Katsui H, Goto T (2016) Effect of heat treatment on the decomposition of TiC-ZrC solid solutions by spark-plasma sintering. *J Eur Ceram Soc* 36(15):3795–3800
1439. Lekakh SN, Medvedeva NI (2015) *Ab initio* study of Fe adsorption on the (001) surface of transition metal carbides and nitrides. *Comput Mater Sci* 106:149–154
1440. Lin Q, Sui R (2015) Wetting of carbide ceramics (B₄C, SiC, TiC and ZrC) by molten Ni at 1753K. *J Alloys Compd* 649:505–514
1441. Khazaei M, Arai M, Sasaki T, Ranjbar A, Liang Y, Yunoki S (2015) OH-terminated two-dimensional transition metal carbides and nitrides as ultra-low work function materials. *Phys Rev B* 92(7):075411
1442. Zha X-H, Luo K, Li Q, Huang Q, He J, Wen X, Du S (2015) Role of the surface effect on the structural, electronic and mechanical properties of the carbide MXenes. *EPL-Europhys Lett* 111:26007 (6 pp.)
1443. Umalas M, Hussainova I, Reedo V, Young D-L, Cura E, Hannula S-P, Löhmus R, Löhmus A (2015) Combined sol-gel and carbothermal synthesis of ZrC-TiC powders for composites. *Mater Chem Phys* 153:301–306
1444. Liu S, Hu W, Xiang J, Wen F, Xu B, Yu D, He J, Tian Y, Liu Z (2014) Mechanical properties of nanocrystalline TiC-ZrC solid solutions fabricated by spark plasma sintering. *Ceram Int* 40:10517–10522
1445. Zainulin YuG (1973) Kontsentratsionnaya oblast ustoychivosti kubicheskogo (tipa NaCl) oksikarbida tsirkoniya pri 1700 °C (The composition region of stability of cubic (NaCl type) zirconium oxycarbide at 1700 °C). In: Shveikin GP, Geld PV (eds) *Trudy Instituta khimii* (Proc. Institute of chemistry), Vol. 25. USSR Academy of Sciences Ural Scientific Centre, Sverdlovsk, pp. 26–32 (in Russian)
1446. Harrison RW, Lee WE (2016) Processing and properties of ZrC, ZrN and ZrCN ceramics. *Adv Appl Ceram* 115(5):294–307
1447. Teber A, Schoenstein F, Têtard F, Abdellaoui M, Jouini N (2012) The effect of Ti substitution by Zr on the microstructure and mechanical properties of the cermet Ti_{1-x}Zr_xC sintered by SPS. *Int J Refract Met Hard Mater* 31:132–137

1448. Teber A, Schoenstein F, Abdellaoui M, Jouini N (2012) Fabrication, microstructure and mechanical properties of novel bulk binderless ($\text{Ti}_{0.8}\text{Zr}_{0.2}\text{C}$) carbides prepared by mechanical alloying and spark plasma sintering. *Ceram Int* 38(6):4929–4933
1449. Kikuchi M, Nagakura S, Oketani S (1971) Crystal structures of transition metal carbides. *J Iron Steel Inst Jpn* 57(6):1009–1053 (in Japanese)
1450. Gusev AI, Rempel AA (1997) Phase diagrams of metal-carbon and metal-nitrogen systems and ordering in strongly nonstoichiometric carbides and nitrides. *Phys Stat Sol A* 163(2):273–304
1451. Krutskii YuL, Dyukova KD, Antonova EV, Bannov AG, Sokolov VV, Pichugin AYU, Maksimovskii EA, Ukhina AV, Krutskaya TM, Netskina OV, Kuznetsova VV (2015) O korrozionnoi stoikosti vysokodispersnykh poroshkov karbidov nekotorykh perekhodnykh metalov (On the corrosion resistance of fine-dispersed powders of some transition metal carbides). *Nauchn Vestn NGTU (Sci Bull NSTU)* 58(1):271–281 (in Russian)
1452. Miller AD, Lye RG, Mueller JI (1967) Electronic band structures in sytem Zr-C-O. *Am Ceram Soc Bull* 46(4):461–463
1453. Kim KH, Shim KB (2003) The effect of lanthanum on the fabrication of ZrB_2 -ZrC composites by spark plasma sintering. *Mater Charact* 50:31–37
1454. Tsuchida T, Yamamoto S (2004) Mechanical activation assisted self-propagating high-temperature synthesis of ZrC and ZrB_2 in air from Zr/B/C powder mixtures. *J Eur Ceram Soc* 24:45–51
1455. Tsuchida T, Yamamoto S (2004) MA-SHS and SPS of ZrB_2 -ZrC composites. *Solid State Ionics* 172:215–216
1456. Stubican VS, Bradt RC, Kennard FL, Minford WJ, Sorrell CC (1986) Ceramic eutectic composites. In: Tressler RE, Messing GL, Pantano CG, Newnham RE (eds) *Tailoring multiphase and composite ceramics*. Plenum Press, New York, pp. 103–114
1457. Zhao L, Jia D, Wang Y, Rao J, Yang ZH, Duan X, Zhou Y (2010) ZrC-ZrB₂ matrix composites with enhanced toughness prepared by reactive hot pressing. *Scripta Mater* 63(8):887–890
1458. Xu L, Huang C, Liu H, Zou B, Zhu H, Zhao G, Wang J (2013) Study on *in-situ* synthesis of ZrB_2 whiskers in ZrB_2 -ZrC matrix powder for ceramic cutting tools. *Int J Refract Met Hard Mater* 37:98–105
1459. Xu L, Huang C, Liu H, Zou B, Zhu H, Zhao G, Wang J (2013) *In-situ* synthesis of ZrB_2 -ZrC_x ceramic tool materials toughened by elongated ZrB_2 grains. *Mater Design* 49:226–233
1460. Ryan NE, Soffa WA, Crawford RC (1968) Orientation and habit plane relationships for carbide and nitride precipitates in molybdenum. *Metallogr* 1:195–220
1461. Tsybulev PN, Serdyuk GN, Molchanovskij IA, Parkhomenko VD, Obushenko TI, Knyazev YuV, Solovev SA (1998) Kataliticheskaya aktivnost pokrytii nitridov i karbidov titana i tsirkoniya v reaktsiyakh okisleniya CH_4 i CO (Catalytic activity of coatings of nitrides and carbides of titanium and zirconium in reactions of oxidation of CH_4 and CO). *J Build Struct* 19(6):105–109 (in Russian)
1462. Rogl P, Bittermann H (1999) Ternary metal boron carbides. *Int J Refract Met Hard Mater* 17:27–32
1463. Takida T, Igarashi T, Saito N, Nakamura M (1999) Stability of grain structures in sintered molybdenum alloys dispersed with carbide particles at high temperatures. *J Jpn Soc Powder Powder Metall* 46(12):1261–1267 (in Japanese)
1464. Kato A, Tamari N (1980) Some common aspects of the growth of TiN, ZrN, TiC and ZrC whiskers in chemical vapour deposition. *J Cryst Growth* 49(1):199–203
1465. Turchanin AG, Fesenko VV (1969) Thermodynamic characteristics of refractory carbides in their homogeneity regions. *Powder Metall Met Ceram* 8(6):466–469
1466. Gusev AI, Rempel AA (2001) Nestekhiometriya, besporyadok i poryadok v tverdom tele (Nonstoichiometry, disorder and order in solids). Ural Division of the Russian Academy of Sciences, Yekaterinburg (in Russian)
1467. Gusev AI (2007) Nestekhiometriya, besporyadok, blizhnii i dalnii poryadok v tverdom tele (Nonstoichiometry, disorder short-range and long-range order in solids). Nauka Fizmatlit, Moscow (in Russian)

1468. Kurlov AS, Gusev AI (2014) High-energy milling of nonstoichiometric carbides: effect of nonstoichiometry on particle size of nanopowders. *J Alloys Compd* 582:108–118
1469. Glushko VP, Gurvich LV, eds (1982) Thermodynamic properties of individual substances, Vol. IV, Parts 1–2. Nauka, Moscow
1470. Sirdeshmukh DB, Sirdeshmukh L, Subhadra KG (2006) Micro- and macro-properties of solids. Springer, Berlin, Heidelberg
1471. Perry DL (2011) Handbook of inorganic compounds, 2nd edn. CRC Press, Boca Raton, London, New York
1472. Nino A, Sasago A, Sugiyama S, Taimatsu H (2016) Preparation of $\text{Si}_3\text{N}_4\text{-TaC}$ and $\text{Si}_3\text{N}_4\text{-ZrC}$ composite ceramics and their mechanical properties. *Int J Refract Met Hard Mater* 61:192–200
1473. Zotov YuP, Kotelnikov RB (1975) Volatilization of zirconium carbide at elevated temperatures in vacuum. *Russ Metall* (2):41–45
1474. Bolgar AS, Verkhoglyadova TS, Samsonov GV (1961) Davlenie para i teplota ispareniya TiC, ZrC i HfC v vakuume pri vysokikh temperaturakh (Vapour pressure and heat of vaporization of TiC, ZrC and HfC in vacuum at high temperatures). *Izv AN SSSR OTN Metall Toplivo* (1):142–145 (in Russian)
1475. Burykina AL, Struk LI, Manzhurnet KV (1967) Stability of refractory compounds in fused basalt. *Powder Metall Met Ceram* 6(2):122–123
1476. Senczyk D (1984) The lattice parameters of MeC-type carbides, nitrides and carbonitrides of transition metals of IV and V groups of the periodic system. In: Proc. 11th conf. applied crystallography, Vol. 1. Kozubnik, Poland, pp. 234–240
1477. Norton JT, Lewis RK (1963) Properties of non-stoichiometric metallic carbides. Technical Report NASA-CR-52083, Contract NASw-663. Advanced Metals Research Corporation, Somerville, Massachusetts, pp. 1–18
1478. Norton JT, Lewis RK (1964) Properties of non-stoichiometric metallic carbides. Final Report NASA-CR-58046, Contract NASw-663. Advanced Metals Research Corporation, Somerville, Massachusetts, pp. 1–42
1479. Zhao J, Zou J, Man Z-Y, Wang X-G, Xue J-X, Zhang G-J (2015) Dopant effects on high-temperature mechanical properties of zirconium carbide ceramics. *Adv Appl Ceram* 114(6):338–343
1480. Holleck H (1986) Material selection for hard coatings. *J Vac Sci Technol A* 4(6):2661–2669
1481. Cape JA, Taylor RE (1962) Thermal properties of refractory materials. Technical Report WADD-TR-60-581, Contract AF 33(616)-6794, Part 2. Atomic International, Canoga Park, California, pp. 1–22
1482. Gorinskii SG, Shabalin IL, Beketov AR, Kokorin AF (1979) Electrical conductivity of carbide-carbon materials. *Inorg Mater* 15(10):1396–1400
1483. Lesnaya MI (1981) Calculation of parameters of electron structure of zirconium carbonitrides. *Inorg Mater* 17(3):293–296
1484. Zhurakovskii EA, Proskurka KS, Lesnaya MI, Sotnik AA, Rozmaritsa AD (1981) Elektronnaya struktura i nekotorye svoistva karbonitrída i dvoynykh karbidnykh rastvorov na osnove titana i tsirkoniya (Electron structure and some properties of carbonitride and binary carbide solutions on the base of titanium and zirconium). *Izv Vyssh Uchebn Zaved Fiz* (12):67–71 (in Russian)
1485. Zhurakovskii EA, Lesnaya MI (1980) Electrophysical and thermophysical properties of the carbide alloys TiC-ZrC and TiC-VC. *High Temp* 18(4):583–586
1486. Alward JF, Fong CY, El-Batanouny M, Wooten F (1975) Band structures and optical properties of two transition metal carbides – TiC and ZrC. *Phys Rev B* 12(4):1105–1117
1487. Delin A, Eriksson O, Ahuja R, Johanson B, Brooks MSS, Gasche T, Auluck S, Wills JM (1996) Optical properties of the group IVB refractory metal compounds. *Phys Rev B* 54(3):1673–1681
1488. Kammori Ô, Sato K, Kurosawa F (1968) Infrared absorption spectra of metal carbides, nitrides and sulfides. *Jpn Analyst* 17(10):1270–1273 (in Japanese)
1489. Wood WD, Deem HW, Lucks CF (1962) Emittance of ceramics and graphites. Defence Metals Information Centre Memo N 148. Battelle Memorial Institute, Columbus, Ohio

1490. Ivashov SN, Fisenko AI (1988) Obrabotka spektrov teplovogo izlucheniya karbidov tsirkoniya i titana pri vysokikh temperaturakh (Processing spectra of thermal radiation of zirconium and titanium carbides at high temperatures). *Zh Prikl Spektrosk* 48(6):1024–1025 (in Russian)
1491. Back T, Fairchild SB, Averett K, Maruyama B, Pierce N, Cahay M, Murray PT (2013) Pulsed-laser deposited transition metal carbides for field emission cathode coatings. *ACS Appl Mater Interfaces* 5:9241–9246
1492. Zaima S, Adachi H, Shibata Y (1984) Promising cathode materials for high brightness electron beams. *J Vac Sci Technol B* 2(1):73–78
1493. Charbonnier FM, Mackie WA, Xie T, Davis PR (1999) Enhanced field emission from carbide-coated field emitters and device applications. *Ultramicroscopy* 79:73–82
1494. Yu ML, Kim HS, Hussey BW, Chang THP, Mackie WA (1996) Energy distributions of field emitted electrons from carbide tips and tungsten tips with diamond-like carbon coatings. *J Vac Sci Technol B* 14(6):3797–3801
1495. Mackie WA, Xie TB, Matthews MR, Routh BP, Davis PR (1998) Field emission from ZrC and ZrC films on Mo field emitters. *J Vac Sci Technol B* 16(4):2057–2062
1496. Yu ML, Lang ND, Hussey BW, Chang THP, Mackie WA (1996) New evidence for localized electronic states on atomically sharp field emitters. *Phys Rev Lett* 77(8):1636–1639
1497. Spindt C, Holland CE, Schwoebel PR (2000) Field emitter array development for field emission displays. In: Shashidhar R, Gnade B (eds) *Liquid crystal materials, devices and flat panel displays*. Proc. the Society of Photo-Optical Instrumentation Engineers (SPIE), San Jose, California, 27–28 Jan 2000, Vol. 3955. SPIE – International Society of Optical Engineering, Bellingham, Washington, pp. 151–158
1498. Charbonnier FM, Mackie WA, Hartman RL, Xie TB (2001) Robust high current field emitter tips and arrays for vacuum microelectronics devices. Proc. 13th Int. vacuum microelectronics conf., Guangzhou, People's Republic of China, 13–17 Aug 2000. *J Vac Sci Technol B* 19(3):1064–1072
1499. Mackie WA, Xie TB, Lee KS, McCallum AT, Kirby MJ, Davis PR (2000) High current field emission from ZrC with differing cone angles. *Mater Res Soc Symp Proc* 558:569–574
1500. Mackie WA, Southall LA, Xie TB, Cabe GL, Charbonnier FM, McClelland PH (2003) Emission fluctuation and slope-intercept plot characterization of Pt and transition metal carbide field emission cathodes in limited current regimes. In: Proc. 15th Int. vacuum microelectronics conf. (IVMC), Lyon, France, 07–11 July 2002. *J Vac Sci Technol B* 21(4):1574–1580
1501. Xu NS, Huq SE (2005) Novel cold cathode materials and applications. *Mater Sci Eng R* 48:47–189
1502. Samsonov GV, Naumenko VYa, Okhremchuk LN, Podchernyaeva IA, Fomenko VC (1972) Termoemissionnye svoistva karbidov perekhodnykh metallov IV-V grupp v oblastiakh ikh gomogenosti (The thermionic emission properties of transition metal carbides IV-V groups in their homogeneity regions). In: Samsonov GV (ed) *Elektronnoe stroenie i fizicheskie svoistva tverdogo tela* (Electron structure and physical properties of solids), Vol. 2. Naukova Dumka, Kyiv, pp. 147–156 (in Russian)
1503. Hannink RHJ, Kohlstedt DL, Murray MJ (1971) Brittle-region slip systems in the transition metal carbides. *Phys Stat Sol A* 6:K25–K28
1504. Hannink RHJ, Murray MJ (1978) Comment on “Slip and microhardness of IVa to VIa refractory materials”. *J Less-Common Met* 60(1):143–145
1505. Brookes CA, O'Neill JB, Redfern BAW (1971) Anisotropy in hardness of single crystals. *Proc R Soc Lond A* 322(1548):73–88
1506. Samsonov GV, Rozina NS (1956) Nekotorye fiziko-khimicheskie svoistva splavov tsirkoniya s uglerodom (Some physico-chemical properties of zirconium alloys with carbon). *Izv Sektora Fiz Khim Analiza AN SSSR* 27:126–132 (in Russian)
1507. Savvatimskiy AI, Onufriev SV (2016) Method and apparatus for studying high-temperature properties of conductive materials in the interests of nuclear power engineering. *Phys Atom Nucl* 79(14):1637–1655

1508. Savvatimskiy AI, Onufriev SV, Muboyadzhyan SA (2017) Measurement of ZrC properties up to 5000 K by fast electrical pulse heating method. *J Mater Res* 32(7):1287–1294
1509. Meerson GA, Umanskii YaS (1953) O tverdosti tugoplavkikh karbidov (On the hardness of refractory carbides). *Izv Sektora Fiz Khim Analiza AN SSSR* 22:104–110 (in Russian)
1510. Jones T (1956) The metallography of certain hot-pressed carbides possessing high melting points. In: Technical papers of the metallographic group meeting held at Bridgeport Brass Company, 7–8 Nov 1956, TID-7567, Part 1. US Atomic Energy Commission, Washington DC, pp. 32–45
1511. Plendl JN, Gielisse PJ (1962) Hardness of nonmetallic solids on an atomic basis. *Phys Rev* 125(3):828–832
1512. Artamonov AYa, Bezykornov AI, Ivanov AI (1966) Abrasive power of refractory compounds. *Powder Metall Met Ceram* 5(9):722–725
1513. Gangler JJ (1971) NASA research on refractory compounds. *High Temp High Press* 3(5):487–502
1514. Frantsevich IN, Voronov FF, Bakuta SA (1982) Uprugie postoyannye i moduli uprugosti metallov i nemetallov (The elastic constants and elasticity moduli of metals and non-metals). *Naukova Dumka, Kyiv* (in Russian)
1515. Kashtalyan YuA (1970) Kharakteristiki uprugosti materialov pri vysokikh temperaturakh (Elasticity characteristics of materials at high temperature). *Naukova Dumka, Kyiv* (in Russian)
1516. Li H, Zhang L, Zeng Q, Guan K, Li K, Ren H, Liu S, Cheng L (2011) Structural, elastic and electronic properties of transition metal carbides TMC (TM = Ti, Zr, Hf and Ta) from first-principles calculations. *Solid State Commun* 151:602–606
1517. Zhao Z, Zhou X-F, Wang L-M, Xu B, He J, Liu Z, Wang H-T, Tian Y (2011) Universal phase transition of B1-structured stoichiometric transition metal carbides. *Inorg Chem* 50(19):9266–9272
1518. Ulrickson M (1979) Material studies related to TFTR limiters and wall armour. *J Nucl Mater* 85–86:231–235
1519. Patriarca P, Rucker DJ (1969) Fuels and materials development program. Quarterly Progress Report ORNL-4420, Contract W-7405-ENG-26. Oak Ridge National Laboratory, Tennessee, pp. 1–270
1520. Topchyan LS, Ogorodnikov VV, Benina LA, Murzin LM (1976) Nizkotemperaturnoe kalorimetricheskoe issledovanie obluchennykh karbidov titana i tsirkoniya (A low-temperature calorimetric study of irradiated titanium and zirconium carbides). *Izv AN SSSR Neorg Mater* 12(11):1800–1803 (in Russian)
1521. Razumovskiy VI, Popov MN, Ding H, Odqvist J (2015) Formation and interaction of point defects in group IVb transition metal carbides and nitrides. *Comput Mater Sci* 104:147–154
1522. Samsonov GV, Panasyuk AD, Kozina GK, Borovikova MS (1977) Vliyanie dobavok ugleroda, bora i kremniya na kontaktnoe vzaimodeistvie v sisteme tugoplavkoe soedinenie – zhidkii splav (The effect of carbon, boron and silicon additions on the contact interaction in the refractory compound – liquid alloy system). In: Shults MM (ed) Zharostoikie pokrytiya dlya zashchity konstruksionnykh materialov (Heat-resistant coatings for the protection of structural materials). *Nauka, Leningrad*, pp. 178–180 (in Russian)
1523. Fedorchenko IM, Frantsevich IN, Radomyselskii ID, Kovalchenko MS, Kislyi PS, Kosolapova TYa, Mai VK, Shcherban NI (1985) Poroshkovaya metallurgiya (Powder metallurgy). *Naukova Dumka, Kyiv* (in Russian)
1524. Zhilyaev VA, Patrakov EI, Pelts AD (1990) Kontaktnoe vzaimodeistvie legirovannykh karbonitridov titana s rasplavami na osnove nikelya (The contact interaction of alloyed titanium carbonitrides with nickel based melts). In: Nauch. soobshcheniya 7-oi Vsesoyuznoi konf. po strukture i svoistvam metallicheskih i shlakovykh rasplavov (Proc. 7th All-Union conf. on structure and properties of metallic and slag melts), Vol. 3, Part 3. Chelyabinsk Polytechnical Institute, Chelyabinsk, pp. 232–235 (in Russian)
1525. Zhilyaev VA, Patrakov EI (2016) Regularities of the contact interaction of double carbides (Ti_{1-n}Me_n^{IV,V})C with the Ni-Mo melt. *Russ J Non-Ferr Met* 57(6):610–617

1526. Xu R, Huang P, Yang H (1988) Investigation on spinodal decomposition of WC-TiC-ZrC-Co cemented carbide. In: Gummeson PU (ed) Proc. Int. powder metallurgy conf., Orlando, Florida, 5–10 June 1988. Metal Powder Industries Federation, Princeton, New Jersey, pp. 15–21
1527. Mortimer DA, Nicholas MG (1973) The wetting of carbon and carbides by copper alloys. *J Mater Sci* 8:640–648
1528. Eustathopoulos N, Nicholas MG, Drevet B (1999) Wettability at high temperatures. Elsevier Science, Oxford
1529. Jeitschko W, Nowotny H, Benesovsky F (1963) Kohlenstoffhaltige ternäre Verbindungen (H-Phase) (Carbonaceous ternary compounds (H-phase)). *Monatsh Chem* 94(4):672–676 (in German)
1530. Jeitschko W, Nowotny H, Benesovsky F (1963) Die H-Phasen Ti_2InC , Zr_2InC , Hf_2InC und Ti_2GeC (The H-phases Ti_2InC , Zr_2InC , Hf_2InC and Ti_2GeC). *Monatsh Chem* 94(6):1201–1205 (in German)
1531. Holleck H, Thümmel F (1967) Ternäre Komplex-carbide, -nitride und -oxide mit teilweise aufgefüllter Ti_2Ni -Struktur (Ternary complex carbides, nitrides and oxides with partial filled Ti_2Ni structure). *Monatsh Chem* 98(1):133–134 (in German)
1532. Pessall N, Gold RE, Johansen HA (1968) A study of superconductivity in interstitial compounds. *J Phys Chem Solids* 29:19–38
1533. Vitryanyuk VK, Arbuzov EA (1972) Manufacture of high-porosity materials from complex carbides. *Powder Metall Met Ceram* 11(3):216–219
1534. Beketov AR, Shabalin IL, Fedorenko OV (1979) Goryachepressovannyye i plavlyennyye karbidno-uglerodnyye materialy (Hot-pressed and fused carbide-carbon materials). *Tsvetnyy Met* (3):39–42
1535. Gorinskii SG, Shabalin IL, Beketov AR, Kokorin AF (1979) Elektrofizicheskie svoystva kompozitsionnykh materialov $Me^{IV}C-SiC-C$ (The electrophysical properties of $Me^{IV}C-SiC-C$ composite materials). In: Shveikin GP (ed) *Realnaya struktura neorganicheskikh zharostoikikh i zharoprochnykh materialov* (Real structure of inorganic heat-resistant and heat-proof materials). USSR Academy of Sciences Ural Scientific Centre, Pervouralsk, Sverdlovsk Area, pp. 344–345 (in Russian)
1536. Paderno VN, Lesnaya MI, Martynenko AN, Chugunova SI (1983) Character of fracture of TiC-ZrC carbide alloys at various temperatures. *Powder Metall Met Ceram* 22(5):375–379
1537. Mroz C (1994) Processing $TiZrC$ and $TiZrB_2$. *Am Ceram Soc Bull* 73(4):78–81
1538. Chae K-W, Hwang C-S, Kim D-Y, Cho S-J (1996) Diffusion induced recrystallization of TiC. *Acta Mater* 44(5):1793–1799
1539. Gusev AI (2000) Order-disorder transformations and phase equilibria in strongly non-stoichiometric compounds. *Phys Usp* 43(1):1–37
1540. Slama C, Teber A, Abdellaoui M (2010) Synthèse et caractérisation structurale de nano-composites riches en $Ti_{1-x}Zr_xC$ (Synthesis and structural characterization of $Ti_{1-x}Zr_xC$ rich nanocomposite). *Phys Chem News* 54:90–94 (in French)
1541. Yung D-L, Cygan S, Antonov M, Jaworska L, Hussainova I (2016) Ultra-high pressure spark plasma sintered ZrC-Mo and ZrC-TiC composites. *Int J Refract Met Hard Mater* 61:201–206
1542. Kubota Y, Tanaka H, Arai Y, Inoue R, Kogo Y, Goto K (2017) Oxidation behaviour of $ZrB_2-SiC-ZrC$ at 1700 °C. *J Eur Ceram Soc* 37(4):1187–1194
1543. Kubota Y, Yano M, Inoue R, Kogo Y, Goto K (2018) Oxidation behaviour of $ZrB_2-SiC-ZrC$ in oxygen-hydrogen torch environment. *J Eur Ceram Soc* 38(4):1095–1102
1544. Cheng EJ, Li Y, Sakamoto J, Han S, Sun H, Noble J, Katsui H, Goto T (2017) Mechanical properties of individual phases of ZrB_2-ZrC eutectic composite measured by nanoindentation. *J Eur Ceram Soc* 37(13):4223–4227
1545. Li Y, Katsui H, Goto T (2017) Preparation of ZrCN-TiCN solid solutions by spark plasma sintering. *Ceram Int* 43(18):16965–16971
1546. Li Y, Katsui H, Goto T (2017) Microstructure evolution of (Ti,Zr)C solid solution at the initial stage of phase decomposition. *Mater Today Proc* 4(11):11449–11452

1547. Bokhonov BB, Dudina DV (2017) Synthesis of ZrC and HfC nanoparticles encapsulated in graphitic shells from mechanically milled Zr-C and Hf-C powder mixtures. *Ceram Int* 43(16):14529–14532
1548. Li K, Zhou X, Zhao Z, Chen C, Wang C, Ren B, Zhang L (2018) Synthesis of zirconium carbide whiskers by a combination of microwave hydrothermal and carbothermal reduction. *J Solid State Chem* 258:383–390
1549. Jia P, Chen L, Rao J, Wang Y, Meng Q, Zhou Y (2017) Evolution of phase, microstructure and ZrC lattice parameter in solid-solution-treated W-ZrC composite. *Sci Rep* 7(1):6531 (8 pp.)
1550. Nino A, Izu Y, Sekine T, Sugiyama S, Taimatsu H (2017) Effects of ZrC and SiC addition on the microstructures and mechanical properties of binderless WC. *Int J Refract Met Hard Mater* 69:259–265
1551. Gasparrini C, Podor R, Horlait D, Chater R, Lee WE (2017) Zirconium carbide oxidation: Maltese cross formation and interface characterization. *Oxid Met* 88(3–4):509–519
1552. Chernetsov MV (2017) Integral materials studies of nuclear fuel at Institute of Reactor Materials. *Atom Energy* 121(4):255–258

Addendum

A.1 Structures

Summarized general data on the structural properties (atomic or molecular weights, phase homogeneity regions, crystal systems, types, space groups and lattice parameters, calculated and experimental densities) of the high-melting elements (carbon and refractory metals) and refractory compounds (carbides of Hf, Nb, Ta and Zr), which were considered separately and comprehensively in the main chapters of the first and second volumes of the book, are given (in alphabetical order) in Table A.1 [1–52, 67, 68, 90].

A.2 Thermal Properties

The most important thermodynamic properties (standard heat of formation, standard molar entropy, molar and specific heat capacities, molar and specific enthalpies (heats) of melting (fusion) and vaporization, molar and specific enthalpy differences $H_T - H_{298}$) of the ultra-high temperature materials considered separately and comprehensively in the first and second volumes of the book are summarized in Tables A.2 and A.3 [1–3, 7–9, 13–20, 28–33, 36–41, 43, 44, 53–66, 71, 85, 90]. For the general comparison, some other thermal properties (melting and boiling points, coefficients of linear thermal expansion, relative thermal expansion, thermal conductivity, vapour pressure and vaporization rate) of ultra-high temperature materials (graphite, refractory metals and Hf, Nb, Ta, Zr carbides) are given in Tables A.4 and

[A.5](#) [1–3, 6–21, 23–32, 35–44, 46, 47, 50–57, 66, 69, 70, 72–75, 79–90]. The values of the heat capacities, enthalpy differences, thermal expansion and thermal conductivity properties and vaporizations parameters of the materials are presented there in the wide range from room (or moderate) to ultra-high temperatures.

A.3 Electro-magnetic and Optical Properties

For the general comparison, the main electro-magnetic and optical properties (specific electrical resistance, temperature coefficient of electroresistance, integral and monochromatic emittances, thermionic emission characteristics and molar magnetic susceptibility) of carbon (graphite), refractory metals and Hf, Nb, Ta, Zr carbides are given in Table [A.6](#) [1, 3, 4, 6–9, 11–15, 18–21, 23, 31–41, 43–47, 56, 76–78, 90–92]. The values of the electrical resistance and integral and monochromatic emittances of the high-melting elements and compounds are summarized in the wide range from room (or moderate) to ultra-high temperatures.

A.4 Physico-mechanical Properties

The relative comparison of some physico-mechanical properties (hardness, tensile and compressive strengths and Young's modulus) of ultra-high temperature materials (graphite, refractory metals and Hf, Nb, Ta, Zr carbides), which were considered above separately and comprehensively in the main chapters of the first and second volumes of the book, can be carried out on the basis of the data presented in Table [A.7](#) [1, 4, 6–15, 18–21, 23, 29–41, 43–47, 57, 83, 90, 93, 94]. The values of the hardness, strength and elasticity of the ultra-high temperature materials are summarized there for the wide range from room to ultra-high temperatures.

A.5 Nuclear Physical Properties

Nuclear physical properties (isotopic mass range, total number of isotopes, thermal neutron macroscopic and microscopic cross sections, moderating ability and capture resonance integral) of the elements (carbon and refractory metals) and Hf, Nb, Ta, Zr carbides are summarized in Table [A.8](#) [1, 2, 95–100].

A.6 Chemical Properties

For the ultra-high temperature materials (elements and compounds) considered in details in the first and second volumes of the book, the characters of interaction with some chemical reagents in the aqueous solutions at room temperature are summarized in Table A.9 [2, 3, 7, 9, 11, 13, 17, 19, 23, 32, 38, 43, 44, 56, 90, 101–104, 220–229]. For the cubic carbides of Hf, Nb, Ta, Zr (NaCl-structured), considered in the second volume, the interaction with isomorphous refractory compounds (carbides, nitrides, oxides, phosphides and sulphides) is considered in Table A.10 [1, 8, 14–21, 24, 28–33, 35–44, 48–50, 64, 67, 90, 230–235].

A.7 Porosity-Property Relationships

The methods of powder metallurgy and particulate technologies, such as conventional sintering, hot pressing, hot isostatic pressing, spark plasma sintering and others, are widely spread for the preparation and production of ultra-high temperature materials, especially for those based on Hf, Nb, Ta, Zr refractory carbides considered in this volume of the book. The effect of porosity on physical properties (thermal conductivity, electrical resistance, strength and elastic characteristics) of sintered metallic and ceramic materials has been the subject of numerous experimental and theoretical studies. Some of the formulae proposed by various researchers for the description of physical properties and characteristics of the materials with residual porosity are given in Table A.11 [105–219]. The diversity of the formulae is associated with the necessity to take into account the shape, size and number of pores, the surface conditions of the test samples, the grain size in the materials, the degree of their local inhomogeneity, the presence of residual stresses and some other factors.

Table A.1 Structural properties (atomic or molecular weight, phase homogeneity region, system, type and space group of crystal structure, calculated and experimental densities)

Materials formula	Atomic or molecular weight	Phase homogeneity region ^a	Crystal structure		Type	Lattice parameters ^b , nm			Density, g cm ⁻³		
			System	Space group		a	c	c/a	Calculated (XRD)	Experimental ^d	
Elements											
C (graphite) ^e	12.01	–	Hexagonal	<i>P6₃/mmc</i>	Graphite	0.2464	0.6711	2.7236	4	2.267	2.26
Ir	192.22	–	Cubic (fcc)	<i>Fm(-3)m</i>	Cu	0.3839	–	–	4	22.56	22.45
Mo	95.94	–	Cubic (bcc)	<i>Im(-3)m</i>	W	0.3147	–	–	2	10.22	10.24
Nb	92.91	–	Cubic (bcc)	<i>Im(-3)m</i>	W	0.3301	–	–	2	8.578	8.59
Os	190.23	–	Hexagonal (hcp)	<i>P6₃/mmc</i>	Mg	0.2734	0.4320	1.580	2	22.60	22.48
Re	186.21	–	Hexagonal (hcp)	<i>P6₃/mmc</i>	Mg	0.2762	0.4457	1.614	2	21.01	21.00
Ta	180.95	–	Cubic (bcc)	<i>Im(-3)m</i>	W	0.3303	–	–	2	16.68	16.60
W	183.84	–	Cubic (bcc)	<i>Im(-3)m</i>	W	0.3165	–	–	2	19.25	19.20
Carbides											
HfC _{1-x}	184.74–190.26	0.02 ≤ x ≤ 0.48	Cubic (fcc)	<i>Fm(-3)m</i>	NaCl	0.4640	–	–	4	12.65	12.60
Nb _{2+x} C	200.62–262.87	0.03 ≤ x ≤ 0.70	Hexagonal ^f	<i>P6₃/mmc</i>	NiAs	0.3127	0.4972	1.590	1	7.80	7.80
NbC _{1-x}	100.60–104.44	0.04 ≤ x ≤ 0.36	Cubic (fcc)	<i>Fm(-3)m</i>	NaCl	0.4470	–	–	4	7.80	7.75
Ta _{2+x} C	341.34–527.72	-0.18 ≤ x ≤ 0.85	Hexagonal ^g	<i>P6₃/mmc</i>	NiAs	0.3105	0.4935	1.589	1	15.05	14.90
TaC _{1-x}	187.80–192.72	0.02 ≤ x ≤ 0.43	Cubic (fcc)	<i>Fm(-3)m</i>	NaCl	0.4457	–	–	4	14.50	14.45
ZrC _{1-x}	97.95–102.99	0.02 ≤ x ≤ 0.44	Cubic (fcc)	<i>Fm(-3)m</i>	NaCl	0.4700	–	–	4	6.60	6.60

^aThe max. variation in the non-metal content of refractory compounds within their temperature intervals of thermal stability according to the phase diagrams

^bConcerning the refractory compounds, it is given for the compositions with the min. deviation from the stoichiometry

^cNumber of formula units in the unit cell

^dPycnometric density

^e2H-Graphite (or α -carbon, α -graphite)

^fThe data are given for the high-temperature modification (Nb semicarbide phases undergo the phase transformations: α -Nb₂C ↔ β -Nb_{2+x}C at ~1200–1230 °C and β -Nb_{2+x}C ↔ γ -Nb_{2+x}C at ~2450–2575 °C, the temperatures of transformations depend on the phase compositions, see Sect. 4.1)

^gThe data are given for the high-temperature modification (Ta semicarbide phases undergo the phase transformation: α -Ta_{2+x}C ↔ β -Ta_{2+x}C at ~1930–2270 °C, the temperatures of transformations depend on the phase compositions, see Sect. 2.1)

Table A.2 Thermodynamic properties (standard heat of formation, standard molar entropy, molar and specific heat capacities)

Materials formula	Standard heat of formation $-\Delta H_{298}^\circ$ $\text{J mol}^{-1} \text{K}^{-1}$	Standard molar entropy S_{298}° $\text{J mol}^{-1} \text{K}^{-1}$	Molar heat capacity c_p , $\text{J mol}^{-1} \text{K}^{-1}$, at temperatures, K (°C)			Specific heat capacity c , $\text{J kg}^{-1} \text{K}^{-1}$, at temperatures, K (°C)							
			298 (25)	1000 (730)	2000 (1730)	3000 (2730)	4000 (3730)	298 (25)	1000 (730)	2000 (1730)	3000 (2730)	4000 (3730)	
C (graphite)	–	5.74	8.5	21.0	25.0	–	–	700	1750	2100	2200	–	
Ir	–	35.5	25.0	29.2	35.2	–	–	130	153	191	–	–	
Mo	–	28.6	24.0	28.7	36.9	41.8	–	250	300	385	435	–	
Nb	–	36.5	24.7	27.7	31.8	33.5	–	265	300	340	360	–	
Os	–	32.6	24.9	27.5	31.2	34.9	37.7	130	145	164	183	198	
Re	–	36.5	25.5	29.0	34.9	42.3	46.0	138	156	188	227	247	
Ta	–	41.5	25.4	27.9	31.0	44.1	–	140	154	171	244	–	
W	–	32.8	24.3	27.6	32.3	37.2	41.8	132	150	176	202	227	
					Elements								
					Carbides ^a								
HfC _{1-x}	235	41.2	37.5	51.6	58.0	63.6	69.2	197	271	305	336	364	
Nb _{2+x} C	195	64.0	63.5	81.1	88.3	94.2	–	317	404	440	470	–	
NbC _{1-x}	141	37.3	36.8	51.2	60.0	66.7	72.5	352	490	575	639	694	
Ta _{2+x} C	208	81.6	61.0	79.5	94.1	108.1	–	163	213	252	289	–	
TaC _{1-x}	145	42.3	36.8	51.1	59.1	66.9	74.2	191	267	307	347	385	
ZrC _{1-x}	197	33.3	37.9	53.4	57.4	60.9	76.2	368	518	557	591	740	

^aAll the data are given for the pure near-stoichiometric compositions

Table A.3 Thermodynamic properties (molar and specific enthalpies (heats) of melting/vaporization, molar and specific enthalpy differences)

Materials formula	Enthalpy (heat) of melting ^a		Enthalpy (heat) of vaporization ^b		Molar enthalpy differences $H_T - H_{298}$, kJ mol ⁻¹ , at temperatures, K (°C)		Specific enthalpy differences $H_T - H_{298}$, kJ kg ⁻¹ , at temperatures, K (°C)									
	Molar, kJ mol ⁻¹	Specific, MJ kg ⁻¹	Molar, MJ mol ⁻¹	Specific, MJ kg ⁻¹	1000 (730)	2000 (1730)	3000 (2730)	4000 (3730)	5000 (4730)	6000 (5730)						
C (graphite)	146	0.71	59.1	12.8	36.6	62.8	—	—	1067	3050	5230	—	—	—		
Ir	41.1	0.214	0.60	3.14	18.9	52.0	118.2	160.1	—	98.3	271	615	833	—		
Mo	37.5	0.290	0.60	6.16	18.5	51.0	123.6	165.4	799	856	192.2	531	1288	1723	8324	8920
Nb	30.0	0.315	0.69	7.32	18.5	48.2	108.2	141.7	175	892	198.5	518	1164	1525	1884	9598
Os	57.9	0.304	0.73	3.84	18.4	47.7	80.7	149.4	187	962	96.6	251	424	786	983	5058
Re	34.1	0.178	0.70	3.74	19.2	51.0	89.5	167.9	214	—	103.0	274	481	902	1149	—
Ta	36.6	0.200	0.75	4.15	19.0	48.2	83.6	150.6	186	—	104.9	266	462	832	1029	—
W	52.3	0.220	0.80	4.33	18.3	48.1	83.8	158.6	200	—	99.3	262	456	867	1090	—
Elements																
HfC _{1-x}	—	—	1.57 ^d	8.24 ^d	32.7	87.7	148.5	214.8 ^e	—	—	171.8	461	780	1128	—	—
Nb _{2+x} C	—	—	—	—	52.4	139.7	229.6 ^f	—	—	—	261.2	696	1144	—	—	—
NbC _{1-x}	92.0 ^g	0.881 ^g	~0.7 ^h	~6.7 ^h	32.6	88.4	151.4	313.6	386	458	312.3	847	1450	2998	3697	4387
Ta _{2+x} C	—	—	2.48 ^d	6.63 ^d	51.0	137.9	239.0	353.7 ^e	—	—	136.4	369	639	946	—	—
TaC _{1-x}	105.0 ^g	0.545 ^g	—	—	32.5	87.7	150.6	221.0	285	352	168.7	455	782	1147	1479	1827
ZrC _{1-x}	83.7 ^{g,i}	0.813 ^g	0.61 ^{d,j}	5.92 ^d	34.3	89.9	149.0	291.0	408	487	333.0	873	1447	2825	3961	4728
Carbides ^c																

(continued)

Table A.3 (continued)

^aFor refractory metals molar and specific enthalpies (heats) of melting are given at the melting points

^bFor refractory metals molar and specific enthalpies (heats) of vaporization are given at the boiling points

^cAll the data are given for the pure near-stoichiometric compositions

^dAt 298.15 K

^eExtrapolated data

^fExtrapolated data (for middle-temperature modification β - Nb_{2+x}C)

^gAt the melting point

^hThe approximate value for the vaporization (dissociation) process of NbC_{1-x} (crystal) = NbC_{1-x-y} (crystal) + $y\text{C}$ (gas) at 2800 K (2530 °C)

ⁱMolar enthalpy (heat) of melting at 298.15 K is 79.5 kJ mol⁻¹

^jMolar enthalpy (heat) of vaporization (dissociation) is 1.52 kJ mol⁻¹ (the value was measured on the basis of Langmuir mode, but also calculated in accordance to the second law of thermodynamics as a sum of average partial enthalpies (heats) of vaporization of C_1 (gas) and Zr (gas) from $\text{ZrC}_{-1,0}$)

Table A.4 Thermal properties (melting and boiling points, coefficients of linear thermal expansion, relative thermal expansion and thermal conductivity)

Materials formula	Melting point, K (°C)	Boiling point, K (°C)	Average coefficient of linear thermal expansion, 10^{-6} K^{-1}	Relative thermal expansion, %				Thermal conductivity, $\text{W m}^{-1} \text{ K}^{-1}$, at temperature, K (°C)							
				20–1700 °C	1000 (730)	1500 (1230)	2000 (1730)	2500 (2230)	3000 (2730)	290 (20)	1000 (730)	1500 (1230)	2000 (1730)	2500 (2230)	3000 (2730)
Elements															
C (graphite ^a)	4200 (3930) ^b	4200 (3930) ^b	2.5–3.5	5.1–5.8	0.25–0.30	0.50–0.58	0.80–0.92	1.13–1.28	1.47–1.70	100–200	60–70	45–60	35–50	35–45	3000
C (graphite ^c)	4200 (3930) ^b	4200 (3930) ^b	0–20	1.5–25	0.08–1.30	0.19–2.40	0.32–3.60	0.49–4.90	–	3–1000	1.5–200	1–150	0.7–100	0.5–70	–
Ir	2720 (2450)	4700 (4430)	6.8	9.2	0.52	0.98	1.55	2.18 ^d	–	145	130	115 ^e	110	100 ^d	–
Mo	2890 (2620)	5100 (4830)	5.4	6.7	0.38	0.74	1.15	1.66	–	135	115	95	80	70	–
Nb	2740 (2470)	5020 (4750)	7.1	8.9	0.56	1.02	1.52	2.00	–	50	60	70	80	90	–
Os	3320 (3050)	5300 (5030)	6.1	~9	0.32 (?)	–	–	–	–	88 ^f	85 ^f	84 ^f	85 ^f	~80	–
Re	3450 (3180)	5870 (5600)	6.6	7.0	0.47	0.85	–	–	–	70	56 ^e	50	45	42	–
Ta	3270 (3000)	5700 (5430)	6.5	7.7	0.50	0.88	1.32	1.82	2.40	60	70	76	80	84	–
W	3680 (3410)	6000 (5730)	4.3	5.0	0.32	0.52	0.88	1.20	1.60	160	120	105	100	95	92
Carbides ^h															
HfC _{1-x}	4220 (3950)	5670 (5400)	5.7	7.0	0.47	0.82	1.19	1.56	1.98	15	21	27	33	39	45
Nb _{2+x} C	3350 (3080)	–	3.4/9/15.7 ⁱ	8.6/9.8 ^j	–	–	–	–	–	12 (?)	–	–	–	–	–
NbC _{1-x}	3870 (3600)	5275 (5000)	6.4	7.3	0.46	0.84	1.28	1.77	2.32	18	25	32	38	43	47
Ta _{2+x} C	3610 (3335)	5740 (5465)	4.2/2.7 ^k	–	–	–	–	–	–	35	–	–	–	–	–
TaC _{1-x}	4260 (3990)	5770 (5500)	5.8	7.0	0.44	0.80	1.20	1.65	2.14	25	30	34	37	39	41
ZrC _{1-x}	3760 (3490)	5370 (5100)	4.5	7.1	0.45	0.85	1.30	1.77	2.27	35	25	30	32	35	40

(continued)

Table A.4 (continued)

^aHigh quality pure industrial polycrystalline (quasi-isotropic) graphite

^bTotal gas pressure over the solid/liquid surface – 10 MPa

^cHighly oriented pyrolytic graphite (HOPG)

^dExtrapolated values

^eInterpolated value

^fAverage values; in different directions the minimal and maximal values are 76 and 111 W m⁻¹ K⁻¹ at 1000 (730) K (°C), 75 and 110 W m⁻¹ K⁻¹ at 1500 (1230) K (°C), 77 and 107 W m⁻¹ K⁻¹ at 2000 (1730) K (°C)

^gAverage value; in different directions the minimal and maximal values are 54 and 60 W m⁻¹ K⁻¹

^hAll the data are given for the pure near-stoichiometric compositions

ⁱThe experimental data for the low-temperature modification α -Nb₂C are given for its main crystallographic directions: *a/b/c*, respectively

^jThe experimental data for the middle-temperature modification β -Nb_{2+x}C given for its main crystallographic directions (for *a* – in the numerator and for *c* – in the denominator, respectively) were extrapolated to the region of higher temperatures

^kThe experimental data for the low-temperature modification α -Ta_{2+x}C are given for its main crystallographic directions: for *a* – in the numerator and for *c* – in the denominator, respectively

Table A.5 Thermal properties (vapour pressure and vaporization rate)

Materials formula	Temperature, K (°C), corresponding to vapour pressure over materials surface, Pa					Temperature, K (°C), corresponding to mass vaporization rate, kg m ⁻² s ⁻¹					Temperature, K (°C), corresponding to linear vaporization rate, m s ⁻¹						
	10 ⁻⁷	10 ⁻⁵	10 ⁻³	10	10 ³	10 ⁵	10 ¹⁰	10 ⁸	10 ⁶	10 ⁻⁴	10 ⁻²	10 ⁻¹⁴	10 ⁻¹²	10 ⁻¹⁰	10 ⁻⁸	10 ⁻⁶	
Elements																	
C (graphite)	1790 (1520)	1950 (1680)	2160 (1890)	2410 (2140)	2740 (2470)	3170 (2900)	3790 (3520)	2000 (1730)	2200 (1930)	2450 (2180)	2800 (2530)	3300 (3030)	1950 (1680)	2130 (1860)	2360 (2090)	2700 (2430)	3100 (2830)
Ir	1750 (1480)	1940 (1670)	2190 (1920)	2510 (2240)	—	—	—	—	—	—	—	—	—	—	—	—	—
Mo	1750 (1480)	1960 (1690)	2210 (1940)	2550 (2280)	3010 (2740)	3770 (3500)	~5100 (~4830)	1750 (1480)	1960 (1690)	2230 (1960)	2560 (2290)	3020 (2750)	1750 (1480)	1960 (1690)	2220 (1950)	2560 (2290)	3030 (2760)
Nb	1930 (1660)	2120 (1850)	2380 (2110)	2720 (2450)	3220 (2950)	3940 (3670)	~4530 (~4260)	1930 (1660)	2130 (1860)	2400 (2130)	2750 (2480)	3250 (2980)	1930 (1660)	2130 (1860)	2390 (2120)	2740 (2470)	3230 (2960)
Os	~1880 (~1610)	~2090 (~1820)	~2370 (~2100)	~2700 (~2430)	~3160 (~2890)	~3850 (~3580)	~4880 (~4610)	~1870 (~1600)	~2080 (~1810)	~2350 (~2080)	~2700 (~2430)	>3150 (>2880)	~1910 (~1640)	~2120 (~1850)	~2410 (~2140)	~2780 (~2510)	~3270 (~3000)
Re	2070 (1800)	2320 (2050)	2630 (2360)	3040 (2770)	3610 (3340)	4460 (4190)	~5920 (~5650)	2060 (1790)	2300 (2030)	2620 (2350)	3040 (2770)	—	2100 (1830)	2350 (2080)	2680 (2410)	3120 (2850)	—
Ta	2110 (1840)	2350 (2080)	2650 (2380)	3050 (2780)	3590 (3320)	4350 (4080)	~5700 (~5430)	2100 (1830)	2340 (2070)	2650 (2380)	3020 (2750)	—	2130 (1860)	2360 (2090)	2670 (2400)	3070 (2800)	—
W	2250 (1980)	2500 (2230)	2820 (2550)	3220 (2950)	3760 (3490)	4520 (4250)	5800 (5530)	2230 (1960)	2480 (2210)	2810 (2540)	3220 (2950)	—	2270 (2000)	2520 (2250)	2860 (2590)	3290 (3020)	—

(continued)

Table A.5 (continued)

Materials formula	Temperature, K (°C), corresponding to vapour pressure over materials surface, Pa				Temperature, K (°C), corresponding to mass vaporization rate, kg m ⁻² s ⁻¹				Temperature, K (°C), corresponding to linear vaporization rate, m s ⁻¹								
	10 ⁻⁷	10 ⁻⁵	10 ⁻³	10 ⁻¹	10 ³	10 ⁵	10 ⁷	10 ⁹	10 ⁻⁶	10 ⁻⁴	10 ⁻²	10 ⁻¹⁴	10 ⁻¹²	10 ⁻¹⁰	10 ⁻⁸	10 ⁻⁶	
HfC _{1-x}	2080 (1810)	2270 (2000)	2550 (2280)	2920 (2650)	3410 (3140)	-	~5670 (~5400)	2070 (1800)	2260 (1990)	2530 (2260)	2910 (2640)	3400 (3130)	2030 (1760)	2270 (2000)	2550 (2280)	2920 (2650)	3410 (3140)
Nb _{2+x} C ^b	-	-	-	-	-	-	-	-	-	-	-	-	-	-	-	-	-
NbC _{1-x}	~1790 (~1520)	~2050 (~1780)	~2400 (~2130)	2770 (2500)	3570 (3300)	-	~5275 (~5000)	~1710 (~1440)	2020 (1750)	2460 (2190)	~3140 (~2870)	-	~1690 (~1420)	1990 (1720)	2440 (2170)	~3120 (~2850)	-
Ta _{2±x} C	-	-	-	-	-	-	-	-	~2420 (~2150)	~2730 (~2460)	~3130 (~2860)	~3660 (~3390)	-	~2440 (~2170)	~2760 (~2490)	~3170 (~2900)	~3710 (~3440)
TaC _{1-x}	~1890 (~1620)	~2140 (~1870)	2470 (2200)	2910 (2640)	~3540 (~3270)	-	-	~1940 (~1670)	2210 (1940)	2570 (2300)	~3070 (~2800)	-	~1950 (~1680)	2220 (1950)	2590 (2320)	~3090 (~2820)	-
(C/Ta) ^c	/2490	/2760	/3100	/3550	-	-	-	-	-	-	-	-	-	-	-	-	-
ZrC _{1-x}	~1970 (~1700)	~2190 (~1920)	2480 (2210)	2850 (2580)	~3340 (~3070)	-	~5370 (~5100)	~1960 (~1690)	2190 (1920)	2460 (2190)	~2820 (~2550)	~3330 (~3060)	~1940 (~1670)	2160 (1890)	2440 (2170)	~2790 (~2520)	~3250 (~2980)
(C/Zr) ^d	/~1950	/~2170	/2460	/2810	/~3280	-	-	-	-	-	-	-	-	-	-	-	-
	(~1680) ^d	(~1900) ^d	(2190) ^d	(2540) ^d	(~3010) ^d	-	-	-	-	-	-	-	-	-	-	-	-

^aAll the data are given for the pure near-stoichiometric compositions

^bNo data on the vaporization of Nb_{2+x}C phases are available

^cThe vapour pressures over TaC_{1-x} materials surface are given separately; in the numerator for C and in the denominator for Ta

^dThe vapour pressures over ZrC_{1-x} materials surface are given separately; in the numerator for C and in the denominator for Zr

Table A.6 (continued)

- ^aMeasured on non-oxidized surfaces
- ^bMeasured at room temperature
- ^cHigh quality industrial polycrystalline (quasi-isotropic) graphite with high purity
- ^dHighly oriented pyrolytic graphite (HOPG)
- ^eInterpolated data
- ^fAverage value; in different directions the minimal and maximal values are 270 and 430 nΩ m, respectively
- ^gAll the data are given for the pure near-stoichiometric compositions
- ^hThe experimental data were extrapolated to the region of lower temperatures
- ⁱThe experimental data were extrapolated to the region of higher temperatures

Table A.7 Physico-mechanical properties (hardness, tensile and compressive strengths and Young's modulus)

Materials formula	Hardness ^a <i>HV</i> , GPa, at temperature, K (°C)		Ultimate tensile strength ^b , MPa, at temperature, K (°C)		Ultimate compressive strength, MPa, at temperature, K (°C)				Young's modulus, GPa, at temperature, K (°C)									
	290 (20)	1000 (730)	2500 (1730)	290 (730)	1000 (730)	2500 (1730)	290 (730)	1000 (730)	1500 (1230)	2000 (1730)	2500 (2230)	290 (730)	1000 (730)	1500 (1230)	2000 (1730)	2500 (2230)		
C (graphite ^c)	0.3–1.0	0.3–1.0	0.4–1.0	6.4–10.0	7.8–15.0	8.8–18.0	10–21	~22	–	68	70	75	95	2.6–8.0	3.3–8.5	4.0–9.5	5.1–10.2	
	1.4–3.7	–	–	5–170	~140 ^e –~160 ^e	120–170 ^e	150–190 ^e	~350 ^e	–	120–470	150–470	170–470	~200	–	~3–40	10–28 ^e	~26–24 ^e	18–21 ^e
Ir	2.0–17.2	~1	–	500–1100	–	–	~75	~20	–	–	–	–	–	52.5–540	–	<420	–	
Mo	1.6–4.0	~0.7	~0.45	~0.14	~0.045	250–800	25–80	~7	–	–	–	–	–	320–330	280–300	~250	~200	
Nb	0.7–2.5	~0.7	~0.12	~0.04	~0.006	200–700	160–300	~20	–	–	–	–	–	104–110	~105	~105	–	
Os	3.0–10.0 ^f	~1.9–4.0 ^f	~1.3–4.0 ^f	–	–	2000–7200 ^f	–	–	–	1000–3600	–	–	–	~560	~500	–	–	
Re	1.3–8.0	~2.0 ^g	~1.25	–	500–2300	500–700	300–400	50–100	~20	–	–	–	–	460–520	~390	~330	–	
Ta	0.4–3.0	~0.5 ^g	~0.2	–	200–1000	~190–85	~35	~15	<6	–	–	–	–	~185	–	–	–	
W	1.4–6.0	0.9–1.6	0.6–1.2	0.3–0.5	~0.1	300–1900	180–800	100–350	60–140	~15	–	–	–	400–415	370	350	330	250

(continued)

Table A.8 Nuclear physical properties (isotopic mass range, total number of isotopes, thermal neutron macroscopic cross sections, moderating ability and capture resonance integral)

Materials formula	Isotopic mass range (minimal and maximal mass numbers)	Total number of isotopes (stable or nearly stable / radioactive / metastable isomers)	Macroscopic (microscopic) thermal neutron cross sections ^a , cm ⁻¹ (b)		Neutron moderating ability (macroscopic slowing-down power) ^b $\xi \Sigma_s, 10^{-3}$	Resonance integral for neutron capture $I_{r,b}$
			$\Sigma_a (\sigma_a)$	capture (absorption) $\Sigma_s (\sigma_s)$		
Elements						
C	8–22	15 (2/13/0)	$\sim 0.32 \times 10^{-3}$ (3.50×10^{-3})	~ 0.43 (~ 4.75)	~ 70	1.57×10^{-3}
Ir	164–199	68 (2/34/32)	29.9 (425.3)	0.984 (14.0)	–	2150
Mo ^d	83–115	41 (7/26/7)	0.163 (2.51–2.55)	0.368 (5.71)	9.27	24
Nb (⁹³ Nb)	81–113	58 (1/32/25)	0.064 (1.15)	0.348 (6.255)	5.82	8.5
Os	162–197	45 (7/28/10)	1.14 (16.0)	1.05 (14.7)	8.2	180
Re ^e	160–194	56 (2/33/21)	6.09 (89.7)	0.781 (11.5)	14.2	831
Ta (¹⁸¹ Ta)	155–190	73 (1/35/37)	1.14 (20.6)	0.333 (6.01)	3.04	660
W ^f	158–192	46 (5/30/11)	1.16 (18.4)	0.292 (4.60)	3.35	352
Carbides ^g						
HfC _{1-x}	153–188 / 8–22	63 (5/31/27) ^h	4.17 (52.6) ⁱ	~ 0.59 (7.5) ⁱ	–	–
Nb _{2+x} C	81–113 / 8–22	58 (1/32/25) ^h	0.055 (0.77) ⁱ	~ 0.41 (5.8) ⁱ	–	–
NbC _{1-x}	81–113 / 8–22	58 (1/32/25) ^h	0.052 (0.59) ⁱ	~ 0.49 (5.5) ⁱ	–	–
Ta _{2+x} C	155–190 / 8–22	73 (1/35/37) ^h	1.00 (13.7) ⁱ	~ 0.41 (5.6) ⁱ	–	–
TaC _{1-x}	155–190 / 8–22	73 (1/35/37) ^h	0.93 (10.4) ⁱ	~ 0.48 (5.4) ⁱ	–	–
ZrC _{1-x}	78–110 / 8–22	39 (5/28/6) ^h	7.27×10^{-3} (0.095) ⁱ	~ 0.43 (5.6) ⁱ	35.8	–

^aFor 2200 m s⁻¹ neutrons

^b ξ – the average logarithmic decrement (or the average change in the logarithm of neutron energy per collision)

Table A.8 (continued)

^cTotal bound scattering cross sections

^dFor ⁹⁸Mo: $\sigma_a = 0.127$ b and $\sigma_s = 5.44$ b, for ⁹⁶Mo: $\sigma_a = 0.5$ b and $\sigma_s = 4.83$ b, for ⁹⁵Mo: $\sigma_a = 13.1$ b and $\sigma_s = 6.5$ b, for ⁹²Mo: $\sigma_a = 0.019$ b and $\sigma_s = 6$ b

^eFor ¹⁸⁷Re $\sigma_a = 76.4$ b and $\sigma_s = 11.9$ b, for ¹⁸⁵Re $\sigma_a = 112$ b and $\sigma_s = 10.7$ b

^fFor ¹⁸⁴W: $\sigma_a = 1.7$ b and $\sigma_s = 7.03$ b, for ¹⁸⁶W: $\sigma_a = 37.9$ b and $\sigma_s = 0.065$ b, for ¹⁸²W: $\sigma_a = 20.7$ b and $\sigma_s = 6.1$ b, for ¹⁸³W: $\sigma_a = 10.1$ b and $\sigma_s = 5.7$ b, for ¹⁸⁰W: $\sigma_a = 30$ b and $\sigma_s = 3$ b

^gAll the data are given for the pure near-stoichiometric compositions

^hThe data are given for the metals forming refractory compounds

ⁱThe formula $\sigma_T = [\sigma_{Me} + (1 - x)\sigma_C]/(2 - x)$ was used to calculate the normalized thermal neutron cross sections for monocarbide MeC_{1-x} compositions

^jThe formula $\sigma_T = [(2 \pm x)\sigma_{Me} + \sigma_C]/(3 \pm x)$ was used to calculate the normalized thermal neutron cross sections for semicarbide Me_{2±x}C compositions

Table A.9 Chemical properties (character of interaction with some chemical reagents in the aqueous solutions at room temperature)

Materials formula	Chemical reagents (formulae, concentrations) ^a																						
	HCl		H ₂ SO ₄		HNO ₃		H ₃ PO ₄		HF		HCl + HNO ₃		HF + HNO ₃		NH ₄ OH		NaOH		KOH		H ₂ O ₂		
	Diluted	Conc.	Diluted	Conc.	Diluted	Conc.	Diluted	Conc.	Diluted	Conc.	Diluted	Conc.	Diluted	Conc.	Diluted	Conc.	Diluted	Conc.	Diluted	Conc.	Diluted	Conc.	
C (graphite)	No	No	No	No	Slight ^b	Oxid.	Oxid.	Slight ^b	No	No	Oxid.	Oxid.	Oxid.	No	No	No	No	No	No	No	No	Slight ^b	
	No	No	No	No	No	No	No	No	No	No	No	No	No	No	No	No	No	No	No	No	No	No	
	No	Slight ^d	No	Slight ^d	Slight	Dissol. ^e	No ^f	Dissol.	Dissol.	Dissol.	Slight ^e	Slight ^e	Slight ^e	Dissol. ^g	No ^h	No ^h	Slight ⁱ	No ^j	No ^j	No ^j	Oxid.	Oxid.	
	No	No	No	No	No	No	No	No	No	No	No	No	No	Dissol.	No	No	No ^k	No ^k	No ^k	No ^k	No	No	No
	Os	No	No	No ^l	No ^l	Slight ^m	—	No	—	No	Slight ^m	—	—	—	No	No ^c	No ^c	No ^c	No ^c	No	No	—	—
	Re	No	No	Slight	Dissol.	Dissol.	Dissol.	—	—	No	Dissol.	Dissol.	Dissol.	Dissol.	Slight	No ⁿ	No ⁿ	No ⁿ	No ⁿ	No ⁿ	Oxid. ⁿ	Oxid. ⁿ	Oxid. ⁿ
	Ta	No	No	No	No	No	No	No	No	Slight	Slight	Slight	Slight	Dissol. ^g	No	No ^o	No ^o	No ^o	No ^o	No ^o	No	No	No
	W	No	No ^p	No	No ^p	Slight	Oxid.	Oxid.	No ^p	No ^q	No ^q	Slight ^m	Slight ^m	Dissol.	No ^h	No ^j	No ^j	No ^j	No ^j	No ^j	No ^j	Oxid.	Oxid.
	Carbides ^r																						
	HfC _{1-x}	No ^s	No	No ^s	No ^s	Slight ^t	Slight ^t	Slight ^t	Slight ^t	Decomp.	Decomp.	Decomp.	Decomp.	Decomp.	—	No	—	—	—	—	—	No	No
Nb _{2+x} C	No	No	No	No	—	—	—	—	Decomp.	Decomp.	—	—	—	—	—	—	—	—	—	—	—	No	No
NbC _{1-x}	No	No ^s	No	No ^t	Slight	No ^s	Slight	Slight	Decomp.	Decomp.	Slight ^t	Slight ^t	Decomp.	—	No	—	—	—	—	—	No	No	Decomp.
Ta _{2+x} C	No	No	No	No	—	—	—	—	Decomp.	Decomp.	—	—	—	—	—	—	—	—	—	—	—	No	No
TaC _{1-x}	No	No	No	No ^t	No	No	No	No	Decomp.	Decomp.	No	Decomp.	Decomp.	No	No	No	No	No	No	No	No	No ^s	No
ZrC _{1-x}	No	No	No ^s	No ^t	Slight ^t	Slight ^t	Slight ^t	Slight ^t	Decomp.	Decomp.	Decomp.	Decomp.	Decomp.	—	No ^u	No ^u	No ^u	No ^u	No ^u	No ^u	No ^u	No	No

^aThe accepted abbreviations: Conc.—concentrated, Oxid.—oxidation, Dissol.—dissolution, Decomp.—decomposition^bOxidized electrochemically^cThe slight interaction in the melts

Table A.9 (continued)

- ^dThe slight dissolution while heating
- ^eBy heating the dissolution intensifies considerably
- ^fThe interaction in the presence of O₂ or some oxidizers
- ^gThe intensive interaction is observed
- ^hThe interaction initiates only in the presence of H₂O₂
- ⁱThe intensive interaction in the presence of oxidizers
- ^jThe interaction with the melts in the presence of O₂
- ^kThe oxidation in the melts
- ^lThe interaction in the presence of O₂
- ^mThe dissolution while heating
- ⁿThe interaction while heating
- ^oThe interaction in the melts
- ^pThe slight interaction while heating
- ^qThe dissolution in the presence of oxidizers
- ^rAll the data are given for the pure near-stoichiometric compositions
- ^sThe partial decomposition while heating
- ^tThe complete decomposition while heating
- ^uThe partial decomposition in the melts

Table A.11 General formulae for the relationships between the various physical properties (thermal conductivity, electrical resistance, strength and elastic characteristics) and porosity of the materials prepared by powder metallurgy methods (sintering, hot pressing, spark plasma sintering and others)

Mathematical expression	Designations	Formula number	Authors
$\lambda = \lambda_0(1 - P)/(1 + 0.5P)$ (universal formula, for matrix systems)	Thermal conductivity, λ^a λ_0 – thermal conductivity of poreless materials, P – volume fraction of porosity	(A.1)	Maxwell and Eucken
$\lambda = \lambda_0(1 - P)$ (applied for refractory carbides, nitrides and oxides)	“ “	(A.2)	Kingery and Loeb
$\lambda = \lambda_0(1 - 1.2P)$ (applied for refractory carbides and oxides)	“ “	(A.3)	Moore and McElroy
$\lambda = \lambda_0(1 - 1.5P)$ (universal formula, for statistical mixture, $0 < P \leq 2/3$)	“ “	(A.4)	Odelevskii
$\lambda = \lambda_0(1 - P)/(1 + P)$ (universal formula, for lengthened pores)	“ “	(A.5)	Odelevskii
$\lambda = \lambda_0(1 - P^{2/3})$ (universal formula)	“ “	(A.6)	Kämpf and Karsten
$\lambda = \lambda_0(1 - P^{2/3})/(1 - P^{2/3} + P)$ (universal formula)	“ “	(A.7)	Kämpf and Karsten
$\lambda = \lambda_0(1 - P)^{3/2}$ (universal formula, for isolated spherical pores)	“ “	(A.8)	Balshin
$\lambda = \lambda_0(1 - P)^2$ (universal formula, for interconnected pores)	“ “	(A.9)	Balshin

(continued)

Table A.11 (continued)

Mathematical expression	Designations	Formula number	Authors
$\lambda = \lambda_0(1 - P)^{5/3}$ (universal formula, for cylindrical pores)	" "	(A.10)	Ondracek et al.
$\lambda = \lambda_0 a(1 - P)$ (proposed for highly porous materials)	a – proportionality constant	(A.11)	Ashby
$\lambda = \lambda_0 \xi(1 - 1.5P)$ (universal formula, for sintered solids with imperfect contacts)	$\xi \approx r/R$, where r – welding (sintered) neck radius and R – particle radius	(A.12)	Skorokhod
$\lambda = \lambda_0(1 - P)^n$ with $n = a/2b + (1 - a)/(1 - b)$ (universal formula, for isolated closed pores with various forms)	a and b – stereometric parameters: orientation and form factors, respectively	(A.13)	Ondracek et al.
$\lambda = \lambda_0(1 - P)/(1 + aP^2)$ (applied for high-temperature materials)	a – constant (for δ -TiN _{1±x} : $a = 6$; for polycrystalline graphite and α -Al ₂ O ₃ : $a = 10$)	(A.14)	Aivazov and Domashnev
$\lambda = \lambda_0(1 - aP + bP^2)$ (applied for refractory metals and compounds)	a and b – constants (for metallic W: $a = 1.56$, $b = 0.311$; for ZrC _{1-x} ($0 < x \leq 0.35$) and NbC _{1-x} ($0.02 \leq x \leq 0.30$): $a = 0.3$ and $b = -5.5$)	(A.15)	Kulcinski et al.
$\rho = \rho_0(1 + 0.5P)/(1 - P)$ (universal formula)	Electrical resistivity, ρ	(A.16)	Maxwell
$\rho = \rho_0(1 + P)/(1 - P)$ (universal formula, for lengthened pores)	ρ_0 – electrical resistance of poreless materials	(A.17)	Odelevskii
$\rho = \rho_0(1 + aP^2)/(1 - P)$ (applied for high-temperature materials)	" "	(A.18)	Aivazov and Domashnev
$\rho = \rho_0(1 + aP + bP^2)$ (applied for refractory metals)	a – constant (for polycrystalline graphite: $a = 8$) a and b – constants (for metallic W: $a = 1.83$, $b = 5.37$)	(A.19)	Kulcinski et al.

(continued)

Table A.11 (continued)

Mathematical expression	Designations	Formula number	Authors
$\sigma = \sigma_0 \exp(-aP)$ (universal formula, for $P \leq 0.5$)	Strength characteristics, σ σ_0 – strength of poreless materials, a – constant (without a clear correlation to the porosity structure)	(A.20)	Ryshkewitch and Duckworth
$\sigma = \sigma_0(1 - aP)$ (universal formula)	a – constant (determined experimentally, without a clear correlation to the porosity structure; for sintered $ZrC_{0.99}$: $a = 2.8$ (for flexural strength) and 3.3 (for compressive strength))	(A.21)	Hasselman
$\sigma = \sigma_0(1 - P)^n$ (universal formula, proposed for sintered metallic materials)	n – exponential constant ($3 \leq n \leq 10$)	(A.22)	Balshin
$\sigma = \sigma_0(1 - P)^n$ (proposed for highly porous materials)	a – proportionality constant dependent on the pore geometry and n – exponential constant dependent on the pore morphology (for interconnected porosity $n = 2$)	(A.23)	Ashby
$\sigma = \sigma_0(1 + aP)/(1 - (a + 1)P)$ (proposed and applied for refractory materials)	a – constant (determined experimentally)	(A.24)	Hasselman
$\sigma = \sigma_0(1 - P)/(1 + aP)$ (proposed and applied for refractory materials)	a – constant (determined experimentally)	(A.25)	Weil
$\sigma = \sigma_0(1 - 1.5P(1 + 2a) + 4.5aP^2)$ (proposed for sintered metallic materials)	a – attenuation coefficient	(A.26)	Pines
$\sigma = \sigma_0[(1 - A)^3/(A^3 + (1 - A)^3)]$ with $A = (3P/4\pi)^{1/5} = r/l$ (proposed for materials with equal-sized pores)	r – radius of pores and l – distance between them	(A.27)	Harvey

(continued)

Table A.11 (continued)

Mathematical expression	Designations	Formula number	Authors
$\sigma = \sigma_0(1 - P)/(1 - 6.25P + aP/2^n \pi)^{1/m}$ (proposed for materials with low porosity ($P < 0.1$) and spherical pores)	a – constant and m – Weibull modulus	(A.28)	Peras and Dauknis
$\sigma = \sigma_0 \{ 1 - [1.5abP(6P/\pi b - 36P/\pi^2)^{1/2}] \}$ (proposed for sintered metallic materials) or $\sigma = \sigma_0[(1 - 1.5P)/(1 + 1.5a'P)]$ (in an approximate form for the practical application)	a – coefficient of the inhomogeneity of pores distribution within a cross-section, b – coefficient of the variation of porosity (for tension $b > 1$ and for compression $b < 1$) and a – parameter that determines the inhomogeneity of stresses within a cross-section (for most of sintered materials $a' \approx 2$)	(A.29)	Troshchenko
$\sigma = \sigma_0(1 - P^2)^2 \exp(-aP)$ (proposed for sintered metallic materials)	a – coefficient determined by the conditions of preparation and testing of the porous materials	(A.30)	Shcherban
$\sigma = \sigma_0[E(1 - P)/E_0]^{1/2}$ (proposed for sintered ceramic materials)	E_0 – Young's modulus of poreless materials	(A.31)	Camiglia
$\sigma = \sigma_0[1 - (P/P_0)^n]$ (applied for the evaluation of compressive strength of gypsum based materials)	n – exponential constant ($n = 3$ for spherical pores and $n = 2$ for cylindrical pores) and P_0 – percolation limit of solid (the porosity value corresponding to $\sigma = 0$)	(A.32)	Schiller
$\sigma = \sigma_0[1 - (P/P_0)^n][1 + a(P/P_0)^p]$ (applied for the evaluation of compressive strength of gypsum based materials)	a, n and p – empirically determined constants	(A.33)	Millard
$\sigma = 3\sigma_0(\xi^2/k)(1 - P)^{2/3}(1 - P_0)$ (applied for ultra-high temperature oxide materials produced from microspheres)	k – the coefficient of concentration of stresses in welding ligament formed due to sintering and $\xi \approx r/R$, where r – welding (sintered) neck radius and R – particle radius	(A.34)	Krasulin et al.

(continued)

Table A.11 (continued)

Mathematical expression	Designations	Formula number	Authors
$E = E_0(1 - P)^3$ (proposed for sintered metallic materials)	Young's modulus, E E_0 – Young's modulus of poreless materials n – exponential constant ($0.5 \leq n \leq 4$, dependent on the tortuosity of the porous structure; for hot-pressed SiC: $n = 3.80$; for Si_3N_4 based materials: $n = 2.6$ – 5.5 ; for UO_{2+x} : $n = 2.27$; for RE oxide materials: $n = 2.0$ – 2.5 , α - Al_2O_3 ; $n = 2.14$; β - Al_2O_3 ; $n = 4.12$) a – proportionality constant dependent on the pore geometry and n – exponential constant dependent on the pore morphology (for cellular materials with open pores (cells) $n = 2$ and with closed pores (cells) $n = 3$) a – constant ($1.4 \leq a \leq 9.0$, determined experimentally, without a clear correlation to the porosity structure; for β -SiC: $a = 2.73$; for B_{4+x}C : $a = 5.46 \pm 0.30$; for AlN: $a = 2.44$; for α - HfO_{2-x} : $a = 4.17$; for MgO: $a = 4.75$; for UO_{2+x} : $a = 2.51$; for α - Al_2O_3 : $a = 1.60$ – 4.35)	(A.35)	Balshin
$E = E_0(1 - P)^n$ (based on porous body modelling approach and applied for refractory materials)			(A.36)
$E = E_0a(1 - P)^n$ (proposed for highly porous materials)		(A.37)	Ashby
$E = E_0 \exp(-aP)$ (universal formula, for $P \leq 0.5$)		(A.38)	Spriggs

(continued)

Table A.11 (continued)

Mathematical expression	Designations	Formula number	Authors
$E = E_0(1 - aP)$ (universal formula)	a – constant (determined experimentally, without a clear correlation to the porosity structure; for UC_{1+x} : $a = 1.9-2.3$; for UN_{1-x} : $a = 2.0-2.7$; for UO_{2+x} : $a = 2.28$; for $\alpha/\beta\text{-Hf(Y)O}_{2-x}$: $a = 2.60$; for $\beta\text{-Hf(Er)O}_{2-x}$: $a = 2.17$; for MgO : $a = 2.7-4.9$; for RE oxide materials: $a = 2.4-2.5$; for glass materials: $a = 2.06$)	(A.39)	Hasselman
$E = E_0 \exp[-a(1 - P)]$ (universal formula, for $P \geq 0.5$)	a – constant (determined experimentally, without a clear correlation to the porosity structure)	(A.40)	Rice
$E = E_0(1 - aP)/(1 + bP)$ (universal formula)	a and b – constants (determined experimentally, without a clear correlation to the porosity structure)	(A.41)	Hasselman
$E = E_0 \exp[-(aP + bP^2 + cP^3 + \dots)]$ (based on a model for packing equal-sized spheres) or $E = E_0 \exp[-(aP + bP^2)]$ (in an approximate form applied for refractory materials)	a, b, c, \dots – non-negative constants (additional high-order terms can be included in the exponential polynomial for wider porosity ranges and for improved accuracy; for $\alpha\text{-Al}_2\text{O}_3$ ($0.05 \leq P \leq 0.32$): $a = 1.46$ and $b = 9.82$)	(A.42)	Wang
$E = E_0(1 + aP + bP^2)/(1 + cP)$ (based on the dependence of sound velocity on the elastic properties of materials)	a, b and c – constants dependent on the shape and size of the average pore and the properties of poreless materials	(A.43)	Kupkova

(continued)

Table A.11 (continued)

Mathematical expression	Designations	Formula number	Authors
$E = E_0(1 - aP)^n$ (based on porous body modelling approach and applied for refractory materials)	a and n – semi-empirical constants; packing geometry factor and grain morphology/pore geometry parameter, respectively (for SiC: $a = 1.0$ and $n = 3.8$; for Si_3N_4 based materials: $a = 1.0$ – 2.3 and $n = 1.1$ – 2.6 ; for UO_{2+x} : $a = 1.0$ – 3.9 and $n = 4.1$; for α - Al_2O_3 : $a = 1.0$ – 3.9 and $n = 0.7$ – 3.4 ; for β - Al_2O_3 : $a = 1.0$ and $n = 4.1$; for RE oxide materials: $a = 1.9$ – 2.7 and $n = 0.7$ – 1.3) $a = 1.21$ and $n = 2/3$	(A.44)	Phani and Niyogi
$E = E_0(1 - aP^m)$ (universal formula, for spherical pores, $P \leq 0.5$) $E = E_0\{1 - \pi b(9aP^2/16\pi^2)^{1/3}[1 + (1/a^2 - 1)]^{1/2}\}$ (proposed for the pores of various shapes in isotropic materials)	$a = z/x$ – the shape factor, defined by the axial ratio of the substitutional spheroids, and $b = \cos^2\alpha$ – the orientation factor, where α is the angle between the stress direction and the rotational axis of the substitutional spheroid (for isotropically oriented porosity: $a = 4.5$ and $b = 0.33$) “ “ “ “	(A.45)	Ondracek
$E = E_0(1 - P^{2/3})^{1.211\Gamma}$ with $\Gamma = a^{1/3}[1 + b(a^{-2} - 1)]^{1/2}$ (proposed for the pores of various shapes in isotropic materials)	a and n – empirical constants taking into account the effect of concentration of stresses by pores	(A.46)	Ondracek
$E = E_0(1 - P^{2/3})/(1 + aP^m)$ (proposed for materials prepared from refractory compounds (carbides, nitrides, borides and silicides) by powder metallurgy methods)	“ “ “ “	(A.47)	Boccacini and Ondracek
$E = E_0(1 - P^{2/3})(1 + P - P^{2/5})$ (based on physico-mechanical analysis for a matrix-inclusion model)	“ “ “ “	(A.48)	Frantsevich
	–	(A.49)	Paul

(continued)

Table A.11 (continued)

Mathematical expression	Designations	Formula number	Authors
$E = E_0(1 - aP + bP^2)$ (based on a model for packing equal-sized spheres and applied for ultra-high temperature carbide and oxide materials)	a and b – constants (without a clear correlation to the porosity structure, to be determined experimentally; for carbide materials: $a \approx 1.9$ – 2.0 and $b \approx 0.9$ – 1.0 , e.g. for ZrC_{1-x} : $a = 1.9$ and $b = 0.9$; for ThO_{2-x} : $a = 2.3$ – 2.7 ; for Y_2O_{3-x} : $a = 1.5$ and $b = -2.7$)	(A.50)	Knudsen et. al
$E = E_0(1 + aP/[1 - (a + 1)P])$ (proposed and applied for refractory materials)	a – constant (determined experimentally; for BeO: $a = -2.0$ – 2.8)	(A.51)	Hasselman
$E = E_0a(1 - P)^2/[P + a(1 - P)]$ (proposed and applied for refractory materials)	a – constant (parameter of structure, $0.4 \leq a \leq 1.0$)	(A.52)	Boccaccini and Fan
$E = E_0(1 - 15P(1 - v_0)/[(7 - 5v_0) + 2P(4 - 5v_0)])$ (based on physico-mechanical approach, applied for ultra-high temperature carbide and carbide-carbon materials)	v_0 – Poisson's ratio of poreless materials	(A.53)	Hashin
$E = E_0[1 - 15P(1 - v_0)/(7 - 5v_0)]$ (based on physico-mechanical approach with the assumption of independence of Poisson's ratio on porosity, applied for ultra-high temperature carbide materials)	“ “	(A.54)	Plyatt et al.
$E = E_0(1 - 3P(9 + 5v_0)(1 - v_0)/[2(7 - 5v_0)])$ (based on physico-mechanical approach with the assumption of independence of Poisson's ratio on porosity)	“ “	(A.55)	Hill
$E = E_0(1 - P)/[1 + (1 + v_0)(13 - 15v_0)/2P(7 - 5v_0)]$ (based on physico-mechanical approach and applied for ceramic materials)	“ “	(A.56)	Weil
$E = E_0(1 - P)^2/[1 + (1 - 5v_0)(3v_0 - 1)P/2(7 - 5v_0)]$ (proposed for an isolated spherical pore geometry)	“ “	(A.57)	Nielsen

(continued)

Table A.11 (continued)

Mathematical expression	Designations	Formula number	Authors
$E = E_0(1 - P)^2/[1 + P(2 - 3v_0)]$ (based on numerical experiments using the finite element method)	“ “	(A.58)	Ramakrishnan and Arunachalam
$E = 3E_0 \exp[-aP/(1 - P)] / (2(1 + v_0) \exp[-bP/(1 - P)] + (1 - v_0))$ (applied for ultra-high temperature carbide materials)	a and b – constants, which express the influence of the shape, size distribution and relative orientation of the pores on the stress conditions (for $ZrC_{0.91}$: $a = 3.26$ and $b = 1.06$; for $ZrC_{0.95}$: $a = 3.49$ and $b = 1.08$; for $NbC_{0.98}$: $a = 2.30$ and $b = 1.18$)	(A.59)	Ordanyan et al.
$G = G_0 \exp(-aP)$ (universal formula, applied for sintered ultra-high temperature oxide materials, for $P \leq 0.5$)	Coulomb's (shear) modulus, G G_0 – Coulomb's (shear) modulus of poreless materials, a – constant (determined experimentally, without a clear correlation to the porosity structure; for MgO $a = 3.90$; for α - Al_2O_3 : $a = 1.7$ – 3.3)	(A.60)	Spriggs
$G = G_0(1 - aP)$ (universal formula)	a – constant (determined experimentally, without a clear correlation to the porosity structure; for $UC_{1 \pm x}$ and UN_{1-x} : $a = 1.92$; for α/β - $Hf(Y)O_{2-x}$: $a = 2.60$; for β - $Hf(Er)O_{2-x}$: $a = 2.15$; for glass materials: $a = 1.94$)	(A.61)	Hasselman
$G = G_0(1 - aP)/(1 + bP)$ (universal formula)	a and b – constants (determined experimentally, without a clear correlation to the porosity structure)	(A.62)	Hasselman

(continued)

Table A.11 (continued)

Mathematical expression	Designations	Formula number	Authors
$G = G_0 \exp[-aP/(1 - P)]$ (applied for ultra-high temperature carbide materials)	a – constant, which express the influence of the shape, size distribution and relative orientation of the pores on the stress conditions (for $ZrC_{0.91}$: $a = 2.20$; for $ZrC_{0.95}$: $a = 2.41$; for $NbC_{0.98}$: $a = 2.12$)	(A.63)	Ordanyan et al.
$G = G_0(1 - aP)^n$ (based on porous body modelling approach and applied for refractory materials)	a and n – semi-empirical constants: packing geometry factor and grain grain morphology / pore geometry parameter, respectively (for Si_3N_4 : $a = 1.0$ and $n = 2.9$)	(A.64)	Phani and Niyogi
$G = G_0(1 - 5P/3)$ (based on physico-mechanical approach)	–	(A.65)	Dewey
$G = G_0(1 - aP + bP^2)$ (applied for ultra-high temperature oxide materials)	a and b – constants (without a clear correlation to the porosity structure, to be determined experimentally; for ThO_{2-x} : $a = 2.5-2.9$)	(A.66)	Knudsen et. al
$G = G_0\{1 - aP/[1 - (a + 1)P]\}$ (applied for refractory materials)	a – constant (determined experimentally; for BeO : $a = 2.0-2.8$)	(A.67)	Hasselman
$G = G_0[1 - 5P(3K_0 + 4G_0)/(9K_0 + 8G_0) + AP^2]$ (for spherical pores, applied for sintered high-temperature materials)	K_0 – bulk (compression) modulus of poreless materials, A – proportionality coefficient for higher powers of porosity, determined by setting $G = 0$ at $P = 1$	(A.68)	MacKenzie
$G = G_0[1 - 5P(3K + G)/(9K + 8G)]$ (universal formula)	–	(A.69)	Kemer
$G = G_0(1 - P)/[1 + 2(4 - 5\nu_0)/P(7 - 5\nu_0)]$ (based on physico-mechanical approach and applied for ceramic materials)	ν_0 – Poisson's ratio of poreless materials	(A.70)	Weil

(continued)

Table A.11 (continued)

Mathematical expression	Designations	Formula number	Authors
$G = G_0[1 - 15P(1 - \nu_0)/(7 - 5\nu_0)]$ (based on physico-mechanical approach with the assumption of independence of Poisson's ratio on porosity)	" "	(A.71)	Hill
$G = G_0(1 - P)^2/[1 + (1 - 5\nu_0)P/(7 - 5\nu_0)]$ (proposed for an isolated spherical pore geometry)	" "	(A.72)	Nielsen
$G = G_0(1 - P)^2/[1 + P(11 - 19\nu_0)/4(1 + \nu_0)]$ (based on numerical experiments using the finite element method)	" "	(A.73)	Ramakrishnan and Arunachalam
Bulk (compression) modulus, K			
$K = K_0(1 - aP)$ (universal formula)	K_0 – bulk (compression) modulus of poreless materials, a – constant (determined experimentally, without a clear correlation to the porosity structure; for $UC_{1\pm x}$: $a = 2.52$; for UN_{1-x} : $a = 2.51$)	(A.74)	Hasselman
$K = K_0(1 - aP)/(1 + bP)$ (universal formula)	a and b – constants (determined experimentally, without a clear correlation to the porosity structure)	(A.75)	Hasselman
$K = K_0(1 - aP)/[1 - (a + 1)P]$ (applied for refractory materials)	a – constant (determined experimentally)	(A.76)	Hasselman
$K = K_0 \exp[-aP/(1 - P)]$ (applied for ultra-high temperature carbide materials)	a – constant, which express the influence of the shape, size distribution and relative orientation of the pores on the stress conditions (for $ZrC_{0.91}$: $a = 3.26$; for $ZrC_{0.95}$: $a = 3.49$; for $NbC_{0.98}$: $a = 2.30$)	(A.77)	Ordanyan et al.
$K = K_0[1 - P(1 + 3K/4G)]$ (universal formula)	–	(A.78)	Kerner

(continued)

Table A.11 (continued)

Mathematical expression	Designations	Formula number	Authors
$K = K_0[1 - 3P(1 - v_0)/2(1 - 2v_0) + P(1 + v_0)]$ (based on physico-mechanical approach)	v_0 – Poisson's ratio of poreless materials	(A.79)	Hashin
$K = K_0(1 - P)/[1 + (1 + v_0)/2P(1 - 2v_0)]$ (based on physico-mechanical approach and applied for ceramic materials)	“ “	(A.80)	Weil
$K = K_0[1 - 15P(1 - v_0)/(7 - 5v_0)]$ (based on physico-mechanical approach with the assumption of independence of Poisson's ratio on porosity)	“ “	(A.81)	Plyatt et al.
$K = K_0(1 - P)^2/[1 + P(5v_0 - 1)/2(1 - 2v_0)]$ (proposed for an isolated spherical pore geometry)	“ “	(A.82)	Nielsen
$K = K_0(1 - P)^2/[1 + P(1 + v_0)/2(1 - 2v_0)]$ (based on numerical experiments using the finite element method)	“ “	(A.83)	Ramakrishnan and Arunachalam
$K = K_0(1 - P)/[1 + PG_0(1 + v_0)/2G(1 - 2v_0)]$ (based on the self-consistent method of mechanics of composites)	“ “	(A.84)	Hill and Budiansky
$K = 2K_0G(1 - 2v_0)/G_0(1 + v_0)[1 + (G/G_0)^{3/5}(1 - 5v_0)/(1 + v_0)]$ (based on the differential method of mechanics of composites)	“ “	(A.85)	Zimmerman
$K = 2K_0(1 - 2v_0)(3 - 5P)(1 - P)/[2(3 - 5P)(1 - 2v_0) + 3P(1 + v_0)]$ (proposed for the materials with low concentration of spherical pores)	“ “	(A.86)	Ondracek
$K = 2(1 - s)K_0(1 - 2v_0)(3 - 5P)(1 - P)/[2(3 - 5P)(1 - 2v_0) + 3P(1 + v_0)] + 2sK_0(1 - 2v_0)(1 - P)/3(1 - v_0)$ with $s = 1/[1 + \exp\{-100(P - 0.4)\}]$ (proposed for the materials with spherical pores for the whole porosity range)	“ “	(A.87)	Boccaccini and Ondracek
$K = 1/[1/K_0(1 - P) + 3P/4G_0(1 - P) + AP^3]$ (proposed for spherical pores, applied for sintered high-temperature materials)	A – proportionality coefficient for the higher powers of porosity	(A.88)	MacKenzie

(continued)

Table A.11 (continued)

Mathematical expression	Designations	Formula number	Authors
$v = v_0 - aP$ (universal formula, applied for sintered ceramic materials, for $P \leq 0.5$)	Poisson's ratio, ν v_0 - Poisson's ratio of poreless materials, a - constant (determined experimentally, without a clear correlation to the porosity structure; for UC ₁₊₂ : $a = 0.17-0.29$; for UN _{1-x} : $a = 0.10-0.37$; for α -Al ₂ O ₃ : $a = 0.30-0.35$)	(A.89)	Spriggs
$v = [2v_0(7 - 5v_0) + P(1 - 5v_0)(3 - v_0)]/[2(7 - 5v_0) + P(1 - 5v_0) \times (3v_0 - 1)]$ (proposed for an isolated spherical pore geometry)	-	(A.90)	Nielsen
$v = (4v_0 + 3P - 7v_0P)/4(1 + 2P - 3v_0P)$ (based on numerical experiments using the finite element method)	-	(A.91)	Ramakrishnan and Arunachalam
$v = 0.5 - (1 - P^{2/3})^{1.21} [2(3 - 5P)(1 - 2v_0) + 3P(1 + v_0)]/4(3 - 5P) \times (1 - P)$ (proposed for spherical pores in isotropic materials)	-	(A.92)	Boccaccini and Ondracek
$v = 0.5 - (1 - P^{2/3})^{1.21} / 4 \{ (1 - s)(3 - 5P)(1 - P)/2(3 - 5P) \times (1 - 2v_0) + 3P(1 + v_0) \} + s(1 - P)/3(1 - v_0)$ with $s = 1/\{1 + \exp[-100(P - 0.4)]\}$ (proposed for the isotropic materials with spherical pores for the whole porosity range)	-	(A.93)	Boccaccini and Ondracek

^aMost of formulae in this section can be applied for the description of resistivity as well

References

1. Kotelnikov RB, Bashlykov SN, Galiakbarov ZG, Kashtanov AI (1968) Osobo tugoplavkie elementy i soedineniya (Extra refractory elements and compounds). Metallurgiya, Moscow (in Russian)
2. Lide DR (ed) (2010) CRC handbook of chemistry and physics, 90th edn. CRC Press, Boca Raton, New York
3. Samsonov GV (ed) (1976) Svoistva elementov (Properties of elements), Vol. 1, 2nd edn. Metallurgiya, Moscow (in Russian)
4. Bushuev YuG, Persin MI, Sokolov VA (1994) Uglerod-uglerodnye kompozitsionnye materialy (Carbon-carbon composite materials). Metallurgiya, Moscow (in Russian)
5. Steurer W (1996) Crystal structure of the metallic elements. In: Cahn RW, Haasen P (eds) Physical metallurgy, Vol. 1, 4th edn. Elsevier Science BV, Amsterdam, pp. 1–46
6. Martienssen W (2005) The elements. In: Martienssen W, Warlimont H (eds) Springer handbook of condensed matter and materials data. Springer, Berlin, Heidelberg, pp. 45–158
7. Goodwin F, Guruswamy S, Kainer KU, Kammer C, Knabl W, Koethe A, Leichtfried G, Schlamp G, Stickler R, Warlimont H (2005) Metals. In: Martienssen W, Warlimont H (eds) Springer handbook of condensed matter and materials data. Springer, Berlin, Heidelberg, pp. 161–430
8. Marmer EN, Gurchich OS, Maltseva LF (1967) Vysokotemperaturnye materialy (High-temperature materials). Metallurgiya, Moscow (in Russian)
9. Portnoi KI, Chubarov VM (1967) Svoistva tugoplavkikh metallov i soedinenii (The properties of refractory metals and compounds). In: Tumanov AT, Portnoi KI (eds) Tugoplavkie materialy v mashinostroenii (Refractory materials in machinery construction). Mashinostroenie, Moscow (in Russian), pp. 7–124
10. Tumanov AT (ed) (1964) Konstruktsionnye materialy (Structural materials). Sovetskaya Entsiklopediya, Moscow (in Russian)
11. Cardarelli F (2008) Materials handbook, 2nd edn. Springer, London
12. Emsley J (1991) The elements, 2nd edn. Clarendon Press, Oxford
13. Gale WF, Totemeir TC (eds) (2004) Smithells metals reference book, 8th edn. Elsevier Butterworth Heinemann, ASM International Materials Information Society, Amsterdam, Boston
14. Umanskii YaS (1947) Karbidy tverdykh splavov (Carbides of hard alloys). Metallurgizdat, Moscow (in Russian)
15. Kieffer R, Schwarzkopf P (1953) Hartstoffe und Hartmetalle (Refractory hard metals). Springer, Vienna (in German)
16. Storms EK (1964) A critical review of refractories. Report LA-TR-2942, Contract W-7405-ENG-36. Los Alamos Scientific Laboratory, New Mexico, pp. 1–255
17. Storms EK (1967) The refractory carbides. Academic Press, New York, London
18. Toth LE (1971) Transition metal carbides and nitrides. Academic Press, New York, London
19. Goldschmidt HJ (1967) Interstitial alloys. Butterworths, London
20. Lengauer W (2000) Transition metal carbides, nitrides and carbonitrides. In: Riedel R (ed) Handbook of ceramic hard materials. Wiley-VCH, Weinheim, New York, pp. 202–252
21. Sheplaine VM, Runck RJ (1956) Carbides. In: Campbell IE (ed) High-temperature technology. Wiley, New York, pp. 114–130
22. Ramqvist L (1968) Variation of lattice parameter and hardness with carbon content of group 4b metal carbides. Jernkontoret Ann 152(10):517–523
23. Warlimont H (2005) Ceramics. In: Martienssen W, Warlimont H (eds) Springer handbook of condensed matter and materials data. Springer, Berlin, Heidelberg, pp. 431–476

24. Rudy E (1969) Compendium of phase diagram data. In: Ternary phase equilibria in transition metal-boron-carbon-silicon systems. Report AFML-TR-65-2, Contracts USAF 33(615)-1249 and USAF 33(615)-67-C-1513, Part 5. Air Force Materials Laboratory, Wright-Patterson Air Force Base, Ohio, pp. 1–689
25. Hansen M, Anderko K (1958) Constitution of binary alloys, 2nd edn. McGraw-Hill, New York, London
26. Massalski TB, Subramanian PR, Okamoto H, Kacprzak L (eds) (1990) Binary alloy phase diagrams, 2nd edn. ASM International, Metals Park, Ohio
27. Lyakishev NP (ed) (1996) Diagrammy sostoyaniya dvoynikh metallicheskih sistem (Phase diagrams of binary metal systems), Vol. 1. Mashinostroenie, Moscow (in Russian)
28. Andrievskii RA, Umanskii YaS (1977) Fazy vnedreniya (Interstitial phases). Nauka, Moscow (in Russian)
29. Andrievskii RA, Lanin AG, Rymashevskii GA (1974) Prochnost tugoplavkikh soedinenii (Strength of refractory compounds). Metallurgiya, Moscow (in Russian)
30. Andrievskii RA, Spivak II (1989) Prochnost tugoplavkikh soedinenii i materialov na ikh osnove (Strength of refractory compounds and materials based on them). Metallurgiya, Chelyabinsk (in Russian)
31. Shaffer PTB (1964) Handbooks of high-temperature materials: No. 1 – Materials index. Plenum Press, Springer, New York
32. Samsonov GV (1964) Handbooks of high-temperature materials: No. 2 – Properties index. Plenum Press, Springer Science, New York
33. Samsonov GV (1953) Fizicheskie svoistva nekotorykh faz vnedreniya (Physical properties of certain interstitial phases). Doklady AN SSSR 93(4):689–692 (in Russian)
34. Samsonov GV, Naumenko VY, Okhremchuk LN (1971) Herstellung und Eigenschaften von Karbiden der Übergangsmetalle in ihren Homogenitätsbereichen (Synthesis and properties of carbides of transition metals in their homogeneity range). Phys Stat Sol A 6(1):201–211 (in German)
35. Samsonov GV, Umanskii YaS (1957) Tverдые soedineniya tugoplavkikh metallov (Hard compounds of refractory metals). Metallurgizdat, Moscow (in Russian)
36. Samsonov GV (1964) Refractory transition metal compounds. Academic Press, New York
37. Samsonov GV, Portnoy KI (1961) Splyavy na osnove tugoplavkikh soedineniy (Alloys based on refractory compounds). Oborongiz, Moscow (in Russian)
38. Samsonov GV, Vinitskii IM (1980) Handbook on refractory compounds. IFI/Plenum, New York
39. Samsonov GV, Épik AP (1973) Tugoplavkie pokrytiya (Refractory coatings). Metallurgiya, Moscow (in Russian)
40. Samsonov GV, Upadkhaya GS, Neshpor VS (1974) Fizicheskoe materialovedenie karbidov (Physical materials science of carbides). Naukova Dumka, Kyiv (in Russian)
41. Upadhyaya GS (1996) Nature and properties of refractory carbides. Nova Science, Commack, New York
42. Holleck H (1984) Binäre und ternäre Carbid- und Nitridsysteme der Übergangsmetalle (Binary and ternary carbide and nitride systems of the transition metals). Gebrüder Bornträger, Berlin, Stuttgart (in German)
43. Kosolapova TYa (1971) Carbides: properties, production and applications. Plenum Press, New York
44. Kosolapova TYa (ed) (1990) Handbook of high-temperature compounds: properties, production and applications. Hemisphere, New York
45. Eisenmann B, Schäfer H (1988) Carbides. In: Hellwege K-H, Hellwege AM (eds) Structure data of elements and intermetallic phases. Subvol. A. Springer, Berlin, Heidelberg, pp. 197–318
46. Krajewski A, D'Alessio L, De Maria G (1998) Physico-chemical and thermophysical properties of cubic binary carbides. Cryst Res Technol 33(3):341–374
47. Tullhoff H (2005) Carbides. In: Ullmann's encyclopedia of industrial chemistry. Wiley, Weinheim

48. Shveikin GP, Alyamovskii SI, Zainulin YuG, Gusev AI, Gubanov VA, Kurmaev ÉZ (1985) Soedineniya peremennogo sostava i ikh tverdye rastvory (Compounds of variable composition and their solid solutions). USSR Academy of Sciences Ural Scientific Centre, Sverdlovsk (in Russian)
49. Gusev AI (1991) Fizicheskaya khimiya nestekhiometricheskikh tugoplavkikh soedinenii (Physical chemistry of non-stoichiometric refractory compounds). Nauka, Moscow (in Russian)
50. Gusev AI, Rempel AA, Magerl AJ (2001) Disorder and order in strongly nonstoichiometric compounds. Springer, Berlin
51. Savitskii EM, Burkhanov GS (1971) Metallovedenie splavov tugoplavkikh i redkikh metallov (Metallography of refractory and less-common metal alloys), 2nd edn. Nauka, Moscow (in Russian)
52. Kalin BA (ed), Platonov PA, Chernov II, Shtrombakh YaI (2008) Fizicheskoe materialovedenie (Physical materials science), Vol. 6, Part 1 – Konstruktsionnye materialy yadernoi tekhniki (Structural materials of nuclear engineering). National Research Nuclear University MEPhI, Moscow (in Russian)
53. Chirkin VS (1959) Teplofizicheskie svoistva materialov (Thermophysical properties of materials). Fizmatgiz, Moscow (in Russian)
54. Chirkin VS (1968) Teplofizicheskie svoistva materialov yadernoi tekhniki (Thermophysical properties of nuclear materials). Atomizdat, Moscow (in Russian)
55. Zefirov AP (ed), Vertyatin UD, Mashirev VP, Ryabtsev NG, Tarasov VI, Rogozkin BD, Korobov IV (1965) Termodinamicheskie svoistva neorganicheskikh veschestv (Thermodynamic properties of inorganic substances). Atomizdat, Moscow (in Russian)
56. Krzhizhanovskii RE, Shtern ZY (1977) Teplofizicheskie svoistva nemetallicheskih materialov (karbidy) (Thermophysical properties of non-metallic materials (carbides)). Energiya, Leningrad (in Russian)
57. Hague JR, Lynch JF, Rudnick A, Holden FC, Duckworth WH (1964) Refractory ceramics for aerospace. Battlle Memorial Institute, The American Ceramic Society, Columbus, Ohio
58. Leider HR, Krikorian OH, Young DA (1973) Thermodynamic properties of carbon up to the critical point. Carbon 11:555–563
59. Barriault RJ, Bender SL, Dreikorn RE, Einwohner TH, Feber RC, Gannon RE, Hanst PL, Ihnat ME, Phaneuf JP, Schick HL, Ward CH (1962) Thermodynamics of certain refractory compounds. Report ASD-TR-61-260, Part 1, Vol. 1. Air Force Materials Laboratory, Wright-Patterson Air Force Base, Ohio, pp. 1–404
60. Schick HL (ed) (1966) Thermodynamics of certain refractory compounds, Vol. 1–2. Academic Press, New York, London
61. Barin I (1995) Thermochemical data of pure substances, 3rd edn. VCH, Weinheim, New York
62. Chase MW, Jr (ed) (1998) NIST-JANAF thermochemical tables, 4th edn. J Phys Chem Ref Data Monograph No. 9. American Institute of Physics, New York (*see also* <http://webbook.nist.gov/chemistry>). Accessed 21 Oct 2016
63. Bolgar AS, Turchanin AG, Fesenko VV (1973) Termodinamicheskie svoistva karbidov (Thermodynamic properties of carbides). Naukova Dumka, Kyiv (in Russian)
64. Turchanin AG, Turchanin MA (1991) Termodinamika tugoplavkikh karbidov i karbonitridov (Thermodynamics of refractory carbides and carbonitrides). Metallurgiya, Moscow (in Russian)
65. Kulikov IS (1988) Termodinamika karbidov i nitridov (Thermodynamics of carbides and nitrides). Metallurgiya, Chelyabinsk (in Russian)
66. Savvatimskii A (2015) Carbon at high temperatures. Springer, Cham, Dordrecht, London
67. Senczyk D (1984) The lattice parameters of MeC-type carbides, nitrides and carbonitrides of transition metals of IV and V groups of the periodic system. In: Proc. 11th conf. applied crystallography, Vol. 1. Kozubnik, Poland, pp. 234–240

68. Vishwanadh B, Murthy TSRCh, Arya A, Tewari R, Dey GK (2016) Synthesis and phase transformation mechanism of Nb₂C carbide phases. *J Alloys Compd* 671:424–434
69. Goldsmith A, Waterman TE, Hirschhorn HJ (1961) Handbook of thermophysical properties of solid materials. Vol. 1 – Elements. Pergamon Press, Oxford, New York
70. Goldsmith A, Waterman TE, Hirschhorn HJ (1961) Handbook of thermophysical properties of solid materials. Vol. 3 – Ceramics. Pergamon Press, Oxford, New York
71. Wicks CE, Block FE (1963) Thermodynamic properties of 65 elements – their oxides, halides, carbides and nitrides. Bulletin N 605. US Bureau of Mines, US Department of the Interior, Washington, DC, pp. 1–146
72. Touloukian YS, Powell RW, Ho CY, Klemens PG (1970) Thermophysical properties of matter. Vol. 1 – Thermal conductivity – metallic elements and alloys. IFI/Plenum Data Corporation, New York, Washington
73. Touloukian YS, Powell RW, Ho CY, Klemens PG (1970) Thermophysical properties of matter. Vol. 2 – Thermal conductivity – nonmetallic solids. IFI/Plenum Data Corporation, New York, Washington
74. Touloukian YS, Buyco EH (1970) Thermophysical properties of matter. Vol. 4 – Specific heat – metallic elements and alloys. IFI/Plenum Data Corporation, New York, Washington
75. Touloukian YS, Buyco EH (1970) Thermophysical properties of matter. Vol. 5 – Specific heat – nonmetallic solids. IFI/Plenum Data Corporation, New York, Washington
76. Touloukian YS, DeWitt DP (1970) Thermophysical properties of matter. Vol. 7 – Thermal radiative properties – metallic elements and alloys. IFI/Plenum Data Corporation, New York, Washington
77. Touloukian YS, DeWitt DP (1972) Thermophysical properties of matter. Vol. 8 – Thermal radiative properties – nonmetallic solids. IFI/Plenum Data Corporation, New York, Washington
78. Touloukian YS, DeWitt DP, Hemicz RS (1972) Thermophysical properties of matter. Vol. 9 – Thermal radiative properties – coatings. IFI/Plenum Data Corporation, New York, Washington
79. Touloukian YS, Powell RW, Ho CY, Nicolaou MC (1973) Thermophysical properties of matter. Vol. 10 – Thermal diffusivity. IFI/Plenum Data Corporation, New York, Washington
80. Touloukian YS, Kirby RK, Taylor RE, Desai PD (1975) Thermophysical properties of matter. Vol. 12 – Thermal expansion – metallic elements and alloys. IFI/Plenum Data Corporation, New York, Washington
81. Touloukian YS, Kirby RK, Taylor RE, Lee TYR (1977) Thermophysical properties of matter. Vol. 13 – Thermal expansion – nonmetallic solids. IFI/Plenum Data Corporation, New York, Washington
82. Touloukian YS, Ho CY (1979) Thermophysical properties of matter. Vol. 14 – Master index to materials and properties. IFI/Plenum Data Corporation, New York, Washington
83. Lynch JF (1979) Engineering property data on selected ceramics. Vol. 2 – Carbides. Report MCIC-HB-07. Metals and Ceramics Information Centre, Battelle Columbus Laboratories, Ohio, pp. 1–136
84. Waseda Y, Hirata K, Ohtani M (1975) High-temperature thermal expansion of platinum, tantalum, molybdenum and tungsten measured by X-ray diffraction. *High Temp High Pressures* 7:221–226
85. Panish MB, Reif L (1961) Vaporization of iridium and rhodium. *J Chem Phys* 34:1915–1918
86. Samsonov GV, Bolgar AS, Guseva EA, Klochkov LA, Kovenskaya BA, Serebryakova TI, Timofeeva II, Turchanin AG, Fesenko VV (1973) Thermophysical properties of transition metal carbides and diborides. *High Temp High Press* 5(1):29–33
87. Fesenko VV, Bolgar AS (1963) Evaporation rate and vapour pressures of carbides, silicides, nitrides and borides. *Powder Metall Met Ceram* 2(1):11–17
88. Fesenko VV, Bolgar AS (1965) Isparenie tugoplavkikh soedinenii (Vaporization of refractory compounds). *Metallurgiya*, Moscow (in Russian)

89. Fesenko VV, Bolgar AS (1969) Study of evaporation rates of carbides of titanium, zirconium, hafnium, niobium and tantalum at high temperatures. *High Temp* 7(2):226–233
90. Pierson HO (1996) Handbook of refractory carbides and nitrides. Noyes Publications, Westwood, New Jersey
91. Fomenko VS, Podchernyaeva IA (1975) Emissionnyye i adsorbtsionnyye svoistva veshchestv i materialov (The thermoionic emission and absorptance properties of substances and materials). Atomizdat, Moscow (in Russian)
92. Fomenko VS (1981) Emissionnyye svoistva materialov (The thermoionic emission properties of materials). Naukova Dumka, Kyiv (in Russian)
93. Gao X-P, Jiang Y-H, Liu Y-Z, Zhou R, Feng J (2014) Stability and elastic properties of Nb_xC_y compounds. *Chin Phys B* 23(9):097704
94. Wu L, Wang Y, Yan Z, Zhang J, Xiao F, Liao B (2013) The phase stability and mechanical properties of Nb-C system: using first-principles calculations and nano-indentation. *J Alloys Compd* 562:220–227
95. Mattes M, Keinert J (2005) Status of thermal neutron scattering data for graphite. IAEA Nuclear Data Section, Vienna
96. Mughabghab SF (2003) Thermal neutron capture cross sections resonance integral and G-factors. IAEA Nuclear Data Section, Vienna
97. Gordeev NV, Kardashev DA, Malyshev AV (1963) Yaderno-fizicheskie konstanty (Nuclear physics constants). Gosatomizdat, Moscow (in Russian)
98. DoE Fundamentals Handbook (1993) Nuclear physics and reactor theory. US Department of Energy, Washington, Oak Ridge
99. Sears VF (1992) Neutron scattering lengths and cross sections. *Neutron News* 3(3):26–37
100. Munter A (2013) Neutron scattering lengths and cross sections. NIST Centre for Neutron Research, National Institute of Standards and Technology, Gaithersburg, Maryland <https://www.ncnr.nist.gov/resources/n-lengths/>. Accessed 1 Nov 2017
101. Robin A, Rosa JL (2000) Corrosion behaviour of niobium, tantalum and their alloys in hot hydrochloric and phosphoric acid solutions. *Int J Refract Met Hard Mater* 18(1):13–21
102. Walker P, Tarn WH (1991) CRC handbook of metal etchants. CRC Press, Boca Raton, Boston, London
103. Samsonov GV (1962) Analiz tugoplavkikh soedinenii (The analysis of refractory compounds). Metallurgizdat, Moscow (in Russian)
104. Kopylova VP (1961) Khimicheskaya ustoychivost karbidov perekhodnykh elementov IV, V i VI grupp (The chemical stability of transition element carbides IV, V and VI groups). *Zh Prikl Khim* 34(9):1936–1939 (in Russian)
105. Maxwell JC (1954) A treatise on electricity and magnetism, 3rd edn. Dover Publications, New York
106. Eucken A (1940) Allgemeine Gesetzmäßigkeiten für das Wärmeleitvermögen verschiedener Stoffarten und Aggregatzustände (General laws for the thermal conductivity of different types of substances and states of aggregation). *Forsch Gebiete Ing* 11(1):6–20 (in German)
107. Loeb AL (1954) Thermal conductivity. VIII. A theory of thermal conductivity of porous materials. *J Am Ceram Soc* 37(2):96–99
108. Francl J, Kingery WD (1954) Thermal conductivity. IX. Experimental investigation of effect of porosity on thermal conductivity. *J Am Ceram Soc* 37(2):99–107
109. Kingery WD, Francl J, Coble RL, Vasilos T (1954) Thermal conductivity. X. Data for several pure oxide materials corrected to zero porosity. *J Am Ceram Soc* 37(2):107–110
110. Vasilos T, Kingery WD (1954) Thermal conductivity. XI. Conductivity of some refractory carbides and nitrides. *J Am Ceram Soc* 37(9):409–414
111. Kulcinski GL, Wagner P, Cowder LR (1964) The effect of porosity and pore interconnection on the thermal conductivity and electrical resistivity of tungsten. *J Less-Common Met* 7(5):383–392
112. Moore JP, McElroy DL (1971) Thermal conductivity of nearly stoichiometric single-crystal and polycrystalline UO_2 . *J Am Ceram Soc* 54(1):40–46

113. Storms EK, Wagner P (1973) Thermal conductivity of sub-stoichiometric ZrC and NbC. *High Temp Sci* 5(6):454–462
114. Taylor RE, Storms EK (1976) Thermal transport in refractory carbides. In: Klemens PG, Chu TK (eds) *Thermal conductivity – 14*. Proc. 14th Int. conf. on thermal conductivity, University of Connecticut, Storrs, 2–4 June 1975. Plenum Press, New York, pp. 161–174
115. Vishnevetskaya IA, Kudryasheva LV, Ordanyan SS, Petrov VA (1983) The effect of processing factors on the thermal and electrical conductivity of zirconium carbides at high temperatures. In: Larsen DC (ed) *Thermal conductivity – 16*. Proc. 16th Int. conf. on thermal conductivity, IIT Research Institute, Chicago, 7–9 Nov 1979. Plenum Press, New York, pp. 351–365
116. Odelevskii VI (1951) Raschet obobshchennoi provodimosti geterogennykh system. 1. Matrichnye dvukhfaznye sistemy s nevytyanutyimi vkladyeniymi (Calculation of the summarized conductivity of heterogeneous systems. 1. Matrix two-phase systems with non-lengthened inclusions). *Zh Tekh Fiz* 21(6):667–677 (in Russian)
117. Odelevskii VI (1951) Raschet obobshchennoi provodimosti geterogennykh system. 2. Statisticheskie smesi nevytyanutykh chastits (Calculation of the summarized conductivity of heterogeneous systems. 2. Statistical mixtures of non-lengthened particles). *Zh Tekh Fiz* 21(6):678–685 (in Russian)
118. Odelevskii VI (1951) Raschet obobshchennoi provodimosti geterogennykh system. 3. Polikristall (Calculation of the summarized conductivity of heterogeneous systems. 3. A polycrystal). *Zh Tekh Fiz* 21(11):1379–1382 (in Russian)
119. Aivazov MI, Domashnev IA (1968) Influence of porosity on the conductivity of hot-pressed titanium nitride specimens. *Powder Metall Met Ceram* 7(9):708–710
120. Ondracek G, Schulz B (1973) The porosity dependence of the thermal conductivity for nuclear fuels. *J Nucl Mater* 46:253–258
121. Ondracek G (1978) Zum Zusammenhang zwischen Eigenschaften und Gefügestruktur mehrphasiger Werkstoffe (On the relationship between the properties and microstructure of multiphase materials). KfK 2688. Institut für Material- und Festkörperforschung, Kernforschungszentrum Karlsruhe (in German)
122. Kämpf H, Karsten G (1970) Effects of different types of void volumes on radial temperature distribution of fuel pins. *Nucl Appl Technol* 9(3):288–299
123. Nikolopoulos P, Ondracek G (1983) Field property bounds for porous sintered ceramics. *J Am Ceram Soc* 66(4):238–241
124. Ondracek G (1986) Microstructure – thermomechanical property correlations of two-phase and porous materials. *Mater Chem Phys* 15:281–313
125. Dulnev GN, Zarichnyak YuP (1974) Teploprovodnost smesei i kompozitsionnykh materialov (Thermal conductivity of mixtures and composite materials). *Energiya*, Leningrad (in Russian)
126. Dulnev GN, Novikov VV (1991) Protsessy perenosa v neodnorodnykh sredakh (The processes of transfer in inhomogeneous media). *Energoatomizdat*, Leningrad (in Russian)
127. Boccacini AR, Fan Z (1997) A new approach for the Young's modulus – porosity correlation of ceramic materials. *Ceram Int* 23:239–245
128. Andrievskii RA (1982) Properties of sintered solids. *Powder Metall Met Ceram* 21(1):33–38
129. Balshin MYu (1948) Poroshkovoe metallovedenie (Powder metals science). *Metallurgizdat*, Moscow (in Russian)
130. Balshin MYu (1949) Zavisimost mekhanicheskikh svoystv poroshkovykh materialov ot poristosti i predelnye svoystva poristykh metallokeramicheskikh materialov (Relation of mechanical properties of powder materials and their porosity and the ultimate properties of porous sintered materials). *Doklady AN SSSR* 67(5):831–834 (in Russian)
131. Pines BI, Sukhinin NI (1956) Some laws of mechanical strength in bodies produced by sintering powdered metals. *Sov Phys Tech Phys* 1(9):2014–2022

132. Pines BI, Sirenko AF, Sukhinin NI (1957) Some correlations regarding the mechanical strength of materials obtained by sintering of powdered metals. 3. Case when powder mixtures contain easily fusible components. *Sov Phys Tech Phys* 2(8):1773–1779
133. Plyatt ShN, Rapoport YuM, Chofnus EG (1958) K voprosu zavisimosti modulei uprugosti nekotorykh geterogennykh sistem ot poristosti (On the problem of the dependence of elastic moduli of some heterogeneous materials on porosity). *Inzh Fiz Zh* 1(6):96–99 (in Russian)
134. Skorokhod VV (1959) Ob elektroprovodnosti dispersnykh smesei provodnikov s neprovodnikami (On electrical conductivity of the disperse mixtures of conductors with non-conductors). *Inzh Fiz Zh* 2(8):51–59 (in Russian)
135. Skorokhod VV (1977) Fiziko-mekhanicheskie svoistva poristyykh materialov (Physico-mechanical properties of porous materials). In: Frantsevich IN (ed) *Poroshkovaya metallurgiya – 77* (Powder metallurgy – 77). Naukova Dumka, Kyiv, pp. 120–129 (in Russian)
136. Troshchenko VT (1960) Nekotorye voprosy prochnosti metallokeramicheskikh materialov na osnovе karbida kremniya (Some problems of the strength of sintered materials based on silicon carbide). *Inzh Fiz Zh* 3(1):103–108 (in Russian)
137. Troshchenko VT (1964) Statystychni teorii mitsnosti ta ih zastosuvannya do spechennykh materialiv (Statistical theories of strength and their application to sintered materials). Ukrainian RSR Academy of Sciences, Kyiv (in Ukrainian)
138. Shcherban NI (1973) Effect of porosity on the mechanical properties of materials produced by powder metallurgy techniques. *Powder Metall Met Ceram* 12(9):736–748
139. Shcherban NI (1973) Effect of technological factors upon the mechanical properties of porous materials produced by powder metallurgy techniques. *Powder Metall Met Ceram* 12(10):834–840
140. Wachtman JB, Jr (1969) Elastic deformation of ceramics and other refractory materials. In: Wachtman JB, Jr (ed) *Mechanical and thermal properties of ceramics*. Proc. symp. on mechanical and thermal properties of ceramics, Gaithersburg, Maryland, 1–2 Apr 1968, Special Publication 303. National Bureau of Standards, US Government Printing Office, Washington, DC, pp. 139–168
141. Ryshkewitch E (1953) Compression strength of porous sintered alumina and zirconia. 9th communication to ceramography. *J Am Ceram Soc* 36(2):65–68
142. Duckworth W (1953) Discussion of Ryshkewitch paper. *J Am Ceram Soc* 36(2):68
143. MacKenzie JK (1950) Elastic constants of a solid containing spherical holes. *Proc Phys Soc Lond B* 63(1):2–11
144. Coble RL, Kingery WD (1956) Effect of porosity on physical properties of sintered alumina. *J Am Ceram Soc* 39(11):377–385
145. Kingery WD, Bowen HK, Uhlmann RD (1976) *Introduction to ceramics*. Wiley, New York
146. Dewey JM (1947) The elastic constants of materials loaded with non-rigid fillers. *J Appl Phys* 18(6):578–581
147. Spriggs RM (1961) Expression for effect of porosity on elastic modulus of polycrystalline refractory materials, particularly aluminium oxide. *J Am Ceram Soc* 44(12):628–630
148. Spriggs RM, Brissette LA (1962) Expression for shear modulus and Poisson's ratio of porous refractory oxides. *J Am Ceram Soc* 45(4):198–199
149. Knudsen FP (1959) Dependence of mechanical strength of brittle polycrystalline specimens on porosity and grain size. *J Am Ceram Soc* 42(8):376–387
150. Knudsen FP (1962) Effect of porosity on Young's modulus of alumina. *J Am Ceram Soc* 45(2):94–95
151. Spinner S, Knudsen FP, Stone L (1963) Elastic constant – porosity relations for polycrystalline thoria. *J Res Nat Bur Stan C* 67(1):39–46
152. Fryxell RE, Chandler BA (1964) Creep, strength, expansion and elastic moduli of sintered BeO as a function of grain size, porosity and grain orientation. *J Am Ceram Soc* 47(6):283–291

153. Hill R (1952) The elastic behaviour of a crystalline aggregate. *Proc Phys Soc Lond A* 65(5):349–355
154. Hill R (1965) A self-consistent mechanics of composite materials. *J Mech Phys Solids* 13(4):213–222
155. Budiansky B (1965) On the elastic moduli of some heterogeneous materials. *J Mech Phys Solids* 13(4):223–227
156. Wu T (1966) The effect of inclusion shape on the elastic moduli of a two-phase material. *Int J Solids Struct* 2(1):1–8
157. Dean EA (1983) Elastic moduli of porous sintered materials as modelled by a variable-aspect-ratio self-consistent oblate-spheroidal-inclusion theory. *J Am Ceram Soc* 66(12):847–854
158. Kerner EH (1956) The elastic and thermo-elastic properties of composite media. *Proc Phys Soc Lond B* 69(8):808–813
159. Hashin Z (1962) Elastic moduli of heterogeneous materials. *J Appl Mech* 29:143–150
160. Hashin Z, Shtrikman S (1963) A variational approach to the theory of the elastic behaviour of multiphase materials. *J Mech Phys Solids* 11(2):127–140
161. Hasselman DPH (1962) On the porosity dependence of the elastic moduli of polycrystalline refractory materials. *J Am Ceram Soc* 45(9):452–453
162. Hasselman DPH (1963) Relation between effects of porosity on strength and on Young's modulus of elasticity of polycrystalline materials. *J Am Ceram Soc* 46(11):565–566
163. Hasselman DPH, Fulrath RM (1964) Effect of small fraction of spherical porosity on elastic moduli of glass. *J Am Ceram Soc* 47(1):52–53
164. Brown SD, Biddulph RB, Wilcox PD (1964) A strength-porosity relation involving different pore geometry and orientation. *J Am Ceram Soc* 47(7):320–322
165. Buch A, Goldschmidt S (1970) Influence of porosity on elastic moduli of sintered materials. *Mater Sci Eng* 5(2):111–118
166. Paul B (1960) Prediction of elastic constants of multiphase materials. *Trans AIME* 218(1):36–41
167. Paul B (1960) The elastic moduli of heterogeneous materials. *J Appl Mech Trans ASME* 29(4):765–766
168. Frantsevich IN, Zhurakovskii EA, Lyashchenko AB (1967) Elastic constants and characteristics of the electron structure of certain classes of refractory compounds obtained by the metal-powder method. *Inorg Mater* 3(1):6–12
169. Frantsevich IN, Voronov FF, Bakuta SA (1982) Uprugie postoyannye i moduli uprugosti metallov i nemetallov (The elastic constants and elasticity moduli of metals and non-metals). *Naukova Dumka, Kyiv* (in Russian)
170. Kats SM (1981) Vysokotemperaturnye teploizolyatsionnye materialy (High-temperature thermal insulation materials). *Metallurgiya, Moscow* (in Russian)
171. Rice RW (1977) Microstructure dependence of mechanical behaviour of ceramics. In: McCrone R (ed) *Treatise on materials science and technology*. Academic Press, New York, pp. 199–381
172. Rice RW (1998) *Porosity of ceramics*. Marcel Dekker, New York, Basel
173. Rice RW (2005) Mechanical properties. In: Scheffler M, Colombo P (eds) *Cellular ceramics: structure, manufacturing, properties and applications*. Wiley, Weinheim, Germany, pp. 291–312
174. Gibson LJ, Ashby MF (1999) *Cellular solids: structure and properties*, 2nd edn. Cambridge University Press, Cambridge, UK
175. Ashby MF (2005) Cellular solids – scaling properties. In: Scheffler M, Colombo P (eds) *Cellular ceramics: structure, manufacturing, properties and applications*. Wiley, Weinheim, Germany, pp. 3–17
176. Ashby MF (2006) The properties of foams and lattices. *Philos Trans R Soc A* 364(1838):15–30
177. Baranov VM, Knyazev VI, Korostin OS (1973) The temperature dependence of the elastic constants of nonstoichiometric zirconium carbides. *Strength Mater* 5(9):1074–1077

178. Avgustinik AI, Ordanyan SS, Fishchev VN, Kudryashova LV (1973) Elastic properties of zirconium and niobium carbides in their homogeneity regions. *Inorg Mater* 9(7):1039–1041
179. Ordanyan SS, Fishchev VN (1976) Porosity as a factor in the elastic modulus of zirconium and niobium monocarbides. *Refract Ind Ceram* 17(1–2):111–113
180. Kotelnikov RB, Bashlykov SN, Kashtanov AI, Menshikova TS (1978) *Vysokotemperaturnoe yadernoe toplivo* (High-temperature nuclear fuel). Atomizdat, Moscow (in Russian)
181. Padel A, De Novion Ch. (1969) Constantes elastiques des carbures, nitrures et oxydes d'uranium et de plutonium (Elastic constants of carbides, nitrides and oxides of uranium and plutonium). *J Nucl Mater* 33:40–51 (in French)
182. Haglund JA, Hunter O, Jr (1973) Elastic properties of polycrystalline monoclinic Gd_2O_3 . *J Am Ceram Soc* 56(6):327–330
183. Hunter O, Jr, Graddy GE, Jr (1976) Porosity dependence of elastic properties of polycrystalline cubic Lu_2O_3 . *J Am Ceram Soc* 59(1–2):82
184. Scheidecker RW, Hunter O, Jr, Calderwood FW (1979) Elastic properties of partially-stabilized HfO_2 compositions. *J Mater Sci* 14(10):2284–2288
185. Dole SL, Hunter O, Jr, Calderwood FW (1980) Elastic properties of stabilized HfO_2 compositions. *J Am Ceram Soc* 63(3–4):136–139
186. Dole SL, Hunter O, Jr (1983) Elastic properties of hafnium and zirconium oxides stabilized with praseodymium or terbium oxides. *J Am Ceram Soc* 66(3):C47–C49
187. Wang JC (1984) Young's modulus of porous materials. Part 1. Theoretical derivation of modulus-porosity correlation. *J Mater Sci* 19(3):801–808
188. Wang JC (1984) Young's modulus of porous materials. Part 2. Young's modulus of porous alumina with changing pore structure. *J Mater Sci* 19(3):809–814
189. Phani KK, Niyogi SK (1986) Porosity dependence of ultrasonic velocity and elastic modulus in sintered uranium dioxide – a discussion. *J Mater Sci Lett* 5(4):427–430
190. Phani KK, Niyogi SK (1987) Elastic modulus – porosity relationship for Si_3N_4 . *J Mater Sci Lett* 6(5):511–515
191. Phani KK, Niyogi SK (1987) Elastic modulus – porosity relation in polycrystalline rare-earth oxides. *J Am Ceram Soc* 70(12):C362–C366
192. Phani KK, Niyogi SK (1987) Young's modulus of porous brittle solids. *J Mater Sci* 22(1):257–263
193. Wagh AS, Poeppel RB, Singh JP (1991) Open pore description of mechanical properties of ceramics. *J Mater Sci* 26(14):3862–3868
194. Boccaccini AR, Ondracek G, Mazilu P, Windelberg D (1993) On the effective Young's modulus of elasticity for porous materials: microstructure modelling and comparison between calculated and experimental values. *J Mech Behav Mater* 4(2):119–128
195. Arnold M, Boccaccini AR, Ondracek G (1996) Prediction of the Poisson's ratio of porous materials. *J Mater Sci* 31:1643–1646
196. Boccaccini AR (1994) Comment on "Effective elastic moduli of porous ceramic materials". *J Am Ceram Soc* 77(10):2779–2781
197. Boccaccini DN, Boccaccini AR (1997) Dependence of ultrasonic velocity on porosity and pore shape in sintered materials. *J Nondestr Eval* 16(4):187–192
198. Janowski KR, Rossi RC (1967) Elastic behaviour of MgO matrix composites. *J Am Ceram Soc* 50(11):600–604
199. Fate WA (1974) Density dependence of shear modulus of Si_3N_4 . *J Am Ceram Soc* 57(8):372
200. Nielsen LF (1982) Elastic properties of two-phase materials. *Mater Sci Eng* 52(1):39–62
201. Norris AN (1985) A differential scheme for the effective moduli of composites. *Mech Mater* 4:1–16
202. Zimmerman RW (1991) Elastic moduli of a solid containing spherical inclusions. *Mech Mater* 12:17–24
203. Ramakrishnan N, Arunachalam VS (1993) Effective elastic moduli of porous ceramic materials. *J Am Ceram Soc* 76(11):2745–2752

204. Ramakrishnan N, Arunachalam VS (1990) Effective elastic moduli of porous solids. *J Mater Sci* 25(9):3930–3937
205. Kupková M (1993) Porosity dependence of materials elastic moduli. *J Mater Sci* 28(19):5265–5268
206. Kupková M, Kupka M (1997) Elastic-wave velocities for porous media with power-law distribution of pore sizes. *Geol Rundsch* 86(1):156–159
207. Kupková M, Parilák L (1997) Young's modulus calculations for systems with periodically distributed identical spheroidal pores of various size, orientation and shape anisotropy. *Kovove Mater* 35(4):237–246
208. Kupková M, Kupka M (2004) Theoretical bounds on the electrical conductivity of sintered materials and their relation to bounds on the Young's modulus. *Metalurgija* 43(2):97–100
209. Kral C, Lengauer W, Rafaja D, Etmayer P (1998) Critical review on the elastic properties of transition metal carbides, nitrides and carbonitrides. *J Alloys Compd* 265:215–233
210. Gong L, Wang Y, Cheng X, Zhang R, Zhang H (2014) A novel effective medium theory for modelling the thermal conductivity of porous materials. *Int J Heat Mass Transf* 68:295–298
211. Jana DC, Sundararajan G, Chattopadhyay K (2017) Effect of porosity on structure, Young's modulus and thermal conductivity of SiC foams by direct foaming and gelcasting. *J Am Ceram Soc* 100(1):312–322
212. Peras AYa, Dauknis VI (1971) The effect of small porosity on the strength of brittle ceramic materials. *Strength Mater* 3(8):921–925
213. Peras AYa, Dauknis VI (1977) Prochnost ognepurnoi keramiki i metody ee issledovaniya (The strength of refractory ceramics and methods of its investigation). *Mokslas, Vilnius* (in Russian)
214. Schiller KK (1958) Porosity and strength of brittle solids (with particular reference to gypsum). In: Warson WH (ed) *Mechanical properties of non-metallic brittle materials*. Interscience, New York, pp. 35–49
215. Carniglia SC (1972) Working model for porosity effects on the uniaxial strength of ceramics. *J Am Ceram Soc* 55(12):610–618
216. Krasulin YuL, Timofeev VN, Barinov SM, Ivanov AB (1980) Strength and fracture of porous ceramics sintered from spherical particles. *J Mater Sci* 15:1402–1406
217. Krasulin YuL, Timofeev VN, Barinov SM, Ivanov AB, Asonov AN, Shnyrev GD (1980) Poristaya konstruktsionnaya keramika (Porous structural ceramics). *Metallurgiya, Moscow* (in Russian)
218. Krasulin YuL, Barinov SM, Ivanov VS (1985) Struktura i razrushenie materialov iz poroshkov tugoplavkikh soedinenii (Microstructure and fracture of materials prepared from the powders of refractory compounds). *Nauka, Moscow* (in Russian)
219. Carson JK, Sekhon JP (2010) Simple determination of the thermal conductivity of the solid phase of particulate materials. *Int Commun Heat Mass Transf* 37:1226–1229
220. Katoh Y, Vasudevamurthy G, Nozawa T, Snead LL (2013) Properties of zirconium carbide for nuclear fuel applications. *J Nucl Mater* 441:718–742
221. Brynza AP, Khmelovskaya SA, Fedorus VB, Silina ZR (1976) Issledovanie khimicheskoi stoikosti i elektrokhimicheskogo povedeniya karbidov (A study of the chemical resistance and electrochemical behaviour of carbides). In: Samsonov GV, Kosolapova TYa, Gnesin GG, Fedorus VB, Domasevich LG (eds) *Karbidy i splyvy na ikh osnove* (Carbides and alloys based on them). *Naukova Dumka, Kyiv*, pp. 199–208 (in Russian)
222. Kotlyar EE, Nazarchuk TN (1966) O nekotorykh khimicheskikh svoistvakh karbidov perekhodnykh metallov IV, V grupp periodicheskoi sistemy (On certain chemical properties of the transition metal carbides of IV, V groups of the periodic table). *Izv AN SSSR Neorg Mater* 2(10):1778–1780 (in Russian)
223. Philipp WH (1966) Chemical reactions of carbides, nitrides and diborides of titanium and zirconium and chemical bonding in these compounds. Report NASA-TN-D-3533. National Aeronautics and Space Administration, Washington DC, pp. 1–23

224. Lukashenko TA, Tikhonov KI (1998) Korroziionnaya stoikost ryada karbidov i nitridov perekhodnykh metallov 4-6 grupp v kontsentrirrovannykh rastvorakh sernoi i fosfornoi kislot (Corrosion resistance of a number of carbides and nitrides of group 4-6 transition metals in concentrated solutions of sulfuric and phosphoric acids). Zh Prikl Khim 71(12):2017–2020 (in Russian)
225. Kopylova VP, Kornilova VI, Nazarchuk TN, Fedorus VB (1980) Reactions of powders of zirconium and niobium carbides in their homogeneity with some acids. Powder Metall Met Ceram 19(1):9–12
226. Kotlyar EE, Nazarchuk TN (1972) Interaction of the carbides of group IV and V transition metals with various acids. In: Samsonov GV (ed) Chemical properties and analysis of refractory compounds. Consultants Bureau, New York, London, pp. 1–5
227. Georgieva GG, Lashko NF, Sorokina KP (1972) Chemical and electrochemical methods of separating the carbides MeC and the carbonitrides Me(C,N) of group IV and V metals. In: Samsonov GV (ed) Chemical properties and analysis of refractory compounds. Consultants Bureau, New York, London, pp. 72–76
228. Ball MC, Brown DS, Page D, Thurman RRT (1967) The action of alkali on transition metal carbides. Trans Brit Ceram Soc 66:307–313
229. Loskutov VF, Khizhnyak VG, Kunitskii YuA, Kindrachuk MV (1991) Diffuzionnye karbidnye pokrytiya (Diffusion carbide coatings). Tékhnika, Kyiv (in Russian)
230. Kieffer R, Benesovsky F (1963) Hartstoffe (Hard materials). Springer, Vienna (in German)
231. Kieffer R (1971) Sondermetalle (Special metals). Springer, Wien (in German)
232. Kieffer R, Nowotny H, Neckel A, Ettmayer P, Usner L (1968) Zur Entmischung von kubischen Mehrstoffcarbiden (On the miscibility of multicomponent cubic carbides). Monatsh Chem 99(3):1020–1027 (in German)
233. Kieffer R, Benesovsky F (1965) Hartmetalle (Hard alloys). Springer, Vienna (in German)
234. Kieffer R, Kölbl F (1949) Tungsten carbide – free hard metals. Powder Metall Bull 4(1):4–17
235. Kieffer R, Ettmayer P, Nowotny H, Dufek G (1972) Neue Ermittlungen zur Mischbarkeit von Übergangsmetallnitride und-carbide (New investigations concerning miscibility of transition metal nitrides and carbides). Metall 26(7):701–708 (in German)

Index (Physical Properties)

A

Atomic weights (masses), 185, 186, 518, 677, 680

B

Boiling points, 17, 18, 151, 257, 435, 677, 682–685

C

Coefficients of linear thermal expansion, 24–29, 159–163, 266–272, 451–457, 677, 684–685

Crystal systems, 6, 11, 12, 147, 251, 252, 425–427, 677, 680

Crystal types, 6, 11, 12, 147, 251, 252, 425–427, 677, 680

D

Densities, 6, 11, 12, 14, 90, 93, 147, 149, 208, 212, 251, 252, 254, 255, 352, 356, 425–427, 432, 571, 583, 677, 680

– calculated (XRD), 11, 12, 14, 147, 251, 252, 254, 255, 425–427, 432, 677, 680

– experimental (pycnometric), 14, 149, 255, 432, 677, 680

Diffusion rate in species pairs (diffusivity), 94–98, 101, 212–214, 356–365, 572, 584–591

E

Electron work function, 37–43, 169–172, 281–285, 469–476, 678, 688

Enthalpies (heat) of melting, 16, 257, 434, 677, 682–683

Enthalpies (heat) of vaporization, 18, 150, 257, 434, 442, 677, 682–683

H

Hafnium monocarbide HfC_{1-x} , 1, 3, 6, 66, 72, 77, 78, 145–248, 319, 333, 530, 538, 546, 677–721

– chemical properties and materials design, 188–218, 694–697

– catalytic activity, 212

– chemical interaction and compatibility, 188–209, 212, 215–218, 679, 694–697

– with elements (solid and liquid metals/non-metals), 188–194

– with reagents (acids, alkalies and salts) in aqueous solutions, 215–218, 694, 695

– with refractory compounds, 195–204, 696, 697

– with gaseous media, 205–209, 212

– oxidation resistance, 206–209, 212

– diffusion characteristics, 212–214

– self-diffusion characteristics, 213–214

– electrochemical behaviour, 212

– quasi-binary systems, 188–204, 696, 697

– quasi-ternary and multi-component systems, 188–196, 198–204

– recommended chemical etching agents, 218

- wettability with liquid metals and alloys, 210–212
- electro-magnetic and optical properties, 163–172, 688, 689
 - colour at the common conditions, 167
 - Hall coefficient, 166
 - integral (total) emittance, 169, 172, 688, 689
 - hemispherical emittance, 169
 - normal emittance, 169
 - molar magnetic susceptibility, 166, 167, 172, 678, 688, 689
 - normal monochromatic emittance (spectral emissivity), 167–169, 172, 688, 689
 - optical spectra, 167, 168
 - reflectance spectra, 167
 - Seebeck coefficient, 166
 - specific electrical resistance (resistivity), 163–166, 688, 689
 - superconductivity, 166
 - thermal coefficient of resistivity, 164, 165, 688, 689
 - thermionic emission characteristics, 169–172, 688, 689
 - brightness characteristics, 172
 - Richardson constant, 170–172, 688, 689
 - work function, 169–172, 688, 689
- nuclear physical properties, 185–187, 678, 692, 693
 - isotopes of metal, 185–187, 678, 692, 693
 - abundance, 185, 186
 - decay mode, 185, 186
 - half-life period, 185, 186
 - mass, 185, 186
 - mass range, 185, 187, 678, 692, 693
 - resonance integral for neutron capture, 187, 678, 692, 693
 - parameters of formation and migration of lattice point defects, 148, 185, 187
 - in metal sublattice, 187
 - in non-metal sublattice, 187
 - interstitial atoms, 148, 185, 187
 - vacancies, 148, 185, 187
 - thermal neutron cross sections, 185, 692, 693
- physico-mechanical properties, 173–184, 690, 691
 - bulk (compression) modulus, 177, 178, 180–184
 - Coulomb's (shear) modulus, 177, 178, 181–184
 - creep characteristics, 177, 179
 - activation energy, 177, 179
 - exponent constant, 177, 179
 - density, 147, 149, 208, 212, 677, 680
 - ductile-to-brittle transition temperature, 177
 - elastic constants, 177, 178, 180–184, 678, 690, 691
 - flexural (bending) strength, 177, 178
 - fracture toughness (critical stress intensity factor), 177
 - hardness characteristics, 173–177, 690, 691
 - in *HK* scale, 173–177
 - in *HRA* scale, 173
 - in *HV* scale, 173–177, 690, 691
 - microhardness, 173–177
 - Poisson's ratio, 177–178, 180–184
 - sound velocities, 178
 - average, 178
 - longitudinal, 178
 - transversal, 178
 - stiffness coefficients, 180–184
 - stress-strain relationship, 180, 183
 - tensile strength, 177, 178
 - tensile/flexural strengths ratio, 177
 - thermal shock/stress resistance (thermal strength), 180, 184
 - volume compressibility, 178
 - Young's modulus, 177, 178, 180–184, 690, 691
- structures, 145–149, 677, 680
 - 2D-molecular MXene, 149
 - bond energy (enthalpy), 146
 - chemical bonding, 146, 187
 - C/Me radii ratio, 145
 - completeness of lattice/sublattices, 146, 148
 - crystal system, 147, 677, 680
 - crystal type, 147, 677, 680
 - densities, 147, 149, 208, 212, 677, 680
 - bulk density, 149, 677, 680
 - XRD density, 147, 677, 680
 - electron structures, 146, 149
 - homogeneity region, 145, 146, 148, 149, 153, 154, 157, 158, 163–167, 174, 677, 680

- lattice parameters, 145–148, 188, 196, 677, 680
 - effect of nitrogen, 146, 196
 - effect of oxygen, 146
 - lattice point defects, 148, 185, 187
 - metal-carbon phase diagram, 145, 146
 - molecular clusters, 145
 - nanostructures, 148, 149, 154, 163, 165, 170–172, 175, 177, 208
 - nanocrystal chains, 149
 - nanofibers, 149
 - nanoparticles, 149
 - nanotubes, 149
 - nanowires, 149
 - thin films/coatings, 149, 154, 163, 165, 168–172, 175–177, 182, 183, 208
 - whiskers, 149
 - order-disorder transformation, 145, 166, 167
 - ordered structures, 145, 166, 167
 - phase transformation under high pressures, 145
 - radii ratio of Me in Me/MeC, 145
 - slip systems, 148
 - thermal properties, 149–163, 677, 681–687
 - boiling point, 151, 677, 684
 - character of vaporization, 150, 151, 153–157, 677, 682, 683, 686, 687
 - linear vaporization rate, 677, 686, 687
 - mass vaporization rate, 154, 157, 677, 686, 687
 - coefficient of linear thermal expansion, 159–163, 677, 684, 685
 - melting point, 146, 149–151, 204, 213, 677, 684, 685
 - molar enthalpy difference, 150, 153, 157, 677, 682, 683
 - molar enthalpy (heat) of atomization from solid state, 151
 - molar enthalpy (heat) of vaporization, 150, 151, 677, 682, 683
 - molar entropy, 150, 151, 153, 677, 681
 - molar heat capacity, 149–152, 157, 677, 681
 - parameters of gaseous phase over monocarbide phase, 153–157, 677, 686, 687
 - partial pressures of carbon over monocarbide phase, 155–157
 - partial pressures of metal over monocarbide phase, 153–157
 - relative thermal expansion, 162, 163, 677, 684, 685
 - specific enthalpy difference, 677, 682, 683
 - specific heat capacity, 150, 152, 153, 677, 681
 - standard heat of formation, 150, 151, 153, 157, 677, 681
 - standard molar entropy, 150, 677, 681
 - standard molar heat capacity, 150, 677, 681
 - thermal conductivity, 157–159, 677, 684, 685
 - thermodynamic properties, 149–153, 157, 677, 681–685
 - Hardnesses, 43–50, 173–177, 285–294, 476–484, 678, 690, 691
- I**
- Integral emittances, 37, 39, 43, 169, 172, 281, 285, 467–469, 476, 678, 688, 689
 - Isotopic mass ranges, 61, 185, 186, 313, 517, 518, 519, 678, 692, 693
- L**
- Lattice parameters, 9–14, 64, 75, 79, 83, 84, 86, 145–148, 188, 196, 249–254, 265, 288, 314–316, 319, 322, 323, 335, 339, 341, 342, 344, 423–430, 519, 524, 525, 533, 537, 545, 551, 552, 555, 556, 563, 566, 677, 680
- M**
- Macroscopic thermal neutron cross sections, 61, 185, 187, 313, 517, 519, 678, 692, 693
 - capture (absorption), 61, 185, 187, 313, 519, 692, 693
 - scattering, 61, 185, 187, 313, 519, 692, 693
 - Melting points, 1–5, 10, 15, 17, 18, 31, 46, 73, 77, 97, 146, 149–151, 204, 213, 250, 255, 257, 258, 275, 364, 365, 424, 432, 434–436, 469, 496, 552, 590, 677, 682–685
 - Microscopic thermal neutron cross sections, 61, 187, 519, 678, 692, 693

- capture (absorption), 187, 519, 678, 692, 693
 - scattering, 187, 519, 678, 692, 693
 - Molar enthalpy differences, 16, 20, 24, 150, 153, 157, 256, 257, 261, 265, 433, 435, 440, 447, 677, 682, 683
 - Molar heat capacities, 15–20, 24, 149–153, 157, 255–260, 265, 432, 433, 435–440, 447, 677, 681
 - Molar magnetic susceptibilities, 33–35, 43, 166, 167, 172, 276, 278, 285, 464, 476, 678, 688, 689
 - Monochromatic emittances, 36, 37, 43, 167–169, 172, 280, 281, 285, 466, 467, 469, 476, 678, 688, 689
- N**
- Neutron moderating abilities (macroscopic slowing down power), 61, 185, 313, 517, 678, 692
 - Niobium monocarbide NbC_{1-x}, 1, 3, 6, 66, 67, 71, 72, 77, 79, 189, 198, 199, 249–422, 447, 529, 530, 536, 538, 546–548, 677–721
 - chemical properties and materials design, 316–368, 679, 694–697
 - catalytic activity, 356
 - chemical interaction and compatibility, 316–353, 366–368, 679, 694–697
 - with gaseous media, 316, 345–353
 - oxidation resistance, 316, 348–353
 - with elements (solid and liquid metals/non-metals), 316–330
 - with reagents (acids, alkalis and salts) in aqueous solutions, 356, 366–368, 679, 694, 695
 - with refractory compounds, 316, 330–345, 679, 696, 697
 - diffusion characteristics, 298, 314, 356–365
 - hetero-diffusion characteristics, 364, 365
 - self-diffusion characteristics, 298, 314, 357–365
 - electrochemical behaviour, 356
 - quasi-binary systems, 317–345, 696, 697
 - quasi-ternary and multi-component systems, 317–326, 330, 331, 333–335, 337–343
 - recommended chemical etching agents, 367, 368
 - wettability with liquid metals and alloys, 353–356
 - electro-magnetic and optical properties, 272–285, 678, 688, 689
 - colour at the common conditions, 280
 - Hall coefficient, 276, 277
 - integral (total) emittance, 281, 285, 678, 688, 689
 - hemispherical emittance, 281
 - normal emittance, 281
 - molar magnetic susceptibility, 276, 278, 678, 688, 689
 - normal monochromatic emittance (spectral emissivity), 280, 281, 285, 678, 688, 689
 - optical constants, 278–280
 - extinction coefficient, 278–280
 - refractive index, 278–280
 - optical spectra, 278–280
 - reflectance spectra, 278, 279
 - spectra in the infrared (IR) ranges, 280
 - spectra in the visible ranges, 280
 - X-ray spectra, 280
 - absorption, 280
 - emission, 280
 - Seebeck coefficient, 276, 277
 - specific electrical resistance (resistivity), 272–276, 316, 678, 688, 689
 - superconductivity, 275, 276, 314, 315
 - thermal coefficient of resistivity, 274–276, 678, 688, 689
 - thermionic emission characteristics, 281–285, 678, 688, 689
 - brightness characteristics, 281, 284
 - Richardson constant, 281–285, 688, 689
 - work function, 281–285, 688, 688
 - nuclear physical properties, 313–316, 678, 692, 693
 - changes in properties after irradiation exposure, 314, 316
 - isotopes of metal, 313, 316, 678, 692, 693
 - abundance, 313
 - decay mode, 313

- half-life period, 313
 - mass range, 313, 316, 678, 692, 693
 - resonance integral for neutron capture, 313, 316, 678, 692
 - parameters of formation and migration of lattice point defects, 313, 314
 - in metal sublattice, 314
 - in non-metal sublattice, 314
 - interstitial atoms, 313, 314, 316
 - vacancies, 313, 314
 - thermal neutron cross sections, 313, 678, 692, 693
 - under bombardment, 313–316
 - by argon ions, 315
 - by fast neutrons, 313, 314
 - by helium ions, 315, 316
 - under gamma irradiation, 314, 315
- physico-mechanical properties, 285–313, 678, 690, 691
 - bulk (compression) modulus, 299, 302–308, 310, 311
 - compressive strength, 294, 297, 313, 678, 690, 691
 - Coulomb's (shear) modulus, 299, 302–308, 310, 311
 - creep characteristics, 296, 298–301
 - activation energy, 298, 300, 301
 - dominating mechanisms, 298
 - exponent constant, 298, 300, 301
 - density, 251–255, 316, 352, 677, 680
 - ductile-to-brittle transition temperature, 296, 297
 - elastic constants, 299, 302–311, 313, 678, 690, 691
 - flexural (bending) strength, 294–296, 316
 - fracture toughness (critical stress intensity factor), 294, 296
 - hardness characteristics, 285–294, 313, 678, 690, 691
 - in *HK* scale, 285, 286, 289, 290, 293, 294
 - in *HRA* scale, 285
 - in *HV* scale, 285–287, 290, 291, 678, 690, 691
 - in Mohs scale, 285
 - microhardness, 285–294, 316
 - Poisson's ratio, 299, 302–307, 310, 311
 - sound velocities, 307, 308
 - average, 308
 - longitudinal, 307, 308
 - transversal, 307, 308
 - stiffness coefficients, 302–307, 311
 - stress-strain relationship, 297
 - tensile/flexural strengths ratio, 294
 - tensile strength, 294, 295, 313, 678, 690, 691
 - thermal shock/stress resistance (thermal strength), 295, 313, 316
 - volume compressibility, 299
 - Young's modulus, 299, 302–311, 313, 316, 678, 690, 691
- structures, 249–255, 677, 680
 - 2D-molecular MXenes, 254, 339, 344
 - bond energy (enthalpy), 254
 - C/Me radii ratio, 249
 - chemical bonding, 254, 314
 - completeness of lattice, 254
 - crystal system, 251–253, 677, 680
 - crystal type, 251–253, 677, 680
 - densities, 251–255, 316, 352, 356, 677, 680
 - bulk density, 255, 677, 680
 - XRD density, 251–255, 677, 680
 - electron structures, 254
 - homogeneity region, 249, 250, 253, 255, 261, 266, 271, 272, 275–278, 285, 286, 295, 298, 310, 311, 345, 349, 361, 677, 680
 - lattice parameters, 249–254, 265, 288, 314–316, 319, 322, 323, 335, 339, 341, 342, 344, 677, 680
 - effect of nitrogen, 254, 335
 - effect of oxygen, 254
 - lattice point defects, 250, 313–315
 - metal-carbon phase diagram, 249, 250
 - minimal Burgers vector, 250
 - molecular clusters, 249
 - nanostructures, 254, 285, 287, 291, 293, 294, 304, 306, 315, 316, 347–350, 365
 - nanofibres, 254
 - nanoparticles, 254, 347, 348
 - nanorods, 254
 - nanosheets, 254
 - nanotubes, 254
 - nanowires, 254

- thin films/coatings, 254, 279, 282, 287, 291, 293, 294, 304, 306, 315, 316, 350, 365–367
 - whiskers, 254
- order-disorder transformation, 253, 256–258, 274, 275, 278, 286, 325
- ordered structures, 249, 250, 252, 253, 256–258, 274, 275, 278, 286
- phase transformation under high pressures, 249
- radii ratio of Me in Me/MeC, 249
- slip systems, 250
- thermal properties, 255–272, 677, 681–687
 - boiling point, 257, 677, 682–685
 - character of vaporization, 257, 261–265
 - linear vaporization rate, 265, 677, 686, 687
 - mass vaporization rate, 265, 677, 686, 687
 - coefficient of linear thermal expansion, 250, 254, 266–272, 677, 684, 685
 - melting point, 249, 250, 255–258, 275, 364, 677, 684, 685
 - molar enthalpy difference, 256, 257, 261, 265, 677, 682, 683
 - molar enthalpy (heat) of atomization from solid state, 257
 - molar enthalpy (heat) of vaporization, 257, 258, 265, 677, 682, 683
 - molar entropy, 256–257, 261, 265, 677, 681
 - molar heat capacity, 255–260, 265, 677, 681
 - parameters of gaseous phase over monocarbide phase, 261–165, 677, 686, 687
 - partial pressures of carbon over monocarbide phase, 261–265
 - partial pressures of metal over monocarbide phase, 261–265
 - relative thermal expansion, 267, 272, 677, 684, 685
 - specific enthalpy difference, 265, 677, 682, 683
 - specific heat capacity, 256–259, 265, 677, 681
 - standard heat of formation, 256–258, 261, 265, 677, 681
 - standard molar entropy, 256–258, 265, 677, 681
 - standard molar heat capacity, 256–258, 265, 677, 681
 - thermal conductivity, 266–268, 272, 677, 684, 685
 - thermodynamic properties, 255–261, 265, 677, 681–685
- Niobium semicarbide Nb_{2±x}C, 1, 3, 6, 71, 78–80, 198, 249–253, 255, 258–263, 265–267, 271, 272, 275, 276, 278, 280, 282, 283, 285, 286, 291, 299, 307, 311, 313, 316–318, 321, 323, 324, 326–339, 341–344, 347, 352, 362, 363, 536, 548, 677–695, 698–721
- chemical properties and materials design, 316–319, 321, 323, 324, 326–339, 341–344, 346, 347, 352, 362, 363, 679, 694, 695
 - catalytic activity, 355
 - chemical interaction and compatibility, 316–319, 321, 323, 324, 326–339, 341–344, 346, 347, 352, 679, 694, 695
 - with elements (solid and liquid metals/non-metals), 316–319, 321, 323, 324, 326–330
 - with gaseous media, 316, 346, 347, 352
 - with refractory compounds, 316, 330–339, 341–345
- diffusion characteristics, 356, 362, 363
 - self-diffusion characteristics, 362, 363
- electrochemical behaviour, 355
- quasi-binary systems, 317, 319, 321, 323, 324, 326–339, 341–345
- quasi-ternary and multi-component systems, 335, 338
- electro-magnetic and optical properties, 272, 275, 276, 278, 280, 282, 283, 285, 678, 688, 689
 - molar magnetic susceptibility, 278, 678, 688, 689
 - optical spectra, 280
 - spectra in the infrared (IR) ranges, 280
 - specific electrical resistance (resistivity), 272, 275, 678, 688, 689
 - superconductivity, 276
 - thermionic emission characteristics, 281, 282, 285, 678, 688, 689
 - work function, 281, 282, 285, 678, 688, 689

- nuclear physical properties, 313, 316, 678, 692, 693
 - isotopes of metal, 313, 316, 678, 692, 693
 - abundance, 313
 - decay mode, 313
 - half-life period, 313
 - mass range, 313, 316, 678, 692, 693
 - resonance integral for neutron capture, 313, 316, 678, 692, 693
 - thermal neutron cross sections, 313, 316, 678, 692, 693
 - physico-mechanical properties, 285, 286, 291, 299, 307, 311, 313, 678, 691
 - bulk (compression) modulus, 299, 307
 - Coulomb's (shear) modulus, 299
 - density, 251–253, 255, 677, 680
 - elastic constants, 299, 307, 311, 313, 678, 691
 - hardness characteristics, 285–287, 291, 313, 678, 691
 - in *HV* scale, 287, 313, 678, 691
 - microhardness, 285–287, 291
 - Poisson's ratio, 299
 - stiffness coefficients, 311
 - Young's modulus, 299, 313, 678, 691
 - structures, 249–253, 255, 677, 680
 - completeness of lattice, 254
 - crystal systems, 251–253, 677, 680
 - crystal types, 251–253, 677, 680
 - densities, 251–253, 257, 677, 680
 - bulk density, 257, 677, 680
 - XRD density, 251–253, 257, 677, 680
 - homogeneity region, 249, 250, 255, 271, 272, 275, 285, 286, 336, 677, 680
 - lattice parameters, 249, 251–253, 677, 680
 - metal-carbon phase diagram, 249, 250
 - nanostructures, 254
 - order-disorder transformation, 249, 250
 - ordered structures, 249, 250, 252, 253
 - phase transformations, 249, 250, 677, 680
 - high-temperature modification, 249, 250, 677, 680
 - low-temperature modification, 249, 250, 677, 680
 - middle-temperature modification, 249, 250, 677, 680
 - thermal properties, 255, 258–263, 265–267, 271, 272, 677, 681–685, 687
 - character of vaporization, 262, 263, 265, 677, 687
 - coefficient of linear thermal expansion, 266, 267, 271, 272, 677, 684, 685
 - melting point, 250, 255, 258, 677, 684, 685
 - molar enthalpy difference, 261, 265, 677
 - molar heat capacity, 258–261, 265, 677, 681
 - parameters of gaseous phase over carbide phases, 262, 263, 265, 677, 687
 - partial pressure of carbon, 263
 - partial pressure of metal, 263, 265
 - specific enthalpy difference, 677, 682, 683
 - specific heat capacity, 258, 677, 681
 - standard heat of formation, 258, 677, 681
 - standard molar entropy, 258, 677, 681
 - standard molar heat capacity, 258, 677, 681
 - thermal conductivity, 266, 272, 677, 684, 685
 - thermodynamic properties, 255, 258–261, 265, 677, 681–685
- P**
- Phase homogeneity regions, 1, 6, 9, 10, 15, 20, 24, 25, 31–35, 44, 47, 51, 145, 146, 149, 153, 154, 157, 158, 163–167, 174, 249, 250, 253, 255, 261, 266, 271, 272, 275–278, 286, 295, 298, 310, 311, 345, 349, 361, 423, 424, 432, 439, 440, 442, 445–448, 456, 462–465, 477, 488, 495, 511–513, 555–558, 561, 562, 677, 680
 - Porosity (effect), 24, 45, 98, 157, 163, 266, 297, 365, 447, 451, 462, 486, 488, 490, 519, 527, 591, 679, 698–710, 715–720
 - property-porosity relationships, 679, 698–710, 715–720
 - for bulk (compression) modulus, 679, 708, 709, 715–720

- for Coulomb's (shear) modulus, 679, 706–708, 715, 720
 - for electrical resistivity, 679, 698, 699, 715–720
 - for Poisson's ratio, 679, 710, 715–720
 - for strength characteristics, 679, 700, 701, 715–720
 - for thermal conductivity, 678, 698, 699, 715–720
 - for Young's modulus, 679, 702–706, 715, 720
- R**
- Relative thermal expansion, 25, 26, 29, 162, 163, 267, 272, 451, 456, 457, 677, 684, 685
- Resonance integral for neutron capture, 61, 63, 185, 187, 313, 316, 517, 519, 524, 678, 692, 693
- Richardson constants, 37, 40–43, 170–172, 281–285, 469–476, 678, 688, 689
- S**
- Space groups, 9, 11, 12, 145, 147, 249, 251–253, 311, 423, 425–428, 677, 680
- Specific electrical resistances, 5, 29–33, 43, 63, 163–166, 172, 272–276, 285, 314, 316, 457–462, 476, 522, 524, 678, 679, 688, 689, 698, 699, 715–720
- Specific enthalpy differences, 24, 157, 265, 447, 677, 682, 683
- Specific heat capacities, 16–18, 24, 150–153, 157, 256–259, 265, 433–435, 439, 447, 677, 681
- Standard molar entropies, 16–18, 20, 24, 150, 151, 153, 157, 256–258, 261, 265, 433–435, 440, 447, 677, 681
- T**
- Tantalum monocarbide TaC_{1-x} , 1, 3, 6, 9–143, 189, 192, 198, 200, 213, 214, 319, 320, 325, 329, 333, 337, 338, 530, 538, 541, 546, 547, 550, 677–721
- chemical properties and materials design, 63–101, 679, 694–697
 - catalytic activity, 101
 - chemical interaction and compatibility, 63–91, 99–101, 679, 694–697
 - with elements (solid and liquid metals/non-metals), 63–75
 - with reagents (acids, alkalis and salts) in aqueous solutions, 99–101, 679, 694, 695
 - with refractory compounds, 63, 76–86, 679, 696, 697
 - with gaseous media, 63, 87–91, 101
 - oxidation resistance, 63, 88–91, 101
 - diffusion characteristics, 51, 62, 94–98, 101
 - hetero-diffusion characteristics, 97, 98
 - self-diffusion characteristics, 51, 62, 94–98
 - electrochemical behaviour, 101
 - quasi-binary systems, 64–86
 - quasi-ternary and multi-component systems, 64–72, 77–79, 82–85
 - recommended chemical etching agents, 101
 - wettability with liquid metals and alloys, 91–93, 101
- electro-magnetic and optical properties, 29–43, 678, 688, 689
- colour at the common conditions, 36
 - Hall coefficient, 33, 34
 - integral (total) emittance, 37, 39, 43, 678, 688, 689
 - hemispherical emittance, 39
 - normal emittance, 39
 - molar magnetic susceptibility, 33–35, 43, 678, 688, 689
 - normal monochromatic emittance (spectral emissivity), 36–38, 43, 678, 688, 689
 - isobestic points (X-points), 37
 - optical spectra, 35, 36
 - photoemission spectra, 35
 - reflectance spectra, 35, 36
 - spectra in the infrared (IR) ranges, 35, 36
 - spectra in the visible ranges, 35, 36
 - X-ray spectra, 35, 36
 - absorption, 35, 36
 - emission, 35, 36
 - photoelectron, 35
 - Seebeck coefficient, 33, 34
 - specific electrical resistance (resistivity), 29–32, 43, 63, 678, 688, 689

- superconductivity, 31
- thermal coefficient of resistivity, 31, 43, 678, 688, 689
- thermoionic emission characteristics, 37–43, 69, 70, 678, 688, 689
 - brightness characteristics, 37, 38, 42
 - Richardson constant, 37, 40–43, 678, 688, 689
 - work function, 37, 39–43, 678, 688, 689
- nuclear physical properties, 61–63, 678, 692, 693
 - changes in properties after irradiation exposure, 62, 63
 - isotopes of metal, 61
 - abundance, 61
 - decay mode, 61
 - half-life period, 61
 - mass range, 61, 63, 678, 692, 693
 - resonance integral for neutron capture, 61, 63, 678, 692, 693
 - parameters of formation and migration of lattice point defects, 62, 63
 - in metal sublattice, 62
 - in non-metal sublattice, 62
 - interstitial atoms, 62, 63
 - vacancies, 62, 63
 - thermal neutron cross sections, 61, 63, 678, 692, 693
 - under bombardment, 63
 - by deuterium ions, 63
 - by electrons, 63
 - by fast neutrons, 62, 63
 - by helium ions, 63
 - by hydrogen ions, 63
 - by protons, 63
- physico-mechanical properties, 43, 61, 678, 690, 691
 - bulk (compression) modulus, 51, 55–60
 - compressive strength, 44, 61, 678, 690, 691
 - Coulomb's (shear) modulus, 51, 54–60
 - creep characteristics, 50, 51, 53–55
 - activation energy, 50, 51, 54
 - exponent constant, 50, 51, 54
 - dominating mechanisms, 51
 - density, 11, 12, 14, 61, 90, 93, 677, 680
 - ductile-to-brittle transition temperature, 46, 50, 52
 - elastic constants, 51, 55–62, 678, 690, 691
 - flexural (bending) strength, 44, 51, 52, 55
 - fracture toughness (critical stress intensity factor), 45, 46, 50
 - hardness characteristics, 43–50, 54, 61, 62, 78, 678, 690, 691
 - in *HK* scale, 43–49
 - in *HRA* scale, 43
 - in *HV* scale, 43–46, 49, 50, 61, 678, 690, 691
 - in Mohs scale, 43
 - microhardness, 43–49, 78
 - Poisson's ratio, 51, 55–61
 - sound velocities, 56
 - average, 56
 - longitudinal, 56
 - transversal, 56
 - stiffness coefficients, 56–60
 - stress-strain relationship, 51, 52, 55
 - tensile strength, 44, 50, 61, 678, 690, 691
 - tensile/flexural strengths ratio, 44
 - thermal shock/stress resistance (thermal strength), 61
 - volume compressibility, 51, 56
 - Young's modulus, 50, 51, 55–61, 678, 690, 691
- structures, 9–14, 677, 680
 - 2D-molecular MXenes, 14
 - chemical bonding, 12, 62
 - C/Me radii ratio, 9
 - completeness of lattice, 12, 14
 - crystal system, 11, 12, 677, 680
 - crystal type, 9, 11, 12, 677, 680
 - densities, 11, 12, 14, 61, 90, 93, 677, 680
 - bulk density, 14, 677, 680
 - XRD density, 11, 12, 14, 677, 680
 - homogeneity region, 9, 10, 13, 15, 20, 24, 25, 31–35, 44, 45, 47, 51, 82, 87, 88, 677, 680
 - lattice parameters, 9–14, 63, 64, 79, 83, 84, 86
 - effect of nitrogen, 12, 14
 - effect of oxygen, 12, 14
- lattice point defects, 10, 62, 63
 - metal-carbon phase diagram, 9, 10
 - minimal Burgers vector, 12

- nanostructures, 9, 12–14, 34, 35, 42–44, 45, 48–50, 57, 59
 - nanofibers, 14
 - nanoparticles, 11, 12–14, 48, 57, 59
 - nanorods, 14
 - nanowires, 14
 - thin films/coatings, 14, 31, 34, 35, 37, 40, 42, 43, 47–49, 63, 88, 89
 - whiskers, 14
- order-disorder transformation, 9–13, 16, 17, 34, 35
- ordered structures, 9–12, 16, 17, 34, 35
- phase transformation under high pressures, 9
- radii ratio of Me in Me/MeC, 9
- slip systems, 12, 13, 43, 46, 50, 52
- thermal properties, 15–17, 19–29, 677, 681–687
 - boiling point, 17, 24, 677, 684, 685
 - character of vaporization, 20–24, 677, 686, 687
 - linear vaporization rate, 24, 677, 686, 687
 - mass vaporization rate, 22, 24, 677, 686, 687
 - coefficient of linear thermal expansion, 24–29, 677, 684, 685
 - melting point, 10, 15–17, 24, 31, 46, 77, 97, 677, 684, 685
 - molar enthalpy difference, 16, 20, 24, 677, 682, 683
 - molar enthalpy (heat) of atomization from solid state, 16, 17
 - molar enthalpy (heat) of melting, 16, 17, 24, 677, 682, 683
 - molar entropy, 16–17, 20, 24, 677, 681
 - molar heat capacity, 15–17, 19, 20, 24, 677, 681
 - partial pressures of carbon over monocarbide phase, 21, 23, 24, 677, 686, 687
 - partial pressures of metal over monocarbide phase, 21–24, 677, 686, 687
 - relative thermal expansion, 25, 29, 677, 684, 685
 - specific enthalpy difference, 24, 677, 682, 683
 - specific enthalpy (heat) of melting, 16, 17, 24, 677, 682, 683
 - specific heat capacity, 16, 17, 24, 677, 681
 - standard heat of formation, 16, 17, 20, 24, 677, 681
 - standard molar entropy, 16, 17, 20, 24, 677, 681
 - standard molar heat capacity, 16, 17, 20, 24, 677, 681
 - thermal conductivity, 24–26, 29, 677, 684, 685
 - thermodynamic properties, 15–17, 19, 20, 24, 677, 681–685
- Tantalum semicarbide $Ta_{2\pm x}C$, 1, 3, 6, 9–12, 14, 15, 18–26, 29, 31, 35, 36, 40–44, 46–50, 52, 55, 56, 61, 63, 65, 68–71, 73–76, 78–83, 85, 86, 88, 90, 95, 97, 98, 100–143, 200, 329, 335, 338, 550, 677–695, 698–721
 - chemical properties and materials design, 63, 65, 68–71, 73–76, 78–83, 85, 86, 88, 90, 95, 97, 98, 100, 101, 679, 694, 695
 - catalytic activity, 101
 - chemical interaction and compatibility, 65, 68–71, 73–76, 78–83, 85, 86, 88, 90, 100, 101, 679, 694, 695
 - with elements (solid and liquid metals/non-metals), 63, 65, 68–71, 73–75
 - with gaseous media, 63, 88, 90
 - oxidation resistance, 63, 90, 101
 - with refractory compounds, 63, 76, 78–83, 85, 86
 - diffusion characteristics, 97, 98, 101
 - self-diffusion characteristics, 97
 - electrochemical behaviour, 101
 - quasi-binary systems, 65, 68–71, 73–76, 78, 79, 81–83, 85, 86
 - quasi-ternary and multi-component systems, 78–80, 85
- electro-magnetic and optical properties, 29, 31, 35, 36, 40–43, 678, 688, 689
 - colour at the common conditions, 36
 - molar magnetic susceptibility, 35, 43, 678, 688, 689
 - optical spectra, 36
 - spectra in the infrared (IR) ranges, 36
 - specific electrical resistance (resistivity), 29, 31, 43, 678, 688, 689
 - superconductivity, 31
 - thermoionic emission characteristics, 37, 40–43, 678, 688, 689

- work function, 37, 40–43, 678, 688, 689
 - nuclear physical properties, 61, 63, 678, 692, 693
 - isotopes of metal, 61
 - abundance, 61
 - decay mode, 61
 - half-life period, 61
 - mass range, 61, 63, 678, 692, 693
 - resonance integral for neutron capture, 61, 63, 678, 692, 693
 - thermal neutron cross sections, 61, 63, 678, 692, 693
 - physico-mechanical properties, 43, 44, 46–50, 52, 55, 56, 61, 678, 690, 691
 - bulk (compression) modulus, 51, 56
 - Coulomb's (shear) modulus, 51, 56
 - density, 11, 12, 14, 46, 52, 61, 677, 680
 - ductile-to-brittle transition temperature, 46, 51, 55
 - elastic constants, 52, 55, 56, 61, 678, 690, 691
 - flexural (bending) strength, 46, 52
 - fracture toughness (critical stress intensity factor), 46, 52
 - hardness characteristics, 43, 44, 47–49, 52, 61, 678, 690, 691
 - in *HK* scale, 44, 47–49, 52
 - in *HV* scale, 43, 44, 52, 61, 678, 690, 691
 - microhardness, 47–49, 52
 - stiffness coefficients, 56, 61
 - stress-strain relationship, 51, 55
 - Young's modulus, 51, 52, 55, 56, 61, 678, 690, 691
 - structures, 9–12, 14, 677, 680
 - chemical bonding, 12
 - completeness of lattice, 12
 - crystal system, 11, 12, 677, 680
 - crystal type, 11, 12, 677, 680
 - densities, 11, 12, 14, 52, 61, 93, 677, 680
 - bulk density, 14, 52, 677, 680
 - XRD density, 11, 12, 14, 677, 680
 - homogeneity region, 9, 10, 82, 90, 677, 680
 - lattice parameters, 10–12, 677, 680
 - metal-carbon phase diagram, 9, 10
 - nanostructures, 14
 - order-disorder transformation, 9–12, 677, 680
 - ordered structures, 9–12, 18, 24–26, 29, 31, 35, 36, 44, 46, 50, 51, 55, 56, 95, 98
 - phase transformations, 9–12, 677, 680
 - high-temperature modification, 9–12, 15, 16, 18, 19, 21–23, 56, 680
 - low-temperature modification, 9–12, 18, 24–26, 29, 31, 35, 36, 44, 46, 50, 51, 55, 56, 95, 98, 680
 - thermal properties, 15, 18–23, 29, 677, 681–687
 - boiling point, 18, 24, 677, 684, 685
 - character of vaporization, 18, 20, 22, 24, 677, 686, 687
 - linear vaporization rate, 24, 677, 686, 687
 - mass vaporization rate, 22, 24, 677, 686, 687
 - coefficient of linear thermal expansion, 24–26, 29, 677, 684, 685
 - melting point, 10, 15, 18, 24, 677, 684, 685
 - molar enthalpy difference, 20, 24, 677, 682, 683
 - molar enthalpy (heat) of vaporization, 18, 24, 677, 682, 683
 - molar heat capacity, 15, 18–20, 24, 677, 681
 - parameters of gaseous phase over carbide phases, 20–23
 - partial pressures of carbon, 20–23
 - partial pressures of metal, 20–23
 - specific enthalpy difference, 20, 677, 682, 683
 - standard heat of formation, 18, 20, 677, 681
 - standard molar entropy, 18, 20, 677, 681
 - standard molar heat capacity, 18, 20, 677, 681
 - thermal conductivity, 24, 25, 29, 677, 684, 685
 - thermodynamic properties, 15, 18–20, 24, 677, 681–685
- Thermal coefficients of electroresistance, 31, 43, 164, 165, 172, 274, 275, 285, 460, 461, 476, 678, 688, 689
- Thermal conductivity, 5, 24–26, 29, 157, 158, 163, 266, 267, 272, 313, 447–451, 457, 516, 524, 525, 677, 679, 684, 685, 698, 699, 715–720

Total numbers of isotopes, 61, 63, 185–187, 313, 316, 517, 518, 524, 678, 692, 693

U

Ultimate compressive strength, 44, 61, 294, 297, 313, 431, 478, 486, 491, 517, 678, 679, 690, 691, 700, 701, 715–720

Ultimate tensile strength, 44, 50, 55, 61, 177, 178, 294–296, 313, 478, 485–516, 517, 487, 678, 679, 690, 691, 700, 701, 715–720

V

Vaporization rates, 20, 21, 22, 24, 153, 154, 157, 261, 265, 440, 442, 446, 447, 677, 686, 687

Vapour pressures, 20–24, 153–157, 261–265, 440–447, 677, 686, 687

Y

Young's moduli, 50–52, 55–61, 177, 180–184, 299, 302–311, 313, 316, 494, 500–508, 510, 511, 513, 516, 517, 523, 678, 679, 690, 691, 701–706, 715–720

Z

Zirconium monocarbide ZrC_{1-x} , 1, 3, 6, 68–70, 72, 78, 79, 82–86, 189, 193, 199–204, 266, 318, 321, 326, 330, 331, 333, 334, 338, 340–345, 423–676, 677–721

– chemical properties and materials design, 527–597, 679, 694–697

– catalytic activity, 572

– chemical interaction and compatibility, 527–576, 592–597, 679, 694–697

– radiochemical compatibility, 527, 572, 574–576

– with elements (solid and liquid metals/non-metals), 527–543

– with reagents (acids, alkalies and salts) in aqueous solutions, 572, 592–597, 679, 694, 695

– for oxycarbide phases, 572, 596

– with reagents (alkalies and salts) in molten states, 572, 593–595

– with refractory compounds, 527, 543–557, 679, 696, 697

– with gaseous media, 527, 557–573

– oxidation resistance, 527, 562–573

– diffusion characteristics, 423, 493, 522, 527, 572, 574–576, 584–591

– fission products diffusion characteristics, 527, 572, 574–576

– hetero-diffusion characteristics, 527, 574–576, 588, 589

– self-diffusion characteristics, 423, 493, 522, 584–591

– electrochemical behaviour, 572

– quasi-binary systems, 528–557

– quasi-ternary and multi-component systems, 528–534, 536, 538–540, 542–554

– recommended chemical etching agents, 596

– wettability with liquid metals and alloys, 543, 572, 577–583

– electro-magnetic and optical properties, 457–476, 678, 688, 689

– colour at the common conditions, 465

– Hall coefficient, 462–464

– integral (total) emittance, 467–469, 476, 678, 688, 689

– hemispherical emittance, 467–469

– normal emittance, 467–469

– molar magnetic susceptibility, 464, 476, 678, 688, 689

– normal monochromatic emittance (spectral emissivity), 466, 467, 469, 476, 678, 688, 689

– isosbestic points (X-points), 469

– optical spectra, 464, 465, 476

– photoemission spectra, 465, 476

– reflectance spectra, 464, 465

– spectra in the infrared (IR) ranges, 465

– spectra in the visible ranges, 465

– X-ray spectra, 464, 465

– absorption, 465

– emission, 465

– Seebeck coefficient, 462–464

– specific electrical resistance (resistivity), 457–462, 476, 522, 524, 562, 678, 688, 689

– superconductivity, 462

– thermal coefficient of resistivity, 460, 461, 476, 678, 688, 689

– thermionic emission characteristics, 469–476, 678, 688, 689

- Richardson constant, 469–476, 678, 688, 689
 - work function, 469–476, 678, 688, 689
 - nuclear physical properties, 517–527, 678, 692, 693
 - changes in properties after irradiation exposure, 522, 524, 525
 - accumulated energy, 524, 526
 - density, 519, 525, 523
 - effective temperature, 524
 - electrical resistivity, 522–524
 - flexural strength, 523, 524
 - heat capacity, 524
 - lattice parameter, 519, 523–525
 - microhardness, 520, 522–525
 - thermal conductivity, 524, 525
 - thermal stress resistance, 523
 - Young's modulus, 523
 - isotopes of metal, 517–519, 524, 678, 692, 693
 - abundance, 517, 518
 - decay mode, 517, 518
 - half-life period, 517, 518
 - mass, 517, 518
 - mass range, 517, 518, 524, 678, 692, 693
 - resonance integral for neutron capture, 517, 519, 524, 678, 692, 693
 - parameters of formation and migration of lattice point defects, 519, 520–522
 - antisites, 519, 520, 522
 - di-vacancies, 519, 520, 522
 - Frenkel pair, 519, 520, 522, 526
 - in metal sublattice, 519, 520–522, 526
 - in non-metal sublattice, 519, 520–522, 526
 - interstitial atoms, 519, 520–522
 - interstitial dimer clusters, 519, 520–522
 - interstitial tetrahedrons, 519, 521, 522
 - interstitial trimer clusters, 519, 521, 522
 - vacancies, 519, 520, 522
 - thermal neutron cross sections, 517, 519, 524, 678, 692, 693
 - under bombardment, 519, 522–527
 - by fast neutrons, 519, 523, 524
 - by gold ions, 526
 - by helium ions, 527, 575, 576, 588
 - by krypton ions, 525, 526, 575, 576
 - by protons, 525
 - by thermal neutrons, 524
 - by xenon ions, 527, 576
 - physico-mechanical properties, 476–517, 678, 690, 691
 - bulk (compression) modulus, 494, 500–507, 509, 510, 512, 513
 - compressive strength, 478, 486, 490, 491, 493, 494, 496, 517, 676, 690, 691
 - Hall-Petch relationship, 491
 - strain values, 491
 - Coulomb's (shear) modulus, 491, 494, 496, 500–508, 510, 511, 513
 - creep characteristics, 490–499, 589, 591
 - activation energy, 492, 493, 496–499
 - exponent constant, 492, 493, 496–499
 - dominating mechanisms, 493
 - long-term rupture strength, 492, 493, 496
 - normalized shear stress – homologous temperature map, 496
 - time-to-rupture, 492, 493
 - density, 425–428, 432, 519, 523, 560, 571, 583, 677, 680
 - ductile-to-brittle transition temperature, 490, 491
 - elastic constants, 483, 491, 494, 496, 500–513, 516–517, 522–524, 678, 690, 691
 - flexural (bending) strength, 486, 488–492, 495, 523, 524
 - effect of surface condition/treatment, 486, 490
 - fracture toughness (critical stress intensity factor), 489, 490, 524, 525
 - hardness characteristics, 431, 476–484, 497–499, 520, 522–525, 542, 585, 678, 690, 691
 - in *HK* scale, 476–481, 483, 484
 - in *HRA* scale, 476
 - in *HV* scale, 476–478, 678, 690, 691
 - in Mohs scale, 476

- microhardness, 476–484, 523, 524, 542, 585
- Poisson's ratio, 494, 500–507, 509, 510, 512, 513–516
- sound velocities, 494, 495
 - average, 495
 - longitudinal, 495
 - transversal, 495
- stiffness coefficients, 500–507
- stress-strain relationship, 478, 486, 487, 503, 506, 507
- tensile/flexural strengths ratio, 489
- tensile strength, 478, 485–487, 492, 494, 514–517, 678, 690, 691
 - elongation, 478, 485–487
 - reduction in area, 478, 485, 486
- thermal shock/stress resistance (thermal strength), 514–517, 523
 - values of figures-of-merit (criteria), 516, 517, 523
- volume compressibility, 494, 502, 506
- Young's modulus, 494, 500–508, 510, 511, 513, 516, 523, 678, 690, 691
- structures, 423–432, 677, 680
 - 2D-molecular MXenes, 432
 - bond energy, 429
 - chemical bonding, 429
 - C/Me radii ratio, 423
 - completeness of lattice, 429–431
 - for oxycarbide phases, 429–431
 - for oxycarbonitride phases, 429, 431
 - crystal system, 425–428, 677, 680
 - crystal type, 423, 425–428, 533, 543, 677, 680
 - densities, 425–428, 432, 519, 523, 560, 571, 583, 677, 680
 - bulk density, 432, 523, 560, 677, 680
 - XRD density, 425–428, 432, 519, 677, 680
 - homogeneity region, 423, 424, 427, 428, 432, 438–440, 442, 445–448, 456, 457, 462–465, 476, 477, 486, 488, 492, 493, 495, 511–513, 535, 551, 555–558, 561, 562, 677, 680
 - lattice parameters, 423–430, 519, 524–526, 533, 537, 545, 551, 552, 555, 556, 563, 677, 680
 - effect of nitrogen, 424–429, 552, 555
 - effect of oxygen, 424–430, 556
 - lattice point defects, 431, 462, 519–522, 526
 - metal-carbon phase diagram, 423, 424
 - minimal Burgers vector, 431
 - nanostructures, 426–429, 431, 432, 458, 460, 464, 466–470, 472–477, 480–484, 490, 502, 503, 505, 506, 519, 527, 532, 539, 540, 551, 553, 554, 562, 568, 569, 571, 579, 583, 588, 592, 593
 - nanofibres, 432
 - nanoparticles, 426–428, 431, 435, 562
 - thin films/coatings, 427, 428, 432, 458, 460, 464, 466–470, 472–477, 480–484, 490, 502, 503, 505, 506, 522, 532, 539, 540, 551, 553, 554, 562, 568, 569, 571, 579, 583, 588, 592, 593
 - whiskers, 426–429, 432
 - order-disorder transformation, 423, 461
 - ordered structures, 423, 461, 562
 - phase transformation under high pressures, 423
 - radii ratio of Me in Me/MeC, 423
 - slip systems, 431, 491
 - thermal properties, 432–457, 677, 681–687
 - boiling point, 435, 447, 677, 684, 685
 - character of vaporization, 434, 435, 440–447, 677, 686, 687
 - linear vaporization rate, 447, 677, 686, 687
 - mass vaporization rate, 442, 446, 447, 677, 686, 687
 - coefficient of linear thermal expansion, 430, 451–457, 677, 684, 685
 - melting point, 424, 432, 434–436, 440, 469, 496, 552, 590, 677, 684, 685
 - molar enthalpy difference, 432, 433, 435, 440, 447, 677, 682, 683
 - molar enthalpy (heat) of atomization from solid state, 435
 - molar enthalpy (heat) of dissociation, 434, 435, 443
 - molar enthalpy (heat) of melting, 434, 447, 677, 682, 683

- molar enthalpy (heat) of vaporization, 434, 435, 447, 677, 682, 683
- molar entropy, 432, 433, 435, 440, 447, 677, 681
- molar heat capacity, 432, 433, 435–440, 447, 524, 677, 681
- parameters of gaseous phase over monocarbide phase, 440–447, 677, 686, 687
- partial pressures of carbon over monocarbide phase, 440–447, 677, 686, 687
- partial pressures of metal over monocarbide phase, 440–447, 677, 686, 687
- relative thermal expansion, 451, 456, 457, 677, 684, 685
- specific enthalpy difference, 447, 677, 682, 683
- specific enthalpy (heat) of melting, 434, 435, 447, 677, 682, 683
- specific heat capacity, 434, 435, 439, 447, 677, 681
- standard heat of formation, 432, 433, 435, 440, 447, 677, 681
- standard molar entropy, 432, 433, 435, 440, 447, 677, 681
- standard molar heat capacity, 432, 433, 435, 438–440, 447, 677, 681
- thermal conductivity, 447–451, 457, 516, 524, 525, 677, 684, 685
- thermodynamic properties, 432–440, 447, 677, 681–685

Index (Chemical Systems)

A

- Ag–Cu–NbC, *see* NbC–Ag–Cu
Ag–Pd–ZrC, *see* ZrC–Ag–Pd
Ag–TaC, *see* TaC–Ag
Ag–ZrC, *see* ZrC–Ag
Al–Al₂O₃–ZrC, *see* ZrC–Al₂O₃–Al
Al–Co–NbC, *see* NbC–Al–Co
Al–Co–TaC, *see* TaC–Al–Co
Al–Cr–NbC, *see* NbC–Al–Cr
Al–Cr–TaC, *see* TaC–Al–Cr
Al–Cu–NbC, *see* NbC–Al–Cu
Al–Cu–TaC, *see* TaC–Al–Cu
Al–Cu–ZrC, *see* ZrC–Al–Cu
Al–Fe–NbC, *see* NbC–Al–Fe
Al–Fe–TaC, *see* TaC–Al–Fe
Al–HfC–SiC–TiC, *see* HfC–SiC–TiC–Al
Al–HfC–SiC, *see* HfC–SiC–Al
Al–HfC, *see* HfC–Al
Al–Mg–NbC, *see* NbC–Al–Mg
Al–Mg–ZrC, *see* ZrC–Al–Mg
Al–Mn–NbC, *see* NbC–Al–Mn
Al–Mn–TaC, *see* TaC–Al–Mn
Al–Nb₂C, *see* Nb₂C–Al
Al–NbC–Ni, *see* NbC–Al–Ni
Al–NbC–SiC–TiC, *see* NbC–SiC–TiC–Al
Al–NbC–TiC, *see* NbC–TiC–Al
Al–NbC, *see* NbC–Al
Al–NbC–V, *see* NbC–Al–V
Al–NbC–VC, *see* NbC–VC–Al
Al–NbC–Zn, *see* NbC–Al–Zn
Al–NbC–ZrC, *see* NbC–ZrC–Al
Al–NbC–ZrC, *see* ZrC–NbC–Al
Al–Ni–TaC, *see* TaC–Al–Ni
AlN–TaC, *see* TaC–AlN
Al–SiC–TiC–ZrC, *see* ZrC–SiC–TiC–Al
Al–SiC–ZrC, *see* ZrC–SiC–Al
Al–Sn–TaC, *see* TaC–Al–Sn
Al–Ta₂C, *see* Ta₂C–Al
Al–TaC, *see* TaC–Al
Al–TaC–TiC, *see* TaC–TiC–Al
Al–TaC–VC, *see* TaC–VC–Al
Al–V–TaC, *see* TaC–Al–V
Al–Zn–TaC, *see* TaC–Al–Zn
Al–ZrC, *see* ZrC–Al
Al–Zr–ZrC, *see* ZrC–Al–Zr
Al₂O₃–Nb₂C, *see* Nb₂C–Al₂O₃
Al₂O₃–NbC, *see* NbC–Al₂O₃
Al₂O₃–Si₃N₄–ZrC, *see* ZrC–Si₃N₄–Al₂O₃
Al₂O₃–Ta₂C, *see* Ta₂C–Al₂O₃
Al₂O₃–TaC, *see* TaC–Al₂O₃
Al₂O₃–ZrC, *see* ZrC–Al₂O₃
Al₄C₃–Ge–ZrC, *see* ZrC–Al₄C₃–Ge
Al₄C₃–HfC, *see* HfC–Al₄C₃
Al₄C₃–HfC–Si, *see* HfC–Al₄C₃–Si
Al₄C₃–HfC–SiC, *see* HfC–Al₄C₃–SiC
Al₄C₃–HfC–SiC–TiC, *see* HfC–Al₄C₃–SiC–TiC
Al₄C₃–HfC–YC, *see* HfC–Al₄C₃–YC
Al₄C₃–HfC–YC₂, *see* HfC–Al₄C₃–YC₂
Al₄C₃–NbC, *see* NbC–Al₄C₃
Al₄C₃–NbC–SiC–TiC, *see* NbC–Al₄C₃–SiC–TiC
Al₄C₃–NbC–TiC, *see* NbC–Al₄C₃–TiC
Al₄C₃–NbC–VC, *see* NbC–Al₄C₃–VC
Al₄C₃–NbC–ZrC, *see* NbC–Al₄C₃–ZrC
Al₄C₃–SiC–TiC–ZrC, *see* ZrC–Al₄C₃–SiC–TiC
Al₄C₃–SiC–ZrC, *see* ZrC–Al₄C₃–SiC
Al₄C₃–Si–ZrC, *see* ZrC–Al₄C₃–Si
Al₄C₃–TaC, *see* TaC–Al₄C₃

Al₄C₃-YC₂-ZrC, *see* ZrC-Al₄C₃-YC₂
 Al₄C₃-YC-ZrC, *see* ZrC-Al₄C₃-YC
 Al₄C₃-ZrC, *see* ZrC-Al₄C₃
 As-NbC, *see* NbC-As
 Au-NbC, *see* NbC-Au
 Au-TaC, *see* TaC-Au

B

B-B₄C-ZrC, *see* ZrC-B₄C-B
 B-HfC, *see* HfC-B
 B-Nb₂C, *see* Nb₂C-B
 B-NbC, *see* NbC-B
 B-Ta₂C, *see* Ta₂C-B
 B-TaC, *see* TaC-B
 B-ZrC, *see* ZrC-B
 B₄C-BN-NbC, *see* NbC-B₄C-BN
 B₄C-BN-ZrC, *see* ZrC-B₄C-BN
 B₄C-HfC, *see* HfC-B₄C
 B₄C-Nb₂C, *see* Nb₂C-B₄C
 B₄C-NbC, *see* NbC-B₄C
 B₄C-SiB₃-ZrC, *see* ZrC-B₄C-SiB₃
 B₄C-Ta₂C, *see* Ta₂C-B₄C
 B₄C-TaC, *see* TaC-B₄C
 B₄C-ZrC, *see* ZrC-B₄C
 Ba-ZrC, *see* ZrC-Ba
 Be-HfC, *see* HfC-Be
 Be-NbC, *see* NbC-Be
 Be-TaC, *see* TaC-Be
 Be-ZrC, *see* ZrC-Be
 Bi-HfC, *see* HfC-Bi
 Bi-NbC, *see* NbC-Bi
 Bi-Pb-ZrC, *see* ZrC-Bi-Pb
 Bi-TaC, *see* TaC-Bi
 Bi-ZrC, *see* ZrC-Bi
 BN-HfC, *see* HfC-BN
 BN-NbC, *see* NbC-BN
 BN-TaC, *see* TaC-BN
 BN-ZrC, *see* ZrC-BN
 Br₂-ZrC, *see* ZrC-Br₂

C

C-Fe-HfC-Mn, *see* HfC-C-Fe-Mn
 C-Fe-HfC, *see* HfC-C-Fe
 C-Fe-Mn-NbC, *see* NbC-C-Fe-Mn
 C-Fe-Mn-TaC, *see* TaC-C-Fe-Mn
 C-Fe-Mn-ZrC, *see* ZrC-C-Fe-Mn
 C-Fe-NbC, *see* NbC-C-Fe
 C-Fe-TaC, *see* TaC-C-Fe
 C-Fe-ZrC, *see* ZrC-C-Fe
 C-HfC, *see* HfC-C
 C-NbC, *see* NbC-C
 C-Ni-ZrC, *see* ZrC-C-Ni
 C-TaC, *see* TaC-C
 C-TiC-WC-ZrC, *see* ZrC-TiC-WC-C

C-VC-WC-ZrC, *see* ZrC-VC-WC-C
 C-ZrC, *see* ZrC-C
 CaO-ZrC, *see* ZrC-CaO
 Cd-HfC, *see* HfC-Cd
 Cd-ZrC, *see* ZrC-Cd
 Ce-Co-Mo₂C-Ni-TaC-TiC-TiN-WC, *see*
 TaC-Mo₂C-TiC-TiN-WC-Ce-Co-Ni
 Ce-ZrC, *see* ZrC-Ce
 CeC₂-UC-ZrC, *see* ZrC-CeC₂-UC
 CeC₂-ZrC, *see* ZrC-CeC₂
 CeN-HfC, *see* HfC-CeN
 CeN-NbC, *see* NbC-CeN
 CeN-TaC, *see* TaC-CeN
 CeN-ZrC, *see* ZrC-CeN
 CeP-HfC, *see* HfC-CeP
 CeP-NbC, *see* NbC-CeP
 CeP-TaC, *see* TaC-CeP
 CeP-ZrC, *see* ZrC-CeP
 CeS-HfC, *see* HfC-CeS
 CeS-NbC, *see* NbC-CeS
 CeS-TaC, *see* TaC-CeS
 CeS-ZrC, *see* ZrC-CeS
 Cl₂-NbC, *see* NbC-Cl₂
 Cl₂-TaC, *see* TaC-Cl₂
 Cl₂-ZrC, *see* ZrC-Cl₂
 Co-Cr₃C₂-Mo₂C-Ni-TaC-TiC-TiN-WC, *see*
 TaC-Cr₃C₂-Mo₂C-TiC-TiN-WC-Co-
 Ni
 Co-Cr₃C₂-NbC-TaC-TiC, *see* TaC-Cr₃C₂-
 NbC-TiC-Co
 Co-HfC-Mo₂C-TaC-TiC-TiN-WC, *see*
 TaC-HfC-TiC-TiN-WC-Mo₂C-Co
 Co-HfC-NbC, *see* HfC-NbC-Co
 Co-HfC-TaC, *see* TaC-HfC-Co
 Co-HfC-TiC, *see* HfC-TiC-Co
 Co-HfC-VC, *see* HfC-VC-Co
 Co-HfC-ZrC, *see* HfC-ZrC-Co
 Co-HfC, *see* HfC-Co
 CO-HfC, *see* HfC-CO
 Co-Mo-NbC-Ni-TaC-TiC-TiN-VC-WC,
see TaC-NbC-TiC-TiN-VC-WC-Co-
 Ni-Mo
 Co-Mo₂C-NbC-Ni-TiC-TiN-WC, *see* NbC-
 Mo₂C-TiC-TiN-WC-Co-Ni
 Co-Mo₂C-NbC, *see* NbC-Mo₂C-Co
 Co-Mo₂C-Ni-TaC-TiC-TiN-VC-WC, *see*
 TaC-Mo₂C-TiC-TiN-VC-WC-Co-Ni
 Co-Mo₂C-Ni-TaC-TiC-TiN-WC, *see* TaC-
 Mo₂C-TiC-TiN-WC-Co-Ni
 Co-Mo₂C-Ni-TaC-TiC-WC, *see* TaC-
 Mo₂C-TiC-WC-Co-Ni
 Co-Nb₂C, *see* Nb₂C-Co
 Co-NbC-Ni-TaC-TiC-TiN, *see* TaC-NbC-
 TiC-TiN-Co-Ni

- Co–NbC–Si, *see* NbC–Co–Si
 Co–NbC–TaC, *see* TaC–NbC–Co
 Co–NbC–TaC–TiC–TiN, *see* TaC–NbC–TiC–TiN–Co
 Co–NbC–TaC–TiC–TiN–WC, *see* TaC–NbC–TiC–TiN–WC–Co
 Co–NbC–TaC–TiC–WC, *see* TaC–NbC–TiC–WC–Co
 Co–NbC–TiC, *see* NbC–TiC–Co
 Co–NbC–VC, *see* NbC–VC–Co
 Co–NbC–VC–WC, *see* NbC–VC–WC–Co
 Co–NbC–WC, *see* NbC–WC–Co
 Co–NbC–ZrC, *see* NbC–ZrC–Co
 Co–NbC, *see* NbC–Co
 CO–NbC, *see* NbC–CO
 Co–Ni–TaC–TiC–TiN–WC, *see* TaC–TiC–TiN–WC–Co–Ni
 Co–Ni–W–ZrC, *see* ZrC–Co–Ni–W
 Co–Ni–ZrC, *see* ZrC–Co–Ni
 Co–Ta₂C, *see* Ta₂C–Co
 Co–TaC–TiC–TiN, *see* TaC–TiC–TiN–Co
 Co–TaC–TiC–WC, *see* TaC–TiC–WC–Co
 Co–TaC–TiC, *see* TaC–TiC–Co
 Co–TaC–VC, *see* TaC–VC–Co
 Co–TaC–WC, *see* TaC–WC–Co
 Co–TaC–ZrC, *see* TaC–ZrC–Co
 Co–TaC, *see* TaC–Co
 CO–TaC, *see* TaC–CO
 Co–TiC–VC–WC–ZrC, *see* ZrC–TiC–VC–WC–Co
 Co–TiC–WC–ZrC, *see* ZrC–TiC–WC–Co
 Co–TiC–ZrC, *see* ZrC–TiC–Co
 Co–VC–WC–ZrC, *see* ZrC–VC–WC–Co
 Co–VC–ZrC, *see* ZrC–VC–Co
 Co–ZrC, *see* ZrC–Co
 CO–ZrC, *see* ZrC–CO
 CO₂–HfC, *see* HfC–CO₂
 CO₂–NbC, *see* NbC–CO₂
 CO₂–TaC, *see* TaC–CO₂
 CO₂–ZrC, *see* ZrC–CO₂
 Cr–Cr₂₃C₆–ZrC, *see* ZrC–Cr₂₃C₆–Cr
 Cr–Cu–Fe–ZrC, *see* ZrC–Cr–Cu–Fe
 Cr–Fe–NbC–Ni, *see* NbC–Cr–Fe–Ni
 Cr–Fe–ZrC, *see* ZrC–Cr–Fe
 Cr–HfC, *see* HfC–Cr
 Cr–Mo₂C–NbC–Ni–TiC–VC, *see* NbC–Mo₂C–TiC–VC–Cr–Ni
 Cr–Nb₂C, *see* Nb₂C–Cr
 Cr–NbC–Ni–TiC–VC–WC, *see* NbC–TiC–VC–WC–Ni–Cr
 Cr–NbC–Ni, *see* NbC–Ni–Cr
 Cr–NbC, *see* NbC–Cr
 Cr–Ni–TaC, *see* TaC–Ni–Cr
 Cr–Ni–ZrC, *see* ZrC–Cr–Ni
 Cr–Ta₂C, *see* Ta₂C–Cr
 Cr–TaC, *see* TaC–Cr
 Cr–ZrC, *see* ZrC–Cr
 Cr₂₃C₆–Nb₂C, *see* Nb₂C–Cr₂₃C₆
 Cr₂₃C₆–NbC, *see* NbC–Cr₂₃C₆
 Cr₂₃C₆–ZrC, *see* ZrC–Cr₂₃C₆
 Cr₂O₃–Nb₂C, *see* Nb₂C–Cr₂O₃
 Cr₂O₃–NbC, *see* NbC–Cr₂O₃
 Cr₂O₃–TaC, *see* TaC–Cr₂O₃
 Cr₂O₃–ZrC, *see* ZrC–Cr₂O₃
 Cr₃C₂–Cr₇C₃–ZrC, *see* ZrC–Cr₃C₂–Cr₇C₃
 Cr₃C₂–HfC–Mo₂C–TiC–TiN–WC, *see* HfC–Cr₃C₂–Mo₂C–TiC–TiN–WC
 Cr₃C₂–HfC, *see* HfC–Cr₃C₂
 Cr₃C₂–Mo–Ni–TaC–TiC–WC, *see* TaC–Cr₃C₂–TiC–WC–Mo–Ni
 Cr₃C₂–Nb₂C, *see* Nb₂C–Cr₃C₂
 Cr₃C₂–NbC, *see* NbC–Cr₃C₂
 Cr₃C₂–TiC–ZrC, *see* ZrC–Cr₃C₂–TiC
 Cr₃C₂–ZrC, *see* ZrC–Cr₃C₂
 Cr₇C₃–Nb₂C, *see* Nb₂C–Cr₇C₃
 Cr₇C₃–NbC, *see* NbC–Cr₇C₃
 Cr₇C₃–TaC, *see* TaC–Cr₇C₃
 Cr₇C₃–ZrC, *see* ZrC–Cr₇C₃
 Cs–HfC, *see* HfC–Cs
 Cs–NbC, *see* NbC–Cs
 Cs–Ta₂C, *see* Ta₂C–Cs
 Cs–TaC, *see* TaC–Cs
 Cs–ZrC, *see* ZrC–Cs
 Cu–Fe–Si–ZrC, *see* ZrC–Cu–Fe–Si
 Cu–Hf–HfC–V, *see* HfC–Cu–Hf–V
 Cu–Hf–HfC, *see* HfC–Cu–Hf
 Cu–HfC, *see* HfC–Cu
 Cu–Nb–NbC–W, *see* NbC–Cu–Nb–W
 Cu–Nb–NbC, *see* NbC–Cu–Nb
 Cu–NbC, *see* NbC–Cu
 Cu–Ni–ZrC, *see* ZrC–Cu–Ni
 Cu–TaC–Zr, *see* TaC–Cu–Zr
 Cu–TaC, *see* TaC–Cu
 Cu–V–Zr–ZrC, *see* ZrC–Cu–V–Zr
 Cu–Zr–ZrC, *see* ZrC–Cu–Zr
 Cu–ZrC, *see* ZrC–Cu
- D**
 Dy₂O₃–ZrC, *see* ZrC–Dy₂O₃
 DyN–HfC, *see* HfC–DyN
 DyN–NbC, *see* NbC–DyN
 DyN–TaC, *see* TaC–DyN
 DyN–ZrC, *see* ZrC–DyN
- E**
 ErN–HfC, *see* HfC–ErN
 ErN–NbC, *see* NbC–ErN
 ErN–TaC, *see* TaC–ErN

ErN–ZrC, *see* ZrC–ErN
 Eu–ZrC, *see* ZrC–Eu
 EuN–HfC, *see* HfC–EuN
 EuN–NbC, *see* NbC–EuN
 EuN–TaC, *see* TaC–EuN
 EuN–ZrC, *see* ZrC–EuN
 EuO–HfC, *see* HfC–EuO
 EuO–NbC, *see* NbC–EuO
 EuO–TaC, *see* TaC–EuO
 EuO–ZrC, *see* ZrC–EuO

F

F₂–HfC, *see* HfC–F₂
 F₂–ZrC, *see* ZrC–F₂
 Fe–HfC, *see* HfC–Fe
 Fe–HfC–Mn, *see* HfC–Fe–Mn
 Fe–Mn–NbC, *see* NbC–Fe–Mn
 Fe–Nb₂C, *see* Nb₂C–Fe
 Fe–NbC–NbN, *see* NbC–NbN–Fe
 Fe–NbC–NbN–Ni–TiC–TiN, *see* NbC–NbN–TiC–TiN–Fe–Ni
 Fe–NbC–NbN–TiC–TiN, *see* NbC–NbN–TiC–TiN–Fe
 Fe–NbC–NbN–TiN, *see* NbC–NbN–TiN–Fe
 Fe–NbC–NbN–TiN–VC–VN, *see* NbC–NbN–TiN–VC–VN–Fe
 Fe–NbC–NbN–VC–VN, *see* NbC–NbN–VC–VN–Fe
 Fe–NbC–Ni, *see* NbC–Fe–Ni
 Fe–NbC–TiC–TiN, *see* NbC–TiC–TiN–Fe
 Fe–NbC–TiC–VC, *see* NbC–TiC–VC–Fe
 Fe–NbC–VC, *see* NbC–VC–Fe
 Fe–NbC, *see* NbC–Fe
 Fe–Ni–ZrC, *see* ZrC–Fe–Ni
 Fe–Si–ZrC, *see* ZrC–Fe–Si
 Fe–Ta₂C, *see* Ta₂C–Fe
 Fe–TaC–TiC–TiN, *see* TaC–TiC–TiN–Fe
 Fe–TaC, *see* TaC–Fe
 Fe–ZrC, *see* ZrC–Fe
 Fe₂O₃–HfC, *see* HfC–Fe₂O₃
 Fe₂O₃–Nb₂C, *see* Nb₂C–Fe₂O₃
 Fe₂O₃–NbC, *see* NbC–Fe₂O₃
 Fe₂O₃–TaC, *see* TaC–Fe₂O₃
 Fe₂O₃–ZrC, *see* ZrC–Fe₂O₃
 Fe₃Al–NbC, *see* NbC–Fe₃Al
 Fe₃C–HfC, *see* HfC–Fe₃C
 Fe₃C–NbC, *see* NbC–Fe₃C
 Fe₃C–TaC, *see* TaC–Fe₃C
 Fe₃C–ZrC, *see* ZrC–Fe₃C

G

Ga–HfC, *see* HfC–Ga
 Ga–NbC, *see* NbC–Ga
 Ga–TaC, *see* TaC–Ga

Ga–ZrC, *see* ZrC–Ga
 GdN–HfC, *see* HfC–GdN
 GdN–NbC, *see* NbC–GdN
 GdN–TaC, *see* TaC–GdN
 GdN–ZrC, *see* ZrC–GdN
 Ge–HfC, *see* HfC–Ge
 Ge–NbC, *see* NbC–Ge
 Ge–TaC, *see* TaC–Ge
 Ge–ZrC, *see* ZrC–Ge

H

H₂–HfC, *see* HfC–H₂
 H₂–Nb₂C, *see* Nb₂C–H₂
 H₂–NbC, *see* NbC–H₂
 H₂–TaC, *see* TaC–H₂
 H₂–ZrC–ZrO, *see* ZrC–ZrO–H₂
 H₂–ZrC, *see* ZrC–H₂
 H₂O–HfC, *see* HfC–H₂O
 H₂O–TaC, *see* TaC–H₂O
 H₂O–ZrC–ZrN, *see* ZrC–ZrN–H₂O
 H₂O–ZrC, *see* ZrC–H₂O
 HBr–ZrC, *see* ZrC–HBr
 HCl–ZrC, *see* ZrC–HCl
 He–ZrC, *see* ZrC–He
 Hf–HfC, *see* HfC–Hf
 Hf–Nb₂C, *see* Nb₂C–Hf
 Hf–NbC, *see* NbC–Hf
 HfB₂–HfC, *see* HfC–HfB₂
 HfB–HfC, *see* HfC–HfB
 HfC–Al, 188
 HfC–Al₄C₃, 195
 HfC–Al₄C₃–Si, 194
 HfC–Al₄C₃–SiC, 195
 HfC–Al₄C₃–SiC–TiC, 195
 HfC–Al₄C₃–YC, 195
 HfC–Al₄C₃–YC₂, 195
 HfC–B, 188
 HfC–B₄C, 195
 HfC–Be, 188
 HfC–Bi, 188
 HfC–BN, 195
 HfC–C, 188
 HfC–C–Fe, 188
 HfC–C–Fe–Mn, 188
 HfC–Cd, 189
 HfC–CeN, 195
 HfC–CeP, 195
 HfC–CeS, 195
 HfC–Co, 189
 HfC–CO, 205
 HfC–CO₂, 205
 HfC–Cr, 189
 HfC–Cr₃C₂, 195
 HfC–Cr₃C₂–Mo₂C–TiC–TiN–WC, 195

- HfC–Cs, 189
 HfC–Cu, 189
 HfC–Cu–Hf, 189
 HfC–Cu–Hf–V, 189
 HfC–DyN, 195
 HfC–ErN, 195
 HfC–EuN, 196
 HfC–EuO, 196
 HfC–F₂, 205
 HfC–Fe, 190
 HfC–Fe–Mn, 190
 HfC–Fe₂O₃, 196
 HfC–Fe₃C, 196
 HfC–Ga, 190
 HfC–GdN, 196
 HfC–Ge, 190
 HfC–H₂, 206
 HfC–H₂O, 206
 HfC–Hf, 190
 HfC–HfB, 196
 HfC–HfB₂, 196
 HfC–HfN, 196
 HfC–HfN–HfO, 196
 HfC–HfO₂, 197
 HfC–HoN, 197
 HfC–In, 190
 HfC–Ir, 190
 HfC–K, 190
 HfC–LaN, 197
 HfC–LaP, 197
 HfC–LaS, 197
 HfC–Li, 190
 HfC–LuN, 197
 HfC–MgO, 197
 HfC–Mn, 190
 HfC–Mn₅C₂, 197
 HfC–Mn₇C₃, 197
 HfC–Mo, 191
 HfC–Mo–Ni, 191
 HfC–Mo–Ni–TiC–TiN, *see* HfC–TiC–TiN–
 Mo–Ni
 HfC–Mo–Ni–TiC, *see* HfC–TiC–Mo–Ni
 HfC–Mo–Ni–TiC, *see* HfC–TiC–Ni–Mo
 HfC–Mo₂C, 198
 HfC–Mo₂C–Ni, 192
 HfC–Mo₂C–Ni–TaC–TiC–TiN–WC, *see* TaC–
 HfC–TiC–TiN–WC–Mo₂C–Ni
 HfC–MoC, 197
 HfC–MoC–TiC, 198
 HfC–MoC–VC, 198
 HfC–MoSi₂, 198
 HfC–N₂, 206
 HfC–Nb, 191
 HfC–Nb₂C, 198
 HfC–NbC, 198
 HfC–NbC–Co, 199
 HfC–NbC–NbN, 199
 HfC–NbC–TaC, 198
 HfC–NbC–ThC, 198
 HfC–NbC–TiC, 198
 HfC–NbC–UC, 198
 HfC–NbC–VC, 199
 HfC–NbC–WC, 199
 HfC–NbC–ZrC, 199
 HfC–NbN, 199
 HfC–NbO, 199
 HfC–Nd₂Fe₁₄B, 199
 HfC–NdN, 199
 HfC–Ni, 192
 HfC–Ni–TaC–TiC–TiN, *see* TaC–HfC–TiC–
 TiN–Ni
 HfC–Ni–TiC–TiN–WC, *see* HfC–TiC–TiN–
 WC–Ni
 HfC–Ni–TiC–TiN, *see* HfC–TiC–TiN–Ni
 HfC–Ni–TiC, *see* HfC–TiC–Ni
 HfC–Ni–WC, *see* HfC–WC–Ni
 HfC–Ni–ZrC, *see* HfC–ZrC–Ni
 HfC–NpC, 199
 HfC–NpN, 199
 HfC–O₂, 206
 HfC–Os, 193
 HfC–Pb, 193
 HfC–Pd, 193
 HfC–PrN, 199
 HfC–Pt, 193
 HfC–PuC, 199
 HfC–PuN, 199
 HfC–PuP, 199
 HfC–PuS, 199
 HfC–Re, 193
 HfC–Rh, 193
 HfC–Ru, 193
 HfC–S, 193
 HfC–Sb, 193
 HfC–ScC, 199
 HfC–ScN, 199
 HfC–Si, 193
 HfC–Si₃N₄, 200
 HfC–SiC, 199
 HfC–SiC–Al, 188
 HfC–SiC–TiC–Al, 188
 HfC–SiO₂, 200
 HfC–SmN, 200
 HfC–Sn, 194
 HfC–Ta, 194
 HfC–Ta₂C, 200
 HfC–TaC, 200
 HfC–TaC–Co, 189

- HfC-TaC-ThC, 200
 HfC-TaC-TiC, 200
 HfC-TaC-TiC-TiN-Ni, 192
 HfC-TaC-TiC-TiN-WC-Mo₂C-Co, 192
 HfC-TaC-TiC-TiN-WC-Mo₂C-Ni, 192
 HfC-TaC-UC, 200
 HfC-TaC-VC, 200
 HfC-TaC-WC, 200
 HfC-TaC-ZrC, 200
 HfC-TaN, 200
 HfC-TbN, 200
 HfC-Tc, 194
 HfC-TcC, 200
 HfC-Th, 194
 HfC-ThC, 200
 HfC-ThC-TiC, 200
 HfC-ThC-UC, 201
 HfC-ThC-VC, 201
 HfC-ThC-ZrC, 201
 HfC-ThN, 201
 HfC-ThP, 201
 HfC-ThS, 201
 HfC-Ti, 194
 HfC-TiC, 201
 HfC-TiC-Co, 189
 HfC-TiC-In, 190
 HfC-TiC-Mo-Ni, 191
 HfC-TiC-NbN, 202
 HfC-TiC-Ni, 192
 HfC-TiC-Ni-Mo, 192
 HfC-TiC-TiN-Mo-Ni, 191
 HfC-TiC-TiN-Ni, 192
 HfC-TiC-TiN-WC-Ni, 193
 HfC-TiC-UC, 201
 HfC-TiC-VC, 201
 HfC-TiC-WC, 202
 HfC-TiC-ZrC, 202
 HfC-TiN, 202
 HfC-TiO, 202
 HfC-Tl, 194
 HfC-U, 194
 HfC-UC, 202
 HfC-UC-VC, 202
 HfC-UC-ZrC, 202
 HfC-UC₂, 202
 HfC-UN, 202
 HfC-UO₂, 203
 HfC-UP, 203
 HfC-US, 203
 HfC-V, 194
 HfC-VC, 203
 HfC-VC-Co, 189
 HfC-VC-WC, 203
 HfC-VC-ZrC, 203
 HfC-VN, 203
 HfC-W, 194
 HfC-W₂B₅, 203
 HfC-W₂C, 204
 HfC-WC, 204
 HfC-WC-Ni, 193
 HfC-WC-ZrC, 204
 HfC-YbN, 204
 HfC-YC, 204
 HfC-YN, 204
 HfC-Zn, 194
 HfC-Zr, 194
 HfC-ZrC, 204
 HfC-ZrC-Co, 189
 HfC-ZrC-Ni, 193
 HfC-ZrN, 204
 HfC-ZrO₂, 204
 HfC-ZrP, 204
 HfN-NbC, *see* NbC-HfN
 HfN-NbC-NbN, *see* NbC-NbN-HfN
 HfN-TaC, *see* TaC-HfN
 HfN-ZrC, *see* ZrC-HfN
 Hf-Ta₂C, *see* Ta₂C-Hf
 Hf-TaC, *see* TaC-Hf
 Hf-ZrC, *see* ZrC-Hf
 HF-ZrC, *see* ZrC-HF
 HI-ZrC, *see* ZrC-HI
 HoN-NbC, *see* NbC-HoN
 HoN-TaC, *see* TaC-HoN
 HoN-ZrC, *see* ZrC-HoN
- I**
- I₂-ZrC, *see* ZrC-I₂
 In-NbC, *see* NbC-In
 In-TaC, *see* TaC-In
 In-TiC-ZrC, *see* ZrC-TiC-In
 In-ZrC, *see* ZrC-In
 Ir-Nb₂C, *see* Nb₂C-Ir
 Ir-NbC, *see* NbC-Ir
 Ir-Ta₂C, *see* Ta₂C-Ir
 Ir-TaC, *see* TaC-Ir
 Ir-ZrC, *see* ZrC-Ir
- K**
- K-NbC, *see* NbC-K
 K-TaC, *see* TaC-K
 K-ZrC, *see* ZrC-K
 Kr-ZrC, *see* ZrC-Kr
- L**
- La-ZrB₂-ZrC, *see* ZrC-ZrB₂-La
 LaB₆-NbC, *see* NbC-LaB₆
 LaB₆-SiC-ZrC, *see* ZrC-LaB₆-SiC
 LaB₆-TaC, *see* TaC-LaB₆

LaB₆-ZrC, *see* ZrC-LaB₆
 LaN-NbC, *see* NbC-LaN
 LaN-TaC, *see* TaC-LaN
 LaN-ZrC, *see* ZrC-LaN
 LaP-NbC, *see* NbC-LaP
 LaP-TaC, *see* TaC-LaP
 LaP-ZrC, *see* ZrC-LaP
 LaS-NbC, *see* NbC-LaS
 LaS-TaC, *see* TaC-LaS
 LaS-ZrC, *see* ZrC-LaS
 Li-ZrC, *see* ZrC-Li
 LuN-NbC, *see* NbC-LuN
 LuN-TaC, *see* TaC-LuN
 LuN-ZrC, *see* ZrC-LuN

M

Mg-ZrC, *see* ZrC-Mg
 MgO-NbC, *see* NbC-MgO
 MgO-Si₃N₄-ZrC, *see* ZrC-Si₃N₄-MgO
 MgO-TaC, *see* TaC-MgO
 MgO-ZrC, *see* ZrC-MgO
 Mn-NbC, *see* NbC-Mn
 Mn-TaC, *see* TaC-Mn
 Mn-ZrC, *see* ZrC-Mn
 Mn₅C₂-NbC, *see* NbC-Mn₅C₂
 Mn₅C₂-TaC, *see* TaC-Mn₅C₂
 Mn₅C₂-ZrC, *see* ZrC-Mn₅C₂
 Mn₇C₃-NbC, *see* NbC-Mn₇C₃
 Mn₇C₃-TaC, *see* TaC-Mn₇C₃
 Mn₇C₃-ZrC, *see* ZrC-Mn₇C₃
 Mo-Nb₂C, *see* Nb₂C-Mo
 Mo-NbC-Ni-TiC-TiN, *see* NbC-TiC-TiN-Mo-Ni
 Mo-NbC-Ni-TiC, *see* NbC-TiC-Mo-Ni
 Mo-NbC-Re, *see* NbC-Mo-Re
 Mo-NbC, *see* NbC-Mo
 Mo-Ni-TaC-TiC-TiN-WC-ZrC, *see* TaC-TiC-TiN-WC-ZrC-Mo-Ni
 Mo-Ni-TaC-TiC-WC, *see* TaC-TiC-WC-Mo-Ni
 Mo-Ni-TaC-TiC, *see* TaC-TiC-Mo-Ni
 Mo-Ni-TiC-TiN-ZrC, *see* ZrC-TiC-TiN-Mo-Ni
 Mo-Ni-TiC-ZrC, *see* ZrC-TiC-Mo-Ni
 Mo-Ni-ZrC, *see* ZrC-Mo-Ni
 Mo-Re-TaC, *see* TaC-Mo-Re
 Mo-Re-ZrC, *see* ZrC-Mo-Re
 Mo-Ta₂C, *see* Ta₂C-Mo
 Mo-TaC, *see* TaC-Mo
 Mo-UC-ZrC, *see* ZrC-UC-Mo
 Mo-W-ZrC, *see* ZrC-Mo-W
 Mo-ZrC, *see* ZrC-Mo
 Mo₂C-Nb₂C-Ta₂C, *see* Nb₂C-Mo₂C-Ta₂C

Mo₂C-Nb₂C, *see* Nb₂C-Mo₂C
 Mo₂C-NbC-Ni-TiC-TiN, *see* NbC-Mo₂C-TiC-TiN-Ni
 Mo₂C-NbC, *see* NbC-Mo₂C
 Mo₂C-Ni-TaC-TiC-TiN-WC, *see* TaC-Mo₂C-TiC-TiN-WC-Ni
 Mo₂C-Ni-TaC-TiC-TiN, *see* TaC-Mo₂C-TiC-TiN-Ni
 Mo₂C-Ni-TaC-TiC, *see* TaC-Mo₂C-TiC-Ni
 Mo₂C-Ni-TiC-ZrC, *see* ZrC-Mo₂C-TiC-Ni
 Mo₂C-Ta₂C-V₂C, *see* Ta₂C-Mo₂C-V₂C
 Mo₂C-Ta₂C, *see* Ta₂C-Mo₂C
 Mo₂C-TaC, *see* TaC-Mo₂C
 Mo₂C-ZrC, *see* ZrC-Mo₂C
 MoC-NbC-UC, *see* NbC-MoC-UC
 MoC-NbC-ZrC, *see* NbC-MoC-ZrC
 MoC-NbC, *see* NbC-MoC
 MoC-TaC, *see* TaC-MoC
 MoC-UC-ZrC, *see* ZrC-MoC-UC
 MoC-ZrC, *see* ZrC-MoC
 MoSi₂-TaC, *see* TaC-MoSi₂
 MoSi₂-ZrC, *see* ZrC-MoSi₂

N

N₂-Nb₂C, *see* Nb₂C-N₂
 N₂-NbC, *see* NbC-N₂
 N₂-Ta₂C, *see* Ta₂C-N₂
 N₂-TaC, *see* TaC-N₂
 N₂-ZrC, *see* ZrC-N₂
 Na-NbC, *see* NbC-Na
 Nb-Nb₂C, *see* Nb₂C-Nb
 Nb-NbC, *see* NbC-Nb
 Nb-Ta₂C, *see* Ta₂C-Nb
 Nb-TaC, *see* TaC-Nb
 Nb-UC-ZrC, *see* ZrC-UC-Nb
 Nb-ZrC, *see* ZrC-Nb
 Nb₂C-Al, 317
 Nb₂C-Al₂O₃, 330
 Nb₂C-B, 318
 Nb₂C-B₄C, 331
 Nb₂C-Co, 321
 Nb₂C-Cr, 321
 Nb₂C-Cr₂₃C₆, 332
 Nb₂C-Cr₂O₃, 332
 Nb₂C-Cr₃C₂, 332
 Nb₂C-Cr₇C₃, 332
 Nb₂C-Fe, 323
 Nb₂C-Fe₂O₃, 332
 Nb₂C-H₂, 347
 Nb₂C-Hf, 323
 Nb₂C-HfC, 333
 Nb₂C-Ir, 323
 Nb₂C-Mo, 324

- Nb₂C–Mo₂C, 334
 Nb₂C–Mo₂C–Ta₂C, 335
 Nb₂C–N₂, 347
 Nb₂C–Nb, 324
 Nb₂C–Nb₂N, 335
 Nb₂C–Nb₂O₅, 336
 Nb₂C–NbB, 335
 Nb₂C–NbO, 336
 Nb₂C–NbSi₂, 336
 Nb₂C–Ni, 326
 Nb₂C–O₂, 351
 Nb₂C–Os, 327
 Nb₂C–Pd, 327
 Nb₂C–Pt, 327
 Nb₂C–Pu, 327
 Nb₂C–Re, 327
 Nb₂C–Rh, 327
 Nb₂C–Ru, 328
 Nb₂C–Si, 328
 Nb₂C–SiC, 337
 Nb₂C–Sn, 328
 Nb₂C–Ta, 329
 Nb₂C–Ta₂C, 338
 Nb₂C–Ta₂C–W₂C, 338
 Nb₂C–TcC, 338
 Nb₂C–Th, 329
 Nb₂C–ThC, 339
 Nb₂C–ThC₂, 339
 Nb₂C–Ti, 329
 Nb₂C–TiC, 339
 Nb₂C–U, 329
 Nb₂C–UC, 341
 Nb₂C–UC₂, 341
 Nb₂C–V, 329
 Nb₂C–V₂C, 342
 Nb₂C–W, 330
 Nb₂C–W₂C, 343
 Nb₂C–Zr, 330
 Nb₂C–ZrC, 344
 Nb₅Si₃–TaC, *see* TaC–Nb₅Si₃
 NbB–Nb₂C, *see* Nb₂C–NbB
 NbB–NbC, *see* NbC–NbB
 NbB₂–NbC, *see* NbC–NbB₂
 NbC–Ag–Cu, 317
 NbC–Al, 317
 NbC–Al–Co, 317
 NbC–Al–Cr, 317
 NbC–Al–Cu, 317
 NbC–Al–Fe, 317
 NbC–Al–Mg, 317
 NbC–Al–Mn, 317
 NbC–Al–Ni, 317
 NbC–Al–V, 317
 NbC–Al–Zn, 317
 NbC–Al₂O₃, 330
 NbC–Al₄C₃, 330
 NbC–Al₄C₃–SiC–TiC, 330
 NbC–Al₄C₃–TiC, 331
 NbC–Al₄C₃–VC, 331
 NbC–Al₄C₃–ZrC, 331
 NbC–As, 318
 NbC–Au, 318
 NbC–B, 318
 NbC–B₄C, 331
 NbC–B₄C–BN, 331
 NbC–Be, 318
 NbC–Bi, 318
 NbC–BN, 331
 NbC–C, 318
 NbC–C–Fe, 318
 NbC–C–Fe–Mn, 318
 NbC–CeN, 331
 NbC–CeP, 331
 NbC–CeS, 331
 NbC–Cl₂, 346
 NbC–Co, 319
 NbC–CO, 345
 NbC–Co–Si, 319
 NbC–CO₂, 345
 NbC–Cr, 321
 NbC–Cr–Fe–Ni, 321
 NbC–Cr₂₃C₆, 332
 NbC–Cr₂O₃, 332
 NbC–Cr₃C₂, 332
 NbC–Cr₇C₃, 332
 NbC–Cs, 321
 NbC–Cu, 321
 NbC–Cu–Nb, 321
 NbC–Cu–Nb–W, 321
 NbC–DyN, 332
 NbC–ErN, 332
 NbC–EuN, 332
 NbC–EuO, 332
 NbC–Fe, 322
 NbC–Fe–Mn, 322
 NbC–Fe–Ni, 322
 NbC–Fe₂O₃, 332
 NbC–Fe₃Al, 332
 NbC–Fe₃C, 332
 NbC–Ga, 323
 NbC–GdN, 333
 NbC–Ge, 323
 NbC–H₂, 346
 NbC–Hf, 323
 NbC–HfC, 333
 NbC–HfC–Co, 319
 NbC–HfC–TaC, 333
 NbC–HfC–ThC, 333

- NbC–HfC–TiC, 333
 NbC–HfC–UC, 333
 NbC–HfC–VC, 333
 NbC–HfC–WC, 333
 NbC–HfC–ZrC, 333
 NbC–HfN, 333
 NbC–HoN, 333
 NbC–In, 323
 NbC–Ir, 323
 NbC–K, 323
 NbC–LaB₆, 333
 NbC–LaN, 333
 NbC–LaP, 333
 NbC–LaS, 333
 NbC–LuN, 333
 NbC–MgO, 334
 NbC–Mn, 323
 NbC–Mn₅C₂, 334
 NbC–Mn₇C₃, 334
 NbC–Mo, 324
 NbC–Mo–Re, 324
 NbC–Mo₂C, 334
 NbC–Mo₂C–Co, 319
 NbC–Mo₂C–TiC–TiN–Ni, 325
 NbC–Mo₂C–TiC–TiN–WC–Co–Ni, 319
 NbC–Mo₂C–TiC–VC–Cr–Ni, 321
 NbC–MoC, 334
 NbC–MoC–UC, 334
 NbC–MoC–ZrC, 334
 NbC–N₂, 347
 NbC–Na, 324
 NbC–Nb, 324
 NbC–Nb₂O₅, 336
 NbC–NbB, 335
 NbC–NbB₂, 335
 NbC–NbN, 335
 NbC–NbN–Fe, 323
 NbC–NbN–HfC, 333
 NbC–NbN–HfN, 335
 NbC–NbN–NbO, 335
 NbC–NbN–TiC, 339
 NbC–NbN–TiC–TiN, 339
 NbC–NbN–TiC–TiN–Fe, 322
 NbC–NbN–TiC–TiN–Fe–Ni, 322
 NbC–NbN–TiN, 335
 NbC–NbN–TiN–Fe, 323
 NbC–NbN–TiN–VC–VN–Fe, 323
 NbC–NbN–TiN–ZrN, 335
 NbC–NbN–VC–VN–Fe, 322
 NbC–NbN–VC–VN, *see* NbC–VC–NbN–VN
 NbC–NbN–VN, 335
 NbC–NbN–WC, 335
 NbC–NbN–ZrN, 335
 NbC–NbO, 336
 NbC–NbSi₂, 336
 NbC–Nd₂Fe₁₄B, 337
 NbC–NdN, 336
 NbC–NH₃, 347
 NbC–Ni, 325
 NbC–Ni–Cr, 326
 NbC–Ni–TaC–TiC–TiN, *see* TaC–NbC–TiC–TiN–Ni
 NbC–Ni–TaC, *see* TaC–NbC–Ni
 NbC–Ni–TiC–TiN–TiO, *see* NbC–TiC–TiN–TiO–Ni
 NbC–Ni–TiC–TiN–WC, *see* NbC–TiC–TiN–WC–Ni
 NbC–Ni–TiC–TiN, *see* NbC–TiC–TiN–Ni
 NbC–Ni–TiC, *see* NbC–TiC–Ni
 NbC–Ni–VC, *see* NbC–VC–Ni
 NbC–Ni–ZrC, *see* NbC–ZrC–Ni
 NbC–NpC, 337
 NbC–NpN, 337
 NbC–O₂, 347
 NbC–Os, 327
 NbC–P, 327
 NbC–Pb, 327
 NbC–Pd, 327
 NbC–PrN, 337
 NbC–Pt, 327
 NbC–Pu, 327
 NbC–PuC, 337
 NbC–PuN, 337
 NbC–PuP, 337
 NbC–PuS, 337
 NbC–Re, 327
 NbC–Rh, 327
 NbC–Ru, 327
 NbC–S, 328
 NbC–Sb, 328
 NbC–ScC, 337
 NbC–ScN, 337
 NbC–Si, 328
 NbC–Si₃N₄, 337
 NbC–SiC, 337
 NbC–SiC–TiC–Al, 317
 NbC–SiO₂–Al₂O₃–CaO–Fe₂O₃ (basalt), 337
 NbC–SmN, 337
 NbC–Sn, 328
 NbC–Ta, 329
 NbC–TaC, 337
 NbC–TaC–Co, 319
 NbC–TaC–Ni, 325
 NbC–TaC–TaN–TiC, 337
 NbC–TaC–ThC, 337
 NbC–TaC–TiC, 337
 NbC–TaC–TiC–TiN–Co, 319
 NbC–TaC–TiC–TiN–Co–Ni, 320

- NbC–TaC–TiC–TiN–Ni, 325
 NbC–TaC–TiC–TiN–VC–WC–Co–Ni–Mo, 320
 NbC–TaC–TiC–TiN–WC–Co, 320
 NbC–TaC–TiC–WC–Co, 319
 NbC–TaC–UC, 338
 NbC–TaC–VC, 338
 NbC–TaC–WC, 338
 NbC–TaC–ZrC, 338
 NbC–Ta₂N, 338
 NbC–TbN, 338
 NbC–Tc, 329
 NbC–TcC, 338
 NbC–Th, 329
 NbC–ThC, 338
 NbC–ThC–TiC, 338
 NbC–ThC–UC, 338
 NbC–ThC–VC, 338
 NbC–ThC–ZrC, 338
 NbC–ThC₂, 339
 NbC–ThN, 339
 NbC–ThP, 339
 NbC–ThS, 339
 NbC–Ti, 329
 NbC–TiC, 339
 NbC–TiC–Al, 318
 NbC–TiC–Co, 320
 NbC–TiC–Mo–Ni, 324
 NbC–TiC–Ni, 325
 NbC–TiC–TiN–Fe, 322
 NbC–TiC–TiN–Mo–Ni, 324
 NbC–TiC–TiN–Ni, 326
 NbC–TiC–TiN–TiO–Ni, 326
 NbC–TiC–TiN–WC–Ni, 326
 NbC–TiC–UC, 340
 NbC–TiC–VC, 340
 NbC–TiC–VC–Fe, 322
 NbC–TiC–VC–WC–Ni–Cr, 326
 NbC–TiC–WC, 340
 NbC–TiC–ZrC, 340
 NbC–TiN, 340
 NbC–TiO, 340
 NbC–Tl, 329
 NbC–U, 329
 NbC–U₂C₃, 341
 NbC–UC, 341
 NbC–UC₂, 341
 NbC–UC–VC, 340
 NbC–UC–WC, 340
 NbC–UC–ZrC, 341
 NbC–UN, 341
 NbC–UP, 341
 NbC–US, 341
 NbC–V, 329
 NbC–VC, 341
 NbC–VC–Al, 318
 NbC–VC–Co, 320
 NbC–VC–Fe, 322
 NbC–VC–NbN–VN, 342
 NbC–VC–Ni, 326
 NbC–VC–VN, 342
 NbC–VC–WC, 342
 NbC–VC–WC–Co, 320
 NbC–VC–ZrC, 342
 NbC–VN, 342
 NbC–W, 329
 NbC–W₂B₅, 342
 NbC–W₃C, 343
 NbC–WC, 342
 NbC–WC–Co, 320
 NbC–WC–ZrC, 343
 NbC–YbN, 343
 NbC–YC, 343
 NbC–YN, 343
 NbC–Zn, 330
 NbC–Zr, 330
 NbC–ZrC, 344
 NbC–ZrC–Al, 318
 NbC–ZrC–Co, 321
 NbC–ZrC–Ni, 326
 NbC–ZrC–ZrN, 344
 NbC–ZrN, 344
 NbC–ZrO₂, 345
 NbC–ZrP, 344
 NbN–TaC, *see* TaC–NbN
 NbN–TiC–ZrC, *see* ZrC–TiC–NbN
 NbN–ZrC, *see* ZrC–NbN
 NbO–TaC, *see* TaC–NbO
 NbO–ZrC, *see* ZrC–NbO
 Nd₂Fe₁₄B–TaC, *see* TaC–Nd₂Fe₁₄B
 Nd₂Fe₁₄B–ZrC, *see* ZrC–Nd₂Fe₁₄B
 NdN–TaC, *see* TaC–NdN
 NdN–ZrC, *see* ZrC–NdN
 NH₃–TaC, *see* TaC–NH₃
 NH₃–ZrC, *see* ZrC–NH₃
 Ni–P–ZrC, *see* ZrC–Ni–P
 Ni–Ta₂C, *see* Ta₂C–Ni
 Ni–TaC–TiC–TiN–WC, *see* TaC–TiC–TiN–WC–Ni
 Ni–TaC–TiC–TiN, *see* TaC–TiC–TiN–Ni
 Ni–TaC–TiC, *see* TaC–TiC–Ni
 Ni–TaC–ZrC, *see* TaC–ZrC–Ni
 Ni–TaC, *see* TaC–Ni
 Ni–TiC–TiN–TiO–ZrC, *see* ZrC–TiC–TiN–TiO–Ni
 Ni–TiC–TiN–WC–ZrC, *see* ZrC–TiC–TiN–WC–Ni
 Ni–TiC–TiN–ZrC, *see* ZrC–TiC–TiN–Ni

Ni–TiC–ZrC, *see* ZrC–TiC–Ni
 Ni–UC–ZrC, *see* ZrC–UC–Ni
 Ni–W–ZrC, *see* ZrC–Ni–W
 Ni–WC–ZrC, *see* ZrC–WC–Ni
 Ni–ZrB₂–ZrC, *see* ZrC–ZrB₂–Ni
 Ni–ZrC, *see* ZrC–Ni
 NiO–ZrC, *see* ZrC–NiO
 NpC–TaC, *see* TaC–NpC
 NpC–ZrC, *see* ZrC–NpC
 NpN–TaC, *see* TaC–NpN
 NpN–ZrC, *see* ZrC–NpN

O

O₂–Ta₂C, *see* Ta₂C–O₂
 O₂–TaC, *see* TaC–O₂
 O₂–ZrC, *see* ZrC–O₂
 Os–Ta₂C, *see* Ta₂C–Os
 Os–TaC, *see* TaC–Os
 Os–ZrC, *see* ZrC–Os

P

Pb–TaC, *see* TaC–Pb
 Pb–ZrC, *see* ZrC–Pb
 Pd–Ta₂C, *see* Ta₂C–Pd
 Pd–TaC, *see* TaC–Pd
 Pd–ZrC, *see* ZrC–Pd
 PrN–TaC, *see* TaC–PrN
 PrN–ZrC, *see* ZrC–PrN
 Pt–Ta₂C, *see* Ta₂C–Pt
 Pt–TaC, *see* TaC–Pt
 Pt–ZrC, *see* ZrC–Pt
 Pu–Ta₂C, *see* Ta₂C–Pu
 Pu–TaC, *see* TaC–Pu
 Pu–UC–ZrC, *see* ZrC–UC–Pu
 Pu–ZrC, *see* ZrC–Pu
 Pu₂C₃–ZrC, *see* ZrC–Pu₂C₃
 PuC–TaC, *see* TaC–PuC
 PuC–UC–ZrC, *see* ZrC–PuC–UC
 PuC–ZrC, *see* ZrC–PuC
 PuN–TaC, *see* TaC–PuN
 PuN–ZrC, *see* ZrC–PuN
 PuP–TaC, *see* TaC–PuP
 PuP–ZrC, *see* ZrC–PuP
 PuS–TaC, *see* TaC–PuS
 PuS–ZrC, *see* ZrC–PuS

R

Rb–ZrC, *see* ZrC–Rb
 Re–Ta₂C, *see* Ta₂C–Re
 Re–TaC, *see* TaC–Re
 Re–UC–ZrC, *see* ZrC–UC–Re
 Re–ZrC, *see* ZrC–Re
 Rh–Ta₂C, *see* Ta₂C–Rh
 Rh–TaC, *see* TaC–Rh

Rh–ZrC, *see* ZrC–Rh
 Ru–Ta₂C, *see* Ta₂C–Ru
 Ru–TaC, *see* TaC–Ru
 Ru–ZrC, *see* ZrC–Ru

S

S–TaC, *see* TaC–S
 S–ZrC, *see* ZrC–S
 Sb–TaC, *see* TaC–Sb
 Sb–ZrC, *see* ZrC–Sb
 Sc–ZrC, *see* ZrC–Sc
 ScC–TaC, *see* TaC–ScC
 ScC–ZrC, *see* ZrC–ScC
 ScN–TaC, *see* TaC–ScN
 ScN–ZrC, *see* ZrC–ScN
 Si–Ta₂C, *see* Ta₂C–Si
 Si–TaC, *see* TaC–Si
 Si–ZrC, *see* ZrC–Si
 Si₃N₄–TaC, *see* TaC–Si₃N₄
 Si₃N₄–ZrC, *see* ZrC–Si₃N₄
 SiC–Ta₂C, *see* Ta₂C–SiC
 SiC–TaC, *see* TaC–SiC
 SiC–WC–ZrC, *see* ZrC–SiC–WC
 SiC–ZrB₂–ZrC, *see* ZrC–SiC–ZrB₂
 SiC–ZrC, *see* ZrC–SiC
 SmN–TaC, *see* TaC–SmN
 SmN–ZrC, *see* ZrC–SmN
 Sn–TaC, *see* TaC–Sn
 Sn–ZrC, *see* ZrC–Sn
 Sr–ZrC, *see* ZrC–Sr

T

Ta–Ta₂C, *see* Ta₂C–Ta
 Ta–TaC–Ta₂N, *see* TaC–Ta₂N–Ta
 Ta–TaC, *see* TaC–Ta
 Ta–UC–ZrC, *see* ZrC–UC–Ta
 Ta–ZrC, *see* ZrC–Ta
 Ta₂C–Al, 65
 Ta₂C–Al₂O₃, 76
 Ta₂C–B, 65
 Ta₂C–B₄C, 76
 Ta₂C–Co, 68
 Ta₂C–Cr, 68
 Ta₂C–Cs, 69
 Ta₂C–Fe, 69
 Ta₂C–Hf, 70
 Ta₂C–HfC, 78
 Ta₂C–Ir, 70
 Ta₂C–Mo, 70
 Ta₂C–Mo₂C, 78
 Ta₂C–Mo₂C–Nb₂C, 78
 Ta₂C–Mo₂C–V₂C, 79
 Ta₂C–N₂, 88
 Ta₂C–Nb, 71

- Ta_2C-Nb_2C , 79
 $Ta_2C-Nb_2C-W_2C$, 80
 Ta_2C-Ni , 73
 Ta_2C-O_2 , 90
 Ta_2C-Os , 73
 Ta_2C-Pd , 73
 Ta_2C-Pt , 73
 Ta_2C-Pu , 73
 Ta_2C-Re , 73
 Ta_2C-Rh , 73
 Ta_2C-Ru , 74
 Ta_2C-Si , 74
 Ta_2C-SiC , 81
 Ta_2C-Ta , 74
 Ta_2C-Ta_2N , 81
 $Ta_2C-Ta_2N-Ta_2O$, 81
 $Ta_2C-Ta_2O_5$, 82
 Ta_2C-TaB_2 , 81
 $Ta_2C-TaSi_2$, 81
 Ta_2C-TcC , 82
 Ta_2C-Th , 74
 Ta_2C-ThC , 82
 Ta_2C-ThC_2 , 82
 Ta_2C-Ti , 83
 Ta_2C-TiC , 83
 Ta_2C-U , 75
 Ta_2C-UC , 84
 Ta_2C-V , 75
 Ta_2C-V_2C , 85
 $Ta_2C-V_2C-W_2C$, 85
 Ta_2C-W , 75
 Ta_2C-W_2C , 85
 Ta_2C-WC , 85
 Ta_2C-Zr , 75
 Ta_2C-ZrC , 86
 Ta_5Si_3-TaC , *see* $TaC-Ta_5Si_3$
 TaB_2-Ta_2C , *see* Ta_2C-TaB_2
 TaB_2-TaC , *see* $TaC-TaB_2$
 $TaC-Ag$, 64
 $TaC-Al$, 64
 $TaC-Al-Co$, 64
 $TaC-Al-Cr$, 64
 $TaC-Al-Cu$, 64
 $TaC-Al-Fe$, 64
 $TaC-Al-Mn$, 64
 $TaC-Al-Ni$, 64
 $TaC-Al-Sn$, 64
 $TaC-Al-V$, 64
 $TaC-Al-Zn$, 64
 $TaC-Al_2O_3$, 76
 $TaC-Al_4C_3$, 76
 $TaC-AlN$, 76
 $TaC-Au$, 65
 $TaC-B$, 65
 $TaC-B_4C$, 76
 $TaC-Be$, 65
 $TaC-Bi$, 65
 $TaC-BN$, 76
 $TaC-C$, 65
 $TaC-C-Fe$, 65
 $TaC-C-Fe-Mn$, 65
 $TaC-CeN$, 76
 $TaC-CeP$, 76
 $TaC-CeS$, 76
 $TaC-Cl_2$, 87
 $TaC-Co$, 66
 $TaC-CO$, 87
 $TaC-CO_2$, 87
 $TaC-Cr$, 68
 $TaC-Cr_2O_3$, 76
 $TaC-Cr_3C_2-Mo_2C-TiC-TiN-WC-Co-Ni$, 66
 $TaC-Cr_3C_2-NbC-TiC-Co$, 66
 $TaC-Cr_3C_2-TiC-WC-Mo-Ni$, 70
 $TaC-Cr_7C_3$, 76
 $TaC-Cs$, 69
 $TaC-Cu$, 69
 $TaC-Cu-Zr$, 69
 $TaC-DyN$, 76
 $TaC-ErN$, 76
 $TaC-EuN$, 76
 $TaC-EuO$, 77
 $TaC-Fe$, 69
 $TaC-Fe_2O_3$, 77
 $TaC-Fe_3C$, 77
 $TaC-Ga$, 69
 $TaC-GdN$, 77
 $TaC-Ge$, 70
 $TaC-H_2O$, 87
 $TaC-H_2$, 87
 $TaC-Hf$, 70
 $TaC-HfC$, 77
 $TaC-HfC-Co$, 66
 $TaC-HfC-Mo_2C-TiC-TiN-WC-Co$, 66
 $TaC-HfC-Mo_2C-TiC-TiN-WC-Ni$, 72
 $TaC-HfC-NbC$, 77
 $TaC-HfC-ThC$, 77
 $TaC-HfC-TiC$, 77
 $TaC-HfC-TiC-TiN-Ni$, 72
 $TaC-HfC-UC$, 77
 $TaC-HfC-VC$, 77
 $TaC-HfC-WC$, 77
 $TaC-HfC-ZrC$, 78
 $TaC-HfN$, 78
 $TaC-HoN$, 78
 $TaC-In$, 70
 $TaC-Ir$, 70
 $TaC-K$, 70
 $TaC-LaB_6$, 78

- TaC–LaN, 78
 TaC–LaP, 78
 TaC–LaS, 78
 TaC–LuN, 78
 TaC–MgO, 78
 TaC–Mn, 70
 TaC–Mn₅C₂, 78
 TaC–Mn₇C₃, 78
 TaC–Mo, 70
 TaC–Mo–Re, 71
 TaC–Mo₂C, 78
 TaC–Mo₂C–TiC–Ni, 72
 TaC–Mo₂C–TiC–TiN–Ni, 72
 TaC–Mo₂C–TiC–TiN–VC–WC–Co–Ni, 66
 TaC–Mo₂C–TiC–TiN–WC–Ce–Co–Ni, 65
 TaC–Mo₂C–TiC–TiN–WC–Co–Ni, 66
 TaC–Mo₂C–TiC–TiN–WC–Ni, 72
 TaC–Mo₂C–TiC–WC–Co–Ni, 67
 TaC–MoC, 78
 TaC–MoSi₂, 79
 TaC–N₂, 88
 TaC–Nb, 71
 TaC–NbC, 79
 TaC–NbC–Co, 67
 TaC–NbC–Ni, 72
 TaC–NbC–ThC, 79
 TaC–NbC–TiC, 79
 TaC–NbC–TiC–TiN–Co, 67
 TaC–NbC–TiC–TiN–Co–Ni, 67
 TaC–NbC–TiC–TiN–Ni, 72
 TaC–NbC–TiC–TiN–VC–WC–Co–Mo–Ni,
 67
 TaC–NbC–TiC–TiN–WC–Co, 67
 TaC–NbC–TiC–WC–Co, 67
 TaC–NbC–UC, 79
 TaC–NbC–VC, 79
 TaC–NbC–WC, 79
 TaC–NbC–WC–Co, 67
 TaC–NbC–ZrC, 79
 TaC–NbN, 80
 TaC–NbO, 80
 TaC–Nb₅Si₃, 80
 TaC–Nd₂Fe₁₄B, 80
 TaC–NdN, 80
 TaC–NH₃, 87
 TaC–Ni, 71
 TaC–Ni–Cr, 71
 TaC–NpC, 80
 TaC–NpN, 80
 TaC–O₂, 88
 TaC–Os, 73
 TaC–Pb, 73
 TaC–Pd, 73
 TaC–PrN, 80
 TaC–Pt, 73
 TaC–Pu, 73
 TaC–PuC, 80
 TaC–PuN, 80
 TaC–PuP, 80
 TaC–PuS, 80
 TaC–Re, 73
 TaC–Rh, 73
 TaC–Ru, 74
 TaC–S, 74
 TaC–Sb, 74
 TaC–ScC, 80
 TaC–ScN, 80
 TaC–Si, 74
 TaC–Si₃N₄, 80
 TaC–SiC, 80
 TaC–SmN, 80
 TaC–Sn, 74
 TaC–Ta, 74
 TaC–Ta₂O₅, 82
 TaC–Ta₅Si₃, 81
 TaC–TaB₂, 81
 TaC–TaN, 81
 TaC–TaN–NbC–TiC, 79
 TaC–TaN–Ta, 74
 TaC–TaN–TaO, 81
 TaC–TaN–TiC–TiN, 81
 TaC–TaSi₂, 81
 TaC–TbN, 82
 TaC–Tc, 74
 TaC–TcC, 82
 TaC–Th, 74
 TaC–ThC, 82
 TaC–ThC–TiC, 82
 TaC–ThC–UC, 82
 TaC–ThC–VC, 82
 TaC–ThC–ZrC, 82
 TaC–ThC₂, 82
 TaC–ThN, 82
 TaC–ThP, 82
 TaC–ThS, 82
 TaC–Ti, 75
 TaC–TiC, 83
 TaC–TiC–Al, 64
 TaC–TiC–Co, 67
 TaC–TiC–Mo–Ni, 70
 TaC–TiC–Ni, 72
 TaC–TiC–TiN, 83
 TaC–TiC–TiN–Co, 67
 TaC–TiC–TiN–Fe, 69
 TaC–TiC–TiN–Ni, 72
 TaC–TiC–TiN–WC–Co–Ni, 68
 TaC–TiC–TiN–WC–Ni, 72
 TaC–TiC–TiN–WC–ZrC–Mo–Ni, 70

TaC–TiC–UC, 83
 TaC–TiC–VC, 83
 TaC–TiC–WC, 83
 TaC–TiC–WC–Co, 68
 TaC–TiC–WC–Mo–Ni, 70
 TaC–TiC–ZrC, 83
 TaC–TiN, 84
 TaC–TiO, 84
 TaC–Ti, 75
 TaC–U, 75
 TaC–UC, 84
 TaC–UC–VC, 84
 TaC–UC–ZrC, 84
 TaC–UC₂, 84
 TaC–UN, 84
 TaC–UP, 84
 TaC–US, 84
 TaC–V, 75
 TaC–VC, 84
 TaC–VC–Al, 65
 TaC–VC–Co, 68
 TaC–VC–WC, 84
 TaC–VC–ZrC, 84
 TaC–VN, 85
 TaC–W, 75
 TaC–W₂B₅, 85
 TaC–W₂C, 85
 TaC–WC, 85
 TaC–WC–Co, 68
 TaC–WC–ZrC, 85
 TaC–YbN, 86
 TaC–YC, 86
 TaC–YN, 86
 TaC–Zr, 75
 TaC–ZrC, 86
 TaC–ZrC–Co, 68
 TaC–ZrC–Ni, 72
 TaC–ZrN, 86
 TaC–ZrO₂, 86
 TaC–ZrP, 86
 TaN–ZrC, *see* ZrC–TaN
 TaSi₂–ZrC, *see* ZrC–TaSi₂
 TbN–ZrC, *see* ZrC–TbN
 Tc–ZrC, *see* ZrC–Tc
 TcC–ZrC, *see* ZrC–TcC
 Th–ZrC, *see* ZrC–Th
 ThC–TiC–ZrC, *see* ZrC–ThC–TiC
 ThC–UC–ZrC, *see* ZrC–ThC–UC
 ThC–VC–ZrC, *see* ZrC–ThC–VC
 ThC–ZrC, *see* ZrC–ThC
 ThC₂–ZrC, *see* ZrC–ThC₂
 ThN–ZrC, *see* ZrC–ThN
 ThO₂–UO₂–ZrC, *see* ZrC–ThO₂–UO₂
 ThO₂–UO₂–ZrC, *see* ZrC–UO₂–ThO₂

ThO₂–ZrC, *see* ZrC–ThO₂
 ThP–ZrC, *see* ZrC–ThP
 ThS–ZrC, *see* ZrC–ThS
 Ti–ZrC, *see* ZrC–Ti
 TiB₂–ZrC, *see* ZrC–TiB₂
 TiC–TiN–ZrC, *see* ZrC–TiC–TiN
 TiC–UC–ZrC, *see* ZrC–TiC–UC
 TiC–VC–ZrC, *see* ZrC–TiC–VC
 TiC–WC–ZrC, *see* ZrC–TiC–WC
 TiC–ZrC, *see* ZrC–TiC
 TiN–ZrC, *see* ZrC–TiN
 TiO–ZrC, *see* ZrC–TiO
 Ti–ZrC, *see* ZrC–Ti

U

U–UC–Zr–ZrC, *see* ZrC–UC–U–Zr
 U–ZrC, *see* ZrC–U
 UC–UC₂–ZrC, *see* ZrC–UC–UC₂
 UC–UN–ZrC, *see* ZrC–UC–UN
 UC–US–ZrC, *see* ZrC–UC–US
 UC–VC–ZrC, *see* ZrC–UC–VC
 UC–W–ZrC, *see* ZrC–UC–W
 UC–WC–ZrC, *see* ZrC–UC–WC
 UC–ZrC, *see* ZrC–UC
 UC₂–ZrC, *see* ZrC–UC₂
 UN–ZrC, *see* ZrC–UN
 UO₂–ZrC, *see* ZrC–UO₂
 UP–ZrC, *see* ZrC–UP
 US–ZrC, *see* ZrC–US

V

V–ZrC, *see* ZrC–V
 VC–WC–ZrC, *see* ZrC–VC–WC
 VC–ZrC, *see* ZrC–VC
 VN–ZrC, *see* ZrC–VN

W

W–W₂C–ZrC, *see* ZrC–W₂C–W
 W–ZrC, *see* ZrC–W
 W₂B₅–ZrC, *see* ZrC–W₂B₅
 W₂C–ZrC, *see* ZrC–W₂C
 WC–ZrC, *see* ZrC–WC

X

Xe–ZrC, *see* ZrC–Xe

Y

YbN–ZrC, *see* ZrC–YbN
 YC–ZrC, *see* ZrC–YC
 YN–ZrC, *see* ZrC–YN

Z

Zn–ZrC, *see* ZrC–Zn
 Zr–ZrB₂–ZrC, *see* ZrC–ZrB₂–Zr

- Zr–ZrC–ZrN, *see* ZrC–ZrN–Zr
Zr–ZrC, *see* ZrC–Zr
ZrB₂–ZrC–ZrN, *see* ZrC–ZrN–ZrB₂
ZrB₂–ZrC, *see* ZrC–ZrB₂
ZrC–Ag, 528
ZrC–Ag–Pd, 528
ZrC–Al, 528
ZrC–Al–Cu, 528
ZrC–Al–Mg, 528
ZrC–Al–Zr, 528
ZrC–Al₂O₃, 544
ZrC–Al₂O₃–Al, 529
ZrC–Al₄C₃, 543
ZrC–Al₄C₃–Ge, 533
ZrC–Al₄C₃–Si, 540
ZrC–Al₄C₃–SiC, 543
ZrC–Al₄C₃–SiC–TiC, 543
ZrC–Al₄C₃–YC, 544
ZrC–Al₄C₃–YC₂, 544
ZrC–B, 529
ZrC–B₄C, 544
ZrC–B₄C–B, 529
ZrC–B₄C–BN, 544
ZrC–B₄C–SiB₃, 544
ZrC–Ba, 529
ZrC–Be, 529
ZrC–Bi, 529
ZrC–Bi–Pb, 529
ZrC–BN, 544
ZrC–Br₂, 557
ZrC–C, 529
ZrC–C–Fe, 530
ZrC–C–Fe–Mn, 530
ZrC–C–Ni, 530
ZrC–CaO, 544
ZrC–Cd, 530
ZrC–Ce, 530
ZrC–CeC₂, 544
ZrC–CeC₂–UC, 544
ZrC–CeN, 544
ZrC–CeP, 544
ZrC–CeS, 544
ZrC–Cl₂, 558
ZrC–Co, 530
ZrC–CO, 557
ZrC–Co–Ni, 530
ZrC–Co–Ni–W, 530
ZrC–Co₂, 558
ZrC–Cr, 531
ZrC–Cr–Cu–Fe, 531
ZrC–Cr–Fe, 532
ZrC–Cr–Ni, 532
ZrC–Cr₂₃C₆, 590
ZrC–Cr₂₃C₆–Cr, 532
ZrC–Cr₂O₃, 545
ZrC–Cr₃C₂, 545
ZrC–Cr₃C₂–Cr₇C₃, 545
ZrC–Cr₃C₂–TiC, 545
ZrC–Cr₇C₃, 545
ZrC–Cs, 532
ZrC–Cu, 532
ZrC–Cu–Fe–Si, 532
ZrC–Cu–Ni, 532
ZrC–Cu–V–Zr, 532
ZrC–Cu–Zr, 532
ZrC–Dy₂O₃, 545
ZrC–DyN, 545
ZrC–ErN, 545
ZrC–Eu, 533
ZrC–EuN, 545
ZrC–EuO, 545
ZrC–F₂, 559
ZrC–Fe, 533
ZrC–Fe–Ni, 533
ZrC–Fe–Si, 533
ZrC–Fe₂O₃, 546
ZrC–Fe₃C, 545
ZrC–Ga, 533
ZrC–GdN, 546
ZrC–Ge, 533
ZrC–H₂, 559
ZrC–H₂O, 560
ZrC–HBr, 561
ZrC–HCl, 561
ZrC–He, 561
ZrC–Hf, 534
ZrC–HF, 561
ZrC–HfC, 546
ZrC–HfC–Co, 530
ZrC–HfC–NbC, 546
ZrC–HfC–Ni, 538
ZrC–HfC–TaC, 546
ZrC–HfC–ThC, 546
ZrC–HfC–TiC, 546
ZrC–HfC–UC, 546
ZrC–HfC–VC, 546
ZrC–HfC–WC, 546
ZrC–HfN, 546
ZrC–HI, 561
ZrC–HoN, 546
ZrC–I₂, 561
ZrC–In, 534
ZrC–Ir, 534
ZrC–K, 534
ZrC–Kr, 561
ZrC–LaB₆, 546
ZrC–LaB₆–SiC, 546
ZrC–LaN, 546

- ZrC–LaP, 546
ZrC–LaS, 546
ZrC–Li, 534
ZrC–LuN, 546
ZrC–Mg, 534
ZrC–MgO, 546
ZrC–Mn, 534
ZrC–Mn₅C₂, 547
ZrC–Mn₇C₃, 547
ZrC–Mo, 535
ZrC–Mo–Ni, 535
ZrC–Mo–Re, 535
ZrC–Mo–W, 535
ZrC–Mo₂C, 538
ZrC–Mo₂C–TiC–Ni, 538
ZrC–MoC, 547
ZrC–MoC–NbC, 547
ZrC–MoC–UC, 547
ZrC–MoSi₂, 547
ZrC–N₂, 561
ZrC–Nb, 536
ZrC–Nb₂C, 548
ZrC–NbC, 547
ZrC–NbC–Al, 529
ZrC–NbC–Co, 530
ZrC–NbC–Ni, 538
ZrC–NbC–TaC, 547
ZrC–NbC–ThC, 547
ZrC–NbC–TiC, 547
ZrC–NbC–UC, 547
ZrC–NbC–VC, 547
ZrC–NbC–WC, 548
ZrC–NbN, 548
ZrC–NbO, 548
ZrC–Nd₂Fe₁₄B, 548
ZrC–NdN, 548
ZrC–NH₃, 562
ZrC–Ni, 537
ZrC–Ni–P, 538
ZrC–Ni–W, 538
ZrC–NiO, 548
ZrC–NpC, 548
ZrC–NpN, 548
ZrC–O₂, 562
ZrC–Os, 539
ZrC–Pb, 539
ZrC–Pd, 539
ZrC–PrN, 548
ZrC–Pt, 539
ZrC–Pu, 539
ZrC–Pu₂C₃, 548
ZrC–PuC, 548
ZrC–PuC–UC, 548
ZrC–PuN, 548
ZrC–PuP, 549
ZrC–PuS, 549
ZrC–Rb, 539
ZrC–Re, 539
ZrC–Rh, 540
ZrC–Ru, 540
ZrC–S, 540
ZrC–Sb, 540
ZrC–Sc, 540
ZrC–ScC, 549
ZrC–ScN, 549
ZrC–Si, 540
ZrC–Si₃N₄, 549
ZrC–Si₃N₄–Al₂O₃, 549
ZrC–Si₃N₄–MgO, 549
ZrC–SiC, 549
ZrC–SiC–Al, 529
ZrC–SiC–TiC–Al, 529
ZrC–SiC–WC, 549
ZrC–SiC–ZrB₂, 549
ZrC–SiO₂–Al₂O₃–CaO–Fe₂O₃(basalt), 549
ZrC–SmN, 550
ZrC–Sn, 541
ZrC–Sr, 541
ZrC–Ta, 541
ZrC–Ta₂C, 550
ZrC–TaC, 550
ZrC–TaC–Co, 530
ZrC–TaC–Ni, 538
ZrC–TaC–ThC, 550
ZrC–TaC–TiC, 550
ZrC–TaC–UC, 550
ZrC–TaC–VC, 550
ZrC–TaC–WC, 550
ZrC–Ta₂N, 550
ZrC–TaSi₂, 550
ZrC–TbN, 550
ZrC–Tc, 541
ZrC–TcC, 550
ZrC–Th, 541
ZrC–ThC, 550
ZrC–ThC–TiC, 551
ZrC–ThC–UC, 551
ZrC–ThC–VC, 551
ZrC–ThC₂, 551
ZrC–ThN, 551
ZrC–ThO₂, 551
ZrC–ThO₂–UO₂, 551
ZrC–ThP, 551
ZrC–ThS, 551
ZrC–Ti, 541
ZrC–TiB₂, 552
ZrC–TiC, 551
ZrC–TiC–Co, 531

- ZrC-TiC-In, 534
ZrC-TiC-Mo-Ni, 536
ZrC-TiC-NbN, 552
ZrC-TiC-Ni, 538
ZrC-TiC-TiN, 552
ZrC-TiC-TiN-Mo-Ni, 536
ZrC-TiC-TiN-Ni, 538
ZrC-TiC-TiN-TiO-Ni, 538
ZrC-TiC-TiN-WC-Ni, 538
ZrC-TiC-UC, 552
ZrC-TiC-VC, 552
ZrC-TiC-VC-WC-Co, 531
ZrC-TiC-WC, 552
ZrC-TiC-WC-C, 530
ZrC-TiC-WC-Co, 531
ZrC-TiN, 552
ZrC-TiO, 552
ZrC-Tl, 541
ZrC-U, 541
ZrC-UC, 552
ZrC-UC-Mo, 536
ZrC-UC-Nb, 537
ZrC-UC-Ni, 539
ZrC-UC-Pu, 539
ZrC-UC-Re, 539
ZrC-UC-Ta, 541
ZrC-UC-U-Zr, 543
ZrC-UC-UC₂, 553
ZrC-UC-UN, 553
ZrC-UC-US, 553
ZrC-UC-VC, 553
ZrC-UC-W, 542
ZrC-UC-WC, 553
ZrC-UC₂, 553
ZrC-UN, 553
ZrC-UO₂, 553
ZrC-UO₂-ThO₂, 554
ZrC-UP, 553
ZrC-US, 554
ZrC-V, 542
ZrC-VC, 554
ZrC-VC-Co, 531
ZrC-VC-WC, 554
ZrC-VC-WC-C, 530
ZrC-VC-WC-Co, 531
ZrC-VN, 554
ZrC-W, 542
ZrC-W₂B₅, 555
ZrC-W₂C, 555
ZrC-W₂C-W, 542
ZrC-WC, 554
ZrC-WC-Ni, 538
ZrC-Xe, 571
ZrC-YbN, 555
ZrC-YC, 555
ZrC-YN, 555
ZrC-Zn, 542
ZrC-Zr, 542
ZrC-ZrB₂, 556
ZrC-ZrB₂-La, 534
ZrC-ZrB₂-Ni, 539
ZrC-ZrB₂-Zr, 543
ZrC-ZrN, 555
ZrC-ZrN-H₂O, 561
ZrC-ZrN-Zr, 543
ZrC-ZrN-ZrB₂, 555
ZrC-ZrN-ZrO, 555
ZrC-ZrO-H₂, 559
ZrC-ZrO₂, 556
ZrC-ZrP, 555